

# CHRONIC INFLAMMATION AND PHARMACOLOGICAL INTERVENTIONS IN CARDIOVASCULAR DISEASES

EDITED BY: Xianwei Wang, Min Zhang and Zufeng Ding

PUBLISHED IN: Frontiers in Pharmacology and  
Frontiers in Cell and Developmental Biology





# frontiers

## Frontiers eBook Copyright Statement

The copyright in the text of individual articles in this eBook is the property of their respective authors or their respective institutions or funders. The copyright in graphics and images within each article may be subject to copyright of other parties. In both cases this is subject to a license granted to Frontiers.

The compilation of articles constituting this eBook is the property of Frontiers.

Each article within this eBook, and the eBook itself, are published under the most recent version of the Creative Commons CC-BY licence.

The version current at the date of publication of this eBook is CC-BY 4.0. If the CC-BY licence is updated, the licence granted by Frontiers is automatically updated to the new version.

When exercising any right under the CC-BY licence, Frontiers must be attributed as the original publisher of the article or eBook, as applicable.

Authors have the responsibility of ensuring that any graphics or other materials which are the property of others may be included in the CC-BY licence, but this should be checked before relying on the CC-BY licence to reproduce those materials. Any copyright notices relating to those materials must be complied with.

Copyright and source acknowledgement notices may not be removed and must be displayed in any copy, derivative work or partial copy which includes the elements in question.

All copyright, and all rights therein, are protected by national and international copyright laws. The above represents a summary only. For further information please read Frontiers' Conditions for Website Use and Copyright Statement, and the applicable CC-BY licence.

ISSN 1664-8714

ISBN 978-2-83250-159-7

DOI 10.3389/978-2-83250-159-7

## About Frontiers

Frontiers is more than just an open-access publisher of scholarly articles: it is a pioneering approach to the world of academia, radically improving the way scholarly research is managed. The grand vision of Frontiers is a world where all people have an equal opportunity to seek, share and generate knowledge. Frontiers provides immediate and permanent online open access to all its publications, but this alone is not enough to realize our grand goals.

## Frontiers Journal Series

The Frontiers Journal Series is a multi-tier and interdisciplinary set of open-access, online journals, promising a paradigm shift from the current review, selection and dissemination processes in academic publishing. All Frontiers journals are driven by researchers for researchers; therefore, they constitute a service to the scholarly community. At the same time, the Frontiers Journal Series operates on a revolutionary invention, the tiered publishing system, initially addressing specific communities of scholars, and gradually climbing up to broader public understanding, thus serving the interests of the lay society, too.

## Dedication to Quality

Each Frontiers article is a landmark of the highest quality, thanks to genuinely collaborative interactions between authors and review editors, who include some of the world's best academicians. Research must be certified by peers before entering a stream of knowledge that may eventually reach the public - and shape society; therefore, Frontiers only applies the most rigorous and unbiased reviews.

Frontiers revolutionizes research publishing by freely delivering the most outstanding research, evaluated with no bias from both the academic and social point of view. By applying the most advanced information technologies, Frontiers is catapulting scholarly publishing into a new generation.

## What are Frontiers Research Topics?

Frontiers Research Topics are very popular trademarks of the Frontiers Journals Series: they are collections of at least ten articles, all centered on a particular subject. With their unique mix of varied contributions from Original Research to Review Articles, Frontiers Research Topics unify the most influential researchers, the latest key findings and historical advances in a hot research area! Find out more on how to host your own Frontiers Research Topic or contribute to one as an author by contacting the Frontiers Editorial Office: [frontiersin.org/about/contact](https://frontiersin.org/about/contact)



# CHRONIC INFLAMMATION AND PHARMACOLOGICAL INTERVENTIONS IN CARDIOVASCULAR DISEASES

Topic Editors:

**Xianwei Wang**, Xinxiang Medical University, China

**Min Zhang**, King's College London, United Kingdom

**Zufeng Ding**, University of Arkansas for Medical Sciences, United States

**Citation:** Wang, X., Zhang, M., Ding, Z., eds. (2022). Chronic Inflammation and Pharmacological Interventions in Cardiovascular Diseases.

Lausanne: Frontiers Media SA. doi: 10.3389/978-2-83250-159-7

# Table of Contents

- 06 Editorial: Chronic Inflammation and Pharmacological Interventions in Cardiovascular Diseases**  
Xiaoping Wang, Min Zhang and Xianwei Wang
- 10 Water-Soluble Tomato Extract Fruitflow Alters the Phosphoproteomic Profile of Collagen-Stimulated Platelets**  
Shenghao Zhang, Huilian Chen, Chuanbao Li, Beidong Chen, Huan Gong, Yanyang Zhao and Ruomei Qi
- 20 The Mechanism Actions of Astragaloside IV Prevents the Progression of Hypertensive Heart Disease Based on Network Pharmacology and Experimental Pharmacology**  
Haoran Jing, Rongsheng Xie, Yu Bai, Yuchen Duan, Chongyang Sun, Ye Wang, Rongyi Cao, Zaisheng Ling and Xiufen Qu
- 33 Circulating Exosomal miRNAs as Novel Biomarkers Perform Superior Diagnostic Efficiency Compared With Plasma miRNAs for Large-Artery Atherosclerosis Stroke**  
Mengying Niu, Hong Li, Xu Li, Xiaoqian Yan, Aijun Ma, Xudong Pan and Xiaoyan Zhu
- 47 Activation of Nrf2 by Lithospermic Acid Ameliorates Myocardial Ischemia and Reperfusion Injury by Promoting Phosphorylation of AMP-Activated Protein Kinase  $\alpha$  (AMPK $\alpha$ )**  
Min Zhang, Li Wei, Saiyang Xie, Yun Xing, Wenke Shi, Xiaofeng Zeng, Si Chen, Shasha Wang, Wei Deng and Qizhu Tang
- 60 Oxytocin Protects Against Isoproterenol-Induced Cardiac Hypertrophy by Inhibiting PI3K/AKT Pathway via a lncRNA GAS5/miR-375-3p/KLF4-Dependent Mechanism**  
Yuqiao Yang, Zhuoran Wang, Mengran Yao, Wei Xiong, Jun Wang, Yu Fang, Wei Yang, Haixia Jiang, Ning Song, Lan Liu and Jinqiao Qian
- 78 LKB1 Regulates Vascular Macrophage Functions in Atherosclerosis**  
Xuewen Wang, Ziwei Liang, Hong Xiang, Yanqiu Li, Shuhua Chen and Hongwei Lu
- 88 Midkine Prevents Calcification of Aortic Valve Interstitial Cells via Intercellular Crosstalk**  
Qian Zhou, Hong Cao, Xiaoyi Hang, Huamin Liang, Miaomiao Zhu, Yixian Fan, Jiawei Shi, Nianguo Dong and Ximiao He
- 104 Mechanism of Improving Aspirin Resistance: Blood-Activating Herbs Combined With Aspirin in Treating Atherosclerotic Cardiovascular Diseases**  
Yixi Zhao, Shengjie Yang and Min Wu
- 114 9-PAHSA Improves Cardiovascular Complications by Promoting Autophagic Flux and Reducing Myocardial Hypertrophy in Db/Db Mice**  
Yan-Mei Wang, Shou-Ling Mi, Hong Jin, Qi-Lin Guo, Zhong-Yu Yu, Jian-Tao Wang, Xiao-Ming Zhang, Qian Zhang, Na-Na Wang, Yan-Yan Huang, Hou-Guang Zhou and Jing-Chun Guo

- 127 ***Role of Higenamine in Heart Diseases: A Mini-Review***  
Jianxia Wen, Mingjie Li, Wenwen Zhang, Haoyu Wang, Yan Bai, Junjie Hao, Chuan Liu, Ke Deng and Yanling Zhao
- 140 ***Traditional Chinese Medicine Targeting Heat Shock Proteins as Therapeutic Strategy for Heart Failure***  
Yanchun Wang, Junxuan Wu, Dawei Wang, Rongyuan Yang and Qing Liu
- 157 ***Research Advances in Cardio-Cerebrovascular Diseases of Ligusticum chuanxiong Hort.***  
Dan Li, Yu Long, Shuang Yu, Ai Shi, Jinyan Wan, Jing Wen, Xiaoqiu Li, Songyu Liu, Yulu Zhang, Nan Li, Chuan Zheng, Ming Yang and Lin Shen
- 183 ***Induction of Heme Oxygenase-1 Modifies the Systemic Immunity and Reduces Atherosclerotic Lesion Development in ApoE Deficient Mice***  
Leyi Yao, Yali Hao, Guanmei Wen, Qingzhong Xiao, Penglong Wu, Jinheng Wang and Jinbao Liu
- 199 ***PAMPs and DAMPs as the Bridge Between Periodontitis and Atherosclerosis: The Potential Therapeutic Targets***  
Xuanzhi Zhu, Hanyao Huang and Lei Zhao
- 211 ***DNA Methylation Aberrant in Atherosclerosis***  
Yao Dai, Danian Chen and Tingting Xu
- 223 ***Pyroptosis-Related Inflammasome Pathway: A New Therapeutic Target for Diabetic Cardiomyopathy***  
Zhengyao Cai, Suxin Yuan, Xingzhao Luan, Jian Feng, Li Deng, Yumei Zuo and Jiafu Li
- 234 ***A Multitarget Therapeutic Peptide Derived From Cytokine Receptors Based on in Silico Analysis Alleviates Cytokine-Stimulated Inflammation***  
Chun-Chun Chang, Shih-Yi Peng, Hao-Hsiang Tsao, Hsin-Ting Huang, Xing-Yan Lai, Hao-Jen Hsu and Shinn-Jong Jiang
- 248 ***Development and Validation of Ischemic Events Related Signature After Carotid Endarterectomy***  
Chunguang Guo, Zaoqu Liu, Can Cao, Youyang Zheng, Taoyuan Lu, Yin Yu, Libo Wang, Long Liu, Shirui Liu, Zhaozhui Hua, Xinwei Han and Zhen Li
- 262 ***Honokiol Inhibits Atrial Metabolic Remodeling in Atrial Fibrillation Through Sirt3 Pathway***  
Guang Zhong Liu, Wei Xu, Yan Xiang Zang, Qi Lou, Peng Zhou Hang, Qiang Gao, Hang Shi, Qi Yun Liu, Hong Wang, Xin Sun, Cheng Liu, Peng Zhang, Hua Dong Liu and Shao Hong Dong
- 275 ***Role of Adiponectin Receptor 1 in Promoting Nitric Oxide-Mediated Flow-Induced Dilation in the Human Microvasculature***  
Katie E. Cohen, Boran Katunaric, Mary E. Schulz, Gopika SenthilKumar, Micaela S. Young, James E. Mace and Julie K. Freed
- 284 ***Farrerol Alleviates Myocardial Ischemia/Reperfusion Injury by Targeting Macrophages and NLRP3***  
Lin Zhou, Shuhui Yang and Xiaoming Zou
- 298 ***Association of TGF- $\beta$  Canonical Signaling-Related Core Genes With Aortic Aneurysms and Aortic Dissections***  
Jicheng Chen and Rong Chang

- 311** *Propofol Protects Myocardium From Ischemia/Reperfusion Injury by Inhibiting Ferroptosis Through the AKT/p53 Signaling Pathway*  
Shengqiang Li, Zhen Lei, Xiaomei Yang, Meng Zhao, Yonghao Hou, Di Wang, Shuhai Tang, Jingxin Li and Jingui Yu
- 322** *Adenosine in Acute Myocardial Infarction-Associated Reperfusion Injury: Does it Still Have a Role?*  
Corrado De Marco, Thierry Charron and Guy Rousseau
- 329** *Qiliqiangxin Modulates the Gut Microbiota and NLRP3 Inflammasome to Protect Against Ventricular Remodeling in Heart Failure*  
Yingdong Lu, Mi Xiang, Laiyun Xin, Yang Zhang, Yuling Wang, Zihuan Shen, Li Li and Xiangning Cui
- 343** *Naltrexone-Induced Cardiac Function Improvement is Associated With an Attenuated Inflammatory Response and Lipid Peroxidation in Volume Overloaded Rats*  
Lukas Dehe, Shaaban A. Mousa, Mohammed Shaqura, Mehdi Shakibaei, Michael Schäfer and Sascha Treskatsch
- 355** *AMPK Activation Alleviates Myocardial Ischemia-Reperfusion Injury by Regulating Drp1-Mediated Mitochondrial Dynamics*  
Jingxia Du, Hongchao Li, Jingjing Song, Tingting Wang, Yibo Dong, An Zhan, Yan Li and Gaofeng Liang
- 365** *AKT/PACS2 Participates in Renal Vascular Hyperpermeability by Regulating Endothelial Fatty Acid Oxidation in Diabetic Mice*  
Zhihao Shu, Shuhua Chen, Hong Xiang, Ruoru Wu, Xuwen Wang, Jie Ouyang, Jing Zhang, Huiqin Liu, Alex F. Chen and Hongwei Lu
- 382** *Cycloviobuxine D Ameliorates Experimental Diabetic Cardiomyopathy by Inhibiting Cardiomyocyte Pyroptosis via NLRP3 in vivo and in vitro*  
Ge Gao, Lingyun Fu, Yini Xu, Ling Tao, Ting Guo, Guanqin Fang, Guangqiong Zhang, Shengquan Wang, Ti Qin, Peng Luo and Xiangchun Shen



## OPEN ACCESS

## EDITED AND REVIEWED BY

Francesco Rossi,  
University of Campania Luigi Vanvitelli,  
Italy

## \*CORRESPONDENCE

Min Zhang,  
min.zhang@kcl.ac.uk  
Xianwei Wang,  
wangxianwei1116@126.com

## SPECIALTY SECTION

This article was submitted to  
Cardiovascular and Smooth Muscle  
Pharmacology,  
a section of the journal  
Frontiers in Pharmacology

RECEIVED 13 July 2022

ACCEPTED 29 July 2022

PUBLISHED 24 August 2022

## CITATION

Wang X, Zhang M and Wang X (2022),  
Editorial: Chronic inflammation and  
pharmacological interventions in  
cardiovascular diseases.  
*Front. Pharmacol.* 13:993569.  
doi: 10.3389/fphar.2022.993569

## COPYRIGHT

© 2022 Wang, Zhang and Wang. This is  
an open-access article distributed  
under the terms of the [Creative  
Commons Attribution License \(CC BY\)](#).  
The use, distribution or reproduction in  
other forums is permitted, provided the  
original author(s) and the copyright  
owner(s) are credited and that the  
original publication in this journal is  
cited, in accordance with accepted  
academic practice. No use, distribution  
or reproduction is permitted which does  
not comply with these terms.

# Editorial: Chronic inflammation and pharmacological interventions in cardiovascular diseases

Xiaoping Wang<sup>1,2</sup>, Min Zhang<sup>3\*</sup> and Xianwei Wang<sup>1,2\*</sup>

<sup>1</sup>Department of Cardiology, The First Affiliated Hospital Xinxiang Medical University, Weihui, China,

<sup>2</sup>Department of Human Anatomy and Histoembryology, Xinxiang Medical University, Xinxiang, China,

<sup>3</sup>School of Cardiovascular and Metabolic Medicine & Sciences, King's College London BHF Centre of Research Excellence, London, United Kingdom

## KEYWORDS

chronic inflammation, cardiovascular diseases, pharmacological interventions, cell-based therapies, cellular and molecular mechanisms

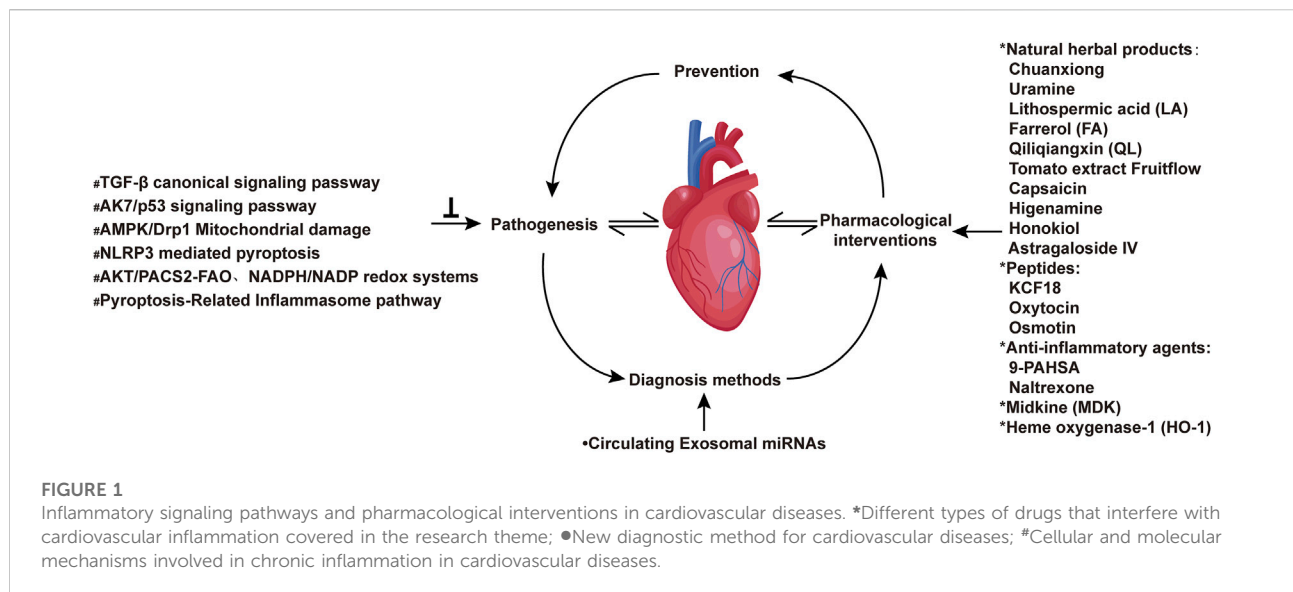
## Editorial on the Research Topic

Chronic inflammation and pharmacological interventions in  
cardiovascular diseases

## Introduction

Cardiovascular diseases (CVDs) are a group of complex and multifactorial disorders and their pathogenesis is still not completely understood. It is recognized that inflammation, especially the chronic inflammation is a common pathogenesis of many CVDs, such as atherosclerosis, myocardial infarction and stroke. Continuous inflammation causes a series of pathological changes of hearts and blood vessels. Clinical trials and basic studies have shown that inflammatory inhibition by pharmacological and other interventions can markedly reduce the degree of pathological changes of hearts or blood vessels, and decrease the morbidity and mortality of CVD events. Thus, the advance of therapies direct or indirect modulating chronic inflammation is an important approach for the prevention and treatment of CVDs.

Pharmacological interventions are the primary therapeutic approaches for CVDs. In the past few decades, plenty of drugs for different targets including anti-inflammatory agents have been developed and used to prevent and treat different CVDs in the clinic. In the past few years, the flood of new drugs including chemical-based drugs and natural herbal products have provided more choices to the treatment of CVDs. Recently, biotherapies and molecular targeted therapies utilizing cell-based products such as stem cells, exosomes, immune cells, cytokines, peptides and monoclonal antibodies have also been used to treat CVDs, and some of them specifically target to



inflammation. The purpose of this Research Topic was to provide interested readers with new advances on prevention and treatment of CVDs, especially on the new therapies targeting chronic inflammation.

The Research Topic themed “Chronic inflammation and pharmacological interventions in cardiovascular diseases” presents a series of articles that highlight the latest studies and strategies that overcome current obstacles in treating chronic inflammation and pharmacological interventions in cardiovascular diseases. This issue collates 30 selected peer-reviewed articles (including 20 original research articles and 10 reviews) covering molecular mechanisms of therapeutic targets, drug intervention targets, and novel diagnostic approaches to cardiovascular diseases (Figure 1).

## Related inflammatory pathways in Cardiovascular Diseases

Atherosclerosis is a serious clinical manifestation of cardiovascular disease (Soehnlein and Libby, 2021), which is the leading cause of premature death in humans (Valanti et al., 2021). Chronic inflammatory response is an important risk factor for the initiation and development of atherosclerosis (Yang et al., 2019), but the inflammatory molecular mechanisms in the occurrence and development of atherosclerotic plaques are not well understood. There are several articles in this Research Topic showed that some chronic inflammatory pathways play critical roles in cardiovascular diseases. Although increasing evidence indicates that genetic factors, particularly the transforming growth factor  $\beta$  (TGF- $\beta$ ) signaling pathway is involved in the development of aortic aneurysms (AAs), the specific action of TGF- $\beta$  signaling in AAs remains controversial (Thatcher, 2016; Tzavlaki and Moustakas, 2020). The review by Chen and Chang

focused on the role of canonical TGF- $\beta$  signaling pathway related to core genes such as TGFBR1, TGFBR2, SMAD2, SMAD3, SMAD4, and SMAD6 in aortic diseases. This review further clarified that the activation of classical TGF- $\beta$  signaling pathway is a determinant of a series of aortic diseases. Wang et al. revealed that liver kinase B1 (LBP1), a serine threonine kinase, played an important role in arteriosclerosis by regulating vascular macrophages after phosphorylation of activating adenosine monophosphate-activated protein kinase (AMPK). Periodontitis is a common chronic disorder that involves oral microbe-related inflammatory bone loss and local destruction of the periodontal ligament and is a risk factor for atherosclerosis (Naderi and Merchant, 2020). Periodontal pathogens produce pathogen associated molecular patterns (PAMPs), including lipopolysaccharide (LPS), PGN, and CpG DNA. Periodontal infection activates neutrophils to form neutrophil extracellular traps (NETs), which together with high mobility group box-1 (HMGB1) and alarmins released by damaged periodontal cells constitute damage-associated molecular patterns (DAMPs) (Gu and Han, 2020). Zhu et al. reported that PAMPs and DAMPs could activate excessive innate immunity by acting on Toll-like receptors (TLRs) and NOD-like receptors (NLRs) in arterial tissue, leading to foam cell formation, endothelial cell and vascular smooth muscle cell dysfunction, and promoting the massive release of inflammatory factors, which all contribute to atherosclerosis.

Diabetic cardiomyopathy (DCM) is one of the serious complications of diabetes, and increasing evidence supports that myocardial inflammation is a key player in the development of DCM (Dillmann, 2019). Pyroptosis is a type of programmed cell death that involves the release of cell contents and inflammatory mediators upon activation, leading to a powerful inflammatory response (Wang et al., 2020). While accumulating evidence implicates pyroptosis as a critical contributor to myocardial inflammation in

the progress of DCM (Yang et al., 2019; Zeng et al., 2020), the molecular mechanisms of cell pyroptosis and its involvement in DCM are not fully understood. Cai et al. reviewed the recent progress in this research field and discussed three main signaling pathways to potentially trigger DCM: 1) Toll like receptor 4 (TLR4)/nuclear factor kappa B (NF- $\kappa$ B) inflammasome/NOD-like receptor, pyrin domain-containing 3 (NLRP3) inflammasome signaling pathway; 2) AMPK/ROS/TXNIP/NLRP3 inflammasome signaling pathway; and 3) AMPK/SIRT1/Nrf2/HO-1/NF- $\kappa$ B inflammasome signaling pathway, all of which could be the possible therapeutic targets for the treatment of DCM in the future. Meanwhile, Gao et al. analyzed the beneficial effect of Cycloxanthine D (CVB-D) on cardiomyocyte pyroptosis associated with DCM, and explored its molecular regulatory mechanism. Their results demonstrated that CVB-D could ameliorate DCM by inhibiting cardiomyocyte pyroptosis via NLRP3 signaling *in vivo* and *in vitro*. These studies once again suggest that the signaling pathways of inflammatory response induced by cell pyroptosis play important roles in cardiovascular diseases.

## Natural drug intervention in cardiovascular diseases

Pharmacological interventions are the main treatment for cardiovascular diseases, and a variety of drugs have been developed for the prevention and treatment of different cardiovascular diseases. Chinese medicine has its unique advantages since it treats patients holistically as well as individually based on the personalised interventions (Fu et al., 2021). In this area, scholars reviewed the effects of traditional Chinese medicine Chuanxiong on cardiovascular and cerebrovascular diseases (Li et al.) and Uramine on heart diseases (Wen et al.). For example, the traditional Chinese medicine is effective to treat heart failure by targeting heat shock proteins (Wen et al.), as well as to treat atherosclerosis and other cardiovascular diseases by promoting blood circulation together with aspirin (Zhao et al.). Some researchers have further explored the signaling pathways of its action. Zhang et al. reported that lithospermic acid (LA) protected against myocardial ischemia-reperfusion (MI/R)-induced cardiac injury by promoting eNOS and Nrf2/HO-1 signaling via phosphorylation of AMPK $\alpha$ . Zhou et al. elucidated the molecular mechanism of action of a Chinese traditional medicine Farrerol (FA) in ischemia-reperfusion (I/R) injury. Their findings showed that FA indirectly protected cardiomyocytes by targeting macrophages, without relying on Nrf2-dependent or autophagy-dependent pathways, but indirectly protected cardiomyocytes through the inhibition of the interaction of NEK7 and NLRP3, thereby abolishing the assembly and activation of NLRP3 inflammasome, resulting in an effective inhibition to alleviate MI/R injury. Liu et al. investigated the effects and mechanisms of Honokiol (HL) in a rabbit atrial fibrillation (AF) model and found that the activation of Sirt3-dependent pathway

participated in atrial metabolic remodeling during AF, which could be inhibited by HL via regulating the Sirtuin-3 (Sirt3) dependent pathway. Sirt3 is widely recognized to be critically involved in diverse cardiovascular diseases including cardiac and vasculature remodeling (Dikalova et al., 2020; Tomczyk et al., 2022). Lu et al. reported that qiliqiangxin (QL) ameliorated ventricular remodeling and heart failure (HF) to some extent in rats by modulating the gut microbiota and NLRP3 inflammasome. Based on network pharmacology and experimental pharmacological analysis, Jing et al. identified that Astragaloside IV, a main active compound from *Astragalus membranaceus*, could be a promising agent to improve L-NAME-induced hypertensive heart disease partly via modulation of eNOS and oxidative stress. In addition, Zhang et al. found that water-soluble tomato extract fruitflow could inhibit platelet activation, which is beneficial to people who are at risk for platelet hyperactivity-associated thrombosis.

## Molecular targeted therapy in cardiovascular diseases

Recently, molecular targeted therapies have been broadly applied to treat CVDs, which include protein and peptide drugs, nucleic acid drugs, and gene editing technologies (Xu and Song, 2021). Apart from Chinese herbal medicine as stated above, the more targeted therapies including peptides have also been studied in the treatment of cardiovascular diseases and chronic inflammation. Yang et al. demonstrated that Oxytocin (OT) ameliorated cardiac hypertrophy by inhibiting PI3K/Akt pathway via lncRNA GAS5/miR-375-3p/KLF4 axis. Based on in Silico analysis, Chang et al. highlighted the importance of the multitarget therapeutic peptide KCF18 which could alleviate inflammation by blocking the interactions of TNF- $\alpha$ , IL-6, and IL-1 $\beta$  with their cognate receptors, thus reducing the translocation of NF- $\kappa$ B and decreasing the inflammatory gene expressions. By lowering the release of cytokines in plasma and directly affecting vascular cells, KCF18 was shown to significantly attenuate vascular inflammation. The property of KCF18 to prevent inflammation may hold a promise as a new treatment strategy for sepsis and other inflammatory vascular diseases.

## New diagnostic methods in cardiovascular diseases

Ischemic stroke is a common serious disease caused by arteriosclerosis (Banerjee and Chimowitz, 2017). Accurate and timely diagnosis of ischemic stroke is the key for the subsequent treatment. Prior studies on biomarkers for ischemic stroke have focused on proteins in plasma such as neuron-specific enolase and interleukin (Tiedt, Prestel et al., 2017). Recently, the applications of miRNAs as the sensitive biomarkers have also attracted significant research attention in a variety of disease settings (Rupaimoole and



Slack, 2017). However, there is scarcely any research to investigate the potential of exosome miRNAs as the diagnostic biomarkers for ischemic stroke. In this issue, Niu et al. reported for the first time that circulating exosome miRNAs including miR-369-3p, miR-493-3p, miR-379-5p, and miR-1296-5p could be the novel biomarkers with higher efficiency compared to conventional plasma factors in the diagnosis of large-artery atherosclerosis stroke (LAA). This is of great interest considering the method as time saving and cost saving. The authors hoped that exosomal miRNAs as new biomarkers can be applied for the prognosis analysis of LAA stroke, which may be helpful to improve the quality of life of stroke patients in the future.

## Summary

The pathogenesis of cardiovascular diseases is complex and interlinked, involving central mechanisms such as cardiomyocyte hypertrophy and death as well as systemic mechanisms such as chronic inflammation. Over last decades, significant evidence from both pre-clinical and clinical studies strongly indicates that targeting inflammation either locally or globally is an effective means for the prevention and treatment of cardiovascular diseases. Here, it is exciting to witness the latest advance, the beautiful works published in this issue elucidate some novel molecular mechanisms, identify some promising peptides, cytokines and natural products, and therefore provide the new insight into the pathogenic role of chronic inflammation in cardiovascular diseases. It is expected that this will continue to be a hot research area, the more

detailed dissection of mechanisms and evaluation of the therapeutic potential by targeting inflammation undoubtedly has great translational significance for the treatment of cardiovascular diseases.

## Author contributions

XwW and MZ are guest editors of this Research Topic. XpW wrote the first draft of the manuscript. XwW and MZ reviewed and revised this editorial. All authors listed have made a substantial, direct, and intellectual contribution to the work and approved it for publication.

## Conflict of interest

The authors declare that the research was conducted in the absence of any commercial or financial relationships that could be construed as a potential conflict of interest.

## Publisher's note

All claims expressed in this article are solely those of the authors and do not necessarily represent those of their affiliated organizations, or those of the publisher, the editors and the reviewers. Any product that may be evaluated in this article, or claim that may be made by its manufacturer, is not guaranteed or endorsed by the publisher.

## References

- Banerjee, C., and Chimowitz, M. I. (2017). Stroke caused by atherosclerosis of the major intracranial arteries. *Circ. Res.* 120 (3), 502–513. doi:10.1161/CIRCRESAHA.116.308441
- Dikalova, A. E., Pandey, A., Xiao, L., Arslanbaeva, L., Sidorova, T., Lopez, M. G., et al. (2020). Mitochondrial deacetylase Sirt3 reduces vascular dysfunction and hypertension while Sirt3 depletion in essential hypertension is linked to vascular inflammation and oxidative stress. *Circ. Res.* 126 (4), 439–452. doi:10.1161/CIRCRESAHA.119.315767
- Dillmann, W. H. (2019). Diabetic cardiomyopathy. *Circ. Res.* 124 (8), 1160–1162. doi:10.1161/CIRCRESAHA.118.314665
- Fu, R., Li, J., Yu, H., Zhang, Y., Xu, Z., and Martin, C. (2021). The yin and yang of traditional Chinese and western medicine. *Med. Res. Rev.* 41 (6), 3182–3200. doi:10.1002/med.21793
- Gu, Y., and Han, Y. (2020). Toll-like receptor signaling and immune regulatory lymphocytes in periodontal disease. *Ijms* 21 (9), 3329. doi:10.3390/ijms21093329
- Naderi, S., and Merchant, A. T. (2020). The association between periodontitis and cardiovascular disease: An update. *Curr. Atheroscler. Rep.* 22 (10), 52. doi:10.1007/s11883-020-00878-0
- Rupaimoole, R., and Slack, F. J. (2017). MicroRNA therapeutics: Towards a new era for the management of cancer and other diseases. *Nat. Rev. Drug Discov.* 16 (3), 203–222. doi:10.1038/nrd.2016.246
- Soehnlein, O., and Libby, P. (2021). Targeting inflammation in atherosclerosis - from experimental insights to the clinic. *Nat. Rev. Drug Discov.* 20 (8), 589–610. doi:10.1038/s41573-021-00198-1
- Thatcher, S. E. (2016). TGF- $\beta$  signaling: New insights into aortic aneurysms. *EBioMedicine* 12, 24–25. doi:10.1016/j.ebiom.2016.09.026
- Tiedt, S., Prestel, M., Malik, R., Schieferdecker, N., Duering, M., Kautzky, V., et al. (2017). RNA-seq identifies circulating miR-125a-5p, miR-125b-5p, and miR-143-3p as potential biomarkers for acute ischemic stroke. *Circ. Res.* 121 (8), 970–980. doi:10.1161/CIRCRESAHA.117.311572
- Tomczyk, M. M., Cheung, K. G., Xiang, B., Tamanna, N., Fonseca Teixeira, A. L., Agarwal, P., et al. (2022). Mitochondrial sirtuin-3 (SIRT3) prevents doxorubicin-induced dilated cardiomyopathy by modulating protein acetylation and oxidative stress. *Circ. Heart Fail* 15 (5), e008547. doi:10.1161/CIRCHEARTFAILURE.121.008547
- Tzavlaki, K., and Moustakas, A. (2020). TGF- $\beta$  signaling. *Biomolecules* 10 (3), 487. doi:10.3390/biom10030487
- Valanti, E. K., Dalakoura-Karagkouni, K., Siasos, G., Kardassis, D., Eliopoulos, A. G., and Sanoudou, D. (2021). Advances in biological therapies for dyslipidemias and atherosclerosis. *Metabolism* 116, 154461. doi:10.1016/j.metabol.2020.154461
- Wang, X., Li, X., Liu, S., Brickell, A. N., Zhang, J., Wu, Z., et al. (2020). PCSK9 regulates pyroptosis via mtDNA damage in chronic myocardial ischemia. *Basic. Res. Cardiol.* 12 (5), a036392. doi:10.1007/s00395-020-00832-w
- Xu, M., and Song, J. (2021). Targeted therapy in cardiovascular disease: A precision therapy era. *Front. Pharmacol.* 12, 623674. doi:10.3389/fphar.2021.623674
- Yao, B. C., Meng, L. B., Hao, M. L., Zhang, Y. M., Gong, T., and Guo, Z. G. (2019). Chronic stress: A critical risk factor for atherosclerosis. *J. Int. Med. Res.* 47 (4), 1429–1440. doi:10.1177/0300060519826820
- Zeng, C., Duan, F., Hu, J., Luo, B., Huang, B., Lou, X., et al. (2020). NLRP3 inflammasome-mediated pyroptosis contributes to the pathogenesis of non-ischemic dilated cardiomyopathy. *Redox Biol.* 34, 101523. doi:10.1016/j.redox.2020.101523





# Water-Soluble Tomato Extract Fruitflow Alters the Phosphoproteomic Profile of Collagen-Stimulated Platelets

Shenghao Zhang, Huilian Chen, Chuanbao Li, Beidong Chen, Huan Gong, Yanyang Zhao and Ruomei Qi\*

The Key Laboratory of Geriatrics, Beijing Institute of Geriatrics, Beijing Hospital, National Center of Gerontology, National Health Commission, Institute of Geriatric Medicine, Chinese Academy of Medical Sciences, Beijing, China

## OPEN ACCESS

### Edited by:

Xianwei Wang,  
Xinxiang Medical University, China

### Reviewed by:

Wei Cui,  
Ningbo University, China  
Asim K. Duttaroy,  
University of Oslo, Norway

### \*Correspondence:

Ruomei Qi  
ruomeiqi@163.com

### Specialty section:

This article was submitted to  
Cardiovascular and Smooth Muscle  
Pharmacology,  
a section of the journal  
Frontiers in Pharmacology

**Received:** 23 July 2021

**Accepted:** 08 September 2021

**Published:** 27 September 2021

### Citation:

Zhang S, Chen H, Li C, Chen B,  
Gong H, Zhao Y and Qi R (2021)  
Water-Soluble Tomato Extract  
Fruitflow Alters the Phosphoproteomic  
Profile of Collagen-  
Stimulated Platelets.  
Front. Pharmacol. 12:746107.  
doi: 10.3389/fphar.2021.746107

Platelet hyperactivity is a risk factor for cardiovascular disease and thrombosis. Recent studies reported that the tomato extract Fruitflow inhibited platelet function, but the molecular mechanism is still unclear. The present study used proteomics to quantitatively analyze the effect of fruitflow on the inhibition of collagen-stimulated platelets and validated the involvement of several signaling molecules. Fruitflow significantly inhibited human platelet aggregation and P-selectin expression that were induced by collagen. Proteomics analysis revealed that compared fruitflow-treated collagen-stimulated platelets with only collagen-stimulated platelets, 60 proteins were upregulated and 10 proteins were downregulated. Additionally, 66 phosphorylated peptides were upregulated, whereas 37 phosphorylated peptides were downregulated. Gene Ontology analysis indicated that fruitflow treatment downregulated phosphoinositide 3-kinase (PI3K)/protein kinase B and guanosine triphosphatase-mediated signal transduction in collagen-activated platelets. Biological validation indicated that fruitflow decreased Akt, glycogen synthase kinase 3 $\beta$ , p38 mitogen-activated protein kinase (MAPK), and heat shock protein (Hsp27) phosphorylation in collagen-stimulated platelets. Fruitflow recovered cyclic adenosine monophosphate levels in collagen-activated platelets and reduced protein kinase A substrate phosphorylation that was induced by collagen. These findings suggest that fruitflow is a functional food that can inhibit platelet function, conferring beneficial effects for people who are at risk for platelet hyperactivity-associated thrombosis.

**Keywords:** fruitflow, platelets, phosphoproteomics, P-selectin, Akt, GSK3 $\beta$

## INTRODUCTION

Platelets are anucleate cells that play diverse roles in hemostasis and thrombosis and also contribute to immunity, inflammation, and wound healing. Platelet hyperactivity is related to hypertension, diabetes, and cardiovascular diseases (Martin et al., 2012; Thomas and Storey, 2015a; Gaiz et al., 2017). Under pathological conditions, platelets promote vascular damage and chronic inflammation by releasing various inflammatory mediators (Rendu and Brohard-Bohn, 2001; Golebiewska and Poole, 2015; Bakogiannis et al., 2019). Accumulating evidence shows that the inhibition of platelet function can decrease biological mediators of platelet secretion. The inhibition of platelet function

has become an effective strategy for reducing the risk of cardiovascular disease (Duchene and von Hundelshausen, 2015; Kirichenko et al., 2016).

Studies of platelet proteomics revealed that platelets contain more than 4,000 proteins, and more than 300 protein products are released when platelets are activated (Burkhardt et al., 2012). Proteomics can identify quantitative changes in the abundance and localization of thousands of proteins and various modifications, including phosphorylation, acetylation, methylation, and glycosylation (Burkhardt et al., 2014; Aebersold and Mann, 2016; Manes and Nita-Lazar, 2018). The modification of phosphorylated proteins is an important biological process during platelet activation. Phosphorylated proteomics can provide useful biological information for drug target screening (Cohen, 2000; García et al., 2005; Dittrich et al., 2008). Quantitative proteomics that uses high-resolution liquid chromatography tandem mass spectrometry (LC-MS/MS) can elucidate cellular signaling cascades. Label-free proteomics utilize the signal intensity and spectral counting of peptides to quantitate both relative and absolute protein abundance, which improves the accuracy and depth of phosphoproteomics research (Megger et al., 2013; Anand et al., 2017; Manes and Nita-Lazar, 2018).

Tomatoes are one of the main vegetables in the Mediterranean diet. Tomatoes contain various nutrients that are beneficial to health. Recent studies demonstrated that the cardioprotective effects of tomato extracts are linked to the modulation of platelet function. Fruitflow is a water-soluble concentrate that mainly contains flavone, adenosine, and chlorogenic acid. O'Kennedy et al. reported that fruitflow reduced human platelet aggregation by 8–23% in an *ex vivo* preparation 3 h after administration (O'Kennedy et al., 2006; O'Kennedy et al., 2017a). Another study showed that tomato juice consumption increased erythrocyte antioxidant enzymes and decreased serum malondialdehyde in overweight and obese females (Ghavipour et al., 2015). These studies suggest that the active ingredients of tomatoes can provide health benefits. However, the inhibitory mechanism of action of fruitflow on platelet function is not fully understood.

Collagen is a powerful platelet activator that plays a critical role in thrombosis. There are three types of collagen receptors on the platelet membrane: glycoprotein Ib, glycoprotein VI, and integrin- $\alpha 2\beta 1$ . Collagen receptor-mediated signal transduction has been shown to be involved in platelet activation (Barnes et al., 1998; Clemetson and Clemetson, 2001; Farndale, 2006; Surin et al., 2008). To obtain further biological information about the effects of fruitflow on platelet function, we used LC-MS/MS to perform a proteomics and phosphoproteomics analysis of the effects of fruitflow in collagen-activated platelets.

## METHODS

### Ethics Statement

Blood was collected from healthy donors, from whom we received written informed consent. The experiments were conducted according to the principles of the Declaration of Helsinki. The blood samples were used for the *in vitro* study. The present study

was approved by the Ethics Committee of Beijing Hospital (no. 2018BJYYEC-195-02).

### Materials

Fruitflow (FF) was provided by By-Health Co., Ltd. (Zhuhai, Guangdong, China). The main biologically active ingredients of FF are adenosine, flavonoids, chlorogenic acid, phytosterols and phenolic acids, etc. (O'Kennedy et al., 2017a).

Collagen was purchased from Chrono-Log Corporation (Havertown, PA, United States). Monoclonal anti-Hsp27 and phospho-Hsp27 antibodies were purchased from Abcam (Boston, MA, United States). Monoclonal anti-glycogen synthase kinase  $\beta$  (GSK3 $\beta$ ), phospho-GSK3 $\beta$ , monoclonal anti-Akt, phospho-Akt, monoclonal anti-p38 MAPK, phospho-p38 MAPK, and phospho-protein kinase A (PKA) substrate (RRXS\*/T\*) antibodies were purchased from Cell Signaling Technology (Danvers, MA, United States). Cyclic adenosine monophosphate (cAMP) kits were obtained from R&D Systems (Minneapolis, MN, United States).

### Platelet Preparation

Venous blood was drawn from health donors who had not taken any medication in the previous 2 weeks. The blood samples were immediately mixed with 3.8% sodium citrate (1 volume of sodium citrate/9 volumes of blood) as an anticoagulant. The blood samples were then centrifuged at  $500 \times g$  for 15 min to obtain platelet-rich plasma. The platelet-rich plasma was diluted 1:1 with Tyrode's/HEPES buffer (128 mM NaCl, 2.8 mM KCl, 1 mM  $MgCl_2$ , 5 mM glucose, 12 mM  $NaHCO_3$ , and 0.4 mM  $NaH_2PO_4$ , pH 7.2). To prevent platelet activation we added 2 mM ethylene glycol tetraacetic acid (EGTA) and ACD (1:10) in platelet suspension during centrifugation. The platelet suspension was centrifuged at  $400 \times g$  for 10 min. Platelet pellets were resuspended in Tyrode's/HEPES buffer and centrifuged under the same conditions for 10 min. The platelet concentration was measured by ABX/HORIBA ABX Diagnostics (Montpellier, France). For Western blot, the platelet concentration was  $3 \times 10^9$  cells/ml.

### Measurement of Platelet Aggregation

Platelet aggregation was measured in a washed platelet suspension using a Chrono-Log aggregometer (Chrono-Log corporation, Havertown, PA, United States). Fruitflow was dissolved in 0.9% NaCl solution to prepare stock solution. The platelet suspension ( $1 \times 10^9$ ) was incubated with fruitflow (100  $\mu g/ml$ ) for 10 min, and the cuvette was then stirred at 1,000 rotations per minute (rpm). Collagen (5  $\mu g/ml$ ) was added to the cuvette for 10 min at 1,000 rpm to induce platelet aggregation.

### Western Blot Analysis

The platelet suspension was incubated with 100  $\mu g/ml$  fruitflow for 10 min before being stimulated with 5  $\mu g/ml$  collagen for 10 min on a Chrono-Log aggregometer. Platelet lysates were analyzed by 10% sodium dodecyl sulfate-polyacrylamide gel electrophoresis and wet electrotransferred to polyvinylidene fluoride membranes. The membranes were blocked with 1%

bovine serum albumin and then incubated with specific primary antibodies overnight. After three washes in PBS that contained 0.5% Tween-20, the membranes were incubated with horseradish peroxidase-conjugated secondary antibodies in TPBS for 2 h. Bands were detected by electrochemiluminescent reagent and the EvolutionCapt system (Vilber Lourmat) and quantified using Image-Pro Plus software.

## Flow Cytometry Analysis of P-Selectin Expression

The washed platelet suspension ( $1 \times 10^6/\text{ml}$ ) was treated with or without fruitflow (100  $\mu\text{g}/\text{ml}$ ) for 10 min. Afterward, collagen (5  $\mu\text{g}/\text{ml}$ ) was added for another 10 min at 37°C. The platelets were fixed by the addition of 4% paraformaldehyde for 10 min. After washing three times, the platelets were incubated with PE-conjugated CD62P and FITC-conjugated CD61 for 30 min. The platelets were analyzed on a FACScan flow cytometer (BD Bioscience) with 10,000 events per gate and analyzed using FlowJo software.

## Preparation and Digestion of Proteins

Washed platelets were used in the present study. The platelet suspension ( $1 \times 10^9/\text{cell}/\text{ml}$ ) was incubated with 100  $\mu\text{g}/\text{ml}$  fruitflow for 10 min, and then 5  $\mu\text{g}/\text{ml}$  collagen was added for 10 min. The samples were centrifuged at  $16,000 \times g$  for 3 min at 4°C and resuspended in 500  $\mu\text{L}$  cold phosphate-buffered saline (PBS), repeated twice, and then 500  $\mu\text{L}$  UA lysis buffer (8 M Urea and 150 mM Tris-HCl, pH 8.0) was added to the samples, followed by storage at  $-80^\circ\text{C}$ .

## Phosphopeptides Enrichment and LC-MS/MS Analysis

Label-free proteomics analysis was performed by Applied Protein Technology (Shanghai, China). LC-MS/MS spectra were searched using a Q Exactive HF/HFX mass spectrometer coupled to Easy nLC (Thermo Fisher Scientific), which is controlled by IntelliFlow technology. Immobilized metal affinity chromatography (IMAC) was used to enrich phosphopeptides. According to the manufacturer's instructions (Thermo Scientific), the enrichment was carried out using High-Select™ Fe-NTA Phosphopeptides Enrichment Kit. The MS raw data for each sample were combined and searched using MaxQuant 1.5.3.17 software for the identification and quantification analysis. A false discovery rate  $<1\%$  was applied. Proteomic samples were analyzed by LC-MS/MS as described in **Supplement S1**. Gene Ontology analysis was performed at <https://david.ncifcrf.gov/home.jsp>.

## Measurement of cAMP by Enzyme-Linked Immunosorbent Assay

Washed platelets were treated with or without fruitflow (100  $\mu\text{g}/\text{ml}$ ) for 10 min, and then collagen (5  $\mu\text{g}/\text{ml}$ ) was added for 10 min. After centrifugation at  $9,600 \times g$  for 10 min, the supernatant was

collected to measure cAMP using enzyme-linked immunosorbent assay (ELISA) kits according to the manufacturer's instructions.

## Statistical Analysis

Quantitative data are presented as the mean  $\pm$  SEM. Significant differences between two groups were analyzed using two-tail paired Student's *t*-test. All of the analyses were performed using Prism 8.3 software (GraphPad, San Diego, CA, United States). Values of  $p < 0.05$  were considered statistically significant.

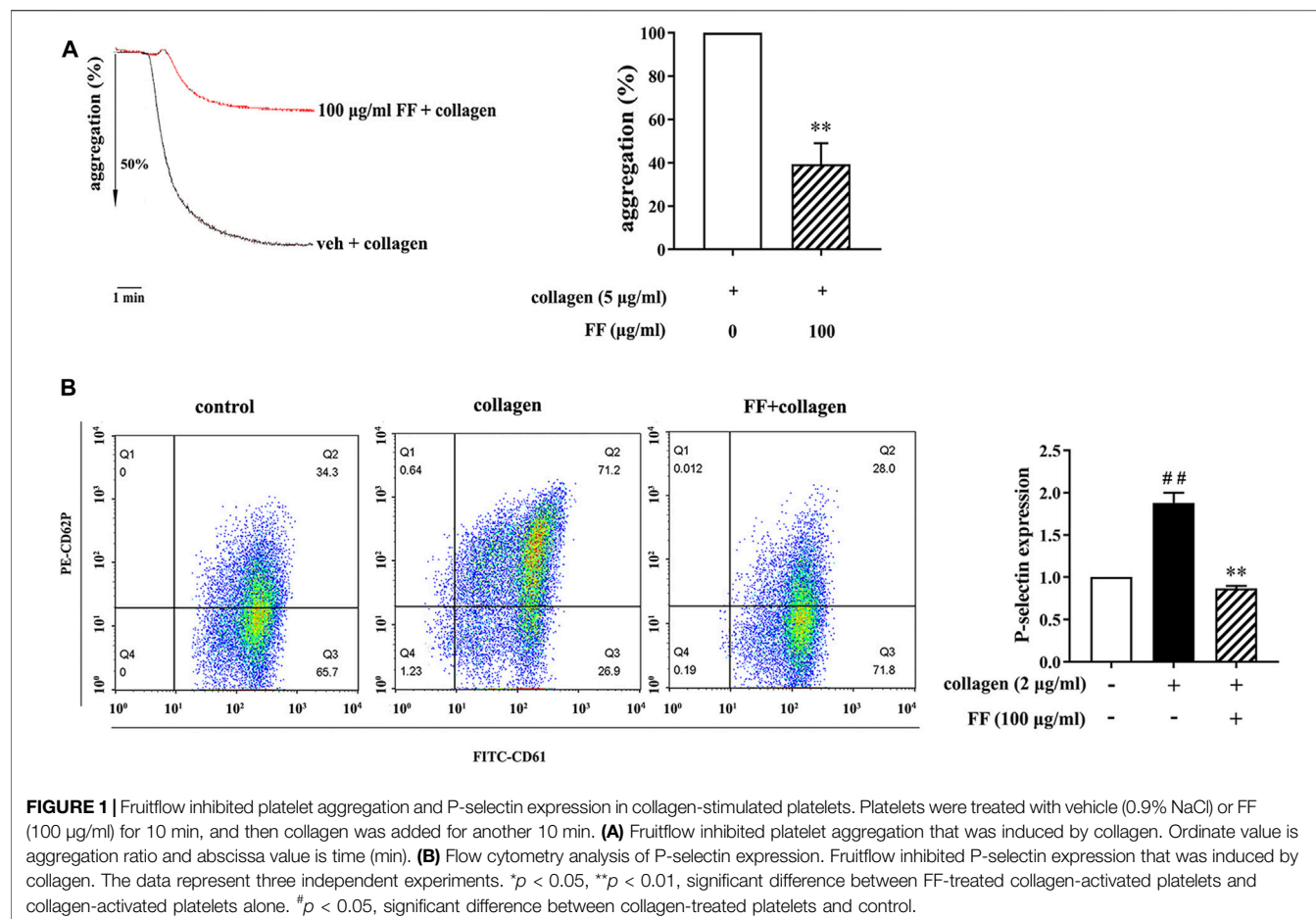
## RESULTS

### Fruitflow Inhibited Platelet Aggregation and P-Selectin Expression in Collagen-Stimulated Platelets

Platelet aggregation and P-selectin expression are important biological processes in platelet activation. We first determined the effect of fruitflow on platelet aggregation and P-selectin expression in collagen-activated platelets. Based on our pre-experiments, in which fruitflow (1, 10, 30, and 100  $\mu\text{g}/\text{ml}$ ) dose-dependently inhibited collagen-induced platelet aggregation, we used 100  $\mu\text{g}/\text{ml}$  fruitflow in the present study. As shown in **Figure 1**, 100  $\mu\text{g}/\text{ml}$  fruitflow significantly inhibited platelet aggregation, in which the aggregation ratio decreased by  $60.7 \pm 9.7\%$ . We also analyzed the effect of fruitflow on P-selectin using flow cytometry. Collagen increased P-selectin expression by 87.9% on the platelet membrane, whereas 100  $\mu\text{g}/\text{ml}$  fruitflow completely suppressed P-selectin expression that was induced by collagen.

### Proteomics Analysis of Fruitflow Treatment and No Treatment in Collagen-Activated Platelets

To explore the mechanism of action fruitflow on platelet function, we performed proteomics analysis of fruitflow treatment and no treatment in collagen-activated platelets. Platelets were pretreated with fruitflow for 10 min, and collagen was then added for 10 min. The proteomics analysis identified 3,856 proteins, and 3,182 proteins were quantified. Different proteomic profiles were found between fruitflow treatment and no treatment in collagen-stimulated platelets. As shown in **Figure 2**, compared fruitflow-treated collagen-stimulated platelets with only collagen-stimulated platelets, 60 proteins were upregulated and 10 proteins were downregulated ( $p < 0.05$ ). The Gene Ontology analysis showed different biological processes that were associated with fruitflow treatment and no treatment in collagen-stimulated platelets. Upregulated biological processes included platelet degranulation, nucleophagy/autophagosome assembly, fibrinolysis, blood coagulation, negative regulation of platelet activation, and negative regulation of fibrinolysis, etc. Detailed data was shown in **Supplement S2 Table 1**.



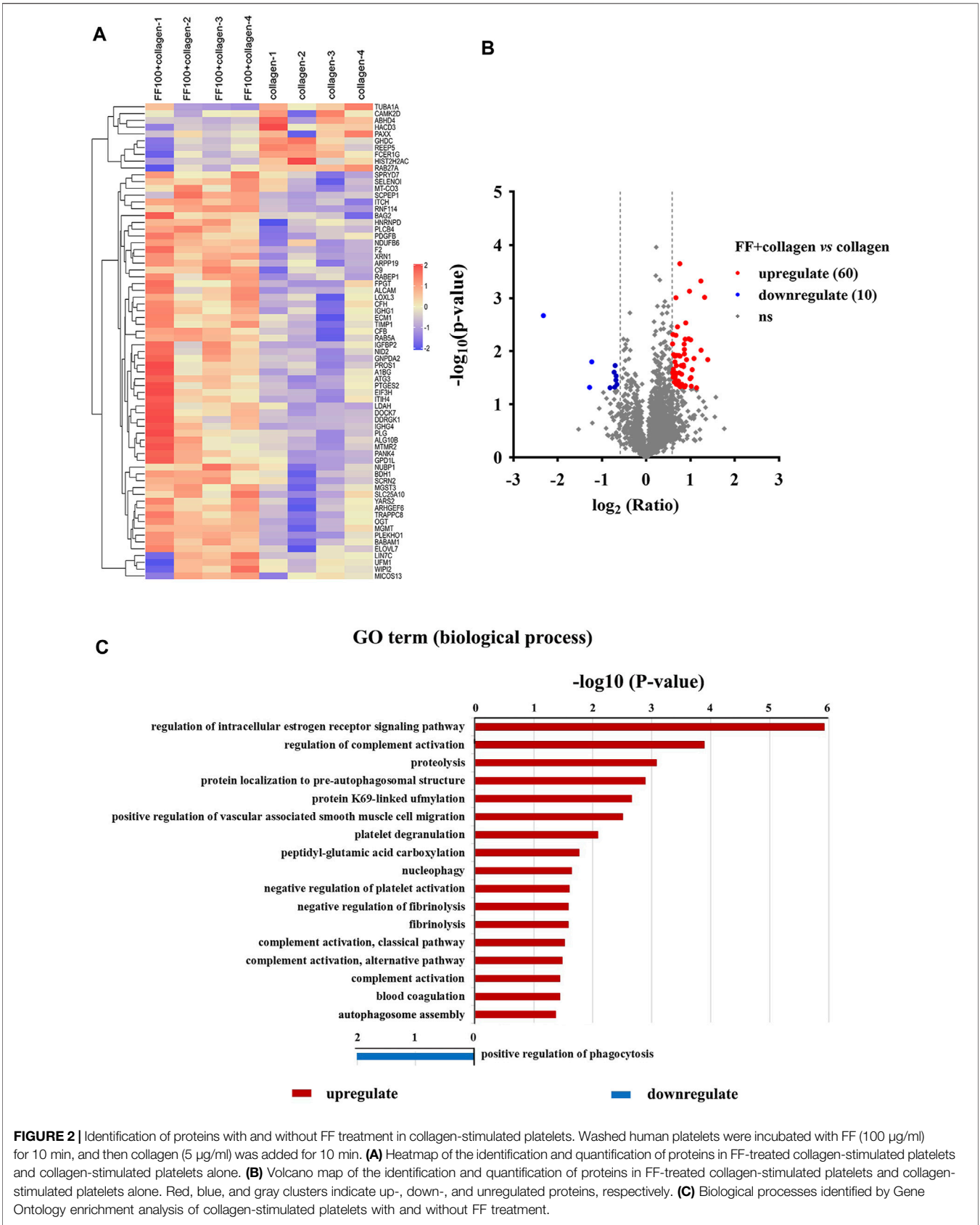
## Phosphoproteomics Analysis of Fruitflow Treatment and No Treatment in Collagen-Activated Platelets

To explore the effect of fruitflow on collagen-stimulated platelets, we conducted a quantitative phosphoproteomics analysis. The quantitative analysis detected 2,099 phosphorylated peptides and 2,376 phosphorylated sites in 1,051 phosphorylated proteins. As shown in **Figure 3**, a significant difference was found between fruitflow treatment and no treatment in collagen-activated platelets. Compared FF-treated collagen-stimulated platelets with only collagen-stimulated platelets, 66 phosphorylated peptides were upregulated two times, whereas 37 phosphorylated peptides were downregulated 0.5 times. As shown in **Table 1**, vasodilator-stimulated phosphoprotein (VASP) phosphorylation levels were upregulated in FF-treated platelets. VASP is a substrate of protein kinase G activation, and it interacts with nitric oxide through the soluble guanylate cyclase (sGC)/cyclic guanosine monophosphate (cGMP) pathway (Li et al., 2003). Most of the phosphorylated proteins that increased are related to calcium mobilization (calcium/calmodulin-dependent protein kinase, CAMK1, tyrosine phosphatase (PTPRJ, PTPN12) and actin polymerization (Rho-associated protein kinase, ROCK). The phosphorylated proteins that decreased included serine/

threonine kinase (STK10), thromboxane receptor (TBXA2R), and heat shock 27 kDa protein 1 (HSPB1, Hsp27). Interestingly, INPP5D (namely SH2 domain-containing inositol-5'-phosphatase 1, SHIP1) and INPPL1 (namely SH2 domain-containing inositol-5'-phosphatase 2, SHIP2) only existed in fruitflow-treated collagen-stimulated platelets, but not in collagen-stimulated platelets (in **Supplement 4 Table 3**). The function of INPPL1 is to specifically hydrolyze the 5-phosphate of phosphatidylinositol-3,4,5-trisphosphate (PtdIns [3,4,5]P<sub>3</sub>) to produce PtdIns(3,4)P<sub>2</sub>, thereby negatively regulating the phosphoinositide-3 kinase (PI3K) pathway (Backers et al., 2003; Durrant et al., 2017; Fu et al., 2019). This suggests that inhibition of the PI3K/protein kinase B (Akt) pathway might be an important mechanism by which fruitflow suppresses platelet function. Detailed phosphoproteomic data was shown in **Supplement 3 Table 2** and **Supplement 4 Table 3**.

## Validation of the Effect of Fruitflow in Collagen-Stimulated Platelets

Based on the research background of collagen-mediated signaling pathway upon platelet activation and the phosphoproteomics data, we verified some important molecular. The phosphoproteomics showed that several phosphorylated peptides were linked to PI3K/Akt pathway. Therefore, we determined the effect of





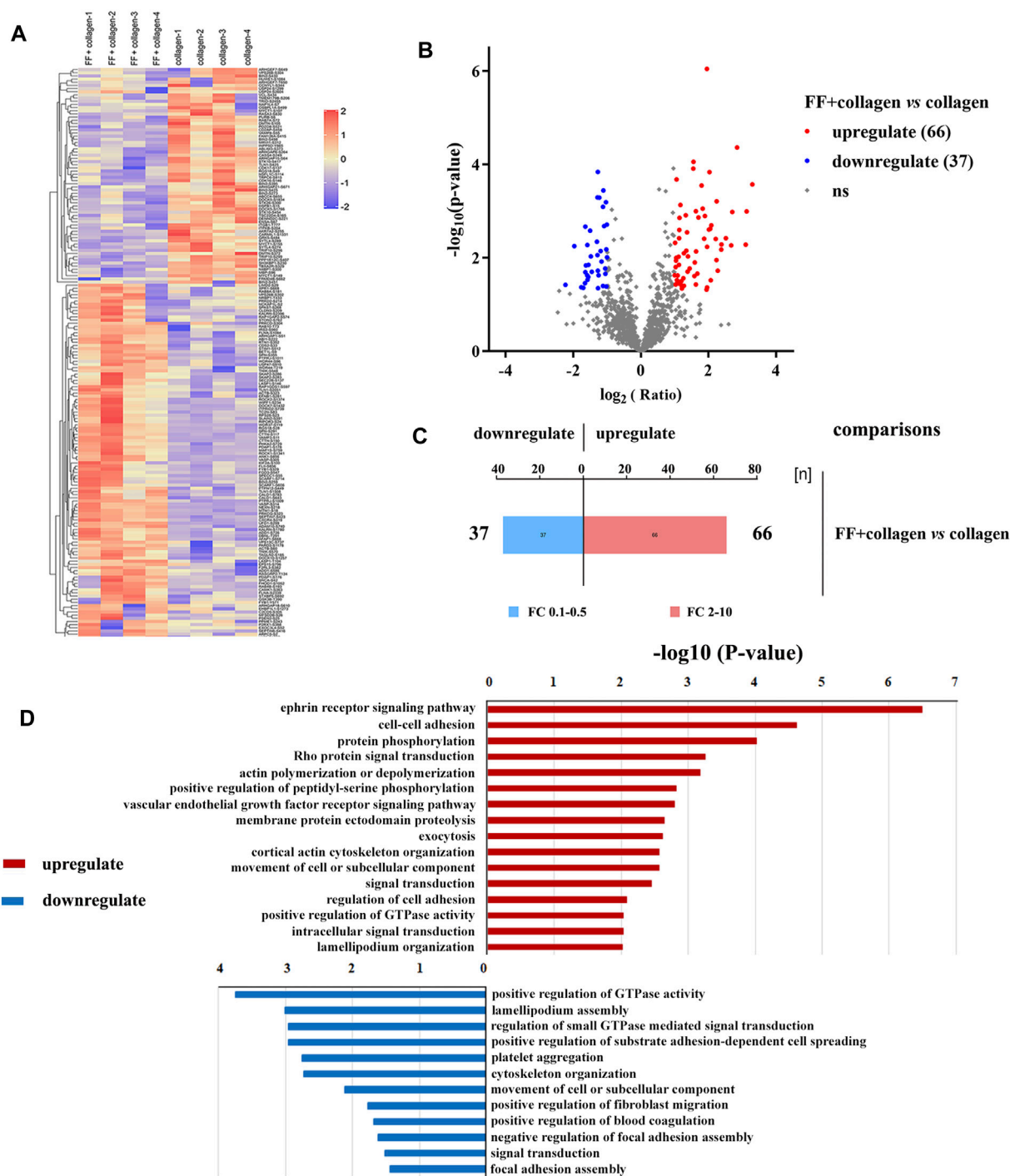


**FIGURE 3 |** Quantitative phosphoproteomics analysis of collagen-stimulated platelets with and without FF treatment. **(A)** Heatmap of different protein phosphorylation profiles with and without FF treatment in collagen-stimulated platelets. **(B)** Volcano map that shows 66 upregulated and 37 downregulated phosphopeptides with and without FF treatment, respectively, in collagen-stimulated platelets. **(C)** Histogram of multiple correlations of collagen-stimulated platelets with and without FF treatment. **(D)** Biological processes identified by Gene Ontology enrichment analysis of collagen-stimulated platelets with and without FF treatment.

fruitflow on the phosphorylation of Akt and its downstream molecular GSK3 $\beta$ . As shown in **Figure 4**, 100  $\mu\text{g/ml}$  fruitflow pretreatment completely suppressed Akt and GSK3 $\beta$  phosphorylation that was induced by collagen.

Moreover, there were four phosphorylated peptides of the MAPK families presented in **Supplement 3 Table 2**. They were MAPKAPK2, MAPK14, MAPKAP1 and MAP4K2. We validated the phosphorylation of p38 MAPK and its downstream molecular HSPB1(Hsp27).

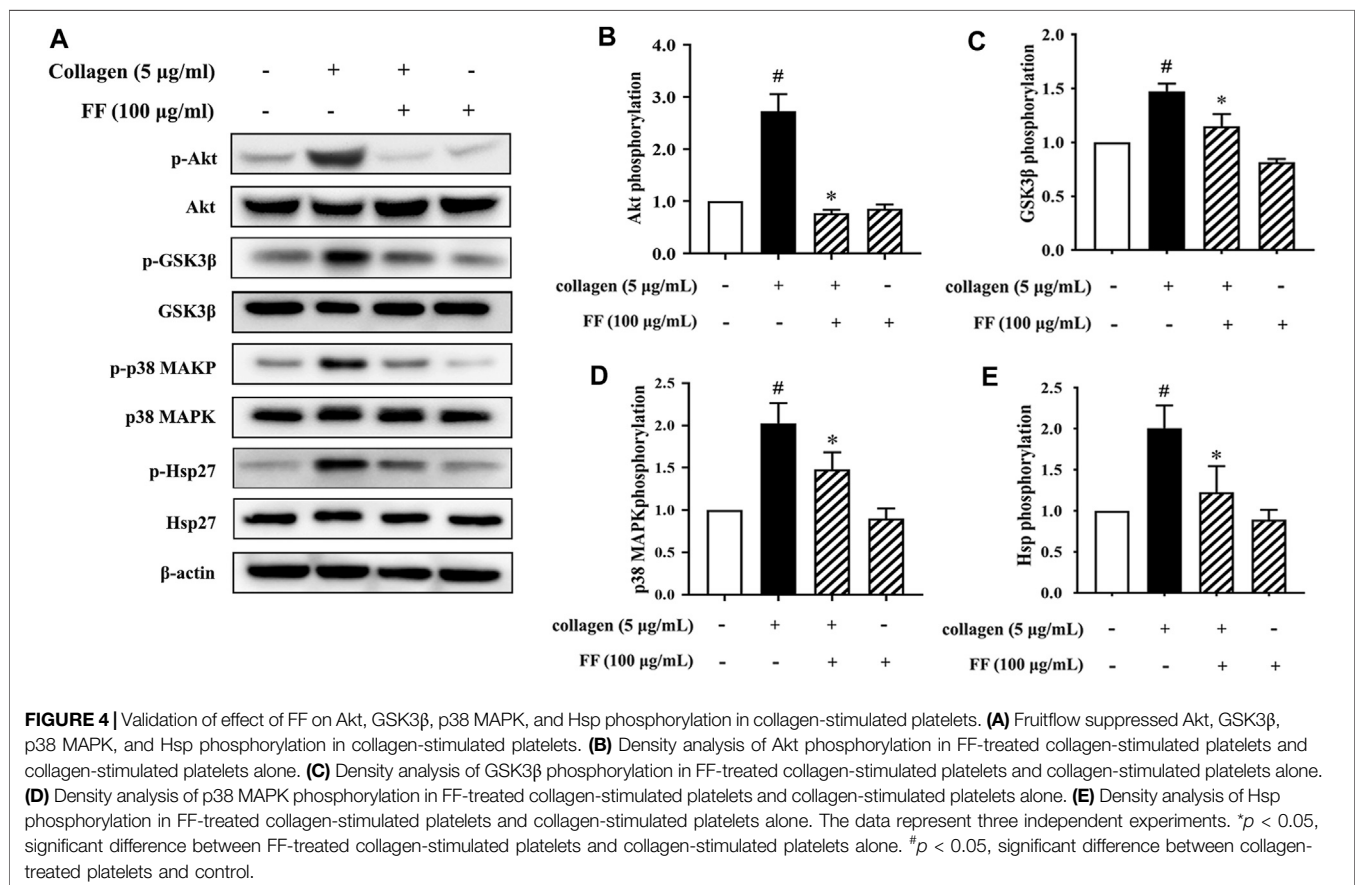
**TABLE 1 |** Different phosphorylated proteins in FF + collagen-vs collagen-treated platelets.

Uniprot	Gene	Site	Regulation
Q13464	ROCK1	Ser1341	up
O75116	ROCK2	Ser1374	up
Q7LDG7	RASGRP2	Ser116	up
P50552	VASP	Ser305/Ser314	up
Q05209	PTPN12	Ser449	up
O15117	FYB1	Ser329	up
O75563	SKAP2	Ser286/Ser283	up
Q684P5	RAP1GAP2	Ser574	up
P49841	GSK3B	Thr390	up
Q12913	PTPRJ	Ser1374	up
Q04759	PRKCQ	Ser1011	up
Q07960	ARHGAP1	Ser51	up
Q14012	CAMK1	Ser363	up
Q13496	MTM1	Ser18	up
Q9BZL6	PRKD2	Ser214	up
P21731	TBXA2R	Ser329	down
P34947	GRK5	Ser484	down
Q14155	ARHGEF7	Ser650	down
Q96B97	SH3KBP1	Ser230	down
O94804	STK10	Ser454/Ser417	down
P04792	HSPB1	Ser15	down
O43182	ARHGAP6	Ser105	down
Q14644	RASA3	Ser830	down

The same dose of fruitflow effectively inhibited p38 MAPK and Hsp27 phosphorylation that was induced by collagen.

### Fruitflow Recovered cAMP Levels and Inhibited the Phosphorylation of PKA Substrates in Collagen-Stimulated Platelets

The phosphoproteomics revealed that several substrates of PKA were significantly different between the FF-treated collagen-stimulated platelets and the collagen-stimulated platelets alone. They were VASP (vasodilation stimulating protein), FLNA (filament protein A), HSP27 (heat shock protein 27) and Rap1GAP2 (activator protein of GTPase-Rap1b) (in **Supplement 3 Table 2**). Protein kinase A (PKA) is a downstream molecule regulated by cyclic adenosine monophosphate (cAMP). cAMP is a second messenger that plays a negative regulatory role in platelet activation (Fuentes and Palomo, 2014; Raslan and Naseem, 2014). We investigated whether fruitflow can affect cAMP/PKA pathway. As shown in **Figure 5**, collagen stimulation decreased cAMP levels, and fruitflow treatment restored cAMP levels that were decreased by collagen. Collagen stimulation increased the phosphorylation of PKA substrates, and 100 µg/ml fruitflow abolished the phosphorylation of PKA substrates.



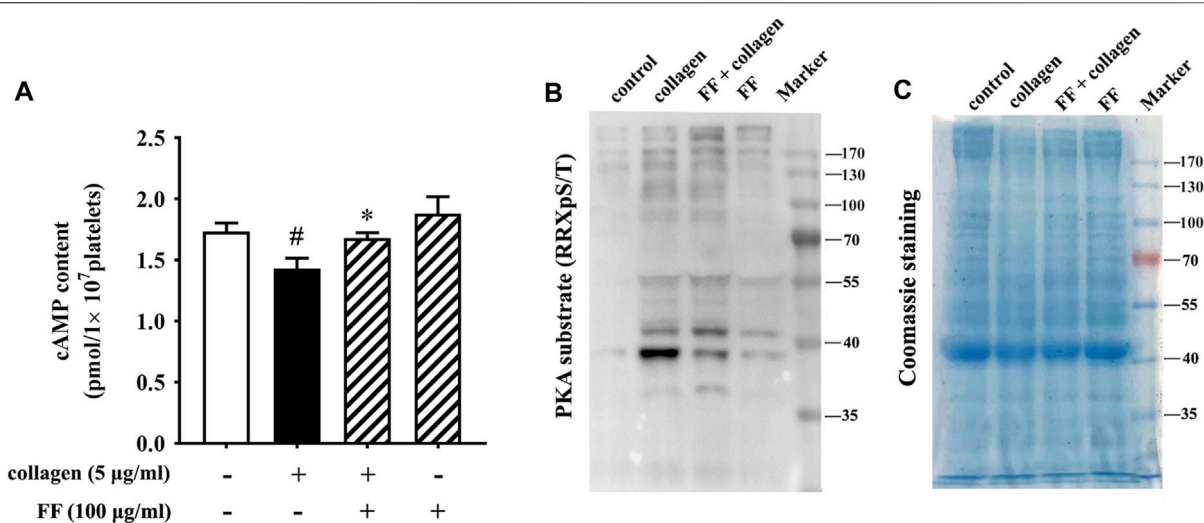


**FIGURE 5 |** Fruitflow recovered cAMP levels and reduced the phosphorylation of PKA substrates in collagen-stimulated platelets. **(A)** Analysis of cAMP levels by ELISA. **(B)** Western blot analysis of the phosphorylation of PKA substrates. **(C)** Coomassie staining showed that protein abundance was equal. The data represent three independent experiments. \* $p < 0.05$ , significant difference between FF-treated collagen-stimulated platelets and collagen-stimulated platelets alone. # $p < 0.05$ , significant difference between collagen-treated platelets and control.

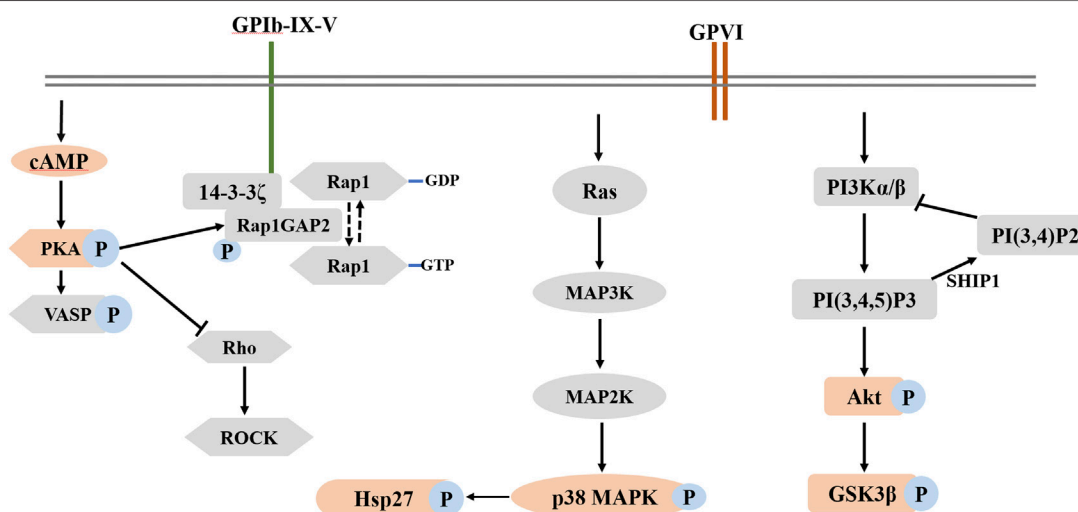


**FIGURE 6 |** Potential mechanism of action of fruitflow in collagen-stimulated platelets.

## DISCUSSION

Several recent studies reported that the water-soluble tomato extract fruitflow inhibits platelet aggregation (Uddin et al., 2018; O'Kennedy et al., 2017b). In the present study, we confirmed that fruitflow inhibited platelet aggregation and P-selectin expression in collagen-activated platelets. P-selectin is an important marker of platelet activation that acts as a bridging molecule to recruit inflammatory cells to adhere to endothelial cells (Thomas and Storey, 2015b; Kappelmayer and Nagy, 2017). Compared with resting platelets, collagen-stimulated platelets exhibited a decrease in cAMP levels and an increase in the phosphorylation of PKA substrates, and

fruitflow reversed these changes. However, the mechanism by which cAMP/PKA signaling regulates platelet function remains unclear.

Interestingly, our results revealed a significant difference in phosphoproteomic profiles between fruitflow treatment and no treatment in collagen-stimulated platelets. The upregulated biological processes included cell-cell adhesion, protein phosphorylation, Rho protein signal transduction, and actin polymerization. The downregulated biological processes included positive regulation of GTPase activity, positive regulation of substrate adhesion-dependent cell spreading, and platelet aggregation. The phosphoproteomics analysis also revealed protein modification-related biological processes, cell



composition changes, and more protein phosphorylated sites. We verified several GTPase signal transduction and PI3K/Akt pathway-related kinase signaling molecules by Western blot. Collagen stimulation increased Akt, GSK3 $\beta$ , p38 MAPK, and Hsp27 phosphorylation, and fruitflow treatment significantly inhibited their phosphorylation. Previous studies showed that Akt, GSK3 $\beta$ , p38 MAPK, and Hsp27 are involved in collagen- and thrombin-induced platelet activation (O'Brien et al., 2012; Moore et al., 2013; Liu et al., 2018; Saklatvala et al., 1996). These findings were consistent with the phosphorylated proteomics analysis. The Gene Ontology analysis revealed that fruitflow treatment downregulated GTPase-mediated signal transduction. This indicates that fruitflow inhibits platelet function through multiple targets. The quantitative phosphoproteomics analysis by MS further provided important biological information to understand the mechanism by which fruitflow inhibits platelet activation. However, the mechanism of action of fruitflow on interactions between signaling molecules needs further investigation.

Tomatoes are the most popular vegetable worldwide, especially in Mediterranean countries. Tomatoes contain various biologically active ingredients, among which lycopene has been shown to exert a protective effect on the enlarged prostate (Campbell et al., 2004; Mordente et al., 2011). Previous studies showed that daily 65 mg fruitflow administration partly suppressed platelet function (O'Kennedy et al., 2017b). Our previous clinic trial showed that daily 150 mg fruitflow intervention for 7 days could reduce ADP and collagen-induced platelet aggregation by 7.7 and 10.2% in elderly subjects. Fruitflow was the first product in Europe to obtain an approved, proprietary health claim under Article 13 (5) of the European Health Claims Regulation 1924/2006 on nutrition and health claim made on foods (19). A previous study showed that an aqueous extract of tomato dose-dependently inhibited plasma anti-angiotensin converting enzyme factor (Biswas et al., 2014). Our data provide some novel evidence of the inhibition of platelet function by fruitflow.

The limitation of the present study was that we have only verified the phosphorylation changes of a few molecules, but the interaction between these proteins is still unclear. The results of proteomics also suggest that fruitflow may affect calcium mobilization, and this mechanism needs to be further explored.

In conclusion, the present study showed that fruitflow inhibited platelet aggregation and P-selectin expression in collagen-stimulated human platelets. We first applied proteomics and phosphoproteomics approaches to comprehensively investigate the effect of fruitflow on collagen-activated platelets. Proteomics analysis revealed that compared fruitflow-treated collagen-stimulated platelets with only collagen-stimulated platelets, 60 proteins were upregulated and 10 proteins were downregulated.

Additionally, 66 phosphorylated peptides were upregulated, whereas 37 phosphorylated peptides were downregulated. Biological verification indicated that the mechanism of action of fruitflow in inhibiting platelet function is related to the suppression of Akt, GSK3 $\beta$ , p38 MAPK, and Hsp27 phosphorylation in collagen-stimulated platelets. Overall, fruitflow can inhibit platelet function and modify proteins in collagen-stimulated platelets, suggesting that fruitflow can provide health benefits for people who are at risk of platelet hyperactivity-related thrombosis though inhibiting platelet function. Potential mechanism of action of fruitflow in collagen-stimulated platelets was shown in **Figure 6**.

## DATA AVAILABILITY STATEMENT

The data presented in the study are deposited to the ProteomeXchange Consortium (<http://proteomecentral.proteomexchange.org>) via the iProX partner repository, accession number PXD027834.

## AUTHOR CONTRIBUTIONS

Conceived and designed the experiments: RQ. Performed the experiments: SZ, HC, CL, BC, and YZ. Analyzed the data: SZ and HC. Wrote the paper: RQ and SZ. All authors reviewed the article.

## FUNDING

This work was supported by the grants from the National Natural Science Foundation of China (grant no. 91649110, 81471051, 81270379, and 81070231). The funding agency had no role in the design of the study; in the collection, analyses, or interpretation of data; in writing the manuscript; or in the decision to publish the results.

## ACKNOWLEDGMENTS

We thank By-Health Co., Ltd. for providing Fruitflow in the present study.

## SUPPLEMENTARY MATERIAL

The Supplementary Material for this article can be found online at: <https://www.frontiersin.org/articles/10.3389/fphar.2021.746107/full#supplementary-material>

## REFERENCES

- Aebbersold, R., and Mann, M. (2016). Mass-spectrometric Exploration of Proteome Structure and Function. *Nature* 537 (7620), 347–355. doi:10.1038/nature19949
- Anand, S., Samuel, M., Ang, C. S., Keerthikumar, S., and Mathivanan, S. (2017). Label-Based and Label-free Strategies for Protein Quantitation. *Methods Mol. Biol.* 1549, 31–43. doi:10.1007/978-1-4939-6740-7\_4
- Backers, K., Blero, D., Paternotte, N., Zhang, J., and Erneux, C. (2003). The Termination of PI3K Signalling by SHIP1 and SHIP2 Inositol 5-phosphatases. *Adv. Enzyme Regul.* 43, 15–28. doi:10.1016/s0065-2571(02)00043-2
- Bakogiannis, C., Sachse, M., Stamatelopoulou, K., and Stellos, K. (2019). Platelet-derived Chemokines in Inflammation and Atherosclerosis. *Cytokine* 122, 154157. doi:10.1016/j.cyt.2017.09.013
- Barnes, M. J., Knight, C. G., and Farndale, R. W. (1998). The Collagen-Platelet Interaction. *Curr. Opin. Hematol.* 5 (5), 314–320. doi:10.1097/00062752-199809000-00002

- Biswas, D., Uddin, M. M., Dizdarevic, L. L., Jørgensen, A., and Duttaroy, A. K. (2014). Inhibition of Angiotensin-Converting Enzyme by Aqueous Extract of Tomato. *Eur. J. Nutr.* 53 (8), 1699–1706. doi:10.1007/s00394-014-0676-1
- Burkhardt, J. M., Gambaryan, S., Watson, S. P., Jurk, K., Walter, U., Sickmann, A., et al. (2014). What Can Proteomics Tell Us about Platelets? *Circ. Res.* 114 (7), 1204–1219. doi:10.1161/CIRCRESAHA.114.301598
- Burkhardt, J. M., Vaudel, M., Gambaryan, S., Radau, S., Walter, U., Martens, L., et al. (2012). The First Comprehensive and Quantitative Analysis of Human Platelet Protein Composition Allows the Comparative Analysis of Structural and Functional Pathways. *Blood* 120 (15), e73–82. doi:10.1182/blood-2012-04-416594
- Campbell, J. K., Canene-Adams, K., Lindshield, B. L., Boileau, T. W., Clinton, S. K., and Erdman, J. W., Jr (2004). Tomato Phytochemicals and Prostate Cancer Risk. *J. Nutr.* 134 (12 Suppl. 1), 3486S–3492S. doi:10.1093/jn/134.12.3486S
- Clemetson, K. J., and Clemetson, J. M. (2001). Platelet Collagen Receptors. *Thromb. Haemost.* 86 (1), 189–197. doi:10.1055/s-0037-1616217
- Cohen, P. (2000). The Regulation of Protein Function by Multisite Phosphorylation-Aa 25 Year Update. *Trends Biochem. Sci.* 25 (12), 596–601. doi:10.1016/s0968-0004(00)01712-6
- Dittrich, M., Birschmann, I., Mietner, S., Sickmann, A., Walter, U., and Dandekar, T. (2008). Platelet Protein Interactions: Map, Signaling Components, and Phosphorylation Groundstate. *Arterioscler Thromb. Vasc. Biol.* 28 (7), 1326–1331. doi:10.1161/atvbaha.107.161000
- Duchene, J., and von Hundelshausen, P. (2015). Platelet-derived Chemokines in Atherosclerosis. *Hamostaseologie* 35 (2), 137–141. doi:10.5482/hamo-14-11-0058
- Durrant, T. N., Hutchinson, J. L., Heesom, K. J., Anderson, K. E., Stephens, L. R., Hawkins, P. T., et al. (2017). In-depth PtdIns(3,4,5)P<sub>3</sub> Signalosome Analysis Identifies DAP1 as a Negative Regulator of GPVI-Driven Platelet Function. *Blood Adv.* 1 (14), 918–932. doi:10.1182/bloodadvances.2017005173
- Farndale, R. W. (2006). Collagen-induced Platelet Activation. *Blood Cell Mol Dis* 36 (2), 162–165. doi:10.1016/j.bcmd.2005.12.016
- Fu, Q., Huang, Y., Ge, C., Li, Z., Tian, H., Li, Q., et al. (2019). SHIP1 Inhibits Cell Growth, Migration, and Invasion in Non-small C-ell L-ung C-ancer through the PI3K/AKT P-athway. *Oncol. Rep.* 41 (4), 2337–2350. doi:10.3892/or.2019.6990
- Fuentes, E., and Palomo, I. (2014). Regulatory Mechanisms of cAMP Levels as a Multiple Target for Antiplatelet Activity and Less Bleeding Risk. *Thromb. Res.* 134 (2), 221–226. doi:10.1016/j.thromres.2014.04.027
- Gaiz, A., Mosawy, S., Colson, N., and Singh, I. (2017). Thrombotic and Cardiovascular Risks in Type Two Diabetes; Role of Platelet Hyperactivity. *Biomed. Pharmacother.* 94, 679–686. doi:10.1016/j.biopha.2017.07.121
- García, A., Watson, S. P., Dwek, R. A., and Zitzmann, N. (2005). Applying Proteomics Technology to Platelet Research. *Mass. Spectrom. Rev.* 24 (6), 918–930. doi:10.1002/mas.20047
- Ghavipour, M., Sotoudeh, G., and Ghorbani, M. (2015). Tomato Juice Consumption Improves Blood Antioxidative Biomarkers in Overweight and Obese Females. *Clin. Nutr.* 34 (5), 805–809. doi:10.1016/j.clnu.2014.10.012
- Golebiewska, E. M., and Poole, A. W. (2015). Platelet Secretion: From Haemostasis to Wound Healing and beyond. *Blood Rev.* 29 (3), 153–162. doi:10.1016/j.blre.2014.10.003
- Kappelmayer, J., and Nagy, B., Jr (2017). The Interaction of Selectins and PSGL-1 as a Key Component in Thrombus Formation and Cancer Progression. *Biomed. Res. Int.* 2017, 6138145. doi:10.1155/2017/6138145
- Kirichenko, T. V., Sobenin, I. A., Nikolic, D., Rizzo, M., and Orekhov, A. N. (2016). Anti-cytokine Therapy for Prevention of Atherosclerosis. *Phytomedicine* 23 (11), 1198–1210. doi:10.1016/j.phymed.2015.12.002
- Li, Z., Ajdic, J., Eigenthaler, M., and Du, X. (2003). A Predominant Role for cAMP-dependent Protein Kinase in the cGMP-Induced Phosphorylation of Vasodilator-Stimulated Phosphoprotein and Platelet Inhibition in Humans. *Blood* 101 (11), 4423–4429. doi:10.1182/blood-2002-10-3210
- Liu, D., Cao, Y., Zhang, X., Peng, C., Tian, X., Yan, C., et al. (2018). Chemokine CC-Motif Ligand 2 Participates in Platelet Function and Arterial Thrombosis by Regulating PKC $\alpha$ -P38mapk-HSP27 Pathway. *Biochim. Biophys. Acta Mol. Basis Dis.* 1864 (9 Pt B), 2901–2912. doi:10.1016/j.bbdis.2018.05.025
- Manes, N. P., and Nita-Lazar, A. (2018). Application of Targeted Mass Spectrometry in Bottom-Up Proteomics for Systems Biology Research. *J. Proteomics* 189, 75–90. doi:10.1016/j.jprot.2018.02.008
- Martin, J. F., Kristensen, S. D., Mathur, A., Grove, E. L., and Choudry, F. A. (2012). The Causal Role of Megakaryocyte-Platelet Hyperactivity in Acute Coronary Syndromes. *Nat. Rev. Cardiol.* 9 (11), 658–670. doi:10.1038/nrcardio.2012.131
- Megger, D. A., Bracht, T., Meyer, H. E., and Sitek, B. (2013). Label-free Quantification in Clinical Proteomics. *Biochim. Biophys. Acta* 1834 (8), 1581–1590. doi:10.1016/j.bbapap.2013.04.001
- Moore, S. F., van den Bosch, M. T., Hunter, R. W., Sakamoto, K., Poole, A. W., and Hers, I. (2013). Dual Regulation of Glycogen Synthase Kinase 3 (GSK3) $\alpha/\beta$  by Protein Kinase C (PKC) $\alpha$  and Akt Promotes Thrombin-Mediated Integrin  $\alpha$ IIb $\beta$ 3 Activation and Granule Secretion in Platelets. *J. Biol. Chem.* 288 (6), 3918–3928. doi:10.1074/jbc.M112.429936
- Mordente, A., Guantario, B., Meucci, E., Silvestrini, A., Lombardi, E., Martorana, G. E., et al. (2011). Lycopene and Cardiovascular Diseases: an Update. *Curr. Med. Chem.* 18 (8), 1146–1163. doi:10.2174/092986711795029717
- O'Brien, K. A., Gartner, T. K., Hay, N., and Du, X. (2012). ADP-stimulated Activation of Akt during Integrin Outside-In Signaling Promotes Platelet Spreading by Inhibiting Glycogen Synthase Kinase-3 $\beta$ . *Arterioscler Thromb. Vasc. Biol.* 32 (9), 2232–2240. doi:10.1161/atvbaha.112.254680
- O'Kennedy, N., Crosbie, L., Song, H. J., Zhang, X., Horgan, G., and Duttaroy, A. K. (2017). A Randomised Controlled Trial Comparing a Dietary Antiplatelet, the Water-Soluble Tomato Extract Fruitflow, with 75 mg Aspirin in Healthy Subjects. *Eur. J. Clin. Nutr.* 71 (6), 723–730. doi:10.1038/ejcn.2016.222
- O'Kennedy, N., Crosbie, L., van Lieshout, M., Broom, J. I., Webb, D. J., and Duttaroy, A. K. (2006). Effects of Antiplatelet Components of Tomato Extract on Platelet Function *In Vitro* and *Ex Vivo*: a Time-Course Cannulation Study in Healthy Humans. *Am. J. Clin. Nutr.* 84 (3), 570–579. doi:10.1093/ajcn/84.3.570
- O'Kennedy, N., Raederstorff, D., and Duttaroy, A. K. (2017). Fruitflow®: the First European Food Safety Authority-Approved Natural Cardio-Protective Functional Ingredient. *Eur. J. Nutr.* 56 (2), 461–482. doi:10.1007/s00394-016-1265-2
- Raslan, Z., and Naseem, K. M. (2014). The Control of Blood Platelets by cAMP Signalling. *Biochem. Soc. Trans.* 42 (2), 289–294. doi:10.1042/bst20130278
- Rendu, F., and Brohard-Bohn, B. (2001). The Platelet Release Reaction: Granules' Constituents, Secretion and Functions. *Platelets* 12 (5), 261–273. doi:10.1080/09537100120068170
- Saklatvala, J., Rawlinson, L., Waller, R. J., Sarsfield, S., Lee, J. C., Morton, L. F., et al. (1996). Role for P38 Mitogen-Activated Protein Kinase in Platelet Aggregation Caused by Collagen or a Thromboxane Analogue. *J. Biol. Chem.* 271 (12), 6586–6589. doi:10.1074/jbc.271.12.6586
- Surin, W. R., Barthwal, M. K., and Dikshit, M. (2008). Platelet Collagen Receptors, Signaling and Antagonism: Emerging Approaches for the Prevention of Intravascular Thrombosis. *Thromb. Res.* 122 (6), 786–803. doi:10.1016/j.thromres.2007.10.005
- Thomas, M. R., and Storey, R. F. (2015). The Role of Platelets in Inflammation. *Thromb. Haemost.* 114 (3), 449–458. doi:10.1160/TH14-12-1067
- Thomas, M. R., and Storey, R. F. (2015). The Role of Platelets in Inflammation. *Thromb. Haemost.* 114 (3), 449–458. doi:10.1160/TH14-12-1067
- Uddin, M., Biswas, D., Ghosh, A., O'Kennedy, N., and Duttaroy, A. K. (2018). Consumption of Fruitflow® Lowers Blood Pressure in Pre-hypertensive Males: a Randomised, Placebo Controlled, Double Blind, Cross-Over Study. *Int. J. Food Sci. Nutr.* 69 (4), 494–502. doi:10.1080/09637486.2017.1376621

**Conflict of Interest:** The authors declare that the research was conducted in the absence of any commercial or financial relationships that could be construed as a potential conflict of interest.

**Publisher's Note:** All claims expressed in this article are solely those of the authors and do not necessarily represent those of their affiliated organizations, or those of the publisher, the editors and the reviewers. Any product that may be evaluated in this article, or claim that may be made by its manufacturer, is not guaranteed or endorsed by the publisher.

Copyright © 2021 Zhang, Chen, Li, Chen, Gong, Zhao and Qi. This is an open-access article distributed under the terms of the Creative Commons Attribution License (CC BY). The use, distribution or reproduction in other forums is permitted, provided the original author(s) and the copyright owner(s) are credited and that the original publication in this journal is cited, in accordance with accepted academic practice. No use, distribution or reproduction is permitted which does not comply with these terms.



# The Mechanism Actions of Astragaloside IV Prevents the Progression of Hypertensive Heart Disease Based on Network Pharmacology and Experimental Pharmacology

Haoran Jing<sup>1</sup>, Rongsheng Xie<sup>1</sup>, Yu Bai<sup>1</sup>, Yuchen Duan<sup>1</sup>, Chongyang Sun<sup>2</sup>, Ye Wang<sup>1</sup>, Rongyi Cao<sup>3</sup>, Zaisheng Ling<sup>4</sup> and Xiufen Qu<sup>1\*</sup>

## OPEN ACCESS

### Edited by:

Min Zhang,  
King's College London,  
United Kingdom

### Reviewed by:

Dharmani Devi Murugan,  
University of Malaya, Malaysia  
Stéfany Cau,  
Universidade Federal de Minas Gerais,  
Brazil

### \*Correspondence:

Xiufen Qu  
quxf021007@163.com

### Specialty section:

This article was submitted to  
Cardiovascular and Smooth Muscle  
Pharmacology,  
a section of the journal  
Frontiers in Pharmacology

**Received:** 09 August 2021

**Accepted:** 13 October 2021

**Published:** 05 November 2021

### Citation:

Jing H, Xie R, Bai Y, Duan Y, Sun C, Wang Y, Cao R, Ling Z and Qu X (2021) The Mechanism Actions of Astragaloside IV Prevents the Progression of Hypertensive Heart Disease Based on Network Pharmacology and Experimental Pharmacology. *Front. Pharmacol.* 12:755653. doi: 10.3389/fphar.2021.755653

<sup>1</sup>Department of Cardiovascular, the First Affiliated Hospital of Harbin Medical University, Harbin, China, <sup>2</sup>Department of CT, the First Affiliated Hospital of Harbin Medical University, Harbin, China, <sup>3</sup>Blood Transfusion Department, the First Affiliated Hospital of Harbin Medical University, Harbin, China, <sup>4</sup>Department of CT, the Second Affiliated Hospital of Harbin Medical University, Harbin, China

Astragaloside IV (AS-IV) has been used to treat cardiovascular disease. However, whether AS-IV exerts a protective effect against hypertensive heart disease has not been investigated. This study aimed to investigate the antihypertensive and cardioprotective effects of AS-IV on L-NAME-induced hypertensive rats via network pharmacology and experimental pharmacology. The network pharmacology and bioinformatics analyses were performed to obtain the potential targets of AS-IV and hypertensive heart disease. The rat hypertension model was established by administrated 50 mg/kg/day of L-NAME for 5 weeks. Meanwhile, hypertension rats were intragastrically administrated with vehicle or AS-IV or fosinopril for 5 weeks. Cardiovascular parameters (systolic blood pressure, diastolic blood pressure, mean arterial pressure, heart rates, and body weight), cardiac function parameters (LVEDd, LVEDs, and fractional shortening), cardiac marker enzymes (creatinine kinase, CK-MB, and lactate dehydrogenase), cardiac hypertrophy markers (atrial natriuretic peptide and brain natriuretic peptide), endothelial function biomarkers (nitric oxide and eNOS), inflammation biomarkers (IL-6 and TNF- $\alpha$ ) and oxidative stress biomarkers (SOD, MDA, and GSH) were measured and cardiac tissue histology performed. Network pharmacological analysis screened the top 20 key genes in the treatment of hypertensive heart disease treated with AS-IV. Besides, AS-IV exerted a beneficial effect on cardiovascular and cardiac function parameters. Moreover, AS-IV alleviated cardiac hypertrophy via down-regulating the expression of ANP and BNP and improved histopathology changes of cardiac tissue. AS-IV improved endothelial function via the up-regulation of eNOS expression, alleviated oxidative stress via increasing antioxidant enzymes activities, and inhibited cardiac inflammation via down-regulating IL-6 and TNF- $\alpha$  expression. Our findings suggested that AS-IV is a

potential therapeutic drug to improve L-NAME-induced hypertensive heart disease partly mediated via modulation of eNOS and oxidative stress.

**Keywords:** cardiac damage, astragaloside IV, hypertensive heart disease, network pharmacology, inflammation, antioxidant

## INTRODUCTION

Hypertension is a common cardiovascular disease and a primary contributory factor for pathological cardiac dysfunction and remodeling, which seriously harms the structure and function of the heart (Santos and Shah, 2014). Besides, persistent hypertension may cause fibrosis and left ventricle hypertrophy, which even resulting in heart failure and renal injury (Gradman and Alfayoumi, 2006; Uraizee et al., 2013). Loss of nitric oxide (NO) bioavailability and deficiency in endogenous NO synthesis are thought to underlie functional and histological cardiac injury during this process (Yang et al., 2015). Abnormal changes in NO bioavailability or synthesis evokes endothelial dysfunction, which is also related to the progression of diabetes, heart failure, and hypertension (Moncada, 1992). It has been reported that NO exerts the cardioprotective effect by alleviating cardiac apoptosis and remodeling after myocardial infarction via inhibition of oxidative stress (Smith et al., 2005). Moreover, Up-regulation of eNOS expression declined fructose-evoked insulin resistance and hypertension in rats (C. X. Zhao et al., 2009). The pathogenesis of hypertension involves complex interplays of pathophysiologic, environmental, and genetic factors. Oxidative stress plays a vital role in the pathophysiologic process of hypertension (Touyz et al., 2020). It contributes to renal injury and vascular dysfunction associated with hypertension (Small et al., 2018). Besides, oxidative stress could decrease the bioavailability of NO, leading to vasoconstriction, which could even cause hypertension (Harrison et al., 2003). The increasing evidence indicated that inflammatory cytokines, including IL-6, TNF- $\alpha$ , IFN- $\gamma$ , and IL-17 secreted from T cells, contributed to both vascular and renal injury and dysfunction, causing organ injury, high blood pressure, and oxidative stress (McMaster et al., 2015; Zimmer et al., 2020). N<sup>ω</sup>-nitro-L-arginine methyl ester (L-NAME), a nitric oxide synthase inhibitor, obviously causes NO deficiency and evokes high blood pressure in an animal model (Biwer et al., 2013). Chronic administration of L-NAME could cause cardiac hypertrophy via up-regulation of brain natriuretic peptide (BNP) and atrial natriuretic peptide (ANP) *in vivo* (Suo et al., 2002). Treating rats with L-NAME could induce vascular endothelial injury, and this animal model is widely used in the study of cardiovascular and hypertension diseases (Ribeiro et al., 1992). Additionally, declined antioxidant defense systems and increased production of reactive oxygen species are present in L-NAME-induced hypertensive rat model (Rincón et al., 2015; Zambrano et al., 2013). Therefore, developing new active ingredients with antioxidant effects that could improve endothelial function, and reduce oxidative stress and inflammation might be beneficial for preventing and treating hypertensive heart disease.

Astragaloside IV (AS-IV) is a major active compound of *Astragalus membranaceus*. It has been useful in the treatment

of nonalcoholic fatty liver disease via regulating inflammatory cytokines (Liu et al., 2020). Additionally, it has been reported that AS-IV could decrease obesity-associated hypertension via improving leptin resistance and suppressing inflammatory reactions (Jiang et al., 2018). AS-IV could alleviate cardiac hypertrophy and improve cardiac function via activating Nrf2 (Nie et al., 2019). However, the effects of AS-IV against hypertension-associated cardiac damage are poorly investigated. Thus, the antihypertensive and cardioprotective effects of AS-IV were explored in the L-NAME-evoked hypertensive model, and the underlying mechanism actions of protection effects were evaluated by measuring oxidative stress and endothelial dysfunction-related biomarkers.

## MATERIALS AND METHODS

### Prediction of AS-IV-Associated Targets

The CTD database (<http://ctdbase.org/>), PubChem database (<https://pubchem.ncbi.nlm.nih.gov/>), and Swiss Target Prediction database (<http://www.swisstargetprediction.ch/>) were used to identify potential targets of AS-IV.

### Prediction of Hypertensive Heart Disease-Associated Targets

The CTD database (<http://ctdbase.org/>) and Genecards database (<https://www.genecards.org/>) were used to identify potential targets of hypertensive heart disease. The hypertensive heart disease-associated targets were obtained by searching the keyword “hypertensive heart disease” in these databases.

Construction of protein-protein interaction (PPI) network and core genes identification.

A Venny2.1.0 tool was used to collect the common targets of the AS-IV and hypertensive heart disease. Then, the PPI network of these common targets was constructed using the STRING database (<https://stringdb.org/>). Then, Cytoscape software ([www.cytoscape.org/](http://www.cytoscape.org/)) was used to visualize and integrate the topological parameters of common targets in the PPI network. The degree of each protein node was calculated using the CytoHubba plugin. Then, the top 20 genes were identified as core genes.

### Enrichment Analysis and Construction of the Compound-Targets-Pathways-Disease Network

KEGG pathway analysis was performed using the Metascape platform (<http://metascape.org/gp/#/main/step1>) to obtain the AS-IV-mediated pathways against hypertensive heart disease. Cytoscape software ([www.cytoscape.org/](http://www.cytoscape.org/)) was used to



construct a compound-targets-pathways-disease network based on the results of PPI and KEGG analysis.

## Experimental Verification

### Animal Experimental Protocol

Male Sprague-Dawley rats (6–8 weeks old and 180–220 g) were purchased from the animal center of Harbin Medical University and housed under temperature- and humidity-controlled animal room, with 12 h light-dark cycles and free access to food and water. All animal experiments were performed by National Institutes of Health guidelines and approved by the Animal Ethics Committee of the First Affiliated Hospital of Harbin Medical University.

After 1 week of acclimation, all animals were randomly divided into the five groups ( $n = 8$  for each group) and treated as follows: Control group (CON), rats only received carboxymethyl cellulose solution (1%) daily; CON + HAS-IV group, rats in the CON group received a high dose of AS-IV (40 mg/kg) daily; L-NAME group (LN), rats received 50 mg/kg of L-NAME in carboxymethyl cellulose solution (1%) daily for 5 weeks to evoke hypertension (Berkban et al., 2015); LN + LAS-IV group, rats in the LN group received a low dose of AS-IV (20 mg/kg) daily; LN + HAS-IV group, rats in the LN group received a high dose of AS-IV (40 mg/kg) daily. LN + fosinopril group, rats in the LN group received fosinopril (4.67 mg/kg) daily. The doses of AS-IV and fosinopril were selected according to the previous report (Jiang et al., 2018; Wang et al., 2020). Drugs were suspended in carboxymethyl cellulose solution (1%). Carboxymethyl cellulose solution (1%) or drugs were intragastrically administered daily for 5 weeks.

### Measurement of Cardiovascular Parameters

After 5 weeks of continuous administration, a non-invasive blood pressure measurement and analysis system (ALC-NIBP, ALCBIO, China) were used to measure the systolic blood pressure (SBP), diastolic blood pressure (DBP), mean arterial pressure (MAP), and heart rates (HR) in conscious rats based on manufacturer's instruction.

### Assessment of Cardiac Function

At the end of the experiment, the rats were fasted for 18 h and anesthetized with 40 mg/kg of sodium pentobarbital by intraperitoneal injection. The Doppler echocardiography (Agilent Sonos5500) was used to measure the left ventricular end-diastolic dimension (LVEDd), left ventricular end-systolic dimension (LVEDs), and fractional shortening (FS) of each group.

### Collection of Tissue and Blood Samples

At the end of the experiment, rats were anesthetized with 40 mg/kg of sodium pentobarbital by intraperitoneal injection and euthanized by inhaling CO<sub>2</sub>. Then, the blood samples were rapidly collected from the abdominal aorta. Hearts and thoracic aortas were rapidly harvested and stored at −20°C for further analysis.

### Measurement of Cardiac Marker Enzymes Activities

Collected blood samples were centrifuged at 3,000 r/min for 15 min at 4°C and the serum was obtained. The activities of creatine kinase (CK), creatine kinase-MB (CK-MB), and lactate dehydrogenase (LDH) were measured using commercially available kits (Jiancheng Bioengineering, Nanjing, China) based on the manufacturer's instruction.

### Assay of Endothelial Function Biomarkers

The plasma, aortic and cardiac NO levels and the eNOS activity were measured by commercially available kits (Jiancheng Bioengineering, Nanjing, China) based on the manufacturer's protocol.

### Measurement of Oxidative Stress Biomarkers

The heart and aorta tissues were homogenized in ice physiological saline using a homogenizer and then centrifuged at 5,000 r/min for 10 min. The supernatant was collected and the protein concentration was measured by the BCA method. The activities of SOD, GSH, and MDA levels in the aortic and cardiac homogenate were measured by corresponding kit (Jiancheng Bioengineering, Nanjing, China) based on the manufacturer's protocols.

### Histopathological Analysis

The cardiac tissue was collected and washed by ice physiological saline, and then fixed by 10% formalin and embedded in paraffin. The pathological changes of the heart were examined using hematoxylin and eosin staining reagent. Cardiomyocyte injury and interstitial edema were evaluated for cardiac pathological score, in which the score was 0 for normal, 1 for mild, 2 for moderate, and 3 for severe damage.

### Cell Experiment

Rat H9C2 cells were purchased from China Infrastructure of Cell Line Resources (Chinese Academy of Medical Sciences) and cultured in Dulbecco's modified Eagle's medium, containing antibiotics and 10% fetal bovine serum at 37°C, 95% air, and 5% CO<sub>2</sub>. We changed the medium daily until the H9C2 cells were at 80–90% confluence. H9C2 cells ( $3 \times 10^4$  cells/ml) were inoculated into a 96-well plate, and then added different concentrations of AS-IV (20, 40, and 80 µg/ml) in the absence or presence of L-NAME (1 mM) for 24 h. Then, cell Counting Kit-8 (CCK-8, Dojindo, Japan) was applied for measuring cell viability.

### Quantitative Real-Time Polymerase Chain Reaction

The whole RNA of H9C2 cells, heart, and aorta tissues was extracted by the TRIzol reagent (Invitrogen, United States) following the manufacturer's protocol. Then, the extracted total RNA was used for cDNA synthesis by the Prime Script RT reagent kit (Takara BioInc, Japan) according to the manufacturer's protocol. qRT-PCR was carried out in the ABI StepOnePlus system (Applied Biosystems,

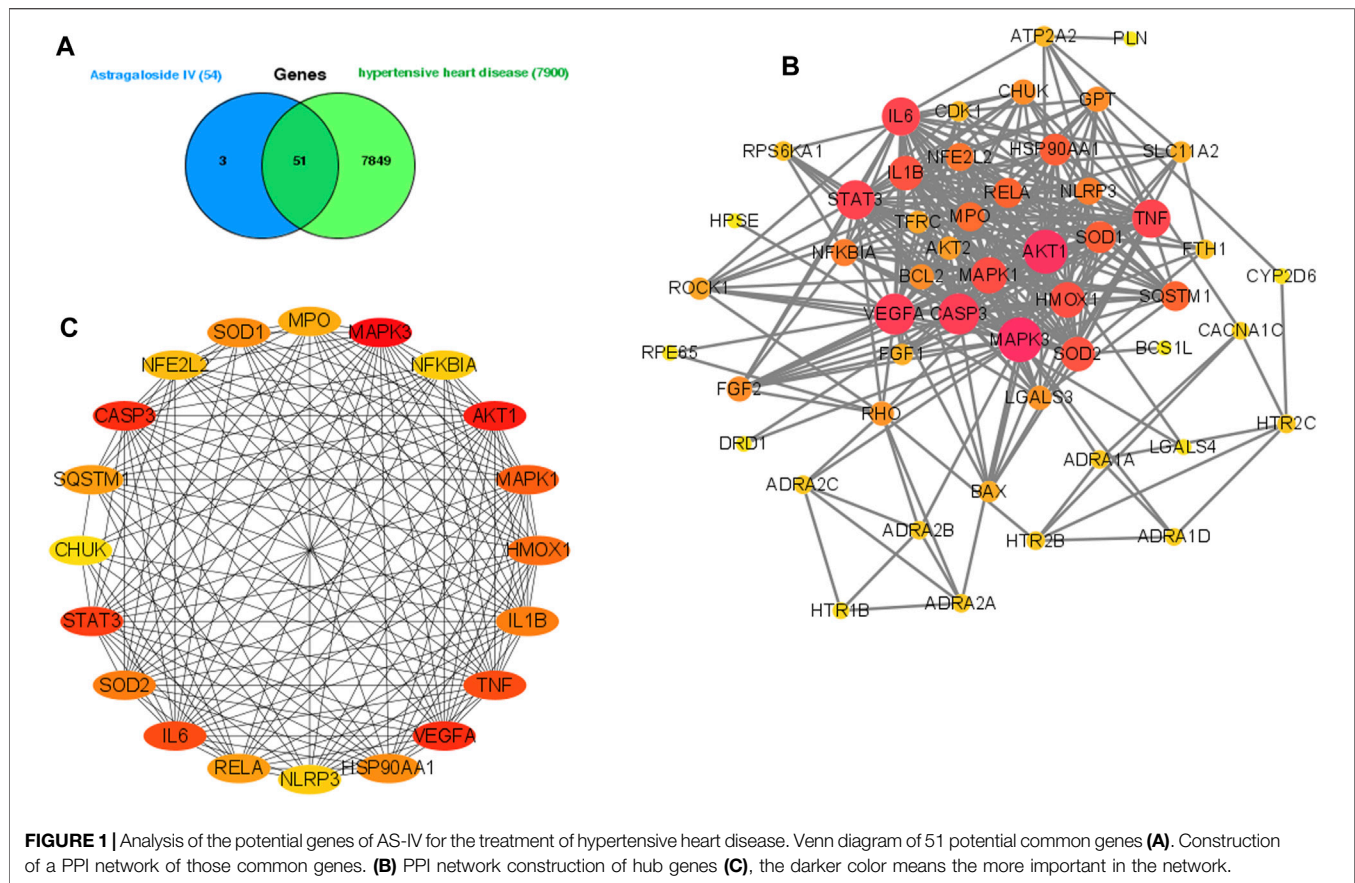


**FIGURE 1 |** Analysis of the potential genes of AS-IV for the treatment of hypertensive heart disease. Venn diagram of 51 potential common genes **(A)**. Construction of a PPI network of those common genes **(B)**. PPI network construction of hub genes **(C)**, the darker color means the more important in the network.

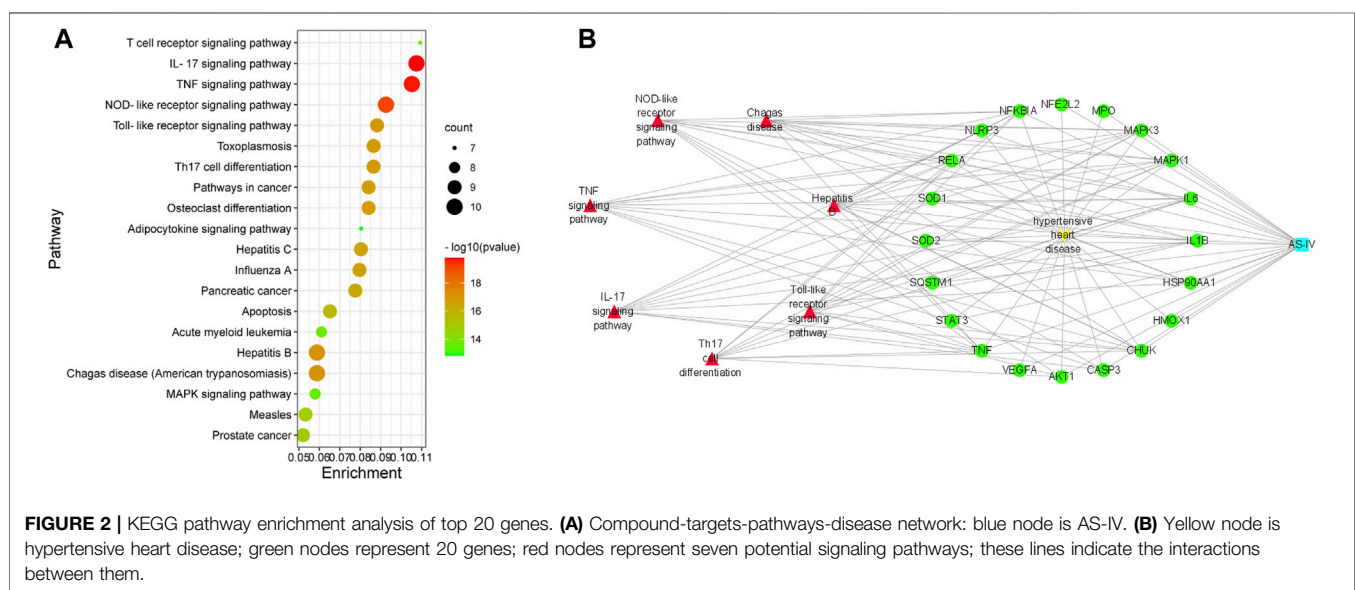
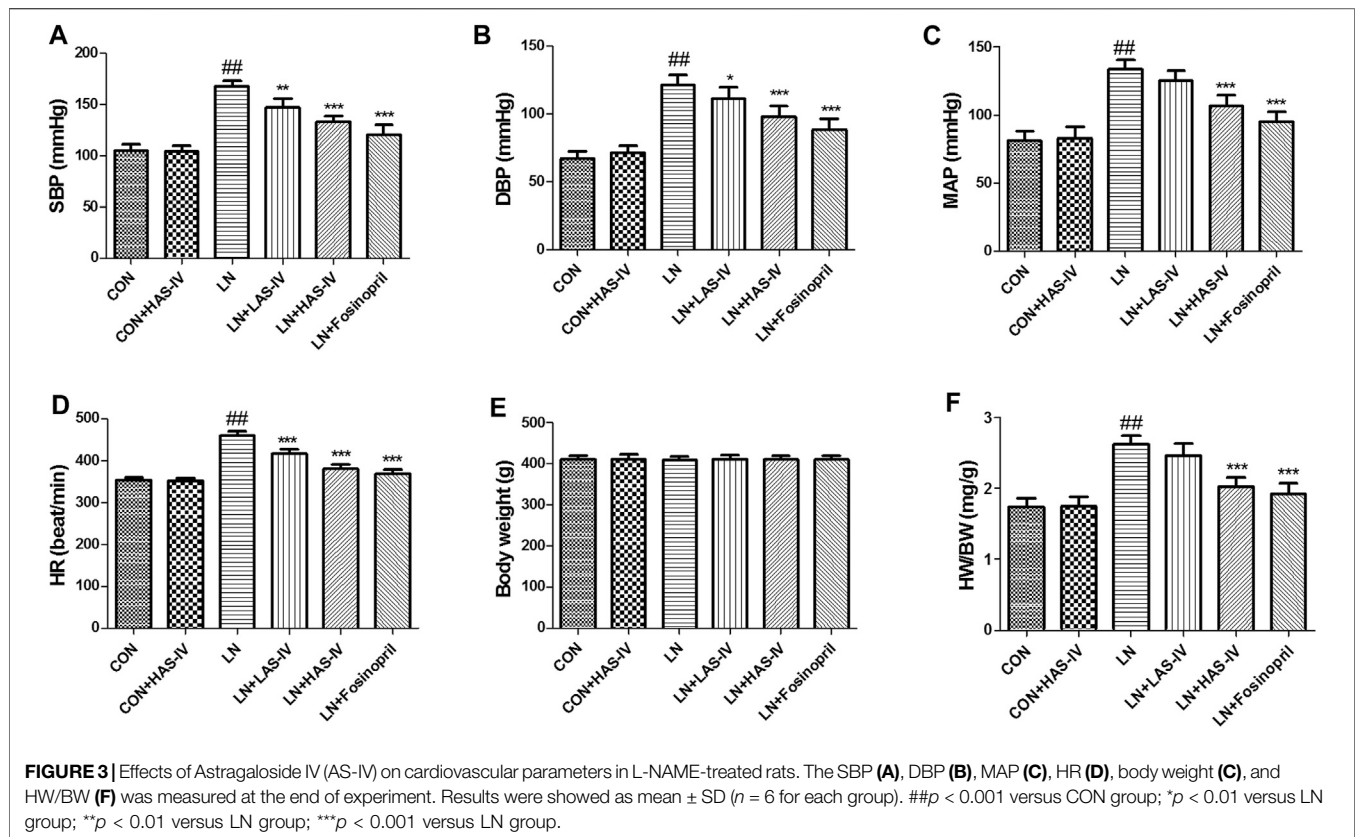


**FIGURE 2 |** KEGG pathway enrichment analysis of top 20 genes. **(A)** Compound-targets-pathways-disease network: blue node is AS-IV. **(B)** Yellow node is hypertensive heart disease; green nodes represent 20 genes; red nodes represent seven potential signaling pathways; these lines indicate the interactions between them.

United States ) using the Sybergreen<sup>TM</sup> reactions. The primers used in the present study were listed in supplementary file **Supplementary Table S1**. The results of mRNA were quantified using the delta Ct method and normalized to glyceraldehyde 3-phosphate dehydrogenase (GAPDH).

## Data Analysis

GraphPad Prism Version (version 7.0) software was used for all data analyses and all results were given as mean  $\pm$  standard deviation (SD). Significant differences were analyzed by one-way analysis of variance (ANOVA) followed by the Mann



Whitney test. A value of  $p < 0.05$  was considered statistically significant.

## RESULTS

### Targets Screening of AS-IV and Hypertensive Heart Disease

As shown in **Figure 1A**, we collected potential genes of AS-IV from CTD, PubChem, and Swiss Target Prediction databases. Those genes were combined and we removed the overlap genes. Then, 54 genes associated with AS-IV were obtained. Besides, potential targets of hypertensive heart disease were predicted from the Genecards and CTD databases. We combined those potential genes and removed the overlap ones. Then, 7,900 hypertensive heart disease-associated genes were collected. Finally, 51 common genes were obtained as potential genes in the therapeutic effect of AS-IV against hypertensive heart disease.

### PPI Network Construction and Hub Genes Screening

As shown in **Figure 1B**, the string database was used to construct the PPI network of 51 common targets. Then, Cytoscape software was used to rearrange those 51 common genes based on the degree value, and the top 20 genes of high-

node degree were selected as the hub genes (**Figure 1C**). Interestingly, we found the inflammation-related (TNF, IL-1 $\beta$ , and IL6) and oxidative stress-related (SOD1 and SOD2) genes in the hub genes.

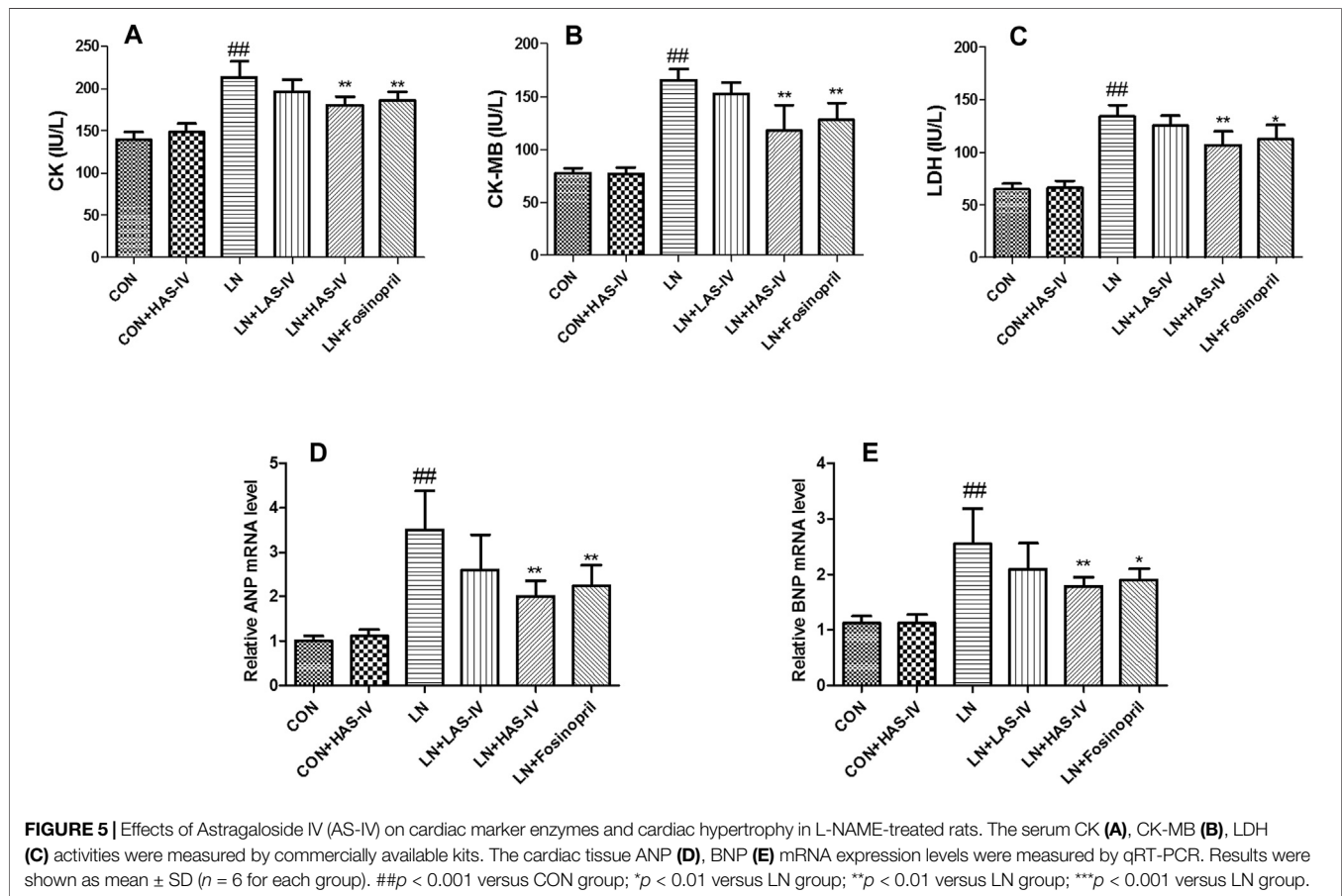
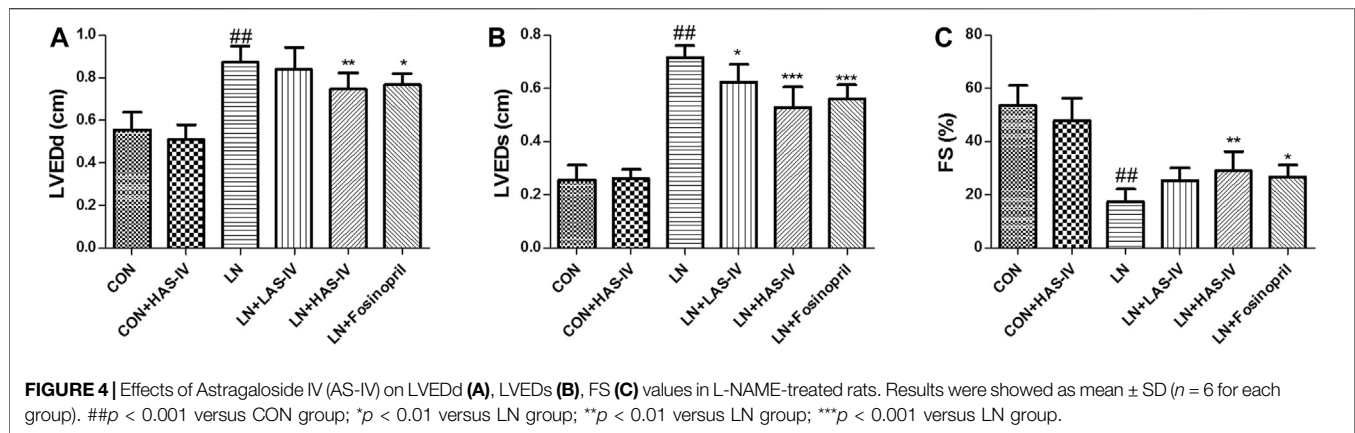
### Enrichment Analysis of Common Genes

The KEGG enrichment analysis indicated how AS-IV acts on this pathway, thus exerting a therapeutic effect in hypertensive heart disease. In the present study, the top 20 hub genes were selected for enrichment analysis, and the top 20 signaling pathways were screened for further analysis based on  $p$ -Value. These signaling pathways were shown in **Figure 2A**. Among them, the IL-17 signaling pathway, TNF signaling pathway, NOD-like receptor signaling pathway, and Toll-like receptor signaling pathway as the top ones.

### Compound-Targets-Pathways-Disease Network

As shown in **Figure 2B**, a multidimensional network of “compound-targets-pathways-disease” was constructed by Cytoscape software, which included 29 nodes (1 compound, 20 genes, 7 signaling pathways, and 1 disease). The purple node is AS-IV; the yellow node is hypertensive heart disease; the green nodes represent 20 genes; the pink to red nodes represent 7 potential signaling pathways; these lines indicate the interactions between them. These findings indicated that





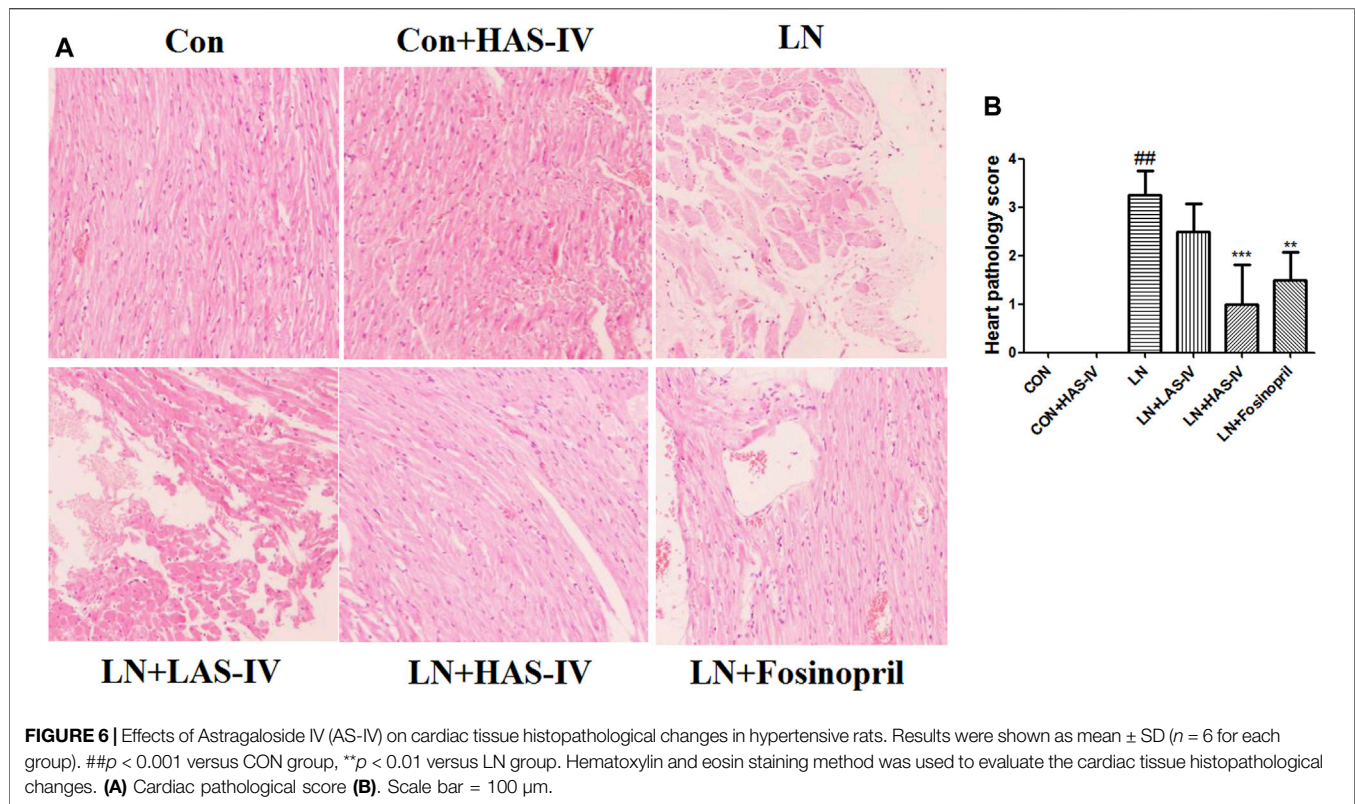
the AS-IV could alleviate hypertension heart disease via regulating multi-targets and multi-signaling pathways.

### Effects of AS-IV on Cardiovascular Parameters and Cardiac Function in L-NAME-Treated Rats

As shown in Figure 3, administration of L-NAME for 5 weeks evoked a significant increase in SBP, DBP, MAP, HR, and HW/

BW compared to the CON group. Treatment with a high dose of AS-IV (40 mg/kg) significantly decreased all these cardiovascular parameters in hypertensive heart disease rats. Fosinopril exerted similar effects as AS-IV (40 mg/kg). It's worth noting that, a low dose of AS-IV (20 mg/kg) also decreased SBP, DBP, and HR in LN + LAS-IV group. Besides, our results indicated that the values of LVEDd and LVEDs in the LN group increased when compared with the CON group, accompanied by a significant decrease of FS (Figure 4). After AS-IV (40 mg/kg) or fosinopril treatment,





LVEDd and LVEDs were decreased, while FS was increased, implying remarkable cardioprotection of AS-IV against L-NAME-induced hypertensive heart disease.

### Effects of AS-IV on Cardiac Marker Enzymes and Cardiac Hypertrophy in L-NAME-Treated Rats

As shown in **Figures 5A–C**, after administration of L-NAME for 5 weeks, the activities of CK, CK-MB, and LDH were significantly increased in the LN group compared to the CON group. Treatment with a high dose of AS-IV (40 mg/kg) or fosinopril significantly reduced these cardiac marker enzymes activities in the model group. ANP and BNP are natriuretic peptides, play a major role in the regulation of cardiovascular, and as markers of myocyte hypertrophy (Gardner, 2003; Kohno et al., 1995). After administration of L-NAME for 5 weeks, the mRNA expression of ANP and BNP were significantly up-regulated in the LN group compared to the CON group (**Figures 5D,E**). Treatment with AS-IV (40 mg/kg) or fosinopril significantly reduced these cardiac hypertrophy markers expressions in the model group. Besides, hematoxylin-eosin (HE) staining was used to evaluate the pathologic features of cardiac tissue. **Figure 6** showed an enlarged cross-sectional area of cardiomyocytes, cardiomyocyte injury, and interstitial edema in the cardiac sections of the LN group. Treatment with AS-IV (40 mg/kg) or fosinopril significantly alleviated these histopathological changes and decreased heart pathology score in the model group (**Figures 6A,B**). However, the low dose of AS-IV (20 mg/kg) has no effect on cardiac

hypertrophy parameters and cardiac damage in L-NAME-treated rats. These findings revealed that the potential protective effects of AS-IV in the treatment of cardiac hypertrophy.

### Effects of AS-IV on Endothelial Function Biomarkers in L-NAME-Treated Rats

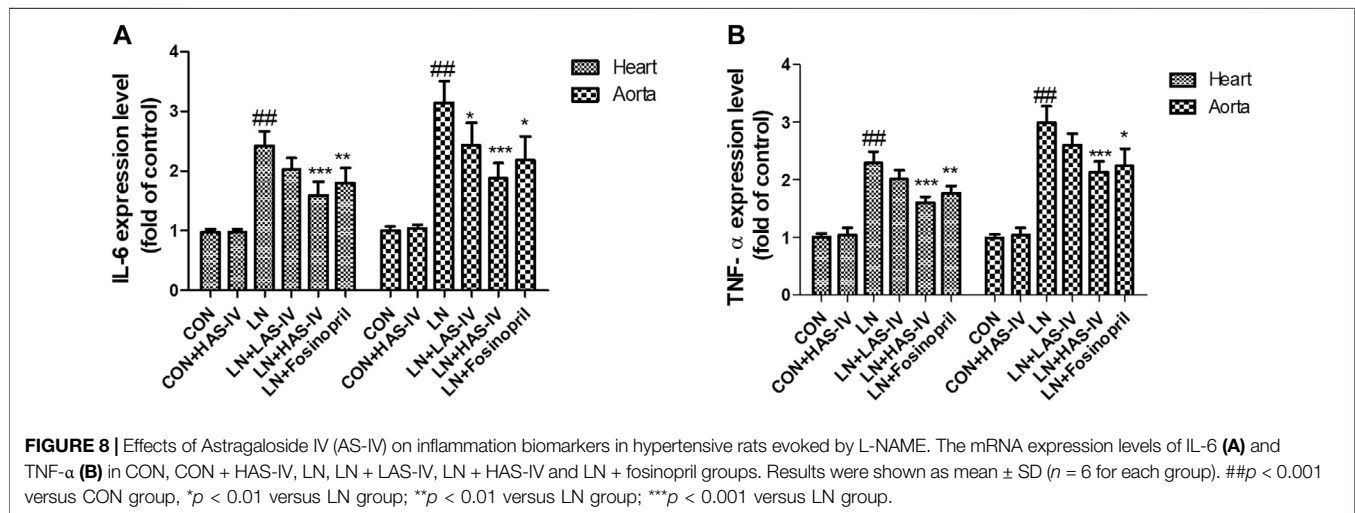
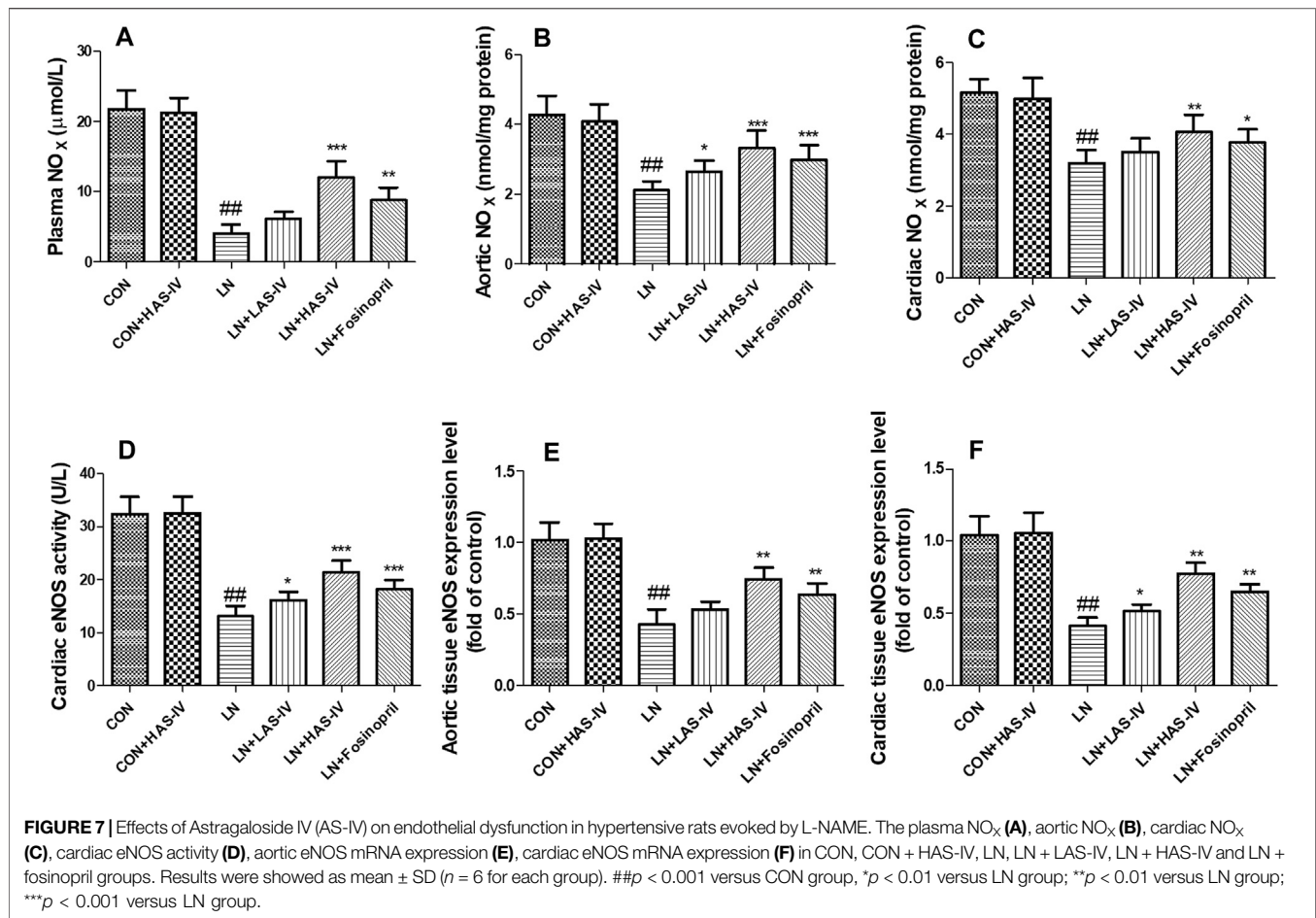
Chronic administration of L-NAME for 5 weeks, the levels of  $\text{NO}_x$  and eNOS in plasma, heart, and aorta were significantly decreased in the LN group compared to the CON group (**Figure 7**). Treatment with AS-IV (40 mg/kg) or fosinopril significantly increased these endothelial function biomarkers in the hypertensive heart disease group.

### Effects of AS-IV on Inflammation Biomarkers in L-NAME-Treated Rats

Chronic administration of L-NAME for 5 weeks, the expression levels of IL-6 and TNF- $\alpha$  in the heart and aorta were significantly increased in the LN group compared to the CON group (**Figure 8**). Hypertensive heart disease rats treated with AS-IV (40 mg/kg) or fosinopril had significantly down-regulated IL-6 and TNF- $\alpha$  expression levels compared with the LN group.

### Effects of AS-IV on Oxidative Stress Biomarkers in L-NAME-Treated Rats

Chronic administration of L-NAME for 5 weeks, the activities of SOD and GSH in the heart and aorta were significantly decreased



in the LN group compared to the CON group (Figures 9A,B). Besides, the levels of MDA were significantly increased in the LN group compared to the CON group (Figure 9C). Hypertensive heart disease rats treated with AS-IV (40 mg/kg) or fosinopril had significantly increased SOD and GSH activities and a significantly

decreased MDA level compared with the LN group. It's worth noting that, a low dose of AS-IV (20 mg/kg) also decreased MDA levels in LN + LAS-IV group. In addition, the qRT-PCR results indicated that AS-IV or fosinopril inhibited the down-regulation levels of SOD1 and SOD2 induced by L-NAME (Figure 9D,E).

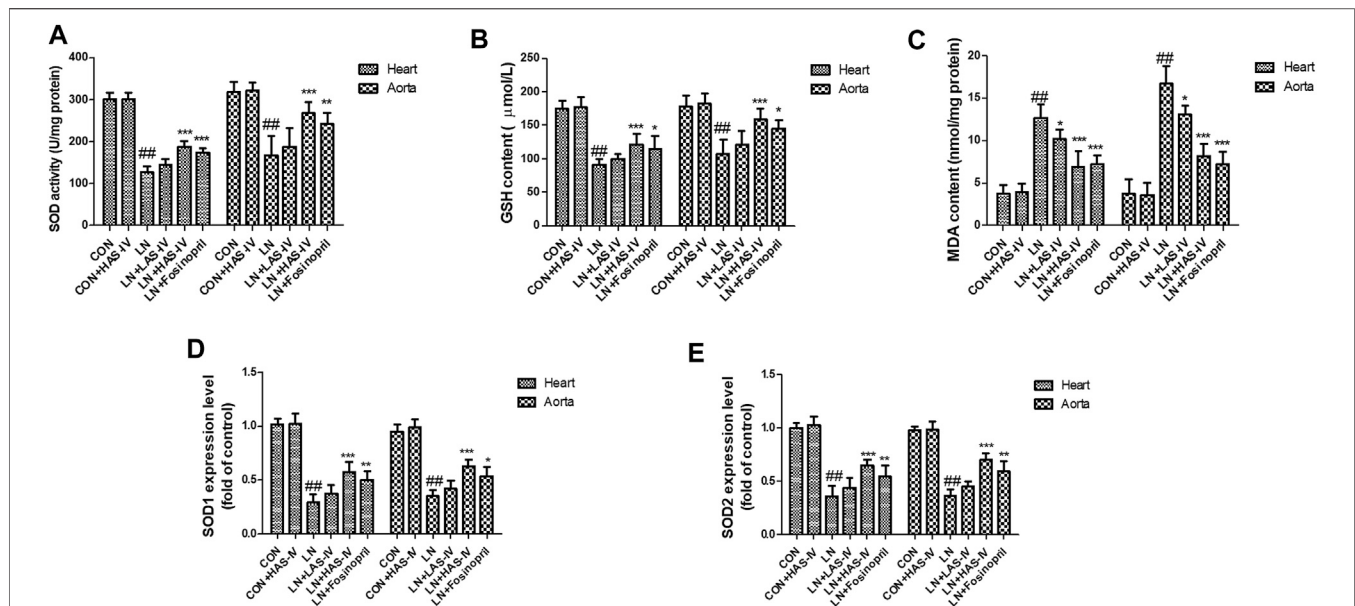


**FIGURE 9** | Effects of Astragaloside IV (AS-IV) on oxidative stress biomarkers in hypertensive rats evoked by L-NAME. The SOD activity **(A)**, GSH content **(B)**, MDA content **(C)**, SOD1 mRNA expression **(D)**, and SOD2 mRNA expression **(E)** in CON, CON + HAS-IV, LN, LN + LAS-IV, LN + HAS-IV and LN + fisinopril groups. Results were shown as mean  $\pm$  SD ( $n = 6$  for each group). ## $p < 0.001$  versus CON group, \* $p < 0.01$  versus LN group; \*\* $p < 0.01$  versus LN group; \*\*\* $p < 0.001$  versus LN group.

## AS-IV Increased Cell Viability in L-NAME-Stimulated H9C2 Cells

As shown in **Figure 10A**, treatment with AS-IV (20–80  $\mu\text{g/ml}$ ) alone did not cause a decrease in cell viability of H9C2 cells. The H9C2 cells were exposed to L-NAME caused the decline of cell viability (**Figure 10B**). Treatment with AS-IV (40–80  $\mu\text{g/ml}$ ) improved cell viability in L-NAME-stimulated H9C2 cells.

## The Protective Effect of AS-IV Against L-NAME-Induced Inflammation and Oxidative Stress in H9C2 Cells

The cells experiment was performed to further validate the results of network pharmacology and animal experiment. As shown in **Figure 11**, the expression of ANP, BNP, and IL-6 was up-regulated in L-NAME-stimulated H9C2 cells. AS-IV significantly down-regulated the expressions of ANP, BNP, and IL-6. The expressions of eNOS and SOD1 were down-regulated in L-NAME-stimulated H9C2 cells. AS-IV significantly up-regulated the expressions of eNOS and SOD1.

## DISCUSSION

Hypertensive heart disease is induced by chronic pressure overload and multiple mechanisms are involved in the progression of this disease (Slivnick and Lampert, 2019). Hyperphosphorylation of titin protein, microtubule disarray, and abnormal calcium handling are involved in this pathological process (Borbély et al., 2009; Shah et al., 2014). Therefore, the detailed etiology of hypertensive heart disease is

not fully understood. Because there is no specific drug to treat hypertensive heart disease; therefore, developing novel agents is very necessary.

Over the past few decades, natural compounds extracted from herbs or Chinese herbal medicine have been one of the most primary resources for drug research and development, especially in the treatment and prevention of cardiovascular disease. AS-IV is the primary active compound extracted from *Astragalus membranaceus*. Previous reports have indicated that AS-IV exerts various protective activities in the brain, kidney, lung, and cardiovascular, and these pharmacological activities are related to multiple signaling pathways, such as Nrf2 antioxidant signaling pathways, NF- $\kappa$ B signaling pathway, and EGFR-Nrf2 signaling pathway (J. Zhang et al., 2020a). However, the underlying mechanism actions of AS-IV against hypertensive heart disease have not been fully understood. Network pharmacology integrates omics, network visualization, and other methods to establish the system network model based on the theory of systems biology (Li and Zhang, 2013). The complex relationship among drugs, diseases, targets, and pathways was revealed via network pharmacology analysis, which is of great significance for understanding the mechanism of action of traditional Chinese medicine, the basis of the medicinal substance, and the research and development of new drugs (Hao da and Xiao, 2014). In the present study, the network pharmacology was used to investigate the therapeutic effect of AS-IV in the treatment of hypertensive heart disease and an animal experiment was performed to verify our speculation.

First, we used network pharmacology and bioinformatics methods to construct a “compound-targets-pathways-disease” network. Our findings indicated that the targeted genes of AS-IV against hypertensive heart disease are involved in oxidative



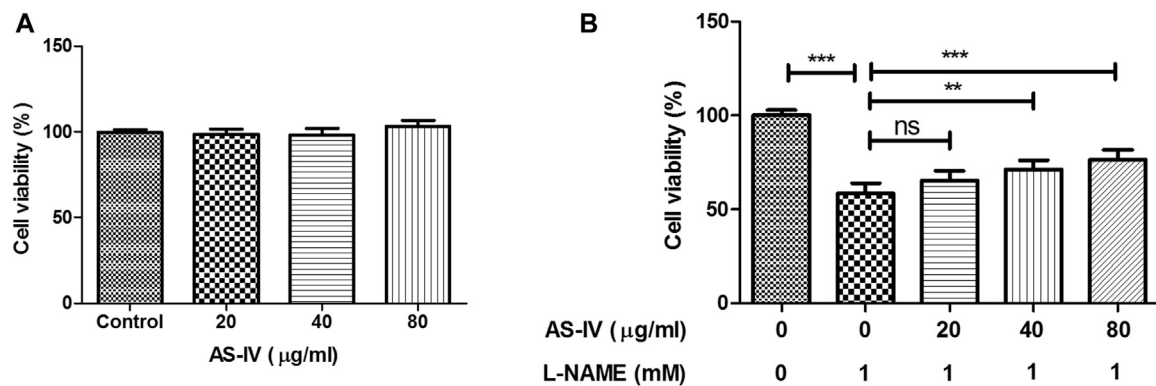


**FIGURE 10 |** Effect of Astragaloside IV (AS-IV) on the cell viability in L-NAME-stimulated H9C2 cells. H9C2 cells were stimulated with different concentrations of AS-IV (20, 40, and 80 µg/ml) in the absence or presence of L-NAME (1 mM) for 24 h. Results were presented as mean ± standard deviation (SD).  $n = 4$ . \*\* $p < 0.01$ , \*\*\* $p < 0.001$ .

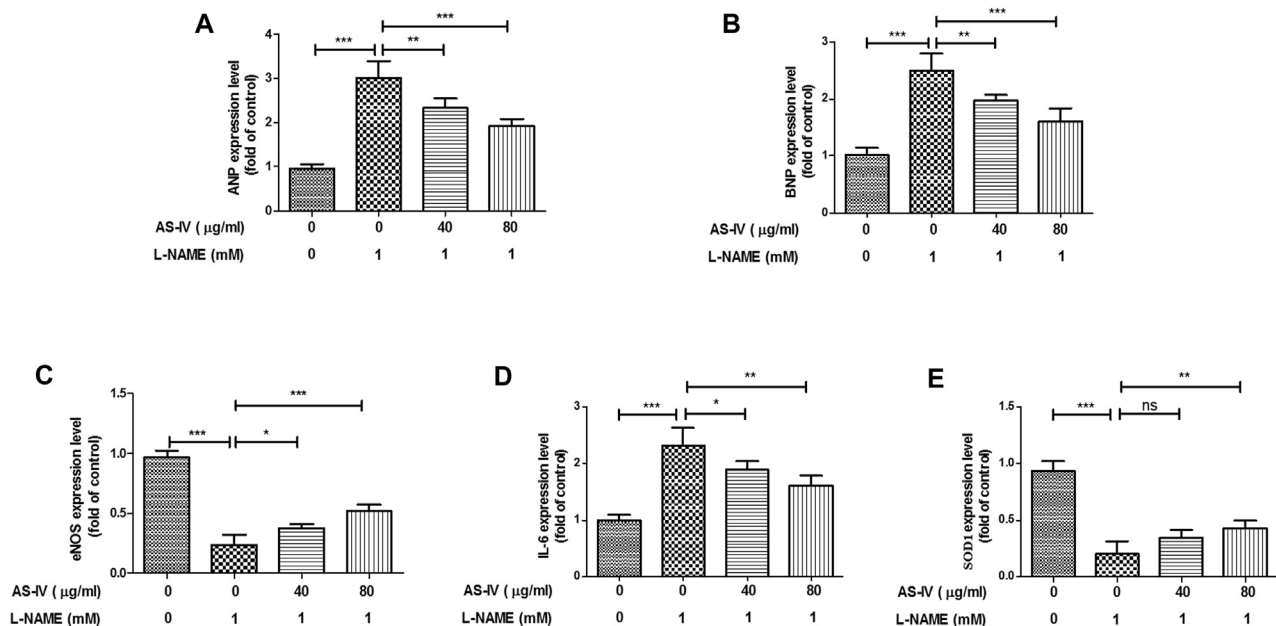


**FIGURE 11 |** The protection effect of Astragaloside IV (AS-IV) against L-NAME-induced inflammation and oxidative stress in H9C2 cells. H9C2 cells were stimulated with different concentrations of AS-IV (40 and 80 µg/ml) in the absence or presence of L-NAME (1 mM) for 24 h mRNA expression of ANP (A), BNP (B), eNOS (C), IL-6 (D), and SOD1 (E) were measured by qRT-PCR. Results were presented as mean ± standard deviation (SD).  $n = 4$ . \* $p < 0.05$ , \*\* $p < 0.01$ , \*\*\* $p < 0.001$ .

stress and inflammation, including SOD2, SOD1, IL-6, TNF, and IL-1 $\beta$ . Next, we investigated the antihypertensive and cardioprotective effects of AS-IV in L-NAME-induced hypertensive heart disease models. And our results revealed that these beneficial effects of AS-IV may be related to the down-regulation of IL-6 and TNF- $\alpha$  and up-regulation of SOD1 and SOD2.

At present, multiple mechanisms have been proposed for the etiology of hypertensive heart disease. One of the most important is the reduction of NO bioavailability or NO synthesis (Davel

et al., 2011; Lee et al., 2016). Previous reports have indicated that the suppression of eNOS resulted in hypertension and high vascular resistance (Nyadjeu et al., 2013; Selamoglu Talas, 2014). Blockade NO synthesis in L-NAME-induced high blood pressure is related to the down-regulation of eNOS expression and elevation of MDA level (Fu et al., 2011; Jan-On et al., 2020). The L-NAME-induced hypertensive heart disease model is similar to that of patients with vascular endothelial dysfunction, who also experience structural and functional cardiac dysfunction due to the loss of bioavailability of NO

(Ndisang et al., 2014). *In vivo*, our findings showed that hypertension heart disease was induced by a decrease of NO<sub>x</sub> level and an increase of oxidative stress. Administration of AS-IV decreased high blood pressure, increased eNOS expression as well as attenuated cardiac dysfunction in the hypertensive heart disease model. Meanwhile, MDA level and oxidative stress markers were also alleviated in the model group after AS-IV administration. Thus, antioxidant properties may be one of the mechanisms by which AS-IV inhibited the progression of hypertensive heart disease. Moreover, the administration of L-NAME also leads to cardiomyocytes injury that induces the secretion of cardiac enzymes (LDH, CK-MB, and CK). The previous report showed that chronic depletion of NO by L-NAME resulted in a significant increase in CK, CK-MB, and LDH levels (Kumar et al., 2014). Consistent with the previous report, our findings of cardiac enzyme measuring and H&E staining showed that the L-NAME administration caused the increase of cardiac enzymes (CK, CK-MB, and LDH) and cardiac structural abnormalities. In the present study, administration of AS-IV reversed those abnormalities induced by L-NAME, implying that AS-IV alleviated symptoms of hypertensive heart disease in L-NAME-treated rats.

Inflammation is a primary factor in the occurrence of disease (Nathan and Ding, 2010). The findings of the PPI network indicated that IL-6, TNF, IL-1 $\beta$ , and NFKBIA were predicted as the main genes of AS-IV against hypertensive heart disease and the KEGG pathways analysis showed that TNF signaling pathway was its key pathway. It has been reported that hypertensive caused chronic systemic inflammation, which stimulates the secretion of pro-inflammatory factors that lead to cardiac damage (Mouton et al., 2020). Chronic cardiac inflammation is involved in the aggravation of cardiac remodeling in hypertensive heart disease (Kai et al., 2009). AS-IV alleviates mechanical stress-induced myocardial hypertrophy *via* decreasing inflammation (T. Zhang et al., 2020b). AS-IV prevents lipopolysaccharide-induced gestational hypertension *via* the suppression of inflammatory responses (Tuerxun et al., 2021). Therefore, we speculated that AS-IV may alleviate systemic inflammation in hypertensive heart disease. In the present study, AS-IV down-regulated the expression of IL-6 and TNF and inhibited the progression of inflammation. This finding explained that AS-IV alleviated cardiac inflammation in hypertensive rats evoked by L-NAME.

Oxidative stress is also one of the pathogenic factors of hypertensive heart disease (Mi et al., 2019). Cardiac oxidative stress induced by excess reactive oxygen species has been indicated to be implicated in the occurrence and development of high blood pressure and pressure overload-induced cardiac damage (W. Zhao et al., 2008). It has been reported that oxidative injury was present in hypertensive myocardial tissue (Worou et al., 2011). Besides, the expression of SOD2 significantly changed in the hypertension-induced cardiac dysfunction (Koyanagi et al., 2008). Therefore, inhibition of oxidative stress is a novel method to treat hypertensive heart disease.

AS-IV alleviates myocardial ischemia injury *via* suppressing reactive oxygen species burst and improving antioxidant potential (Luo et al., 2019). The findings of the PPI network indicated that SOD1 and SOD2 were predicted as the potential genes of AS-IV in the treatment of hypertensive heart disease. And the network pharmacological results were verified by *in vivo* and *in vitro* experiments. In the present study, we found that AS-IV up-regulated the expression of SOD1 and SOD2, improved the activities of SOD and GSH, and decreased the MDA level, indicating that AS-IV inhibited the progression of hypertensive heart disease *via* inhibition of oxidative stress.

## CONCLUSION

In the present report, the network pharmacology and experimental validation were performed to investigate the therapeutic effects of AS-IV against hypertensive heart disease. Our findings demonstrated that AS-IV prevents the progression of hypertensive heart disease *via* activation of eNOS and inhibition of oxidative stress. Our results not only provide a theoretical foundation for exploring the mechanism actions of AS-IV against hypertensive heart disease but also develop a promising treatment for hypertensive heart disease.

## DATA AVAILABILITY STATEMENT

The original contributions presented in the study are included in the article/**Supplementary Files**, further inquiries can be directed to the corresponding author.

## ETHICS STATEMENT

The animal study was reviewed and approved by the First Affiliated Hospital of Harbin Medical University. Written informed consent was obtained from the owners for the participation of their animals in this study.

## AUTHOR CONTRIBUTIONS

HJ and RX designed the experiments and wrote the manuscript. YB, YD, CS, WY, and RC carried out the experiments and analyzed the data. ZL and XQ supervised and corrected the manuscript.

## SUPPLEMENTARY MATERIAL

The Supplementary Material for this article can be found online at: <https://www.frontiersin.org/articles/10.3389/fphar.2021.755653/full#supplementary-material>

## REFERENCES

- Berkban, T., Boonprom, P., Bunbupha, S., Welbat, J. U., Kukongviriyapan, U., Kukongviriyapan, V., et al. (2015). Ellagic Acid Prevents L-NAME-Induced Hypertension via Restoration of eNOS and P47phox Expression in Rats. *Nutrients* 7 (7), 5265–5280. doi:10.3390/nu7075222
- Biwer, L. A., Broderick, T. L., Xu, H., Carroll, C., and Hale, T. M. (2013). Protection against L-NAME-Induced Reduction in Cardiac Output Persists Even after Cessation of Angiotensin-Converting Enzyme Inhibitor Treatment. *Acta Physiol. (Oxf)* 207 (1), 156–165. doi:10.1111/j.1748-1716.2012.02474.x
- Borbély, A., Falcao-Pires, I., van Heerebeek, L., Hamdani, N., Edes, I., Gavina, C., et al. (2009). Hypophosphorylation of the Stiff N2B Titin Isoform Raises Cardiomyocyte Resting Tension in Failing Human Myocardium. *Circ. Res.* 104 (6), 780–786. doi:10.1161/CIRCRESAHA.108.193326
- Davel, A. P., Wenceslau, C. F., Akamine, E. H., Xavier, F. E., Couto, G. K., Oliveira, H. T., et al. (2011). Endothelial Dysfunction in Cardiovascular and Endocrine-Metabolic Diseases: an Update. *Braz. J. Med. Biol. Res.* 44 (9), 920–932. doi:10.1590/s0100-879x2011007500104
- Fu, J. Y., Qian, L. B., Zhu, L. G., Liang, H. T., Tan, Y. N., Lu, H. T., et al. (2011). Betulinic Acid Ameliorates Endothelium-dependent Relaxation in L-NAME-Induced Hypertensive Rats by Reducing Oxidative Stress. *Eur. J. Pharm. Sci.* 44 (3), 385–391. doi:10.1016/j.ejps.2011.08.025
- Gardner, D. G. (2003). Natriuretic Peptides: Markers or Modulators of Cardiac Hypertrophy. *Trends Endocrinol. Metab.* 14 (9), 411–416. doi:10.1016/s1043-2760(03)00113-9
- Gradman, A. H., and Alfayoumi, F. (2006). From Left Ventricular Hypertrophy to Congestive Heart Failure: Management of Hypertensive Heart Disease. *Prog. Cardiovasc. Dis.* 48 (5), 326–341. doi:10.1016/j.pcad.2006.02.001
- Hao, da. C., and Xiao, P. G. (2014). Network Pharmacology: a Rosetta Stone for Traditional Chinese Medicine. *Drug Dev. Res.* 75 (5), 299–312. doi:10.1002/ddr.21214
- Harrison, D. G., Cai, H., Landmesser, U., and Griendling, K. K. (2003). Interactions of Angiotensin II with NAD(P)H Oxidase, Oxidant Stress and Cardiovascular Disease. *J. Renin Angiotensin Aldosterone Syst.* 4 (2), 51–61. doi:10.3317/jraas.2003.014
- Jan-On, G., Sangartit, W., Pakdechote, P., Kukongviriyapan, V., Sattayasai, J., Senaphan, K., et al. (2020). Virgin rice Bran Oil Alleviates Hypertension through the Upregulation of eNOS and Reduction of Oxidative Stress and Inflammation in L-NAME-Induced Hypertensive Rats. *Nutrition* 69, 110575. doi:10.1016/j.nut.2019.110575
- Jiang, P., Ma, D., Wang, X., Wang, Y., Bi, Y., Yang, J., et al. (2018). Astragaloside IV Prevents Obesity-Associated Hypertension by Improving Pro-inflammatory Reaction and Leptin Resistance. *Mol. Cell* 41 (3), 244–255. doi:10.14348/molcells.2018.2156
- Kai, H., Kudo, H., Takayama, N., Yasuoka, S., Kajimoto, H., and Imaizumi, T. (2009). Large Blood Pressure Variability and Hypertensive Cardiac Remodeling-Role of Cardiac Inflammation. *Circ. J.* 73 (12), 2198–2203. doi:10.1253/circj.cj-09-0741
- Kohno, M., Horio, T., Yokokawa, K., Yasunari, K., Ikeda, M., Minami, M., et al. (1995). Brain Natriuretic Peptide as a Marker for Hypertensive Left Ventricular Hypertrophy: Changes during 1-year Antihypertensive Therapy with Angiotensin-Converting Enzyme Inhibitor. *Am. J. Med.* 98 (3), 257–265. doi:10.1016/S0002-9343(99)80372-6
- Koyanagi, T., Wong, L. Y., Inagaki, K., Petrauskene, O. V., and Mochly-Rosen, D. (2008). Alteration of Gene Expression during Progression of Hypertension-Induced Cardiac Dysfunction in Rats. *Am. J. Physiol. Heart Circ. Physiol.* 295 (1), H220–H226. doi:10.1152/ajpheart.00289.2008
- Kumar, S., Prahalathan, P., and Raja, B. (2014). Vanillic Acid: a Potential Inhibitor of Cardiac and Aortic wall Remodeling in L-NAME Induced Hypertension through Upregulation of Endothelial Nitric Oxide Synthase. *Environ. Toxicol. Pharmacol.* 38 (2), 643–652. doi:10.1016/j.etap.2014.07.011
- Lee, J., Bae, E. H., Ma, S. K., and Kim, S. W. (2016). Altered Nitric Oxide System in Cardiovascular and Renal Diseases. *Chonnam Med. J.* 52 (2), 81–90. doi:10.4068/cmj.2016.52.2.81
- Li, S., and Zhang, B. (2013). Traditional Chinese Medicine Network Pharmacology: Theory, Methodology and Application. *Chin. J. Nat. Med.* 11 (2), 110–120. doi:10.1016/S1875-5364(13)60037-0
- Liu, Y. L., Zhang, Q. Z., Wang, Y. R., Fu, L. N., Han, J. S., Zhang, J., et al. (2020). Astragaloside IV Improves High-Fat Diet-Induced Hepatic Steatosis in Nonalcoholic Fatty Liver Disease Rats by Regulating Inflammatory Factors Level via TLR4/NF-KB Signaling Pathway. *Front. Pharmacol.* 11, 605064. doi:10.3389/fphar.2020.605064
- Luo, Y., Wan, Q., Xu, M., Zhou, Q., Chen, X., Yin, D., et al. (2019). Nutritional Preconditioning Induced by Astragaloside IV on Isolated Hearts and Cardiomyocytes against Myocardial Ischemia Injury via Improving Bcl-2-Mediated Mitochondrial Function. *Chem. Biol. Interact.* 309, 108723. doi:10.1016/j.cbi.2019.06.036
- McMaster, W. G., Kirabo, A., Madhur, M. S., and Harrison, D. G. (2015). Inflammation, Immunity, and Hypertensive End-Organ Damage. *Circ. Res.* 116 (6), 1022–1033. doi:10.1161/CIRCRESAHA.116.303697
- Mi, C., Qin, X., Hou, Z., and Gao, F. (2019). Moderate-intensity Exercise Allows Enhanced protection against Oxidative Stress-Induced Cardiac Dysfunction in Spontaneously Hypertensive Rats. *Braz. J. Med. Biol. Res.* 52 (6), e8009. doi:10.1590/1414-431X20198009
- Moncada, S. (1992). Nitric Oxide Gas: Mediator, Modulator, and Pathophysiologic Entity. *J. Lab. Clin. Med.* 120 (2), 187–191.
- Mouton, A. J., Li, X., Hall, M. E., and Hall, J. E. (2020). Obesity, Hypertension, and Cardiac Dysfunction: Novel Roles of Immunometabolism in Macrophage Activation and Inflammation. *Circ. Res.* 126 (6), 789–806. doi:10.1161/CIRCRESAHA.119.312321
- Nathan, C., and Ding, A. (2010). Nonresolving Inflammation. *Cell* 140 (6), 871–882. doi:10.1016/j.cell.2010.02.029
- Ndisang, J. F., Chibbar, R., and Lane, N. (2014). Heme Oxygenase Suppresses Markers of Heart Failure and Ameliorates Cardiomyopathy in L-NAME-Induced Hypertension. *Eur. J. Pharmacol.* 734, 23–34. doi:10.1016/j.ejphar.2014.03.026
- Nie, P., Meng, F., Zhang, J., Wei, X., and Shen, C. (2019/2019). Astragaloside IV Exerts a Myocardial Protective Effect against Cardiac Hypertrophy in Rats, Partially via Activating the Nrf2/HO-1 Signaling Pathway. *Oxid. Med. Cell Longev.* 2019, 4625912. doi:10.1155/2019/4625912
- Nyadjeu, P., Nguetefack-Mbuyo, E. P., Atsamo, A. D., Nguetefack, T. B., Dongmo, A. B., and Kamanyi, A. (2013). Acute and Chronic Antihypertensive Effects of Cinnamomum Zeylanicum Stem Bark Methanol Extract in L-NAME-Induced Hypertensive Rats. *BMC Complement. Altern. Med.* 13, 27. doi:10.1186/1472-6882-13-27
- Ribeiro, M. O., Antunes, E., de Nucci, G., Lovisolo, S. M., and Zatz, R. (1992). Chronic Inhibition of Nitric Oxide Synthesis. A New Model of Arterial Hypertension. *Hypertension* 20 (3), 298–303. doi:10.1161/01.hyp.20.3.298
- Rincón, J., Correia, D., Arcaya, J. L., Finol, E., Fernández, A., Pérez, M., et al. (2015). Role of Angiotensin II Type 1 Receptor on Renal NAD(P)H Oxidase, Oxidative Stress and Inflammation in Nitric Oxide Inhibition Induced-Hypertension. *Life Sci.* 124, 81–90. doi:10.1016/j.lfs.2015.01.005
- Santos, M., and Shah, A. M. (2014). Alterations in Cardiac Structure and Function in Hypertension. *Curr. Hypertens. Rep.* 16 (5), 428. doi:10.1007/s11906-014-0428-x
- Selamoglu Talas, Z. (2014). Propolis Reduces Oxidative Stress in L-NAME-Induced Hypertension Rats. *Cell Biochem Funct* 32 (2), 150–154. doi:10.1002/cbf.2986
- Shah, S. J., Aistrup, G. L., Gupta, D. K., O'Toole, M. J., Nahhas, A. F., Schuster, D., et al. (2014). Ultrastructural and Cellular Basis for the Development of Abnormal Myocardial Mechanics during the Transition from Hypertension to Heart Failure. *Am. J. Physiol. Heart Circ. Physiol.* 306 (1), H88–H100. doi:10.1152/ajpheart.00642.2013
- Slivnick, J., and Lampert, B. C. (2019). Hypertension and Heart Failure. *Heart Fail. Clin.* 15 (4), 531–541. doi:10.1016/j.hfc.2019.06.007
- Small, H. Y., Migliarino, S., Czesnikiewicz-Guzik, M., and Guzik, T. J. (2018). Hypertension: Focus on Autoimmunity and Oxidative Stress. *Free Radic. Biol. Med.* 125, 104–115. doi:10.1016/j.freeradbiomed.2018.05.085
- Smith, R. S., Jr., Agata, J., Xia, C. F., Chao, L., and Chao, J. (2005). Human Endothelial Nitric Oxide Synthase Gene Delivery Protects against Cardiac Remodeling and Reduces Oxidative Stress after Myocardial Infarction. *Life Sci.* 76 (21), 2457–2471. doi:10.1016/j.lfs.2004.11.028
- Suo, M., Kalliovalkama, J., Pörsti, I., Jolma, P., Tolvanen, J. P., Vuolteenaho, O., et al. (2002). N(G)-nitro-L-arginine Methyl Ester-Induced Hypertension and Natriuretic Peptide Gene Expression: Inhibition by Angiotensin II Type 1

- Receptor Antagonism. *J. Cardiovasc. Pharmacol.* 40 (3), 478–486. doi:10.1097/00005344-200209000-00017
- Touyz, R. M., Rios, F. J., Alves-Lopes, R., Neves, K. B., Camargo, L. L., and Montezano, A. C. (2020). Oxidative Stress: A Unifying Paradigm in Hypertension. *Can. J. Cardiol.* 36 (5), 659–670. doi:10.1016/j.cjca.2020.02.081
- Tuerxun, D., Aierken, R., Zhang, Y. M., Huang, Y., Sui, S., Li, X. Y., et al. (2021). Astragaloside IV Alleviates Lipopolysaccharide-Induced Preeclampsia-like Phenotypes via Suppressing the Inflammatory Responses. *Kaohsiung J. Med. Sci.* 37 (3), 236–244. doi:10.1002/kjm2.12313
- Uraizee, I., Cheng, S., Hung, C. L., Verma, A., Thomas, J. D., Zile, M. R., et al. (2013). Relation of N-Terminal Pro-B-type Natriuretic Peptide with Diastolic Function in Hypertensive Heart Disease. *Am. J. Hypertens.* 26 (10), 1234–1241. doi:10.1093/ajh/hpt098
- Wang, X., Meng, H., Wang, Q., Shao, M., Lu, W., Chen, X., et al. (2020). Baoyuan Decoction Ameliorates Apoptosis via AT1-CARP Signaling Pathway in H9C2 Cells and Heart Failure post-acute Myocardial Infarction Rats. *J. Ethnopharmacol.* 252, 112536. doi:10.1016/j.jep.2019.112536
- Worou, M. E., Belmokhtar, K., Bonnet, P., Vourc'h, P., Machet, M. C., Khamis, G., et al. (2011). Hemin Decreases Cardiac Oxidative Stress and Fibrosis in a Rat Model of Systemic Hypertension via PI3K/Akt Signalling. *Cardiovasc. Res.* 91 (2), 320–329. doi:10.1093/cvr/cvr072
- Yang, L., Gao, J. Y., Ma, J., Xu, X., Wang, Q., Xiong, L., et al. (2015). Cardiac-specific Overexpression of Metallothionein Attenuates Myocardial Remodeling and Contractile Dysfunction in L-NAME-Induced Experimental Hypertension: Role of Autophagy Regulation. *Toxicol. Lett.* 237 (2), 121–132. doi:10.1016/j.toxlet.2015.06.005
- Zambrano, S., Blanca, A. J., Ruiz-Armenta, M. V., Miguel-Carrasco, J. L., Revilla, E., Santa-María, C., et al. (2013). The Renoprotective Effect of L-Carnitine in Hypertensive Rats Is Mediated by Modulation of Oxidative Stress-Related Gene Expression. *Eur. J. Nutr.* 52 (6), 1649–1659. doi:10.1007/s00394-012-0470-x
- Zhang, J., Wu, C., Gao, L., Du, G., and Qin, X. (2020a). Astragaloside IV Derived from Astragalus Membranaceus: A Research Review on the Pharmacological Effects. *Adv. Pharmacol.* 87, 89–112. doi:10.1016/bs.apha.2019.08.002
- Zhang, T., Wang, H., Lu, M., Zhao, K., Yin, J., Liu, Y., et al. (2020b). Astragaloside IV Prevents Myocardial Hypertrophy Induced by Mechanical Stress by Activating Autophagy and Reducing Inflammation. *Am. J. Transl. Res.* 12 (9), 5332–5342.
- Zhao, C. X., Xu, X., Cui, Y., Wang, P., Wei, X., Yang, S., et al. (2009). Increased Endothelial Nitric-Oxide Synthase Expression Reduces Hypertension and Hyperinsulinemia in Fructose-Treated Rats. *J. Pharmacol. Exp. Ther.* 328 (2), 610–620. doi:10.1124/jpet.108.143396
- Zhao, W., Zhao, T., Chen, Y., Ahokas, R. A., and Sun, Y. (2008). Oxidative Stress Mediates Cardiac Fibrosis by Enhancing Transforming Growth Factor-Beta1 in Hypertensive Rats. *Mol. Cell Biochem* 317 (1-2), 43–50. doi:10.1007/s11010-008-9803-8
- Zimmer, A., Teixeira, R. B., Bonetto, J. H. P., Bahr, A. C., Türk, P., de Castro, A. L., et al. (2020). Role of Inflammation, Oxidative Stress, and Autonomic Nervous System Activation during the Development of Right and Left Cardiac Remodeling in Experimental Pulmonary Arterial Hypertension. *Mol. Cell Biochem* 464 (1-2), 93–109. doi:10.1007/s11010-019-03652-2

**Conflict of Interest:** The authors declare that the research was conducted in the absence of any commercial or financial relationships that could be construed as a potential conflict of interest.

**Publisher's Note:** All claims expressed in this article are solely those of the authors and do not necessarily represent those of their affiliated organizations, or those of the publisher, the editors, and the reviewers. Any product that may be evaluated in this article, or claim that may be made by its manufacturer, is not guaranteed or endorsed by the publisher.

Copyright © 2021 Jing, Xie, Bai, Duan, Sun, Wang, Cao, Ling and Qu. This is an open-access article distributed under the terms of the Creative Commons Attribution License (CC BY). The use, distribution or reproduction in other forums is permitted, provided the original author(s) and the copyright owner(s) are credited and that the original publication in this journal is cited, in accordance with accepted academic practice. No use, distribution or reproduction is permitted which does not comply with these terms.



# Circulating Exosomal miRNAs as Novel Biomarkers Perform Superior Diagnostic Efficiency Compared With Plasma miRNAs for Large-Artery Atherosclerosis Stroke

Mengying Niu<sup>1†</sup>, Hong Li<sup>1†</sup>, Xu Li<sup>2</sup>, Xiaoqian Yan<sup>3</sup>, Aijun Ma<sup>1\*</sup>, Xudong Pan<sup>1,2\*</sup> and Xiaoyan Zhu<sup>3\*</sup>

## OPEN ACCESS

### Edited by:

Xianwei Wang,  
Xinxiang Medical University, China

### Reviewed by:

Anxin Wang,  
Capital Medical University, China  
Juan Du,  
The Chinese University of Hong Kong,  
SAR China

### \*Correspondence:

Aijun Ma  
drmaj@126.com  
Xudong Pan  
drpan022@163.com  
Xiaoyan Zhu  
zxysdjm@163.com

<sup>†</sup>These authors have contributed  
equally to this work

### Specialty section:

This article was submitted to  
Cardiovascular and Smooth Muscle  
Pharmacology,  
a section of the journal  
Frontiers in Pharmacology

**Received:** 08 October 2021

**Accepted:** 08 November 2021

**Published:** 26 November 2021

### Citation:

Niu M, Li H, Li X, Yan X, Ma A, Pan X  
and Zhu X (2021) Circulating Exosomal  
miRNAs as Novel Biomarkers Perform  
Superior Diagnostic Efficiency  
Compared With Plasma miRNAs for  
Large-Artery Atherosclerosis Stroke.  
*Front. Pharmacol.* 12:791644.  
doi: 10.3389/fphar.2021.791644

<sup>1</sup>Department of Neurology, The Affiliated Hospital of Qingdao University, Qingdao, China, <sup>2</sup>Institute of Cerebrovascular Diseases, The Affiliated Hospital of Qingdao University, Qingdao, China, <sup>3</sup>Department of Critical Care Medicine, The Affiliated Hospital of Qingdao University, Qingdao, China

Recently, exosomal miRNAs have been reported to be associated with some diseases, and these miRNAs can be used for diagnosis and treatment. However, diagnostic biomarkers of exosomal miRNAs for ischemic stroke have rarely been studied. In the present study, we aimed to identify exosomal miRNAs that are associated with large-artery atherosclerosis (LAA) stroke, the most common subtype of ischemic stroke; to further verify their diagnostic efficiency; and to obtain promising biomarkers. High-throughput sequencing was performed on samples from 10 subjects. Quantitative real-time polymerase chain reaction (qRT-PCR) was performed on exosomes and plasma in the discovery phase (66 subjects in total) and the validation phase (520 subjects in total). We identified 5 candidate differentially expressed miRNAs (miR-369-3p, miR-493-3p, miR-379-5p, miR-1296-5p, and miR-1277-5p) in the discovery phase according to their biological functions, 4 of which (miR-369-3p, miR-493-3p, miR-379-5p, and miR-1296-5p) were confirmed in the validation phase. These four exosomal miRNAs could be used to distinguish LAA samples from small artery occlusion (SAO) samples, LAA samples from atherosclerosis (AS) samples, and LAA samples from control samples and were superior to plasma miRNAs. In addition, composite biomarkers achieved higher area under the curve (AUC) values than single biomarkers. According to our analysis, the expression levels of exosomal miR-493-3p and miR-1296-5p were negatively correlated with the National Institutes of Health Stroke Scale (NIHSS) score. The four identified

**Abbreviations:** AS, atherosclerosis; AUC, area under the curve; CTA, computed tomography angiography; CAMs, cell adhesion molecules; CT, computed tomography; FC, fold change; GO, Gene Ontology; KEGG, Kyoto Encyclopedia of Genes and Genomes; FDR, false discovery rate; LAA, large-artery atherosclerosis stroke; MRI, magnetic resonance imaging; MRA, magnetic resonance angiography; NPV, negative predictive value; NIHSS score, National Institutes of Health Stroke Scale score; NTA, nanoparticle tracking analysis; PPV, positive predictive value; PBS, phosphate-buffered saline; qRT-PCR, quantitative real-time polymerase chain reaction; ROC, receiver operating characteristic curves; SAO, small artery occlusion stroke; SD, standard deviation; TOAST, Trial of Org 10,172 in Acute Stroke Treatment; TEM, transmission electron microscopy; TPM, transcripts per million.



exosomal miRNAs are promising biomarkers for the diagnosis of LAA stroke, and their diagnostic efficiency is superior to that of their counterparts in plasma.

**Keywords:** ischemic stroke, biomarkers, exosomes, miRNA, atherosclerosis

## INTRODUCTION

Stroke is the leading cause of long-term disability and one of the leading causes of death worldwide and is a growing global burden (Barrington et al., 2017; Ornello et al., 2018; Raju et al., 2020; Zuo et al., 2020). Ischemic stroke accounts for 80% of stroke incidence (Tiedt et al., 2017). According to the Trial of Org 10,172 in Acute Stroke Treatment (TOAST), large-artery atherosclerosis (LAA) stroke is the most common type (Ornello et al., 2018). The primary cause of this type of ischemic stroke is narrowing or obstruction of the main brain trunk or cortical artery branches due to atherosclerosis (AS) (Adams et al., 1993). AS is a condition in which fatty and/or fibrous material accumulates in the lining of the arteries (Lu and Rothenberg, 2018). Proper diagnosis of ischemic stroke is important for subsequent treatment (Prabhakaran et al., 2015; Powers, 2020).

Previous studies have found that miRNAs play important roles in a variety of diseases (Rupaimoole and Slack, 2017). The expression of miRNAs varies greatly between normal and pathological states and can be disease-specific (Liu et al., 2019). miRNAs are endogenous molecules with lengths of 20–25 nucleotides that regulate gene expression after transcription (Lu and Rothenberg, 2018; Treiber et al., 2019). miRNAs have a wide range of functions in cells and can be released into the peripheral circulation in small extracellular vesicles or bound to proteins (Tiedt et al., 2017). miRNAs can serve as valuable diagnostic biomarkers in a variety of diseases, but studies have rarely been conducted on their use as biomarkers in ischemic stroke (Tiedt et al., 2017). In addition, miRNAs are unstable in the presence of RNase and are therefore easily degraded in plasma (Matsuura et al., 2016; Min et al., 2019). However, exosomes provide a relatively stable environment for miRNAs and can protect miRNAs from degradation, which has attracted considerable research interest (van Niel et al., 2018; Kalluri and LeBleu, 2020).

Exosomes are endosomal-derived phospholipid bilayer vesicles that are 40–160 nm (on average 100 nm) in diameter. Exosomes play very important roles not only in physiological processes, such as cell-to-cell communication, material transport, and the immune response, but also in pathological processes, such as cardiovascular and cerebrovascular diseases (Tiedt et al., 2017; van Niel et al., 2018; Kalluri and LeBleu, 2020). Exosomes contain a variety of substances, including noncoding RNAs such as miRNAs, mRNAs, and proteins (van Niel et al., 2018; Kalluri and LeBleu, 2020). However, scarcely any research has been performed on diagnostic biomarkers for ischemic stroke in exosomes (Kalluri and LeBleu, 2020).

The purposes of our study were to verify the association of exosomal miRNAs with LAA stroke, the major subtype of ischemic stroke, and to find promising diagnostic biomarkers. In this study, we characterized total miRNA profiles in plasma

exosomes of LAA stroke patients and healthy controls using high-throughput sequencing. Furthermore, we identified exosomal miRNAs that distinguish LAA stroke patients from controls, validated these biomarkers in a large independent cohort, and compared their diagnostic performance with plasma miRNAs.

## MATERIALS AND METHODS

### Participant Information and Sample Collection

A total of 596 subjects recruited from the Affiliated Hospital of Qingdao University Neurology Department from June 2018 to March 2020 were included in our study, including 10 for high-throughput sequencing, 66 for the discovery phase, and 520 for the validation phase. Patients were enrolled in our study cohort within 72 h of symptom onset when computed tomography (CT) or magnetic resonance imaging (MRI) demonstrated a new infarction. Patient diagnosis was based on the TOAST criteria and a combination of CT, MRI, and magnetic resonance angiography (MRA)/CT angiography (CTA) findings. The inclusion and exclusion criteria are shown in the **Supplementary Materials** (Glisic et al., 2018; Fernandez et al., 2019; Shen et al., 2019; Zuo et al., 2020). Informed consent was obtained from all participants. This study was approved by the ethics committee of Qingdao University Affiliated Hospital. All procedures followed were in accordance with the ethical standards of the responsible committee on human experimentation (institutional and national) and with the Helsinki Declaration as revised in 2013. Peripheral blood samples from each participant were collected in EDTA tubes following a regular venipuncture procedure in the morning under fasted conditions without water intake within 24 h of hospital admission. After centrifugation at 3,000 ×g for 15 min at 4°C, the plasma was immediately stored at –80°C until use.

### Exosome Isolation

For exosome isolation, we used total exosome separation reagent for plasma (Cat 4484450, Invitrogen Carlsbad, United States) (Tian et al., 2020). In brief, each plasma sample was centrifuged at room temperature for 20 min at 2000 ×g to remove cells and debris and then centrifuged at 10,000 ×g for 20 min to remove debris for a second time. Then, 1 ml of plasma was added to 0.5 ml of phosphate-buffered saline (PBS). The sample was vortexed for thorough mixing; then, 50 µl of proteinase K was added to the mixture, and the mixture was incubated at 37°C for 10 min. Next, 300 µl of exosome precipitation reagent was added to the supernatant. After thorough mixing, the mixture was incubated for 30 min at 4°C and then centrifuged at 10,000 ×g for 5 min. The isolated exosomes were contained in the pellet at the bottom of the tube. Finally, the pellet was resuspended in PBS.

## Transmission Electron Microscopy

Exosome-enriched solution was placed on a copper grid and incubated at room temperature for 2 min. Then, the exosomes were placed in 2% phosphotungstic acid for 2 min and washed with sterile distilled water. The morphology of the exosomes was observed by using TEM (Hitachi, Tokyo, Japan) (Min et al., 2019).

## Nanoparticle Tracking Analysis

Exosome pellets were resuspended in 1 ml of PBS and examined with a ZetaView PMX 110 instrument (Particle Metrix, Meerbusch, Germany). We used NTA software (ZetaView) to analyze the particle size and quantity (Min et al., 2019).

## Western Blot Analysis

We extracted total protein from exosomes with RIPA and PMSF buffers at a ratio of 99:1 (MCE, United States), and the concentration of the total protein was normalized after a BCA assay was performed. The protein samples were then subjected to 10% SDS-PAGE and transferred onto a membrane. The PVDF membrane was incubated with primary antibodies against CD9, CD63, TSG101 and GRP94 (ab92726, ab134045, ab125011, and ab238126, respectively; Abcam, Cambridge, United Kingdom) at 4°C overnight and then with HRP-conjugated secondary antibodies (Abcam, Cambridge, United Kingdom) for an hour.

## RNA Isolation and RNA Analysis

According to a published protocol, we used an miRNeasy Serum/Plasma Advanced kit to extract and purify total RNA from plasma exosome-enriched fractions (Androvic et al., 2019; Peng et al., 2020). RNA concentration, purity, and integrity were assessed using the RNA Nano 6000 Assay Kit of an Agilent Bioanalyzer 2,100 System (Agilent Technologies, CA, United States) (Min et al., 2019).

## Library Preparation and Sequencing

A total of 5 µg of RNA was used as input material for RNA library preparation. Sequencing libraries were created with an NEBNext® Ultra™ Directional RNA Library Prep Kit for Illumina R (NEB, United States) according to the manufacturer's recommendations. First-strand cDNA was synthesized using random hexamer primers and M-MuLV Reverse transcriptase (RNase H). Then, second-strand cDNA was synthesized by using DNA polymerase I and RNase H. Once the 3' ends of the DNA fragments were adenylated, they were attached to NEBNext adaptors with hairpin loop structures to prepare for hybridization. The library fragments were purified using an AMPure XP system (Beckman Coulter, Beverly, United States), and cDNA fragments with a length of 150–200 bp were selected. PCR was then performed using Phusion High-Fidelity DNA polymerase, universal PCR primers, and Index (X) primers. Finally, the products were purified (AMPure XP system), and the library quality was evaluated by using the Agilent Bioanalyzer 2,100 system.

The index-encoded samples were clustered using a cBot Cluster Generation System with a TruSeq PE Cluster Kit V3-cBot-HS (Illumina) according to the manufacturer's instructions.

After cluster generation, the Illumina HiSeq 4,000 platform was used for sequencing, and 150 bp paired-end reads were generated.

## miRNA Quantification and Differential Expression Analysis

First, the transcripts per million (TPM) values were used to normalize the raw counts. Transcripts with a *padj* (*p*-value after adjust) < 0.05 and a fold change (FC) > 2.0 or < -2.0 were considered to be differentially expressed. The differentially expressed miRNAs were visualized with volcano plots.

## Target Gene Prediction and Gene Ontology/Kyoto Encyclopedia of Genes and Genomes Pathway Enrichment Analysis

For all miRNAs that were differentially expressed between LAA stroke samples and control samples, the potential target genes that were predicted by both miRanda and RNAhybrid were included in subsequent analyses. We used DAVID and KOBAS to enrich the biological functions of the target genes (Low et al., 2019; Min et al., 2019).

## Quantification of miRNA Expression With qRT-PCR

Total RNA was extracted and purified from plasma exosomes according to the manufacturer's protocols (Androvic et al., 2019). Reverse transcription of miRNAs was performed using a Mir-X miRNA First-Strand Synthesis Kit (Takara, Japan). TB-Green Premix Ex Taq™ II (Takara, Japan) was used for quantitative amplification. The expression levels of U6 were used to normalize the relative expression levels of miRNA, and the  $2^{-\Delta\Delta Ct}$  method was used for quantification (Raouf et al., 2018). The primer sequences are listed in the **Supplementary Materials**.

## Statistical Analysis

Statistical analyses were performed using SPSS 22.0. The false discovery rate (FDR) was controlled for multiple comparisons, and *p* < 0.05 was considered to indicate a significant difference. Normally distributed data was presented as the mean ± standard deviation (SD) while non-normally distributed data was presented as the median (interquartile range). Statistical significance (*p* < 0.05) was determined by means of independent-samples *t*-tests, chi-square tests and Kruskal-Wallis tests. We constructed the regression model by binary logistic regression. Receiver operating characteristic (ROC) curves were generated, and the area under the curve (AUC) was also calculated to assess the diagnostic efficiency of candidate miRNAs.

## RESULTS

### Participant Characteristics

In this study, a total of 596 subjects were recruited. Of these participants, 348 patients were diagnosed with ischemic stroke at

**TABLE 1 |** Demographic and clinical characteristics of the subjects. (TG, triglycerides; TC, total cholesterol; LDL, low-density lipoprotein; HDL, low-density lipoprotein).

Characteristic	LAA (n = 193)	SAO (n = 155)	As (n = 105)	Controls (n = 143)	p-val
Age, mean (SD), y	62.9 (10.5)	62.9 (11.8)	63.4 (9.6)	64.7 (8.9)	0.38
Female, n (%)	88 (45.6%)	69 (44.5%)	55 (52.4%)	65 (45.5%)	0.61
Risk factors, n (%)					
Hypertension	122 (63.2%)	91 (58.7%)	57 (54.3%)	99 (69.2%)	0.08
Smoking history	58 (30.1%)	52 (33.5%)	28 (26.7%)	35 (24.5%)	0.34
Drinking history	56 (29.0%)	36 (23.2%)	23 (21.9%)	31 (21.7%)	0.37
Diabetes mellitus	57 (29.5%)	38 (24.5%)	26 (24.8%)	29 (20.3%)	0.27
TG, mean (SD)	1.4 (1.2)	1.3 (0.8)	1.5 (1.1)	1.4 (0.7)	0.06
TC, mean (SD)	4.3 (1.2)	4.2 (1.1)	4.8 (1.1)	4.7 (1.1)	<0.01
LDL, mean (SD)	2.4 (0.8)	2.6 (0.9)	2.5 (0.3)	2.9 (0.9)	<0.01
HDL, mean (SD)	1.2 (0.3)	1.3 (0.3)	2.6 (0.9)	1.3 (0.3)	<0.01
Hypertension med use (%)	18 (9.3%)	17 (11.0%)	35 (33.3%)	29 (20.3%)	<0.01
Diabetes med use (%)	11 (5.7%)	15 (9.7%)	21 (20.0%)	8 (5.6%)	<0.01
Lipid-lowering drug (%)	1 (0.5%)	3 (1.9%)	6 (5.7%)	4 (2.8%)	0.04
Anti-platelet drugs (%)	6 (3.1%)	1 (0.6%)	6 (5.7%)	10 (7.0%)	0.02

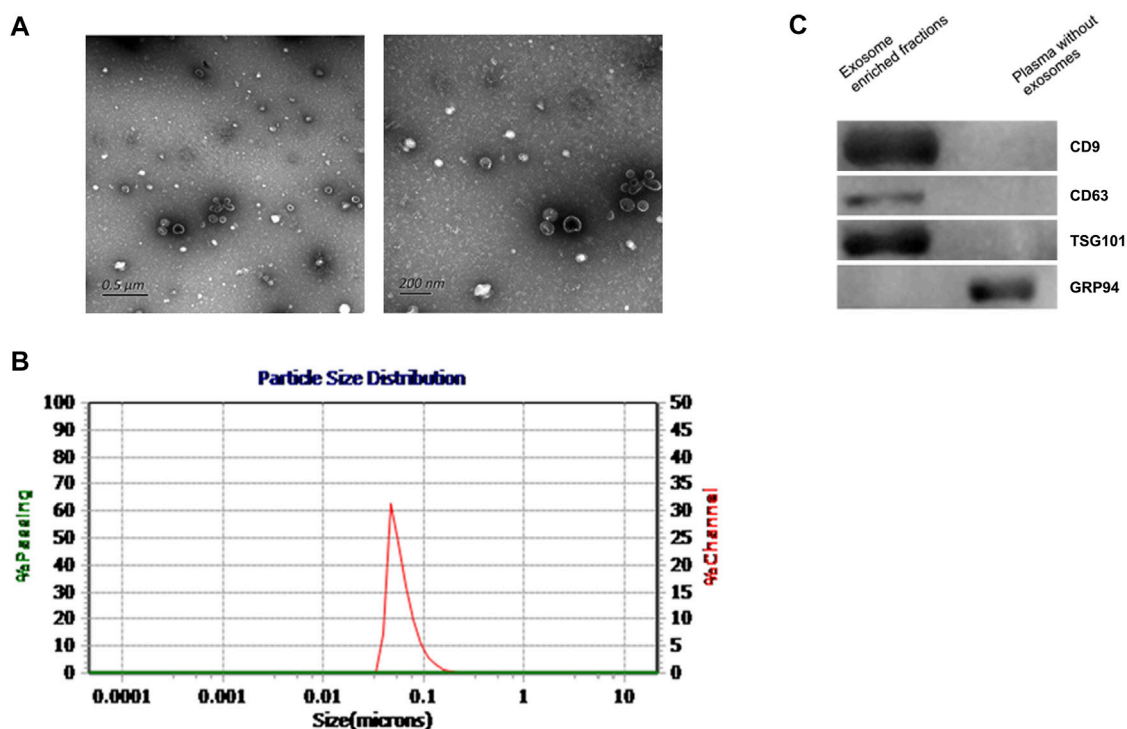


**FIGURE 1 |** Characteristics of plasma exosomes from participants. **(A)** TEM images showing that the exosomes were bilayer vesicles (left image: wide field containing multiple exosomes; right: close-up image of a single exosome). **(B)** NTA results showing that the diameter of the enriched plasma exosomes was approximately 30–150 nm. **(C)** Western blot showing that CD9, CD63 and TSG101 were detected in the enriched exosome samples isolated from plasma, while the negative exosomal marker GRP94 was not detected in these samples.

a tertiary hospital, among which 193 patients were diagnosed with LAA and 155 patients were diagnosed with small artery occlusion (SAO). Another 105 patients were diagnosed with AS but did not develop stroke, and 143 of the subjects were healthy controls. The demographics and clinical features of the subjects are shown in **Table 1**. There were no significant differences in the

age or sex distributions of the participants, which was consistent with the clinical manifestations ( $p > 0.05$ ).

### Characteristics of Exosomes

According to previous literature, we verified the enriched exosomes via TEM, NTA, and western blot analysis. We

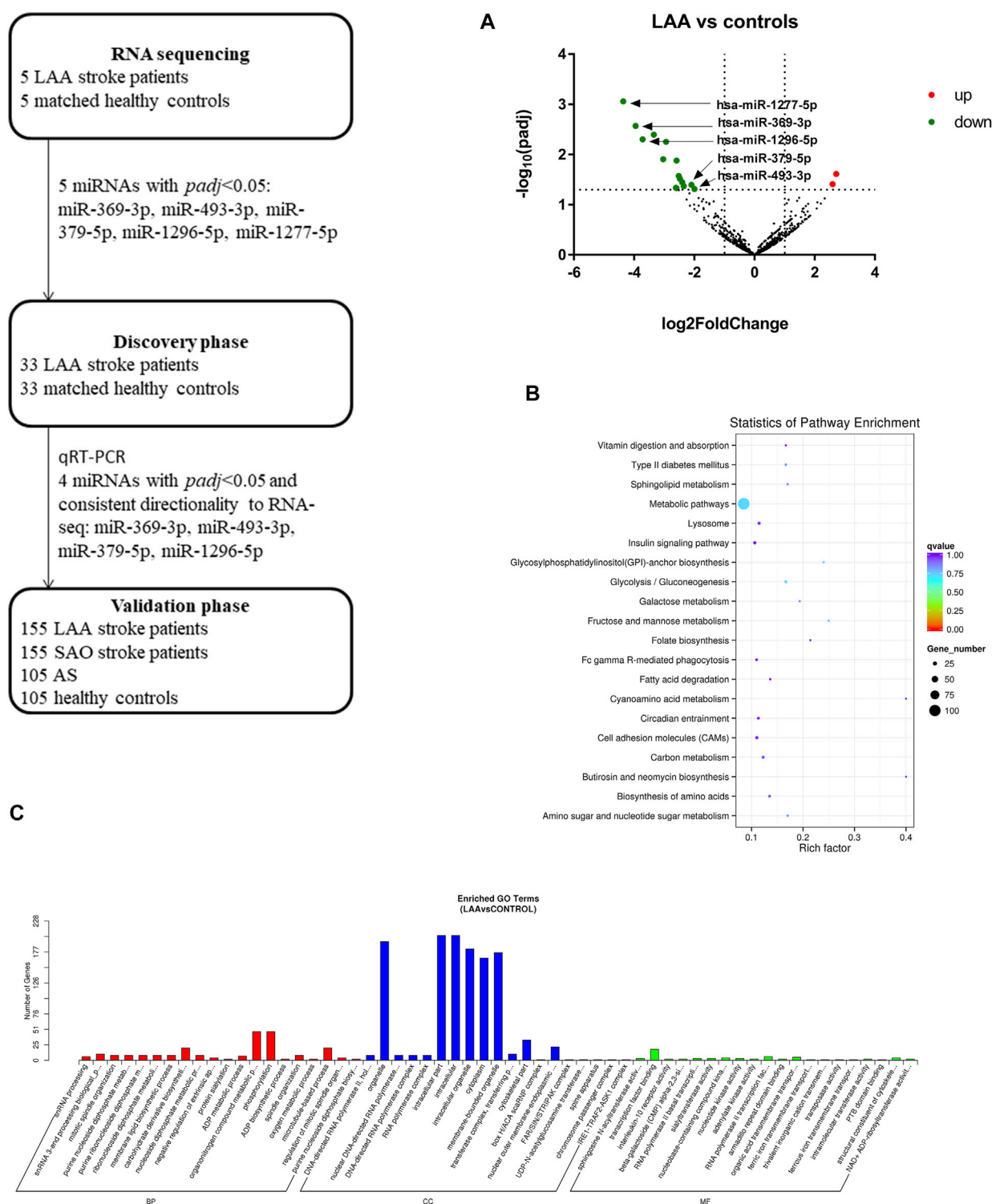


**FIGURE 2 |** Workflow and RNA sequencing results. Target analysis of miRNAs differentially expressed in enriched exosome fractions from LAA and control plasma samples. GO/KEGG enrichment was performed on differentially expressed miRNAs identified in exosome-enriched plasma, and miRNA analysis was performed. **(A)**. Volcano map showing the high-throughput sequencing results for LAA vs. healthy control samples; red indicates upregulation, and green indicates downregulation. **(B)**. Bubble plot of the KEGG pathway enrichment results. **(C)**. Bar plot of the GO enrichment results (biological process, cellular component, and molecular function categories).

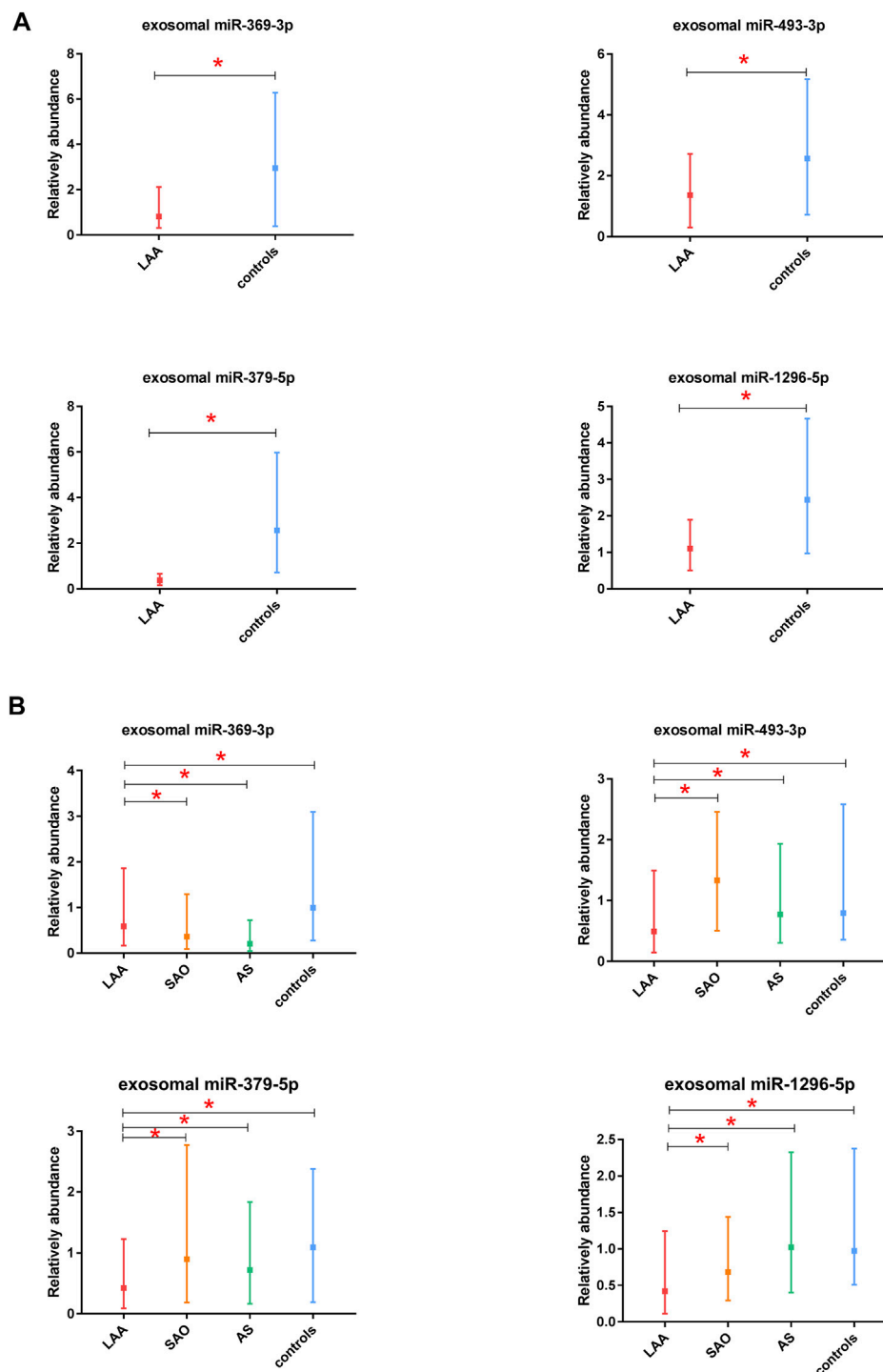


**FIGURE 3 |** Discovery and validation of exosomal miR-369-3p, miR-493-3p, miR-379-5p, miR-1296-5p. **(A).** Results from the discovery phase. **(B).** Results from the validation phase (median  $\pm$  interquartile range, Mann-Whitney  $U$  test. \* $p < 0.05$ ).

extracted and identified total plasma-derived exosomes according to the methods recommended by the International Society for Extracellular Vesicles (Théry et al., 2018). In this study, the exosomes we extracted were observed via electron microscopy to be phospholipid bilayer vesicles

with an average diameter of 100 nm, and NTA showed that exosomes in diameter were 30–150 nm (Figures 1A,B). Western blotting verified 3 positive markers of exosomes (CD9, CD63, and TSG101) (van Niel et al., 2018; Kalluri and LeBleu, 2020). In addition, a negative marker of



exosomes, GRP94, was absent (**Figure 1C**). The above findings suggested that we successfully obtained exosomes.

## RNA Sequencing Analysis

To obtain overall profiles of the miRNAs derived from exosomes in plasma, we performed high-throughput sequencing on 10 samples (5 LAA samples and 5 control samples) and obtained 830 miRNAs. Among the miRNAs there were 18 differentially expressed miRNAs (16 miRNAs were downregulated, and 2 miRNAs were upregulated) (**Figure 2A**). The functions of the genes targeted by these miRNAs were analyzed with the KEGG database, and the top 20 functions were enriched (**Figure 2B**). As shown in the figure, the function terms associated with the genes targeted by these miRNAs included the metabolic pathways, cell adhesion molecules (CAMs), and insulin signaling pathway terms, which suggests that the genes may be associated with the occurrence of disease. Through GO analysis, we found enrichment of numerous terms in the biological process category, such as the organonitrogen compound metabolic process and phosphorylation terms. The enriched terms in the cellular component category included the intracellular part, cytoplasm, membrane-bounded organelle and intracellular organelle terms. In the molecular function category, the enriched terms included the transcription factor binding and RNA polymerase II transcription factor binding terms (**Figure 2C**).

## Expression of Candidate miRNAs in Exosomes in the Discovery Phase

In this study, we selected 5 miRNAs according to their biological functions and differential expression in the discovery phase: miR-369-3p, miR-493-3p, miR-379-5p, miR-1296-5p, and miR-1277-5p ( $|\log_2(\text{FC})| > 1$ ,  $p < 0.05$ ). These five miRNAs were all downregulated on the basis of previous sequencing results. A total of 66 subjects were recruited in the discovery phase (33 LAA subjects, 33 controls). Interestingly, we found significant differences in expression between the two groups for all miRNAs except miR-1277-5p (**Figure 3A**, **Supplementary Figure S1**). The other four miRNAs derived from exosomes were able to distinguish LAA subjects from control subjects (unadjusted raw  $p$ -value  $< 0.05$ ) (**Figure 3A**). The sequencing results were verified with experiments in the discovery phase.

## Identification of Exosomal miRNAs as Candidate Biomarkers in the Validation Phase

In the validation phase, we verified the four exosomal miRNAs screened out as potential biomarkers in the discovery phase. miR-1277-5p was excluded because it did not perform well in differentiating the LAA group from the control group in the discovery phase. miR-369-3p, miR-493-3p, miR-379-5p, miR-1296-5p were ultimately selected for verification in 520 participants (310 ischemic stroke patients, 105 AS patients, and 105 healthy controls), and their expression levels were analyzed by qRT-PCR. To obtain the most robust and reliable biomarker, we further subdivided the stroke group into two

groups: the LAA group (155 patients) and the SAO group (155 patients). In addition, we performed ROC curve analysis and calculated the AUC values to further confirm the diagnostic efficiency of these biomarkers. The results obtained were consistent with those from previous experiments: all four of the miRNAs could distinguish the LAA subjects from control subjects. Moreover, significant differences in the expression of exosome-derived miR-369-3p were observed in the LAA group vs. the SAO group and in the LAA group vs. the AS group. Likewise, exosomal miR-493-3p, miR-379-5p, miR-1296-5p showed the same differential expression patterns ( $p < 0.05$ ) (**Figure 3B**). Intergroup analysis of exosomal miRNAs in LAA and SAO groups ruled out such changes due to acute ischemic stroke. While analysis of LAA and AS groups demonstrated that the differential expression of exosomal miRNAs was probably due to the rupture of atherosclerotic plaques.

In addition, we calculated the AUC values for the four miRNAs. The AUC values for exosomal miR-369-3p, miR-493-3p, miR-379-5p and miR-1296-5p were 0.841, 0.852, 0.857, and 0.838, respectively (95% CI, 0.783–0.898; 0.793–0.910; 0.801–0.913; 0.777–0.900;  $p < 0.05$ ) (78.46% PPV and 76.18% NPV; 83.15% PPV and 75.62% NPV; 80.82% PPV and 77.28% NPV; 81.23% PPV and 78.65% NPV) (**Figure 4**), which shows the potential value of these four miRNAs as biomarkers for discriminating patients with LAA from other groups.

## Comparison of Exosomal miRNAs and Plasma miRNAs

We also tested the expression of miRNAs in plasma via qRT-PCR. According to the correlation analysis, there was no correlation between the expression of exosomal miRNAs and the expression of their counterparts in plasma ( $p > 0.05$ ) (**Figure 5**). Plasma miR-369-3p, miR-493-3p, and miR-379-5p failed to distinguish between the LAA group and the control group (**Figure 6A**). In addition, miR-1296-5p in plasma exhibited an AUC of 0.611 (95% CI, 0.542–0.680), while the exosomal miRNA exhibited an AUC of 0.838 (NRI = 0.36) (**Figure 6B**). Thus, the diagnostic efficiency of miRNAs in exosomes is better than that of miRNAs in plasma.

## Diagnostic Efficiency of Composite Biomarkers

Considering that a single marker is not typically used for the final diagnosis in clinical practice, we tested the diagnostic efficiency of composite biomarkers by using a logistic model and ROC curve analysis (Min et al., 2019). The AUCs of exosomal miRNAs were as high as 0.867 (95% CI, 0.812–0.922) when different combinations of two biomarkers were used, higher than the value achieved for a single miRNA. Further, a combination of three miRNAs achieved an AUC of 0.872 (95% CI, 0.819–0.925); thus, adding miRNAs improved the diagnostic efficiency of a single biomarker to some extent. However, the AUC did not increase further a fourth miRNA was added (0.868 (95% CI, 0.813–0.922)) (**Figures 7A–C**).



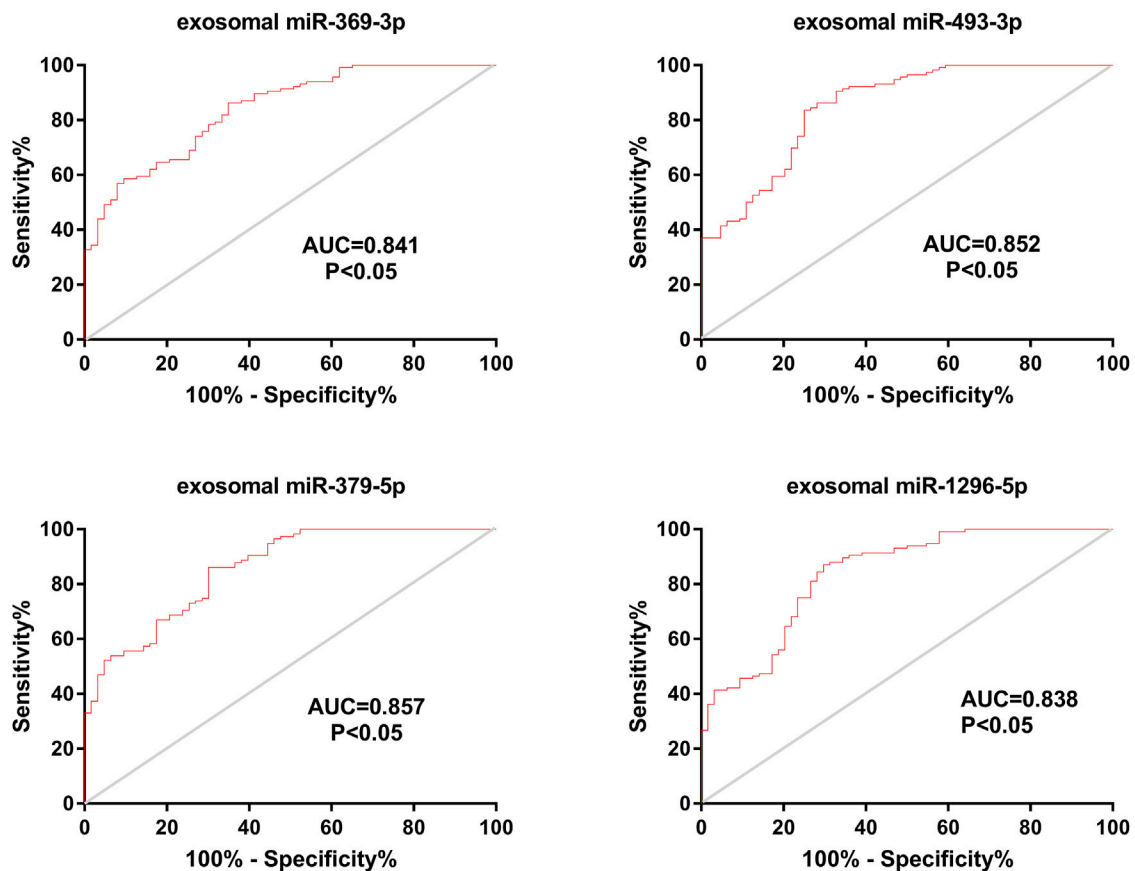


**FIGURE 4 |** Diagnostic efficiency of exosomal miRNAs in the validation phase. ROC curve analyses were performed. The AUCs of the 4 exosomal miRNAs were calculated and are shown in red.

## Correlations Between miRNA Expression Levels and NIHSS Scores

In addition, we analyzed the relationship between NIHSS score and miRNA expression in exosomes. Patients' conditions were clinically evaluated according to their NIHSS scores: a higher score indicated a more serious condition (Kwah and Diong, 2014). We classified patients according to their NIHSS scores as having mild stroke ( $\text{NIHSS} \leq 5$ ) or moderate to severe stroke ( $\text{NIHSS} > 5$ ) (Kvistad et al., 2019; Johnston et al., 2020). Spearman rank correlation was used to analyze the relationships between NIHSS scores and miRNA expression levels (Matsuura et al., 2016). The results suggested that the expression levels of exosomal miR-493-3p and miR-1296-5p were negatively correlated with the NIHSS score. Interestingly, exosomal miR-493-3p and miR-1296-5p expression was lower in patients with moderate to severe stroke than in patients with mild stroke ( $p < 0.05$ ) (Figure 8).

## DISCUSSION

In this study, we compared the diagnostic efficiency of miRNAs in exosomes and plasma among LAA, SAO, AS, and control groups. To the best of our knowledge, this is the first study to

show that exosomal miRNAs can be used as biomarkers with better efficiency than plasma miRNAs for ischemic stroke. We screened out four identified exosomal miRNAs, namely, miR-369-3p, miR-493-3p, miR-379-5p, and miR-1296-5p, which are promising biomarkers for the diagnosis of LAA stroke, and their diagnostic efficiency is superior to that of their counterparts in plasma. In addition, we found that the expression levels of exosomal miR-493-3p and miR-1296-5p expression were negatively correlated with NIHSS score.

Ischemic stroke is a very urgent, serious, and heterogeneous disease, especially LAA stroke, which accounts for a considerable proportion of the incidence of ischemic stroke (Ornello et al., 2018). Therefore, proper identification and diagnosis of LAA are of vital importance for the success of follow-up treatment and for the quality of life of patients (Prabhakaran et al., 2015). The etiological diagnosis of ischemic stroke is mainly based on medical history, clinical evaluation, and cerebral angiography etc. (Jauch et al., 2017). When patients are unable to cooperate with examinations, diagnostic biomarkers can help solve the problem. Here, diagnosis of LAA stroke is undoubtedly time saving and cost saving, which is of great significance for the rational allocation of medical resources and further treatment (Tu et al., 2017b). In addition, we report a noninvasive method that

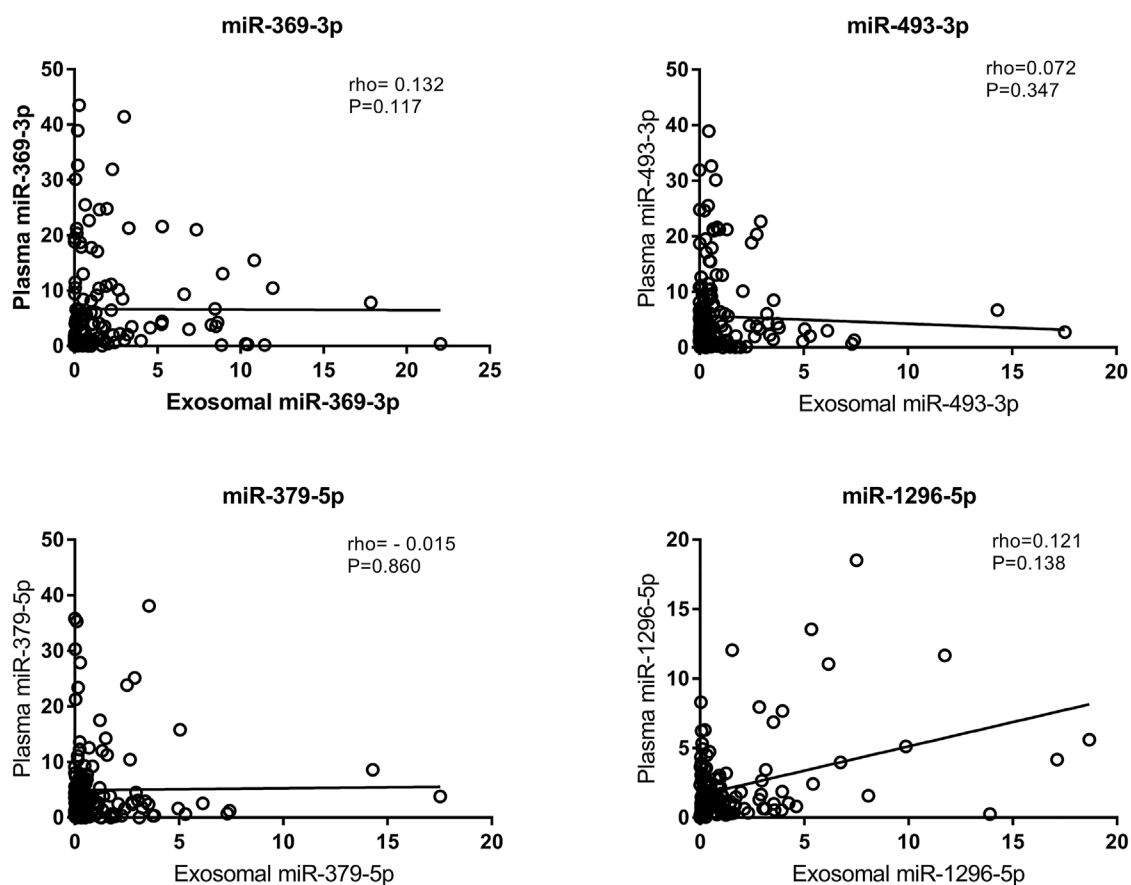


**FIGURE 5 |** Correlation of exosomal miRNA expression levels with plasma miRNA expression levels as assessed using Spearman's correlation coefficient ( $\rho$ ).

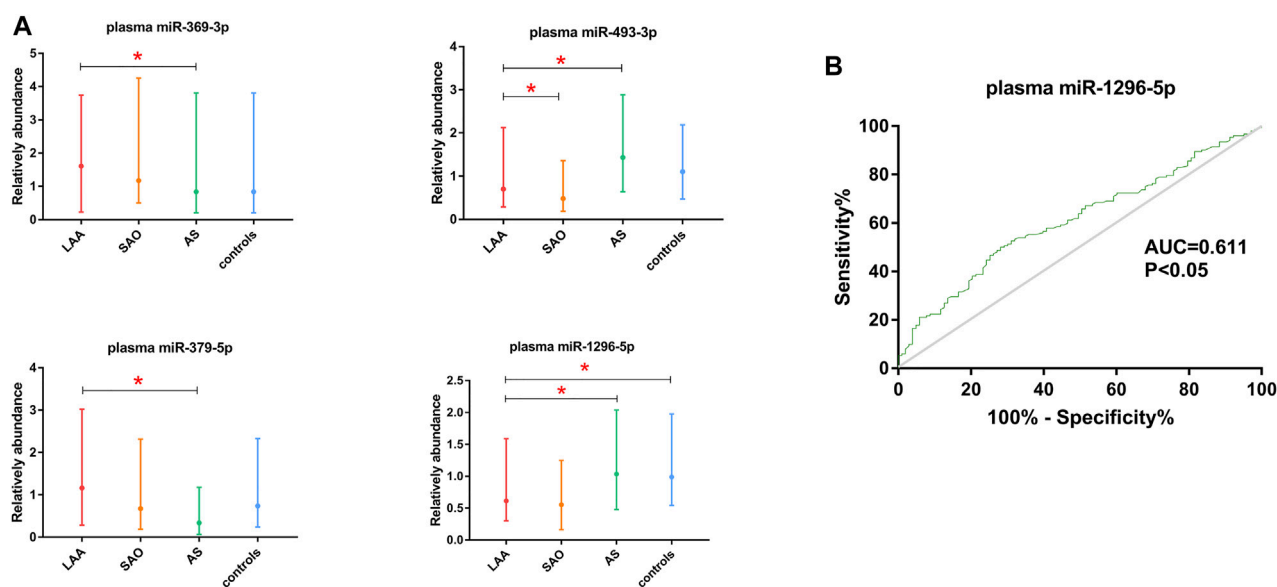
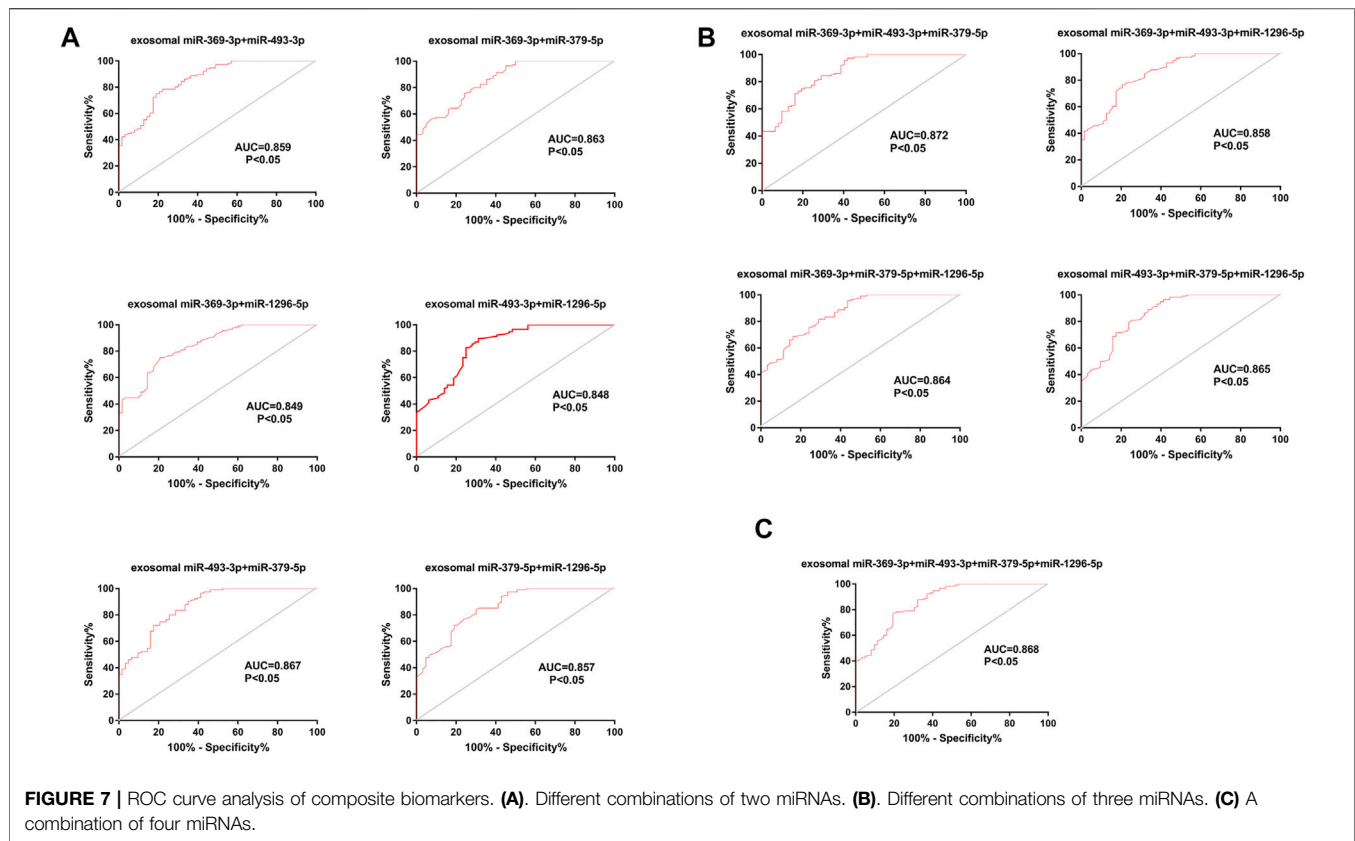


**FIGURE 6 |** Validation of plasma miR-369-3p, miR-493-3p, miR-379-5p, and miR-1296-5p. **(A)**. qRT-PCR of miRNAs in plasma. **(B)**. ROC curve of plasma miR-1296-5p. The AUC was calculated and is shown in green (\* $p < 0.05$ ).

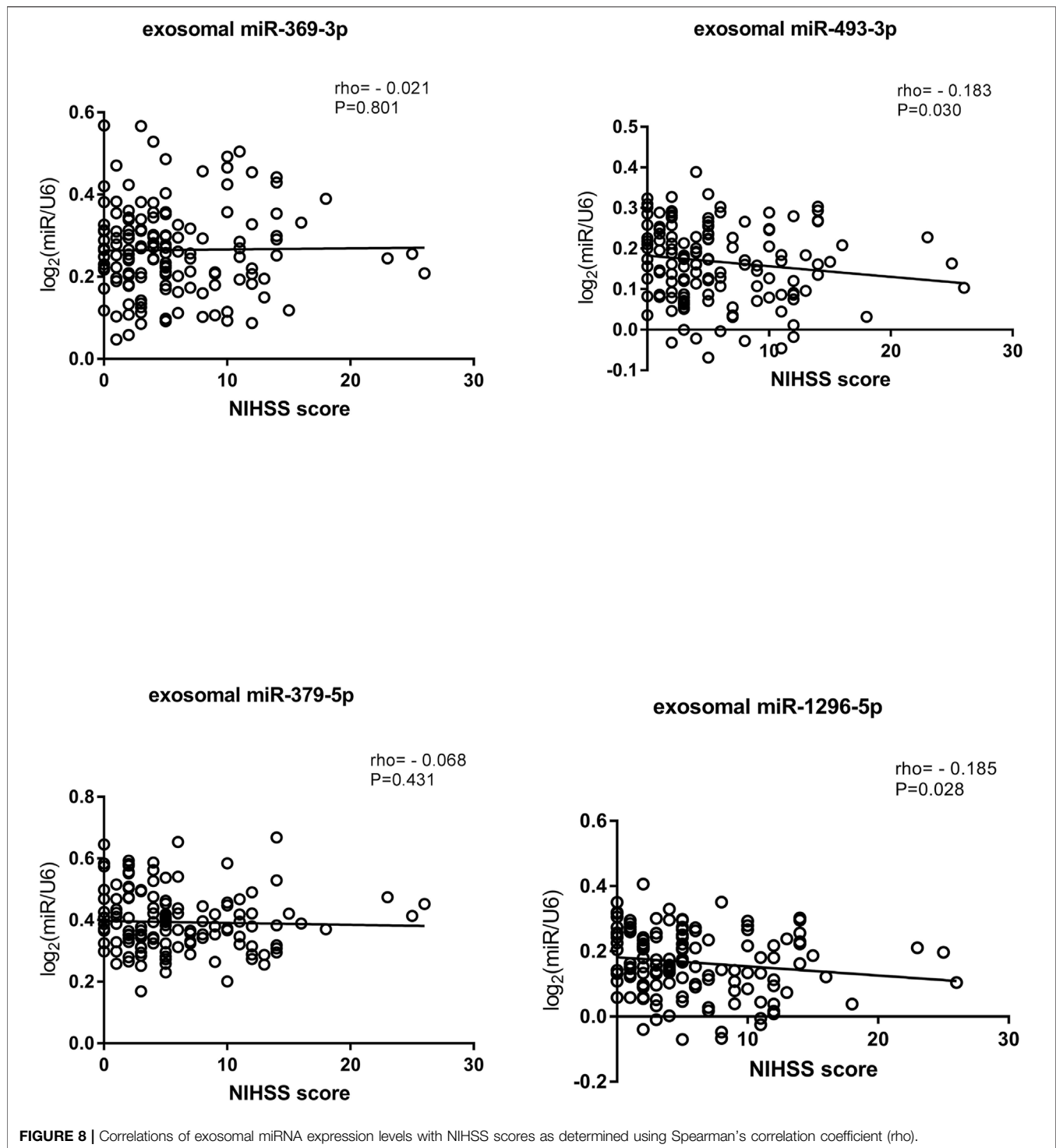


can potentially be used for diagnosis. This method is feasible even when clinical resources are limited.

Exosomes are involved in cell-to-cell communication, material transport, immune responses, and other processes, and miRNAs are involved in multiple processes associated with stroke occurrence and progression (Krupinski and Slevin, 2013; Mirzaei et al., 2018; Raju et al., 2020). miRNAs are selectively packaged into exosomes, suggesting that they may carry specific information, and the numbers of exosomes and miRNAs secreted are affected by disease state and progression (Liu et al., 2019). Prior studies have shown that about 70% of miRNAs are expressed in the central nervous system, and a growing number of exosomal miRNAs play an important role in central nervous system diseases, such as ischemic stroke (Yu et al., 2021).

Previous studies have shown that miRNAs can serve as biomarkers for diagnosis of diseases, especially cancer (Min et al., 2019). In this work, we used high-throughput sequencing to gain an overall understanding of miRNA profiles. LAA is closely associated with inflammation and involves a cascade of inflammatory cytokines (Wolf and Ley, 2019). GO and KEGG analyses were used to screen out 5 miRNAs (miR-369-3p, miR-493-3p, miR-379-5p, miR-1296-5p, miR-1277-5p) according to the functions of their targeting genes. Among them, miR-369-3p is associated with low-density lipoprotein and monocyte-to-macrophage differentiation. And it has been reported to play a role in the inflammatory process, and its targeted genes are associated with inflammatory cytokines

(Galleggiante et al., 2019). miR-1296-5p is associated with CAMs, white blood cell migration across endothelial cells, which are known as playing crucial roles in atherosclerosis (Libby et al., 2019). LAA is associated with a chronic inflammatory process involving CAMs (Zeng et al., 2021). Inflammatory cells can bind to cell adhesion molecules expressed by endothelial cells. In addition, during inflammation, cells migrate via chemotaxis in response to inflammatory cytokines (del Zoppo et al., 2000; Libby et al., 2019; Wolf and Ley, 2019). In addition, miR-493-3p has been found to modulate angiogenesis in a rat model of ischemic stroke (Li et al., 2016). miR-379-5p and miR-493-3p are related to metabolic pathways and fatty acid metabolism, which play essential roles in the pathophysiology of LAA (Libby et al., 2019). Besides, miR-493-3p is also related to antigen processing and presentation. Previous studies have shown that atherosclerotic plaque rupture correlates with the level of immune cells, and that antigen processing and presentation play important roles in regulating the function and level of immune cells (Kobiyama and Ley, 2018). In previous studies, miR-379-5p has been reported to be associated with autoimmune diseases of the central nervous system, multiple sclerosis, and its target genes are associated with cell death and inflammation, and miR-1296-5p inhibits liver cancer metastasis through the PI3K/Akt pathway and is downregulated in breast cancer (Xu et al., 2017; Baulina et al., 2018). What's more, PI3K/Akt pathway has been confirmed to be associated with ischemic stroke (Qi et al., 2021). miR-1277-5p has been associated with inflammatory response and oxidative stress in previous study (Zhou et al.,



2021). We speculate that the factors we screened play roles in the occurrence and progression of LAA. In total, 4 miRNAs (miR-369-3p, miR-493-3p, miR-379-5p, and miR-1296-5p) were selected for a large-sample validation phase. These factors have not often been studied in the context of cerebrovascular diseases, including ischemic stroke. Although these miRNAs have been identified as biomarkers for diagnosis and prognosis of other

diseases, we are the first to identify them as biomarkers for ischemic stroke.

We analyzed our experimental results by calculating the relative expression levels of miRNAs based on the study of Rana Raoof et al (Raoof et al. (2018)). Our analysis revealed that the intergroup differences for exosomal miR-369-3p, miR-493-3p, miR-379-5p, and miR-1296-5p were significant. These

miRNAs could distinguish the LAA group from the control group, the LAA group from the SAO group, and the LAA group from the AS group. The significant difference between the LAA and the control group distinguished patients with ischemic stroke from those without stroke. Differential expressions were also observed in LAA and SAO groups. However, the presence or absence of vascular stenosis was the main difference between the LAA and SAO groups, and SAO usually shows no signs of cortical dysfunction (Adams et al., 1993). Differentially expressed miRNAs between these two groups can be helpful for the classification of ischemic stroke. Additionally, LAA is generally caused by rupture of atherosclerotic plaques, and our results showed a significant difference between the LAA group and the AS group, which consisted of patients with unruptured atherosclerotic plaques, suggesting that plaques rupture may play a role in the pathogenesis of stroke (Chistiakov et al., 2015). Identification of the etiology of acute ischemic stroke (AIS) is of much importance for guiding the secondary prevention. That is, candidate biomarkers are important for early prevention, diagnosis and treatment of the disease. The screened candidate diagnostic biomarkers can potentially identify the etiology, in other words, the occurrence of stroke events caused by ruptured atherosclerotic plaque, which is helpful for early treatment of the etiology and guidance of clinical medication.

Notably, the experimental grouping in this experiment was more detailed than those in previous studies. Here, we included ischemic stroke patients, patients with AS, and healthy controls. Previous studies on ischemic stroke have divided participants into two groups: a stroke group and a control group (Jickling et al., 2014; Tiedt et al., 2017). We further refined the groups in this study. Since there are multiple subtypes of ischemic stroke, we focused on LAA and SAO. Moreover, strict exclusion criteria were adopted in the current study to ensure the rigor and accuracy of the experiment (Tiedt et al., 2017; Jia et al., 2019; Min et al., 2019). It has been previously reported that miRNAs in exosomes can be used as biomarkers of atherosclerosis in cardiovascular diseases (Liu et al., 2019). We made a more detailed grouping and applied exosomal miRNAs to the diagnosis of LAA stroke. As a result, we identified candidate biomarkers for LAA stroke. It is indicated that different exosomal miRNAs could be used as diagnostic biomarkers and play roles in different atherosclerotic diseases, while needs to be further studied. In this study, we focus on the diagnostic value of exosomal miRNAs in the acute stage of ischemic stroke. The occurrence of an ischemic stroke usually indicates the need for immediate evaluation of therapeutic interventions. Biomarkers, especially in the acute phase, can play a valuable role in the treatment of stroke. Longfei Jia, Steffen Tiedt, Li Min et al. have conducted cross-sectional studies in their respective fields, and similarly, we have adopted the same research methods to obtain alternative diagnostic biomarkers.

In order to validate the results, we calculated the AUCs of the four factors. The results suggested that compared with plasma miRNAs, the exosomal miRNAs (miR-369-3p, miR-493-3p, miR-379-5p, and miR-1296-5p) showed greater diagnostic efficiency with much higher AUCs. The AUC was also calculated for a panel of four potential biomarkers. A large number of studies have shown that the diagnostic efficiency of combined biomarkers is

better than that of single biomarkers (Jia et al., 2019; Min et al., 2019). In line with these findings, composite biomarkers achieved higher AUCs than single biomarkers in this study. We verified the diagnostic efficiency of the four miRNAs in exosomes with a relatively large sample size of subjects to obtain clinical support. A study by Li Min et al. has verified that exosomal miRNAs are more effective than plasma miRNAs for the diagnosis of colon cancer (Min et al., 2019). Consistent with this finding, our experimental results showed that exosomal miRNAs were superior to their plasma counterparts for the diagnosis of LAA. In addition, there were significant differences in exosomal miRNAs among the four groups. In contrast, plasma miRNAs did not exhibit the same differential expression patterns, confirming that exosomes protect miRNAs from RNA-degrading enzymes in plasma. And according to our results, plasma miRNAs were not correlated with exosomal miRNAs. Diehl et al. found that miRNAs profiles in microvesicles were significantly different from those in maternal cells, suggesting that the selective packaging of miRNAs from cells into microvesicles is an active mechanism, which may indirectly prove the protective effect of exosomes, and partly explains the incorrelation between plasma and exosomal miRNAs in our results (Matsuura et al., 2016).

Prior studies on biomarkers for ischemic stroke have focused on proteins in plasma such as neuron-specific enolase and interleukin (AUC = 0.82 and 0.69 respectively) (Tiedt et al., 2017). According to Wang et al.'s study, exo-miRNAs perform better than traditional protein biomarkers, such as CEA and Cyfra21-1, in the diagnosis of non-small cell lung cancer (Wang et al., 2020). By contrast, in our study, we focused on exosomal miRNAs that can be used as diagnostic biomarkers in LAA stroke. Compared with previous studies, we investigated new factors for diagnostic biomarkers of LAA stroke that had not been previously studied. It is indicated in previous literature that miRNAs in plasma are easily degraded by RNase (Moreno-Moya et al., 2014). As a result, we not only studied the potential value of new factors in the diagnosis of ischemic stroke but also compared the diagnostic power of plasma factors and exosomal factors. The diagnostic efficiency of miRNAs in plasma vs. exosomes has been reported before (Min et al., 2019). Our results indicated that the diagnostic efficiency of exosomal miRNAs was superior to that of plasma miRNAs for ischemic stroke. We confirmed the protective effects of exosomes on miRNAs and the diagnostic value of exosomal miRNAs for ischemic stroke. Furthermore, we analyzed the identified miRNAs for the first time.

We also analyzed the correlations between miRNA expression levels in exosomes and NIHSS scores according to the methods in a previous study by Kentaro M. et al. (Matsuura et al., 2016). Early in the disease, a higher NIHSS score usually predicts a poorer prognosis to some extent (Powers, 2020). We classified ischemic stroke patients according to their NIHSS scores and found that exosomal miR-493-3p and miR-1296-5p levels were negatively correlated with NIHSS score. Therefore, we speculate that the expression levels of miRNAs in exosomes reflect the severity of disease to some extent. Although the two correlations were weak, the results provide new ideas for further exploration of the expression of miRNAs in the future. miRNA expression



decreased with increasing disease severity, which confirms that miRNAs play important roles in disease progression. Our findings provide insights for determination of disease severity through quantitative detection of miRNAs in the future. Besides, it has been previously reported that baseline NIHSS score is an important parameter to predict the prognosis of acute ischemic stroke (Tu et al., 2017a; Tu et al., 2017b). Therefore, we speculated that exosomal miRNAs as biomarkers can be used for the prognosis analysis of LAA stroke, which may be helpful to improve the quality of life of stroke patients in the future.

There were some limitations to our study. First, we only included Chinese Han ethnicity as the research object of our study, which restricted the generalization of our experimental conclusions to other populations. In addition, more clinical trials are needed to confirm the diagnostic efficiency of the candidate miRNAs.

## CONCLUSION

In summary, our study sheds new light on the use of exosomal miRNAs as noninvasive diagnostic biomarkers for LAA. We also provide a new alternative diagnostic method. Exosomal miR-369-3p, miR-493-3p, miR-379-5p, and miR-1296-5p are potential biomarkers, and composite biomarkers achieve higher diagnostic efficiency than the single biomarkers, making them more suitable for clinical diagnosis. In addition, we found that the NIHSS score is negatively correlated with exosomal miRNA expression, which provides a new perspective for future studies (Xu et al., 2019).

## DATA AVAILABILITY STATEMENT

The data that support the findings of this study are available from the corresponding author upon reasonable request.

## REFERENCES

- Adams, H. P., Bendixen, B. H., Kappelle, L. J., Biller, J., Love, B. B., Gordon, D. L., et al. (1993). Classification of Subtype of Acute Ischemic Stroke. Definitions for Use in a Multicenter Clinical Trial. TOAST. Trial of Org 10172 in Acute Stroke Treatment. *Stroke* 24, 35–41. doi:10.1161/01.str.24.1.35
- Androvic, P., Romanyuk, N., Urdzikova-Machova, L., Rohlova, E., Kubista, M., and Valihrach, L. (2019). Two-tailed RT-qPCR Panel for Quality Control of Circulating microRNA Studies. *Sci. Rep.* 9, 4255. doi:10.1038/s41598-019-40513-w
- Barrington, J., Lemarchand, E., and Allan, S. M. (2017). A Brain in Flame; Do Inflammasomes and Pyroptosis Influence Stroke Pathology? *Brain Pathol.* 27, 205–212. doi:10.1111/bpa.12476
- Chistiakov, D. A., Orekhov, A. N., and Bobryshev, Y. V. (2015). Contribution of Neovascularization and Intraplaque Haemorrhage to Atherosclerotic Plaque Progression and Instability. *Acta Physiol. (Oxf)* 213, 539–553. doi:10.1111/apha.12438
- del Zoppo, G., Ginis, I., Hallenbeck, J. M., Iadecola, C., Wang, X., and Feuerstein, G. Z. (2000). Inflammation and Stroke: Putative Role for Cytokines, Adhesion Molecules and iNOS in Brain Response to Ischemia. *Brain Pathol.* 10, 95–112. doi:10.1111/j.1750-3639.2000.tb00247.x
- Eldh, M., Lötvall, J., Malmhäll, C., and Ekström, K. (2012). Importance of RNA Isolation Methods for Analysis of Exosomal RNA: Evaluation of Different Methods. *Mol. Immunol.* 50, 278–286. doi:10.1016/j.molimm.2012.02.001

## ETHICS STATEMENT

This study was approved by the ethics committee of Qingdao University Affiliated Hospital. Informed consent was obtained from all participants.

## AUTHOR CONTRIBUTIONS

Conceived and designed the experiments: MN, XP, and XZ. Performed the experiments, and analyzed the data: MN, HL, XL, XY, AM, XP, and XZ. All included authors made contributions to the manuscript and approved the version submitted.

## FUNDING

This work was supported by Natural Science Foundation of Shandong Province (ZR2020MH138).

## ACKNOWLEDGMENTS

We thank all members of the Department of Neurology at The Affiliated Hospital of Qingdao University, especially all nurses, for assistance with blood withdrawal.

## SUPPLEMENTARY MATERIAL

The Supplementary Material for this article can be found online at: <https://www.frontiersin.org/articles/10.3389/fphar.2021.791644/full#supplementary-material>

- Fernandez, D. M., Rahman, A. H., Fernandez, N. F., Chudnovskiy, A., Amir, E. D., Amadori, L., et al. (2019). Single-cell Immune Landscape of Human Atherosclerotic Plaques. *Nat. Med.* 25, 1576–1588. doi:10.1038/s41591-019-0590-4
- Galleghante, V., De Santis, S., Liso, M., Verna, G., Sommella, E., Mastronardi, M., et al. (2019). Quercetin-Induced miR-369-3p Suppresses Chronic Inflammatory Response Targeting C/EBP- $\beta$ . *Mol. Nutr. Food Res.* 63, e1801390. doi:10.1002/mnfr.201801390
- Glisic, M., Mujaj, B., Rueda-Ochoa, O. L., Asllanaj, E., Laven, J. S. E., Kavousi, M., et al. (2018). Associations of Endogenous Estradiol and Testosterone Levels with Plaque Composition and Risk of Stroke in Subjects with Carotid Atherosclerosis. *Circ. Res.* 122, 97–105. doi:10.1161/CIRCRESAHA.117.311681
- Jauch, E. C., Barreto, A. D., Broderick, J. P., Char, D. M., Cucchiara, B. L., Devlin, T. G., et al. (2017). Biomarkers of Acute Stroke Etiology (BASE) Study Methodology. *Transl Stroke Res.* doi:10.1007/s12975-017-0537-3
- Jia, L., Qiu, Q., Zhang, H., Chu, L., Du, Y., Zhang, J., et al. (2019). Concordance between the Assessment of A $\beta$ 42, T-Tau, and P-T181-Tau in Peripheral Blood Neuronal-Derived Exosomes and Cerebrospinal Fluid. *Alzheimers Dement* 15, 1071–1080. doi:10.1016/j.jalz.2019.05.002
- Jickling, G. C., Ander, B. P., Zhan, X., Noblett, D., Stamova, B., and Liu, D. (2014). microRNA Expression in Peripheral Blood Cells Following Acute Ischemic Stroke and Their Predicted Gene Targets. *PLoS one* 9, e99283. doi:10.1371/journal.pone.0099283

- Johnston, S. C., Amarenco, P., Denison, H., Evans, S. R., Himmelmann, A., James, S., et al. (2020). Ticagrelor and Aspirin or Aspirin Alone in Acute Ischemic Stroke or TIA. *N. Engl. J. Med.* 383, 207–217. doi:10.1056/NEJMoa1916870
- Kalluri, R., and LeBleu, V. S. (2020). The Biology, Function, and Biomedical Applications of Exosomes. *Science* 367. doi:10.1126/science.aau6977
- Kobiyama, K., and Ley, K. (2018). Atherosclerosis. *Circ. Res.* 123, 1118–1120. doi:10.1161/circresaha.118.313816
- Krupinski, J., and Slevin, M. (2013). Emerging Molecular Targets for Brain Repair after Stroke. *Stroke Res. Treat.* 2013, 473416. doi:10.1155/2013/473416
- Kvistad, C. E., Novotny, V., Kurz, M. W., Rønning, O. M., Thommessen, B., Carlsson, M., et al. (2019). Safety and Outcomes of Tenecteplase in Moderate and Severe Ischemic Stroke. *Stroke* 50, 1279–1281. doi:10.1161/STROKEAHA.119.025041
- Kwah, L. K., and Diong, J. (2014). National Institutes of Health Stroke Scale (NIHSS). *J. Physiother.* 60, 61. doi:10.1016/j.jphys.2013.12.012
- Li, Q., He, Q., Baral, S., Mao, L., Li, Y., Jin, H., et al. (2016). MicroRNA-493 Regulates Angiogenesis in a Rat Model of Ischemic Stroke by Targeting MIF. *FEBS J.* 283, 1720–1733. doi:10.1111/febs.13697
- Libby, P., Buring, J. E., Badimon, L., Hansson, G. K., Deanfield, J., Bittencourt, M. S., et al. (2019). Atherosclerosis. *Nat. Rev. Dis. Primers* 5, 56. doi:10.1038/s41572-019-0106-z
- Liu, T., Zhang, Q., Zhang, J., Li, C., Miao, Y. R., Lei, Q., et al. (2019). EVmiRNA: a Database of miRNA Profiling in Extracellular Vesicles. *Nucleic Acids Res.* 47, D89–D93. doi:10.1093/nar/gky985
- Low, E. N. D., Mokhtar, N. M., Wong, Z., and Raja Ali, R. A. (2019). Colonic Mucosal Transcriptomic Changes in Patients with Long-Duration Ulcerative Colitis Revealed Colitis-Associated Cancer Pathways. *J. Crohns Colitis* 13, 755–763. doi:10.1093/ecco-jcc/jjz002
- Lu, T. X., and Rothenberg, M. E. (2018). MicroRNA. *J. Allergy Clin. Immunol.* 141, 1202–1207. doi:10.1016/j.jaci.2017.08.034
- Matsuura, K., De Giorgi, V., Schechterly, C., Wang, R. Y., Farci, P., Tanaka, Y., et al. (2016). Circulating Let-7 Levels in Plasma and Extracellular Vesicles Correlate with Hepatic Fibrosis Progression in Chronic Hepatitis C. *Hepatology* 64, 732–745. doi:10.1002/hep.28660
- Min, L., Zhu, S., Chen, L., Liu, X., Wei, R., Zhao, L., et al. (2019). Evaluation of Circulating Small Extracellular Vesicles Derived miRNAs as Biomarkers of Early colon Cancer: a Comparison with Plasma Total miRNAs. *J. Extracell. Vesicles* 8, 1643670. doi:10.1080/20013078.2019.1643670
- Mirzaei, H., Momeni, F., Saadatpour, L., Sahebkar, A., Goodarzi, M., Masoudifar, A., et al. (2018). MicroRNA: Relevance to Stroke Diagnosis, Prognosis, and Therapy. *J. Cel Physiol* 233, 856–865. doi:10.1002/jcp.25787
- Ornello, R., Degan, D., Tiseo, C., Di Carmine, C., Perciballi, L., Pistoia, F., et al. (2018). Distribution and Temporal Trends from 1993 to 2015 of Ischemic Stroke Subtypes: A Systematic Review and Meta-Analysis. *Stroke* 49, 814–819. doi:10.1161/STROKEAHA.117.020031
- Peng, X. X., Yu, R., Wu, X., Wu, S. Y., Pi, C., Chen, Z. H., et al. (2020). Correlation of Plasma Exosomal microRNAs with the Efficacy of Immunotherapy in EGFR/ALK Wild-type Advanced Non-small Cell Lung Cancer. *J. Immunother. Cancer* 8. doi:10.1136/jitc-2019-000376
- Powers, W. J. (2020). Acute Ischemic Stroke. *N. Engl. J. Med.* 383, 252–260. doi:10.1056/NEJMcp1917030
- Prabhakaran, S., Ruff, I., and Bernstein, R. A. (2015). Acute Stroke Intervention: a Systematic Review. *JAMA* 313, 1451–1462. doi:10.1001/jama.2015.3058
- Raju, S., Fish, J. E., and Howe, K. L. (2020). MicroRNAs as Sentinels and Protagonists of Carotid Artery Thromboembolism. *Clin. Sci. (Lond)* 134, 169–192. doi:10.1042/CS20190651
- Raouf, R., Bauer, S., El Naggar, H., Connolly, N. M. C., Brennan, G. P., Brindley, E., et al. (2018). Dual-center, Dual-Platform microRNA Profiling Identifies Potential Plasma Biomarkers of Adult Temporal Lobe Epilepsy. *EBioMedicine* 38, 127–141. doi:10.1016/j.ebiom.2018.10.068
- Rupaimoole, R., and Slack, F. J. (2017). MicroRNA Therapeutics: towards a new era for the Management of Cancer and Other Diseases. *Nat. Rev. Drug Discov.* 16, 203–222. doi:10.1038/nrd.2016.246
- Shen, Y., Peng, C., Bai, Q., Ding, Y., Yi, X., Du, H., et al. (2019). Epigenome-Wide Association Study Indicates Hypomethylation of MTRNR2L8 in Large-Artery Atherosclerosis. *Stroke* 50, 1330–1338. doi:10.1161/STROKEAHA.118.023436
- Tian, Y., Gong, M., Hu, Y., Liu, H., Zhang, W., Zhang, M., et al. (2020). Quality and Efficiency Assessment of Six Extracellular Vesicle Isolation Methods by Nano-Flow Cytometry. *J. Extracell. Vesicles* 9, 1697028. doi:10.1080/20013078.2019.1697028
- Tiedt, S., Prestel, M., Malik, R., Schieferdecker, N., Duering, M., Kautzky, V., et al. (2017). RNA-seq Identifies Circulating miR-125a-5p, miR-125b-5p, and miR-143-3p as Potential Biomarkers for Acute Ischemic Stroke. *Circ. Res.* 121, 970–980. doi:10.1161/CIRCRESAHA.117.311572
- Treiber, T., Treiber, N., and Meister, G. (2019). Regulation of microRNA Biogenesis and its Crosstalk with Other Cellular Pathways. *Nat. Rev. Mol. Cel Biol* 20, 5–20. doi:10.1038/s41580-018-0059-1
- Tu, W. J., Ma, G. Z., Ni, Y., Hu, X. S., Luo, D. Z., Zeng, X. W., et al. (2017a). Copeptin and NT-proBNP for Prediction of All-Cause and Cardiovascular Death in Ischemic Stroke. *Neurology* 88, 1899–1905. doi:10.1212/WNL.0000000000003937
- Tu, W. J., Zeng, X. W., Deng, A., Zhao, S. J., Luo, D. Z., Ma, G. Z., et al. (2017b). Circulating FABP4 (Fatty Acid-Binding Protein 4) Is a Novel Prognostic Biomarker in Patients with Acute Ischemic Stroke. *Stroke* 48, 1531–1538. doi:10.1161/STROKEAHA.117.017128
- van Niel, G., D'Angelo, G., and Raposo, G. (2018). Shedding Light on the Cell Biology of Extracellular Vesicles. *Nat. Rev. Mol. Cel Biol* 19, 213–228. doi:10.1038/nrm.2017.125
- Wolf, D., and Ley, K. (2019). Immunity and Inflammation in Atherosclerosis. *Circ. Res.* 124, 315–327. doi:10.1161/CIRCRESAHA.118.313591
- Xu, Q., Liu, X., Liu, Z., Zhou, Z., Wang, Y., Tu, J., et al. (2017). MicroRNA-1296 Inhibits Metastasis and Epithelial-Mesenchymal Transition of Hepatocellular Carcinoma by Targeting SRPK1-Mediated PI3K/AKT Pathway. *Mol. Cancer* 16, 103. doi:10.1186/s12943-017-0675-y
- Xu, X., Wang, Y., Mojumdar, K., Zhou, Z., Jeong, K. J., Mangala, L. S., et al. (2019). AD-to-I-edited miRNA-379-5p Inhibits Cancer Cell Proliferation through CD97-Induced Apoptosis. *J. Clin. Invest.* 129, 5343–5356. doi:10.1172/JCI123396
- Zeng, Q., Zeng, Y., Slevin, M., Guo, B., Shen, Z., Deng, B., et al. (2021). C-reactive Protein Levels and Clinical Prognosis in LAA-type Stroke Patients: A Prospective Cohort Study. *Biomed. Res. Int.* 2021. doi:10.1155/2021/66710436671043
- Zhou, S., Zhang, D., Guo, J., Chen, Z., Chen, Y., and Zhang, J. (2021). Deficiency of NEAT1 Prevented MPP+ induced Inflammatory Response, Oxidative Stress and Apoptosis in Dopaminergic SK-N-SH Neuroblastoma Cells via miR-1277-5p/ARHGAP26 axis. *Brain Res.* 1750, 147156. doi:10.1016/j.brainres.2020.147156
- Zuo, L., Zhang, L., Zu, J., Wang, Z., Han, B., Chen, B., et al. (2020). Circulating Circular RNAs as Biomarkers for the Diagnosis and Prediction of Outcomes in Acute Ischemic Stroke. *Stroke* 51, 319–323. doi:10.1161/STROKEAHA.119.027348

**Conflict of Interest:** The authors declare that the research was conducted in the absence of any commercial or financial relationships that could be construed as a potential conflict of interest.

**Publisher's Note:** All claims expressed in this article are solely those of the authors and do not necessarily represent those of their affiliated organizations, or those of the publisher, the editors and the reviewers. Any product that may be evaluated in this article, or claim that may be made by its manufacturer, is not guaranteed or endorsed by the publisher.

Copyright © 2021 Niu, Li, Li, Yan, Ma, Pan and Zhu. This is an open-access article distributed under the terms of the Creative Commons Attribution License (CC BY). The use, distribution or reproduction in other forums is permitted, provided the original author(s) and the copyright owner(s) are credited and that the original publication in this journal is cited, in accordance with accepted academic practice. No use, distribution or reproduction is permitted which does not comply with these terms.



# Activation of Nrf2 by Lithospermic Acid Ameliorates Myocardial Ischemia and Reperfusion Injury by Promoting Phosphorylation of AMP-Activated Protein Kinase $\alpha$ (AMPK $\alpha$ )

Min Zhang<sup>1,2†</sup>, Li Wei<sup>3†</sup>, Saiyang Xie<sup>1,2</sup>, Yun Xing<sup>1,2</sup>, Wenke Shi<sup>1,2</sup>, Xiaofeng Zeng<sup>1,2</sup>, Si Chen<sup>1,2</sup>, Shasha Wang<sup>1,2</sup>, Wei Deng<sup>1,2</sup> and Qizhu Tang<sup>1,2\*</sup>

<sup>1</sup>Department of Cardiology, Renmin Hospital of Wuhan University, Wuhan, China, <sup>2</sup>Hubei Key Laboratory of Metabolic and Chronic Diseases, Wuhan, China, <sup>3</sup>Department of Pediatrics, Renmin Hospital of Wuhan University, Wuhan, China

## OPEN ACCESS

### Edited by:

Xianwei Wang,  
Xinxiang Medical University, China

### Reviewed by:

Chao Guo,  
Fourth Military Medical University,  
China  
Gauhar Rehman,  
Abdul Wali Khan University Mardan,  
Pakistan

### \*Correspondence:

Qizhu Tang  
qztang@whu.edu.cn

<sup>†</sup>These authors have contributed  
equally to this work

### Specialty section:

This article was submitted to  
Cardiovascular and Smooth Muscle  
Pharmacology,  
a section of the journal  
Frontiers in Pharmacology

Received: 14 October 2021

Accepted: 29 October 2021

Published: 26 November 2021

### Citation:

Zhang M, Wei L, Xie S, Xing Y, Shi W,  
Zeng X, Chen S, Wang S, Deng W and  
Tang Q (2021) Activation of Nrf2 by  
Lithospermic Acid Ameliorates  
Myocardial Ischemia and Reperfusion  
Injury by Promoting Phosphorylation of  
AMP-Activated Protein Kinase  
 $\alpha$  (AMPK $\alpha$ ).  
Front. Pharmacol. 12:794982.  
doi: 10.3389/fphar.2021.794982

**Background:** As a plant-derived polycyclic phenolic carboxylic acid isolated from *Salvia miltiorrhiza*, lithospermic acid (LA) has been identified as the pharmacological management for neuroprotection and hepatoprotection. However, the role and mechanism of lithospermic acid in the pathological process of myocardial ischemia-reperfusion injury are not fully revealed.

**Methods:** C57BL/6 mice were subjected to myocardial ischemia and reperfusion (MI/R) surgery and pretreated by LA (50 mg/kg, oral gavage) for six consecutive days before operation. The *in vitro* model of hypoxia reoxygenation (HR) was induced by hypoxia for 24 h and reoxygenation for 6 h in H9C2 cells, which were subsequently administrated with lithospermic acid (100  $\mu$ M). Nrf2 siRNA and dorsomorphin (DM), an inhibitor of AMPK $\alpha$ , were used to explore the function of AMPK $\alpha$ /Nrf2 in LA-mediated effects.

**Results:** LA pretreatment attenuates infarct area and decreases levels of TnT and CK-MB in plasm following MI/R surgery in mice. Echocardiography and hemodynamics indicate that LA suppresses MI/R-induced cardiac dysfunction. Moreover, LA ameliorates oxidative stress and cardiomyocytes apoptosis following MI/R operation or HR *in vivo* and *in vitro*. In terms of mechanism, LA selectively activates eNOS, simultaneously increases nuclear translocation and phosphorylation of Nrf2 and promotes Nrf2/HO-1 pathway *in vivo* and *in vitro*, while cardioprotection of LA is abolished by pharmacological inhibitor of AMPK or Nrf2 siRNA in H9C2 cells.

**Conclusion:** LA protects against MI/R-induced cardiac injury by promoting eNOS and Nrf2/HO-1 signaling via phosphorylation of AMPK $\alpha$ .

**Keywords:** lithospermic acid, myocardial ischemia-reperfusion injury (MIRI), Nrf2, oxidative stress, ampk $\alpha$

**Abbreviations:** AMI, Acute myocardial infarction; AMPK $\alpha$ , AMP-activated protein kinase alpha; DHE, Dihydroethidium; DM, Dorsomorphin; eNOS, Endothelial nitric oxide synthase; 4-HNE, 4-Hydroxynonenal; HO-1, Heme oxygenase-1; HR, Hypoxia reoxygenation; LA, Lithospermic acid; MI/R, Myocardial ischemia and reperfusion; NS, Normal saline; Nrf2, Nuclear factor E2-related factor 2; ROS, Reactive oxygen species.

## 1 INTRODUCTION

Myocardial ischemia-reperfusion (MI/R) injury has a significant impact on the prognosis of patients with revascularization (Jennings, 2013). Moreover, MI/R injury largely contributed to cardiac dysfunction through additional oxidative stress and apoptosis in the heart (Lu et al., 2018; Chen et al., 2019). Therefore, reducing MI/R injury following acute myocardial infarction (AMI) greatly improves morbidity and mortality. Unfortunately, the pathogenesis and molecular mechanisms of MI/R injury in the heart are poorly understood (Lejay et al., 2016). A considerable number of patients with MI/R injury still have a poor prognosis after conventional treatment. Hence, a better understanding of the mechanism of MI/R injury would make it possible to propose more effective interventions.

As a well-known Chinese herbal medicine, *Salvia miltiorrhiza* has been widely utilized to prevent cardiovascular diseases (CVDs) in China and Asia (Wang et al., 2017; Jia et al., 2019). Lithospermic acid (LA), a catechol derivative extracted from *Salvia miltiorrhiza*, is a natural compound with diversified biological activities. Cheng et al. revealed that LA attenuated diabetes and target organ damage in rats (Jin et al., 2014). Moreover, LA has been suggested to prevent Parkinson's disease by suppressing apoptosis and inflammation in the nervous system (Lin et al., 2015). In addition, LA has been shown to exert a hepatoprotective effect against carbon tetrachloride (CCl<sub>4</sub>)-induced hepatic oxidative damage (Chan and Ho, 2015). Importantly, previous clinical trials showed that LA injection improved coronary heart diseases angina pectoris (Zhang et al., 2006). However, the exact contribution of LA in MI/R injury following AMI remains largely elusive.

As a master transcription factor expressed in multiple tissues, nuclear factor erythroid 2-related factor 2 (Nrf2) is implicated in antioxidant defense mechanisms in the myocardium, which is usually activated by increased reactive oxygen species (ROS) production (Chen and Maltagliati, 2018; Vashi and Patel, 2020). Nrf2 upregulates detoxicant genes in response to the stimulatory signal, leading to cardioprotection (Boo, 2020). Accumulating evidence reveals that Nrf2 reduces oxidative stress and myocardial inflammation in heart tissues by activation of the Nrf2-antioxidant response element (ARE) pathway (Buendia et al., 2016; Guo and Mo, 2020). Previous studies have also uncovered the cardioprotection of the Nrf2 pathway. Most recently, Guo et al. reported that inhibition of the Nrf2-ARE pathway promoted oxidative stress-induced necrosis and ischemia/reperfusion injury (Guo et al., 2020). Furthermore, activation of the Nrf2-ARE pathway suppresses oxidative stress, and ameliorates isoproterenol-mediated pathological cardiac hypertrophy progression (Velusamy et al., 2020). Additionally, phosphorylation of Nrf2 has been suggested to inhibit oxidative stress and apoptosis in human dermal fibroblasts (Huang et al., 2019). Manuel et al. suggested that AMP-activated protein kinase (AMPK) triggered phosphorylation of Nrf2 and promoted transactivation of antioxidative genes (Matzinger et al., 2020).

In the present study, we demonstrate that LA improves cardiac function and attenuates myocardial injury during MI/R. Moreover, LA suppresses oxidative stress and apoptosis by

promoting activation of endothelial nitric oxide synthase (eNOS) and Nrf2/HO-1 pathway via phosphorylation of AMPK $\alpha$  in MI/R injury. Table

## 2 METHODS

All animal experimental procedures followed the National Institutes of Health (NIH) guidelines and were approved by the Animal Care and Use Committee of Renmin Hospital of Wuhan University. Lithospermic acid (>98% purity, CAS. 28831-65-4) was obtained from Shanghai Winberb Medical Technology Co., Ltd (Shanghai, China).

### 2.1 Animals

C57BL/6 male mice (2 months old, 24.5  $\pm$  2.0 g), obtained from the Institute of Laboratory Animal Science, Chinese Academy of Medical Sciences (Beijing, China), were randomly separated into 4 groups: Sham-NS (normal saline) ( $n$  = 10), Sham-LA ( $n$  = 10), MI/R-NS ( $n$  = 15) and MI/R-LA ( $n$  = 15). Mice were pretreated with LA (50 mg/kg, oral gavage) for six consecutive days before MI/R surgery or sham, and poured into the normal saline control group processing.

A myocardial ischemia-reperfusion mouse model was constructed as previously described (Fan et al., 2017). Briefly, mice were anesthetized with pentobarbital (50 mg/kg, i.p.). Afterward, mice subjected to skin preparation were intubated and connected to a small animal ventilator. Subsequently, surgical scissors were used to cut the fourth intercostal space on the left side to fully expose the heart. Then, the left anterior descending coronary artery (LAD) was ligated with 6-0 silk thread at 2 mm below the left atrial appendage. Mice were exposed to 45 min of LAD occlusion, followed by 24 h of reperfusion. Meanwhile, the small animal electrocardiogram (ECG) monitoring system was utilized to record ST-segment elevation. Finally, the rodents were euthanized with an overdose of pentobarbital (200 mg/kg, i.p.), and their hearts were harvested for further analysis.

### 2.2 Echocardiography and Hemodynamics

Mice subjected to 24 h of reperfusion were anesthetized by inhalation of 1.5–2% isoflurane (Fan et al., 2017). The cardiac structure and function were monitored using a MyLab 30CV system (Biosound Esaote, Inc.) equipped with a 15 MHz probe in a small animal ultrasound instrument. Parameters were obtained from more than three beats and then averaged. Left ventricular internal diameter at end-diastole (LVIDd), left ventricular internal diameter at end-systole (LVIDs) and left ventricular fractional shortening (LVFS) were tested. Hemodynamic parameters were obtained using a 1.4-French catheter-tip micromanometer catheter (SPR-839; Millar Instruments, Houston, TX, United States), which was inserted into the left ventricle (LV) through the right carotid artery. Subsequently, pressure-volume parameters were recorded using an ARIA pressure-volume conductance system (MPVS-300 Signal Conditioner, Millar Instruments, Houston, TX, United States) coupled to a Power Lab/4SPA/D converter, and then analyzed by Lab Chart 8 software.



## 2.3 Histological Analysis

Double staining with Evans blue and 2,3,5-triphenyltetrazolium chloride (TTC) was utilized to determine the area at risk and infarcted area following MI/R operation. More details are provided in the supplement material. The isolated heart tissue was immobilized with 4% paraformaldehyde and dehydrated with gradient alcohol. Then, 5  $\mu$ m-thick sections were paraffin-embedded. Immunohistochemistry (IHC) of 4-hydroxynonenal and Nrf2 was performed to detect oxidative stress and the location of Nrf2 in the heart. Dihydroethidium (DHE) fluorescence was also performed to assess oxidative. Moreover, a terminal-deoxynucleotidyl transferase-mediated nick end labeling (TUNEL) assay was used to determine apoptotic cells in the heart after MI/R surgery. The density of IHC and DHE staining was assessed using Image-Pro Plus version 6.0. More details are provided in the supplement material.

## 2.4 Western Blot

The heart sample was collected after reperfusion for 24 h. Protein was extracted from heart homogenates by radioimmunoprecipitation assay (RIPA) lysis buffer. Nuclear protein was obtained *in vivo* and *in vitro* using the Nuclear and Cytoplasmic Protein Extraction kit (P0028, Beyotime, Shanghai, China) and protein concentration was determined by bicinchoninic acid assay (Thermo Scientific, 23,227). Subsequently, 10% sodium dodecyl sulfate-polyacrylamide gel electrophoresis (SDS-PAGE) was performed to separate protein samples (40  $\mu$ g), and then proteins were transferred to polyvinylidene difluoride (PVDF) membranes. After incubation with blocking buffer and targeted antibodies overnight, the PVDF membranes were subsequently incubated with a corresponding secondary antibody. Afterward, targeted protein bands were examined using a chemiluminescence method, and the density of target bands was evaluated by AlphaEaseFC software processing system (Bio-Rad, ChemiDoc XRS) and Image Lab software. Primary antibodies used in this study are provided in **Supplement Table S1**.

## 2.5 Real-Time Polymerase Chain Reaction (RT-PCR)

Total RNA was extracted from mouse hearts and H9C2 cells using Trizol reagent (Invitrogen, 15596-026) and cDNA was produced using the Transcriptor First Strand cDNA synthesis kit (04897030001, Roche Diagnostics, Basel, Switzerland). Meanwhile, SYBR Green (04707516001) was utilized to amplify transcripts, and GAPDH was the endogenous reference. All primers used are listed in **Supplement Table S2**.

## 2.6 Culture and Treatment of Cardiomyocytes

H9C2 cells were obtained from the Cell Bank of the Chinese Academy of Sciences (Shanghai, China) and cultured in Dulbecco's modified Eagle's medium (DMEM, GIBCO, C11995). Afterward, H9C2 cells in good growth condition were divided into 4 groups: Normoxia (Nor)-PBS group, Nor-LA group, hypoxia-reoxygenation (HR)-PBS group and HR-LA

group. For Nor, cells were incubated under 5% CO<sub>2</sub> at 37°C, whereas for HR, cells were subjected to hypoxia for 24 h and reoxygenation for 6 h with 5% CO<sub>2</sub>, 94% N<sub>2</sub> and 1% O<sub>2</sub> at 37°C in tri-gas incubators. H9C2 cells in the LA group were subjected to LA (100  $\mu$ M) treatment for 24 h after Nor or HR.

For small interfering RNA (siRNA)-mediated knockdown experiments, Nrf2-siRNA (sc-156128) or Scr-siRNA was transfected with Lipofectamine 6,000 (Lipo6000, Beyotime, C0526) at 40 nM concentration in culture medium following the manufacturer's protocol. Western blot analysis was performed to assess the efficiency of knockdown. For the AMPK inhibitor, dorsomorphin (DM, 10  $\mu$ M, Cat No. HY-13418A, purchased from MedChemExpression) was incubated with H9C2 cells for 18 h after Nor or HR. Immunoblotting was performed to assess the efficiency of blockage.

## 2.7 Cellular Immunofluorescence

After washing with phosphate-buffered saline (PBS), H9C2 cells were fixed by 4% paraformaldehyde for over 15 min. Afterward, permeabilization was performed with 0.1% Triton X-100 (Amresco) in PBS. Then cells were incubated with 10% goat serum and subsequently stained with anti-Nrf2 overnight at 4°C. Next, cells scrubbed with PBS were then subjected to the secondary antibody goat anti-rabbit Alexa Fluor™ 488 (Invitrogen, A10266) for 1 h. SlowFade® Gold anti-fade reagent with DAPI (Invitrogen, S36939) was utilized for mounting as previously described (Wu et al., 2018).

## 2.8 Data and Statistical Analysis

Data are expressed as mean  $\pm$  standard error of the mean (SEM) and evaluated using SPSS version 22.0 (SPSS Inc, Chicago). Comparison of multiple groups was performed using one-way analysis of variance (ANOVA) and two group comparisons were analyzed by unpaired Student's t-test. A *p*-value <0.05 was considered statistically significant.

# 3 RESULTS

## 3.1 LA Ameliorates MI/R-Induced Myocardial Injury *in vivo*

MI/R injury is characterized by a significant increase in oxidative stress, inflammation and apoptosis in the heart tissues (Sun et al., 2021). LA has been previously verified as a potential antioxidant drug (Kang et al., 2021). To determine whether LA might reduce myocardial injury, plasma levels of troponin T (TnT) and creatine kinase MB (CK-MB) and myocardial infarct area were measured. It was found that the myocardial infarct area was reduced following MI/R surgery, suggesting a cardioprotective effect of LA (**Figures 1A–C**). In addition, plasma levels of TnT and CK-MB were elevated following MI/R operation, which were significantly reduced by LA pretreatment (**Figures 1D,E**).

## 3.2 LA Improves MI/R-Mediated Cardiac Dysfunction *in vivo*

To determine the effects of LA on cardiac function, echocardiography and hemodynamic assessment were



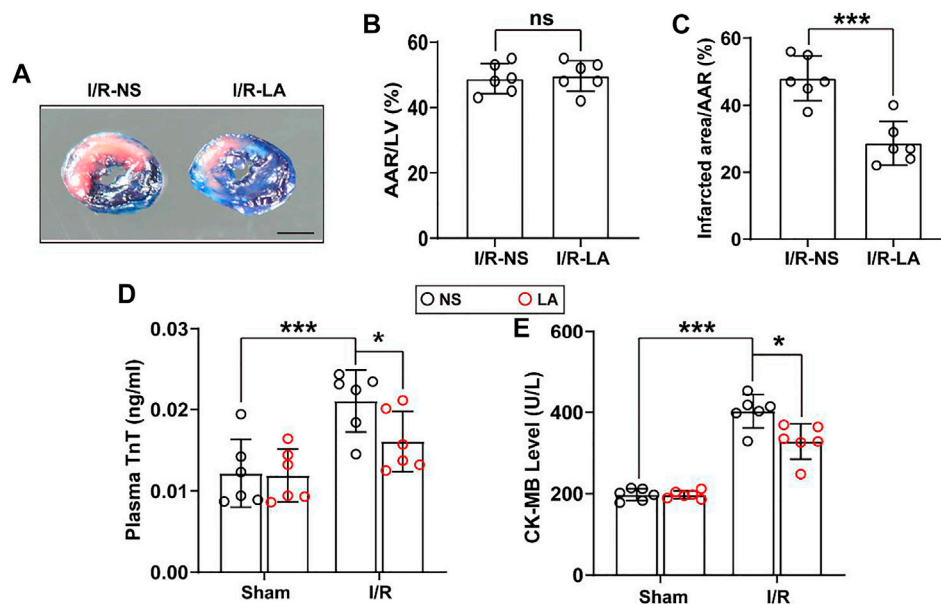


**FIGURE 1** | LA ameliorates MI/R-induced myocardial injury **(A)**. Left ventricular (LV) tissue sections of both LA and NS pretreated mice stained with Evans blue and 2,3,5-triphenyltetrazolium chloride (TTC) at 24 h after MI/R, in order to delineate the area at risk (AAR) and the infarcted region (Scale bar, 1 mm) **(B,C)**. The ratios of AAR/LV and infarct area/AAR were compared between LA and NS pretreated mice ( $n = 6$ ) **(D,E)**. The enzyme activity of CK-MB and TnT in serum were accessed in LA and NS pretreated mice 24 h after MI/R operation by Elisa assay ( $n = 6$ ). Data are presented as the mean  $\pm$  SEM, with each point representing a mouse. \* indicates  $p < 0.05$ , \*\*\* indicates  $p < 0.001$ , ns indicates no significance.

performed in mice. It was found that LA attenuated MI/R-induced left ventricle systolic dysfunction (**Figure 2A**; **Table 1**). However, LA pretreatment partly restored LVEF, LVFS and LVIDs after MI/R surgery (**Figures 2B–D**). Moreover, LA administration significantly attenuated MI/R-mediated disturbance in hemodynamic parameters; the left ventricular pressure-volume (P-V) loop, end-systolic volume (ESV) and end-diastolic volume (EDV) remained relatively unchanged (**Figures 2E–G**). However, LA administration had a limited effect on hemodynamic parameters in sham mice (**Supplementary Figure S1**). Collectively, these data indicated that LA ameliorated MI/R-mediated cardiac dysfunction *in vivo*.

### 3.3 LA Attenuates Oxidative Stress and Apoptosis in the Heart Following MI/R Surgery

To evaluate whether LA regulates oxidative stress and apoptosis in the MI/R heart, immunohistochemistry staining of 4-hydroxynonenal (4-HNE) in the heart section was performed. The results showed a higher expression of 4-HNE after MI/R operation, which was significantly suppressed by LA pretreatment (**Figures 3A,B**). Similarly, DHE staining showed that LA pretreatment reduced MI/R-mediated ROS production (**Figures 3A,C**). Next, protein and transcriptional levels of oxidative stress markers were investigated. Immunoblot analysis revealed that p47 phox and GP91 were upregulated, whereas anti-oxidative marker SOD2 in mitochondria was decreased in response to MI/R in the heart. However, pretreatment with LA conferred protective effects against

oxidative stress (**Figures 3D,E**). Likewise, RT-PCR analysis showed increased expression of oxidative factors such as GP91, NOX4 and p67 phox, while anti-oxidative markers such as Gpx, SOD2 and NQO1 were downregulated following MI/R surgery. However, LA treatment promoted the transcription of anti-oxidative genes and blocked the expression of oxidative genes in the heart (**Supplementary Figure S2**).

TUNEL staining was employed to determine the role of LA MI/R-induced apoptosis in heart tissues. TUNEL-positive cells were remarkably increased after MI/R surgery; however, LA treatment attenuated MI/R-induced apoptosis in the heart (**Figures 3F,G**). Subsequently, Caspase-3 activity was examined, and it was found that LA treatment reduced Caspase-3 activity following MI/R operation in the heart (**Figure 3H**). Similarly, immunoblotting analysis revealed that LA treatment alleviated MI/R-induced expression of cleaved Caspase-3 and Bax and contributed to Bcl2 production in the heart (**Figures 3I,J**). As expected, RT-PCR analysis revealed that LA treatment decreased mRNA levels of Bax and promoted transcription of Bcl2 in the heart (**Supplementary Figure S3**). These data suggested that LA treatment attenuated oxidative stress and apoptosis after MI/R surgery in the heart.

### 3.4 LA Counters Oxidative Stress and Apoptosis in Hypoxia Reoxygenation (HR) in H9C2 Cells

To further explore the role of LA in H9C2 cells, *in vitro* experiments were performed with the HR model (**Supplementary Figure S3**). ROS levels were assessed using

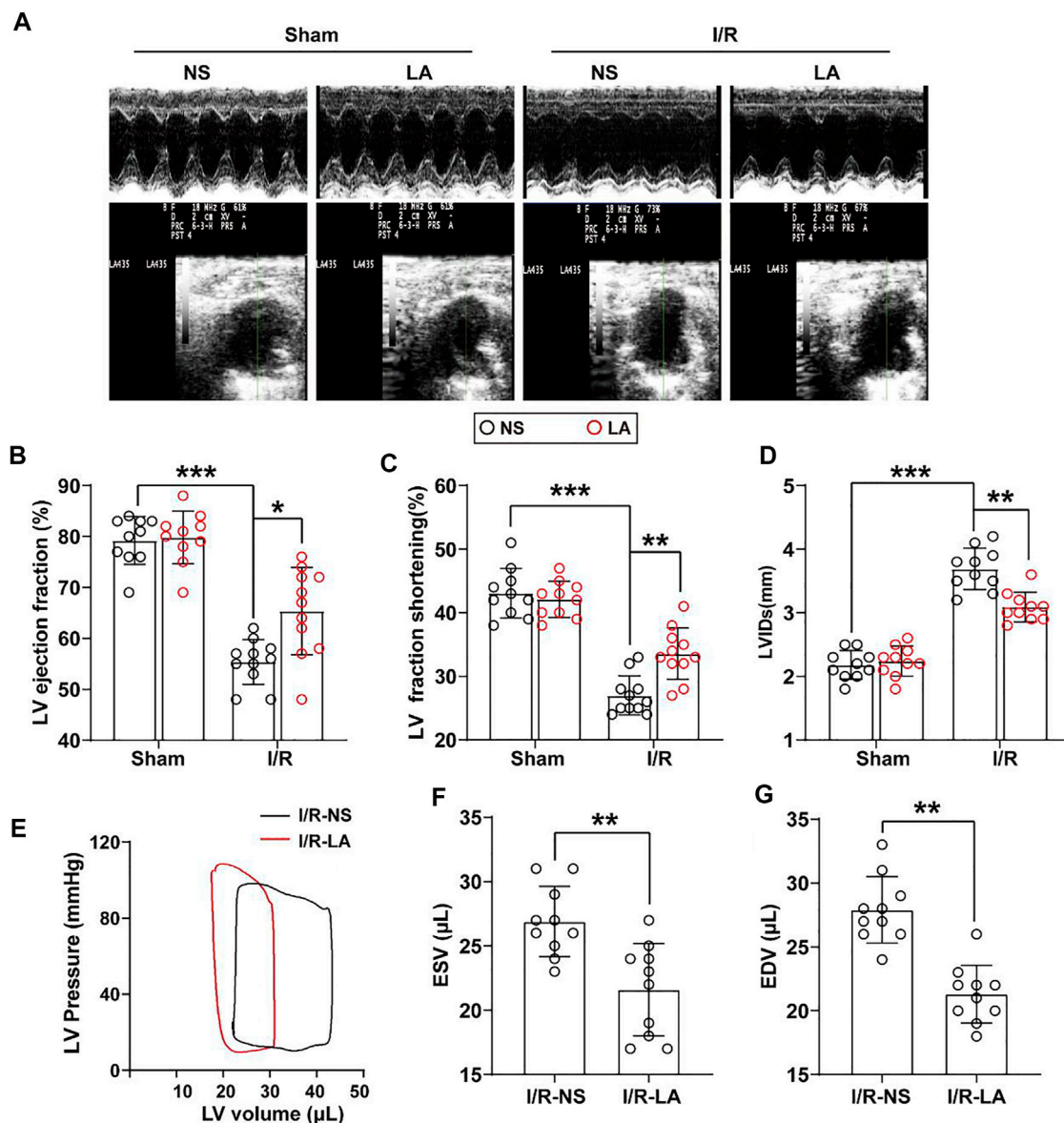


**FIGURE 2 |** LA improves MI/R-induced cardiac dysfunction *in vivo*. LA and NS pretreated mice were subjected to MI/R operation or sham (A). Representative M-mode and B-mode echocardiography of left ventricular chamber (B–D). Measurement of left ventricle ejection fraction (LVEF), left ventricle fraction shortening (LVFS) and left ventricular end systolic diameter (LVIDs),  $n = 10$ –11 per group (E). Representative PV loops of LA and NS pretreated mice following MI/R, and (F,G), analysis of end systolic volume (ESV) and end diastolic volume (EDV) ( $n = 10$ ). Data are presented as the mean  $\pm$  SEM, with each point representing a mouse. \* indicates  $p < 0.05$ , \*\* indicates  $p < 0.01$ , \*\*\* indicates  $p < 0.001$ .

the 2',7'-dihydro-dichlorofluorescein diacetate (DCFH-DA) probe in H9C2 cells. It was found that HR contributed to ROS production, whereas LA pretreatment decreased the expression of ROS in cardiomyocytes (Figures 4A,B). Similarly, Western blotting indicated that HR elevated the levels of p47 phox and GP91, and suppressed protein levels of SOD2 in H9C2 cells. Consistent with *in vivo* experiments, LA decreased protein levels of p47 phox and GP91 and promoted SOD2 production inside mitochondria in cardiomyocytes (Figures 4C,D). In addition, LA attenuated HR-induced

upregulation of GP91 and p67 phox and triggered the transcription of SOD2 in H9C2 cells (Supplementary Figure S4).

Importantly, the extent of apoptosis in H9C2 cells following HR was also assessed. TUNEL staining showed that LA alleviated HR-induced apoptosis (Figures 4E,F). Subsequently, lactate dehydrogenase (LDH) release assay showed that HR resulted in the upregulation of LDH and LA protected against cell damage (Figure 4G). Consistent with *in vivo* experiments, LA decreased the expression of cleaved Caspase-3 and Bax and contributed to Bcl2 production in H9C2 cells following HR (Figures 4H,I). Moreover,

**TABLE 1 |** Physiological, Echocardiographic and Hemodynamic parameters after MI/R.

	Sham-NS (n = 10) Mean ± SEM	Sham-LA (n = 10) Mean ± SEM	MI/R-NS (n = 14) Mean ± SEM	MI/R-LA (n = 15) Mean ± SEM
Physiological parameter				
HW (mg)	126.52 ± 7.24	128.36 ± 5.03	126.28 ± 4.96	129.63 ± 6.71
BW (g)	25.12 ± 1.63	24.85 ± 1.26	24.86 ± 3.38	25.03 ± 3.02
TL (mm)	18.24 ± 0.26	18.59 ± 0.15	18.46 ± 0.44	17.95 ± 0.52
HW/BW	4.95 ± 0.18	5.04 ± 0.23	4.96 ± 0.24	5.11 ± 0.42
HW/TL	6.98 ± 0.32	6.85 ± 0.39	6.93 ± 0.52	7.03 ± 0.47
Echocardiographic and Hemodynamic parameters				
HR, bpm	474 ± 17	467 ± 22	475 ± 24	464 ± 28
LVIDs, mm	2.35 ± 0.08	2.33 ± 0.11	3.71 ± 0.09*	3.09 ± 0.09#
IVSs, mm	0.69 ± 0.11	0.71 ± 0.09	0.81 ± 0.11*	0.75 ± 0.08#
EF (%)	80 ± 1	79 ± 1	54 ± 2*	64 ± 1#
FS (%)	43 ± 1	42 ± 2	26 ± 2*	32 ± 1#
CO (μL)	10,644 ± 3.56	10,574 ± 3.32	5,854 ± 3.39*	7,946 ± 3.51#
ESP (mmHg)	92 ± 1.9	91 ± 2.3	121 ± 2.5*	122 ± 2.7
dp/dt max (mmHg/s)	9,648 ± 116	9,736 ± 152	6,036 ± 106*	7,541 ± 126#
dp/dt min (mmHg/s)	-9,726 ± 129	-9,802 ± 96	-5,979 ± 103*	-7,265 ± 131#

Mean ± SEM, vs Sham-NS: \*p < 0.05. vs MI/R-NS: #p < 0.05.; Abbreviations: HW: heart weight/tibial length; BW: body weight; TL: tibial length; HR, heart rate; left ventricular end-systolic diameter; IVSs, interventricular septal thickness at end-systole; FS, fractional shortening; EF, ejection fraction; CO, cardiac output; ESP, end-systolic pressure.

LA prevented HR-induced upregulation of Bax and triggered the transcription of Bcl2 in H9C2 cells (Supplementary Figure S5).

### 3.5 LA Promotes the Expression of eNOS *in vivo* and *in vitro*

Furthermore, we investigated how LA alleviated oxidative stress and apoptosis. LA administration promoted nitric oxide (NO) production in heart tissues (Figure 5A), which was derived mainly from several isoforms of NO synthase (NOS), including neuronal NOS (nNOS), inducible NOS (iNOS) and eNOS isoforms (Crane et al., 2010). Therefore, the expression of iNOS, eNOS and nNOS in the heart was evaluated by RT-PCR. It was found that LA selectively activated eNOS (Figure 5B). Consistent Western blotting, LA increased the expression of eNOS but not iNOS and nNOS in the heart following MI/R surgery (Figures 5C,D). To assess the effects of LA on NOS in H9C2 cells, mRNA levels of the three isoforms of NOS in the HR model were measured by Western blotting and RT-PCR. Congruent with *in vivo* experiments, it was found that LA selectively increased transcription of eNOS in H9C2 cells following HR (Figure 5E), which was also observed in protein levels (Figures 5F,G). Overall, these data suggested that LA selectively promoted the expression of eNOS *in vivo* and *in vitro*.

### 3.6 LA Contributes to the Activation of the Nrf2/HO-1 Pathway and Nuclear Translocation of Nrf2 *in vivo* and *in vitro*

To further elucidate how LA regulates oxidative stress, the role of Nrf2 signaling, a transcriptional coactivator that mediates anti-oxidative gene expression in the heart, was investigated (Dai et al., 2020). Immunoblot analysis revealed that MI/R largely contributed to the protein downregulation of Nrf2 and HO-1 in the heart; however, LA treatment restored the expression of the Nrf2/

HO-1 pathway (Figures 6A,B). The transcription activity of Nrf2 is reported to depend largely on the nuclear translocation of Nrf2 (Silva-Islas and Maldonado, 2018). Hence, the nuclear translocation of Nrf2 after MI/R and LA treatment was explored. IHC analysis revealed that MI/R reduced the levels of Nrf2 in the nuclear, and LA pretreatment partly restored the nuclear translocation of Nrf2 in the heart (Figures 6C,D). Subsequently, nuclear protein from fresh heart tissue was isolated and Western blotting showed that LA triggered nuclear levels of Nrf2 in response to MI/R (Figure 6E). Furthermore, the effects of LA on the Nrf2/HO-1 pathway *in vitro* were evaluated. Congruous with *in vivo* experiments, Western blotting showed that LA promoted the activation of the Nrf2/HO-1 pathway in H9C2 cells under HR (Figures 6F,G). Similarly, immunofluorescence of Nrf2 in H9C2 cells also showed that LA increased nuclear levels of Nrf2 in response to HR (Figure 6H). Additionally, Western blotting showed that LA promoted nuclear translocation of Nrf2 in H9C2 cells under HR (Figures 6I,J). In summary, these data suggested that LA contributed to the activation of Nrf2/HO-1 signaling and nuclear translocation of Nrf2 *in vivo* and *in vitro*.

### 3.7 LA-Mediated Activation of Nrf2/HO-1 Pathway Depends on the Phosphorylation of AMPKα

Previous studies reported that AMPK triggered phosphorylation of Nrf2 and promoted the transactivation of antioxidative genes (Matzinger et al., 2020). Herein, the effect of LA on the activation of AMPKα and phosphorylation of Nrf2 was further investigated. The results of Western blot showed that LA accelerated the activation and phosphorylation of AMPKα, which further resulted in phosphorylation of Nrf2 and activation of the Nrf2/HO-1 pathway *in vitro* (Figures 7A,B). To verify the role of Nrf2 and AMPKα in H9C2 cells, Nrf2 siRNA and DM, an inhibitor of AMPKα, were used to explore the function of

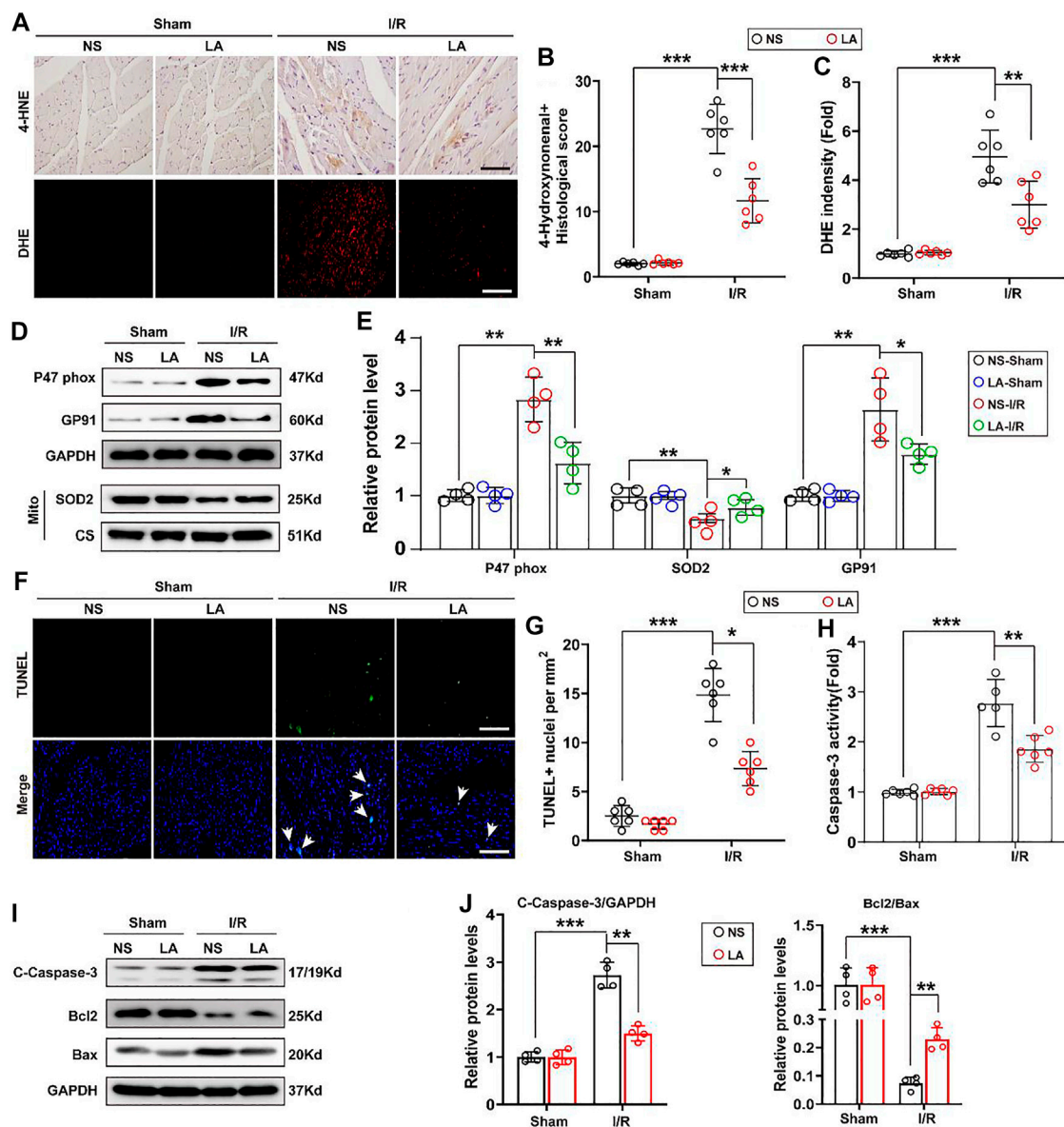


**FIGURE 3 |** LA attenuates oxidative stress and apoptosis following MI/R operation in heart. LA and NS pretreated mice were subjected to MI/R operation or sham, and then hearts were harvested for histology and molecular analysis (A–C). Representative immunohistochemistry of 4-hydroxynonenal and DHE staining in hearts, and intensity analysis ( $n = 6$ ). Scale bar: 100  $\mu$ m (D,E). Representative western blot and analysis of p47 phox, SOD2 and GP91 in hearts, normalized to GAPDH ( $n = 4$ ) (F,G). Representative TUNEL and positive cells analysis in hearts ( $n = 6$ ). Scale bar: 100  $\mu$ m (H). Caspase-3 activity was tested in heart tissues ( $n = 6$ ) (I,J). Representative western blot and analysis of cleaved-caspase-3 (C-caspase-3), Bax and Bcl2 in hearts, normalized to GAPDH ( $n = 4$ ) (I,J). Data are presented as the mean  $\pm$  SEM, with each point representing a mouse. \* indicates  $p < 0.05$ , \*\* indicates  $p < 0.01$ , \*\*\* indicates  $p < 0.001$ .

AMPK $\alpha$ /Nrf2 in LA-mediated effects. We firstly tested ROS production in H9C2 cells using the DCFH-DA probe and found that LA-mediated blockage of ROS production was abolished by silencing Nrf2 or inhibiting AMPK $\alpha$  in H9C2 cells under HR (Figures 7C,D and Supplementary Figure S7A–D). Similarly, Western blotting revealed that inhibition of AMPK $\alpha$  decreased phosphorylated-modification and nuclear translocation of Nrf2 in H9C2 cells under HR (Figures 7E–G) and blockage of AMPK $\alpha$  countered LA-mediated upregulation of eNOS in response to HR (Supplementary Figure S7E,F). Overall,

these data indicated that LA-mediated activation of Nrf2/HO-1 signaling and nuclear translocation of Nrf2 depended on the phosphorylation of AMPK $\alpha$ .

## 4 DISCUSSION

Morbidity and mortality from AMI remain high, and reperfusion strategies are the current standard therapy for AMI. However, MI/R injury leads to increased oxidative stress and apoptosis, which



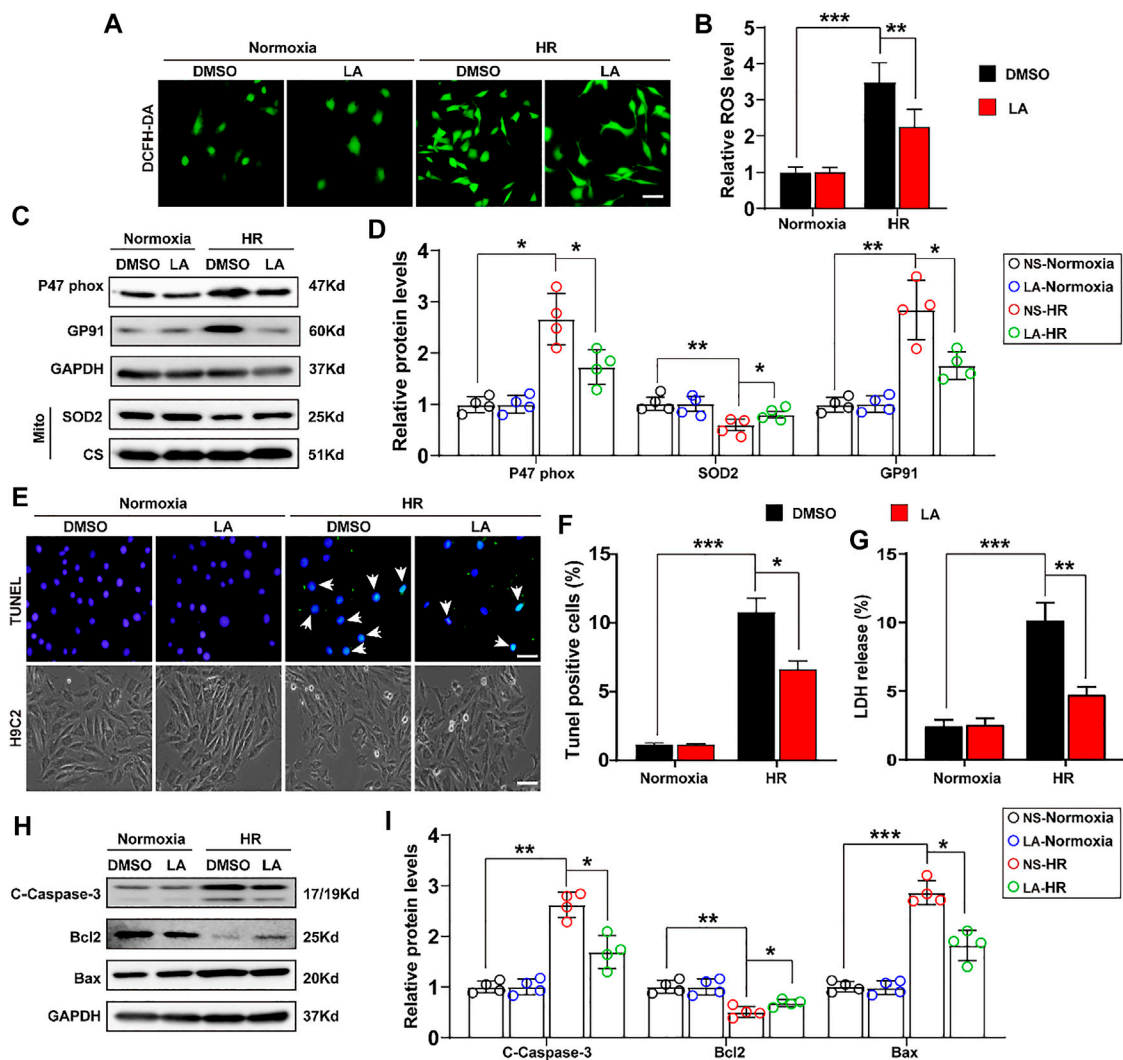


**FIGURE 4 |** LA counters oxidative stress and apoptosis in hypoxia reoxygenation (HR) in H9C2 cells. LA and DMSO pretreated H9C2 cells were subjected to HR or Normoxia (A,B). Representative ROS levels of H9C2 cells were measured by incubating with DCFH-DA probe, and then analysis fluorescence intensity, Scar bar: 50  $\mu$ m (C,D). Representative western blot and analysis of p47 phox, SOD2 and GP91 in H9C2 cells, normalized to GAPDH ( $n = 4$ ) (E,F). Representative TUNEL and cell morphology, and positive cells analysis in H9C2 cells, Scar bar: 50  $\mu$ m (G). LDH release was detected by LDH assay kits (H-I). Representative western blot and analysis of cleaved-caspase-3 (C-caspase-3), Bax and Bcl2 in H9C2 cells, normalized to GAPDH ( $n = 4$ ) (I). Data are presented as the mean  $\pm$  SEM, with each point representing a mouse. \* indicates  $p < 0.05$ , \*\* indicates  $p < 0.01$ , \*\*\* indicates  $p < 0.001$ .

further contribute to cellular injury, exacerbating the final infarct size (Toldo et al., 2018). Myocardial infarct size is a key factor of prognosis in patients with AMI. Therefore, cardioprotective strategies aim to reduce the infarct size (Heusch, 2020). In addition, LA has been considered as a potential antioxidant and anti-apoptotic drug (Kang et al., 2021). Herein, we found that LA pretreatment alleviated oxidative stress and apoptosis and improved cardiac function in the MI/R injury mouse model. LA may yield novel interventional strategies attenuating reperfusion injury in AMI. Lithospermic acid (LA) is a catechol derivative extracted from *Salvia miltiorrhiza*, which is a traditional Chinese herb widely used to treat multiple disorders (Shih et al., 2019). Liu et al. showed that LA is an oxidase inhibitor that strongly exerts anti-inflammatory and hypouricemic effects (Liu et al., 2008).

Izabela et al. demonstrated that LA exhibited cytotoxicity against MCF-7 cell lines and suppressed breast cancer growth and metastasis (Berdowska et al., 2013). Furthermore, previous clinical trials showed that LA injection improved coronary heart diseases angina pectoris in a clinical trial (Zhang et al., 2006). The current study found that LA prevented cardiac dysfunction in MI/R injury, and may provide a potential therapeutic strategy for AMI treatment.

Recently, oxidative stress has been implicated in heart failure in different sources of stress and characterized by overproduction of ROS relative to anti-oxidant defenses (van der Pol et al., 2019; Aimò et al., 2020). Moreover, increased production of ROS caused cellular dysfunction such as lipid peroxidation, and increased DNA damage, resulting in cell death (Seddon et al., 2007). In the present study, LA significantly blocked oxidative



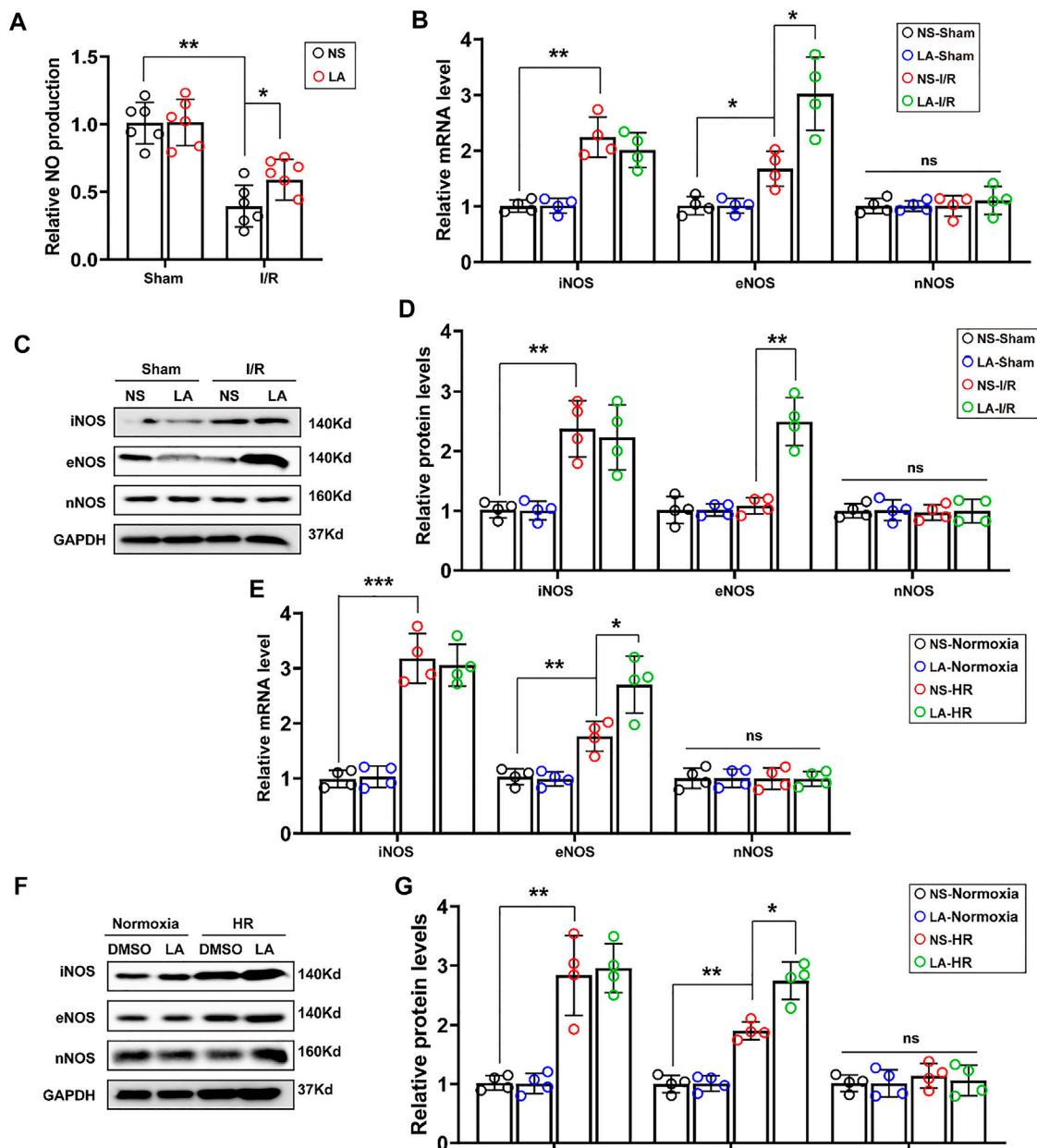


**FIGURE 5 |** LA promotes expression of eNOS *in vivo* and *in vitro* (A). NO production in the indicated groups 24 h post-MI/R operation ( $n = 6$ ) (B). The mRNA expression levels of iNOS, eNOS and nNOS in the indicated groups 24 h post-MI/R operation ( $n = 4$ ). Normalized to GAPDH (C,D). Representative western blot and analysis of iNOS, eNOS and nNOS in hearts following MI/R or sham, normalized to GAPDH ( $n = 4$ ) (E). The mRNA expression levels of iNOS, eNOS and nNOS in LA or DMSO pretreated H9C2 cells with or without HR (F,G). Representative western blot and analysis of iNOS, eNOS and nNOS in H9C2 cells, normalized to GAPDH ( $n = 4$ ). Data are presented as the mean  $\pm$  SEM, with each point representing a mouse or a cell sample. \* indicates  $p < 0.05$ , \*\* indicates  $p < 0.01$ , \*\*\* indicates  $p < 0.001$ , ns indicated no significance.

stress in the MI/R mouse model. Besides, as an important free radical, NO is synthesized by several NOS, and three isoforms of NOS are produced in the heart (Tang et al., 2014). Interestingly, both iNOS and eNOS were upregulated, and eNOS was unchanged in the MI/R heart. However, LA pretreatment increased eNOS but not iNOS or nNOS levels. Our previous study suggested that eNOS/Nrf2 pathway regulates pressure overload-induced cardiac remodeling (Liu et al., 2019). In addition, previous studies reported that the

transcription activity of Nrf2 depends largely on the nuclear translocation of Nrf2 (Silva-Islas and Maldonado, 2018). Therefore, the effects of Nrf2 signaling on LA-mediated cardioprotection in MI/R injury were investigated. As anticipated, LA promoted the Nrf2/HO-1 pathway and contributed to the nuclear translocation of Nrf2 *in vivo* and *in vitro*.

As a member of the serine/threonine (Ser/Thr) kinase group, AMPK is widely distributed in various organs (Jiang et al., 2018).

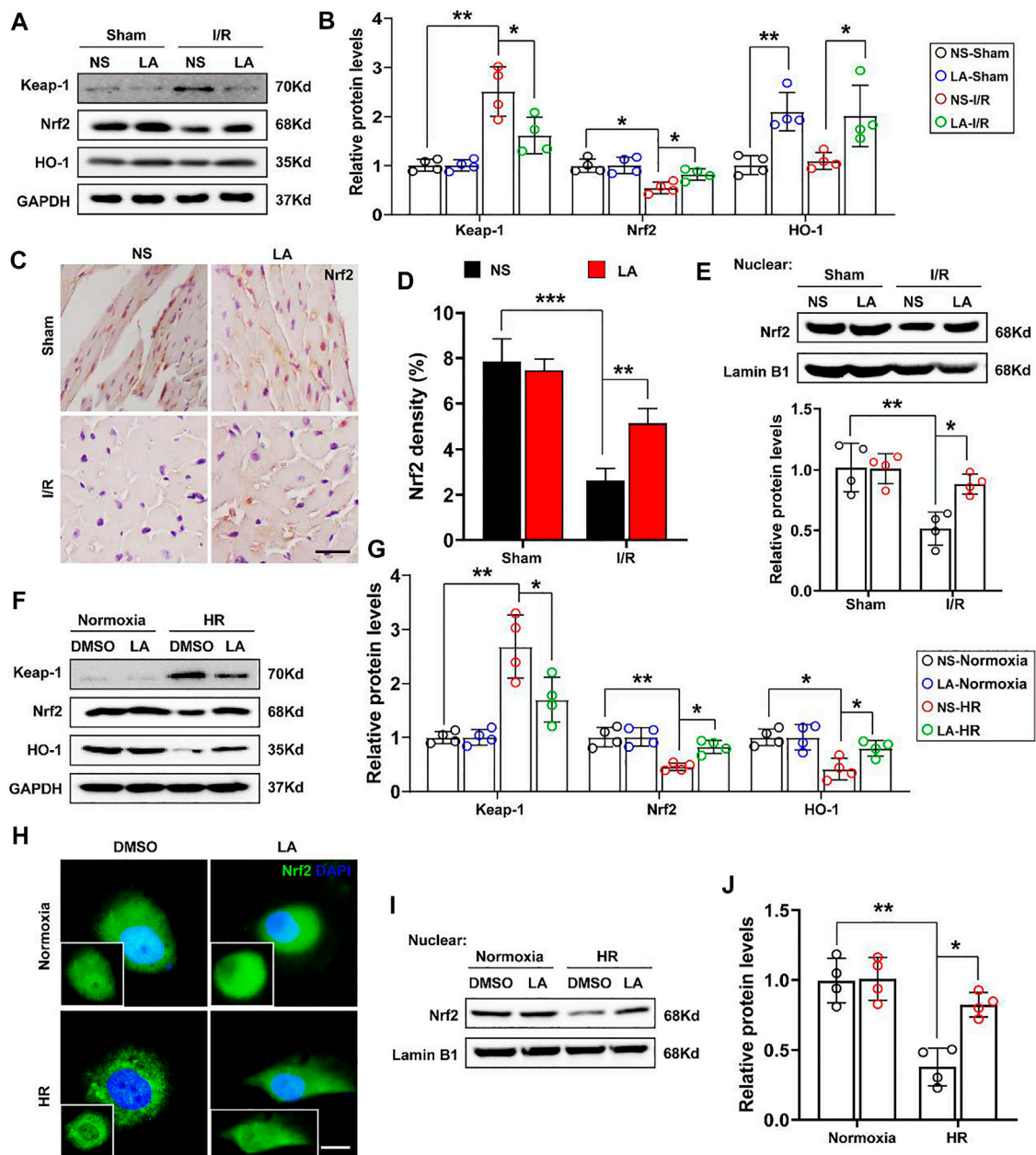


**FIGURE 6** | LA contributes to activation of Nrf2/HO-1 pathway and nuclear translocation of Nrf2 *in vivo* and *in vitro* (**A,B**). Representative western blot and analysis of Keap-1, Nrf2 and HO-1 in hearts following MI/R or sham, normalized to GAPDH ( $n = 4$ ) (**C,D**). Representative immunohistochemistry and density analysis of Nrf2 in heart tissues ( $n > 25$  from 3 mice per group). Scar bar: 100  $\mu$ m (**E**). Representative western blot and analysis of Nrf2 in nuclear from fresh heart tissues, normalized to Lamin B1 ( $n = 4$ ) (**F,G**). Representative western blot and analysis of Keap-1, Nrf2 and HO-1 in H9C2 cells, normalized to GAPDH ( $n = 4$ ) (**H**). Representative immunofluorescence of Nrf2 in LA or DMSO pretreated H9C2 cells with or without HR. Scar bar: 10  $\mu$ m (**I,J**). Representative western blot and analysis of Nrf2 in nuclear from H9C2 cells, normalized to Lamin B1 ( $n = 4$ ). Data are presented as the mean  $\pm$  SEM, with each point representing a mouse or a cell sample. \* indicates  $p < 0.05$ , \*\* indicates  $p < 0.01$ , \*\*\* indicates  $p < 0.001$ .

AMPK is closely associated with cellular metabolism and energy status, which is characterized by increased AMP/ATP and ADP/ATP ratios (Lin and Hardie, 2018). In addition, as a key controller of cellular homeostasis, AMPK plays a critical role in cardiovascular disease, diabetes and cancer (Qi and Young, 2015). A recent study suggested that AMPK-eNOS signaling

regulated endothelial dysfunction and hypertension in the heart (Cheng et al., 2020). Moreover, AMPK $\alpha$  has been reported to be highly expressed in the heart (Fan et al., 2018). Therefore, the activation and phosphorylation of AMPK $\alpha$  were assessed. It was found that LA promoted phosphorylation of AMPK $\alpha$  and Nrf2 *in vivo* and *in vitro*, which corresponds with a

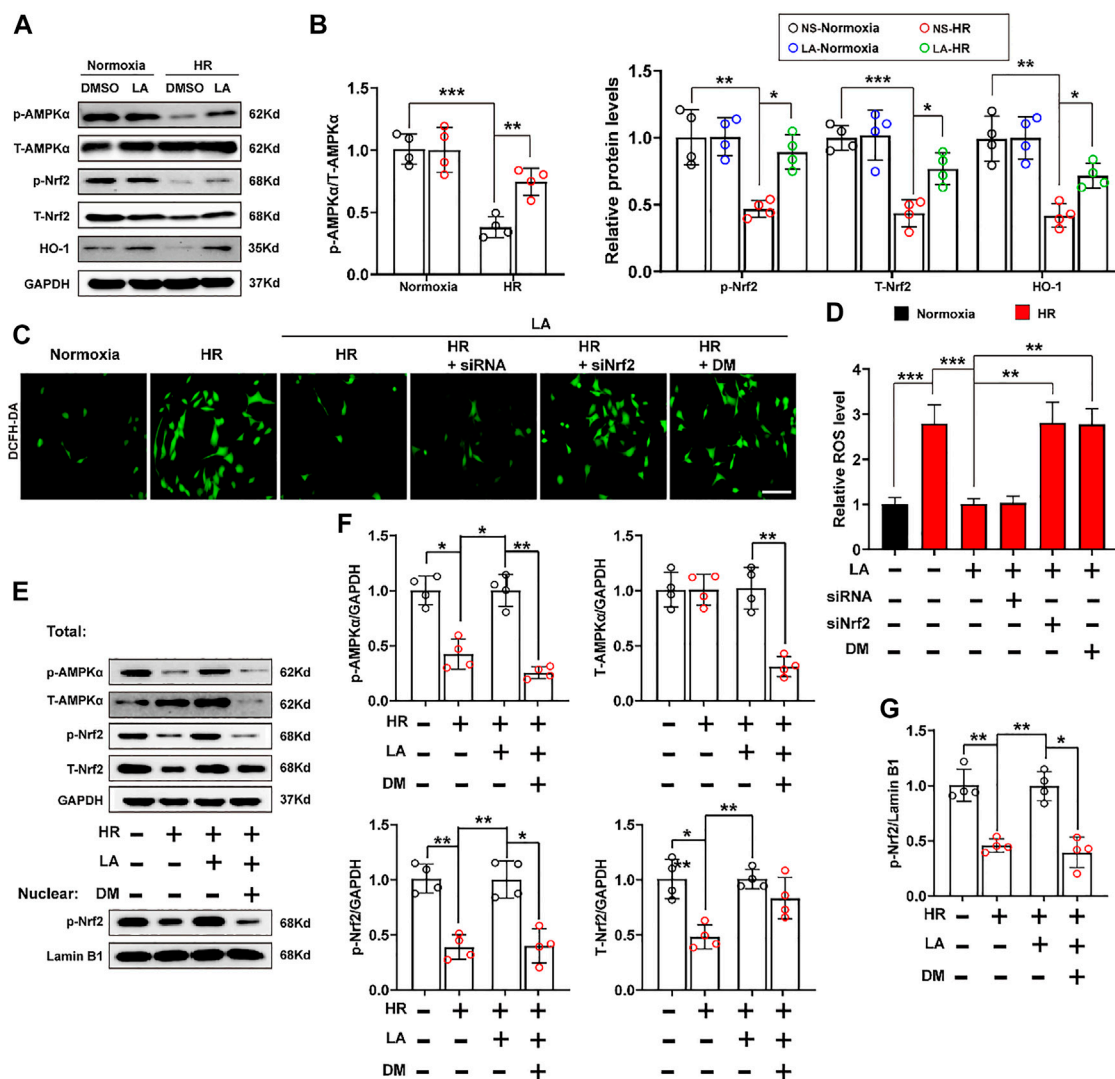


**FIGURE 7 |** LA-mediated activation of Nrf2/HO-1 pathway depends on phosphorylation of AMPK $\alpha$ . Nrf2 siRNA and dorsomorphin, an inhibitor of AMPK $\alpha$ , LA and DMSO pretreated H9C2 cells were subjected to HR or Normoxia (A,B). Representative western blot and analysis of p-AMPK $\alpha$ , AMPK $\alpha$ , p-Nrf2, Nrf2 and HO-1 in H9C2 cells, normalized to GAPDH ( $n = 4$ ) (C,D). Representative ROS levels of H9C2 cells were measured by incubating with DCFH-DA probe, and then analysis fluorescence intensity. Scale bar: 50  $\mu$ m (E,G). (E) and (F). Representative western blot and analysis of p-AMPK $\alpha$ , AMPK $\alpha$ , p-Nrf2, Nrf2 and HO-1 in H9C2 cells, normalized to GAPDH ( $n = 4$ ). (E) and (G). Representative western blot and analysis of p-Nrf2 in nuclear from H9C2 cells, normalized to Lamin B1 ( $n = 4$ ). Data are presented as the mean  $\pm$  SEM, with each point representing a mouse or a cell sample. \* indicates  $p < 0.05$ , \*\* indicates  $p < 0.01$ , \*\*\* indicates  $p < 0.001$ .

recent study showing that AMPK triggered phosphorylation of Nrf2 and promoted transactivation of antioxidative genes (Matzinger et al., 2020). Furthermore, we demonstrated that LA-mediated activation of Nrf2/HO-1 pathway and nuclear translocation of Nrf2 depended on the phosphorylation of AMPK $\alpha$ . Although LA countered oxidative stress and apoptosis after MI/R by activating AMPK $\alpha$ /Nrf2 and eNOS pathway, evidence on direct interaction between AMPK $\alpha$  and Nrf2 warrants further exploration. Moreover, how AMPK $\alpha$  regulates eNOS should be further investigated.

In summary, this study demonstrates that LA improves cardiac function and attenuates myocardial injury in mice. It

also suppresses oxidative stress and apoptosis following hypoxia-reoxygenation. Mechanistically, LA promotes the activation of the eNOS and Nrf2/HO-1 pathway by enhancing phosphorylation of AMPK $\alpha$ , providing a novel therapeutic strategy for reperfusion in AMI patients.

## DATA AVAILABILITY STATEMENT

The original contributions presented in the study are included in the article/Supplementary Material further inquiries can be directed to the corresponding author.

## ETHICS STATEMENT

The animal study was reviewed and approved by the Renmin Hospital of Wuhan University.

## AUTHOR CONTRIBUTIONS

MZ and QT contributed to the conception and design of the experiments; SX, XZ, SC, and SW carried out the experiments; LW revised the document. WD analyzed the experimental results; YX and WS wrote the manuscript.

## FUNDING

This work was supported by grants from the National Natural Science Foundation of China (Nos: 81860080,

81500184 and 81700254); the Key Project of the National Natural Science Foundation (No. 81530012); Development Center for Medical Science and Technology National Health and Family Planning Commission of the People's Republic of China (The prevention and control project of cardiovascular disease,2016ZX-008-01); National Key R and D Program of China (2018YFC1311300); National Major Scientific Instrument and Equipment Development Projects,2013YQ03092306; the Fundamental Research Funds for the Central Universities (2042018kf1032).

## SUPPLEMENTARY MATERIAL

The Supplementary Material for this article can be found online at: <https://www.frontiersin.org/articles/10.3389/fphar.2021.794982/full#supplementary-material>

## REFERENCES

- Aimo, A., Castiglione, V., Borrelli, C., Saccaro, L. F., Franzini, M., Masi, S., et al. (2020). Oxidative Stress and Inflammation in the Evolution of Heart Failure: From Pathophysiology to Therapeutic Strategies. *Eur. J. Prev. Cardiol.* 27 (5), 494–510. doi:10.1177/2047487319870344
- Berdowska, I., Zieliński, B., Fecka, I., Kulbacka, J., Saczko, J., and Gamian, A. (2013). Cytotoxic Impact of Phenolics from Lamiaceae Species on Human Breast Cancer Cells. *Food Chem.* 141 (2), 1313–1321. doi:10.1016/j.foodchem.2013.03.090
- Boo, Y. C. (2020). Natural Nrf2 Modulators for Skin Protection. *Antioxidants (Basel)* 9 (9). doi:10.3390/antiox9090812
- Buendia, I., Michalska, P., Navarro, E., Gameiro, I., Egea, J., and León, R. (2016). Nrf2-ARE Pathway: An Emerging Target against Oxidative Stress and Neuroinflammation in Neurodegenerative Diseases. *Pharmacol. Ther.* 157, 84–104. doi:10.1016/j.pharmthera.2015.11.003
- Chan, K. W., and Ho, W. S. (2015). Anti-oxidative and Hepatoprotective Effects of Lithospermic Acid against Carbon Tetrachloride-Induced Liver Oxidative Damage *In Vitro* and *In Vivo*. *Oncol. Rep.* 34 (2), 673–680. doi:10.3892/or.2015.4068
- Chen, J., Luo, Y., Wang, S., Zhu, H., and Li, D. (2019). Roles and Mechanisms of SUMOylation on Key Proteins in Myocardial Ischemia/reperfusion Injury. *J. Mol. Cell Cardiol.* 134, 154–164. doi:10.1016/j.yjmcc.2019.07.009
- Chen, Q. M., and Maltagliati, A. J. (2018). Nrf2 at the Heart of Oxidative Stress and Cardiac protection. *Physiol. Genomics* 50 (2), 77–97. doi:10.1152/physiolgenomics.00041.2017
- Cheng, L., Wang, L., Guo, M., He, J., Deng, Y., Liu, J., et al. (2020). Clinically Relevant High Levels of Human C-Reactive Protein Induces Endothelial Dysfunction and Hypertension by Inhibiting the AMPK-eNOS axis. *Clin. Sci. (Lond)* 134 (13), 1805–1819. doi:10.1042/CS20200137
- Crane, B. R., Sudhamsu, J., and Patel, B. A. (2010). Bacterial Nitric Oxide Synthases. *Annu. Rev. Biochem.* 79, 445–470. doi:10.1146/annurev-biochem-062608-103436
- Dai, X., Yan, X., Wintergerst, K. A., Cai, L., Keller, B. B., and Tan, Y. (2020). Nrf2: Redox and Metabolic Regulator of Stem Cell State and Function. *Trends Mol. Med.* 26 (2), 185–200. doi:10.1016/j.molmed.2019.09.007
- Fan, D., Yang, Z., Yuan, Y., Wu, Q. Q., Xu, M., Jin, Y. G., et al. (2017). Sesamin Prevents Apoptosis and Inflammation after Experimental Myocardial Infarction by JNK and NF- $\kappa$ B Pathways. *Food Funct.* 8 (8), 2875–2885. doi:10.1039/c7fo00204a
- Fan, Y., Lu, H., Liang, W., Garcia-Barrio, M. T., Guo, Y., Zhang, J., et al. (2018). Endothelial TFEB (Transcription Factor EB) Positively Regulates Postischemic Angiogenesis. *Circ. Res.* 122 (7), 945–957. doi:10.1161/CIRCRESAHA.118.312672
- Guo, X., Hong, S., He, H., Zeng, Y., Chen, Y., Mo, X., et al. (2020). NF $\kappa$ B Promotes Oxidative Stress-Induced Necrosis and Ischemia/reperfusion Injury by Inhibiting Nrf2-ARE Pathway. *Free Radic. Biol. Med.* 159, 125–135. doi:10.1016/j.freeradbiomed.2020.07.031
- Guo, Z., and Mo, Z. (2020). Keap1-Nrf2 Signaling Pathway in Angiogenesis and Vascular Diseases. *J. Tissue Eng. Regen. Med.* 14 (6), 869–883. doi:10.1002/term.3053
- Heusch, G. (2020). Myocardial Ischaemia-Reperfusion Injury and Cardioprotection in Perspective. *Nat. Rev. Cardiol.* 17 (12), 773–789. doi:10.1038/s41569-020-0403-y
- Huang, K. F., Ma, K. H., Jhap, T. Y., Liu, P. S., and Chueh, S. H. (2019). Ultraviolet B Irradiation Induced Nrf2 Degradation Occurs via Activation of TRPV1 Channels in Human Dermal Fibroblasts. *Free Radic. Biol. Med.* 141, 220–232. doi:10.1016/j.freeradbiomed.2019.06.020
- Jennings, R. B. (2013). Historical Perspective on the Pathology of Myocardial Ischemia/reperfusion Injury. *Circ. Res.* 113 (4), 428–438. doi:10.1161/CIRCRESAHA.113.300987
- Jia, Q., Zhu, R., Tian, Y., Chen, B., Li, R., Li, L., et al. (2019). Salvia Miltiorrhiza in Diabetes: A Review of its Pharmacology, Phytochemistry, and Safety. *Phytomedicine* 58, 152871. doi:10.1016/j.phymed.2019.152871
- Jiang, S., Li, T., Ji, T., Yi, W., Yang, Z., Wang, S., et al. (2018). AMPK: Potential Therapeutic Target for Ischemic Stroke. *Theranostics* 8 (16), 4535–4551. doi:10.1371/journal.pone.0098232
- Jin, C. J., Yu, S. H., Wang, X. M., Woo, S. J., Park, H. J., Lee, H. C., et al. (2014). The Effect of Lithospermic Acid, an Antioxidant, on Development of Diabetic Retinopathy in Spontaneously Obese Diabetic Rats. *PLoS One* 9 (6), e98232. doi:10.1371/journal.pone.0098232
- Kang, T. K., Le, T. T., Kim, K.-A., Kim, Y.-J., Lee, W.-B., and Jung, S. H. (2021). Roots of Lithospermum Erythrorhizon Promotes Retinal Cell Survival in Optic Nerve Crush-Induced Retinal Degeneration. *Exp. Eye Res.* 203, 108419. doi:10.1016/j.exer.2020.108419
- Lejay, A., Fang, F., John, R., Van, J. A., Barr, M., Thaveau, F., et al. (2016). Ischemia Reperfusion Injury, Ischemic Conditioning and Diabetes Mellitus. *J. Mol. Cell Cardiol.* 91, 11–22. doi:10.1016/j.yjmcc.2015.12.020
- Lin, S. C., and Hardie, D. G. (2018). AMPK: Sensing Glucose as Well as Cellular Energy Status. *Cell Metab.* 27 (2), 299–313. doi:10.1016/j.cmet.2017.10.009
- Lin, Y. L., Tsay, H. J., Lai, T. H., Tzeng, T. T., and Shiao, Y. J. (2015). Lithospermic Acid Attenuates 1-Methyl-4-Phenylpyridine-Induced Neurotoxicity by Blocking Neuronal Apoptotic and Neuroinflammatory Pathways. *J. Biomed. Sci.* 22, 37. doi:10.1186/s12929-015-0146-y
- Liu, C., Wu, Q. Q., Cai, Z. L., Xie, S. Y., Duan, M. X., Xie, Q. W., et al. (2019). Zingerone Attenuates Aortic Banding-Induced Cardiac Remodelling via Activating the eNOS/Nrf2 Pathway. *J. Cell Mol. Med.* 23 (9), 6466–6478. doi:10.1111/jcmm.14540



- Liu, X., Chen, R., Shang, Y., Jiao, B., and Huang, C. (2008). Lithospermic Acid as a Novel Xanthine Oxidase Inhibitor Has Anti-inflammatory and Hypouricemic Effects in Rats. *Chem. Biol. Interact.* 176 (2-3), 137–142. doi:10.1016/j.cbi.2008.07.003
- Lu, Y., Feng, Y., Liu, D., Zhang, Z., Gao, K., Zhang, W., et al. (2018). Thymoquinone Attenuates Myocardial Ischemia/Reperfusion Injury through Activation of SIRT1 Signaling. *Cell Physiol Biochem* 47 (3), 1193–1206. doi:10.1159/000490216
- Matzinger, M., Fischhuber, K., Pölöske, D., Mechtler, K., and Heiss, E. H. (2020). AMPK Leads to Phosphorylation of the Transcription Factor Nrf2, Tuning Transactivation of Selected Target Genes. *Redox Biol.* 29, 101393. doi:10.1016/j.redox.2019.101393
- Qi, D., and Young, L. H. (2015). AMPK: Energy Sensor and Survival Mechanism in the Ischemic Heart. *Trends Endocrinol. Metab.* 26 (8), 422–429. doi:10.1016/j.tem.2015.05.010
- Seddon, M., Looi, Y. H., and Shah, A. M. (2007). Oxidative Stress and Redox Signalling in Cardiac Hypertrophy and Heart Failure. *Heart* 93 (8), 903–907. doi:10.1136/hrt.2005.068270
- Shih, Y. E., Chen, C. H., Lin, N. H., and Tzen, J. T. C. (2019). Development of Indirect Competitive ELISA for Lithospermic Acid B of *Salvia Miltiorrhiza* with its Specific Antibodies Generated via Artificial Oil Bodies. *Molecules* 24 (10), 1952. doi:10.3390/molecules24101952
- Silva-Islas, C. A., and Maldonado, P. D. (2018). Canonical and Non-canonical Mechanisms of Nrf2 Activation. *Pharmacol. Res.* 134, 92–99. doi:10.1016/j.phrs.2018.06.013
- Sun, W., Wang, Z., Sun, M., Huang, W., Wang, Y., and Wang, Y. (2021). Aloin Antagonizes Stimulated Ischemia/reperfusion-Induced Damage and Inflammatory Response in Cardiomyocytes by Activating the Nrf2/HO-1 Defense Pathway. *Cell Tissue Res* 384, 735–744. doi:10.1007/s00441-020-03345-z
- Tang, L., Wang, H., and Ziolo, M. T. (2014). Targeting NOS as a Therapeutic Approach for Heart Failure. *Pharmacol. Ther.* 142 (3), 306–315. doi:10.1016/j.pharmthera.2013.12.013
- Toldo, S., Mauro, A. G., Cutter, Z., and Abbate, A. (2018). Inflammasome, Pyroptosis, and Cytokines in Myocardial Ischemia-Reperfusion Injury. *Am. J. Physiol. Heart Circ. Physiol.* 315 (6), H1553–H1568. doi:10.1152/ajpheart.00158.2018
- van der Pol, A., van Gilst, W. H., Voors, A. A., and van der Meer, P. (2019). Treating Oxidative Stress in Heart Failure: Past, Present and Future. *Eur. J. Heart Fail.* 21 (4), 425–435. doi:10.1002/ehf.1320
- Vashi, R., and Patel, B. M. (2020). NRF2 in Cardiovascular Diseases: a Ray of Hope! *J. Cardiovasc. Trans. Res.* 14, 573–586. doi:10.1007/s12265-020-10083-8
- Velusamy, P., Mohan, T., Ravi, D. B., Kishore Kumar, S. N., Srinivasan, A., Chakrapani, L. N., et al. (2020). Targeting the Nrf2/ARE Signalling Pathway to Mitigate Isoproterenol-Induced Cardiac Hypertrophy: Plausible Role of Hesperetin in Redox Homeostasis. *Oxidative Med. Cell Longevity* 2020, 1–13. doi:10.1155/2020/9568278
- Wang, L., Ma, R., Liu, C., Liu, H., Zhu, R., Guo, S., et al. (2017). *Salvia Miltiorrhiza*: A Potential Red Light to the Development of Cardiovascular Diseases. *Curr. Pharm. Des.* 23 (7), 1077–1097. doi:10.2174/1381612822666161010105242
- Wu, Q. Q., Xiao, Y., Duan, M. X., Yuan, Y., Jiang, X. H., Yang, Z., et al. (2018). Aucubin Protects against Pressure Overload-Induced Cardiac Remodelling via the  $\beta_3$ -Adrenoceptor-Neuronal NOS Cascades. *Br. J. Pharmacol.* 175 (9), 1548–1566. doi:10.1111/bph.14164
- Zhang, Q., Liu, A. D., and Huang, Y. S. (2006). Clinical Non-inferiority Trial on Treatment of Coronary Heart Disease Angina Pectoris of Xin-Blood Stasis Syndrome Type with Lyophilized *Salvia* Salt of Lithospermic Acid Powder for Injection. *Chin. J. Integr. Med.* 12 (1), 12–18. doi:10.1007/BF02857423

**Conflict of Interest:** The authors declare that the research was conducted in the absence of any commercial or financial relationships that could be construed as a potential conflict of interest.

**Publisher's Note:** All claims expressed in this article are solely those of the authors and do not necessarily represent those of their affiliated organizations, or those of the publisher, the editors and the reviewers. Any product that may be evaluated in this article, or claim that may be made by its manufacturer, is not guaranteed or endorsed by the publisher.

Copyright © 2021 Zhang, Wei, Xie, Xing, Shi, Zeng, Chen, Wang, Deng and Tang. This is an open-access article distributed under the terms of the Creative Commons Attribution License (CC BY). The use, distribution or reproduction in other forums is permitted, provided the original author(s) and the copyright owner(s) are credited and that the original publication in this journal is cited, in accordance with accepted academic practice. No use, distribution or reproduction is permitted which does not comply with these terms.





# Oxytocin Protects Against Isoproterenol-Induced Cardiac Hypertrophy by Inhibiting PI3K/AKT Pathway via a lncRNA GAS5/miR-375-3p/KLF4-Dependent Mechanism

## OPEN ACCESS

### Edited by:

Xianwei Wang,  
Xinxiang Medical University, China

### Reviewed by:

Lu Gao,  
The First Affiliated Hospital of  
Zhengzhou University, China  
Yong Zhang,  
Harbin Medical University, China  
Panxia Wang,  
Sun Yat-sen University, China

### \*Correspondence:

Jinqiao Qian  
qianjinqiao@126.com

<sup>†</sup>These authors have contributed  
equally to this work

### Specialty section:

This article was submitted to  
Cardiovascular and Smooth Muscle  
Pharmacology,  
a section of the journal  
Frontiers in Pharmacology

**Received:** 28 August 2021

**Accepted:** 11 November 2021

**Published:** 03 December 2021

### Citation:

Yang Y, Wang Z, Yao M, Xiong W,  
Wang J, Fang Y, Yang W, Jiang H,  
Song N, Liu L and Qian J (2021)  
Oxytocin Protects Against  
Isoproterenol-Induced Cardiac  
Hypertrophy by Inhibiting PI3K/AKT  
Pathway via a lncRNA GAS5/miR-375-  
3p/KLF4-Dependent Mechanism.  
Front. Pharmacol. 12:766024.  
doi: 10.3389/fphar.2021.766024

Yuqiao Yang<sup>1†</sup>, Zhuoran Wang<sup>1†</sup>, Mengran Yao<sup>1†</sup>, Wei Xiong<sup>1</sup>, Jun Wang<sup>1</sup>, Yu Fang<sup>1</sup>,  
Wei Yang<sup>1</sup>, Haixia Jiang<sup>1</sup>, Ning Song<sup>1</sup>, Lan Liu<sup>2</sup> and Jinqiao Qian<sup>1\*</sup>

<sup>1</sup>Department of Anesthesiology, First Affiliated Hospital of Kunming Medical University, Kunming, China, <sup>2</sup>Department of Pathology, Kunming Medical University, Kunming, China

Cardiac hypertrophy is caused by cardiac volume or pressure overload conditions and ultimately leads to contractile dysfunction and heart failure. Oxytocin (OT), an endocrine nonapeptide, has been identified as a cardiovascular homeostatic hormone with anti-hypertrophic effects. However, the underlying mechanism remains elusive. In this study, we aimed to investigate the role and mechanism of OT in cardiac hypertrophy. The rats with cardiac hypertrophy induced by isoproterenol (ISO) were treated with or without oxytocin. Cardiac functional parameters were analyzed by echocardiography. The changes in cell surface area were observed using wheat germ agglutinin (WGA) or immunofluorescence staining. The expressions of cardiac hypertrophy markers (B-Natriuretic Peptide, BNP and  $\beta$ -myosin heavy chain,  $\beta$ -MHC), long non-coding RNA Growth (LcRNA) Arrest-Specific transcript 5 (lncRNA GAS5), miR-375-3p, and Kruppel-like factor 4 (*Klf4*) were detected by qRT-PCR. KLF4 protein and PI3K/AKT pathway related proteins were detected by Western blot. The interactions among lncRNA GAS5, miR-375-3p, and *Klf4* were verified by dual-luciferase reporter assays. The findings showed that OT significantly attenuated cardiac hypertrophy, increased expressions of lncRNA GAS5 and KLF4, and decreased miR-375-3p expression. *In vitro* studies demonstrated that either knock-down of lncRNA GAS5 or *Klf4*, or over-expression of miR-375-3p blunted the anti-hypertrophic effects of OT. Moreover, down-regulation of lncRNA GAS5 promoted the expression of miR-375-3p and inhibited KLF4 expression. Similarly, over-expression of miR-375-3p decreased the

**Abbreviations:** OT, oxytocin; ISO, isoproterenol; microRNA, miRNA; lncRNA, long non-coding RNA; GAS5, Growth Arrest-Specific transcript 5; KLF4, Kruppel like factor 4; PI3K, phosphatidylinositol 3-kinase; AKT, Protein Kinase B; BNP, B-Natriuretic Peptide;  $\beta$ -MHC,  $\beta$ -myosin heavy chain; HF, heart failure; AngII, angiotensin II; OXTR, oxytocin receptor; I/R, ischemia-reperfusion; ncRNAs, non-coding RNAs; H&E, hematoxylin-eosin; NRCMs, Neonatal rat cardiomyocytes; CMs, Cultured cardiomyocytes; LV, left ventricular; LVPWd, left ventricular posterior wall thickness at end-diastole; LVPWs, left ventricular posterior wall thickness at end-systole; LVIDd, left ventricular internal diameter at end-diastole; LVIDs, left ventricular internal diameter at end-systole; LVEF, left ventricular ejection fraction; LVFS, left ventricular fractional shortening; WGA, wheat germ agglutinin.

expression of KLF4. Dual-luciferase reporter assays validated that lncRNA GAS5 could sponge miR-375-3p and *Klf4* was a direct target gene of miR-375-3p. In addition, OT could inactivate PI3K/AKT pathway. The functional rescue experiments further identified OT regulated PI3K/AKT pathway through lncRNA GAS5/miR-375-3p/KLF4 axis. In summary, our study demonstrates that OT ameliorates cardiac hypertrophy by inhibiting PI3K/AKT pathway via lncRNA GAS5/miR-375-3p/KLF4 axis.

**Keywords:** oxytocin, cardiac hypertrophy, lncRNA GAS5, miR-375-3p, KLF4, PI3K/AKT

## INTRODUCTION

The prevalence of heart failure (HF) is increasing at an alarming rate worldwide (Benjamin et al., 2019). Pathological cardiac hypertrophy is an independent predictor of HF, commonly induced by hypertension, myocardial injury, valvular heart diseases or excessive neurohumoral stimulation. It is characterized by myocardial fibrosis, apoptosis and necrosis, leading to cardiac dysfunction and consequently to heart failure (Azevedo et al., 2016). Alleviating pathological cardiac hypertrophy is of great importance to postpone the progression of heart failure. Although the current pharmaceutical therapies, such as angiotensin-converting enzyme inhibitors, angiotensin II (AngII) type 1 receptor antagonists, and  $\beta$ -adrenergic receptor blockers, exhibit some anti-hypertrophic effects (Mcnamara, 2008), the therapeutic effects are not satisfied in clinic practice.

Oxytocin (OT) is a pivotal cardiovascular homeostatic hormone with definite cardiovascular regulation and protection effects. Knowledge of the oxytocin and oxytocin receptor (OXTR) system present in heart tissue suggests an autocrine and paracrine roles of the hormone. Dozens of researches have delineated the cardioprotective effects of this endogenous hormone, including alleviation of ischemia-reperfusion (I/R) injury (Alizadeh et al., 2010; Gonzalez-Reyes et al., 2015; Polshakan et al., 2019), cardiomyocyte hypertrophy (Menaouar et al., 2014), myocardial infarction (Kobayashi et al., 2009), and diabetic cardiomyopathy (Plante et al., 2015), as well as mitigation of development of atherosclerosis (Wang et al., 2019). The cardioprotective properties of oxytocin make this endogenous hormone of special potential to be a “natural medicine” against cardiovascular diseases. However, due to lack of deep knowledge of its molecular mechanism, therapeutic potential of OT in treating cardiovascular disease is largely unexplored.

Enormous studies have corroborated that non-coding RNAs (ncRNAs) are quite indispensable epigenetic regulators which are closely related to the occurrence and development of cardiac hypertrophy (Jusic and Devaux, 2020; Zhu et al., 2021). MicroRNAs (miRNA) and long non-coding RNAs (lncRNAs) are well-known ncRNAs and implicated in the complex pathophysiological process of cardiac hypertrophy. In the nervous system, Almansoub et al. (2020) reported that miR-26a is epigenetically tuned by oxytocin to mediate the neuroprotective effects. Whether OT administration regulates ncRNAs in heart is still unknown. Although the beneficial effects of OT in the prevention of pathological cardiac

hypertrophy have been well documented (Menaouar et al., 2014; Plante et al., 2015; Garrott et al., 2017), the mechanisms responsible for these actions are unclear, especially the roles of non-coding RNAs (ncRNAs) in the effect.

lncRNA Growth Arrest-Specific transcript 5 (lncRNA GAS5) is identified as a novel regulator of hypertension-related vascular remodeling (Wang et al., 2016) and also closely associated with cardiac fibrosis and cardiomyocyte apoptosis, as evidenced by over-expression of lncRNA GAS5 significantly attenuates cardiac fibrosis (Liu et al., 2019) and cardiomyocyte apoptosis (Hao et al., 2018) induced by isoproterenol (ISO).

In our preliminary experiments, we detected that OT ameliorated cardiac hypertrophy induced by ISO along with lncRNA GAS5 remarkably upregulated, as well as miR-375-3p down-regulated. lncRNA GAS5 has been shown to bind to miR-375-3p by bioinformatic prediction. High expression of miR-375-3p has been found to be associated with cardiomyocyte hypertrophy and heart failure. Knock-down of miR-375-3p suppresses cardiomyocyte hypertrophy induced by AngII (Feng et al., 2019). Garikipati et al. (2017) demonstrated that therapeutic inhibition of miR-375 attenuates inflammatory response and cardiomyocyte death, as well as enhancement of angiogenesis and cardiac function in a mouse myocardial infarction model.

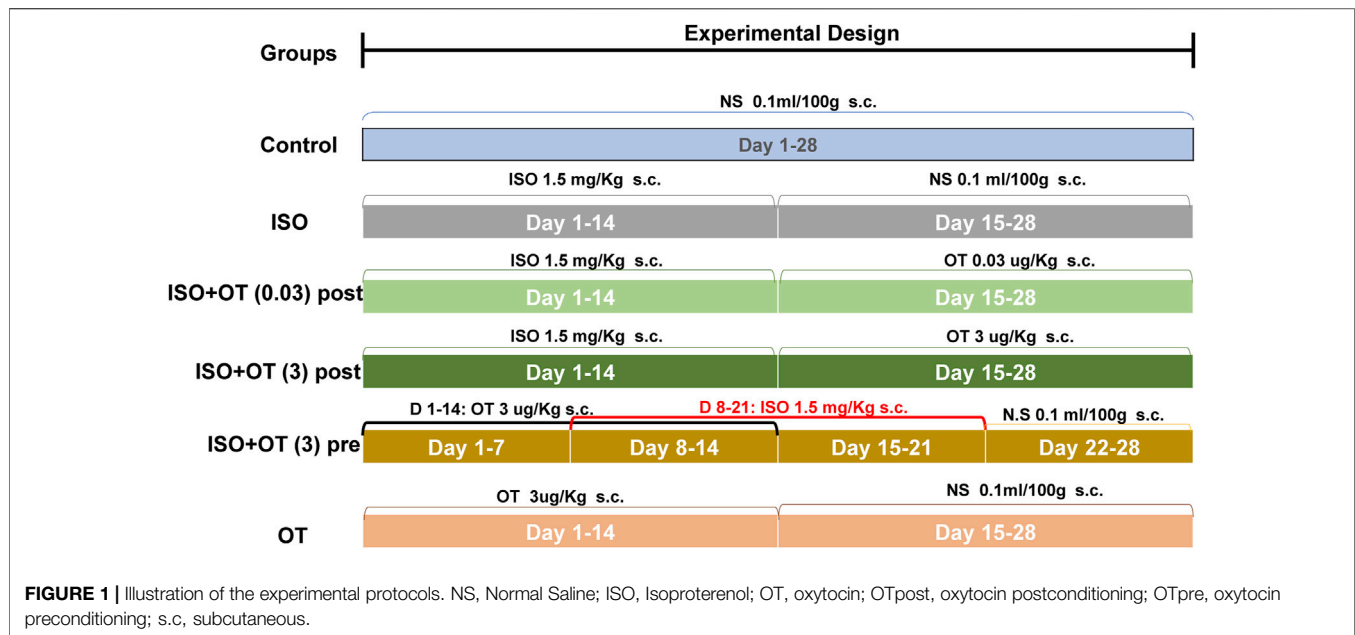
Kruppel-like factor 4 (KLF4) plays an important role in cardiac hypertrophy. Cardiomyocyte-specific knockout of KLF4 aggravates ISO-induced cardiac hypertrophy, which suggests that control of KLF4 is a potential therapeutic target for cardiac hypertrophy (Yoshida et al., 2014). Based on bioinformatic prediction, *Klf4* is one of the target gene of miR-375-3p.

Hence, in this study, we hypothesized that lncRNA GAS5 sequesters miR-375-3p to promote KLF4 expression, mediating the anti-hypertrophic actions of OT. We attempted to identify gene transcription changes and their functions that respond to the treatment of oxytocin in cardiac hypertrophy. Our results will provide insights into discovery of potential therapeutic targets for cardiac hypertrophy.

## MATERIALS AND METHODS

### Ethics Statement

In this study, all experimental procedures involving animals were approved by the Animal Care and Ethics Committee of Kunming Medical University (Kunming, China, Approval



number: No. Kmmu2020350). All animal experiments complied with the National Institutes of Health Guide for the Care and Use of Laboratory animals. Significant efforts were made to minimize the sufferings and the number of the rats used.

## Experimental Animals and Drug Administration Protocol

Male Sprague-Dawley (SD) rats weighing 220–250 g were purchased from Hunan SJA Laboratory Animal Co., Ltd., China. After 1 week acclimatization under laboratory conditions, a natural light cycle at a controlled temperature  $25 \pm 2^\circ\text{C}$  with food and water available ad libitum, the rats were randomly divided into six groups (eight rats/group) and treated as **Figure 1**. In brief, the control group received a daily subcutaneous (s.c) injection of normal saline (0.1 ml/100 g) for 28 days. The ISO group received a daily s.c injection of isoproterenol (1.5 mg/kg/day) at day 1 to day 14, followed by a daily s.c injection of normal saline (0.1 ml/100 g) for another 14 days. The ISO+OT postconditioning group received a daily s.c injection of isoproterenol (1.5 mg/kg) for the first 14 days, followed by a daily s.c injection of 0.03 and 3 ug/kg oxytocin acetate (purchased from MedChemExpress) for the second 14 days, respectively. In ISO+OT preconditioning group, oxytocin acetate (3 ug/kg) was administered subcutaneously for 7 days, followed by co-administration of oxytocin and ISO for 7 days, and ISO administration alone for another 7 days. The time interval of administration between oxytocin acetate and ISO was more than 8 h. OT group received a daily s.c injection of oxytocin acetate (3 ug/kg) for the first 14 days, followed by a daily s.c injection of normal saline (0.1 ml/100 g) for the second 14 days. The dose of oxytocin acetate was based on Plante's study (Plante et al., 2015). After 28-day treatment,

echocardiography examinations were performed to assess changes in cardiac morphology and functions. At the end of the study, all animals were anesthetized using isoflurane in a sealed glass jar and hearts excised. Heart weights were measured after the hearts were rinsed with ice-cold saline and dried with filter papers. Some heart samples were immediately stored in liquid nitrogen, while the other samples were fixed in 4% paraformaldehyde.

## Echocardiography

Transthoracic echocardiograms were performed on rats using a PHILIPS EPIQ7C ultrasound system for cardiology. Rats were isolated in a glass chamber, anesthetized by inhalation of 1.5 to 2% isoflurane mixed with 100% oxygen, and then supinely placed on an operational warming platform. The chest hair was depilated with a hair removal cream. M-mode cine loops were recorded and analyzed by high-frequency ultrasound imaging software to assess myocardial parameters and cardiac functions of left ventricle (LV), including left ventricular posterior wall thickness at end-diastole (LVPWd), left ventricular posterior wall thickness at end-systole (LVPWs), left ventricular internal diameter at end-diastole (LVIDd), left ventricular internal diameter at end-systole (LVIDs), left ventricular ejection fraction (LVEF), and left ventricular fractional shortening (LVFS).

## Histomorphology Analysis

Heart tissues were fixed in 4% paraformaldehyde for 48 h and then embedded in paraffin. The embedded hearts were cut into 5- $\mu\text{m}$  thickness sections, which were mounted on glass slide and stained with hematoxylin-eosin (H&E) and Masson's trichrome stainings. The sections were assessed under light microscopic fields by digital image analysis (BH-Z, Olympus Corporation, Tokyo, Japan).

The tissue sections underwent dewaxing and rehydrated, then be boiled in EDTA buffer for 10 min, and phosphate-buffered saline was used to washing the slides three times. Slides were incubated for 30 min with 5  $\mu$ M wheat germ agglutinin (WGA) dye (sigma) in the dark. The cell nucleus were stained with 4',6-diamidino-2-phenylindole (DAPI). The slides were sealed with antifade mounting medium and then observed using a fluorescence microscope (Olympus BX53).

Masson's trichrome staining was used to evaluate the myocardial fibrosis and WGA staining was used to evaluate the cardiomyocyte cross-sectional area. Myocardial fibrosis and cardiomyocyte cross-section areas were quantitatively analyzed with Image J software. Three images for each group and 40 cells for each image were randomly selected to determine the cross-section areas of cardiomyocyte. Five images for each group were randomly selected to measure the collagen content, which was presented by collagen volume fraction (collagen area/field area  $\times$  100%).

## Cell Culture and Treatment

Neonatal rat cardiomyocytes (NRCMs) were prepared from the hearts of 1- to 3-day-old SD rats. In brief, the hearts were excised from neonatal rats and washed in ice-cold phosphate buffered saline (PBS). Then the ventricles were finely separated and minced into 1–2 mm<sup>3</sup> pieces, which were digested in 0.25% trypsin at 37°C. The cell suspension was centrifuged and the pellets re-suspended and then transferred into Dulbecco's modified Eagle's medium (DMEM) with 10% fetal bovine serum (FBS) and 1% penicillin/streptomycin (P/S) culture medium. Fibroblast growth inhibitor (sciencell) was added to the cell suspension. Immunofluorescence staining was performed to detect the expression of cardiac troponin T (cTnT) and immunofluorescence microscopy to identify primary cardiomyocytes. The cultured cardiomyocytes (CMs) were treated with vehicle alone, ISO (10  $\mu$ M) alone or OT (10 nM) + ISO (10  $\mu$ M) respectively and further incubated for 24 h before harvest. In OT + ISO group, the cells were pretreated with OT for 30 min prior to stimulation with ISO.

## Cell Transfection

lncRNA GAS5 and *Klf4* gene knock-down were achieved using RNA interference. shRNA-GAS5, shRNA-*Klf4* and its corresponding scramble negative control siRNA (siNC) were purchased from TsingKe Biological Technology (Beijing, China). miR-375-3p mimics, miR-375-3p inhibitor and the corresponding negative control were synthesized by RIBOBIO (Guangzhou, China). The *Klf4* over-expression plasmid (pcDNA-*Klf4*) and empty pcDNA3.1 plasmid (control) were purchased from RIBOBIO (Guangzhou, China).

Plasmids were transfected into the cultured CMs using Lipofectamine 3000 (Cat: L3000-015 Invitrogen) according to the manufacturer's protocol. The transfection efficiency was detected by qRT-PCR and Western blotting. After 24-h transfection, the cells were incubated in DMEM medium supplemented with 10% FBS and 10  $\mu$ M ISO for 24 h followed by 30 min OT pretreatment.

## Real-Time Quantitative Polymerase Chain Reaction

Total RNA was extracted from the cultured CMs and LV tissues using Trizol reagent (Lifetech 15596026). Reversely transcribed to complementary DNA (cDNA) for miR-375-3p and lncRNA GAS5 and PCR amplification were performed using a Bulge-Loop™ miRNA qRT-PCR Starter Kit, a Bulge-Loop™ miRNA qRT-PCR Primer Set and a lncDETECT™ lncRNA qRT-PCR kit (RiboBio, Guangzhou, China) according to the manufacturer's instructions. U6 and  $\beta$ -actin served as internal normalized references for miR-375-3p and lncRNA GAS5, respectively. The relative mRNA levels of the target genes were evaluated by qRT-PCR with SYBR Green master mix (KAPA KK4601, Roche, United States) using the LightCycle 96 (Roche, United States). *In vitro* experiment, all qRT-PCR assays were conducted at least in triplicate. Fold-changes were calculated according to cycle quantitation (Ct) values with  $2^{-\Delta\Delta Ct}$  method. List of the primers used for qRT-PCR is presented in Table 1.

## Western Blot Analysis

NRCMs or tissue samples were lysed by radioimmunoprecipitation assay (RIPA) lysis buffer (Beyotime Biotechnology, China). The total protein concentrations were determined by BCA protein assay kit (Beyotime Biotechnology, China). A total of 30  $\mu$ g proteins were separated by 10% sodium dodecyl sulfate polyacrylamide gel electrophoresis (SDS-PAGE) and subsequently transferred onto polyvinylidene difluoride (PVDF) membranes. The blots were blocked with 5% non-fat milk and incubated overnight with the primary antibodies against BNP (1:500, rabbit #ab19645 abcam),  $\beta$ -MHC (1:1,000, rabbit #ab172967 abcam), KLF4 (1:1,000, rabbit #bs-1064R BLOSS), PI3K (1:1,000, rabbit #ab182651 abcam), p-PI3K (1:1,000, rabbit #205841-1-AP Proteintech), AKT1 (1:1,000, rabbit #bs-0115M BLOSS), p-AKT1 (1:1,000, rabbit #bs-0876R BLOSS),  $\beta$ -actin (1:1,000, rabbit #abmart P30002) and GAPDH (1:2,000, rabbit #2118S CST). Then, the membranes were washed and treated with horseradish peroxidase-conjugated secondary antibodies (CST 7074) at room temperature for 2 h. ECL System was employed to examine the protein bands and the intensity of protein bands measured by ImageJ software.

## Dual-Luciferase Reporter Gene Assay

lncRNA GAS5 or *Klf4* containing the predicted miR-375-3p binding sites were cloned into pGL3-WT-lncRNA Gas5, pGL3-MUT-lncRNA GAS5, pGL3-WT *Klf4* or pGL3-MUT *Klf4*, respectively. The WT or MUT reporter plasmid were co-transfected with the miR-375-3p mimics (50 nM) or the negative control into 293T cells using Lipofectamine 2000 (ThermoFisher), and the luciferase intensity was assessed by the double-luciferase reporter assay kit (Promega, United States) on SpectraMax Gemini EM (Molecular Devices, United States).



**TABLE 1 |** Primers for qRT-PCR.

Sequence (5'–3')	Primer names
TATGGAATCCTGTGGCATC	$\beta$ -actin-F
GTGTTGGCATAGAGGTCTT	$\beta$ -actin-R
AATCTCACAGGCAGTTCT	GAS5-F
ATGGCTTTGTTTCAGTTATCC	GAS5-R
AACCTATACGAAGATTCTCAT	KLF4-F
CCAGTCACAGTGGTAAGG	KLF4-R
ACACTCCAGCTGGGTTTGTTCGTTTCGGCTC	mo-miR-375-3p-F
CTCAACTGGTGTGCTGGAGTCGGCAATTCAGTTGAG	mo-miR-375-3p-R
TCACGCGA	BNP-F
GATGATTCTGCTCCTGCTTTTCC	BNP-R
CAGCTTCTGCATCGTGGATT	$\beta$ -MHC-F
CAGCTCAGTCATGCCAACCG	$\beta$ -MHC-R
GCTCCACGATGGCGATGTT	$\alpha$ -SMA-F
ACCATCGGGGAATGAACGCTT	$\alpha$ -SMA-R
CTGTGAGCAATGCCTGGGTA	GAPDH-F
CTGGAGAAACCTGCCAAGTATG	GAPDH-R
GGTGAAGAATGGGAGTTGCT	

F, forward primer; R, reverse primer; qRT-PCR, real-time quantitative polymerase chain reaction.

## Immunofluorescent Staining

After transfection and treatment, cultured cardiomyocytes were washed with cold PBS for three times and subsequently fixed with 4% paraformaldehyde for 30 min. After that, the cells were permeabilized with 3% Triton X-100 for 20 min. Then, washed three times with PBS, the cardiomyocytes were incubated with anti-cTnT antibody (1:300, rabbit bs-10648R) at 4°C overnight and were further incubated with fluorophore-conjugated secondary antibodies at a normal temperature for 1 h, and then stained with 4',6-diamidino-2-phenylindole (DAPI) solution for 15 min. Immunofluorescence was analyzed under an inverted fluorescence microscope (Olympus BX53).

## Statistical Analysis

SPSS 20.0 (IBM Corp. Armonk, NY, United States) and Prism 8 (GraphPad Software, CA, United States) were used for statistical analysis and plotting. Data were expressed as mean  $\pm$  standard deviation (sd). Unpaired Student's *t*-test was used to determine the significance between two groups.

## RESULTS

### Oxytocin Attenuated Hypertrophic Responses in ISO-Treated Cardiomyocytes

First, to investigate the effects of OT pretreatment on cardiac hypertrophy, NRCMs were incubated and pretreated with OT for 30 min and then stimulated with 10  $\mu$ M ISO for 24 h. Cardiomyocyte hypertrophy was evaluated by cell surface area and expressions of BNP and  $\beta$ -MHC, which have been well-established as cardiac hypertrophy markers. As shown in **Figure 2**, ISO triggered significant hypertrophic responses in NRCMs, as indicated by the increased cell surface area (**Figures 2A,B**) and elevated protein levels of BNP and  $\beta$ -MHC (**Figures 2C,D,K**), which were reduced by pretreatment of OT. At the

same time, we observed the expressions of lncRNA GAS5 (**Figure 2E**), *Klf4* mRNA (**Figure 2G**) and KLF4 protein (**Figures 2H,K**) were down-regulated in ISO group when compared with control group, while up-regulated significantly after OT treatment. Inversely, the expression of miR-375-3p (**Figure 2F**) was increased significantly in ISO group when compared with control group and decreased after OT treatment. We also observed that OT modulated PI3K/AKT signaling pathway in a cardiomyocyte hypertrophy model. As shown in **Figures 2I–K**, the ratios of phosphorylated-PI3K/PI3K (p-PI3K/PI3K) and phosphorylated-AKT1/AKT1 (p-AKT1/AKT1) were significantly increased in ISO-induced hypertrophic cardiomyocytes and significantly decreased after OT treatment.

These results indicated that oxytocin could attenuate cardiomyocyte hypertrophic responses, promote the expressions of lncRNA GAS5 and KLF4 protein, repress miR-375-3p expression, and modulate PI3K/AKT signaling pathway.

### Oxytocin Protected Rats From ISO-Induced Cardiac Hypertrophy and Up-Regulated lncRNA GAS5 Expressions

To evaluate the effects of OT on cardiac hypertrophy *in vivo*, we established a rat cardiac hypertrophy model by ISO subcutaneous infusion for 14 days and treated rats with different dosages of OT before (preconditioning) and after (postconditioning) ISO infusions. Heart weight/body weight (HW/BW) ratio served as a measurement of cardiac hypertrophy. HW/BW ratio was significantly increased in ISO group compared to control group, but significant lower in ISO+OT (3) post group than that in ISO group (**Figure 3A**). HW/BW ratio was not significantly different in ISO+OT (0.03) post group and in ISO+OT (3) pre group when compared with ISO group (**Figure 3A**). Furthermore, no significant difference in HW/BW ratio was found between control group and OT (3) group (**Figure 3A**). Besides, ISO markedly increased the expressions of pathological cardiac hypertrophy markers (BNP,  $\beta$ -MHC) and fibrosis marker (Alpha-smooth muscle actin,  $\alpha$ -SMA) compared with control group, whereas different concentrations of OT preconditioning or postconditioning inhibited ISO-induced increases in BNP,  $\beta$ -MHC and  $\alpha$ -SMA (**Figures 3B–D**). Likewise, only high dosage (3  $\mu$ g/kg) of OT postconditioning could significantly reduce expressions of hypertrophic and fibrosis markers (**Figures 3B–D**). From HE staining (**Figure 3G**), we observed a large number of inflammatory cells and fibroblasts gathered around endocardium region in ISO group and OT treatment alleviated it. Masson's trichrome staining (**Figure 3G**) showed a significant increase in collagen deposition in ISO-infusion group and reduced in OT (3  $\mu$ g/kg) postconditioning group (**Figures 3E,G**). To elucidate the mechanisms underlying the anti-hypertrophic effects of OT, lncRNA GAS5 expressions were detected in left ventricular tissues of different groups. As shown in **Figure 3F**, lncRNA GAS5 expressions in hypertrophic heart tissues were decreased, while up-regulated significantly in rat hearts treated with OT.



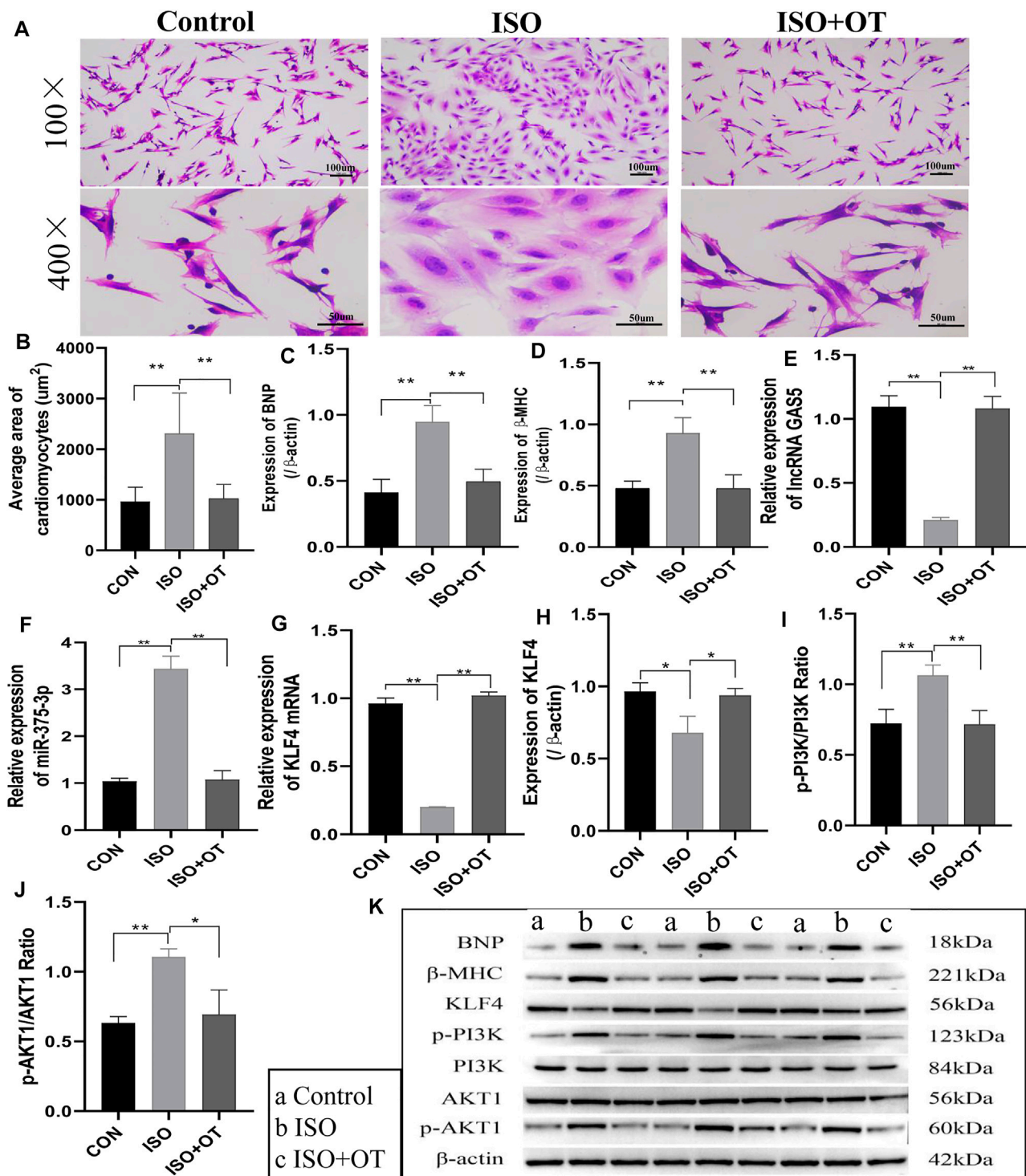


**FIGURE 2 |** Antihypertrophic effects of OT *in vitro*. Neonatal rat cardiomyocytes stimulated with ISO for 24 h in the presence or absence of OT. **(A)** The cell morphology was evaluated by H&E staining. **(B)** Statistical results of measurement of cell surface areas. **(C,D)** Effects of OT on the protein expressions of BNP and β-MHC. **(E)** Effects of OT on the expression of lncRNA GAS5. **(F)** Effects of OT on the expression of miR-375-3p. **(G,H)** Effects of OT on the mRNA and protein expressions of KLF4. **(I)** Effects of OT on the p-PI3K/PI3K ratio. **(J)** Effects of OT on the p-AKT1/AKT1 ratio. **(K)** Western blot images of BNP, β-MHC, KLF4, p-PI3K, PI3K, AKT1, p-AKT1, and β-actin levels. Data are shown as the mean ± sd of three independent experiments. \*,  $p < 0.05$ ; \*\*,  $p < 0.01$ .

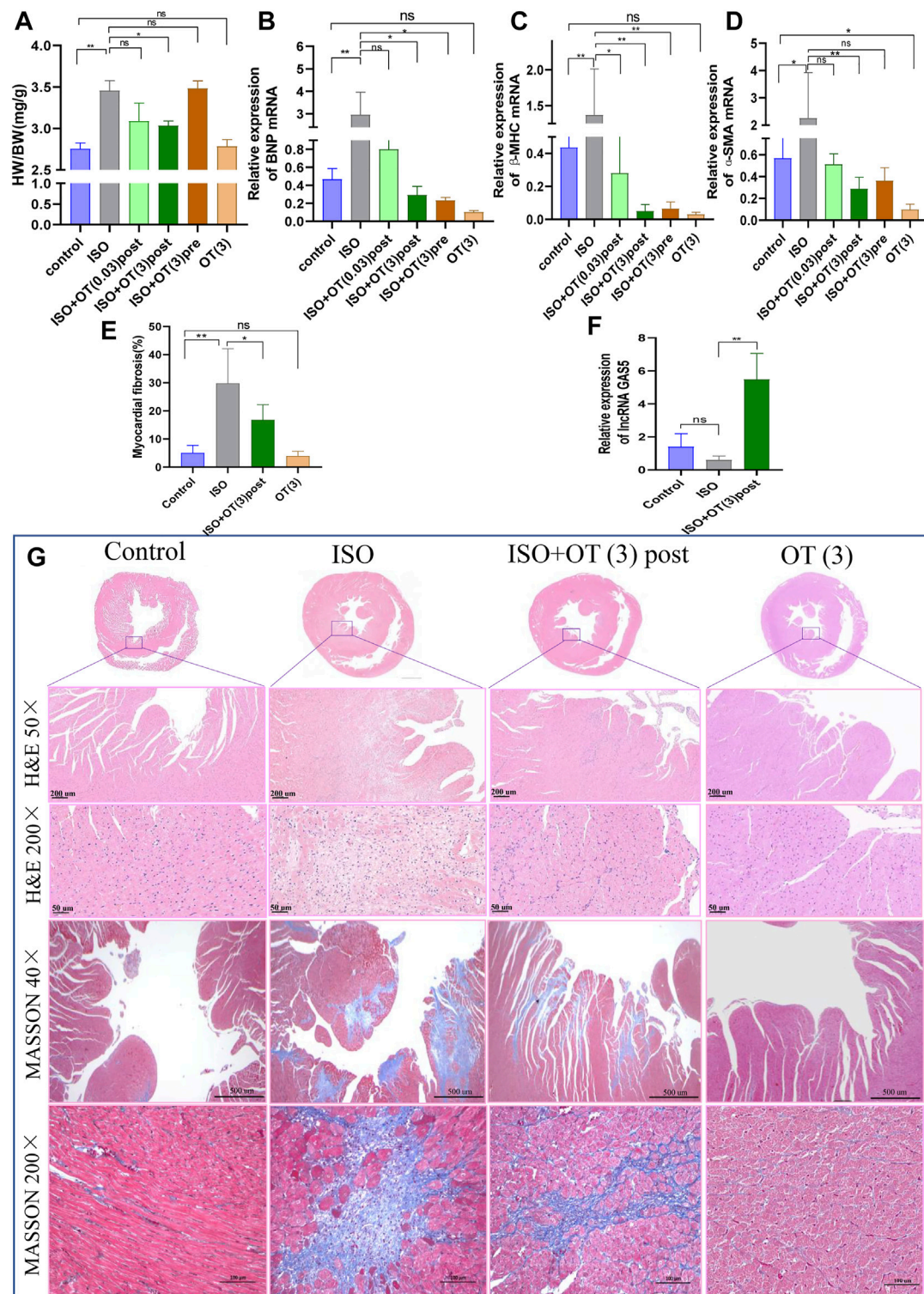


**FIGURE 3** | OT alleviated cardiac hypertrophy caused by ISO administration along with up-regulation of lncRNA GAS5 expression. SD rats were treated with ISO and different concentrations of OT as described. **(A)** HW/BW ratio. **(B–D)** The expressions of BNP,  $\beta$ -MHC and  $\alpha$ -SMA mRNA detected by qRT-PCR. **(E)** Quantitative morphometric analysis of Masson's trichrome staining representing myocardial fibrosis. **(F)** Effects of OT (3 ug/kg) postconditioning on the expression of lncRNA GAS5. **(G)** Representative histopathological images of heart tissue sections stained with H&E, Masson's Trichrome staining from the indicated groups.  $n = 3$ –6 rats per experimental group. Data shown as mean  $\pm$  sd, \* $p < 0.05$  \*\* $p < 0.01$ .



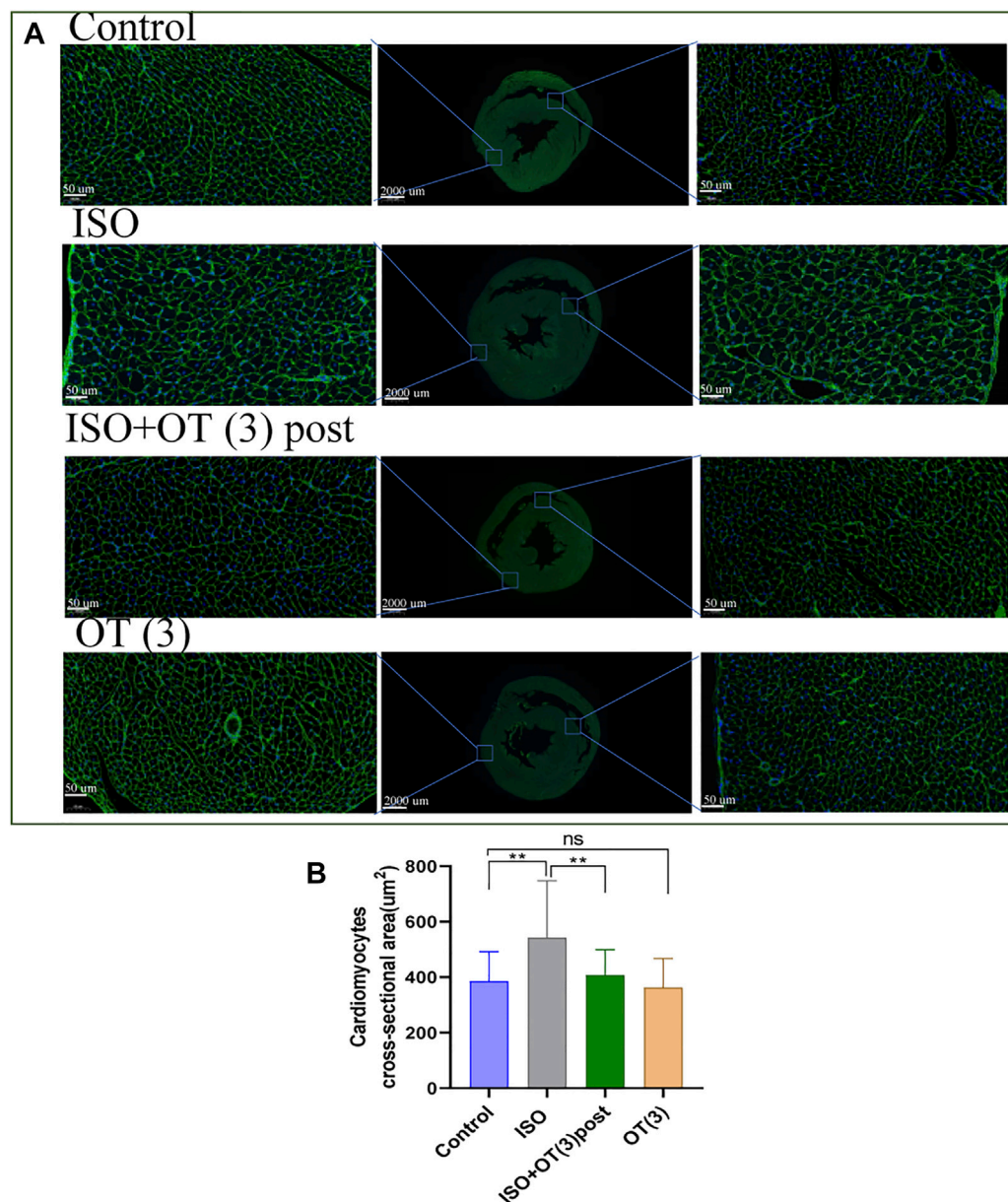


**FIGURE 4 |** The cross sections of hearts were stained with WGA. **(A)** The representative images of WGA staining in the cardiomyocyte cross-sectional area. **(B)** Statistical results of measurement of cross-sectional areas of cardiomyocytes. Data are shown as mean  $\pm$  sd, \* $p < 0.05$  \*\* $p < 0.01$ .

The results of WGA staining (**Figure 4A**) showed that the cardiomyocytes were not orderly arranged and the cross-sectional areas of cardiomyocytes were significantly enlarged after ISO insulted, while OT (3 ug/kg) postconditioning could prevent these pathomorphological changes (**Figure 4B**).

## The Effects of OT on Cardiac Structure and Functional Parameters

We performed transthoracic echocardiography to evaluate cardiac function and left ventricular remodeling (**Figure 5A**).

ISO infusion induced cardiac hypertrophy of rats, as evidenced by increased LVPWd (**Figure 5B**) and LVPWs (**Figure 5C**) in ISO group compared with control group. OT (3 ug/kg) postconditioning treatment effectively prevented left ventricular wall from thickening (**Figures 5B,C**). There were no significant differences in LVIDd (**Figure 5D**), LVIDs (**Figure 5E**), LVEF (**Figure 5F**), and LVFS (**Figure 5G**) between ISO group and control group, suggesting that cardiac hypertrophy induced in our study was not typical concentric hypertrophy and left ventricular function was not worsened by ISO and not affected by OT.

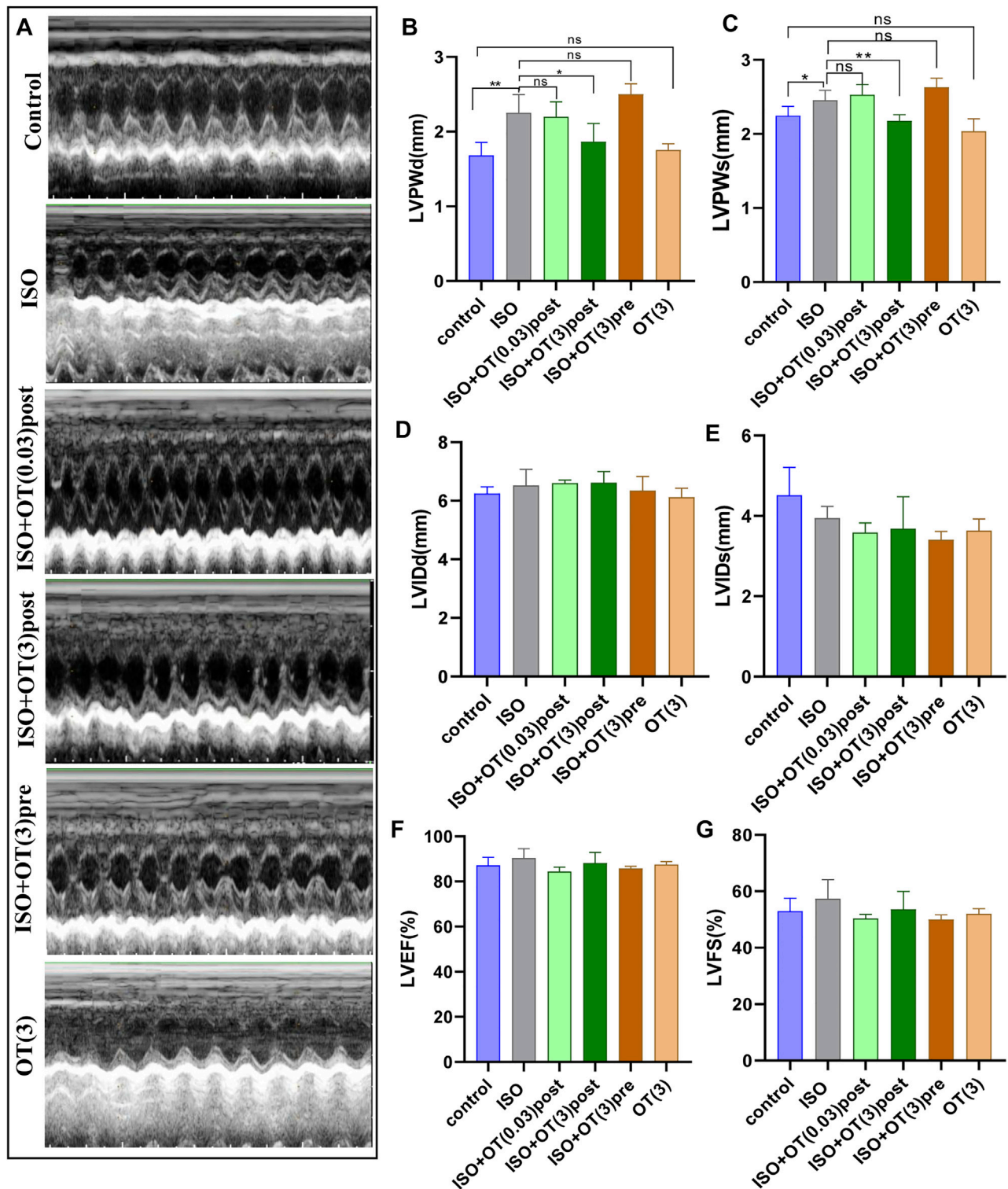


**FIGURE 5 |** Effects of OT on cardiac structure and functional parameters assessed by Echocardiography. **(A)** Representative echo images of each group. **(B)** LVPWd. **(C)** LVPWs. **(D)** LVIDd. **(E)** LVIDs. **(F)** LVEF. **(G)** LVFS.  $n = 4-6$  rats per experimental group. \* $p < 0.05$ ; \*\* $p < 0.01$ ; ns, not significant. LVPWd, left ventricular posterior wall thickness at end-diastole; LVPWs, left ventricular posterior wall thickness at end-systole; LVIDd, Left ventricular internal diameter end-diastole; LVIDs, Left ventricular internal diameter end-systole; LVEF, left ventricular ejection fraction; LVFS, left ventricular fractional shortening.

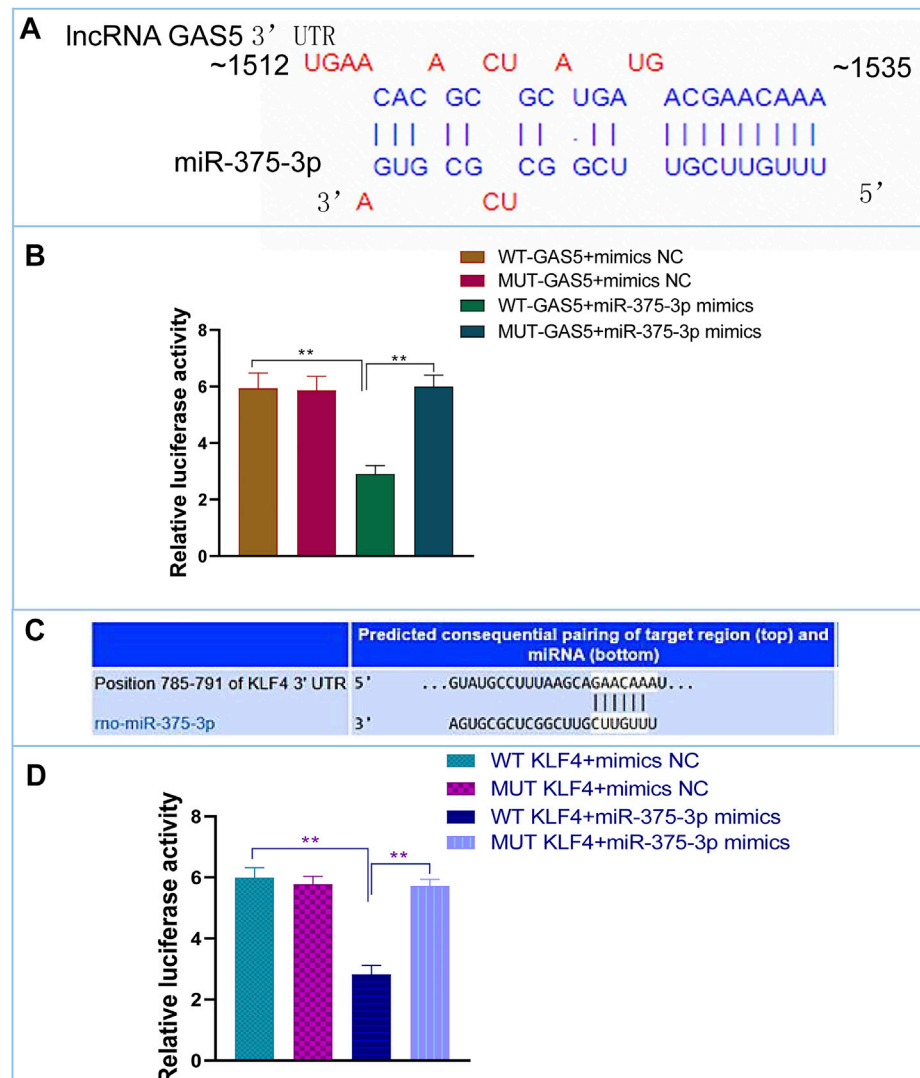


**FIGURE 6 |** The interactions of miR-375-3p with lncRNA GAS5 and KLF4. **(A,C)** Predicted duplex formation between lncRNA GAS5 and miR-375-3p **(A)**, and KLF4 3'-UTR and miR-375-3p **(C)**. **(B)** The WT (MUT) GAS5 vector and miR-375-3p mimics or mimics NC were co-transfected into 293T cells. Dual luciferase gene reporter assay was performed to indicate that miR-375-3p could directly bind with the WT GAS5. **(D)** The WT (MUT) KLF4 3'-UTR vector and miR-375-3p mimics or mimics NC were co-transfected into 293T cells. Dual luciferase gene reporter assay was performed to indicate that miR-375-3p could directly bind with the WT KLF4. All the experiments were repeated three times. \*\* $p < 0.01$ . WT, wild-type; MUT, mutant type; NC, negative control.

## The Interactions of miR-375-3p With lncRNA GAS5 and *Klf4*

Based on bioinformatic prediction (**Figures 6A,C**), we performed dual-luciferase reporter gene assays to validate the interactions between lncRNA GAS5 and miR-375-3p as well as miR-375-3p and *Klf4*. The results revealed that luciferase values were decreased in WT GAS5+miR-375-3p mimics group, but there was no significant alteration in MUT-GAS5+miR-375-3p mimics group or in mimics-NC+WT-GAS5/MUT-GAS5 groups (**Figure 6B**). Similarly, after co-transfection of WT *Klf4* and miR-375-3p mimics, the luciferase value was decreased significantly when compared with co-transfection of WT *Klf4* and miR-375-3p mimics NC

group. There was no significant difference in luciferase value between MUT *Klf4*+mimics NC and MUT *Klf4*+miR-375-3p mimics groups (**Figure 6D**). These results confirmed that lncRNA GAS5 could sponge miR-375-3p and *Klf4* was a direct target gene of miR-375-3p.

## Knock-Down of lncRNA GAS5 Inhibited Anti-Hypertrophic Effects of Oxytocin via Upregulation of miR-375-3p

To validate the regulatory relationships among lncRNA GAS5, miR-375-3p and KLF4 in the *in vitro* model under OT action, NRCMs were transfected with shRNA GAS5



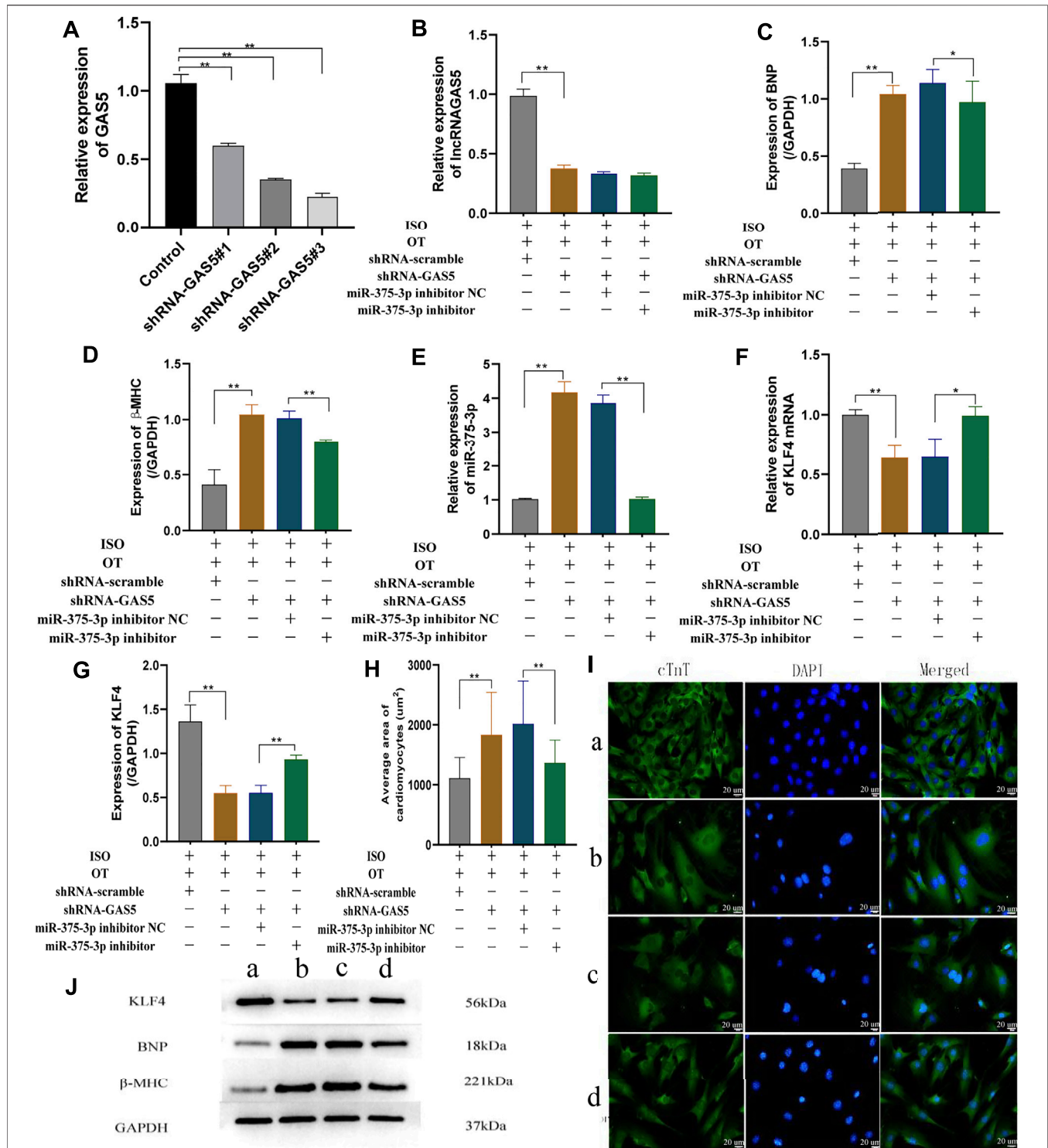


**FIGURE 7 |** Down-regulation of lncRNA GAS5 inhibits the anti-hypertrophic effects of OT via miR-375-3p in ISO-treated primary cardiomyocytes. **(A)** qRT-PCR was performed to quantitatively measure lncRNA GAS5 expression after transfection of shRNA-GAS5#1, shRNA-GAS5#2, shRNA-GAS5#3 in cardiomyocytes. **(B)** Expression of lncRNA GAS5 was determined by qRT-PCR. **(C,D)** Expressions of BNP and β-MHC proteins were measured by Western blot analysis. **(E)** Expression of miR-375-3p was determined by qRT-PCR. **(F)** Expression of KLF4 mRNA was determined by qRT-PCR. **(G)** Expression of KLF4 protein was determined by Western blot analysis. **(H)** Statistical results of measurement of cell surface areas. **(I)** Cardiomyocyte surface areas were measured by immunofluorescent staining. Scale bars represent 20 μm. Images were captured at ×400 magnification **(J)** Representative Western blot images of KLF4, BNP, β-MHC and GAPDH. (a) ISO+OT+shRNA-scramble group. (b) ISO+OT+shRNA-GAS5 group. (c) ISO+OT+shRNA-GAS5+miR-375-3p inhibitor NC group. (d) ISO+OT+shRNA-GAS5+miR-375-3p inhibitor group. Data are shown as the mean ± sd of three independent experiments. \*,  $p < 0.05$ ; \*\*,  $p < 0.01$ .

followed by OT pretreatment and ISO stimulation, and expressions of lncRNA GAS5, miR-375-3p and *Klf4* mRNA, as well as the protein levels of KLF4, BNP and  $\beta$ -MHC were evaluated. At the beginning, we assessed the transfection efficiency of shRNA GAS5#1, shRNA GAS5#2, shRNA GAS5#3 in cardiomyocytes and selected the shRNA GAS5#3 (shRNA-GAS5) for the subsequent experiments due to the highest efficiency (Figure 7A). The expression of lncRNA GAS5 was significantly decreased in ISO+OT+shRNA-GAS5 group compared with ISO+OT+shRNA-scramble group (Figure 7B), suggesting that knock-down of lncRNA GAS5 was effective and sustained. Compared to ISO+OT+shRNA-scramble group, the expressions of BNP,  $\beta$ -MHC were significantly increased in ISO+OT+shRNA-GAS5 group (Figures 7C,D,J). Meanwhile, we also found that after lncRNA GAS5 knock-down, the expression of miR-375-3p was increased (Figure 7E), while *Klf4* mRNA (Figure 7F) and protein (Figures 7G,J) levels were decreased. These results indicated that knock-down of lncRNA GAS5 inhibited anti-hypertrophic effects of oxytocin and that lncRNA GAS5 negatively regulated miR-375-3p and positively regulated *Klf4* mRNA and protein.

Subsequently, we co-transfected shRNA GAS5 and miR-375-3p inhibitor to NRCMs followed by OT and ISO treatment. The expression of miRNA-375-3p was markedly down-regulated in ISO+OT+shRNA-GAS5+miR-375-3p inhibitor group compared with ISO+OT+shRNA-GAS5+miR-375-3p inhibitor NC group (Figure 7E). The inhibiting effects of shRNA-GAS5 on *Klf4* mRNA and protein expressions were reversed by transfection of miR-375-3p inhibitor (Figures 7F,G,J). Meanwhile, the expressions of hypertrophic markers (BNP and  $\beta$ -MHC) (Figures 7C,D,J) as well as the size of the cardiomyocytes evaluated by immunofluorescent staining (Figures 7H,I) were significantly decreased in ISO+OT+shRNA-GAS5+miR-375-3p inhibitor group compared with ISO+OT+shRNA-GAS5+miR-375-3p inhibitor NC group. These results indicated that miR-375-3p inhibitor rescued the pro-hypertrophic effects of shRNA-GAS5.

Taken together, these data demonstrated that lncRNA GAS5 mediated anti-hypertrophic effects of OT through negative regulation of miR-375-3p expression.

### Upregulation of miR-375-3p Blunted Anti-Hypertrophic Effects of Oxytocin via Downregulation of KLF4 and Modulation of PI3K/AKT Signaling Pathway

To further verify whether down-regulation of miR-375-3p mediated the anti-hypertrophic effects of OT, we upregulated miR-375-3p by transfection of miR-375-3p mimics into NRCMs followed by OT pretreatment and ISO insult. The transfection efficiency of miR-375-3p mimics in cardiomyocytes was detected and demonstrated to be effective (Figure 8A). Forced expression of miR-375-3p was observed in ISO+OT+miR-375-3p mimics group, but not in ISO+OT+miR-375-3p mimics NC group

(Figure 8B). As compared with ISO+OT+miR-375-3p mimics NC group, ISO+OT+miR-375-3p mimics group presented notable increases in BNP and  $\beta$ -MHC expressions (Figures 8C,D,J), along with remarkable decreases in *Klf4* gene (Figure 8E) and protein (Figures 8F,J), suggesting that upregulation of miR-375-3p dampened anti-hypertrophic effects of OT and miR-375-3p could negatively regulate expressions of KLF4. Rescue assays were carried out to test whether upregulation of *Klf4* could abolish the effects conferred by miR-375-3p mimics. We co-transfected miR-375-3p mimics and pcDNA-*Klf4* vector or empty pcDNA vector into NRCMs followed by OT and ISO treatments. The results showed that the expression of *Klf4* mRNA was significantly increased in ISO+OT+miR-375-3p mimics+pcDNA-*Klf4* group compared to ISO+OT+miR-375-3p mimics+pcDNA-NC group (Figure 8E), whereas the expressions of KLF4 protein of two groups were not statistically significant (Figures 8F,J).  $\beta$ -MHC protein was reduced observably in ISO+OT+miR-375-3p mimics+pcDNA-*Klf4* group compared with ISO+OT+miR-375-3p mimics+pcDNA-NC group (Figures 8D,J), while BNP protein was not significantly reversed (Figures 8C,J). Immunofluorescent staining was also used to detect the changes in cardiomyocyte sizes (Figure 8K). Cardiomyocytes were markedly enlarged in ISO+OT+miR-375-3p mimics group compared with ISO+OT+miR-375-3p mimics NC group. Compared with ISO+OT+miR-375-3p mimics+pcDNA NC group, the sizes of cardiomyocytes were diminished notably in ISO+OT+miR-375-3p mimics+pcDNA-*Klf4* group (Figures 8I,K).

Furthermore, we also evaluated the protein expressions of p-PI3K, PI3K, p-AKT1, AKT1 after transfection of miR-375-3p mimics and co-transfection of miR-375-3p mimics and pcDNA-*Klf4*, respectively. The ratios of p-PI3K/PI3K (Figures 8G,J) and p-AKT1/AKT1 (Figures 8H,J) were significantly increased in ISO+OT+miR-375-3p mimics group compared with ISO+OT+miR-375-3p mimics NC group, suggesting that PI3K/AKT signaling pathway was also regulated by miR-375-3p. When the cells were simultaneously transfected with miR-375-3p mimics and pcDNA-*Klf4*, the ratio of p-AKT1/AKT1 (Figures 8H,J) was significantly reduced, whereas p-PI3K/PI3K (Figures 8G,J) was reduced but not statistically significant.

### *Klf4* Knock-Down Inhibited Anti-Hypertrophic Effects of Oxytocin via PI3K/AKT Pathway

We first assessed the interference efficiency of shRNA *Klf4*#1, shRNA *Klf4*#2, and shRNA *Klf4*#3 in cardiomyocytes and then selected the shRNA *Klf4*#3 for the subsequent experiments based on its highest efficiency of interference (Figures 9A–C). We transfected shRNA-*Klf4* #3 (shRNA-*Klf4*) and its negative scramble into NRCMs followed by OT pretreatment and ISO stimulation. The expressions of *Klf4* mRNA and protein were significantly lower in ISO+OT+shRNA-*Klf4* group than those in ISO+OT+shRNA-NC group (Figures 9D,E,L). The anti-hypertrophic effects of OT was dampened in ISO+OT+shRNA-*Klf4* group compared with ISO+OT+shRNA-NC group, as shown by higher protein expressions of BNP and

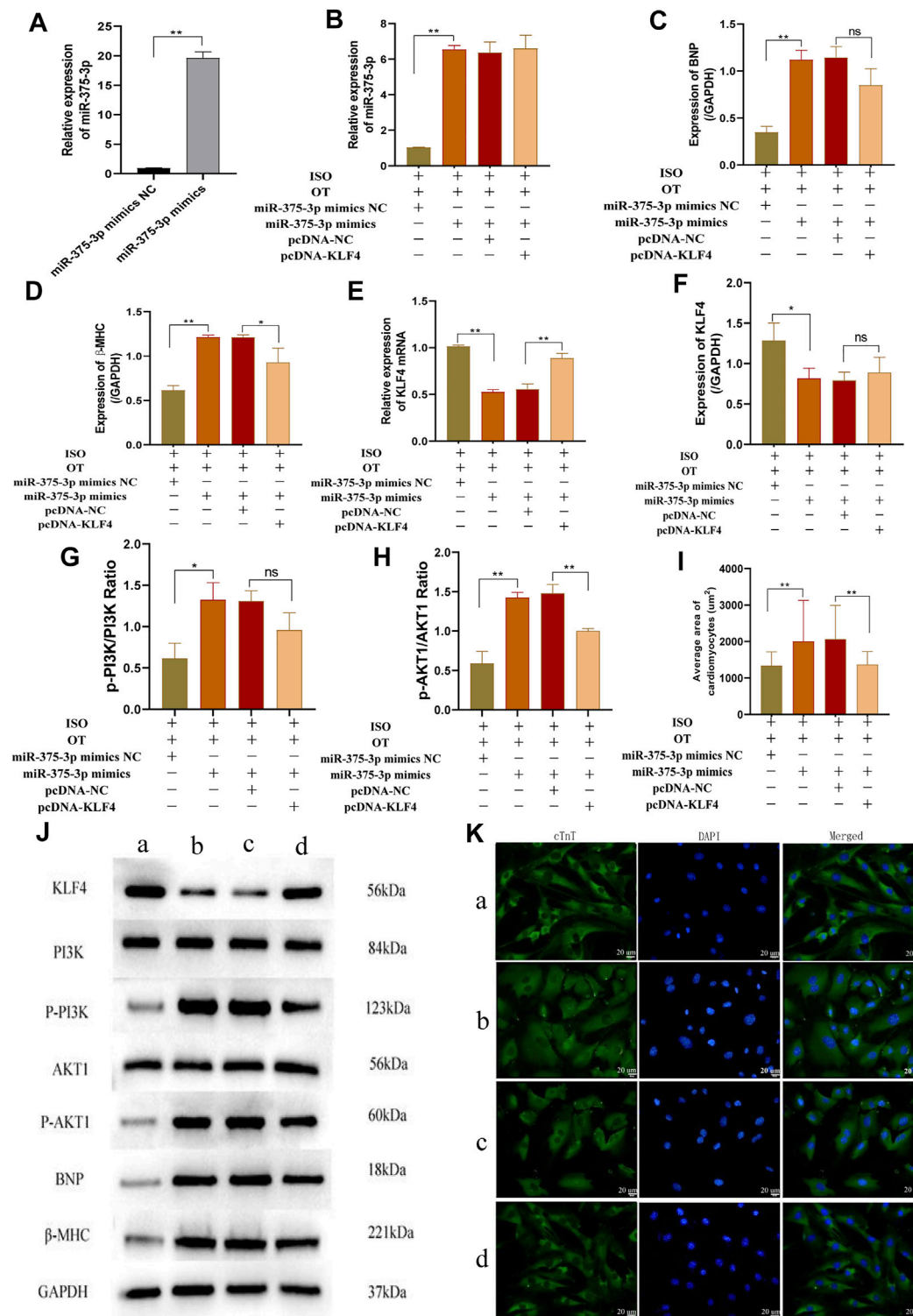


**FIGURE 8 |** Over-expression of miR-375-3p blunted anti-hypertrophic effects of oxytocin via KLF4 and modulated the PI3K/AKT signaling pathway. **(A)** Expression of miR-375-3p in cardiomyocytes following transfection of miR-375-3p mimics and miR-375-3p mimics NC. **(B)** Expression of miR-375-3p was detected by qRT-PCR. **(C,D)** Expressions of BNP and β-MHC proteins were measured by Western blot analysis. **(E)** Expression of KLF4 mRNA was detected by qRT-PCR. **(F)** Expression of KLF4 protein was measured by Western blot analysis. **(G)** p-PI3K/PI3K ratio. **(H)** p-AKT1/AKT1 ratio. **(I)** Statistical results of measurement of cell surface areas. **(J)** Representative western blot images of KLF4, PI3K, p-PI3K, AKT1, p-AKT1, BNP, β-MHC and GAPDH levels. **(K)** Cardiomyocyte surface areas were measured by immunofluorescent staining. Scale bars represent 20 μm. Images were captured at ×400 magnification. (a) ISO+OT+miR-375-3p mimics NC group. (b) ISO+OT+miR-375-3p mimics group. (c) ISO+OT+miR-375-3p mimics+pcDNA-NC group. (d) ISO+OT+miR-375-3p mimics+pcDNA-KLF4 group. Data are shown as the mean ± sd of three independent experiments. \*,  $p < 0.05$ ; \*\*,  $p < 0.01$ .

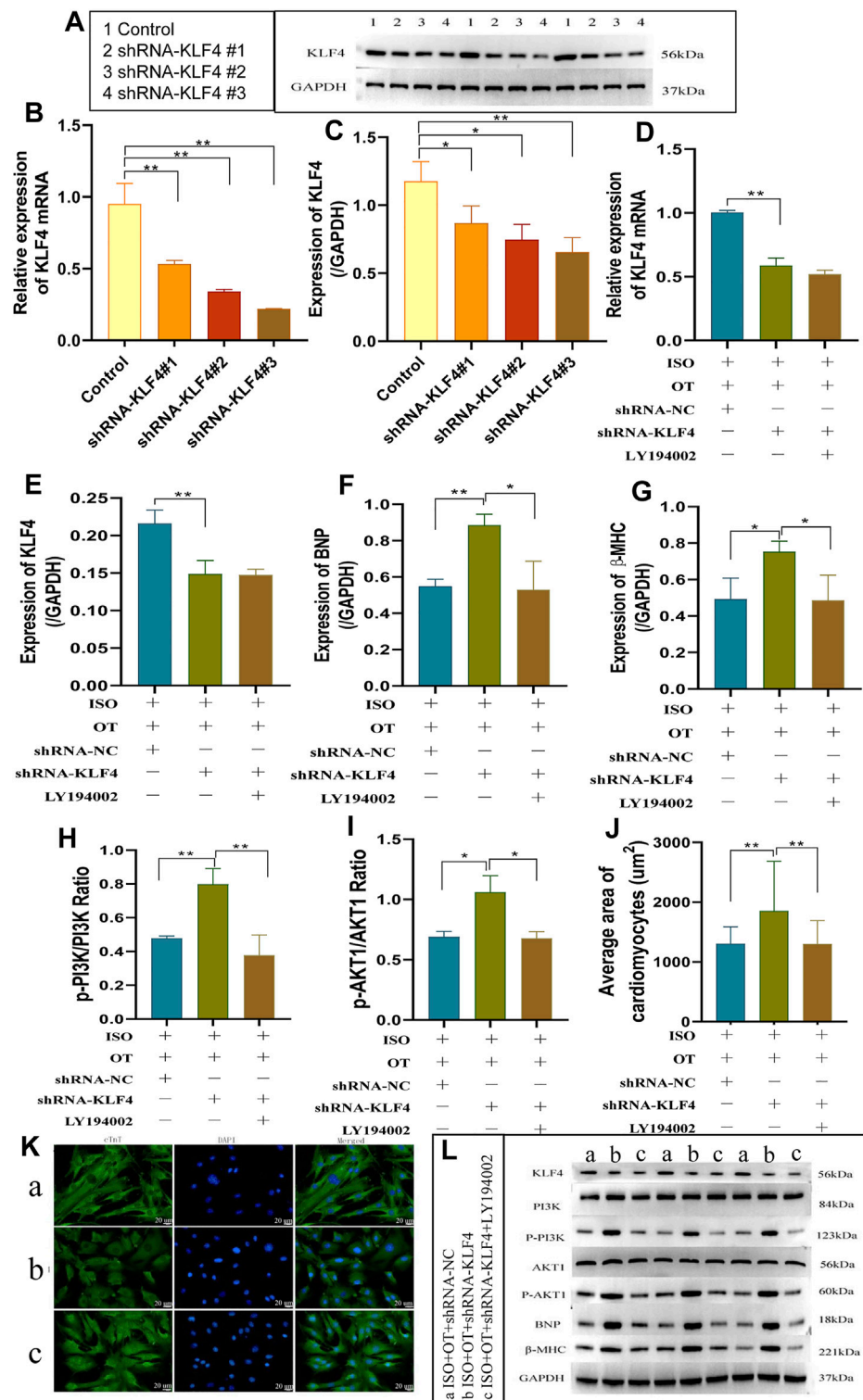


**FIGURE 9** | knock-down of KLF4 blunted anti-hypertrophic effects of oxytocin via PI3K/AKT pathway. **(A–C)** Detection of relative shRNA-KLF4 interference effects. The changes in KLF4 mRNA and protein levels were detected by qRT-PCR and Western blotting after transfection of shRNA-KLF4 #1, shRNA-KLF4 #2, shRNA-KLF4 #3 in primary cardiomyocytes. **(D)** Expression of KLF4 mRNA was determined by qRT-PCR. **(E)** Expression of KLF4 protein was measured by Western blot analysis. **(F,G)** Expressions of BNP,  $\beta$ -MHC proteins were measured by Western blot analysis. **(H)** p-PI3K/PI3K ratio. **(I)** p-AKT1/AKT1 ratio. **(J)** Statistical results of measurement of cell surface areas. **(K)** Cardiomyocyte surface areas were measured by immunofluorescent staining. Scale bars represent 20  $\mu\text{m}$ . Images were captured at  $\times 400$  magnification. **(L)** Western blot images of KLF4, PI3K, p-PI3K, AKT1, p-AKT1, BNP,  $\beta$ -MHC and GAPDH levels. (a) ISO+OT+shRNA-NC group. (b) ISO+OT+shRNA-KLF4 group. (c) ISO+OT+shRNA-KLF4+LY194002 group. Data are shown as the mean  $\pm$  sd of three independent experiments. \*,  $p < 0.05$ ; \*\*,  $p < 0.01$ .



$\beta$ -MHC (Figures 9F,G,L), and larger surface areas of cardiomyocytes observed in ISO+OT+shRNA-*Klf4* group (Figures 9J,K).

The ratios of p-PI3K/PI3K (Figures 9H,I) and p-AKT1/AKT1 (Figures 9I,L) in ISO+OT+shRNA-*Klf4* group were significantly higher than those in ISO+OT+shRNA-NC group, suggesting PI3K/AKT pathway was modulated by KLF4. After transfecting shRNA-*Klf4* into NRCMs, we pretreated NRCMs with 10  $\mu$ M LY194002 (a PI3K inhibitor that prevents PI3K phosphorylation) and then treated with OT and ISO. The results revealed that the ratios of p-PI3K/PI3K (Figures 9H,I) and p-AKT1/AKT1 (Figures 9I,L) were notably lower in ISO+OT+shRNA-*Klf4*+LY194002 group than those in ISO+OT+shRNA-*Klf4* group. The expressions of BNP and  $\beta$ -MHC (Figures 9F,G,L) as well as the sizes of cardiomyocytes were remarkably reduced in ISO+OT+shRNA-*Klf4*+LY194002 group compared with ISO+OT+shRNA-*Klf4* group (Figures 9J,K). These findings suggested that blockade of PI3K/AKT signaling pathway rescued the pro-hypertrophic effects of shRNA-*Klf4*.

The above results indicated that KLF4 mediated the anti-hypertrophic effects of OT, and PI3K/AKT is the downstream signaling pathway of miR-375-3p/KLF4 axis.

## DISCUSSION

Oxytocin has a broad spectrum of beneficial roles in regulating cardiovascular homeostasis (Reiss et al., 2019; Jankowski et al., 2020). An *ex vivo* experiment well documented that OT treatment exerts anti-hypertrophic responses in cardiomyocytes exposed to endothelin-1 and AngII (Menaouar et al., 2014). We constructed cardiomyocyte hypertrophic model by ISO challenge and found that OT exerted cardioprotection against hypertrophy, which is consistent with a previous report (Menaouar et al., 2014). In an *in vivo* study, Plante et al. (2015) reported that chronic subcutaneous infusion OT prevents the development of cardiomyocyte hypertrophy, fibrosis associated with obesity and diabetes in db/db mice. Similarly, Garrott et al. (2017) showed that chronic activation of hypothalamic oxytocin neurons blunts cellular hypertrophy and myocardial collagen density in rats undergoing *trans*-ascending aortic constriction through increase of parasympathetic tone. Our *in vivo* findings are in accordance with aforementioned studies (Plante et al., 2015; Garrott et al., 2017). In contrast, a recent study demonstrated that OT accelerated AngII-induced cardiac hypertrophy and fibrosis when the rats were simultaneously infused AngII and OT for 28 days (Phie et al., 2015). This discrepancy over anti-hypertrophic effects of OT *in vivo* studies may be attributed to the different administration routes (central or peripheral) or different concentrations of OT.

Our study showed that different doses of OT preconditioning or postconditioning inhibited hypertrophic responses induced by ISO and that OT (3  $\mu$ g/kg) postconditioning exhibited more significantly anti-hypertrophic and anti-fibrotic effects. The

delivery route, dose, and timing of OT possibly affected therapeutic effects. In our preliminary experiment, we initially investigated the actions of OT preconditioning, in spite of that the infusion time interval of OT and ISO was more than 2 h, the mortality of rats receiving these two agents was still high. Accordingly, we adjusted the infusion time interval to more than 8 h and the survival rate of rats was improved in preconditioning group. Oxytocin is a vasoactive hormone, which could induce both vasoconstriction or vasodilation depending on doses used, and decrease the LV preload and the inotropic state (Carter et al., 2020). Phie et al. (2015) documented that OT elicited a detrimental effect when AngII was simultaneously infused. The possible reasons may be due to that the rats hearts undergo complex effects caused by disturbances of parasympathetic and sympathetic system in response to AngII and OT, some of which are harmful rather than cardioprotective, and therefore counteract the beneficial effects of OT.

Oxytocin has been well documented to be implicated in stress-buffering via regulation of autonomic nervous system (Tracy et al., 2018; Carter et al., 2020; Belém-Filho et al., 2021). It is well known that chronic stresses, including social, emotional, and physical stresses, increase activity of sympathetic nervous system. Recently, Belém-Filho et al. (2021) reported that OT attenuates tachycardiac responses evoked by restraint via increasing parasympathetic activity, promoting cardioprotection by reducing the stress-evoked heart rate increase. Jovanovic et al. (2019) provided evidence that oxytocin treatment decreases the heart/body weight ratio and prevents the hypertrophy of cardiomyocytes in the wall of the left ventricle of the stressed rats. The present study showed that the expression levels of hypertrophy and fibrosis markers in OT alone group were lower than those in control group, which may be associated with the anxiolytic effects of Oxytocin, because daily infusion of normal saline or OT for 28 days was a kind of chronic stressor for rats. The underlying mechanisms by which OT regulates cardiac hypertrophy remain largely unknown. Over the past decade, some non-coding RNAs have been identified to mediate the development of cardiac hypertrophy, whereas the roles of non-coding RNAs in OT-evoked antihypertrophic effects are not well established. In our study, we identified oxytocin modulated lncRNA GAS5 and miR-375-3p expressions in the hypertrophic cardiomyocytes, and validated that *Klf4* is a direct target gene of miR-375-3p. lncRNA GAS5 is a potential regulator of hypertension-related vascular remodeling: Downregulation of lncRNA GAS5 was observed in spontaneously hypertensive rats, which had elevated blood pressure and increased medial thickness and luminal diameter (Wang et al., 2016). lncRNA GAS5 expression is downregulated in cardiomyocytes in pathological cardiac hypertrophy induced by ISO (Liu et al., 2019) and in diabetic cardiomyopathy (Xu et al., 2020a). Therefore up-regulation of lncRNA GAS5 attenuates cardiac fibrosis, myocardial hypertrophy and improved cardiac function (Liu et al., 2019; Xu et al., 2020a). The present study showed that anti-hypertrophic effects of OT were accompanied by up-regulation of lncRNA GAS5 and that downregulation of



lncRNA GAS5 minimized anti-hypertrophic effects of OT. These results were in line with previous studies (Wang et al., 2016; Liu et al., 2019; Xu et al., 2020a).

MiR-375-3p was recently found to promote cardiac hypertrophy by reducing protein expression of lactate dehydrogenase B chain, a regulator of cell metabolism (Feng et al., 2019). In addition, miR-375 is significantly up-regulated in post-myocardial infarction mice hearts (Garikipati et al., 2015) and failing human hearts (Garikipati et al., 2017). Therapeutic inhibition of miR-375 decreases inflammatory response, reduces cardiomyocyte apoptosis in ischemic myocardia, and attenuates LV remodeling after myocardial infarction (Garikipati et al., 2017). KLF4, a novel anti-hypertrophic transcriptional regulator, inhibits cardiomyocyte hypertrophy induced by phenylephrine in cultured cardiomyocytes or by partial aortic constriction in mice (Kee and Kook, 2009; Liao et al., 2010). It has been documented that KLF4 mediates anti-hypertrophic effects of histone deacetylase inhibitors (Kee and Kook, 2009), berberine (Ding et al., 2021), and lncRNA-Mhrt (Xu et al., 2020b). In this study, miR-375-3p was up-regulated in hypertrophic cardiomyocytes, but downregulated by OT treatment. The expressions of *Klf4* mRNA and protein were notably decreased in hypertrophic cardiomyocytes but increased after OT treatment. We hypothesized lncRNA GAS5/miR-375-3p/KLF4 axis mediated the anti-hypertrophic actions of OT. We transfected shRNA-GAS5, miR-375-3p mimics and shRNA-*Klf4* followed by OT treatment and ISO stimulation respectively to evaluate the changes in anti-hypertrophic effects of OT. Our data showed that shRNA-GAS5, shRNA-*Klf4*, and miR-375-3p mimics could minimize anti-hypertrophic effects of OT. Meanwhile, after lncRNA GAS5 knock-down, miR-375-3p was up-regulated and KLF4 levels significantly downregulated. Over-expression of miR-375-3p resulted in inhibition of KLF4 expression. Through dual-luciferase reporter gene assays, we confirmed the regulatory relationship between lncRNA GAS5 and miR-375-3p, as well as miR-375-3p and *Klf4*. Additionally, we conducted the rescue experiments to further confirm the functions of lncRNA GAS5, miR-375-3p, and KLF4, respectively. lncRNA GAS5 knock-down-induced hypertrophy was reversed after co-transfection with miR-375-3p inhibitor. Similarly, miR-375-3p over-expression increased expression of hypertrophic fetal genes, which was partially reversed after co-transfection with *Klf4* pcDNA. To sum up, our data elaborate the regulatory relationships among lncRNA GAS5, miR-375-3p and KLF4, which imply that lncRNA GAS5 functions as a decoy of miR-375-3p, leads to enhanced KLF4 expression, and mediates anti-hypertrophic effects of OT.

From **Figure 8E**, we confirmed the pcDNA-*Klf4* transfection efficiency, as the expression of *Klf4* mRNA is significantly increased in ISO+OT+miR-375-3p mimics+pcDNA-*Klf4* group compared to ISO+OT+miR-375-3p mimics+pcDNA-NC group. However, the expressions of KLF4 protein showed a slightly but not significantly increased in ISO+OT+miR-375-3p mimics+pcDNA-*Klf4* group compared with ISO+OT+miR-375-3p mimics+pcDNA-NC group (**Figure 8F**). The reason can be explained by the presence of miR-375-3p mimics. We co-transfected miR-375-3p mimics and pcDNA-*Klf4* into the cardiomyocytes, due to *Klf4* mRNA is the

direct target gene of miR-375-3p, miR-375-3p mimics mediated the post-transcriptional silence effects on *Klf4* mRNA, so KLF4 protein expressions were repressed. Due to the insufficient expressions of KLF4 proteins, the downstream signaling pathway was affected. The p-PI3K/PI3K ratio (**Figure 8G**) was not significantly decreased as expected in ISO+OT+miR-375-3p mimics+pcDNA-*Klf4* group than in ISO+OT+miR-375-3p mimics+pcDNA-NC group. Similarly, the rescue effects of up-regulation of KLF4 on inhibiting hypertrophic markers, the BNP expression (**Figure 8C**), was not significant.

It is well established that PI3K/AKT signaling pathway is a key pathway in the process of cardiac hypertrophy. Excessive activation of PI3K/AKT cascade contributes to the progress of cardiac hypertrophy, which has been observed in cardiac-selective transgenic over-expression of AKT in mice (Condorelli et al., 2002) and other cardiac hypertrophy models (Zhu et al., 2009; Gao et al., 2017). Effectively suppressing PI3K/AKT signaling by pharmacological agents could be resistant to cardiac hypertrophy when mouse hearts are exposed to chronic pressure overload, as evidenced by that Isorhamnetin (Gao et al., 2017) and Astragaloside IV (Liu et al., 2018) protect against cardiac hypertrophy through inactivation of PI3K/AKT pathway. Consistently, we found the expressions of p-PI3K and p-AKT were increased by ISO treatment, while significantly decreased by OT treatment. PI3K/AKT signaling pathway has been proposed to be implicated in the cardioprotective effect of OT by several studies: OT increases myocardial glucose uptake via triggering PI3K phosphorylation (Florian et al., 2010); OT protects H9c2 cells against I/R by recruiting p-AKT accumulated in the perinuclear region (Gonzalez-Reyes et al., 2015). Both of these cardioprotective effects exerted by OT were abrogated by PI3K inhibitor Wortmannin, which suggests that PI3K/AKT signaling pathway, a salvage kinase pathway, is responsible for cardioprotection of OT (Florian et al., 2010; Gonzalez-Reyes et al., 2015).

PI3K/AKT was shown to be a downstream signaling pathway of KLF4 in the study of carcinoma (Chang et al., 2015; Tang et al., 2018). Therefore, we further determined whether PI3K/AKT pathway is regulated by miR-375-3p/KLF4 axis under OT treatment in the *in vitro* hypertrophic model. We checked the expressions of PI3K/AKT pathway-related proteins after miR-375-3p over-expression and *Klf4* knock-down, respectively, and found that either miR-375-3p over-expression or *Klf4* knock-down significantly up-regulated phosphorylated PI3K and AKT in cultured cardiomyocytes. Furthermore, LY194002, an inhibitor of PI3K, abrogated sh-*Klf4*-evoked cardiac hypertrophy. These results indicate that inactivation of PI3K/AKT signaling by OT may therefore play a causal role in its anti-hypertrophic action.

## LIMITATIONS

In our *in vivo* study, we showed the anti-hypertrophic effects of exogenous oxytocin administration on ISO-induced cardiac hypertrophy. Since oxytocin is an endogenous hormone and oxytocin and oxytocin receptors are located in the heart, oxytocin concentrations in hypertrophic heart tissues should have been assayed. Moreover, a lack of evaluation of cardiac diastolic function of rats is the limitation of this study. Our study

revealed the role of lncRNA GAS5 and KLF4 in cardiac hypertrophy in an *in vitro* model, not in an *in vivo* one. Therefore, much more work needs to be done to validate lncRNA GAS5 and KLF4 as potential mediating factors in the anti-hypertrophic effects of OT in an *in vivo* model.

## CONCLUSION

Taken together, OT-conferred anti-hypertrophic effects are mediated via inhibiting PI3K/AKT signaling pathway through up-regulating lncRNA GAS5 and KLF4 and down-regulating miR-375-3p. Our findings provide not only new evidence that OT could be an agent to ameliorate cardiac hypertrophy, but also insights into the potential therapeutic targets for cardiac hypertrophy.

## DATA AVAILABILITY STATEMENT

The original contributions presented in the study are included in the article/**Supplementary Material**, further inquiries can be directed to the corresponding author.

## ETHICS STATEMENT

The animal study was reviewed and approved by the Animal Care and Ethics Committee of Kunming Medical University.

## REFERENCES

- Alizadeh, A. M., Faghihi, M., Sadeghipour, H. R., Mohammadghasemi, F., Imani, A., Houshmand, F., et al. (2010). Oxytocin Protects Rat Heart against Ischemia-Reperfusion Injury via Pathway Involving Mitochondrial ATP-dependent Potassium Channel. *Peptides* 31 (7), 1341–1345. doi:10.1016/j.peptides.2010.04.012
- Almansoub, H. A. M. M., Tang, H., Wu, Y., Wang, D. Q., Mahaman, Y. A. R., Salissou, M. T. M., et al. (2020). Oxytocin Alleviates MPTP-Induced Neurotoxicity in Mice by Targeting MicroRNA-26a/Death-Associated Protein Kinase 1 Pathway. *J. Alzheimers Dis.* 74 (3), 883–901. doi:10.3233/JAD-191091
- Azevedo, P. S., Polegato, B. F., Minicucci, M. F., Paiva, S. A., and Zornoff, L. A. (2016). Cardiac Remodeling: Concepts, Clinical Impact, Pathophysiological Mechanisms and Pharmacologic Treatment. *Arq Bras Cardiol.* 106 (1), 62–69. doi:10.5935/abc.20160005
- Belém-Filho, I. J. A., Brasil, T. F. S., Fortaleza, E. A. T., Antunes-Rodrigues, J., and Corrêa, F. M. A. (2021). A Functional Selective Effect of Oxytocin Secreted under Restraint Stress in Rats. *Eur. J. Pharmacol.* 904, 174182. doi:10.1016/j.ejphar.2021.174182
- Benjamin, E. J., Muntner, P., Alonso, A., Bittencourt, M. S., Callaway, C. W., Carson, A. P., et al. (2019). Heart Disease and Stroke Statistics-2019 Update: A Report from the American Heart Association. *Circulation* 139 (10), e56–e528. doi:10.1161/cir.0000000000000659
- Carter, C. S., Kenkel, W. M., Maclean, E. L., Wilson, S. R., Perkeybile, J. R., Yee, J. R., et al. (2020). Is Oxytocin "Nature's Medicine". *Pharmacol. Rev.* 72 (4), 829–861. doi:10.1124/pr.120.019398
- Chang, Y. L., Zhou, P. J., Wei, L., Li, W., Ji, Z., Fang, Y. X., et al. (2015). MicroRNA-7 Inhibits the Stemness of Prostate Cancer Stem-like Cells and Tumorigenesis by Repressing KLF4/PI3K/Akt/p21 Pathway. *Oncotarget* 6 (27), 24017–24031. doi:10.18632/oncotarget.4447

## AUTHOR CONTRIBUTIONS

YY, ZW, MY contributed to conception, methodology, data curation, and writing-original draft. WX performed the statistical analysis and visualization. JW, YF and WY wrote sections of the manuscript. HJ, NS and LL contributed to project administration. JQ contributed to supervision, funding acquisition, and writing-review and editing. All authors contributed to manuscript revision, read, and approved the submitted version.

## FUNDING

This work was supported by the National Natural Science Foundation of China (82060060, 81860050), Yunnan Health Training Project of High Levels Talents (L-2018007), Program for Innovative Research Team of Kunming Medical University (CXTD201802), Yunnan Provincial Ten Thousand-Talent Program-Famous Doctor (YNWR-MY-2018-043). Innovative fund of Kunming medical university (2021D07) (Yunnan Provincial Science and Technology Department (202101AY070001-132)).

## SUPPLEMENTARY MATERIAL

The Supplementary Material for this article can be found online at: <https://www.frontiersin.org/articles/10.3389/fphar.2021.766024/full#supplementary-material>

- Condorelli, G., Drusco, A., Stassi, G., Bellacosa, A., Roncarati, R., Iaccarino, G., et al. (2002). Akt Induces Enhanced Myocardial Contractility and Cell Size *In Vivo* in Transgenic Mice. *Proc. Natl. Acad. Sci. U S A.* 99 (19), 12333–12338. doi:10.1073/pnas.172376399
- Ding, L., Li, S., Wang, F., Xu, J., Li, S., Wang, B., et al. (2021). Berberine Improves Dietary-Induced Cardiac Remodeling by Upregulating Kruppel-like Factor 4-dependent Mitochondrial Function. *Biol. Chem.* 402 (7), 795–803. doi:10.1515/hsz-2020-0267
- Feng, H., Wu, J., Chen, P., Wang, J., Deng, Y., Zhu, G., et al. (2019). MicroRNA-375-3p Inhibitor Suppresses Angiotensin II-Induced Cardiomyocyte Hypertrophy by Promoting Lactate Dehydrogenase B Expression. *J. Cell Physiol* 234 (8), 14198–14209. doi:10.1002/jcp.28116
- Florian, M., Jankowski, M., and Gutkowska, J. (2010). Oxytocin Increases Glucose Uptake in Neonatal Rat Cardiomyocytes. *Endocrinology* 151 (2), 482–491. doi:10.1210/en.2009-0624
- Gao, L., Yao, R., Liu, Y., Wang, Z., Huang, Z., Du, B., et al. (2017). Isorhamnetin Protects against Cardiac Hypertrophy through Blocking PI3K-AKT Pathway. *Mol. Cell Biochem* 429 (1–2), 167–177. doi:10.1007/s11010-017-2944-x
- Garikipati, V. N., Krishnamurthy, P., Verma, S. K., Khan, M., Abramova, T., Mackie, A. R., et al. (2015). Negative Regulation of miR-375 by Interleukin-10 Enhances Bone Marrow-Derived Progenitor Cell-Mediated Myocardial Repair and Function after Myocardial Infarction. *Stem Cells* 33 (12), 3519–3529. doi:10.1002/stem.2121
- Garikipati, V. N., Verma, S. K., Joladarashi, D., Cheng, Z., Ibeti, J., Cimini, M., et al. (2017). Therapeutic Inhibition of miR-375 Attenuates post-myocardial Infarction Inflammatory Response and Left Ventricular Dysfunction via PDK-1-AKT Signalling axis. *Cardiovasc. Res.* 113 (8), 938–949. doi:10.1093/cvr/cvx052
- Garrott, K., Dyavanapalli, J., Cauley, E., Dwyer, M. K., Kuzmiak-Glancy, S., Wang, X., et al. (2017). Chronic Activation of Hypothalamic Oxytocin Neurons Improves Cardiac Function during Left Ventricular Hypertrophy-Induced Heart Failure. *Cardiovasc. Res.* 113 (11), 1318–1328. doi:10.1093/cvr/cvx084

- Gonzalez-Reyes, A., Menaouar, A., Yip, D., Danalache, B., Plante, E., Noiseux, N., et al. (2015). Molecular Mechanisms Underlying Oxytocin-Induced Cardiomyocyte protection from Simulated Ischemia-Reperfusion. *Mol. Cell Endocrinol* 412, 170–181. doi:10.1016/j.mce.2015.04.028
- Hao, S., Liu, X., Sui, X., Pei, Y., Liang, Z., and Zhou, N. (2018). Long Non-coding RNA GAS5 Reduces Cardiomyocyte Apoptosis Induced by MI through Sema3a. *Int. J. Biol. Macromol* 120 (Pt A), 371–377. doi:10.1016/j.jbiomac.2018.08.039
- Jankowski, M., Broderick, T. L., and Gutkowska, J. (2020). The Role of Oxytocin in Cardiovascular Protection. *Front. Psychol.* 11, 2139. doi:10.3389/fpsyg.2020.02139
- Jovanovic, P., Spasojevic, N., Puskas, N., Stefanovic, B., and Dronjak, S. (2019). Oxytocin Modulates the Expression of Norepinephrine Transporter,  $\beta_3$ -adrenoceptors and Muscarinic M2 Receptors in the Hearts of Socially Isolated Rats. *Peptides* 111, 132–141. doi:10.1016/j.peptides.2018.06.008
- Jusic, A., and Devaux, Y. (2020). Mitochondrial Noncoding RNA-Regulatory Network in Cardiovascular Disease. *Basic Res. Cardiol.* 115 (3), 23. doi:10.1007/s00395-020-0783-5
- Kee, H. J., and Kook, H. (2009). Krüppel-like Factor 4 Mediates Histone Deacetylase Inhibitor-Induced Prevention of Cardiac Hypertrophy. *J. Mol. Cell Cardiol* 47 (6), 770–780. doi:10.1016/j.jmcc.2009.08.022
- Kobayashi, H., Yasuda, S., Bao, N., Iwasa, M., Kawamura, I., Yamada, Y., et al. (2009). Postinfarct Treatment with Oxytocin Improves Cardiac Function and Remodeling via Activating Cell-Survival Signals and Angiogenesis. *J. Cardiovasc. Pharmacol.* 54 (6), 510–519. doi:10.1097/FJC.0b013e3181bfac02
- Liao, X., Haldar, S. M., Lu, Y., Jeyaraj, D., Paruchuri, K., Nahori, M., et al. (2010). Krüppel-like Factor 4 Regulates Pressure-Induced Cardiac Hypertrophy. *J. Mol. Cell Cardiol* 49 (2), 334–338. doi:10.1016/j.jmcc.2010.04.008
- Liu, H. L., Chen, C. H., and Sun, Y. J. (2019). Overexpression of lncRNA GAS5 Attenuates Cardiac Fibrosis through Regulating PTEN/MMP-2 Signal Pathway in Mice. *Eur. Rev. Med. Pharmacol. Sci.* 23 (10), 4414–4418. doi:10.26355/eurev\_201905\_17949
- Liu, Z. H., Liu, H. B., and Wang, J. (2018). Astragaloside IV Protects against the Pathological Cardiac Hypertrophy in Mice. *Biomed. Pharmacother.* 97, 1468–1478. doi:10.1016/j.biopha.2017.09.092
- Mcnamara, D. M. (2008). Emerging Role of Pharmacogenomics in Heart Failure. *Curr. Opin. Cardiol.* 23 (3), 261–268. doi:10.1097/HCO.0b013e3282fcd662
- Menaouar, A., Florian, M., Wang, D., Danalache, B., Jankowski, M., and Gutkowska, J. (2014). Anti-hypertrophic Effects of Oxytocin in Rat Ventricular Myocytes. *Int. J. Cardiol.* 175 (1), 38–49. doi:10.1016/j.ijcard.2014.04.174
- Phie, J., Haleagrahara, N., Newton, P., Constantinou, C., Saranyai, Z., Chilton, L., et al. (2015). Prolonged Subcutaneous Administration of Oxytocin Accelerates Angiotensin II-Induced Hypertension and Renal Damage in Male Rats. *PLoS one* 10 (9), e0138048. doi:10.1371/journal.pone.0138048
- Plante, E., Menaouar, A., Danalache, B. A., Yip, D., Broderick, T. L., Chiasson, J. L., et al. (2015). Oxytocin Treatment Prevents the Cardiomyopathy Observed in Obese Diabetic Male Db/db Mice. *Endocrinology* 156 (4), 1416–1428. doi:10.1210/en.2014-1718
- Polshakan, M., Khor, V., Alizadeh, A., Ghayour-Mobarhan, M., Saeidi, M., Jand, Y., et al. (2019). The SAFE Pathway Is Involved in the Postconditioning Mechanism of Oxytocin in Isolated Rat Heart. *Peptides* 111, 142–151. doi:10.1016/j.peptides.2018.04.002
- Reiss, A. B., Glass, D. S., Lam, E., Glass, A. D., De Leon, J., and Kasselman, L. J. (2019). Oxytocin: Potential to Mitigate Cardiovascular Risk. *Peptides* 117, 170089. doi:10.1016/j.peptides.2019.05.001
- Tang, J., Zhong, G., Wu, J., Chen, H., and Jia, Y. (2018). SOX2 Recruits KLF4 to Regulate Nasopharyngeal Carcinoma Proliferation via PI3K/AKT Signaling. *Oncogenesis* 7 (8), 61. doi:10.1038/s41389-018-0074-2
- Tracy, L. M., Gibson, S. J., Labuschagne, I., Georgiou-Karistianis, N., and Giummarra, M. J. (2018). Intranasal Oxytocin Reduces Heart Rate Variability during a Mental Arithmetic Task: A Randomised, Double-Blind, Placebo-Controlled Cross-Over Study. *Prog. Neuropsychopharmacol. Biol. Psychiatry* 81, 408–415. doi:10.1016/j.pnpbp.2017.08.016
- Wang, P., Wang, S., Yang, H., Lv, C., Jia, S., Wang, X., et al. (2019). Therapeutic Potential of Oxytocin in Atherosclerotic Cardiovascular Disease: Mechanisms and Signaling Pathways. *Front. Neurosci.* 13 (undefined), 454. doi:10.3389/fnins.2019.00454
- Wang, Y. N., Shan, K., Yao, M. D., Yao, J., Wang, J. J., Li, X., et al. (2016). Long Noncoding RNA-GAS5: A Novel Regulator of Hypertension-Induced Vascular Remodeling. *Hypertension* 68 (3), 736–748. doi:10.1161/hypertensionaha.116.07259
- Xu, Y., Luo, Y., Liang, C., and Zhang, T. (2020). lncRNA-Mhrt Regulates Cardiac Hypertrophy by Modulating the miR-145a-5p/KLF4/myocardin axis. *J. Mol. Cell Cardiol* 139, 47–61. doi:10.1016/j.jmcc.2019.12.013
- Xu, Y., Fang, H., Xu, Q., Xu, C., Yang, L., and Huang, C. (2020). lncRNA GAS5 Inhibits NLRP3 Inflammasome Activation-Mediated Pyroptosis in Diabetic Cardiomyopathy by Targeting miR-34b-3p/AHR. *Cell Cycle* 19, 3054–3065. doi:10.1080/15384101.2020.1831245
- Yoshida, T., Yamashita, M., Horimai, C., and Hayashi, M. (2014). Kruppel-like Factor 4 Protein Regulates Isoproterenol-Induced Cardiac Hypertrophy by Modulating Myocardin Expression and Activity. *J. Biol. Chem.* 289 (38), 26107–26118. doi:10.1074/jbc.M114.582809
- Zhu, L., Li, N., Sun, L., Zheng, D., and Shao, G. (2021). Non-coding RNAs: The Key Detectors and Regulators in Cardiovascular Disease. *Genomics* 113, 1233–1246. doi:10.1016/j.ygeno.2020.10.024
- Zhu, W., Trivedi, C. M., Zhou, D., Yuan, L., Lu, M. M., and Epstein, J. A. (2009). Inpp5f Is a Polyphosphoinositide Phosphatase that Regulates Cardiac Hypertrophic Responsiveness. *Circ. Res.* 105 (12), 1240–1247. doi:10.1161/circresaha.109.208785

**Conflict of Interest:** The authors declare that the research was conducted in the absence of any commercial or financial relationships that could be construed as a potential conflict of interest.

**Publisher's Note:** All claims expressed in this article are solely those of the authors and do not necessarily represent those of their affiliated organizations, or those of the publisher, the editors and the reviewers. Any product that may be evaluated in this article, or claim that may be made by its manufacturer, is not guaranteed or endorsed by the publisher.

Copyright © 2021 Yang, Wang, Yao, Xiong, Wang, Fang, Yang, Jiang, Song, Liu and Qian. This is an open-access article distributed under the terms of the Creative Commons Attribution License (CC BY). The use, distribution or reproduction in other forums is permitted, provided the original author(s) and the copyright owner(s) are credited and that the original publication in this journal is cited, in accordance with accepted academic practice. No use, distribution or reproduction is permitted which does not comply with these terms.



# LKB1 Regulates Vascular Macrophage Functions in Atherosclerosis

Xuwen Wang<sup>1,2†</sup>, Ziwei Liang<sup>3†</sup>, Hong Xiang<sup>4</sup>, Yanqiu Li<sup>1</sup>, Shuhua Chen<sup>5\*</sup> and Hongwei Lu<sup>1,2,4\*</sup>

<sup>1</sup>Health Management Center, The Third Xiangya Hospital of Central South University, Changsha, China, <sup>2</sup>Department of Cardiology, The Third Xiangya Hospital of Central South University, Changsha, China, <sup>3</sup>Department of Clinical Laboratory, Yueyang people's Hospital, Yueyang, China, <sup>4</sup>Center for Experimental Medicine, The Third Xiangya Hospital of Central South University, Changsha, China, <sup>5</sup>Department of Biochemistry, School of Life Sciences of Central South University, Changsha, China

## OPEN ACCESS

### Edited by:

Xianwei Wang,  
Xinxiang Medical University, China

### Reviewed by:

Geoff H. Werstuck,  
McMaster University, Canada  
Tzong-Shyuan Lee,  
National Taiwan University, Taiwan

### \*Correspondence:

Hongwei Lu  
hongweilu@csu.edu.cn  
Shuhua Chen  
shuhuachen@csu.edu.cn

<sup>†</sup>These authors have contributed  
equally to this work and share first  
authorship

### Specialty section:

This article was submitted to  
Cardiovascular and Smooth Muscle  
Pharmacology,  
a section of the journal  
Frontiers in Pharmacology

**Received:** 06 November 2021

**Accepted:** 29 November 2021

**Published:** 15 December 2021

### Citation:

Wang X, Liang Z, Xiang H, Li Y, Chen S  
and Lu H (2021) LKB1 Regulates  
Vascular Macrophage Functions  
in Atherosclerosis.  
Front. Pharmacol. 12:810224.  
doi: 10.3389/fphar.2021.810224

Liver kinase B1 (LKB1) is known to shape the regulation of macrophage function by participating in multiple processes including cell metabolism, growth, and polarization. However, whether LKB1 also affects the functional plasticity of macrophages in atherosclerosis has not attracted much attention. Abnormal macrophage function is a pathophysiological hallmark of atherosclerosis, characterized by the formation of foam cells and the maintenance of vascular inflammation. Mounting evidence supports that LKB1 plays a vital role in the regulation of macrophage function in atherosclerosis, including affecting lipid metabolism reprogramming, inflammation, endoplasmic reticulum stress, and autophagy in macrophages. Thus, decreased expression of LKB1 in atherosclerosis aggravates vascular injury by inducing excessive lipid deposition in macrophages and the formation of foam cells. To systematically understand the role and potential mechanism of LKB1 in regulating macrophage functions in atherosclerosis, this review summarizes the relevant data in this regard, hoping to provide new ideas for the prevention and treatment of atherosclerosis.

**Keywords:** liver kinase B1, atherosclerosis, macrophage function, AMPK, inflammatory

## INTRODUCTION

Atherosclerosis is a systemic vascular disease, which is the pathological basis of cardiovascular and cerebrovascular diseases such as coronary heart disease and stroke (Ibanez et al., 2021; Shea et al., 2021). With the gradual increase in prevalence, atherosclerosis-related diseases have brought a heavy burden to patients and society, and become a major risk of death (Valanti et al., 2021). Atherosclerotic lesions are characterized by lipid deposition in the arterial intima, focal fibrosis, inflammation, and intimal plaque formation (Nakagawa et al., 2021). In the early stage of atherosclerosis, circulating chemokines derived from blood monocytes increase, which promote the migration of cells to the intima to become macrophages (Cochain and Zernecke, 2017). Meanwhile, a substantial amount of low-density lipoprotein (LDL) is deposited in the arterial wall and is oxidized into oxidized LDL (Ox-LDL). This oxidized form of LDL cannot be recognized by the LDL receptors and internalized into cells for decomposition but is mainly recognized and taken up by macrophages through the scavenger receptors (SR) (Shen et al., 2020). Cholesterol-laden macrophages then turn into foam cells, whose formation is a key marker of atherosclerotic plaque development (Bäck et al., 2019; Xia et al., 2020).



In addition to the formation and accumulation of foam cells, sustained inflammatory response is another indispensable contributor to atherosclerotic lesion (Jeon et al., 2020). As the main innate immune cells, macrophages play a key role in maintaining the inflammatory response of blood vessels and regulating the stability of atherosclerotic plaques by producing pro-inflammatory cytokines (Kim et al., 2021). Moreover, macrophages promote the development of atherosclerosis in other ways, such as through endoplasmic reticulum (ER) stress and autophagy (Zhou et al., 2021). Although the exact mechanism behind macrophage regulation of atherosclerosis is unclear, certain kinases seem to hold the key to determine macrophage phenotype and function.

Liver kinase B1 (LKB1) is a serine/threonine kinase that is widely present in various tissues and cells and regulates cell proliferation, metabolism, polarity, and migration (Zhang Y. et al., 2021). LKB1 mainly acts by phosphorylating and activating adenosine monophosphate-activated protein kinase (AMPK) (Hollstein et al., 2019). Through AMPK, LKB1 regulates lipid metabolism, glycolysis, and other metabolic pathways to maintain the phenotype and function of normal cells (Zhang Y. et al., 2021; Molina et al., 2021). LKB1 is also a negative regulator of inflammatory response (Wu et al., 2021). Studies have shown that LKB1 exerts anti-inflammatory effects by activating AMPK in macrophages to inhibit the production of pro-inflammatory mediators and chemokines (Filippov et al., 2013). Moreover, LKB1 may participate in the regulation of ER stress and autophagy of macrophages through other pathways (Khayati et al., 2020; Zuo et al., 2020). With the deepening of understanding, the pathophysiological value of LKB1 in cardiovascular and metabolic diseases has attracted much attention (Liang et al., 2021; Liu et al., 2021). It has been observed that LKB1 expression is down-regulated in atherosclerotic macrophages and is involved in the regulation of atherosclerosis (Liu et al., 2017). Given that the particular regulatory importance of LKB1 in macrophage function in atherosclerosis has not been systematically described, here we review the role and possible mechanism of LKB1 in shaping macrophage function to reveal the potential target for the treatment of atherosclerosis.

## Functional Plasticity of Macrophages in Atherosclerosis

The etiology of atherosclerosis is more complex than previously thought, and its risk factors include hypertension, hyperlipidemia, heavy smoking, diabetes, and genetic predisposition (Lien et al., 2020; Wang and Ge, 2021; Zhao et al., 2021). Generally, different factors interact and converge to affect the formation of foam cells and the maintenance of vascular inflammation, thereby promoting the occurrence of atherosclerosis (Poznyak et al., 2020a). There is no doubt that the phenotypic and functional changes of macrophage are the hub of the pathological process of atherosclerosis (Zhang et al., 2019). The phenotypic and functional plasticity of atherosclerotic macrophages mainly involves lipid metabolism reprogramming, maintenance of inflammatory response, ER stress, and autophagy

(Sukhorukov et al., 2020a; Cui et al., 2021). Among these, how lipid metabolism affects the phenotype and function of atherosclerotic macrophage has been extensively studied (Zhang Y. X. et al., 2021; Kotlyarov and Kotlyarova, 2021). Under normal conditions, macrophages can process intracellular lipids through uptake, synthesis, storage, and outflow to ensure the dynamic equilibrium of lipid metabolism (Sukhorukov et al., 2020b). However, when lipid intake exceeds the tolerance limit of macrophages, or relevant receptors and pathways are dysfunctional, the lipid metabolism of the cells will be disrupted and reprogrammed, resulting in the transformation of macrophages into foam cells and then the occurrence of atherosclerosis (Poznyak et al., 2020a).

The vascular inflammation of atherosclerosis is also one of the current research hotspots. Macrophages participate in atherosclerotic lesions by releasing pro-inflammatory cytokines and anti-inflammatory cytokines to maintain vascular inflammation (Cai D. et al., 2021). Excessive infiltration of macrophages will not only lead to focal arterial inflammation, but also increase the risk of systemic vascular inflammation; either way it will accelerate the progression of atherosclerosis (Lavin et al., 2020). Macrophage polarization is involved in maintaining vascular inflammation and has been shown to be necessary for the occurrence and development of atherosclerosis (Liu et al., 2020). Under different conditions, macrophages polarize into different subtypes to participate in the inflammatory response. Macrophages in atherosclerosis may polarize into the classically activated macrophage (M1) and alternatively activated macrophage (M2) phenotypes (Murray et al., 2014). The M2 phenotype can be further divided into subtypes M2a, M2b, M2c, and M2d (Colin et al., 2014). In addition, macrophages in atherosclerosis can differentiate into Mox, Mhem, M4, and M(Hb) phenotypes under the stimulation of certain factors. According to their functionality, M1, Mox, and M4 mainly have pro-inflammatory effects and promote the formation of atherosclerosis, while M2, Mhem, and M(Hb) can produce anti-inflammatory effects and prevent the formation of foam cells (Colin et al., 2014; Jinnouchi et al., 2020). M1 and M2 macrophages are the most important polarization subtypes in atherosclerosis. In the initial stage of vascular inflammation, circulating monocytes are recruited into vascular tissues, and are mainly polarized into M1 under the stimulation of pro-inflammatory factors. M1 macrophages further secrete tumor necrosis factor- $\alpha$  (TNF- $\alpha$ ), (human)  $\beta$ -Interleukin 1 (IL-1 $\beta$ ), interleukin-6 (IL-6), Interferon- $\gamma$  (IFN- $\gamma$ ), and other pro-inflammatory mediators, which in turn aggravate vascular inflammation (Saha et al., 2017). Relatively, macrophages polarize into M2 during the self-repair of blood vessels, and inhibit M1-mediated vascular inflammation by up-regulating transforming growth factor- $\beta$  (TGF- $\beta$ ), interleukin-10 (IL-10), and other anti-inflammatory cytokines (Murray, 2016). Although M1 and M2 can be seen in both early and late atherosclerotic lesions, as atherosclerosis progresses, the number of M1 gradually increases and the number of M2 gradually decreases (Bisgaard et al., 2016).

ER stress in macrophages is also closely related to the occurrence of atherosclerosis (Yang B. et al., 2020). ER stress



aggravates atherosclerosis by inducing foam cell formation, apoptosis, and the release of pro-inflammatory cytokines (Tian et al., 2019; Wang T. et al., 2020). Increased expression of the ER stress-associated apoptosis signaling molecule C/EBP homologous protein (CHOP) indicates macrophage apoptosis (Yang et al., 2020b). Pathologically, macrophage apoptosis instigates the formation of inflammatory necrotic core, which is not conducive to the stability of advanced atherosclerotic plaques and thus underlies plaque rupture (Qiu et al., 2021).

On the contrary, autophagy of macrophages can delay cell death by repairing damaged macrophages, thereby protecting against atherosclerosis. Also, the autophagic machinery helps nearby phagocytes to effectively eliminate damaged cells (Liao et al., 2012). Thus, it is expected that dysregulated macrophage autophagy will contribute to the occurrence and development of atherosclerosis through promoting dyslipidemia, foam cell formation, and inflammation (Kumar et al., 2021; Shan et al., 2021). However, it has been observed that macrophage autophagy has a dual regulatory effect on the inflammatory response (Zhang J. et al., 2021). Under normal circumstances, autophagy can effectively inhibit the excessive activation of inflammasomes, thereby alleviating severe inflammatory response. However, when this self-digesting mechanism is inhibited or damaged, cathepsin will leak from the damaged lysosomes, further activates the inflammasomes, thus exacerbating the inflammatory response (Takahama et al., 2018). Generally, functional changes of lipid metabolism reprogramming, inflammation maintenance, ER stress and autophagy in macrophages are dynamic and interconnected, but any abnormal alterations in these cellular functions may eventually lead to atherosclerotic progression at multiple levels.

## LKB1 and Lipid Metabolism Reprogramming of Macrophages in Atherosclerosis

Lipid metabolism reprogramming is one of the main causes of early atherosclerosis formation. There are many types of lipids in the body, among which total cholesterol (TC) and triglyceride (TG) are mainly related to atherosclerosis. TC consists of free cholesterol (FC) and cholesterol ester (CE) (Cai Y. et al., 2021). Due to poor water solubility, lipids often exist in the form of highly soluble lipoproteins. The main lipoproteins closely related to atherosclerosis are LDL and chemically modified LDL, such as Ox-LDL (Malekmohammad et al., 2021). The circulating LDL binds to the LDL receptors on normal cell membranes, but Ox-LDL does not. Ox-LDL is recognized by SR on the surface membrane of macrophages and taken up into the cell for metabolism. This internalization and process involves SR class A type 1 (SR-A1), SR class B type 1 (SR-B1), ATP-binding cassette transporter A1 (ABCA1), and adenosine triphosphate-binding cassette (ABC) transporter G1 (ABCG1) (Jia et al., 2019; Kobayashi et al., 2021; Tao et al., 2021). Lipids in macrophages are normally metabolized through uptake, synthesis, storage, and outflow (Chistiakov et al., 2017). This metabolic mechanism is essential for maintaining the steady state of lipid metabolism. The imbalance of lipid metabolism will

initiates the reprogramming of lipid metabolism and the differentiation of macrophages into foam cells, which is a prerequisite for the formation of atherosclerosis (Poznyak et al., 2020a; Poznyak et al., 2020b).

LKB1 can inhibit the formation of atherosclerosis by reprogramming lipid metabolism of macrophages. On the one hand, LKB1 can affect the lipid uptake of macrophages. Macrophage membrane molecule SR-A is closely related to pathological intracellular lipid deposition, and its primary function is to recognize and uptake Ox-LDL and mediate the formation of foam cells. However, LKB1, as the upstream kinase of SR-A, can phosphorylate SR-A for degradation (Liu et al., 2017). It has been found that in the process of atherosclerotic plaque progression, the membrane expression of SR-A is high, while the expression of LKB1 in macrophages is decreased (Lin et al., 2016; Liu et al., 2017). These findings indicate that in the absence of phosphorylation and degradation of SR-A, SR-A can increase pathological lipid deposition and promote foam cell formation. On the other hand, LKB1 may affect lipid efflux from macrophages. Macrophages lipid efflux is dependent on the expression of ABCA1, ABCG1, and SR-B1 on the membrane surface. The high expression of these transporters and receptors will facilitate lipid efflux and reduce foam cell formation. It has been confirmed that the activation of AMPK/SIRT1/LXR $\alpha$  and AMPK/STAT1/STING signaling pathways in macrophages can up-regulate the expressions of ABCA1, ABCG1, and SR-B1, promote intracellular cholesterol outflow, reduce lipid accumulation, and ultimately prevent the occurrence of atherosclerosis (Lin et al., 2015; Cai D. et al., 2021). Interestingly, LKB1 is the main upstream kinase of AMPK, so it may participate in cellular lipid metabolism by activating AMPK (Xi et al., 2018). Nevertheless, more evidence is needed to evaluate that macrophage LKB1 participates in intracellular lipid outflow and negatively regulates atherosclerotic plaque formation by activating AMPK/SIRT1/LXR  $\alpha$  and AMPK/STAT1/STING signaling pathways (Figure1).

## LKB1 and Maintenance of Macrophage Inflammatory Response in Atherosclerosis

Inflammatory immune response is an essential part of the pathogenesis of atherosclerosis (Liao et al., 2021). More specifically, vascular inflammation is the main driving force for the formation and growth of atherosclerotic lesions and the development of unstable ruptured plaques (Romanenko et al., 2021). Mechanistically, inflammatory response mainly relies on various cytokines and mediators to participate in the whole process of atherosclerosis development. Especially in the late stage of atherosclerosis, pro-inflammatory cytokines cause abnormal functions of macrophages, endothelial cells, and lymphocytes, thus accelerating the destruction of plaques (Poznyak et al., 2021). Cytokines are synthesized by various immune cells and secreted in autocrine and paracrine manners. As the most abundant immune cells in atherosclerotic lesions, macrophages have a vital role in the entire disease process from the onset of the lesion to the rupture of the plaque (Chen et al., 2020). Under the long-term

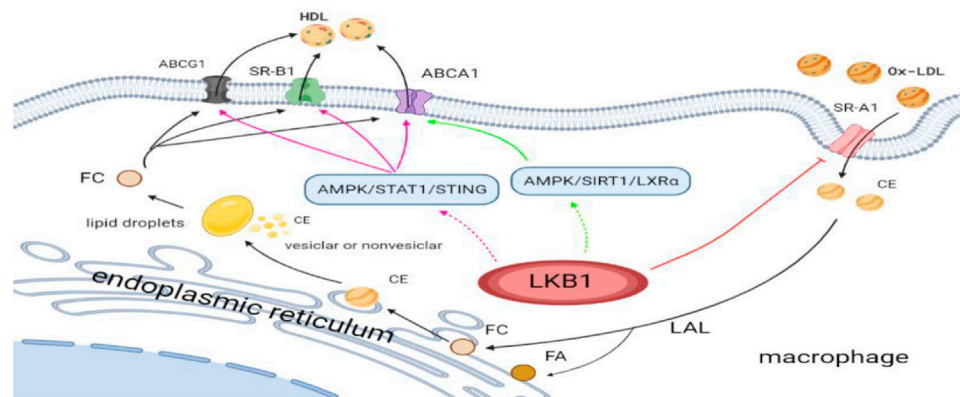


**FIGURE 1 |** LKB1 and lipid metabolism reprogramming of macrophages in atherosclerosis. Ox-LDL, oxidized low-density lipoprotein; SR-A1, scavenger receptor class A type 1; CE, cholesterol ester; FA, fatty acid; FC, free cholesterol; LAL, lysosomal acid lipase; HDL, high-density lipoprotein; SR-B1, scavenger receptor class B type 1; ABCG1, adenosine triphosphate (ATP)-binding cassette (ABC) transporter G1; ABCA1, ATP-binding cassette transporter A1.

effect of various interactive factors such as dyslipidemia, the arterial intimal damage is aggravated, the expression of adhesion factors increases, the number of monocytes attached to the endothelial cells gradually increases, and the number of intimal macrophage increases (Shen et al., 2020). Atherogenic macrophages produce and secrete a variety of pro-inflammatory cytokines [i.e., TNF- $\alpha$ , IL-1 $\beta$ , interleukin-18 (IL-18), IL-6, interleukin-23 (IL-23)] to maintain vascular inflammation and promote the growth of atherosclerotic plaques (Poznyak et al., 2021).

LKB1 is closely related to the release of a variety of pro-inflammatory cytokines (Wang et al., 2019). It was found that activating LKB1/AMPK and LKB1/MARK2 signaling pathways can reduce the release of TNF- $\alpha$ , IL-6, and IL-1 $\beta$  from macrophages, thereby inhibiting the inflammatory response (Wu et al., 2018; Deng et al., 2020). AMPK is a cellular energy sensor, and its  $\alpha$  subunit is mainly distributed in the heart, brain, and liver (Molina et al., 2021). Studies have shown that LKB1 down-regulates the expression of IL-1 $\beta$ , IL-18, and IL-23 through AMPK $\alpha$  phosphorylation, thereby relieving the inflammatory damage at the affected sites (Liu et al., 2019; Guo et al., 2021). However, whether LKB1 inhibits the release of pro-inflammatory cytokines from macrophages through the Mitogen-activated protein kinase2 (MARK2) and AMPK signaling pathways and further regulates the process of atherosclerosis is not fully understood.

In addition, as mentioned above, the ability of macrophages to orchestrate an inflammatory response is related to their polarization phenotypes. Different polarization phenotypes have distinct cytokine secretion profiles, which exhibit opposite effects on the formation of atherosclerosis. It has been reported that up-regulation of LKB1 expression can reduce macrophage infiltration and M1 polarization (Yang et al., 2020c). Furthermore, the LKB1/AMPK signaling pathway can promote the transformation of macrophages from M1 to M2, although further studies are needed to determine the involvement of LKB1 in the regulation of atherosclerotic inflammation by altering macrophage polarization phenotypes (Ji et al., 2018). While the metabolic

signatures of M1 macrophages are increased glucose uptake and enhanced anaerobic glycolysis, activated M2 macrophages show significantly increased oxygen consumption through fatty acid oxidation and oxidative phosphorylation (Jha et al., 2015; Andrejeva and Rathmell, 2017). In view of this, it has been suggested that the metabolic transformations between glycolysis and mitochondrial oxidative phosphorylation are related to the direction of macrophage polarization (Mouton et al., 2020). Moreira et al. found that the LKB1 signaling pathway plays a vital role in the energy metabolism of macrophages, and the LKB1/AMPK signaling pathway regulates the transformation of energy metabolism from glycolysis to oxidative phosphorylation during inflammation (Moreira et al., 2015). This energy transformation regulated by LKB1 is likely to be the reason why macrophages polarize to M2 and participate in the atherosclerotic process. In any case, the energy transformation in the process of macrophage phenotype changes is worthy of further exploration (Figure 2).

## LKB1 and Macrophage ER Stress in Atherosclerosis

Various pathological conditions can lead to the accumulation of unfolded or misfolded proteins in the ER lumen. This phenomenon is called ER stress and usually causes ER dysfunction (Qiao et al., 2021). ER stress performs many pathophysiological functions through the activating transcription factor-6 (ATF-6), transmembrane inositol-requiring enzyme-1 (IRE1), protein kinase RNA-like ER kinase (PERK), and their downstream signaling pathways (Ren et al., 2021). Recent studies have found that ER stress plays a vital role in the occurrence and development of atherosclerosis, which is manifested as a significant upregulation of the ER stress marker CHOP in atherosclerotic plaque macrophages (Ma et al., 2020; Yang B. et al., 2020). It is precisely by mediating the ER stress of intravascular macrophages, endothelial cells, and smooth muscle cells that a variety of factors participate in and exacerbate the pathogenesis of atherosclerosis (Yang et al., 2020b). Among these intravascular cells, macrophage ER stress mainly aggravates atherosclerotic

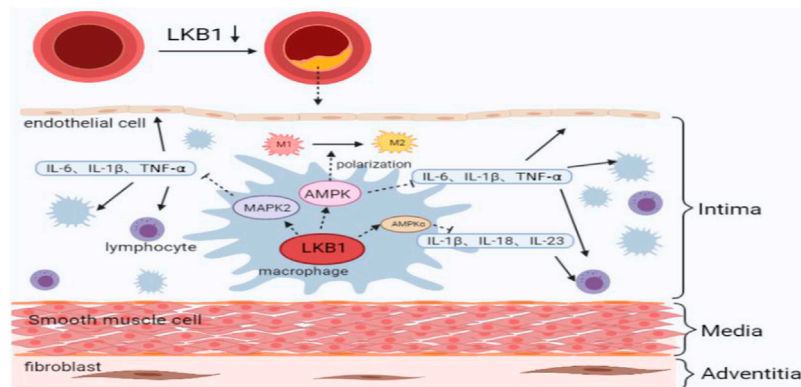


**FIGURE 2 |** LKB1 and maintenance of macrophage inflammatory response in atherosclerosis. M1, classically activated macrophage; M2, alternatively activated macrophage; IL, interleukin; TNF, tumor necrosis factor; AMPK, adenosine 5'-monophosphate activated protein kinase; MAPK, mitogen-activated protein kinase.

vascular damage by inducing foam cell formation and activating the apoptotic signaling pathway (Zahid et al., 2020).

Note that ER stress cross-regulates the production of pro-inflammatory cytokines, which are the main force for maintaining vascular inflammation (Chen et al., 2018). The synergistic effect of ER stress and inflammation substantially affects the formation and stability of dynamic atherosclerotic plaques, which is an essential condition for the development of atherosclerosis. In addition, excessive accumulation of FC in cells is one of the main causes of ER stress in macrophages (Zhu et al., 2008). ER stress in turn actively regulates lipid metabolism in macrophages by coordinating the uptake and outflow of lipids, but ultimately leads to an increase in lipid content in cells. This event clearly involves two mechanisms. On the one hand, ER stress up-regulates the expression of SR-A and the cluster of differentiation 36 (CD36) to increase lipid intake. On the other hand, ER stress increases the expression of CHOP and inhibits the expressions of ABCG1, ABCA1, and SR-B1, thereby reducing lipid efflux (Wang Z. et al., 2020). These two strategies work synergistically to effectively promote the transformation of macrophages into foam cells (Sukhorukov et al., 2020a).

LKB1 has the ability to negatively regulate the ER stress of macrophages, so it is an important part of the atherosclerotic process. It has been found that activation of LKB1/AMPK signaling can reduce ER stress and help improve cardiovascular diseases (Li et al., 2015; Zuo et al., 2020). As mentioned above, LKB1 affects the expression of SR such as SR-A1 on the surface of macrophages, regulates lipid metabolism, inhibits the formation of foam cells, and thus exerts strong anti-atherosclerotic effects. Therefore, the inhibition of ER stress by LKB1/AMPK signaling may be through regulation of lipid metabolism. However, it is not clear whether this effect is achieved through direct interaction with ER stress or caused by indirect and complex cross-regulation mechanisms. In addition, macrophages produce different pro-inflammatory cytokines to maintain the inflammatory response when ER stress occurs. For example, activation of the PERK/ATF4/CHOP signaling pathway promotes the release of TNF- $\alpha$  and IL-1 $\beta$ , and activation of IRE1 $\alpha$ /JNK signaling pathway stimulates the release of IL-1 $\beta$ , IL-6, and IL-8 (Li D. et al., 2021; Song et al.,

2021). However, activating the LKB1/AMPK signaling pathway robustly inhibits ER stress, reduces the production of pro-inflammatory cytokines, and alleviates cellular inflammatory responses (Rao et al., 2019). Therefore, LKB1 may block the release of pro-inflammatory cytokines by inhibiting the ER stress of macrophages, thus exhibiting anti-atherosclerotic effects.

In addition, there are some adaptive mechanisms related to ER stress, including ER-associated degradation and unfolded protein response (UPR). Moderate activation of these mechanisms can counteract excessive ER stress (Ren et al., 2021). UPR is an important regulatory response of the ER stress process, which refers to the degradation of unfolded or faulty proteins in the ER. Interestingly, LKB1/AMPK signaling pathway relieves ER stress by regulating UPR (Meares et al., 2011; Karunakaran et al., 2021). However, UPR may initiate apoptosis under prolonged ER stress. This is because excessive saturated fatty acids and FC in the ER activate CHOP through IRE1 $\alpha$ /JNK, IRE1 $\alpha$ /XBP1, ATF6/XBP1, and PERK/eIF2 $\alpha$ /ATF4 pathways, thus inducing macrophage apoptosis (Tian et al., 2019). Macrophage apoptosis is the basis for the formation of atherosclerosis vulnerable plaques. There are reasons to believe that LKB1 can reduce macrophage apoptosis and slow the progression of atherosclerosis by inhibiting ER stress, but this needs to be verified.

In general, the function of LKB1 is partially related to the ER stress of vascular macrophages. LKB1 can regulate the lipid metabolism of macrophages through the ER stress regulation of SR-A, ABCG1, ABCA1, and SR-B1. Furthermore, LKB1 regulates vascular inflammation and macrophage apoptosis by affecting ER stress. These regulatory mechanisms may work together and form an overlapping regulatory network in atherosclerosis, which needs to be further explored in the future (Figure 3).

## LKB1 and Macrophage Autophagy in Atherosclerosis

Macrophage autophagy seems to have a dual role in atherosclerosis: dysregulated autophagy promotes

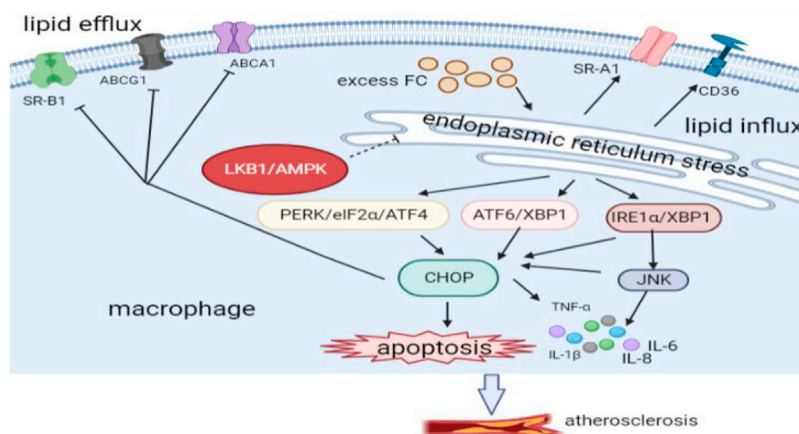


**FIGURE 3 |** LKB1 and endoplasmic reticulum stress of macrophages in atherosclerosis. CD, Cluster differentiation; PERK, protein kinase RNA-like ER kinase; ATF4, activating transcription factor 4; ATF6, activating transcription factor 6; XBP1, the transcription factor X-box-binding protein 1; IRE1 $\alpha$ , inositol-requiring protein 1 $\alpha$ ; JNK, c-JUN N-terminal kinase; CHOP, C/EBP homologous protein.

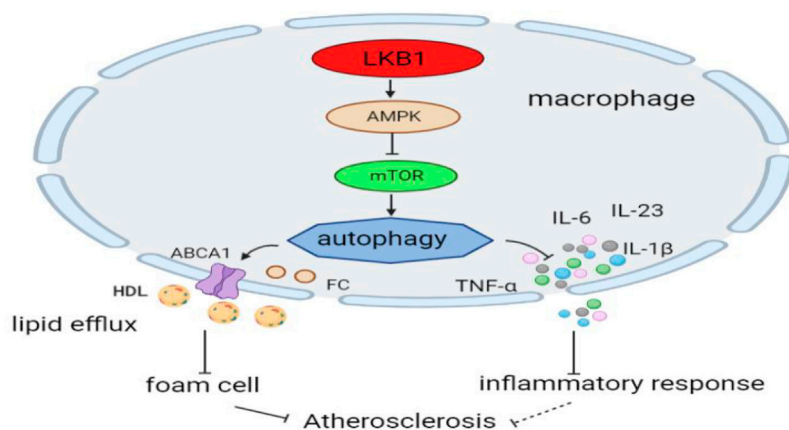


**FIGURE 4 |** LKB1 and macrophage autophagy in atherosclerosis. Activation of the LKB1/AMPK/mTOR signaling pathway can induce autophagic activity in macrophages.

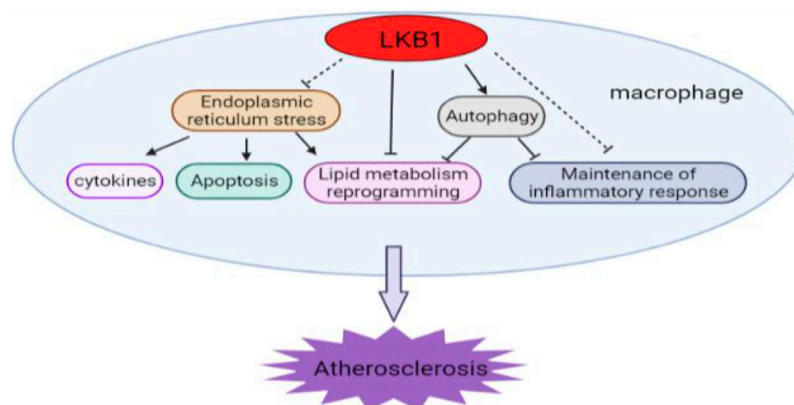


**FIGURE 5 |** The diverse and complex roles of LKB1 in the development of atherosclerosis. LKB1 participates in multiple regulatory activities in vascular macrophages.



atherosclerosis, and moderate autophagy inhibits plaque progression (Zahid et al., 2021). Autophagy is a conservative degradation mode of cells, which is essential for maintaining the main functions of cell metabolism (Chen et al., 2021). When cells suffer from nutrient deficiency, oxidative stress, and organelle dysfunction, autophagy degrades unwanted materials through a lysosomal-dependent pathway to maintain cell homeostasis (Duan et al., 2020). Autophagy of macrophages play an anti-atherosclerotic effect by inhibiting the formation of foam cells and eliminating inflammation (Wang Z. et al., 2020; Tao et al., 2021). Also, autophagy promotes the transformation of foam cells into alternately activated macrophages to alleviate late-stage atherosclerosis (Robichaud et al., 2021). When autophagy is dysregulated, inflammasomes will be overactivated and promote the development of atherosclerosis (Razani et al., 2012). Even in advanced atherosclerosis, dysregulation of macrophage autophagy can increase the number of plaque lesions and the area of necrotic foci (He et al., 2020).

LKB1 affects the occurrence and development of atherosclerosis by regulating the autophagy of macrophages. On the one hand, LKB1 regulates lipid metabolism in macrophages by altering autophagy (Liang et al., 2021). The LKB1/AMPK/mTOR pathway can induce increased autophagy, inhibit lipid synthesis, and promote fatty acid oxidation (Li W. et al., 2021). Moreover, this pathway in macrophages can improve intracellular cholesterol accumulation by promoting cholesterol outflow and reduce the formation of foam cells in atherosclerosis (Li et al., 2019). On the other hand, LKB1 suppresses inflammation by inducing autophagy in macrophages (Liu et al., 2019). The LKB1/AMPK/mTOR signaling pathway reduces the synthesis and release of pro-inflammatory cytokines, such as IL-6, IL-23, IL-1 $\beta$ , and TNF- $\alpha$  (Alexander et al., 2010; Li et al., 2019). However, whether LKB1 has a similar regulatory effect in atherosclerotic macrophages needs to be tested (Figure 4).

## CONCLUSION

LKB1 is a serine-threonine kinase expressed in a variety of cells and is involved in regulating cell metabolism, polarity, and growth. LKB1 is a negative feedback regulator of atherosclerosis, which inhibits foam cell formation and

vascular inflammation in many ways. LKB1's regulation of macrophage lipid metabolism and its inhibition of foam cell formation are achieved by directly affecting the expression of SR or indirectly regulating autophagy. It can also regulate the release of pro-inflammatory cytokines in a variety of ways to inhibit vascular inflammation. Moreover, macrophage ER stress is closely related to the occurrence and development of atherosclerosis. LKB1 may participate in this disease process by affecting the ER stress of macrophages. Together, these different regulatory mechanisms of LKB1 may form an overlapping and complex network that determines the progression and outcome of atherosclerosis (Figure 5). Additionally, activation of LKB1 can alleviate atherosclerosis. This has been initially verified in clinical applications. For example, metformin, an important LKB1/AMPK activator, has been found to improve atherosclerosis (Vasamsetti et al., 2015; Ramachandran et al., 2018). Nevertheless, so far, our understanding of the exact regulatory mechanism of LKB1 in the functional changes of macrophage in atherosclerosis is rather limited. Given the important role of LKB1 in vascular macrophages, this regulator is worthy of further study and has great potential as a new target for the treatment of atherosclerosis.

## AUTHOR CONTRIBUTIONS

Conceptualization, XW and ZL; investigation, YL; resources, HX; writing—original draft preparation, XW; writing—review and editing, ZL; project administration, HL and SC; funding acquisition, HL and SC. All authors have read and agreed to the published version of the manuscript.

## FUNDING

This research was funded by the National Natural Science Foundation of China (grant no. 81870352, 81970252), the Key Research and Development Project of Hunan Province (grant no. 2020SK 2087, 2019SK 2041) and the Fundamental Research Funds for the Central Universities of Central South University (2021zzts0408).

## REFERENCES

- Alexander, A., Cai, S. L., Kim, J., Nanez, A., Sahin, M., MacLean, K. H., et al. (2010). ATM Signals to TSC2 in the Cytoplasm to Regulate mTORC1 in Response to ROS. *Proc. Natl. Acad. Sci. U S A.* 107, 4153–4158. doi:10.1073/pnas.0913860107
- Andrejeva, G., and Rathmell, J. C. (2017). Similarities and Distinctions of Cancer and Immune Metabolism in Inflammation and Tumors. *Cell. Metab.* 26, 49–70. doi:10.1016/j.cmet.2017.06.004
- Bäck, M., Yurdagül, A., Tabas, I., Öörni, K., and Kovanen, P. T. (2019). Inflammation and its Resolution in Atherosclerosis: Mediators and Therapeutic Opportunities. *Nat. Rev. Cardiol.* 16, 389–406. doi:10.1038/s41569-019-0169-2
- Bisgaard, L. S., Mogensen, C. K., Rosendahl, A., Cucak, H., Nielsen, L. B., Rasmussen, S. E., et al. (2016). Bone Marrow-Derived and Peritoneal Macrophages Have Different Inflammatory Response to oxLDL and M1/M2 Marker Expression - Implications for Atherosclerosis Research. *Sci. Rep.* 6, 35234. doi:10.1038/srep35234
- Cai, D., Liu, H., Wang, J., Hou, Y., Pang, T., Lin, H., et al. (2021a). Balasubramide Derivative 3C Attenuates Atherosclerosis in Apolipoprotein E-Deficient Mice: Role of AMPK-STAT1-STING Signaling Pathway. *Aging (Albany NY)* 13, 12160–12178. doi:10.18632/aging.202929
- Cai, J., Wen, J., Ma, S., Mai, Z., Zhan, Q., Wang, Y., et al. (2021b). Huang-Lian-Jie-Du Decoction Attenuates Atherosclerosis and Increases Plaque Stability in High-Fat Diet-Induced ApoE<sup>-/-</sup> Mice by Inhibiting M1 Macrophage Polarization and Promoting M2 Macrophage Polarization. *Front. Physiol.* 12, 666449. doi:10.3389/fphys.2021.666449
- Chen, J., Zhang, M., Zhu, M., Gu, J., Song, J., Cui, L., et al. (2018). Paeoniflorin Prevents Endoplasmic Reticulum Stress-Associated Inflammation in Lipopolysaccharide-Stimulated Human Umbilical Vein Endothelial Cells via

- the IRE1 $\alpha$ /NF-K $\kappa$ B Signaling Pathway. *Food Funct.* 9, 2386–2397. doi:10.1039/c7fo01406f
- Chen, X., Wang, J., Tahir, M., Zhang, F., Ran, Y., Liu, Z., et al. (2021). Current Insights into the Implications of m6A RNA Methylation and Autophagy Interaction in Human Diseases. *Cell. Biosci.* 11, 147. doi:10.1186/s13578-021-00661-x
- Chen, Y. T., Yuan, H. X., Ou, Z. J., and Ou, J. S. (2020). Microparticles (Exosomes) and Atherosclerosis. *Curr. Atheroscler. Rep.* 22, 23. doi:10.1007/s11883-020-00841-z
- Chistiakov, D. A., Melnichenko, A. A., Myasoedova, V. A., Grechko, A. V., and Orekhov, A. N. (2017). Mechanisms of Foam Cell Formation in Atherosclerosis. *J. Mol. Med. (Berl)* 95, 1153–1165. doi:10.1007/s00109-017-1575-8
- Cochain, C., and Zerneck, A. (2017). Macrophages in Vascular Inflammation and Atherosclerosis. *Pflugers. Arch.* 469, 485–499. doi:10.1007/s00424-017-1941-y
- Colin, S., Chinetti-Gbaguidi, G., and Staels, B. (2014). Macrophage Phenotypes in Atherosclerosis. *Immunol. Rev.* 262, 153–166. doi:10.1111/imr.12218
- Cui, X., Xing, R., Tian, Y., Wang, M., Sun, Y., Xu, Y., et al. (2021). The G2A Receptor Deficiency Aggravates Atherosclerosis in Rats by Regulating Macrophages and Lipid Metabolism. *Front. Physiol.* 12, 659211. doi:10.3389/fphys.2021.659211
- Deng, J., Wen, C., Ding, X., Zhang, X., Hou, G., Liu, A., et al. (2020). LKB1-MARK2 Signaling Mediates Lipopolysaccharide-Induced Production of Cytokines in Mouse Macrophages. *J. Cel. Mol. Med.* 24, 11307–11317. doi:10.1111/jcmm.15710
- Duan, R., Xie, H., and Liu, Z. Z. (2020). The Role of Autophagy in Osteoarthritis. *Front. Cel. Dev. Biol.* 8, 608388. doi:10.3389/fcell.2020.608388
- Filippov, S., Pinkosky, S. L., Lister, R. J., Pawloski, C., Hanselman, J. C., Cramer, C. T., et al. (2013). ETC-1002 Regulates Immune Response, Leukocyte Homing, and Adipose Tissue Inflammation via LKB1-dependent Activation of Macrophage AMPK. *J. Lipid. Res.* 54, 2095–2108. doi:10.1194/jlr.M035212
- Guo, J., Peng, L., Zeng, J., Zhang, M., Xu, F., Zhang, X., et al. (2021). Paeoniflorin Suppresses Allergic and Inflammatory Responses by Promoting Autophagy in Rats with Urticaria. *Exp. Ther. Med.* 21, 590. doi:10.3892/etm.2021.10022
- He, L., Zhao, X., and He, L. (2020). LINC01140 Alleviates the Oxidized Low-Density Lipoprotein-Induced Inflammatory Response in Macrophages via Suppressing miR-23b. *Inflammation* 43, 66–73. doi:10.1007/s10753-019-01094-y
- Hollstein, P. E., Eichner, L. J., Brun, S. N., Kamireddy, A., Svensson, R. U., Vera, L. I., et al. (2019). The AMPK-Related Kinases SIK1 and SIK3 Mediate Key Tumor-Suppressive Effects of LKB1 in NSCLC. *Cancer Discov.* 9, 1606–1627. doi:10.1158/2159-8290.CD-18-1261
- Ibanez, B., Fernández-Ortiz, A., Fernández-Friera, L., García-Lunar, I., Andrés, V., and Fuster, V. (2021). Progression of Early Subclinical Atherosclerosis (PESA) Study: JACC Focus Seminar 7/8. *J. Am. Coll. Cardiol.* 78, 156–179. doi:10.1016/j.jacc.2021.05.011
- Jeon, S., Kim, T. K., Jeong, S. J., Jung, I. H., Kim, N., Lee, M. N., et al. (2020). Anti-Inflammatory Actions of Soluble Ninturin-1 Ameliorate Atherosclerosis. *Circulation* 142, 1736–1751. doi:10.1161/CIRCULATIONAHA.120.046907
- Jha, A. K., Huang, S. C., Sergushichev, A., Lampropoulou, V., Ivanova, Y., Loginicheva, E., et al. (2015). Network Integration of Parallel Metabolic and Transcriptional Data Reveals Metabolic Modules that Regulate Macrophage Polarization. *Immunity* 42, 419–430. doi:10.1016/j.immuni.2015.02.005
- Ji, J., Xue, T. F., Guo, X. D., Yang, J., Guo, R. B., Wang, J., et al. (2018). Antagonizing Peroxisome Proliferator-Activated Receptor  $\gamma$  Facilitates M1-To-M2 Shift of Microglia by Enhancing Autophagy via the LKB1-AMPK Signaling Pathway. *Aging Cel.* 17, e12774. doi:10.1111/accel.12774
- Jia, Q., Cao, H., Shen, D., Li, S., Yan, L., Chen, C., et al. (2019). Quercetin Protects against Atherosclerosis by Regulating the Expression of PCSK9, CD36, PPAR $\gamma$ , LXR $\alpha$  and ABCA1. *Int. J. Mol. Med.* 44, 893–902. doi:10.3892/ijmm.2019.4263
- Jinnouchi, H., Guo, L., Sakamoto, A., Torii, S., Sato, Y., Cornelissen, A., et al. (2020). Diversity of Macrophage Phenotypes and Responses in Atherosclerosis. *Cell Mol. Life Sci.* 77, 1919–1932. doi:10.1007/s00018-019-03371-3
- Karunakaran, U., Elumalai, S., Moon, J. S., and Won, K. C. (2021). Pioglitazone-induced AMPK-Glutaminase-1 Prevents High Glucose-Induced Pancreatic  $\beta$ -cell Dysfunction by Glutathione Antioxidant System. *Redox Biol.* 45, 102029. doi:10.1016/j.redox.2021.102029
- Khayati, K., Bhatt, V., Hu, Z. S., Fahumy, S., Luo, X., and Guo, J. Y. (2020). Autophagy Compensates for Lkb1 Loss to Maintain Adult Mice Homeostasis and Survival. *Elife* 9, e62377. doi:10.7554/eLife.62377
- Kim, C. W., Oh, E. T., and Park, H. J. (2021). A Strategy to Prevent Atherosclerosis via TNF Receptor Regulation. *FASEB. J.* 35, e21391. doi:10.1096/fj.202000764R
- Kobayashi, M., Watanabe, K., Suzuki, T., Dohmae, N., Fujiyoshi, M., Uchida, M., et al. (2021). Analysis of the Acrolein-Modified Sites of Apolipoprotein B-100 in LDL. *Biochim. Biophys. Acta Mol. Cel. Biol. Lipids* 1866, 158809. doi:10.1016/j.bbalip.2020.158809
- Kotlyarov, S., and Kotlyarova, A. (2021). The Role of ABC Transporters in Lipid Metabolism and the Comorbid Course of Chronic Obstructive Pulmonary Disease and Atherosclerosis. *Int. J. Mol. Sci.* 22, 6711. doi:10.3390/ijms22136711
- Kumar, S., Nanduri, R., Bhagyaraj, E., Kalra, R., Ahuja, N., Chacko, A. P., et al. (2021). Vitamin D3-VDR-PTPN6 axis Mediated Autophagy Contributes to the Inhibition of Macrophage Foam Cell Formation. *Autophagy* 17, 2273–2289. doi:10.1080/15548627.2020.1822088
- Lavin Plaza, B., Phinikaridou, A., Andia, M. E., Potter, M., Lorrio, S., Rashid, I., et al. (2020). Sustained Focal Vascular Inflammation Accelerates Atherosclerosis in Remote Arteries. *Arterioscler. Thromb. Vasc. Biol.* 40, 2159–2170. doi:10.1161/ATVBAHA.120.314387
- Li, D., Cui, Y., Wang, X., Liu, F., and Li, X. (2021a). Apple Polyphenol Extract Alleviates Lipid Accumulation in Free-Fatty-Acid-Exposed HepG2 Cells via Activating Autophagy Mediated by SIRT1/AMPK Signaling. *Phytother. Res.* 35, 1416–1431. doi:10.1002/ptr.6902
- Li, W., Zhou, X., Cai, J., Zhao, F., Cao, T., Ning, L., et al. (2021b). Recombinant Treponema pallidum Protein Tp0768 Promotes Proinflammatory Cytokine Secretion of Macrophages through ER Stress and ROS/NF- $\kappa$ B Pathway. *Appl. Microbiol. Biotechnol.* 105, 353–366. doi:10.1007/s00253-020-11018-8
- Li, Y., Yang, J., Chen, M. H., Wang, Q., Qin, M. J., Zhang, T., et al. (2015). Ilexgenin A Inhibits Endoplasmic Reticulum Stress and Ameliorates Endothelial Dysfunction via Suppression of TXNIP/NLRP3 Inflammasome Activation in an AMPK Dependent Manner. *Pharmacol. Res.* 99, 101–115. doi:10.1016/j.phrs.2015.05.012
- Li, Y., Sun, T., Shen, S., Wang, L., and Yan, J. (2019). LncRNA DYNLRB2-2 Inhibits THP-1 Macrophage Foam Cell Formation by Enhancing Autophagy. *Biol. Chem. Undefined* 400, 1047–1057. doi:10.1515/hsz-2018-0461
- Liang, Y., Zhang, Z., Tu, J., Wang, Z., Gao, X., Deng, K., et al. (2021).  $\gamma$ -Linolenic Acid Prevents Lipid Metabolism Disorder in Palmitic Acid-Treated Alpha Mouse Liver-12 Cells by Balancing Autophagy and Apoptosis via the LKB1-AMPK-mTOR Pathway. *J. Agric. Food Chem.* 69, 8257–8267. doi:10.1021/acs.jafc.1c02596
- Liao, M., Hu, F., Qiu, Z., Li, J., Huang, C., Xu, Y., et al. (2021). Pim-2 Kinase Inhibits Inflammation by Suppressing the mTORC1 Pathway in Atherosclerosis. *Aging (Albany NY)* 13, 22412–22431. doi:10.18632/aging.203547
- Liao, X., Sluimer, J. C., Wang, Y., Subramanian, M., Brown, K., Pattison, J. S., et al. (2012). Macrophage Autophagy Plays a Protective Role in Advanced Atherosclerosis. *Cel. Metab.* 15, 545–553. doi:10.1016/j.cmet.2012.01.022
- Lien, C.-F., Chen, S.-J., Tsai, M.-C., and Lin, C.-S. (2020). Potential Role of Protein Kinase C in the Pathophysiology of Diabetes-Associated Atherosclerosis. *Front. Pharmacol.* 12, 716332. doi:10.3389/fphar.2021.716332
- Lin, X. L., Liu, M. H., Hu, H. J., Feng, H. R., Fan, X. J., Zou, W. W., et al. (2015). Curcumin Enhanced Cholesterol Efflux by Upregulating ABCA1 Expression through AMPK-SIRT1-Lxr $\alpha$  Signaling in THP-1 Macrophage-Derived Foam Cells. *DNA. Cel. Biol.* 34, 561–572. doi:10.1089/dna.2015.2866
- Lin, Y. T., Jian, D. Y., Kwok, C. F., Ho, L. T., and Juan, C. C. (2016). Visfatin Promotes Foam Cell Formation by Dysregulating Cd36, Sra, Abca1, and Abcg1 Expression in Raw264.7 Macrophages. *Shock* 45, 460–468. doi:10.1097/SHK.0000000000000529
- Liu, N., Kataoka, M., Wang, Y., Pu, L., Dong, X., Fu, X., et al. (2021). LncRNA LncHrt Preserves Cardiac Metabolic Homeostasis and Heart Function by Modulating the LKB1-AMPK Signaling Pathway. *Basic Res. Cardiol.* 116, 48. doi:10.1007/s00395-021-00887-3
- Liu, W., Bai, F., Wang, H., Liang, Y., Du, X., Liu, C., et al. (2019). Tim-4 Inhibits NLRP3 Inflammasome via the LKB1/AMPK $\alpha$  Pathway in Macrophages. *J. Immunol.* 203, 990–1000. doi:10.4049/jimmunol.1900117
- Liu, X., Wu, J., Tian, R., Su, S., Deng, S., and Meng, X. (2020). Targeting Foam Cell Formation and Macrophage Polarization in Atherosclerosis: The Therapeutic

- Potential of Rhubarb. *Biomed. Pharmacother.* 129, 110433. doi:10.1016/j.biopha.2020.110433
- Liu, Z., Zhu, H., Dai, X., Wang, C., Ding, Y., Song, P., et al. (2017). Macrophage Liver Kinase B1 Inhibits Foam Cell Formation and Atherosclerosis. *Circ. Res.* 121, 1047–1057. doi:10.1161/CIRCRESAHA.117.311546
- Malekmohammad, K., Bezsonov, E. E., and Rafieian-Kopaei, M. (2021). Role of Lipid Accumulation and Inflammation in Atherosclerosis: Focus on Molecular and Cellular Mechanisms. *Front. Cardiovasc. Med.* 8, 707529. doi:10.3389/fcvm.2021.707529
- Meares, G. P., Hughes, K. J., Naatz, A., Papa, F. R., Urano, F., Hansen, P. A., et al. (2011). IRE1-dependent Activation of AMPK in Response to Nitric Oxide. *Mol. Cell Biol.* 31, 4286–4297. doi:10.1128/MCB.05668-11
- Molina, E., Hong, L., and Chefetz, I. (2021). Ampka-Like Proteins as LKB1 Downstream Targets in Cell Physiology and Cancer. *J. Mol. Med. (Berl)* 99, 651–662. doi:10.1007/s00109-021-02040-y
- Moreira, D., Rodrigues, V., Abengozar, M., Rivas, L., Rial, E., Laforge, M., et al. (2015). Leishmania Infantum Modulates Host Macrophage Mitochondrial Metabolism by Hijacking the SIRT1-AMPK axis. *Plos. Pathog.* 11, e1004684. doi:10.1371/journal.ppat.1004684
- Mouton, A. J., Li, X., Hall, M. E., and Hall, J. E. (2020). Obesity, Hypertension, and Cardiac Dysfunction: Novel Roles of Immunometabolism in Macrophage Activation and Inflammation. *Circ. Res.* 126, 789–806. doi:10.1161/CIRCRESAHA.119.312321
- Murray, P. J., Allen, J. E., Biswas, S. K., Fisher, E. A., Gilroy, D. W., Goerdt, S., et al. (2014). Macrophage Activation and Polarization: Nomenclature and Experimental Guidelines. *Immunity* 41, 14–20. doi:10.1016/j.immuni.2014.06.008
- Murray, P. J. (2016). Macrophage Polarization. *Annu. Rev. Physiol.* 79, 541–566. doi:10.1146/annurev-physiol-022516-034339
- Nakagawa, K., Tanaka, M., Hahm, T. H., Nguyen, H. N., Matsui, T., Chen, Y. X., et al. (2021). Accumulation of Plasma-Derived Lipids in the Lipid Core and Necrotic Core of Human Atheroma: Imaging Mass Spectrometry and Histopathological Analyses. *Arterioscler Thromb. Vasc. Biol.* 41, e498–e511. doi:10.1161/ATVBAHA.121.316154
- Poznyak, A. V., Bharadwaj, D., Prasad, G., Grechko, A. V., Sazonova, M. A., and Orekhov, A. N. (2021). Anti-Inflammatory Therapy for Atherosclerosis: Focusing on Cytokines. *Int. J. Mol. Sci.* 22, 7061. doi:10.3390/ijms22137061
- Poznyak, A. V., Nikiforov, N. G., Markin, A. M., Kashirskikh, D. A., Myasoedova, V. A., Gerasimova, E. V., et al. (2020a). Overview of OxLDL and its Impact on Cardiovascular Health: Focus on Atherosclerosis. *Front. Pharmacol.* 11, 613780. doi:10.3389/fphar.2020.613780
- Poznyak, A. V., Zhang, D., Orekhova, V., Grechko, A. V., Wetzker, R., and Orekhov, A. N. (2020b). A Brief Overview of Currently Used Atherosclerosis Treatment Approaches Targeting Lipid Metabolism Alterations. *Am. J. Cardiovasc. Dis.* 10, 62–71.
- Qiao, D., Zhang, Z., Zhang, Y., Chen, Q., Chen, Y., Tang, Y., et al. (2021). Regulation of Endoplasmic Reticulum Stress-Autophagy: A Potential Therapeutic Target for Ulcerative Colitis. *Front. Pharmacol.* 12, 697360. doi:10.3389/fphar.2021.697360
- Qiu, J., Fu, Y., Chen, Z., Zhang, L., Li, L., Liang, D., et al. (2021). BTK Promotes Atherosclerosis by Regulating Oxidative Stress, Mitochondrial Injury, and ER Stress of Macrophages. *Oxid. Med. Cell. Longev.* 2021, 9972413. doi:10.1155/2021/9972413
- Ramachandran, S., Anandan, V., Kutty, V. R., Mullasari, A., Pillai, M. R., and Kartha, C. C. (2018). Metformin Attenuates Effects of Cyclophilin A on Macrophages, Reduces Lipid Uptake and Secretion of Cytokines by Repressing Decreased AMPK Activity. *Clin. Sci. (Lond)* 132, 719–738. doi:10.1042/CS20171523
- Rao, Y., Lu, Y. T., Li, C., Song, Q. Q., Xu, Y. H., Xu, Z., et al. (2019). Bouchardatine Analogue Alleviates Non-alcoholic Hepatic Fatty Liver Disease/non-Alcoholic Steatohepatitis in High-Fat Fed Mice by Inhibiting ATP Synthase Activity. *Br. J. Pharmacol.* 176, 2877–2893. doi:10.1111/bph.14713
- Razani, B., Feng, C., Coleman, T., Emanuel, R., Wen, H., Hwang, S., et al. (2012). Autophagy Links Inflammasomes to Atherosclerotic Progression. *Cel. Metab.* 15, 534–544. doi:10.1016/j.cmet.2012.02.011
- Ren, J., Bi, Y., Sowers, J. R., Hetz, C., and Zhang, Y. (2021). Endoplasmic Reticulum Stress and Unfolded Protein Response in Cardiovascular Diseases. *Nat. Rev. Cardiol.* 18, 499–521. doi:10.1038/s41569-021-00511-w
- Robichaud, S., Fairman, G., Vijithakumar, V., Mak, E., Cook, D. P., Pelletier, A. R., et al. (2021). Identification of Novel Lipid Droplet Factors that Regulate Lipophagy and Cholesterol Efflux in Macrophage Foam Cells. *Autophagy* 17, 3671–3689. doi:10.1080/15548627.2021.1886839
- Romanenko, A. V., Amelina, I. P., and Solovyeva, E. Y. (2021). Vascular Inflammation Underlies the Development of Atherothrombotic Stroke. *Zh Nevrol Psikhiatr Im S S Korsakova* 121, 22–29. doi:10.17116/jnevro202112108222
- Saha, S., Shalova, I. N., and Biswas, S. K. (2017). Metabolic Regulation of Macrophage Phenotype and Function. *Immunol. Rev.* 280, 102–111. doi:10.1111/imr.12603
- Shan, R., Liu, N., Yan, Y., and Liu, B. (2021). Apoptosis, Autophagy and Atherosclerosis: Relationships and the Role of Hsp27. *Pharmacol. Res.* 166, 105169. doi:10.1016/j.phrs.2020.105169
- Shea, S., Navas-Acien, A., Shimbo, D., Brown, E. R., Budoff, M., Bancks, M. P., et al. (2021). Spatially Weighted Coronary Artery Calcium Score and Coronary Heart Disease Events in the Multi-Ethnic Study of Atherosclerosis. *Circ. Cardiovasc. Imaging* 14, e011981. doi:10.1161/CIRCIMAGING.120.011981
- Shen, C. Y., Wang, T. X., Jiang, J. G., Huang, C. L., and Zhu, W. (2020). Bergaptol from Blossoms of Citrus Aurantium L. Var. Amara Engl Inhibits LPS-Induced Inflammatory Responses and Ox-LDL-Induced Lipid Deposition. *Food Funct.* 11, 4915–4926. doi:10.1039/c9fo00255c
- Song, C., Chen, J., Li, X., Yang, R., Cao, X., Zhou, L., et al. (2021). Limonin Ameliorates Dextran Sulfate Sodium-Induced Chronic Colitis in Mice by Inhibiting PERK-ATF4-CHOP Pathway of ER Stress and NF-Kb Signaling. *Int. Immunopharmacol.* 90, 107161. doi:10.1016/j.intimp.2020.107161
- Sukhorukov, V. N., Khotina, V. A., Bagheri Ekta, M., Ivanova, E. A., Sobenin, I. A., and Orekhov, A. N. (2020a). Endoplasmic Reticulum Stress in Macrophages: The Vicious Circle of Lipid Accumulation and Pro-inflammatory Response. *Biomedicines* 8, 210. doi:10.3390/biomedicines8070210
- Sukhorukov, V. N., Khotina, V. A., Chegodaev, Y. S., Ivanova, E., Sobenin, I. A., and Orekhov, A. N. (2020b). Lipid Metabolism in Macrophages: Focus on Atherosclerosis. *Biomedicines* 8, 262. doi:10.3390/biomedicines8080262
- Takahama, M., Akira, S., and Saitoh, T. (2018). Autophagy Limits Activation of the Inflammasomes. *Immunol. Rev.* 281, 62–73. doi:10.1111/imr.12613
- Tao, H., Yancey, P. G., Blakemore, J. L., Zhang, Y., Ding, L., Jerome, W. G., et al. (2021). Macrophage SR-BI Modulates Autophagy via VPS34 Complex and PPARα Transcription of Tfeb in Atherosclerosis. *J. Clin. Invest.* 131, e94229. doi:10.1172/JCI94229
- Tian, H., Li, Y., Kang, P., Wang, Z., Yue, F., Jiao, P., et al. (2019). Endoplasmic Reticulum Stress-dependent Autophagy Inhibits Glycated High-Density Lipoprotein-Induced Macrophage Apoptosis by Inhibiting CHOP Pathway. *J. Cel. Mol. Med.* 23, 2954–2969. doi:10.1111/jcmm.14203
- Valanti, E. K., Dalakoura-Karagkouni, K., Siasos, G., Kardassis, D., Eliopoulos, A. G., and Sanoudou, D. (2021). Advances in Biological Therapies for Dyslipidemias and Atherosclerosis. *Metabolism* 116, 154461. doi:10.1016/j.metabol.2020.154461
- Vasamsetti, S. B., Karnewar, S., Kanugula, A. K., Thatipalli, A. R., Kumar, J. M., and Kotamraju, S. (2015). Metformin Inhibits Monocyte-To-Macrophage Differentiation via AMPK-Mediated Inhibition of STAT3 Activation: Potential Role in Atherosclerosis. *Diabetes* 64, 2028–2041. doi:10.2337/db14-1225
- Wang, T., Zhao, Y., You, Z., Li, X., Xiong, M., Li, H., et al. (2020a). Endoplasmic Reticulum Stress Affects Cholesterol Homeostasis by Inhibiting LXRA Expression in Hepatocytes and Macrophages. *Nutrients* 12, 3088. doi:10.3390/nu12103088
- Wang, X., and Ge, J. (2021). Hypertension Aggravates Atherosclerosis: A Matter of Pressure Remodeling of Myofibroblasts or LDL Accumulation? *J. Am. Coll. Cardiol.* 77, 2619–2620. doi:10.1016/j.jacc.2021.03.305
- Wang, Y., Du, X., Wei, J., Long, L., Tan, H., Guy, C., et al. (2019). LKB1 Orchestrates Dendritic Cell Metabolic Quiescence and Anti-tumor Immunity. *Cell. Res.* 29, 391–405. doi:10.1038/s41422-019-0157-4
- Wang, Z., Sequeira, R. C., Zabalawi, M., Madenspacher, J., Boudyguina, E., Ou, T., et al. (2020b). Myeloid Atg5 Deletion Impairs N-3 PUFA-Mediated Atheroprotection. *Atherosclerosis* 295, 8–17. doi:10.1016/j.atherosclerosis.2020.01.004
- Wu, W., Wang, S., Liu, Q., Wang, X., Shan, T., and Wang, Y. (2018). Cathelicidin-WA Attenuates LPS-Induced Inflammation and Redox Imbalance through

- Activation of AMPK Signaling. *Free Radic. Biol. Med.* 129, 338–353. doi:10.1016/j.freeradbiomed.2018.09.045
- Wu, Z., Xi, P., Zhang, Y., Wang, H., Xue, J., Sun, X., et al. (2021). LKB1 Up-Regulation Inhibits Hypothalamic Inflammation and Attenuates Diet-Induced Obesity in Mice. *Metabolism* 116, 154694. doi:10.1016/j.metabol.2020.154694
- Xi, P., Du, J., Liang, H., Han, J., Wu, Z., Wang, H., et al. (2018). Intraventricular Injection of LKB1 Inhibits the Formation of Diet-Induced Obesity in Rats by Activating the AMPK-POMC Neurons-Sympathetic Nervous System Axis. *Cell Physiol Biochem* 47, 54–66. doi:10.1159/000489746
- Xia, X., Xu, Q., Liu, M., Chen, X., Liu, X., He, J., et al. (2020). Deubiquitination of CD36 by UCHL1 Promotes Foam Cell Formation. *Cell. Death Dis.* 11, 636. doi:10.1038/s41419-020-02888-x
- Yang, B., Qin, Q., Xu, L., Lv, X., Liu, Z., Song, E., et al. (2020a). Polychlorinated Biphenyl Quinone Promotes Atherosclerosis through Lipid Accumulation and Endoplasmic Reticulum Stress via CD36. *Chem. Res. Toxicol.* 33, 1497–1507. doi:10.1021/acs.chemrestox.0c00123
- Yang, S., Ma, C., Wu, H., Zhang, H., Yuan, F., Yang, G., et al. (2020b). Tectorigenin Attenuates Diabetic Nephropathy by Improving Vascular Endothelium Dysfunction through Activating AdipoR1/2 Pathway. *Pharmacol. Res.* 153, 104678. doi:10.1016/j.phrs.2020.104678
- Yang, S., Wu, M., Li, X., Zhao, R., Zhao, Y., Liu, L., et al. (2020c). Role of Endoplasmic Reticulum Stress in Atherosclerosis and its Potential as a Therapeutic Target. *Oxid. Med. Cel. Longev.* 2020, 9270107. doi:10.1155/2020/9270107
- Zahid, M. D. K., Rogowski, M., Ponce, C., Choudhury, M., Moustaid-Moussa, N., and Rahman, S. M. (2020). CCAAT/enhancer-binding Protein Beta (C/EBP $\beta$ ) Knockdown Reduces Inflammation, ER Stress, and Apoptosis, and Promotes Autophagy in oxLDL-Treated RAW264.7 Macrophage Cells. *Mol. Cel. Biochem.* 463, 211–223. doi:10.1007/s11010-019-03642-4
- Zahid, M. K., Sufian, H. B., Choudhury, M., Yamasaki, M., Al-Harrasi, A., Moustaid-Moussa, N., et al. (2021). Role of Macrophage Autophagy in Atherosclerosis: Modulation by Bioactive Compounds. *Biochem. J.* 478, 1359–1375. doi:10.1042/BCJ20200894
- Zhang, J., Ma, C. R., Hua, Y. Q., Li, L., Ni, J. Y., Huang, Y. T., et al. (2021). Contradictory Regulation of Macrophages on Atherosclerosis Based on Polarization, Death and Autophagy. *Life Sci.* 276, 118957. doi:10.1016/j.lfs.2020.118957
- Zhang, Q., Hu, J., Wu, Y., Luo, H., Meng, W., Xiao, B., et al. (2019). Rheb (Ras Homolog Enriched in Brain 1) Deficiency in Mature Macrophages Prevents Atherosclerosis by Repressing Macrophage Proliferation, Inflammation, and Lipid Uptake. *Arterioscler. Thromb. Vasc. Biol.* 39, 1787–1801. doi:10.1161/ATVBAHA.119.312870
- Zhang, Y., Meng, Q., Sun, Q., Xu, Z. X., Zhou, H., and Wang, Y. (2021). LKB1 Deficiency-Induced Metabolic Reprogramming in Tumorigenesis and Non-neoplastic Diseases. *Mol. Metab.* 44, 101131. doi:10.1016/j.molmet.2020.101131
- Zhang, Y. X., Qu, S. S., Zhang, L. H., Gu, Y. Y., Chen, Y. H., Huang, Z. Y., et al. (2021). The Role of Ophiopogonin D in Atherosclerosis: Impact on Lipid Metabolism and Gut Microbiota. *Am. J. Chin. Med.* 49, 1449–1471. doi:10.1142/S0192415X21500683
- Zhao, Z., Wang, X., Zhang, R., Ma, B., Niu, S., Di, X., et al. (2021). Melatonin Attenuates Smoking-Induced Atherosclerosis by Activating the Nrf2 Pathway via NLRP3 Inflammasomes in Endothelial Cells. *Aging (Albany NY)* 13, 11363–11380. doi:10.18632/aging.202829
- Zhou, Y., Murugan, D. D., Khan, H., Huang, Y., and Cheang, W. S. (2021). Roles and Therapeutic Implications of Endoplasmic Reticulum Stress and Oxidative Stress in Cardiovascular Diseases. *Antioxidants* 10, 1167. doi:10.3390/antiox10081167
- Zhu, X., Lee, J. Y., Timmins, J. M., Brown, J. M., Boudyguina, E., Mulya, A., et al. (2008). Increased Cellular Free Cholesterol in Macrophage-specific Abca1 Knock-Out Mice Enhances Pro-inflammatory Response of Macrophages. *J. Biol. Chem.* 283, 22930–22941. doi:10.1074/jbc.M801408200
- Zuo, A., Zhao, X., Li, T., Li, J., Lei, S., Chen, J., et al. (2020). CTRP9 Knockout Exaggerates Lipotoxicity in Cardiac Myocytes and High-Fat Diet-Induced Cardiac Hypertrophy through Inhibiting the LKB1/AMPK Pathway. *J. Cel. Mol. Med.* 24, 2635–2647. doi:10.1111/jcmm.14982

**Conflict of Interest:** The authors declare that the research was conducted in the absence of any commercial or financial relationships that could be construed as a potential conflict of interest.

**Publisher's Note:** All claims expressed in this article are solely those of the authors and do not necessarily represent those of their affiliated organizations, or those of the publisher, the editors and the reviewers. Any product that may be evaluated in this article, or claim that may be made by its manufacturer, is not guaranteed or endorsed by the publisher.

Copyright © 2021 Wang, Liang, Xiang, Li, Chen and Lu. This is an open-access article distributed under the terms of the Creative Commons Attribution License (CC BY). The use, distribution or reproduction in other forums is permitted, provided the original author(s) and the copyright owner(s) are credited and that the original publication in this journal is cited, in accordance with accepted academic practice. No use, distribution or reproduction is permitted which does not comply with these terms.





# Midkine Prevents Calcification of Aortic Valve Interstitial Cells via Intercellular Crosstalk

Qian Zhou<sup>1,2,3†</sup>, Hong Cao<sup>4†</sup>, Xiaoyi Hang<sup>1,2,3</sup>, Huamin Liang<sup>1,2,3</sup>, Miaomiao Zhu<sup>1,2,3</sup>, Yixian Fan<sup>1,2,3</sup>, Jiawei Shi<sup>4</sup>, Nianguo Dong<sup>4\*</sup> and Ximiao He<sup>1,2,3\*</sup>

<sup>1</sup>Department of Physiology, School of Basic Medicine, Tongji Medical College, Huazhong University of Science and Technology, Wuhan, China, <sup>2</sup>Center for Genomics and Proteomics Research, School of Basic Medicine, Tongji Medical College, Huazhong University of Science and Technology, Wuhan, China, <sup>3</sup>Hubei Key Laboratory of Drug Target Research and Pharmacodynamic Evaluation, Huazhong University of Science and Technology, Wuhan, China, <sup>4</sup>Department of Cardiovascular Surgery, Union Hospital, Tongji Medical College, Huazhong University of Science and Technology, Wuhan, China

## OPEN ACCESS

### Edited by:

Xianwei Wang,  
Xinxiang Medical University, China

### Reviewed by:

Michel Puceat,  
Institut National de la Santé et de la  
Recherche Médicale (INSERM), France  
Dimitris Beis,  
Biomedical Research Foundation of  
the Academy of Athens (BRFAA),  
Greece

### \*Correspondence:

Ximiao He  
XimiaoHe@hust.edu.cn  
Nianguo Dong  
dongnianguo@hotmail.com

<sup>†</sup>These authors share senior  
authorship

### Specialty section:

This article was submitted to  
Molecular and Cellular Pathology,  
a section of the journal  
Frontiers in Cell and Developmental  
Biology

**Received:** 13 October 2021

**Accepted:** 24 November 2021

**Published:** 15 December 2021

### Citation:

Zhou Q, Cao H, Hang X, Liang H,  
Zhu M, Fan Y, Shi J, Dong N and He X  
(2021) Midkine Prevents Calcification  
of Aortic Valve Interstitial Cells via  
Intercellular Crosstalk.  
Front. Cell Dev. Biol. 9:794058.  
doi: 10.3389/fcell.2021.794058

Calcified aortic valve disease (CAVD), the most common valvular heart disease, lacks pharmaceutical treatment options because its pathogenesis remains unclear. This disease with a complex macroenvironment characterizes notable cellular heterogeneity. Therefore, a comprehensive understanding of cellular diversity and cell-to-cell communication are essential for elucidating the mechanisms driving CAVD progression and developing therapeutic targets. In this study, we used single-cell RNA sequencing (scRNA-seq) analysis to describe the comprehensive transcriptomic landscape and cell-to-cell interactions. The transitional valvular endothelial cells (tVECs), an intermediate state during the endothelial-to-mesenchymal transition (EndMT), could be a target to interfere with EndMT progression. Moreover, matrix valvular interstitial cells (mVICs) with high expression of midkine (MDK) interact with activated valvular interstitial cells (aVICs) and complement-activated valvular interstitial cells (cVICs) through the MK pathway. Then, MDK inhibited calcification of VICs that calcification was validated by Alizarin Red S staining, real-time quantitative polymerase chain reaction (RT-qPCR), and Western blotting assays *in vitro*. Therefore, we speculated that mVICs secreted MDK to prevent VICs' calcification. Together, these findings delineate the aortic valve cells' heterogeneity, underlining the importance of intercellular cross talk and MDK, which may offer a potential therapeutic strategy as a novel inhibitor of CAVD.

**Keywords:** CAVD, scRNA-seq, cell communication, VICs' calcification, midkine (MDK)

## INTRODUCTION

Calcified aortic valve disease (CAVD), the most prevalent form of aortic valve stenosis, affects approximately 3% of the population aged over 60 years, and so far, it has lacked pharmacological treatment (Osnabrugge et al., 2013). Previously considered a degenerative disease, CAVD is now thought to be an active cellular process driven by intricate cell-to-cell interactions with complex mechanisms. The progression of the disease includes three phases: 1) initial endothelial dysfunction and injury, 2) low-density lipoprotein cholesterol deposition, and 3) immune cell infiltration, oxidative stress, and pro-inflammatory cytokine stimulations (Akai, Borggrefe, and Kaden 2009; Li, Xu, and Gotlieb 2011; Towler 2013). Such changes give rise to innate and adaptive immune cell infiltration, valvular endothelial cells' (VECs') transformation, and

valvular interstitial cells' (VICs') activation, leading to a complicated aortic valve microenvironment. Moreover, cell-to-cell interactions are closely related to the maintenance of normal aortic valve physiological functions and the development of CAVD. For instance, macrophages and VICs communicate with VICs through IL6 and CDH11 molecules, respectively, to accelerate the osteogenic differentiation of VICs (Hutcheson et al., 2013; Grim et al., 2020). Comparing VICs and VECs' co-culture in the osteogenic medium with only VICs in the osteogenic medium, it was found that expressions of osteogenic markers (RUNX2 and  $\alpha$ SMA) in the co-culture medium were reduced, indicating that VECs inhibited the VICs' calcification (Akat, Borggreffe, and Kaden 2009). Although cell-cell interactions were examined from bulk RNA-seq and experimental data, there was a lack of comprehensive and systematic research on cell heterogeneity and cell-to-cell communication in CAVD.

Recently, single-cell RNA sequencing (scRNA-seq) technologies have allowed the identification of calcified-associated cell types and trends of cell fate, and provided unprecedented details of the valve heterogeneity and interactions among cell subpopulations (Xu et al., 2020).

In this study, we characterized the cell types with functional states of biological relevance. There were two special and novel cell subsets. First, the VECs' subset was an intermediate state in the process of VECs to VICs' transformation, that is, in the process of endothelial-to-mesenchymal transition (EndMT), so they are named transitional valvular endothelial cells (tVECs). Second, the T-cell subset was derived from a normal aortic valve and involved in extracellular matrix (ECM) organization, which has never been reported. Furthermore, we systematically analyzed cell-to-cell interactions mediated by ligand-receptor interactions across all cell subsets in the aortic valve microenvironment. Intriguingly, matrix valvular interstitial cells (mVICs) highly expressed midkine (MDK) and mainly interacted with activated valvular interstitial cells (aVICs) and complement-activated valvular interstitial cells (cVICs) through MDK-NCL ligand-receptor. Subsequently, we validated that MDK inhibited calcification of VICs that calcification by Alizarin Red S staining, real-time quantitative polymerase chain reaction (RT-qPCR), and Western blotting assay *in vitro*. In summary, we determined the functional status of each cell type, VICs' heterogeneity, and intercellular cross talk among all cell subsets. We identified that MDK prevented VICs' calcification as well, which provided a potential therapeutic target for CAVD treatment.

## MATERIALS AND METHODS

### Gene Expression Data

The scRNA-seq data of two normal and four calcific samples were sequenced by our group (Xu et al., 2020). The sample collection and harvesting of single cells were described in detail in the study by Xu et al. (2020). Briefly, after the operation, these valves were

separated and washed with cold  $1 \times$  PBS, and then mechanically dissociated using eye scissors. Dissociated samples were digested in DMEM with collagenase type I, 2 mg/ml (Sigma-Aldrich, Saint Louis, MO) to prepare a single-cell suspension because the extracellular matrix of the aortic valve is mainly composed of type I collagen that completely degrades extracellular matrix. Healthy aortic valve tissue specimens were harvested from patients undergoing repair of aortic dissection requiring aortic valve replacement. The standards for healthy aortic valves included the following: 1) heart color Doppler echocardiography showed no obvious thickening of valve leaflets and no nodules; 2) histopathological examination showed no calcium nodules. The data also can be downloaded from the GEO database with accession number PRJNA562645. Microarray data of human aortic valves were downloaded from the GEO database with accession number GSE51472 and microarray data of human VICs were downloaded from the GEO database with accession number GSE88803.

scRNA-seq matrix: [https://www.jianguoyun.com/p/DRQVbtkQp8\\_2CRiVrZME](https://www.jianguoyun.com/p/DRQVbtkQp8_2CRiVrZME)

scRNA-seq annotation: [https://www.jianguoyun.com/p/DX5htpQQp8\\_2CRjZrJME](https://www.jianguoyun.com/p/DX5htpQQp8_2CRjZrJME).

Bulk RNA-seq data: [https://www.jianguoyun.com/p/DbnawFYQp8\\_2CRjyq5ME](https://www.jianguoyun.com/p/DbnawFYQp8_2CRjyq5ME).

Experimental data: [https://www.jianguoyun.com/p/DRV3dbEQp8\\_2CRiDrJME](https://www.jianguoyun.com/p/DRV3dbEQp8_2CRiDrJME).

### scRNA-Seq Analysis and Identification of the Major Cell Types

Raw gene expression matrices of scRNA-seq data were integrated and regenerated to a Seurat object by the Seurat R package (version 3.2.0) (Stuart et al., 2019). Cells with fewer than 2000 UMIs, over 6,000 or below 500 expressed genes, over 20% UMIs derived from mitochondrial genome, and  $\log_{10}$  UMIs of per gene lower than 0.8 were removed. We then used the `NormalizeData` function to normalize the library size of each cell with default parameters and the `FindVariableFeatures` function to select the top three thousand genes that are the most variably expressed genes of each sample. The `FindIntegrationAnchors` and `IntegrateData` functions were used to integrate data with default parameters, which made a normalized Seurat object. Principal components analysis was performed and the first 30 PCs were used to further generate t-SNE dimensionality reductions of the `RunTSNE` function. Graph-based clustering was run using `FindNeighbors` and `FindClusters` functions with a resolution of 0.3. Cell clusters were annotated using canonical marker genes.

### Gene Set Variation Analysis

To estimate the purity of diverse cell subsets in the aortic valve from bulk RNA-seq and scRNA-seq data, we calculated stromal and immune scores using single-sample gene set enrichment analysis (ssGSEA) (Barbie et al., 2009). Stromal and immune gene sets are from curated datasets in ESTIMATE software (Yoshihara et al., 2013). To assign pathway activity of individual cell subset, we used GSVA (Hanzelmann, Castelo, and Guinney 2013) with

standard parameters. Immune and stromal score data: [https://www.jianguoyun.com/p/DSpzs1gQp8\\_2CRiGrJME](https://www.jianguoyun.com/p/DSpzs1gQp8_2CRiGrJME).

## Differential Expression Genes Analysis

Microarray data were normalized and log2-transformed using the limma R package (version 3.44.1) (Ritchie et al., 2015). We then used this package to filter the differential expression genes between disease and normal samples. The cutoff thresholds: adjusted *p* values <0.05 and |log2fold change (FC)| > 1. For scRNA-seq data, in order to compare the transcriptional characteristics of normal and calcified groups in the major cell types, we used the FindMarkers function (Seurat v3) (Stuart et al., 2019) to screen the differential expression genes from each group in the three major cell types. The cutoff thresholds: in the calcified group or normal group, the gene is expressed in more than 25% of cells, adjusted *p* values <0.05, log2fold change (FC) > 0.5.

## Gene Ontology Analysis

Gene Ontology (GO) analysis was performed using Metascape (<https://metascape.org/>) (Zhou et al., 2019). REVIGO (Supek et al., 2011) was used to remove redundant GO terms. Ultimately, top 5 pathways were remained to visualize.

## Subclustering of the Major Cell Types

We performed integrated analyses of three main cell types so as to subdivide the subsets of each main cell type. The number of PCs was determined by dataset specificity. Based on the graph-based clustering approach of the FindClusters function, the resolution of VECs, immune cells, and VICs was 0.4, 0.2, and 0.2, respectively. For visualization purposes, these informative PCs were converted into t-SNE plots as above. Then, the FindAllMarkers function was used to define the expression of corresponding marker genes.

## Trajectory Analysis

Pseudotime ordering of VECs was performed using monocle 2 (version 2.16.0) (Trapnell et al., 2014). Differential gene expression analysis used the differentialGeneTest function. Dimensional reduction and cell ordering were performed using the DDRTree method and orderCells function.

## Transcription Factors Analysis

Motifs of transcriptional factors were found by the SCENIC package (version 1.1.3) (Aibar et al., 2017). Transcriptional factors of hg19 as a reference were downloaded using RcisTarget. Gene regulatory networks were inferred using GENIE3 and according to the gene expression matrix of each cell subset.

## Cell-To-Cell Communication Analysis

To investigate potential interactions among cell subsets in the aortic valve microenvironment, cell-to-cell communication analysis was performed using CellChatDB (Jin et al., 2021) and CellChat R package (version 0.0.2).

## Cell Culture and Processing

Isolation and culture of VICs follow the previous method (Zhou et al., 2020). The experiments were divided into four

groups, namely, the control group with the DMEM containing 2% fetal bovine serum (FBS), VICs cultured in OM (Cyagen Biosciences, HUXMA-90021), the MDK group supplemented with 100 ng/ml MDK (PEPROTECH, 450-16), and both OM and MDK.

## Calcification Analysis

Alizarin Red S staining was used to evaluate the degree of osteogenic differentiation of VICs. Cells were plated on a 12-well cell culture plate at a density of 30,000/cm<sup>2</sup>. Before treatment, starving with serum-free medium for 24 h, the four groups were cultured for about 21 days. After the treatment, the cell culture plate was washed twice with phosphate-buffered saline (PBS) solution, fixed with 4% paraformaldehyde (PFA) for 10 min, and then stained with 2% Alizarin Red S for 30 min at room temperature. After dyeing, it was rinsed with deionized water three times.

## Western Blot Analysis

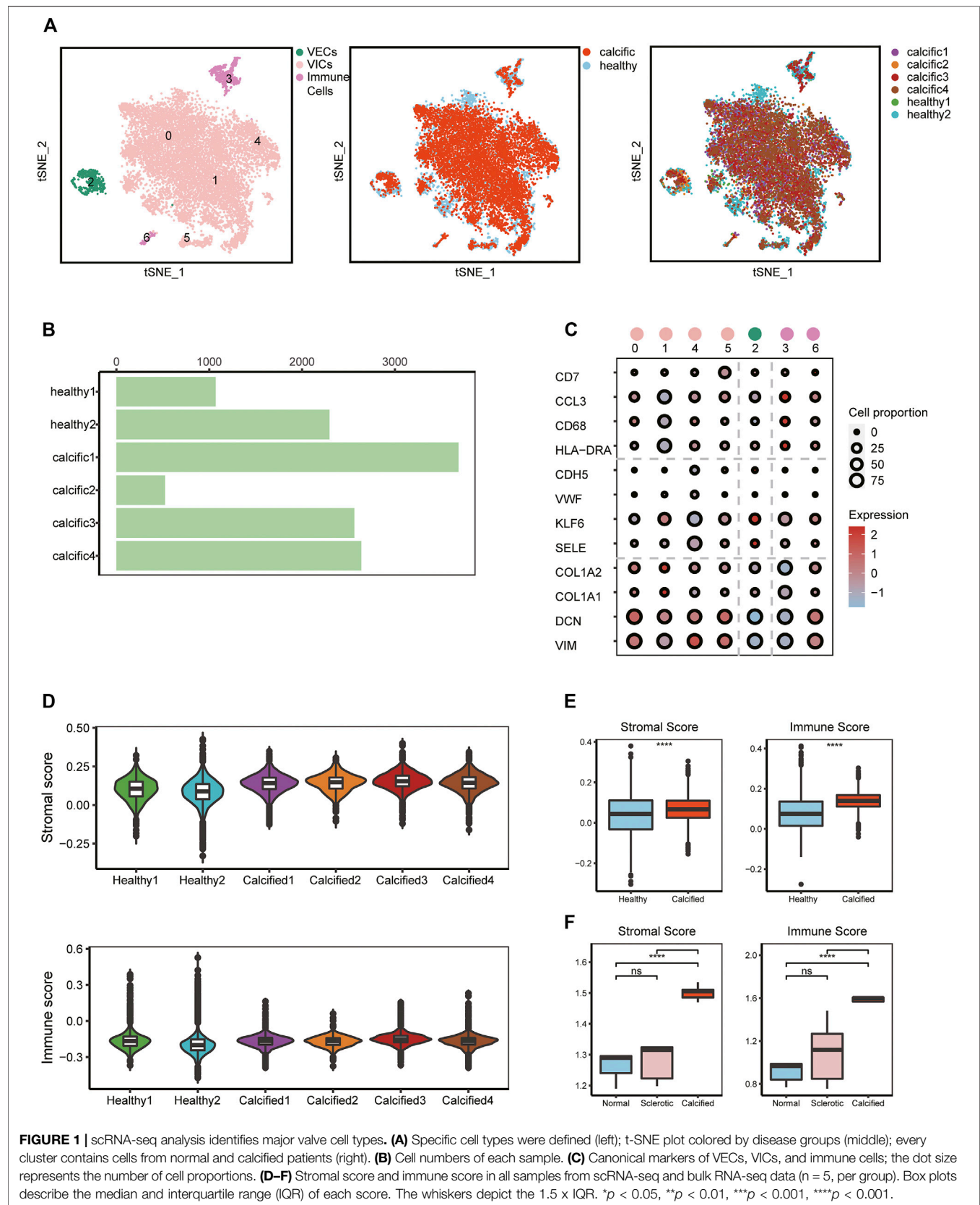
After the cells were cultured for five days, the protein was collected by RIPA containing protease inhibitors. After the protein concentration was measured by the kit, a quarter volume of the loading buffer (Servicebio, G2013) was added, denaturing at 95°C for 10 min. The protein samples were resolved by SDS-PAGE (4–20% gels) and then transferred to PVDF membranes using a protein transfer instrument (eBlotL1, GENSCRIPT). After 15 min of QuickBlock™ Western blocking solution (Beyotime, P0252) at room temperature, the membrane was incubated overnight with the primary antibody at 4°C for RUNX2 (CST, 8486s), ALP (Zenbio, 220,678), and GAPDH (Proteintech, 60004-1-I). qRT-PCR assay using Cell Total RNA isolation kit (FOREGENE, RE-O3113) was utilized to extract mRNA. HiScript III RT SuperMix (Vazyme, R323-01) was used to perform reverse transcription of mRNA. Then, the reverse transcription product was used as a template to perform qRT-PCR on a StepOnePlus thermal cycler (Applied Biosystems, Foster City, CA) using ChamQ Universal SYBR qPCR Master Mix (Vazyme, Q711-02) to analyze the difference in gene expression. The primers used were designed at the NCBI and synthesized by Tsingke Biological technology.

Primer.

Homo ALP-F	GACAACTGGGGCCTGAGATA
HOMO ALP-R	CTGACTTCCCTGCTTTCTTGG
HOMO GAPDH-F	GAGAAGGCTGGGGCTCATTT
HOMO GAPDH-R	AGTGATGGCATGGACTGTGG
HOMO RUNX2-F	GCGCATTOCTCATCCAGTA
HOMO RUNX2-R	GGCTCAGGTAGGAGGGGTAA

## Statistical Analysis

To determine statistical significance in the analysis of immune score and stromal score for each sample, we used a two-sided Student's *t*-test with Bonferroni correction. Statistical significance between multiple samples was determined using a one-way analysis of variance (ANOVA). All statistical analyses were used R (version 4.0.2).





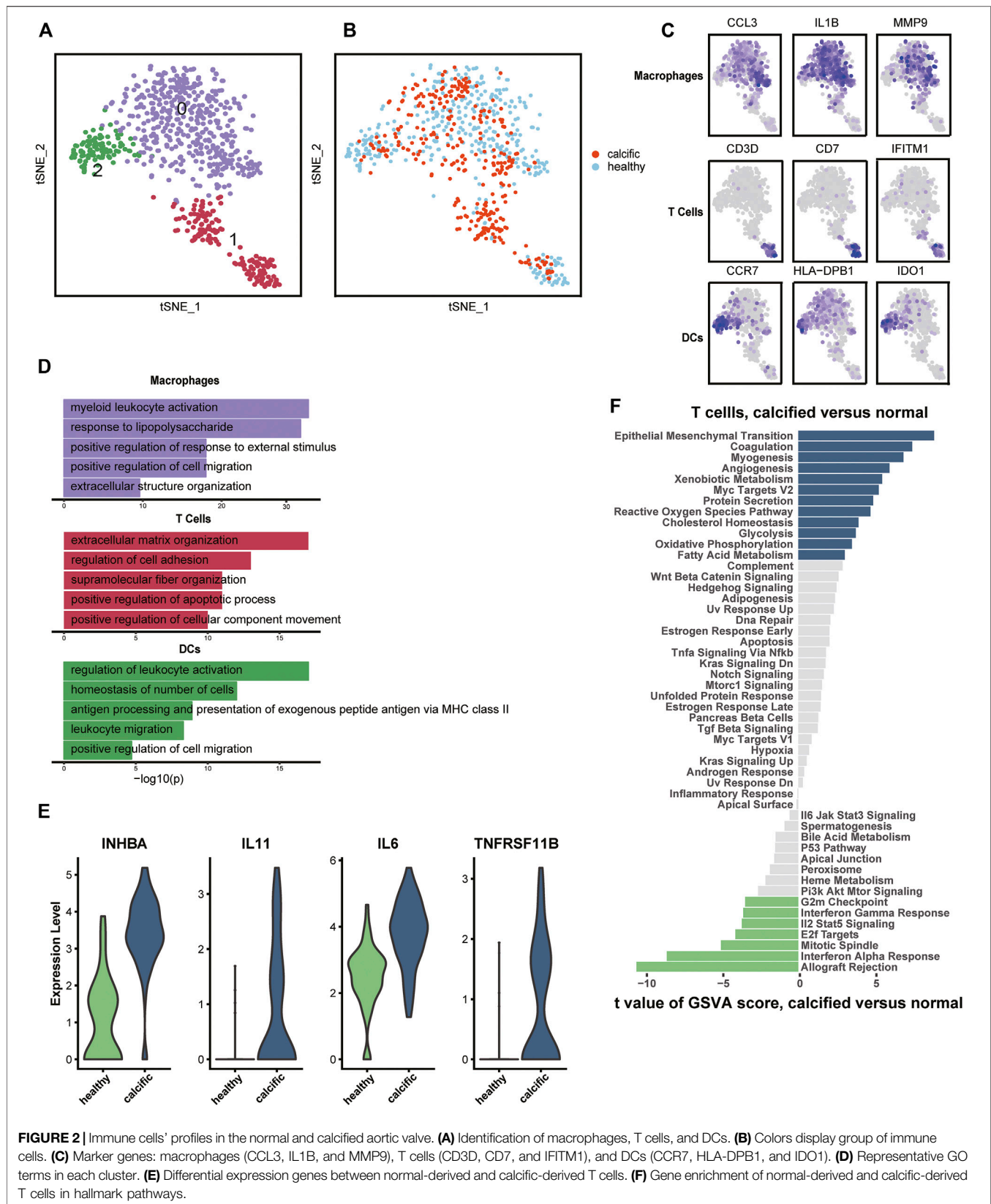


**FIGURE 2 |** Immune cells' profiles in the normal and calcified aortic valve. **(A)** Identification of macrophages, T cells, and DCs. **(B)** Colors display group of immune cells. **(C)** Marker genes: macrophages (CCL3, IL1B, and MMP9), T cells (CD3D, CD7, and IFITM1), and DCs (CCR7, HLA-DPB1, and IDO1). **(D)** Representative GO terms in each cluster. **(E)** Differential expression genes between normal-derived and calcific-derived T cells. **(F)** Gene enrichment of normal-derived and calcific-derived T cells in hallmark pathways.

## RESULTS

### Major Cell Types Are Identified in Aortic Valve Microenvironment

To investigate cellular heterogeneity and cell-to-cell interactions in aortic valves microenvironment at single-cell resolution, we used scRNA-seq data previously from our research group, including two normal and four calcific samples (Xu et al., 2020) (Supplementary Figure S1). After stringent filtering (Supplementary Figure S2), 16,275 unique genes were obtained from 12,776 cells. Of these, 3,366 cells (26%) originated from normal samples and 9,410 cells (74%) from calcified samples (Figure 1B). Based on the known cell markers, there were three main populations in the aortic valve: immune cells (691 cells, 5.4%, marked with HLA-DRA, CD68, CCL3, and CD7); VECs (599 cells, 4.7%, marked with SELE, KLF6, VWF, and CDH5); VICs (11486 cells, 89.9%, marked with VIM, DCN, COL1A1, and COL1A2) (Figures 1A,C). There was no sample preference in different cell populations (Figure 1A), suggesting that batch effects were removed by the integrated analysis of scRNA-seq data.

To verify cell clustering, we reconfirmed features of major cell types based on scRNA-seq and bulk RNA-seq data. From the scRNA-seq data, for each main cell population, differential genes analysis was performed between calcific-derived and normal-derived cells (Supplementary Figure S3A-C). GO analysis, selecting upregulated genes of each calcific group, showed that VECs were involved in metabolic-related processes (Supplementary Figure S3D), immune cells were associated with immune-related processes (Supplementary Figure S3E), and VICs were connected with ECM remodeling processes (Supplementary Figure S3F). From bulk RNA-seq data, comparing calcific and normal tissues, there were 472 downregulated genes and 250 upregulated genes (Supplementary Figure S3G), of which upregulated genes were also involved in immune-related and ECM remodeling pathways (Supplementary Figures S3H,I). Considering ECM remodeling and immune activities were closely connected with valve calcification, we used stromal and immune scores to comprehensively estimate samples profiles. These two scores not only significantly increased in calcified samples from bulk RNA-seq data but also slightly raised in calcific samples from scRNA-seq data (Figures 1D,E). Consequently, we were convinced that all cell types were accurately identified and that three key cell populations existed in the aortic valve microenvironment, including VECs, VICs, and immune cells.

### The Environment Is Prominent in Shaping T-Cell Traits

Regarding inflammation and lipid infiltration, diverse immune cells infiltrate into the aortic valve, so we re-clustered immune cells from normal and calcific valves. The most immune cells were macrophages (IL1B, CCL3, and MMP9), followed by T cells (CD3D, CD7, and IFITM1) and were dendritic cells (DCs) (CCR7, HLA-DBP1, and IDO1) (Figures 2A,C, Supplementary Figure S4A). Macrophages and DCs activated leukocytes, which

were the main features of early CAVD (Figure 2D). However, T cells had the ability to organize extracellular matrix, which aroused our curiosity (Figure 2D). To explore whether transcription factors caused biological differences, we used Single-Cell Regulatory Network Inference and Clustering (SCENIC) (Aibar et al., 2017) to evaluate the transcription factors activities of each subset. The activity of transcription factors varied greatly among cell types (Supplementary Figure S4B). The heatmap presented increased expressions of TFDP1 and RB1 in macrophages and DCs, while that of CEBPG, MECP2, and SAP30 decreased in the same clusters (Supplementary Figure S4B). In contrast, the expressions of these transcription factors showed an opposite trend in T cells (Supplementary Figure S4B).

Surprisingly, an interesting discovery in the t-SNE graph (Figure 2B) was that there was an evident dichotomy between normal-derived and calcific-derived T cells. This meant that T cells also resided in the normal aortic valve, which was not reported before. According to expression profiles, the genes relevant to calcification induction, such as INHBA, IL11, IL6, and TNFRSF11B, were specifically expressed in calcific-derived T cells (Figure 2E). Furthermore, EndMT pathways connected with CAVD were enriched in calcific-derived T cells (Figure 2F). These results suggested that T cells derived from distinctive environments promote aortic valve homeostasis or CAVD in some way.

### scRNA-Seq Reveals a Novel Cluster of VECs Correlated With EndMT in CAVD

VECs, from normal and calcific samples, were re-clustered. It was evident from the t-SNE graph that there were three subsets of VECs (Figure 3A). The largest number of cells was normal-derived VECs (nVECs) with high expression of END1, followed by calcified-derived VECs (cVECs), then a few cluster2 cells (Figures 3B,C). Comparing nVECs with cVECs, the noticeable enrichment of upregulated genes in nVECs was in response to tumor necrosis factor and cytokine stimulation (Figure 3D). On the other hand, transcription factors activity presented various profiles between these two populations. The expressions of IRF1, CEBPD, and NFkB1 increased in cVECs and those of JUNB and GATA2 decreased (Figure 3E). However, these transcription factors showed completely opposite expressions in nVECs.

EndMT driven by TGF $\beta$ , inflammation, and shear stress plays an essential role in the damage of valve endothelium in CAVD (Kovacic et al., 2019). Therefore, it was essential to explore the differentiation trajectory of VECs in EndMT by single-cell pseudotime analysis using monocle (Trapnell et al., 2014). The pseudotime analysis illustrated that nVECs were distributed at the beginning end of the pseudotemporal trajectory, whereas cVECs and cluster2 cells were located at the other two ends (Figure 3F). Interestingly, the expression of mesenchymal marker genes (MMP9, FN1, and S100A4) in cluster2 rose dramatically compared with other clusters (Figure 3G). Considering the features of cluster2 cells, we inferred that the cluster cells were in a transitional state from VECs to VICs, named tVECs. In conclusion, a novel cluster of VECs was found to exist in EndMT, which was regarded as a potential target for intervention in the process of conversion of VECs to VICs.

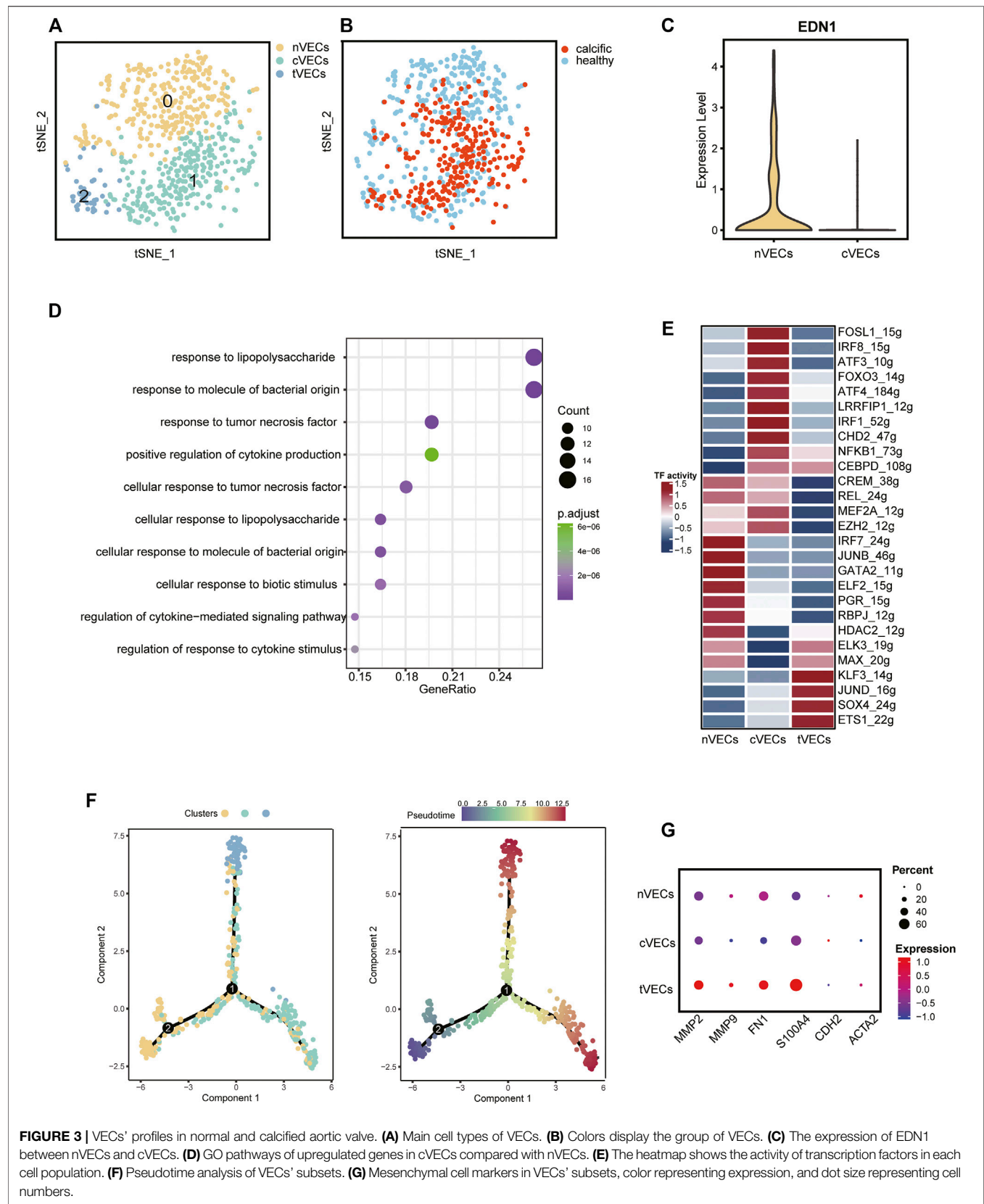


**FIGURE 3 |** VECs' profiles in normal and calcified aortic valve. **(A)** Main cell types of VECs. **(B)** Colors display the group of VECs. **(C)** The expression of EDN1 between nVECs and cVECs. **(D)** GO pathways of upregulated genes in cVECs compared with nVECs. **(E)** The heatmap shows the activity of transcription factors in each cell population. **(F)** Pseudotime analysis of VECs' subsets. **(G)** Mesenchymal cell markers in VECs' subsets, color representing expression, and dot size representing cell numbers.

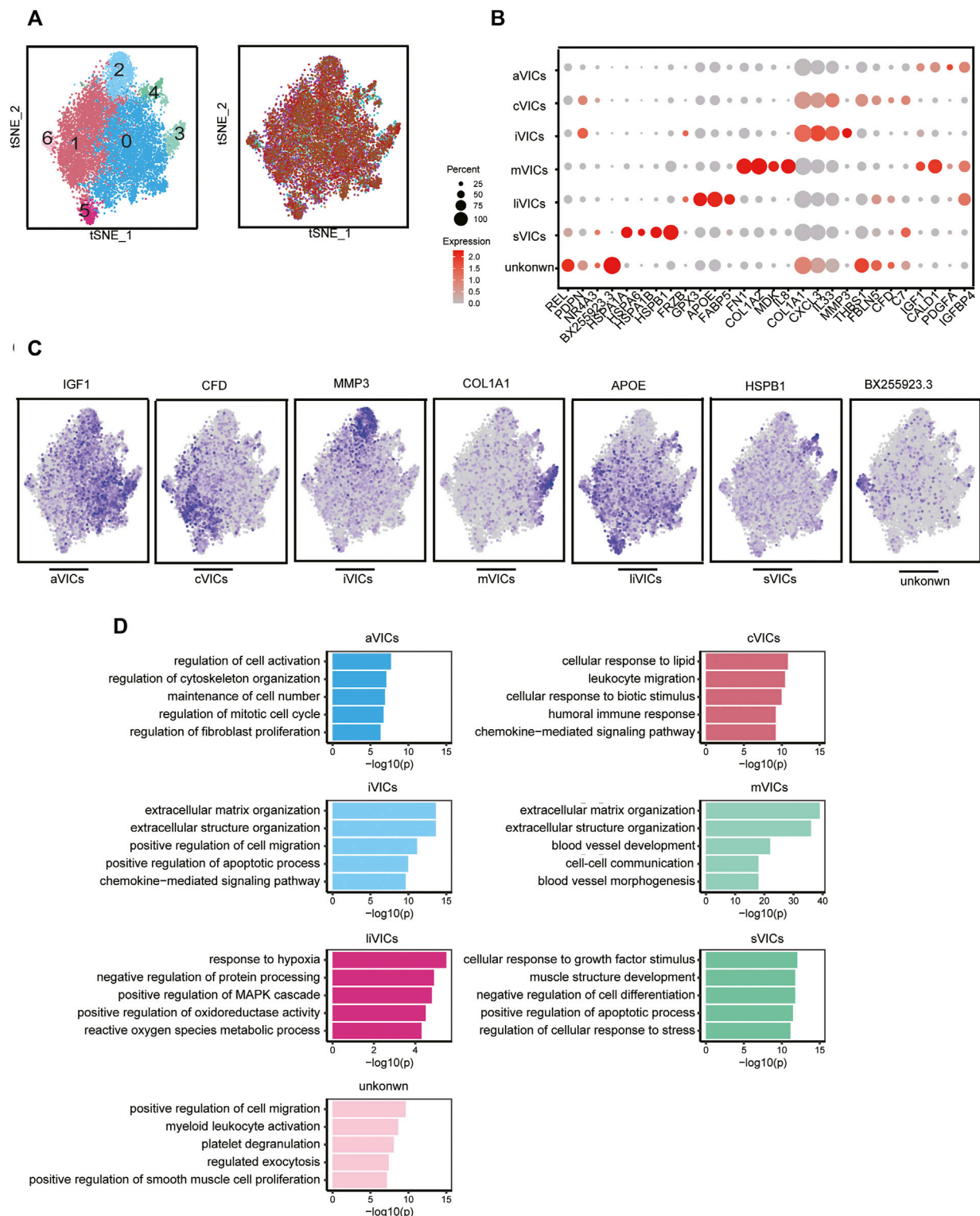
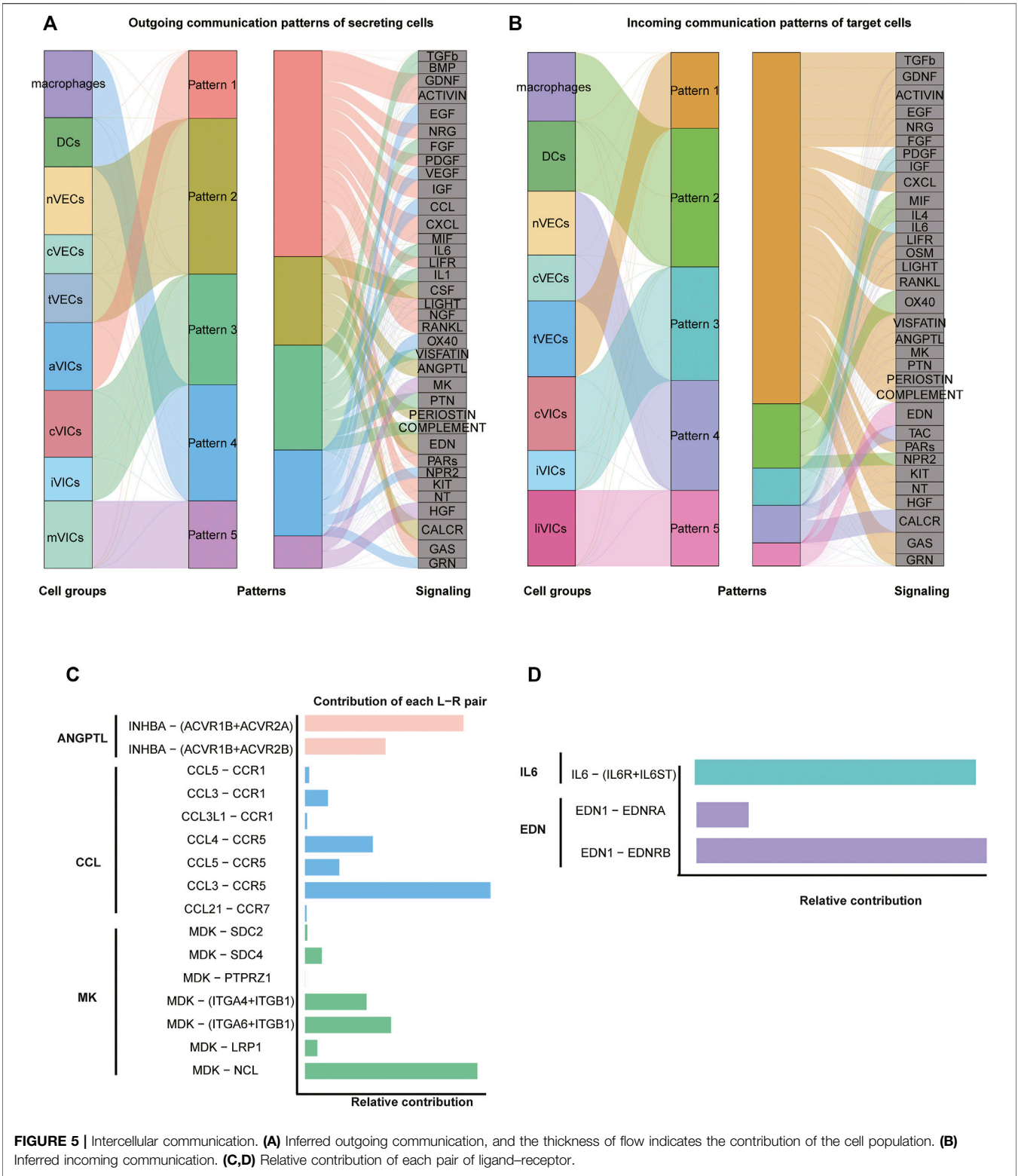


**FIGURE 4 |** VICs heterogeneity. **(A)** VICs' subsets colored by sample origin. **(B)** Markers expression of each cell subset. **(C)** Differential expression genes: aVICs (IGF1), cVICs (CFD), iVICs (MMP3), mVICs (COL1A1), liVICs (APOE), and sVICs (HSPB1). **(D)** GO terms of each subset.





**VICs Exhibit a High Degree of Heterogeneity**  
CAVD is now considered to be an active disease process, mainly controlled by resident VICs (Rutkovskiy et al., 2017). Disease-induced stimuli transform VICs from quiescent fibroblast-like

into active myofibroblast-like cells, thereby forming an intricate environment. Therefore, it is urgent to elucidate the heterogeneity of VICs in CAVD. We identified seven main subsets, of which cluster0 and cluster1 were the most abundant subsets, accounting

for 78% (**Figures 4A,C**). Cluster0 VICs still expressed several myofibroblast-related genes (for example, IGF1, IGFBP4, CALD1, and PDGFA), which was in line with GO analysis showing cell activation and fibroblast proliferation (**Figures 4B–D**). These cells were termed aVICs. Cluster1 VICs presented gene signatures related to the cellular response to lipid and leukocyte migration (for example, C7 and CFD), which was also confirmed by GO analysis, so these cells were named cVICs (**Figures 4B–D**). Interestingly, both cluster2 and cluster3 VICs specialized in an extracellular matrix organization (**Figure 4D**). Cluster2 VICs were also involved in inflammatory responses except for remodeling ECM, with a signature expression of IL33, CXCL3, and MMP3, while cluster3 VICs only expressed stromal-related genes (for example, COL1A1, COL1A2, and FN1) (**Figures 4B–D**). Hence, the two clusters were termed inflammation-associated valvular interstitial cells (iVICs) and mVICs, respectively. Cluster4 VICs specifically expressed lipid metabolism-related genes (for example, FABP5, APOE, GPX3, and FRZB) and were named lipid-associated valvular interstitial cells (liVICs) (**Figures 4B–D**), suggesting that this cluster of VICs responded to lipid infiltration. The GO terms of this cluster were enriched in response to hypoxia and reactive oxygen species metabolism, which also confirmed our inference (**Figure 4D**). Cluster5 VICs, with characteristics of heat shock protein-related genes (for example, HSPB1, HSPA1B, HSPA6, and HSPA1A), were rich in the cellular response to growth factor stimulation and were named stress valvular interstitial cells (sVICs) (**Figures 4B–D**). However, cluster6 VICs were uncertain and we only observed that these cells may be related to inflammation (**Figures 4B–D**).

## Complex Intercellular Interactions in Aortic Valve Microenvironment

Cell-to-cell communication is an important regulator for maintaining the homeostasis of the aortic valves environment, including communication between the same cells and between different cells (Wang, Leinwand, and Anseth 2014). Therefore, we systematically explored potential communication among VICs, VECs, and immune cells.

Intercellular interactions were examined from two aspects of the outgoing signals (all cell subsets as senders) (**Figure 5A; Supplementary Figure S5A**) and the incoming signals (all cell subsets as receivers) (**Figure 5B; Supplementary Figure S5B**). Firstly, as for outgoing signals, the results showed that immune cells (including macrophages and DCs) sent signals through pattern4, which is a collection of many pathways mostly composed of CCL and EGF pathways (**Figure 5A; Supplementary Figure S5B**). VECs sent signals via pattern2, primarily including EDN, CALCR, and CSF approaches (**Figure 5A; Supplementary Figure S5A**). VICs sent out signals through three modes: pattern1, 3, and 5. That is, pattern1 was primarily composed of IGF, CXCL and GAS pathways; pattern3 consisted predominantly of FGF and PTN pathways; and

pattern5 was primarily made up of MK and HGF pathways (**Figure 5A; Supplementary Figure S5A**). Secondly, from the perspective of afferent signals, immune cells received signals through pattern2 represented by the OX40 pathway (**Figure 5B; Supplementary Figure S5B**). VECs received signals through pattern4 represented by TAC and CALAR channels (**Figure 5B; Supplementary Figure S5B**). VICs received signals were pattern3 and pattern5, including CXCL, ACTIVIN and PDGF, and EDN channels, respectively (**Figure 5B; Supplementary Figure S5B**).

Since VICs play an important role in CAVD (Rutkovskiy et al., 2017), our investigation of cell communication focused on VICs: macrophages got in touch with VICs through CCL3 ligands and CCR5 receptors that belonged to the CCL pathway (**Figure 5C; Supplementary Figures S6C,D**). As for VECs, tVICs communicated with VICs through INHBA ligands and ACVR1B and ACVR2A receptors that were in the ANGPTL pathway (**Figure 5C; Supplementary Figures S6A,B**); nVICs interacted with VICs through EDN1 ligands and EDNRB receptors that were members of the EDN signaling pathway (**Figure 5D; Supplementary Figures S7C,D**). Correspondingly, EDN1 is also highly expressed in nVICs (**Figure 3C**). For communication among all VICs' subsets, two interesting pathways were observed. aVICs and cVICs, as the main subsets secreting IL6 cytokines, affected other VICs' subsets through paracrine (**Supplementary Figures S7A,B**). It was previously reported that macrophages secreted IL6 to affect VICs (Grim et al., 2020); however, here, we observed that activated VICs' subsets could also secrete IL6 to induce other VICs' subsets. In addition, cVICs released the inflammatory cytokine IL1 that had an impact on all VICs' subsets (**Supplementary Figures S6E,F**).

## MDK From mVICs Inhibits VICs' Calcification

After analyzing cell-to-cell interactions among all cell populations, we discovered a special signaling pathway MDK. This signal network indicated that MDK was only derived from mVICs and acted on all other VICs' subsets in a paracrine manner, mainly aVICs and cVICs (**Figures 6A,B**). Moreover, MDK is significantly expressed in mVICs (**Figure 6C**). These results displayed that MDK had a key effect on VICs' calcification. In order to better understand the influences of MDK in VICs' calcification, relevant experiments were used for verification. VICs, isolated from aortic valve tissues of non-CAVD patients, were cultured in normal medium, osteogenic induced medium (OM), MDK-add medium, and MDK-add OM, respectively. Strikingly, there was no calcified nodule in all media except for OM, suggesting that MDK could reverse the formation of OM-induced calcified nodules (**Figure 6D**). In addition, regardless of the protein or transcription level, osteogenic differentiation markers RUNX2 and ALP were reduced in VICs after MDK treatment (**Figures 6E,F**), which was consistent with the above phenomena. Therefore, it was clearly indicated that MDK inhibited the osteogenic differentiation of VICs.

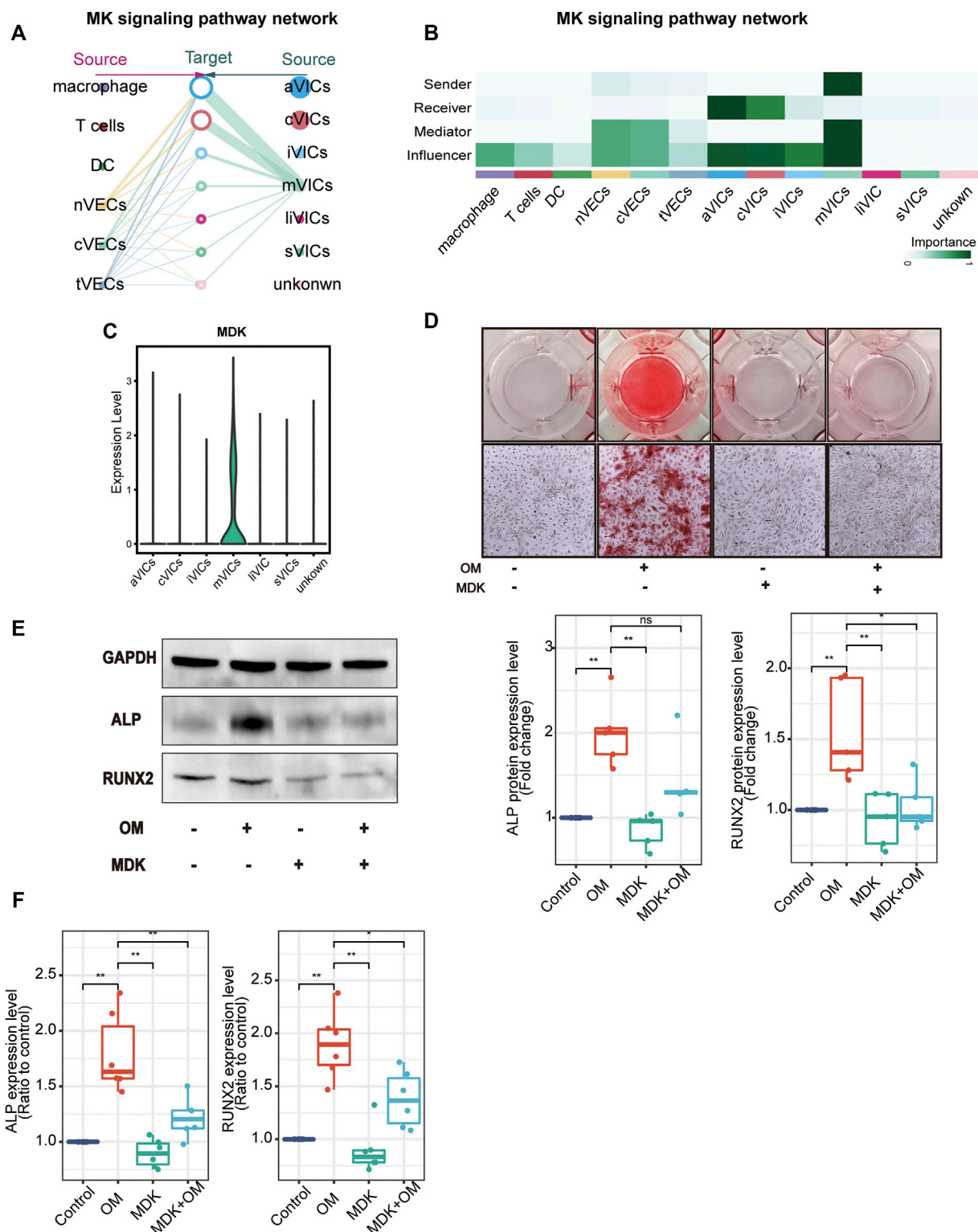


**FIGURE 6 | MDK inhibits VICs' calcification. (A)** The hierarchical plot shows the intercellular communication network of the MK pathway. The left portion describes the paracrine activity and the right portion describes autocrine activity; the solid and open circles represent the source and the target, respectively; the size of the circle represents the proportion of cell numbers in each cell subset; the width of the edge represents the communication probability; the edge color is the same as the source. **(B)** The relative importance of each subset with different roles. **(C)** The expression of MDK in VICs' subsets. **(D)** Alizarin Red S staining of VICs with different treatments: control (normal culture medium), OM (osteogenic medium), MDK (normal culture medium-plus MDK treatment), and OM + MDK (osteogenic medium-plus MDK treatment). **(E)** The protein expression level of RUNX2 and ALP with different treatments ( $n = 5$  per group). **(F)** The RNA expression level of osteogenesis-specific genes (RUNX2 and ALP) with different treatments ( $n = 6$  per group). \* $p < 0.05$ , \*\* $p < 0.01$ .

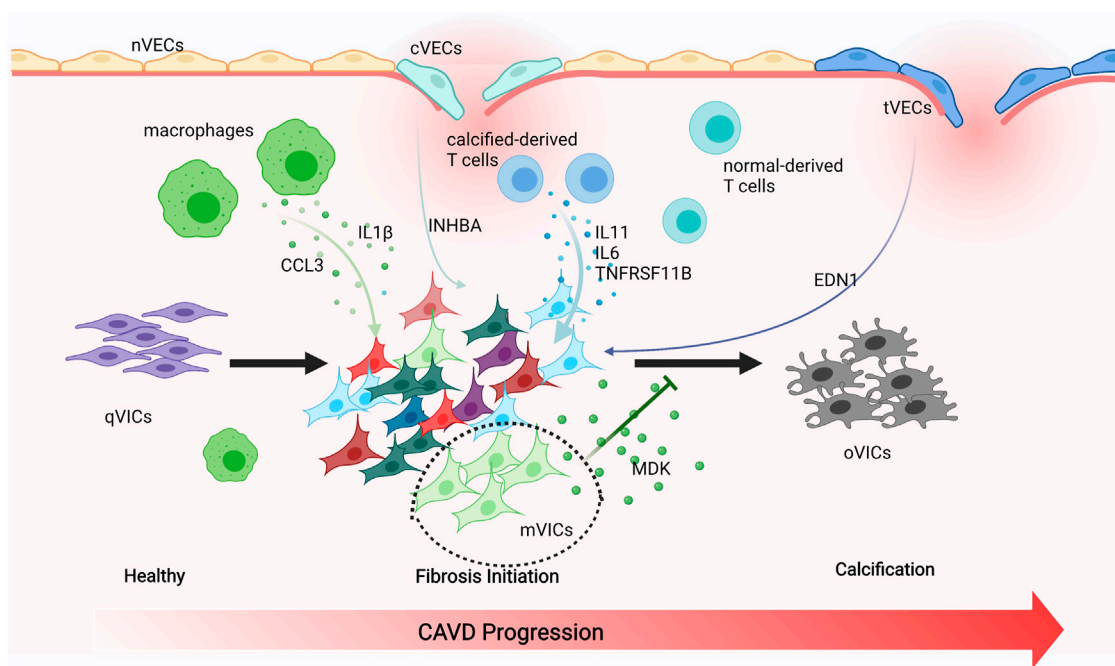


**FIGURE 7 |** Schematic illustration of intercellular cross talk among valve cells. Macrophages secreting IL1 $\beta$  and CCL3 to activate VICs' subsets. cVECs secreting INHBA and tVECs secreting EDN1 to affect VICs. Calcified-derived T cells secreting IL11, IL6, and TNFRSF11B to activate VICs. mVICs secreting MDK to inhibit VICs' calcification.

## DISCUSSION

Endothelial cells tightly cover the surface of the heart valve to avoid the influx of foreign cells and substances into the valve and to maintain valve homeostasis (Takx et al., 2015; Singh et al., 2008; Freeman and Otto 2005). However, VECs' dysfunction and damage are motivated by hemodynamic changes that initiate the onset and progression of CAVD (Richards et al., 2013; Fernandez Esmerats, Heath, and Jo 2016; Yabusaki et al., 2016). VECs have the unique capacity to undergo EndMT, which plays a crucial role in valve calcification and is important during valvulogenesis (Yu et al., 2014; Kovacic et al., 2019; Balachandran et al., 2011). VECs within adult valves can replenish VICs and reshape the valve leaflets through the EndMT process (Paruchuri et al., 2006). On the other hand, VECs can also contribute to VICs' calcification through EndMT that is TGF $\beta$ -dependent through the inflammation-mediated process (Mahler, Farrar, and Butcher 2013). The diverse VECs' populations found in our research have been directly linked to EndMT. We observed that nVECs derived from normal valve interact with VICs through the EDN signaling pathway, and tVECs expressed mesenchymal markers interplay with VICs through the ANGPTL signaling pathway, which includes a wide assay of molecules attributed to the TGF family. The comparison between the two indicates that VECs undergo EndMT to achieve VICs' replenishment through the EDN pathway and to cause VICs' calcification through the ANGPTL pathway (Figure 7). With the disturbance of endothelium, cVECs derived from calcific valve also raise expression of inflammatory cytokines, which is lined with

previous studies (Mahler, Farrar, and Butcher 2013). In summary, effects on EndMT differ from VECs to VECs, which are driven by the particular VECs' subpopulation through precise approaches.

The pathobiology of CAVD is intricate, encompassing genetic factors, lipid infiltration, and oxidative damage; the complicated immune cell networks are now being accepted to play an essential role in disease continuation (Bartoli-Leonard, Zimmer, and Aikawa 2021). Our research found that there were three types of immune cells in the aortic valve, namely, macrophages, T cells, and DCs. Macrophages have been connected with the progression and severity of valve calcification and atherosclerosis, considered to be crucial drivers of early valve inflammation (Moore and Tabas 2011; Passos et al., 2020). With extracellular matrix remodeling and hemodynamic obstruction, macrophages differentiate into pro-inflammatory (M1) and anti-inflammatory (M2) macrophages (Malyshev and Malyshev 2015). However, only pro-inflammatory macrophages were observed in our study and they produced CCL3, IL1 $\beta$ , and MMP9, all of which attract monocytes to the local region propagate inflammatory responses. On the other hand, pro-inflammatory cytokines such as IL1 $\beta$  were proven to promote osteogenic differentiation of VICs through the NF $\kappa$ B pathway (Chinetti-Gbaguidi et al., 2017; Hjortnaes et al., 2010). Thus, targeted therapies could focus on reducing M1 macrophages, leading to a cell-mediated decrease of calcification. DCs express CCR7 and IDO1 within the calcific valve and present lipid-related antigens to T cells in a way that depends on MHC class II, triggering a pro-inflammatory phenotype, and promoting the



development of inflammation and mineralization (Ait-Oufella et al., 2014). Previous reports also demonstrated that DCs were colocalized with oxidized lipid, suggesting a regulatory role associated with lipid infiltration in CAVD (Choi et al., 2009). T cells have long been noted in the aged and calcific valve and even have been considered to be an indicator of aortic stenosis severity (Steiner et al., 2012; Olsson et al., 1994; Otto et al., 1994). More recently, researches have proved that T cells gathered around regions of calcification (Olsson et al., 1994; Otto et al., 1994; Steiner et al., 2012), while their functions in normal human aortic valves tissue have not yet been studied. We observed that IL11, IL6, and TNFRSF11B (OPG) encoding osteoprotegerin, which are inextricably linked to EndMT and VIC calcification, were downregulated in normal-derived T cells (**Figure 7**) (Rattazzi et al., 2018; Gonzalez Rodriguez et al., 2021). Therefore, we inferred that normal-derived T cells play a vital role in maintaining aortic valve homeostasis and calcific-derived T cells play a crucial role in contributing to CAVD development.

VICs are the foundation for understanding the pathophysiology of CAVD (Rutkovskiy et al., 2017) and actively drive valve calcification by acquiring osteogenic phenotypes (Yip and Simmons 2011). The shift of VICs into osteoclast-like cells is ascribed to pathological stimuli, including endothelial cells injury, chronic inflammation, low-density lipoprotein cholesterol deposition, and reactive oxygen species. VICs were categorized into six subsets, namely, aVICs, cVICs, iVICs, mVICs, liVICs, and sVICs, and every cluster reflected relevant biological functions of disease progression. Identification of VICs' subsets could provide therapeutic targets to alleviate CAVD. Cell-to-cell interactions rely on the secretion of cytokines that play a crucial role in CAVD, with recent researches underscoring the complexity and interconnectivity of the resident cells (Schlotter et al., 2018). IL6 is implicated as an active driver in valve calcification (Akahori et al., 2018), with IL6 silencing shown to prevent mineralization *in vitro* (El Hussein et al., 2014). IL1 $\beta$  promotes the expression of matrix metalloproteinases (MMPs) (Matilla et al., 2020), both of which exacerbate osteogenic differentiation of VICs and increase the production of inflammatory mediators through the NF $\kappa$ B axis. Further evidence confirmed that IL1 $\beta$  receptor agonist (IL1RA) deficiency could significantly improve the progression of CAVD (Isoda et al., 2010). So far, however, these important cytokines are secreted by which subsets have not been specified. In this study, there were comprehensive descriptions that IL6 is secreted by cVICs and aVICs affecting all VICs' subsets and IL1 $\beta$  originated from cVICs is critical to the inflammation within the valve (**Figure 7**).

Impressively, mVICs were the most specific VICs' subset and highly expressed MDK from bioinformatics analysis. It was the first report that MDK prevented VICs' calcification, which was demonstrated through the experiment *in vitro*. MDK as a heparin-binding growth factor could interact with different receptors, including syndecans, integrins, protein tyrosine phosphatase  $\zeta$ , anaplastic lymphoma kinase (ALK), low-density lipoprotein (LDL) receptor-related protein (PRP), and Notch2 receptor (Filippou, Karagiannis, and Constantinidou 2020), and has multifaceted functions, including contribution to diseases

development and maintenance of normal tissue homeostasis (Filippou, Karagiannis, and Constantinidou 2020). For example, MDK-Notch signaling, Notch2 as a functional receptor of MDK, regulates the epithelial-mesenchymal transition and chemotherapy resistance in pancreatic cancer (Gungor et al., 2011) and promotes the development of neuroblastoma (Kishida et al., 2013). Therefore, MDK can induce tumorigenesis through Notch signaling. The Notch pathway has an inevitable connection with CAVD because NOTCH1 mutation causes valve calcification (Garg et al., 2005). However, the details of the Notch dysfunction causing CAVD have not been fully clarified. Activation of the Notch pathway seems to restrain VICs' calcification (Nigam and Srivastava 2009; Acharya et al., 2011). On the other hand, activation of the Notch pathway promotes VICs' osteogenic differentiation (Zeng et al., 2013), and interactions between VICs and VECs increase NOTCH1 and HEY1 expressions in VICs, accelerating their osteogenic transformation (Kostina et al., 2019). Furthermore, Notch-dependent mechanisms of valve calcification are different in calcific bicuspid and tricuspid aortic valve; VICs, derived from CAVD patients, tend to undergo osteogenic differentiation owing to the activation of the Notch pathway (Kostina et al., 2018). In our study, the expressions of DLL4, NOTCH1, CSL, HES1, and HEY1 were downregulated after treatment of MDK, which indicated that the Notch pathway was suppressed (**Supplementary Figure S8**). Therefore, we convincingly determined that the MDK-Notch axis plays an important role in preventing human VICs' osteogenic differentiation (**Figure 7**).

Taken together, our results provided a comprehensive landscape of cell-to-cell interactions among all cell subsets, which could provide potential reference and guidance for experimental design and may advance the identification of potential therapeutic targets for precision medicine.

## DATA AVAILABILITY STATEMENT

The original contributions presented in the study are included in the article/**Supplementary Material**; further inquiries can be directed to the corresponding authors.

## ETHICS STATEMENT

The studies involving human participants were reviewed and approved by the Institutional Review Board of Union Hospital and Tongji Medical College. The patients/participants provided their written informed consent to participate in this study.

## AUTHOR CONTRIBUTIONS

XHE, ND, and QZ designed this study, performed bioinformatic analysis, and wrote the article. HC performed experimental data. XHA, MZ, YF, HL, and JS revised the article. XHE and ND supervised this study and provided resources.

## FUNDING

This study was supported by the grants from the National Key R&D Program of China (No. 2016YFA0101100) and Fundamental Research Funds for the Central Universities, HUST (Nos. 2020JYCXJJ006 and 2021GCRC073).

## ACKNOWLEDGMENTS

The authors sincerely thank Chenghao Gao for his technical support and valuable discussions.

## SUPPLEMENTARY MATERIAL

The Supplementary Material for this article can be found online at: <https://www.frontiersin.org/articles/10.3389/fcell.2021.794058/full#supplementary-material>

**Supplementary Figure 1** | Workflow of single-cell transcriptome analysis and experimental verification.

**Supplementary Figure 2** | Quality control of scRNA-seq data. (A) Density distribution plots reflect the gene numbers, mitochondrial ratio, UMI numbers,

and log10 Genes per UMI in each sample. (B) The bar plot shows original cell numbers in each sample. (C) Cell cycle distribution. (D) The plot shows gene numbers versus the number of UMIs colored by the fraction of mitochondrial reads.

**Supplementary Figure 3** | Differential genes analysis of scRNA-seq and bulk RNA-seq data. (A–C) Differential genes were performed as comparing cells from normal and calcified aortic valve tissue within VECs, immune cells, and VICs. The full table of genes is found in the Supplementary Table. (D–F) Functional enrichment analysis of significantly upregulated genes in cells from the calcified compared with the normal aortic valve tissue. (G) The volcano plot shows the number of upregulated and downregulated genes in bulk RNA-seq data. (H) The heatmap shows significantly differential genes. (I) Pathway enrichment of upregulated genes.

**Supplementary Figure 4** | Characteristics of immune cell. (A) The heatmap indicates top 10 marker genes in macrophages, T cells, and DCs. (B) Transcription factor activity of these cell types.

**Supplementary Figure 5** | Cell-to-cell communication patterns. (A,B) Heatmaps show the expression level of each pattern genes in each cluster (left), as well as the strength of each pathway gene expression in each pattern (right).

**Supplementary Figure 6** | Outgoing pathways. (A,C,E) Hierarchical plots show inferred intercellular communication networks for ANGPTL, CCL, and IL1 pathways. (B,D,F) Heatmaps show the relative importance of each cell subset.

**Supplementary Figure 7** | Incoming pathways. (A,C) Hierarchical plots show inferred intercellular communication networks for IL6 and EDN pathways. (B,D) Heatmaps show the relative importance of each cell subsets.

**Supplementary Figure 8** | RNA expression of genes in the Notch pathway.

## REFERENCES

- Acharya, A., Hans, C. P., Koenig, S. N., Nichols, H. A., Galindo, C. L., Garner, H. R., et al. (2011). Inhibitory Role of Notch1 in Calcific Aortic Valve Disease. *PLoS One* 6 (11), e27743. doi:10.1371/journal.pone.0027743
- Aibar, S., González-Blas, C. B., Moerman, T., Huynh-Thu, V. A., Imrichova, H., Hulselmans, G., et al. (2017). SCENIC: Single-Cell Regulatory Network Inference and Clustering. *Nat. Methods* 14 (11), 1083–1086. doi:10.1038/nmeth.4463
- Ait-Oufella, H., Sage, A. P., Mallat, Z., and Tedgui, A. (2014). Adaptive (T and B Cells) Immunity and Control by Dendritic Cells in Atherosclerosis. *Circ. Res.* 114 (10), 1640–1660. doi:10.1161/CIRCRESAHA.114.302761
- Akabori, H., Tsujino, T., Masuyama, T., and Ishihara, M. (2018). Mechanisms of Aortic Stenosis. *J. Cardiol.* 71 (3), 215–220. doi:10.1016/j.jcc.2017.11.007
- Akat, K., Borggreffe, M., and Kaden, J. J. (2009). Aortic Valve Calcification: Basic Science to Clinical Practice. *Heart* 95 (8), 616–623. doi:10.1136/hrt.2007.134783
- Balachandran, K., Alford, P. W., Wylie-Sears, J., Goss, J. A., Grosberg, A., Bischoff, J., et al. (2011). Cyclic Strain Induces Dual-Mode Endothelial-Mesenchymal Transformation of the Cardiac Valve. *Proc. Natl. Acad. Sci.* 108 (50), 19943–19948. doi:10.1073/pnas.1106954108
- Barbie, D. A., Tamayo, P., Boehm, J. S., Kim, S. Y., Moody, S. E., Dunn, I. F., et al. (2009). Systematic RNA Interference Reveals that Oncogenic KRAS-Driven Cancers Require TBK1. *Nature* 462 (7269), 108–112. doi:10.1038/nature08460
- Bartoli-Leonard, F., Zimmer, J., and Aikawa, E. (2021). Innate and Adaptive Immunity: the Understudied Driving Force of Heart Valve Disease. *Cardiovasc. Res.* 1, cvab273. doi:10.1093/cvr/cvab273
- Chinetti-Gbaguidi, G., Daoudi, M., Rosa, M., Vinod, M., Louvet, L., Copin, C., et al. (2017). Human Alternative Macrophages Populate Calcified Areas of Atherosclerotic Lesions and Display Impaired RANKL-Induced Osteoclastic Bone Resorption Activity. *Circ. Res.* 121 (1), 19–30. doi:10.1161/CIRCRESAHA.116.310262
- Choi, J.-H., Do, Y., Cheong, C., Koh, H., Boscardin, S. B., Oh, Y.-S., et al. (2009). Identification of Antigen-Presenting Dendritic Cells in Mouse Aorta and Cardiac Valves. *J. Exp. Med.* 206 (3), 497–505. doi:10.1084/jem.20082129
- El Hussein, D., Boulanger, M.-C., Mahmut, A., Bouchareb, R., Laflamme, M.-H., Fournier, D., et al. (2014). P2Y2 Receptor Represses IL-6 Expression by Valve Interstitial Cells through Akt: Implication for Calcific Aortic Valve Disease. *J. Mol. Cell Cardiol.* 72, 146–156. doi:10.1016/j.yjmcc.2014.02.014
- Fernández Esmerats, J., Heath, J., and Jo, H. (2016). Shear-Sensitive Genes in Aortic Valve Endothelium. *Antioxid. Redox Signaling* 25 (7), 401–414. doi:10.1089/ars.2015.6554
- Filippou, P. S., Karagiannis, G. S., and Constantinidou, A. (2020). Midkine (MDK) Growth Factor: a Key Player in Cancer Progression and a Promising Therapeutic Target. *Oncogene* 39 (10), 2040–2054. doi:10.1038/s41388-019-1124-8
- Freeman, R. V., and Otto, C. M. (2005). Spectrum of Calcific Aortic Valve Disease. *Circulation* 111 (24), 3316–3326. doi:10.1161/CIRCULATIONAHA.104.486738
- Garg, V., Muth, A. N., Ransom, J. F., Schluterman, M. K., Barnes, R., King, I. N., et al. (2005). Mutations in NOTCH1 Cause Aortic Valve Disease. *Nature* 437 (7056), 270–274. doi:10.1038/nature03940
- Gonzalez Rodriguez, A., Schroeder, M. E., Grim, J. C., Walker, C. J., Speckl, K. F., Weiss, R. M., et al. (2021). Tumor Necrosis Factor- $\alpha$  Promotes and Exacerbates Calcification in Heart Valve Myofibroblast Populations. *FASEB j.* 35 (3), e21382. doi:10.1096/fj.202002013RR
- Grim, J. C., Aguado, B. A., Vogt, B. J., Batan, D., Andrichik, C. L., Schroeder, M. E., et al. (2020). Secreted Factors from Proinflammatory Macrophages Promote an Osteoblast-like Phenotype in Valvular Interstitial Cells. *Atvb* 40 (11), e296–e308. doi:10.1161/ATVBAHA.120.315261
- Güngör, C., Zander, H., Effenberger, K. E., Vashist, Y. K., Kalinina, T., Izicki, J. R., et al. (2011). Notch Signaling Activated by Replication Stress-Induced Expression of Midkine Drives Epithelial-Mesenchymal Transition and Chemoresistance in Pancreatic Cancer. *Cancer Res.* 71 (14), 5009–5019. doi:10.1158/0008-5472.CAN-11-0036
- Hänzelmann, S., Castelo, R., and Guinney, J. (2013). GSVA: Gene Set Variation Analysis for Microarray and RNA-Seq Data. *BMC Bioinformatics* 14, 7. doi:10.1186/1471-2105-14-7
- Hjortnaes, J., Butcher, J., Figueiredo, J.-L., Riccio, M., Kohler, R. H., Kozloff, K. M., et al. (2010). Arterial and Aortic Valve Calcification Inversely Correlates with Osteoporotic Bone Remodelling: a Role for Inflammation. *Eur. Heart J.* 31 (16), 1975–1984. doi:10.1093/eurheartj/ehq237
- Hutcheson, J. D., Chen, J., Sewell-Loftin, M. K., Ryzhova, L. M., Fisher, C. I., Su, Y. R., et al. (2013). Cadherin-11 Regulates Cell-Cell Tension Necessary for Calcific Nodule Formation by Valvular Myofibroblasts. *Atvb* 33 (1), 114–120. doi:10.1161/ATVBAHA.112.300278
- Isoda, K., Matsuki, T., Kondo, H., Iwakura, Y., and Ohsuzu, F. (2010). Deficiency of Interleukin-1 Receptor Antagonist Induces Aortic Valve Disease in BALB/c Mice. *Atvb* 30 (4), 708–715. doi:10.1161/ATVBAHA.109.201749

- Jin, S., Guerrero-Juarez, C. F., Zhang, L., Chang, I., Ramos, R., Kuan, C.-H., et al. (2021). Inference and Analysis of Cell-Cell Communication Using CellChat. *Nat. Commun.* 12 (1), 1088. doi:10.1038/s41467-021-21246-9
- Kishida, S., Mu, P., Miyakawa, S., Fujiwara, M., Abe, T., Sakamoto, K., et al. (2013). Midkine Promotes Neuroblastoma through Notch2 Signaling. *Cancer Res.* 73 (4), 1318–1327. doi:10.1158/0008-5472.CAN-12-3070
- Kostina, A., Semenova, D., Kostina, D., Uspensky, V., Kostareva, A., and Malashicheva, A. (2019). Human Aortic Endothelial Cells Have Osteogenic Notch-dependent Properties in Co-culture with Aortic Smooth Muscle Cells. *Biochem. Biophysical Res. Commun.* 514 (2), 462–468. doi:10.1016/j.bbrc.2019.04.177
- Kostina, A., Shishkova, A., Ignatieva, E., Irtyuga, O., Bogdanova, M., Levchuk, K., et al. (2018). Different Notch Signaling in Cells from Calcified Bicuspid and Tricuspid Aortic Valves. *J. Mol. Cell Cardiol.* 114, 211–219. doi:10.1016/j.jymcc.2017.11.009
- Kovacic, J. C., Dimmeler, S., Harvey, R. P., Finkel, T., Aikawa, E., Krenning, G., et al. (2019). Endothelial to Mesenchymal Transition in Cardiovascular Disease. *J. Am. Coll. Cardiol.* 73 (2), 190–209. doi:10.1016/j.jacc.2018.09.089
- Li, C., Xu, S., and Gotlieb, A. I. (2011). The Response to Valve Injury. A Paradigm to Understand the Pathogenesis of Heart Valve Disease. *Cardiovasc. Pathol.* 20 (3), 183–190. doi:10.1016/j.carpath.2010.09.008
- Mahler, G. J., Farrar, E. J., and Butcher, J. T. (2013). Inflammatory Cytokines Promote Mesenchymal Transformation in Embryonic and Adult Valve Endothelial Cells. *Atvb* 33 (1), 121–130. doi:10.1161/ATVBAHA.112.300504
- Malyshev, I., and Malyshev, Y. (2015). Current Concept and Update of the Macrophage Plasticity Concept: Intracellular Mechanisms of Reprogramming and M3 Macrophage "Switch" Phenotype. *Biomed. Res. Int.* 2015, 1–22. doi:10.1155/2015/341308
- Matilla, L., Roncal, C., Ibarrola, J., Arrieta, V., García-Peña, A., Fernández-Celis, A., et al. (2020). A Role for MMP-10 (Matrix Metalloproteinase-10) in Calcific Aortic Valve Stenosis. *Atvb* 40 (5), 1370–1382. doi:10.1161/ATVBAHA.120.314143
- Moore, K. J., and Tabas, I. (2011). Macrophages in the Pathogenesis of Atherosclerosis. *Cell* 145 (3), 341–355. doi:10.1016/j.cell.2011.04.005
- Nigam, V., and Srivastava, D. (2009). Notch1 Represses Osteogenic Pathways in Aortic Valve Cells. *J. Mol. Cell Cardiol.* 47 (6), 828–834. doi:10.1016/j.jymcc.2009.08.008
- Olsson, M., Dalsgaard, C.-J., Haegerstrand, A., Rosenqvist, M., Rydén, L., and Nilsson, J. (1994). Accumulation of T Lymphocytes and Expression of Interleukin-2 Receptors in Nonrheumatic Stenotic Aortic Valves. *J. Am. Coll. Cardiol.* 23 (5), 1162–1170. doi:10.1016/0735-1097(94)90606-8
- Osnabrugge, R. L. J., Mylotte, D., Head, S. J., Van Mieghem, N. M., Nkomo, V. T., LeReun, C. M., et al. (2013). Aortic Stenosis in the Elderly. *J. Am. Coll. Cardiol.* 62 (11), 1002–1012. doi:10.1016/j.jacc.2013.05.015
- Otto, C. M., Kuusisto, J., Reichenbach, D. D., Gown, A. M., and O'Brien, K. D. (1994). Characterization of the Early Lesion of 'degenerative' Valvular Aortic Stenosis. Histological and Immunohistochemical Studies. *Circulation* 90 (2), 844–853. doi:10.1161/01.cir.90.2.844
- Paruchuri, S., Yang, J.-H., Aikawa, E., Melero-Martin, J. M., Khan, Z. A., Loukogeorgakis, S., et al. (2006). Human Pulmonary Valve Progenitor Cells Exhibit Endothelial/Mesenchymal Plasticity in Response to Vascular Endothelial Growth Factor-A and Transforming Growth Factor- $\beta$  2. *Circ. Res.* 99 (8), 861–869. doi:10.1161/01.RES.0000245188.41002.2c
- Passos, L. S. A., Lupieri, A., Becker-Greene, D., and Aikawa, E. (2020). Innate and Adaptive Immunity in Cardiovascular Calcification. *Atherosclerosis* 306, 59–67. doi:10.1016/j.atherosclerosis.2020.02.016
- Rattazzi, M., Faggini, E., Bertacco, E., Buso, R., Puato, M., Plebani, M., et al. (2018). RANKL Expression Is Increased in Circulating Mononuclear Cells of Patients with Calcific Aortic Stenosis. *J. Cardiovasc. Trans. Res.* 11 (4), 329–338. doi:10.1007/s12265-018-9804-2
- Richards, J., El-Hamamsy, I., Chen, S., Sarang, Z., Sarathchandra, P., Yacoub, M. H., et al. (2013). Side-Specific Endothelial-dependent Regulation of Aortic Valve Calcification. *Am. J. Pathol.* 182 (5), 1922–1931. doi:10.1016/j.ajpath.2013.01.037
- Ritchie, M. E., Phipson, B., Wu, D., Hu, Y., Law, C. W., Shi, W., et al. (2015). Limma powers Differential Expression Analyses for RNA-Sequencing and Microarray Studies. *Nucleic Acids Res.* 43 (7), e47. doi:10.1093/nar/gkv007
- Rutkovskiy, A., Malashicheva, A., Sullivan, G., Bogdanova, M., Kostareva, A., Stensløkken, K. O., et al. (2017). Valve Interstitial Cells: The Key to Understanding the Pathophysiology of Heart Valve Calcification. *Jaha* 6 (9). doi:10.1161/JAHA.117.006339
- Schlottter, F., Halu, A., Goto, S., Blaser, M. C., Body, S. C., Lee, L. H., et al. (2018). Spatiotemporal Multi-Omics Mapping Generates a Molecular Atlas of the Aortic Valve and Reveals Networks Driving Disease. *Circulation* 138 (4), 377–393. doi:10.1161/CIRCULATIONAHA.117.032291
- Singh, R., Strom, J. A., Ondrovic, L., Joseph, B., and VanAuker, M. D. (2008). Age-related Changes in the Aortic Valve Affect Leaflet Stress Distributions: Implications for Aortic Valve Degeneration. *J. Heart Valve Dis.* 17 (3), 290–299. ; discussion 299.
- Šteiner, I., Krbal, L., Rozkoš, T., Harrer, J., and Laco, J. (2012). Calcific Aortic Valve Stenosis: Immunohistochemical Analysis of Inflammatory Infiltrate. *Pathol. - Res. Pract.* 208 (4), 231–234. doi:10.1016/j.prp.2012.02.009
- Stuart, T., Butler, A., Hoffman, P., Hafemeister, C., Papalexi, E., Mauck, W. M., 3rd, et al. (2019). Comprehensive Integration of Single-Cell Data. *Cell* 177 (7), 1888–1902. e21. doi:10.1016/j.cell.2019.05.031
- Supek, F., Bošnjak, M., Škunca, N., and Šmuc, T. (2011). REVIGO Summarizes and Visualizes Long Lists of Gene Ontology Terms. *PLoS One* 6 (7), e21800. doi:10.1371/journal.pone.0021800
- Takx, R. A. P., Zanen, P., Leiner, T., van der Graaf, Y., and de Jong, P. A. Smart study group (2015). The Interdependence between Cardiovascular Calcifications in Different Arterial Beds and Vascular Risk Factors in Patients at High Cardiovascular Risk. *Atherosclerosis* 238 (1), 140–146. doi:10.1016/j.atherosclerosis.2014.11.024
- Towler, D. A. (2013). Molecular and Cellular Aspects of Calcific Aortic Valve Disease. *Circ. Res.* 113 (2), 198–208. doi:10.1161/CIRCRESAHA.113.300155
- Trapnell, C., Cacchiarelli, D., Grimsby, J., Pokharel, P., Li, S., Morse, M., et al. (2014). The Dynamics and Regulators of Cell Fate Decisions Are Revealed by Pseudotemporal Ordering of Single Cells. *Nat. Biotechnol.* 32 (4), 381–386. doi:10.1038/nbt.2859
- Wang, H., Leinwand, L. A., and Anseth, K. S. (2014). Cardiac Valve Cells and Their Microenvironment-Insights from *In Vitro* Studies. *Nat. Rev. Cardiol.* 11 (12), 715–727. doi:10.1038/nrcardio.2014.162
- Xu, K., Xie, S., Huang, Y., Zhou, T., Liu, M., Zhu, P., et al. (2020). Cell-Type Transcriptome Atlas of Human Aortic Valves Reveal Cell Heterogeneity and Endothelial to Mesenchymal Transition Involved in Calcific Aortic Valve Disease. *Atvb* 40 (12), 2910–2921. doi:10.1161/ATVBAHA.120.314789
- Yabusaki, K., Hutcheson, J. D., Vyas, P., Bertazzo, S., Body, S. C., Aikawa, M., et al. (2016). Quantification of Calcified Particles in Human Valve Tissue Reveals Asymmetry of Calcific Aortic Valve Disease Development. *Front. Cardiovasc. Med.* 3, 44. doi:10.3389/fcvm.2016.00044
- Yip, C. Y. Y., and Simmons, C. A. (2011). The Aortic Valve Microenvironment and its Role in Calcific Aortic Valve Disease. *Cardiovasc. Pathol.* 20 (3), 177–182. doi:10.1016/j.carpath.2010.12.001
- Yoshihara, K., Shahmoradgoli, M., Martínez, E., Vegesna, R., Kim, H., Torres-Garcia, W., et al. (2013). Inferring Tumour Purity and Stromal and Immune Cell Admixture from Expression Data. *Nat. Commun.* 4, 2612. doi:10.1038/ncomms3612
- Yu, W., Liu, Z., An, S., Zhao, J., Xiao, L., Gou, Y., et al. (2014). The Endothelial-Mesenchymal Transition (EndMT) and Tissue Regeneration. *Cscr* 9 (3), 196–204. doi:10.2174/1574888x09666140213154144
- Zeng, Q., Song, R., Ao, L., Weyant, M. J., Lee, J., Xu, D., et al. (2013). Notch1 Promotes the Pro-osteogenic Response of Human Aortic Valve Interstitial Cells via Modulation of ERK1/2 and Nuclear Factor-Kb Activation. *Arterioscler Thromb. Vasc. Biol.* 33 (7), 1580–1590. doi:10.1161/ATVBAHA.112.300912
- Zhou, T., Wang, Y., Liu, M., Huang, Y., Shi, J., Dong, N., et al. (2020). Curcumin Inhibits Calcification of Human Aortic Valve Interstitial Cells by Interfering NF- $\kappa$ B, AKT, and ERK Pathways. *Phytotherapy Res.* 34 (8), 2074–2081. doi:10.1002/ptr.6674

Zhou, Y., Zhou, B., Pache, L., Chang, M., Khodabakhshi, A. H., Tanaseichuk, O., et al. (2019). Metascape Provides a Biologist-Oriented Resource for the Analysis of Systems-Level Datasets. *Nat. Commun.* 10 (1), 1523. doi:10.1038/s41467-019-09234-6

**Conflict of Interest:** The authors declare that the research was conducted in the absence of any commercial or financial relationships that could be construed as a potential conflict of interest.

**Publisher's Note:** All claims expressed in this article are solely those of the authors and do not necessarily represent those of their affiliated organizations, or those of

the publisher, the editors, and the reviewers. Any product that may be evaluated in this article, or claim that may be made by its manufacturer, is not guaranteed or endorsed by the publisher.

*Copyright © 2021 Zhou, Cao, Hang, Liang, Zhu, Fan, Shi, Dong and He. This is an open-access article distributed under the terms of the Creative Commons Attribution License (CC BY). The use, distribution or reproduction in other forums is permitted, provided the original author(s) and the copyright owner(s) are credited and that the original publication in this journal is cited, in accordance with accepted academic practice. No use, distribution or reproduction is permitted which does not comply with these terms.*





# Mechanism of Improving Aspirin Resistance: Blood-Activating Herbs Combined With Aspirin in Treating Atherosclerotic Cardiovascular Diseases

Yixi Zhao<sup>1,2</sup>, Shengjie Yang<sup>1</sup> and Min Wu<sup>1\*</sup>

<sup>1</sup>Comprehensive Department, Guang'anmen Hospital, China Academy of Chinese Medical Sciences, Beijing, China, <sup>2</sup>Graduate School, Beijing University of Chinese Medicine, Beijing, China

## OPEN ACCESS

### Edited by:

Xianwei Wang,  
Xinxiang Medical University, China

### Reviewed by:

Gao Zhu Ye,  
China Academy of Chinese Medical  
Sciences, China  
Jing Tang,  
University of Helsinki, Finland

### \*Correspondence:

Min Wu  
wumin19762000@126.com

### Specialty section:

This article was submitted to  
Cardiovascular and Smooth Muscle  
Pharmacology,  
a section of the journal  
Frontiers in Pharmacology

**Received:** 13 October 2021

**Accepted:** 29 November 2021

**Published:** 17 December 2021

### Citation:

Zhao Y, Yang S and Wu M (2021)  
Mechanism of Improving Aspirin  
Resistance: Blood-Activating Herbs  
Combined With Aspirin in Treating  
Atherosclerotic  
Cardiovascular Diseases.  
Front. Pharmacol. 12:794417.  
doi: 10.3389/fphar.2021.794417

Atherosclerotic thrombotic disease continues to maintain a high morbidity and mortality rate worldwide at present. Aspirin, which is reckoned as the cornerstone of primary and secondary prevention of atherosclerotic cardiovascular diseases (ASCVDs), has been applied in clinics extensively. However, cardiovascular events continue to occur even though people utilize aspirin appropriately. Therefore, the concept of aspirin resistance (AR) was put forward by scholars, which is of great significance for the prediction of the clinical outcome of diseases. The pathogenesis of AR may be incorporated with low patient compliance, insufficient dose, genetic polymorphism, increased platelet transformation, inflammation, and the degenerative changes and calcification of platelets. The improvement of AR in the treatment of ASCVDs has gradually become a research hot spot in recent years. Traditional Chinese medicine (TCM) regards individuals as a whole and treats them from a holistic view, which has been found to have advantages in clinical studies on the treatment of AR. Many kinds of blood-activating TCM have the effect of improving AR. The potential mechanism for the improvement of AR by blood-activating herbs combined with aspirin was explored. The combination of blood-activating herbs and aspirin to improve AR is likely to turn into a hot topic of research in the future.

**Keywords:** blood-activating, traditional Chinese medicine, aspirin resistance, atherosclerotic cardiovascular diseases, mechanism

## INTRODUCTION

Atherosclerotic cardiovascular diseases (ASCVDs) have a high incidence in the world and are the main cause of morbidity and mortality in China (The interpretation of, 2017). The increase in platelet reactivity, platelet activation, aggregation, and interaction with surface molecules is closely related to ischemic stroke, thrombosis, and cardiovascular diseases (CVDs) (Kannan et al., 2019; Khodadi, 2020; Wiśniewski et al., 2020). Aspirin, an acetylated salicylate, can irreversibly inhibit the conversion of arachidonic acid (AA) to thromboxane A<sub>2</sub> (TXA<sub>2</sub>) by acetylating the serine 529 site of platelet cyclooxygenase-1 (COX-1), and then inhibit platelet production and play an antithrombotic role. Aspirin is widely used in clinics as the cornerstone of primary and secondary prevention of CVDs (Welsh et al., 2019; Nudy et al., 2020; Rocca and Patrono, 2020; Mogul et al., 2021). Nevertheless, a large number of studies have shown that about 2–4% of

cardiovascular ischemic events, such as myocardial infarction, stroke, and death still reoccur every year after the rational use of drugs (Eikelboom et al., 2017; Sabatine et al., 2017; Schwartz et al., 2018). Patients with CVD who are at high risk of aspirin-induced bleeding were challenged by novel evidence of aspirin tolerance poses (Santos-Gallego and Badimon, 2021). The conception of aspirin resistance (AR) has been proposed, and the improvement of AR in the treatment of ASCVDs has gradually become a research hot spot in recent years (Locâne et al., 2019).

## CONCEPTION OF AR AND CURRENT RESEARCH STUDIES

### Conception of AR

Aspirin is the representative medicine of antiplatelet aggregation (Ornelas et al., 2017). However, thrombosis events still occur after patients take aspirin in clinical practice, which is called AR (Paven et al., 2020). Henry et al. (2010) evaluated the 2- to 24-h peak and trough biological efficacy of daily low-dose aspirin in 150 patients with stable coronary heart disease (CHD). Light transmittance concentration (LTA) induced by 0.5 mg/ml AA was measured. It was found that AR appeared in one quarter of the patients. At present, AR is generally defined as the expected effect of antiplatelet aggregation which does not appear after patients regularly take conventional dose of aspirin, and laboratory indicators show that platelet activity or accumulation rate is not ideal, resulting in increased risk of cardiovascular events (Paseban et al., 2020). A study conducted on 126 Asian Indian patients with stable CHD found that 36% of patients had no response to aspirin (Chadha et al., 2016). In a systematic review and meta-analysis of 65 studies involving 10,729 patients, the overall prevalence of AR in CVD patients defined by the laboratory was 24.7% (95% CI 21.4–28.4). The risk of it was higher in women than in men, with a ratio of 1.16 (95% CI 0.87–1.54) (Ebrahimi et al., 2020). These pieces of evidence suggest that AR is common clinically and may affect the therapeutic efficacy.

### Detection and Significance of AR

There are no official diagnostic or regulatory guidelines for the AR concept (Ferreira et al., 2020). The determination of platelet function is a significant method to estimate the clinical prognosis of patients with AR. The *in vivo* platelet function test is prothrombin time. The *in vitro* platelet function test included the determination of the thromboxane and aspirin metabolite thromboxane B2 (TXB2) (Yassin et al., 2019). However, the AR standard most commonly used and accepted by researchers is that the average aggregation of 10  $\mu$ mol/L adenosine diphosphate (ADP) is greater than 70%, and the average aggregation of 0.5 mg/ml AA is greater than 20% as proposed by Gum et al. (2001). Mohring et al. (2017) detected the formation of thromboxane induced by AA through enzyme-linked immunosorbent assay (ELISA) and the AA-induced antiplatelet effect of aspirin by the LTA method. The results showed that there was a non-linear correlation between the formation of thromboxane and the maximum value of AA-

induced LTA aggregation (Spearman's rho  $R = 0.7396$ ; 95% CI 0.7208–0.7573,  $p < 0.0001$ ). Receiver characteristics analysis and Youden's J statistics showed that 209.8 ng/ml was the optimal cutoff value for thromboxane ELISA to detect high on-treatment platelet reactivity to aspirin (area under the curve: 0.92,  $p < 0.0001$ , sensitivity: 82.7%, specificity: 90.3%). This study showed that the thromboxane formation examined by ELISA is reliable for detecting high on-treatment platelet reactivity to aspirin.

The detection of AR has important implications to predict the clinical outcome of the disease. A 5-year follow-up study of 465 patients treated with aspirin found that multivariate logistic regression analysis showed a high association between AR and cardiovascular events (adjusted odds ratio, 4.28; 95% CI: 1.64–11.20;  $p = 0.03$ ) (Chen and Chou, 2017). Wang et al. (2019) conducted a systematic review and meta-analysis of 35 clinical trials involving 19,025 patients with CHD to explore the relationship between the laboratory test AR and endpoint events. They found that the risk of all-cause death [7.9 vs. 2.5%, OR = 2.42 (95% CI 1.86–3.15,  $p < 0.00001$ )] and target vessel reconstruction [4.5 vs. 1.7%, OR = 2.20 (95% CI 1.19–4.08,  $p = 0.01$ )] in aspirin non-responders was higher than that in aspirin responders, indicating that AR has a good predictive effect on clinical outcomes. Li et al. conducted a systematic review of nine prospective studies including 1889 confirmed adherence patients with CHD who insisted on taking aspirin to explore the relationship between AR and the risk of major adverse cardiovascular events (MACEs). The results illustrated that the incidence of MACEs in patients with AR was significantly higher than that in patients with aspirin sensitivity (odds ratio 2.44, 95% CI 1.81 to 3.30;  $p < 0.000001$ ). The risk of MACEs in the laboratory AR patients with CHD was 2.4 times higher than that in aspirin-sensitive patients (Li et al., 2014).

### Mechanism of AR Formation

AR may be caused by many factors and involves multiple complex mechanisms. AR was found to be related to patients' low compliance and insufficient drug dosage in clinics. Molecular studies have shown that the mechanisms of AR involves platelet gene polymorphism, increased platelet conversion rate, inflammation, and other mechanisms (Figure 1) (Floyd and Ferro, 2014; Du et al., 2016).

### Patients' Incompliance to Aspirin

Grinstein and Cannon (2012) considered that low patient adherence to aspirin was the main reason for the failure of aspirin treatment and thus affected the analysis of AR. Dawson et al. (2011) used aspirin to investigate compliance in 90 ischemic stroke patients and 90 control subjects. Platelet function was assessed using standard definitions of resistance using platelet function analyzer (PFA)-100 and rapid platelet function analyzer (RPFA) devices. Urine levels of aspirin metabolites were measured by high-performance liquid chromatography to confirm treatment adherence. The results indicated that poor compliance accounted for nearly half of the cases of aspirin failure. The key point of AR research is to evaluate the compliance objectively. Cuisset et al. (2009) recruited 136 patients who underwent coronary stenting to explore the

compliance of aspirin. The maximum intensity of AA-induced aggregation (AA-Ag) during hospitalization and a month after discharge was detected; aspirin non-responders were defined as AA-Ag > 30%. 19 patients (14%) were identified as non-responsive 1 month after discharge, and AA-Ag in the population was significantly higher than that during hospitalization ( $15.3 \pm 23$  vs.  $7.5 \pm 10\%$ ,  $p = 0.0004$ ). Only one person did not respond after receiving aspirin, suggesting that these changes were due to non-adherence. Schwartz, K. A. defines this class of patients as “inadequately responsive to aspirin” and believes that such patients are at increased risk of vascular events, and suggests that future studies should focus on improving compliance and reducing the risk of future cardiovascular events (Schwartz, 2011).

### Inadequate Dose of Aspirin

Doses of aspirin for primary and secondary prophylaxis of thrombosis in ASCVD vary from country to country and are usually aimed at achieving analgesic effects rather than achieving antithrombotic effects by complete acetylation of COX-1 (Linden and Tran, 2012).

Low-dose aspirin (75–150 mg) is a long-term effective antiplatelet aggregation therapy (Collaboration, 2002). Quinn, M. J. et al. compared the effects of low-dose (<150 mg) and medium-dose ( $\geq 150$  mg) aspirin on the incidence of patients with unstable angina pectoris or acute myocardial infarction (AMI) within 6 months in the Global Use of Strategies to Open Occluded Coronary Arteries (GUSTO) IIb and Platelet Glycoprotein IIb/IIIa in Unstable Angina: Receptor Suppression Using Integrelin Therapy (PURSUIT) trials. It was found that high-dose aspirin was associated with a reduced incidence of MI [HR 0.79 (95% CI 0.64 to 0.98),  $p = 0.03$ ] (Quinn et al., 2004). Lee, P.Y. et al. observed 468 patients with stable CHD who regularly took aspirin 80–325 mg for 4 weeks and found that the incidence of AR was higher with daily aspirin dose  $\leq 100$  mg than with daily aspirin dose of 150 and 300 mg (30.2 vs. 16.7% vs. 0%,  $p = 0.0062$ ) (Lee et al., 2005). Vivas, D. et al. researched the effect of an additional dose of 100 mg aspirin on platelet function and the proportion of aspirin non-responders in 141 patients with CHD who took 100 mg aspirin on a long-term treatment using PFA-100. The incidence of aspirin non-response decreased from 50.7% (95% CI 42.4–59) to 35.0% (95% CI 27.3–43.2), illustrating that the additional dose of aspirin had a significant effect on aspirin non-response (Vivas et al., 2011). Perrier-Cornet, A. et al. observed that the AR rate decreased from 94 to 47% in patients with myeloid proliferative tumor after changing the aspirin dose from 75 mg once daily to twice daily (Perrier-Cornet et al., 2018).

The dosage of aspirin is still controversial. Haley, S.P. et al. reviewed 12 randomized controlled trials (RCTs) and found that aspirin was not dose-dependent on the incidence of bleeding or ASCVD events, indicating that the dose might not be critical (Haley and Chessman, 2020).

### Platelet Receptor Gene Polymorphism

Platelet receptor gene polymorphism is considered to be closely related to platelet activation, adhesion, aggregation, and the

development of thrombotic diseases (Haybar et al., 2018). Singh, S. et al. explored the expression of MiR-19b-1-5p from the buffy coat of 945 patients with acute coronary syndrome (ACS) through reverse transcription quantitative polymerase chain reaction (PCR). Platelet function was detected by multiplate aggregometry testing. The results showed that after adjusting for age, gender, race, and history of previous stroke, platelet aggregation continues in the presence of aspirin [-Log-MiR-19b-1-5p (unstandardized beta, 44.50; 95% CI, 2.20–86.80;  $p < 0.05$ )], illustrating that AR is related to the lower expression of MiR-19b-1-5p (Singh et al., 2021). Wang, J. et al. evaluated the expression of long chain non-coding RNA H19 in ischemic stroke patients in order to explore the relationship between H19 and AR. 150 acute ischemic stroke patients were recruited, and urine 11-dehydrogenation thromboxane B2 (11dhTXB2) level, plasma H19, and 8-iso-prostaglandin F2 $\alpha$  (8-iso-PGF2 $\alpha$ ) levels were determined. The results showed that plasma H19 levels were elevated significantly in patients with AR ( $p = 0.0203$ ). The H19 level was positively related with urine 11dhTXB2/creatinine ( $R = 0.04364$ ,  $p = 0.0106$ ) and 8-iso-PGF2 $\alpha$  ( $R = 0.04561$ ,  $p = 0.0089$ ). It was considered that H19 might induce AR by increasing the production of 8-iso-PGF2 $\alpha$  (Wang et al., 2020). Xue, M. et al. explored genetic markers in Chinese patients with chronic stable angina pectoris (SAP) after percutaneous coronary intervention (PCI). 207 subjects were recruited to receive 100 mg aspirin daily. The inhibitory effect of platelets was evaluated by LTA. TXB2 and hypersensitive C-reactive protein (hs-CRP) were determined by radioimmunoassay. Genotyping was performed using Taqmanprobe technology (rs5787 and rs5911) and gene sequencing technology (rs3842788). The results showed that rs5911 A/C, C/C and A/A genotype (OR = 5.546, 95% CI = 1.812–11.404), and rs3842788 A/G and G/G genotype (OR = 8.358, 95% CI = 2.470–28.286) were correlated with AR. TXB2 and hs-CRP were significantly increased in the AR group, and the plasma TXB2 level was significantly increased in rs3842788a/G genotype carriers. This suggested that rs5911 and rs3842788 were specific genetic markers for AR in Chinese patients with chronic SAP (Xue et al., 2017).

### Increased Turnover of Platelet

The regeneration of platelet COX-1 improves the ability of circulating platelet pools to produce TXA2 and then promotes platelet aggregation (Floyd and Ferro, 2014). High platelet turnover can be triggered by reduction of abnormal megakaryocytopenia from primary thrombocythemia or peripheral consumption caused by inflammation (Coccheri, 2012). Restoration of thromboxane synthesis capacity in circulating blood reflects the number of platelets with uninhibited COX activity by aspirin. Data had shown that the time during which platelets with normal COX activity entered the circulation in diabetic patients was shorter than that of healthy individuals (Di Minno, 2011). Grove, E. L. et al. investigated the effect of platelet turnover on the antiplatelet effect of aspirin in 177 patients with stable CHD. Platelet turnover was measured by immature platelets and thrombopoietin. Platelet aggregation was measured using the VerifyNow aspirin test and MEA. The results showed that the

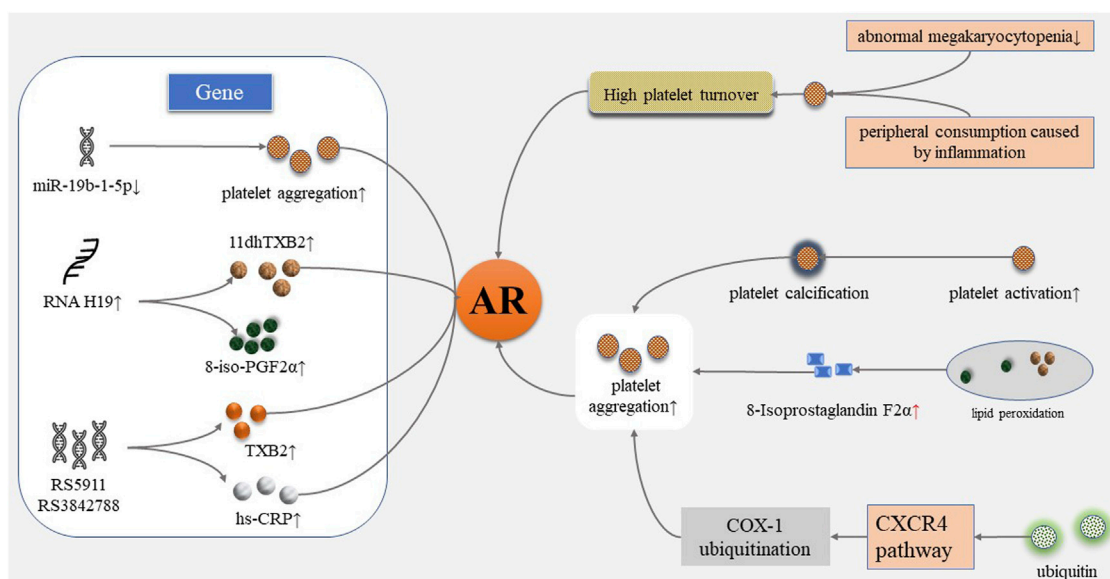


**FIGURE 1 |** Mechanism of aspirin resistance. AR, aspirin resistance; 11dhTXB2, 11-dehydrogenation thromboxane B2; 8-iso-PGF2α, 8-iso-prostaglandin F2α; hs-CRP, high-sensitivity C-reactive protein; CXCR4, CXC chemokine receptor 4; COX-1, cyclooxygenase-1.

**TABLE 1 |** Research studies on improving aspirin resistance by blood-activating herbs.

Intervention	Number of subjects	Findings	References
TCM for promoting blood circulation and removing blood stasis	1,055 subjects	Incidence of AR↓; the maximum platelet aggregation rate induced by ADP and AA↓	Guan et al. (2020)
Blood-activating TCM combined with aspirin	327 subjects	Platelet aggregation rate induced by ADP and AA↓; adverse events and endpoint events were low	Liu et al. (2016)
TCM extracts with water, 90% ethanol, and ethyl acetate	31 kinds of TCM	Chuanxiong ( <i>Rhizoma Chuanxiong</i> ), yanhusuo ( <i>Rhizoma Corydalis yanhusuo</i> ), and Danshen ( <i>Radix Salvia miltiorrhiza</i> ) had similar or higher antiplatelet aggregation effect than aspirin	Chen and Chou (2017)
Assess the efficacy and safety of Chinese herbal medicine for AR	1,011 subjects	Tongxinluo capsule and Danshen-based prescriptions were the most frequently used herbal prescriptions, while Danshen root, milkvetch root, leech, and rosewood were the most frequently used single herbs	Liu et al. (2014)
SMDS extract from <i>Salvia miltiorrhiza</i> -combined aspirin	135 patients with SAP	Improvement of AA% sensitivity of the SMDS-combined aspirin group is the highest; TCM symptoms of the SMDS-combined aspirin group are higher than those of the aspirin group	Lyn et al. (2021)
Compound Danshen Dripping Pills combined with aspirin	40 patients with CHD	Platelet aggregation rate induced by ADP and AA↓	Lin (2016)
Compound Danshen dripping pills (10 grains, tid) with aspirin (100 mg/d)	72 patients with SAP	Platelet aggregation rate↓	Chen (2019)
Danhong injection in combination with aspirin	100 CHD patients with AR	The rate of platelet aggregation, salicylic acid levels, the accumulation of salicylic acid, TXB2, TXB2/6-keto-PGF1α↓; plasma CAT, GPx, plasma SOD activity, and serum G-17 levels↑	Wang and Xu (2018)
Danhong injection combined with aspirin	50 CHD patients with AR	Platelet reactive units and readmission rate↓	Wang et al. (2017)
Tongxinluo capsule combined with aspirin	330 CHD patients	Platelet aggregation values induced by COL and ADP↓	Yin et al. (2010)
Naoxintong capsule combined with aspirin	151 elderly Chinese patients with NVAf and VKORC1 gene variation	Incidence of severe bleeding↓	Wang et al. (2016)

TCM, traditional Chinese medicine; ADP, adenosine diphosphate; AA, arachidonic acid; AR, aspirin resistance; SAP, stable angina pectoris; *Salvia miltiorrhiza* deposite salt, SMDS; arachidonic acid induction rate, AA%; SAP, stable angina pectoris; TXB2, thromboxane B2; catalase, CAT; GPx, glutathione peroxidase; superoxide dismutase, SOD; gastrin-17, G-17; collagen, COL; NVAf, non-valvular atrial fibrillation; vitamin K epoxide reductase, VKORC.

level of immature platelets was closely related to MEA ( $r = 0.31-0.36$ ,  $p < 0.0001$ ), and sP-selector which is the marker of platelet activation ( $r = 0.19$ ,  $p = 0.014$ ). The antiplatelet effect of aspirin decreased within the increase of the platelet turnover

rate, and AR was obvious consequently (Grove et al., 2011). The clinical association between accelerated platelet turnover and AR increased the risk of thrombotic disease events (Di Minno et al., 2012).



**TABLE 2 |** Research studies on Chinese herbs that have been tested for aspirin resistance.

Chinese herb	Scientific name	Chemical composition	Findings	References
<i>Chuanxiong</i>	<i>Rhizoma Chuanxiong</i>	Chuanxiongazine	ADP-, AA-, and THR-induced platelet aggregation↓	Cen et al. (2017)
<i>Huaihua</i>	<i>Flos Sophorae</i>	Rutin, sophorae glycol	Stronger anti-aggregation effect even than that of aspirin	
<i>Niuxi</i>	<i>Radix Achyranthis Bidentatae</i>	Polysaccharide, saponin, and sterone	Strong anti-aggregation effect at lower concentrations with THR and AA as aggregation inducers	
<i>Chishao</i>	<i>Radix Paeoniae Rubra</i>	Paeoniflorins and paeonols	Strong anti-aggregation effect at lower concentrations with AA as the aggregation inducer	
<i>Danshen</i>	<i>Radix Salvia miltiorrhiza</i>	Salvia miltiorrhiza depside salt	Rate of sensitivity in AA%↑	Lyu et al. (2021)
<i>Danhong injection</i>	<i>Radix Salvia miltiorrhiza</i> and <i>Carthamus tinctorius</i> L	Tanshinone, phenolic acid, safflor yellow pigment, and flavone	Platelet aggregation rate, TXB2 and TXB2/6-keto-PGF1α↓	Wang and Xu (2018)
<i>Danhong injection</i>	<i>Radix Salvia miltiorrhiza</i> and <i>Carthamus tinctorius</i> L	Tanshinone, phenolic acid, safflor yellow pigment, and flavone	Platelet reactive units and readmission rate↓	Wang et al. (2017)
Compound <i>Danshen</i> Dropping Pills	<i>Radix Salvia miltiorrhiza</i>	Water-soluble Danshen	AA-induced platelet aggregation rate↓	Zhang (2015)
Tongqiao Huoxue Decoction	—	—	ADP- and AA-induced platelet aggregation rate↓	Liu (2019)
<i>Ginkgo biloba</i>	<i>Ginkgo biloba</i> L	Ginkgo flavone and ginkgolide	ADP- and AA-induced platelet aggregation rate↓	Feng et al. (2016)
<i>Tongxinluo</i> capsule	—	—	ADP- and AA-induced platelet aggregation↓	Yin et al. (2010)
<i>Naoxintong</i> capsule	—	—	Incidence of severe bleeding↓	Wang et al. (2016)
<i>Xuefu Zhuyu</i> Capsule	—	Peach kernel water extract, safflor yellow pigment, tangerine peel, and saikosaponin a	Platelet aggregation rate↓	Zhu et al. (2018)
<i>Taoren-Honghua</i>	<i>Persicae Semen</i> and <i>Carthamus tinctorius</i> L	Amygdalin and hydroxysafflor yellow A	WBV, PV and PCV↓, TT, APTT and PT↑, FIB↓	Liu et al. (2012)

AA, arachidonic acid; ADP, adenosine diphosphate; THR, thrombin; WBV, whole blood viscosity; PV, plasma viscosity; PCV, packed cell volume; TT, prolonged thrombin time; APTT, activated partial thromboplastin time; PT, prothrombin time; FIB, fibrinogen content.

## Inflammation

Chronic inflammation is the underlying pathological mechanism of atherosclerosis-induced CVDs. The complex process involves the interaction of vascular endothelial cells, immune cells, and molecular transmitters, and promotes the development of atherosclerotic thrombotic disease by activating the rupture of atherosclerotic plaque (Shah, 2019). Inflammatory cytokines contribute to the formation of AR through platelet transformation, activation, and adhesion processes (Du et al., 2016). The pre-thrombotic state can be generated by the production and release of thromboxane A2 due to the increased expression of cyclooxygenase-2, which is associated with inflammation (Yalcinkaya and Celik, 2014). Reactivity to aspirin therapy may be reduced by inflammation-induced AR (Shan et al., 2010).

## Other Mechanisms

Kyyak, Y. H. et al. observed the functional status and ultrastructure of platelets in 36 patients with ACS under electron microscopy. The majority of platelets were found to be under an activated state, with pseudopodence, partial platelet aggregation, osmiophilism, vacuolation, and even calcification and apoptosis. Therefore, the researchers considered that AR may be caused by the degenerative changes and calcification of platelets (Kyyak et al., 2019).

Recent studies have shown that 8-isoprostaglandin F2α induced by oxidative stress can mediate the occurrence of AR.

8-Isoprostaglandin F2α as an agonist binding to the thromboxane platelet receptor and promoting vasoconstriction and platelet activation. 8-Isoprostaglandin F2α produced by the lipid peroxidation pathway is independent of COX activity, which means it is not affected by aspirin (Bauer et al., 2014). Therefore, platelet aggregation still occurs after TXA2 is inhibited by aspirin and leads to AR (Guo et al., 2019).

Tan, C. et al. observed platelet function and serum ubiquitin levels in 250 patients with AMI before and after taking aspirin to explore the possible mechanism of AR. They found that AR occurred in 47 patients, and serum ubiquitin levels were higher in AR patients than in healthy patients. Patients with high serum ubiquitin levels showed high levels of platelet ubiquitination, ubiquitinated proteins, and ubiquitinated cyclooxygenase-1. Serum ubiquitin promoted COX-1 ubiquitination through the CXC chemokine receptor 4 (CXCR4) pathway and prevented aspirin from acetylation of its target *in vitro* studies, thereby reducing the antiplatelet effect of aspirin, which might be involved in the mechanism of AR (Tan et al., 2015). In addition, there are also drug interactions and the influence of patient comorbidities in clinical practice which deserve more exploration.

## Current Clinical Researches on AR

Olas, B. investigated the antiplatelet effects of fish and vegetable oils and their constituent fatty acids. Studies in patients with a variety of CVDs have shown that both fish and vegetable oils

contain protective components with antiplatelet activity. And, vegetable oils contain compounds known as phytosterols that protect the heart from hypercholesterolemia. Therefore, the author considered that vegetable oils might play a key role in the prevention and treatment of CVDs associated with platelet overactivation (Olas, 2020). Al-Azzam, S. I. et al. conducted a cross-sectional study of 418 patients taking aspirin and found that the use of statin was associated with the improvement of AR (Al-Azzam et al., 2012). Flavonoids have been found to have antiplatelet activity. In recent years, they have been focused on research and considered favorable drug candidates in the future (Khan et al., 2018). Some researchers considered that lifestyle changes such as smoking cessation, exercise, and weight loss might improve aspirin response, and prevention and treatment of complications related to AR such as hyperlipidemia, diabetes, and hypertension might also help improve AR (Kasmeridis et al., 2013; Ardeshna et al., 2019). In addition, other antiplatelet drugs, such as clopidogrel and P2Y<sub>12</sub> inhibitor ticagrelor in combination with aspirin have also been studied (Divani et al., 2013). TCM treatment is based on a holistic perspective and treats the patient as a whole rather than just targeting a certain disease. In recent years, studies on the improvement of AR by TCM have been paid more and more attention, and the advantages of TCM have been reflected in clinical studies (Table 1) (Chen, 2019).

## RESEARCHES ON IMPROVING AR BY BLOOD-ACTIVATING HERBS COMBINED WITH ASPIRIN

Low compliance, insufficient dose, and the interaction between non-steroidal inflammatory drugs (NSAIDs) and platelets are important factors leading to AR and the risk of thrombus. Blood-activating herbs have good effects on improving microcirculation, antiplatelet aggregation, and anti-thrombosis in CVDs (Wang et al., 2014).

A systematic review of 1,055 subjects studying the improvement of AR by TCM for promoting blood circulation and removing blood stasis showed that the incidence of AR [RR = 0.41, 95% CI (0.32, 0.52),  $p < 0.00001$ ], the maximum platelet aggregation rate induced by ADP [MD = -6.20, 95% CI (-7.83, -4.57),  $p < 0.0001$ ], and the maximum platelet aggregation rate induced by AA [MD = -4.8, 95% CI (-8.16, -1.44),  $p = 0.005$ ] were significantly decreased after treatment, indicating a very positive efficacy of blood-activating herbs in improving AR (Guan et al., 2020). Liu et al. conducted a meta-analysis of the RCTs of blood-activating TCM combined with aspirin versus aspirin alone in the treatment of AR and found that the combined therapy significantly reduced the ADP-induced platelet aggregation rate [SMD = -1.78, 95% CI (-2.95, 0.61),  $p < 0.003$ ] and AA-induced platelet aggregation rate [SMD = -2.31, 95% CI (-3.41, -1.21),  $p < 0.0001$ ], and there was no increase in endpoint events [R = 0.26, 95% CI (0.05, 1.35),  $p > 0.05$ ], indicating the good safety of blood-activating TCM (Liu et al., 2016). Chen Cen. et al. prepared 31 kinds of TCM extracts with water, 90% ethanol, and ethyl acetate. The antiplatelet aggregation effects of various TCM for blood activation and

stasis removal were measured on the platelet aggregator *in vitro* using 5'-ADP, bovine thrombin, and AA as inducers, respectively, and aspirin was taken as the positive control. It was found that *Chuanxiong* (*Rhizoma Chuanxiong*), *yanhusuo* (*Rhizoma Corydalis yanhusuo*), and *Danshen* (*Radix Salvia miltiorrhiza*) had at least similar or higher antiplatelet aggregation effect than the aspirin group (Cen et al., 2017). Liu et al. conducted a systematic review of 16 RCTs with a total of 1,011 subjects to evaluate the therapeutic effect of Chinese herbal medicine on AR. The results indicated that *Tongxinluo* capsules and prescriptions based on *Danshen* (*Radix Salvia miltiorrhiza*) were the most commonly used TCM prescriptions, and the most commonly used single TCM included *Danshen* (*Radix Salvia miltiorrhiza*), *Leech* (*Whitmania pigra Whitman*), and *Rosewood* (*Pterocarpus indicus Willd*). It was suggested that Chinese herbal medicines as potential agents for improving AR merit further more rigorous designs of RCTs to provide further evidence (Liu et al., 2014).

Lyu, J. et al. explored the curative effect of the *Salvia miltiorrhiza* Depside Salt (SMDS) extract from *Danshen* (*Radix Salvia miltiorrhiza*) for SAP. A total of 135 subjects were randomly assigned to the SMDS group, aspirin group, and SMDS-combined aspirin group. Thromboelastography, visual analog scale score of TCM symptoms, and platelet aggregation detected by light transmittance aggregometry were determined at baseline and after 10-day treatment, respectively. The results showed that the improvement of arachidonic acid induction rate (AA%) sensitivity of the SMDS-combined aspirin group was the highest among the three groups [ $p < 0.001$ , 95% CI (0.00–0.00)], and TCM symptoms of the SMDS-combined aspirin group was higher than those of the aspirin group [MD = 1.71, 95% CI (0.15–3.27),  $p = 0.032$ ]. Those findings indicated that SMDS combined with aspirin is an effective intervention for SAP (Lyu et al., 2021).

Research on compound *Danshen* dripping pills combined with aspirin in treating patients with CHD showed that the platelet aggregation rate induced by ADP and AA was lower than that of aspirin alone ( $74.2 \pm 1.4$  vs.  $70.1 \pm 1.3$ ,  $p < 0.05$ ;  $26.4 \pm 5.3$  vs.  $24.3 \pm 3.1$ ,  $p < 0.05$ ), illustrating the high clinical application value (Lin, 2016). Chen et al. recruited 72 patients with SAP who took aspirin (100 mg/d) continuously for more than 4 weeks and were confirmed as AR by thromboelastography. The control group took 100 mg/d orally according to the original dose, and the experimental group took compound *Danshen* dripping pills (10 grains, tid) additionally. After 1-month treatment, the platelet aggregation rate of the experimental group was significantly lower than that of the control group [ $(69 \pm 6)\%$  vs.  $(44 \pm 5)\%$ ,  $p < 0.05$ ], suggesting that the compound *Danshen* dripping pill has a preferable effect on reducing platelet aggregation (Si-rui et al., 2016).

Wang et al. observed the effect of *Danhong* injection on the antiplatelet effect of aspirin and gastric mucosa damage in patients with CHD. *Danhong* injection in combination with aspirin decreased the rate of platelet aggregation, the salicylic acid levels, and the accumulation of salicylic acid, TXB<sub>2</sub>, and TXB<sub>2</sub>/6-keto-PGF<sub>1</sub> $\alpha$ . The activity of plasma catalase (CAT), glutathione peroxidase (GPx), and plasma superoxide

dismutase (SOD), and the serum gastrin-17 (G-17) level were higher than those of the control group ( $p < 0.05$ ), suggesting that the combination of aspirin strengthened the inhibition of COX-1, promoted gastric mucus secretion, and enhanced the body's antioxidant capacity (Wang and Xu, 2018). In addition, *Danhong* injection combined with aspirin was also found to reduce platelet reactive units ( $540.39 \pm 54.39$  vs.  $654.49 \pm 39.48$ ,  $p < 0.01$ ) and readmission rate (20 vs. 40%,  $p = 0.029$ ) in CHD patients with AR (Wang et al., 2017).

Yin et al. observed the *Tongxinluo* capsule on platelet aggregation in AR patients with CHD. Platelet aggregation values were determined by collagen (COL) and ADP as inducers. Results showed that after 1-month treatment, platelet aggregation values of the *Tongxinluo* capsule group and *Tongxinluo* capsule-combined aspirin group were significantly decreased, while those of the aspirin group did not, suggesting that *Tongxinluo* capsule inhibits the function of platelets and prevented the progress of the disease (Yin et al., 2010).

Wang et al. compared the effect of *Naoxintong* capsule combined with aspirin with warfarin at adjusted doses on thrombus risk in elderly Chinese patients with non-valvular atrial fibrillation (NVAF) and vitamin K epoxide reductase (VKORC1) gene variation. It was observed that combination therapy reduced the incidence of severe bleeding (0 vs. 7.9%, OR: 0.921, 95% CI: 0.862–0.984,  $p = 0.028$ ), demonstrating the antithrombotic effect of blood-activating herbs (Wang et al., 2016).

## POTENTIAL MECHANISMS ON IMPROVING AR BY BLOOD-ACTIVATING HERBS COMBINED WITH ASPIRIN

The mechanism of traditional Chinese medicine to improve aspirin resistance is not clear. The studies of Chinese herbal medicine that have been tested for aspirin resistance are shown in Table 2.

Lai et al. explored the potential active ingredients and mechanism of *Danhong* injection in improving AR based on network pharmacology. The Traditional Chinese Medicine Database and Analysis Platform was used to collect the main active components and action targets of *Danshen* (*Salviae miltiorrhizae radix et rhizome*) and *Honghua* (*Carthamus tinctorius* L.). The main active ingredients were screened, and 60 active ingredients were obtained, including 51 components of *Danshen* (*Salviae miltiorrhizae radix et rhizome*), 11 components of *Honghua* (*Carthamus tinctorius* L.), two components of *Danshen* (*Salviae miltiorrhizae radix et rhizome*) and *Honghua* (*Carthamus tinctorius* L.), and 159 target genes. The results of gene enrichment analysis suggested that *Danhong* injection mainly improved AR through multicomponent, multi-target, and multichannel pathways involving coagulation process, inflammatory response, and metabolic regulation (Lai et al., 2019).

Xue et al. observed the effect of *Xuefu Zhuyu* Capsule on AR and explored its mechanism. Patients with AR were randomly divided into three groups: aspirin high-dose group (300 mg/d,

qd), *Xuefu Zhuyu* Capsule group (six grains each time, bid), and *Xuefu Zhuyu* Capsule (six grains each time, bid) in combination with aspirin (100 mg/d, qd). AA and platelet aggregation rate, TXB<sub>2</sub>, 6-Keto-prostaglandin F<sub>1</sub> alpha (6-Keto-PGF<sub>1α</sub>), and hs-CRP induced by ADP were measured. The platelet aggregation rate in the combination group (AA-induced:  $23.57 \pm 4.1$  vs.  $25.76 \pm 3.76$ ; ADP-induced:  $72.18 \pm 7.57$  vs.  $77.01 \pm 9.83$ ), TXB<sub>2</sub> ( $279.81 \pm 52.49$  vs.  $304.53 \pm 47.3$ ), and Hs-CRP ( $3.69 \pm 0.99$  vs.  $4.3 \pm 1.24$ ) was significantly lower than that in the aspirin group. The effect of increasing 6-Keto-PGF<sub>1α</sub> in the combination group was better than that of the high-dose aspirin group. The mechanism of *Xuefu Zhuyu* Capsule to improve AR was considered to be associated with TXB<sub>2</sub>, hs-CRP, and 6-Keto-PGF<sub>1α</sub> (Zhu et al., 2018).

*Taoren* (*Persicae Semen*) and *Honghua* (*Carthamus tinctorius* L.), which is also called *Taoren-Honghua* (TH), is a commonly used herb group for promoting blood circulation and removing blood stasis in TCM. Liu et al. explored the effects of its main components amygdalin and hydroxysafflor yellow A (HSYA) on hemorheology in rats. The intervention methods include TH, amygdalin, HSYA, amygdalin combined with HSYA, and aspirin. Rats were administered every 12 h. After the fifth administration, during the interval between the two injections of adrenaline hydrochloride, the rats except the control group with blood stasis syndrome were placed in ice water to establish the model; blood samples were collected 30 min after the last administration the next day. The results indicated that TH significantly reduced whole blood viscosity (WBV), plasma viscosity (PV), and packed cell volume (PCV); prolonged thrombin time (TT), activated partial thromboplastin time (APTT), and increased prothrombin time (PT); and decreased fibrinogen content (FIB). Amygdalin mainly reduced PV and FIB and prolonged APTT while HSYA mainly reduced WBV and PV. This reveals that TH plays a synergistic role in reducing blood viscosity and improving coagulation parameters (Liu et al., 2012).

## CONCLUSION AND PROSPECTIVE

Platelet activation and coagulation regulation play an important role in vascular injury and atherosclerotic thrombus events (Tomaiuolo et al., 2017). Aspirin as an antiplatelet drug is an important part of the secondary prevention of atherosclerotic thrombosis; however, the antiplatelet aggregation effect of aspirin is different among the crowd. AR is defined as the state in which platelet reactivity does not reach the ideal reduction after aspirin treatment (Ping-ping et al., 2019). Research had shown that AR is an independent predictor of cardiovascular adverse risk (Pasala et al., 2016). In recent years, more and more studies have been conducted on AR, and the improvement of AR may become a research hot spot in the future (Xue et al., 2014; Al-Jabi, 2017; AJin et al., 2019; Baş et al., 2020).

It has been found that the combination of blood-activating herbs and aspirin can improve AR and reduce the rate of platelet aggregation (Yulong and Zhongjun, 2014). Monomers including *Danshen* (*Radix Salvia miltiorrhiza*) and *Honghua* (*Carthamus*

*tinctorius* L.) and compounds including *Danshen* Dropping Pills, *Danhong* injection, *Tongxinluo* capsule, *Naoxintong* capsule, and *Xuefu Zhuyu* capsule have advantages in antiplatelet aggregation, which were the research hot spots in recent years. However, the effectiveness of blood-activating TCM in CVDs still needs further rigorous large-scale clinical trials to provide further strong evidence. There are many studies on the role of blood-activating traditional Chinese medicine, but scattered studies have not formed a unified therapeutic target network. Researchers have used different computational approaches to construct network models of Chinese herbal medicine to explore the interaction of ingredients of disease pathways (Jafari et al., 2020; Wang et al., 2021). The network model construction of Chinese herbal medicine may further reveal the intervention targets and potential treatment orientation of diseases. The mechanism of blood-activating herbs on improving AR remains unclear, and there is still a lack of relevant research at home and abroad. Studies have found that blood-activating herbs

may improve AR through multicomponent, multi-target, and multichannel pathways such as coagulation process, inflammatory reaction, and metabolic regulation, which are worthy of further exploration and may become a potential target for future treatment.

## AUTHOR CONTRIBUTIONS

MW designed and directed the manuscript. YZ wrote the manuscript. SY revised the manuscript.

## FUNDING

This work was supported by the National Natural Science Foundation of China (Grant No. 81202805 and 82074254), the Beijing Natural Science Foundation (No.7172185).

## REFERENCES

- AJin, C., Jin, C. M., Young-Ki, L., Hoon, H. C., Koo, J. R., Yoon, J. W., et al. (2019). Effects of Aspirin Resistance and Mean Platelet Volume on Vascular Access Failure in Hemodialysis Patients. *Korean J. Intern. Med.* 34, 1304–1312. doi:10.3904/kjim.2018.111
- Al-Azzam, S. I., Alzoubi, K. H., Khabour, O., Alowidi, A., and Tawalbeh, D. (2012). The Prevalence and Factors Associated with Aspirin Resistance in Patients Premedicated with Aspirin. *Acta Cardiol.* 67, 445–448. doi:10.1080/ac.67.4.2170686
- Al-Jabi, S. W. (2017). Global Trends in Aspirin Resistance-Related Research from 1990 to 2015: A Bibliometric Analysis. *Basic Clin. Pharmacol. Toxicol.* 5, 1–19. doi:10.1111/bcpt.12840
- Ardeshtna, D., Khare, S., Jagadish, P. S., Bhattad, V., Cave, B., and Khouzam, R. N. (2019). The Dilemma of Aspirin Resistance in Obese Patients. *Ann. Transl Med.* 7, 404. doi:10.21037/atm.2019.07.52
- Baş, H. A., Aksoy, F., Bağcı, A., Varol, E., and Altınbaş, A. (2020). Incidence of Aspirin Resistance Is Higher in Patients with Acute Coronary Syndrome and Atrial Fibrillation Than without Atrial Fibrillation. *Rev. Assoc. Med. Bras* 66, 800–805. doi:10.1590/1806-9282.66.6.800
- Bauer, J., Ripberger, A., Frantz, S., Ergün, S., Schwedhelm, E., and Benndorf, R. A. (2014). Pathophysiology of Isoprostanes in the Cardiovascular System: Implications of Isoprostane-Mediated Thromboxane A<sub>2</sub> Receptor Activation. *Br. J. Pharmacol.* 171, 3115–3131. doi:10.1111/bph.12677
- Cen, C., Fengqin, W., Wen, X., Zhining, X., Guang, H., Jianbo, W., et al. (2017). Effect on Platelet Aggregation Activity: Extracts from 31 Traditional Chinese Medicines with the Property of Activating Blood and Resolving Stasis. *J. Traditional Chin. Med.* 37, 64–75. doi:10.1016/s0254-6272(17)30028-6
- Chadha, D. S., Sumana, B., Karthikeyan, G., Jayaprasad, V., and Arun, S. S. (2016). Prevalence of Aspirin Resistance in Asian-Indian Patients with Stable Coronary Artery Disease. *Catheter Cardiovasc. Interv.* 88, E126–E131. doi:10.1002/ccd.25420
- Chen, H. (2019). Integrative Medicine on Optimizing Clopidogrel and Aspirin Therapy. *Chin. J. Integr. Med.* 25, 395–400. doi:10.1007/s11655-017-2551-4
- Chen, H. Y., and Chou, P. (2017). Pfa-100-measured Aspirin Resistance Is the Predominant Risk Factor for Hospitalized Cardiovascular Events in Aspirin-Treated Patients: A 5-year Cohort Study. *J. Clin. Pharm. Ther.*, 1–7.
- Coccheri, S. (2012). Antiplatelet Therapy: Controversial Aspects. *Thromb. Res.* 129, 225–229. doi:10.1016/j.thromres.2011.10.036
- Collaboration, A. T. (2002). Collaborative Meta-Analysis of Randomised Trials of Antiplatelet Therapy for Prevention of Death, Myocardial Infarction, and Stroke in High Risk Patients. *BMJ* 324, 71–86. doi:10.1136/bmj.324.7329.71
- Cuisset, T., Frere, C., Quilici, J., Gaborit, B., Bali, L., Poyet, R., et al. (2009). Aspirin Noncompliance Is the Major Cause of "aspirin Resistance" in Patients Undergoing Coronary Stenting. *Am. Heart J.* 157, 889–893. doi:10.1016/j.ahj.2009.02.013
- Dawson, J., Quinn, T., Rafferty, M., Higgins, P., Ray, G., Lees, K. R., et al. (2011). Aspirin Resistance and Compliance with Therapy. *Cardiovasc. Ther.* 29, 301–307. doi:10.1111/j.1755-5922.2010.00188.x
- Di Minno, G. (2011). Aspirin Resistance and Platelet Turnover: A 25-year Old Issue. *Nutr. Metab. Cardiovasc. Dis.* 21, 542–545. doi:10.1016/j.numecd.2011.04.002
- Di Minno, M. N., Lupoli, R., Palmieri, N. M., Russolillo, A., Buonauro, A., and Di Minno, G. (2012). Aspirin Resistance, Platelet Turnover, and Diabetic Angiopathy: A 2011 Update. *Thromb. Res.* 129, 341–344. doi:10.1016/j.thromres.2011.11.020
- Divani, A. A., Zantek, N. D., Borhani-Haghighi, A., and Rao, G. H. (2013). Antiplatelet Therapy: Aspirin Resistance and All that Jazz!. *Clin. Appl. Thromb. Hemost.* 19, 5–18. doi:10.1177/1076029612449197
- Du, G., Lin, Q., and Wang, J. (2016). A Brief Review on the Mechanisms of Aspirin Resistance. *Int. J. Cardiol.* 220, 21–26. doi:10.1016/j.ijcard.2016.06.104
- Ebrahimi, P., Farhadi, Z., Behzadifar, M., Shabaninejad, H., Abolghasem Gorji, H., Taheri Mirghaied, M., et al. (2020). Prevalence Rate of Laboratory Defined Aspirin Resistance in Cardiovascular Disease Patients: A Systematic Review and Meta-Analysis. *Caspian J. Intern. Med.* 11, 124–134. doi:10.22088/cjim.11.2.124
- Eikelboom, J. W., Connolly, S. J., Bosch, J., Dagenais, G. R., Hart, R. G., Shestakovska, O., et al. (2017). Rivaroxaban with or without Aspirin in Stable Cardiovascular Disease. *N. Engl. J. Med.* 377, 1319–1330. doi:10.1056/NEJMoa1709118
- Feng, Y., Yao, M. H., and Wu, L. J. (2016). Effect of Ginkgo Biloba on Platelet Aggregation Rate and Aspirin Resistance in Patients with Acute Cerebral Infarctions. *Chin. J. Coal Industry Med.* 19, 1476–1479.
- Ferreira, M., Freitas-Silva, M., Assis, J., Pinto, R., Nunes, J. P., and Medeiros, R. (2020). The Emergent Phenomenon of Aspirin Resistance: Insights from Genetic Association Studies. *Pharmacogenomics* 21, 125–140. doi:10.2217/pgs-2019-0133
- Floyd, C. N., and Ferro, A. (2014). Mechanisms of Aspirin Resistance. *Pharmacol. Ther.* 141, 69–78. doi:10.1016/j.pharmthera.2013.08.005
- Grinstein, J., and Cannon, C. P. (2012). Aspirin Resistance: Current Status and Role of Tailored Therapy. *Clin. Cardiol.* 35, 673–681. doi:10.1002/clc.22031
- Grove, E. L., Hvas, A. M., Mortensen, S. B., Larsen, S. B., and Kristensen, S. D. (2011). Effect of Platelet Turnover on Whole Blood Platelet Aggregation in Patients with Coronary Artery Disease. *J. Thromb. Haemost.* 9, 185–191. doi:10.1111/j.1538-7836.2010.04115.x
- Guan, B. Y., Gao, J., and Ma, X. J. (2020). Clinical Efficacy of Blood-Activating and Stasis-Removing Chinese Medicines on Aspirin Resistance: A Meta-Analysis Chinese. *J. Integr. Med. Cardio-cerebrovascular Dis.* 18, 6–12.
- Gum, P. A., Kottke-Marchant, K., Poggio, E. D., Gurm, H., Welsh, P. A., Brooks, L., et al. (2001). Profile and Prevalence of Aspirin Resistance in Patients with



- Cardiovascular Disease. *Am. J. Cardiol.* 88, 230–235. doi:10.1016/s0002-9149(01)01631-9
- Guo, J., Wang, J., and Feng, J. (2019). Aspirin Resistance Mediated by Oxidative Stress-Induced 8-isoprostaglandin F<sub>2</sub>. *J. Clin. Pharm. Ther.* 44, 823–828. doi:10.1111/jcpt.12838
- Haley, S. P., and Chessman, A. (2020). Treatment Effect of Aspirin for Primary Prevention Does Not Differ According to Baseline Ascvd Risk. *Ann. Intern. Med.* 173, JC39–39. doi:10.7326/ACPJ202010200-039
- Haybar, H., Khodadi, E., Zibara, K., and Saki, N. (2018). Platelet Activation Polymorphisms in Ischemia. *Cardiovasc. Hematol. Disord. Drug Targets* 18, 153–161. doi:10.2174/1871529X18666180326121239
- Henry, P., Vermillet, A., Boval, B., Guyetand, C., Petroni, T., Dillinger, J. G., et al. (2010). 24-hour Time-dependent Aspirin Efficacy in Patients with Stable Coronary Artery Disease. *Thromb. Haemost.* 105, 336–344. doi:10.1160/TH10-02-0082
- Jafari, M., Wang, Y., Amiryousefi, A., and Tang, J. (2020). Unsupervised Learning and Multipartite Network Models: A Promising Approach for Understanding Traditional Medicine. *Front. Pharmacol.* 11, 1319. doi:10.3389/fphar.2020.01319
- Kannan, M., Ahmad, F., and Saxena, R. (2019). Platelet Activation Markers in Evaluation of Thrombotic Risk Factors in Various Clinical Settings. *Blood Rev.* 37, 1–9. doi:10.1016/j.blre.2019.05.007
- Kasmeridis, C., Apostolakis, S., and Lip, G. Y. (2013). Aspirin and Aspirin Resistance in Coronary Artery Disease. *Curr. Opin. Pharmacol.* 13, 242–250. doi:10.1016/j.coph.2012.12.004
- Khan, H., Jawad, M., Kamal, M. A., Baldi, A., Xiao, J., Nabavi, S. M., et al. (2018). Evidence and Prospective of Plant Derived Flavonoids as Antiplatelet Agents: Strong Candidates to Be Drugs of Future. *Food Chem. Toxicol.* 119, 355–367. doi:10.1016/j.fct.2018.02.014
- Khodadi, E. (2020). Platelet Function in Cardiovascular Disease: Activation of Molecules and Activation by Molecules. *Cardiovasc. Toxicol.* 20, 1–10. doi:10.1007/s12012-019-09555-4
- Kyyak, Y. H., Barnett, O. Y., Halkevych, M. P., Labinska, O. Y., Kyyak, H. Y., Kysil, O. Y., et al. (2019). Impact of Risk Factors of Ischemic Heart Disease on the Development of Acute Coronary Syndrome, Platelet Ultrastructure, and Aspirin Resistance. *Wiad Lek* 72, 1–9.
- Lai, R. M., Ju, J. Q., Zhao, Y. H., and Xu, H. (2019). Network Pharmacology-Based Study on Mechanisms of Danhong Injection in Treatment of Aspirin Resistance. *Zhongguo Zhong Yao Za Zhi* 44, 2719–2726. doi:10.19540/j.cnki.cjcmm.20190215.001
- Lee, P. Y., Chen, W. H., Ng, W., Cheng, X., Kwok, J. Y., Tse, H. F., et al. (2005). Low-dose Aspirin Increases Aspirin Resistance in Patients with Coronary Artery Disease. *Am. J. Med.* 118, 723–727. doi:10.1016/j.amjmed.2005.03.041
- Li, J., Song, M., Jian, Z., Guo, W., Chen, G., Jiang, G., et al. (2014). Laboratory Aspirin Resistance and the Risk of Major Adverse Cardiovascular Events in Patients with Coronary Heart Disease on Confirmed Aspirin Adherence. *J. Atheroscler. Thromb.* 21, 239–247. doi:10.5551/jat.19521
- Lin, B. (2016). Clinical Effect of Compound Salvia Miltiorrhiza Dropping Pills on Aspirin Resistance of Coronary Heart Disease. *World Latest Med. Inf. (Electronic Version)* 16, 122–123.
- Linden, M. D., and Tran, H. A. (2012). Overcoming Aspirin Treatment Failure in Diabetes. *Crit. Rev. Clin. Lab. Sci.* 49, 183–198. doi:10.3109/10408363.2012.731377
- Liu, A. J., Li, H. Q., Li, J. H., Wang, Y. Y., Chen, D., Wang, Y., et al. (2014). Chinese Herbal Medicine for Aspirin Resistance: A Systematic Review of Randomized Controlled Trials. *Evid. Based Complement. Alternat Med.* 2014, 1–16. doi:10.1155/2014/890950
- Liu, L., Duan, J. A., Tang, Y., Guo, J., Yang, N., Ma, H., et al. (2012). Taoren-honghua Herb Pair and its Main Components Promoting Blood Circulation through Influencing on Hemorheology, Plasma Coagulation and Platelet Aggregation. *J. Ethnopharmacol* 139, 381–387. doi:10.1016/j.jep.2011.11.016
- Liu, Q. Q., Jiang, K., and Chen, X. H. (2016). Meta-analysis of Aspirin Combined with Traditional Chinese Medicine to Promote Blood Circulation and Remove Blood Stasis on Aspirin Resistance. *J. Yunnan Univ. Traditional Chin. Med.* 39, 54–58.
- Liu, W. C. (2019). Preventive Effect of Tongqiao Huoxue Decoction on Aspirin Resistance in Elderly Patients with Coronary Heart Disease. *Chin. Med. Sci. Technol.* 26, 106–107.
- Locâne, S., Pucite, E., Miglâne, E., Millers, A., Novasa, A., Levina, R., et al. (2019). Antiplatelet Resistance in Patients with Atherosclerosis. *Proc. Latvian Acad. Sci. Section B Nat. Exact, Appl. Sci.* 73, 373–378. doi:10.2478/prolas-2019-0058
- Lyu, J., Xue, M., Li, J., Lyu, W., Wen, Z., Yao, P., et al. (2021). Clinical Effectiveness and Safety of Salvia Miltiorrhiza Depside Salt Combined with Aspirin in Patients with Stable Angina Pectoris: A Multicenter, Pragmatic, Randomized Controlled Trial. *Phytomedicine* 81, 153419–153512. doi:10.1016/j.phymed.2020.153419
- Mogul, A., Leppien, E. E., Laughlin, E., and Spinler, S. A. (2021). Aspirin for Primary Prevention of Cardiovascular Disease: A Review of Recent Literature and Updated Guideline Recommendations. *Expert Opin. Pharmacother.* 22, 83–91. doi:10.1080/14656566.2020.1817389
- Mohring, A., Piayda, K., Dannenberg, L., Zako, S., Schneider, T., Bartkowski, K., et al. (2017). Thromboxane Formation Assay to Identify High On-Treatment Platelet Reactivity to Aspirin. *Pharmacology* 100, 127–130. doi:10.1159/000477303
- Nudy, M., Cooper, J., Ghahramani, M., Ruzieh, M., Mandrolia, J., and Foy, A. J. (2020). Aspirin for Primary Atherosclerotic Cardiovascular Disease Prevention as Baseline Risk Increases: A Meta-Regression Analysis. *Am. J. Med.* 133, 1056–1064. doi:10.1016/j.amjmed.2020.04.028
- Olas, B. (2020). Biochemistry of Blood Platelet Activation and the Beneficial Role of Plant Oils in Cardiovascular Diseases. *Adv. Clin. Chem.* 95, 219–243. doi:10.1016/bs.acc.2019.08.006
- Ornelas, A., Zacharias-Millward, N., Menter, D. G., Davis, J. S., Lichtenberger, L., Hawke, D., et al. (2017). Beyond Cox-1: The Effects of Aspirin on Platelet Biology and Potential Mechanisms of Chemoprevention. *Cancer Metastasis Rev.* 36, 289–303. doi:10.1007/s10555-017-9675-z
- Pasala, T., Hoo, J. S., Lockhart, M. K., Waheed, R., Sengodan, P., Alexander, J., et al. (2016). Aspirin Resistance Predicts Adverse Cardiovascular Events in Patients with Symptomatic Peripheral Artery Disease. *Tex. Heart Inst. J.* 43, 482–487. doi:10.14503/THIJ-14-4986
- Paseban, M., Marjaneh, R. M., Banach, M., Riahi, M. M., Bo, S., and Sahebkar, A. (2020). Modulation of Micromas by Aspirin in Cardiovascular Disease. *Trends Cardiovasc. Med.* 30, 249–254. doi:10.1016/j.tcm.2019.08.005
- Paven, E., Dillinger, J. G., Bal Dit Sollier, C., Vidal-Trecan, T., Berge, N., Dautry, R., et al. (2020). Determinants of Aspirin Resistance in Patients with Type 2 Diabetes. *Diabetes Metab.* 46, 370–376. doi:10.1016/j.diabet.2019.11.002
- Perrier-Cornet, A., Ianotto, J. C., Mingant, F., Perrot, M., Lippert, E., and Galinat, H. (2018). Decreased Turnover Aspirin Resistance by Bidaily Aspirin Intake and Efficient Cytochrome Reduction in Myeloproliferative Neoplasms. *Platelets* 29, 723–728. doi:10.1080/09537104.2017.1361018
- Ping-ping, G., Xiao-xia, C., and Xiao-rong, W. (2019). Progress in the Mechanism and Clinical Treatment of Antiplatelet Resistance of Aspirin and Clopidogrel. *Chin. J. Clin. Neurosci.* 27, 321–328.
- Quinn, M. J., Aronow, H. D., Califf, R. M., Bhatt, D. L., Sapp, S., Kleiman, N. S., et al. (2004). Aspirin Dose and Six-Month Outcome after an Acute Coronary Syndrome. *J. Am. Coll. Cardiol.* 43, 972–978. doi:10.1016/j.jacc.2003.09.059
- Rocca, B., and Patrono, C. (2020). Aspirin in the Primary Prevention of Cardiovascular Disease in Diabetes Mellitus: A New Perspective. *Diabetes Res. Clin. Pract.* 160, 108008. doi:10.1016/j.diabres.2020.108008
- Sabatine, M. S., Giugliano, R. P., Keech, A. C., Honarpour, N., Wiviott, S. D., Murphy, S. A., et al. (2017). Evolocumab and Clinical Outcomes in Patients with Cardiovascular Disease. *N. Engl. J. Med.* 376, 1713–1722. doi:10.1056/NEJMoa1615664
- Santos-Gallego, C. G., and Badimon, J. (2021). Overview of Aspirin and Platelet Biology. *Am. J. Cardiol.* 144 (Suppl. 1), 2–9. doi:10.1016/j.amjcard.2020.12.018
- Schwartz, G. G., Steg, P. G., Szarek, M., Bhatt, D. L., Bittner, V. A., Diaz, R., et al. (2018). Alirocumab and Cardiovascular Outcomes after Acute Coronary Syndrome. *N. Engl. J. Med.* 379, 2097–2107. doi:10.1056/NEJMoa1801174
- Schwartz, K. A. (2011). Aspirin Resistance: A Clinical Review Focused on the Most Common Cause, Noncompliance. *Neurohospitalist* 1, 94–103. doi:10.1177/1941875210395776
- Shah, P. K. (2019). Inflammation, Infection and Atherosclerosis. *Trends Cardiovasc. Med.* 29, 468–472. doi:10.1016/j.tcm.2019.01.004
- Shan, Y., Zhao, R., Geng, W., Lin, N., Wang, X., Du, X., et al. (2010). Protective Effect of Sulforaphane on Human Vascular Endothelial Cells against Lipopolysaccharide-Induced Inflammatory Damage. *Cardiovasc. Toxicol.* 10, 139–145. doi:10.1007/s12012-010-9072-0

- Si-rui, C., Li-hua, Z., and Jun1, L. (2016). Risk Factors and Impact of Danshen Compound Dripping Pill on Aspirin Resistance in Patients with Stable Angina Pectoris. *Chin. Heart J.* 28, 435–438.
- Singh, S., de Ronde, M. W. J., Creemers, E. E., Van der Made, I., Meijering, R., Chan, M. Y., et al. (2021). Low Mir-19b-1-5p Expression Is Related to Aspirin Resistance and Major Adverse Cardio- Cerebrovascular Events in Patients with Acute Coronary Syndrome. *J. Am. Heart Assoc.* 10, e017120–9. doi:10.1161/JAHA.120.017120
- Tan, C., Lu, X., Chen, W., and Chen, S. (2015). Serum Ubiquitin via Cxc Chemokine Receptor 4 Triggered Cyclooxygenase-1 Ubiquitination Possibly Involved in the Pathogenesis of Aspirin Resistance. *Clin. Hemorheol. Microcirc.* 61, 59–81. doi:10.3233/CH-141900
- The Interpretation of (2017). The Interpretation of “Aspirin Use in Patients with Atherosclerotic Cardiovascular Disease: the 2016 Chinese Expert Consensus Statement”. *Zhonghua Nei Ke Za Zhi*, 56, 4–6. doi:10.3760/cma.j.issn.0578-1426.2017.01.002
- Tomaiuolo, M., Brass, L. F., and Stalker, T. J. (2017). Regulation of Platelet Activation and Coagulation and its Role in Vascular Injury and Arterial Thrombosis. *Interv. Cardiol. Clin.* 6, 1–12. doi:10.1016/j.iccl.2016.08.001
- Vivas, D., Bernardo, E., García-Rubira, J. C., Azcona, L., Núñez-Gil, I., González-Ferrer, J. J., et al. (2011). Can Resistance to Aspirin Be Reversed after an Additional Dose? *J. Thromb. Thrombolysis* 32, 356–361. doi:10.1007/s11239-011-0596-3
- Wang, H., Zhou, Xk., Zheng, L. F., Wu, X. Y., and Chen, H. (2016). Comparison of Aspirin and Naixintong Capsule with Adjusted-Dose Warfarin in Elderly Patients with High-Risk of Non-valvular Atrial Fibrillation and Genetic Variants of Vitamin K Epoxide Reductase. *Chin. J. Integr. Med.* 24, 247–253. doi:10.1007/s11655-015-2443-4
- Wang, J., Cao, B., Gao, Y., Han, D., Zhao, H., Chen, Y., et al. (2020). Long Non-coding Rna H19 Positively Associates with Aspirin Resistance in the Patients of Cerebral Ischemic Stroke. *Front. Pharmacol.* 11, 1–7. doi:10.3389/fphar.2020.580783
- Wang, J., Liu, J., Zhou, Y., Wang, F., Xu, K., Kong, D., et al. (2019). Association Among Plal/a2 Gene Polymorphism, Laboratory Aspirin Resistance and Clinical Outcomes in Patients with Coronary Artery Disease: An Updated Meta-Analysis. *Sci. Rep.* 9, 13177–13179. doi:10.1038/s41598-019-49123-y
- Wang, J., Xiong, X., and Feng, B. (2014). Aspirin Resistance and Promoting Blood Circulation and Removing Blood Stasis: Current Situation and Prospectives. *Evid. Based Complement. Alternat Med.* 2014, 1–11. doi:10.1155/2014/954863
- Wang, Y., Kong, L. J., and Wang, S. H. (2017). Effect of Danhong Injection on Aspirin Reaction Units and Clinical Prognosis in Patients with Coronary Heart Disease. *CHINESE ARCHIVES TRADITIONAL CHINESE MEDICINE* 35, 1243–1246.
- Wang, Y., Yang, H., Chen, L., Jafari, M., and Tang, J. (2021). Network-based Modeling of Herb Combinations in Traditional Chinese Medicine. *Brief Bioinform* 22. doi:10.1093/bib/bbab106
- Wang, Y. Y., and Xu, Q. S. (2018). Effect of Danhong Injection on Aspirin Antiplatelet and Gastric Mucosa Injury in Patients with Coronary Heart Disease. *Shandong Med. J.* 58, 44–47.
- Welsh, R. C., Peterson, E. D., De Caterina, R., Bode, C., Gersh, B., and Eikelboom, J. W. (2019). Applying Contemporary Antithrombotic Therapy in the Secondary Prevention of Chronic Atherosclerotic Cardiovascular Disease. *Am. Heart J.* 218, 100–109. doi:10.1016/j.ahj.2019.09.006
- Wiśniewski, A., Sikora, J., Sławińska, A., Filipka, K., Karczmarska-Wódzka, A., Serafin, Z., et al. (2020). High On-Treatment Platelet Reactivity Affects the Extent of Ischemic Lesions in Stroke Patients Due to Large-Vessel Disease. *J. Clin. Med.* 9, 251–264.
- Xue, M., Xue, L. N., and Shi, D. Z. (2014). Progress and Prospective of Prevention and Treating Aspirin Resistance by Integrative Medicine. *Zhongguo Zhong Xi Yi Jie He Za Zhi* 34, 245–249.
- Xue, M., Yang, X., Yang, L., Kou, N., Miao, Y., Wang, M., et al. (2017). Rs5911 and Rs3842788 Genetic Polymorphism, Blood Stasis Syndrome, and Plasma Txb2 and Hs-Crp Levels Are Associated with Aspirin Resistance in Chinese Chronic Stable Angina Patients. *Evid. Based Complement. Alternat Med.* 2017, 9037094–9037098. doi:10.1155/2017/9037094
- Yalcinkaya, E., and Celik, M. (2014). Evaluation of Inflammatory Conditions Associated with Aspirin Resistance. *Ups J. Med. Sci.* 119, 292–293. doi:10.3109/03009734.2014.918679
- Yassin, A. S., Abubakar, H., Mishra, T., Subahi, A., Hartman, M., Ahmed, A., et al. (2019). Aspirin Resistance: Cardiovascular Risk Game Changer. *Am. J. Ther.* 26, 593–599. doi:10.1097/MJT.0000000000000780
- Yin, C. H., Bi, D. P., and Du, M. (2010). Effect of Tongxinluo Capsule on Platelet Aggregation Function in Patients with Aspirin Resistance. *Zhongguo Zhong Xi Yi Jie He Za Zhi* 30, 380–382.
- Youlong, X., and Zhongjun, L. (2014). Application of Different Traditional Chinese Medicine in Antiplatelet Resistance. *J. Changchun Univ. Traditional Chin. Med.* 30, 34–36.
- Zhang, J. C. (2015). Effect of Compound Danshen Dropping Pills on Aspirin Resistance in Patients with Coronary Heart Disease. *Med. Inf.* 28, 337–338.
- Zhu, X., Youqin, D., and Zhibing, H. (2018). Clinical Observation and Mechanism of Xuefu Zhuyu Capsule on Aspirin Resistance. *CHINA MEDICINE PHARMACY* 8, 194–197.

**Conflict of Interest:** The authors declare that the research was conducted in the absence of any commercial or financial relationships that could be construed as a potential conflict of interest.

**Publisher's Note:** All claims expressed in this article are solely those of the authors and do not necessarily represent those of their affiliated organizations, or those of the publisher, the editors, and the reviewers. Any product that may be evaluated in this article, or claim that may be made by its manufacturer, is not guaranteed or endorsed by the publisher.

Copyright © 2021 Zhao, Yang and Wu. This is an open-access article distributed under the terms of the Creative Commons Attribution License (CC BY). The use, distribution or reproduction in other forums is permitted, provided the original author(s) and the copyright owner(s) are credited and that the original publication in this journal is cited, in accordance with accepted academic practice. No use, distribution or reproduction is permitted which does not comply with these terms.



# 9-PAHSA Improves Cardiovascular Complications by Promoting Autophagic Flux and Reducing Myocardial Hypertrophy in Db/Db Mice

## OPEN ACCESS

### Edited by:

Xianwei Wang,  
Xinxiang Medical University, China

### Reviewed by:

Lu Lu,  
Guangzhou University of Chinese  
Medicine, China  
Zhongbing Lu,  
Chinese Academy of Sciences (CAS),  
China

### \*Correspondence:

Hou-Guang Zhou  
zhouhouguang@huashan.org.cn  
Jing-Chun Guo  
jingchunguo@shmu.edu.cn  
Yan-Yan Huang  
hyiwen94@hotmail.com

<sup>†</sup>These authors have contributed  
equally to this work

### Specialty section:

This article was submitted to  
Cardiovascular and Smooth Muscle  
Pharmacology,  
a section of the journal  
Frontiers in Pharmacology

**Received:** 06 August 2021

**Accepted:** 11 October 2021

**Published:** 15 November 2021

### Citation:

Wang Y-M, Mi S-L, Jin H, Guo Q-L,  
Yu Z-Y, Wang J-T, Zhang X-M,  
Zhang Q, Wang N-N, Huang Y-Y,  
Zhou H-G and Guo J-C (2021) 9-  
PAHSA Improves Cardiovascular  
Complications by Promoting  
Autophagic Flux and Reducing  
Myocardial Hypertrophy in Db/  
Db Mice.  
Front. Pharmacol. 12:754387.  
doi: 10.3389/fphar.2021.754387

Yan-Mei Wang<sup>1†</sup>, Shou-Ling Mi<sup>2†</sup>, Hong Jin<sup>3†</sup>, Qi-Lin Guo<sup>1</sup>, Zhong-Yu Yu<sup>1</sup>, Jian-Tao Wang<sup>1</sup>,  
Xiao-Ming Zhang<sup>1</sup>, Qian Zhang<sup>1</sup>, Na-Na Wang<sup>1</sup>, Yan-Yan Huang<sup>1\*</sup>, Hou-Guang Zhou<sup>1\*</sup> and  
Jing-Chun Guo<sup>1\*</sup>

<sup>1</sup>Department of Geriatrics of Huashan Hospital, National Clinical Research Center for Aging and Medicine, Department of Translational Neuroscience, Jing'an District Centre Hospital of Shanghai, State Key Laboratory of Medical Neurobiology and MOE Frontiers Center for Brain Science, Institutes of Brain Science, Fudan University, Shanghai, China, <sup>2</sup>Department of Cardiology, Zhongshan Hospital, Fudan University, Shanghai, China, <sup>3</sup>Shanghai Stomatological Hospital & Institutes of Biomedical Sciences, Fudan University, Shanghai, China

Atherosclerotic cardiovascular disease is a common and severe complication of diabetes. There is a large need to identify the effective and safety strategies on diabetic cardiovascular disease (DCVD). 9-PAHSA is a novel endogenous fatty acid, and has been reported to reduce blood glucose levels and attenuate inflammation. We aim to evaluate the effects of 9-PAHSA on DCVD and investigate the possible mechanisms underlying it. Firstly, serum 9-PAHSA levels in human were detected by HPLC-MS/MS analysis. Then 9-PAHSA was synthesized and purified. The synthesized 9-PAHSA was gavaged to db/db mice with 50 mg/kg for 4 weeks. The carotid arterial plaque and cardiac structure was assessed by ultrasound. Cardiac autophagy was tested by western blot analysis, electron microscope and iTRAQ. The results showed that 9-PAHSA, in patients with type 2 diabetes mellitus (T2DM), was significantly lower than that in non-diabetic subjects. Administration of 9-PAHSA for 2 weeks reduced blood glucose levels. Ultrasound observed that continue administration of 9-PAHSA for 4 weeks ameliorated carotid vascular calcification, and attenuated myocardial hypertrophy and dysfunction in db/db mice. Electron microscopy showed continue 9-PAHSA treatment significantly increased autolysosomes, while dramatically decreased greases in the myocardial cells of the db/db mice. Moreover, iTRAQ analysis exhibited that continue 9-PAHSA treatment upregulated BAG3 and HSPB8. Furthermore, western blot analysis confirmed that 9-PAHSA down-regulated Akt/mTOR and activated PI3KIII/BECN1 complex in diabetic myocardium. Thus, 9-PAHSA benefits DCVD in diabetic mice by ameliorating carotid vascular calcification, promoting autophagic flux and reducing myocardial hypertrophy.

**Keywords:** diabetic cardiovascular complications, autophagy, 9-PAHSA, myocardial hypertrophy, vascular calcification

## INTRODUCTION

Diabetic cardiovascular complication (DCVC) is a common and severe complication of diabetes mellitus. DCVC is characterized by diastolic dysfunctions, followed by systolic impairment and left ventricle abnormalities. It often leads to high mortality with properties of severer infarction and poorer prognosis than those without diabetes (Voulgari et al., 2010; Tarquini et al., 2011; Kovacic et al., 2014). The pathogenesis of DCVC is complex and multifactorial, and hyperglycemia and inflammation are two of the important factors. Besides, accumulating evidence has recently suggested that autophagy play a key role in the pathophysiology of metabolic dysregulation and related cardiovascular complications (Xu and Brink, 2016; Luo et al., 2019). Autophagy-lysosomal pathway is a major cellular clearance machinery, which maintains metabolic homeostasis by degradation and clearance of long-lived or damaged proteins. Moreover, autophagy in cardiomyocytes play a key role in mediating hyperglycemia-induced cell dysfunction and damage. To this end, autophagy offers promising targets for novel strategies to prevent and treat DCVC. Targeting autophagy using pharmacological or natural agents is an emerging strategy for DCVC.

Palmitic-acid-9-hydroxy-stearic-acid (9-PAHSA) is a recently discovered endogenous lipid that is highly elevated in the adipose tissue of transgenic mice overexpressing glucose transporter 4 (GLUT4) (Shepherd et al., 1993; Carvalho et al., 2005; Yore et al., 2014; Syed et al., 2018a). 9-PAHSA levels correlate highly with insulin sensitivity and are reduced in adipose tissue and serum of insulin-resistant humans. 9-PAHSA administration in mice lowered ambient glycemia and improved glucose tolerance while stimulating glucagon-like peptide-1 (GLP-1) and insulin secretion (Yore et al., 2014). 9-PAHSA also exhibited anti-inflammatory effects. For example, it decreased high fat diet (HFD)-induced adipose inflammation in obese, insulin-resistant mice and attenuated lipopolysaccharide (LPS)-induced dendritic cell activation and cytokine production *in vitro* (Moraes-Vieira et al., 2016). Notably, 9-PAHSA may also play a major role in mediating autophagy. We found 9-PAHSA treatment regulated autophagy-related pathway using iTRAQ approach in the study. Thus, the novel lipid 9-PAHSA opens up new opportunities of treatment for diabetes and cardiovascular complications.

In the study, we evaluated the effects of 9-PAHSA on DCVC and investigated the possible mechanisms underlying it. We found that 9-PAHSA ameliorated vascular calcification and myocardial dysfunction in db/db mice, possibly through promoting autophagic flux and reducing myocardial hypertrophy.

## MATERIALS AND METHODS

### Human Samples Preparation

For the detection of serum 9-PAHSA levels, human blood samples were collected from 60 subjects including type 2 diabetes mellitus (T2DM) elderly patients ( $n = 30$ ) and

healthy elderly control subjects (control,  $n = 30$ ). They were recruited randomly in the year of 2016 from the same group of the physical examination population of Huashan Hospital, Fudan University. The diagnosis of diabetes was according to the WHO criteria (fasting plasma glucose  $\geq 7.0$  mmol/L or 2 h plasma glucose  $\geq 11.1$  mmol/L during an oral glucose tolerance test). Subjects with type 1 diabetes, hypertension, severe psychological disorders, dementia, tumors, stroke, coronary heart disease, and acute or chronic inflammation were all excluded.

Data was collected on age, gender, body weight, height, waistline, hipline, blood pressure, serum lipid, blood glucose, and Hemoglobin A1C (HbA1C). Body mass index (BMI) was calculated based on body weight (kg) and height (m). Fasting blood samples were drawn after an overnight fast. Circulating HbA1C, glucose levels, and serum lipids were determined by the standard methods in the Huashan Hospital laboratory. Informed consent was provided by the participants. The experiments were performed in accordance with the Declaration of Helsinki of the World Medical Association, and approved by the ethics committee of Huashan Hospital, Fudan University (No. 2015-127).

### Animal Grouping and Intervention

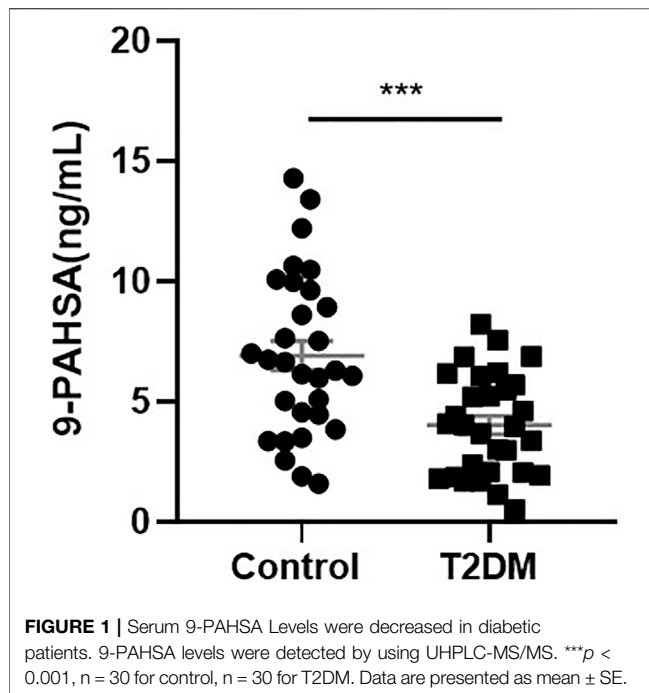
Age matched male C57BL6/J and db/db mice were purchased from Nanjing University Biological Center (Nanjing, China), and housed in colony cages with free access to water and regular diet in a 12-h light/dark cycle and temperature-controlled environment. All the experimental procedures conformed to the NIH Guide for the Care and Use of Laboratory Animals. The Institutional Animal Care and Use Committee of Fudan University approved the experiments.

32-week-old mice were randomly assigned into groups as follows: ctrl + veh, db/db + veh, db/db+9-PAHSA (50 mg/kg per day) ( $n = 9$  mice for each group). 9-PAHSA was given to mice by gavage once a day for 4 weeks. The veh groups were given with the same volume of vehicle (50% PEG400, 0.5% Tween-80, 49.5% H<sub>2</sub>O) at the corresponding time points.

### Serum Detection for 9-PAHSA

Serum samples were collected from human. Detection for serum 9-PAHSA levels in diabetic and non-diabetic human was performed by HPLC-MS/MS analysis. After centrifugation and pretreatment with phosphate-buffered saline, methanol and chloroform (1:1:1.5), the organic phase in the lower layer were collected and purified by using SPE column. Then, samples were separated and analyzed by using a Thermo Tsq Vantage HPLC-MS/MS (waters UHPLC T3) via multiple reaction monitoring in negative ionization mode (spray voltage 3,000 kV, atomization temperature 300°C, sheath gas pressure 40 psi, auxiliary gas pressure 15 psi, ion transmission tube temperature 350 °C). For gradient elution analysis, mobile phases contained (A) 5 mM ammonium acetate and (B) methanol consisted of 0.01% ammonium hydroxide. 9-PAHSA-d4 (10 ng/ml, Cayman) was used as internal standard.





## 9-PAHSA Synthesis

To investigate whether that supplement of 9-PAHSA benefit diabetic mice, the compound 9-PAHSA was synthesized by Prof. Jichang Xiao of Shanghai Institute of Organic Chemistry, Chinese Academy of Sciences with purity of >99% according to the previous paper (Yore et al., 2014). The characterization of synthesized 9-PAHSA was outlined in Figure 2.

## Detection for Fasting Glycemia

Fasting blood glucose (FBG) was tested three times in each mouse: prior to the administration of 9-PAHSA, and at 14 and 28 days after the administration of 9-PAHSA. In order to avoid glycemic fluctuations, mice were placed in a safe and quiet environment; this practice avoided provoking the animals. Venous blood was collected by cutting the tail vein of each mouse at 9:00 am every time. The oral glucose tolerance test (OGTT) was performed at 9:00 am after a single time intervention. Glucose levels were determined using Accu-Check active bands and a glucometer (Roche Diagnostics, Basel, Switzerland).

## Ultrasound Assessment of the Carotid Arterial Plaque

Mice were anesthetized by a mixed gas of oxygen and 2% isoflurane via nose cone. A heat lamp was used to keep mice warm during anesthesia. The neck of mice was shaved to reduce artifacts and then slightly hyperextended, after which each supine mouse was assessed via color doppler sonography using the Visual Sonics Vevo 770 high-resolution *in vivo* micro-imaging system with a micro-visualization scan head probe (RMV-707B) which had a focal length of 12.7 mm, a center frequency of 30 MHz, a -3 dB bandwidth of 15–45 MHz, an axial resolution of 55  $\mu$ m, and a lateral resolution of 115  $\mu$ m.

## Transthoracic Echocardiography

Transthoracic echocardiography was performed in sedated mice by using Vevo 770 high-resolution *in vivo* imaging system (30-MHz transducer; Visualsonics, Toronto, ON, Canada). Mice were anesthetized with 2% isoflurane. Basic hemodynamic parameters, such as left ventricular (LV) mass, left ventricular end-systolic internal diameter (LVIDs), left ventricular end-diastolic internal diameter (LVIDd), left ventricular end-systolic posterior wall thickness (LVPWs) and left ventricular end-diastolic posterior wall thickness (LVPWd) were measured by using M-mode.

## Detection for NT-Pro BNP

Abdominal aorta blood of mice was collected and detected for NT-pro BNP, by using ELISA kit (Sigma). Briefly, all samples were centrifuged, and plasma was tested according to the protocol of ELISA kit.

## Histopathology of Carotid Artery

After the animals were anesthetized and sacrificed, the left common carotid artery was obtained. Then, the samples were cut and stained with hematoxylin and eosin (HE) or alizarin red.

## Immunohistochemistry of Carotid Artery

The left common carotid artery was embedded in paraffin and sectioned at 5  $\mu$ m. Nonspecific binding was blocked with 10% normal rabbit serum. After incubation with polyclonal anti-vascular cell adhesion molecule-1 (VCAM-1) antibody (Santa Cruz Biotechnology, 4  $\mu$ g/mL; 1:500) followed by anti-rabbit IgG secondary antibody, the slices were colored by diaminobenzidine to visualize positive immunoreactivity and counterstained with Hematoxylin.

## In-Solution Digestion/High pH RPLC

Cardiac protein samples of mice were reduced by 5 mM DTT at 56°C for 30 min and alkylated by 10 mM MMTS at room temperature for 30 min, then diluted with 50 mM ammonium bicarbonate until the urea concentration < 1 M. Lys-C was added at the mass ratio of 1:50 (enzyme: protein) for 3 h at 37°C. Then, trypsin was added at the mass ratio of 1:50 (enzyme: protein) for 12 h. For label-free quantification, the digested peptides were desalted using C18 column (Sep-Pak Vac C18, Waters Corporation), concentrated using SpeedVac, and then resuspended in 2% ACN with 0.1% FA. For iTRAQ samples, iTRAQ-8pLex labeling reagents (AB Sciex) were added to the peptide, which were incubated at room temperature for 120 min. The reaction was stopped by water, followed concentration using SpeedVac and desalts. The digested protein samples were fractionated by using high pH reversed phase liquid chromatography.

## Western Blot Analysis

Heart tissues (50–100 mg) were cut into small pieces and lysed with RIPA buffer (Roche, Switzerland), which consists of 50 mM Tris-HCl (pH 7.4), 150 mM NaCl, 0.5% sodium deoxycholate, 1% NP-40, 1% sodium dodecyl sulfate (SDS), and protease inhibitor cocktail, at 4°C, then ruptured by homogenizer on ice. The supernatant was collected

**TABLE 1 |** Physiological parameters of the study population in healthy control and T2DM group (n = 30 for each group, mean ± SE).

Variables	Control (n = 30)	T2DM (n = 30)	p-value <sup>a</sup>
Age (years)	74.5 ± 6.7	74.5 ± 6.6	1.000
Male (n)	18	16	0.998
Female (n)	12	14	0.998
Body weight (kg)	64.4 ± 5.8	63.6 ± 6.0	0.764
Waistline (cm)	81.6 ± 6.0	85.5 ± 7.7	0.223
Hipline (cm)	94.5 ± 4.3	97.9 ± 4.3	0.097
BMI (kg/m <sup>2</sup> )	22.6 ± 1.5	22.6 ± 1.6	0.976
SBP (mmHg)	137.6 ± 17.2	138.1 ± 11.6	0.905
DBP (mmHg)	75.3 ± 8.0	73.8 ± 9.7	0.570
BG (mmol/L)	5.3 ± 0.5	6.7 ± 1.1	0.001***
HbA1C (%)	5.6 ± 0.3	6.8 ± 0.9	0.001***
TC (mmol/L)	4.8 ± 0.8	4.6 ± 1.0	0.303
LDL (mmol/L)	2.8 ± 0.7	2.7 ± 0.9	0.723
TG (mmol/L)	1.1 ± 0.4	1.3 ± 0.9	0.354

<sup>a</sup>p-value for comparisons between control and T2DM group by an independent samples t-test or Chi-square test. \*\*\*p < 0.001. BMI—body mass index; SBP—systolic blood pressure; DBP—diastolic blood pressure; BG—blood glucose; HbA1C—glycosylated hemoglobin; TC—total cholesterol; LDL—low-density lipoprotein; TG—triglyceride.

after centrifugation at 14,000×g for 30 min at 4°C. The protein concentration of the cell lysate was quantified by using the bicinchoninic acid assay (Beyotime Biotechnology, Beijing, China).

Cardiac proteins from mice were subjected to polyacrylamide gel electrophoresis and then transferred onto polyvinylidene difluoride membranes. The membranes were then probed with antibodies, including LC3-phosphatidyl ethanolamine conjugate (1:200), mTOR (1:1,000), GAPDH (1:2000) and PI3KIII (1:1,000) (all purchased from Cell signaling Technology, United States); BECN1 (1:500) and p-Akt (1:1,000) (all purchased from Santa Cruz); p62 (1:1,000), BAG3 (1:500) and HspB8 (1:500) (all purchased from Abcam, United Kingdom). Peroxidase activity was visualized with ECL (SantaCruz, United States). The bands were quantified using Quantity One.

## Transmission Electron Microscopy

Heart tissues of mice were perfused and fixed with 2.5% glutaraldehyde perfusate. Following the fixation and dehydration steps, the tissues were embedded in paraffin, sliced, and stained with 3% uranyl acetate and lead citrate. Cardiac ultrastructure was examined under transmission electron microscope (CM-120, Philips; Amsterdam, Netherlands). Six random fields of each slice were analyzed to calculate the relative area of autolysosomes and greases.

## Data and Statistical Analysis

All data are expressed as mean ± SEM and statistically analyzed by using the Graph Prism 7 software (GraphPad Software) and SPSS. ANOVA were used to evaluate the differences among multiple groups. Non-paired t-test was used to analyze two groups after homogeneity of variance test. Logistic regression was used to analyze the association between serum 9-PAHSA and T2DM. In the first model, we adjusted solely for age and gender. In Model 2 we further adjusted for BMI. We then added waistline, hipline in Model 3. In Model 4, fully-adjusted, model we adjusted for potential confounding factors, including SBP, DBP, TC, TG and LDL. *p* < 0.05 was considered statistically significant.

## RESULTS

### Serum 9-PAHSA Levels Were Reduced in Elderly Diabetic Patients

To determine if 9-PAHSA was regulated in diabetic state, we firstly detected serum 9-PAHSA levels from type 2 diabetic humans using HPLC-MS/MS analysis. The results showed that serum 9-PAHSA was reduced in diabetic patients compared to the nondiabetic humans (Figure 1). The baseline characteristics of the T2DM and control groups are listed (Table 1). Briefly, T2DM patients have significantly higher blood glucose and HbA1C levels compared to nondiabetic humans. There were no differences in age, gender, BMI, blood pressure, waistline, hipline, and serum lipids.

Serum 9-PAHSA was a protective factor for T2DM (Table 2, OR 0.71, 95%CI: 0.58, 0.87). After adjusting for age and gender, 9-PAHSA was still a protective factor for T2DM (Model 1, OR 0.69, 95%CI: 0.53, 0.89). Further adjustment for BMI, waistline and hipline, only minimally changed this association (Model 2 and 3). Moreover, the estimated association between serum 9-PAHSA and T2DM also appeared slightly changed when we adjusted for SBP, DBP, TC and LDL (Model 4, OR 0.50, 95%CI: 0.30, 0.83).

### 9-PAHSA Was Successfully Synthesized and Characterized

Since 9-PAHSA levels were decreased in diabetic state, we synthesized 9-PAHSA compound for the following exogenous supplement experiments. Detailed procedure for synthesize of 9-PAHSA was available in Supplementary Materials (S1). 9-

**TABLE 2 |** Multiple logistic regression analysis of correlation between serum 9-PAHSA and T2DM.

Group	Unadjusted		Model 1		Model 2		Model 3		Model 4	
	OR	95%-CI	OR	95%-CI	OR	95%-CI	OR	95%-CI	OR	95%-CI
Control	...	...	...	...	...	...	...	...	...	...
T2DM	0.71	(0.58, 0.87)	0.69	(0.53, 0.89)	0.68	(0.53, 0.89)	0.55	(0.34, 0.89)	0.50	(0.30, 0.83)

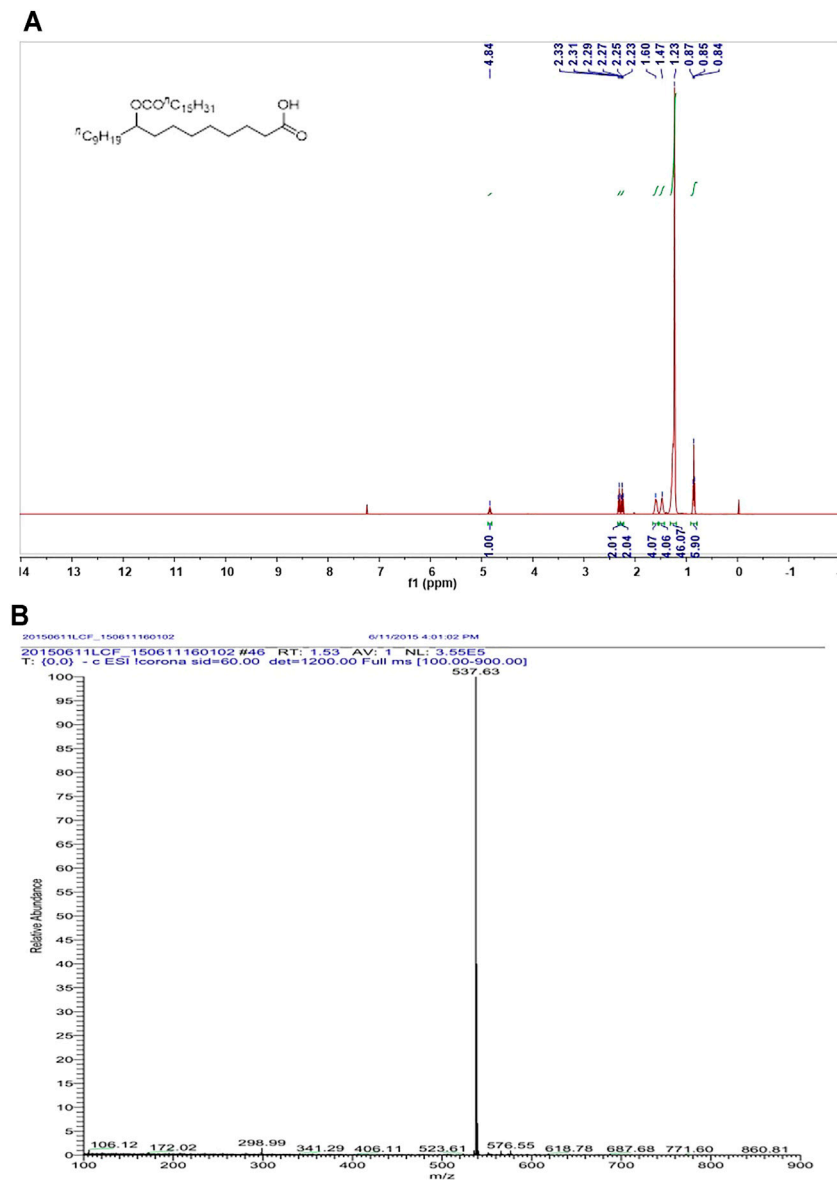
OR = odds ratio for type 2 diabetes mellitus; CI = confidence interval.

Model 1: adjusted for age and gender.

Model 2: adjusted for age, gender and BMI.

Model 3: adjusted for age, gender, BMI, waistline and hipline.

Model 4: adjusted for age, gender, BMI, waistline, hipline, SBP, DBP, TC and LDL.



In order to investigate the effect of 9-PAHSA on vascular atherosclerosis in db/db mice, we conducted two-dimensional





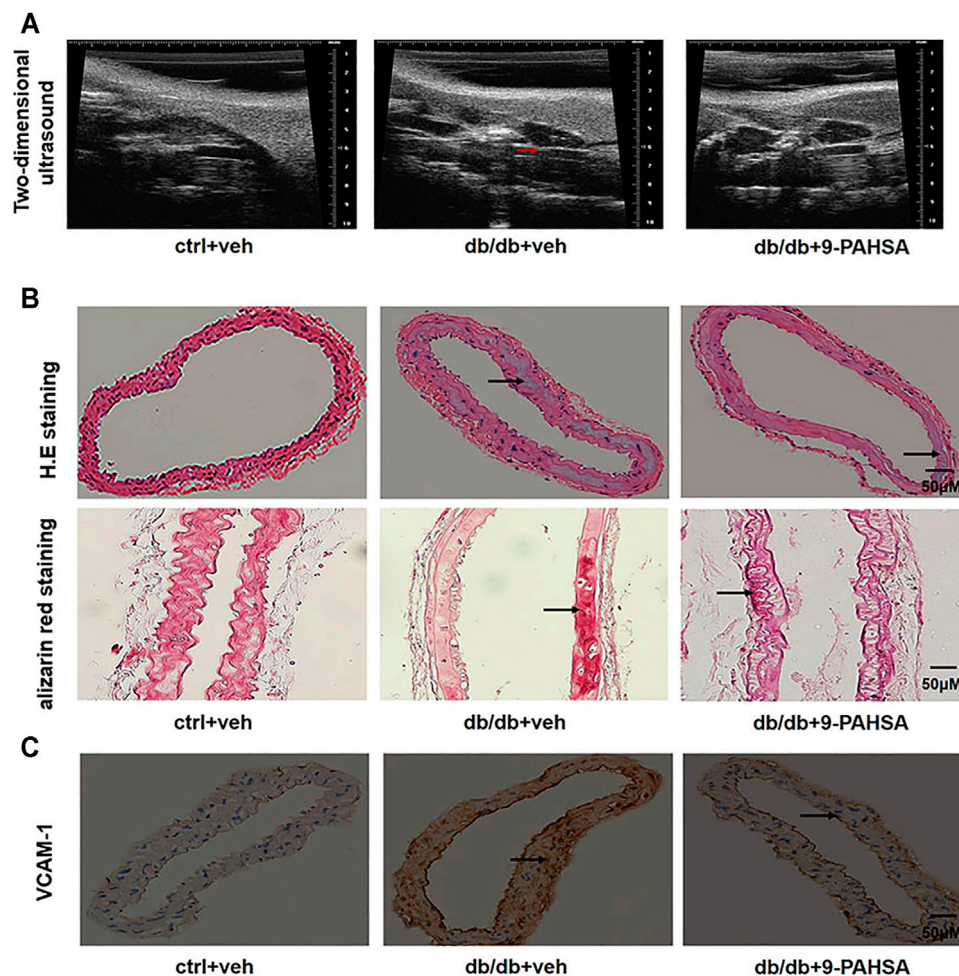


**FIGURE 4 |** Effects of 9-PAHSA on carotid arterial atherosclerosis in db/db mice. **(A)** Two-dimensional ultrasound assessments of arterial wall plaque in the left common carotid artery. Arrows represent arterial wall plaque. **(B)** H.E and alizarin red staining cross-sections of the left common carotid arteries to assess vascular calcification. Arrows represent vascular calcification. **(C)** Immunohistochemistry showed VCAM-1 expression in the left common carotid arteries.  $n = 6$  for each group. Arrows represent VCAM-1 expression.

Nevertheless, to gain a better understanding of the physiological roles of 9-PAHSA on diabetic cardiomyopathy, we further confirmed the changes of two proteins among the above 82 proteins list. They were Bcl2-associated athanogene 3 (BAG3) and heat shock protein beta-8 (HSPB8), which were upregulated after 9-PAHSA intervention by iTRAQ analysis (Figure 6A), and further confirmed by western blotting analysis (Figure 6B). BAG3/HSPB8 complex is involved in enhancing myocardial autophagy. The impairment of autophagy contributes to the progress of diabetes-induced cardiac abnormalities (Bartlett et al., 2017). It is hypothesized that 9-PAHSA could improve diabetic cardiomyopathy in db/db mice by increasing cardiac autophagy. To determine whether 9-PAHSA mediated cardiac autophagy in db/db mice, we examined the morphological images by using electron microscopy. In control mice, the cardiomyocytes were regularly arranged, with few autophagosomes and lysosomes in the cytosol. In contrast, small decreased autolysosomes but

apparent increased greases were observed in the myocardial cells of the db/db mice. However, 9-PAHSA treatment significantly increased autolysosomes, while dramatically decreased greases in the myocardial cells of the db/db mice (Figures 6C–E).

In addition, results of western blotting analysis showed the decreased ratio of LC3II/LC3I and increased P62 protein level in db/db mice compared to control mice. However, 9-PAHSA treatment partly reversed the expression of these proteins in db/db mice (Figure 6F). These results suggested that 9-PAHSA enhanced cardiac autophagy in db/db mice.

### 9-PAHSA Increased Cardiac Autophagy Through p-AKT/mTOR/PI3KIII-BECN-1 Pathway in Db/Db Mice

In order to elucidate the possible autophagic signaling pathways involved in the effect of 9-PAHSA, we detected the cardiac levels

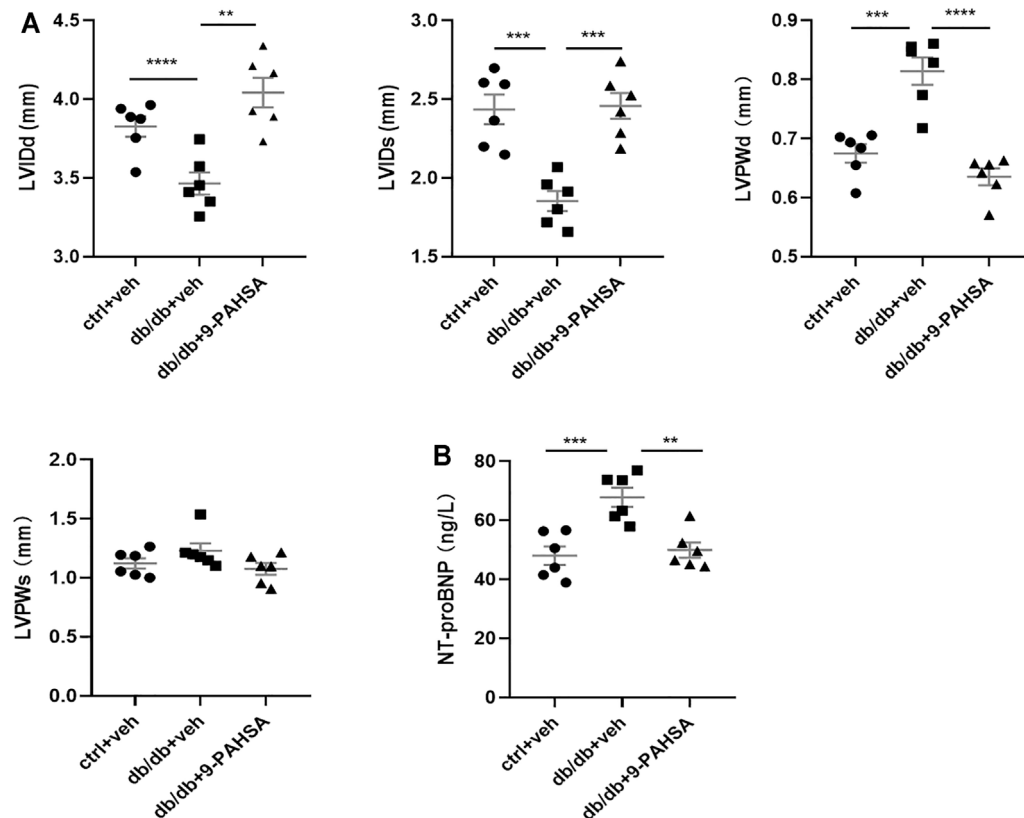


**FIGURE 5 |** Effects of 9-PAHSA on myocardial hypertrophy and LV function in db/db mice. Cardiac structure **(A)** was assessed by transthoracic echocardiography **(B)** The contents of serum NT-proBNP were detected by ELISA kit. \*\* $p < 0.01$ , \*\*\* $p < 0.001$ , \*\*\*\* $p < 0.0001$ ,  $n = 6$  for each group. Data are presented as mean  $\pm$  SE. Left ventricular internal diameter end diastole (LVIDd), left ventricular internal diameter end systole (LVIDs), left ventricular posterior wall end diastole (LVPWd), left ventricular posterior wall end systole (LVPWs).

of several proteins which related to autophagic pathways. Our results showed that cardiac BECN1 and PI3KIII levels were reduced in db/db mice while significantly increased after 9-PAHSA treatment (**Figure 7A**). Meanwhile, the expression of mTOR in the myocardium increased in db/db mice, while reduced in 9-PAHSA-treated db/db mice (**Figure 7B**). Besides, 9-PAHSA exert mild tendency of reduction in p-Akt level when compared with db/db mice (**Figure 7B**). These results suggested that 9-PAHSA treatment increased cardiac autophagy possibly via up-regulation of PI3KIII and BECN1, and down-regulation of mTOR and p-Akt in diabetic myocardium.

## DISCUSSION

In this study, we demonstrated a new role of 9-PAHSA, that is, continued administration of 9-PAHSA alleviates cardiovascular complications by promoting autophagic flux and reducing myocardial hypertrophy in db/db mice. As one of the endogenous metabolic products of palmitic acid, 9-PAHSA has been reported to reduce hyperglycemia (Yore et al., 2014). In our study, we found that 9-PAHSA levels are reduced in T2DM.

Therefore, it is supposed that the exogenous supplementation of 9-PAHSA might be an effective means for the therapy of T2DM. A single oral dose of 9-PAHSA improves glucose tolerance in insulin resistant mice (Yore et al., 2014). Our data showed that 9-PAHSA played a role in glucose-lowering in db/db mice after 2 weeks administration. But this action disappeared after 4 weeks administration. Unconsistent with it, it is reported that chronic PAHSA treatment in 15-week-old HFD mice improved insulin sensitivity and glucose tolerance and these effects were sustained for at least 4.5 months (Syed et al., 2018b). Such discrepancy might due to the age of the mice we used are much closer to the senile period of diabetic mice, because the occurrence of T2DM is highly associated with aging (Saeedi et al., 2019). Although our results seem to be more similar to the real clinic cases, the hypoglycemic effect of 9-PAHSA in elderly patients need further investigation.

Cardiovascular complication remains to be the principal cause of death and disability among patients with diabetes mellitus. Multi-factorial risk is highly associated with diabetic associated cardiac disorders, such as hypertension, hyperglycemia, hyperlipemia and atherosclerosis (Bornfeldt, 20132014; Low Wang et al., 2016). Therefore, it is not adequate to modulate

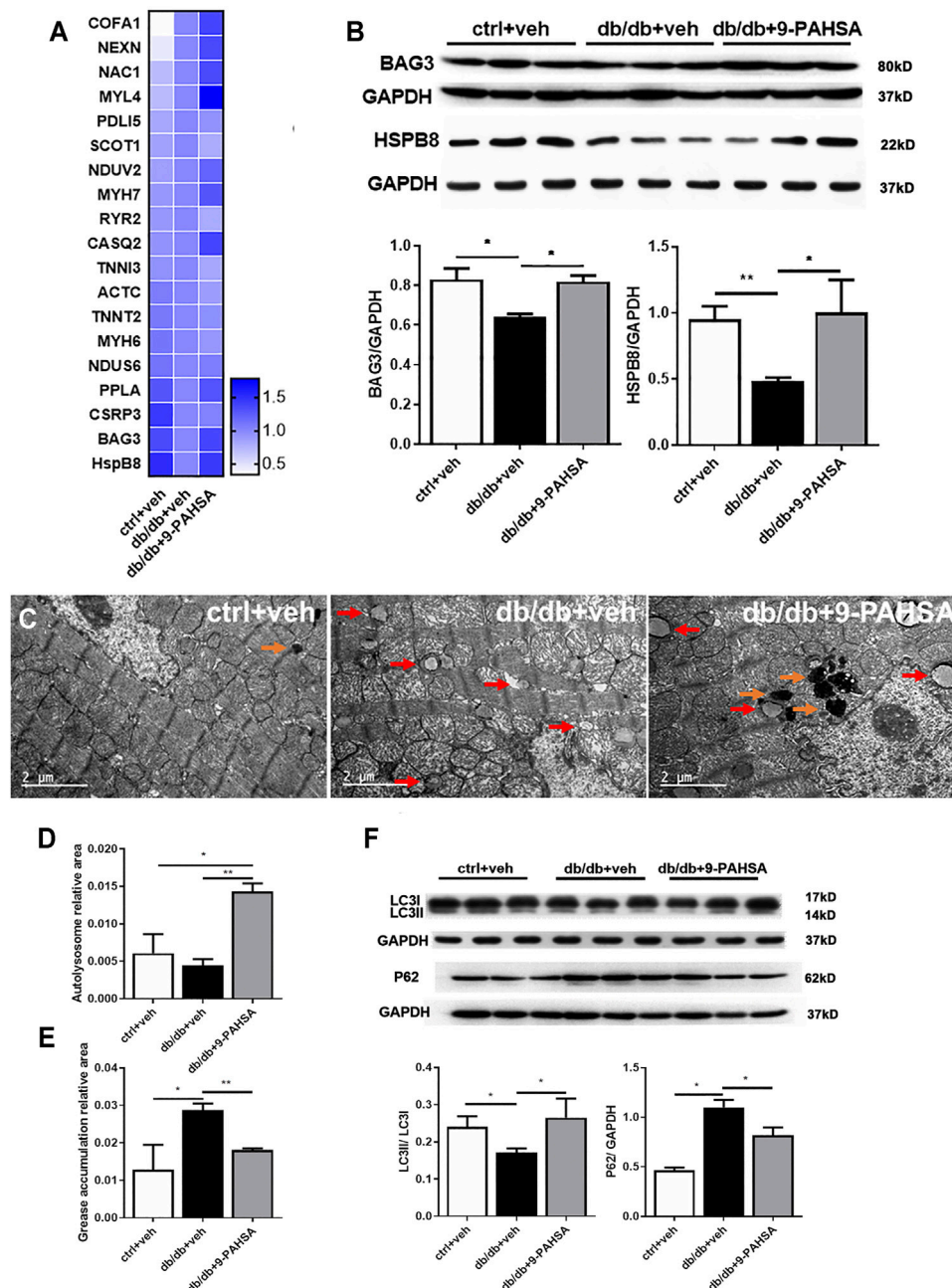


**FIGURE 6 |** Effects of 9-PAHSA treatment on cardiac autophagy. **(A)** Representative altered proteins after 9-PAHSA treatment by using iTRAQ analysis. **(B)** Western blotting analysis detected the expression levels of BAG3 and HSPB8. **(C)** Representative cardiomyocyte electron micrographs of ctrl + veh, db/db + veh and db/db+9-PAHSA mice. 9-PAHSA intervention increased the number of autolysosomes (orange arrow) and reduced the grease aggregation (red arrow) in db/db cardiomyocytes. **(D and E)** Statistical column graphs representing the ratio of autolysosome area **(D)** and grease aggregates area **(E)**. **(F)** Representative western blotting images and statistical columns of cardiac LC3 and P62 protein levels, which showed that cardiac autophagy levels were enhanced under 9-PAHSA administration in db/db mice. \* $p < 0.05$ , \*\* $p < 0.01$ ,  $n = 3$  mice for each group. Data are presented as mean  $\pm$  SE.

cardiovascular disorder by therapeutic strategies focusing solely on optimal glycemic control. Developing drugs that focus on cardiovascular management, but not simply on glycemic control is of the utmost importance for DCVC patients. As a novel endogenous fatty acid, we demonstrated new roles of 9-PAHSA

in relieving atherosclerosis and cardiac failure in aging diabetic mice. It has been extensively documented that certain fatty acids play beneficial roles in cardiovascular diseases (Sokola-Wysoczanska et al., 2018). Polyunsaturated fatty acids (PUFAs) belong to fatty acids family and activate the

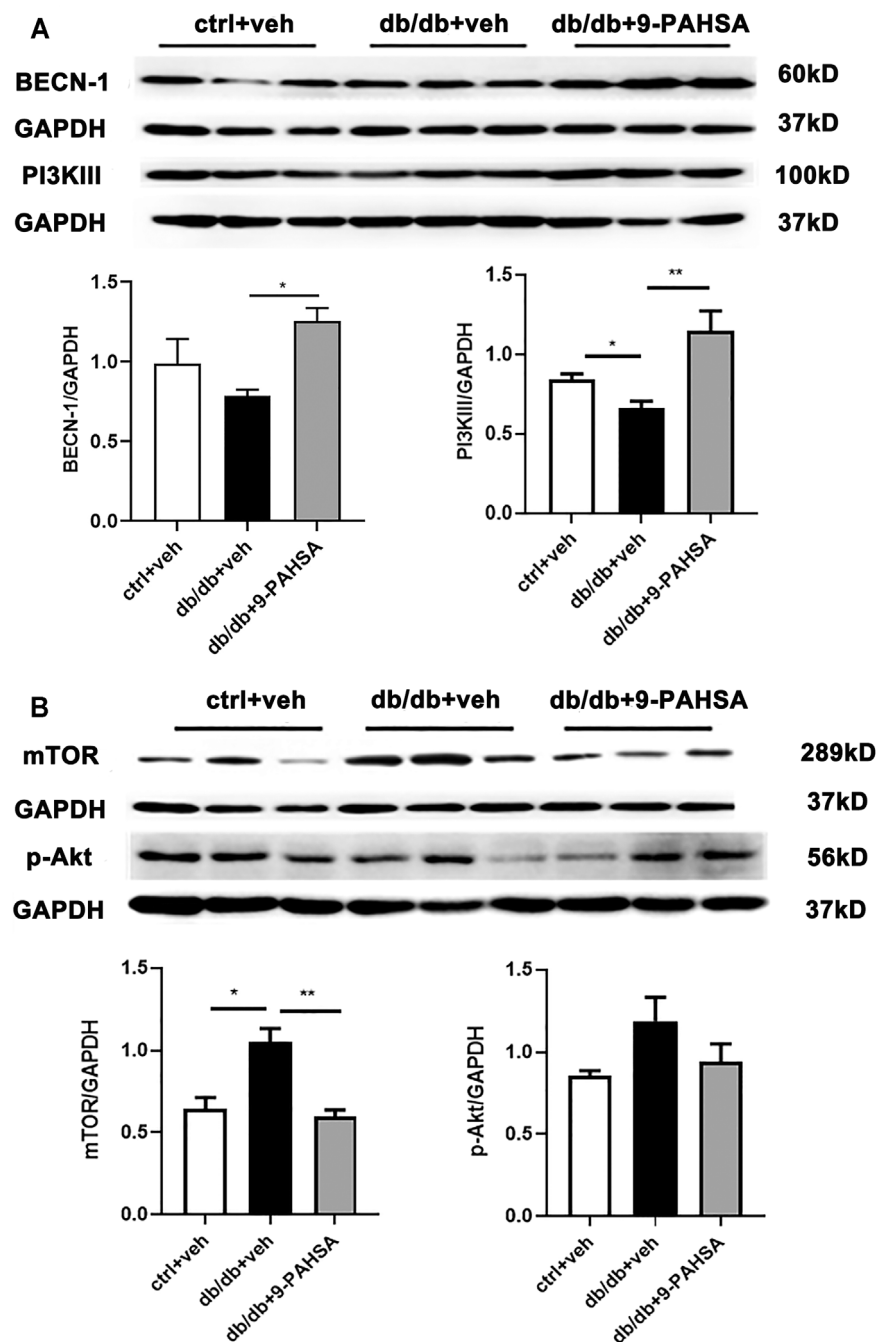


**FIGURE 7 |** Effects of 9-PAHSA on the expression of autophagy-related proteins in cardiomyocytes of db/db mice. Western blot analysis was used to detect protein levels of cardiac BECN-1, PI3K III, mTOR, p-Ak after 9-PAHSA treatment in db/db mice. \* $p < 0.05$ , \*\* $p < 0.01$ ,  $n = 3$  for each group. Data are presented as mean  $\pm$  SE.

G-protein coupled receptor (GPR) 120/free fatty acid receptor (FFAR) 4 (GPR120/FFAR4) signaling (Harper and Jacobson, 2001; Oh et al., 2010). The supplement of omega-3 PUFAs could improve cardiac structures (Harper and Jacobson, 2001). Similar to PUFA, 9-PAHSA is the ligand of GPR120 and also exerts anti-diabetic and cardiac protective effects.

Autophagy plays an important role in the maintenance of normal heart function. Autophagy could be triggered by metabolic clues. Accumulating evidence suggested that autophagy was impaired in the heart with insulin resistance and T2DM (Xu et al., 2013; Kanamori et al., 2015; Munasinghe et al., 2016). However, whether the suppression



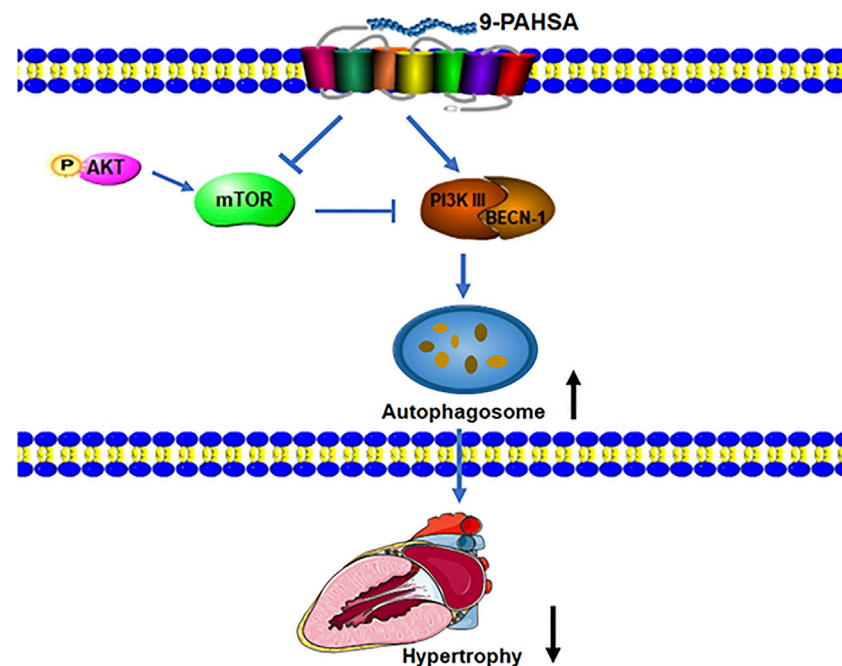


**FIGURE 8** | 9-PAHSA increased autophagy to ameliorate cardiac hypertrophy via up-regulation of PI3KIII and BECN1 and down-regulation of mTOR and p-Akt in diabetic myocardium.

of cardiac autophagy has beneficial or detrimental functional consequences in T2DM is largely unknown. Studies showed that inhibition of autophagy lead to ventricular hypertrophy (Kenessey and Ojamaa, 2016; Zeng et al., 2017; Zhang et al., 2017). In contrast, it is also reported that the reduced cardiac autophagy in diabetic mice promoted the progression of cardiac aging (Eisenberg et al., 2016; Shirakabe et al., 2016). Studies involving autophagy assessment in the hearts of diabetic mice have been controversial. This may be due in part to the different mouse models using in studies and metabolic complexity of these conditions. Our study used the db/db mouse, a genetic model of T2DM. Consistently, we found that cardiac autophagic level is reduced in db/db mice, as evidenced by the decreased expression of cardiac HSPB8, BECN1 and PI3KIII proteins and enhanced level of cardiac mTOR protein. Moreover, we showed that enhanced autophagy regulated by 9-PAHSA alleviated diabetic cardiomyopathy in db/db mice.

Akt/mTOR signaling activation inhibits cell autophagy. In the study, we found that the pathway was elevated in hearts of db/db mice. mTOR inhibits autophagy through suppressing the activation of PI3KIII/BECN1 complex (Kim et al., 2011; Heras-Sandoval et al., 2014). Besides, the reduced levels of cardiac BAG3 and HSPB8 were identified in db/db mice. BAG3 is one of a family of co-chaperones characterized by a C-terminal BAG domain that binds the HSP70/HSPA ATPase domain to regulate the fate of HSP70 substrates. BAG3 functions as a chaperone interacting with HspB8 and targets misfolded proteins to macroautophagy. Studies have reported that

BAG3/HSPB8 complex is involved in autophagic signaling (Carra et al., 2008; Li et al., 2017). BAG3 would promote the sequestration and targeting of HSP70/HSC70-associated protein aggregates to the aggresome, a perinuclear compartment with high autophagic activity. While overexpression of HSPB8 can stimulate autophagy in a BAG3-dependent manner, it seems to be dispensable for the function of BAG3 in the aggresome-autophagy pathways during proteotoxic stress (Fuchs et al., 2015). It is further demonstrated that autophagic flux was impaired in the heart of db/db mice. It is worth noting that 9-PAHSA treatment down-regulated Akt/mTOR and activated PI3KIII/BECN1 complex in diabetic myocardium, suggesting that 9-PAHSA could promote cardiac autophagy.

Taken together, our results demonstrated that continued administration of 9-PAHSA alleviated diabetic cardiomyopathy in db/db mice. 9-PAHSA treatment increased cardiac autophagy possibly via up-regulation of PI3KIII and BECN1 and down-regulation of mTOR and p-Akt in diabetic myocardium (Figure 8). The exogenous supplementation of 9-PAHSA might be an effective strategy for the T2DM-related cardiomyopathy.

## DATA AVAILABILITY STATEMENT

The data that support the findings of this study are available from the corresponding author upon reasonable request.

## ETHICS STATEMENT

The studies involving human participants were reviewed and approved by the ethics committee of Huashan Hospital, Fudan University. The patients/participants provided their written informed consent to participate in this study. The animal study was reviewed and approved by The Institutional Animal Care and Use Committee of Fudan University.

## AUTHOR CONTRIBUTIONS

Conceptualization, Y-MW, H-GZ, J-CG, Y-YH; Methodology, Y-MW, S-LM, HJ, Q-LG, Z-YY, J-TW, X-MZ, QZ, N-NW; Investigation, Y-MW, S-LM, HJ; Writing, Y-MW, Q-LG; Funding Acquisition, H-GZ, J-CG; Supervision, H-GZ, J-CG, Y-YH.

## REFERENCES

- Bartlett, J. J., Trivedi, P. C., and Pulinilkunnil, T. (2017). Autophagic Dysregulation in Doxorubicin Cardiomyopathy. *J. Mol. Cel Cardiol* 104, 1–8. doi:10.1016/j.jmcc.2017.01.007
- Bornfeldt, K. E. (2013/2014). 2013 Russell Ross Memorial Lecture in Vascular Biology: Cellular and Molecular Mechanisms of Diabetes Mellitus-Accelerated Atherosclerosis. *Arterioscler Thromb. Vasc. Biol.* 34, 705–714. doi:10.1161/ATVBAHA.113.301928
- Carra, S., Seguin, S. J., and Landry, J. (2008). HspB8 and Bag3: a New Chaperone Complex Targeting Misfolded Proteins to Macroautophagy. *Autophagy* 4, 237–239. doi:10.4161/auto.5407
- Carvalho, E., Kotani, K., Peroni, O. D., and Kahn, B. B. (2005). Adipose-specific Overexpression of GLUT4 Reverses Insulin Resistance and Diabetes in Mice Lacking GLUT4 Selectively in Muscle. *Am. J. Physiol. Endocrinol. Metab.* 289, E551–E561. doi:10.1152/ajpendo.00116.2005
- Eisenberg, T., Abdellatif, M., Schroeder, S., Primessnig, U., Stekovic, S., Pendl, T., et al. (2016). Cardioprotection and Lifespan Extension by the Natural Polyamine Spermidine. *Nat. Med.* 22, 1428–1438. doi:10.1038/nm.4222
- Fuchs, M., Luthold, C., Guilbert, S. M., Varlet, A. A., Lambert, H., Jetté, A., et al. (2015). A Role for the Chaperone Complex BAG3-HSPB8 in Actin Dynamics, Spindle Orientation and Proper Chromosome Segregation during Mitosis. *Plos Genet.* 11, e1005582. doi:10.1371/journal.pgen.1005582
- Harper, C. R., and Jacobson, T. A. (2001). The Fats of Life: the Role of omega-3 Fatty Acids in the Prevention of Coronary Heart Disease. *Arch. Intern. Med.* 161, 2185–2192. doi:10.1001/archinte.161.18.2185
- Heras-Sandoval, D., Pérez-Rojas, J. M., Hernández-Damián, J., and Pedraza-Chaverri, J. (2014). The Role of PI3K/AKT/mTOR Pathway in the Modulation of Autophagy and the Clearance of Protein Aggregates in Neurodegeneration. *Cell Signal* 26, 2694–2701. doi:10.1016/j.cellsig.2014.08.019
- Kanamori, H., Takemura, G., Goto, K., Tsujimoto, A., Mikami, A., Ogino, A., et al. (2015). Autophagic Adaptations in Diabetic Cardiomyopathy Differ between Type 1 and Type 2 Diabetes. *Autophagy* 11, 1146–1160. doi:10.1080/15548627.2015.1051295
- Kenessey, A., and Ojamaa, K. (2016). Thyroid Hormone Stimulates Protein Synthesis in the Cardiomyocyte by Activating the Akt-mTOR and p70S6K Pathways. *J. Biol. Chem.* 281, 20666–20672. doi:10.1074/jbc.M512671200
- Kim, J., Kundu, M., Viollet, B., and Guan, K. L. (2011). AMPK and mTOR Regulate Autophagy through Direct Phosphorylation of Ulk1. *Nat. Cel Biol* 13, 132–141. doi:10.1038/ncb2152
- Kovacic, J. C., Castellano, J. M., Farkouh, M. E., and Fuster, V. (2014). The Relationships between Cardiovascular Disease and Diabetes: Focus on Pathogenesis. *Endocrinol. Metab. Clin. North. Am.* 43, 41–57. doi:10.1016/j.ecl.2013.09.007
- Li, X. C., Hu, Q. K., Chen, L., Liu, S. Y., Su, S., Tao, H., et al. (2017). HSPB8 Promotes the Fusion of Autophagosome and Lysosome during Autophagy in Diabetic Neurons. *Int. J. Med. Sci.* 14, 1335–1341. doi:10.7150/ijms.20653
- Low Wang, C. C., Hess, C. N., Hiatt, W. R., and Goldfine, A. B. (2016). Clinical Update: Cardiovascular Disease in Diabetes Mellitus: Atherosclerotic Cardiovascular Disease and Heart Failure in Type 2 Diabetes Mellitus - Mechanisms, Management, and Clinical Considerations. *Circulation* 133, 2459–2502. doi:10.1161/CIRCULATIONAHA.116.022194
- Luo, G., Jian, Z., Zhu, Y., Zhu, Y., Chen, B., Ma, R., et al. (2019). Sirt1 Promotes Autophagy and Inhibits Apoptosis to Protect Cardiomyocytes from Hypoxic Stress. *Int. J. Mol. Med.* 43, 2033–2043. doi:10.3892/ijmm.2019.4125
- Moraes-Vieira, P. M., Saghatelian, A., and Kahn, B. B. (2016). GLUT4 Expression in Adipocytes Regulates De Novo Lipogenesis and Levels of a Novel Class of Lipids with Antidiabetic and Anti-inflammatory Effects. *Diabetes* 65, 1808–1815. doi:10.2337/db16-0221
- Munasinghe, P. E., Riu, F., Dixit, P., Edamatsu, M., Saxena, P., Hamer, N. S., et al. (2016). Type-2 Diabetes Increases Autophagy in the Human Heart through Promotion of Beclin-1 Mediated Pathway. *Int. J. Cardiol.* 202, 13–20. doi:10.1016/j.ijcard.2015.08.111
- Oh, D. Y., Talukdar, S., Bae, E. J., Imamura, T., Morinaga, H., Fan, W., et al. (2010). GPR120 Is an omega-3 Fatty Acid Receptor Mediating Potent Anti-inflammatory and Insulin-Sensitizing Effects. *Cell* 142, 687–698. doi:10.1016/j.cell.2010.07.041
- Ponnuswamy, P., Schrötle, A., Ostermeier, E., Grüner, S., Huang, P. L., Ertl, G., et al. (2012). eNOS Protects from Atherosclerosis Despite Relevant Superoxide Production by the Enzyme in apoE Mice. *PLoS One* 7, e30193. doi:10.1371/journal.pone.0030193
- Saeedi, P., Petersohn, I., Salpea, P., Malanda, B., Karuranga, S., Unwin, N., et al. , Global and Regional Diabetes Prevalence Estimates for 2019 and Projections for 2030 and 2045: Results from the International Diabetes Federation Diabetes Atlas, 9th Edition, 9(th) edition. *Diabetes Res. Clin. Pract.*, 2019. 157:107843. doi:10.1016/j.diabres.2019.107843
- Shepherd, P. R., Gnudi, L., Tozzo, E., Yang, H., Leach, F., and Kahn, B. B. (1993). Adipose Cell Hyperplasia and Enhanced Glucose Disposal in Transgenic Mice Overexpressing GLUT4 Selectively in Adipose Tissue. *J. Biol. Chem.* 268, 22243–22246. doi:10.1016/s0021-9258(18)41516-5
- Shirakabe, A., Ikeda, Y., Sciarretta, S., Zablocki, D. K., and Sadoshima, J. (2016). Aging and Autophagy in the Heart. *Circ. Res.* 118, 1563–1576. doi:10.1161/CIRCRESAHA.116.307474
- Sokola-Wysoczanska, E., Wysoczanski, T., Wagner, J., CzyżBodkowski, R., Lochyński, S., et al. (2018). Polyunsaturated Fatty Acids and Their Potential Therapeutic Role in Cardiovascular System Disorders-A Review. *Nutrients* 10: 1561. doi:10.3390/nu10101561

## FUNDING

This work was supported by the National scientific foundation of China (81671392 to J.-C.G. 81571361and 81871098 to H.-G.Z.). Projects of Shanghai Health and Health Committee on Integration of Traditional Chinese and Western Medicine (ZY (2018- 2020)-FWTX-3007, ZHYY-ZXYJHZZ-201915), Shanghai Medical Park New Star-Outstanding Young Medical Talents Program, and Shanghai Municipal Key Clinical Specialty (Geriatrics, No. shslczdzk02802).

## SUPPLEMENTARY MATERIAL

The Supplementary Material for this article can be found online at: <https://www.frontiersin.org/articles/10.3389/fphar.2021.754387/full#supplementary-material>

- Syed, I., Lee, J., Peroni, O. D., Yore, M. M., Moraes-Vieira, P. M., et al. (2018). Methodological Issues in Studying PAHSA Biology: Masking PAHSA Effects. *Cell Metab.* 28, 543–546. doi:10.1016/j.cmet.2018.09.007
- Syed, I., Lee, J., Moraes-Vieira, P. M., Donaldson, C. J., Sontheimer, A., Aryal, P., et al. (2018). Palmitic Acid Hydroxystearic Acids Activate GPR40, Which Is Involved in Their Beneficial Effects on Glucose Homeostasis. *Cel Metab* 27, 419–e4. doi:10.1016/j.cmet.2018.01.001
- Tarquini, R., Lazzeri, C., Pala, L., Rotella, C. M., and Gensini, G. F. (2011). The Diabetic Cardiomyopathy. *Acta Diabetol.* 48, 173–181. doi:10.1007/s00592-010-0180-x
- Voulgari, C., Papadogiannis, D., and Tentolouris, N. (2010). Diabetic Cardiomyopathy: from the Pathophysiology of the Cardiac Myocytes to Current Diagnosis and Management Strategies. *Vasc. Health Risk Manag.* 6, 883–903. doi:10.2147/VHRM.S11681
- Xu, L., and Brink, M. (2016). mTOR, Cardiomyocytes and Inflammation in Cardiac Hypertrophy. *Biochim. Biophys. Acta* 1863, 1894–1903. doi:10.1016/j.bbamcr.2016.01.003
- Xu, X., Kobayashi, S., Chen, K., Timm, D., Volden, P., Huang, Y., et al. (2013). Diminished Autophagy Limits Cardiac Injury in Mouse Models of Type 1 Diabetes. *J. Biol. Chem.* 288, 18077–18092. doi:10.1074/jbc.M113.474650
- Yore, M. M., Syed, I., Moraes-Vieira, P. M., Zhang, T., Herman, M. A., Homan, E. A., et al. (2014). Discovery of a Class of Endogenous Mammalian Lipids with Anti-diabetic and Anti-inflammatory Effects. *Cell* 159, 318–332. doi:10.1016/j.cell.2014.09.035
- Zeng, X., Yu, X., Xiao, S., Yao, H., and Zhu, J. (2017). Effects of 1,25-dihydroxyvitamin D3 on Pathological Changes in Rats with Diabetic Cardiomyopathy. *Lipids Health Dis.* 16, 109. doi:10.1186/s12944-017-0498-2
- Zhang, Y., Ling, Y., Yang, L., Cheng, Y., Yang, P., Song, X., et al. (2017). Liraglutide Relieves Myocardial Damage by Promoting Autophagy via AMPK-mTOR Signaling Pathway in Zucker Diabetic Fatty Rat. *Mol. Cel Endocrinol* 448, 98–107. doi:10.1016/j.mce.2017.03.029

**Conflict of Interest:** The authors declare that the research was conducted in the absence of any commercial or financial relationships that could be construed as a potential conflict of interest.

**Publisher's Note:** All claims expressed in this article are solely those of the authors and do not necessarily represent those of their affiliated organizations, or those of the publisher, the editors and the reviewers. Any product that may be evaluated in this article, or claim that may be made by its manufacturer, is not guaranteed or endorsed by the publisher.

Copyright © 2021 Wang, Mi, Jin, Guo, Yu, Wang, Zhang, Zhang, Wang, Huang, Zhou and Guo. This is an open-access article distributed under the terms of the Creative Commons Attribution License (CC BY). The use, distribution or reproduction in other forums is permitted, provided the original author(s) and the copyright owner(s) are credited and that the original publication in this journal is cited, in accordance with accepted academic practice. No use, distribution or reproduction is permitted which does not comply with these terms.



# Role of Higenamine in Heart Diseases: A Mini-Review

Jianxia Wen<sup>1</sup>, Mingjie Li<sup>2</sup>, Wenwen Zhang<sup>1</sup>, Haoyu Wang<sup>1</sup>, Yan Bai<sup>1</sup>, Junjie Hao<sup>3\*</sup>, Chuan Liu<sup>1\*</sup>, Ke Deng<sup>1\*</sup> and Yanling Zhao<sup>4\*</sup>

<sup>1</sup>School of Food and Bioengineering, Xihua University, Chengdu, China, <sup>2</sup>Department of Pathology, First Affiliated Hospital of Guangxi Medical University, Nanning, China, <sup>3</sup>College of Pharmaceutical Science, Yunnan University of Chinese Medicine, Kunming, China, <sup>4</sup>Department of Pharmacy, Chinese PLA General Hospital, Beijing, China

## OPEN ACCESS

### Edited by:

Xianwei Wang,  
Xinxiang Medical University, China

### Reviewed by:

Zhi Yong Du,  
Capital Medical University, China  
Wenying Wei,  
Renmin Hospital of Wuhan University,  
China

### \*Correspondence:

Junjie Hao  
2005102238@163.com  
Chuan Liu  
1220210030@mail.xhu.edu.cn  
Ke Deng  
ke.deng@siat.ac.cn  
Yanling Zhao  
zhaoyl2855@126.com

### Specialty section:

This article was submitted to  
Cardiovascular and Smooth Muscle  
Pharmacology,  
a section of the journal  
Frontiers in Pharmacology

Received: 20 October 2021

Accepted: 29 November 2021

Published: 10 January 2022

### Citation:

Wen J, Li M, Zhang W, Wang H, Bai Y,  
Hao J, Liu C, Deng K and Zhao Y  
(2022) Role of Higenamine in Heart  
Diseases: A Mini-Review.  
Front. Pharmacol. 12:798495.  
doi: 10.3389/fphar.2021.798495

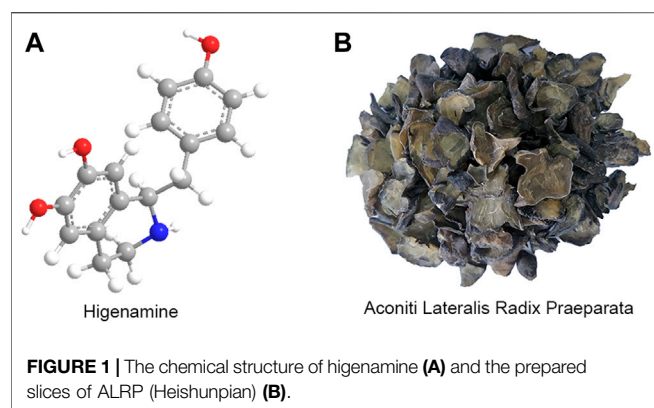
Higenamine, a natural product with multiple targets in heart diseases, is originally derived from *Aconitum*, which has been traditionally used in China for the treatment of heart disease, including heart failure, arrhythmia, bradycardia, cardiac ischemia/reperfusion injury, cardiac fibrosis, etc. This study is aimed to clarify the role of higenamine in heart diseases. Higenamine has effects on improving energy metabolism of cardiomyocytes, anti-cardiac fibroblast activation, anti-oxidative stress and anti-apoptosis. Accumulating evidence from various studies has shown that higenamine exerts a wide range of cardiovascular pharmacological effects *in vivo* and *in vitro*, including alleviating heart failure, reducing cardiac ischemia/reperfusion injury, attenuating pathological cardiac fibrosis and dysfunction. In addition, several clinical studies have reported that higenamine could continuously increase the heart rate levels of healthy volunteers as well as patients with heart disease, but there are variable effects on systolic blood pressure and diastolic blood pressure. Moreover, the heart protection and therapeutic effects of higenamine on heart disease are related to regulating LKB1/AMPK $\alpha$ /Sirt1, mediating the  $\beta$ 2-AR/PI3K/AKT cascade, induction of heme oxygenase-1, suppressing TGF- $\beta$ 1/Smad signaling, and targeting ASK1/MAPK (ERK, P38)/NF- $\kappa$ B signaling pathway. However, the interventional effects of higenamine on heart disease and its underlying mechanisms based on experimental studies have not yet been systematically reviewed. This paper reviewed the potential pharmacological mechanisms of higenamine on the prevention, treatment, and diagnosis of heart disease and clarified its clinical applications. The literature shows that higenamine may have a potent effect on complex heart diseases, and proves the profound medicinal value of higenamine in heart disease.

**Keywords:** higenamine, heart diseases, pharmacological effects, biological mechanism, mini-review

## INTRODUCTION

Natural products represent an important source of compounds used in the discovery of new therapeutic agents (Harvey et al., 2015), which have relatively single compounds with good drug characteristics, including structural diversity and complexity, high selectivity and specific pharmacological activities, as well as novel therapeutic effects and mechanisms of action (Barnett and Stallforth, 2018; Ekiert and Szopa, 2020). The importance of natural products in the prevention and treatment of heart disease is universally known. In the past few decades, a large number of studies have shown that natural products and their related synthetic compounds have





good clinical effects on the prevention, treatment and diagnosis of heart disease. Previous studies have revealed that higenamine showed better therapeutic effects on heart disease, including coronary artery disease (CAD), bradyarrhythmia, chronic heart failure (CHF), cardiac ischemia/reperfusion (I/R) injury, cardiac fibrosis, cardiorenal syndrome (CRS), etc., which have aroused great interest of researchers (Chen Z. et al., 2019). In the oriental Asian countries, herbal medicines containing higenamine have been used to treat heart disease for thousands of years. Recently, with extensive studies and clinical reports on higenamine, researchers have proved its beneficial therapeutic effects on various diseases, most prominently on heart disease (Zhang et al., 2017). Based on the effectiveness and safety of clinical medicine practice, higenamine has attracted much attention as a promising chemical compound and natural product for the prevention, diagnosis, and treatment of heart disease.

Higenamine (1-(4-Hydroxybenzyl)-1,2,3,4-tetrahydroisochinolin-6,7-diol), also called as dldemethylcoclaurine or norcoclaurine, is a plant-based benzylisoquinoline alkaloid, which was originally isolated from the root of *Aconitum* (a commonly used traditional Chinese herbal medicine) as an active cardiogenic compound by Kosuge in 1976 (Kosuge and Yokota, 1976). Its molecular formula is  $C_{16}H_{17}NO_3$ , and its relative molecular mass is 271.311. Its chemical structure is shown in **Figure 1A**. The 2-(3,4-dimethoxybenzene) acetonitrile could be used as the starting material for the synthesis of higenamine-D4, and heavy water as the stable isotope labeling source (Han et al., 2021). Preliminary studies have found that higenamine has similar pharmacological effects and biological mechanisms to the traditional Chinese medicine (TCM) *Aconiti Lateralis Radix Praeparata* (ALRP) (**Figure 1B**), and may be one of the active effect substances of ALRP against CHF. Higenamine also exists in many other medicinal plants, such as *Scutellariae barbatae herba*, *Gnetum montanum* Markgr., *Asari radix et rhizoma*, *Nandina domestica*, and so on (Kosuge and Yokota, 1976; Li et al., 2020). Besides, higenamine is also commonly used as a dietary supplement, which has a heart-stimulating effect. It is one of the homologous drugs of medicine and food (Calvert et al., 2015; Nuntawong et al., 2020). Structurally, higenamine is similar to catecholamines and can activate  $\alpha_1$ -,  $\alpha_2$ -,  $\beta_1$ -, and  $\beta_2$ -adrenergic

receptors (AR). Higenamine is a non-selective  $\beta$  receptor agonist, which has a wide range of effects on heart, brain, vasculature, lung, smooth muscle, striate muscle and so on (Ueki et al., 2011). Higenamine has been identified as a new type of  $\alpha_1$ -AR antagonist, which contributes to its antihypertensive effect and inhibits platelet aggregation (Zhang et al., 2019). Higenamine acts as a  $\beta$ -AR receptor agonist by acting on dobutamine receptors. Studies have shown that the positive inotropic effect of higenamine and the effect of increasing heart rate (HR) are shorter than that of dobutamine hydrochloride (Shin et al., 1999). Higenamine can play the role of positive chronotropic effect and positive ionotropic effect by regulating  $\beta_1$ -AR (Kimura et al., 1994). By regulating the  $\beta_2$ -AR, higenamine has the effect of reducing the tension of smooth muscles, thus reflecting the effect of cardiac stimulation (Hudzik et al., 2021). Furthermore, higenamine enhances myocardial contractile response and reduces myocardial cell apoptosis by activating  $\beta_2$ -AR (Chen Y. et al., 2019). In the other hand, higenamine also decreases pulmonary inflammation and increases glucose uptake (muscle) (Hudzik et al., 2021). Pharmacologically, higenamine has multiple pharmacological effects, such as positive inotropic effect, vasodilation, tracheal relaxation, anti-thrombosis, anti-platelet aggregation, anti-inflammatory, anti-apoptosis, anti-oxidative stress, anti-fibrosis, and immune regulation (Pyo et al., 2007; Tsukiyama et al., 2009; Chen et al., 2013; Bai et al., 2019; Guan et al., 2019; Yang et al., 2020). Currently, higenamine has been clinically used for the diagnosis, prevention and treatment of CAD, myocardial perfusion imaging, myocardial I/R injury, bradyarrhythmia, diffuse intravascular coagulation and bronchoconstrictive diseases (Wu et al., 2016; Zhang et al., 2017; Yang et al., 2020).

The chloride salt of higenamine, higenamine hydrochloride [1-(4-Hydroxybenzyl)-1,2,3,4-tetrahydroisochinolin-6,7-diol hydrochloride], is a white powder, which is more stable than higenamine, and more soluble in water, so it is often used for clinical purposes. Higenamine hydrochloride injection is an original and innovative drug with independent intellectual property rights in China. Higenamine hydrochloride can be used as a cardiac stress test drug for radionuclide myocardial perfusion imaging to assist in the diagnosis and evaluation of myocardial ischemia. It is worth mentioning that higenamine has been approved for clinical research by the China Food and Drug Administration (CFDA). It has been approved by clinical trials to detect coronary artery stenosis and myocardial ischemia by myocardial perfusion imaging with certain specificity and safety (Zheng et al., 2005). Higenamine can be used for radionuclide myocardial perfusion imaging to assist in the diagnosis and assessment of coronary heart disease (CHD) and myocardial ischemia. At present, the phase III clinical trials (2004L02567) of higenamine have been completed and are currently in the evaluation stage of National Medical Products Administration (Zhang et al., 2017). These properties indicate that higenamine has a clear pharmacological effect on the cardiovascular system in clinical practice, but its underlying mechanism is still unclear. Studies specifically designed to evaluate the potential pharmacological effects and biological mechanisms of higenamine in the prevention, diagnosis, and

treatment of heart disease are necessary for researchers. Hence, this study provided a synthetic summary of the recent research progress of higenamine on cardiovascular pharmacology and its mechanism of action, thereby contributing to the further clinical practice and application of the drug.

## METHODOLOGY

The databases, including PubMed, EMBASE, SinoMed, China National Knowledge Infrastructure (CNKI), VIP medicine information system (VMIS), Wanfang, and Chinese Biomedical Database (CBM), were comprehensively searched. The following search terms were used: “higenamine” [Mesh terms] OR “norcoclaurine” [Mesh terms]. Studies concerning the role of higenamine in heart disease were picked out manually. The related studies were downloaded for further evaluation.

## Ethics Approval and Consent to Participate

Due to this study does not involve animal and patient experiments, the ethics approval and consent to participate are not applicable.

## Pharmacokinetics of Higenamine

Studies have explored the pharmacokinetics of higenamine from humans, rabbits, rats, and dogs in recent years. Feng et al. (2012), gave 10 subjects a continuous intravenous infusion of higenamine, and the dose of higenamine was gradually increased from 0.5 to  $4.0 \mu\text{g kg}^{-1} \text{ min}^{-1}$ , with each administration being 3 min. The pharmacokinetics of higenamine in humans were evaluated by detecting the HR of subjects. The results showed that the peak concentration ( $C_{\text{max}}$ ) of higenamine ranges from 15.1 to  $44.0 \text{ ng mL}^{-1}$ . The half-life of higenamine was 0.133 h, and the area under the concentration-time curve (AUC) extrapolated to infinity was  $5.39 \text{ ng h mL}^{-1}$ . The volume of distribution (V) is 48 L. The total clearance (CL) is  $249 \text{ L h}^{-1}$ . Within 8 h, 9.3% of higenamine was recovered in the urine. Studies have shown that higenamine has desirable pharmacokinetic properties. Lo and Chen (1996), administered higenamine to rabbits by intravenous bolus, oral and intravenous infusion, and studied the pharmacokinetics of higenamine in rabbits. The results indicate that AUC increases proportionally with the dose increase of higenamine, and when the dose continues to increase, the percentage of higenamine excreted in the urine remains unchanged. Lo and Chen (1994) found that higenamine is quickly absorbed from the gastrointestinal tract after oral administration. The  $T_{\text{max}}$  is about 10 min. The cumulative urinary excretion of the same rabbit within 24 h after intravenous ( $20 \text{ mg kg}^{-1}$ ) and oral administration ( $50 \text{ mg kg}^{-1}$ ) of higenamine are 4.73 and 0.82%, respectively. Wang et al. (2020), used a non-compartmental model to derive the pharmacokinetic parameters of higenamine in the plasma of rats. Oral administration of higenamine in the dose of  $3.0\text{--}30.0 \text{ mg kg}^{-1}$  could quickly reach its maximum concentration, and the  $T_{\text{max}}$  for all doses was 0.42 h. The higher the total level of the athlete's intake of food, the longer it takes for the metabolism to eliminate higenamine. Zheng et al. (2004), gave intravenous injection of higenamine to beagle dog. This study found that the dog's metabolism under this condition

conforms to the two-compartment model, with  $t_{1/2}$  of 8.60 min, indicating that the pharmacokinetics of higenamine in different species of animals may be different. However, animal experiments have certain limitations, and further research on health and pharmacokinetics in patients is needed. The pharmacokinetics parameter of higenamine in different kinds of animals is shown in Table 1.

## EFFECTS OF HIGENAMINE ON HEART DISEASE IN VIVO

### Anti-Heart Failure

Heart failure (HF) is myocardial damage caused by any cause such as myocardial infarction (MI), cardiomyopathy, hemodynamic overload, inflammation, etc., resulting in changes in myocardial structure and function, and finally resulting in hypofunction of ventricular pumping or filling. The main clinical manifestations are dyspnea, fatigue and fluid retention. CHF is the terminal stage of various heart disease, which refers to a state of persistent HF that can be stabilized, worsened, or decompensated (Wen et al., 2020b). Due to high morbidity and high mortality, CHF is still a clinical cause that seriously endangers the health of patients with various heart disease (Dini et al., 2018). In recent years, the relationship between CHF and myocardial energy metabolism has become a hot spot in clinical research. Even though the drugs used to treat CHF are diverse, the drugs themselves can enhance the energy metabolism of myocardial mitochondria and may also have the preventing and therapeutic effects on CHF (Wen et al., 2019a) (Table 2).

A number of studies by our team showed that higenamine exerts a therapeutic effect on doxorubicin (DOX)-induced CHF *via* the cardiotonic effect and promoting myocardial energy metabolism. Higenamine had effects on ameliorating heart function, down-regulation serum indices, alleviating histological damage of heart tissue and reducing the apoptosis of myocardial cells (Wen et al., 2020b; Wen et al., 2020c). Specifically, higenamine increased the haemodynamic parameter levels of left ventricular systolic pressure (LVSP) and maximum rate of increase in left ventricular pressure ( $+dp/dt_{\text{max}}$ ), but decreased left ventricular end-diastolic pressure (LVEDP) and maximum rate of decrease in left ventricular pressure ( $-dp/dt_{\text{max}}$ ). Moreover, higenamine decreases serum level of neuro-humoral factor, such as renin, angiotension II (Ang-II), aldosterone (ALD), and endothelin-1 (ET-1); serum level of myocardial biomarkers, such as brain natriuretic peptide (BNP), NT-proBNP, lactate dehydrogenase (LDH), creatine kinase-MB (CK-MB), and aspartate aminotransferase (AST); but increases the serum level of adenosine phosphate, such as adenosine triphosphate (ATP), ATPase, nicotinamide adenine dinucleotide (NAD), and NADH in CHF rats induced by DOX (Wen et al., 2020b; Wen et al., 2020c). Serum metabolomics analyses indicated that the therapeutic effects of higenamine on CHF rats were primarily related to the comprehensively regulation of mitochondrial energy metabolism metabolites, including acetylphosphate, coenzyme A, 3-Carboxy-1-hydroxypropylthiamine

**TABLE 1 |** Pharmacokinetics parameters of higenamine in different kinds of animals.

Species	Dose of higenamine	Pharmacokinetics parameter	Findings
Human Feng et al. (2012)	22.5 $\mu\text{g kg}^{-1}$ , <i>i.v.</i>	$AUC_{\text{last}}$ 5.31 $\pm$ 1.21 ng h mL <sup>-1</sup> $AUC_{0-\text{inf}}$ 5.39 $\pm$ 1.23 ng h mL <sup>-1</sup> $C_{\text{max}}$ 31.3 $\pm$ 9.24 $\mu\text{g L}^{-1}$ $CL$ 249 $\pm$ 42.78 L h <sup>-1</sup> $CL_r$ 22.9 $\pm$ 4.41 L h <sup>-1</sup> $t_{1/2}$ 0.133 $\pm$ 0.02 h $V$ 48 $\pm$ 13.83 L $A_e$ 120.6 $\pm$ 34.5 $\mu\text{g fe}\%$ 9.3 $\pm$ 2.2% $t_{1/2}$ 22 min	Two-compartment pharmacokinetic model
Rabbits Lo and Chen (1996)	NR	total body clearance 127.7 ml min <sup>-1</sup> kg <sup>-1</sup> mean residence time 9.28 min volume of distribution at steady state 1.44 L kg <sup>-1</sup> fraction of urinary excretion 5.48%	Two-compartment open pharmacokinetic model
Rabbits Lo and Chen (1994)	50 mg kg <sup>-1</sup> , <i>p.o.</i> 20 mg kg <sup>-1</sup> , intravenous	$T_{\text{max}}$ 10 min Cumulative urinary excretion 0.82% Cumulative urinary excretion 4.73%	Two-compartment model
Rats Wang et al. (2020)	30.0 mg kg <sup>-1</sup> , <i>i.g.</i>	$AUC_{(0-t)}$ 11,482.55 $\pm$ 1,291.49 ng mL <sup>-1</sup> min <sup>-1</sup> $AUC_{(0-\infty)}$ 13,030.94 $\pm$ 714.93 ng mL <sup>-1</sup> min <sup>-1</sup> $t_{1/2z}$ 53.67 $\pm$ 26.11 min $T_{\text{max}}$ 25.83 $\pm$ 2.04 min $C_{\text{max}}$ 256.38 $\pm$ 37.33 Ng mL <sup>-1</sup> $MRT_{(0-t)}$ 53.02 $\pm$ 1.66 min $MRT_{(0-\infty)}$ 76.16 $\pm$ 19.93 min $VRT_{(0-t)}$ 1,146.09 $\pm$ 89.10 min <sup>2</sup> $VRT_{(0-\infty)}$ 3,183.12 $\pm$ 763.67 min <sup>2</sup> $Vz/F$ 180.47 $\pm$ 93.67 L kg <sup>-1</sup> $CLz/F$ 2.31 $\pm$ 0.12 L min <sup>-1</sup> kg <sup>-1</sup>	High concentrations of topical or oral use of higenamine-rich materials may cause positive test of higenamine in the urine of athletes
	15.0 mg kg <sup>-1</sup> , <i>i.g.</i>	$AUC_{(0-t)}$ 3,824.53 $\pm$ 332.08 ng mL <sup>-1</sup> min <sup>-1</sup> $AUC_{(0-\infty)}$ 4,051.78 $\pm$ 280.95 ng mL <sup>-1</sup> min <sup>-1</sup> $t_{1/2z}$ 36.00 $\pm$ 9.10 min $T_{\text{max}}$ 25.00 $\pm$ 0.00 min $C_{\text{max}}$ 119.00 $\pm$ 23.05 ng mL <sup>-1</sup> $MRT_{(0-t)}$ 47.77 $\pm$ 1.75 min $MRT_{(0-\infty)}$ 55.76 $\pm$ 5.66 min $VRT_{(0-t)}$ 1,000.72 $\pm$ 76.25 min <sup>2</sup> $VRT_{(0-\infty)}$ 2,354.15 $\pm$ 878.73 min <sup>2</sup> $CLz/F$ 3.72 $\pm$ 0.26 L min <sup>-1</sup> kg <sup>-1</sup> $Vz/F$ 194.31 $\pm$ 54.11 L kg <sup>-1</sup>	
	3.0 mg kg <sup>-1</sup> , <i>i.g.</i>	$AUC_{(0-t)}$ 801.78 $\pm$ 65.96 ng mL <sup>-1</sup> min <sup>-1</sup> $AUC_{(0-\infty)}$ 849.59 $\pm$ 76.10 ng mL <sup>-1</sup> min <sup>-1</sup> $t_{1/2z}$ 34.69 $\pm$ 12.13 min $T_{\text{max}}$ 25.00 $\pm$ 0.00 min $C_{\text{max}}$ 24.46 $\pm$ 3.44 ng mL <sup>-1</sup> $MRT_{(0-t)}$ 44.75 $\pm$ 1.98 min $MRT_{(0-\infty)}$ 50.89 $\pm$ 2.57 min $VRT_{(0-t)}$ 890.10 $\pm$ 104.91 min <sup>2</sup> $VRT_{(0-\infty)}$ 1944.89 $\pm$ 551.80 min <sup>2</sup> $CLz/F$ 3.55 $\pm$ 0.32 L min <sup>-1</sup> kg <sup>-1</sup> $Vz/F$ 174.90 $\pm$ 49.02 L kg <sup>-1</sup>	
	3.0 mg kg <sup>-1</sup> , <i>i.v.</i>	$AUC_{(0-t)}$ 25,966.04 $\pm$ 759.68 $\mu\text{g L}^{-1}$ min <sup>-1</sup> $AUC_{(0-\infty)}$ 26,185.37 $\pm$ 787.28 $\mu\text{g L}^{-1}$ min <sup>-1</sup> $t_{1/2z}$ 26.92 $\pm$ 3.31 min $T_{\text{max}}$ 2.00 $\pm$ 0.00 min $C_{\text{max}}$ 2,762.33 $\pm$ 113.72 $\mu\text{g L}^{-1}$ $MRT_{(0-t)}$ 11.21 $\pm$ 0.25 min $MRT_{(0-\infty)}$ 12.37 $\pm$ 0.29 min $VRT_{(0-t)}$ 283.75 $\pm$ 13.36 min <sup>2</sup> $VRT_{(0-\infty)}$ 464.88 $\pm$ 34.75 min <sup>2</sup> $Vz/F$ 4.45 $\pm$ 0.55 L kg <sup>-1</sup> $CLz/F$ 0.11 $\pm$ 0.003 L min <sup>-1</sup> kg <sup>-1</sup>	
Dog Zheng et al. (2004)	10 mg kg <sup>-1</sup> , single <i>i.v.</i>	$AUC_{(0-30)}$ 0.076 $\pm$ 0.00027 mg min L <sup>-1</sup> $t_{1/2\beta}$ 8.60 $\pm$ 0.26 min $CL_T$ 0.13 $\pm$ 0.0058 L min <sup>-1</sup> kg <sup>-1</sup> $V/F$ 0.95 $\pm$ 0.0038 L kg <sup>-1</sup>	Two-compartment pharmacokinetic model

Notes: NR, not report; AUC, area under the concentration-time curve; CL, total clearance.

**TABLE 2 |** *In vivo* pharmacological activities of higenamine in heart disease.

Effects	Animals	Experimental model	Doses of higenamine	Pathways
CHF Wen et al. (2020b), Wen et al. (2020c)	Rats	DOX (15 mg kg <sup>-1</sup> , <i>i.p.</i> )-induced CHF	5 mg kg <sup>-1</sup>	Regulating LKB1/AMPKα/Sirt1 signaling pathway
Anti-I/R injury Wu et al. (2016)	Mice	I/R-induced MI	10 mg kg <sup>-1</sup>	Mediating the β2-AR/PI3K/AKT cascade
Myocardial damages Lee et al. (2006)	Rats	Myocardial I/R injury	1–10 mg kg <sup>-1</sup> ( <i>i.p.</i> )	Induction of heme oxygenase-1
Cardiac fibrosis Zhu et al. (2021)	Mice	TAC or ISO (50 mg kg <sup>-1</sup> <i>i.p.</i> )-induced cardiac fibrosis	10 mg kg <sup>-1</sup>	Suppressing TGF-β1/Smad signaling
CRS Deng et al. (2020)	Rats	Left anterior descending coronary artery ligation combined with 5/6 STNx	0.5–4.5 mg kg <sup>-1</sup>	Targeting ASK1/MAPK (ERK, P38)/NF-κB signaling pathway

Notes: CHF, chronic heart failure. I/R, ischemia/reperfusion. CRS, cardiorenal syndrome; DOX, doxorubicin; ISO, isoproterenol; TAC, transverse aortic constriction; STNx, subtotal nephrectomy. *i.p.*, intraperitoneal injection.

**TABLE 3 |** *In vitro* pharmacological activities of higenamine in heart disease.

Effects	Cells/tissues	Experimental model	Concentrations of higenamine	Targets/pathways
Treatment of blood pressure Zhang et al. (2019)	HEK293 cell lines	Stably transfected with α1A-, α1B-, and α1D-AR/Flag and treatment with 10 μM PE	10 μM	Antagonist for α1-AR
Improve energy metabolism of cardiomyocytes Wen et al. (2019a), Wen et al. (2020c)	H9c2 cells	5 μM DOX-induced H9c2 cells injury	5–20 μM	Upregulation the PPARα/PGC-1α/Sirt3 pathway
Treatment of CHF Chen et al. (2019a)	SK/SK-β2 cells adult rat cardiomyocytes cells	0.001 μg mL <sup>-1</sup> PTX Perfused with Ca <sup>2+</sup> -free perfusion buffer	0.1 μM	Stimulating the Gs and Gi pathways in β2-AR signaling
Anti-cardiac fibroblast activation Zhu et al. (2021)	AMCM NRCF	10 μM PE-induce hypertrophic growth of AMCM NRCF cells were stimulated with 10 ng mL <sup>-1</sup> TGF-β1	100 μM	Inhibiting TGF-β1/Smad signaling
Anti-cardiorenal fibrosis Deng et al. (2020)	NRCM NRCF	10 μM IS 10 ng mL <sup>-1</sup> TGF-β1	0.01–100 μM	Mediating ASK1 and its downstream MAPK (pERK, p-P38) and p-NF-κB pathways
Anti-oxidative stress and apoptosis in cardiomyocytes Chen et al. (2013)	NRCM/H9c2 cells	5 μM DOX-induced cardiotoxicity	0.5–50 μM	Activating the PI3K/Akt signaling pathway
Anti-myocyte apoptosis Wu et al. (2016)	NRCM/AMVM	H <sub>2</sub> O <sub>2</sub> (250 μM for 24 h) in NRVM H <sub>2</sub> O <sub>2</sub> (20 μM for 24 h) in AMVM	100 μM in NRVMs/ 100 μM in AMVMs	β2-AR/PI3K/AKT signaling pathway

Notes: CHF, chronic heart failure; AMCM, adult mouse cardiac myocytes; AMVM, adult mouse ventricular myocytes; NRCF, neonatal rat cardiac fibroblasts; NRCM, neonatal rat cardiac myocyte; NRVM, neonatal rat ventricular myocytes. SK, SK-N-MC, cell.

diphosphate, PE (O-18:1 (1Z)/20:4 (5Z, 8Z, 11Z, 14Z)), lysoPC(18:1 (9Z)), oleic acid, palmitic acid, and PC(16:0/16:0). Pathway analysis showed that higenamine on CHF treatment was related to energy metabolism signaling pathways, including glycerophospholipid metabolism, linoleic acid metabolism, fatty acid metabolism, citrate cycle (TCA cycle), arachidonic acid metabolism, pantothenate and CoA biosynthesis, and pyruvate metabolism (Wen et al., 2020b). The potential mechanism of these activities was partially related to down-regulating renin-angiotensin-aldosterone system (RAAS) pathway-related molecules and up-regulating LKB1/AMPKα/Sirt1-related pathway (Wen et al., 2020c) (Table 2). Moreover, studies focused on ALRP, one of the sources of higenamine, was in accordance with these results showing the alleviating of mitochondrial energy metabolism. ALRP could significantly improve the left ventricular function and cardiac enzyme

activities *via* activating the PPARα/PGC-1α/Sirt3 signaling pathway, which promotes mitochondrial energy metabolism and protects against CHF (Wen et al., 2019b) (Table 2). Another study further indicated that ALRP could regulate the metabolites related to the mitochondrial energy metabolism pathway, which increases the relative gene expression level of energy metabolism, including *PPARδ*, *PPARγ*, *Lpl*, *Scd*, *Fasn*, and *Pla2g2e* (Wen J. X. et al., 2020). These findings all indicate that higenamine plays a role in the treatment of CHF by regulating the mitochondria energy metabolism of myocardial.

## Reducing Cardiac Ischemia/Reperfusion Injury

Cardiac I/R injury after myocardial ischemia is a partial or complete acute obstruction of the coronary artery and recanalization after a



certain period of time. Although the ischemic myocardium can be restored to normal perfusion, the tissue damage is a progressive pathological process (Tibaut et al., 2017). A series of damaging changes such as myocardial ultrastructure, energy metabolism, cardiac function and electrophysiology caused by ischemic period will be more prominent after vascular recanalization, and severe arrhythmia may even occur and cause sudden death. In the process of I/R, myocardial cell apoptosis will aggravate the development of ischemic heart injury and HF. I/R injury significantly increases morbidity and mortality after MI (Herr et al., 2020). Wu et al. (2016), reported that higenamine reduces I/R-induced MI in mice *in vivo*. In addition, higenamine stimulates AKT phosphorylation and activates PI3K to play an anti-apoptotic effect in cardiomyocytes. These results indicated that the heart protection effects of higenamine are mediated by the  $\beta_2$ -AR/PI3K/AKT cascade (Table 2). Lee et al. (2006), found that administration of higenamine (bolus injection, intraperitoneal injection) 1 h before I/R injury dramatically reduced the release of cytochrome c, caspase-3 activity and Bax expression in the left ventricle of rats, but increased the expression of heme oxygenase-1 (HO-1). I/R-induced myocardial injury is related to mitochondrial-dependent apoptosis. This study also confirmed the key role of HO-1 in the protective effect of higenamine in the myocardial injury induced by I/R (Table 2). Therefore, higenamine is expected to become a potential agent for the treatment of myocardial ischemic injury.

## Attenuating Pathological Cardiac Fibrosis and Dysfunction

Cardiac fibrosis is the result of persistent and/or repeated myocardial ischemia and hypoxia caused by moderate to severe coronary atherosclerotic stenosis, leading to the gradual development of chronic ischemic heart disease (IHD). Myocardial fibrosis is the inevitable process of the development of various clinical heart disease to the final stage, and is the main manifestation of cardiac structural remodeling. It is currently believed to be closely related to arrhythmia, cardiac dysfunction and even sudden cardiac death. It is mainly characterized by the proliferation of fibroblasts and the deposition of extracellular matrix (ECM). The deposition of ECM causes an increase in the stiffness of the heart and a decrease in compliance, which affects the normal diastolic and contractile functions of the heart (Frey and Olson, 2003). It is currently believed that the pathogenesis of cardiac fibrosis involves multiple influencing factors, including the endothelial-to-mesenchymal transition (EndMT), left ventricle pressure overload, inflammation activation, the effector cells and cellular mediators of immune system in cardiac tissue (Burke et al., 2019; Martinez-Martinez et al., 2019; Liu et al., 2020; Wilhelmi et al., 2020).

In the transverse aortic constriction (TAC) and isoproterenol (ISO) injection-induced cardiac fibrosis model, higenamine in the dose of  $10 \text{ mg kg}^{-1}$  in mice could abolish the decreased fractional shortening (FS) and ejection fraction (EF) as well as increased systolic left ventricular internal diameter (LVIDs) and systolic left ventricular volumes (LVVs) in cardiac fibrosis mice induced by TAC and ISO. Moreover, the extremely increased heart size, ratio

of heart weight to tibia length (HW/TL), and ratio of heart weight to body weight (HW/BW) induced by TAC and ISO was also decreased by higenamine treatment. In addition, higenamine exerts a therapeutic effect on TAC-induced cardiac dysfunction, as well as ISO-induced cardiac remodeling and fibrosis in mice by attenuating serum level of hypertrophic markers, such as  $\beta$ -myosin heavy chain ( $\beta$ -MHC), A-type natriuretic peptide (ANP), and BNP. These results indicated that HG remarkably inhibits myocardial fibrosis in different models by inhibiting cardiac fibrosis activation. The potential mechanism of higenamine exerting these pharmacological activities is related to the inhibition of TGF- $\beta$ 1/Smad signaling pathway (Zhu et al., 2021) (Table 2).

## Ameliorating Cardiac and Renal Fibrosis

Cardiorenal syndrome (CRS) is a clinical syndrome characterized by the co-pathogenicity of the heart and kidneys. It refers to the acute or chronic dysfunction of one organ resulting in progressive dysfunction of the other organ, and ultimately caused to the failure of both organs (Rangaswami et al., 2019). Currently, higenamine is considered to be effective in the treatment of CRS. A study from Deng (Deng et al., 2020) revealed that compared with type 2 CRS rats, rats treated with higenamine ( $0.5\text{--}4.5 \text{ mg kg}^{-1}$ ) showed significantly increased LV ejection fraction (LVEF%) and left ventricular fraction shortening (LVFS%), decreased LV end systolic volume (LVESV), LV posterior wall thickness LVPW, Cardiac weight index (CWI) and kidney weight index (KWI). In addition, higenamine markedly decreased serum creatinine (Scr), blood urea nitrogen (BUN), indole sulfate (IS), and 24-h urine protein level as well as memorably diminished cardiac and renal fibrosis in CRS rats, accompanied with the reduced protein level of  $\alpha$ -smooth muscle actin ( $\alpha$ -SMA), transforming growth factor- $\beta$ 1 (TGF- $\beta$ 1), and collagen I. Moreover, it dramatically improved left ventricular remodeling and systolic function in CRS. This heart and renal therapeutic effects are strongly relevant to directly inhibited the protein expression of phosphorylated apoptosis signal-regulated kinase 1 (p-ASK1) and its downstream mitogen-activated protein kinases (MAPK) (ERK, P38)/NF- $\kappa$ B in cardiorenal tissues of CRS rats. This study finally found that higenamine alleviated ventricular remodeling and renal fibrosis *via* targeting ASK1/MAPK (ERK, P38)/NF- $\kappa$ B signaling pathway (Table 2).

## EFFECTS OF HIGENAMINE ON HEART DISEASE IN VITRO

Most studies of higenamine in the treatment of heart disease *in vitro* are based on its role as  $\alpha$  and  $\beta$  receptor agonists. Higenamine could increase the contractility, contraction frequency and contraction amplitude of guinea pig ventricular papillary muscle, mouse left atrium and mouse right atrium in a concentration-dependent range of  $0.1\text{--}800 \text{ }\mu\text{M}$ , and increase the left atrial tension of rabbit. However, these effects were competitively blocked by the non-selective  $\beta$ -AR blocker propranolol, indicating that higenamine exerted a cardiotonic

effect by stimulating  $\beta$ -AR (Park et al., 1984; Kimura et al., 1989; Kimura et al., 1994; Kimura et al., 1996). Higenamine in the concentration of 10 and 100  $\mu$ M could increase the contraction frequency and contraction amplitude of primary cultured neonatal rat ventricular myocytes (Han et al., 1981). Chen et al. (2019b), investigated the contractility of higenamine and ISO on adult rat cardiomyocytes. Studies have found that the stimulation of higenamine on cardiomyocytes was dose-dependent. The  $EC_{50}$  of its contractile response was 0.33  $\mu$ M, which was equivalent to the  $EC_{50}$  measured by cAMP of 0.129  $\mu$ M, but it was not as effective as ISO. The  $\beta$ 1- or  $\beta$ 2-receptor antagonists completely blocked the positive inotropic effect of higenamine on cardiomyocytes. Wang et al. (2019) found that higenamine controlled the electrophysiology of the heart by having a dominant effect on the sinus node without inducing ectopic activities that cause arrhythmia, which might help treat bradycardia. Higenamine could inhibit the apoptosis of ventricular myocytes in primary neonatal rats and adult mice, and its anti-apoptotic effect could be completely eliminated by  $\beta$ 2-AR, but could not be antagonized by  $\beta$ 1-AR. Higenamine reduces myocardial damage caused by ischemia/reperfusion in a  $\beta$ 2-AR-dependent manner, thereby exerting anti-apoptosis and protecting the heart (Wu et al., 2016) (Table 3). Studies have also indicated that higenamine at a concentration of more than 30  $\mu$ M could inhibit the proliferation and migration of rat aortic smooth muscle cells in a concentration-dependent manner. It was speculated that higenamine might have the effect of preventing the restenosis of blood vessels in various heart disease, such as atherosclerosis, allograft vascular disease, hypertension, and angioplasty (Weng and Sun, 2020). Zhang et al. (2019), indicated that higenamine can inhibit the production of inositol monophosphate. It also inhibits the influx and entry of calcium ions induced by phenylephrine (PE) and the phosphorylation of extracellular signal-regulated kinases 1 and 2. In addition, higenamine has similar affinities (pKi) to the cloned  $\alpha$ 1A-,  $\alpha$ 1B- and  $\alpha$ 1D-AR, which may contribute to its antihypertensive effect (Table 3).

## Improve Energy Metabolism of Cardiomyocytes

The heart is an energy-intensive organ that consumes large amounts of ATP every day to provide fuel for pumping functions (Jiang et al., 1980; Neubauer, 2007). Since mitochondria are organelles that coordinate multiple metabolic systems and enzymes involved in substrate utilization and oxidative phosphorylation, mitochondrial metabolic dysfunction plays a key role in energy metabolism. Therefore, drugs that enhance myocardial mitochondrial energy metabolism and respiratory function of cardiomyocytes may have the potential effects on treating heart disease (Doenst et al., 2013). In our previous studies, 5  $\mu$ M DOX was used to establish a cardiomyocyte injury model to simulate myocardial cell energy metabolism disorder and respiratory injury during CHF *in vitro*. Cell metabolomics analyses indicated that the protective effects of higenamine on DOX-induced mitochondrial energy metabolism disorder and respiratory dysfunction were closely associated with the mitochondrial energy metabolism metabolites, including pantothenic acid, palmitic acid, eicosanoyl-CoA, coenzyme A,

1,4-beta-D-Glucan, oleic acid, and so on. Metabolic pathway analysis indicated that these potential metabolites were related to energy metabolism signaling pathways, including citrate cycle (TCA cycle), biosynthesis of unsaturated fatty acids, fatty acid metabolism, fatty acid biosynthesis, pentose and glucuronate interconversions, and so on (Wen et al., 2020c). Besides, higenamine could meliorate DOX-induced mitochondrial dysfunction and elevate cell mitochondrial oxygen consumption rate (OCR) as well as extracellular acidification rate (ECAR), thus enhancing the mitochondrial function of H9c2 cardiomyocytes (Wen et al., 2019a; Wen et al., 2020c) (Table 3). Molecular biological mechanism research suggests that the protective mechanism of higenamine on ameliorating DOX-induced mitochondrial function impairment in H9c2 cells may be related to the upregulation of the PPAR $\alpha$ /PGC-1 $\alpha$ /Sirt3 pathway, which promotes mitochondrial energy metabolism and protects against heart disease (Wen et al., 2019a) (Table 3). In addition, Chen Y. et al. (2019), applied contractility experiments to prove that higenamine exerts a positive inotropic effect by stimulating  $\beta$ 1/ $\beta$ 2-AR, and has no preference for stimulating the Gs and Gi pathways in  $\beta$ 2-AR signaling. The pharmacological effects of higenamine in the treatment of CHF and the mechanism of its cardiotoxicity have been elucidated.

## Anti-Cardiac Fibroblast Activation

Cardiomyocyte hypertrophy is crucial in pathological heart remodeling as well as HF. Zhu et al. (Liu et al., 2020), investigated the effect of higenamine on cardiomyocytes hypertrophy in adult mouse cardiac myocytes (AMCM) *in vitro*. Studies have found that higenamine has no significant effects on the cardiomyocytes hypertrophy induced by PE, but it could dose-dependently inhibit the relative mRNA and protein expression of  $\alpha$ -SMA in TGF- $\beta$ 1 stimulated neonatal rat cardiac fibroblasts (NRCF). In addition, higenamine could reduce the relative mRNA expressions of collagen I, collagen III and fibronectin in the TGF- $\beta$ 1 stimulated NRCF. These results indicated that higenamine improves cardiomyocyte fibrosis and dysfunction by inhibiting TGF- $\beta$ 1/Smad signaling and cardiac fibroblasts activation. Deng et al. (2020), also found that higenamine dramatically inhibits the collagen synthesis of NRCF and inhibits the hypertrophy of neonatal rat cardiomyocytes. It mainly mediates ASK1 pathways to relieve cell fibrosis (Table 3).

## Anti-Oxidative Stress and Apoptosis

Recently, studies have shown that higenamine could protect cardiomyocytes through its anti-oxidative stress injury and anti-apoptosis effects (Chen et al., 2013; Wu et al., 2016). Chen et al. (2013) (Table 3), studied the cardioprotective mechanism of higenamine in DOX-induced cytotoxic neonatal rat cardiac myocyte (NRCM) and H9c2 cells *in vitro*. The results showed that higenamine could increase the cell viability of DOX-injured cardiomyocytes, increase SOD activity, reduce the generation of ROS and the formation of MDA, and inhibit the release of LDH and the inherent mitochondrial-dependent apoptosis pathway of cardiomyocytes. Molecular biology studies indicated that higenamine played a cardioprotective effect on DOX-induced cardiotoxicity by activating the PI3K/

**TABLE 4 |** Clinical research of higenamine in heart disease.

Subjects	Cases	Effects	Intervention	HR	SBP	DBP	Cardiac output
Healthy volunteers Feng et al. (2012)	10	Pharmacokinetic and pharmacodynamics study	Higenamine intravenous infusions escalating from 0.5 to 4 mg kg <sup>-1</sup> min <sup>-1</sup> for 3 min	↑	-	↓	NR
Healthy volunteers Du et al. (2007)	32	Tolerability study	Higenamine intravenous infusions escalating from 0.5 to 4 mg kg <sup>-1</sup> min <sup>-1</sup>	↑	-	↓	NR
Confirmed or suspected heart disease Du et al. (2014)	120	Pharmacological stress agent	Higenamine intravenous infusions escalating from 0.5 to 4 mg kg <sup>-1</sup> min <sup>-1</sup>	↑	-	↓	NR
Suspected heart disease Cao et al. (2012a)	71	Suitability as pharmacological stress agent	Higenamine intravenous infusions escalating from 0.5 to 4 mg kg <sup>-1</sup> min <sup>-1</sup>	↑	-	↓	NR
heart disease Liu et al. (1983)	15	Tolerability study	2.5 mg Higenamine intravenous slow infusion	↑	NR	NR	↑
heart disease Jiang et al. (1981b)	19	effect on the function of left ventricle	2.5 mg higenamine intravenous slow infusion	↑	↑	↓	↑
Sick sinus syndrome Jiang et al. (1981a)	22	Effects on sick sinus syndrome	2.5 mg higenamine intravenous slow infusion	↑	NR	NR	NR
Heart block Bao et al. (1982)	14	effect on patients with heart block	5 mg higenamine intravenous slow infusion	↑	↑↓	↑↓	NR
Heart block Jiang et al. (1980)	68	effect on patients with heart bloc	2.5 mg higenamine intravenous slow infusion	↑	↑↓	↑↓	NR

Notes: HR, heart rate; SBP, systolic blood pressure; DBP, diastolic blood pressure. -, no change. NR, not report. Min, minute(s). ↑, increased. ↓, decreased. ↑↓, variable effects.

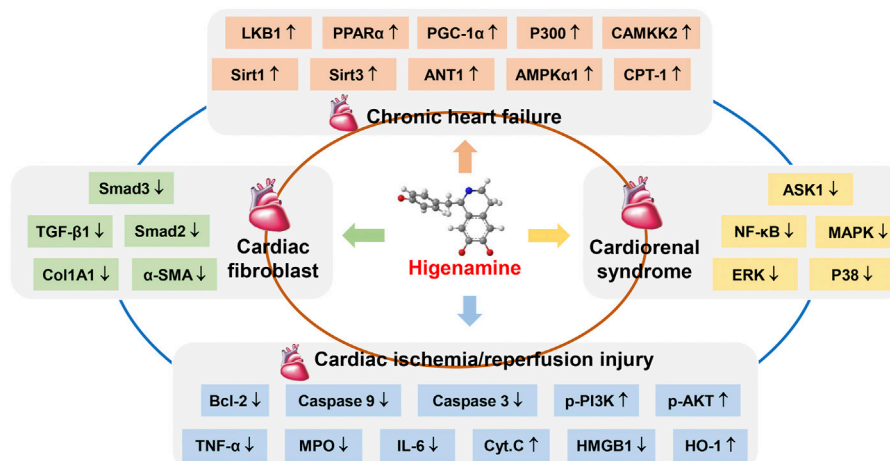


**FIGURE 2 |** The pharmacological effect of higenamine on heart disease through multiple targets. ↑, Higenamine has an agonistic effect on this target. ↓, Higenamine has an inhibitory effect on this target.

Akt signaling pathway. Wu et al. (2016), reported that higenamine inhibits apoptosis of primary neonatal rat cells and adult mouse ventricular myocytes, and reduces the levels of cleaved caspase-3 and 9 as a biochemical marker of apoptosis *in vitro*. Higenamine stimulates AKT phosphorylation and requires PI3K activation to exert anti-apoptotic effects in cardiomyocytes. The anti-apoptotic effect of higenamine is mediated by the  $\beta_2$ -AR/PI3K/AKT cascade (Table 3).

## EFFECTS OF HIGENAMINE ON HEART DISEASE IN CLINICAL

Higenamine has been clinically studied in China, which can be used as a pharmacological agent for cardiac stress test and for

the treatment of a variety of heart disease. The subjects of the clinical study included healthy volunteers, sick sinus syndrome, heart block, hypertension and other heart disease patients (Feng et al., 2012; Jiang et al., 1980; Jiang et al., 1981a; Jiang et al., 1981b; Bao et al., 1982; Liu et al., 1983; Du et al., 2007; Cao et al., 2012a; Du et al., 2014). Clinical studies on higenamine intervention in heart disease are listed in Table 4. The number of subjects included in the study ranged from 10 to 120 (Jiang et al., 1980; Jiang et al., 1981a; Jiang et al., 1981b; Bao et al., 1982; Liu et al., 1983; Du et al., 2007; Cao et al., 2012a; Feng et al., 2012; Du et al., 2014). The research objectives include pharmacokinetic and pharmacodynamics study, tolerability study, pharmacological stress agent, suitability as pharmacological stress agent, effect on the function of left ventricle, effects on sick sinus syndrome,

effect on patients with heart block, effect on patients with heart block and so on. The intervention of higenamine include intravenous infusions escalating from 0.5 to 4 mg kg<sup>-1</sup> min<sup>-1</sup> (Du et al., 2007; Cao et al., 2012a; Feng et al., 2012; Du et al., 2014), 2.5 or 5 mg higenamine intravenous slow infusion (Jiang et al., 1980a; Jiang et al., 1980b; Jiang et al., 1981; Bao et al., 1982; Liu et al., 1983). The results of the study found that higenamine could continuously increase the HR levels of subjects, but there are variable effects on systolic blood pressure (SBP), diastolic blood pressure (DBP). Higenamine has increasing effects on cardiac output, and several studies have not reported it (Table 4).

## Safety of Higenamine in the Treatment of Heart Disease

The toxic effects of higenamine mainly affect the cardiovascular and nervous systems (Chan, 2009; Chen et al., 2012). Cardiovascular features include high blood pressure, chest pain, palpitations, and bradycardia. Studies have shown that in isolated mouse atria, higenamine can enhance myocardial contractility and aconitine-induced tachyarrhythmia (Kimura et al., 1994), and increase the pulsation of cultured cardiomyocytes. Higenamine produces positive inotropic effects by acting on cardiac AR, which can enhance myocardial contractile response and reduce myocardial cell apoptosis to play a pharmacological role in the treatment of CHF (Park et al., 1984). However, higenamine caused the activation of  $\beta_1$ -AR to induce CAMKII-dependent cell death and cardiac remodeling. It shows that the toxicity of aconitum is at least partly caused by aconitine.

The median lethal dose (LD<sub>50</sub>) of higenamine in intravenous injection, intraperitoneal injection and oral administration are 58.9 mg kg<sup>-1</sup>, 300 mg kg<sup>-1</sup>, and 3.35 g kg<sup>-1</sup> in mice, respectively. Regarding cardiovascular regulation, higenamine can significantly increase blood pressure, enhance myocardial contractility, speed up HR and expand coronary blood vessels. However, the effect of higenamine in accelerating the HR and increasing myocardial oxygen consumption limits its clinical use. On the other hand, the rapid and controllable features of higenamine can be used to diagnose myocardial ischemia clinically. A study reported that 48 human subjects in the higenamine group took it daily for 8 weeks. This study found that a daily higenamine supplement for 8 weeks alone or in combination with caffeine and yohimbe bark extract do not cause substantially changes in resting HR, breathing rate, blood pressure, and liver enzyme activity of men. It shows the safety of higenamine to human subjects. It is worth noting that the saturation pharmacodynamic model fully describes the increase in the HR of healthy Chinese volunteers after giving higenamine. Zhang et al. (2002), found that the hemodynamic effects of higenamine and dobutamine on dogs were similar, and they were still tolerable even at a dose of 500  $\mu$ g kg<sup>-1</sup> min<sup>-1</sup>, and there were no serious adverse reactions. It had good safety and could be used as a substitute for dobutamine. Continuously taking higenamine capsules (50 mg per capsule) for 8 weeks, it had no significant effect on men's resting breathing rate, HR, blood pressure, urine test indicators, complete blood count, metabolic

indicators, liver enzyme activity, and blood lipids, indicating that oral higenamine has a certain degree of safety (Bloomer et al., 2015). Clinical studies have found that patients receiving higenamine treatment have been reported to have varying degree of dyspnea, palpitations, dizziness, headache, chest tightness and other adverse reactions (Cao et al., 2012b; Zhou et al., 2012). The toxic effects of higenamine mainly affect the cardiovascular and nervous systems (Chan, 2009; Chen et al., 2012). Cardiovascular features include high blood pressure, chest pain, palpitations, and bradycardia (Du et al., 2014). Higenamine can enhance myocardial contractility and aconitine-induced tachyarrhythmia, and increase the pulsation of cultured cardiomyocytes in isolated mouse atria (Kimura et al., 1994). Thus, it should be comprehensively evaluated while using higenamine for preventing, treating and diagnosing heart disease according to the actual situation during clinical use.

## CONCLUSION AND PERSPECTIVE

Higenamine hydrochloride injection is an original innovative drug with independent intellectual property rights in China, and it can be used as a diagnostic drug for cardiac stress test. Currently, higenamine has obtained the implicit permission of clinical trials. It has certain specificity and safety in the detection of coronary artery stenosis and myocardial ischemia by myocardial perfusion imaging (Zheng et al., 2005). It can be used for radionuclide myocardial perfusion imaging to assist diagnosis and evaluation of CHD and myocardial ischemia, and has completed the phase III clinical study (2004L02567), and is in the review stage of the National Medical Products Administration (Zhang et al., 2017).

This study reviewed the pharmacological effects and biological mechanisms of higenamine intervention in heart disease. Taken together, higenamine has a significant alleviate effect on heart disease such as CHF, cardiac fibroblast, CRS, and cardiac I/R injury, which could significantly increase the relative mRNA and protein expression levels of LKB1, AMPK  $\alpha$ 1, Sirt1, Sirt3, ANT1, P300, PGC-1 $\alpha$  and other targets in rat myocardial tissues and myocardial cells, and play a crucial role in the treatment of CHF by regulating PPAR $\alpha$ /PGC-1 $\alpha$  and LKB1/AMPK $\alpha$ /Sirt1 signaling pathway, which promotes mitochondrial energy metabolism and protects against CHF (Wen et al., 2019a; Wen et al., 2020c). In treatment cardiac fibroblast, higenamine inhibits the relative mRNA and protein expression of  $\alpha$ -SMA, Acta2,  $\beta$ -MHC, Smad2, and Smad3 in TGF- $\beta$ 1-induced cardiac fibroblast. In addition, higenamine reduces the expression of ECM molecules collagen I and collagen III, thereby improving pathological cardiac fibrosis and dysfunction (Zhu et al., 2021). Higenamine can improve the left ventricular remodeling and contractile function of CRS rats by reducing the expression of TGF- $\beta$ 1,  $\alpha$ -SMA, and Col1A1. In addition, higenamine significantly inhibits the relative protein expression of p-ASK1, MAPK, ERK, p38, and NF- $\kappa$ B in the heart tissues of CRS rats and cardiomyocytes. Thus, higenamine improves the heart and kidney function of CRS rats by targeting the ASK1/MAPK (ERK, P38)/NF- $\kappa$ B signaling pathway (Deng et al., 2020). Higenamine inhibits the apoptosis biochemical markers caspase 3



and 9 in primary neonatal rats and adult mouse ventricular myocytes. In intact mouse hearts, higenamine reduces I/R-induced myocardial damage and reduced lytic caspase levels in a  $\beta_2$ -AR-dependent manner. Overall, higenamine exerts anti-apoptotic and cardioprotective effects by regulating the  $\beta_2$ -AR/PI3K/AKT cascade<sup>[23]</sup> (Figure 2).

In conclusion, higenamine has a variety of cardiovascular pharmacological activities *in vivo* and *in vitro*, which has positive inotropic and positive heart strengthening effects, as well as relaxing tracheal and vascular functions. It could alleviate the conduction function of sinoatrial node cells by stimulating  $\beta$ -AR in the sinoatrial node to play the role of treating bradyarrhythmia. Higenamine exerts vasodilatory, anti-apoptotic and anti-oxidative stress effects by inhibiting  $\alpha_1$ -AR and agonizing  $\beta_2$ -AR. The vasodilator effect is used for cardiac stress test diagnosis. The anti-apoptotic and anti-oxidative stress effects can reduce myocardial I/R injury. In addition, It is often used in the treatment of HF and bradycardia and served as a cardiac stress test to diagnose coronary artery stenosis and myocardial deficiency.

Higenamine is a drug with important research value and development prospects. There are various of reports about its heart strengthening and anti-HF effects, and it has clear pharmacological effects on the cardiovascular system. At

present, it is necessary for researchers to strengthen the research on the pharmacological effects of higenamine and the deep-seated mechanism of action to help its development and clinical application.

## AUTHOR CONTRIBUTIONS

JW provided important information for the completion, wrote and amended the manuscript. ML and WZ reviewed the drafts and searched the references. HW and YB carefully checked the references. JH strictly modified the paper. CL and KD checked crucial information of this manuscript. YZ conceived and designed the study. All data were generated in-house, and no paper mill was used. All authors agree to be accountable for all aspects of work ensuring integrity and accuracy.

## FUNDING

This study was supported by the National Natural Science Foundation of China (81573631), Xihua University Talent Introduction Project (Z211060), and National Key R&D Program of China (No. 2018YFC1704500).

## REFERENCES

- Bai, X., Ding, W., Yang, S., and Guo, X. (2019). Higenamine Inhibits IL-1 $\beta$ -induced Inflammation in Human Nucleus Pulposus Cells. *Biosci. Rep.* 39, BSR20190857. doi:10.1042/BSR20190857
- Bao, Y. X., Yu, G. R., Xu, J. M., Xu, Y. Q., Bian, Y. T., and Zheng, D. S. (1982). Effect of Acute Higenamine Administration on Bradyarrhythmias and HIS Bundle. A Clinical Study of 14 Cases and Animal experiment on Dogs. *Chin. Med. J. (Engl)* 95, 781–784.
- Barnett, R., and Stallforth, P. (2018). Natural Products from Social Amoebae. *Chemistry* 24, 4202–4214. doi:10.1002/chem.201703694
- Bloomer, R. J., Schrieffer, J. M., and Gunnels, T. A. (2015). Clinical Safety Assessment of Oral Higenamine Supplementation in Healthy, Young Men. *Hum. Exp. Toxicol.* 34, 935–945. doi:10.1177/0960327114565490
- Burke, R. M., Lighthouse, J. K., Mickelsen, D. M., and Small, E. M. (2019). Sacubitril/Valsartan Decreases Cardiac Fibrosis in Left Ventricle Pressure Overload by Restoring PKG Signaling in Cardiac Fibroblasts. *Circ. Heart Fail.* 12, e005565. doi:10.1161/CIRCHEARTFAILURE.118.005565
- Calvert, R., Vohra, S., Ferguson, M., and Wiesenfeld, P. (2015). A Beating Heart Cell Model to Predict Cardiotoxicity: Effects of the Dietary Supplement Ingredients Higenamine, Phenylethylamine, Ephedrine and Caffeine. *Food Chem. Toxicol.* 78, 207–213. doi:10.1016/j.fct.2015.01.022
- Cao, Y., Wang, F., Li, B. L., Shao, G. Q., Zhang, L. L., and Wang, X. W. (2012a). Influence of Higenamine Hydrochloride Myocardial Stress Test on Heart Rate, Blood Pressure, Myocardial Oxygen Consumption. *Chin. Hosp. Pharm. J.* 32, 1353–1355. doi:10.13286/j.cnki.chinhosppharmacy.2012.17.006
- Cao, Y., Wang, F., Zhang, L. L., Wang, X. W., Shao, G. Q., Meng, Q. L., et al. (2012b). Detection of Coronary Heart Disease with 99mTc-MIBI Myocardial Perfusion Imaging Stressed by Intravenous Infusion of Higenamine Hydrochloride. *Chin. J. Nucl. Med. Mol. Imaging* 32, 203–205.
- Chan, T. Y. (2009). Aconite Poisoning. *Clin. Toxicol. (Phila)* 47, 279–285. doi:10.1080/15563650902904407
- Chen, S. P., Ng, S. W., Poon, W. T., Lai, C. K., Ngan, T. M., Tse, M. L., et al. (2012). Aconite Poisoning over 5 years: a Case Series in Hong Kong and Lessons towards Herbal Safety. *Drug Saf.* 35, 575–587. doi:10.2165/11597470-000000000-00000
- Chen, Y., Guo, B., Zhang, H., Hu, L., and Wang, J. (2019a). Higenamine, a Dual Agonist for  $\beta_1$ - and  $\beta_2$ -Adrenergic Receptors Identified by Screening a Traditional Chinese Medicine Library. *Planta. Med.* 85, 738–744. doi:10.1055/a-0942-4502
- Chen, Y. L., Zhuang, X. D., Xu, Z. W., Lu, L. H., Guo, H. L., Wu, W. K., et al. (2013). Higenamine Combined with [6]-Gingerol Suppresses Doxorubicin-Triggered Oxidative Stress and Apoptosis in Cardiomyocytes via Upregulation of PI3K/Akt Pathway. *Evid. Based. Complement. Alternat. Med.* 2013, 970490. doi:10.1155/2013/970490
- Chen, Z., Liu, Z., Peng, Y., Leng, L., Du, L., Xu, T., et al. (2019c). Cardiovascular Diseases and Natural Products. *Curr. Protein Pept. Sci.* 20, 962–963. doi:10.2174/138920372010190920124756
- Deng, T., Wei, Z., Gael, A., Deng, X., Liu, Y., Lai, J., et al. (2020). Higenamine Improves Cardiac and Renal Fibrosis in Rats with Cardiorenal Syndrome via ASK1 Signaling Pathway. *J. Cardiovasc. Pharmacol.* 75, 535–544. doi:10.1097/FJC.0000000000000822
- Dini, F. L., Bajraktari, G., Zara, C., Mumoli, N., and Rosa, G. M. (2018). Optimizing Management of Heart Failure by Using Echo and Natriuretic Peptides in the Outpatient Unit. *Adv. Exp. Med. Biol.* 1067, 145–159. doi:10.1007/5584\_2017\_137
- Doenst, T., Nguyen, T. D., and Abel, E. D. (2013). Cardiac Metabolism in Heart Failure: Implications beyond ATP Production. *Circ. Res.* 113, 709–724. doi:10.1161/CIRCRESAHA.113.300376
- Du, Y. R., Wang, Q., Li, D. F., Long, M. Q., Liu, Y. M., and Li, B. L. (2014). Efficacy and Safety of a Novel Pharmacological Stress Test Agent – Higenamine in Radionuclide Myocardial Perfusion Imaging: Phase II Clinical Trial. *Chin. J. Nucl. Med. Mol. Imaging* 34, 34–38.
- Du, Y. R., Xu, R. Y., Zhang, Y., Ouyang, M., and Jing, H. L. (2007). Tolerability of Higenamine Hydrochloride in Healthy Volunteers. *Chin. J. Clin. Pharmacol.* 23, 258–260. doi:10.13699/j.cnki.1001-6821.2007.04.012
- Ekiert, H. M., and Szopa, A. (2020). Biological Activities of Natural Products. *Molecules* 25, 5769. doi:10.3390/molecules25235769
- Feng, S., Jiang, J., Hu, P., Zhang, J. Y., Liu, T., Zhao, Q., et al. (2012). A Phase I Study on Pharmacokinetics and Pharmacodynamics of Higenamine in Healthy Chinese Subjects. *Acta Pharmacol. Sin.* 33, 1353–1358. doi:10.1038/aps.2012.114
- Frey, N., and Olson, E. N. (2003). Cardiac Hypertrophy: the Good, the Bad, and the Ugly. *Annu. Rev. Physiol.* 65, 45–79. doi:10.1146/annurev.physiol.65.092101.142243

- Guan, J., Lin, H., Xie, M., Huang, M., Zhang, D., Ma, S., et al. (2019). Higenamine Exerts an Antispasmodic Effect on Cold-Induced Vasoconstriction by Regulating the PI3K/Akt, ROS/ $\alpha$ 2C-AR and PTK9 Pathways Independently of the AMPK/eNOS/NO axis. *Exp. Ther. Med.* 18, 1299–1308. doi:10.3892/etm.2019.7656
- Han, H. W., Wang, J. Z., and Sun, F. L. (1981). Effect of DL-Demethylcoclaurine on Cultured Rat Heart Cells Author's Transl. *Zhongguo Yao Li Xue Bao* 2, 111–114.
- Han, S. L., Chen, J. L., Yang, L. F., and Zhang, L. (2021). Synthesis and Characterization of Stable Isotope Deuterium-Labelled Higenamine. *J. Isotopes* 34, 317–324. doi:10.7538/tws.2021.34.04.0317
- Harvey, A. L., Edrada-Ebel, R., and Quinn, R. J. (2015). The Re-emergence of Natural Products for Drug Discovery in the Genomics Era. *Nat. Rev. Drug Discov.* 14, 111–129. doi:10.1038/nrd4510
- Herr, D. J., Singh, T., Dhammu, T., and Menick, D. R. (2020). Regulation of Metabolism by Mitochondrial Enzyme Acetylation in Cardiac Ischemia-Reperfusion Injury. *Biochim. Biophys. Acta Mol. Basis. Dis.* 1866, 165728. doi:10.1016/j.bbdis.2020.165728
- Hudzik, T. J., Patel, M., and Brown, A. (2021).  $\beta$ 2-Adrenoceptor Agonist Activity of Higenamine. *Drug Test. Anal.* 13, 261–267. doi:10.1002/dta.2992
- Jiang, W. Q., Liu, X. J., Tao, S. Q., Li, J. M., Zhao, S. H., and Guo, X. Z. (1981). Clinical Study of the Effect of Higenamine on Ejection Fraction and Bradycardia. *Chin. J. Integr. Trad. West. Med.* 161, 667–668.
- Jiang, W. Q., Tao, S. C., Chen, K. J., Zang, W. C., Zun, Q. Y., GuQian, F. S., et al. (1980). Effects of Acute Administration of Higenamine on Bradycardia: a Preliminary Clinical Study Author's Transl. *Zhonghua Xin Xue Guan Bing Za Zhi* 8, 95–98.
- Jiang, W. Q., Tao, S. Q., Li, J. M., Zhao, S. H., and Guo, X. Z. (1981a). Clinical Electrophysiology Study of the Effects of Higenamine (Fuji One) on Sick Sinus Syndrome. *Chin. J. Integr. Trad. West. Med.* 4, 30–31.
- Kimura, I., Chui, L. H., Fujitani, K., Kikuchi, T., and Kimura, M. (1989). Inotropic Effects of (+/-)-higenamine and its Chemically Related Components, (+)-R-Coclaurine and (+)-S-Reticuline, Contained in the Traditional Sino-Japanese Medicines "bushi" and "Shin-I" in Isolated guinea Pig Papillary Muscle. *Jpn. J. Pharmacol.* 50, 75–78. doi:10.1254/jjp.50.75
- Kimura, I., Islam, M. A., and Kimura, M. (1996). Potentiation by Higenamine of the Aconitine-Induced Positive Chronotropic Effect in Isolated Right Atria of Mice: the Effects of Cholera Toxin, Forskolin and Pertussis Toxin. *Biol. Pharm. Bull.* 19, 1032–1037. doi:10.1248/bpb.19.1032
- Kimura, I., Makino, M., Takamura, Y., Islam, M. A., and Kimura, M. (1994). Positive Chronotropic and Inotropic Effects of Higenamine and its Enhancing Action on the Aconitine-Induced Tachycardia in Isolated Murine Atria. *Jpn. J. Pharmacol.* 66, 75–80. doi:10.1254/jjp.66.75
- Kosuge, T., and Yokota, M. (1976). Letter: Studies on Cardiac Principle of Aconite Root. *Chem. Pharm. Bull. (Tokyo)* 24, 176–178. doi:10.1248/cpb.24.176
- Lee, Y. S., Kang, Y. J., Kim, H. J., Park, M. K., Seo, H. G., Lee, J. H., et al. (2006). Higenamine Reduces Apoptotic Cell Death by Induction of Heme Oxygenase-1 in Rat Myocardial Ischemia-Reperfusion Injury. *Apoptosis* 11, 1091–1100. doi:10.1007/s10495-006-7110-y
- Li, Y. L., Tian, M., Yu, J., Shang, M. Y., and Cai, S. Q. (2020). Studies on morphology and aristolochic acid analogue constituents of Asarum campaniflorum and a comparison with two official species of Asari radix et rhizoma. *J. Nat. Med.* 64, 442–451. doi:10.1007/s11418-010-0433-6
- Liu, X. J., Wagner, H. N., Jr., and Tao, S. (1983). Measurement of Effects of the Chinese Herbal Medicine Higenamine on Left Ventricular Function Using a Cardiac Probe. *Eur. J. Nucl. Med.* 8, 233–236. doi:10.1007/BF00522511
- Liu, Y., Xu, J., Wu, M., Kang, L., and Xu, B. (2020). The Effector Cells and Cellular Mediators of Immune System Involved in Cardiac Inflammation and Fibrosis after Myocardial Infarction. *J. Cel. Physiol.* 235, 8996–9004. doi:10.1002/jcp.29732
- Lo, C. F., and Chen, C. M. (1994). Determination of Higenamine in Plasma and Urine by High-Performance Liquid Chromatography with Electrochemical Detection. *J. Chromatogr. B. Biomed. Appl.* 655, 33–39. doi:10.1016/0378-4347(94)00023-9
- Lo, C. F., and Chen, C. M. (1996). Pharmacokinetics of Higenamine in Rabbits. *Biopharm. Drug Dispos.* 17, 791–803. doi:10.1002/(SICI)1099-081X(199612)17:9<791::AID-BDD993>3.0.CO;2-T
- Martínez-Martínez, E., Brugnolaro, C., Ibarrola, J., Ravassa, S., Buonafina, M., López, B., et al. (2019). CT-1 (Cardiotrophin-1)-Gal-3 (Galectin-3) Axis in Cardiac Fibrosis and Inflammation. *Hypertension* 73, 602–611. doi:10.1161/HYPERTENSIONAHA.118.11874
- Neubauer, S. (2007). The Failing Heart-Aan Engine Out of Fuel. *N. Engl. J. Med.* 356, 1140–1151. doi:10.1056/NEJMra063052
- Nuntawong, P., Tanaka, H., Sakamoto, S., and Morimoto, S. (2020). ELISA for the Detection of the Prohibited Doping Agent Higenamine. *Planta. Med.* 86, 760–766. doi:10.1055/a-1181-2084
- Park, C. W., Chang, K. C., and Lim, J. K. (1984). Effects of Higenamine on Isolated Heart Adrenoceptor of Rabbit. *Arch. Int. Pharmacodyn. Ther.* 267, 279–288. doi:10.1016/0378-7796(84)90012-9
- Pyo, M. K., Kim, J. M., Jin, J. L., Chang, K. C., Lee, D. H., and Yun-Choi, H. S. (2017). Effects of Higenamine and its 1-naphthyl Analogs, YS-49 and YS-51, on Platelet TXA2 Synthesis and Aggregation. *Thromb. Res.* 120, 81–86. doi:10.1016/j.thromres.2006.07.006
- Rangaswami, J., Bhalla, V., Blair, J. E. A., Chang, T. I., Costa, S., Lentine, K. L., et al. (2019). Cardiorenal Syndrome: Classification, Pathophysiology, Diagnosis, and Treatment Strategies: A Scientific Statement from the American Heart Association. *Circulation* 139, e840–e878. doi:10.1161/CIR.0000000000000664
- Shin, J. S., Yun-Choi, H. S., Kim, E. I., and Lee, M. K. (1999). Inhibitory Effects of Higenamine on Dopamine Content in PC12 Cells. *Planta. Med.* 65, 452–455. doi:10.1055/s-2006-960810
- Tibaut, M., Mekis, D., and Petrovic, D. (2017). Pathophysiology of Myocardial Infarction and Acute Management Strategies. *Cardiovasc. Hematol. Agents Med. Chem.* 14, 150–159. doi:10.2174/1871525714666161216100553
- Tsukiyama, M., Ueki, T., Yasuda, Y., Kikuchi, H., Akaishi, T., Okumura, H., et al. (2009). Beta2-adrenoceptor-mediated Tracheal Relaxation Induced by Higenamine from Nandina Domestica Thunberg. *Planta. Med.* 75, 1393–1399. doi:10.1055/s-0029-1185743
- Ueki, T., Akaishi, T., Okumura, H., Morioka, T., and Abe, K. (2011). Biphasic Tracheal Relaxation Induced by Higenamine and Nantenine from Nandina Domestica THUNBERG. *J. Pharmacol. Sci.* 115, 254–257. doi:10.1254/jphs.10251SC
- Wang, R., Xiong, X., Yang, M., He, S., and Xu, X. (2020). A Pharmacokinetics Study of Orally Administered Higenamine in Rats Using LC-MS/MS for Doping Control Analysis. *Drug Test. Anal.* 12, 485–495. doi:10.1002/dta.2756
- Wang, Y., Geng, J., Jiang, M., Li, C., Han, Y., and Jiang, J. (2019). The Cardiac Electrophysiology Effects of Higenamine in guinea Pig Heart. *Biomed. Pharmacother.* 109, 2348–2356. doi:10.1016/j.biopha.2018.10.022
- Wen, J., Ma, X., Niu, M., Hao, J., Huang, Y., Wang, R., et al. (2020b). Metabolomics Coupled with Integrated Approaches Reveal the Therapeutic Effects of Higenamine Combined with [6]-gingerol on Doxorubicin-Induced Chronic Heart Failure in Rats. *Chin. Med.* 15, 120. doi:10.1186/s13020-020-00403-0
- Wen, J., Wang, J., Li, P., Wang, R., Wang, J., Zhou, X., et al. (2019a). Corrigendum to "Protective Effects of Higenamine Combined with [6]-gingerol against Doxorubicin-Induced Mitochondrial Dysfunction and Toxicity in H9c2 Cells and Potential Mechanisms" [Biomed. Pharmacother. 115 (2019) 108881]. *Biomed. Pharmacother.* 115, 108936. doi:10.1016/j.biopha.2019.108881
- Wen, J., Zhang, L., Wang, J., Wang, J., Wang, L., Wang, R., et al. (2020c). Therapeutic Effects of Higenamine Combined with [6]-gingerol on Chronic Heart Failure Induced by Doxorubicin via Ameliorating Mitochondrial Function. *J. Cel. Mol. Med.* 24, 4036–4050. doi:10.1111/jcmm.15041
- Wen, J., Zou, W., Wang, R., Liu, H., Yang, Y., Li, H., et al. (2019b). Cardioprotective Effects of Aconiti Lateralis Radix Praeparata Combined with Zingiberis Rhizoma on Doxorubicin-Induced Chronic Heart Failure in Rats and Potential Mechanisms. *J. Ethnopharmacol.* 238, 111880. doi:10.1016/j.jep.2019.111880
- Wen, J. X., Li, R. S., Wang, J., Hao, J. J., Qin, W. H., Yang, T., et al. (2020a). Therapeutic Effects of Aconiti Lateralis Radix Praeparata Combined with Zingiberis Rhizoma on Doxorubicin-Induced Chronic Heart Failure in Rats Based on an Integrated Approach. *J. Pharm. Pharmacol.* 72, 279–293. doi:10.1111/jphp.13191
- Weng, J. H., and Sun, S. M. (2020). Effects of Noraconitine on the Proliferation and Migration of Rat Aortic Smooth Muscle Cells. *Jiangsu J. Traditional Chin. Med.* 52, 87–90. doi:10.3969/j.issn.1672-397X.2020.01.027

- Wilhelmi, T., Xu, X., Tan, X., Hulshoff, M. S., Maamari, S., Sossalla, S., et al. (2020). Serelaxin Alleviates Cardiac Fibrosis through Inhibiting Endothelial-To-Mesenchymal Transition via RXFP1. *Theranostics* 10, 3905–3924. doi:10.7150/thno.38640
- Wu, M. P., Zhang, Y. S., Zhou, Q. M., Xiong, J., Dong, Y. R., and Yan, C. (2016). Higenamine Protects Ischemia/reperfusion Induced Cardiac Injury and Myocyte Apoptosis through Activation of  $\beta_2$ -AR/PI3K/AKT Signaling Pathway. *Pharmacol. Res.* 104, 115–123. doi:10.1016/j.phrs.2015.12.032
- Yang, S., Chu, S., Ai, Q., Zhang, Z., Gao, Y., Lin, M., et al. (2020). Anti-inflammatory Effects of Higenamine (Hig) on LPS-Activated Mouse Microglia (BV2) through NF-Kb and Nrf2/HO-1 Signaling Pathways. *Int. Immunopharmacol.* 85, 106629. doi:10.1016/j.intimp.2020.106629
- Zhang, N., Lian, Z., Peng, X., Li, Z., and Zhu, H. (2017). Applications of Higenamine in Pharmacology and Medicine. *J. Ethnopharmacol.* 196, 242–252. doi:10.1016/j.jep.2016.12.033
- Zhang, N., Qu, K., Wang, M., Yin, Q., Wang, W., Xue, L., et al. (2019). Identification of Higenamine as a Novel  $\alpha_1$ -adrenergic Receptor Antagonist. *Phytother. Res.* 33, 708–717. doi:10.1002/ptr.6261
- Zhang, Z., Liu, X., Tao, Z., Shi, R., Zhang, X., Yao, Z., et al. (2002). Effects of Higeramine on Hemodynamics and its Tolerability and Safety, an Experimental Study. *Zhonghua Yi Xue Za Zhi* 82, 352–355. doi:10.3760/j.issn:0376-2491.2002.05.019
- Zheng, Y. L., Shen, R., Yang, M. F., Gu, D. L., Fang, L., Zhang, Z., et al. (2005). Experimental Study of Pharmaceutic Stress Myocardial Perfusion Imaging with Higenamine. *Zhonghua Xin Xue Guan Bing Za Zhi* 33, 473–475. doi:10.3760/j.issn:0253-3758.2005.05.019
- Zheng, Y. L., Zhang, Z., Chen, B. L., Wang, K., Xue, L. M., Fang, L., et al. (2004). Determination of Higenamine in Plasma by HPLC-ECD and Study on its Pharmacokinetics. *Chin. Pharm. J.* 39, 848–850. doi:10.3321/j.issn:1001-2494.2004.11.017
- Zhou, W., Wang, F., Zhang, L. L., Jiang, Y., Wang, M., and Ye, F. (2012). Myocardial Perfusion Imaging with Higenamine Hydrochloride Stress Studies in Diagnosis of Coronary Artery Disease. *Chin. J. Nucl. Med. Mol. Imaging* 32, 408–412. doi:10.3760/cma.j.issn.2095-2848.2012.06.002
- Zhu, J. X., Ling, W., Xue, C., Zhou, Z., Zhang, Y. S., Yan, C., et al. (2021). Higenamine Attenuates Cardiac Fibroblast Abstract and Fibrosis via Inhibition of TGF- $\beta$ 1/Smad Signaling. *Eur. J. Pharmacol.* 900, 174013. doi:10.1016/j.ejphar.2021.174013

**Conflict of Interest:** The authors declare that the research was conducted in the absence of any commercial or financial relationships that could be construed as a potential conflict of interest.

**Publisher's Note:** All claims expressed in this article are solely those of the authors and do not necessarily represent those of their affiliated organizations, or those of the publisher, the editors and the reviewers. Any product that may be evaluated in this article, or claim that may be made by its manufacturer, is not guaranteed or endorsed by the publisher.

Copyright © 2022 Wen, Li, Zhang, Wang, Bai, Hao, Liu, Deng and Zhao. This is an open-access article distributed under the terms of the Creative Commons Attribution License (CC BY). The use, distribution or reproduction in other forums is permitted, provided the original author(s) and the copyright owner(s) are credited and that the original publication in this journal is cited, in accordance with accepted academic practice. No use, distribution or reproduction is permitted which does not comply with these terms.

## GLOSSARY

**CAD** Coronary artery disease

**CHF** Chronic heart failure

**I/R** Ischemia/reperfusion

**CRS** Cardiorenal syndrome

**TCM** Traditional Chinese medicine

**ALRP** Aconiti lateralis radix praeparata

**AR** Adrenergic receptors

**HR** Heart rate

**CFDA** China food and drug administration

**CHD** Coronary heart disease

**CNKI** China national knowledge infrastructure

**VMIS** VIP medicine information system

**CBM** Chinese biomedical database

**AUC** Area under the concentration-time curve

**CL** Total clearance

**NR** Not report

**HF** Heart failure

**DOX** Doxorubicin

**LVSP** Left ventricular systolic pressure

**+dp/dtmax** Left ventricular pressure

**LVEDP** Left ventricular end-diastolic pressure

**Ang-II** Angiotension II

**ALD** Aldosterone

**ET-1** Endothelin-1

**BNP** Brain natriuretic peptide

**LDH** Lactate dehydrogenase

**CK-MB** Creatine kinase-MB

**AST** Aspartate aminotransferase

**ATP** Adenosine triphosphate

**NAD** Nicotinamide adenine dinucleotide

**RAAS** Renin-angiotensin-aldosterone system

**MI** Myocardial infarction

**HO-1** Heme oxygenase-1

**IHD** Ischemic heart disease

**ECM** Extracellular matrix

**EndMT** Endothelial-to-mesenchymal transition

**TAC** Transverse aortic constriction

**ISO** Isoproterenol

**STNx** Subtotal nephrectomy

**i.p** Intraperitoneal injection

**FS** Fractional shortening

**EF** Ejection fraction

**LVVs** Left ventricular volumes

**HW/TL** Heart weight to tibia length

**HW/BW** Ratio of heart weight to body weight

**β-MHC** β-Myosin heavy chain

**ANP** A-Type natriuretic peptide

**LVEF%** LV ejection fraction

**LVFS%** Left ventricular fraction shortening

**LVESV** LV end systolic volume

**LVPW** LV posterior wall thickness

**CWI** Cardiac weight index

**KWI** Kidney weight index

**Scr** Serum creatinine

**BUN** Blood urea nitrogen

**IS** Indole sulfate

**α-SMA** α-Smooth muscle actin

**TGF-β1** Transforming growth factor-β1

**p-ASK1** Phosphorylated apoptosis signal-regulated kinase 1

**MAPK** Mitogen-activated protein kinases

**PE** Phenylephrine

**OCR** Oxygen consumption rate

**ECAR** Extracellular acidification rate

**AMCM** Adult mouse cardiac myocytes

**AMVM** Adult mouse ventricular myocytes

**NRCF** Neonatal rat cardiac fibroblasts

**NRCM** Neonatal rat cardiac myocyte

**NRVM** Neonatal rat ventricular myocytes

**SK** SK-N-MC cell

**SBP** Systolic blood pressure

**DBP** Diastolic blood pressure

**LD50** Median lethal dose





# Traditional Chinese Medicine Targeting Heat Shock Proteins as Therapeutic Strategy for Heart Failure

Yanchun Wang<sup>1</sup>, Junxuan Wu<sup>2</sup>, Dawei Wang<sup>2\*</sup>, Rongyuan Yang<sup>3\*</sup> and Qing Liu<sup>3\*</sup>

<sup>1</sup>Shenyang the Tenth People's Hospital, Shenyang, China, <sup>2</sup>Shunde Hospital of Guangzhou University of Chinese Medicine, Foshan, China, <sup>3</sup>The Second Clinical School of Medicine, Guangzhou University of Chinese Medicine, Guangdong Provincial Hospital of Chinese Medicine-Zhuhai Hospital, Zhuhai, China

## OPEN ACCESS

### Edited by:

Xianwei Wang,  
Xinxiang Medical University, China

### Reviewed by:

Yusuf Tutar,  
University of Health Sciences, Turkey  
Min Wu,  
China Academy of Chinese Medical  
Sciences, China  
Hongcai Shang,  
Beijing University of Chinese Medicine,  
China

### \*Correspondence:

Qing Liu  
851757626@qq.com  
Dawei Wang  
davidwang33@139.com  
Rongyuan Yang  
yangrongyuan@163.com

### Specialty section:

This article was submitted to  
Cardiovascular and Smooth Muscle  
Pharmacology,  
a section of the journal  
Frontiers in Pharmacology

**Received:** 13 November 2021

**Accepted:** 21 December 2021

**Published:** 18 January 2022

### Citation:

Wang Y, Wu J, Wang D, Yang R and  
Liu Q (2022) Traditional Chinese  
Medicine Targeting Heat Shock  
Proteins as Therapeutic Strategy for  
Heart Failure.  
Front. Pharmacol. 12:814243.  
doi: 10.3389/fphar.2021.814243

Heart failure (HF) is the terminal stage of multifarious heart diseases and is responsible for high hospitalization rates and mortality. Pathophysiological mechanisms of HF include cardiac hypertrophy, remodeling and fibrosis resulting from cell death, inflammation and oxidative stress. Heat shock proteins (HSPs) can ameliorate folding of proteins, maintain protein structure and stability upon stress, protect the heart from cardiac dysfunction and ameliorate apoptosis. Traditional Chinese medicine (TCM) regulates expression of HSPs and has beneficial therapeutic effect in HF. In this review, we summarized the function of HSPs in HF and the role of TCM in regulating expression of HSPs. Studying the regulation of HSPs by TCM will provide novel ideas for the study of the mechanism and treatment of HF.

**Keywords:** heat shock proteins, heart failure, traditional Chinese medicine, myocardial injury, therapeutic targets

## INTRODUCTION

Heart failure (HF) is a clinical syndrome that is characterized by impaired myocardial structure or ventricular contraction/diastolic function and it causes insufficient cardiac output (Yancy et al., 2013). HF is a critical health problem that affects 26 million people worldwide, and an estimated 17–45% of patients with HF admitted to hospital die within 1 year of admission. Most patients die within 5 years after admission (Ambrosy et al., 2014; Ponikowski et al., 2014). The recommended pharmacological treatments for HF include angiotensin-converting enzyme inhibitors (ACEI), angiotensin receptor blockers (ARB), angiotensin receptor neprilysin inhibitor (ARNI), I<sub>f</sub> channel inhibitor,  $\beta$ -adrenergic blockers and diuretics. Recommended treatments are able to reduce hospitalizations, morbidity and mortality, but can have severe side effects like angioedema, electrolyte depletion and fluid depletion (Yancy et al., 2017). Therefore, developing new therapeutic methods and medicine will be of great significance in the treatment of HF.

Heat shock proteins (HSPs) are a group of conserved proteins with multiple biological activities (Stetler et al., 2010). Previous studies reveal the vital role played by HSPs in HF (Ranek et al., 2018). Therefore, it would be imperative to focus on regulation of HSPs in the treatment of HF. Traditional Chinese Medicine (TCM) contains numerous chemical components and active ingredients, which can regulate expression of HSPs in various diseases (Yang et al., 2017a; Kunde et al., 2017; Zhou et al., 2018; Zhao et al., 2020). Furthermore, TCM can improve cardiac function and ameliorate damage caused by HF (Wang et al., 2017a). Recent studies suggest that TCM can alter expression of HSPs in HF (Wang et al., 2014; Zhang et al., 2018a; Nie et al., 2019). Consequently, TCM may regulate expression of HSPs to treat HF. We therefore summarized the role of HSPs in the pathogenesis of HF,

effects of TCM in regulating HSPs and action of TCM targeting HSPs in treating HF to enhance our understanding of the mechanisms in HF, and provide novel ideas for its application as a therapeutic strategy of HF.

## HSPS FAMILY

HSPs widely occur in eukaryotic cells and can respond to multiple stimuli, high temperature, lack of nutrients, energy depletion, aging, oxidative stress, acute and chronic inflammatory reactions, viral and bacterial infections, ischemia, heavy metals and excessive exercise (Kregel, 1985; 2002). HSPs have a variety of biological functions. The most crucial role is they act as molecular chaperones which ensure correct folding of newly synthesized proteins, facilitating refolding of misfolded proteins upon stress, and maintaining protein structure and stability (Stetler et al., 2010). HSPs is divided into the following six families according to their relative molecular masses; HSP110, HSP90, HSP70, HSP60, HSP40, and small HSPs (HSPs).

HSP110 is a high molecular weight HSP belonging to HSP70 superfamily. Its expression is also induced by stress, and it cooperates with other HSPs to facilitate refolding of proteins and cell survival (Zuo et al., 2016).

HSP90 is a highly conserved ATP-dependent molecular chaperone that is involved in homeostasis and folding of proteins (Wu et al., 2017). The HSP90 family has two isoforms which occur in the cytoplasm: 1) stress-inducible HSP90 $\alpha$  and 2) a constitutively expressed HSP90 $\beta$ .

HSP70 family is by far the most widely studied group of HSPs which generally occur in the cytoplasm and nucleus (Shrestha and Young, 2016). HSP70 acts in an ATP-dependent manner, and its family includes inducible HSP70, constitutively expressed HSP70 and glucose-regulated protein 78 (GRP78). The chaperone protein, HSP70 is principally dedicated to the degradation of unstable and misfolded proteins and refolding of proteins, preventing and dissolving protein complexes, and stabilizing cellular homeostasis (Daugaard et al., 2007). GRP78 belongs to the HSP70 family and plays an essential role in attenuating endoplasmic reticulum (ER) stress. ER is a cellular organelle responsible for storage of calcium, protein synthesis and folding, and lipid metabolism (Schwarz and Blower, 2016). Ischemia, hypoxia, disruption of calcium homeostasis, ATP depletion, and oxidative stress result in accumulation of unfolded proteins in the ER subsequently causing endoplasmic reticulum (ER) stress. This initiates unfolded protein response (UPR) to maintain homeostasis in the ER (Minamino et al., 2010). However, sustained UPR can cause cell death. Consequently, expression of GRP78 is increased acting as a quality control system.

HSP60 is a chaperone protein that forms a complex with the chaperone protein, HSP10 to promote protein folding. HSP60 mainly exists in the mitochondria, but can also be distributed within the cytoplasm, cell membrane and extracellular matrix (Rizzo et al., 2011).

Small HSPs are a group of proteins which are small size (12–42 kDa) and are present in the cytoplasm and nucleus.

Small HSPs include HSP20, HSP27, heme oxygenase-1 (HO-1), and  $\alpha$ B-crystallin (CRYAB). HSPs are involved in the regulation of anti-oxidants, anti-apoptosis, muscle contraction and cell motility, which can prevent irreversible aggregation of damaged proteins in an ATP-independent manner and protect cells under unfavorable conditions (Mymrikov et al., 2011).

## FUNCTION OF HSPS IN HF

HSPs participate in a wide range of biological activities, can contribute to intracellular homeostasis in cells and counteract pathological factors. Previous studies have investigated changes in the expression of HSPs in HF and the effects of overexpressed/deficient HSPs in HF. In this review, we have summarized recent advances in functions of HSPs in HF (**Figure 1**; **Table 1**).

### HSP110

HSPA4 is a member of the HSP110 family that acts as a nucleotide exchange factor for HSP70 chaperones. Expression of HSPA4 was significantly elevated in hearts of mice subjected to TAC (Mohamed et al., 2012). HSPA4 is essential in ensuring proper folding of proteins and maintaining homeostasis in cardiomyocytes. Deletion of HSPA4 accelerates cardiac hypertrophy and fibrosis (Mohamed et al., 2012).

### HSP90

Expression of HSP90 was decreased in animals treated with fluoride (Panneerselvam et al., 2017), and no significant change was observed after CAL in comparison with control group (Tanonaka et al., 2001a), whereas expression of HSP90 increased in patients with DCM (Kapustian et al., 2013). DCM alters distribution of HSP90 in cells: mitochondrial HSP90 content was increased in the left ventricular myocardium of individuals with DCM (Kapustian et al., 2013). HSP90 can have a detrimental effect on HF and cardiac hypertrophy. Inhibiting functional expression of HSP90 can attenuate cardiac hypertrophy and reduce collagen deposition. HSP90 facilitates regulation of Raf/Mek/ERK, transformation of growth factor- $\beta$  (TGF- $\beta$ ) and NF- $\kappa$ B pathways in cardiac hypertrophy which are either induced by MI or pressure overload (Lee et al., 2010; Datta et al., 2015; Tamura et al., 2019). Mice with cardiac-specific overexpressed HSP75 (a member of HSP90 family located in the mitochondria) may attenuate hypertrophy and fibrosis in response to pressure overload. Protection depends on the inhibitory effect of HSP75 in regulating MAPK and Akt pathways by reducing phosphorylation of p38, JNK and Akt (Zhang et al., 2011).

### HSP70

Previous studies have proven the protective function of HSP70s in HF. Expression of HSP70 in HF varies with models. Levels of intracellular HSP70 were elevated in patients with HF of arrhythmogenic right ventricular cardiomyopathy (ARVC), ischemic cardiomyopathy (ICM) and DCM (Wei et al., 2009). Nonetheless, expression of HSP70 remained unchanged at 8 w after CAL in rats in comparison with the control group,

**TABLE 1 |** The functions of heat shock proteins in heart failure.

HSP family	Function	Model	Protective/ adverse effects of HSPs in HF	Ref
HSP110	HSPA4 deletion leads to cardiac hypertrophy and fibrosis	HSPA4 knockout mice that subjected to transverse aortic constriction and volume overload	protective	Mohamed et al. (2012)
HSP90	Inhibition of HSP90 improves cardiac function	Rats that subjected to CAL.	adverse	Tamura et al. (2019)
	HSP90 can regulate cardiac hypertrophy and collagen deposition	Mice overexpression of HSP75 (a member of HSP90 family located in the mitochondria)	adverse	Lee et al. (2010); Datta et al. (2015); Tamura et al. (2019), Zhang et al. (2011)
	HSP90 facilitates regulation of Raf/Mek/ERK, TGF- $\beta$ and NF- $\kappa$ B pathways in cardiac hypertrophy	Mice overexpression of HSP75	adverse	Lee et al. (2010); Datta et al. (2015); Tamura et al. (2019), Zhang et al. (2011)
	Interacts with TGF $\beta$ receptor-II and exerts profibrotic effect	Rats that subjected to renal artery ligation; Cardiac fibroblasts that subjected to Ang II and Celastrol	adverse	Datta et al. (2015)
	Interacts with IKK complex, leads to NF- $\kappa$ B activation	Ang II-induced cardiac myocytes	adverse	Lee et al. (2010)
	HSP75 downregulates TAK, p38, JNK, and Akt phosphorylation levels	Cardiac-specific HSP75 transgenic mice that subjected to aortic banding	protective	Zhang et al. (2011)
HSP70	Maintains cardiac contractility and calcium handling	HSP70-knockout mice that subjected to I/R	protective	Kim et al. (2006)
	Inhibits p53 activation and its downstream bax, caspase-3 and caspase-9	DOX-induced HSP70 overexpress transgenic mice	protective	Naka K et al. (2014)
	Does not improve cardiac function in failing hearts with atrial fibrillation	Cardiac-specific MURC mice and MURC-HSP70 mice	Undetermined	Bernardo et al. (2015)
	Both intracellular and extracellular HSP70 regulates myocardial hypertrophy, cardiac dysfunction and cardiac fibrosis	Mice that subjected to abdominal aortic constriction (AAC)	adverse	Cai et al. (2010)
	Extracellular HSP70 promotes cardiac hypertrophy and fibrosis	Mice that subjected to abdominal aortic constriction (AAC)	adverse	Cai et al. (2010)
	Extracellular HSP70 activates TLR2 signaling	TLR2/4 knockout mice that subjected to transverse aortic constriction (TAC). Mice treated with anti-HSP70 antibody and DOX.	adverse	Higashikuni et al. (2013), Liu et al. (2019)
	GRP78 attenuates ER stress and cell death	Neonatal cardiomyocytes that subjected to MG132, epoxomicin or tunicamycin	protective	Fu et al. (2008)
HSP60	Inhibits caspase-3 activation, interacts with bax and bcl-x	HSP60 and HSP10 overexpressed myocytes that subjected to DOX.	protective	Shan et al. (2003)
	Interacts with bak and bax in cytoplasm	Myocytes that subjected to antisense phosphorothioate oligonucleotide to reduce HSP60	protective	Kirchhoff et al. (2002)
	Maintains mitochondrial homeostasis function	Cardiac-specific HSP60 knockout mice	protective	Fan et al. (2020)
	Extracellular HSP60 activates TLR4 and triggers inflammation	Cardiomyocytes of rats that subjected to LAD.	adverse	Liu et al. (2015)
small HSPs—HSP27	Enhances the SOD activity, increases cell survival	DOX-induced cardiac H9c2 cells and mouse embryonic fibroblasts	protective	Turakhia et al. (2007)
	Improves cardiac function, suppresses oxidative stress and decreases apoptosis	DOX-induced cardiac specific-overexpressed HSP27 mice	protective	Liu et al. (2007a)
	Increases phosphorylation of Akt and GSK-3 $\beta$ , decreases NF- $\kappa$ B activation	LPS-induced cardiac-specific expression of Hsp27 and H9c2	protective	You et al. (2009)
	Preserves mitochondrial function	Rats that subjected to coronary artery ligation (CAL)	protective	Marunouchi et al. (2013c), (Marunouchi et al. (2014)
	Interacts with SIRT1; increases p53 acetylation and bax when be downregulated	Transfected H9c2 cells that subjected to DOX.	protective	Zhang et al. (2016a)
	High level HSP27 causes reductive stress and develops cardiac dysfunction	HSP27 transgenic mice	adverse	Yu et al. (2015), Zhang et al. (2010)
	Binds to p53 and increases bax contents	DOX-induced HSF-1 knockout mice	protective	Vedam et al. (2010)

(Continued on following page)

**TABLE 1 |** (Continued) The functions of heat shock proteins in heart failure.

HSP family	Function	Model	Protective/ adverse effects of HSPs in HF	Ref
small HSPs—HSP20	HSP20 reverse cardiac remodeling, fibrosis and hypertrophy	ISO-induced cardiac-specific overexpressed HSP20 mice and H9c2 cells	protective	Fan et al. (2006)
	Ameliorates cardiac dysfunction and suppresses ASK1 activation	ISO-induced cardiac-specific overexpressed HSP20 mice and H9c2 cells	protective	Fan et al. (2006)
	Inhibits NF- $\kappa$ B activation and caspase-3 activity	LPS-induced Ad. HSP20-AS-infected rat cardiomyocytes	protective	Wang et al. (2009)
	Preserves Akt activation, improves cardiac function	DOX-induced cardiac-specific overexpressed HSP20 mice	protective	Fan et al. (2008)
small HSPs—HO-1	Reduces oxidative stress and preserves mitochondrial function	Cardiac-specific HO-1 transgenic mice that subjected to CAL.	protective	Wang et al. (2010b)
	Preserves cardiac function	AAV-human HO-1 treated rats that subjected to LAD.	protective	Liu et al. (2007b)
	Increases Akt activation and decreases apoptosis	Ang II-induced myocytes that transfected with human HO-1	protective	Foo et al. (2006)
	Exerts either protective or detrimental effect	Cardiac-specific HO-1 mice that subjected to either TAC or ISO.	Dual	Allwood et al. (2014)

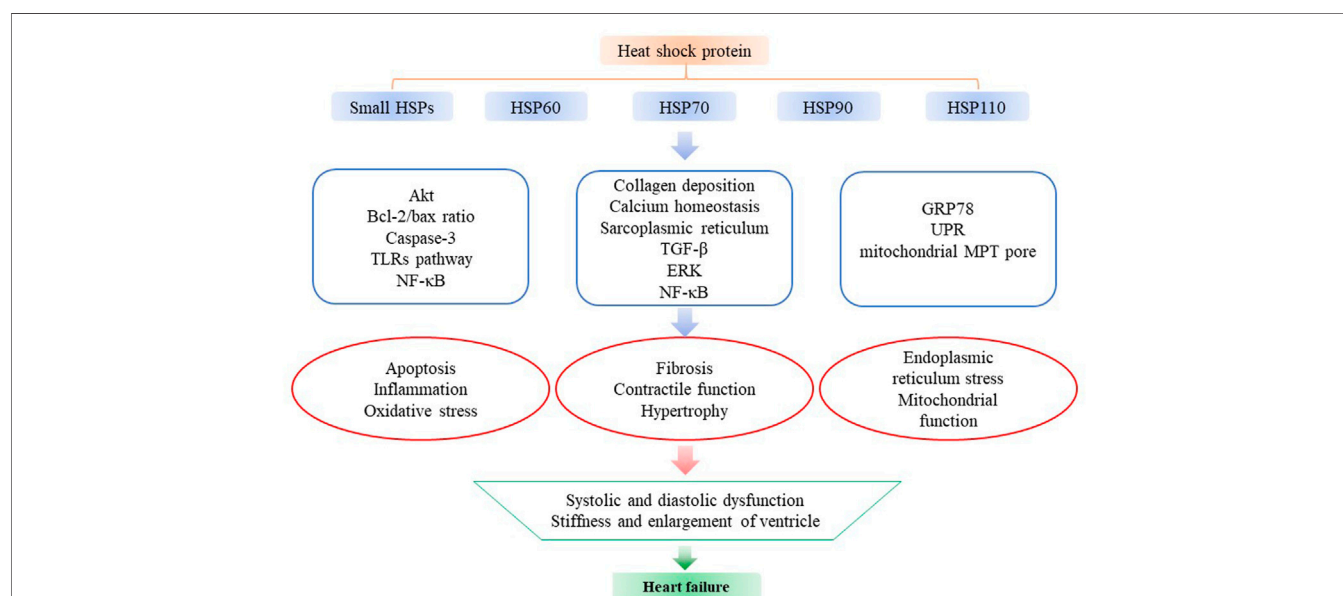


**FIGURE 1 |** The functions of heat shock proteins in HF. Small HSPs (HSP27, HSP20, HO-1), HSP60, HSP70, HSP90, and HSP110 are the most studied HSPs in HF. They can affect apoptosis, inflammation, oxidative stress, fibrosis, contractile function, hypertrophy, ER stress and mitochondrial function by regulating multiple pathways like Akt, caspase-3, ERK and various cellular functions like ER and mitochondria in the progression of HF, including modulating the systolic and diastolic function and the stiffness and enlargement of ventricle.

accompanied by decreased cardiac contractility and function. HSP70 was not induced even under heat stress (Tanonaka et al., 2001b; Tanonaka et al., 2001c). Myocardial dysfunction of CAL-induced HF was partially due to impaired induction of HSP70 and the mechanisms can be elucidated as follows: 1) total expression of HSF-1 is enhanced in CAL-induced HF rat model, whereas phosphorylated HSF-1 at ser303 is accumulated in the cytoplasm and fails to translocate to the nucleus thereby becoming incapable of inducing HSP70 (Marunouchi et al., 2013a), 2) interaction of HSP90 and

HSF-1 is enhanced in the cytoplasm hindering nuclear translocation of HSF-1 (Marunouchi et al., 2013b), 3) downregulated mitochondrial aldehyde dehydrogenase2 (ALDH2) and the upregulated 4-hydroxy-2-nonenol (4-HNE) suppress expression of HSP70 in response to hypoxia, and this process is independent of HSF-1 (Sun et al., 2014). HSP70 can inhibit apoptosis and enhance tolerance to harmful stimuli to protect the heart from further damage. HSP70 knockout mice are more susceptible to ischemia/reperfusion (I/R) injury and more likely to develop myocardial hypertrophy resulting in decreased



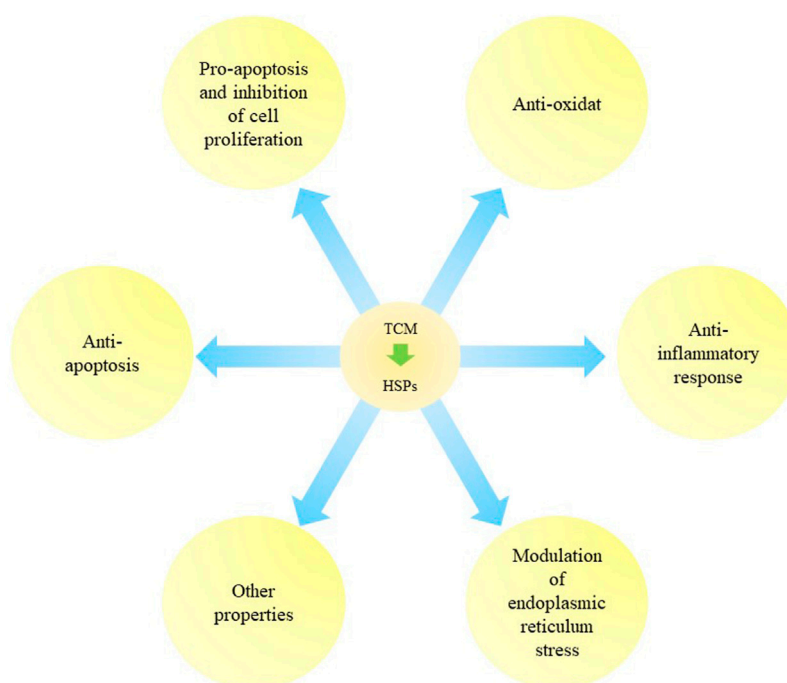


**FIGURE 2 |** The regulation of Traditional Chinese Medicine on heat shock proteins. Traditional Chinese medicine (TCM) can exert various biological functions like anti-apoptosis, pro-apoptosis and inhibition of cell proliferation, anti-oxidant, anti-inflammatory response, modulation of ER stress and other properties via regulating HSPs.

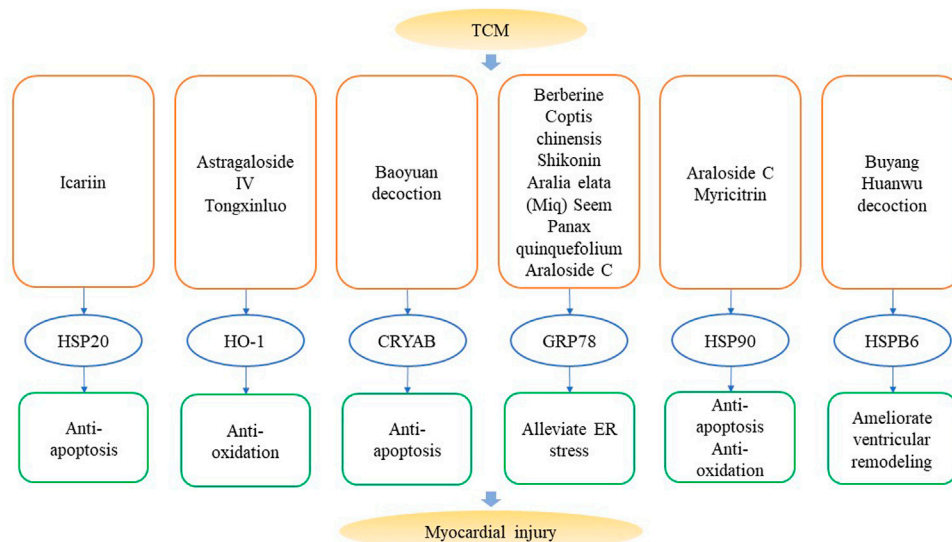


**FIGURE 3 |** Traditional Chinese Medicine that target heat shock proteins in myocardial injuries. Components like icariin, astragaloside IV, berberine and decoctions like Baoyuan decoction and Buying Huanwu decoction can alleviate myocardial injury via anti-apoptosis, anti-oxidation, reducing ER stress and cardiac remodeling by regulating the expression of HSPs.

$\text{Ca}^{2+}$  in the sarcoplasmic reticulum, damaged myocardial contractility, activation of JNK, p38, Raf-1 and extracellular regulated protein kinases (ERKs) pathways (Kim et al., 2006). Overexpressed HSP70 can protect mice from HF induced by

DOX by inactivating p53 and its downstream bax, caspase-3 and caspase-9 (Naka K et al., 2014). However, long-term overexpression of HSP70 does not mitigate cardiac dysfunction and reverses remodeling in failing hearts with

atrial fibrillation (AF). This indicates that HSP70 can be beneficial during acute cardiac condition but it cannot adequately inhibit chronic stimuli (Bernardo et al., 2015; Bernardo et al., 2016).

Intracellular HSP70 and extracellular HSP70 have differential effects on pressure overload-induced HF. Inhibition of HSP70 expression (both intracellular and extracellular) through inactivation of HSF-1 can promote myocardial hypertrophy and cardiac dysfunction but ameliorate cardiac fibrosis; functional inhibition of extracellular HSP70 using anti-HSP70 attenuates cardiac hypertrophy and fibrosis (Cai et al., 2010). Results of a study indicated the protective effect of intracellular HSP70 in cardiac function, and that the potential mechanism of anti-HSP70 lies in its inhibitory effect on ERK and p38 pathway through neutralization of extracellular HSP70. Concentration of plasma HSP70 was increased in both TAC-induced pressure overload and DOX-induced HF mice models. Extracellular HSP70 activates TLR2/NF- $\kappa$ B pathway, triggers inflammation and causes cardiac hypertrophy and fibrosis (Higashikuni et al., 2013; Liu et al., 2019). Furthermore, anti-HSP70 antibodies attenuate cardiac dysfunction induced by TAC or DOX by blocking extracellular HSP70-mediated activation of TLR2 pathway (Higashikuni et al., 2013; Liu et al., 2019). Plasma HSP70 was significantly increased in patients with HF and ARVC, ICM or DCM (Genth-Zotz et al., 2004; Gombos et al., 2008; Wei et al., 2009). Plasma HSP70 can be an independent prognostic biomarker for early diagnosis and is suitable for predicting long-term survival of patients with HF (Li et al., 2013a; Jenei et al., 2013).

Stress-induced UPR in the endoplasmic reticulum plays crucial role in the development and progression of HF (Minamino et al., 2010). Increased expression levels of GRP78, a marker of ER stress can also be an indicator of impaired UPR during progression of HF (Okada et al., 2004; Dally et al., 2009; Sawada et al., 2010). However, overexpressed GRP78 has a protective function in myocytes (Fu et al., 2008).

## HSP60

Unlike other HSPs, expression of HSP60 was elevated at 8w after CAL, and elevated HSP60 expression was driven by loss in the transcriptional activity of NF- $\kappa$ B for heat shock factor-1 (HSF-1) and failure to induce HSP72 in CAL-induced HF (Tanonaka et al., 2001a; Toga et al., 2007; Wang et al., 2010a). In addition, HF and DCM induced mitochondrial translocation of HSP60 (Sidorik et al., 2005; Lin et al., 2007). The potential protective mechanisms of HSP60 in the myocardium are involvement in anti-apoptosis and preservation of mitochondrial function. HSP60 can increase b-cell lymphoma-2 (bcl-2)/bcl-2-associated x (bax) ratio, inhibit caspase-3 and poly (ADP-ribose) polymerase (PARP) (Kirchhoff et al., 2002; Shan et al., 2003). HSP60 deletion causes HF in mice and impairs mitochondrial protein homeostasis (Fan et al., 2020). HSP60 transfers to the plasma and plasma membrane in HF, and its surface translocation is highly associated with apoptosis (Lin et al., 2007). Extracellular HSP60 can trigger toll-like receptor4 (TLR4) pathway and induce inflammatory response (Liu et al., 2015). The plasma HSP60 is positively correlated with occurrence of adverse cardiac events in both acute and chronic HF, implicating its potential of being a

biomarker of HF (Niizeki et al., 2008; Zhang et al., 2008; Bonanad et al., 2013).

## Small HSPs—HSP27

HSP27 (also called HSP25 in murine) is involved in numerous cellular functions; it can counteract apoptosis and oxidative stress, and inhibit cardiac remodeling and dysfunction of a failing heart (Liu et al., 2007a; Turakhia et al., 2007; You et al., 2009; Marunouchi et al., 2013c; Marunouchi et al., 2014). Expression levels of HSP27 are increased in failing hearts, and this is induced by doxorubicin (DOX) and fluoride (Vedam et al., 2010; Panneerselvam et al., 2017) as a response to harmful stimuli. HSP27 may possibly have a dual effect on HF; it not only acts as an antioxidant to protect the heart from damages and improve cardiac function (Liu et al., 2007a; Turakhia et al., 2007; You et al., 2009), but also augments injury in a failing heart (Vedam et al., 2010; Zhang et al., 2010; Yu et al., 2015). Overexpression and phosphorylation of HSP27 counteracts the cardiotoxic effect of DOX, mitigates cardiac dysfunction in dilated cardiomyopathy (DCM) and congestive HF (Liu et al., 2007a; Turakhia et al., 2007). Cardiac-specific overexpressed HSP27 enhances phosphorylation of serine/threonine kinase (Akt), attenuates activation of glycogen synthase kinase-3 $\beta$  (GSK-3 $\beta$ ) and nuclear factor kappa-B (NF- $\kappa$ B) to ameliorate cardiac dysfunction induced by lipopolysaccharide (LPS) (You et al., 2009). Expression and phosphorylation of HSP27 in the cytoplasm and mitochondria increased at 2w after coronary artery ligation (CAL) but decreased in the mitochondria at 8w. This indicates that mitochondrial HSP27 and phosphorylated HSP27 significantly contribute to mitochondrial function in HF (Marunouchi et al., 2013c; Marunouchi et al., 2014). The co-chaperones of HSP27 alter its function. Downregulation of HSP27 hinders interaction of silent information regulator1 (SIRT1)-p53 and endowed p53 acetylation, augmenting apoptosis in DOX-induced H9c2 cells (Zhang et al., 2016a). However, inducible HSP27 can be pro-apoptotic by binding to and transactivating p53 resulting in loss of cardiomyocytes in HF (Vedam et al., 2010). Moderate level of HSP27 is beneficial, whereas higher levels of HSP27 can induce reductive stress and aggravate cardiomyopathy (Zhang et al., 2010; Yu et al., 2015). Plasma HSP27 is regarded as a novel candidate biomarker for diagnosing chronic HF and an independent predictor of HF-related mortality (Liu et al., 2016a; Traxler et al., 2017).

## Other Small HSPs

Other HSPs are also involved in the pathophysiology of HF. HSP20 has anti-apoptotic and anti-oxidative effects in cardiomyocytes which improve cardiac function. HSP20 can reverse cardiac remodeling, fibrosis and hypertrophy induced by isoproterenol (ISO) by inhibiting apoptosis signal regulating kinase1 (ASK1)/Jun N-terminal kinase (JNK)/p38 pathways (Fan et al., 2006). HSP20 decreases activity of NF- $\kappa$ B to attenuate apoptosis and myocardial dysfunction induced by LPS (Wang et al., 2009). HSP20 maintains activity of Akt signaling pathway and suppresses oxidative stress to alleviate damage of DOX (Fan et al., 2008). Expression of HO-1 was elevated at both protein

**TABLE 2 |** The regulation of Traditional Chinese Medicine on heat shock proteins.

Property	TCM or active ingredients	Targets	Model	Ref
Anti-apoptosis	Resveratrol	↑ HSP27	Ultraviolet B-treated HaCaT cells	Zhou et al. (2018)
	Hydroxysafflor yellow A, extract of <i>Carthamus tinctorius</i> L	↓ phosphorylation of HSP27 at ser 78	Heat stress-induced neural stem cells	Li et al. (2019a)
	Zanthoxylum bungeanum Maxim	↑ HO-1	D-Galactose-Induced Aging Mice	Zhao et al. (2020)
	Icariin	↑ HSP70	Calvaria osteoblasts of rats	Qian et al. (2018)
	EGb761, extract of Ginkgo biloba leaves	↑ HSP70 and GRP78	Aβ <sub>1-42</sub> oligomer-induced SH-SY5Y cells	Liu et al. (2016b)
	Ginsenosides Rg1 and Rb1 (extracts of <i>panax notoginseng</i> )	↑ HSP70	MCAO mice	Zeng et al. (2014)
	Tanshinone IIA	↑ HSP70	Rats that subjected to spinal I/R injury	Zhang et al. (2012)
	Gualou Guizhi decoction	↑ HSP70	Rats that subjected to MCAO.	Nan et al. (2020)
	Qinghuobaiduyin formula	↑ HSP70	Rats that subjected to burn injury	Zhu et al. (2013)
Pro-apoptosis and inhibit cells proliferation	Xiaotan Tongfu granule	↑ HSP70	Rats that subjected to cold-restraint model	Yan et al. (2013)
	Barbaloin, extract of <i>Aloe barnadensis</i> Miller leaves	↓ HSP27	NSCLC cell line A549	Zhang et al. (2017)
	Lariciresinol	↓ HSP27	HepG2 cells	Ma et al. (2016)
	Bufalin	↓ HSP27	Pancreatic cancer cells	Li et al. (2014)
	Tanshinone IIA, extract of <i>Salvia miltiorrhiza</i>	↑ phosphorylation of HSP27 at ser 82	Human gastric cell line AGS	Yin et al. (2020)
	Curcumin, extract of <i>Curcuma longa</i>	↓ HSP27	Human colon cancer HCT-8 and HCT-8/5-FU (5-FU-resistant cell line)	He et al. (2019a)
	Synergistic application of triptolide and celastrol	↓ HSP27, HSP70 and HSP90	Human cancer cell lines and human normal embryonic kidney cell line HEK293T	Jiang et al. (2015)
	Homogeneous <i>Schisandra chinensis</i> polysaccharide-0-1	↓ HSP90	HepG2 cells	Chen et al. (2016)
	Patrinia heterophylla	↓ HSP90	Leukemia K562 cells	Wei et al. (2012)
Anti-oxidative property	Platycodin D, extract of <i>Platycodonis Radix</i>	↓ Hsp90/Cdc37 interactions	Human lung cancer cells	Li et al. (2017)
	Zanthoxylum bungeanum Maxim	↑ HO-1	D-Galactose-Induced Aging Mice	Zhao et al. (2020)
	Celastrol (extract of <i>Tripterygium wilfordii</i> Hook)	↑ HO-1 and HSP70	Lipopolysaccharide (LPS)-induced rats	Wang et al. (2015a)
	Protopanaxtriol	↑ HO-1 and HSP70	Rats that subjected to 3-nitropropionic acid	Gao et al. (2015)
	Radix Bupleuri extract	↑ HO-1, ↓ HSP70	H <sub>2</sub> O <sub>2</sub> -induced Tilapia	Jia et al. (2019)
	Water extract and ethanol extract of <i>Cordyceps cicadae</i>	↑ HO-1	Cisplatin-induced mouse	Deng et al. (2020)
	Diethyl blechnic, a compound isolated from Danshen	↑ HO-1	LPS-induced RAW264.7 cells	He et al. (2019b)
Anti-inflammation	Celastrol, extract of <i>Tripterygium wilfordii</i> Hook	↑ HO-1 and HSP70	LPS-induced rats	Wang et al. (2015a)
	Radix Bupleuri extract	↑ HO-1, ↓ HSP70	H <sub>2</sub> O <sub>2</sub> -induced Tilapia	Jia et al. (2019)
	Momordica grosvenori	↑ HO-1	LPS-induced RAW264.7 cells	Li et al. (2019b)
	Liquiritigenin and liquiritin	↓ extracellular release of HSP60	Monocrotaline-induced Hepatic sinusoidal obstruction syndrome in rats	Huang et al. (2019)
	Rhodiola rosea L. root and rhizome extract	↑ HSP70	CRH-stimulated BV2 microglial cells	Borgonetti et al. (2020)
	Xiaotan Tongfu granule	↑ HSP70	Rats that subjected to cold-restraint model	Yan et al. (2013)
	Emodin-8-O-glucuronic acid, isolated from qinghuobaiduyin decoction	↑ HSP70	LPS-stimulated raw 264.7 cells	Wang et al. (2016)

(Continued on following page)

**TABLE 2 |** (Continued) The regulation of Traditional Chinese Medicine on heat shock proteins.

Property	TCM or active ingredients	Targets	Model	Ref
Modulate ER stress	Bitter melon	↓ GRP78	Human colonic adenocarcinoma LS174T cells	Kunde et al. (2017)
	Gambogenic acid, a compound of <i>Garcinia hanburyi</i> HOOK	↓ GRP78	Human nasopharyngeal carcinoma cells	Su et al. (2019)
	Glycyrrhetic acid, a component of <i>glycyrrhiza</i>	↑ GRP78	Human NSCLC cells	Zhu et al. (2015)
	Rhein, a compound of rhubarb	↓ GRP78	MCF-7 and HepG2 cells	Wang et al. (2015b)
	Xuefuzhuyu capsules	↓ GRP78	Rats subjected to hindlimb unload	Zhang et al. (2018b)
	Bushen Zhuangjin decoction	↓ GRP78	Tunicamycin induced-articular chondrocytes	Lin et al. (2015)
Others	Licorice, extract of <i>Glycyrrhiza uralensis</i> Fisch	↓ phosphorylation of HSP27, alters the interaction of HSP27 and actin	Oxytocin-induced uterine contraction	Yang et al. (2017a)
	Schisandrin B, isolated from a <i>Schisandra chinensis</i>	↑ HSP27 and HSP70	D-galactosamine-induced liver injury in mice	Gao et al. (2016)
	Combination use of ferulic acid, ligustrazine and tetrahydropalmatine	↓ HSP90	Endometriosis rats	Tang et al. (2014)
	Uncaria rhynchophylla	↓ HSP90	MPP <sup>+</sup> -induced SHSY5Y cells and MPTP-induced mice	Lan et al. (2018)
	Zhenbao Pill	↑ HSP27	Rats that subjected to acute spinal cord injury	He et al. (2018)
	YangZheng XiaoJi formula	↓ phosphorylation of HSP27	Human gastric cancer, pancreatic cancer, ovarian cancer), lung cancer, breast cancer, prostate cancer, ovarian cancer cells	Owen et al. (2016)

and mRNA levels in the right-sided HF and post-myocardial infarction (MI) HF (Raju et al., 1999; Wang et al., 2010b). HO-1 induces anti-oxidant and anti-apoptotic effects, and enhances tolerance to HF. HO-1 can attenuate cardiac hypertrophy, fibrosis, oxidative stress, mitochondrial MPT pore (mPTP) opening and promote angiogenesis to preserve left ventricular function and attenuates remodeling of post-MI HF (Liu et al., 2007b; Wang et al., 2010b). Overexpressed HO-1 activates Akt pathway to reduce apoptosis in myocytes which is induced by angiotensin II (Ang II) (Foo et al., 2006). However, the protective role of HO-1 seems to depend on the type of stimulation. HO-1 significantly attenuated ISO-induced cardiac dysfunction, fibrosis and hypertrophy, but was detrimental in aging and transverse aortic constriction (TAC) models (Allwood et al., 2014).

In conclusion, HSPs make significant contributions in HF and most HSPs can exhibit protective effects whereas a few HSPs may accelerate damage based on a specific condition. Functions of HSPs seem to vary with their location: intracellular HSPs exhibit anti-apoptotic, anti-inflammatory and anti-oxidative effects, whereas extracellular HSPs are on the contrary. Moreover, HSPs modulate several signaling pathways to initiate biological effects. Consequently, regulation of the expression of HSPs is a promising treatment for HF.

## TCM REGULATES EXPRESSION OF HSPS

TCM can regulate expression of HSPs to initiate anti-apoptotic, pro-apoptotic and anti-inflammatory responses. TCM can be used as anti-oxidants and for modulating ER stress in cancer, diseases of the nervous system, ischemic diseases, hepatopathy, gastroenteropathy and uterine diseases. Regulatory effects of

TCM on HSPs are summarized and listed in **Figure 2** and **Table 2**.

## Anti-Apoptosis

Resveratrol inhibits apoptosis in ultraviolet B-treated HaCaT cells, and can upregulate HSP27 expression, increase bcl-2/bax ratio, and inhibit caspase-3 activity and p65 expression (Zhou et al., 2018). Hydroxysafflor yellow A is extracted from the flowers of *Carthamus tinctorius* L.; it can inhibit phosphorylation of p38 and HSP27 Ser78, and prevent apoptosis in heat stress-induced neural stem cells (NSCs) (Li et al., 2019a). Icariin upregulates HSP70 and serpin family F-1 (PEDF-1) to promote proliferation, calcium deposition and inhibits osteoblast apoptosis (Qian et al., 2018). Pretreatment with EGb761, an extract of *Ginkgo biloba* leaves can increase levels of HSP70 and GRP78 to reduce apoptosis and neurotoxicity in Aβ<sub>1-42</sub> oligomer-induced SH-SY5Y cells (Liu et al., 2016b). Ginsenosides Rg1 and Rb1, extracts of *Panax notoginseng* increased HSP70 levels and restored the Akt/NF-κB signaling pathway in the hippocampus, causing neuroprotective effects against cerebral I/R (Zeng et al., 2014). Tanshinone IIA can attenuate spinal I/R injury and promote expression of HSP70 and bcl-2 (Zhang et al., 2012). Some formula can also be anti-apoptotic. Gualou Guizhi decoction increases expression of HSP70 in middle cerebral artery occlusion (MCAO) rat model and alleviates neuronal apoptosis by inhibiting PARP-1/apoptosis inducing factor (AIF) signaling pathway (Nan et al., 2020). Qinghuobaiduyin formula (contains extracts of *Astragalus membranaceus*, *Lonicera japonica*, *Scutellaria baicalensis* Georgi, *Ophiopogon japonicus* and *Rheum rhabarbarum*) increases HSP70 levels and induces anti-apoptotic effects on the intestinal mucosa following burn injury (Zhu et al., 2013). Granules of Xiaotan Tongfu promote cell proliferation,



inhibit gastric mucosal cell apoptosis and local inflammation, and increase expression of HSP70 in rats with stress ulceration (Yan et al., 2013).

## Pro-Apoptosis and Inhibition of Cell Proliferation

Induction of apoptosis in cancer cells is vital and certain types of TCM can inactivate HSPs resulting in increased cell death. Barbaloin which is extracted from leaves of *Aloe barbadensis* Miller, inactivates p38 mitogen-activated protein kinase (MAPK)/HSP27 pathway, induces apoptosis and inhibits growth of human non-small cell lung cancer (NSCLC) cell line, A549 (Zhang et al., 2017). Laricresinol downregulates HSP27 and initiates apoptosis in HepG2 cells (Ma et al., 2016). Bufalin induces apoptosis by partially targeting HSP27, eliminates anti-apoptotic effect of HSP27 in pancreatic cancer cells, and induces caspase-3 and caspase-9 (Li et al., 2014). Temporal treatment with tanshinone IIA (a diterpene quinone extract from *Salvia miltiorrhiza*) increases phosphorylation of HSP27 at Ser 82, and subsequent overexpression of HSP27 limits tanshinone IIA-induced cell death in gastric cells (Yin et al., 2020). Curcumin is a hydrophobic polyphenol derived from the rhizomes of *Curcuma longa*, which can inhibit cell proliferation and decrease expression of HSP27 at mRNA levels in human colon cancer (HCT)-8 and HCT-8/5-FU (5-FU-resistant cell line) (He et al., 2019a). Triptolide reduces protein levels of HSP27, HSP70 and HSP90 whereas celastrol increases protein levels of HSP27 and HSP70. Synergistic application of triptolide and celastrol can mitigate effect of increased HSP27 and HSP70, inhibit growth of cancer cells, and induce apoptosis in cancer cells (Jiang et al., 2015). Homogeneous polysaccharide-0-1 (SCP-0-1) from *Schisandra chinensis* induces mitochondrial apoptosis in human hepatocellular liver carcinoma, a mechanism involved in the downregulation of HSP90 and inhibition of Akt pathway (Chen et al., 2016). *Patrinia heterophylla*, a member of Valerianaceae family, inhibits expression of HSP90 $\alpha$  to induce apoptosis in leukemia K562 cells (Wei et al., 2012). Platycodin D is a saponin isolated from *Platycodonis radix*, which can disrupt Hsp90/Cdc37 co-chaperone interactions without affecting ATPase activity of HSP90 and reduces Akt phosphorylation in human lung cancer cells (Li et al., 2017).

## Anti-Oxidant

*Zanthoxylum bungeanum* Maxim is a plant that can be used both as a condiment and as medicine. Its extracts in water and volatile oil can activate Akt/nuclear factor E2-related factor 2 (Nrf2)/HO-1 pathway to prevent cognitive dysfunction and hippocampal neuronal cell damage which are induced by D-galactose (Zhao et al., 2020). Celastrol is extracted from the root of *Tripterygium wilfordii* Hook, and it possesses anti-oxidant and anti-inflammatory effects which can attenuate cardiac iNOS, tumor necrosis factor- $\alpha$  (TNF- $\alpha$ ), NF- $\kappa$ B and activity of caspase-3. Celastrol can also increase contents of HO-1 and HSP70 in the heart and aorta to prevent circulatory failure in sepsis (Wang et al., 2015a). Protopanaxtriol increases expression of HO-1 to induce anti-oxidative effect, relatively increases reactive

oxygen species (ROS) and HSP70, and alleviates behavior disorders in 3-nitropropionic acid-induced rat model of Huntington's disease (Gao et al., 2015). Pretreatment with extracts from *Radix bupleuri* can reverse increased HSP70 at mRNA levels in liver injury induced by H<sub>2</sub>O<sub>2</sub>. The primary beneficial effects of *Radix bupleuri* extracts of inhibiting oxidative stress is due to its role in enhancing Nrf2/HO-1 signaling pathway and inhibiting TLRs/MyD88/NF- $\kappa$ B signaling pathway (Jia et al., 2019). Water and t and ethanol extracts of *Cordyceps cicadae* increase production of Nrf2, HO-1 and other antioxidants, inhibit activation of NF- $\kappa$ B, attenuates oxidative stress and inflammation to prevent cisplatin-induced kidney injury (Deng et al., 2020). Diethyl blechnic, a compound isolated from *Salvia miltiorrhiza*, increases expression of Nrf2/HO-1 and inhibits TLR4/MyD88 signaling pathway to ameliorate oxidative stress in LPS-induced RAW264.7 cells (He et al., 2019b).

## Anti-Inflammatory Response

*Momordica grosvenori* attenuates phosphorylation of Akt1 pathway, increases expression of HO-1 to initiate anti-inflammatory effect on LPS-induced RAW264.7 cells (Li et al., 2019b). Liquiritigenin and liquiritin are two key compounds in *Glycyrrhizae radix et Rhizoma*, which have the ability to alleviate liver inflammatory injury. These compounds can prevent release of HSP60 to the extracellular matrix in monocrotaline-induced rat models and block exogenous HSP60-activated NF- $\kappa$ B in RAW264.7 cells (Huang et al., 2019). Root and rhizome extracts of *Rhodiola rosea* L. increase expression of HSP70 in corticotropin releasing hormone (CRH)-stimulated BV2 microglial cells, counteract neuroinflammatory effect and enhance cell survival (Borgonetti et al., 2020). Emodin-8-O-glucuronic acid, a compound isolated from qinghuobaiduyin decoction (TCM), increases expression of HSP70 to inhibit inflammatory cytokines in the LPS-stimulated Raw 264.7 cells (Wang et al., 2016).

## Modulation of Endoplasmic Reticulum Stress

The chaperone heat shock protein GRP78, together with C/EBP homologous protein (CHOP) are commonly used as markers of endoplasmic reticulum (ER) stress. As an ER chaperone, GRP78 functions as a potent anti-apoptotic factor and confers drug resistance, whereas CHOP is a key initiating factor of ER stress-related cell death. Moreover, as a master of UPR in ER of normal cells, GRP78 force the unfolded proteins to refold or degrade by cellular degradation mechanisms. While under stress, the overexpression of GRP78 on the cell membrane mediates the vast amount of disordered proteins (Ibrahim et al., 2019).

Gambogic acid is a component of Gamboge, a dry resin obtained from *Garcinia hanburyi* HOOK. f. (Guttiferae), which downregulates GRP78 and upregulates CHOP to induce apoptosis in poorly differentiated human nasopharyngeal carcinoma cells (Su et al., 2019). Glycyrrhetic acid, a bioactive component of *glycyrrhiza*, upregulates GRP78 and CHOP to modulate ER stress and suppresses proliferation of

human NSCLC cells (Zhu et al., 2015). Rhein, a compound of rhubarb can adequately induce GRP78 and inhibit expression of GRP78 induced by ER stress, disrupting the anti-apoptotic pathway in cancer cells (Wang et al., 2015b). Bitter melon ameliorates ER stress in epithelial cells of the colon thus decreasing expression of GRP78 and CHOP (Kunde et al., 2017). Capsules of Xuefu Zhuyu decrease expression of GRP78 and CHOP to alleviate ER stress. Capsules also attenuate loss of muscle mass and cross-sectional areas induced by hindlimb unloading (Zhang et al., 2018b). A decoction of Bushen Zhuangjin downregulates expression of GRP78 and inhibits ER stress to suppress tunicamycin induced-chondrocyte apoptosis (Lin et al., 2015).

## Other Properties

Licorice is derived from the roots and rhizomes of *Glycyrrhiza uralensis* Fisch, and it reduces levels of phosphorylated HSP27 at Ser15, altering interaction of HSP27 and actin, and it decreases actin polymerization to enhance spasmolytic effects in oxytocin-stimulated uterus (Yang et al., 2017a). Schisandrin B is isolated from *Schisandra chinensis* and it attenuates D-galactosamine-induced liver injury in mice. Hepatoprotective effect of schisandrin B is partially attributed to increased levels of HSP27 and HSP70 (Gao et al., 2016). Combined use of ferulic acid, ligustrazine and tetrahydropalmatine enhance downregulation of hypothalamus–pituitary–ovarian axis (HPOA), estrogen response element (ERE) pathway and expression of HSP90 in rat model of endometriosis (Tang et al., 2014). *Uncaria rhynchophylla* inhibits expression of HSP90 and activates Akt pathway to induce neuroprotective effect in mouse model of Parkinson's disease (Lan et al., 2018). Zhenbao pills promote expression of HSP27, affect Treg cell differentiation and ameliorate acute spinal cord injury in rats (He et al., 2018). YangZheng XiaoJi formula is able to inhibit phosphorylation of HSP27 and reduce migration of cancer cells (Owen et al., 2016).

## THERAPEUTIC FUNCTIONS OF TCM IN HF

TCM is widely distributed in nature and the various forms of TCM include signal herbs, formula, decoctions, capsules and others. Discovery and application of TCM is based on TCM theories. TCM with particular therapeutic effects have been applied in the treatment of HF in China for thousands of years. A systematic review has revealed that Shengmai (comprising herbs from *Panax ginseng*, *Ophiopogon japonicus* and *Schisandra chinensis*) improves ejection fraction, cardiac output, cardiac index, left ventricular end-systolic volume and myocardial contractility (Zhou et al., 2014). Clinical studies have mostly been conducted by the Chinese and recent studies come to emphasize a uniform standard.

Studies have summarized the commonly prescribed herbs for treating different HF syndromes as follows: Radix aconiti carmichaeli (Fuzi), Atractylodes (Baizhu), Cassia twig (Guizhi), Dried ginger (Ganjiang), Radix pseudostellariae (Taizishen), Radix astragali (Huangqi), Codonopsis pilosula (Dangshen),

Ginseng (Renshen), *Panax notoginseng* (Sanqi), Chinese angelica (Danggui), Safflower (Honghua), Ligusticum wallichii (Chuanxiong), Salvia miltiorrhiza (Danshen), Red paeony root (Chishao), Peach kernel (Taoren), Hawthorn (Shanzha), Semen lepidii (Tinglizhi), Alisma (Xieze), Poria cocos (Fuling), Radix Ophiopogonis (Maidong), Fructus schisandrae (Wuweizi), Radix rehmanniae (Shengdi), Pinellia (Banxia), Trichosanthes Kirilowii (Gualou), Dried tangerine or orange peel (Chenpi), and Scallions white (Xiebai), etc (Wang et al., 2017a). Moreover, there are several most commonly prescribed formulae that have been proven effective clinically for the treatment of HF. These decoctions prescribed by physicians include: Zhenwu tang, Shengmai san, Baoyuan tang, Xuefuzhuyu tang, Tinglidazaoxiefei tang, Danshen yin, and Taohongsiwu tang etc. Meanwhile, several Chinese patent drugs have been successfully produced by standardized procedures and are widely used in health care industry. Drugs in the form of capsules or pills include: Qishenyiqi dripping pill (QSYQ), Fufang danshen dripping pill, Danqi pill (DQP), Qili qiangxin capsule, and Shengmai capsule, etc. The produced injections include: Shenmai injection, Shengmai injection, Huangqi injection, Shenfu injection, and Danhong injection, etc (Jian, 2002). Among these patent medicine above, a randomized clinical trial indicates QSYQ could promote left ventricular function, increase exercise capacity and reduce re-admission rate (Hou et al., 2013; Shang et al., 2013). A clinical trial of Qili qiangxin capsule demonstrated superior performance in comparison to the placebo in terms of NYHA functional classification, 6-min walking distance, LVEF and quality of life (Li et al., 2013b). The underlying mechanisms includes regulating TGF- $\beta$ 1 in the progression of fibrosis (Zhang et al., 2016b), or modulates the expressions of collagen I (Col I), collagen III (Col III), matrix metalloproteinase-2 (MMP-2), and MMP-9, which are the main contributors to extracellular matrix remodeling (Zhang et al., 2015).

I/R injury in myocardial infarction is an important inducing or exacerbating factor for acute HF. The underlying mechanisms of TCM in the treatment of HF include anti-fibrosis, anti-inflammation, anti-oxidant, anti-apoptosis, pro-angiogenesis effects and regulation of metabolism, thus directly mitigate the I/R injury or indirectly reducing the adverse cardiac remodeling which could induce or exacerbate HF. For example, dioscin attenuates apoptosis and oxidative stress by regulating bcl-2/bax ratio and SOD (). Shensong Yangxin and Sini Tang (comprising *Aconitum carmichaelii* Debeaux, *Cinnamomum cassia* (L.) J. Presl, *Zingiber officinale* Roscoe and *Glycyrrhiza uralensis* Fisch. ex DC.) can enhance cardiac function by suppressing cardiac collagen hyperplasia in rabbits and TGF- $\beta$ 1 expression in MI-induced rat models (Liu et al., 2014; Dang et al., 2016).

TCM is usually used together with western medicine to treat HF. The multiple effects of TCM can counteract adverse effects of pharmacological treatment, making it a potential therapeutic option. However, application of TCM is limited because of lack of large-scale multi-center clinical trials and experiments. Therefore, further research on the mechanism of TCM in treating HF is necessary to enhance its applicability worldwide.

**TABLE 3 |** Traditional Chinese Medicine that target heat shock proteins in myocardial injuries.

Target	TCM	Function	Model	Ref
HSP20	Icariin	Upregulates HSP20 and suppresses apoptosis	H9C2 with H/R	Ren et al. (2018)
HO-1	Astragaloside IV, a component of <i>Astragalus membranaceus</i>	Activates Nrf2/HO-1 pathway, attenuates cardiac hypertrophy, improves left ventricular function and structure	Abdominal aortic constriction (AAC)-induced rats; Ang II-induced cardiomyocyte	Nie et al. (2019/2019)
	Tongxinluo	Upregulates cardiac expression of HO-1 and activates VEGF/Akt/eNOS pathway	TAC-induced HF in mice	Wang et al. (2014)
CRYAB	Baoyuan decoction	Activates CRYAB to inhibit apoptosis, rescues cardiac function	Rats that subjected to LAD; LPS-induced RAW 264.7 Cell; macrophage-conditioned media-stimulated H9C2 cells	Zhang et al. (2018a)
GRP78	Berberine, <i>Coptis chinensis</i>	Reduce apoptosis and ER stress, improve cardiac function and remodeling	Rats that subjected to LAD.	Liao et al. (2018)
	Shikonin	Inhibits $\alpha$ -SMA/collagen, TLR4/NF- $\kappa$ B signaling and ER stress pathway, decreases GRP78	ISO-induced mice and H9C2 cells	Yang et al. (2017b)
	<i>Aralia elata</i> (Miq) Seem	Alleviates ER stress-induced apoptosis, reduces GRP78	Rats that subjected to LAD.	Wang et al. (2018)
	<i>Panax quinquefolium</i>	Inhibits excessive ER stress and reduces GRP78	H/R-induced Ventricular cardiomyocytes	Wang et al. (2012)
	Araloside C	Attenuates ER stress-dependent apoptotic pathways	H/R-induced H9C2 cells. I/R-induced rat hearts	Du et al. (2018), Wang et al. (2017b)
HSP90	Araloside C	Reduces apoptosis by increasing HSP90 expression	H/R-induced H9C2 cells. I/R-induced rat hearts	Du et al. (2018), Wang et al. (2017b)
	Myricitrin	Increases expression of HSP90 to alleviate apoptosis and oxidative stress	H/R-induced H9C2 cells	Wang et al. (2017c)
HSPB6	Buyang Huanwu decoction	Increases the expression and phosphorylation of HSPB6, ameliorates ventricular remodeling	Rats with left anterior descending (LAD) artery ligation	Zhou et al. (2012)

## TCM Regulates Expression of HSPs in HF

Based on the functions of HSPs in HF, regulation of HSPs and the protective effects of TCM in treating HF, it can be hypothesized that TCM regulate HSPs to enhance therapeutic effects on HF. A fraction of TCM has been proven to regulate HSPs in the myocardium and protect the heart from fibrosis, remodeling and hypertrophy. Functions of TCM which target HSPs in myocardial injuries are summarized in **Figure 3** and **Table 3**.

On the one side, TCM could directly relieve HF by regulating HSPs and HSPs-mediated ER stress. Astragaloside IV is an active component of *Astragalus membranaceus*, can activate Nrf2/HO-1 pathway to protect the heart from hypertrophy and fibrosis (Nie et al., 2019/2019). Shikonin is extracted from the red-root gromwell, and it ameliorates ISO-induced myocardial damage, and cardiac hypertrophy by inhibiting  $\alpha$ -smooth muscle actin ( $\alpha$ -SMA)/collagen, TLR4/NF- $\kappa$ B signaling and ER stress pathways. Suppression of ER stress is reflected as decreased expression of GRP78 (Yang et al., 2017b). Tongxinluo is a TCM compound, which can increase cardiac expression of HO-1 and activate vascular endothelial growth factor (VEGF)/Akt/eNOS pathway to prevent TAC-induced HF in mice (Wang et al., 2014).

On the other side, as I/R injury in myocardial infarction is an important inducing or exacerbating factor for acute HF, TCM could also indirectly prevent HF pathogenesis by decreasing I/R injury and impeding fibrosis and cardiac remodeling in myocardial infarction. Berberine, a key active ingredient of *Coptis chinensis* can improve cardiac function and remodeling, reduce apoptosis and ER stress (marked as decreased GRP78 and CHOP) in post-MI HF (Liao et al., 2018). Icariin suppresses apoptosis by reversing downregulation of HSP20 in H9c2 cells induced by hypoxia/reoxygenation (H/R) injury (Ren et al., 2018). Araloside C, a compound isolated from *Aralia elata* (Miq) Seem, icariin and

*Panax quinquefolius* L. can ameliorate apoptosis and ER stress, reduce expression of GRP78 in myocytes induced by either I/R or tunicamycin (Wang et al., 2012; Zhang et al., 2013; Wang et al., 2017b; Du et al., 2018; Wang et al., 2018). In addition, Araloside C can increase expression of HSP90 and alleviate apoptosis in either H9c2 with H/R injury or rat with I/R injury (Wang et al., 2017b; Du et al., 2018). Myricitrin can also alleviate apoptosis and oxidative stress induced by H/R injury by increasing expression of HSP90, and the protective function of myricitrin partially depends on phosphatidylinositol 3-kinase (PI3K)/Akt pathway (Wang et al., 2017c). Buyang Huanwu decoction ameliorates I/R-induced ventricular remodeling by upregulating expression of HSPB6 and peroxiredoxin-6 (PRDX6), and downregulating atrial natriuretic factor (ANF) thereby decreasing activities of bax and caspase-3 (Zhou et al., 2012). Baoyuan decoction is a TCM formula composed of *astragalus*, *ginseng*, *liquorice* and *cinnamon*. It can activate CRYAB to inhibit apoptosis and enhance cardiac function in post-MI-induced HF (Zhang et al., 2018a). Scutellarin can alleviate apoptosis in H/R induced human cardiac microvascular endothelial cells (HCMECs) and increased expression of HSP60 might be a crucial factor for its protective effect (Shi et al., 2015/2015). Emodin restores activity of peroxisome proliferators-activated receptor- $\gamma$  (PPAR- $\gamma$ ), eNOS phosphorylation, and interaction of HSP90/eNOS to alleviate H/R-induced injury in HAECs (Shou et al., 2018).

## Other Cardio-Protective Effects of TCM by Regulating HSPs

Besides HF and myocardial infarction, studies indicates TCM could also prohibit pathological process of atherosclerosis by regulating HSPs. Decoctions like Xiaoyaosan can inhibit

expression of HSP27, HSP60 and HSP90, and promote interaction of HSP90 with glucocorticoid receptor (GR) and CD36 to prevent development of atherosclerotic vulnerable plaque in mouse model of atherosclerosis induced by high-fat food coupled with chronic stress (Fu et al., 2019). Ligustrazine increases NO production in human umbilical vein endothelial cells (HUVECs), downregulates intercellular cell adhesion molecule-1 (ICAM-1) and HSP60 expression levels to induce immunomodulatory effect on TNF- $\alpha$ -stimulated HUVECs (Wu et al., 2012). Baicalin increases HSP72 expression at both mRNA and protein levels in a cow's mammary epithelial cells (CMECs) and inactivates NF- $\kappa$ B pathway to alleviate LPS-induced apoptosis (Yang et al., 2016). Catalpol, an extract of *Radix rehmannia*, inhibits homocysteine-induced apoptosis in the human aorta endothelial cells (HAECs) by suppressing Nox4/ROS/NF- $\kappa$ B pathway and GRP78/dsRNA-activated protein kinase-like endoplasmic reticulum kinase (PERK) pathway to alleviate ER stress (Hu et al., 2019).

## CONCLUSION AND PERSPECTIVES

HF describes the terminal stage of multifarious heart diseases such as dilated cardiomyopathy, myocardial infarction and myocarditis. Pathogenesis of HF is characterized by cardiomyocyte apoptosis, oxidative stress, inflammation and mitochondrial dysfunction, all of which cause myocardial fibrosis and remodeling. HSPs have various functions, including regulation of apoptosis, anti-oxidant and anti-inflammation effects, and are capable of ameliorating cardiac dysfunction in HF. However, not all the HSPs are protective in HF, some HSPs exerts detrimental effects in HF progressive. Even some HSPs can modulate HF pathogenesis with dual effects. Thus, further studies are still required to explore accurate functions of HSPs in HF with different cell and molecular microenvironment. New treatment methods that focuses on the regulation of

HSPs would have a promising application prospect in the prevention and treatment of HF.

TCM has been applied in the treatment of HF in China for thousands of years. Small sample clinical trials indicate the single compounds extracted from herbal medicine and formula, as well as patent medicine, are able to regulate HSPs in HF. Consequently, TCM is a potential therapeutic medium for modulating HSPs in HF and improving cardiac function. Studies on effects of various forms of TCM have confirmed the hypothesis that TCM alters expression of HSPs in HF but such studies are few. Thus, the application of TCM is limited in clinic because of lack of large-scale multi-center and randomized clinical trials. Therefore, further investigations on the effects of TCM in relieving HF by targeting HSPs are needed, and the underlying mechanisms involved in TCM regulating HSPs are also encouraged to be explored in future.

## AUTHOR CONTRIBUTIONS

QL designed the study. YW, JW and DW drafted the manuscript. QL finalized the manuscript. Critical comments and typesetting correction on the final version were made by RY and QL. All authors read, revised and approved the final manuscript.

## FUNDING

This study is supported by Guangdong Provincial Bureau of Traditional Chinese Medicine Fund Project (No. 202106082257336500, to Q.L.), Guangdong Medical Science and Technology Research Fund Project (No. B2020155, to Q.L.), Zhuhai Medical Science and Technology Research Fund Project (No. ZH24013310210002PWC, to Q.L.). National Natural Science Foundation of China (82174156), Guangzhou Science and Technology Plan Project (202002030432).

## REFERENCES

- Allwood, M. A., Kinobe, R. T., Ballantyne, L., Romanova, N., Melo, L. G., Ward, C. A., et al. (2014). Heme Oxygenase-1 Overexpression Exacerbates Heart Failure with Aging and Pressure Overload but Is Protective against Isoproterenol-Induced Cardiomyopathy in Mice. *Cardiovasc. Pathol.* 23, 231–237. doi:10.1016/j.carpath.2014.03.007
- Ambrosy, A. P., Fonarow, G. C., Butler, J., Chioncel, O., Greene, S. J., Vaduganathan, M., et al. (2014). The Global Health and Economic burden of Hospitalizations for Heart Failure: Lessons Learned from Hospitalized Heart Failure Registries. *J. Am. Coll. Cardiol.* 63, 1123–1133. doi:10.1016/j.jacc.2013.11.053
- Bernardo, B. C., Sapra, G., Patterson, N. L., Cemerlang, N., Kiriazis, H., Ueyama, T., et al. (2015). Long-Term Overexpression of Hsp70 Does Not Protect against Cardiac Dysfunction and Adverse Remodeling in a MURC Transgenic Mouse Model with Chronic Heart Failure and Atrial Fibrillation. *PloS one* 10, e0145173. doi:10.1371/journal.pone.0145173
- Bernardo, B. C., Weeks, K. L., Patterson, N. L., and McMullen, J. R. (2016). HSP70: Therapeutic Potential in Acute and Chronic Cardiac Disease Settings. *Future Med. Chem.* 8, 2177–2183. doi:10.4155/fmc-2016-0192
- Bonanad, C., Núñez, J., Sanchis, J., Bodi, V., Chaustre, F., Chillet, M., et al. (2013). Serum Heat Shock Protein 60 in Acute Heart Failure: a New Biomarker? *Congest. Heart Fail.* 19, 6–10. doi:10.1111/j.1751-7133.2012.00299.x
- Borgonetti, V., Governa, P., Biagi, M., Dalia, P., and Corsi, L. (2020). Rhodiola Rosea L. Modulates Inflammatory Processes in a CRH-Activated BV2 Cell Model. *Phytomedicine* 68, 153143. doi:10.1016/j.phymed.2019.153143
- Cai, W. F., Zhang, X. W., Yan, H. M., Ma, Y. G., Wang, X. X., Yan, J., et al. (2010). Intracellular or Extracellular Heat Shock Protein 70 Differentially Regulates Cardiac Remodelling in Pressure Overload Mice. *Cardiovasc. Res.* 88, 140–149. doi:10.1093/cvr/cvq182
- Chen, Y., Shi, S., Wang, H., Li, N., Su, J., Chou, G., et al. (2016). A Homogeneous Polysaccharide from Fructus Schisandra Chinensis (Turz.) Baill Induces Mitochondrial Apoptosis through the Hsp90/AKT Signalling Pathway in HepG2 Cells. *Int. J. Mol. Sci.* 17. doi:10.3390/ijms17071015
- Dally, S., Monceau, V., Corvazier, E., Bredoux, R., Raies, A., Bobe, R., et al. (2009). Compartmentalized Expression of Three Novel Sarco/endoplasmic Reticulum Ca2+ATPase 3 Isoforms Including the Switch to ER Stress, SERCA3f, in Non-failing and Failing Human Heart. *Cell Calcium* 45, 144–154. doi:10.1016/j.ceca.2008.08.002
- Dang, S., Huang, C. X., Wang, X., Wang, X., Hu, J., and Huang, H. (2016). Shensong Yangxin (SSYX) Ameliorates Disordered Excitation Transmission by Suppressing Cardiac Collagen Hyperplasia in Rabbits with Chronic Myocardial



- Infarction. *J. Huazhong Univ. Sci. Technolog Med. Sci.* 36, 162–167. doi:10.1007/s11596-016-1560-4
- Datta, R., Bansal, T., Rana, S., Datta, K., Chattopadhyay, S., Chawla-Sarkar, M., et al. (2015). Hsp90/Cdc37 Assembly Modulates TGF $\beta$  Receptor-II to Act as a Profibrotic Regulator of TGF $\beta$  Signaling during Cardiac Hypertrophy. *Cell Signal.* 27, 2410–2424. doi:10.1016/j.cellsig.2015.09.005
- Daugaard, M., Rohde, M., and Jäättelä, M. (2007). The Heat Shock Protein 70 Family: Highly Homologous Proteins with Overlapping and Distinct Functions. *FEBS Lett.* 581, 3702–3710. doi:10.1016/j.febslet.2007.05.039
- Deng, J. S., Jiang, W. P., Chen, C. C., Lee, L. Y., Li, P. Y., Huang, W. C., et al. (2020). Cordyceps Cicadae Mycelia Ameliorate Cisplatin-Induced Acute Kidney Injury by Suppressing the TLR4/NF-Kb/MAPK and Activating the HO-1/Nrf2 and Sirt-1/AMPK Pathways in Mice. *Oxid Med. Cel Longev* 2020, 7912763. doi:10.1155/2020/7912763
- Du, Y., Wang, M., Liu, X., Zhang, J., Xu, X., Xu, H., et al. (2018). Araloside C Prevents Hypoxia/Reoxygenation-Induced Endoplasmic Reticulum Stress via Increasing Heat Shock Protein 90 in H9c2 Cardiomyocytes. *Front. Pharmacol.* 9, 180. doi:10.3389/fphar.2018.00180
- Fan, F., Duan, Y., Yang, F., Trexler, C., Wang, H., Huang, L., et al. (2020). Deletion of Heat Shock Protein 60 in Adult Mouse Cardiomyocytes Perturbs Mitochondrial Protein Homeostasis and Causes Heart Failure. *Cell Death Differ* 27, 587–600. doi:10.1038/s41418-019-0374-x
- Fan, G. C., Yuan, Q., Song, G., Wang, Y., Chen, G., Qian, J., et al. (2006). Small Heat-Shock Protein Hsp20 Attenuates Beta-Agonist-Mediated Cardiac Remodeling through Apoptosis Signal-Regulating Kinase 1. *Circ. Res.* 99, 1233–1242. doi:10.1161/01.RES.0000251074.19348.af
- Fan, G. C., Zhou, X., Wang, X., Song, G., Qian, J., Nicolaou, P., et al. (2008). Heat Shock Protein 20 Interacting with Phosphorylated Akt Reduces Doxorubicin-Triggered Oxidative Stress and Cardiotoxicity. *Circ. Res.* 103, 1270–1279. doi:10.1161/CIRCRESAHA.108.182832
- Foo, R. S., Siow, R. C., Brown, M. J., and Bennett, M. R. (2006). Heme Oxygenase-1 Gene Transfer Inhibits Angiotensin II-Mediated Rat Cardiac Myocyte Apoptosis but Not Hypertrophy. *J. Cel Physiol* 209, 1–7. doi:10.1002/jcp.20723
- Fu, H. Y., Minamino, T., Tsukamoto, O., Sawada, T., Asai, M., Kato, H., et al. (2008). Overexpression of Endoplasmic Reticulum-Resident Chaperone Attenuates Cardiomyocyte Death Induced by Proteasome Inhibition. *Cardiovasc. Res.* 79, 600–610. doi:10.1093/cvr/cvn128
- Fu, W., Chen, M., Ou, L., Li, T., Chang, X., Huang, R., et al. (2019). Xiaoyaosan Prevents Atherosclerotic Vulnerable Plaque Formation through Heat Shock Protein/glucocorticoid Receptor axis-mediated Mechanism. *Am. J. Transl Res.* 11, 5531–5545.
- Gao, Y., Chu, S. F., Li, J. P., Zhang, Z., Yan, J. Q., Wen, Z. L., et al. (2015). Protopanaxtriol Protects against 3-nitropropionic Acid-Induced Oxidative Stress in a Rat Model of Huntington's Disease. *Acta Pharmacol. Sin* 36, 311–322. doi:10.1038/aps.2014.107
- Gao, Z., Zhang, J., Li, L., Shen, L., Li, Q., Zou, Y., et al. (2016). Heat Shock Proteins 27 and 70 Contribute to the protection of Schisandrin B against D-Galactosamine-Induced Liver Injury in Mice. *Can. J. Physiol. Pharmacol.* 94, 373–378. doi:10.1139/cjpp-2015-0419
- Genth-Zotz, S., Bolger, A. P., Kalra, P. R., von Haehling, S., Doehner, W., Coats, A. J., et al. (2004). Heat Shock Protein 70 in Patients with Chronic Heart Failure: Relation to Disease Severity and Survival. *Int. J. Cardiol.* 96, 397–401. doi:10.1016/j.ijcard.2003.08.008
- Gombos, T., Föhrész, Z., Pozsonyi, Z., Jánoskúti, L., and Prohászka, Z. (2008). Interaction of Serum 70-kDa Heat Shock Protein Levels and HspA1B (+1267) Gene Polymorphism with Disease Severity in Patients with Chronic Heart Failure. *Cell Stress Chaperones* 13, 199–206. doi:10.1007/s12192-007-0001-5
- He, J., Han, S., Li, X. X., Wang, Q. Q., Cui, Y., Chen, Y., et al. (2019). Diethyl Blechnic Exhibits Anti-inflammatory and Antioxidative Activity via the TLR4/MyD88 Signaling Pathway in LPS-Stimulated RAW264.7 Cells. *Molecules* 24, doi:10.3390/molecules24244502
- He, W. T., Zhu, Y. H., Zhang, T., Abulimiti, P., Zeng, F. Y., Zhang, L. P., et al. (2019). Curcumin Reverses 5-Fluorouracil Resistance by Promoting Human Colon Cancer HCT-8/5-FU Cell Apoptosis and Down-Regulating Heat Shock Protein 27 and P-Glycoprotein. *Chin. J. Integr. Med.* 25, 416–424. doi:10.1007/s11655-018-2997-z
- He, Y., Li, M., Leng, W., Lv, B., Huan, Y., Liu, B., et al. (2018). Zhenbao Pill Reduces Treg Cell Proportion in Acute Spinal Cord Injury Rats by Regulating TUG1/miR-214/HSP27 axis. *Biosci. Rep.* 38. doi:10.1042/BSR20180895
- Higashikuni, Y., Tanaka, K., Kato, M., Nureki, O., Hirata, Y., Nagai, R., et al. (2013). Toll-like Receptor-2 Mediates Adaptive Cardiac Hypertrophy in Response to Pressure Overload through Interleukin-1 $\beta$  Upregulation via Nuclear Factor  $\kappa$ B Activation. *J. Am. Heart Assoc.* 2, e000267. doi:10.1161/Jaha.113.000267
- Hou, Y. Z., Wang, S., Zhao, Z. Q., Wang, X. L., Li, B., Soh, S. B., et al. (2013). Clinical Assessment of Complementary Treatment with Qishen Yiqi Dripping Pills on Ischemic Heart Failure: Study Protocol for a Randomized, Double-Blind, Multicenter, Placebo-Controlled Trial (CACT-IHF). *Trials* 14, 138. doi:10.1186/1745-6215-14-138
- Hu, H., Wang, C., Jin, Y., Meng, Q., Liu, Q., Liu, Z., et al. (2019). Catalpol Inhibits Homocysteine-Induced Oxidation and Inflammation via Inhibiting Nox4/NF-Kb and GRP78/PERK Pathways in Human Aorta Endothelial Cells. *Inflammation* 42, 64–80. doi:10.1007/s10753-018-0873-9
- Huang, Z., Zhao, Q., Chen, M., Zhang, J., and Ji, L. (2019). Liquiritigenin and Liquiritin Alleviated Monocrotaline-Induced Hepatic Sinusoidal Obstruction Syndrome via Inhibiting HSP60-Induced Inflammatory Injury. *Toxicology* 428, 152307. doi:10.1016/j.tox.2019.152307
- Ibrahim, I. M., Abdelmalek, D. H., and Elfiky, A. A. (2019). GRP78: A Cell's Response to Stress. *Life Sci.* 226, 156–163. doi:10.1016/j.lfs.2019.04.022
- Jenei, Z. M., Gombos, T., Föhrész, Z., Pozsonyi, Z., Karádi, L., Jánoskúti, L., et al. (2013). Elevated Extracellular HSP70 (HSPA1A) Level as an Independent Prognostic Marker of Mortality in Patients with Heart Failure. *Cell Stress Chaperones* 18, 809–813. doi:10.1007/s12192-013-0425-z
- Jia, R., Gu, Z., He, Q., Du, J., Cao, L., Jeney, G., et al. (2019). Anti-oxidative, Anti-inflammatory and Hepatoprotective Effects of Radix Bupleuri Extract against Oxidative Damage in tilapia (*Oreochromis niloticus*) via Nrf2 and TLRs Signaling Pathway. *Fish. Shellfish Immunol.* 93, 395–405. doi:10.1016/j.fsi.2019.07.080
- Jian, M. (2002). Clinical Observation of Congestive Heart Failure Treated by Integrated Traditional Chinese and Western Medicine. *Zhongguo Zhong Xi Yi Jie He Za Zhi* 22, 542–544.
- Jiang, Q. W., Cheng, K. J., Mei, X. L., Qiu, J. G., Zhang, W. J., Xue, Y. Q., et al. (2015). Synergistic Anticancer Effects of Triptolide and Celastrol, Two Main Compounds from Thunder God Vine. *Oncotarget* 6, 32790–32804. doi:10.18632/oncotarget.5411
- Kapustian, L. L., Vigontina, O. A., Rozhko, O. T., Ryabenko, D. V., Michowski, W., Lesniak, W., et al. (2013). Hsp90 and its Co-chaperone, Sgt1, as Autoantigens in Dilated Cardiomyopathy. *Heart Vessels* 28, 114–119. doi:10.1007/s00380-011-0226-1
- Kim, Y. K., Suarez, J., Hu, Y., McDonough, P. M., Boer, C., Dix, D. J., et al. (2006). Deletion of the Inducible 70-kDa Heat Shock Protein Genes in Mice Impairs Cardiac Contractile Function and Calcium Handling Associated with Hypertrophy. *Circulation* 113, 2589–2597. doi:10.1161/Circulationaha.105.598409
- Kirchhoff, S. R., Gupta, S., and Knowlton, A. A. (2002). Cytosolic Heat Shock Protein 60, Apoptosis, and Myocardial Injury. *Circulation* 105, 2899–2904. doi:10.1161/01.cir.0000019403.35847.23
- Kregel, K. C. (19852002). Heat Shock Proteins: Modifying Factors in Physiological Stress Responses and Acquired Thermotolerance. *J. Appl. Physiol.* (1985) 92, 2177–2186. doi:10.1152/japplphysiol.01267.2001
- Kunde, D. A., Chong, W. C., Nerurkar, P. V., Ahuja, K. D., Just, J., Smith, J. A., et al. (2017). Bitter Melon Protects against ER Stress in LS174T Colonic Epithelial Cells. *BMC Complement. Altern. Med.* 17, 2. doi:10.1186/s12906-016-1522-1
- Lan, Y. L., Zhou, J. J., Liu, J., Huo, X. K., Wang, Y. L., Liang, J. H., et al. (2018). Uncaria Rhynchophylla Ameliorates Parkinson's Disease by Inhibiting HSP90 Expression: Insights from Quantitative Proteomics. *Cell Physiol Biochem* 47, 1453–1464. doi:10.1159/000490837
- Lee, K. H., Jang, Y., and Chung, J. H. (2010). Heat Shock Protein 90 Regulates I $\kappa$ B Kinase Complex and NF-Kb Activation in Angiotensin II-Induced Cardiac Cell Hypertrophy. *Exp. Mol. Med.* 42, 703–711. doi:10.3858/em.2010.42.10.069
- Li, H., Liu, Y., Wen, M., Zhao, F., Zhao, Z., Liu, Y., et al. (2019). Hydroxysafflor Yellow A (HSYA) Alleviates Apoptosis and Autophagy of Neural Stem Cells Induced by Heat Stress via P38 MAPK/MK2/Hsp27-78 Signaling Pathway. *Biomed. Pharmacother.* 114, 108815. doi:10.1016/j.biopha.2019.108815

- Li, M., Yu, X., Guo, H., Sun, L., Wang, A., Liu, Q., et al. (2014). Bufalin Exerts Antitumor Effects by Inducing Cell Cycle Arrest and Triggering Apoptosis in Pancreatic Cancer Cells. *Tumour Biol.* 35, 2461–2471. doi:10.1007/s13277-013-1326-6
- Li, T., Chen, X., Dai, X. Y., Wei, B., Weng, Q. J., Chen, X., et al. (2017). Novel Hsp90 Inhibitor Platycodin D Disrupts Hsp90/Cdc37 Complex and Enhances the Anticancer Effect of mTOR Inhibitor. *Toxicol. Appl. Pharmacol.* 330, 65–73. doi:10.1016/j.taap.2017.07.006
- Li, X., Zhang, J., Huang, J., Ma, A., Yang, J., Li, W., et al. (2013). A Multicenter, Randomized, Double-Blind, Parallel-Group, Placebo-Controlled Study of the Effects of Qili Qiangxin Capsules in Patients with Chronic Heart Failure. *J. Am. Coll. Cardiol.* 62, 1065–1072. doi:10.1016/j.jacc.2013.05.035
- Li, Y., Zou, L., Li, T., Lai, D., Wu, Y., and Qin, S. (2019). Mogroside V Inhibits LPS-Induced COX-2 Expression/ROS Production and Overexpression of HO-1 by Blocking Phosphorylation of AKT1 in RAW264.7 Cells. *Acta Biochim. Biophys. Sin. (Shanghai)* 51, 365–374. doi:10.1093/abbs/gmz014
- Li, Z., Song, Y., Xing, R., Yu, H., Zhang, Y., Li, Z., et al. (2013). Heat Shock Protein 70 Acts as a Potential Biomarker for Early Diagnosis of Heart Failure. *PLoS One* 8, e67964. doi:10.1371/journal.pone.0067964
- Liao, Y., Chen, K., Dong, X., Li, W., Li, G., Huang, G., et al. (2018). Berberine Inhibits Cardiac Remodeling of Heart Failure after Myocardial Infarction by Reducing Myocardial Cell Apoptosis in Rats. *Exp. Ther. Med.* 16, 2499–2505. doi:10.3892/etm.2018.6438
- Lin, L., Kim, S. C., Wang, Y., Gupta, S., Davis, B., Simon, S. I., et al. (2007). HSP60 in Heart Failure: Abnormal Distribution and Role in Cardiac Myocyte Apoptosis. *Am. J. Physiol. Heart Circ. Physiol.* 293, H2238–H2247. doi:10.1152/ajpheart.00740.2007
- Lin, P., Weng, X., Liu, F., Ma, Y., Chen, H., Shao, X., et al. (2015). Bushen Zhuangjin Decoction Inhibits TM-Induced Chondrocyte Apoptosis Mediated by Endoplasmic Reticulum Stress. *Int. J. Mol. Med.* 36, 1519–1528. doi:10.3892/ijmm.2015.2387
- Liu, J., Peter, K., Shi, D., Zhang, L., Dong, G., Zhang, D., et al. (2014). Traditional Formula, Modern Application: Chinese Medicine Formula Sini Tang Improves Early Ventricular Remodeling and Cardiac Function after Myocardial Infarction in Rats. *Evid. Based Complement. Alternat Med.* 2014, 141938. doi:10.1155/2014/141938
- Liu, L., Wang, Y., Cao, Z. Y., Wang, M. M., Liu, X. M., Gao, T., et al. (2015). Up-regulated TLR4 in Cardiomyocytes Exacerbates Heart Failure after Long-Term Myocardial Infarction. *J. Cel Mol Med* 19, 2728–2740. doi:10.1111/jcmm.12659
- Liu, L., Zhang, C., Kalionis, B., Wan, W., Murthi, P., Chen, C., et al. (2016). EGB761 Protects against Aβ1-42 Oligomer-Induced Cell Damage via Endoplasmic Reticulum Stress Activation and Hsp70 Protein Expression Increase in SH-Sy5y Cells. *Exp. Gerontol.* 75, 56–63. doi:10.1016/j.exger.2016.01.003
- Liu, L., Zhang, X., Qian, B., Min, X., Gao, X., Li, C., et al. (2007). Over-expression of Heat Shock Protein 27 Attenuates Doxorubicin-Induced Cardiac Dysfunction in Mice. *Eur. J. Heart Fail.* 9, 762–769. doi:10.1016/j.ejheart.2007.03.007
- Liu, P., Bao, H. Y., Jin, C. C., Zhou, J. C., Hua, F., Li, K., et al. (2019). Targeting Extracellular Heat Shock Protein 70 Ameliorates Doxorubicin-Induced Heart Failure through Resolution of Toll-like Receptor 2-Mediated Myocardial Inflammation. *J. Am. Heart Assoc.* 8, e012338. doi:10.1161/Jaha.119.012338
- Liu, S., Iskandar, R., Chen, W., Zhang, J., Wang, Y., Chen, X., et al. (2016). Soluble Glycoprotein 130 and Heat Shock Protein 27 as Novel Candidate Biomarkers of Chronic Heart Failure with Preserved Ejection Fraction. *Heart Lung Circ.* 25, 1000–1006. doi:10.1016/j.hlc.2016.02.011
- Liu, X., Simpson, J. A., Brunt, K. R., Ward, C. A., Hall, S. R., Kinobe, R. T., et al. (2007). Preemptive Heme Oxygenase-1 Gene Delivery Reveals Reduced Mortality and Preservation of Left Ventricular Function 1 Yr after Acute Myocardial Infarction. *Am. J. Physiol. Heart Circ. Physiol.* 293, H48–H59. doi:10.1152/ajpheart.00741.2006
- Ma, Z. J., Wang, X. X., Su, G., Yang, J. J., Zhu, Y. J., Wu, Y. W., et al. (2016). Proteomic Analysis of Apoptosis Induction by Laricresinol in Human HepG2 Cells. *Chem. Biol. Interact.* 256, 209–219. doi:10.1016/j.cbi.2016.07.011
- Marunouchi, T., Abe, Y., Murata, M., Inomata, S., Sanbe, A., Takagi, N., et al. (2013). Changes in Small Heat Shock Proteins HSPB1, HSPB5 and HSPB8 in Mitochondria of the Failing Heart Following Myocardial Infarction in Rats. *Biol. Pharm. Bull.* 36, 529–539. doi:10.1248/bpb.b12-00796
- Marunouchi, T., Araki, M., Murata, M., Takagi, N., and Tanonaka, K. (2013). Possible Involvement of HSP90-HSF1 Multichaperone Complex in Impairment of HSP72 Induction in the Failing Heart Following Myocardial Infarction in Rats. *J. Pharmacol. Sci.* 123, 336–346. doi:10.1254/jphs.13109fp
- Marunouchi, T., Inomata, S., Sanbe, A., Takagi, N., and Tanonaka, K. (2014). Protective Effect of Geranylgeranylacetone via Enhanced Induction of HSPB1 and HSPB8 in Mitochondria of the Failing Heart Following Myocardial Infarction in Rats. *Eur. J. Pharmacol.* 730, 140–147. doi:10.1016/j.ejphar.2014.02.037
- Marunouchi, T., Murata, M., Takagi, N., and Tanonaka, K. (2013). Possible Involvement of Phosphorylated Heat-Shock Factor-1 in Changes in Heat Shock Protein 72 Induction in the Failing Rat Heart Following Myocardial Infarction. *Biol. Pharm. Bull.* 36, 1332–1340. doi:10.1248/bpb.b13-00196
- Minamino, T., Komuro, I., and Kitakaze, M. (2010). Endoplasmic Reticulum Stress as a Therapeutic Target in Cardiovascular Disease. *Circ. Res.* 107, 1071–1082. doi:10.1161/CIRCRESAHA.110.227819
- Mohamed, B. A., Barakat, A. Z., Zimmermann, W. H., Bittner, R. E., Mühlfeld, C., Hünlich, M., et al. (2012). Targeted Disruption of Hspa4 Gene Leads to Cardiac Hypertrophy and Fibrosis. *J. Mol. Cel Cardiol* 53, 459–468. doi:10.1016/j.jmcc.2012.07.014
- Mymrikov, E. V., Seit-Nebi, A. S., and Gusev, N. B. (2011). Large Potentials of Small Heat Shock Proteins. *Physiol. Rev.* 91, 1123–1159. doi:10.1152/physrev.00023.2010
- Naka K, K., Veziraki, P., Kalaitzakis, A., Zerikiotis, S., Michalis, L., and Angelidis, C. (2014). Hsp70 Regulates the Doxorubicin-Mediated Heart Failure in Hsp70-Transgenic Mice. *Cell Stress Chaperones* 19, 853–864. doi:10.1007/s12192-014-0509-4
- Nan, L., Xie, Q., Chen, Z., Zhang, Y., Chen, Y., Li, H., et al. (2020). Involvement of PARP-1/AIF Signaling Pathway in Protective Effects of Gualou Guizhi Decoction against Ischemia-Reperfusion Injury-Induced Apoptosis. *Neurochem. Res.* 45, 278–294. doi:10.1007/s11064-019-02912-3
- Nie, P., Meng, F., Zhang, J., Wei, X., and Shen, C. (20192019). Astragaloside IV Exerts a Myocardial Protective Effect against Cardiac Hypertrophy in Rats, Partially via Activating the Nrf2/HO-1 Signaling Pathway. *Oxid Med. Cel Longev* 2019, 4625912. doi:10.1155/2019/4625912
- Niizeki, T., Takeishi, Y., Watanabe, T., Nitobe, J., Miyashita, T., Miyamoto, T., et al. (2008). Relation of Serum Heat Shock Protein 60 Level to Severity and Prognosis in Chronic Heart Failure Secondary to Ischemic or Idiopathic Dilated Cardiomyopathy. *Am. J. Cardiol.* 102, 606–610. doi:10.1016/j.amjcard.2008.04.030
- Okada, K., Minamino, T., Tsukamoto, Y., Liao, Y., Tsukamoto, O., Takashima, S., et al. (2004). Prolonged Endoplasmic Reticulum Stress in Hypertrophic and Failing Heart after Aortic Constriction: Possible Contribution of Endoplasmic Reticulum Stress to Cardiac Myocyte Apoptosis. *Circulation* 110, 705–712. doi:10.1161/01.Cir.0000137836.95625.D4
- Owen, S., Zhao, H., Dart, A., Wang, Y., Ruge, F., Gao, Y., et al. (2016). Heat Shock Protein 27 Is a Potential Indicator for Response to YangZheng XiaoJi and Chemotherapy Agents in Cancer Cells. *Int. J. Oncol.* 49, 1839–1847. doi:10.3892/ijo.2016.3685
- Panneerselvam, L., Raghunath, A., and Perumal, E. (2017). Differential Expression of Myocardial Heat Shock Proteins in Rats Acutely Exposed to Fluoride. *Cell Stress Chaperones* 22, 743–750. doi:10.1007/s12192-017-0801-1
- Ponikowski, P., Anker, S. D., AlHabib, K. F., Cowie, M. R., Force, T. L., Hu, S., et al. (2014). Heart Failure: Preventing Disease and Death Worldwide. *ESC Heart Fail.* 1, 4–25. doi:10.1002/ehf2.12005
- Qian, W., Su, Y., Zhang, Y., Yao, N., Gu, N., Zhang, X., et al. (2018). Secretome Analysis of Rat Osteoblasts during Icarin Treatment Induced Osteogenesis. *Mol. Med. Rep.* 17, 6515–6525. doi:10.3892/mmr.2018.8715
- Raju, V. S., Imai, N., and Liang, C. S. (1999). Chamber-specific Regulation of Heme Oxygenase-1 (Heat Shock Protein 32) in Right-Sided Congestive Heart Failure. *J. Mol. Cel Cardiol* 31, 1581–1589. doi:10.1006/jmcc.1999.0995
- Ranek, M. J., Stachowski, M. J., Kirk, J. A., and Willis, M. S. (2018). The Role of Heat Shock Proteins and Co-chaperones in Heart Failure. *Philos. Trans. R. Soc. Lond. B Biol. Sci.* 373. doi:10.1098/rstb.2016.0530
- Ren, Z. H., Ke, Z. P., Luo, M., and Shi, Y. (2018). Icarin Protects against Ischemia-reperfusion I-njury in H9C2 C-ells by U-pregulating H-eat S-hock P-rotein 20. *Mol. Med. Rep.* 17, 3336–3343. doi:10.3892/mmr.2017.8251
- Rizzo, M., Macario, A. J., de Macario, E. C., Gouni-Berthold, I., Berthold, H. K., Rini, G. B., et al. (2011). Heat Shock Protein-60 and Risk for Cardiovascular Disease. *Curr. Pharm. Des.* 17, 3662–3668. doi:10.2174/138161211798220981

- Sawada, T., Minamino, T., Fu, H. Y., Asai, M., Okuda, K., Isomura, T., et al. (2010). X-box Binding Protein 1 Regulates Brain Natriuretic Peptide through a Novel AP1/CRE-like Element in Cardiomyocytes. *J. Mol. Cel Cardiol* 48, 1280–1289. doi:10.1016/j.yjmcc.2010.02.004
- Schwarz, D. S., and Blower, M. D. (2016). The Endoplasmic Reticulum: Structure, Function and Response to Cellular Signaling. *Cell Mol Life Sci* 73, 79–94. doi:10.1007/s00018-015-2052-6
- Shan, Y. X., Liu, T. J., Su, H. F., Samsamshariat, A., Mestrl, R., and Wang, P. H. (2003). Hsp10 and Hsp60 Modulate Bcl-2 Family and Mitochondria Apoptosis Signaling Induced by Doxorubicin in Cardiac Muscle Cells. *J. Mol. Cel Cardiol* 35, 1135–1143. doi:10.1016/s0022-2828(03)00229-3
- Shang, H., Zhang, J., Yao, C., Liu, B., Gao, X., Ren, M., et al. (2013). Qi-shen-yi-qi Dripping Pills for the Secondary Prevention of Myocardial Infarction: a Randomised Clinical Trial. *Evid. Based Complement. Alternat Med.* 2013, 738391. doi:10.1155/2013/738391
- Shi, M., Liu, Y., Feng, L., Cui, Y., Chen, Y., Wang, P., et al. (20152015). Protective Effects of Scutellarin on Human Cardiac Microvascular Endothelial Cells against Hypoxia-Reoxygenation Injury and its Possible Target-Related Proteins. *Evid. Based Complement. Alternat Med.* 2015, 278014. doi:10.1155/2015/278014
- Shou, X., Zhou, R., Zhu, L., Ren, A., Wang, L., Wang, Y., et al. (2018). Emodin, A Chinese Herbal Medicine, Inhibits Reoxygenation-Induced Injury in Cultured Human Aortic Endothelial Cells by Regulating the Peroxisome Proliferator-Activated Receptor- $\gamma$  (PPAR- $\gamma$ ) and Endothelial Nitric Oxide Synthase (eNOS) Signaling Pathway. *Med. Sci. Monit.* 24, 643–651. doi:10.12659/msm.908237
- Shrestha, L., and Young, J. C. (2016). Function and Chemotypes of Human Hsp70 Chaperones. *Curr. Top. Med. Chem.* 16, 2812–2828. doi:10.2174/1568026616666160413142028
- Sidorik, L., Kyyamova, R., Bobyk, V., Kapustian, L., Rozhko, O., Vigontina, O., et al. (2005). Molecular Chaperone, HSP60, and Cytochrome P450 2E1 Co-expression in Dilated Cardiomyopathy. *Cell Biol Int* 29, 51–55. doi:10.1016/j.cellbi.2004.11.011
- Stetler, R. A., Gan, Y., Zhang, W., Liou, A. K., Gao, Y., Cao, G., et al. (2010). Heat Shock Proteins: Cellular and Molecular Mechanisms in the central Nervous System. *Prog. Neurobiol.* 92, 184–211. doi:10.1016/j.pneurobio.2010.05.002
- Su, J., Xu, T., Jiang, G., Hou, M., Liang, M., Cheng, H., et al. (2019). Gambogenic Acid Triggers Apoptosis in Human Nasopharyngeal Carcinoma CNE-2Z Cells by Activating Volume-Sensitive Outwardly Rectifying Chloride Channel. *Fitoterapia* 133, 150–158. doi:10.1016/j.fitote.2019.01.002
- Sun, A., Zou, Y., Wang, P., Xu, D., Gong, H., Wang, S., et al. (2014). Mitochondrial Aldehyde Dehydrogenase 2 Plays Protective Roles in Heart Failure after Myocardial Infarction via Suppression of the Cytosolic JNK/p53 Pathway in Mice. *J. Am. Heart Assoc.* 3, e000779. doi:10.1161/JAHA.113.000779
- Tamura, S., Marunouchi, T., and Tanonaka, K. (2019). Heat-shock Protein 90 Modulates Cardiac Ventricular Hypertrophy via Activation of MAPK Pathway. *J. Mol. Cel Cardiol* 127, 134–142. doi:10.1016/j.yjmcc.2018.12.010
- Tang, Q., Shang, F., Wang, X., Yang, Y., Chen, G., Chen, Y., et al. (2014). Combination Use of Ferulic Acid, Ligustrazine and Tetrahydropalmatine Inhibits the Growth of Ectopic Endometrial Tissue: a Multi-Target Therapy for Endometriosis Rats. *J. Ethnopharmacol* 151, 1218–1225. doi:10.1016/j.jep.2013.12.047
- Tanonaka, K., Furuhashi, K. I., Yoshida, H., Kakuta, K., Miyamoto, Y., Toga, W., et al. (2001). Protective Effect of Heat Shock Protein 72 on Contractile Function of Perfused Failing Heart. *Am. J. Physiol. Heart Circ. Physiol.* 281, H215–H222. doi:10.1152/ajpheart.2001.281.1.H215
- Tanonaka, K., Toga, W., Yoshida, H., Furuhashi, K., and Takeo, S. (2001). Effect of Long-Term Treatment with Trandolapril on Hsp72 and Hsp73 Induction of the Failing Heart Following Myocardial Infarction. *Br. J. Pharmacol.* 134, 969–976. doi:10.1038/sj.bjp.0704323
- Tanonaka, K., Yoshida, H., Toga, W., Furuhashi, K., and Takeo, S. (2001). Myocardial Heat Shock Proteins during the Development of Heart Failure. *Biochem. Biophys. Res. Commun.* 283, 520–525. doi:10.1006/bbrc.2001.4801
- Toga, W., Tanonaka, K., and Takeo, S. (2007). Changes in Hsp60 Level of the Failing Heart Following Acute Myocardial Infarction and the Effect of Long-Term Treatment with Trandolapril. *Biol. Pharm. Bull.* 30, 105–110. doi:10.1248/bpb.30.105
- Traxler, D., Lainscak, M., Simader, E., Ankersmit, H. J., and Jug, B. (2017). Heat Shock Protein 27 Acts as a Predictor of Prognosis in Chronic Heart Failure Patients. *Clin. Chim. Acta* 473, 127–132. doi:10.1016/j.cca.2017.08.028
- Turakhia, S., Venkatakrishnan, C. D., Dunsmore, K., Wong, H., Kuppusamy, P., Zweier, J. L., et al. (2007). Doxorubicin-induced Cardiotoxicity: Direct Correlation of Cardiac Fibroblast and H9c2 Cell Survival and Aconitase Activity with Heat Shock Protein 27. *Am. J. Physiol. Heart Circ. Physiol.* 293, H3111–H3121. doi:10.1152/ajpheart.00328.2007
- Vedam, K., Nishijima, Y., Druhan, L. J., Khan, M., Moldovan, N. I., Zweier, J. L., et al. (2010). Role of Heat Shock Factor-1 Activation in the Doxorubicin-Induced Heart Failure in Mice. *Am. J. Physiol. Heart Circ. Physiol.* 298, H1832–H1841. doi:10.1152/ajpheart.01047.2009
- Wang, B., Yang, Q., Bai, W. W., Xing, Y. F., Lu, X. T., Sun, Y. Y., et al. (2014). Tongxinluo Protects against Pressure Overload-Induced Heart Failure in Mice Involving VEGF/Akt/eNOS Pathway Activation. *PLoS One* 9, e98047. doi:10.1371/journal.pone.0098047
- Wang, C., Li, Y. Z., Wang, X. R., Lu, Z. R., Shi, D. Z., and Liu, X. H. (2012). Panax Quinquefolium Saponins Reduce Myocardial Hypoxia-Reoxygenation Injury by Inhibiting Excessive Endoplasmic Reticulum Stress. *Shock* 37, 228–233. doi:10.1097/SHK.0b013e31823f15c4
- Wang, G., Hamid, T., Keith, R. J., Zhou, G., Partridge, C. R., Xiang, X., et al. (2010). Cardioprotective and Antiapoptotic Effects of Heme Oxygenase-1 in the Failing Heart. *Circulation* 121, 1912–1925. doi:10.1161/CIRCULATIONAHA.109.905471
- Wang, J., Liu, S., Yin, Y., Li, M., Wang, B., Yang, L., et al. (2015). FOXO3-mediated Up-Regulation of Bim Contributes to Rhein-Induced Cancer Cell Apoptosis. *Apoptosis* 20, 399–409. doi:10.1007/s10495-014-1071-3
- Wang, M., Sun, G. B., Du, Y. Y., Tian, Y., Liao, P., Liu, X. S., et al. (2017). Myricitrin Protects Cardiomyocytes from Hypoxia/Reoxygenation Injury: Involvement of Heat Shock Protein 90. *Front. Pharmacol.* 8, 353. doi:10.3389/fphar.2017.00353
- Wang, M., Tian, Y., Du, Y. Y., Sun, G. B., Xu, X. D., Jiang, H., et al. (2017). Protective Effects of Araloside C against Myocardial Ischaemia/reperfusion Injury: Potential Involvement of Heat Shock Protein 90. *J. Cel Mol Med* 21, 1870–1880. doi:10.1111/jcmm.13107
- Wang, P., He, Q., and Zhu, J. (2016). Emodin-8-O-glucuronic A-cid, from the T-traditional Chinese M-edicine Q-inghuobaiduyin, Affects the S-secretion of I-inflammatory C-ytokines in LPS-stimulated R-aw 264.7 C-ells via HSP70. *Mol. Med. Rep.* 14, 2368–2372. doi:10.3892/mmr.2016.5512
- Wang, R., Yang, M., Wang, M., Liu, X., Xu, H., Xu, X., et al. (2018). Total Saponins of Aralia Elata (Miq) Seem Alleviate Calcium Homeostasis Imbalance and Endoplasmic Reticulum Stress-Related Apoptosis Induced by Myocardial Ischemia/Reperfusion Injury. *Cel Physiol Biochem* 50, 28–40. doi:10.1159/000493954
- Wang, X., Zingarelli, B., O'Connor, M., Zhang, P., Adeyemo, A., Kranias, E. G., et al. (2009). Overexpression of Hsp20 Prevents Endotoxin-Induced Myocardial Dysfunction and Apoptosis via Inhibition of NF-kappaB Activation. *J. Mol. Cel Cardiol* 47, 382–390. doi:10.1016/j.yjmcc.2009.05.016
- Wang, Y., Chen, L., Hagiwara, N., and Knowlton, A. A. (2010). Regulation of Heat Shock Protein 60 and 72 Expression in the Failing Heart. *J. Mol. Cel Cardiol* 48, 360–366. doi:10.1016/j.yjmcc.2009.11.009
- Wang, Y., Wang, Q., Li, C., Lu, L., Zhang, Q., Zhu, R., et al. (2017). A Review of Chinese Herbal Medicine for the Treatment of Chronic Heart Failure. *Curr. Pharm. Des.* 23, 5115–5124. doi:10.2174/1381612823666170925163427
- Wang, Y. L., Lam, K. K., Cheng, P. Y., and Lee, Y. M. (2015). Celastrol Prevents Circulatory Failure via Induction of Heme Oxygenase-1 and Heat Shock Protein 70 in Endotoxemic Rats. *J. Ethnopharmacol* 162, 168–175. doi:10.1016/j.jep.2014.12.062
- Wei, D. F., Wei, Y. X., Cheng, W. D., Yan, M. F., Su, G., Hu, Y., et al. (2012). Proteomic Analysis of the Effect of Triterpenes from Patrinia Heterophylla on Leukemia K562 Cells. *J. Ethnopharmacol* 144, 576–583. doi:10.1016/j.jep.2012.09.043
- Wei, Y. J., Huang, Y. X., Shen, Y., Cui, C. J., Zhang, X. L., Zhang, H., et al. (2009). Proteomic Analysis Reveals Significant Elevation of Heat Shock Protein 70 in Patients with Chronic Heart Failure Due to Arrhythmogenic Right Ventricular Cardiomyopathy. *Mol. Cel Biochem* 332, 103–111. doi:10.1007/s101010-009-0179-1



- Wu, H. J., Hao, J., Wang, S. Q., Jin, B. L., and Chen, X. B. (2012). Protective Effects of Ligustrazine on TNF- $\alpha$ -Induced Endothelial Dysfunction. *Eur. J. Pharmacol.* 674, 365–369. doi:10.1016/j.ejphar.2011.10.046
- Wu, J., Liu, T., Rios, Z., Mei, Q., Lin, X., and Cao, S. (2017). Heat Shock Proteins and Cancer. *Trends Pharmacol. Sci.* 38, 226–256. doi:10.1016/j.tips.2016.11.009
- Yan, B., Shi, J., Xiu, L. J., Liu, X., Zhou, Y. Q., Feng, S. H., et al. (2013). Xiaotan Tongfu Granules Contribute to the Prevention of Stress Ulcers. *World J. Gastroenterol.* 19, 5473–5484. doi:10.3748/wjg.v19.i33.5473
- Yancy, C. W., Jessup, M., Bozkurt, B., Butler, J., Casey, D. E., Jr., Colvin, M. M., et al. (2017/2017). 2017 ACC/AHA/HFSA Focused Update of the 2013 ACCF/AHA Guideline for the Management of Heart Failure: A Report of the American College of Cardiology/American Heart Association Task Force on Clinical Practice Guidelines and the Heart Failure Society of America. *Circulation* 136, e137–e161. doi:10.1161/CIR.0000000000000509
- Yancy, C. W., Jessup, M., Bozkurt, B., Butler, J., Casey, D. E., Jr., Drazner, M. H., et al. (2013/2013). 2013 ACCF/AHA Guideline for the Management of Heart Failure: a Report of the American College of Cardiology Foundation/American Heart Association Task Force on Practice Guidelines. *J. Am. Coll. Cardiol.* 62, e147–239. doi:10.1016/j.jacc.2013.05.019
- Yang, J., Wang, Z., and Chen, D. L. (2017). Shikonin Ameliorates Isoproterenol (ISO)-induced Myocardial Damage through Suppressing Fibrosis, Inflammation, Apoptosis and ER Stress. *Biomed. Pharmacother.* 93, 1343–1357. doi:10.1016/j.biopha.2017.06.086
- Yang, L., Chai, C. Z., Yan, Y., Duan, Y. D., Henz, A., Zhang, B. L., et al. (2017). Spasmolytic Mechanism of Aqueous Licorice Extract on Oxytocin-Induced Uterine Contraction through Inhibiting the Phosphorylation of Heat Shock Protein 27. *Molecules* 22. doi:10.3390/molecules22091392
- Yang, W., Li, H., Cong, X., Wang, X., Jiang, Z., Zhang, Q., et al. (2016). Baicalin Attenuates Lipopolysaccharide Induced Inflammation and Apoptosis of Cow Mammary Epithelial Cells by Regulating NF-Kb and HSP72. *Int. Immunopharmacol.* 40, 139–145. doi:10.1016/j.intimp.2016.08.032
- Yin, C. F., Kao, S. C., Hsu, C. L., Chang, Y. W., Cheung, C. H. Y., Huang, H. C., et al. (2020). Phosphoproteome Analysis Reveals Dynamic Heat Shock Protein 27 Phosphorylation in Tanshinone IIA-Induced Cell Death. *J. Proteome Res.* 19, 1620–1634. doi:10.1021/acs.jproteome.9b00836
- You, W., Min, X., Zhang, X., Qian, B., Pang, S., Ding, Z., et al. (2009). Cardiac-specific Expression of Heat Shock Protein 27 Attenuated Endotoxin-Induced Cardiac Dysfunction and Mortality in Mice through a PI3K/Akt-dependent Mechanism. *Shock* 32, 108–117. doi:10.1097/SHK.0b013e318199165d
- Yu, P., Zhang, Y., Li, C., Li, Y., Jiang, S., Zhang, X., et al. (2015). Class III PI3K-Mediated Prolonged Activation of Autophagy Plays a Critical Role in the Transition of Cardiac Hypertrophy to Heart Failure. *J. Cel Mol Med* 19, 1710–1719. doi:10.1111/jcmm.12547
- Zeng, X. S., Zhou, X. S., Luo, F. C., Jia, J. J., Qi, L., Yang, Z. X., et al. (2014). Comparative Analysis of the Neuroprotective Effects of Ginsenosides Rg1 and Rb1 Extracted from Panax Notoginseng against Cerebral Ischemia. *Can. J. Physiol. Pharmacol.* 92, 102–108. doi:10.1139/cjpp-2013-0274
- Zhang, C., Qu, S., Wei, X., Feng, Y., Zhu, H., Deng, J., et al. (2016). HSP25 Down-Regulation Enhanced P53 Acetylation by Dissociation of SIRT1 from P53 in Doxorubicin-Induced H9c2 Cell Apoptosis. *Cell Stress Chaperones* 21, 251–260. doi:10.1007/s12192-015-0655-3
- Zhang, G., Yang, G., Deng, Y., Zhao, X., Yang, Y., Rao, J., et al. (2016). Ameliorative Effects of Xue-Fu-Zhu-Yu Decoction, Tian-Ma-Gou-Teng-Yin and Wen-Dan Decoction on Myocardial Fibrosis in a Hypertensive Rat Mode. *BMC Complement. Altern. Med.* 16, 56. doi:10.1186/s12906-016-1030-3
- Zhang, L., Gan, W., and An, G. (2012). Influence of Tanshinone IIA on Heat Shock Protein 70, Bcl-2 and Bax Expression in Rats with Spinal Ischemia/reperfusion Injury. *Neural Regen. Res.* 7, 2882–2888. doi:10.3969/j.issn.1673-5374.2012.36.005
- Zhang, Q., Li, H., Wang, S., Liu, M., Feng, Y., and Wang, X. (2013). Icariin Protects Rat Cardiac H9c2 Cells from Apoptosis by Inhibiting Endoplasmic Reticulum Stress. *Int. J. Mol. Sci.* 14, 17845–17860. doi:10.3390/ijms140917845
- Zhang, S., Yuan, M., Cheng, C., Xia, D. H., and Wu, S. W. (2018). Chinese Herbal Medicine Effects on Muscle Atrophy Induced by Simulated Microgravity. *Aerosp Med. Hum. Perform.* 89, 883–888. doi:10.3357/AMHP.5079.2018
- Zhang, X., He, M., Cheng, L., Chen, Y., Zhou, L., Zeng, H., et al. (2008). Elevated Heat Shock Protein 60 Levels Are Associated with Higher Risk of Coronary Heart Disease in Chinese. *Circulation* 118, 2687–2693. doi:10.1161/CIRCULATIONAHA.108.781856
- Zhang, X., Min, X., Li, C., Benjamin, I. J., Qian, B., Zhang, X., et al. (2010). Involvement of Reductive Stress in the Cardiomyopathy in Transgenic Mice with Cardiac-specific Overexpression of Heat Shock Protein 27. *Hypertension* 55, 1412–1417. doi:10.1161/HYPERTENSIONAHA.109.147066
- Zhang, Y., Jiang, D. S., Yan, L., Cheng, K. J., Bian, Z. Y., and Lin, G. S. (2011). HSP75 Protects against Cardiac Hypertrophy and Fibrosis. *J. Cel Biochem* 112, 1787–1794. doi:10.1002/jcb.23091
- Zhang, Y., Li, C., Meng, H., Guo, D., Zhang, Q., Lu, W., et al. (2018). BYD Ameliorates Oxidative Stress-Induced Myocardial Apoptosis in Heart Failure Post-Acute Myocardial Infarction via the P38 MAPK-CRYAB Signaling Pathway. *Front. Physiol.* 9, 505. doi:10.3389/fphys.2018.00505
- Zhang, Y., Wang, H., Cui, L., Zhang, Y., Liu, Y., Chu, X., et al. (2015). Continuing Treatment with Salvia Miltiorrhiza Injection Attenuates Myocardial Fibrosis in Chronic Iron-Overloaded Mice. *PLoS one* 10, e0124061. doi:10.1371/journal.pone.0124061
- Zhang, Z., Rui, W., Wang, Z. C., Liu, D. X., and Du, L. (2017). Anti-proliferation and Anti-metastasis Effect of Barbaloin in Non-small Cell Lung Cancer via Inactivating p38MAPK/Cdc25B/Hsp27 Pathway. *Oncol. Rep.* 38, 1172–1180. doi:10.3892/or.2017.5760
- Zhao, M., Tang, X., Gong, D., Xia, P., Wang, F., and Xu, S. (2020). Bungeanum Improves Cognitive Dysfunction and Neurological Deficits in D-Galactose-Induced Aging Mice via Activating PI3K/Akt/Nrf2 Signaling Pathway. *Front. Pharmacol.* 11, 71. doi:10.3389/fphar.2020.00071
- Zhou, F., Huang, X., Pan, Y., Cao, D., Liu, C., Liu, Y., et al. (2018). Resveratrol Protects HaCaT Cells from Ultraviolet B-Induced Photoaging via Upregulation of HSP27 and Modulation of Mitochondrial Caspase-dependent Apoptotic Pathway. *Biochem. Biophys. Res. Commun.* 499, 662–668. doi:10.1016/j.bbrc.2018.03.207
- Zhou, Q., Qin, W. Z., Liu, S. B., Kwong, J. S., Zhou, J., and Chen, J. (2014). *Shengmai (A Traditional Chinese Herbal Medicine) for Heart Failure*. Oxford, UK: The Cochrane database of systematic reviews, Cd005052.
- Zhou, Y. C., Liu, B., Li, Y. J., Jing, L. L., Wen, G., Tang, J., et al. (2012). Effects of Buyang Huanwu Decoction on Ventricular Remodeling and Differential Protein Profile in a Rat Model of Myocardial Infarction. *Evid. Based Complement. Alternat Med.* 2012, 385247. doi:10.1155/2012/385247
- Zhu, J., Chen, M., Chen, N., Ma, A., Zhu, C., Zhao, R., et al. (2015). Glycyrrhetic Acid Induces G1-phase C-ell C-cycle A-rrest in H-uman N-on-small C-ell L-ung C-ancer C-ells through E-ndoplasmic R-eticulum S-tress P-athway. *Int. J. Oncol.* 46, 981–988. doi:10.3892/ijo.2015.2819
- Zhu, J., Wang, P., He, Q., Zhou, J., and Luo, C. (2013). Evidence of an Anti-apoptotic Effect of Qinghuobaiduyin on Intestinal Mucosa Following Burn Injury. *Exp. Ther. Med.* 6, 1390–1396. doi:10.3892/etm.2013.1314
- Zuo, D., Subjeck, J., and Wang, X. Y. (2016). Unfolding the Role of Large Heat Shock Proteins: New Insights and Therapeutic Implications. *Front. Immunol.* 7, 75. doi:10.3389/fimmu.2016.00075

**Conflict of Interest:** The authors declare that the research was conducted in the absence of any commercial or financial relationships that could be construed as a potential conflict of interest.

**Publisher's Note:** All claims expressed in this article are solely those of the authors and do not necessarily represent those of their affiliated organizations, or those of the publisher, the editors and the reviewers. Any product that may be evaluated in this article, or claim that may be made by its manufacturer, is not guaranteed or endorsed by the publisher.

Copyright © 2022 Wang, Wu, Wang, Yang and Liu. This is an open-access article distributed under the terms of the Creative Commons Attribution License (CC BY). The use, distribution or reproduction in other forums is permitted, provided the original author(s) and the copyright owner(s) are credited and that the original publication in this journal is cited, in accordance with accepted academic practice. No use, distribution or reproduction is permitted which does not comply with these terms.



## GLOSSARY

<b>4-HNE</b>	4-hydroxy-2-nonenol	<b>HSF-1</b>	Heat shock factor-1
<b>AAC</b>	Abdominal aortic constriction;	<b>HSPs</b>	Heat shock proteinsSmall heat shock proteins
<b>ACEI</b>	Angiotensin-converting enzyme inhibitors	<b>HUVECs</b>	Human umbilical vein endothelial cells
<b>AF</b>	Atrial fibrillation	<b>I/R</b>	Ischemia/reperfusion
<b>AIF</b>	Apoptosis inducing factor	<b>ICAM-1</b>	Intercellular cell adhesion molecule-1
<b>Akt</b>	Serine/threonine kinase	<b>ICM</b>	Ischemic cardiomyopathy
<b>ALDH2</b>	Aldehyde dehydrogenase 2	<b>ISO</b>	Isoproterenol
<b>ANF</b>	Atrial natriuretic factor	<b>JNK</b>	Jun N-terminal kinase
<b>Ang II</b>	Angiotensin II	<b>LAD</b>	Left anterior descending
<b>ARB</b>	Angiotensin receptor blockers	<b>LPS</b>	Lipopolysaccharide
<b>ARNI</b>	Angiotensin receptor neprilysin inhibitor	<b>MAPK</b>	Mitogen-activated protein kinase
<b>ARVC</b>	Arrhythmogenic right ventricular cardiomyopathy	<b>MCAO</b>	Middle cerebral artery occlusion
<b>ASK1</b>	Apoptosis signal regulating kinase1	<b>MI</b>	Myocardial infarction
<b>bax</b>	Bcl-2-associated x	<b>mPTP</b>	Mitochondrial MPT pore
<b>bcl-2</b>	B-cell lymphoma-2	<b>NF-κB</b>	Nuclear factor kappa-B
<b>CAL</b>	Coronary artery ligation	<b>Nrf2</b>	Nuclear factor E2-related factor2
<b>CHOP</b>	C/EBP-homologous protein	<b>NSCLC</b>	Non-small cell lung carcinoma
<b>CMECs</b>	Cow mammary epithelial cells	<b>NSCs</b>	Neural stem cells
<b>CRH</b>	Corticotropin releasing hormone	<b>PARP</b>	Poly (ADP-ribose) polymerase
<b>CRYAB</b>	αB-crystallin	<b>PEDF-1</b>	Serpin family F-1
<b>DCM</b>	dilated cardiomyopathy	<b>PERK</b>	dsRNA-activated protein kinase-like endoplasmic reticulum kinase
<b>DOX</b>	Doxorubicin	<b>PI3K</b>	Phosphatidylinositol 3-kinase
<b>ER</b>	Endoplasmic reticulum	<b>PPAR-γ</b>	Peroxisome proliferators-activated receptor-γ
<b>ERE</b>	Estrogen response element	<b>PRDX6</b>	Peroxiredoxin 6
<b>ERKs</b>	Extracellular regulated protein kinases	<b>ROS</b>	Reactive oxygen species
<b>GR</b>	Glucocorticoid receptor	<b>SCP-0-1</b>	Homogeneous Schisandra chinensis polysaccharide-0-1
<b>GRP78</b>	Glucose regulated protein 78	<b>HSPs</b>	Heat shock proteinsSmall heat shock proteins
<b>GSK-3β</b>	Glycogen synthase kinase-3β	<b>SIRT1</b>	Silent information regulator1
<b>H/R</b>	Hypoxia/reoxygenation	<b>TAC</b>	Transverse aortic constriction
<b>HAECs</b>	Human aorta endothelial cells	<b>TCM</b>	Traditional Chinese Medicine
<b>HCMECs</b>	Human cardiac microvascular endothelial cells	<b>TGF-β</b>	Transforming growth factor-β
<b>HF</b>	Heart failure	<b>TLR4</b>	Toll-like receptor 4
<b>HO-1</b>	Heme oxygenase-1	<b>TNF-α</b>	Tumor necrosis factor-α
<b>HPOA</b>	Hypothalamus-pituitary-ovarian axis	<b>UPR</b>	Unfolded protein response
		<b>VEGF</b>	Vascular endothelial growth factor
		<b>α-SMA</b>	α-smooth muscle actin.



# Research Advances in Cardio-Cerebrovascular Diseases of *Ligusticum chuanxiong* Hort.

Dan Li<sup>1</sup>, Yu Long<sup>1</sup>, Shuang Yu<sup>1</sup>, Ai Shi<sup>1</sup>, Jinyan Wan<sup>1</sup>, Jing Wen<sup>1</sup>, Xiaoqiu Li<sup>1</sup>, Songyu Liu<sup>1</sup>, Yulu Zhang<sup>1</sup>, Nan Li<sup>1\*</sup>, Chuan Zheng<sup>1\*</sup>, Ming Yang<sup>2\*</sup> and Lin Shen<sup>3</sup>

<sup>1</sup>State Key Laboratory of Southwestern Chinese Medicine Resources, Chengdu University of Traditional Chinese Medicine, Chengdu, China, <sup>2</sup>Key Laboratory of Modern Preparation of Traditional Chinese Medicine, Ministry of Education, Jiangxi University of Traditional Chinese Medicine, Nanchang, China, <sup>3</sup>Second Affiliated Hospital of Tianjin University of Traditional Chinese Medicine, Tianjin, China

## OPEN ACCESS

### Edited by:

Xianwei Wang,  
Xinxiang Medical University, China

### Reviewed by:

Junfei Gu,  
Nanjing University of Chinese  
Medicine, China  
Chang Chen,  
China Academy of Chinese Medical  
Sciences, China

### \*Correspondence:

Nan Li  
55743198@qq.com  
Chuan Zheng  
zhengchuan@cdutcm.edu.cn  
Ming Yang  
yangming16@126.com

### Specialty section:

This article was submitted to  
Cardiovascular and Smooth Muscle  
Pharmacology,  
a section of the journal  
Frontiers in Pharmacology

**Received:** 10 December 2021

**Accepted:** 28 December 2021

**Published:** 31 January 2022

### Citation:

Li D, Long Y, Yu S, Shi A, Wan J,  
Wen J, Li X, Liu S, Zhang Y, Li N,  
Zheng C, Yang M and Shen L (2022)  
Research Advances in Cardio-  
Cerebrovascular Diseases of  
*Ligusticum chuanxiong* Hort.  
Front. Pharmacol. 12:832673.  
doi: 10.3389/fphar.2021.832673

Cardio-cerebrovascular diseases (CVDs) are a serious threat to human health and account for 31% of global mortality. *Ligusticum chuanxiong* Hort. (CX) is derived from umbellifer plants. Its rhizome, leaves, and fibrous roots are similar in composition but have different contents. It has been used in Japanese, Korean, and other traditional medicine for over 2000 years. Currently, it is mostly cultivated and has high safety and low side effects. Due to the lack of a systematic summary of the efficacy of CX in the treatment of CVDs, this article describes the material basis, molecular mechanism, and clinical efficacy of CX, as well as its combined application in the treatment of CVDs, and has been summarized from the perspective of safety. In particular, the pharmacological effect of CX in the treatment of CVDs is highlighted from the point of view of its mechanism, and the complex mechanism network has been determined to improve the understanding of CX's multi-link and multi-target therapeutic effects, including anti-inflammatory, antioxidant, and endothelial cells. This article offers a new and modern perspective on the impact of CX on CVDs.

**Keywords:** *Ligusticum chuanxiong* Hort., cardio-cerebrovascular diseases, material basis, molecular mechanism, clinical efficacy

## 1 INTRODUCTION

Cardio-cerebrovascular diseases (CVDs) are the general name of cardiovascular and cerebrovascular diseases (Liu et al., 2021). They generally refer to the ischemic or hemorrhagic diseases of the heart, brain, and the whole body caused by hyperlipidemia, blood viscosity, atherosclerosis (AS), hypertension, etc. These include coronary heart disease (CHD), myocardial infarction, angina pectoris, coronary artery insufficiency, aortic AS, and other cardiovascular diseases, as well as ischemic stroke, hemorrhagic stroke, transient cerebral ischemia and other cerebrovascular diseases (Qin, 2020). CVDs can occur alone, but often exist at the same time in different degrees. CVDs is a common and serious threat to human health, with the characteristics of high morbidity, high disability rate, high recurrence rate, and high mortality. More than 31% of deaths worldwide are attributable to cardiovascular diseases, and more than any the other causes of death, this is the main cause of incidence rate and mortality rate in developing and developed countries (Stephanieh and Sarahh, 2020). The burden of global CVDs is increasing day by day, which has become a major public health problem. At present, there are more than 290 million patients with CVDs in China, accounting for 42.5 and 44.6% of the deaths in urban and rural areas (Zhou et al., 2019a). More than 80% of the cardiovascular disease burden could be attributed to known modifiable risk factors such as hypertension, dietary risks, high low-density lipoprotein cholesterol, and impaired kidney function

(Paolo et al., 2020). Hypertension, high cholesterol, and diabetes are the three major risk factors for CVDs, among which hypertension is the primary factor (Wang, 2016).

As we enter a golden age of drug discovery based on natural products, the growing interest in natural products has led to the discovery of new chemical entities for the treatment of various human diseases in the past decades. Natural drugs extracted from herbal medicines are valuable sources of chemical entities and provide important ways to discover new drugs. Complementary and alternative medicine (CAM) can be used to maintain human health for a long time because of less side effects. In addition, an increasing number of patients with CVDs have resorted to the use of CAM, which shows a great application prospect and scope of exploration.

At present, in the exploration of natural drugs for the treatment of CVDs, including *Ligusticum chuanxiong* Hort. (Chuanxiong, CX) (Wang et al., 2018b), *Paeonia veitchii* Lynch. (Chishao, CS) (Ke et al., 2017), *Carthamus tinctorius* L. (Honghua, HH) (Jin et al., 2016), *Salvia miltiorrhiza* Bunge (Danshen, DS) (Lim et al., 2017), *Panax notoginseng* (Sanqi, SQ) (Fan et al., 2016), *Prunus persica* (L.) Batsch (Taoren, TR) (Li et al., 2020a), *Leonurus heterophyllus* Sweet (Yimucao, YMC) (Liu et al., 2019a), *Curcuma zedoaria* Roscoe (Ezhu, EZ) (Wu et al., 2019), etc., it has been found that they play a certain role in hemorheology (Wang et al., 2011), hemodynamics, platelet function (Chen et al., 2020), anticoagulation, antithrombotic (Zhou et al., 2016) and microcirculation functions, regulation of blood lipids (Xu et al., 2019), dilation of blood vessels (Yang et al., 2020a), regulation of energy metabolism (Ke et al., 2017), and other aspects. The above problems are often accompanied by the course of CVDs. These drugs focus on the whole in the prevention and treatment of complex diseases such as hypertension, showing the advantages of “multi-link and multi-target.” As one of the most frequently used drugs, CX can play its role in CVDs by expanding blood vessels and reducing the release of inflammatory mediators (He et al., 2018).

Evidence in the published literature suggests that CX is a herb with great potential to reduce the risk of CVDs and is already widely used clinically. Because CX has received good feedback in the treatment of CVDs, but there is no systematic summary of it, it is difficult to provide concise and clear reference significance for subsequent research and development. The purpose of this review is to summarize the current commonly used CVD drugs, and it has been found that CX has a huge competitive advantage in this aspect. Under the premise that the molecular mechanism of CX is still unclear, the material basis, pharmacological action, and clinical data of the cardiovascular and cerebrovascular aspects of CX are used as a support to provide a state-of-the-art overview of the chemistry and pharmacology about this valuable plant species and explore new perspectives and outline future challenges.

## 2 CHARACTERISTICS OF *LIGUSTICUM CHUANXIONG* HORT.

*Ligusticum chuanxiong* Hort. (Chuanxiong), also known as *Ligusticum wallichii* Franchat, belongs to Angiospermae, family

Umbelliferae, Ligusticum. It is a perennial herb with well-developed rhizomes and irregular nodules. The stem is upright, with vertical and longitudinal lines, many branches in the upper part, and the lower stem nodes expand into a disk shape. The lower part of the stem is petiolate, and the base expands into a sheath. Leaves are oval triangular, 12–15 cm long, and 10–15 cm wide, with 3–4 pinnate lobes. Compound umbellate catkin terminal or lateral seen (Song, 2015). It is cultivated in Sichuan, Guizhou, Yunnan, Guangxi, and other places in China, and its cultivation history can be traced back to 1,500 years ago (Yin, 2013). In addition, according to different producing areas, it can be divided into “Chuanxiong (CX)” produced in Sichuan, “Yunxiong (YX)” produced in Yunnan and Guizhou, “Dongxiong (DX)” produced in the East, and “Fuxiong (FX)” produced in the northeast (Liu, 2020).

As a natural drug, CX was introduced into Europe through Arabia in the 10th century. At present, it is used in more than 20 countries and regions and has become one of the important drug resources in the world, with Japan and South Korea as the main export places (Ma et al., 2001; Li and Yu, 2020). It is known as “Senkyu” (Shizu et al., 2012) and “Tousenkyu” (Yi et al., 2006) in Japan, “chungung” (Rhyu et al., 2004) in South Korea, “*Ligusticum chuanxiong* Hort.” (Lai, 2014) in Thailand, and “Szechuan lovage root” (Li et al., 2012) in Britain.

CX has always been used as medicine for its dry roots, but in recent years, it has been found that the stems, leaves, and fibrous roots of CX also have medicinal value. Compared with the rhizomes, only the content is different (Jiang et al., 2008). In the Bencao Huiyan, the aboveground part of CX is called “Mi Wu,” accounting for 75% of the fresh weight of the whole plant (Jiang et al., 2008; Tang et al., 2021). At the same time, CX is also one of the drugs that can be used for health food announced by the Ministry of Health of China in 2017 (Yu, 2017). In addition, CX is widely used in health-care products, food, cosmetics, and other fields. Its tender stems and leaves can be eaten as vegetables, and its rhizomes can also be stewed with beef and mutton for use (Yang et al., 2013). It has the characteristics of strong safety and wide application fields (Wen et al., 2019).

CX has been used by Chinese medicinal physicians for more than 2,000 years (Shan and Hao, 2011); its pharmacological effect was first mentioned in the Shen Nong Ben Cao Jing (a compilation of information regarding Chinese herbs dating back to 2800 BC) (Ran et al., 2011). It has therapeutic effects on the cardiovascular and cerebrovascular system, liver and kidney system, nervous system, respiratory system, urinary system, and many other systems (Zhang et al., 2020b). CX is widely used in CVDs, which provides a certain theoretical basis for solving the problem of high global mortality and disability (Figure 1). It is an effective drug for the treatment of CVDs. Moreover, CX is widely cultivated and inexpensive. Strengthening its application and development is conducive to reducing the economic burden of patients with CVDs.

## 3 PHARMACODYNAMIC SUBSTANCE BASIS OF *LIGUSTICUM CHUANXIONG* HORT.

Up to now, more than 263 substances have been isolated from different parts (rhizomes, fibrous roots, and aboveground parts)

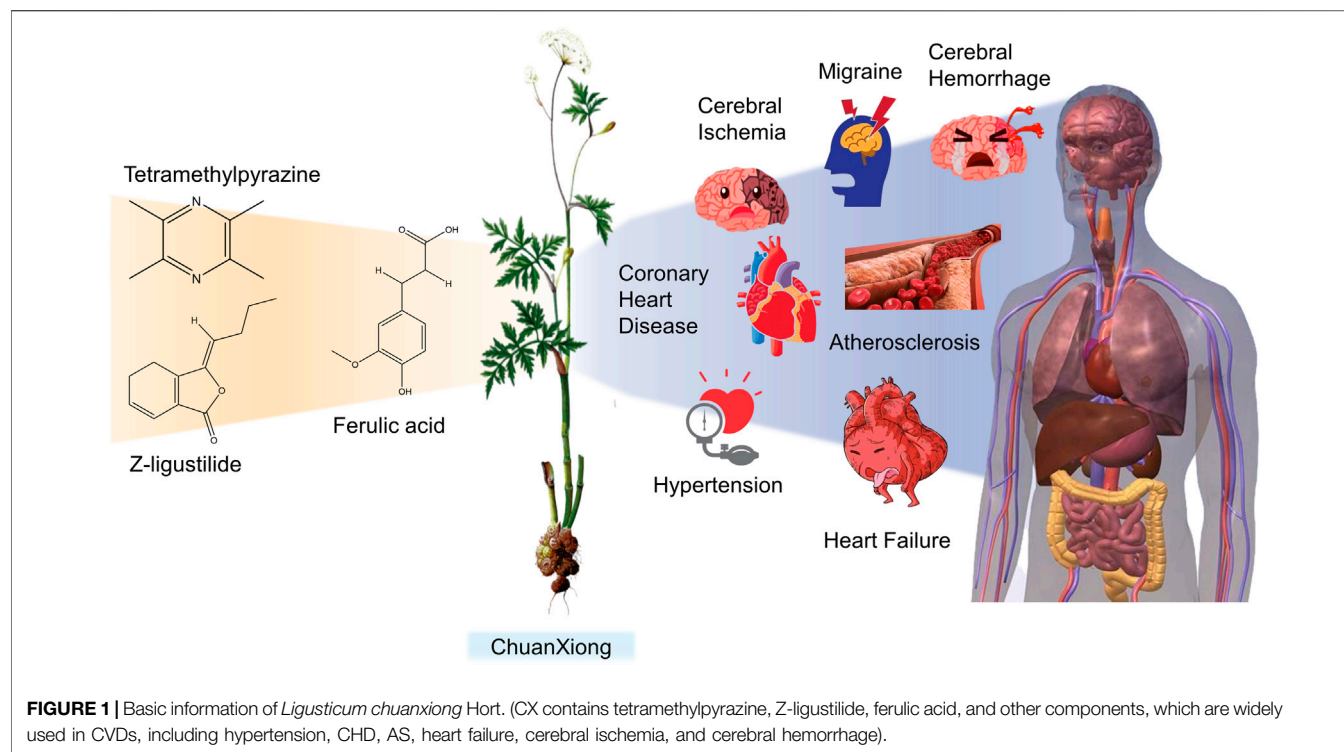


**FIGURE 1 |** Basic information of *Ligusticum chuanxiong* Hort. (CX contains tetramethylpyrazine, Z-ligustilide, ferulic acid, and other components, which are widely used in CVDs, including hypertension, CHD, AS, heart failure, cerebral ischemia, and cerebral hemorrhage).

of CX, such as volatile oils, organic acids, phenolic acids, phthalides, alkaloids, polysaccharides, ceramides, cerebrosides (Ran et al., 2011; Hung and Wu, 2016), and terpenoids (Chen et al., 2018). More than 80 compounds of which belong to various different structural types that have been identified (Li et al., 2012), including tetramethylpyrazine (TMP), ligustilide, senkyunolide A, ferulic acid, and other substances. At present, researches on active components of CX mainly focus on phthalides, alkaloids, and phenolic acids, while researches on other components are relatively few (Li, 2017). TMP and ferulic acid are the more functional and structural representatives of CX (Guo et al., 2016), among which TMP is the most active compound (Zhi-Gang et al., 2015). Based on the study of compounds isolated from CX, 42 compounds that have been proved to have CVD's protective effects are summarized in this article (Table 1).

### 3.1 Volatile Oil

CX contains 1% volatile oil, of which phthalides are the most important compounds, widely existing in *Angelica sinensis* (Oliv.) Diels (Danggui, DG), CX, and other umbelliferous plants, with low polarity and unstable heating characteristics (Fang et al., 2020). The phthalides in CX include more than 30 kinds of phthalides such as Z-ligustilide, E-ligustilide, senkyunolide A, and butylphthalide (Li et al., 2012). Modern pharmacological studies have found that phthalides have a variety of pharmacological activities, and the potential mechanism of cardio-cerebrovascular protection is related to the antithrombotic and antiplatelet effects, neuroprotective effects, improving blood fluidity, and inhibition of the abnormal proliferation of vascular smooth muscle cells (VSMCs) (León et al., 2017). Ligustilide is the most important phthalide in CX,

which can play a neuroprotective role in cerebral ischemic diseases through its antioxidant and anti-apoptosis (Long et al., 2020). Butylphthalide was listed as one of the drugs that can be used in the treatment of ischemic stroke in 2005 by the food and Drug Administration of China (Zou et al., 2018).

### 3.2 Alkaloids

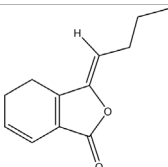
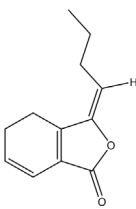
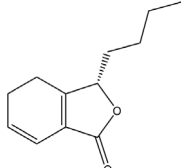
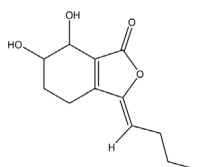
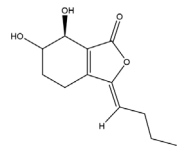
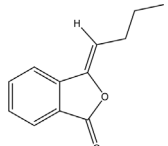
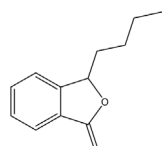
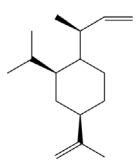
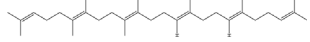
Up to now, 20 kinds of alkaloids have been found from CX, among which TMP is the most studied alkaloid, in addition to adenine, Senkyunolide A and other components (Pu et al., 2020a). TMP widely exists in *Ligusticum* species (Donkor et al., 2016). It was first extracted from CX in 1937 (Cai et al., 2014), and also used as one of the quality evaluation materials of CX (Pu et al., 2020a). It has been used effectively since the 1970s to treat ischemic heart disease, cerebrovascular and thrombotic vascular diseases (Hintz and Ren, 2003). Modern pharmacological studies have found that alkaloids have a variety of pharmacological activities. The potential mechanisms of cardio-cerebrovascular protection are related to antiplatelet aggregation, antithrombotic, antioxidant, anti-inflammatory, inhibition of abnormal proliferation of VSMCs, and neuroprotection (Pu et al., 2020b).

### 3.3 Phenolic Acids

The total phenolic acids of CX is the basis of the pharmacodynamic substance in CX, containing not less than 18 kinds of phenolic acids (Li et al., 2012), which are given priority to with ferulic and chlorogenic acids (Pu et al., 2018). Ferulic acid is an effective component in CX and DG (Luo et al., 2019a), and its content is high in CX. It is often used as the quality control index of CX (Zhang et al., 2018b). According to the

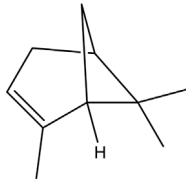
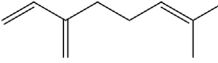
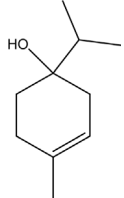
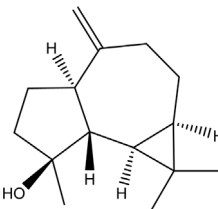
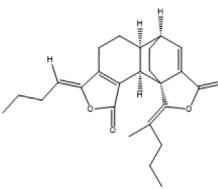
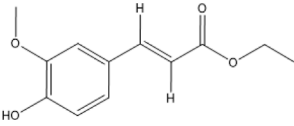
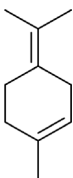
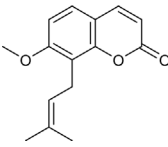
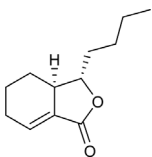


**TABLE 1 |** The pharmacodynamic material basis of *Ligusticum chuanxiong* Hort. in the treatment of CVDs.

Number	Component	Classification	Structural form	CAS	Molecular formula	Molecular weight	Reference
1	Z-Ligustilide	Volatile oil		4431-01-0	C <sub>12</sub> H <sub>14</sub> O <sub>2</sub>	190.24 g/mol	Yi et al. (2006), Zhou et al. (2019b)
2	E-Ligustilide	Volatile oil		81944-08-3	C <sub>12</sub> H <sub>14</sub> O <sub>2</sub>	190.24 g/mol	Yi et al. (2006), Zhou et al. (2019b)
3	Senkyunolide A	Volatile oil		63038-10-8	C <sub>12</sub> H <sub>16</sub> O <sub>2</sub>	192.25 g/mol	Or et al. (2011), Zheng et al. (2018)
4	Senkyunolide H	Volatile oil		94596-27-7	C <sub>12</sub> H <sub>16</sub> O <sub>4</sub>	224.25 g/mol	Yi et al. (2006), Han et al. (2018)
5	Senkyunolide I	Volatile oil		224.25 g/mol	C <sub>12</sub> H <sub>16</sub> O <sub>4</sub>	224.25 g/mol	Yi et al. (2006), Wang et al. (2012)
6	3-Butyridenephthalide	Volatile oil		72917-31-8/551-08-6	C <sub>12</sub> H <sub>12</sub> O <sub>2</sub>	188.22 g/mol	Yi et al. (2006), Boo et al. (2009), Nam et al. (2013)
7	Butylphthalide	Volatile oil		6066-49-5	C <sub>12</sub> H <sub>14</sub> O <sub>2</sub>	190.24 g/mol	Yi et al. (2006), He et al. (2021)
8	β-Elemene	Volatile oil		515-13-9	C <sub>15</sub> H <sub>24</sub>	204.35 g/mol	Liu et al. (2017b), Zhang et al. (2019)
9	Squalene	Volatile oil		111-02-4	C <sub>30</sub> H <sub>50</sub>	410.7 g/mol	Zhang et al. (2019), 'Izzah Ibrahim et al. (2020)

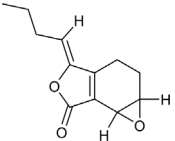
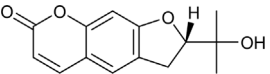
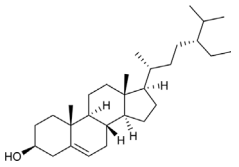
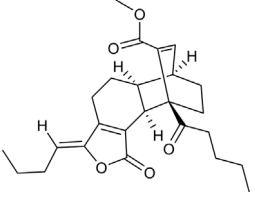
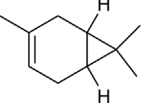
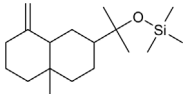
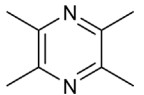
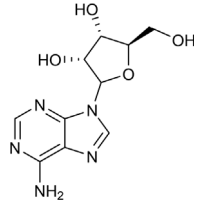
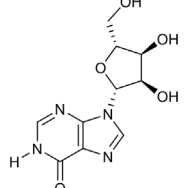
(Continued on following page)

**TABLE 1 |** (Continued) The pharmacodynamic material basis of *Ligusticum chuanxiong* Hort. in the treatment of CVDs.

Number	Component	Classification	Structural form	CAS	Molecular formula	Molecular weight	Reference
10	$\alpha$ -Pinene	Volatile oil		80-56-8	C <sub>10</sub> H <sub>16</sub>	136.23 g/mol	Zhang et al. (2019); Khoshnazar et al. (2020)
11	$\beta$ -Myrcene	Volatile oil		123-35-3	C <sub>10</sub> H <sub>16</sub>	136.23 g/mol	Burcu et al. (2016), Zhang et al. (2019)
12	Terpinen-4-ol	Volatile oil		562-74-3	C <sub>10</sub> H <sub>18</sub> O	154.25 g/mol	Maia-Joca et al. (2014), Zhang et al. (2019)
13	Spathulenol	Volatile oil		6750-60-3	C <sub>15</sub> H <sub>24</sub> O	220.35 g/mol	Suručić et al. (2017), Zhang et al. (2019)
14	Levistilide A	Volatile oil		88182-33-6	C <sub>24</sub> H <sub>28</sub> O <sub>4</sub>	380.5 g/mol	Tong, (2021)
15	Ethyl ferulate	Volatile oil		4046-02-0	C <sub>12</sub> H <sub>14</sub> O <sub>4</sub>	222.24 g/mol	Ya-Xian et al. (2021)
16	Terpinolene	Volatile oil		586-62-9	C <sub>10</sub> H <sub>16</sub>	136.23 g/mol	Labdelli et al. (2019)
17	Osthole	Volatile oil		484-12-8	C <sub>15</sub> H <sub>16</sub> O <sub>3</sub>	224.28 g/mol	Shengzhong et al. (2019)
18	Neocnidilide	Volatile oil		4567-33-3	C <sub>12</sub> H <sub>18</sub> O <sub>2</sub>	194.27 g/mol	Tang et al. (2021)

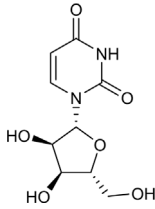
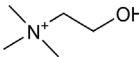
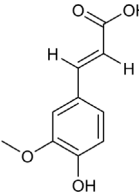
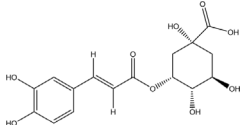
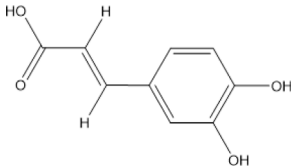
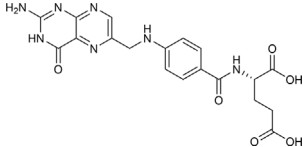
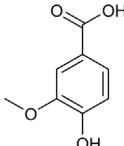
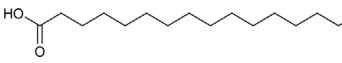
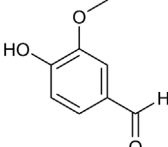
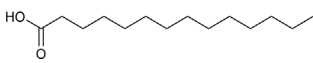
(Continued on following page)

**TABLE 1 |** (Continued) The pharmacodynamic material basis of *Ligusticum chuanxiong* Hort. in the treatment of CVDs.

Number	Component	Classification	Structural form	CAS	Molecular formula	Molecular weight	Reference
19	Z-6,7-Epoxyiligustilide	Volatile oil		106533-40-8	C <sub>12</sub> H <sub>14</sub> O <sub>3</sub>	206.24 g/mol	Liu et al. (2004)
20	Marmesin	Volatile oil		13848-08-6	C <sub>14</sub> H <sub>28</sub> O <sub>2</sub>	246.26 g/mol	Kim et al. (2015)
21	β-Sitosterol	Volatile oil		83-46-5	C <sub>29</sub> H <sub>50</sub> O	414.7 g/mol	Koc et al. (2020)
22	Wallichilide	Volatile oil		—	C <sub>25</sub> H <sub>32</sub> O <sub>5</sub>	412.5 g/mol	Kaillin et al. (2021)
23	3-Carene	Volatile oil		—	—	—	Sedigheh et al. (2013)
24	β-Eudesmol	Volatile oil		—	—	—	Acharya et al. (2021)
25	Tetramethylpyrazine	Alkaloid		1124-11-4	C <sub>8</sub> H <sub>12</sub> N <sub>2</sub>	136.19 g/mol	Li and Chen (2004), Mi et al. (2020)
26	Adenosine	Alkaloid		58-61-7	C <sub>10</sub> H <sub>13</sub> N <sub>5</sub> O <sub>4</sub>	267.24 g/mol	Guieu et al. (2020)
27	Inosine	Alkaloid		58-63-9	C <sub>10</sub> H <sub>12</sub> N <sub>4</sub> O <sub>5</sub>	268.63 g/mol	Lima et al. (2020)

(Continued on following page)

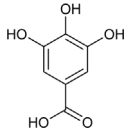
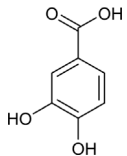
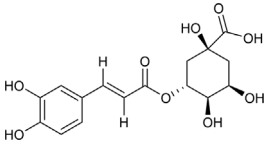
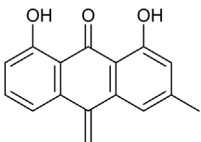
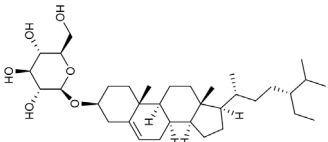
**TABLE 1 |** (Continued) The pharmacodynamic material basis of *Ligusticum chuanxiong* Hort. in the treatment of CVDs.

Number	Component	Classification	Structural form	CAS	Molecular formula	Molecular weight	Reference
28	Uridine	Alkaloid		58-96-8	C <sub>9</sub> H <sub>12</sub> N <sub>2</sub> O <sub>6</sub>	244.2 g/mol	Krylova et al. (2021)
29	Choline	Alkaloid		62-49-7	C <sub>5</sub> H <sub>14</sub> NO <sup>+</sup>	104.17 g/mol	Longzhu et al. (2017)
30	Ferulic acid	Phenolic acid		1135-24-6	C <sub>10</sub> H <sub>10</sub> O <sub>4</sub>	194.18 g/mol	Yi et al. (2006), Zhou et al. (2019b)
31	Neochlorogenic acid	Phenolic acid		906-33-2	C <sub>16</sub> H <sub>18</sub> O <sub>9</sub>	354.31 g/mol	Liu et al. (2017a), Zhang et al. (2017)
32	Caffeic acid	Phenolic acid		331-39-5/ 501-16-6	C <sub>9</sub> H <sub>8</sub> O <sub>4</sub>	180.16 g/mol	Gang (2018)
33	Folic acid	Phenolic acid		59-30-3	C <sub>19</sub> H <sub>19</sub> N <sub>7</sub> O <sub>6</sub>	441.4 g/mol	Ning et al. (2020)
34	Vanillic acid	Phenolic acid		121-34-6	C <sub>8</sub> H <sub>8</sub> O <sub>4</sub>	168.15 g/mol	Xiuya et al. (2020)
35	Palmitic acid	Phenolic acid		57-10-3	C <sub>16</sub> H <sub>32</sub> O <sub>2</sub>	256.42 g/mol	Haibo et al. (2021)
36	Vanillin	Phenolic acid		121-33-5	C <sub>8</sub> H <sub>8</sub> O <sub>3</sub>	152.15 g/mol	Sirangelo et al. (2020)
37	Tetradecanoic acid	Phenolic acid		544-63-8	C <sub>14</sub> H <sub>28</sub> O <sub>2</sub>	228.37 g/mol	Oliviero et al. (2020)

(Continued on following page)



**TABLE 1 |** (Continued) The pharmacodynamic material basis of *Ligusticum chuanxiong* Hort. in the treatment of CVDs.

Number	Component	Classification	Structural form	CAS	Molecular formula	Molecular weight	Reference
38	Gallic acid	Phenolic acid		149-91-7	C <sub>7</sub> H <sub>6</sub> O <sub>5</sub>	170.12 g/mol	Jin et al. (2018)
39	Protocatechuic acid	Phenolic acid		99-50-3	C <sub>7</sub> H <sub>6</sub> O <sub>4</sub>	154.12 g/mol	Liyan et al. (2021)
40	Chlorogenic	Phenolic acid		327-97-9	C <sub>16</sub> H <sub>18</sub> O <sub>9</sub>	354.31 g/mol	Bhandarkar et al. (2018)
41	Chrysophanic acid	Phenolic acid		481-74-3	C <sub>15</sub> H <sub>10</sub> O <sub>4</sub>	254.24 g/mol	Lian et al. (2017)
42	Daucosterol	Others		474-58-8	C <sub>35</sub> H <sub>60</sub> O <sub>6</sub>	576.8 g/mol	Wang et al. (2018)

Chinese Pharmacopoeia 2020, the content of ferulic acid in dried CX should not be less than 0.01%. Modern pharmacological studies have found that CX phenolic acid has a variety of pharmacological activities. The potential mechanism of cardio-cerebrovascular protection is related to neuroprotective effect and regulation of inflammatory metabolism (He et al., 2018; Bao et al., 2019).

### 3.4 Polysaccharides

Polysaccharides widely exist in higher animals, plants, algae, and fungi. As a kind of biological macromolecule, its biological activity is related to its complex structure (Zhang, 2011). Research on the chemical composition of CX has been carried out since the 1950s, while research on CX polysaccharide only started in 2008. CX polysaccharide is composed of glucose, galactose, arabinose, xylose, rhamnose, and mannose (Li et al., 2017a). Modern pharmacological studies have found that CX polysaccharide has a variety of pharmacological activities. The potential mechanism of cardio-cerebrovascular protection is related to antioxidant and anti-inflammatory (Zhao et al., 2017).

### 3.5 Other Categories

Glycosides, ceramides, cerebroside, terpenoids, steroids, flavonoids, and other components were also found in CX (Li, 2017). Wang et al.

(2018) found that daucosterol was one of the effective components in the treatment of cerebrovascular diseases when analyzing the active components of *Erigeron breviscapus* (Vant.) Hand.-Mazz.

## 4 PHARMACOLOGICAL ACTION OF *LIGUSTICUM CHUANXIONG* HORT.

Better understanding of the CX effective components has revealed a complex regulatory mechanism, and these interactions are influenced by each other and form a wide, complex, and multi-directional regulatory network. These effects include anti-inflammatory, antioxidant, maintenance of endothelial cell stability, etc., which are usually associated with the course of CVDs. A systematic understanding of the mechanism of CX is conducive to guiding its clinical application. Here, we sorted out the complex network mechanism of CX in the CVDs, which is a powerful means to enrich our understanding of the “multi-link and multi-target” therapeutic mechanism of CX (Figure 2).

### 4.1 Inhibition of Inflammatory Mediators

Inflammation is a common pathophysiological sign of complex diseases, including AS and myocardial damage, that has recently

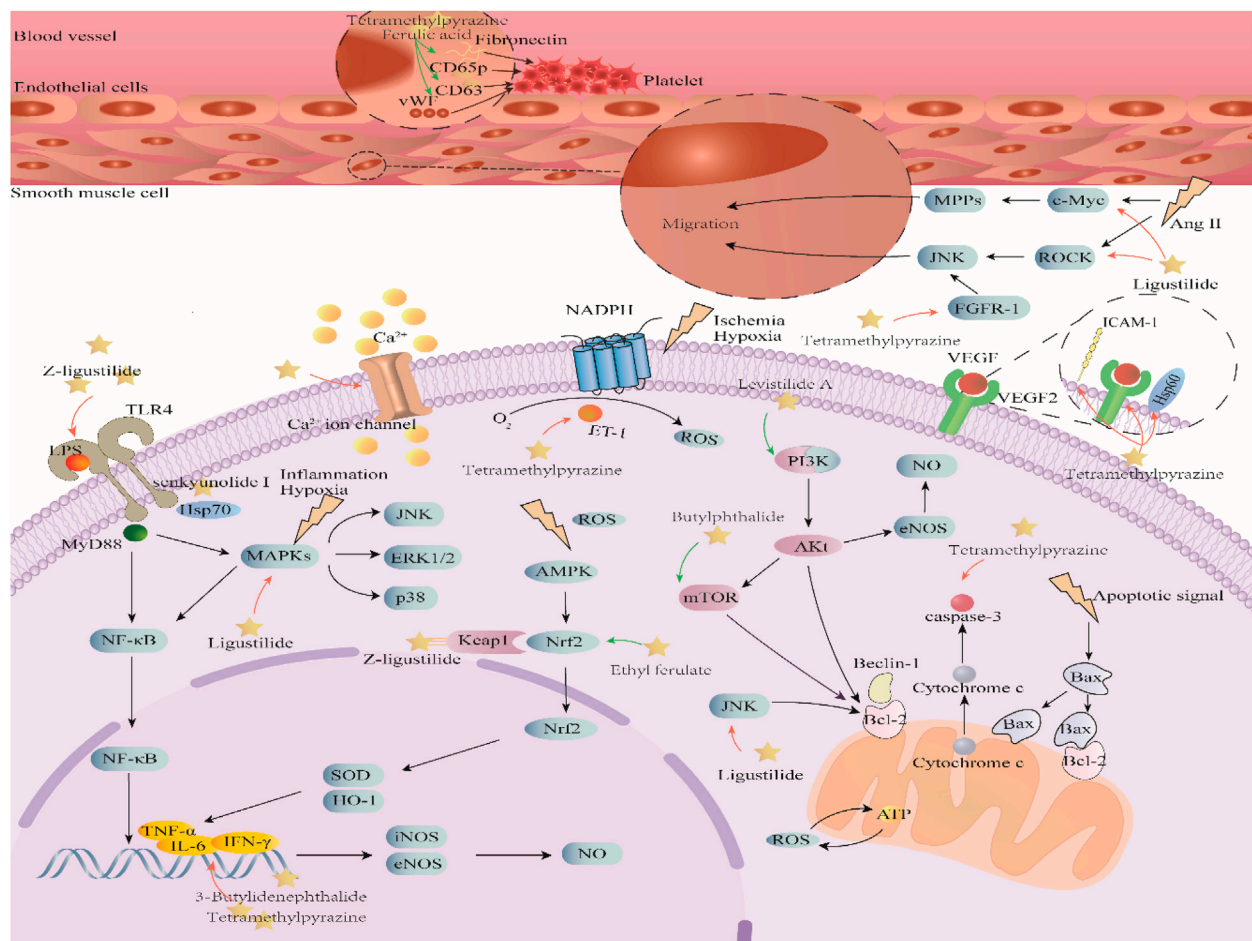


**FIGURE 2 |** Mechanism and pathway of *Ligusticum chuanxiong* Hort. in the treatment of CVDs.

emerged as an important contributor for CVDs development. In addition, it further exacerbates its harmful cardiovascular effects by interacting with the cardiovascular risk factors, thus creating a vicious cycle (Luca et al., 2020). The continuous increase of inflammatory mediators and the decrease of circulating anti-inflammatory cytokines may aggravate the remodeling of vascular extracellular matrix (ECM) and arteriosclerosis, thus expanding pulse pressure, promoting systolic blood pressure, and aggravating cardiovascular conditions (Hirofumi et al., 2017).

In CX, phthalides, such as senkyunolide A, senkyunolide I, and Z-ligustilide, ethyl ferulate, and other components can inhibit the expression of inflammatory factors and achieve anti-inflammatory effect. This effect may be realized through the Hsp70/TLR4/NF-κB, MAPK, and AMPK/Nrf2 pathways. The microglia are resident macrophages in the brain, which are activated during ischemia and produce various inflammatory mediators, including tumor necrosis factor-α (TNF-α), NO, interleukin-6 (IL-6), and interleukin-1 (IL-1). Among them, TNF-α induces post-stroke injury in a variety of ways (Or et al., 2011). Senkyunolide A and Z-ligustilide inhibit the expression of iNOS and TNF-α-mRNA in the microglia and protect neuro-2A cells from activated microglia-induced

cytotoxicity (Or et al., 2011). The contents of NO, TNF-α, and interleukin-1 β (IL-1β) in the lipopolysaccharide (LPS)-induced rat brain microglia were decreased and the activation of the microglia was inhibited by butenylphthalide (Nam et al., 2013). Toll-like receptors (TLRs) are highly conserved members of the interleukin-1 receptor superfamily, which can result in the activation of innate immune responses. Most TLRs are activated by the protein products produced by myeloid differentiation primary gene 88 (MyD88). Activation of the TLRs makes the nuclear factor kappa-B (NF-κB) activated, moves it to the nucleus, and initiates the transcription of immune-related genes, including interferon-γ (IFN-γ), IL-6, TNF-α, and so on (Mayra et al., 2015). The extracellular heat shock protein 70 (Hsp70) is an endogenous ligand of TLR4 and can inhibit TLR4 through negative regulation to play a protective role. Senkyunolide I inhibits oxygen glucose deprivation/reoxygenation-induced TLR4 elevation, and decreases MyD88 expression and NF-κB nuclear translocation. At the same time, the Hsp70 gene is silenced by siRNA before senkyunolide I treatment. It has been found that downregulation of Hsp70 enhanced the expression of TLR4 and weakened the inhibitory effect of senkyunolide I on NF-κB (Hu et al., 2016b). In addition,

TLRs can also activate MAPK, and p38 mitogen-activated protein kinase (p38MAPK), c-Jun terminal kinases (JNKs), and ERK1/2 that have been identified as three major subgroups of MAPKs. p38 and JNK, as two major pathways of MAPK signal transduction, play an important role in inflammatory diseases (Zhou et al., 2019b). Hypoxia and inflammatory factors can activate the p38MAPK and JNK signaling pathways, but the downregulation of p38 MAPK and JNKs can reduce brain injury and neurologic deficit of focal cerebral ischemia and contribute to nerve protection (Gu et al., 2018). Ligustilide can reverse nitroprusside-induced activation of JNK and P38MAPK (Zhou et al., 2019b). In addition, adenosine monophosphate-activated protein kinase (AMPK) can reduce the inflammatory response, and ethyl ferulate can enhance the phosphorylation of AMPK, increase the expression of downstream Nrf2 gene, and promote its nuclear translocation. AMPK inhibitor could reverse the increase of Nrf2 expression caused by ethyl ferulate, and ethyl ferulate did not show the effect of increasing Nrf2 expression in Nrf2 knockout mice (Ya-Xian et al., 2021). The above data can well explain the anti-inflammatory effect of ethyl ferulate, which can be realized through activation of the AMPK/Nrf2 pathway.

## 4.2 Antioxidant

Oxidative stress (OS) greatly leads to endothelial dysfunction and increases the risk of cardiovascular and cerebrovascular events (Heitzer et al., 2001). Excessive reactive oxygen species (ROS) are its direct primers, including the forms of hydroxyl radical (OH $\cdot$ ), superoxide anion (O $^{2-}$ ) and hydrogen peroxide (H $_2$ O $_2$ ), which have become key mediators in the pathogenesis of vascular diseases such as stroke (Davis et al., 2019). Absolute and relative ischemia and hypoxia cause the decrease of oxygen supply and energy supply, which is the primary factor causing OS (Yang and Shanshan, 2015). Under the induction of cerebral ischemia, the energy consumption in the brain can promote the activity of OS. The highly activated nicotinamide adenine dinucleotide phosphate (NADPH) oxidase will produce excessive ROS to aggravate the damage (Ni et al., 2014). In addition, a large number of ROS can cause changes in mitochondrial membrane potential, enhancing its permeability and damaging mitochondria. The loss of ATP synthesis further exacerbates ROS production, creating a vicious cycle (Yang and Shanshan, 2015). Excessive ROS can cause fatal influence to the cells and organs, transforming the redox equilibrium state into a pro-oxidation state. ROS can block blood circulation, destroy epithelial cells and inhibit vasodilation by affecting blood vessels (Lin et al., 2019).

A variety of components in CX can exert antioxidant effects, which may be realized through the Nrf2 pathway and inhibition of NADPH enzyme. Superoxide dismutase (SOD) is an important enzyme for ROS removal in the body; the total antioxidant capacity (T-AOC) is the overall level of antioxidants in the body, which can reflect the antioxidant capacity of the body; malondialdehyde (MDA) is the final product of ROS lipid peroxidation, which can reflect the degree of lipid peroxidation. CX extract can reverse the decrease of SOD and T-AOC and the increase of MDA in the myocardial ischemia

model, showing its antioxidant ability (Wang et al., 2017b). When OS occurs, the synthesis of redox sensitive transcription factor NF-E2-related factor 2 (Nrf2) is increased and Nrf2 is activated, increasing Nrf2 transfer from the cytoplasm to the nucleus. The upregulation of heme oxygenase-1 (HO-1) and SOD expression results in NF- $\kappa$ B failure and alleviates OS injury (Li et al., 2017b). Studies have shown that, as an antioxidant, TMP can exert its antioxidant effect by directly scavenging ROS or inhibiting the activity of the main source of ROS, namely NADPH oxidase (Jiang et al., 2011). Angiotensin II (AngII) can stimulate NADPH oxidase to produce ROS in VSMCs, which can be induced by endothelin-1 (ET-1). TMP can significantly inhibit the expression of ET-1 mRNA induced by AngII, reduce the activity of NADPH enzyme, and reduce the expression of ROS (Wong et al., 2007).

## 4.3 Protection of Endothelial Cells

Vascular events are caused by many factors of complex events. Endothelial cells play an important role in the regulation of vascular homeostasis and are closely related to the regulation of vascular tone, platelet activity, leukocyte adhesion, and thrombosis (Heitzer et al., 2001). Endothelial dysfunction is almost the common denominator of most vascular events (Ni et al., 2014), which is the earliest indicator of the development of cardiovascular disease. Vascular endothelium is a selective blood and tissue barrier that promotes angiogenesis and is necessary for tissues to adequately meet their metabolic and functional needs over the long term. Vascular endothelial cells (VECs) can promote angiogenesis and further aggravate inflammation-related injuries, causing plaque dilation, internal bleeding, and rupture, and promoting atherosclerotic lesions (Zhang et al., 2014; Wang et al., 2015). Therefore, inhibition of VECs growth can help treat AS.

TMP, levistilide A, and other components of CX play an important role in maintaining normal physiological functions of VECs, which may be achieved by inhibiting proliferation of endothelial cells, inhibiting the VEGF/VEGFR2 pathway, activating the PI3K-Akt-ENOS pathway, reducing ROS and icAM-1 and HSP60 expressions. Vascular endothelial growth factor (VEGF) is a key pro-angiogenic factor that promotes angiogenesis by activating VEGF2 receptors on the endothelial cells. Yuan et al. (2018) found that in the model of human umbilical vein endothelial cells (HUVECs) when induced by low concentrations of oxidized low-density lipoprotein (LDL), the number of vascular branch points increased and angiogenesis-related proteins VEGF and VEGF2 were upregulated. After TMP treatment, VEGF2 was downregulated, but VEGF was not affected. These data suggest that TMP can play a therapeutic role in reducing angiogenesis by inhibiting the VEGF/VEGFR2 pathway and inhibiting endothelial cell generation. NO is the key to maintaining endothelial function, and it can protect VECs by vasodilating in the physiological state. The activation of the PI3K-Akt pathway can affect the level of eNOS and thus increase the content of NO. Levistilide A can improve the continuity and integrity of damaged VECs and enhance their vitality. In addition to protecting VECs, the expression levels of PI3K, AKT, and eNOS proteins were increased (Tong, 2021). In addition, excessive ROS produced by

VEC stress can also lead to endothelial dysfunction.  $O_2^{2-}$  is an ROS associated with the cytotoxicity of VECs, and  $H_2O_2$  can produce  $O_2^{2-}$  by activating NADPH oxidase. Ni et al. (2014) found that TMP could improve Ach-induced relaxation of VECs and reverse  $O_2^{2-}$  induced by  $H_2O_2$ , which is consistent with the inhibition effect of NADPH oxidase. Under normal physiological functions, the expression levels of intracellular adhesion molecular-1 (ICAM-1) and heat shock protein 60 (HSP60) in VECs are low. However, when VECs are stimulated by inflammatory factors such as TNF- $\alpha$ , the expressions of ICAM-1 and HSP60 are upregulated, which induces the expression of cell adhesion molecules and produces autoantibodies and autoimmune responses, which are one of the pathogenesis of AS. Wu et al. (2012) detected the levels of ICAM-1 and HSP60 in HUVECs under the influence of TNF- $\alpha$ . It was found that the levels of ICAM-1 and HSP60 of HUVECs stimulated by TNF- $\alpha$  were significantly reduced before and after TMP administration, thus achieving protective effect against VECs disorders and reducing leukocyte adhesion.

#### 4.4 Influence on Autophagy and Apoptosis

Apoptosis is a gene-controlled leukocyte death process—also known as programmed cell death under physiological conditions, is one of the mechanisms to maintain the stability of the internal environment, and is also an important mechanism of cerebral ischemia reperfusion and other diseases. Autophagy, also known as type ii programmed cell death, is often used as a protective mechanism. Under normal physiological conditions, it can remove damaged organelles, protein aggregates, and invading pathogens and maintain cell homeostasis. Under pathological conditions, the over-activation or inhibition of autophagy is often accompanied by a variety of diseases, including AS, myocardial ischemia-reperfusion injury, heart failure, and other cardiovascular diseases (Wang et al., 2017a; Demin et al., 2018). Autophagy and apoptosis are a double-edged sword and are balanced by Beclin-1 and Bcl-2. Beclin-1 can promote autophagy under the regulation of a variety of proteins, but this pro-autophagy binding can be blocked by anti-apoptotic Bcl-2 protein. Activation of PI3K/Akt phosphatidylinositol 3-kinase/serine/threonine kinase (PI3K/Akt) pathway can promote the interaction between Beclin-1 and Bcl-2 protein, thereby inhibiting autophagy (Wang et al., 2017a). Phosphorylation of Beclin-1 and Bcl-2 alone can lead to the separation of the two proteins, for example, phosphorylation of Bcl-2 by JNK promotes autophagy. In addition, JNK and P38 are major pathways of MAPK signaling and play important roles in stimulating apoptotic signals and inflammation. It has been found that Bcl-2 family plays an important role in apoptosis caused by mitochondrial dysfunction. Bax can promote apoptosis, and Bcl-2 can resist apoptosis (Jun et al., 2015). When the mitochondrial membrane potential changes, cytochrome c will be released to the cytoplasm, which stimulates Caspase-3. Bcl-2 located on the outer membrane of the mitochondria can prevent the release of pro-apoptotic proteins such as cytochrome c. After receiving the apoptosis signal, the inactive monomer protein Bax, which is free in the cytoplasm, moves to the outer membrane of the mitochondria and forms a channel, damaging the integrity of

the mitochondrial membrane and antagonizing bcl-2 to prevent it from exerting the anti-apoptotic effect.

The volatile oil components in CX, including ligustilide, butylphthalide, senkyunolide A, H, and I, and TMP can play a therapeutic role in myocardial ischemia and cerebral ischemia-reperfusion injury by regulating autophagy and apoptosis. This role may be related to the PI3K/Akt/mTOR pathway, the MAPK pathway, and mitochondrial dependence. Cystine protease P32, also known as Caspase-3, is one of the most important pro-apoptotic factors of the Caspase family members and the common effector of multiple apoptotic pathways. Butylphthalide pretreatment can inhibit the expression of Caspase-3 and increase the level of p-Akt, an Akt phosphorylation product, in the brain of rats with cerebral ischemia-reperfusion injury (Yan, 2013). It shows that butylphthalide may achieve the effect of anti-apoptosis by activating the PI3K/Akt pathway. The mammalian target of rapamycin (mTOR) is a negative regulator of autophagy. Ligustilide can upregulate the expression of p-p13k, p-Akt, and p-mTOR proteins in the brain of rats with cerebral ischemia-reperfusion and show the activation of the PI3K/Akt/mTOR pathway. It also upregulated Bcl-2 protein and downregulated the levels of pro-apoptotic protein Bax and Caspase-3 mRNA (Bo et al., 2021). The lactone components of CX (senkyunolide I: senkyunolide H: senkyunolide A: ligustilide = 1.00: 1.30: 6.90: 13.24) significantly increased the PI3K protein expression and Akt and mTOR protein phosphorylation levels, decreased Beclin-1 expression, and reduced the number of autophagic vesicles. The anti-autophagy effect of lactone components of CX can be terminated by PI3K inhibitor LY94002, which shows that it can play a role by activating PI3K/Akt/mTOR pathway (Gang, 2018). In addition, TMP downregulated the level of Caspase-3 and increased the ratio of Bcl-2/Bax. This effect can be reversed by LY294002, a specific inhibitor of the PI3K/Akt signaling pathway (Su et al., 2019). Ligustilide can increase the expression of Bcl-2 and reduce the levels of Caspase-3, Bax, and iNOS. The effect of ligustilide can be reversed by JNK and p38MAPK agonist anisomycin (Zhou et al., 2019b). This shows that the inhibitory effect of ligustilide on apoptosis may be achieved by inhibiting JNK and p38 MAPK. Xuesong et al. (2019) found that the ratio of cytochrome c and Cox IV in the mitochondria decreased and that in the cytoplasm increased in the model group. In addition, TUNEL and DAPI staining showed that the apoptosis in the model group reached 41%, accompanied by the upregulation of Caspase-3 and Bax/Bcl-2. TMP attenuated the change of mitochondrial membrane potential, inhibited the release of cytochrome c from the mitochondria to the cytoplasm, and decreased the expression of Caspase-3 and Bax/Bcl-2.

#### 4.5 Inhibition of Smooth Muscle Cell Proliferation

VSMCs, endothelial cells, and ECM are the same components of the vascular wall. In line with endothelial cells, VSMCs can control the diameter of the lumen by coordinating the contraction and relaxation of the vessels, thus maintaining



blood pressure (Wei and Wu, 2020). The proliferation, migration, and phenotypic transformation of VSMCs are one of the characteristics of vascular stenosis and the main pathological basis of vascular diseases. In addition, the phenotypic plasticity of VSMCs enables them to quickly adapt to environmental changes and plays an important role in CVDs (Park et al., 2019). NF- $\kappa$ B is a transcription factor commonly found in eukaryotes. When the body has an immune or stress response, NF- $\kappa$ B is activated and then transferred to the nucleus where it can stimulate or inhibit the transcription of some genes (Wei, 2020).

Ligustilide and TMP in CX can inhibit the proliferation of VSMCs and maintain the normal function of blood vessels. This effect may be related to JNK phosphorylation, and the c-Myc/MMP2 and ROCK/JNK pathway. Ligustilide can inhibit Ang II-induced VSMC migration and downregulate migration-related proteins c-Myc, MMP2, ROCK1, ROCK2, p-JNK, and JNK (Luo et al., 2019b). The increased expression of fibroblast growth factor receptor-1 (FGFR-1) can activate the phosphorylation of JNK and affect the migration of VSMCs. TMP can reduce the proliferation of VSMCs induced by PM2.5, accompanied by the decrease of FGFR-1 and JNK phosphorylation levels. This effect is consistent with the results of JNK inhibitor treatment, suggesting that TMP can inhibit the proliferation of VSMCs by reducing the phosphorylation level of JNK (Qiang et al., 2017). c-Myc gene regulates cell proliferation and migration, and its high expression can enhance cell motility. The matrix metalloproteinases (MMPs) can degrade most of the components of the extracellular matrix, destroy the basement membrane formed during migration, and damage its migration inhibition, so as to make cells migrate smoothly. Ang II increased the expression of protein and mRNA of c-Myc and MMPs. Transwell cell migration experiment also found that cell migration was enhanced. The treatment with ligustilide and c-Myc inhibitor showed the downregulation of the expression of c-Myc and MMPs, accompanied by the decrease of cell migration. It can be preliminarily determined that ligustilide can inhibit the migration of VSMCs through the c-Myc/MMP2 signaling pathway. Rho-GTP has an important relationship with cell migration. Rho-associated kinase (ROCK) is the related kinase of Rho and is necessary to mediate the actin structure and contraction response of VSMCs. Ligustilide can inhibit the expression of ROCK1 and ROCK2 induced by Ang II, activate Rho/ROCK pathway, reduce the expression of JNK, and form signal interaction, but the role of them is not clear. After treatment with ROCK-specific inhibitors, it was found that the decrease of ROCK1 and ROCK2 was accompanied by the decrease of JNK expression, suggesting that ligustilide can inhibit the migration of VSMCs by regulating the ROCK/JNK signaling pathway (Luo et al., 2019b).

## 4.6 Adjust NO

Nitric oxide synthase (NOS) is the only rate-limiting enzyme for NO production. It can be divided into endothelial NOS (eNOS), neuronal NOS (nNOS), and inducible NOS (iNOS). eNOS is mainly expressed in endothelial cells. Under normal conditions, eNOS produces a small amount of NO, which can dilate blood vessels and has a neuroprotective effect. Under pathological conditions, nNOS and iNOS produce a large

amount of NO, play a neurotoxic role, and cause cerebrovascular dysfunction.

TMP and other components in CX can regulate NO, which may be achieved by inhibiting NOS. And IL-1 $\beta$ , IL-2, IL-6, TNF- $\alpha$ , IFN- $\beta$ , and other proinflammatory cytokines can induce high expression of iNOS. TMP can inhibit the expression of eNOS and iNOS induced by LPS to downregulate the level of NO in the rat brain. The expression of IL-6, TNF- $\alpha$ , and IL-1 $\beta$  was decreased (Sheng et al., 2020). It shows that CX can reduce the expression of NO by affecting proinflammatory cytokines and inhibiting NOS.

## 4.7 Influence on Calcium Ions

Intracellular Ca<sup>2+</sup> homeostasis is necessary to maintain cell function. When cardiomyocytes are activated, changes in the cell membrane potential will open up L-type calcium current (ICA-L) and increase the amount of Ca<sup>2+</sup> entering the cytoplasm from the outside of the cell. Large amounts of Ca<sup>2+</sup> will bind to troponin, causing excitatory contraction of the myocardium and myocardial injury (Zhao et al., 2020). Therefore, calcium overload can be alleviated by inhibiting calcium channels and intracellular Ca<sup>2+</sup> homeostasis can be maintained to achieve cardiac protection.

The regulating effect of TMP and other components in CX on calcium ions may be related to regulating calcium channels. TMP reduces Ca<sup>2+</sup> increase in cells by selectively opening KATP or SKCa channels (Wong et al., 2003). Wu et al. (1989) found that at low doses, TMP predominantly prevents the mobilization of intracellular calcium, but at a higher dose, it inhibits the influx of extracellular calcium. Ren et al. (2012) found that TMP can dose-dependently reduce the ICA-L of rabbit cardiomyocytes, and this inhibition can be restored after elimination of the drug. At the same time, TMP can inhibit the transient and contraction of calcium in rabbit cardiomyocytes under physiological and pathological conditions.

## 4.8 Anti-Platelet Aggregation

Platelet activation and aggregation play a crucial role in AS. Platelet proteomics revealed that platelet gelsolin is a differential functional protein between patients with CHD and healthy people and is highly expressed in patients (Liu et al., 2013). In addition, platelet aggregation also plays an important role in thrombosis, which is related to AS, stroke, and various inflammatory reactions. Inhibition of platelet aggregation can effectively prevent and slow down the formation of thrombosis (Chen et al., 2017a).

TMP, ferulic acid, and other components in CX can inhibit platelet aggregation, which may be achieved by reducing platelet activation and the expression of adhesion molecules. TMP was used to treat patients with acute coronary syndrome (ACS) after percutaneous coronary intervention (PCI). It was found that the two platelet activation indexes of CD65p and CD63 decreased significantly before and after the treatment (Xu and Li, 2019). TMP can reduce the expression of two adhesion molecules the von Willebrand Factor (vWF) and fibronectin in endothelial cells, inhibit platelet activation and aggregation, promote blood circulation and reduce platelet adhesion (Wang et al., 2016).

Xu and Li (2019) used TMP to treat ACS patients after PCI using CD65p, CD63 (two platelet activation markers), platelet adhesion

**TABLE 2 |** Application of classical prescription containing *Ligusticum chuanxiong* Hort. in CVDs.

Classics	Prescription	Therapeutic effect	Indication	Reference
Golden Mirror of Medicine	Taohong Siwu decoction	1. Reduce the area of cerebral infarction and reduce neurological damage; 2. Promote blood circulation; 3. Promote angiogenesis and reduce apoptosis; 4. Anticoagulation and lipid lowering; 5. Inhibit apoptosis; 6. Reduce myocardial fibrosis	1. Cerebral ischemia-reperfusion injury; 2. Acute blood stasis; 3. Myocardial infarction; 4. CHD; 5. Middle cerebral artery occlusion reperfusion; 6. Myocardial infarction	Li et al. (2015b), Tan et al. (2021)
Correction on Errors in Medical Classics	Buyang Huanwu decoction	1. Inhibit the proliferation of VSMCs; 2. Improve hemorheological disorders and energy metabolism; 3. Neuroprotective effect; 4. Reduce and inhibit excitatory amino acids; 5. Improve synaptic plasticity and promote nerve repair; 6. Protect blood-brain barrier	1. CHD; 2. Ischemic stroke	Chen et al. (2011), Pan et al. (2017), Chen et al. (2019c)
Correction on Errors in Medical Classics	Decoction for activating blood circulation	Dilate blood vessels, improve microenvironment, and inhibit inflammatory reaction	1. Cerebral infarction; 2. Hypertension	Yang (2020b)
Danxi's Mastery of Medicine	Yueju pill	1. Improve myocardial tissue antioxidant; 2. Reduce inflammatory factors	1. Myocardial ischemia; 2. Angina pectoris; 3. Hypertension; 4. Hyperlipidemia; 5. CHD	Gui et al. (2016), Hu et al. (2017)
Essential Recipes for Emergent Use Worth A Thousand Gold	Xiao Xu Ming decoction	1. Inhibit autophagy-related protein and promote the recovery of neural function; 2. Reduce the damage of blood-brain barrier and cerebral ischemia; 3. Improve cerebral artery blood supply and hemodynamics, and promote the recovery of neural function; 4. Improve hemorheology, reduce blood viscosity, and improve the increase of cell aggregation; 5. Dilate blood vessels, inhibit vascular motor left, or sympathetic nervous system	1. Cerebral ischemia-reperfusion; 2. Acute cerebral infarction; 3. Hyperlipidemia; 4. Hypertension	Lan et al. (2013), Cheng et al. (2019), Wu and Wang (2020)
Clear Synopsis on Recipes	Dachuanxiong pill	1. Regulate hemorheology and hemodynamics; 2. Upregulate the level of VEGF	Cerebral ischemia	Zhang et al. (2006)
Correction on Errors in Medical Classics	Xuefu Zhuyu decoction	1. Inhibit inflammation and inhibit apoptosis; 2. Improve blood lipid and inhibit AS; 3. Improve cerebral infarction, improve neurological deficit; 4. Reverse myocardial fibrosis; 5. Reduce blood lipid and whole blood viscosity, improve heart energy supply, and regulate amino acid metabolism; 6. Improve vascular endothelial function, promote angiogenesis, and improve hemorheology	1. Thromboembolic stroke; 2. Hyperlipidemia; 3. Acute ischemic stroke; 4. Hypertension; 5. CHD; 6. AS	Lee et al. (2011), Shen et al. (2015)
Clear Synopsis on Recipes	Miraculous power of <i>Ledebouriella</i>	Promote and improve the level of lipid metabolism, and improve and regulate lipid metabolism and disorder	Hyperlipidemia	Xing (2002)
Prescriptions of the Bureau of Taiping People's Welfare Pharmacy	Decoction of 10 powerful tonics	Reduce the load of heart, improve the congestion of organs	1. Heart failure after acute myocardial infarction; 2. CHF	Pan and Liu, (2017), Yang (2020a)
General principles of Medicine	Chaihu Shugan powder	1. Reduce neurogenic inflammation; 2. Improve heart function and inflammatory reaction, and reduce adverse reactions	1. Stable angina pectoris of CHD; 2. Hypertension; 3. Acute myocardial infarction	Hu et al. (2016a), Yang et al. (2020b)

(Continued on following page)

**TABLE 2 |** (Continued) Application of classical prescription containing *Ligusticum chuanxiong* Hort. in CVDs.

Classics	Prescription	Therapeutic effect	Indication	Reference
Correction on Errors in Medical Classics	Infradiaphragmatic stasis-expelling decoction	1. Improve hemorheology, reduce vascular resistance, inhibit platelet aggregation and release, increase plasmin activity, promote fibrinolysis, improve microcirculation; 2. Improve platelet aggregation, reduce inflammatory reaction, and myocardial injury	1. Angina pectoris of CHD; 2. Myocardial infarction	Liu et al. (2012), Liu et al. (2018)
Synopsis of Golden Chamber	Danggui Shaoyao powder	1. Improve the level of lipid peroxidation and hemorheology; 2. Improve the level of blood lipids; 3. Reduce the concentration of vasoconstrictors; 4. Increase the blood supply to the brain	1. Hyperlipidemia; 2. AS; 3. Hypertension; 4. Acute myocardial infarction	Ren et al. (2017)
SuWenBingJiQiYiBaoMingJi	Daqinjiao decoction	1. Improve blood pressure level and blood pressure rhythm; 2. Improve hemorheology and nerve function; 3. Improve the degree of nerve function defect	1. Hypertension; 2. Acute cerebral infarction; 3. Acute ischemic stroke	Song et al. (2018), Gao et al. (2019)

**TABLE 3 |** Application of *Ligusticum chuanxiong* Hort. preparation in CVDs.

Category	Name	Indication	Reference
Capsule	Compound Chuanxiong capsule	AS	Kang et al. (2015)
	Xinnaokang capsule	Angina pectoris	Li et al. (2019)
	Naointong capsule	Heart failure, myocardial infarction, cerebral ischemia-reperfusion, cerebral infarction	Wang et al. (2017c)
	Niuhuang Jiangya capsule	Hypertension	Ma (2018a)
	Zhengxin Tai capsule	Angina pectoris	Zhang and Qi (2015)
	Xueshuan Xinmaining capsule	Acute cerebral infarction	Ma et al. (2019)
	Xuemaitong capsule	Cerebral hemorrhage, acute myocardial infarction, AS, CHD, and angina pectoris	Wang et al. (2006), Ye et al. (2013)
	Shuxin Tongmai capsule	CHD	Zhang and Gao (2019)
Granule	Guanxin Kang capsule	Heart failure, acute myocardial ischemia, CHD, and angina pectoris	Pan et al. (2007)
	Mailuotong granules	Cerebral infarction	Wang et al. (2020)
	Zhengxintai granules	Angina pectoris	Li et al. (2005)
	Yixin Tongmai granules	Angina pectoris	Wang and Shi (2015)
Pill	Guanxin Kang granules	Angina pectoris	Liu (2011)
	Guanxin pill	Angina pectoris	Feng (2006)
	Angong Jiangya pill	Hypertension	Li and Wang (2019)
	Suxiao Jiuxin pill	AS, acute myocardial ischemia, CHD, myocardial infarction	Li et al. (2011)
Tablet	Niuhuang Jiangya pills	Hypertension	Yin (2018)
	ShuXinNing tablets	Hypertension, high cholesterol, CHD, angina pectoris	Wang et al. (2018a)
	Zhengxintai tablets	Angina pectoris	Xu (2007)
	Xiaoshuan Tongluo tablets	Focal cerebral ischemia	Li et al. (2016)
Oral liquid	Xueshuan Xinmaining tablets	CHD angina, CHD	Tan et al. (2018), Shan and Leng (2019)
	Guanxin'an oral liquid	Myocardial ischemia	Wang et al. (2005)
	Ruanmailing oral liquid	AS	Wu et al. (2013)
Injection	Tongtian oral liquid	Acute cerebral infarction	Chen et al. (2019b)
	Guanxining injection	Myocardial ischemia-reperfusion, CHD, angina pectoris, ischemic stroke	Xiao et al. (2021)
	Danshen ligustrazin for injection	Myocardial ischemia, cerebral ischemia-reperfusion injury	Huang et al. (2016)

test (PADT), and gelsolin to evaluate the therapeutic effect of postoperative antiplatelet aggregation. It was found that the differences of CD65p, CD63, PADT, and gelsolin before and after operation in the TMP treatment group was greater than in the control group, which showed that TMP could significantly

inhibit platelet activation. Wang et al. (2016) used TMP in the treatment of allergic asthma rats induced by ovalbumin and found that the adhesion of platelet to HUVECs was inhibited by TMP, and the expression of two adhesion molecules, vWF and fibronectin, expressed in endothelial cells, was reduced in the asthmatic rats

### Chuanxiong in Cardio-cerebrovascular diseases

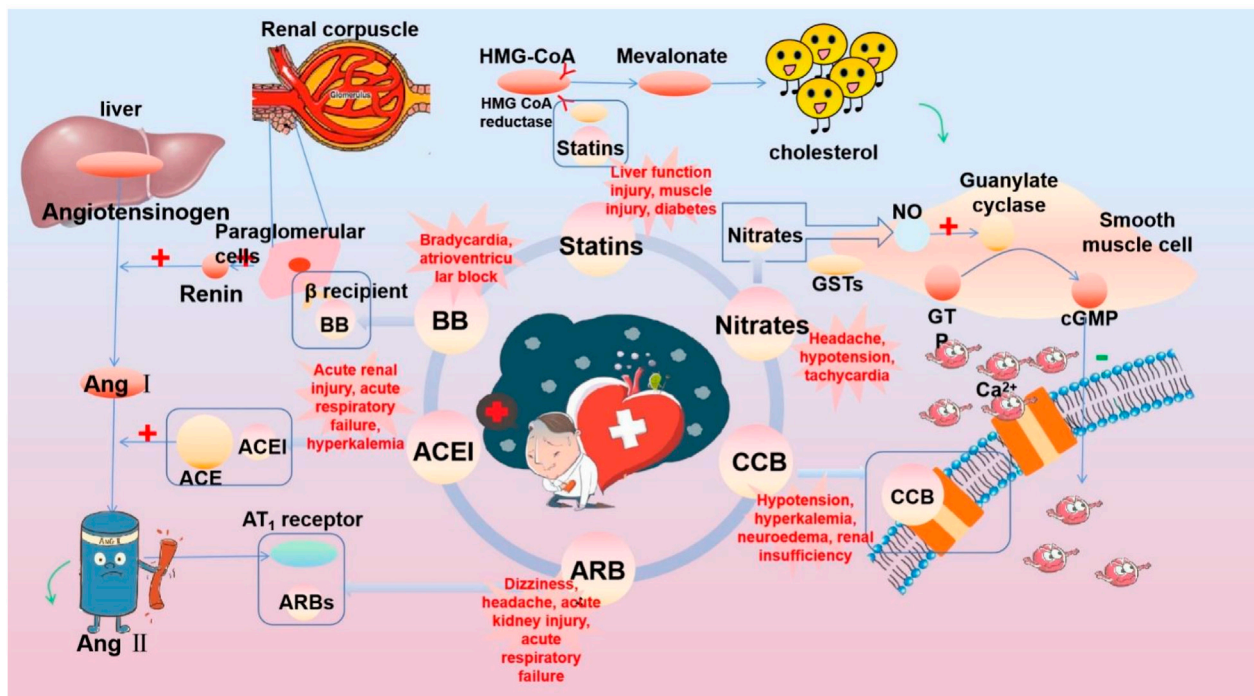


**FIGURE 3 |** Commonly used drugs for CVD and their mechanisms (the green symbol indicates the effect after administration, and the red symbol indicates the pathological condition. Commonly used drugs for CVDs include statins, BB, ACEI, ARBs, CCB, and nitrates. Angiotensin produced by the liver is converted to Ang I under the action of renin secreted by juxtaglomerular cells, and then to Ang II under the action of ACE. Ang II can bind to AT<sub>1</sub> receptor and produce vasoconstriction. BB can bind to  $\beta$  receptor of adjacent glomerular cells and reduce the secretion of renin. ACEI can inhibit ACE and reduce Ang II. ARBs can bind to AT<sub>1</sub> receptor and competitively inhibit the binding of Ang II to AT<sub>1</sub> receptor. BB, ACEI, and ARBs play a role in the renin-angiotensin system, thereby inhibiting vasoconstriction, reducing blood volume, and lowering blood pressure. CCB can directly block the Ca<sup>2+</sup> channel on the endothelial cell membrane and reduce Ca<sup>2+</sup> influx, thereby reducing blood pressure and myocardial contractility. HMG-CoA is transformed into mevalonate by HMG-CoA reductase, and then into cholesterol. Statins can significantly reduce blood cholesterol and LDL by inhibiting HMG-CoA reductase, thus achieving the effect of lowering blood lipid. Nitrates catalyzed the release of NO in the smooth muscle cells by GSTs, and NO activates guanylate cyclase, increasing the content of intracellular second messenger cGMP, and then activating cGMP-dependent protein kinase, which reduces intracellular Ca<sup>2+</sup> release and extracellular Ca<sup>2+</sup> influx and relaxes smooth muscle cells).

treated with TMP. It is confirmed that TMP markedly inhibited platelets activation and aggregation, and promoted blood circulation, and platelet adhesion was significantly attenuated. Zhang et al. (2020a) demonstrated that TMP can partially inhibit the p38MAPK and NF- $\kappa$ B signaling pathways, thereby reducing platelet adhesion of mouse micro-VECs induced by oxygen-glucose deprivation/reoxygenation injury. Choi et al. (2018) through the study of ferulic acid in *in vivo* and *in vitro* experiments found that ferulic acid can inhibit platelet aggregation to play a role in weakening platelet activation by stimulation and can play an antithrombotic role in the acute thromboembolism model.

## 5 LIGUSTICUM CHUANXIONG HORT. IN THE TREATMENT OF CARDIO-CEREBROVASCULAR DISEASES

Under the guidance of the current situation that CX is widely used in CVDs, the effects of CX on hypertension, CHD, AS, heart failure, cerebral hemorrhage, and cerebral ischemia are described.

Supported by clinical data and combined with network pharmacology research, the signaling pathway and mechanism of CX in the treatment of CVDs are constantly explored to promote its more comprehensive application.

## 5.1 Cardiovascular Disease

### 5.1.1 Hypertension

According to the American Heart Association, hypertension is one of the five major risk factors for disease burden in areas other than Oceania and the eastern, central, and western parts of sub-Saharan Africa (Virani et al., 2021). It is one of the most important risk factors for CVDs and is closely related to stroke, heart failure, and other CVDs. Currently, the prevalence rate of hypertension in China is 50% and the United States is 46% (Chen et al., 2019a).

Through the analysis of network pharmacology of CX and hypertension, it was found that CX could be based on the calcium signaling, VEGF signaling, PI3K-Akt signaling, cGMP-PKG signaling, TNF signaling, and estrogen, insulin resistance, and prostate cancer pathways. CX can be involved in the treatment of



hypertension by blocking vasoconstrictor molecules, increasing the number of smooth muscle cells, reducing the number of intracellular  $\text{Ca}^{2+}$  and other mechanisms (Yan et al., 2020).

According to the statistics, Tian et al. (2021) analyzed the clinical data of TCM in the treatment of hypertension patients and found that among the hypertension diseases with different syndrome types, CX was used the most frequently, and according to different syndrome types, it was combined with *Gastrodia elata* Blume (Tianma, TM), *Dioscorea opposita* Thumb. (Shanyao, SY), DG, *Pinellia ternate* (Thunb.) Breit. (Banxia, BX), etc.

### 5.1.2 Coronary Heart Disease

CHD, also known as coronary atherosclerotic heart disease, is a kind of heart disease caused by myocardial ischemia, hypoxia, or necrosis caused by coronary artery stenosis, spasm, or occlusion (Therapy, 2021). Angina pectoris refers to chest discomfort caused in the heart (Joseph and Colin, 2020), which is one of the common complications of patients with CHD. About 80% of patients with CHD will have angina pectoris (Wei, 2021).

Through the analysis of network pharmacology of CX in the treatment of CHD, seven compounds were selected from CX. It was found that they could be used in 31 targets such as vascular hemophilic molecule, coagulation factor 2, transmembrane receptor protein 1, cardiac cell enhancement factor 2A, SOD 1, nitric oxide synthase 2, etc. Based on these targets, CX can play the role of anti-oxidation, anti-inflammation, anticoagulation, promoting angiogenesis, dilating blood vessels, regulating blood pressure, and other functions to realize the treatment of CHD (Zhao-et al., 2019).

Bi et al. (2020) investigated the clinical medication data of 1986 patients with CHD in 11 provinces, cities, and autonomous regions of China. Among them, drugs for property of activating blood and resolving stasis were used 2,173 times. In addition, in the application of single drug in the treatment of CHD, the frequency of use of CX reached 447 times, 56.58%, second only to Danshen. Ma (2018b) investigated the clinical efficacy of CX injection in patients with CHD and angina pectoris. The control group received angiotensin II receptor antagonists (ARBs), aspirin, nitrate drugs, and  $\beta$ -receptor blockers (BB), while the observation group was given ligustrazine injection on the basis of the control group. The clinical results showed that the frequency and duration of angina pectoris in the observation group were significantly lower than in the control group, and the total effective rate in the observation group (94.44%) was significantly higher than that of the control group (82.22%). As far as the clinical data of ligustrazine injection are concerned, they show that ligustrazine injection has a better disease control effect.

### 5.1.3 Atherosclerosis

AS is the main pathological basis of cardiovascular disease. It refers to a progressive pathological process in which the structure or function of the endothelial cells of the large and medium arteries are damaged, the permeability of the intima is increased, and cholesterol and cholesterol lipid accumulate in or under the intima of the artery under the combined action of a variety of risk factors (Ma, 2016). The potential mechanisms include endothelial

dysfunction, lipid deposition, OS injury, immune inflammatory response, and platelet migration and aggregation (Xin et al., 2020).

Through the analysis of network pharmacology of CX in the treatment of AS, 20 compounds were screened from CX and 37 targets were found in the treatment of AS. Through KEGG analysis of these targets, it was found that CX could exert anti-inflammatory, anti-OS, protect endothelial cells, inhibit the proliferation and migration of VSMCs, improve vasoconstriction, and inhibit platelet aggregation by affecting 14 pathways, including TNF, insulin resistance, vascular smooth muscle contraction, calcium ion, VEGF, TRP channel regulated by inflammatory mediators, and platelet activation, so as to achieve the therapeutic effect on AS (Tian et al., 2018).

Deng et al. (2017) analyzed the clinical efficacy of Danshen combined with CX in the treatment of elderly patients with AS. The control group was given routine treatment of AS, and the observation group was given Danshen: CX decoction (5:4). The levels of inflammatory factors and blood lipids in the venous blood of the patients were detected after 30 days. The levels of inflammatory factors including C-reactive protein (CRP), IL-1 $\beta$ , IL-6, TNF- $\alpha$ , monocyte chemotactic protein-1, and blood lipids total, including total cholesterol (TC), triglyceride, high-density lipoprotein cholesterol, and LDL cholesterol in the venous blood of the patients after 30 days were measured. It was found that there was no significant difference in the blood lipid level between the control and observation groups, whereas the inflammatory factor level of the observation group was significantly lower than that of the control group. The data showed that Danshen combined with CX had an obvious anti-infection effect in the treatment of elderly patients with AS and a better disease control effect on patients with AS. Zuo et al. (2020) studied the clinical efficacy of Xingnao Zhitan capsule (including CX) in the treatment of the carotid artery in patients with acute cerebral infarction. During the 3-month treatment, the control group was given atorvastatin calcium tablets and the observation group was given atorvastatin calcium tablets combined with Xingnao Zhitan capsule. After research, it was found that TC and LDL in the observation group were significantly lower than those in the control group, and FIB, D-D, hs CRP, IMT, Crouse scores were significantly improved, and the total effective rate in the observation group (82.1%) was significantly higher than that in the control group (60.5%). According to the analysis of the clinical data, the capsule can control AS by regulating blood lipid and reducing inflammation and plate volume.

### 5.1.4 Heart Failure

Chronic heart failure (CHF) is a clinical syndrome with abnormal cardiac structure and function caused by a variety of risk factors (Jia et al., 2020b). It has the characteristics of high incidence rate, high mortality rate, and high medical expenditure (Li et al., 2020b). Only in the United States, heart failure accounted for 10% of the total medical expenses in medical spending, and patients with heart failure in 2030 are expected to increase to eight million.

Through the analysis of network pharmacology of CX in the treatment of heart failure, it was found that CX could realize the

therapeutic effect of heart failure through 12 targets, one of which was related to chest and flank prickling pain. Through KEGG enrichment analysis of these targets, it has been found that CX can activate the cancer signaling pathway, apoptosis, HIF-1, and the other signaling pathways to achieve the functions of inhibiting inflammation, regulating apoptosis, and improving vasoconstriction to treat heart failure (Jia et al., 2020a).

Zhang (2019) analyzed the clinical efficacy of Danshen–ligustrazin for injection in the treatment of heart failure. The control group was given conventional treatment methods such as oxygen inhalation, cardiotonic, low salt diet, vasodilation, and bed rest. The observation group was given Danshen–ligustrazin for injection on the basis of the control group. After 14 days of treatment, the relevant levels of the patients were detected. It was found that the left ventricular ejection fraction (LVEF) of the observation group was significantly higher than that of the control group, and the brain natriuretic peptide (BNP) level was significantly lower. The total effective rate in the observation group (90%) was significantly higher than that in the control group (78%). Through clinical data analysis, Danshen–ligustrazin for injection can effectively improve cardiac function and hemodynamics and has a good control effect on heart failure. Sui et al. (2020) analyzed the clinical efficacy of Danshen–ligustrazin for injection in the treatment of blood stasis syndrome of CHF. The control group received conventional treatment of heart failure by limiting salt and water, using digitalis preparation, BB, angiotensin converting enzyme inhibitors (ACEI)/ARB, and aldosterone receptor antagonist and diuretic, and the observation group was given Danshen–ligustrazin for injection on the basis of the control group. It was found that compared with the control group, the levels of NT-proBNP and myocardial energy consumption were significantly decreased and LVEF was significantly increased in the observation group. In addition, the total effective rate of the observation group (80%) was significantly higher than that of the control group (57.17%). Through the analysis of clinical data, Danshen–ligustrazin for injection can relieve the clinical symptoms of CHF patients with blood stasis and improve cardiac function, so as to play a good therapeutic effect on heart failure.

## 5.2 Cerebrovascular Disease

In 2017, the Cerebrovascular Division of the Neurology Society of the Chinese Medical Association released the “Classification of Cerebrovascular Diseases in China 2015,” which explained cerebrovascular diseases and believed that cerebrovascular diseases are transient or permanent neurological dysfunction caused by various risk factors. Stroke is the second leading cause of death worldwide and increases the global medical burden (Shakiba et al., 2021), especially acute cerebrovascular disease, which is a focal vasogenic neurological deficit syndrome that can lead to death or permanent neurological defects (Fan, 2018). Stroke is characterized by high morbidity, high disability, high mortality, and high recurrence rate (Jin et al., 2021), including ischemic cerebrovascular disease and hemorrhagic cerebrovascular disease (Chen et al., 2017b). Ischemic strokes

are more common, accounting for 87% of strokes in the United States. In Asian countries, cerebral hemorrhage accounts for 24–55% of all strokes, while in China, the rate is 24%, significantly higher than in developed countries (Li, 2019). Ischemic stroke refers to the blood clots in the blood that stop enough blood supply to the brain, and hemorrhagic stroke refers to the primary non-traumatic hemorrhage that cause bleeding within the brain parenchyma of the microvascular burst (Zheng and Deng, 2020). Hemorrhagic stroke is gender related, with women having a higher rate of stroke-related deaths than do men, averaging six out of 10 women (Derek and Hiranmoy, 2020).

### 5.2.1 Cerebral Ischemia

Song et al. (2015) analyzed the material basis and molecular mechanism of CX in the treatment of cerebral ischemia through molecular docking technology. Through molecular docking of 45 components selected from CX with cerebral ischemia target proteins of four existing drugs on the market, it was found that 12 components of CX scored higher than the existing drugs on the market, and ferulic acid scored the highest. Other studies have proven that CX can inhibit the expression of Uba3a, thereby inhibiting the NF- $\kappa$ B signaling pathway and relieving neuron cell damage (Yu et al., 2017). Z-ligustilide nasal administration can prevent cerebral ischemia through the Nrf2 and HSP70 signaling pathways (Li et al., 2017b).

Cheng and Luo (2020) analyzed the clinical effect of TMP on elderly patients with early cerebral ischemia after intracranial aneurysm clipping. The control group was given edaravone injection, and the observation group was given TMP injection. After 14 days of treatment, it was found that the Barthel Index (BI) and SOD level of the observation group were higher than those of the control group, and the NIHSS score and plasma MDA level of the observation group were lower than those of the control group. The clinical data show that TMP can improve OS and reduce rebleeding in elderly patients with early cerebral ischemia after intracranial aneurysm clipping, which has important clinical value.

### 5.2.2 Cerebral Hemorrhage

In the treatment of intracerebral hemorrhage, studies have shown that Danshen–ligustrazin for injection can reduce cell apoptosis by reducing the release of IL-6 and TNF- $\alpha$ , increasing the expression of NOS, decreasing the expression of Caspase-3, and increasing the expression of Bcl-2, thus playing a role in the treatment of intracerebral hemorrhage (Zhang et al., 2018a).

Sun et al. (2008) analyzed the clinical efficacy of ligusticum (sodium ferulic acid) for intracerebral hemorrhage. The control group was given routine treatments such as dehydration, brain cell activator, regulation of blood pressure and blood glucose, and management of stress complications, and the observation group was given intravenous infusion of ligusticum on the basis of the control group. Zhao (2020) analyzed the clinical efficacy of Taoren–Chuanxiong decoction on cerebral hemorrhage. The control group was treated with Piracetam tablet, and the observation group was treated with Taoren–Chuanxiong decoction on the basis of the control group. It was found that the whole blood high-shear viscosity, whole blood low-shear

viscosity, plasma viscosity, and HCT of the observation group were significantly lower than those of the control group, and the NHISS, FMA, and BI scores of the patients were better than those of the control group, and the total effective rate in the observation group (88.89%) was significantly higher than that in the control group (71.11%). This shows that Taoren–Chuanxiong decoction has an obvious improvement effect on the nerve function defect and hemodynamics of the patients and can effectively control the condition of the patients with cerebral hemorrhage.

## 6 COMBINED APPLICATION OF *LIGUSTICUM CHUANXIONG* HORT. AGAINST CARDIO-CEREBROVASCULAR DISEASE

### 6.1 Study on the mechanism of compound containing *Ligusticum chuanxiong* Hort.

So far, CX has been widely used in cardiovascular and cerebrovascular diseases and together with a variety of drugs, which provide a certain idea and feasibility for the prevention and treatment of CVDs and also a new direction for drug research and development. Modern pharmacological studies have found that it can reduce arterial resistance, increase cerebral blood flow, improve microcirculation, reduce capillary permeability, and has a protective effect on brain injury, so it plays an important role in the prevention and treatment of CVDs (Zeng et al., 2013). In previous studies, CX and other drug combinations were collected and identified for CVDs therapy, in order to provide theoretical support for the subsequent studies on CX resistance to CVDs (Table 2).

### 6.2 Modern Application of Preparations Containing *Ligusticum chuanxiong* Hort.

Compared with chemical medicine, natural medicine has the advantages of less side effects, multiple links, and multiple targets. Its preparation into capsules, granules, pills, tablets, oral liquid, injection, and other dosage forms is conducive to improve its bioavailability, enhances the convenience in its production, transportation, taking, carrying, and storage, and makes it better in playing its pharmacodynamic role. A total of 1640 modern preparations have been collected in the Chinese Pharmacopoeia, of which 9.21% are CX (Li, 2017). This article summarizes the current modern preparations containing CX, and their applications in CVDs are counted, in order to provide some reference for follow-up research of other scholars (Table 3).

## 7 THE SECURITY TOXICITY OF *LIGUSTICUM CHUANXIONG* HORT.

At present, the clinical treatment of CVDs still mainly uses BB, calcium channel blockers (CCB), ACEI, ARBs, statins, nitrates, etc (Liu et al., 2019b). In a survey of patients with CHD in 24 European countries, the European Heart Association found that

of the cardioprotective drugs, BB accounted for 82.6%, ACEI/ARBs for 75.1%, and statins for 85.7% (Kornelia et al., 2016). Statin is the first ideal choice to treat hypercholesterolemia. In addition, drugs such as ACEI, ARBs, BB, CCB, and nitrate are also commonly used for CVDs. However, while it plays a therapeutic role in several ways, it affects normal cells, proteins, and factors, resulting in various toxic effects and side effects (Figure 3); for example, nearly one-third of statin users generally have side effects depending on the dose, and the risk of myopathy is higher at higher doses (Li et al., 2015a).

CAM has gained popularity among health professionals over the past few years because of its preventive mechanisms against the side effects of chemotherapy drugs. On the basis of several acute toxicology studies, CX was found to be highly safe in both gavage experiments and intraperitoneal injection. In the CX gavage experiment, mice's LD<sub>50</sub> is 7.26 g/kg, or 1460 times the maximum clinical dose of CX. In the CX intraperitoneal injection, mice's LD<sub>50</sub> is 2.52 g/kg, which is equivalent to 5,091 times of the maximum clinical dose of CX (Ran, 2012). Xia et al. (2018) found that under the 16-fold clinical dose, the decoction of CX may increase mouse fetal stillbirth and absorption fetus, cause sternum and limb bone deformities, and have weak embryotoxicity. Zhang (2014) measured that the LD<sub>50</sub> of mice was 1594.92 mg/kg after a single intragastric administration of CX volatile oil. In addition, CX has few adverse reactions in clinical application, mainly facial flushing and emotional agitation, which can improve without additional intervention (Pan, 2012). It is demonstrated that CX is highly safe at normal clinical doses.

The above results are mainly based on the preclinical and clinical research of CX. In life, CX is often boiled together with beef and mutton as health food (Donkor et al., 2016). In Yunnan, China, the tender stems and leaves of CX are often eaten as vegetables (Yang et al., 2013). The characteristics of high safety of CX were explained from the medicinal and edible perspective. However, although natural drugs are generally considered to be safe and non-toxic, they have the characteristics of “multi-links and multi-targets,” they inevitably cause us to think about whether they will produce unknown or uncontrollable effects, and they affect the uptake and transport of drugs and then cause damage. Therefore, as a “homology medicine and food” drug, when evaluating the safety of CX, we must pay attention to being rigorous and objective. We cannot simply identify its high safety. We should study the potential safety hazards from the whole and in part.

## 8 SUMMARY AND PROSPECT

As a natural medicine, CX has less toxic and side effects than other artificial drugs. It has rich effective ingredients, has extensive pharmacological effects, and can be used in many parts, with good quality and at low price. Based on these characteristics, the rhizomes, leaves, and fibrous roots of CX can be used as food and medicine. However, at present, the rhizomes are mostly used and the aboveground parts are abandoned, which not only causes a waste of resources but

also makes it difficult to control its quality. At the same time, due to its planting, harvesting, processing, and other links, there are many influencing factors resulting in the differences in its efficacy, including soil fertility, water and nutrients in growth, harvesting method, season, origin, and so on, make its quality differences. Therefore, the establishment of strict quality control and safety testing means can not only strengthen the utilization of resources but also realize its industrialization and internationalization, realize the unified control of CX's quality, and enhance its safety identification. With the development of drug safety research, metabolomics can be used to identify related biomarkers, monitor the overall dynamic changes of metabolites, judge the effect of drugs on the target site, and then realize the scientific prediction of drug safety. In addition, quality markers can also be used to control drug quality to avoid the impact of evaluation based on single component or multiple component indexes on the overall quality monitoring. At present, the safety study of CX is not perfect, so it can be studied by means of metabonomics, equivalent component group discovery technology, serum pharmacochimistry, network pharmacology, quality markers, etc., to provide a basis for safety evaluation and quality control of CX.

Finally, CX has rich pharmacological effects and a wide range of applications. Its basic research is abundant, mainly in the field of CVDs. However, current studies on the direct target and mechanisms of CVDs treatment are still lacking. It requires researchers to carry out more in-depth research from the molecular, cellular, and animal perspectives and provides more comprehensive treatment ideas for CX in the treatment of CVDs through the combination of molecular biology, genomics, metabonomics, and other methods which further promote the progress of human health career. At the same time, in order to optimize the efficacy of CX, studies can also be carried out from

the perspectives of preparation and drug delivery way. The preparation of modern new nanometer preparation and the expansion of drug delivery way can improve drug loading, optimize drug delivery efficiency, solve the problems of first-pass effect and blood-brain barrier, achieve more efficient accurate effects, and promote modern CX research from the CVDs point of view.

## AUTHOR CONTRIBUTIONS

DL, NL, CZ, and MY designed the study; YL, SY, AS, JyW, JgW, XL, SL, and YZ supplied materials and analytic tools; DL, YL, and SL wrote the article.

## FUNDING

This work was supported by the Xinglin Scholar Discipline Promotion Talent Program of Chengdu University of Traditional Chinese Medicine (No. XGZX 2010); national talent project of traditional Chinese medicine characteristic technology inheritance (No. T20194828003); major science and technology research and development projects in Jiangxi Province (No. 20194ABC28009); and 2021 "three districts" talent plan (No. 319021057).

## SUPPLEMENTARY MATERIAL

The Supplementary Material for this article can be found online at: <https://www.frontiersin.org/articles/10.3389/fphar.2021.832673/full#supplementary-material>

## REFERENCES

- Acharya, B., Chaijaroenkul, W., and Na-Bangchang, K. (2021). Therapeutic Potential and Pharmacological Activities of  $\beta$ -eudesmol. *Chem. Biol. Drug Des.* 97, 984–996. doi:10.1111/cbdd.13823
- Bao, Y. R., Wang, S., Yang, X. X., Li, T. J., and Shengmeng, X. (2019). Extraction and Purification Process of Chuanxiong Phenolic Acid and its Effects on Hypoxic Nerve Cell Injury. *Herald Med.* 38, 1199–1203. doi:10.3870/j.issn.1004-0781.2019.09.018
- Bhandarkar, N. S., Brown, L., and Panchal, S. K. (2018). Chlorogenic Acid Attenuates High-Carbohydrate, High-Fat Diet-Induced Cardiovascular, Liver, and Metabolic Changes in Rats. *Nutr. Res.* 62, 78–88. doi:10.1016/j.nutres.2018.11.002
- Bi, Y. F., Wang, X. L., Zhao, Z. Q., Hou, Y. Z., Wang, C., Zhao, G. Y., et al. (2020). Investigation on Clinical Application of Traditional Chinese Medicine in 1986 Patients with Coronary Heart Disease. *Chin. J. Integr. Med. Cardio-Cerebrovasc. Dis.* 18, 2959–2962+2973. doi:10.12102/j.issn.1672-1349.2020.18.004
- Bo, C. J., Jing, Y., Fu, W. P., Ming, Z. L., Lin, H. B., and Chen, D. J. (2021). Study on Neuroprotective Mechanism of Ligustilide-Mediated PI3K/AKT/mTOR Signal Pathway in Rats with Cerebral Ischemia-Reperfusion Injury. *J. N. Sichuan Med. Coll.* 36, 826–831. doi:10.3969/j.issn.1005-3697.2021.07.003
- Boo, J. J., Yeong, J. S., Ho, P. J., Rak, L. J., Won, Y. K., Tae, K. S., et al. (2009). Antioxidant Activity in Essential Oils of *Cnidium Officinale* Makino and *Ligusticum Chuanxiong* Hort and Their Inhibitory Effects on DNA Damage and Apoptosis Induced by Ultraviolet B in Mammalian Cell. *Cancer Epidemiol.* 33, 41–46. doi:10.1016/j.canep.2009.04.010
- Burcu, G., Osman, C., Asli, C., Namik, O., and Neşe, B. (2016). The Protective Cardiac Effects of B-myrcene after Global Cerebral Ischemia/reperfusion in C57BL/J6 Mouse. *Acta Cir. Bras.* 31, 456–462. doi:10.1590/S0102-865020160070000005
- Cai, X. X., Chen, Z., Pan, X. K., Xia, L., Chen, P., Yang, Y., et al. (2014). Inhibition of Angiogenesis, Fibrosis and Thrombosis by Tetramethylpyrazine: Mechanisms Contributing to the SDF-1/CXCR4 axis. *PLoS One* 9, e88176. doi:10.1371/journal.pone.0088176
- Chen, C., Guo, C., Gao, J., Shi, K. F., Cheng, J. T., Zhang, J., et al. (2019a). Vasorelaxant and Antihypertensive Effects of Tianshu Capsule on Rats: An *In Vitro* and *In Vivo* Approach. *Biomed. Pharmacother.* 111, 188–197. doi:10.1016/j.biopha.2018.12.061
- Chen, C., Wang, F. Q., Xiao, W., Xia, Z. N., Hu, G., Wan, J. B., et al. (2017a). Effect on Platelet Aggregation Activity: Extracts from 31 Traditional Chinese Medicines with the Property of Activating Blood and Resolving Stasis. *J. Tradit. Chin. Med.* 37, 64–75. doi:10.1016/s0254-6272(17)30028-6
- Chen, G., Wu, L., and Deng, C.-Q. (2011). The Effects of BuYang HuanWu Decoction and its Effective Components on Proliferation-Related Factors and ERK1/2 Signal Transduction Pathway in Cultured Vascular Smooth Muscle Cells. *J. Ethnopharmacol.* 135, 7–14. doi:10.1016/j.jep.2011.02.011
- Chen, H. C., Chen, L. L., and Liu, T. J. (2019b). The Effect of Tongtian Oral Liquid Combined with Bubphthalide Sodium Chloride Injection in the Treatment of Acute Cerebral Infarction. *Pract. Clin. J. Integr. Tradit. Chin. West. Med.* 19, 97–99. doi:10.13638/j.issn.1671-4040.2019.10.048



- Chen, Y., Hu, F. Y., and Wu, B. (2017b). Interpretation of "Chinese Classification of Cerebrovascular Diseases (2015). *Chin. J. Contemp. Neurol. Neurosurg.* 17, 865–868. doi:10.3969/j.issn.1672-6731.2017.12.002
- Chen, Z.-Z., Gong, X., Guo, Q., Zhao, H., and Wang, L. (2019c). Bu Yang Huan Wu Decoction Prevents Reperfusion Injury Following Ischemic Stroke in Rats via Inhibition of HIF-1  $\alpha$ , VEGF and Promotion  $\beta$ -ENaC Expression. *J. Ethnopharmacol.* 228, 70–81. doi:10.1016/j.jep.2018.09.017
- Chen, Z. J., Zhang, C., Gao, F., Fu, Q., Fu, C. M., He, Y., et al. (2018). A Systematic Review on the Rhizome of Ligusticum Chuanxiong Hort. (Chuanxiong). *Food Chem. Toxicol.* 119, 309–325. doi:10.1016/j.fct.2018.02.050
- Chen, Z. M., Hu, L., Liao, Y. J., Zhang, X., Yang, Z., Hu, C. J., et al. (2020). Different Processed Products of Curcuma Radix Regulate Pain-Related Substances in a Rat Model of Qi Stagnation and Blood Stasis. *Front. Pharmacol.* 11, 242. doi:10.3389/fphar.2020.00242
- Cheng, F., and Luo, C. (2020). Clinical Observation of Ligustrazine on Elderly Patients with Early Cerebral Ischemia after Intracranial Aneurysm Clipping. *Chin. J. Health Lab. Technol.* 30, 1104–1106. CNKI:SUN:ZWJZ.0.2020-09-025.
- Cheng, Y. S., Cheng, X. X., Zhao, Y. C., and Zhao, H. (2019). Effect of Xiaoxuming Decoction on Acute Cerebral Infarction and Effect on Levels of SOD, MCP-1 and BDNF. *Chin. Arc Tradit Chin. Med.* 37, 435–437. doi:10.13193/j.issn.1673-7717.2019.02.045
- Choi, J.-H., Park, J.-K., Kim, K.-M., Lee, H.-J., and Kim, S. (2018). *In Vitro* and *In Vivo* Antithrombotic and Cytotoxicity Effects of Ferulic Acid. *J. Biochem. Mol. Toxicol.* 32 (1), e22004. doi:10.1002/jbt.22004
- Davis, N., Koichi, F., Zubaerul, F. M., Zahid, H. M., Hiroki, O., and Toru, N. (2019). Dual Inhibition of NADPH Oxidases and Xanthine Oxidase Potently Prevents Salt-Induced Stroke in Stroke-Prone Spontaneously Hypertensive Rats. *Hypertens. Res.* 42, 981–989. doi:10.1038/s41440-019-0246-2
- Demin, L., Hongyu, J., Wenjing, C., Haijuan, H., and Yi, C. (2018). The Progress of Autophagy and Oxidative Stress in Cardiovascular Diseases. *J. Clin. Cardiol.* 34, 402–407. doi:10.13201/j.issn.1001-1439.2018.04.021
- Deng, M. L., Zheng, W. L., and Ju, L. T. (2017). Clinical Efficacy of Salvia Miltiorrhiza Combined with Ligusticum Chuanxiong in the Treatment of Elderly Patients with Atherosclerosis. *Chin. J. Gerontol.* 37, 3445–3447. doi:10.3969/j.issn.1005-9202.2017.14.028
- Derek, B., and Hiranmoy, D. (2020). Current Advances in Ischemic Stroke Research and Therapies. *Biochim. Biophys. Acta Mol. Basis Dis.* 1866, 165260. doi:10.1016/j.bbdis.2018.09.012
- Donkor, P. O., Chen, Y., Ding, L. Q., and Qiu, F. (2016). Locally and Traditionally Used Ligusticum Species - A Review of Their Phytochemistry, Pharmacology and Pharmacokinetics. *J. Ethnopharmacol.* 194, 530–548. doi:10.1016/j.jep.2016.10.012
- Fan, J. S., Liu, D. N., He, C., Li, X. H., and He, F. T. (2016). Inhibiting Adhesion Events by Panax Notoginseng Saponins and Ginsenoside Rb1 Protecting Arteries via Activation of Nr2f2 and Suppression of P38 - VCAM-1 Signal Pathway. *J. Ethnopharmacol.* 192, 423–430. doi:10.1016/j.jep.2016.09.022
- Fan, W. X. (2018). Research Progress on the Mechanism of Ischemic Stroke. *J. Chin. Pharm. Univ.* 49, 751–759. doi:10.11665/j.issn.1000-7369.2019.05.015
- Fang, X., Ma, Q., Zhang, K.-X., Yao, S.-Y., Feng, Y., Jin, Y.-S., et al. (2020). Synthesis of Phthalide Derivatives and Evaluation on Their Antiplatelet Aggregation and Antioxidant Activities. *J. Asian Nat. Prod. Res.* 22, 1176–1187. doi:10.1080/10286020.2019.1681982
- Feng, W. H. (2006). Clinical Observation on 32 Cases of Coronary Heart Disease with Angina Pectoris Treated by Guanxin Pill. *J. New Chin. Med.* 36-37. doi:10.13457/j.cnki.jncm.2006.06.020
- Gang, W. (2018). *Study on Structural Characteristics of Ligusticum CHUANXIONG in the Prevention and Treatment of Myocardial Ischemia Injury and Biopharmaceutical Properties of CHUANXIONG Lactone Components*. Hefei: Anhui University of traditional Chinese Medicine. master.
- Gao, J. H., Yu, L., and Wang, C. J. (2019). Clinical Observation of Daqinjiao Decoction in the Treatment of Cervical Spondylotic Hypertension. *Shaanxi J. Tradit Chin. Med.* 40, 597–599. doi:10.3969/j.issn.1000-7369.2019.05.015
- Gu, J. F., Su, S. L., Guo, J. M., Zhu, Y., Zhao, M., and Duan, J.-A. (2018). Anti-inflammatory and Anti-apoptotic Effects of the Combination of Ligusticum Chuanxiong and Radix Paeoniae against Focal Cerebral Ischaemia via TLR4/MyD88/MAPK/NF- $\kappa$ B Signalling Pathway in MCAO Rats. *J. Pharm. Pharmacol.* 70, 268–277. doi:10.1111/jph.12841
- Gui, M. T., Xu, L. S., Fu, D. Y., Yao, L., Lu, B., Zhou, X. J., et al. (2016). Application Progress of Yueju Pill in Cardiovascular Disease. *People's Milit Sur.* 59, 506–507. CNKI:SUN:RMJZ.0.2016-05-044.
- Guieu, R., Deharo, J.-C., Maille, B., Crotti, L., Torresani, E., Brignole, M., et al. (2020). Adenosine and the Cardiovascular System: The Good and the Bad. *J. Clin. Med.* 9, 1366. doi:10.3390/jcm9051366
- Guo, M., Liu, Y., and Shi, D. Z. (2016). Cardiovascular Actions and Therapeutic Potential of Tetramethylpyrazine (Active Component Isolated from Rhizoma Chuanxiong): Roles and Mechanisms. *Biomed. Res. Inter.* 2016, 2430329. doi:10.1155/2016/2430329
- Haibo, T., Weiwei, S., Sha, L., Qing, S., Tiangang, Z., Yidan, W., et al. (2021). Molecular Mechanism of Palmitic Acid on Myocardial Contractility in Hypertensive Rats and its Relationship with Neural Nitric Oxide Synthase Protein in Cardiomyocytes. *Biomed. Res. Int.* 2021, 6657476. doi:10.1155/2021/6657476
- Han, L., Liu, D.-L., Zeng, Q.-K., Shi, M.-Q., Zhao, L.-X., He, Q., et al. (2018). The Neuroprotective Effects and Probable Mechanisms of Ligustilide and its Degradative Products on Intracerebral Hemorrhage in Mice. *Int. Immunopharmacol.* 63, 43–57. doi:10.1016/j.intimp.2018.06.045
- He, L., Bao, Y. R., Meng, X. S., Wang, S., Li, T. J., and Fu, L. (2018). Potential Mechanism of Chuanxiong Phenolic Acid Components for Rat Migraine by Promoting Blood Circulation and Removing Blood Stasis. *Centr South Pharma* 16, 45–49. doi:10.7539/j.issn.1672-2981.2018.01.008
- He, Y., Gui, S. Q., Huang, X. J., and Zhu, D. L. (2021). Effect of DL-3-N-Butylphthalide on the Improvement of Neurological Function in Rats with Traumatic Brain Injury. *China Pharmaceuticals* 30, 32–35. doi:10.3969/j.issn.1006-4931.2021.08.009
- Heitzer, T., Schlinzig, T., Krohn, K., Meinertz, T., and Münzel, T. (2001). Endothelial Dysfunction, Oxidative Stress, and Risk of Cardiovascular Events in Patients with Coronary Artery Disease. *Circulation* 104, 2673–2678. doi:10.1161/hc4601.099485
- Hintz, K. K., and Ren, J. (2003). Tetramethylpyrazine Elicits Disparate Responses in Cardiac Contraction and Intracellular Ca(2+) Transients in Isolated Adult Rat Ventricular Myocytes. *Vascul. Pharmacol.* 40, 213–217. doi:10.1016/j.vph.2003.08.002
- Hirofumi, T., Kazuki, S., Chisa, M.-N., Toshiharu, N., Shunsuke, K., Kazutaka, K., et al. (2017). The Contribution of Inflammation to the Development of Hypertension Mediated by Increased Arterial Stiffness. *J. Am. Heart Assoc.* 6, e005729. doi:10.1161/JAHA.117.005729
- Hu, J. L., Zhi, L., Zhang, L. F., Shi, M. G. H., Ding, J. S., and Yang, S. H. (2016a). Effect of Chaihu Shugan San on NF-Kb, C-FOS and 5-HT in Migraine Rats. *Sci. Technol. Engineer* 16, 205–210. CNKI:SUN:KXJS.0.2016-12-035.
- Hu, R., Wang, J. Y., and Zhou, S. (2017). Effect of Yueju Pill on Protective Mechanism of Experimental Rats with Myocardial Ischemia. *Chin. J. Ethnomed Ethnopharm* 26, 47–49. CNKI:SUN:MZMJ.0.2017-14-018.
- Hu, Y.-Y., Wang, Y., Liang, S., Yu, X.-L., Zhang, L., Feng, L.-Y., et al. (2016b). Senkyunolide I Attenuates Oxygen-Glucose Deprivation/reoxygenation-Induced Inflammation in Microglial Cells. *Brain Res.* 1649, 123–131. doi:10.1016/j.brainres.2016.08.012
- Huang, W. D., Yang, Y. F., Zeng, Z., Su, M. L., Gao, Q., and Zhu, B. H. (2016). Effect of Salvia Miltiorrhiza and Ligustrazine Injection on Myocardial Ischemia/reperfusion and Hypoxia/reoxygenation Injury. *Mol. Med. Rep.* 14, 4537–4544. doi:10.3892/mmr.2016.5822
- Hung, H.-Y., and Wu, T.-S. (2016). Recent Progress on the Traditional Chinese Medicines that Regulate the Blood. *J. Food Drug Anal.* 24, 221–238. doi:10.1016/j.jfda.2015.10.009
- Izzah Ibrahim, N., Fairus, S., Zulfarina, M. S., and Naina Mohamed, I. (2020). The Efficacy of Squalene in Cardiovascular Disease Risk-A Systematic Review. *Nutrients* 12, 414. doi:10.3390/nu12020414
- Jia, C. X., Chen, J. X., Gao, K., Li, J. Z., Zhang, F. L., Wang, J. P., et al. (2020a). Network Pharmacology of Chuanxiong in the Treatment of Heart Failure. *World Chin. Med.* 15, 1093–1097. doi:10.3969/j.issn.1673-7202.2020.08.001
- Jia, Q. J., Wang, L. R., Zhang, X. N., Ding, Y. J., Li, H., Yang, Y. X., et al. (2020b). Prevention and Treatment of Chronic Heart Failure through Traditional Chinese Medicine: Role of the Gut Microbiota. *Pharmacol. Res.* 151, 104552. doi:10.1016/j.phrs.2019.104552

- Jiang, F. R., Qian, J. C., Chen, S. Y., Zhang, W. B., and Liu, C. (2011). Ligustrazine Improves Atherosclerosis in Rat via Attenuation of Oxidative Stress. *Pharm. Biol.* 49, 856–863. doi:10.3109/13880209.2010.551776
- Jiang, G. H., Chen, S. L., and Wen, W. (2008). Histology Study on Aerial Parts of Rhizoma Chuanxiong. *West. China J. Pharm. Sci.* 5, 508–510. doi:10.13375/j.cnki.wcjps.2008.05.006
- Jin, L., Sun, S., Ryu, Y., Piao, Z. H., Liu, B., Choi, S. Y., et al. (2018). Gallic Acid Improves Cardiac Dysfunction and Fibrosis in Pressure Overload-Induced Heart Failure. *Sci. Rep.* 8, 9302. doi:10.1038/s41598-018-27599-4
- Jin, X. L., Chen, H. Z., Shi, H., Fu, K. L., Li, J. W., Tian, L., et al. (2021). Lipid Levels and the Risk of Hemorrhagic Stroke: A Dose-Response Meta-Analysis. *Nutr. Metab. Cardiovasc. Dis. : NMCD* 31, 23–35. doi:10.1016/j.numecd.2020.10.014
- Jin, Y., Wu, L., Tang, Y. P., Cao, Y. J., Li, S. J., Shen, J., et al. (2016). UFLC-Q-TOF/MS Based Screening and Identification of the Metabolites in Plasma, Bile, Urine and Feces of normal and Blood Stasis Rats after Oral Administration of Hydroxysafflor Yellow A. *J. Chromatogr. B Analyt. Technol. Biomed. Life Sci.* 1012–1013, 124–129. doi:10.1016/j.jchromb.2016.01.023
- Joseph, F. T., and Colín, B. (2020). Angina: Contemporary Diagnosis and Management. *Heart (British Cardiac Soc.)* 106, 387–398. doi:10.1136/heartjnl-2018-314661
- Jun, P., Jiang-Feng, S., Guo-Qin, J., and Zhi-Xue, Y. (2015). Ligustrazine Induces Apoptosis of Breast Cancer Cells *In Vitro* and *In Vivo*. *J. Journal of Cancer Research and Therapeutics. J. Cancer Res. Ther.* 11, 454–8. doi:10.4103/0973-1482.147378
- Kailin, Y., Liuting, Z., Anqi, G., Yaqiao, Y., Shanshan, W., Jinwen, G., et al. (2021). Exploring the Oxidative Stress Mechanism of Buyang Huanwu Decoction in Intervention of Vascular Dementia Based on Systems Biology Strategy. *Oxid. Med. Cel. Longev.* 2021, 20218879060. doi:10.1155/2021/8879060
- Kang, Q. F., Liu, W. H., Liu, H. X., and Zhou, M. (2015). Effect of Compound Chuanxiong Capsule on Inflammatory Reaction and PI3K/Akt/NF-Kb Signaling Pathway in Atherosclerosis. *Evid Based. Complement. Altern. Med. : eCAM* 2015, 584596. doi:10.1155/2015/584596
- Ke, Z. C., Wang, G., Yang, L., Qiu, H. H., Wu, H., Du, M., et al. (2017). Crude Terpene Glycoside Component from Radix Paeoniae Rubra Protects against Isoproterenol-Induced Myocardial Ischemic Injury via Activation of the PI3K/AKT/mTOR Signaling Pathway. *J. Ethnopharmacol.* 206, 160–169. doi:10.1016/j.jep.2017.05.028
- Khoshnazar, M., Parvardeh, S., and Bigdeli, M. (2020). Alpha-pinene Exerts Neuroprotective Effects via Anti-inflammatory and Anti-apoptotic Mechanisms in a Rat Model of Focal Cerebral Ischemia-Reperfusion. *J. Stroke Cerebrovasc. Dis.* 29, 104977. doi:10.1016/j.jstrokecerebrovasdis.2020.104977
- Kim, J. H., Kim, J.-K., Ahn, E.-K., Ko, H.-J., Cho, Y.-R., Lee, C. H., et al. (2015). Marmesin Is a Novel Angiogenesis Inhibitor: Regulatory Effect and Molecular Mechanism on Endothelial Cell Fate and Angiogenesis. *Cancer Lett.* 369, 323–330. doi:10.1016/j.canlet.2015.09.021
- Koc, K., Geyikoglu, F., Cakmak, O., Koca, A., Kutlu, Z., Aysin, F., et al. (2020). The Targets of  $\beta$ -sitosterol as a Novel Therapeutic against Cardio-Renal Complications in Acute Renal Ischemia/reperfusion Damage. *Naunyn-schmiedeberg's Arch. Pharmacol.* 394, 469–479. doi:10.1007/s00210-020-01984-1
- Kornelia, K., David, W., Dirk, D. B., Guy, D. B., Lars, R., Catriona, J., et al. (2016). EUROASPIRE IV: A European Society of Cardiology Survey on the Lifestyle, Risk Factor and Therapeutic Management of Coronary Patients from 24 European Countries. *Anal. Tech. Biomed. Life Sci.* 23, 636–648. doi:10.1177/2047487315569401
- Krylova, I. B., Selina, E. N., Bulion, V. V., Rodionova, O. M., Evdokimova, N. R., Belosludtseva, N. V., et al. (2021). Uridine Treatment Prevents Myocardial Injury in Rat Models of Acute Ischemia and Ischemia/reperfusion by Activating the Mitochondrial ATP-dependent Potassium Channel. *Sci. Rep.* 11, 16999. doi:10.1038/s41598-021-96562-7
- Labdelli, A., Zemour, K., Simon, V., Cerny, M., Adda, A., and Merah, O. (2019). Pistacia Atlantica Desf., a Source of Healthy Vegetable Oil. *Appl. Sci.* 9, 2552. doi:10.3390/app9122552
- Lai, D. P. (2014). "Application of Ligusticum Chuanxiong in Thailand," in China guangzhou international health conference (International Health Association; Guangdong Health Association; Guangzhou University of Chinese Medicine).
- Lan, R., Xiang, J., Wang, G.-H., Li, W.-W., Zhang, W., Xu, L.-L., et al. (2013). Xiao-Xu-Ming Decoction Protects against Blood-Brain Barrier Disruption and Neurological Injury Induced by Cerebral Ischemia and Reperfusion in Rats. *Evid Based. Complement. Altern. Med. : eCAM* 2013, 629782. doi:10.1155/2013/629782
- Lee, J.-J., Hsu, W.-H., Yen, T.-L., Chang, N.-C., Luo, Y.-J., Hsiao, G., et al. (2011). Traditional Chinese Medicine, Xue-Fu-Zhu-Yu Decoction, Potentiates Tissue Plasminogen Activator against Thromboembolic Stroke in Rats. *J. Ethnopharmacol.* 134, 824–830. doi:10.1016/j.jep.2011.01.033
- León, A., Del-Ángel, M., Ávila, J. L., and Delgado, G. (2017). Phthalides: Distribution in Nature, Chemical Reactivity, Synthesis, and Biological Activity. *Prog. Chem. Org. Nat. Prod.* 104, 127–246. doi:10.1007/978-3-319-45618-8\_2
- Li, B., Mao, X. M., and Mao, J. Y. (2005). Clinical Observation of Zhengxintai Granule in Treating Angina Pectoris of Coronary Heart Disease. *Tianjin J. Tradit. Chin. Med.* 2005, 294–296. doi:10.3969/j.issn.1672-1519.2005.04.011
- Li, C.-S., Qu, Z.-Q., Wang, S.-S., Hao, X.-W., Zhang, X.-Q., Guan, J., et al. (2011). Effects of Suxiao Jiuxin Pill (See Test) on Oxidative Stress and Inflammatory Response in Rats with Experimental Atherosclerosis. *J. Tradit. Chin. Med.* 31, 107–111. doi:10.1016/s0254-6272(11)60022-8
- Li, D., Kim, R., McArthur, E., Fleet, J. L., Bailey, D. G., Juurlink, D., et al. (2015a). Risk of Adverse Events Among Older Adults Following Co-prescription of Clarithromycin and Statins Not Metabolized by Cytochrome P450 3A4. *Can. Med. Assoc. J.* 187, 174–180. doi:10.1503/cmaj.140950
- Li, D. Y., and Yu, Z. B. (2020). Analysis of Import & Export of Chinese Medicinal Materials in First Half of 2020. *Mod. Chin. Med.* 22, 12–15. doi:10.13313/j.issn.1673-4890.20200921001
- Li, G. H., Ji, P. C., and Wang, Y. J. (2019). Effect of Xinnaokang Capsule on Hemorheology and Serum Cytokines in Patients with Chronic Stable Angina Pectoris. *Chin. J. Coal Ind. Med.* 22, 191–194. doi:10.11723/mtgyyx.1007-9564.201902016
- Li, H. B., and Chen, F. (2004). Preparative Isolation and Purification of Chuanxiongine from the Medicinal Plant Ligusticum Chuanxiong by High-Speed Counter-current Chromatography. *J. Chromatogr. A.* 1047, 249–253. doi:10.1016/j.chroma.2004.07.006
- Li, J., Wu, Y. S., and Qiu, S. X. (2017a). Research Progress on Polysaccharide from Ligusticum Chuanxiong Hort. *Anim. Husb. Feed Sci* 38, 71–72. doi:10.16003/j.cnki.issn1672-5190.2017.05.017
- Li, J., Yu, J., Ma, H., Yang, N., Li, L., Zheng, D.-D., et al. (2017b). Intranasal Pretreatment with Z-Ligustilide, the Main Volatile Component of Rhizoma Chuanxiong, Confers Prophylaxis against Cerebral Ischemia via Nrf2 and HSP70 Signaling Pathways. *J. Agric. Food Chem.* 65, 1533–1542. doi:10.1021/acs.jafc.6b04979
- Li, L.-L., Liu, Y.-R., Sun, C., Yan, Y.-G., Tang, Z.-S., Sun, J., et al. (2020a). Taorendahuang Herb Pair Reduces Eicosanoid Metabolite Shifts by Regulating ADORA2A Degradation Activity in Ischaemia/reperfusion Injury Rats. *J. Ethnopharmacol.* 260, 113014. doi:10.1016/j.jep.2020.113014
- Li, L. J. (2017). *Studies on the Chemical Constituents of Ligusticum Chuanxiong*. Tianjin: Tianjin University. master.
- Li, L., Yang, N., Nin, L., Zhao, Z. L., Chen, L., Yu, J., et al. (2015b). Chinese herbal medicine formula tao hong si Wu decoction protects against cerebral ischemia-reperfusion injury via PI3K/Akt and the Nrf2 signaling pathway. *J. Nat. Med.* 69, 76–85. doi:10.1007/s11418-014-0865-5
- Li, W. X., Tang, Y. P., Chen, Y. Y., and Duan, J.-A. (2012). Advances in the Chemical Analysis and Biological Activities of Chuanxiong. *Molecules (Basel, Switzerland)* 17, 10614–10651. doi:10.3390/molecules170910614
- Li, Y. Q. (2019). *Analysis of Drug Use Rules Os TCM for Cerebral Edema after Cerebral Hemorrhage Based on Data Mining*. Guangzhou: Guangzhou University of traditional Chinese Medicine. master.
- Li, Y., and Wang, D. C. (2019). Efficacy of An'Gong Jiangya Wan on Clinical Symptoms of Blood Pressure Fluctuations in Patients with Hypertension. *Clini J. Chin. Med.* 11, 71–73+76. doi:10.3969/j.issn.1674-7860.2019.07.027
- Li, Y., Zhang, X. H., Chen, X. X., Chen, D. Z., Yu, Q., Yang, S. L., et al. (2020b). Chinese Herbal Preparations for Chronic Heart Failure: Study Protocol for an Umbrella Review of Systematic Reviews and Meta-Analyses. *Medicine* 99, e18966. doi:10.1097/MD.00000000000018966
- Li, Z. Q., Zong, S. B., Zhou, J., Wang, Z. Z., and Xiao, W. (2016). A Comparison Study of the Difference in Effect between Adjusted XiaoShuan TongLuo and

- Marketed XiaoShuan TongLuo Tablets on Rats with Focal Cerebral Ischemia. *Anhui Med. Pharm. J.* 20, 1250–1253. doi:10.3969/j.issn.1009-6469.2016.7.007
- Lian, Y., Xia, X., Zhao, H., and Zhu, Y. (2017). The Potential of Chrysophanol in Protecting against High Fat-Induced Cardiac Injury through Nrf2-Regulated Anti-inflammation, Anti-oxidant and Anti-fibrosis in Nrf2 Knockout Mice. *Biomed. Pharmacother.* 93, 1175–1189. doi:10.1016/j.biopha.2017.05.148
- Lim, C., Lim, S., Lee, B., Kim, B., and Cho, S. (2017). Effect of Methanol Extract of *Salviae Miltiorrhizae Radix* in High-Fat Diet-Induced Hyperlipidemic Mice. *Chin. Med.* 12, 29. doi:10.1186/s13020-017-0150-0
- Lima, G. F., Lopes, R. D. O., Mendes, A. B. A., Brazão, S. C., Autran, L. J., Motta, N. A. V., et al. (2020). Inosine, an Endogenous Purine Nucleoside, Avoids Early Stages of Atherosclerosis Development Associated to eNOS Activation and P38 MAPK/NF- $\kappa$ B Inhibition in Rats. *Eur. J. Pharmacol.* 882, 173289. doi:10.1016/j.ejphar.2020.173289
- Lin, D. F., Wang, L. L., Yan, S. Q., Zhang, Q., Zhang, J. H., and Shao, A. W. (2019). The Role of Oxidative Stress in Common Risk Factors and Mechanisms of Cardio-Cerebrovascular Ischemia and Depression. *Oxid. Med. Cel. Longev.* 2019, 2491927. doi:10.1155/2019/2491927
- Liu, F. H., Chen, S. J., and Juanni, W. (2017a). Study on the Computer Virtual Screening of Antithrombotic Active Ingredients in Chuanxiong Rhizoma. *Chin. Pharm.* 28, 2182–2186. doi:10.6039/j.issn.1001-0408.2017.16.0610.1002/cav.1776
- Liu, G. W., Liu, G., Lei, Z. Y., Zheng, X. L., and Yang, H. J. (2018). Effect of Gexiazhuo Decoction on Platelet Aggregation Rate and Mace Incidence in Patients with Non ST Segment Elevation Myocardial Infarction after PCI. *J. Sichuan Tradit. Chin. Med.* 36, 68–70. CNKI:SCZY.0.2018-11-024. doi:10.1097/01.hjh.0000548566.68605.1a
- Liu, J. J. (2011). Curative Effect Analysis of Guanxinkang Granule in Treating 146 Cases of Angina Pectoris of Coronary Heart Disease. *Chin. Manip Rehab Med.* 000, 74–75.
- Liu, L., Cheng, Y., and Zhang, H. (2004). Phytochemical Analysis of Anti-atherogenic Constituents of Xue-Fu-Zhu-Yu-Tang Using HPLC-DAD-ESI-MS. *Chem. Pharm. Bull. (Tokyo)* 52, 1295–1301. doi:10.1248/cpb.52.1295
- Liu, M., Chen, X. T., Ma, J., Hassan, W., Wu, H. L., Ling, J. W., et al. (2017b).  $\beta$ -Elemene Attenuates Atherosclerosis in Apolipoprotein E-Deficient Mice via Restoring NO Levels and Alleviating Oxidative Stress. *Biomed. Pharmacother.* 95, 1789–1798. doi:10.1016/j.biopha.2017.08.092
- Liu, S. Y., Long, Y., Yu, S., Zhang, D. K., Yang, Q. Y., Ci, Z. M., et al. (2021). Borneol in Cardio-Cerebrovascular Diseases: Pharmacological Actions, Mechanisms, and Therapeutics. *Pharmacol. Res.* 169, 105627. doi:10.1016/j.phrs.2021.105627
- Liu, T. (2020). Identification of Ligusticum Chuanxiong and Analysis of Clinical Safe Medication. *Guid Chin. Med.* 18, 135–136.
- Liu, X., Shan, X. L., Chen, H. H., Li, Z., Zhao, P., Zhang, C., et al. (2019a). Stachydrine Ameliorates Cardiac Fibrosis through Inhibition of Angiotensin II/Transformation Growth Factor  $\beta$ 1 Fibrogenic Axis. *Front. Pharmacol.* 10, 538. doi:10.3389/fphar.2019.00538
- Liu, Y. J., Li, Z., Shen, D. D., Song, Y. Q., Huang, M. N., Xue, X. X., et al. (2019b). Adjuvant Treatment of Coronary Heart Disease Angina Pectoris with Chinese Patent Medicine: A Prospective Clinical Cohort Study. *Medicine* 98, e16884. doi:10.1097/MD.00000000000016884
- Liu, Y., Yin, H. J., Jiang, Y. R., Xue, M., Guo, C. Y., Shi, D. Z., et al. (2013). Correlation between Platelet Gelsolin and Platelet Activation Level in Acute Myocardial Infarction Rats and Intervention Effect of Effective Components of Chuanxiong Rhizome and Red Peony Root. *Evid Based. Complement. Altern. Med. : eCAM* 2013, 985746. doi:10.1155/2013/985746
- Liu, Z. Y., Deng, P., and Hu, D. (2012). Modern Clinical Application of Gexia Zhuyu Decoction. *Jiangxi Tradit. Chin. Med.* 43, 75–80. doi:10.3969/j.issn.0411-9584.2012.01.03410.1002/chin.201210215
- Liyan, B., Jin, K. H., Xiong, Y., Tingwei, Z., Jung, K. S., and Ho, J. M. (2021). Protocatechuic Acid Attenuates Isoproterenol-Induced Cardiac Hypertrophy via Downregulation of ROCK1–Sp1–PKC $\gamma$  axis. *Sci. Rep.* 11, 17343. doi:10.1038/s41598-021-96761-2
- Long, Y., Yang, Q., Xiang, Y., Zhang, Y., and Peng, W. (2020). Nose to Brain Drug Delivery - A Promising Strategy for Active Components from Herbal Medicine for Treating Cerebral Ischemia Reperfusion. *Pharmacol. Res.* 159, 104795. doi:10.1016/j.phrs.2020.104795
- Longzhu, L., Yi, L., Xueyuan, B., Man, X., Xiaojiang, Y., Runqing, X., et al. (2017). Choline Ameliorates Cardiovascular Damage by Improving Vagal Activity and Inhibiting the Inflammatory Response in Spontaneously Hypertensive Rats. *Sci. Rep.* 7, 42553. doi:10.1038/srep42553
- Luca, L., Fabrizio, M., Jean-Claude, T., Peter, L., and Giovanni, G., C. (2020). Inflamm-aging: the Role of Inflammation in Age-dependent Cardiovascular Disease. *Eur. Heart J.* 41, 2974–2982. doi:10.1093/eurheartj/ehz961
- Luo, M., Chen, P.-P., Yang, L., Wang, P., Lu, Y.-L., Shi, F.-G., et al. (2019a). Sodium Ferulate Inhibits Myocardial Hypertrophy Induced by Abdominal Coarctation in Rats: Involvement of Cardiac PKC and MAPK Signaling Pathways. *Biomed. Pharmacother.* 112, 108735. doi:10.1016/j.biopha.2019.108735
- Luo, Z. H., Deng, H. J., Fang, Z. C., Zeng, A., Chen, Y. K., Zhang, W., et al. (2019b). Ligustilide Inhibited Rat Vascular Smooth Muscle Cells Migration via C-Myc/MMP2 and ROCK/JNK Signaling Pathway. *J. Food Sci.* 84, 3573–3583. doi:10.1111/1750-3841.14936
- Ma, H. Q. (2018a). Effect of Niu Huang Jiangya Capsule Combined with Amlodipine in the Treatment of Primary Hypertension. *J. Huaihai Med.* 36, 718–719. doi:10.14126/j.cnki.1008-7044.2018.06.034
- Ma, Q. (2016). *Clinical Study on Distribution of TCM Syndrome Elements and Traditional Chinese Medicine in Atherosclerotic Cardio Cerebrovascular Disease*. Beijing: Beijing University of traditional Chinese Medicine. master.
- Ma, Y. B., Chen, G. Q., and Ni, Z. H. (2019). Clinical Study on Xueshuan Xinmaining Capsules Combined with Nimodipine in Treatment of Acute Cerebral Infarction. *Drugs Clinic* 34, 970–974. doi:10.7501/j.issn.1674-5515.2019.04.018
- Ma, Y. G., Zhou, M. S., and Zhang, M. F. (2001). Analysis on the Current Situation and Prospect of Chinese Herbal Medicine export. *World Agri* 9, 27–28. doi:10.3969/j.issn.1002-4433.2001.09.008
- Ma, Y. X. (2018b). Clinical Observation of Ligustrazine Injection in the Treatment of Angina Pectoris of Coronary Heart Disease. *Med. Health Care* 26, 125–126. doi:10.3969/j.issn.1004-8650.2018.09.073
- Maia-Joca, R.-P., Joca, H. C., Ribeiro, F. J., do Nascimento, R. V., Silva-Alves, K.-S., Cruz, J. S., et al. (2014). Investigation of Terpinen-4-Ol Effects on Vascular Smooth Muscle Relaxation. *Life Sci.* 115, 52–58. doi:10.1016/j.lfs.2014.08.022
- Mayra, T.-S., Cirino, D. S. R., Vieira, K. F., Vieira, A. M., Gustavo, M. C., Visconde, B. G., et al. (2015). Knockout of Toll-like Receptors 2 and 4 Prevents Renal Ischemia-Reperfusion-Induced Cardiac Hypertrophy in Mice. *PLoS One* 10, e0139350. doi:10.1371/journal.pone.0139350
- Mi, Y. H., Wang, M. J., Liu, M. P., Cheng, H., and Li, S. Q. (2020). Pharmacokinetic Comparative Study of GAS with Different Concentration of Tetramethylpyrazine and Ferulic Acid on Liver-Yang Hyperactivity Migraine Model by Blood-Brain Microdialysis Method. *J. Pharm. Biomed. Anal.* 191, 113643. doi:10.1016/j.jpba.2020.113643
- Nam, K. N., Kim, K.-P., Cho, K.-H., Jung, W.-S., Park, J.-M., Cho, S.-Y., et al. (2013). Prevention of Inflammation-Mediated Neurotoxicity by Butylenephthalide and its Role in Microglial Activation. *Cell Biochem Funct* 31, 707–712. doi:10.1002/cbf.2959
- Ni, X. J., Wong, S. L., Wong, C. M., Chi, W. L., Shi, X. G., Cai, Y. F., et al. (2014). Tetramethylpyrazine Protects against Hydrogen Peroxide-Provoked Endothelial Dysfunction in Isolated Rat Aortic Rings: Implications for Antioxidant Therapy of Vascular Diseases. *Evid Based. Complement. Altern. Med. : eCAM* 2014, 627181. doi:10.1155/2014/627181
- Ning, G., Yuzhen, Z., Lei, L., Li, L., Ping, C., Xuan, Z., et al. (2020). Low Doses of Folic Acid Can Reduce Hyperhomocysteinemia-Induced Glomerular Injury in Spontaneously Hypertensive Rats. *Hypertens. Res.* 43, 1182–1191. doi:10.1038/s41440-020-0471-8
- Oliviero, O., Giulia, S., Annalisa, C., Patrizia, P., Silvia, U., Francesca, P., et al. (2020). The Positive Association between Plasma Myristic Acid and ApoCIII Concentrations in Cardiovascular Disease Patients Is Supported by the Effects of Myristic Acid in HepG2 Cells. *J. Nutr.* 150, 2707–2715. doi:10.1093/jn/nxaa202
- Or, T. C., Yang, C. L., Law, A. H., Li, J. C., and Lau, A. S. (2011). Isolation and Identification of Anti-inflammatory Constituents from Ligusticum Chuanxiong and Their Underlying Mechanisms of Action on Microglia. *Neuropharmacology* 60, 823–831. doi:10.1016/j.neuropharm.2010.12.002
- Pan, R., Cai, J., Zhan, L. C., Guo, Y. H., Huang, R.-Y., Li, X., et al. (2017). Buyang Huanwu Decoction Facilitates Neurorehabilitation through an Improvement of Synaptic Plasticity in Cerebral Ischemic Rats. *BMC Complement. Altern. Med.* 17, 173. doi:10.1186/s12906-017-1680-9



- Pan, X. C. (2012). Clinical Effect of Ligustrazine in the Treatment of Chronic Pulmonary Heart Disease. *Chin. Comm. Doc* 14, 174.
- Pan, X. J., and Liu, H. (2017). The Application Value of Shiquan Dabu Decoction in the Treatment of Chronic Heart Failure. *Chin. Comm. Doc* 33, 106–107. doi:10.3969/j.issn.1007-614x.2017.34.61
- Pan, Z., Duan, F. J., and Wei, X. H. (2007). Protective Effect and Mechanism of Guanxinkang Capsule on Myocardial Injury in Experimental Acute Myocardial Ischemia Rats. *Chin. Pharmacol. Bull.* 9, 1185–1188. doi:10.3321/j.issn:1001-1978.2007.09.017
- Paolo, C., Carla, F., Fabiana, M., Sara, C., Mohsen, N., Boris, B., et al. (2020). Trends in Cardiovascular Diseases burden and Vascular Risk Factors in Italy: The Global Burden of Disease Study 1990–2017. *Anal. Tech. Biomed. Life Sci.* 28, 385–396. doi:10.1177/2047487320949414
- Park, M., Choi, S., Kim, S., Kim, J., Lee, D.-K., Park, W., et al. (2019). NF- $\kappa$ B-responsive miR-155 Induces Functional Impairment of Vascular Smooth Muscle Cells by Downregulating Soluble Guanylyl Cyclase. *Exp. Mol. Med.* 51, 1–12. doi:10.1038/s12276-019-0212-8
- Pu, Z.-H., Dai, M., Xiong, L., and Peng, C. (2020a). Total Alkaloids from the Rhizomes of a Review of Chemical Analysis and Pharmacological Activities. *Nat. Prod. Res.* 9, 1–18. doi:10.1080/14786419.2020.1830398
- Pu, Z. H., Dai, M., Peng, C., and Xiong, L. (2020b). Research Progress on Material Basis and Pharmacological Action of Alkaloids from Ligusticum Chuanxiong Hort. *Chin. Pharm.* 31, 1020–1024. doi:10.6039/j.issn.1001-0408.2020.08.22
- Pu, Z. H., Peng, Y. Z., Peng, C., Liu, J., Xiong, L., and Li, W. B. (2018). Optimization of Extraction Process of Total Phenolic Acids from Ligusticum Chuanxiong Hort. *Chin. Tradit. Pat. Med.* 40, 1506–1509. doi:10.3969/j.issn.1001-1528.2018.07.012
- Qiang, W., Ping, Y. Y., Xue, Y., Tao, C. H., Jun, W. C., and Ri, X. (2017). Ligustrazine Inhibits pm2.5-induced Proliferation of Vascular Smooth Muscle Cells by Down Regulating JNK Phosphorylation. *Chin. J. Pharmacol. Toxicol.* 31, 707–713. doi:10.3867/j.issn.1000-3002.2017.07.002
- Qin, K. (2020). Current Situation and Development of Cardiovascular and Cerebrovascular Disease Surveillance in China. *Appl. Prevent Med.* 26, 265–268. doi:10.3969/j.issn.1673-758X.2020.03.031
- Ran, X., Ma, L., Peng, C., Zhang, H., and Qin, L.-P. (2011). Ligusticum Chuanxiong Hort: a Review of Chemistry and Pharmacology. *Pharm. Biol.* 49, 1180–1189. doi:10.3109/13880209.2011.576346
- Ran, X. (2012). *The Therapeutic Effect of Essential Oil of Ligusticum Chuanxiong Hort. On Human Hypertrophic Scar Nd its Safety Evaluation*. Shanghai: East China Normal University. master.
- Ren, P., Kang, Q. F., Zhou, M. X., Zhang, L., Li, S. N., and Liu, W. H. (2017). Intervention Effect of Danggui Shaoyao Powder on Atherosclerosis in Mice and Expression of DNA Methyltransferase 1 and PPAR- $\gamma$  the Influence of Expression. *Glob. Tradit. Chin. Med.* 10, 1328–1332. doi:10.3969/j.issn.1674-1749.2017.11.009
- Ren, Z. Q., Ma, J. H., Zhang, P. H., Luo, A. T., Zhang, S., Kong, L. H., et al. (2012). The Effect of Ligustrazine on L-type Calcium Current, Calcium Transient and Contractility in Rabbit Ventricular Myocytes. *J. Ethnopharmacol.* 144, 555–561. doi:10.1016/j.jep.2012.09.037
- Rhyu, M., Kim, E., and Kim, B. (2004). Nitric Oxide-Mediated Vasorelaxation by Rhizoma Ligustici Wallichii in Isolated Rat Thoracic Aorta. *Phytomedicine: Int. J. Phytother. Phytopharmacol.* 11, 51–55. doi:10.1078/0944-7113-00334
- Sedigheh, A., Ali, N. G., Reza, S. A. M., Amirhossein, S., Atousa, A., Sanaz, A., et al. (2013). Chemical Analysis and Biological Activities of Cupressus Sempervirens Var. Horizontalis Essential Oils. *Pharm. Biol.* 51, 137–144. doi:10.3109/13880209.2012.715168
- Shakiba, A., Zahra, S., Samira, A., Tahereh, F., Mahmood, S., Fatemeh, A., et al. (2021). Therapeutic Potential of Saffron (L.) in Ischemia Stroke. *Evid. Based. Complement. Altern. Med. : eCAM* 2021, 6643950. doi:10.1155/2021/6643950
- Shan, F., and Hao, J. D. (2011). The Origin of Rhizoma Chuanxiong. *Chin. J. Chin. Mater. Med.* 36, 2306–2310. doi:10.4268/cjcm.2011.36.23
- Shan, L. N., and Leng, L. (2019). Effect of Xueshuanxinmaining Tablet on Vascular Endothelial Function and Hemorheology in Patients with Coronary Heart Disease and Angina Pectoris. *Mod. J. Integr. Tradit. Chin. West. Med.* 28, 2560–2563. doi:10.3969/j.issn.1008-8849.2019.23.013
- Shen, Y.-C., Lu, C.-K., Liou, K.-T., Hou, Y.-C., Lin, Y.-L., Wang, Y.-H., et al. (2015). Common and Unique Mechanisms of Chinese Herbal Remedies on Ischemic Stroke Mice Revealed by Transcriptome Analyses. *J. Ethnopharmacol.* 173, 370–382. doi:10.1016/j.jep.2015.07.018
- Sheng, H. Z., Qi, X. D., Jun, X. L., Shun, H. C., Min, Z., Jun, C. Y., et al. (2020). Tetramethylpyrazine Ameliorates Lipopolysaccharide-Induced Sepsis in Rats via Protecting Blood-Brain Barrier, Impairing Inflammation and Nitrous Oxide Systems. *Front. Pharmacol.* 11, 562084. doi:10.3389/fphar.2020.00376
- Shengzhong, L., Ying, H., Jun, S., Lulu, L., Hao, M., Li, H., et al. (2019). Downregulation of miRNA-30a Enhanced Autophagy in Osthole-Alleviated Myocardium Ischemia/reperfusion Injury. *J. Cel. Physiol.* 1–10. doi:10.1002/jcp.28556
- Shizu, K., Saki, N., Yutaka, Y., Kang, D., Takeshi, B., and Eiichiro, F. (2012). Metabolic Profiling and Identification of the Genetic Varieties and Agricultural Origin of Cnidium Officinale and Ligusticum Chuanxiong. *J. Biosci. Bioeng.* 114, 86–91. doi:10.1016/j.jbiosc.2012.02.015
- Sirangelo, L., Sapio, L., Ragone, A., Naviglio, S., Iannuzzi, C., Barone, D., et al. (2020). Vanillin Prevents Doxorubicin-Induced Apoptosis and Oxidative Stress in Rat H9c2 Cardiomyocytes. *Nutrients* 12, 2317. doi:10.3390/nu12082317
- Song, T. (2015). *Transcriptome Sequencing and Analysis of Rhizome and Leaf in Ligusticum Chuanxiong Hort.* Chengdu: Southwest Jiaotong University. master.
- Song, X. G., Zhou, W., Cheng, C., Wang, S. M., and Liang, S. W. (2015). Study on Material Base of Ligusticum Wallichii for Treating Brain Ischemia and its Molecular Mechanism Based on Molecular Docking. *Chin. J. Chin. Mater. Med.* 40, 2195–2198. doi:10.4268/cjcm.2015.40.24
- Song, X., Li, Y., Zhao, X., Fan, J. M., and Zhao, J. W. (2018). Influence of Daqinjiao Prescription on Recent Hemorheology Hcy and Neurological Functin in Patients with Acute Cerebral Infarction. *Shaanxi J. Tradit. Chin. Med.* 39, 699–702. doi:10.3969/j.issn.1000-7369.2018.06.005
- Stephanieh, R., and Sarahh, W. (2020). Prevention of Premature Cardiovascular Death Worldwide. *Lancet (London, England)* 395, 758–760. doi:10.1016/S0140-6736(19)32034-3
- Su, Q., Lv, X., and Ye, Z. (2019). Ligustrazine Attenuates Myocardial Injury Induced by Coronary Microembolization in Rats by Activating the PI3K/Akt Pathway. *Oxid. Med. Cel. Longev* 2019, 6791457. doi:10.1155/2019/6791457
- Sui, Y. B., Sun, B. H., Zhang, D. D., Liu, L., and Zhang, X. (2020). Clinical Study of Danshen Ligustrazine Injection on Patients with Chronic Heart Failure and Blood Stasis Syndrome. *J. Emerg. Tradit. Chin. Med.* 29, 806–809. doi:10.3969/j.issn.1004-745X.2020.05.015
- Sun, Y. M., Lou, J. T., and Huang, G. Q. (2008). Clinical Study on Early Application of Ligusticin in Cerebral Hemorrhage. *Chin. J. Chin. Mater. Med.* 33, 2545–2548. doi:10.3321/j.issn:1001-5302.2008.21.027
- Suručić, R., Kundaković, T., Lakušić, B., Drakul, D., Milovanović, S. R., and Kovačević, N. (2017). Variations in Chemical Composition, Vasorelaxant and Angiotensin I-Converting Enzyme Inhibitory Activities of Essential Oil from Aerial Parts of Seseli Pallasii Besser (Apiaceae). *Chem. Biodivers.* 14 (5), e1600407. doi:10.1002/cbdv.201600407
- Tan, J., Wang, C. Z., Zhu, H. L., Zhou, B. S., Xiong, L. X., Wang, F., et al. (2018). Comprehensive Metabolomics Analysis of Xueshuan Xinmaining Tablet in Blood Stasis Model Rats Using UPLC-Q/TOF-MS. *Molecules (Basel, Switzerland)* 23, 1650. doi:10.3390/molecules23071650
- Tan, Z., Jiang, X. L., Zhou, W., Deng, B., Cai, M., Deng, S. H., et al. (2021). Taohong Siwu Decoction Attenuates Myocardial Fibrosis by Inhibiting Fibrosis Proliferation and Collagen Deposition via TGFBR1 Signaling Pathway. *J. Ethnopharmacol.* 270, 113838. doi:10.1016/j.jep.2021.113838
- Tang, F., Yan, Y.-M., Yan, H.-L., Wang, L.-X., Hu, C.-J., Wang, H.-L., et al. (2021). Chuanxiongdiolides R4 and R5, Phthalide Dimers with a Complex Polycyclic Skeleton from the Aerial Parts of Ligusticum Chuanxiong and Their Vasodilator Activity. *Bioorg. Chem.* 107, 104523. doi:10.1016/j.bioorg.2020.104523
- Therapy, S. P. T. O. C. a. G. F. P. D. O. C. P. M. (2021). Guidelines for Clinical Application of Chinese Patent Medicine in the Treatment of Coronary Heart Disease (2020 Edition). *Chin. J. Integr. Tradit. West. Med.* 41 (04), 1–27.
- Tian, J. F., Lv, S. Z., Song, X. T., Li, L. Z., and Liu, Y. (2018). Study on Action Mechanism of Chuanxiong in Attenuation of Atherosclerosis Based on Network Pharmacology. *China Med.* 13, 1894–1898. doi:10.3760/j.issn.1673-4777.2018.12.032
- Tian, Y., Zhou, P., Lu, F., Fu, C., Gao, C., Xie, H. T., et al. (2021). Analysis of Clinical Characteristics and Chinese Herbal Medicine Prescription of Hypertension Inpatients Based on Real-World Study. *Chin. Tradit. Herbal Drugs* 52, 469–482. doi:10.7501/j.issn.0253-2670.2021.02.021



- Tong, L. X. (2021). *Effects of Levistilide A on Hemorheology and Endothelial Cell Injury Protection in Rats with Blood Stasis*. Southwest Medical University. master.
- Virani, S. S., Alonso, A., Aparicio, H. J., Benjamin, E. J., Bittencourt, M. S., Callaway, C. W., et al. (2021). Heart Disease and Stroke Statistics-2021 Update: A Report from the American Heart Association. *Circulation* 143, e254–e743. doi:10.1161/CIR.0000000000000950
- Wang, D. L., Dai, M., and Li, H. K. (2006). Effect of Xuemaitong Capsule on Hemorheology of Experimental Atherosclerosis Rabbits. *Chin. J. Tradit Med. Sci. Technol.* 1, 28–29. doi:10.3969/j.issn.1005-7072.2006.01.014.k
- Wang, F. C., Feng, X. R., Yang, L. X., Li, D. H., and Ma, X. (2018a). Simultaneous Determination of Hydroxysafflor Yellow A and Ferulic Acid in ShuXinNing Tablets by HPLC. *Gansu Med. J.* 37, 271–272. doi:10.15975/j.cnki.gsyj.2018.03.031
- Wang, F., Jia, J., and Rodrigues, B. (2017a). Autophagy, Metabolic Disease, and Pathogenesis of Heart Dysfunction. *Can. J. Cardiol.* 33. doi:10.1016/j.cjca.2017.01.002
- Wang, G., Dai, G. L., Song, J., Zhu, M. M., Liu, Y., Hou, X. F., et al. (2018b). Lactone Component from Alleviates Myocardial Ischemia Injury through Inhibiting Autophagy. *Front. Pharmacol.* 9, 301. doi:10.3389/fphar.2018.00301
- Wang, G., Liu, Y., Hou, X. F., Ke, Z. C., Feng, L., and Jia, X. B. (2017b). Prevention Effect of Ligusticum Chuanxiong Extraction against Oxidative Stress Injury Induced by Myocardial Ischemia through Activation of Nrf2 Signaling Pathway. *Chin. J. Chin. Mater. Med.* 42, 4834–4840. doi:10.19540/j.cnki.cjcmm.20171010.001
- Wang, H., Qiu, L. Z., Ma, Y. K., Zhang, L. S., Chen, L., Li, C. X., et al. (2017c). Naoxintong Inhibits Myocardial Infarction Injury by VEGF/eNOS Signaling-Mediated Neovascularization. *J. Ethnopharmacol.* 209, 13–23. doi:10.1016/j.jep.2017.06.040
- Wang, J., Zhang, L., Liu, B., Wang, Q., Chen, Y., Wang, Z., et al. (2018). Systematic Investigation of the Erigeron Breviscapus Mechanism for Treating Cerebrovascular Disease. *J. Ethnopharmacol.* 224, 429–440. doi:10.1016/j.jep.2018.05.022
- Wang, L., Li, G. Q., Chen, Q. W., and Ke, D. Z. (2015). Octanoylated Ghrelin Attenuates Angiogenesis Induced by oxLDL in Human Coronary Artery Endothelial Cells via the GHSR1a-Mediated NF- $\kappa$ B Pathway. *Metabolism* 64, 1262–1271. doi:10.1016/j.metabol.2015.07.008
- Wang, N. N., Xing, Y. M., Wei, M. L., Li, R. H., and Chen, J. (2020). Clinical Study on Mailuotong Granules Combined with Urinary Kallidinogenase in Treatment of Cerebral Infarction. *Drugs & Clinic* 35, 904–908. doi:10.7501/j.issn.1674-5515.2020.05.017
- Wang, W.-R., Lin, R., Zhang, H., Lin, Q.-Q., Yang, L.-N., Zhang, K.-F., et al. (2011). The Effects of Buyang Huanwu Decoction on Hemorheological Disorders and Energy Metabolism in Rats with Coronary Heart Disease. *J. Ethnopharmacol.* 137, 214–220. doi:10.1016/j.jep.2011.05.008
- Wang, X. F., and Shi, X. (2015). Clinical Observation on Yixintongmai Granule in Treating Angina Pectoris of Coronary Heart Disease with Qi Deficiency and Blood Stasis Syndrome. *Shanxi J. Tradit Chin. Med.* 31, 33–35. doi:10.3969/j.issn.1000-7156.2015.12.017
- Wang, X. P. (2016). International Development of New Cardiovascular Medicines. *Chin. J. New Drugs* 25, 1726–1732. doi:10.1088/0964-1726/25/9/095018
- Wang, Y.-H., Hong, Y.-L., Feng, Y., Xu, D.-S., Liang, S., Lin, X., et al. (2012). Comparative Pharmacokinetics of Senkyunolide I in a Rat Model of Migraine versus normal Controls. *Eur. J. Drug Metab. Pharmacokinet.* 37, 91–97. doi:10.1007/s13318-011-0073-6
- Wang, Y. J., Zhu, H. Z., Tong, J. B., and Li, Z. G. (2016). Ligustrazine Improves Blood Circulation by Suppressing Platelet Activation in a Rat Model of Allergic Asthma. *Environ. Toxicol. Pharmacol.* 45, 334–339. doi:10.1016/j.etap.2016.06.016
- Wang, Y. X., Li, J. R., and Shen, H. (2005). Experimental Study on Anti Myocardial Ischemia Effect of Guanxin'an Oral Liquid. *Chin. J. Exp. Tradit Med. Form* 1, 52–54. doi:10.13422/j.cnki.syfjx.2005.01.024
- Wei, L. C. (2020). *Effect of NF- $\kappa$ B on the Proliferation and Apoptosis of Vascular Smooth Muscle Cells and Related Mechanisms*. Zhenjiang: Jiangsu University. master.
- Wei, L. C., and Wu, M. (2020). Effect of Overexpression of NF- $\kappa$ B on Proliferation and Apoptosis of Vascular Smooth Muscle Cells. *J. Med. Res.* 49, 132–136. doi:10.11969/j.issn.1673-548X.2020.08.031
- Wei, Y. Y. (2021). Effect of Clopidogrel Bisulfate on Patients with Coronary Heart Disease and Angina Pectoris. *Conti Med. Edu* 35, 166–167. doi:10.3969/j.issn.1004-6763.2021.03.089
- Wen, Y. Q., Chen, Y., Li, G., Luo, L., and Chen, P. P. (2019). Analysis of the Current Situation of Chuanxiong Patent protection in china. *Pharm. Clin. Chin. Mater. Med.* 10, 1–4. CNKI:SUN:LCZY.0.2019-Z1-002.
- Wong, K.-L., Chan, P., Huang, W.-C., Yang, T.-L., Liu, I. M., Lai, T.-Y., et al. (2003). Effect of Tetramethylpyrazine on Potassium Channels to Lower Calcium Concentration in Cultured Aortic Smooth Muscle Cells. *Clin. Exp. Pharmacol. Physiol.* 30, 793–798. doi:10.1046/j.1440-1681.2003.03913.x
- Wong, K.-L., Wu, K.-C., Wu, R. S.-C., Chou, Y.-H., Cheng, T.-H., and Hong, H.-J. (2007). Tetramethylpyrazine Inhibits Angiotensin II-Increased NAD(P)H Oxidase Activity and Subsequent Proliferation in Rat Aortic Smooth Muscle Cells. *Am. J. Chin. Med.* 35, 1021–1035. doi:10.1142/s0192415x0700548x
- Wu, C., Chiou, W., and Yen, M. (1989). A Possible Mechanism of Action of Tetramethylpyrazine on Vascular Smooth Muscle in Rat Aorta. *Eur. J. Pharmacol.* 169, 189–195. doi:10.1016/0014-2999(89)90015-0
- Wu, H.-J., Hao, J., Wang, S.-Q., Jin, B.-L., and Chen, X.-B. (2012). Protective Effects of Ligustrazine on TNF- $\alpha$ -Induced Endothelial Dysfunction. *Eur. J. Pharmacol.* 674, 365–369. doi:10.1016/j.ejphar.2011.10.046
- Wu, H. Y., and Wang, Y. (2020). Effect of Xiao Xumingtang Combined with Ultrapuncture along Governor Meridian on Autophagy-Related Protein NF- $\kappa$ B P65 in Cerebral Ischemia Reperfusion Model. *Chin. J. Exp. Tradit Med. Form* 26, 30–35. doi:10.13422/j.cnki.syfjx.20201606
- Wu, T. H., Yin, F., Kong, H. M., and Peng, J. (2019). Germacrone Attenuates Cerebral Ischemia/reperfusion Injury in Rats via Antioxidative and Antiapoptotic Mechanisms. *J. Cel Biochem* 120, 18901–18909. doi:10.1002/jcb.29210
- Wu, T. M., Chen, J. S., and Zeng, X. Y. (2013). Effect of Ruanmailing Oral Liquid on Angiogenesis in Atherosclerotic Plaque of Apolipoprotein E Gene Knock-Out Mice. *Chin. J. Info Tradit Chin. Med.* 20, 37–39. doi:10.3969/j.issn.1005-5304.2013.09.013
- Xia, Q., Bao, Q., Jiang, D. J., and Yi, H. (2018). Evaluation of Embryotoxicity of Chuanxiong Rhizoma Decoction Based on Mouse Embryonic Stem Cell Test Model. *Chin. Tradi Pat Med.* 40, 1910–1915. doi:10.3696/j.issn.1001-1528.2018.09.003
- Xiao, G. X., Lyu, M., Li, Z. X., Cao, L. H., Liu, X. Y., Wang, Y. L., et al. (2021). Restoration of Early Deficiency of Axonal Guidance Signaling by Guanxinling Injection as a Novel Therapeutic Option for Acute Ischemic Stroke. *Pharmacol. Res.* 165, 105460. doi:10.1016/j.phrs.2021.105460
- Xin, L. Y., Gao, J. L., Lin, H. C., Qu, Y., Shang, C., Wang, Y. L., et al. (2020). Regulatory Mechanisms of Baicalin in Cardiovascular Diseases: A Review. *Front. Pharmacol.* 11, 583200. doi:10.3389/fphar.2020.583200
- Xing, X. Y. (2002). 40 Cases of Hyperlipidemia Treated with Fangfeng Tongsheng Powder. *J. New Chin. Med* 5, 58. doi:10.3969/j.issn.0256-7415.2002.05.03
- Xiuya, Y., Shoufeng, J., Mingming, Q., Wenfeng, H., Bo, Y., and Dan, L. (2020). Vanillic Acid Alleviates Acute Myocardial Hypoxia/Reoxygenation Injury by Inhibiting Oxidative Stress. *Oxid. Med. Cel. Longev.* 2020, 20208348035. doi:10.1155/2020/8348035
- Xu, C. C., Wang, W. W., Wang, B., Zhang, T., Cui, X. M., Pu, Y. Q., et al. (2019). Analytical Methods and Biological Activities of Panax Notoginseng Saponins: Recent Trends. *J. Ethnopharmacol.* 236, 443–465. doi:10.1016/j.jep.2019.02.035
- Xu, L. C., and Li, G. H. (2019). Effect of Ligustrazine on Platelet Activation and Gelsolin Level in ACS Patients after PCI. *Anhui Med. J.* 40, 775–777. doi:10.3969/j.issn.1000-0399.2019.07.016
- Xu, P. (2007). Effect of Zhengxintai Tablet on Angina Pectoris of Coronary Heart Disease. *Chin. Comm. Doc* 24, 131.
- Xuesong, F., Enshi, W., Jianxun, H., Lei, Z., Xiaoli, Z., Yuan, G., et al. (2019). Ligustrazine Protects Homocysteine-Induced Apoptosis in Human Umbilical Vein Endothelial Cells by Modulating Mitochondrial Dysfunction. *J. Cardiovas. Transl. Res.* 12, 591–599. doi:10.1007/s12265-019-09900-6
- Ya-Xian, W., Ying-Ying, W., Zhiqi, G., Dan, C., Gang, L., Binbin, W., et al. (2021). Ethyl Ferulate Protects against Lipopolysaccharide-Induced Acute Lung Injury by Activating AMPK/Nrf2 Signaling Pathway. *Acta Pharmacol. Sin* 42, 2069–2081. doi:10.1038/s41401-021-00742-0
- Yan, X. J. (2013). *Neuroprotective Mechanism of Butylphthalide Injection Pretreatment through the PI3-k/AKT Signaling Pathway in Cerebral Ischemia Reperfusion Injury on Sprague-Dawley Rats*. Dalian: Dalian medical university. master.

- Yan, X. R., Ding, Y. D., Li, S. L., Yang, D. D., He, X. H., and Jiang, W. W. (2020). Study on Mechanism for Treating Hypertension of Ligusticum Chuanxiong Hort. Based on Network Pharmacology. *Chin. J. Ethnomed. Ethnopharm.* 29, 18–24. CNKI:SUN:MZMJ.0.2020-14-004.
- Yang, D. K. (2020a). Dabu Decoction Combined with Nitroglycerin in the Treatment of Heart Failure after Acute Myocardial Infarction. *Syst. Med.* 5, 115–117. doi:10.19368/j.cnki.2096-1782.2020.12.115
- Yang, J. F., Wang, R., Cheng, X. H., Qu, H. C., Qi, J., Li, D., et al. (2020a). The Vascular Dilatation Induced by Hydroxysafflor Yellow A (HSYA) on Rat Mesenteric Artery through TRPV4-dependent Calcium Influx in Endothelial Cells. *J. Ethnopharmacol.* 256, 112790. doi:10.1016/j.jep.2020.112790
- Yang, M. J., Liu, F. W., Zhang, L. Q., Qin, R., Gong, Y. Q., Feng, S. L., et al. (2013). Annual Cultivation Techniques of Ligusticum Chuanxiong in Kunming. *Yunnan Agri Sci. Technol.* (2), 45. doi:10.3969/j.issn.1000-0488.2013.02.018
- Yang, S. L., Huang, L., Liu, Y. J., and Tan, Q. (2020b). Effect of Chaihu Shugan Powder on Acute Myocardial Infarction of Qi Stagnation Cardiothoracic Type and its Influence on H-FABP Level of Patients. *Acta Chin. Med. Pharm.* 48, 29–33. doi:10.19664/j.cnki.1002-2392.200064
- Yang, X. D. (2020b). Clinical Analysis of Tongqiao Huoxue Decoction in the Treatment of Acute Cerebral Infarction. *Psychologies* 15, 221. doi:10.19738/j.cnki.psy.2020.01.204
- Yang, Y., and Shanshan, P. (2015). Latest Advances in the Research on the Influence of Reactive Oxygen Species-Mediated Oxidative Stress on Myocardial Mitochondria and Autophagy in Cardiovascular Stress and Exercise. *China Sport Sci.* 35, 71–77+97. doi:10.16469/j.css.201505010
- Ye, L., Zhang, Q., Hu, Y., Huang, Y. P., and Liu, Z. (2013). Protective Effects of Xuemaitong Capsule on Rats with Acute Myocardial Infarction and its Mechanism. *J. Chongqing Med. Univ.* 38, 1433–1437. doi:10.11699/cyxb20131209
- Yi, T., Leung, K. S.-Y., Lu, G.-H., Chan, K., and Zhang, H. (2006). Simultaneous Qualitative and Quantitative Analyses of the Major Constituents in the Rhizome of Ligusticum Chuanxiong Using HPLC-DAD-MS. *Chem. Pharm. Bull. (Tokyo)* 54, 255–259. doi:10.1248/cpb.54.255
- Yin, L. (2013). *Study on the Chuanxiong Quality Evaluation Based on the Evolution of Origin*. Chengdu: Chengdu University of Traditional Chinese Medicine. master.
- Yin, M. L. (2018). Clinical Effect of Niu Huang Jiangya Pill in the Treatment of Essential Hypertension. *Inner Mongolia J. Tradit. Chin. Med.* 37, 20–21. doi:10.3969/j.issn.1006-0979.2018.02.016
- Yu, J. (2017). List of Pharmaceutical and Food Homologous Raw Materials (2017 Edition). *Oral Care Ind.* 27, 24–28. doi:10.3969/j.issn.2095-3607.2017.06.007
- Yu, R. Y., Guo, Y. Q., and Lin, L. L. (2017). Protective Effects of Ligusticum Wallichii Extract on Cerebral Ischemia and the Correlation Study with NF- $\kappa$ B Pathway. *J. Nanjing Univ. Tradit. Chin. Med.* 33, 74–77. doi:10.14148/j.issn.1672-0482.2017.0074
- Yuan, R., Shi, W. L., Xin, Q. Q., Yang, B. R., Hoi, M. P., Lee, S. M., et al. (2018). Tetramethylpyrazine and Paeoniflorin Inhibit Oxidized LDL-Induced Angiogenesis in Human Umbilical Vein Endothelial Cells via VEGF and Notch Pathways. *Evid. Based. Complement. Altern. Med. : eCAM* 2018, 3082507. doi:10.1155/2018/3082507
- Zeng, M. F., Pan, L. M., Qi, S. M., Cao, Y. T., Zhu, H. X., Guo, L. W., et al. (2013). Systematic Review of Recent Advances in Pharmacokinetics of Four Classical Chinese Medicines Used for the Treatment of Cerebrovascular Disease. *Fitterapia* 88, 50–75. doi:10.1016/j.fitter.2013.04.006
- Zhang, B., Wu, W. J., Zhong, Z. J., Qian, C. Z., Wang, S., Chen, Y., et al. (2018a). Impact of Danshen Ligustrazine for Injection on Neurological Function, Cerebral Edema and Neuronal Apoptosis in Rats with Cerebral Hemorrhage. *Pract. J. Card. Cereb. Pneumal Vasc. Dis.* 26, 62–66. doi:10.3969/j.issn.1008-5971.2018.11.015
- Zhang, D. Y. (2011). *The Study on Separation, Purification and Structure Analysis of the Polysaccharide from the Ligusticum Chuanxiong Hort.* Changchun: Northeast Normal University. master.
- Zhang, H., Tang, W. W., Wang, S., Zhang, J. H., and Fan, X. (2020a). Tetramethylpyrazine Inhibits Platelet Adhesion and Inflammatory Response in Vascular Endothelial Cells by Inhibiting P38 MAPK and NF- $\kappa$ B Signaling Pathways. *Inflammation* 43, 286–297. doi:10.1007/s10753-019-01119-6
- Zhang, J. F., and Qi, B. K. (2015). Clinical Analysis of 89 Cases of Angina Pectoris of Chronic Coronary Heart Disease Treated with Zhengxintai Capsule. *Qinghai Med. J.* 6, 56–57.
- Zhang, J. J. (2019). Objective to Analyze the Clinical Efficacy of Salvia Miltiorrhiza Ligustrazine Injection in the Treatment of Heart Failure. *Chin. J. Mod. Drug Appl.* 13, 95–96. doi:10.14164/j.cnki.cn11-5581/r.2019.07.052
- Zhang, L. J. (2014). *The Research of Pilot-Scale Production, Toxicological and Pharmacological of Chuanxiong Volatile Oil Soft Capsule*. Shanghai: Second Military Medical University. master.
- Zhang, L., Zhou, X., Lu, T. T., Mu, C. L., Wang, X. L., Tang, L. J., et al. (2019). Optimization of Extraction Process of Volatile Oil from Ligusticum Chuanxiong and GC-MS Analysis of its Overground Part. *J. Chin. Med. Mater.* 42, 607–611. doi:10.13863/j.issn1001-4454.2019.03.029
- Zhang, M. S., Gao, F., Teng, F. M., and Zhang, C. B. (2014). Tetramethylpyrazine Promotes the Proliferation and Migration of Brain Endothelial Cells. *Mol. Med. Rep.* 10, 29–32. doi:10.3892/mmr.2014.2169
- Zhang, Q., Yang, Y.-X., Li, S.-Y., Wang, Y.-L., Yang, F.-Q., Chen, H., et al. (2017). An Ultrafiltration and High Performance Liquid Chromatography Coupled with Diode Array Detector and Mass Spectrometry Approach for Screening and Characterizing Thrombin Inhibitors from Rhizoma Chuanxiong. *J. Chromatogr. B Analyt. Technol. Biomed. Life Sci.* 1061–1062, 421–429. doi:10.1016/j.jchromb.2017.07.050
- Zhang, X., Han, B., Feng, Z.-M., Yang, Y.-N., Jiang, J.-S., and Zhang, P.-C. (2018b). Ferulic Acid Derivatives from Ligusticum Chuanxiong. *Fitterapia* 125, 147–154. doi:10.1016/j.fitter.2018.01.005
- Zhang, X. J., Zhang, Y. L., and Zuo, D. D. (2020b). Research Progress on Chemical Constituents and Pharmacological Effects of Ligusticum Chuanxiong Hort. *Inf. Tradit. Chin. Med.* 37, 128–133. doi:10.19656/j.cnki.1002-2406.200177
- Zhang, X. L., and Gao, Z. W. (2019). Clinical Study on Shuxin Tongmai Capsules Combined with Atorvastatin in Treatment of Coronary Heart Disease. *Drugs & Clinic* 34, 2306–2310. doi:10.7501/j.issn.1674-5515.2019.08.012
- Zhang, Z. J., Kong, S. Y., Zhou, D., and He, L. (2006). Effect of Dachuanxiongwan on the Expression of Vascular Epithelial Growth Factor in Rats with Cerebral Ischemia. *J. Sichuan Univ. Med. Sci.* 37, 246–249. doi:10.3969/j.issn.1672-173X.2006.02.021
- Zhao, C. (2020). Clinical Evaluation of Taoren Chuanxiong Decoction in Treating 45 Cases of Cerebral Hemorrhage Sequelae. *Chin. Pract. Med.* 15, 134–136. doi:10.14163/j.cnki.11-5547/r.2020.11.060
- Zhao, Y., Lu, L. D., and Zhen, X. H. (2017). The Effect of Ligusticum Chuanxiong Polysaccharide on the Cerebral Ischemia-Reperfusion Injury and the Expression of High Mobility Group Protein B1 in Rats. *Chin. J. Gerontol.* 37, 2878–2880. doi:10.3969/j.issn.1005-9202.2017.12.007
- Zhao, Z. F., Zheng, B., Li, J. H., Wei, Z. H., Chu, S. J., Han, X., et al. (2020). Influence of Crocetin, a Natural Carotenoid Dicarboxylic Acid in Saffron, on L-type Ca Current, Intracellular Ca Handling and Contraction of Isolated Rat Cardiomyocytes. *Biol. Pharm. Bull.* 43, 1367–1374. doi:10.1248/bpb.b20-00298
- Zhao-, X. W., Xu, W. H., Zhao, Y., Wu, Y. H., Luo, W., Zhu, Z. M., et al. (2019). Action Mechanisms of Chuanxiong Rhizoma in Treating Coronary Heart Disease Based on Network Pharmacology. *Chin. Tradit. Pat. Med.* 41, 2096–2101. doi:10.3969/j.issn.1001-1528.2019.09.015
- Zheng, J. R., and Deng, J. L. (2020). Research Progress in Animal Models of Cerebral Hemorrhage. *Med. Recapitulate* 26, 960–964. doi:10.3969/j.issn.1006-2084.2020.05.025
- Zheng, Q., Tang, Y., Hu, P.-Y., Liu, D., Zhang, D. L., Yue, P. F., et al. (2018). The Influence and Mechanism of Ligustilide, Senkyunolide I, and Senkyunolide A on Echinacoside Transport through MDCK-MDR1 Cells as Blood-Brain Barrier In Vitro Model. *Phytotherapy Res. : PTR* 32, 426–435. doi:10.1002/ptr.5985
- Zhi-Gang, Z., Xiao-Lan, Z., Xian-Yue, W., Zhu-Rong, L., and Jing-Chun, S. (2015). Inhibition of Acid Sensing Ion Channel by Ligustrazine on Angina Model in Rat. *Am. J. Transl. Res.* 7, 1798–1811.
- Zhou, M. G., Wang, H. D., Zeng, X. Y., Yin, P., Zhu, J., Chen, W. Q., et al. (2019a). Mortality, Morbidity, and Risk Factors in China and its Provinces, 1990–2017: a Systematic Analysis for the Global Burden of Disease Study 2017. *Lancet (London, England)* 394, 1145–1158. doi:10.1016/S0140-6736(19)30427-1
- Zhou, Y., Ming, J. H., Li, Y. M., Deng, M., Chen, Q., Ma, Y. G., et al. (2019b). Ligustilide Attenuates Nitric Oxide-Induced Apoptosis in Rat Chondrocytes and Cartilage Degradation via Inhibiting JNK and P38 MAPK Pathways. *J. Cel. Mol. Med.* 23, 3357–3368. doi:10.1111/jcmm.14226
- Zhou, Y., Xie, M., Song, Y., Wang, W. P., Zhao, H. R., Tian, Y., et al. (2016). Two Traditional Chinese Medicines Curcumae Radix and Curcumae Rhizoma: An

- Ethnopharmacology, Phytochemistry, and Pharmacology Review. *Evid Based. Complement. Altern. Med. : eCAM* 2016, 4973128. doi:10.1155/2016/4973128
- Zou, J., Chen, G.-D., Zhao, H., Huang, Y., Luo, X., Xu, W., et al. (2018). Triligustilides A and B: Two Pairs of Phthalide Trimers from *Angelica Sinensis* with a Complex Polycyclic Skeleton and Their Activities. *Org. Lett.* 20, 884–887. doi:10.1021/acs.orglett.8b00017
- Zuo, B. T., Qu, Y. Q., Wang, L. G., Li, L., Zhang, H., and Yang, X. J. (2020). Clinical Study on Xingnao Zhitan Capsule in the Treatment of Carotid Atherosclerosis in Patients with Acute Cerebral Infarction. *Res. Pract. Chin. Med.* 34, 73–77. doi:10.13728/j.1673-6427.2020.01.016

**Conflict of Interest:** The authors declare that the research was conducted in the absence of any commercial or financial relationships that could be construed as a potential conflict of interest.

**Publisher's Note:** All claims expressed in this article are solely those of the authors and do not necessarily represent those of their affiliated organizations, or those of the publisher, the editors, and the reviewers. Any product that may be evaluated in this article, or claim that may be made by its manufacturer, is not guaranteed or endorsed by the publisher.

Copyright © 2022 Li, Long, Yu, Shi, Wan, Wen, Li, Liu, Zhang, Li, Zheng, Yang and Shen. This is an open-access article distributed under the terms of the Creative Commons Attribution License (CC BY). The use, distribution or reproduction in other forums is permitted, provided the original author(s) and the copyright owner(s) are credited and that the original publication in this journal is cited, in accordance with accepted academic practice. No use, distribution or reproduction is permitted which does not comply with these terms.



# Induction of Heme Oxygenase-1 Modifies the Systemic Immunity and Reduces Atherosclerotic Lesion Development in ApoE Deficient Mice

Leyi Yao<sup>1,2†</sup>, Yali Hao<sup>1†</sup>, Guanmei Wen<sup>1,3†</sup>, Qingzhong Xiao<sup>4</sup>, Penglong Wu<sup>5</sup>, Jinheng Wang<sup>1\*</sup> and Jinbao Liu<sup>1\*</sup>

## OPEN ACCESS

### Edited by:

Xianwei Wang,  
Xinxiang Medical University, China

### Reviewed by:

Silvia Castany,  
Linköping University, Sweden  
Mohamed Ameen Ismahil,  
Washington University in St. Louis,  
United States

### \*Correspondence:

Jinheng Wang  
wangjh89@gzhmu.edu.cn  
Jinbao Liu  
jliu@gzhmu.edu.cn

<sup>†</sup>These authors have contributed  
equally to this work

### Specialty section:

This article was submitted to  
Cardiovascular and Smooth Muscle  
Pharmacology,  
a section of the journal  
Frontiers in Pharmacology

**Received:** 05 November 2021

**Accepted:** 03 January 2022

**Published:** 24 February 2022

### Citation:

Yao L, Hao Y, Wen G, Xiao Q, Wu P,  
Wang J and Liu J (2022) Induction of  
Heme Oxygenase-1 Modifies the  
Systemic Immunity and Reduces  
Atherosclerotic Lesion Development in  
ApoE Deficient Mice.  
Front. Pharmacol. 13:809469.  
doi: 10.3389/fphar.2022.809469

<sup>1</sup>Guangzhou Municipal and Guangdong Provincial Key Laboratory of Protein Modification and Degradation, School of Basic Medical Sciences, Affiliated Cancer Hospital and Institute of Guangzhou Medical University, Guangzhou Medical University, Guangzhou, China, <sup>2</sup>Institute of Digestive Disease of Guangzhou Medical University, Qingyuan People's Hospital, The Sixth Affiliated Hospital of Guangzhou Medical University, Qingyuan, China, <sup>3</sup>Guangdong Key Laboratory of Vascular Diseases, State Key Laboratory of Respiratory Disease, Guangzhou Institute of Cardiovascular Disease, The Second Affiliated Hospital, Guangzhou Medical University, Guangzhou, China, <sup>4</sup>Clinical Pharmacology, Barts and The London School of Medicine and Dentistry, William Harvey Research Institute, Queen Mary University of London, London, United Kingdom, <sup>5</sup>Hospital of Xiamen University, School of Medicine, Xiamen University, Xiamen, China

Heme oxygenase-1 (HO-1) has been reported to protect against oxidation and inflammation in atherosclerosis. It remains unclear how the immune system participates in the cytoprotective function of HO-1 in the context of atherosclerosis. In this study, we attempted to investigate the potential effect of a HO-1 inducer, hemin, and a HO-1 inhibitor, Tin-protoporphyrin IX (SnPP), on the progression of atherosclerosis in ApoE deficient mice. Using mass cytometry, 15 immune cell populations and 29 T cell sub-clusters in spleen and peripheral blood were thoroughly analyzed after hemin or SnPP treatment. SnPP elevated risk factors of atherosclerosis, whereas hemin reduced them. In-depth analysis showed that hemin significantly modified the immune system in both spleen and peripheral blood. Hemin increased dendritic (DC) and myeloid-derived suppressor cells (MDSCs), but decreased natural killer (NK) cells. An opposite effect was observed with SnPP treatment in terms of NK cells. NK cells and MDSCs were positively and negatively correlated with total cholesterol and low-density lipoprotein, respectively. Moreover, the T cell profiles were significantly reshaped by hemin, whereas only minor changes were observed with SnPP. Several hemin-modulated T cell clusters associated with atherosclerosis were also identified. In summary, we have unraveled an important regulatory role for HO-1 pathway in immune cell regulation and atherosclerosis. Our finding suggests that modulating HO-1 signaling represents a potential therapeutic strategy against atherosclerosis.

**Keywords:** heme oxygenase-1, atherosclerosis, systemic immunity, hemin, SNPP



## INTRODUCTION

Heme oxygenase-1 (HO-1) is a well-characterized inducible isoform of the rate-limiting monooxygenase, ferrous iron, and biliverdin. While some immune cells including iron-recycling macrophages in the spleen and liver and tolerogenic immune cells constitutively express HO-1, most other tissues and cells express little or no HO-1 under homeostatic conditions (Campbell et al., 2021). In response to pro-oxidant stimuli, HO-1 is highly upregulated in most cell types, protecting them from oxidative damage. As a result of its antioxidant properties, HO-1 has cytoprotective effects in various pathological conditions such as atherosclerosis, diabetes, and occlusive vascular disease (Durante, 2011).

Atherosclerosis is a chronic inflammatory disease associated with multifactorial mechanisms, which are primarily driven by oxidative stress and inflammation (Agudiez et al., 2020; Dinh et al., 2017; Le, 2004; Wang et al., 2014). Apolipoprotein E knockout (ApoE<sup>-/-</sup>) mice and low-density lipoprotein (LDL) receptor deficient (LDLR<sup>-/-</sup>) mice are widely used as murine models for atherosclerosis (Mukhopadhyay, 2013). Both *in vivo* and *in vitro* evidence have demonstrated the protective properties of HO-1 against atherosclerosis. In a co-culture system of human aortic endothelial cells and smooth muscle cells, pretreatment with HO-1 inducer hemin chloride suppressed monocyte chemotaxis induced by oxidized low-density lipoprotein (Ishikawa et al., 1997). By inhibiting MCP-1 production (Shokawa et al., 2006), foam cell formation, and pro-inflammatory cytokine production or by upregulating anti-inflammatory mediators, HO-1 may act as an anti-atherogenic molecule (Ma et al., 2007). In an animal model, HO-1 deficiency resulted in more advanced atherosclerotic lesions in ApoE<sup>-/-</sup> mice (Wu et al., 2006). The inhibition of HO-1 by pharmacological agents like Tin-protoporphyrin IX (SnPP), exacerbates atherosclerosis in LDLR<sup>-/-</sup> mice (Ishikawa et al., 2001b) or heritable hyperlipidemic rabbits (Ishikawa et al., 2001a). Overexpression of HO-1 *via* adenovirus-mediated gene transfer in vascular cells attenuates the development of atherosclerosis in ApoE<sup>-/-</sup> mice (Juan et al., 2001). The level of HO-1 expression is positively associated with the risk and severity of atherosclerosis. A higher level of HO-1 in monocyte-derived macrophages was related to the unstable phenotype of atherosclerotic plaques featured with higher content of macrophage, thin fibrous caps, and thrombosis (Fiorelli et al., 2019). HO-1's anti-atherogenic properties may also be mediated through free radicals scavenging, fatty acid oxidation inhibition, lipid composition modification, or influence on the nitric oxide pathway (Durante, 2011; Bellner et al., 2020). In addition to its antioxidant effects, HO-1 has been widely reported to have anti-inflammatory effects in atherosclerosis. HO-1 is upregulated during inflammation and subsequently suppresses vascular inflammation by affecting a variety of immune cells, including macrophages, dendritic cells, T cells, and mast cells (Ryter, 2021). HO-1 has been well documented for its cardioprotective properties, but its effects on systemic immunity are not well understood. As a chronic inflammatory disease, atherosclerosis is closely associated with immune modulation.

Mass cytometry, an emerging technology, has been widely applied in recent years to analyze immune systems at the single cell level (Bandura et al., 2009; Bodenmiller et al., 2012). Traditional flow cytometry is restricted by a limited number of detection channels (generally <15) and cumbersome compensation caused by spectral overlap, whereas mass cytometry can simultaneously measure more than 40 parameters in millions of individual cells (Bendall et al., 2011). The expansion of channels enables us to quantify more surface and intracellular proteins in single cell and thus facilitate in-depth analyses of cellular heterogeneity and comprehensive dissections of immune systems (McGuire et al., 2020). Mass cytometry has already been used to expand our understanding of complex processes in cellular development (Bendall et al., 2014), tumor immunology (Wang et al., 2020a; Wang et al., 2020b), and immune modulation in cardiovascular disease (Cole et al., 2018).

ApoE<sup>-/-</sup> mice exhibit higher plasma total cholesterol level than LDLR<sup>-/-</sup> mice on a chow diet, and develop severe atherosclerotic lesions and proinflammatory changes as soon as a few weeks, making them good candidates for studying inflammation of atherosclerosis (Lo Sasso et al., 2016). In this study, we used the well-characterized HO-1 inducer hemin and inhibitor SnPP to examine the protective role of HO-1 in the ApoE<sup>-/-</sup> atherosclerosis mouse model. Following hemin or SnPP treatment, mass cytometry was utilized to simultaneously assess the expression of 26 immune cell markers on spleen and peripheral blood immune cells at the single cell level. Additionally, high-dimensional analysis was used to uncover the effects of HO-1 on systemic immune regulation in the context of atherosclerosis.

## METHODS AND MATERIALS

### Animals

8-week-old male ApoE<sup>-/-</sup> mice (C57BL/6.129P2-APOE/J) were purchased from Beijing Vital River Laboratory Animal Technology. These mice were housed and treated following the protocols approved by the Institutional Committee for the Use and Care of Laboratory Animals of Guangzhou Medical University (2017-014). All animals were fed on a western diet supplemented with 21% fat (wt/wt) and 0.15% cholesterol (wt/wt) at 8 weeks of age and this diet was continued for 10 weeks. ApoE<sup>-/-</sup> mice were simultaneously intraperitoneally injected with HO-1 inducer hemin (Hemin group, 51280, Sigma, 5 mg/kg/d, *n* = 6) or HO-1 inhibitor SnPP (SnPP group, B6432, APEX BIO, 10 mg/kg/d, *n* = 10) or vehicle (Control group, *n* = 8) every other day for 10 weeks, during which time the body weight and the daily intake of food and water were monitored at weekly interval. The mice were euthanized with an overdose of pentobarbital sodium (200 mg/kg, Sigma, St. Louis, MO, United States) for blood and tissue collection.

### Biochemical Assays

Peripheral blood was collected into a heparin-coated tube by cardiac puncture at the end (10 weeks) of the study for biochemical assay. All metabolic parameters, including glucose,

lipid or lipoprotein profile, and hepatic enzymes in plasma, were determined by following the instructions of the commercial kits (Kehua Bio-Engineering, Shanghai, China).

## Histological and Morphometric Analyses

The hearts perfused with 5 ml phosphate-buffered saline were dissected and snap-frozen in liquid nitrogen followed by OCT embedment. The entire aorta between the heart and iliac bifurcation was carefully dissected. Aorta segments, including the ascending aorta, aorta arch, descending thoracic and abdominal aortas, were separated and fixed in formaldehyde solution at room temperature (RT) for 24 h. Under a stereomicroscope (SXZ 16, OLYMPUS, JAPAN), the brachiocephalic trunk was dissected from the aorta arch. The rest of the aorta segments were dissected free of fat tissue and opened longitudinally. To prepare the stock solution, 0.25 g of oil red O (ORO, O026, Sigma, St. Louis, MO, United States) was dissolved in 100 ml of distilled water. The working solution is prepared by adding four parts of distilled water to six parts of the stock solution. After rinsing with 60% isopropyl alcohol for 5 min, the fixed arterial tree was incubated in a working solution at room temperature for 30 min. The sample was then rinsed in 60% IPA, followed by distilled water. After staining with ORO, the aorta was pinned onto a black wax plate and photographed under a Stereomicroscope at standardized magnification and illumination. The aorta lesion area was quantified as the percentage of ORO red positive area over the total aorta area using ImageJ software. The heart and brachiocephalic trunk were serially sectioned into 5  $\mu$ m cryosections. The first section of the aortic sinus was harvested when all three aortic valves became visible in the lumen of the aorta. The cryosections were subjected to hematoxylin and eosin (H&E, KGA223, KeyGEN, Jiangshu, China) staining for morphological analysis, ORO staining for lipid load measurement, and Masson's Trichrome (DC0033, LEAGENE, Beijing, China) staining for collagen detection, respectively. Microscopic atherosclerotic lesions in the aortic sinus were standardized as the ratio of intima area to the media area. All images were captured by a digital pathology slide scanner (Leica, Aperio CS2, Germany).

## Peripheral Blood and Spleen Cell Preparation

After injection of pentobarbital sodium, peripheral blood was collected from the heart. The spleen of mice was removed after sacrifice, and the spleen cell suspension was separated by gently crushing the spleen. Fix I buffer (Fluidigm) was used for 10 min at room temperature to fix cells from peripheral blood or spleen. After washing with cold phosphate buffered solution, erythrocytes were removed from these samples using red blood cell lysis buffer. Cells were then resuspended in cell staining buffer supplemented with 10% dimethyl sulphoxide and stored at  $-80^{\circ}\text{C}$  until cell staining was performed.

## Immunostaining and Mass Cytometry

To eliminate sample-specific staining variation,  $0.5 \times 10^6$  peripheral blood or spleen cells from each mouse were

barcoded separately using the Cell-ID 20-Plex Pd Barcoding Kit (Fluidigm) containing premade combinations of six different palladium isotopes for 30 min at room temperature. After washing twice with cell staining buffer, samples were pooled together. To reduce nonspecific antibody binding, samples were incubated for 10 min at RT with anti-CD16/32 antibody (FcR III/II, Biolegend, CA, United States). A cocktail of 26 metal isotope-conjugated antibodies (**Supplementary Table S1**) was incubated with these cells for 30 min at room temperature after washing twice with staining buffer. Cell-ID Intercalator-Ir (Fluidigm) was used to stain the cell nucleus. After washing with cell staining buffer and ddH<sub>2</sub>O, cells were resuspended in ultrapure water supplemented with 10% EQ Four Element Calibration Beads (Fluidigm). The sample was filtered through a 40- $\mu$ m cell strainer and analyzed using Helios mass cytometer (Fluidigm).

## Data Processing and Analysis

Flow cytometry standard (FCS) files were generated by mass cytometry, and data were normalized, randomized, and debarcoded using the CyTOF 6.7 software (Fluidigm). These files were uploaded to cytobank. cn for cytometry-based single cell analysis. Cell debris and doublets were excluded and the single cell data were used for high-dimensional analysis with viSNE algorithm. We directly gated clear cell populations based on marker expression on cells in the viSNE map and on phenotypes of immune cell populations or T cell subsets. Also, two dimensional plots were used to distinguish the other cell populations from the rest of the cells in the viSNE map.

## Statistical Analysis

One-way ANOVA followed by Tukey's multiple comparison test was used for comparing multiple groups. Person's correlation coefficient was used for correlation analyses.  $|R| > 0.4$  with  $p < 0.05$  was regarded as statistical correlation. Data presented as the mean  $\pm$  SD.  $p < 0.05$  was regarded as statistically significant.

## RESULTS

### The HO-1 Inducer Hemin Improves Atherogenesis and its Inhibitor SnPP Exacerbates Atherogenesis

In order to determine whether endogenous HO-1 system is involved in atherogenesis *in vivo*, we treated ApoE<sup>-/-</sup> mice on a western-type diet with well-proven HO-1 inducer hemin or inhibitor SnPP, respectively. We found that hemin slightly but not significantly decreased the body weight, whereas SnPP significantly increased it (**Figure 1A**). As assessed by immunostaining in aortic lesions, HO-1 expression was higher in mice treated with hemin, but lower in those treated with SnPP (**Supplementary Figure S1A**). HO-1 expression in liver was increased by hemin and inhibited by SnPP, indicating a successful induction or inhibition of HO-1 (**Supplementary Figure S1B**). Hemin or SnPP did not affect blood glucose or triglyceride (**Figure 1B**), but hemin significantly reduced total cholesterol, LDL cholesterol, and HDL cholesterol levels.

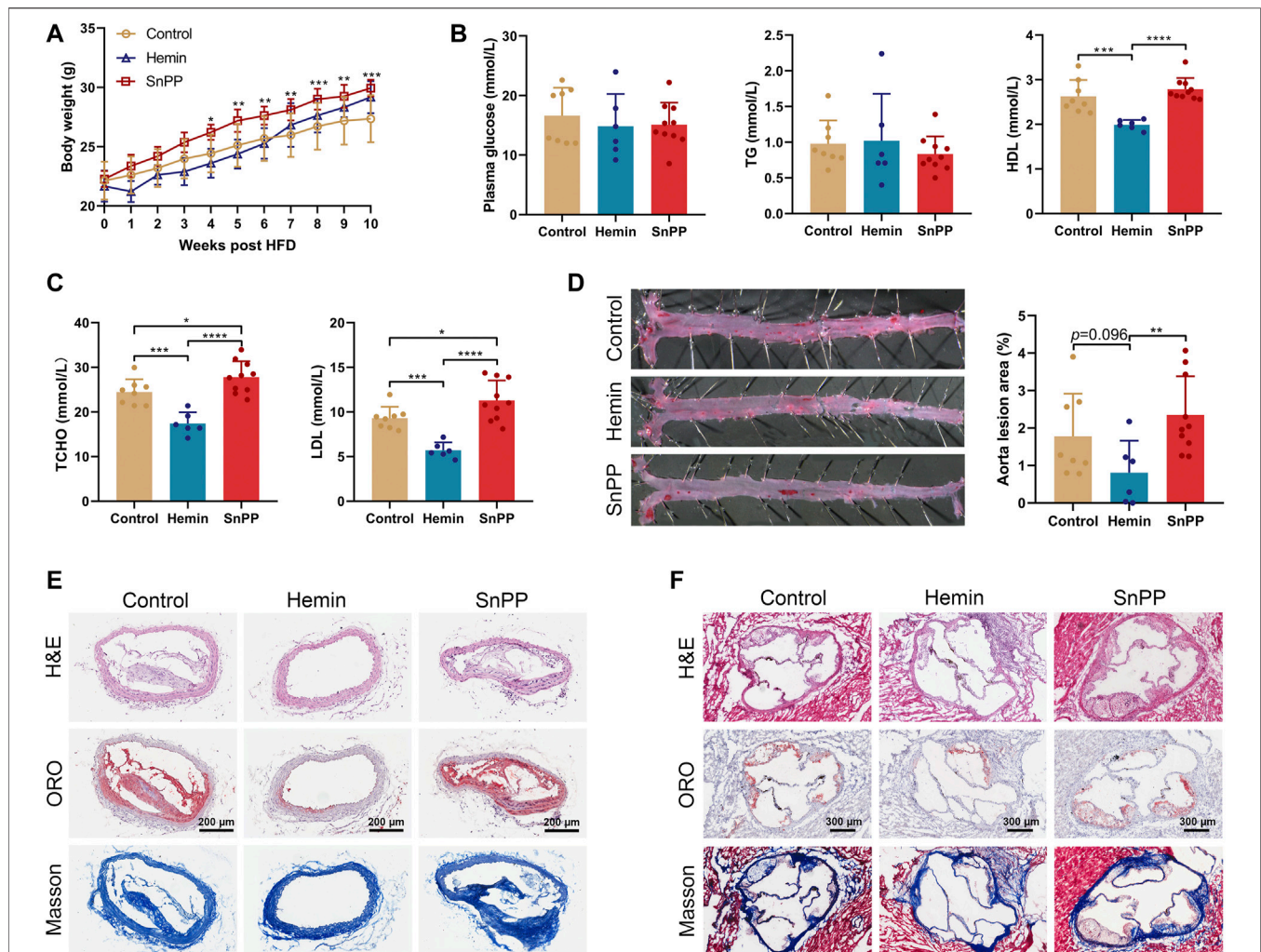


**FIGURE 1 |** HO-1 inducer hemin ameliorates atherosclerosis in ApoE<sup>-/-</sup> mice. Male 8-week old ApoE<sup>-/-</sup> mice fed on a western-type diet (high-fat diet, HFD) were received an intraperitoneal injection of hemin (hemin group, 30 mg/kg/day,  $n = 6$ ), Tin-protoporphyrin IX (SnPP group, 10 mg/kg/day,  $n = 10$ ) and vehicle (control group,  $n = 8$ ) once every other day for 10 weeks. **(A)** Weekly body weight of mice on HFD and under pharmacological challenges. **(B,C)** Plasma lipids profiles. Plasma collected from peripheral blood was subjected to the biochemical analysis of glucose, total triglyceride (TG), high-density lipoprotein cholesterol (HDL), low-density lipoprotein cholesterol (LDL), and total cholesterol (TCHO). **(D)** Aortas, **(E)** brachiocephalic arteries, and **(F)** aortic roots collected from three groups were subjected to histological and morphometric analysis. **(D)** Representative images of En face oil red O (ORO) staining (left) and quantitative analysis of the ORO (+) staining area over total aorta. Aorta lesions are identified by dark red areas after ORO staining. Data are expressed as mean  $\pm$  SD. **(E)** Representative images of lesion morphology in brachiocephalic artery. Cells were stained with H&E (upper panel), lipid content (red) was stained with ORO (middle panel), and collagen (blue) was stained with Masson's Trichrome (lower panel). **(F)** Morphometric and histological analyses of the lesions in aortic sinus/roots. Representative cross-sections of the aortic roots were shown. Cells were stained with H&E (upper panel), lipid content was stained with ORO (middle panel), and collagen was stained with Masson's Trichrome (lower panel). Data were expressed as mean  $\pm$  SD.  $n$  (control) = 8,  $n$  (hemin) = 6,  $n$  (SnPP) = 10. \* $p < 0.05$ , \*\* $p < 0.01$ , \*\*\* $p < 0.001$ , \*\*\*\* $p < 0.0001$  (One-way ANOVA).

Compared to the control group, HO-1 inhibitor SnPP increased the levels of total and LDL cholesterol (**Figures 1B,C**).

After administration of hemin or SnPP, en face Oil Red O staining was then used to evaluate atherosclerotic lesions in aortas in ApoE<sup>-/-</sup> mice. As shown in **Figure 1D**, mice treated with hemin had a smaller lesion area than mice treated with SnPP ( $p = 0.009$ ) or vehicle ( $p = 0.096$ ). The brachiocephalic artery (BCA) is a highly reproducible site of lesion formation and after treatment with hemin, no visible lesions were found in the BCA of mice (**Figure 1E**). Moreover, hemin-treated mice showed a small atherosclerotic plaque in aortic roots

(**Figure 1F** and **Supplementary Figure S1C**). Importantly, HO-1 induction by hemin caused a more stable plaque phenotype characterized by reduced lipid content and increased collagen deposition both in BCA and aortic sinus (**Figures 1E,F**, and **Supplementary Figure S1C**). Hemin and SnPP did not have a significant effect on AST and ALT activity (**Supplementary Figure S1D**), suggesting that they do not cause liver damage. These results indicate that HO-1 induction significantly reduces circulating lipid and ameliorates atherogenesis, whereas HO-1 inhibition exacerbates them.



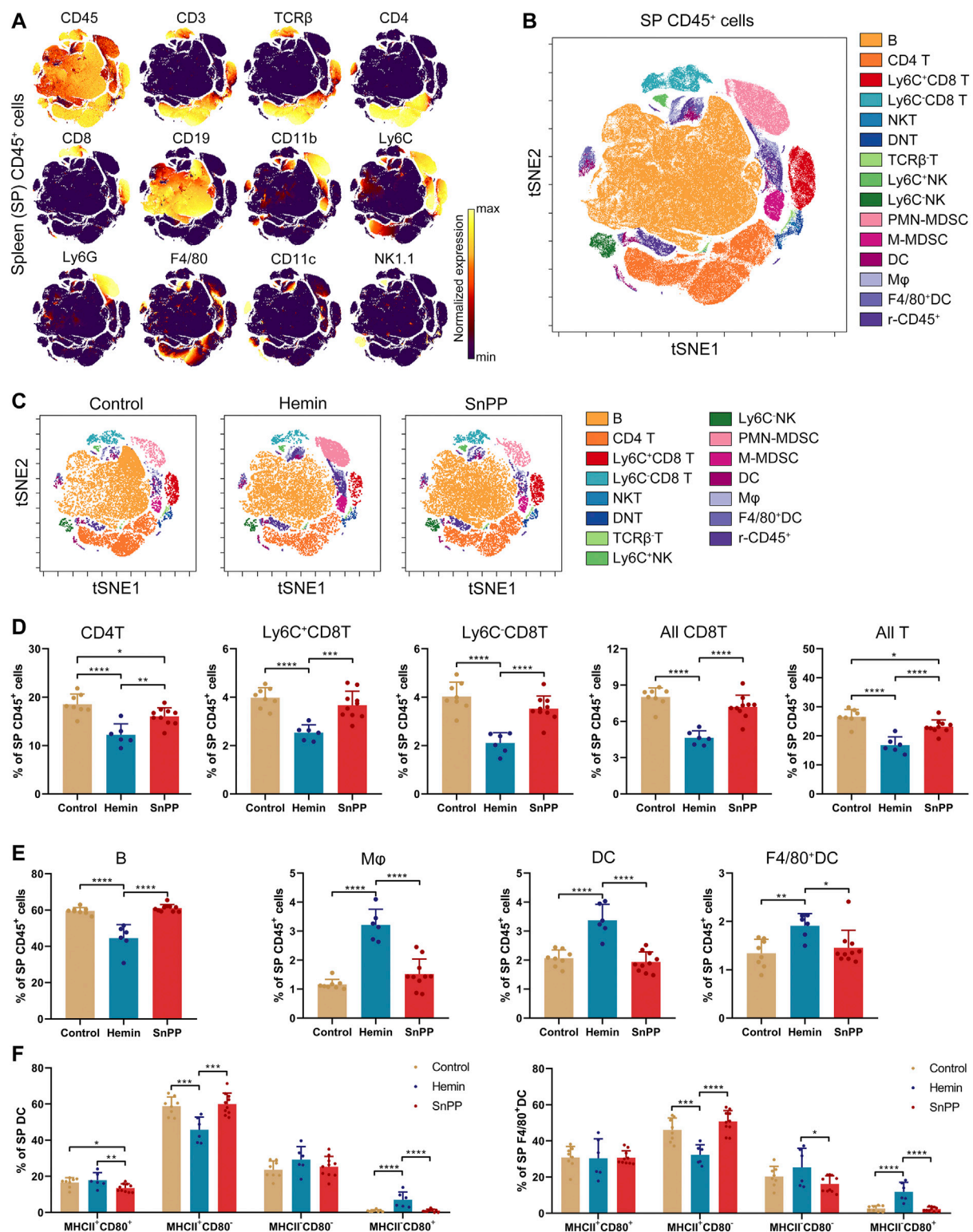


**FIGURE 2 |** Alterations of immune cell component by HO-1 inducer and inhibitor in the spleen. ApoE<sup>-/-</sup> mice fed with a western-type diet were treated with hemin ( $n = 6$ ) or SnPP ( $n = 10$ ) or vehicle (control,  $n = 8$ ) for 10 weeks. The spleen (SP) cells were collected from mice and subjected to mass cytometry analysis after staining with 26 metal isotope-labeled antibodies. **(A)** tSNE map showing the distribution of the spleen CD45<sup>+</sup> immune cells from all three groups. Cells on the tSNE map were colored according to their expression profiles of the indicated surface markers. The color bar indicates the normalized expression of each marker. **(B)** 15 cell populations were identified and colored on the tSNE map. **(C)** Representative tSNE maps of spleen CD45<sup>+</sup> immune cells from each group. **(D,E)** Bar plots showing the cell frequencies as indicated. **(F)** Bar plots showing the frequencies of indicated cell subsets in spleen DCs (left) or F4/80<sup>+</sup>DCs (right). Only significant changed cell populations are shown. Bar graphs represent mean  $\pm$  SD. Dots represent individual samples.  $n$  (control) = 8,  $n$  (hemin) = 6,  $n$  (SnPP) = 10. \* $p < 0.05$ , \*\* $p < 0.01$ , \*\*\* $p < 0.001$ , \*\*\*\* $p < 0.0001$  (One-way ANOVA). r-CD45, rest of CD45<sup>+</sup> cells.



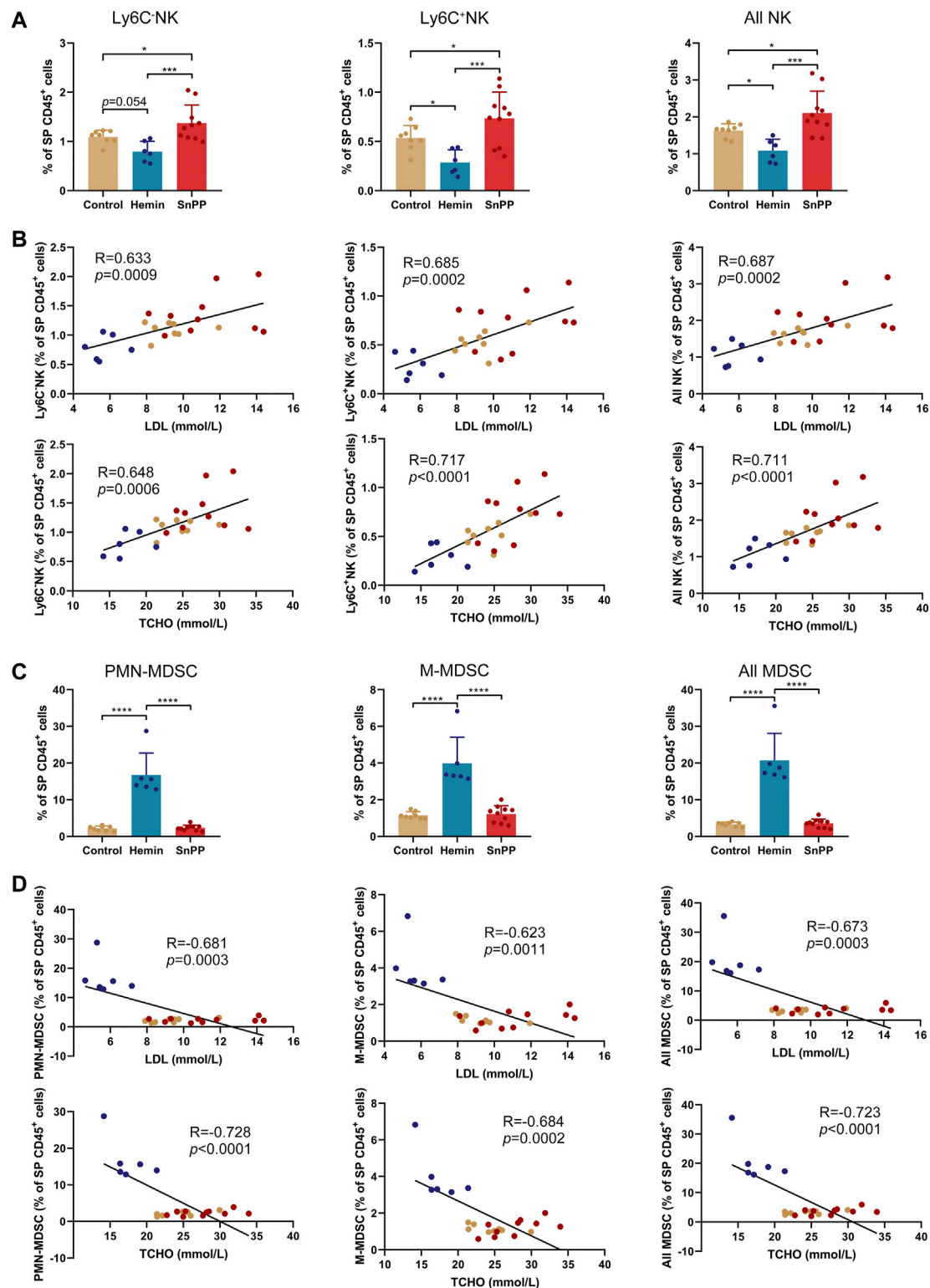


**FIGURE 3 |** HO-1 inducer and inhibitor affect the NK and MDSC in the spleen. **(A)** Bar plots showing the frequencies of Ly6C<sup>+</sup>NK, Ly6C<sup>-</sup>NK, and all NK cells in spleen (SP) CD45<sup>+</sup> cells obtained from ApoE<sup>-/-</sup> mice treated with hemin or SnPP or vehicle, respectively. **(B)** Dot plots ( $n = 24$ ) showing the Pearson correlation coefficients for relationships between the concentrations of total (TCHO) or LDL cholesterol in peripheral blood and the frequencies of indicated NK cell subsets in the spleen. **(C)** Bar plots showing the frequencies of PMN-MDSCs, M-MDSCs, and all MDSCs in spleen CD45<sup>+</sup> cells obtained from ApoE<sup>-/-</sup> mice treated with hemin or SnPP or vehicle, respectively. **(D)** Dot plots ( $n = 24$ ) showing the Pearson correlation coefficients for relationships between the concentrations of total (TCHO) or LDL cholesterol in peripheral blood and the frequencies of indicated MDSC subsets in the spleen. Bar graphs represent mean  $\pm$  SD. Dots represent individual samples.  $n$  (control) = 8,  $n$  (hemin) = 6,  $n$  (SnPP) = 10. \* $p < 0.05$ , \*\*\* $p < 0.001$ , \*\*\*\* $p < 0.0001$  (One-way ANOVA).

## HO-1 Induction Decreases the Percentage of T and Natural Killer Cells, and Increases the Proportion of Dendritic Cells and Myeloid-Derived Suppressor Cells in the Spleen

Modulation of the immune system is closely associated with the progression of atherosclerosis. Since hemin reduced both total and LDL cholesterol in atherosclerosis, we next systemically investigated the immune component of the spleen and peripheral blood using a high-throughput single-cell technique, mass cytometry. After analyzing the 26 surface markers on the spleen cells, viSNE was used to visualize high-dimensional data in two dimensions (**Figures 2A–C**). Based on the expression profiles of 12 markers (**Figure 2A**) and phenotypes used for immune cell gating (**Supplementary Figure S2A**), 15 immune cell populations, including 7 T cell subsets, two NK cell populations, two MDSC subsets, two DC subsets, macrophages, and rest of the CD45<sup>+</sup> cells, were identified on the viSNE map (**Figures 2B,C** and **Supplementary Figure S2B**). The HO-1 inducer, hemin, significantly reduced the proportions of CD4T, Ly6C<sup>+</sup>CD8T, Ly6C<sup>−</sup>CD8T, all CD8T, all T, and B cells (**Figures 2D,E**). Except for CD4T, all of these cell populations correlated positively with the levels of blood LDL and total cholesterol (**Supplementary Figures S2C,D**). SnPP, as a HO-1 inhibitor, also slightly decreased CD4T and all T cells without affecting the rest of the T cell subpopulations (**Figure 2D**). Additionally, hemin increased the percentage of DC, F4/80<sup>+</sup>DC, and macrophages in the spleen, whereas SnPP had no significant effect on these cell populations (**Figure 2E**). Among these cell populations, DC and macrophage proportions were significantly and negatively related to blood LDL and total cholesterol levels (**Supplementary Figure S2D**). MHCII and CD80 are markers for DC maturation (Ye et al., 2020). Hemin treatment decreased the proportion of MHCII<sup>+</sup>CD80<sup>−</sup> cells and increased the proportions of and MHCII<sup>−</sup>CD80<sup>+</sup> cells in DC and F4/80<sup>+</sup>DC populations, whereas SnPP had no significant effects on these cell sub-population (**Figure 2F**). The proportions of NK cells, as well as their subsets, Ly6C<sup>+</sup>NK and Ly6C<sup>−</sup>NK, were decreased by hemin treatment, but significantly increased by SnPP (**Figure 3A**). NK cells and their subsets exhibited moderate ( $|R| > 0.4$ ) to strong ( $|R| > 0.7$ ), significant, and positive correlations with LDL and total cholesterol concentrations (**Figure 3B**). Furthermore, hemin caused a 14.5 and 2.8% increase in the percentages of PMN-MDSCs and M-MDSCs, respectively, whereas SnPP had no effect (**Figure 3C**). The percentages of PMN-MDSCs and M-MDSCs, as well as all MDSCs, were significantly and negatively related to the concentrations of LDL and total cholesterol with a moderate correlation ( $|R| > 0.4$ ) (**Figure 3D**). These results clearly demonstrate the regulatory role of HO-1 induction in spleen immune cells. Hemin significantly regulate NK and MDSCs, which are closely associated with the risk factors for atherosclerosis, suggesting that NK and MDSCs might play a important role in HO-1-induced atherogenesis improvement.

## HO-1 Induction Significantly Affects T Cell Subsets in the Spleen

Inflammation is largely modulated by T cells and we next comprehensively analyzed the effect of the HO-1 pathway on spleen T clusters using 12 markers and viSNE. Based on the expression patterns of these 12 markers on T cells (**Supplementary Figure S3A**), 29 T cell sub-populations, including 13 CD4 T, eight CD8 T, 2 double-negative T (DNT), 4 NKT, and 2 TCRβ<sup>−</sup> T cell clusters, were identified in spleen T cells (**Figures 4A–C**). Their phenotypes and name were displayed in **Figure 4C**. The proportions of T1 (Ly6C<sup>−</sup>Treg), T11 (rest of effector memory CD4 T, EM r-CD4T), T19 (EM Ly6C<sup>+</sup>CD8T), T26 (TCRβ<sup>−</sup>Ly6C<sup>−</sup>NKT), and T28 (Ly6C<sup>−</sup>TCRβ<sup>−</sup> T) were significantly increased by hemin treatment, while SnPP did not affect these clusters (**Figure 4D**). Among them, T11 and T26 were significantly and negatively correlated with the levels of LDL and total cholesterol. T19 displayed a negative correlation with total cholesterol levels with a trend close to significant ( $p = 0.0516$ ) (**Figure 4E**). Hemin also dramatically decreased T2 (Ly6C<sup>+</sup>Treg), T5 (central memory Ly6C<sup>+</sup>Th1, CM Ly6C<sup>+</sup>Th1), T16 (naive Ly6C<sup>−</sup>CD8T), and T20 (naive Ly6C<sup>+</sup>CD8T), but no such effect was observed with SnPP (**Figure 5A**). Among these clusters, T2, T5, T16, and T20 were positively correlated with LDL concentrations in the blood. T16 and T20 were also positively correlated with total cholesterol levels in the blood (**Figure 5B**). Both hemin and SnPP increased the percentage of T9 (Th17 + Th22), T13 (naive r-CD4T), T22 (Ly6C<sup>−</sup>DNT), and T24 (TCRβ<sup>+</sup>Ly6C<sup>−</sup>NKT), and decreased the proportion of T3 (CM Ly6C<sup>−</sup>Th1) and T4 (EM Ly6C<sup>−</sup>Th1, **Figure 5C** and **Supplementary Figure S3B**). The percentage of T15 (EM Ly6C<sup>−</sup>CD8T) and T10 (CM r-CD4T) was decreased by SnPP and hemin, respectively (**Figure 5C** and **Supplementary Figure S3B**). Among these clusters, T4 and T10 showed positive correlations with blood triglyceride levels and LDL levels, respectively (**Figure 5D**). The rest of the T cell clusters were not affected by either hemin or SnPP. The data suggest that hemin has a significant role in regulating T cells and HO-1 induction can reshape the T cell components in the spleen, improving blood lipid metabolism and reducing atherosclerosis.

## HO-1 Induction Reduces the Proportion of T, B, and NK Cells, and Increases the Proportion of DCs and MDSCs in the Peripheral Blood

We further comprehensively analyzed the immune cell changes in the peripheral blood. Similar to spleen, 15 main immune cell populations were identified in the peripheral blood (**Figures 6A–C**, and **Supplementary Figure S4A**). Similar to the results observed in the spleen, hemin decreased the proportions of CD4 T, two CD8 T subsets, all T cells, and B cells (**Figures 6D,E**). All of them except CD4T were significantly and positively correlated with the levels of LDL and total cholesterol (**Supplementary Figures S4B,C**). Meanwhile, hemin increased the percentages of DCs and M-MDSCs (**Figure 6E**), and DC levels were correlated negatively with the levels of blood LDL and total cholesterol

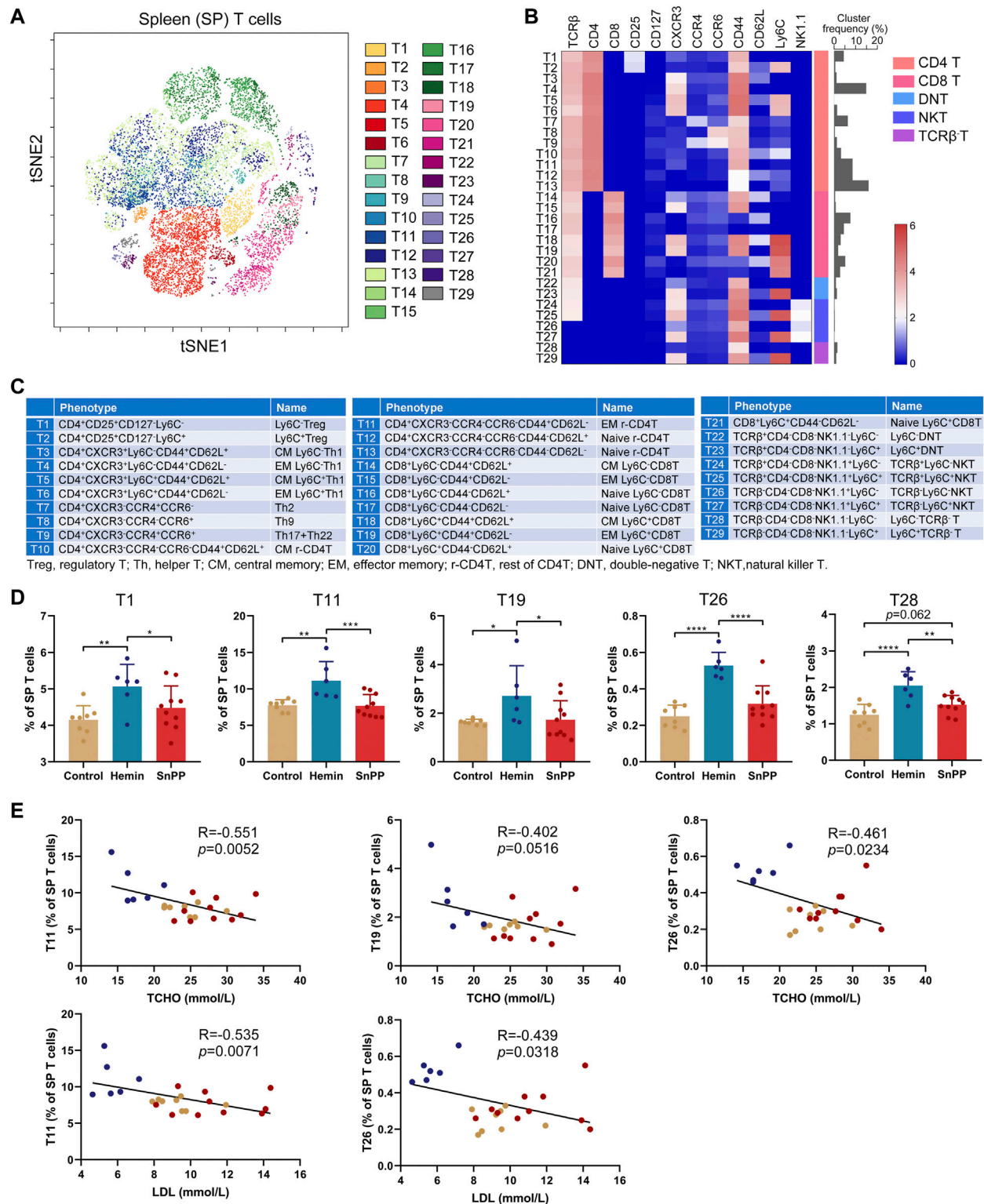
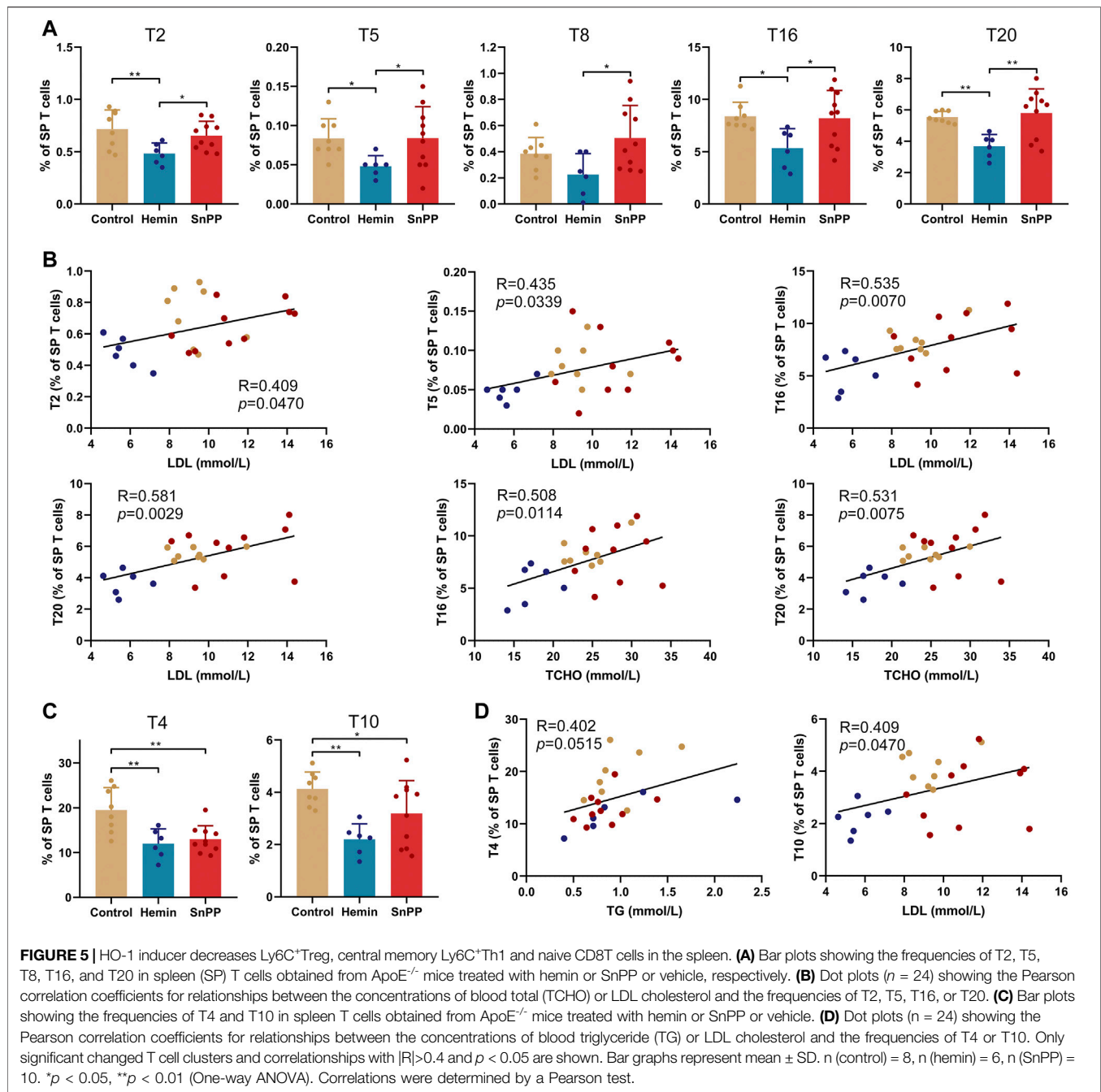


**FIGURE 4** | HO-1 inducer increases the proportion of Ly6C<sup>-</sup>Treg, effector memory T and NKT cells in the spleen. After measuring the expression of 26 surface markers on the spleen (SP) cells using mass cytometry, all the T cells (CD3<sup>+</sup>) were analyzed using viSNE. **(A)** viSNE map showing the distribution of the splenic T cells from all three groups. 29 T cell clusters were identified and colored on the viSNE map based on the expression profiles of 12 T cell markers. **(B)** A heatmap showing the normalized expression of 12 indicated markers in 29 T cell clusters. **(C)** Phenotypes and names of 29 T cell clusters. **(D)** Bar plots showing the frequencies of T1, T11, T19, T26, and T28 in spleen. **(E)** Dot plots ( $n = 24$ ) showing the Pearson correlation coefficients for relationships between the concentrations of blood total (TCHO) or LDL cholesterol and the frequencies of T11, T19, or T26. Only significant changed T cell clusters and correlations with  $|R| > 0.4$  and  $p < 0.05$  are shown. Bar graphs represent mean  $\pm$  SD.  $n$  (control) = 8,  $n$  (hemin) = 6,  $n$  (SnPP) = 10. \* $p < 0.05$ , \*\* $p < 0.01$ , \*\*\* $p < 0.001$ , \*\*\*\* $p < 0.0001$  (One-way ANOVA). Correlations were determined by a Pearson test.



(Supplementary Figure S4C). Hemin treatment resulted in a significant decrease in the proportion of MHCII<sup>+</sup>CD80<sup>-</sup> cells, but an increase in MHCII<sup>+</sup>CD80<sup>+</sup> cells in both DC and F4/80<sup>+</sup>DCs (Figure 6F). In F4/80<sup>+</sup>DCs, hemin increased the proportion of both MHCII<sup>+</sup>CD80<sup>+</sup> and MHCII<sup>+</sup>CD80<sup>-</sup> cells. Except for the percentage of MHCII<sup>+</sup>CD80<sup>-</sup> cells in DCs, no significant alternations in the other subsets were observed with SnPP treatment (Figure 6).

Moreover, hemin significantly decreased Ly6C<sup>+</sup>NK, Ly6C<sup>+</sup>NK, and all NK cells, whereas SnPP increased them

with either significant or a trend close to significant except for Ly6C<sup>+</sup>NK cells (Figure 7A). The percentage of NK cells, as well as their two subsets, displayed significant and positive correlations with blood LDL and total cholesterol levels (Figure 7B). Hemin also increased the proportions of PMN-MDSCs and all MDSCs, which were negatively correlated with blood LDL and total cholesterol concentrations (Figures 7C,D). All of these data suggest that HO-1 induction can significantly reshape peripheral immune cells, especially NK and MDSCs, which are closely associated with atherosclerosis risk factors.



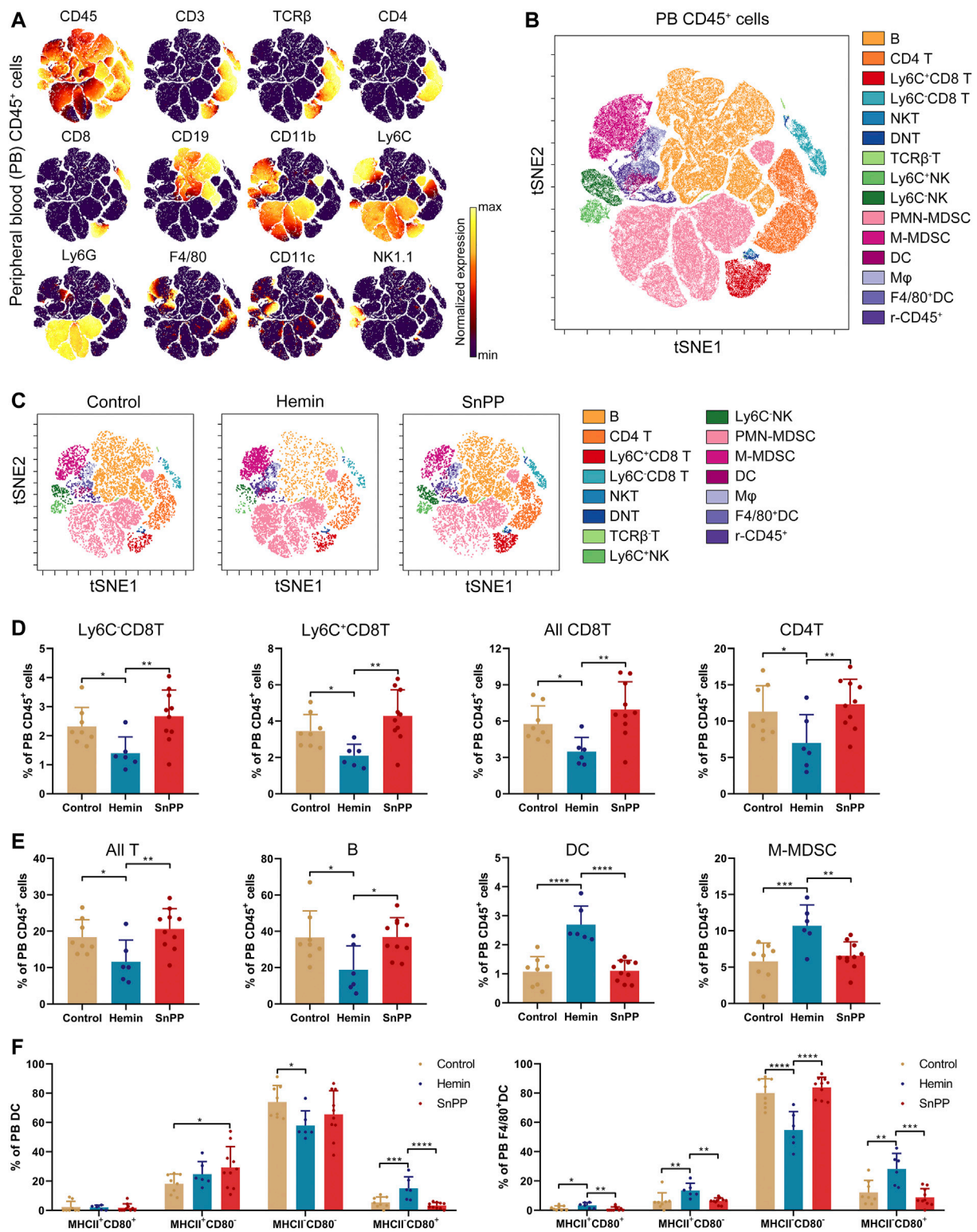


**FIGURE 6 |** Hemin and SnPP differently alter the immune cell populations in peripheral blood. ApoE<sup>-/-</sup> mice fed with a western-type diet were treated with hemin ( $n = 6$ ) or SnPP ( $n = 10$ ) or vehicle (control,  $n = 8$ ) for 10 weeks. The peripheral blood (PB) cells were collected and subjected to mass cytometry analysis after staining with 26 metal isotope-labeled antibodies. **(A)** viSNE map showing the distribution of the PB CD45<sup>+</sup> immune cells from all three groups. Cells on the viSNE map were colored according to the expression profiles of indicated surface markers. The color bar indicates the normalized expression of each marker. **(B)** 15 cell populations were identified and colored on the viSNE map. **(C)** Representative viSNE maps of PB CD45<sup>+</sup> immune cells from each group. **(D,E)** Bar plots showing the frequencies of the indicated cell populations and sub-clusters. **(F)** Bar plots showing the frequencies of indicated subsets in PB DCs and F4/80<sup>+</sup>DCs. Only significant changed cell populations are shown. Bar graphs represent mean  $\pm$  SD. Dots represent individual samples.  $n$  (control) = 8,  $n$  (hemin) = 6,  $n$  (SnPP) = 10. \* $p < 0.05$ , \*\* $p < 0.01$ , \*\*\* $p < 0.001$ , \*\*\*\* $p < 0.0001$  (One-way ANOVA).

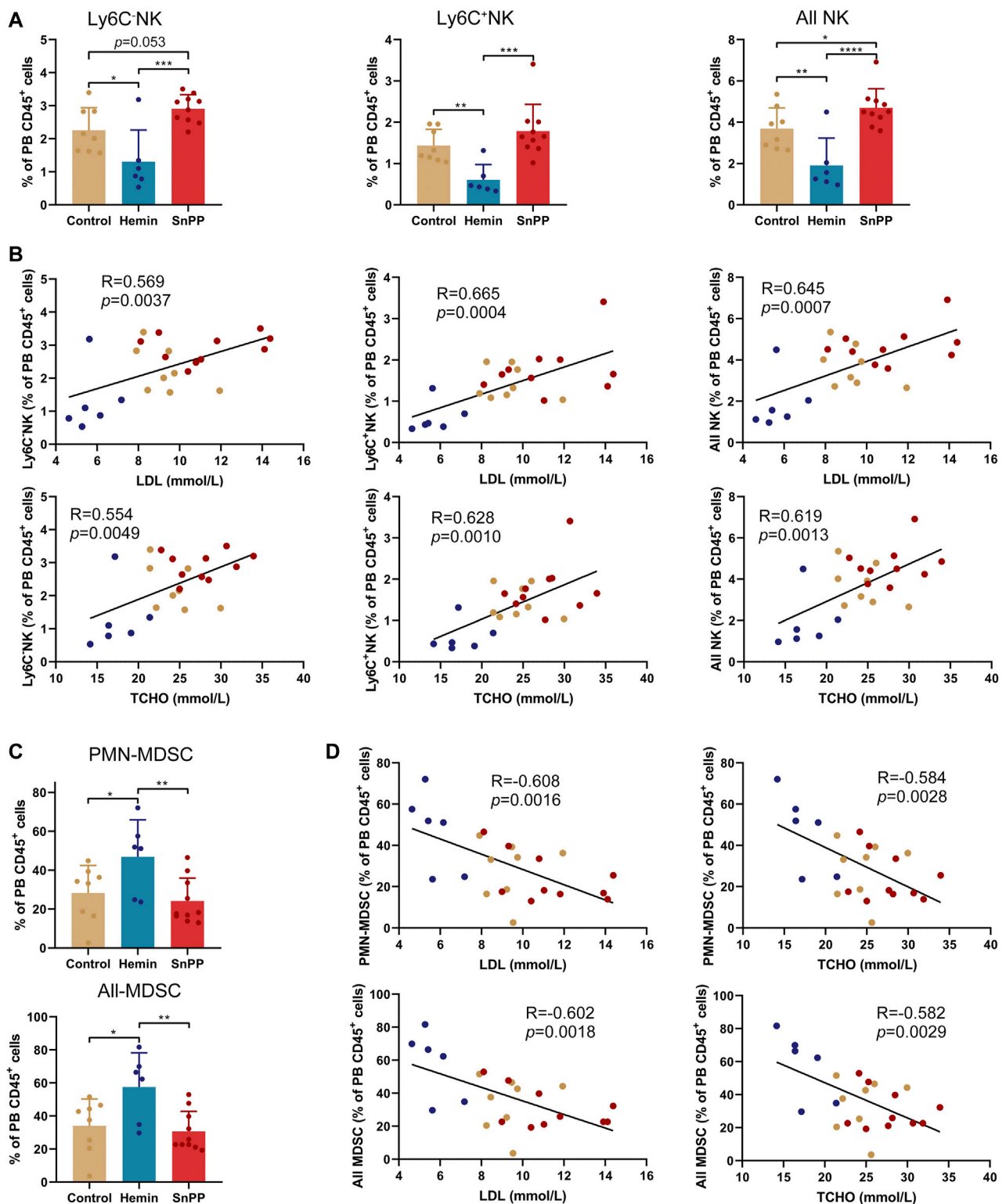
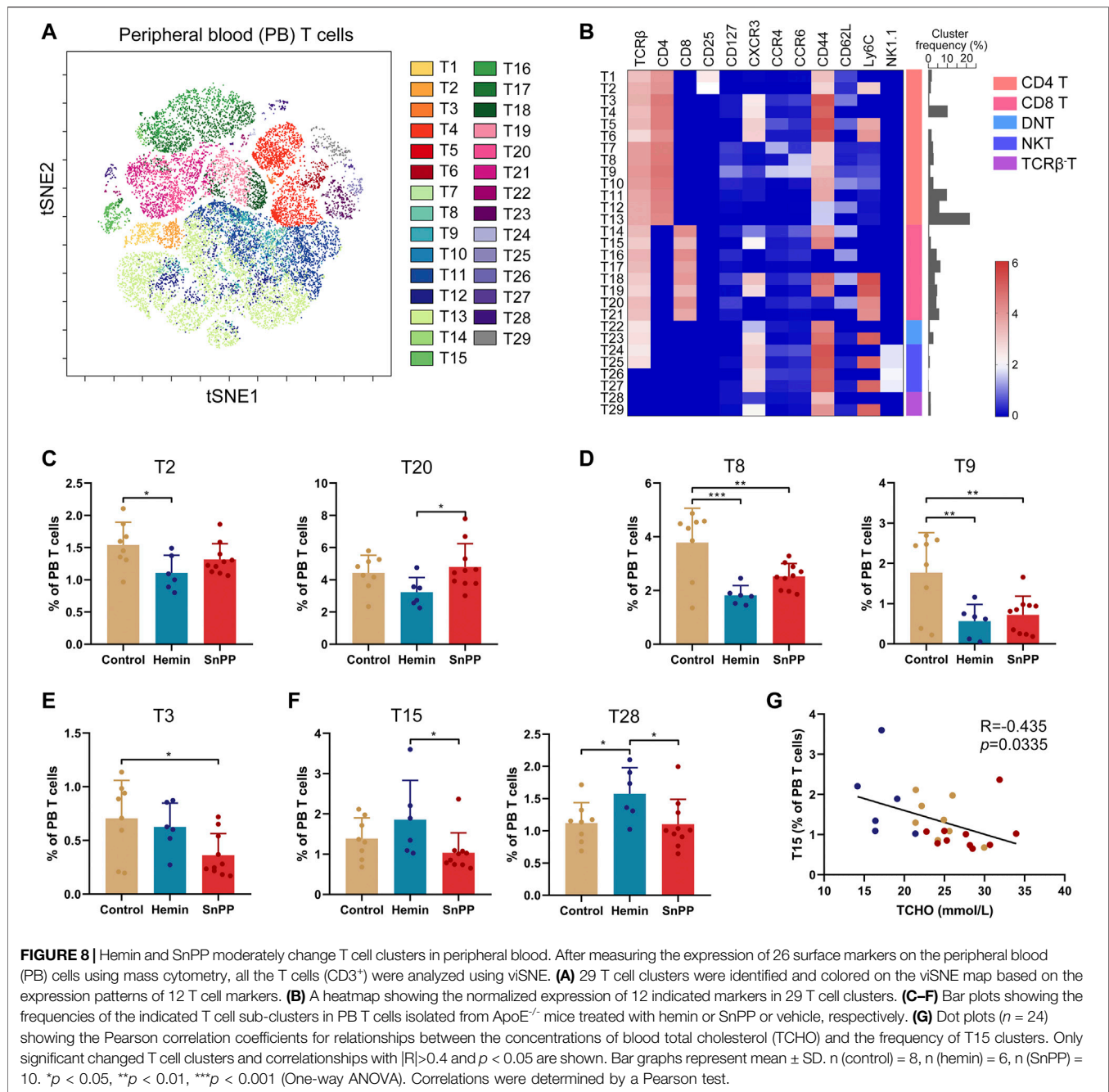


**FIGURE 7** | HO-1 inducer and inhibitor significantly affect the peripheral NK and MDSCs. **(A)** Bar plots showing the frequencies of Ly6C<sup>-</sup>NK, Ly6C<sup>+</sup>NK, and all NK cells in peripheral blood (PB) CD45<sup>+</sup> cells with various treatments as indicated. **(B)** Dot plots ( $n = 24$ ) showing the Pearson correlation coefficients for relationships between the concentrations of total (TCHO) or LDL cholesterol in peripheral blood and the frequencies of indicated NK cell subsets in PB CD45<sup>+</sup> cells. **(C)** Bar plots showing the frequencies of PMN-MDSCs and all MDSCs in PB CD45<sup>+</sup> cells obtained from ApoE<sup>-/-</sup> mice treated with hemin or SnPP or vehicle, respectively. **(D)** Dot plots ( $n = 24$ ) showing the Pearson correlation coefficients for relationships between the concentrations of blood total (TCHO) or LDL cholesterol and the frequencies of indicated MDSC subsets in PB CD45<sup>+</sup> cells. Bar graphs represent mean  $\pm$  SD. Dots represent individual samples.  $n$  (control) = 8,  $n$  (hemin) = 6,  $n$  (SnPP) = 10. \* $p < 0.05$ , \*\* $p < 0.01$ , \*\*\* $p < 0.001$ , \*\*\*\* $p < 0.0001$  (One-way ANOVA).



## HO-1 Induction Moderately Affects T Cell Subsets in Peripheral Blood

The peripheral blood T cells were then further analyzed by viSNE (Figure 8A and Supplementary Figure S5A) and 29 T cell clusters were identified (Figure 8B) according to the phenotypes of T cell clusters (Figure 4C). However, only four clusters, including T2 (Ly6C<sup>+</sup>Treg), T8 (Th9), T9 (Th17 + Th22), and T28 (Ly6C<sup>+</sup>TCR $\beta$ <sup>+</sup>T), were dramatically affected by hemin. Specifically, hemin treatment significantly decreased T2, T8, and T9, but increased T28 (Figures 8C–F). On the other

hand, T3, T8, and T9 were significantly decreased by SnPP (Figures 8D,E). T3 (CM Ly6C<sup>+</sup>Th1) was correlated negatively with blood LDL and total cholesterol levels (Supplementary Figure S5B), while T15 (EM Ly6C<sup>+</sup>CD8T) was correlated negatively with blood total cholesterol (Figure 8G). The rest of the T cell clusters were not significantly affected by either hemin or SnPP. Taken together, hemin or SnPP had only moderate effects on peripheral blood T cells, suggesting that peripheral blood T cells may play a minor role in HO-1-mediated atherogenesis.

## DISCUSSION

Due to its antioxidant and anti-inflammatory properties, HO-1 provides protection against atherosclerosis and other cardiovascular diseases (Campbell et al., 2021; Durante, 2011). As an HO-1 inducer, hemin attenuates atherosclerotic lesion formation in LDLr deficient mice by inhibiting lipid peroxidation and affecting the nitric oxide pathway (Ishikawa et al., 2001b). A deficiency of HO-1 accelerates and exacerbates atherosclerotic lesion formation (Yet et al., 2003). Immunity, including monocytes/macrophages, dendritic cells, T cells, NK cells, mast cells, platelets, and a number of inflammatory mediators and pathways, are involved in the initiation, progression, and rupture of atherosclerotic plaques. Using HO-1 inducer and inhibitor, we confirmed the protective role of HO-1 in murine atherosclerosis and demonstrated its profound effect on systemic immunity using mass cytometry-based single-cell analysis. Through in-depth analyses, we discovered that the HO-1 inducer hemin effectively ameliorates atherosclerosis by lowering circulating cholesterol levels and reshaping immune cells in the spleen and peripheral blood. Our data further support HO-1 as a promising therapeutic target in atherosclerosis treatment.

Oxidized LDL is a major determinant in the pathogenesis of atherosclerosis since it is taken up by immune cells attaching to the injured (or activated) artery wall, leading to the transformation into foam cells and initiation of atherosclerotic plaques (Libby et al., 2002). A previous study have shown that hemin decreased the plasma lipid hydroperoxide levels and SnPP increased them in LDLr<sup>-/-</sup> mice (Ishikawa et al., 2001b). Byproducts of HO-1, such as biliverdin, bilirubin, and CO, function as antioxidants by scavenging oxygen free radicals and organic peroxy radicals. Among them, bilirubin protects cells from lipid-induced damage and prevents LDL peroxidation (Stocker et al., 1987; Boon et al., 2012), thereby slowing down the process of atherosclerosis. After hemin administration, they are catalyzed by HO-1 to generate biliverdin, carbon monoxide (CO), and ferrous iron (Verheij et al., 2021). Biliverdin is subsequently transformed into bilirubin. Since biliverdin and bilirubin are antioxidants, the anti-atherogenic properties of hemin is likely mediated by these byproducts.

The innate immune response as well as the adaptive immune response are critical for the pathogenesis of atherosclerosis. Macrophages play a major role in eliminating oxidized LDL, while excessive LDL uptake induced apoptosis (Elliott et al., 2017). An increase in apoptotic macrophages in the plaques results in secondary necrosis and thereafter the formation of a necrotic core (Martinet et al., 2011; Gonzalez and Trigatti, 2017). A reduction in circulating macrophages reduces the clearance of oxidized LDL, which can exacerbate atherosclerotic lesion formation. In our study, we found that hemin treatment resulted in an increase of macrophages in the spleen by more than three times, suggesting an increased capacity for removing LDL. Indeed, our data showed that increased spleen macrophages were associated with lower levels of total and LDL cholesterol in the blood.

As a link between the innate and adaptive immune systems, DCs are crucial to the artery-specific immune response. These cells either promote or inhibit atherogenesis through regulating lipid uptake, antigen presentation, and cytokine secretion (Herrero-Fernandez

et al., 2019; Jongstra-Bilen et al., 2006; Liu et al., 2008). DCs can protect against atherosclerosis by activating Treg cells, which suppress the inflammatory response (Choi et al., 2011). Here, we observed a significant increase in DCs in both the spleen and peripheral blood after hemin treatment. Moreover, hemin increased the proportion of T1 cells, which are Ly6C<sup>+</sup> Treg cells, in the spleen. Since DCs can induce Treg cells, hemin-induced DCs may be responsible for the increase in Treg cells. An inflammatory environment promotes the maturation of dendritic cells along with the upregulation of MHCII and co-stimulatory molecules (Durante, 2011). Mature DCs present antigens to T cells through surface MHCII and activate them through co-stimulatory molecules. Although the proportions of DCs and F4/80<sup>+</sup>DCs were increased by hemin in the spleen, the MHCII<sup>+</sup> cells in these two DC subsets were reduced, suggesting that hemin attenuates their capacity to present antigens and therefore reduces the T cell-mediated inflammation. In the spleen, the proportion of T cells, including CD4 T and CD8 T cells, was significantly decreased by hemin treatment, possibly due to the decreased ability of DCs to present antigens. DCs found in peripheral blood are immature because they lack MHCII and co-stimulatory molecule CD80, making them incapable of presenting antigens. Furthermore, the proportion of DCs in both the spleen and peripheral blood was negatively correlated with the levels of blood total and LDL cholesterol, indicating that hemin-induced DCs may contribute to the decrease in circulating cholesterol.

NK cells, derived from common bone marrow progenitor cells, are characterized by their ability to eliminate aberrant cells without any priming or prior activation. These cells exhibit both innate and adaptive immune features and present a critical component of the innate immune system (van Erp et al., 2020; Yang et al., 2021). As revealed by single-cell RNA sequencing- and mass cytometry-based single-cell analysis, NK cells have been detected in human atherosclerotic plaques and mouse atherosclerotic aorta (Fernandez et al., 2019; Winkels et al., 2018). The accumulation of NK cells in atherosclerotic lesions leads to the expansion of necrotic cores and accelerates atherosclerosis through the release of perforin, granzyme B, and pro-inflammation factor IFN- $\gamma$  (Selathurai et al., 2014). It is well documented that the HO-1 pathway regulates inflammation in atherosclerosis *via* either direct or indirect effects on a variety of immune cells, including macrophages, DCs, Th1, Th17, Treg, and monocytes (Campbell et al., 2021; Durante, 2011). However, the direct connection between NK cells and the HO-1 pathway in atherosclerosis has not yet been reported. After hemin treatment, we observed a significant decrease in NK cells in both the spleen and peripheral blood as well as a reduction in atherosclerosis. In previous studies, depletion of NK cells by anti-Asialo-GM1 antibody decreased atherosclerosis in ApoE<sup>-/-</sup> mice (Selathurai et al., 2014) and transgenic elimination of functional NK cells also ameliorated atherosclerosis in LDLr<sup>-/-</sup> mice (Whitman et al., 2004). NK cells and circulating cholesterol have a clear positive correlation, so a decrease in NK cells caused by hemin may directly contribute to the relief of atherosclerosis symptoms. Meanwhile, SnPP, as a HO-1 inhibitor, persistently and exclusively increased the NK cells in both the spleen and peripheral blood, and exacerbated



atherosclerotic lesion in ApoE<sup>-/-</sup> mice, further highlighting the contribution of NK cells to atherosclerosis. A previous study has shown that the elevated NK cells *via* adoptive transfer doubled atherosclerotic lesion size in ApoE<sup>-/-</sup>Rag2<sup>-/-</sup>IL2rg<sup>-/-</sup> mice (Whitman et al., 2004), indicating that SnPP can exacerbate atherosclerosis through NK cells. This previous evidence, together with ours, highlights the critical role of NK cells in the pathogenesis of atherosclerosis. Importantly, our findings propose that the protective role of HO-1 in atherosclerosis may be closely associated with the regulation of NK cells as its inducer (hemin) and inhibitor (SnPP) oppositely affect NK cells and atherosclerosis.

MDSCs represent a heterogeneous population of immature myeloid cells and negatively regulate the immune response through producing immunosuppressive factors, including IL-10, transforming growth factor- $\beta$ , inducible nitric oxide synthase, and reactive oxygen species (De Veirman et al., 2014). As a result of MDSC activation, T cell activation and proliferation, antigen recognition, and NK cell cytotoxicity are suppressed, and regulatory T cells are induced, eventually leading to immunosuppression (Gabrilovich and Nagaraj, 2009). In mice, expression of both Gr-1 (Ly6C/Ly6G) and CD11b are widely used to define MDSCs. Two subsets of MDSCs, PMN-MDSC (CD11b<sup>+</sup>Ly6G<sup>+</sup>Ly6C<sup>lo</sup>) and M-MDSC (CD11b<sup>+</sup>Ly6G<sup>-</sup>Ly6C<sup>hi</sup>), are classified according to their different phenotypic and morphological features (Bronte et al., 2016; Wang et al., 2016). MDSCs have been implicated in chronic inflammation-related diseases, including obesity and atherosclerosis (Foks et al., 2016; Xia et al., 2011). Because of their potent immunosuppressive function, adoptive transfer of MDSCs has been shown to significantly alleviate atherosclerosis through suppression of T cell-mediated pro-inflammatory immune responses (Foks et al., 2016). A six-fold increase in spleen MDSCs and an apparent increase of peripheral blood MDSCs were observed in mice treated with hemin, implying an enhanced immunosuppression by hemin. Elevated MDSCs by hemin in both spleen and peripheral blood was accompanied by lower cholesterol, supporting the role of MDSCs in atherosclerosis. Several studies have reported that MDSCs, induced by endotoxin or histone deacetylase inhibitor or baicalein, inhibit immune responses *via* HO-1 (De Wilde et al., 2009; Rosborough et al., 2012; Li et al., 2019). Here, we provided *in vivo* evidence for the important and effective role of HO-1 in MDSC induction and anti-inflammatory effects in atherosclerosis. Despite many changes in immune cell composition in mice treated with hemin, the precise mechanisms driving these changes remain unknown. Therefore, future investigations will need to provide mechanistic insights into how systemic immunity is remodeled by the HO-1 pathway to enable the development of novel therapeutic strategies for atherosclerosis.

In summary, we confirmed the critical regulatory role of the HO-1 pathway in reshaping systemic immunity in the context of

atherosclerosis. Importantly, using mass cytometry-based single cell analysis, we thoroughly dissected the profiles of immune cell lineages and respective cell subsets modulated by hemin- and SnPP in both spleen and peripheral blood. This study increases our understanding of the HO-1 pathway, and provides a potential new strategy to treat atherosclerosis by targeting HO-1.

## DATA AVAILABILITY STATEMENT

The original contributions presented in the study are included in the article/**Supplementary Material**, further inquiries can be directed to the corresponding authors.

## ETHICS STATEMENT

The animal study was reviewed and approved by Institutional Committee for the Use and Care of Laboratory Animals of Guangzhou Medical University.

## AUTHOR CONTRIBUTIONS

JL designed and supervised the experiments. LY, YH, GW, and PW performed the experiments and analyzed the data. JW performed the mass cytometry and analyzed the data. JL, JW and GW wrote the manuscript. QX provided critical suggestions and revised the manuscript. All authors read and approved the final manuscript.

## FUNDING

This work was supported by the National Natural Science Foundation of China (81900365); The National Funds for Developing Local Colleges and Universities (B16056001); Natural Science Foundation research team of Guangdong Province (2018B030312001); and Natural Science Foundation of Guangdong Province (2018A0303130024 and 2017A030313662).

## SUPPLEMENTARY MATERIAL

The Supplementary Material for this article can be found online at: <https://www.frontiersin.org/articles/10.3389/fphar.2022.809469/full#supplementary-material>

## REFERENCES

Agudiez, M., Martinez, P. J., Martin-Lorenzo, M., Heredero, A., Santiago-Hernandez, A., Molero, D., et al. (2020). Analysis of Urinary Exosomal Metabolites Identifies Cardiovascular Risk Signatures with Added Value

to Urine Analysis. *BMC Biol.* 18 (1), 192. doi:10.1186/s12915-020-00924-y

Bandura, D. R., Baranov, V. I., Ornatsky, O. I., Antonov, A., Kinach, R., Lou, X., et al. (2009). Mass Cytometry: Technique for Real Time Single Cell Multitarget Immunoassay Based on Inductively Coupled Plasma Time-Of-Flight Mass Spectrometry. *Anal. Chem.* 81 (16), 6813–6822. doi:10.1021/ac901049w

- Bellner, L., Lebovics, N. B., Rubinstein, R., Buchen, Y. D., Sinatra, E., Sinatra, G., et al. (2020). Heme Oxygenase-1 Upregulation: A Novel Approach in the Treatment of Cardiovascular Disease. *Antioxid. Redox Signal.* 32 (14), 1045–1060. doi:10.1089/ars.2019.7970
- Bendall, S. C., Simonds, E. F., Amir, E. L.-A. D., Finck, R., Qiu, P., Krutzik, P. O., et al. (2011). Single-cell Mass Cytometry of Differential Immune and Drug Responses across a Human Hematopoietic Continuum. *Science* 332 (6030), 687–696. doi:10.1126/science.1198704
- Bendall, S. C., Davis, K. L., Amir, E. L.-A. D., Tadmor, M. D., Simonds, E. F., Chen, T. J., et al. (2014). Single-cell Trajectory Detection Uncovers Progression and Regulatory Coordination in Human B Cell Development. *Cell* 157 (3), 714–725. doi:10.1016/j.cell.2014.04.005
- Bodenmiller, B., Zunder, E. R., Finck, R., Chen, T. J., Savig, E. S., Bruggner, R. V., et al. (2012). Multiplexed Mass Cytometry Profiling of Cellular States Perturbed by Small-Molecule Regulators. *Nat. Biotechnol.* 30 (9), 858–867. doi:10.1038/nbt.2317
- Boon, A. C., Hawkins, C. L., Bisht, K., Coombes, J. S., Bakrania, B., Wagner, K. H., et al. (2012). Reduced Circulating Oxidized LDL Is Associated with Hypocholesterolemia and Enhanced Thiol Status in Gilbert Syndrome. *Free Radic. Biol. Med.* 52 (10), 2120–2127. doi:10.1016/j.freeradbiomed.2012.03.002
- Bronte, V., Brandau, S., Chen, S. H., Colombo, M. P., Frey, A. B., Greten, T. F., et al. (2016). Recommendations for Myeloid-Derived Suppressor Cell Nomenclature and Characterization Standards. *Nat. Commun.* 7, 12150. doi:10.1038/ncomms12150
- Campbell, N. K., Fitzgerald, H. K., and Dunne, A. (2021). Regulation of Inflammation by the Antioxidant Haem Oxygenase 1. *Nat. Rev. Immunol.* 21 (7), 411–425. doi:10.1038/s41577-020-00491-x
- Choi, J. H., Cheong, C., Dandamudi, D. B., Park, C. G., Rodriguez, A., Mehendru, S., et al. (2011). Flt3 Signaling-dependent Dendritic Cells Protect against Atherosclerosis. *Immunity* 35 (5), 819–831. doi:10.1016/j.immuni.2011.09.014
- Cole, J. E., Park, I., Ahern, D. J., Kassiteridi, C., Danso Abeam, D., Goddard, M. E., et al. (2018). Immune Cell Census in Murine Atherosclerosis: Cytometry by Time of Flight Illuminates Vascular Myeloid Cell Diversity. *Cardiovasc. Res.* 114 (10), 1360–1371. doi:10.1093/cvr/cvy109
- De Veirman, K., Van Valckenborgh, E., Lahmar, Q., Geeraerts, X., De Bruyne, E., Menu, E., et al. (2014). Myeloid-derived Suppressor Cells as Therapeutic Target in Hematological Malignancies. *Front. Oncol.* 4, 349. doi:10.3389/fonc.2014.00349
- De Wilde, V., Van Rompaey, N., Hill, M., Lebrun, J. F., Lemaître, P., Lhommé, F., et al. (2009). Endotoxin-induced Myeloid-Derived Suppressor Cells Inhibit Alloimmune Responses via Heme Oxygenase-1. *Am. J. Transpl.* 9 (9), 2034–2047. doi:10.1111/j.1600-6143.2009.02757.x
- Dinh, Q. N., Chrissobolis, S., Diep, H., Chan, C. T., Ferens, D., Drummond, G. R., et al. (2017). Advanced Atherosclerosis Is Associated with Inflammation, Vascular Dysfunction and Oxidative Stress, but Not Hypertension. *Pharmacol. Res.* 116, 70–76. doi:10.1016/j.phrs.2016.12.032
- Durante, W. (2011). Protective Role of Heme Oxygenase-1 against Inflammation in Atherosclerosis. *Front. Biosci. (Landmark Ed.)* 16, 2372–2388. doi:10.2741/3860
- Elliott, M. R., Koster, K. M., and Murphy, P. S. (2017). Efferocytosis Signaling in the Regulation of Macrophage Inflammatory Responses. *J. Immunol.* 198 (4), 1387–1394. doi:10.4049/jimmunol.1601520
- Fernandez, D. M., Rahman, A. H., Fernandez, N. F., Chudnovskiy, A., Amir, E. D., Amadori, L., et al. (2019). Single-cell Immune Landscape of Human Atherosclerotic Plaques. *Nat. Med.* 25 (10), 1576–1588. doi:10.1038/s41591-019-0590-4
- Fiorelli, S., Porro, B., Cosentino, N., Di Minno, A., Manega, C. M., Fabbicchi, F., et al. (2019). Activation of Nrf2/HO-1 Pathway and Human Atherosclerotic Plaque Vulnerability: an *In Vitro* and *In Vivo* Study. *Cells* 8 (4), 356. doi:10.3390/cells8040356
- Foks, A. C., Van Puijvelde, G. H., Wolbert, J., Kröner, M. J., Frodermann, V., Van Der Heijden, T., et al. (2016). CD11b+Gr-1+ Myeloid-Derived Suppressor Cells Reduce Atherosclerotic Lesion Development in LDLr Deficient Mice. *Cardiovasc. Res.* 111 (3), 252–261. doi:10.1093/cvr/cvw114
- Gabrilovich, D. I., and Nagaraj, S. (2009). Myeloid-derived Suppressor Cells as Regulators of the Immune System. *Nat. Rev. Immunol.* 9 (3), 162–174. doi:10.1038/nri2506
- Gonzalez, L., and Trigatti, B. L. (2017). Macrophage Apoptosis and Necrotic Core Development in Atherosclerosis: A Rapidly Advancing Field with Clinical Relevance to Imaging and Therapy. *Can. J. Cardiol.* 33 (3), 303–312. doi:10.1016/j.cjca.2016.12.010
- Herrero-Fernandez, B., Gomez-Bris, R., Somovilla-Crespo, B., and Gonzalez-Granado, J. M. (2019). Immunobiology of Atherosclerosis: A Complex Net of Interactions. *Int. J. Mol. Sci.* 20 (21), 5293. doi:10.3390/ijms20215293
- Ishikawa, K., Navab, M., Leitinger, N., Fogelman, A. M., and Lusis, A. J. (1997). Induction of Heme Oxygenase-1 Inhibits the Monocyte Transmigration Induced by Mildly Oxidized LDL. *J. Clin. Invest.* 100 (5), 1209–1216. doi:10.1172/JCI119634
- Ishikawa, K., Sugawara, D., Goto, J., Watanabe, Y., Kawamura, K., Shiomi, M., et al. (2001a). Heme Oxygenase-1 Inhibits Atherogenesis in Watanabe Heritable Hyperlipidemic Rabbits. *Circulation* 104 (15), 1831–1836. doi:10.1161/hc3901.095897
- Ishikawa, K., Sugawara, D., Wang Xp, X., Suzuki, K., Itabe, H., Maruyama, Y., et al. (2001b). Heme Oxygenase-1 Inhibits Atherosclerotic Lesion Formation in Ldl-Receptor Knockout Mice. *Circ. Res.* 88 (5), 506–512. doi:10.1161/01.res.88.5.506
- Jongstra-Bilen, J., Haidari, M., Zhu, S. N., Chen, M., Guha, D., and Cybulsky, M. I. (2006). Low-grade Chronic Inflammation in Regions of the normal Mouse Arterial Intima Predisposed to Atherosclerosis. *J. Exp. Med.* 203 (9), 2073–2083. doi:10.1084/jem.20060245
- Juan, S. H., Lee, T. S., Tseng, K. W., Liou, J. Y., Shyue, S. K., Wu, K. K., et al. (2001). Adenovirus-mediated Heme Oxygenase-1 Gene Transfer Inhibits the Development of Atherosclerosis in Apolipoprotein E-Deficient Mice. *Circulation* 104 (13), 1519–1525. doi:10.1161/hc3801.095663
- Le, N. A. (2004). Inflammation, Oxidative Stress, and Atherosclerosis. *Curr. Opin. Lipidol.* 15 (2), 227–229. doi:10.1097/00041433-200404000-00018
- Li, D., Shi, G., Wang, J., Zhang, D., Pan, Y., Dou, H., et al. (2019). Baicalein Ameliorates Pristane-Induced Lupus Nephritis via Activating Nrf2/HO-1 in Myeloid-Derived Suppressor Cells. *Arthritis Res. Ther.* 21 (1), 105. doi:10.1186/s13075-019-1876-0
- Libby, P., Ridker, P. M., and Maseri, A. (2002). Inflammation and Atherosclerosis. *Circulation* 105 (9), 1135–1143. doi:10.1161/hc0902.104353
- Liu, P., Yu, Y. R., Spencer, J. A., Johnson, A. E., Vallanat, C. T., Fong, A. M., et al. (2008). CX3CR1 Deficiency Impairs Dendritic Cell Accumulation in Arterial Intima and Reduces Atherosclerotic burden. *Arterioscler Thromb. Vasc. Biol.* 28 (2), 243–250. doi:10.1161/ATVBAHA.107.158675
- Lo Sasso, G., Schlage, W. K., Boué, S., Veljkovic, E., Peitsch, M. C., and Hoeng, J. (2016). The Apoe(-/-) Mouse Model: a Suitable Model to Study Cardiovascular and Respiratory Diseases in the Context of Cigarette Smoke Exposure and Harm Reduction. *J. Transl. Med.* 14 (1), 146. doi:10.1186/s12967-016-0901-1
- Ma, J. L., Yang, P. Y., Rui, Y. C., Lu, L., Kang, H., and Zhang, J. (2007). Hemin Modulates Cytokine Expressions in Macrophage-Derived Foam Cells via Heme Oxygenase-1 Induction. *J. Pharmacol. Sci.* 103 (3), 261–266. doi:10.1254/jphs.fp0060270
- Martinet, W., Schrijvers, D. M., and De Meyer, G. R. (2011). Necrotic Cell Death in Atherosclerosis. *Basic Res. Cardiol.* 106 (5), 749–760. doi:10.1007/s00395-011-0192-x
- McGuire, H. M., Rizzetto, S., Withers, B. P., Clancy, L. E., Avdic, S., Stern, L., et al. (2020). Mass Cytometry Reveals Immune Signatures Associated with Cytomegalovirus (CMV) Control in Recipients of Allogeneic Haemopoietic Stem Cell Transplant and CMV-specific T Cells. *Clin. Transl. Immunol.* 9 (7), e1149. doi:10.1002/cti2.1149
- Mukhopadhyay, R. (2013). Mouse Models of Atherosclerosis: Explaining Critical Roles of Lipid Metabolism and Inflammation. *J. Appl. Genet.* 54 (2), 185–192. doi:10.1007/s13353-013-0134-4
- Rosborough, B. R., Castellana, A., Natarajan, S., Thomson, A. W., and Turnquist, H. R. (2012). Histone Deacetylase Inhibition Facilitates GM-CSF-Mediated Expansion of Myeloid-Derived Suppressor Cells *In Vitro* and *In Vivo*. *J. Leukoc. Biol.* 91 (5), 701–709. doi:10.1189/jlb.0311119
- Ryter, S. W. (2021). Heme Oxygenase-1, a Cardinal Modulator of Regulated Cell Death and Inflammation. *Cells* 10 (3), 515. doi:10.3390/cells10030515
- Selathurai, A., Deswaerte, V., Kanellakis, P., Tipping, P., Toh, B. H., Bobik, A., et al. (2014). Natural Killer (NK) Cells Augment Atherosclerosis by Cytotoxic

- dependent Mechanisms. *Cardiovasc. Res.* 102 (1), 128–137. doi:10.1093/cvr/cvu016
- Shokawa, T., Yoshizumi, M., Yamamoto, H., Omura, S., Toyofuku, M., Shimizu, Y., et al. (2006). Induction of Heme Oxygenase-1 Inhibits Monocyte Chemoattractant Protein-1 mRNA Expression in U937 Cells. *J. Pharmacol. Sci.* 100 (2), 162–166. doi:10.1254/jphs.sc0040188
- Stocker, R., Yamamoto, Y., McDonagh, A. F., Glazer, A. N., and Ames, B. N. (1987). Bilirubin Is an Antioxidant of Possible Physiological Importance. *Science* 235 (4792), 1043–1046. doi:10.1126/science.3029864
- van Erp, E. A., Lakerveld, A. J., de Graaf, E., Larsen, M. D., Schepp, R. M., Hipgrave Ederveen, A. L., et al. (2020). Natural Killer Cell Activation by Respiratory Syncytial Virus-specific Antibodies Is Decreased in Infants with Severe Respiratory Infections and Correlates with Fc-Glycosylation. *Clin. Transl. Immunol.* 9 (2), e1112. doi:10.1002/cti2.1112
- Verheij, M., Zeerleder, S., and Voermans, C. (2021). Heme Oxygenase-1: Equally Important in Allogeneic Hematopoietic Stem Cell Transplantation and Organ Transplantation? *Transpl. Immunol.* 68, 101419. doi:10.1016/j.trim.2021.101419
- Wang, Y., Wang, G. Z., Rabinovitch, P. S., and Tabas, I. (2014). Macrophage Mitochondrial Oxidative Stress Promotes Atherosclerosis and Nuclear Factor- $\kappa$ B-Mediated Inflammation in Macrophages. *Circ. Res.* 114 (3), 421–433. doi:10.1161/CIRCRESAHA.114.302153
- Wang, J., De Veirman, K., Faict, S., Frassanito, M. A., Ribatti, D., Vacca, A., et al. (2016). Multiple Myeloma Exosomes Establish a Favourable Bone Marrow Microenvironment with Enhanced Angiogenesis and Immunosuppression. *J. Pathol.* 239 (2), 162–173. doi:10.1002/path.4712
- Wang, J., Tu, C., Zhang, H., Zhang, J., Feng, Y., Deng, Y., et al. (2020a). Loading of Metal Isotope-Containing Intercalators for Mass Cytometry-Based High-Throughput Quantitation of Exosome Uptake at the Single-Cell Level. *Biomaterials* 255, 120152. doi:10.1016/j.biomaterials.2020.120152
- Wang, J., Zheng, Y., Tu, C., Zhang, H., Vanderkerken, K., Menu, E., et al. (2020b). Identification of the Immune Checkpoint Signature of Multiple Myeloma Using Mass Cytometry-Based Single-Cell Analysis. *Clin. Transl. Immunol.* 9 (5), e01132. doi:10.1002/cti2.1132
- Whitman, S. C., Rateri, D. L., Szilvassy, S. J., Yokoyama, W., and Daugherty, A. (2004). Depletion of Natural Killer Cell Function Decreases Atherosclerosis in Low-Density Lipoprotein Receptor Null Mice. *Arterioscler Thromb. Vasc. Biol.* 24 (6), 1049–1054. doi:10.1161/01.ATV.0000124923.95545.2c
- Winkels, H., Ehinger, E., Vassallo, M., Buscher, K., Dinh, H. Q., Kobiyama, K., et al. (2018). Atlas of the Immune Cell Repertoire in Mouse Atherosclerosis Defined by Single-Cell RNA-Sequencing and Mass Cytometry. *Circ. Res.* 122 (12), 1675–1688. doi:10.1161/CIRCRESAHA.117.312513
- Wu, B. J., Kathir, K., Witting, P. K., Beck, K., Choy, K., Li, C., et al. (2006). Antioxidants Protect from Atherosclerosis by a Heme Oxygenase-1 Pathway that Is Independent of Free Radical Scavenging. *J. Exp. Med.* 203 (4), 1117–1127. doi:10.1084/jem.20052321
- Xia, S., Sha, H., Yang, L., Ji, Y., Ostrand-Rosenberg, S., and Qi, L. (2011). Gr-1+ CD11b+ Myeloid-Derived Suppressor Cells Suppress Inflammation and Promote Insulin Sensitivity in Obesity. *J. Biol. Chem.* 286 (26), 23591–23599. doi:10.1074/jbc.M111.237123
- Yang, Y., Day, J., Souza-Fonseca Guimaraes, F., Wicks, I. P., and Louis, C. (2021). Natural Killer Cells in Inflammatory Autoimmune Diseases. *Clin. Transl. Immunol.* 10 (2), e1250. doi:10.1002/cti2.1250
- Ye, Y., Gaugler, B., Mohty, M., and Malard, F. (2020). Plasmacytoid Dendritic Cell Biology and its Role in Immune-Mediated Diseases. *Clin. Transl. Immunol.* 9 (5), e1139. doi:10.1002/cti2.1139
- Yet, S. F., Layne, M. D., Liu, X., Chen, Y. H., Ith, B., Sibinga, N. E., et al. (2003). Absence of Heme Oxygenase-1 Exacerbates Atherosclerotic Lesion Formation and Vascular Remodeling. *FASEB J.* 17 (12), 1759–1761. doi:10.1096/fj.03-0187fje

**Conflict of Interest:** The authors declare that the research was conducted in the absence of any commercial or financial relationships that could be construed as a potential conflict of interest.

**Publisher's Note:** All claims expressed in this article are solely those of the authors and do not necessarily represent those of their affiliated organizations, or those of the publisher, the editors, and the reviewers. Any product that may be evaluated in this article, or claim that may be made by its manufacturer, is not guaranteed or endorsed by the publisher.

Copyright © 2022 Yao, Hao, Wen, Xiao, Wu, Wang and Liu. This is an open-access article distributed under the terms of the Creative Commons Attribution License (CC BY). The use, distribution or reproduction in other forums is permitted, provided the original author(s) and the copyright owner(s) are credited and that the original publication in this journal is cited, in accordance with accepted academic practice. No use, distribution or reproduction is permitted which does not comply with these terms.



# PAMPs and DAMPs as the Bridge Between Periodontitis and Atherosclerosis: The Potential Therapeutic Targets

Xuanzhi Zhu<sup>1</sup>, Hanyao Huang<sup>2\*</sup> and Lei Zhao<sup>1\*</sup>

<sup>1</sup>State Key Laboratory of Oral Diseases, Department of Periodontics, National Clinical Research Center for Oral Diseases, West China Hospital of Stomatology, Sichuan University, Chengdu, China, <sup>2</sup>State Key Laboratory of Oral Diseases, Department of Oral and Maxillofacial Surgery, National Clinical Research Center for Oral Diseases, West China Hospital of Stomatology, Sichuan University, Chengdu, China

## OPEN ACCESS

### Edited by:

Xianwei Wang,  
Xinxiang Medical University, China

### Reviewed by:

Sasanka Chukkappalli,  
Texas A&M University College Station,  
United States

Caroline Genco,  
Tufts University School of Medicine,  
United States

### \*Correspondence:

Hanyao Huang  
huanghanyao\_cn@scu.edu.cn  
Lei Zhao  
jollyzldoc@163.com

### Specialty section:

This article was submitted to  
Molecular and Cellular Pathology,  
a section of the journal  
Frontiers in Cell and Developmental  
Biology

**Received:** 16 January 2022

**Accepted:** 11 February 2022

**Published:** 25 February 2022

### Citation:

Zhu X, Huang H and Zhao L (2022)  
PAMPs and DAMPs as the Bridge  
Between Periodontitis and  
Atherosclerosis: The Potential  
Therapeutic Targets.  
Front. Cell Dev. Biol. 10:856118.  
doi: 10.3389/fcell.2022.856118

Atherosclerosis is a chronic artery disease characterized by plaque formation and vascular inflammation, eventually leading to myocardial infarction and stroke. Innate immunity plays an irreplaceable role in the vascular inflammatory response triggered by chronic infection. Periodontitis is a common chronic disorder that involves oral microbe-related inflammatory bone loss and local destruction of the periodontal ligament and is a risk factor for atherosclerosis. Periodontal pathogens contain numerous pathogen-associated molecular patterns (PAMPs) such as lipopolysaccharide, CpG DNA, and Peptidoglycan, that initiate the inflammatory response of the innate immunity depending on the recognition of pattern-recognition receptors (PRRs) of host cells. The immune-inflammatory response and destruction of the periodontal tissue will produce a large number of damage-associated molecular patterns (DAMPs) such as neutrophil extracellular traps (NETs), high mobility group box 1 (HMGB1), alarmins (S100 protein), and which can further affect the progression of atherosclerosis. Molecular patterns have recently become the therapeutic targets for inflammatory disease, including blocking the interaction between molecular patterns and PRRs and controlling the related signal transduction pathway. This review summarized the research progress of some representative PAMPs and DAMPs as the molecular pathological mechanism bridging periodontitis and atherosclerosis. We also discussed possible ways to prevent serious cardiovascular events in patients with periodontitis and atherosclerosis by targeting molecular patterns.

**Keywords:** PAMPs, DAMPs, PRRs, innate immunity, periodontitis, atherosclerosis

## 1 INTRODUCTION

Cardiovascular disease (CVD), mainly coronary atherosclerotic heart disease, and is the number one cause of premature death in humans (Roth et al., 2020). Chronic infection and the inflammatory response caused by this infection are important risk factors for the formation of atherosclerosis (AS), the primary pathology of CVD (Soehnlein and Libby, 2021). Innate immunity is the host's first line of defense against pathogenic microorganisms, it plays a vital role in the vascular inflammatory response triggered by chronic infection (Thaiss et al., 2016). Different from adaptive immune



response relies on antigen-specific T/B lymphocytes *in vivo* to activate, proliferate, and differentiate into effector cells after receiving antigen stimulation (Chavarria-Smith et al., 2018), the activation of innate immunity depends on the interaction between pattern-recognition receptors (PRRs) of host cells and molecular patterns, such as pathogen-associated molecular patterns (PAMPs), and damage-associated molecular patterns (DAMPs) (Olive, 2012). The pathogen itself or its metabolites together, as PAMPs, constitute a class of molecular patterns involved in the activation of innate immunity. PAMPs are relatively non-specific, highly conserved, pathogenic molecular structures expressed in pathogens, and their products (Mogensen, 2009). DAMPs are a large number of related intracellular proteins or nucleic acids released by necrotic cells at the site of necrosis. DAMPs participate in the occurrence and development of acute and chronic inflammation and are critical factors in the outbreak of acute severe inflammation (Gong et al., 2020).

Periodontitis (PD) is an infectious inflammatory disease with plaque biofilm as the initiating factor. It mainly destroys the supporting tissues around the teeth (including gingiva, periodontal ligament, alveolar bone, and cementum). The microbial dysbiosis and the host immune response jointly promote the progression of PD (Slots, 2017), in which PAMPs and DAMPs are representatives of this process. Representative PD-related PAMPs include lipopolysaccharide (LPS), peptidoglycan (PGN), and DNA sequence containing unmethylated CpG-motif (CpG DNA). LPS and PGN, which are located on the surface of periodontal pathogenic bacteria, can be released after the bacteria are cleared and lysed, accompanied by the release of CpG DNA (Song et al., 2017). The release of PD-related DAMPs, represented by neutrophil extracellular traps (NETs), high mobility group box 1 (HMGB1) and alarmins (S100A8, S100A9, and S100A12), mainly comes from the ablation and apoptosis of periodontal tissue cells and the activation and rupture of immune cells (Gu and Han, 2020). PAMPs and DAMPs interact with the PRRs in the periodontal tissues. With the persistent activation of the innate immune system by PAMPs and DAMPs, inflammatory responses continuously exist and lead to the destruction of the periodontal tissue (Song et al., 2017; Gu and Han, 2020).

In periodontal tissues, PAMPs are recognized by PRRs and initiate the innate immune response within a short period, such as eliminating pathogens by macrophages and complement. After PRRs recognize PAMPs, neutrophils, T lymphocytes, macrophages, and plasma cells successively infiltrate periodontal tissue; immune cells secrete IL-1 $\beta$  (interleukin-1 $\beta$ ), IL-6, TNF- $\alpha$  (tumor necrosis factor- $\alpha$ ) or other cytokines which mediate inflammation (Karki and Kanneganti, 2021), promote osteoclast production, and cause periodontal tissue damage (Chen et al., 2021). DAMPs released in PD were also confirmed to capture bacteria and activate inflammation in PD (Gu and Han, 2020).

PD is regarded as a significant independent risk factor for AS (Holmlund et al., 2017; Sanz et al., 2020). *Porphyromonas gingivalis* (*P. gingivalis*), one primary pathogen of PD (Slots, 2017), can adhere to and invade the arterial vessel wall after entering the bloodstream. By inhibiting the proliferation of

endothelial cells, it promotes the adhesion and chemotaxis of monocytes, and activates the inflammatory signaling pathway (Hajishengallis, 2015), eventually leading to vascular endothelial dysfunction (Higashi et al., 2008), aggravating vascular inflammation, and promoting the formation of AS (Gibson et al., 2004). Meanwhile, studies have confirmed that many of these PAMPs and DAMPs related to PD are involved in the progression of AS, and most of them have adverse effects. These substances and the activated innate immunity bridge the gap between PD and AS, and enable us further to understand the relationship between oral diseases and systemic diseases (Figure 1). These substances may also become new targets for treating patients with AS who are aggravated by PD. This review summarizes representative PD-derived PAMPs and DAMPs and their receptors that are most closely related to AS and introduces potential treatments.

## 2 REPRESENTATIVE PERIODONTITIS-RELATED PAMPS AND DAMPS AND THEIR ROLES IN ATHEROSCLEROSIS

### 2.1 Representative Periodontitis-Related PAMPS

#### 2.1.1 Lipopolysaccharide

LPS is a unique component of the outer membrane of Gram-negative bacteria, composed of lipid A, a short core oligosaccharide and O-antigen. It is also called endotoxin due to its ability to induce a robust inflammatory response. LPS is the most representative virulence factor among periodontal pathogens. Clinical studies have shown that LPS levels were positively correlated with periodontal clinical parameters and inflammatory factors before and after periodontal treatment (Lee et al., 2008; Shaddox et al., 2013).

After the periodontal microbial homeostasis is disrupted, *P. gingivalis* proliferates in large numbers, and excessive proliferation and death cause the release of LPS (Zheng et al., 2021). *P. gingivalis* LPS is recognized by the Toll-like receptor 4 (TLR4) of macrophages and activates the NF- $\kappa$ B and MAPK signaling pathways, thereby inducing the release of inflammatory cytokines (Nativel et al., 2017). These factors can promote the expression of matrix metalloproteinases and osteoclast factors and then destroy soft tissue and bone.

*P. gingivalis* LPS can induce macrophage foam cell formation. It promotes the binding of macrophages to low-density lipoproteins (LDL) and induces macrophages to modify native LDL (Qi et al., 2003). *P. gingivalis* LPS promotes monocyte chemotaxis and adhesion to vascular endothelial cells through Akt and NF- $\kappa$ B signaling pathways (Wang et al., 2020). *P. gingivalis* LPS can also promote the high expression of angiotensin II and IL-6 in vascular endothelial cells and accelerates endothelial dysfunction (Viafara-Garcia et al., 2019). In animal models, *P. gingivalis* LPS increased the secretion of TNF- $\alpha$  from macrophages and up-regulated the expression of endothelial cell adhesion molecules, which

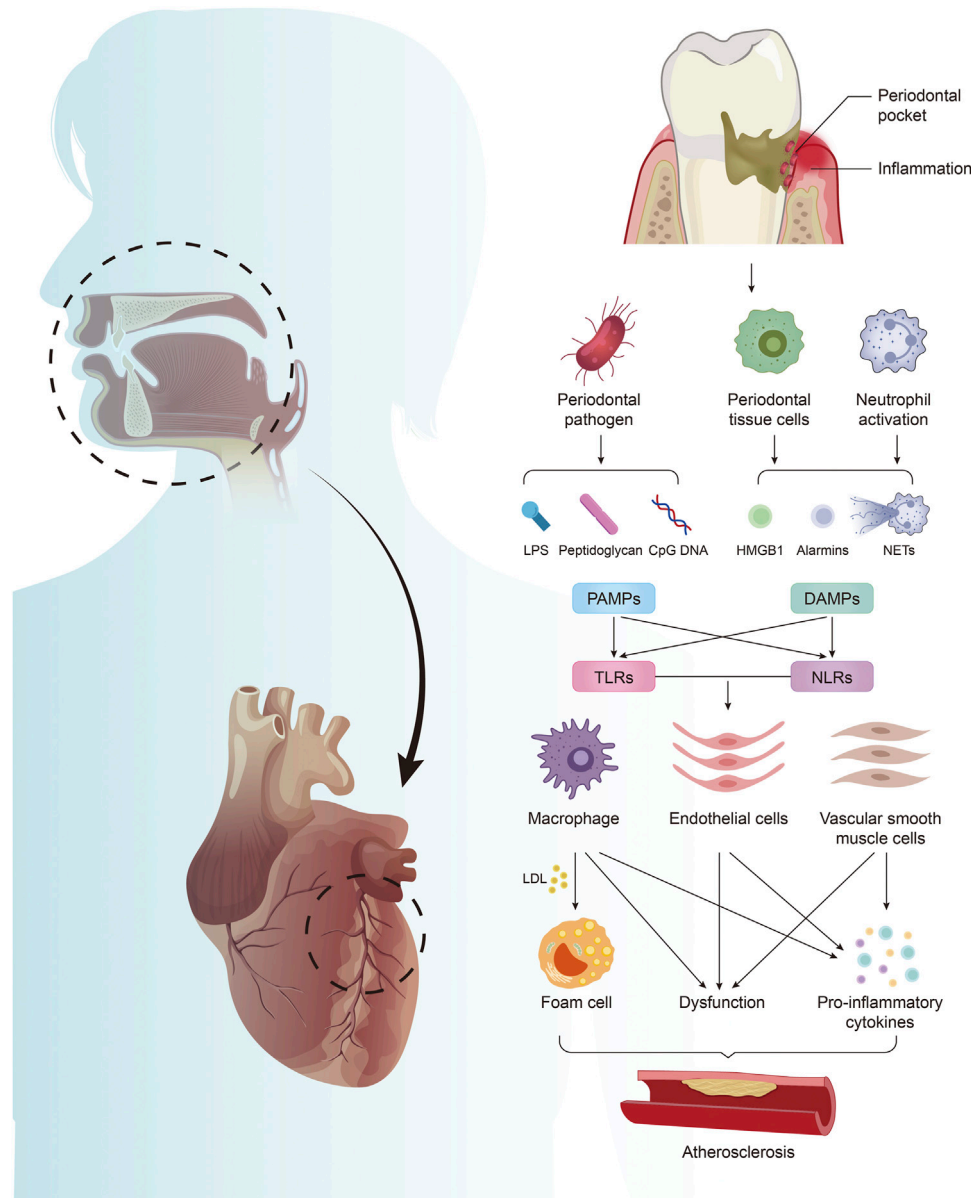


**FIGURE 1 |** Periodontitis mediates the formation of atherosclerosis by producing PAMPs and DAMPs. Periodontal pathogens produce PAMPs, including LPS, PGN, and CpG DNA. Periodontal infection activates neutrophils to form NETs, which together with HMGB1 and alarmins released by damaged periodontal cells constitute DAMPs. PAMPs and DAMPs activate excessive innate immunity by acting on TLRs and NLRs in arterial tissue, leading to foam cell formation, endothelial cell and vascular smooth muscle cell dysfunction, and promoting the massive release of inflammatory factors, which are involved in the regulation of AS.

aggravated the exacerbated effect of ligature-induced PD on AS (Suh et al., 2019). However, the role of other periodontal pathogenic LPS in AS, such as *Treponema denticola* (*T. denticola*) and *Tannerella forsythia* (*T. forsythia*), is still unknown.

From a broader perspective, PD related low-grade endotoxemia (LGE) causes phenotypic and transcriptional changes in myeloid cell populations that enhance their response to pathogens, a process known as trained immunity (Netea et al., 2020). LPS from periodontal pockets continue to enter the peripheral blood at low levels, activating neutrophil

hyperresponsiveness (Vitkov et al., 2021) (The role of neutrophils in this process will be discussed in detail later). Therefore, periodontal pathogenic bacteria-derived LPS represented by *P. gingivalis* LPS and its induced LGE may be the link between PD and AS.

### 2.1.2 CpG DNA

CpG DNA is a type of DNA sequence with immune activation function containing unmethylated CpG motif, including artificially synthesized oligodeoxynucleotides containing CpG (CpG ODN) and genomic DNA of bacteria, viruses, and

invertebrates (Zhou and Deng, 2021). CpG DNA triggers immunostimulatory activity through TLR9 (Ohto et al., 2015). TLR9 is highly expressed in the gingival tissue of PD patients (Narayan et al., 2018), suggesting that CpG DNA could be actively involved in the progression of PD.

It was found *in vitro* that macrophages recognize CpG DNA from periodontal pathogens through TLR9 and then highly express IL-1 $\beta$  and TNF- $\alpha$  to induce osteoclastogenesis (Zou et al., 2002). In addition, TLR9-related autophagy may also be involved in the progression of PD (Wei et al., 2020). However, there are also studies showing that CpG ODN sometimes may positively affect PD. CpG ODNs can promote the proliferation and differentiation of MC3T3 cells in the early stage and up-regulate the expression levels of bone differentiation genes SP7 and OCN (Yu et al., 2020).

AS can associate with PD through CpG DNA. In ApoE<sup>-/-</sup> mice infected by *P. gingivalis*, alveolar bone resorption and aortic plaque increased significantly (Xuan et al., 2017). The genomic DNA of *P. gingivalis* can be detected in the oral epithelium and the aorta (Velsko et al., 2014). In polymicrobial infection-induced periodontal disease, ApoE<sup>-/-</sup> mice had enlarged aortic plaques, accumulation of macrophages around the arteries, increased serum cholesterol and triglycerides, while genomic DNA of *P. gingivalis*, *T. denticola*, and *T. forsythia* can be detected in the aorta and liver (Rivera et al., 2013). Intravenous injection of *P. gingivalis* in ApoE<sup>-/-</sup> mice can also aggravate AS, and the ribosomal DNA of *P. gingivalis* can be detected in the aorta, liver and heart (Li et al., 2002). However, *P. gingivalis* DNA in the periodontal pocket may not be transferred to the heart valve area, causing the aortic valve and mitral valve to degenerate (Radwan-Oczko et al., 2014). Therefore, periodontal pathogens represented by *P. gingivalis* might colonize the arterial wall through blood circulation, and the CpG DNA released after bacterial cell lysis may regulate the development of AS by activating the corresponding TLR9 pathway.

However, the role of CpG DNA/ODN on AS is still controversial. The genetic deletion of the TLR9 gene exacerbated AS lesions in ApoE<sup>-/-</sup> mice, and the use of CpG ODN 1668 can reduce this effect (Koulis et al., 2014). In other words, CpG ODN and TLR9 may protect the aorta in specific circumstances. Further studies demonstrated that TLR9 plays a negative role in vascular injury (Hirata et al., 2013), and systemic stimulation of TLR9 with high-dose CpG ODN will aggravate the development of AS (Krogmann et al., 2016). There are differences between CpG DNA released in PD and synthetic CpG ODN. The difference in concentration and sequence may lead to changes in the activation of the downstream inflammatory pathway of TLR9 in AS lesions. Therefore, it is necessary to screen PD-related CpG DNA to clarify its role in AS in future studies.

### 2.1.3 Peptidoglycan

Peptidoglycan (PGN) is a common component of bacterial cell walls. Transcriptional pathways for peptidoglycan synthesis are significantly up-regulated in tongue and subgingival plaque in patients with periodontitis (Yost et al., 2015; Belstrom et al., 2021). PGN can be recognized by TLR2 on the cell membrane and the endogenous NOD1, NOD2, and NLRP3. The expression of

NOD1 and NOD2 can be detected in human periodontal ligament cells (hPDLC). Under the stimulation of PGN, the production of IL-6 and IL-8 in hPDLC increased, and the NF- $\kappa$ B and MAPK signaling pathways were activated (Jeon et al., 2012). Injecting PGN into the gums of mice can induce osteoclastogenesis, and TLR2, NOD1, and NOD2 are activated (Kishimoto et al., 2012). N-acetylglucosamine can be recognized by the glycolytic enzyme hexokinase in the cytoplasm and subsequently activate the NLRP3 inflammasome, which may be involved in the progression of PD (Wolf et al., 2016). In summary, periodontal pathogens may activate excessive innate immunity through PGN, an exogenous pathogen-associated molecular pattern, and cause PD. The destruction of periodontal tissue damages the barrier function of the oral mucosa. The decisive invasion and migration capabilities of periodontal pathogens make it enter the circulation and spread the PGN in the cell wall to the cardiovascular system.

Although there are few studies on the relation between periodontal PGN and AS, as a ubiquitous substance in bacteria, PGN produced by lysis or ectopic colonization of periodontal pathogens around blood vessels can cause chronic inflammation. The long-term chronic inflammation of the vascular microenvironment is obviously beneficial to the formation of AS. Early studies found that PGN induced the production of pro-inflammatory cytokines through TLR2 and increased the vulnerability of AS plaques (Nijhuis et al., 2004). While the vascular endothelial dysfunction appeared in rats modeled by surgery and a high-cholesterol diet, the concentration of serum PGN was significantly increased (Tsunooka et al., 2005). It has been confirmed that TLR2 is expressed in macrophages in AS lesions. PGN activated monocytes to overexpress intercellular adhesion molecule-1 (ICAM-1) through the TLR2 and NF- $\kappa$ B pathways, promoting monocyte adhesion and chemotaxis to vascular diseases (Nijhuis et al., 2007; Xie et al., 2016). Using PGN to stimulate human coronary artery endothelial cells that were knocked out TLR2 through CRISPR-Cas9 technology, the expression levels of ICAM-1, IL-6, and IL-8 were significantly down-regulated (Wang et al., 2018). PGN can also be recognized by PGN recognition protein-1 (PGLYRP-1) in the innate immune system. The level of circulating PGLYRP-1 is associated with AS, coronary artery calcification, thickening of the abdominal aorta, and acute coronary syndrome (Brownell et al., 2016; Han et al., 2021). PGLYRP1 may promote the formation of AS plaques by regulating the overexpression of adhesion molecules in endothelial cells (Jin et al., 2021). PGN also triggers the up-regulation of vascular cell adhesion molecule-1 (VCAM-1) through the NOD1-RIP2-NF- $\kappa$ B axis, promotes the recruitment of myeloid cells, and leads to endothelial dysfunction (Gonzalez-Ramos et al., 2019).

## 2.2 Representative Periodontitis-Related DAMPs

### 2.2.1 Neutrophil Extracellular Traps

Neutrophil extracellular traps (NETs) are an extracellular fibrous network structure produced by neutrophils after being

stimulated, mainly composed of chromatin and cellular proteins (Brinkmann et al., 2004). The process of neutrophils forming NETs is called NETosis, including suicidal NETosis and survival vital NETosis, which is considered a cell death program different from apoptosis and necrosis (Yipp and Kubes, 2013). NETs recognize, trap, and restrict the spread of bacteria and other pathogens and highly express antimicrobial peptides and other antibacterial ingredients to delete pathogens ultimately (Papayannopoulos, 2018).

Numerous clinical studies have confirmed that NETs are closely related to the progression of PD. NETs expression in the inflamed gingival tissue was higher than that in the healthy control group (White P. C. et al., 2016). The expression of NETs in the gingival tissue of patients with periodontitis was higher than that of patients with gingivitis, indicating that the level of NETs is related to the severity of periodontal inflammation (Magan-Fernandez et al., 2019). The gingival biopsy samples of patients with PD and the purulent exudate in the periodontal pockets (Vitkov et al., 2009) found high expression of NETs, showing a fibrous network structure. There are many bacteria in the NETs and their mechanical entanglement, and they are closely arranged on the surface of the epithelium. A case-control study (Kaneko et al., 2018) found that the NETs level was positively correlated with the average probing depth and clinical attachment loss in patients with PD. NETs were detected in supragingival plaque biofilms, and NETs-related protein Myeloperoxidase (MPO) was found in saliva and biofilms, which confirmed that oral bacteria isolated from plaque biofilms could stimulate the formation of NETs (Hirschfeld et al., 2015). Neutrophils in PD are recruited by fibrin through myeloid integrin  $\alpha_m\beta_2$ -binding motif and activated to generate NETs (Silva et al., 2021). Studies have found that *P. gingivalis* (Jayaprakash et al., 2015) and *Fusobacterium nucleatum* (*F. nucleatum*) (White et al., 2014) can stimulate neutrophils to produce reactive oxygen species (ROS). *Streptococcus sanguis* also increased the level of NETs marker citH3 and up-regulated the level of MPO (Oveisi et al., 2019). In summary, specific periodontal pathogens can stimulate neutrophils to produce ROS and release NETs.

Multivariate logistic regression analysis showed that the peripheral blood NET level was significantly positively associated with moderate to severe PD (Kaneko et al., 2018). Degradation of NETs in plasma is increased after periodontal therapy in PD patients (Moonen et al., 2020). Periodontal pathogens and excessive NETs produced during PD may participate in the progression of AS after entering the circulation. After entering the bloodstream, *P. gingivalis* binds to erythrocytes to avoid ROS destruction, thereby further activating the Rho GTPase signaling pathway, up-regulating CD11b/CD18, and promoting the activation of neutrophils (Borgeson et al., 2011; Damgaard et al., 2017). Periodontal pathogen DNA can be detected in carotid plaque. *T. forsythia* is significantly related to intraplaque hemorrhage and neutrophil activation, reflected in the increased release of MPO, cell-free DNA, and NETs (Range et al., 2014). The systemic inflammatory state caused by PD promotes the adhesion of neutrophils and endothelial cells by increasing oxidative stress parameters

(superoxide and mitochondrial membrane potential) (Martinez-Herrera et al., 2018). However, studies are still limited to the relationship between periodontal NETs and AS. The differences between the histone composition and DNA sequence of periodontal NETs and other systemic inflammatory NETs, as well as the mechanism of periodontal NETs in AS plaque formation, deserve more efforts to reveal both *in vivo* and *in vitro*.

## 2.2.2 High Mobility Group Box 1

High mobility group Box 1 (HMGB1) is a non-histone chromosome binding protein widely distributed in the nucleus of various cells. It plays an important role in stabilizing the structure of nucleosomes, regulating transcription factors, and DNA replication repair (Vijayakumar et al., 2019). HMGB1 can be released by necrotic or ruptured cells and activated immune cells (Andersson and Tracey, 2011). High levels of HMGB1 can be detected in the gingival crevicular fluid of patients with moderate to severe chronic PD (Luo et al., 2011; Paknejad et al., 2016), and it was positively correlated with periodontal clinical parameters (including plaque index, bleeding index, probing depth, and clinical attachment level) (Yu et al., 2019). Human gingival epithelial cells can increase the secretion of HMGB1 under the stimulation of TNF- $\alpha$  (Morimoto et al., 2008). Similarly, IL-1 $\beta$  promoted the secretion of HMGB1 in fibroblasts (Ito et al., 2012). Under the constant stimulation of periodontal infection, tissue cells continuously secrete HMGB1, which causes macrophages to be further activated and secrete cytokines, and amplifying the destruction of inflammation. This process can be inhibited by HMGB1 antibody (Yoshihara-Hirata et al., 2018). Excessive HMGB1 secreted by periodontal cells in PD or released by apoptosis can enter the circulation through osmosis and transmit the damage signal to the artery.

In AS, HMGB1 plays an important role. The increase of HMGB1 level directly leads to the mass production of cytokines, including IFN- $\gamma$ , TNF- $\alpha$ , IL-1 $\beta$ , and IL-6, which promotes the formation of AS and reduces the stability of plaque (Su et al., 2015). In the AS model of rabbits, administration of HMGB1 and TNF- $\alpha$  can significantly aggravate the inflammation of advanced plaques (Kim J.-S. et al., 2016). In the ApoE<sup>-/-</sup> mouse AS model induced by the Western diet, anti-HMGB1 antibodies were more than six times higher than regular diet ApoE<sup>-/-</sup> mice and ApoE<sup>+/+</sup> mice, indicating that HMGB1 autoimmunity is involved in the progression of AS (Pan et al., 2016). It was speculated that HMGB1 produced by PD might be involved in systemic diseases by acting on monocytes, macrophages and vascular endothelial cells (Morimoto-Yamashita et al., 2012). Bioinformatics analysis shows that HMGB1 is a potential molecular mechanism of the association between PD and AS (Ning et al., 2021). There have been reports that *P. gingivalis* elevated HMGB1 levels after myocardial infarction in mice (Srisuwantha et al., 2017). In addition, the circular RNA PPP1CC of *P. gingivalis* can regulate the apoptosis of vascular smooth muscle cells through the HMGB1/TLR9/AIM2 axis (Liu J. et al., 2021). The role of HMGB1 produced by PD in the AS model remains to be discovered.



### 2.2.3 Alarmins

S100 protein is a group of calcium-binding proteins. Its family has more than 20 members and participates in the metabolism of the cytoskeleton under physiological conditions (Vogl et al., 2014). When cells are damaged or phagocytes are activated, macrophages secrete S100A8, S100A9, and S100A12 (Foell et al., 2007). These proteins combine with PRRs as “alarmins”, activating immune cells and endothelial cells to promote inflammation (Goyette and Geczy, 2011). The levels of S100A8, S100A9, and S100A12 in saliva and gingival crevicular fluid of patients with PD were significantly increased (Kojima et al., 2000; Shin et al., 2019; Lira-Junior et al., 2020; Jimenez et al., 2021). Microbial infection can cause abnormal expression of S100 protein in gingival tissues and destroy the epithelial barrier function (Nishii et al., 2013). Immunohistochemistry and RNA sequencing showed that S100A8 and S100A9 were highly expressed in the ligature-induced PD (Maekawa et al., 2019). After mouse osteocyte-like cells (MLO-Y4-A2) were treated with S100A9, the expression of IL-6 and RANKL increased, and the p38/ERK/STAT3 signaling pathway was activated, indicating that alarmins were involved in periodontal bone destruction (Takagi et al., 2020). It is worth noting that the levels of S100A12 and C-reactive protein in the gingival crevicular fluid and serum of patients with PD are elevated and positively correlated with periodontal parameters (Pradeep et al., 2014), suggesting that alarmins may be the link between PD and AS.

The expression of S100A9 and SMemb protein (a phenotypic marker of smooth muscle cell proliferation) increased in aneurysm specimens from patients infected with *P. gingivalis* (Hokamura et al., 2010). This phenotype has been verified in mice. Studies have also found that *P. gingivalis* infection can up-regulate the expression of S100A9 in human aortic smooth muscle cells (hAOSMC), which makes hAOSMC change from a contractile to proliferative phenotype (Inaba et al., 2009). These may lead to a potential mechanism for PD to promote aortic intimal hyperplasia. Therefore, PD can accelerate AS through alarmins.

## 3 PERIODONTITIS-RELATED PAMPS AND DAMPS RECOGNITION RECEPTORS EXIST IN ATHEROSCLEROSIS

### 3.1 Toll-like Receptors

Toll-like receptors (TLRs) are a type of PRRs that exist on the cell surface or endosome/lysosome membrane (Minton, 2019). So far, 10 TLRs have been found in humans. TLRs are mainly divided into two categories. TLR1, TLR2, TLR4, TLR5, TLR6, and TLR10 significantly recognize lipids and proteins, while TLR3, TLR7, TLR8, and TLR9 mainly recognize nucleic acids (Fitzgerald and Kagan, 2020). TLR1, TLR2, TLR4, TLR7, and TLR9 are highly expressed in the gingival tissue of patients with PD (Becerik et al., 2011; Scheres et al., 2011; Duarte et al., 2012; Ribeiro et al., 2012; Beklen et al., 2014; Chen et al., 2014). Under the infection of periodontal pathogens (such as *P.*

*gingivalis*), LPS, flagella, and CpG DNA, etc., stimulate the corresponding TLRs, activate excessive innate immunity, and destroy periodontal tissue. These molecular patterns transfer chronic inflammatory signals from the oral cavity to cardiovascular tissues by releasing them into the blood or ectopic bacterial colonization, driving the activation of innate immunity in the vascular microenvironment and participating in the progression of AS.

The high degree of conservation of TLRs determines that TLRs closely related to PD are widely distributed in blood vessels and surrounding immune cells. Macrophages play a vital role in the pathology of AS. Under *P. gingivalis* stimulation, macrophages recognized LPS and flagella through TLR2 and TLR4, and CpG DNA through TLR9, secreted more IL-1 $\beta$ , IL-6, TNF- $\alpha$ , and adhesion molecules, and formed foam cells and participated in plaque formation (Gibson and Genco, 2007; Brown et al., 2015; Crump and Sahingur, 2016). At the same time, cholesterol crystals in blood vessels will amplify the activation of TLR2 and TLR4 signaling pathways of monocytes stimulated by *P. gingivalis*, and the mechanism may be related to the NLRP3 inflammasome (Kollgaard et al., 2017). Interestingly, mice lacking TLR2 and TLR4 have significantly reduced alveolar bone resorption compared with the control group under the condition of periodontal red-complex infection, and the serum oxidized low-density lipoprotein, nitric oxide, and lipid fractions levels were not altered. The AS lesions of the aortic arch in the experimental group also did not aggravate (Chukkapalli et al., 2017). After TLR9-deficient mice were stimulated with CpG DNA, the activation of NF- $\kappa$ B was down-regulated compared with wild-type, and the contractility of cardiomyocytes was increased (Knuefermann et al., 2008). Activating TLR9 in endothelial cells can promote neutrophil chemotaxis and vascular inflammation (El Kebir et al., 2009).

### 3.2 NOD-like Receptors

NLRs are similar to TLRs in that they are both signal transduction pattern recognition receptors. 23 NLR family members have been found in humans, including NOD1, NOD2, and NLRP3, etc (Zhen and Zhang, 2019). NOD1 and NOD2 are the first two NLRs discovered. They contain an N-terminal caspase recruitment domain and a C-terminal leucine-rich repeat sequence (Kim Y. K. et al., 2016). In healthy gingival tissue, NOD1 and NOD2 are more abundant than TLRs. Both *P. gingivalis* and *F. nucleatum* infection can induce high expression of NOD1 and NOD2 in periodontal tissues (Liu et al., 2014; Alyami et al., 2019). After NOD1 and NOD2 are activated, they recruit a series of downstream molecules and activate NF- $\kappa$ B and MAPK pathways (Jeon et al., 2012). PD aggravates vascular endothelial dysfunction through NOD1 and NOD2. *P. gingivalis* can stimulate the activation of endothelial cells and promote the up-regulation of E-selectin, NOD1, NOD2, and TLR2. This change depends on the NF- $\kappa$ B/p38/MAPK pathway. The use of small interfering RNA targeting NOD1 can suppress related signals (Wan et al., 2015). Compared with cells treated with NOD1 and NOD2 ligand stimulants, *P.*

*gingivalis*-infected endothelial cells showed rapid lysis of receptor-interacting protein 1 (RIPK1) and RIPK2, suggesting that tumor necrosis factor receptor-1 (TNF-R1)-induced cell activation or death was involved in the invasion of arteries by periodontal pathogens (Madrigal et al., 2012).

NOD-like receptor protein 3 (NLRP3) NLRP3 is an essential member of the NOD-like receptor family. Its inflammasome complex consists of NLRP3, apoptosis-associated speck-like protein (ASC) containing a caspase recruitment domain (CARD) and pro-cysteiny aspartate specific proteinase-1 (pro-caspase-1) composition. NLRP3 is encoded by autoinflammatory syndrome 1 (CIAS1) and has an N-terminal pyrin domain (PYD), a central nucleoside triphosphatase domain (NACHT domain), and a C-terminal leucine-rich repeat (LRR). When NLRP3 senses a danger signal, it interacts with the PYD of ASC. Then ASC recruits pro-caspase-1 through the same CARD and then aggregates it into NLRP3 inflammasomes. The activated inflammasomes prompt ASC to cleave pro-caspase-1 into active caspase-1, which promotes the maturation of IL-1 $\beta$  and IL-18, and induces inflammation and cell death (Haneklaus and O'Neill, 2015; Shao et al., 2015).

NLRP3 is a crucial mediator of periodontal infections involved in AS. The latest clinical study showed that NLRP3 was positively correlated with periodontal parameters, and periodontal treatment can effectively reduce the level of NLRP3 in gingival crevicular fluid (Shahbeik et al., 2021). The detection of high levels of NLRP3, ASC and IL-1 $\beta$  in saliva reflected the severity of periodontal inflammation (Isaza-Guzman et al., 2017). Further *in vivo* (Yamaguchi et al., 2017) and *in vitro* (Lu et al., 2017; Lian et al., 2018; Zhang et al., 2021) experiments proved that NLRP3 was involved in the regulation of periodontal inflammation. The saliva and serum levels of NLRP3 in patients with PD were elevated, suggesting that NLRP3 may be a mediator of periodontal infection and systemic diseases (Isola et al., 2021). In a clinical trial of 90 subjects, the level of NLRP3 in the serum of patients with coronary heart disease was significantly higher than that in the control group. It was positively correlated with the levels of serum IL-1 $\beta$  and IL-18 (Satoh et al., 2014). A study of 22 patients with chronic PD showed that the relative expression levels of ASC, NLRP3, and caspase-1 mRNA in peripheral blood decreased after initial periodontal treatment (Higuchi et al., 2020). It was suggested that periodontal treatment might prevent AS by reversing the release of inflammasome from periodontal tissue to the cardiovascular system. Compared with KDP136 (gingipain null mutant) or KDP150 (FimA defective mutant), wild-type (WT) ApoE<sup>-/-</sup> mice infected with pg showed loss of alveolar bone and increased AS plaque area, and periodontal macrophages secreted more IL-1 $\beta$ , IL-18, and TNF- $\alpha$ . The expression of NLRP3 mRNA in the gingival tissue and the aorta were increased (Yamaguchi et al., 2015). *P. gingivalis* can also act synergistically with cholesterol crystals to stimulate the NLRP3 inflammasome to promote the secretion of AS-promoting cytokines by monocytes (Kollgaard et al., 2017). However, a study showed that *P. gingivalis* LPS could stimulate the increase of NLRP3 levels in endothelial cells instead of *P. gingivalis* stimulation (Huck et al., 2015), which seems to contradict *in vivo* studies. Therefore, the mechanism of

NLRP3 in periodontal inflammation-promoting AS remains to be explored.

#### 4 BLOCKING PAMPs AND DAMPs HAS THE POTENTIAL TO INHIBIT THE SYSTEMIC EFFECTS CAUSED BY PERIODONTITIS

With the continuous progress of periodontal inflammation, PAMPs and DAMPs can be released into the circulation, promoting the development of systemic diseases such as AS, rheumatoid arthritis, and inflammatory bowel disease, etc. As mentioned above, periodontal treatment can decrease systemic inflammation, which can be explained as the control of oral infections reduces the microbial burden caused by the release of PAMPs. The healing and reconstruction of damaged tissues cut off the source of DAMPs release.

In order to antagonize infection and inflammation, there have been attempts to find or synthesize inhibitors targeting molecular patterns. For example, the ubiquitous 14-3-3  $\beta/\alpha$ -A protein in zebrafish embryos specifically neutralizes PGN and protects the early embryonic host from pathogenic attacks (Wang et al., 2021). The artificially synthesized monoclonal antibody 2E7 targeting on muramyl-L-alanyl-D-isoglutamine (a highly conserved domain of PGN), suppressed the development of autoimmune arthritis and experimental autoimmune encephalomyelitis in mice by blocking NOD2-related pathways (Huang et al., 2019). It is suggested that the specific neutralization of PAMPs has potential value in regulating inflammatory diseases.

Synthetic Anti-lipopolysaccharide Peptides (SALPs) as effective inhibitors of PAMPs have been used to treat bacterial infectious diseases. SALPs capture the negatively charged phosphate and carboxylate in the LPS head group through the positively charged N-terminal residue, and then the C-terminal region interacts with the non-polar hydrophobic interaction of the lipid A acyl chain portion (Correa et al., 2019). The binding affinity of SALPs and LPS surpasses that of LPS-binding protein (LBP), showing excellent antibacterial properties. SALPs have a significant inhibitory effect on LPS-induced TNF- $\alpha$  secretion in monocytes. SALPs can also neutralize LPS-induced shock *in vivo* and have little impact on healthy organs (Gutsmann et al., 2010). In the cecum ligation and puncture (CLP)-induced mice model, SALPs can improve the contractile function of cardiomyocytes and reduce cardiac dysfunction (Martin et al., 2015; Martin et al., 2016). This indicated that SALPs have the potential to block the activation of periodontal-related LPS on innate immunity in AS.

Specific molecular patterns neutralizer such as SALPs have two disadvantages. First, there are many types of innate immune activation receptors, each of which recognizes a specific molecular pattern. We cannot guarantee to know the exact molecular pattern of each disease. There may be many models involved in the inflammatory response of the same disease. Secondly, these molecular patterns may be interrelated. Blocking only one of the specific pathways may not effectively suppress the inflammatory response. Both PAMPs and DAMPs include nucleic acids, such as DNA fragments in NETs and CpG DNA. Deoxyribonuclease I

(DNase I) is the first DNA hydrolase to be discovered. In physiological conditions, DNase I contributes to the digestion of food, apoptosis, and elimination of necrotic cells (Mannherz et al., 1995). DNase I has been used as a common neutralizing agent to disrupt NETs structure to prevent DAMPs from over-activating innate immunity, and has preliminary applications in cancer treatment (Cools-Lartigue et al., 2013; White P. et al., 2016). In the periodontal destruction caused by plasminogen deficiency, the use of DNase I to remove NETs recruited and activated by excessive fibrin can significantly reduce alveolar bone resorption (Silva et al., 2021). The level of plasma DNase I of PD patients was significantly lower than healthy controls (White P. et al., 2016), indicating that the use of DNase I may contribute to the balance of nucleic acid metabolism in the circulation. In socially defeated ApoE<sup>-/-</sup> mice, the aggravation of arterial plaque area was wholly diminished by DNase I treatment (Yamamoto et al., 2018). Therefore, DNase I may block the pathway of PD acting on AS by hydrolyzing DNA and its complexes. However, how to define the usage and dosage in the course of treatment and its potential damage to normal tissues remain to be considered.

Nucleic acids are generally negatively charged in their natural state. NA-binding polymers (NABP) represented by PAMAM-G3 are typically used in non-viral gene delivery. Recently, NABP, as a positively charged nucleic acid scavenger, and has been used in various inflammatory diseases to block the excessive activation of innate immunity by molecular patterns (Lee et al., 2011). Compared with the soluble polycations (like PAMAM-G3), the improved NABP nanoparticles have better biological safety and NA scavenging capacity, and demonstrates an excellent therapeutic effect in rheumatoid arthritis (Liang et al., 2018; Peng et al., 2019), sepsis (Dawulieti et al., 2020; Liu F. et al., 2021), and inflammatory bowel disease (Shi et al., 2022). Therefore, it can be feasible to regulate inflammation through non-specific clearance of DAMPs and PAMPs. At present, the research and development of such materials are still in their infancy, and it is expected to be applied to PD and AS models in the future.

## REFERENCES

- Alyami, H. M., Finoti, L. S., Teixeira, H. S., Aljefri, A., Kinane, D. F., and Benakanakere, M. R. (2019). Role of NOD1/NOD2 Receptors in Fusobacterium Nucleatum Mediated NETosis. *Microb. Pathogenesis* 131, 53–64. doi:10.1016/j.micpath.2019.03.036
- Andersson, U., and Tracey, K. J. (2011). HMGB1 Is a Therapeutic Target for Sterile Inflammation and Infection. *Annu. Rev. Immunol.* 29, 139–162. doi:10.1146/annurev-immunol-030409-101323
- Becerik, S., Özsan, N., Gürkan, A., Öztürk, V. Ö., Atilla, G., and Emingil, G. (2011). Toll like Receptor 4 and Membrane-Bound CD14 Expressions in Gingivitis, Periodontitis and CsA-Induced Gingival Overgrowth. *Arch. Oral Biol.* 56 (5), 456–465. doi:10.1016/j.archoralbio.2010.11.008
- Beklen, A., Sarp, A., Uckan, D., and Tsous Memet, G. (2014). The Function of TLR4 in Interferon Gamma or Interleukin-13 Exposed and Lipopolysaccharide Stimulated Gingival Epithelial Cell Cultures. *Biotech. Histochem.* 89 (7), 505–512. doi:10.3109/10520295.2014.903299
- Belström, D., Constancias, F., Markvart, M., Sikora, M., Sørensen, C. E., and Givskov, M. (2021). Transcriptional Activity of Predominant Streptococcus

## 5 CONCLUSION AND PERSPECTIVES

The chronic inflammatory state of PD is closely related to cardiovascular disease. LPS, PGN, and CpG DNA released by periodontal pathogen infection, NETs, HMGB1, and alarmins cast by periodontal tissue destruction can enter the circulation and participate in vasoconstriction, endothelial dysfunction and the transformation of macrophage to foam cells. These molecule patterns join in the development of AS and affect the occurrence of CVD through TLR, NLR and other innate immune signaling pathways. PD and cardiovascular disease are two high-prevalence diseases in humans. Studying the mechanism of action between the two has significant public health significance. In this review, PAMPs and DAMPs are discussed as a complex mechanism of PD affecting AS. This shows that chronic inflammation represented by innate immune activation plays an important role in connecting oral cavity and systemic diseases. Naturally, we will consider whether eliminating molecule patterns will block this process. Through specific and non-specific removal of PAMPs or DAMPs, there have been preliminary applications in the regulation of inflammation. Similar methods will have application prospects in studying the relationship between PD and AS in the future.

## AUTHOR CONTRIBUTIONS

XZ, HH designed, wrote, and revised the manuscript. LZ revised the manuscript. All authors contributed to the article and approved the submitted version.

## FUNDING

This study was supported by the Research and Develop Program, West China Hospital of Stomatology Sichuan University Grant RD-02-202107 (HH) and the National Natural Science Foundation of China Grant 81970944 (LZ).

- Species at Multiple Oral Sites Associate with Periodontal Status. *Front. Cell. Infect. Microbiol.* 11, 752664. doi:10.3389/fcimb.2021.752664
- Börjeson, E., Lönn, J., Bergström, I., Brodin, V. P., Ramström, S., Nayeri, F., et al. (2011). Lipoxin A 4 Inhibits Porphyromonas Gingivalis -Induced Aggregation and Reactive Oxygen Species Production by Modulating Neutrophil-Platelet Interaction and CD11b Expression. *Infect. Immun.* 79 (4), 1489–1497. doi:10.1128/IAI.00777-10
- Brinkmann, V., Reichard, U., Goosmann, C., Fauler, B., Uhlemann, Y., Weiss, D. S., et al. (2004). Neutrophil Extracellular Traps Kill Bacteria. *Science* 303 (5663), 1532–1535. doi:10.1126/science.1092385
- Brown, P. M., Kennedy, D. J., Morton, R. E., and Febbraio, M. (2015). CD36/SR-B2-TLR2 Dependent Pathways Enhance Porphyromonas Gingivalis Mediated Atherosclerosis in the Ldlr KO Mouse Model. *PLoS One* 10 (5), e0125126. doi:10.1371/journal.pone.0125126
- Brownell, N. K., Khera, A., de Lemos, J. A., Ayers, C. R., and Rohatgi, A. (2016). Association between Peptidoglycan Recognition Protein-1 and Incident Atherosclerotic Cardiovascular Disease Events. *J. Am. Coll. Cardiol.* 67 (19), 2310–2312. doi:10.1016/j.jacc.2016.02.063
- Chavarria-Smith, J., Hazenbos, W. L. W., and van Lookeren Campagne, M. (2018). Humoral Immunity Goes Hormonal. *Nat. Immunol.* 19 (10), 1044–1046. doi:10.1038/s41590-018-0216-x



- Chen, Y.-C., Liu, C.-M., Jeng, J.-H., and Ku, C.-C. (2014). Association of Pocket Epithelial Cell Proliferation in Periodontitis with TLR9 Expression and Inflammatory Response. *J. Formos. Med. Assoc.* 113 (8), 549–556. doi:10.1016/j.jfma.2012.07.043
- Chen, Y., Yang, Q., Lv, C., Chen, Y., Zhao, W., Li, W., et al. (2021). NLRP3 Regulates Alveolar Bone Loss in Ligature-induced Periodontitis by Promoting Osteoclastic Differentiation. *Cell Prolif* 54 (2), e12973. doi:10.1111/cpr.12973
- Chukkappalli, S. S., Velsko, I. M., Rivera-Kweh, M. F., Larjava, H., Lucas, A. R., and Kesavalu, L. (2017). Global TLR2 and 4 Deficiency in Mice Impacts Bone Resorption, Inflammatory Markers and Atherosclerosis to Polymicrobial Infection. *Mol. Oral Microbiol.* 32 (3), 211–225. doi:10.1111/omi.12165
- Cools-Lartigue, J., Spicer, J., McDonald, B., Gowing, S., Chow, S., Giannias, B., et al. (2013). Neutrophil Extracellular Traps Sequester Circulating Tumor Cells and Promote Metastasis. *J. Clin. Invest.* 123, 3446–3458. doi:10.1172/JCI67484
- Correa, W., Heinbockel, L., Martinez-de-Tejada, G., Sánchez, S., Garidel, P., Schürholz, T., et al. (2019). Synthetic Anti-lipopolysaccharide Peptides (SALPs) as Effective Inhibitors of Pathogen-Associated Molecular Patterns (PAMPs). *Adv. Exp. Med. Biol.* 1117, 111–129. doi:10.1007/978-981-13-3588-4\_8
- Crump, K. E., and Sahingur, S. E. (2016). Microbial Nucleic Acid Sensing in Oral and Systemic Diseases. *J. Dent Res.* 95 (1), 17–25. doi:10.1177/0022034515609062
- Damgaard, C., Kantarci, A., Holmstrup, P., Hasturk, H., Nielsen, C. H., and Van Dyke, T. E. (2017). Porphyromonas Gingivalis-Induced Production of Reactive Oxygen Species, Tumor Necrosis Factor- $\alpha$ , Interleukin-6, CXCL8 and CCL2 by Neutrophils from Localized Aggressive Periodontitis and Healthy Donors: Modulating Actions of Red Blood Cells and Resolvin E1. *J. Periodont Res.* 52 (2), 246–254. doi:10.1111/jre.12388
- Dawulieti, J., Sun, M., Zhao, Y., Shao, D., Yan, H., Lao, Y.-H., et al. (2020). Treatment of Severe Sepsis with Nanoparticulate Cell-free DNA Scavengers. *Sci. Adv.* 6 (22), eaay7148. doi:10.1126/sciadv.aay7148
- Duarte, P. M., Szeremeske Miranda, T., Lima, J. A., Dias Gonçalves, T. E., Santos, V. R., Bastos, M. F., et al. (2012). Expression of Immune-Inflammatory Markers in Sites of Chronic Periodontitis in Patients with Type 2 Diabetes. *J. Periodontol.* 83 (4), 426–434. doi:10.1902/jop.2011.110324
- El Kebir, D., József, L., Pan, W., Wang, L., and Filep, J. G. (2009). Bacterial DNA Activates Endothelial Cells and Promotes Neutrophil Adherence through TLR9 Signaling. *J. Immunol.* 182 (7), 4386–4394. doi:10.4049/jimmunol.0803044
- Fitzgerald, K. A., and Kagan, J. C. (2020). Toll-like Receptors and the Control of Immunity. *Cell* 180 (6), 1044–1066. doi:10.1016/j.cell.2020.02.041
- Foell, D., Wittkowski, H., Vogl, T., and Roth, J. (2007). S100 Proteins Expressed in Phagocytes: a Novel Group of Damage-Associated Molecular Pattern Molecules. *J. Leukoc. Biol.* 81 (1), 28–37. doi:10.1189/jlb.0306170
- Gibson, F. C., 3rd, Hong, C., Chou, H.-H., Yumoto, H., Chen, J., Lien, E., et al. (2004). Innate Immune Recognition of Invasive Bacteria Accelerates Atherosclerosis in Apolipoprotein E-Deficient Mice. *Circulation* 109 (22), 2801–2806. doi:10.1161/01.CIR.0000129769.17895.F0
- Gibson III, F., 3rd, and Genco, C. (2007). Porphyromonas Gingivalis Mediated Periodontal Disease and Atherosclerosis: Disparate Diseases with Commonalities in Pathogenesis through TLRs. *Cpd* 13 (36), 3665–3675. doi:10.2174/138161207783018554
- Gong, T., Liu, L., Jiang, W., and Zhou, R. (2020). DAMP-sensing Receptors in Sterile Inflammation and Inflammatory Diseases. *Nat. Rev. Immunol.* 20 (2), 95–112. doi:10.1038/s41577-019-0215-7
- González-Ramos, S., Paz-García, M., Rius, C., Monte-Monge, A., Rodríguez, C., Fernández-García, V., et al. (2019). Endothelial NOD1 Directs Myeloid Cell Recruitment in Atherosclerosis through VCAM-1. *FASEB J.* 33 (3), 3912–3921. doi:10.1096/fj.201801231RR
- Goyette, J., and Geczy, C. L. (2011). Inflammation-associated S100 Proteins: New Mechanisms that Regulate Function. *Amino Acids* 41 (4), 821–842. doi:10.1007/s00726-010-0528-0
- Gu, Y., and Han, X. (2020). Toll-Like Receptor Signaling and Immune Regulatory Lymphocytes in Periodontal Disease. *Ijms* 21 (9), 3329. doi:10.3390/ijms21093329
- Gutsmann, T., Razquin-Olazarán, I., Kowalski, I., Kaonis, Y., Howe, J., Bartels, R., et al. (2010). New Antiseptic Peptides to Protect against Endotoxin-Mediated Shock. *Antimicrob. Agents Chemother.* 54 (9), 3817–3824. doi:10.1128/AAC.00534-10
- Hajishengallis, G. (2015). Periodontitis: from Microbial Immune Subversion to Systemic Inflammation. *Nat. Rev. Immunol.* 15 (1), 30–44. doi:10.1038/nri3785
- Han, Y., Hua, S., Chen, Y., Yang, W., Zhao, W., Huang, F., et al. (2021). Circulating PGLYRP1 Levels as a Potential Biomarker for Coronary Artery Disease and Heart Failure. *J. Cardiovasc. Pharmacol.* Publish Ahead of Print (5), 578–585. doi:10.1097/FJC.0000000000000996
- Haneklaus, M., and O'Neill, L. A. J. (2015). NLRP3 at the Interface of Metabolism and Inflammation. *Immunol. Rev.* 265 (1), 53–62. doi:10.1111/imr.12285
- Higashi, Y., Goto, C., Jitsuiki, D., Umemura, T., Nishioka, K., Hidaka, T., et al. (2008). Periodontal Infection Is Associated with Endothelial Dysfunction in Healthy Subjects and Hypertensive Patients. *Hypertension* 51 (2), 446–453. doi:10.1161/HYPERTENSIONAHA.107.101535
- Higuchi, K., Sm, Z., Yamashita, Y., Ozaki, Y., and Yoshimura, A. (2020). Initial Periodontal Treatment Affects Nucleotide-Binding Domain Leucine-Rich Repeat-Containing Protein 3 Inflammasome Priming in Peripheral Blood Mononuclear Cells. *Arch. Oral Biol.* 110, 104625. doi:10.1016/j.archoralbio.2019.104625
- Hirata, Y., Kurobe, H., Higashida, M., Fukuda, D., Shimabukuro, M., Tanaka, K., et al. (2013). HMGB1 Plays a Critical Role in Vascular Inflammation and Lesion Formation via Toll-like Receptor 9. *Atherosclerosis* 231 (2), 227–233. doi:10.1016/j.atherosclerosis.2013.09.010
- Hirschfeld, J., Dommisch, H., Skora, P., Horvath, G., Latz, E., Hoerauf, A., et al. (2015). Neutrophil Extracellular Trap Formation in Supragingival Biofilms. *Int. J. Med. Microbiol.* 305 (4-5), 453–463. doi:10.1016/j.ijmm.2015.04.002
- Hokamura, K., Inaba, H., Nakano, K., Nomura, R., Yoshioka, H., Taniguchi, K., et al. (2010). Molecular Analysis of Aortic Intimal Hyperplasia Caused by Porphyromonas Gingivalis Infection in Mice with Endothelial Damage. *J. Periodont Res.* 45 (3), 337–344. doi:10.1111/j.1600-0765.2009.01242.x
- Holmlund, A., Lampa, E., and Lind, L. (2017). Oral Health and Cardiovascular Disease Risk in a Cohort of Periodontitis Patients. *Atherosclerosis* 262, 101–106. doi:10.1016/j.atherosclerosis.2017.05.009
- Huang, Z., Wang, J., Xu, X., Wang, H., Qiao, Y., Chu, W. C., et al. (2019). Antibody Neutralization of Microbiota-Derived Circulating Peptidoglycan Dampens Inflammation and Ameliorates Autoimmunity. *Nat. Microbiol.* 4 (5), 766–773. doi:10.1038/s41564-019-0381-1
- Huck, O., Elkaim, R., Davideau, J.-L., and Tenenbaum, H. (2015). Porphyromonas Gingivalis-Impaired Innate Immune Response via NLRP3 Proteolysis in Endothelial Cells. *Innate Immun.* 21 (1), 65–72. doi:10.1177/1753425914523459
- Inaba, H., Hokamura, K., Nakano, K., Nomura, R., Katayama, K., Nakajima, A., et al. (2009). Upregulation of S100 Calcium-Binding Protein A9 Is Required for Induction of Smooth Muscle Cell Proliferation by a Periodontal Pathogen. *FEBS Lett.* 583 (1), 128–134. doi:10.1016/j.febslet.2008.11.036
- Isaza-Guzmán, D. M., Medina-Piedrahita, V. M., Gutiérrez-Henao, C., and Tobón-Arroyave, S. I. (2017). Salivary Levels of NLRP3 Inflammasome-Related Proteins as Potential Biomarkers of Periodontal Clinical Status. *J. Periodontol.* 88 (12), 1329–1338. doi:10.1902/jop.2017.170244
- Isola, G., Polizzi, A., Santonocito, S., Alibrandi, A., and Williams, R. C. (2021). Periodontitis Activates the NLRP3 Inflammasome in Serum and Saliva. *J. Periodontol.* 93, 135–145. doi:10.1002/JPER.21-0049
- Ito, Y., Bhawal, U. K., Sasahira, T., Toyama, T., Sato, T., Matsuda, D., et al. (2012). Involvement of HMGB1 and RAGE in IL-1 $\beta$ -induced Gingival Inflammation. *Arch. Oral Biol.* 57 (1), 73–80. doi:10.1016/j.archoralbio.2011.08.001
- Jayaprakash, K., Demirel, I., Khalaf, H., and Bengtsson, T. (2015). The Role of Phagocytosis, Oxidative Burst and Neutrophil Extracellular Traps in the Interaction between Neutrophils and the Periodontal pathogen Porphyromonas Gingivalis. *Mol. Oral Microbiol.* 30 (5), 361–375. doi:10.1111/omi.12099
- Jeon, D.-I., Park, S.-R., Ahn, M.-Y., Ahn, S.-G., Park, J.-H., and Yoon, J.-H. (2012). NOD1 and NOD2 Stimulation Triggers Innate Immune Responses of Human Periodontal Ligament Cells. *Int. J. Mol. Med.* 29 (4), 699–703. doi:10.3892/ijmm.2012.878
- Jiménez, C., Carvajal, D., Hernández, M., Valenzuela, F., Astorga, J., and Fernández, A. (2021). Levels of the Interleukins 17A, 22, and 23 and the S100 Protein Family in the Gingival Crevicular Fluid of Psoriatic Patients with or without Periodontitis. *Anais Brasileiros de Dermatologia* 96 (2), 163–170. doi:10.1016/j.abd.2020.08.008



- Jin, Y., Huang, H., Shu, X., Liu, Z., Lu, L., Dai, Y., et al. (2021). Peptidoglycan Recognition Protein 1 Attenuates Atherosclerosis by Suppressing Endothelial Cell Adhesion. *J. Cardiovasc. Pharmacol.* 78 (4), 615–621. doi:10.1097/FJC.0000000000001100
- Kaneko, C., Kobayashi, T., Ito, S., Sugita, N., Murasawa, A., Nakazono, K., et al. (2018). Circulating Levels of Carbamylated Protein and Neutrophil Extracellular Traps Are Associated with Periodontitis Severity in Patients with Rheumatoid Arthritis: A Pilot Case-Control Study. *PLoS One* 13 (2), e0192365. doi:10.1371/journal.pone.0192365
- Karki, R., and Kanneganti, T.-D. (2021). The 'cytokine Storm': Molecular Mechanisms and Therapeutic Prospects. *Trends Immunol.* 42 (8), 681–705. doi:10.1016/j.it.2021.06.001
- Kim, J.-S., Lee, S.-G., Oh, J., Park, S., Park, S.-I., Hong, S.-Y., et al. (2016a). Development of Advanced Atherosclerotic Plaque by Injection of Inflammatory Proteins in a Rabbit Iliac Artery Model. *Yonsei Med. J.* 57 (5), 1095–1105. doi:10.3349/ymj.2016.57.5.1095
- Kim, Y. K., Shin, J.-S., and Nahm, M. H. (2016b). NOD-like Receptors in Infection, Immunity, and Diseases. *Yonsei Med. J.* 57 (1), 5–14. doi:10.3349/ymj.2016.57.1.5
- Kishimoto, T., Kaneko, T., Ukai, T., Yokoyama, M., Ayon Haro, R., Yoshinaga, Y., et al. (2012). Peptidoglycan and Lipopolysaccharide Synergistically Enhance Bone Resorption and Osteoclastogenesis. *J. Periodontol. Res.* 47 (4), 446–454. doi:10.1111/j.1600-0765.2011.01452.x
- Knuefermann, P., Schwederski, M., Velten, M., Krings, P., Ehrentraut, H., Rudiger, M., et al. (2008). Bacterial DNA Induces Myocardial Inflammation and Reduces Cardiomyocyte Contractility: Role of Toll-like Receptor 9. *Cardiovasc. Res.* 78 (1), 26–35. doi:10.1093/cvr/cvn011
- Kojima, T., Andersen, E., Sanchez, J. C., Wilkins, M. R., Hochstrasser, D. F., Pralong, W. F., et al. (2000). Human Gingival Crevicular Fluid Contains MRP8 (S100A8) and MRP14 (S100A9), Two Calcium-Binding Proteins of the S100 Family. *J. Dent Res.* 79 (2), 740–747. doi:10.1177/00220345000790020701
- Køllgaard, T., Enevold, C., Bendtzen, K., Hansen, P. R., Givskov, M., Holmstrup, P., et al. (2017). Cholesterol Crystals Enhance TLR2- and TLR4-Mediated Pro-inflammatory Cytokine Responses of Monocytes to the Proatherogenic Oral Bacterium *Porphyromonas gingivalis*. *PLoS One* 12 (2), e0172773. doi:10.1371/journal.pone.0172773
- Koulics, C., Chen, Y.-C., Hausding, C., Ahrens, I., Kyaw, T. S., Tay, C., et al. (2014). Protective Role for Toll-like Receptor-9 in the Development of Atherosclerosis in Apolipoprotein E-Deficient Mice. *Atvb* 34 (3), 516–525. doi:10.1161/ATVBAHA.113.302407
- Krogmann, A. O., Lüsebrink, E., Steinmetz, M., Asdonk, T., Lahrmann, C., Lütjohann, D., et al. (2016). Proinflammatory Stimulation of Toll-like Receptor 9 with High Dose CpG ODN 1826 Impairs Endothelial Regeneration and Promotes Atherosclerosis in Mice. *PLoS One* 11 (1), e0146326. doi:10.1371/journal.pone.0146326
- Lee, J., Sohn, J. W., Zhang, Y., Leong, K. W., Pisetky, D., and Sullenger, B. A. (2011). Nucleic Acid-Binding Polymers as Anti-inflammatory Agents. *Proc. Natl. Acad. Sci.* 108 (34), 14055–14060. doi:10.1073/pnas.1105777108
- Lee, M. K., Ide, M., Coward, P. Y., and Wilson, R. F. (2008). Effect of Ultrasonic Debridement Using a Chlorhexidine Irrigant on Circulating Levels of Lipopolysaccharides and Interleukin-6. *J. Clin. Periodontol.* 35 (5), 415–419. doi:10.1111/j.1600-051X.2008.01221.x
- Li, L., Messas, E., Batista, E. L., Jr., Levine, R. A., and Amar, S. (2002). *Porphyromonas gingivalis* Infection Accelerates the Progression of Atherosclerosis in a Heterozygous Apolipoprotein E-Deficient Murine Model. *Circulation* 105 (7), 861–867. doi:10.1161/hc0702.104178
- Lian, D., Dai, L., Xie, Z., Zhou, X., Liu, X., Zhang, Y., et al. (2018). Periodontal Ligament Fibroblasts Migration Injury via ROS/TXNIP/Nlrp3 Inflammasome Pathway with *Porphyromonas gingivalis* Lipopolysaccharide. *Mol. Immunol.* 103, 209–219. doi:10.1016/j.molimm.2018.10.001
- Liang, H., Peng, B., Dong, C., Liu, L., Mao, J., Wei, S., et al. (2018). Cationic Nanoparticle as an Inhibitor of Cell-free DNA-Induced Inflammation. *Nat. Commun.* 9 (1), 4291. doi:10.1038/s41467-018-06603-5
- Lira-Junior, R., Holmström, S. B., Clark, R., Zwicker, S., Majster, M., Johannsen, G., et al. (2020). S100A12 Expression Is Modulated during Monocyte Differentiation and Reflects Periodontitis Severity. *Front. Immunol.* 11, 86. doi:10.3389/fimmu.2020.00086
- Liu, F., Sheng, S., Shao, D., Xiao, Y., Zhong, Y., Zhou, J., et al. (2021a). A Cationic Metal-Organic Framework to Scavenge Cell-free DNA for Severe Sepsis Management. *Nano Lett.* 21 (6), 2461–2469. doi:10.1021/acs.nanolett.0c04759
- Liu, J., Duan, J., Wang, Y., and Ouyang, X. (2014). Intracellular Adhesion Molecule-1 Is Regulated by *Porphyromonas gingivalis* Through Nucleotide Binding Oligomerization Domain-Containing Proteins 1 and 2 Molecules in Periodontal Fibroblasts. *J. Periodontol.* 85 (2), 358–368. doi:10.1902/jop.2013.130152
- Liu, J., Wang, Y., Liao, Y., Zhou, Y., and Zhu, J. (2021b). Circular RNA PPP1CC Promotes *Porphyromonas gingivalis*-Lipopolysaccharide-Induced Pyroptosis of Vascular Smooth Muscle Cells by Activating the HMGB1/TLR9/AIM2 Pathway. *J. Int. Med. Res.* 49 (3), 030006052199656. doi:10.1177/0300060521996564
- Lu, W. L., Song, D. Z., Yue, J. L., Wang, T. T., Zhou, X. D., Zhang, P., et al. (2017). NLRP3 Inflammasome May Regulate Inflammatory Response of Human Periodontal Ligament Fibroblasts in an Apoptosis-Associated Speck-like Protein Containing a CARD (ASC)-dependent Manner. *Int. Endod. J.* 50 (10), 967–975. doi:10.1111/iej.12722
- Luo, L., Xie, P., Gong, P., Tang, X.-h., Ding, Y., and Deng, L.-X. (2011). Expression of HMGB1 and HMGN2 in Gingival Tissues, GCF and PICF of Periodontitis Patients and Peri-Implantitis. *Arch. Oral Biol.* 56 (10), 1106–1111. doi:10.1016/j.archoralbio.2011.03.020
- Madrigal, A. G., Barth, K., Papadopoulos, G., and Genco, C. A. (2012). Pathogen-mediated Proteolysis of the Cell Death Regulator RIPK1 and the Host Defense Modulator RIPK2 in Human Aortic Endothelial Cells. *Plos Pathog.* 8 (6), e1002723. doi:10.1371/journal.ppat.1002723
- Maekawa, S., Onizuka, S., Katagiri, S., Hatasa, M., Ohsugi, Y., Sasaki, N., et al. (2019). RNA Sequencing for Ligature Induced Periodontitis in Mice Revealed Important Role of S100A8 and S100A9 for Periodontal Destruction. *Sci. Rep.* 9 (1), 14663. doi:10.1038/s41598-019-50959-7
- Magán-Fernández, A., O'Valle, F., Abadía-Molina, F., Muñoz, R., Puga-Guil, P., and Mesa, F. (2019). Characterization and Comparison of Neutrophil Extracellular Traps in Gingival Samples of Periodontitis and Gingivitis: A Pilot Study. *J. Periodont Res.* 54 (3), 218–224. doi:10.1111/jre.12621
- Mannherz, H. G., Peitsch, M. C., Zanotti, S., Paddenberger, R., and Polzar, B. (1995). A New Function for an Old Enzyme: the Role of DNase I in Apoptosis. *Curr. Top. Microbiol. Immunol.* 198, 161–174. doi:10.1007/978-3-642-79414-8\_10
- Martin, L., De Santis, R., Koczera, P., Simons, N., Haase, H., Heinbockel, L., et al. (2015). The Synthetic Antimicrobial Peptide 19-2.5 Interacts with Heparanase and Heparan Sulfate in Murine and Human Sepsis. *PLoS One* 10 (11), e0143583. doi:10.1371/journal.pone.0143583
- Martin, L., Horst, K., Chiazza, F., Oggero, S., Collino, M., Brandenburg, K., et al. (2016). The Synthetic Antimicrobial Peptide 19-2.5 Attenuates Septic Cardiomyopathy and Prevents Down-Regulation of SERCA2 in Polymicrobial Sepsis. *Sci. Rep.* 6, 37277. doi:10.1038/srep37277
- Martinez-Herrera, M., López-Domènech, S., Silvestre, F. J., Silvestre-Rangil, J., Bañuls, C., Victor, V. M., et al. (2018). Chronic Periodontitis Impairs Polymorphonuclear Leucocyte-Endothelium Cell Interactions and Oxidative Stress in Humans. *J. Clin. Periodontol.* 45 (12), 1429–1439. doi:10.1111/jcpe.13027
- Minton, K. (2019). Regulation of Endosomal TLRs. *Nat. Rev. Immunol.* 19 (11), 660–661. doi:10.1038/s41577-019-0229-1
- Mogensen, T. H. (2009). Pathogen Recognition and Inflammatory Signaling in Innate Immune Defenses. *Clin. Microbiol. Rev.* 22 (2), 240–273. Table of Contents. doi:10.1128/CMR.00046-08
- Moonen, C. G., Buurma, K. G., Faruque, M. R., Balta, M. G., Lieferink, E., Bizzarro, S., et al. (2020). Periodontal Therapy Increases Neutrophil Extracellular Trap Degradation. *Innate Immun.* 26 (5), 331–340. doi:10.1177/1753425919889392
- Morimoto, Y., Kawahara, K.-I., Tanchareon, S., Kikuchi, K., Matsuyama, T., Hashiguchi, T., et al. (2008). Tumor Necrosis Factor- $\alpha$  Stimulates Gingival Epithelial Cells to Release High Mobility-Group Box 1. *J. Periodontol. Res.* 43 (1), 76–83. doi:10.1111/j.1600-0765.2007.00996.x
- Morimoto-Yamashita, Y., Ito, T., Kawahara, K.-i., Kikuchi, K., Tatsuyama-Nagayama, S., Kawakami-Morizono, Y., et al. (2012). Periodontal Disease and Type 2 Diabetes Mellitus: Is the HMGB1-RAGE axis the Missing Link? *Med. Hypotheses* 79 (4), 452–455. doi:10.1016/j.mehy.2012.06.020
- Narayan, I., Gowda, T., Mehta, D., and Kumar, B. (2018). Estimation of Toll-like Receptor 9 in Gingival Tissues of Patients with Chronic Periodontitis with or

- without Hyperlipidemia and its Association with the Presence of *Porphyromonas gingivalis*. *J. Indian Soc. Periodontol.* 22 (4), 298–303. doi:10.4103/jisp.jisp\_124\_18
- Nativel, B., Couret, D., Giraud, P., Meilhac, O., d'Hellencourt, C. L., Viranaïcken, W., et al. (2017). *Porphyromonas gingivalis* Lipopolysaccharides Act Exclusively through TLR4 with a Resilience between Mouse and Human. *Sci. Rep.* 7 (1), 15789. doi:10.1038/s41598-017-16190-y
- Netea, M. G., Domínguez-Andrés, J., Barreiro, L. B., Chavakis, T., Divangahi, M., Fuchs, E., et al. (2020). Defining Trained Immunity and its Role in Health and Disease. *Nat. Rev. Immunol.* 20 (6), 375–388. doi:10.1038/s41577-020-0285-6
- Nijhuis, M. M. O., Pasterkamp, G., Sluis, N. I., de Kleijn, D. P. V., Laman, J. D., and Ulfman, L. H. (2007). Peptidoglycan Increases Firm Adhesion of Monocytes under Flow Conditions and Primes Monocyte Chemotaxis. *J. Vasc. Res.* 44 (3), 214–222. doi:10.1159/000100420
- Nijhuis, M. M. O., van der Graaf, Y., Melief, M.-J., Schoneveld, A. H., de Kleijn, D. P. V., Laman, J. D., et al. (2004). IgM Antibody Level against Proinflammatory Bacterial Peptidoglycan Is Inversely Correlated with Extent of Atherosclerotic Disease. *Atherosclerosis* 173 (2), 245–251. doi:10.1016/j.atherosclerosis.2003.12.005
- Ning, W., Ma, Y., Li, S., Wang, X., Pan, H., Wei, C., et al. (2021). Shared Molecular Mechanisms between Atherosclerosis and Periodontitis by Analyzing the Transcriptomic Alterations of Peripheral Blood Monocytes. *Comput. Math. Methods Med.* 2021, 1–28. doi:10.1155/2021/1498431
- Nishii, K., Usui, M., Yamamoto, G., Yajima, S., Tsukamoto, Y., Tanaka, J., et al. (2013). The Distribution and Expression of S100A8 and S100A9 in Gingival Epithelium of Mice. *J. Periodontol. Res.* 48 (2), 235–242. doi:10.1111/jre.12000
- Ohto, U., Shibata, T., Tanji, H., Ishida, H., Krayukhina, E., Uchiyama, S., et al. (2015). Structural Basis of CpG and Inhibitory DNA Recognition by Toll-like Receptor 9. *Nature* 520 (7549), 702–705. doi:10.1038/nature14138
- Olive, C. (2012). Pattern Recognition Receptors: Sentinels in Innate Immunity and Targets of New Vaccine Adjuvants. *Expert Rev. Vaccin.* 11 (2), 237–256. doi:10.1586/erv.11.189
- Oveis, M., Shifman, H., Fine, N., Sun, C., Glogauer, N., Senadheera, D., et al. (2019). Novel Assay to Characterize Neutrophil Responses to Oral Biofilms. *Infect. Immun.* 87 (2), 1. doi:10.1128/IAI.00790-18
- Paknejad, M., Sattari, M., Roozbahani, Z., Ershadi, M., and Mehrfard, A. (2016). Relationships between High-Mobility Group Protein B1 and Triggering Receptor Expressed on Myeloid Cells Concentrations in Gingival Crevicular Fluid and Chronic Periodontitis. *Iran J. Allergy Asthma Immunol.* 15 (5), 381–385.
- Pan, Y., Ke, H., Yan, Z., Geng, Y., Asner, N., Palani, S., et al. (2016). The Western-type Diet Induces Anti-HMGB1 Autoimmunity in ApoE<sup>-/-</sup> Mice. *Atherosclerosis* 251, 31–38. doi:10.1016/j.atherosclerosis.2016.05.027
- Papayannopoulos, V. (2018). Neutrophil Extracellular Traps in Immunity and Disease. *Nat. Rev. Immunol.* 18 (2), 134–147. doi:10.1038/nri.2017.105
- Peng, B., Liang, H., Li, Y., Dong, C., Shen, J., Mao, H. Q., et al. (2019). Tuned Cationic Dendronized Polymer: Molecular Scavenger for Rheumatoid Arthritis Treatment. *Angew. Chem. Int. Ed.* 58 (13), 4254–4258. doi:10.1002/anie.201813362
- Pradeep, A. R., Martande, S. S., Singh, S. P., Suke, D. K., Raju, A. P., and Naik, S. B. (2014). Correlation of Human S100A12 (EN-RAGE) and High-Sensitivity C-Reactive Protein as Gingival Crevicular Fluid and Serum Markers of Inflammation in Chronic Periodontitis and Type 2 Diabetes. *Inflamm. Res.* 63 (4), 317–323. doi:10.1007/s00011-013-0703-3
- Qi, M., Miyakawa, H., and Kuramitsu, H. K. (2003). *Porphyromonas gingivalis* Induces Murine Macrophage Foam Cell Formation. *Microb. Pathogenesis* 35 (6), 259–267. doi:10.1016/j.micpath.2003.07.002
- Radwan-Oczko, M., Jaworski, A., Duś, I., Plonek, T., Szulc, M., and Kustrzycki, W. (2014). *Porphyromonas gingivalis* Periodontal Pockets and Heart Valves. *Virulence* 5 (4), 575–580. doi:10.4161/viru.28657
- Rangé, H., Labreuche, J., Louedec, L., Rondeau, P., Planes, C., Sebbag, U., et al. (2014). Periodontal Bacteria in Human Carotid Atherothrombosis as a Potential Trigger for Neutrophil Activation. *Atherosclerosis* 236 (2), 448–455. doi:10.1016/j.atherosclerosis.2014.07.034
- Ribeiro, F., Santos, V., Bastos, M., De Miranda, T., Vieira, A., De Figueiredo, L., et al. (2012). A Preliminary Study on the FAM5C Expression in Generalized Chronic Periodontitis. *Oral Dis.* 18 (2), 147–152. doi:10.1111/j.1601-0825.2011.01855.x
- Rivera, M. F., Lee, J.-Y., Aneja, M., Goswami, V., Liu, L., Velsko, I. M., et al. (2013). Polymicrobial Infection with Major Periodontal Pathogens Induced Periodontal Disease and Aortic Atherosclerosis in Hyperlipidemic ApoE<sup>0/0</sup> Mice. *PLoS One* 8 (2), e57178. doi:10.1371/journal.pone.0057178
- Roth, G. A., Mensah, G. A., Johnson, C. O., Addolorato, G., Ammirati, E., Baddour, L. M., et al. (2020). Global Burden of Cardiovascular Diseases and Risk Factors, 1990–2019: Update from the GBD 2019 Study. *J. Am. Coll. Cardiol.* 76 (25), 2982–3021. doi:10.1016/j.jacc.2020.11.010
- Sanz, M., Marco Del Castillo, A., Jepsen, S., Gonzalez-Juanatey, J. R., D'Aiuto, F., Bouchard, P., et al. (2020). Periodontitis and Cardiovascular Diseases: Consensus Report. *J. Clin. Periodontol.* 47 (3), 268–288. doi:10.1111/jcpe.13189
- Satoh, M., Tabuchi, T., Itoh, T., and Nakamura, M. (2014). NLRP3 Inflammasome Activation in Coronary Artery Disease: Results from Prospective and Randomized Study of Treatment with Atorvastatin or Rosuvastatin. *Clin. Sci. (Lond)* 126 (3), 233–241. doi:10.1042/CS20130043
- Scheres, N., Laine, M. L., Sipos, P. M., Bosch-Tijhof, C. J., Crielaard, W., de Vries, T. J., et al. (2011). Periodontal Ligament and Gingival Fibroblasts from Periodontitis Patients Are More Active in Interaction with *Porphyromonas gingivalis*. *J. Periodontol. Res.* 46 (4), 407–416. doi:10.1111/j.1600-0765.2011.01353.x
- Shaddox, L. M., Gonçalves, P. F., Vovk, A., Allin, N., Huang, H., Hou, W., et al. (2013). LPS-induced Inflammatory Response after Therapy of Aggressive Periodontitis. *J. Dent Res.* 92 (8), 702–708. doi:10.1177/0022034513495242
- Shahbeik, S., Taleghani, F., Sattari, M., Mohammadi, M. M., and Moravej, M. (2021). Evaluation of NLRP3 and IL-18 Levels after Periodontal Therapy. *Ijai* 20 (6), 764–770. doi:10.18502/ijai.v20i6.8028
- Shao, B.-Z., Xu, Z.-Q., Han, B.-Z., Su, D.-F., and Liu, C. (2015). NLRP3 Inflammasome and its Inhibitors: a Review. *Front. Pharmacol.* 6, 262. doi:10.3389/fphar.2015.00262
- Shi, C., Dawulieti, J., Shi, F., Yang, C., Qin, Q., Shi, T., et al. (2022). A Nanoparticulate Dual Scavenger for Targeted Therapy of Inflammatory Bowel Disease. *Sci. Adv.* 8 (4), eabj2372. doi:10.1126/sciadv.abj2372
- Shin, M.-S., Kim, Y.-G., Shin, Y. J., Ko, B. J., Kim, S., and Kim, H.-D. (2019). Deep Sequencing Salivary Proteins for Periodontitis Using Proteomics. *Clin. Oral Invest.* 23 (9), 3571–3580. doi:10.1007/s00784-018-2779-1
- Silva, L. M., Doyle, A. D., Greenwell-Wild, T., Dutzan, N., Tran, C. L., Abusleme, L., et al. (2021). Fibrin Is a Critical Regulator of Neutrophil Effector Function at the Oral Mucosal Barrier. *Science* 374 (6575), eabl5450. doi:10.1126/science.abl5450
- Slots, J. (2017). Periodontitis: Facts, Fallacies and the Future. *Periodontol* 75 (1), 7–23. doi:10.1111/prd.12221
- Soehnlein, O., and Libby, P. (2021). Targeting Inflammation in Atherosclerosis - from Experimental Insights to the Clinic. *Nat. Rev. Drug Discov.* 20 (8), 589–610. doi:10.1038/s41573-021-00198-1
- Song, B., Zhang, Y., Chen, L., Zhou, T., Huang, W., Zhou, X., et al. (2017). The Role of Toll-like Receptors in Periodontitis. *Oral Dis.* 23 (2), 168–180. doi:10.1111/odi.12468
- Srisuwantha, R., Shiheido, Y., Aoyama, N., Sato, H., Kure, K., Laosrisin, N., et al. (2017). *Porphyromonas gingivalis* Elevated High-Mobility Group Box 1 Levels after Myocardial Infarction in Mice. *Int. Heart J.* 58 (5), 762–768. doi:10.1536/ihj.16-500
- Su, Z., Lu, H., Jiang, H., Zhu, H., Li, Z., Zhang, P., et al. (2015). IFN- $\gamma$ -producing Th17 Cells Bias by HMGB1-T-bet/RUNX3 axis Might Contribute to Progression of Coronary Artery Atherosclerosis. *Atherosclerosis* 243 (2), 421–428. doi:10.1016/j.atherosclerosis.2015.09.037
- Suh, J. S., Kim, S., Boström, K. I., Wang, C.-Y., Kim, R. H., and Park, N.-H. (2019). Periodontitis-induced Systemic Inflammation Exacerbates Atherosclerosis Partly via Endothelial-Mesenchymal Transition in Mice. *Int. J. Oral Sci.* 11 (3), 21. doi:10.1038/s41368-019-0054-1
- Takagi, R., Sakamoto, E., Kido, J.-i., Inagaki, Y., Hiroshima, Y., Naruishi, K., et al. (2020). S100A9 Increases IL-6 and RANKL Expressions through MAPKs and STAT3 Signaling Pathways in Osteocyte-like Cells. *Biomed. Res. Int.* 2020, 1–12. doi:10.1155/2020/7149408
- Thaiss, C. A., Zmora, N., Levy, M., and Elinav, E. (2016). The Microbiome and Innate Immunity. *Nature* 535 (7610), 65–74. doi:10.1038/nature18847
- Tsunooka, N., Nakagawa, H., Doi, T., Yukumi, S., Sato, K., Horiuchi, A., et al. (2005). Pitavastatin Prevents Bacterial Translocation after Nonpulsatile/low-Pressure Blood Flow in Early Atherosclerotic Rat: Inhibition of Small Intestine

- Inducible Nitric Oxide Synthase. *Eur. Surg. Res.* 37 (5), 302–311. doi:10.1159/000089242
- Velsko, I. M., Chukkappalli, S. S., Rivera, M. F., Lee, J.-Y., Chen, H., Zheng, D., et al. (2014). Active Invasion of Oral and Aortic Tissues by Porphyromonas Gingivalis in Mice Causally Links Periodontitis and Atherosclerosis. *PLoS One* 9 (5), e97811. doi:10.1371/journal.pone.0097811
- Viafara-García, S. M., Morantes, S. J., Chacon-Quintero, Y., Castillo, D. M., Lafaurie, G. I., and Buitrago, D. M. (2019). Repeated Porphyromonas Gingivalis W83 Exposure Leads to Release Pro-inflammatory Cytokines and Angiotensin II in Coronary Artery Endothelial Cells. *Sci. Rep.* 9 (1), 19379. doi:10.1038/s41598-019-54259-y
- Vijayakumar, E. C., Bhatt, L. K., and Prabhavalkar, K. S. (2019). High Mobility Group Box-1 (HMGB1): A Potential Target in Therapeutics. *Cdt* 20 (14), 1474–1485. doi:10.2174/1389450120666190618125100
- Vitkov, L., Klappacher, M., Hannig, M., and Krautgartner, W. D. (2009). Extracellular Neutrophil Traps in Periodontitis. *J. Periodontol. Res.* 44 (5), 664–672. doi:10.1111/j.1600-0765.2008.01175.x
- Vitkov, L., Muñoz, L. E., Knopf, J., Schauer, C., Oberthaler, H., Minnich, B., et al. (2021). Connection between Periodontitis-Induced Low-Grade Endotoxemia and Systemic Diseases: Neutrophils as Protagonists and Targets. *Ijms* 22 (9), 4647. doi:10.3390/ijms22094647
- Vogl, T., Eisenblätter, M., Völler, T., Zenker, S., Hermann, S., van Lent, P., et al. (2014). Alarmin S100A8/S100A9 as a Biomarker for Molecular Imaging of Local Inflammatory Activity. *Nat. Commun.* 5, 4593. doi:10.1038/ncomms5593
- Wan, M., Liu, J. R., Wu, D., Chi, X. P., and Ouyang, X. Y. (2015). E-selectin Expression Induced by Porphyromonas Gingivalis in Human Endothelial Cells via Nucleotide-Binding Oligomerization Domain-like Receptors and Toll-like Receptors. *Mol. Oral Microbiol.* 30 (5), 399–410. doi:10.1111/omi.12102
- Wang, X., Liu, Y., Zhang, S., Ouyang, X., Wang, Y., Jiang, Y., et al. (2020). Crosstalk between Akt and NF- $\kappa$ B Pathway Mediates Inhibitory Effect of Gas6 on Monocytes-endothelial Cells Interactions Stimulated by P. gingivalis-LPS. *J. Cell Mol Med* 24 (14), 7979–7990. doi:10.1111/jcmm.15430
- Wang, X., Ren, Y., Li, J., Ji, Z., Chen, F., and Wang, X. (2021). Identification of the 14-3-3  $\beta/\alpha$ -A Protein as a Novel Maternal Peptidoglycan-Binding Protein that Protects Embryos of Zebrafish against Bacterial Infections. *Dev. Comp. Immunol.* 114, 103867. doi:10.1016/j.dci.2020.103867
- Wang, Y., Chen, L., Tian, X., Shen, X., Wang, X., Wu, H., et al. (2018). CRISPR-Cas9 Mediated Gene Knockout in Human Coronary Artery Endothelial Cells Reveals a Pro-inflammatory Role of TLR2. *Cell Biol Int* 42 (2), 187–193. doi:10.1002/cbin.10885
- Wei, W., Ren, J., Yin, W., Ding, H., Lu, Q., Tan, L., et al. (2020). Inhibition of Ctsk Modulates Periodontitis with Arthritis via Downregulation of TLR9 and Autophagy. *Cell Prolif* 53 (1), e12722. doi:10.1111/cpr.12722
- White, P. C., Chicca, I. J., Cooper, P. R., Milward, M. R., and Chapple, I. L. C. (2016b). Neutrophil Extracellular Traps in Periodontitis. *J. Dent Res.* 95 (1), 26–34. doi:10.1177/0022034515609097
- White, P., Cooper, P., Milward, M., and Chapple, I. (2014). Differential Activation of Neutrophil Extracellular Traps by Specific Periodontal Bacteria. *Free Radic. Biol. Med.* 75 (Suppl. 1), S53. doi:10.1016/j.freeradbiomed.2014.10.827
- White, P., Sakellari, D., Roberts, H., Risafi, I., Ling, M., Cooper, P., et al. (2016a). Peripheral Blood Neutrophil Extracellular Trap Production and Degradation in Chronic Periodontitis. *J. Clin. Periodontol.* 43 (12), 1041–1049. doi:10.1111/jcpe.12628
- Wolf, A. J., Reyes, C. N., Liang, W., Becker, C., Shimada, K., Wheeler, M. L., et al. (2016). Hexokinase Is an Innate Immune Receptor for the Detection of Bacterial Peptidoglycan. *Cell* 166 (3), 624–636. doi:10.1016/j.cell.2016.05.076
- Xie, Y., Li, Y., Cai, X., Wang, X., and Li, J. (2016). Interleukin-37 Suppresses ICAM-1 Expression in Parallel with NF-Kb Down-Regulation Following TLR2 Activation of Human Coronary Artery Endothelial Cells. *Int. Immunopharmacology* 38, 26–30. doi:10.1016/j.intimp.2016.05.003
- Xuan, Y., Shi, Q., Liu, G.-J., Luan, Q.-X., and Cai, Y. (2017). Porphyromonas Gingivalis Infection Accelerates Atherosclerosis Mediated by Oxidative Stress and Inflammatory Responses in ApoE-/- Mice. *Clin. Lab.* 63 (10), 1627–1637. doi:10.7754/Clin.Lab.2017.170410
- Yamaguchi, Y., Kurita-Ochiai, T., Kobayashi, R., Suzuki, T., and Ando, T. (2015). Activation of the NLRP3 Inflammasome in Porphyromonas Gingivalis-Accelerated Atherosclerosis. *Pathog. Dis.* 73 (4), 1. doi:10.1093/femspd/ftv011
- Yamaguchi, Y., Kurita-Ochiai, T., Kobayashi, R., Suzuki, T., and Ando, T. (2017). Regulation of the NLRP3 Inflammasome in Porphyromonas Gingivalis-Accelerated Periodontal Disease. *Inflamm. Res.* 66 (1), 59–65. doi:10.1007/s00011-016-0992-4
- Yamamoto, K., Yamada, H., Wakana, N., Kikai, M., Terada, K., Wada, N., et al. (2018). Augmented Neutrophil Extracellular Traps Formation Promotes Atherosclerosis Development in Socially Defeated apoE-/- Mice. *Biochem. Biophysical Res. Commun.* 500 (2), 490–496. doi:10.1016/j.bbrc.2018.04.115
- Yipp, B. G., and Kubes, P. (2013). NETosis: How Vital Is it? *Blood* 122 (16), 2784–2794. doi:10.1182/blood-2013-04-457671
- Yoshihara-Hirata, C., Yamashiro, K., Yamamoto, T., Aoyagi, H., Ideguchi, H., Kawamura, M., et al. (2018). Anti-HMGB1 Neutralizing Antibody Attenuates Periodontal Inflammation and Bone Resorption in a Murine Periodontitis Model. *Infect. Immun.* 86 (5), 1. doi:10.1128/IAI.00111-18
- Yost, S., Duran-Pinedo, A. E., Teles, R., Krishnan, K., and Frias-Lopez, J. (2015). Functional Signatures of Oral Dysbiosis during Periodontitis Progression Revealed by Microbial Metatranscriptome Analysis. *Genome Med.* 7 (1), 27. doi:10.1186/s13073-015-0153-3
- Yu, L., Zhou, C., Wei, Z., and Shi, Z. (2019). Effect of Combined Periodontal-Orthodontic Treatment on NOD-like Receptor Protein 3 and High Mobility Group Box-1 Expressions in Patients with Periodontitis and its Clinical Significance. *Medicine (Baltimore)* 98 (44), e17724. doi:10.1097/MD.00000000000017724
- Yu, W., Zheng, Y., Li, H., Lin, H., Chen, Z., Tian, Y., et al. (2020). The Toll-like Receptor Ligand, CpG Oligodeoxynucleotides, Regulate Proliferation and Osteogenic Differentiation of Osteoblast. *J. Orthop. Surg. Res.* 15 (1), 327. doi:10.1186/s13018-020-01844-x
- Zhang, W., Jia, L., Zhao, B., Xiong, Y., Wang, Y.-N., Liang, J., et al. (2021). Quercetin Reverses TNF- $\alpha$  I-induced O-steogenic D-amage to H-human P-eriodontal L-igament S-tem C-ells by S-uppressing the NF- $\kappa$ B/NLRP3 I-nflammasome P-athway. *Int. J. Mol. Med.* 47 (4), 1. doi:10.3892/ijmm.2021.4872
- Zhen, Y., and Zhang, H. (2019). NLRP3 Inflammasome and Inflammatory Bowel Disease. *Front. Immunol.* 10, 276. doi:10.3389/fimmu.2019.00276
- Zheng, S., Yu, S., Fan, X., Zhang, Y., Sun, Y., Lin, L., et al. (2021). Porphyromonas Gingivalis Survival Skills: Immune Evasion. *J. Periodontol. Res.* 56 (6), 1007–1018. doi:10.1111/jre.12915
- Zhou, J., and Deng, G. M. (2021). The Role of Bacterial DNA Containing CpG Motifs in Diseases. *J. Leukoc. Biol.* 109 (5), 991–998. doi:10.1002/JLB.3MR1220-748RRRRR
- Zou, W., Schwartz, H., Endres, S., Hartmann, G., and Bar-Shavit, Z. (2002). CpG Oligonucleotides: Novel Regulators of Osteoclast Differentiation. *FASEB j.* 16 (3), 274–282. doi:10.1096/fj.01-0586com

**Conflict of Interest:** The authors declare that the research was conducted in the absence of any commercial or financial relationships that could be construed as a potential conflict of interest.

**Publisher's Note:** All claims expressed in this article are solely those of the authors and do not necessarily represent those of their affiliated organizations, or those of the publisher, the editors and the reviewers. Any product that may be evaluated in this article, or claim that may be made by its manufacturer, is not guaranteed or endorsed by the publisher.

Copyright © 2022 Zhu, Huang and Zhao. This is an open-access article distributed under the terms of the Creative Commons Attribution License (CC BY). The use, distribution or reproduction in other forums is permitted, provided the original author(s) and the copyright owner(s) are credited and that the original publication in this journal is cited, in accordance with accepted academic practice. No use, distribution or reproduction is permitted which does not comply with these terms.



# DNA Methylation Aberrant in Atherosclerosis

Yao Dai\*, Danian Chen and Tingting Xu

Department of Cardiology, The First Affiliated Hospital of Anhui Medical University, Hefei, China

Atherosclerosis (AS) is a pathological process involving lipid oxidation, immune system activation, and endothelial dysfunction. The activated immune system could lead to inflammation and oxidative stress. Risk factors like aging and hyperhomocysteinemia also promote the progression of AS. Epigenetic modifications, including DNA methylation, histone modification, and non-coding RNA, are involved in the modulation of genes between the environment and AS formation. DNA methylation is one of the most important epigenetic mechanisms in the pathogenesis of AS. However, the relationship between the progression of AS and DNA methylation is not completely understood. This review will discuss the abnormal changes of DNA methylation in AS, including genome-wide hypermethylation dominating in AS with an increase of age, hypermethylation links with methyl supply and generating hyperhomocysteinemia, and the influence of oxidative stress with the demethylation process by interfering with the hydroxyl-methylation of TET proteins. The review will also summarize the current status of epigenetic treatment, which may provide new direction and potential therapeutic targets for AS.

## OPEN ACCESS

### Edited by:

Xianwei Wang,  
Xinxiang Medical University, China

### Reviewed by:

Zuo Wang,  
University of South China, China  
Bela Molnar,  
Semmelweis University, Hungary

### \*Correspondence:

Yao Dai  
daiyaoh@163.com

### Specialty section:

This article was submitted to  
Cardiovascular and Smooth Muscle  
Pharmacology,  
a section of the journal  
Frontiers in Pharmacology

Received: 16 November 2021

Accepted: 24 January 2022

Published: 03 March 2022

### Citation:

Dai Y, Chen D and Xu T (2022) DNA  
Methylation Aberrant  
in Atherosclerosis.  
Front. Pharmacol. 13:815977.  
doi: 10.3389/fphar.2022.815977

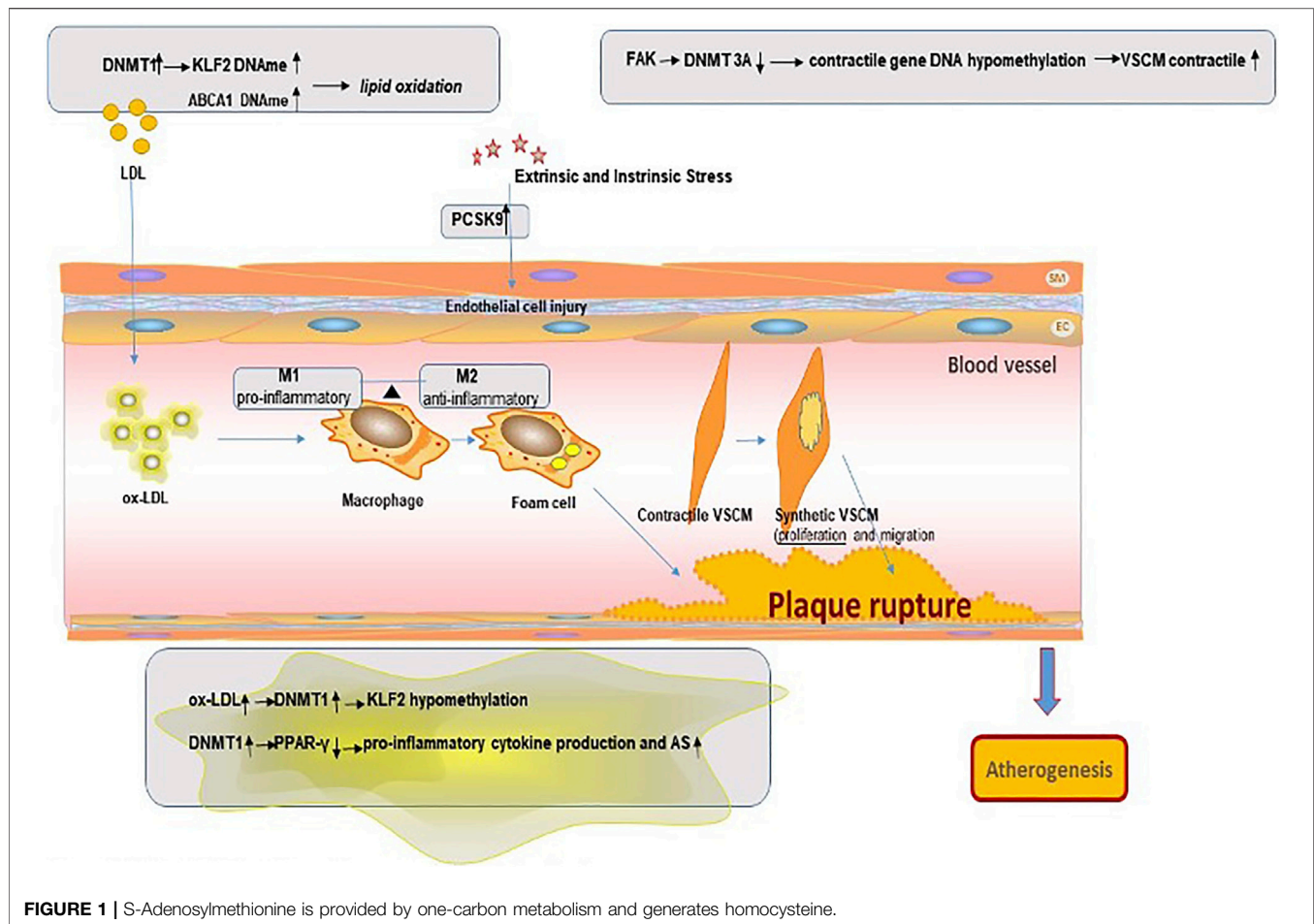
**Keywords:** atherosclerosis, DNA methylation, hyperhomocysteinemia, oxidative stress, aging

## INTRODUCTION

Atherosclerosis (AS) is the pathological basis in heavy cardiovascular diseases like unstable angina pectoris, acute myocardial infarction, and abdominal aortic aneurysm (Tabas et al., 2015). Due to hidden onset, these diseases are difficult to detect and diagnose in the early stage, and serious damage has been caused and a heavy economic burden is imposed once discovered (Zhao et al., 2019). AS is a complex pathological processes beginning with the accumulation of lipids in damaged vessel walls and oxidative modification to oxidized low-density lipoproteins (ox-LDLs), activation immune system, rapid reaction inflammatory, followed with endothelial cell (ECs) activation, arterial smooth muscle cell (SMC) proliferation, activation of macrophages, and formation of foam cells (Tabaei and Tabae, 2019). In this process, monocytes/macrophages, vascular smooth muscle cells (VSMCs), and vascular endothelial cells (VECs) are all involved in the pathological process (Yuan et al., 2020; Botts et al., 2021). In clinical practice, AS is associated with certain diseases like hyperlipidemia, diabetes mellitus, hyperhomocysteinemia, and hyperuricemia (Jiang et al., 2021). On the other hand, male, smoking history, obesity, aging, and poor lifestyle can also lead to AS (Rizzacasa et al., 2019).

The epigenetic modifications mostly include DNA methylation, histone modification, and non-coding RNAs. Nowadays, genotyping methods supported by statistical and computational approaches enabled large-scale genome-wide association studies (GWAS), in which a large number of genetic variants are investigated in a search for links with the trait of interest. Genetic variants that are too rare to be detected by GWAS are aggregated into subsets, and their frequency is compared between patients and control. More recently, next-generation sequencing (NGS) technologies have also better improved this problem (Veljkovic et al., 2018).





Epigenetic modifications have been proved in so many medical research, such as breast cancer, lung cancer, and thyroid cancer, and already contributed major new molecular biology markers, genes, or pathways (Patani et al., 2020). Among these, DNA methylation is the most well-studied epigenetic mark partly due to the development of multiple approaches to assay it, including microarrays and bisulfite sequencing, and its relative stability allowing for profiling of previously collected stored DNA samples (Rask-Andersen et al., 2016). In recent years, GWAS of coronary heart disease (CHD) have identified some genetic risk factors. On the other hand, the association between phenotype and DNA methylation changes across the genome is assessed through epigenome-wide association studies (EWASs) (Xia et al., 2021). So, in this article, we want to illustrate the specific regulatory mechanisms of DNA methylation in the pathogenesis of AS. The main objectives of this review are (1) to describe the dynamic balance and adjustment process of methylation and demethylation, (2) to study the DNA methylation changes in lipid oxidation, vascular smooth muscle cells, vascular endothelial cells, mononuclear-macrophage activation, oxidative stress, and vascular aging, (3) to analyze the influence of linked risk factors like homocysteine, aging, and metabolism on DNA methylation in AS, and (4) to

explore current clinical methylation studies on therapy in AS patients.

## DNA Methylation/Demethylation

DNA methylation (DNAm) is one of the most well-understood epigenetic modifications concentrating to happen in the CPG islands region (CGIs) (Papin et al., 2020). The presence of DNAm in promoter and enhancer will be associated with gene silencing (Stratton et al., 2019). The level of methylation is inversely proportional to the level of gene expression, and the position of methylation in a transcription unit affects its relationship to gene control.

Nowadays, accumulating evidence has suggested that DNAm may be reversible in mammalian cells. The regulation by DNAm is at times quite dynamic (Parry et al., 2021). Abnormal increases or decreases in DNA methylation contribute to or are closely related to different diseases like cancers and atherosclerosis (Ehrlich, 2019). The DNAm turnover depends on the DNA methyltransferases (DNMTs) writing the methylation mode, and ten-eleven translocation (TET) enzymes remove their activity (Parry et al., 2021).

DNAm is an epigenetic modification catalyzed by DNA methyltransferases (DNMTs). Adding methyl ( $\text{CH}_3$ ) from

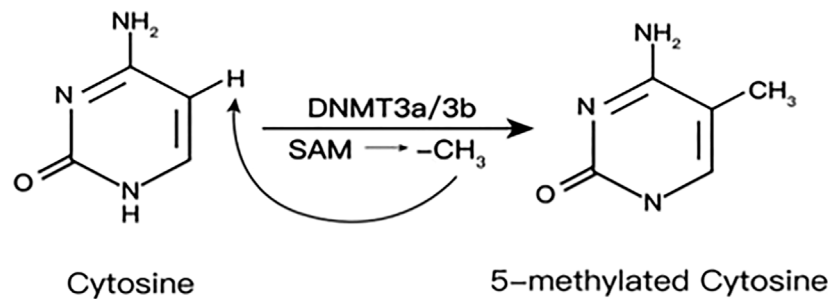


**FIGURE 2 |** Mechanism of DNA methylation in the pathogenesis of atherosclerosis plaque.

S-adenosylmethionine (SAM) to the C5 position of the cytosine base will convert cytosine–guanosine into CpGs (Schiano et al., 2020). SAM is provided by one carbon metabolism and generates homocysteine (HCys) (Shen et al., 2020) (**Figure 1**)

DNMTs family include DNMT1, 2, 3A, 3B, and 3L. DNMT1 is the key enzyme to maintain DNAm, which is responsible for maintaining the existing methylation patterns (Gujar et al., 2019). DNMT2 lacks DNA methyltransferase activity, mainly catalyzing the methylation of RNA as a transfer RNA (tRNA) methyltransferase. DNMT3A and DNMT3B mediate *de novo* methylation in undifferentiated cells, which contribute to the formation and subsequent maintenance of DNAm marks. DNMT3L mainly regulates DNAm during early embryogenesis, actually expressed only in germ cells and embryonic stem cells but not in somatic cells (Veland et al., 2019).

In the process of catalytic methylation, the various enzymes interact with each other. Research shows that knockout Dnmt3a and Dnmt3b in mouse embryonic cells will result in a gradual loss of DNAm over time, indicating that the involvement of Dnmt3a/Dnmt3b also plays an important role in maintaining DNAm profiles during embryonic development (Chen et al., 2003) (**Figure 2**).

In recent years, the discovery of 5-hydroxymethyl cytosine (5-hmC) has opened a new horizon of the process in removing methyl marks from DNA (Bhutani et al., 2011). The TET family, including TET1, 2, and 3, catalyzes the oxidation of 5-mC to 5-hmC to get the methyl marks removed.

TET2 dominates a protective role in preventing AS by repressing the VSMC phenotype transformation, protecting ECs from damage and dysfunction and inhibiting inflammation (Liu et al., 2018). All of the TETs are Fe(II)-dependent dioxygenases and require Fe (II) as cofactors. Oxidative stress will block the reduction of Fe(III) back to Fe(II), causing less regeneration of active enzyme (Niu et al., 2015).

## DNA Methylation Abnormalities in AS

Multiple studies have shown that DNA methylation is associated with atherosclerotic phenotypes. Aberrant DNA methylation, including hypermethylation and hypomethylation, plays an important role in AS (Chistiakov et al., 2017). In healthy individuals, CGIs in the promoter region of genes are, in general, hypomethylated, whereas CpGs in the non-promoter

region are hypermethylated (Khyzha et al., 2017). Global DNA hypomethylation (which is known as DNA hypomethylation of non-promoter regions) can cause structural changes and the instability of chromosomes because of the initiation of transcription at incorrect regions and the high transcriptional activity in sites that are usually silent (Zhang et al., 2021). Genome-wide DNA hypomethylation leads to the expression of potentially harmful genes and also the high expression of genes that are meant to be silent. Conversely, genome-wide DNA hypermethylation causes the inactivation of disease-suppressor genes or protective genes, gene mutation, and allelic loss.

In total, DNA methylation is catalyzed by DNA methylation transferases (DNMT1, DNMT3A, and DNMT3B) and reversed by TET proteins (TET1, TET2, and TET3), which maintain a state of dynamic equilibrium over the course of life (Bhutani et al., 2011).

## Genome-Wide Hypermethylation in AS

Views on genome-wide DNAm state in AS are varied. Hypermethylation may dominate in AS lesions as pointed out in recent reports. With lesion progression, DNAm drifted toward hypermethylation (Valencia-Morales et al., 2015; Lacey et al., 2019)—for example, a recent study finds that DNMT3B-mediated CREG gene hypermethylation becomes a novel mechanism, which may contribute to endothelial dysfunction and atherosclerosis development (Liu et al., 2020).

Silvio Zaina et al. (2014) have examined DNAm levels using whole-genome bisulfite sequencing. They observed that the atherosclerotic portion of the aorta was hypermethylated across many genomic loci in comparison with the matched healthy counterpart. This study using a high-throughput DNA methylation microarray and covering more than 450,000 CpG sites found the repeat element *Alu* to be also hypermethylated. The study also found that TET2 is decreased in atherosclerotic lesion. A deficiency of this study may be its use of post-mortem donor-matched atherosclerotic and non-atherosclerotic portions, which could not better reflect the dynamic changes of arteriosclerosis *in vivo* and do not specifically describe the level of gene methylation in live exact tissues.

Another study (Sharma et al., 2014) collected blood samples from angiographically confirmed CAD patients and healthy controls. It has identified 72 different methylated regions that were hypermethylated in CAD patients in the background of

**TABLE 1** | Summary of differences in genome-wide methylation in AS.

Authors	Measurement	DNAm		Reference
Valencia-Morales Mdel P	Microarray	Hypermethylation	2015	Valencia-Morales et al. (2015)
Lacey M	Bisulfite sequencing	Hypermethylation	2019	Lacey et al. (2019)
Liu Y	Bisulfate sequencing	Hypermethylation	2020	Liu et al. (2020)
Zaina et al.	Whole-genome bisulfite sequencing	Hypermethylation	2014	Zaina et al. (2014)
Sharma	Bisulfite 454 sequencing	Hypermethylation	2014	Sharma et al. (2014)
Wang X	NGS, microarrays	Hypomethylation	2018	Wang et al. (2018)

varying homocysteine levels and found methylation to be significantly higher in CAD cases. Though this study took blood from living persons as research objects, a high level of homocysteine could enhance the DNMT expression level, which leads to hypermethylation and affects the judgment results.

## Genome-Wide Hypomethylation in AS

The occurrence of DNA methylation patterns exists in inter-individual variation; genome-wide hypomethylation also exists in AS. Wang et al. (2018) collected various tissues from six patients who underwent coronary artery bypass surgery, including atherosclerotic plaques, great saphenous vein, and internal mammary artery. They have found that the genes which participated in immune response-associated pathways (cytokine–cytokine receptor interactions and the MAPK signaling pathway) in AS were enriched by the hypomethylated genes. However, the limitations of this study are the relatively small sample size and the fact that data may be biased because of the possible effects of the drugs given to the patients for treatment. Other studies have found that genes hypomethylated in AS may include keratin gene, ATP-binding proteins, cells of the skeleton, and chromatin regulatory protein-related genes (Aavik et al., 2015).

In conclusion, analyzing multiple cell types involved in atherosclerotic lesions at the single-cell DNAm level for the global methylation status appears to be rather difficult. The DNAm status on gene expression depends on its position in the whole genome, one of the reasons of which is that methylation near transcriptional start sites (TSSs) blocks initiation, but genomic methylation does not block initiation and may even stimulate transcriptional lengthening (Jones, 2012).

Genome-wide methylation in AS only reflected probable methylation levels, but specific “target” genes need to be studied moving forward. More testing tools that have been used, such as NGS, may help to distinguish patterns of DNA methylation of various atherosclerotic tissues and specific epigenetic characteristics (Zhong et al., 2021). (Table 1)

## DNA Methylation Link With Lipid Oxidation

AS is a set of processes driven by lipid plaque formation. Hyperlipidemia is considered as the major contributor for the development of atherosclerotic cardiovascular diseases (Zafeiropoulos et al., 2021). Multiple EWASs have explored total cholesterol, low-density lipoprotein cholesterol (LDL-C), and triacylglycerol (TG), which are pro-atherogenic, and high-density lipoprotein cholesterol (HDL-C), which is anti-

atherogenic (Hedman et al., 2017). Genes related to lipid metabolism include Kruppel-like factor 2 (KLF2), ATP-binding cassette transporter A1 (ABCA1), and so on.

Lipid oxidation is the initiating factor in the atherogenesis process. The pivotal role of low-density lipoprotein cholesterol (LDL-C) has been well studied and widely recognized. Epigenetic regulation has been observed in low-density lipoprotein oxidation—for example, the upregulated expression of DNMT1 causes methylation of the promoter region of KLF2 in human umbilical vein endothelial cells (HUVECs) treated with oxidized low-density lipoprotein (ox-LDL) (Yan et al., 2017).

The ATP-binding cassette transporter A1 (ABCA1), an important gene associated with lipid metabolism, which could mediate the outflow of phospholipid and cholesterol, binds apolipoprotein A-I (apoA-I) on the cell surface, forms high-density lipoprotein (HDL), reduces the lipid content of plasma membrane free cholesterol, reduces the taxis ability of macrophages, and delays the pathological progress of AS (Ghaznavi et al., 2018). At the same time, ABCA1-mediated cholesterol efflux can change the lipid microenvironment of the cell membrane, activate the anti-inflammatory signaling pathway, and play an important anti-inflammatory role. ABCA1 is a key regulator of cholesterol reverse transport from peripheral tissues back to the liver and participates in the initial stage of cholesterol reverse transport (RCT). Functional defects of ABCA1 may impair the activity of RCT and lead to the formation of foam cells (Annema and Tietge, 2012). In a study of patients with familial hypercholesterolemia, ABCA1 promoter methylation was confirmed to be related to the occurrence of hypercholesterolemia (Peng et al., 2014). In addition, studies have also reported that there is a significant correlation between the methylation level of ABCA1 gene promoter and aging. The abnormally increased methylation level of the ABCA1 gene promoter in elderly patients with stable angina pectoris may be related to the fact that most elderly patients have a long history of atherosclerosis and hyperlipidemia. Prolonged disease states can lead to the accumulation of epigenetic changes (Ghaznavi et al., 2018).

That notwithstanding, the exact molecular mechanisms underlying DNA methylation modulation by lipid oxidation and the association between the global DNA methylation and regulation of atherosclerosis-specific genes are not fully understood. Further investigations to resolve these issues may lead to the identification of novel therapeutic targets to treat atherosclerosis induced by lipid oxidation.

## DNA Methylation Link With Vascular Endothelial Cells in AS

Vascular endothelial cells (ECs) play a key role in local vasodilation, oxygen-free radical generation, and blood vessel homeostasis (Lovren and Verma, 2013). Endothelial dysfunction is one of the main factors causing AS. Studies have found that in all patients, no matter with mild coronary artery disease (CAD) or advanced CAD, endothelium-dependent vasodilation disorder was observed, indicating that endothelial function can be disordered and involved in the entire development of atherosclerosis (Ludmer et al., 1986). Flow shear stress plays an important role in endothelial cell phenotype. In addition, decreased NO bioavailability, vascular oxidative stress, inflammatory response, vascular aging, and hemodynamics can induce endothelial dysfunction and the typical features of early atherosclerotic lesions (Davies et al., 2013).

Unsurprisingly, DNA methylation changes are readily detectable in atherosclerotic tissues—for example, a significant hypomethylation of CpG dinucleotides was measured in the coding region of extracellular superoxide dismutase from rabbit aortic atherosclerotic lesion when compared with normal intima-media (Laukkanen et al., 2002). Proprotein convertase subtilisin/kexin type 9 (PCSK9) plays an important role in cholesterol and fatty acid metabolism. PCSK9 expression in vascular smooth muscle cells (SMCs) and endothelial cells (ECs) reached a maximal value at low shear stress and then began to decline with an increase in shear stress. Researchers found that the PCSK9 promoter DNA methylation may be linked with CAD (Shyamala et al., 2021).

## DNA Methylation and Inflammation in AS

AS is widely known as an inflammatory disease involving immune cell subsets of various lineages, like T cells, B cells, foam cells, and monocytes-macrophages, in which macrophage plays a major role in the progression of lesions (Swirski et al., 2007). During the formation of atherosclerotic plaques, macrophage phagocytosis of oxidized low-density lipoprotein becomes a major contributor to the inflammatory response by secreting pro-inflammatory mediators, eventually dying from necrosis or apoptosis (Davis and Gallagher, 2019). Dying macrophages release their lipid content and tissue factors, then leading to the formation of necrotic prethrombotic cores as a key component of unstable plaques (Davis and Gallagher, 2019).

Macrophages are characterized by a remarkable degree of plasticity, influenced by the affected sites and microenvironment in atherosclerotic lesions, which can be differentiated into M1 and M2 phenotypes through different activation pathways, while the two phenotypes keep a dynamic equilibrium (Jia et al., 2017). M1 macrophage performs a pro-inflammatory character, expressing high levels of pro-inflammatory cytokines such as tumor necrosis factor  $\alpha$ , interleukin-6, and interleukin-1 $\beta$ , which predominate in the progression of atherosclerotic lesions and vulnerable plaques (Bakshi et al., 2019). On the contrary, M2-type usually expresses high levels of anti-inflammatory cytokines, such as interleukin-10 and recombinant human arginase-1, plays an

anti-inflammatory role, and predominates in stable plaque and early atherosclerosis (Tabas and Bornfeldt, 2016). A significant hallmark of atherosclerosis is the accumulation of pro-inflammatory metabolites in coronary arteries that respond to pro-atherogenic stimuli, such as free fatty acids (FFAs) and oxidized LDLs (ox-LDLs), and the failure to digest lipids that contribute to the formation of foam cells in atherosclerotic plaques (Eshghjoo et al., 2021).

In recent years, growing research has focused on changes in DNA methylation as observed in AS-associated inflammation—for instance, Kumar A and colleagues showed that oxidized LDL (ox-LDL) stimulation of endothelial cells could upregulate DNMT1 and lead to the methylation of the promoter of the gene encoding KLF2. KLF2 plays an important role in vascular endothelial cell immunity and homeostasis. In addition, this effect of ox-LDL on KLF2 methylation can be reversed by treating endothelial cells with the DNMT inhibitor 5-azacytidine (5-azacine) (Kumar et al., 2013). Another important immune regulator, peroxisome proliferator-activated receptor-gamma (PPAR- $\gamma$ ), has anti-inflammatory effects; its dysfunction can lead to lipid accumulation. PPAR- $\gamma$  is able to promote macrophages to polarize towards M2-like phenotypes and inhibit M1 macrophage polarization. Additional PPAR- $\gamma$  or pharmacological activation of PPAR- $\gamma$  effectively prevented DNMT1-induced pro-inflammatory cytokine production in macrophages and AS development in the mouse model. A study in a mouse model found that the DNA methylation status of the proximal PPAR- $\gamma$  promoter was regulated by DNMT1 in macrophages. The DNMT1-PPAR $\gamma$  pathway in macrophages can regulate chronic inflammation and AS development in mice (Yu et al., 2016).

Similarly, DNA methylation can also affect the development, polarization, and activation of macrophages. It has been observed that the DNA methylation status has changed in monocytes and macrophages during atherogenesis, which may have an influence on monocyte-to-macrophage differentiation and the activation of these two types of cell (Jia et al., 2017). One study compared the gene-specific promoter DNA methylation status of macrophage polarization genes in peripheral blood mononuclear cells (PBMCs) between coronary atherosclerotic heart disease (CHD) cases and controls, showing that the DNA methylation level of M1 macrophage genes was decreased in patients with CAD (Bakshi et al., 2019). This may indicate that the M1 type of pro-inflammatory macrophages may play a dominant role in CHD. Another study involved monocyte chemoattractant protein-1 (MCP-1), which is related to the migration and gathering of monocytes, and found MCP-1 expression due to DNA hypomethylation induced by Hcys mediated by NF- $\kappa$ B/DNMT1 (Wang et al., 2013).

In summary, the methylation of inflammatory cells in AS is mainly manifested as hypomethylation of pro-inflammatory factors and hypermethylation of anti-inflammatory factors, which is particularly consistent with the aggregation of inflammatory cells and adhesion to ECs in the progression of AS.

## Aberrant DNA Methylation in VSMCs

Vascular smooth muscle cell (VSMC) is one of the main cell types in blood vessel wall, and VSMC proliferation and apoptosis are



involved in the development of atherosclerosis (Clarke and Bennett, 2006). During the development of AS, VSMCs can convert to multiple phenotypes, including calcification (osteogenesis, chondrogenesis, and osteocytosis) and macrophage surface type. On the one hand, some VSMCs acquire macrophages during phenotypic transformation, characteristically differentiating into lipid-loaded foam cell-like macrophages through healthy low ability to clear lipids, dead cells, and necrotic debris and the exacerbation of inflammation to promote atherosclerosis. On the other hand, VSMCs tend to calcify phenotypic transformation. Phenotypic plasticity and osteochondral differentiation in VSMCs play a key role in atherosclerotic intima calcification (Harith et al., 2016). Intimal calcification and atherosclerotic adverse events, such as plaque rupture, myocardial infarction, stroke and other important relationship. VSMCs regulate phenotypes promotes cell proliferation, which is involved in the whole process of AS (Elia et al., 2019).

Recently, studies have demonstrated that methylation modulated the atherogenic profile also of VSMCs. They handled primary VSMCs with platelet-derived growth factor-BB strongly expressed UHRF1, in cooperation with DNMT1, and found positively modulated the methylation status of different genes associated with VSMC differentiation, such as smooth muscle actin 2, smooth muscle-myosin heavy chain 11 and some proteins (Elia et al., 2018). Strong plasticity and phenotypic transformation of VSMCs play an important role in the formation of AS. Focal adhesion kinase (FAK) could activation elicits VSMC dedifferentiation by stabilizing DNA methyltransferase 3A (DNMT3A). Reduced DNMT3A protein led to DNA hypomethylation in contractile gene promoters, which increased VSMC contractile protein expression. It was also observed that VSMCs in human atherosclerotic lesions show reduced nuclear FAK, which is associated with increased DNMT3A levels and decreased contractile gene expression (Jeong et al., 2021).

To sum up, DNA methylation was observed in nearly all of the pathogenesis of atherosclerosis plaque. The findings of DNA methylation changes may open avenues for novel treatment for CAD management.

## Risk Factors Associated With AS and Methylation

AS is a common clinical disease often associated with other diseases as their end-stage complication—for example, hyperlipidemia, diabetes mellitus, hyperhomocysteinemia, and hyperuricemia (Jiang et al., 2021). In this article, we want to highlight some relevant risk factors that are well known in current studies.

## DNA Methylation Changes Associated With Oxidative Stress

Oxidative stress has been widely accepted as another important risk factor for atherosclerotic cardiovascular diseases (CVD) (Salvayre et al., 2016). Many CVD have been associated, in

part or completely, with oxidative stress. Oxidative stress is a process which is damaging to various organs and tissues and caused by reactive oxygen species at the cellular level.

Reactive oxygen species (ROS) accounted for an important proportion. ROS, one important product generated by redox reaction with one or more unpaired electrons in the external shell, includes super oxygen anion ( $O_2^-$ ) and hydrogen peroxide ( $H_2O_2$ ) (Chen et al., 2007). Various metabolic disorders in the body and aging contribute to the imbalance between oxidative and antioxidant mechanisms, leading to ROS-mediated damage (Izzo et al., 2021).

In the cardiovascular system, the excessive formation of  $O_2^-$  leads to the oxidative inactivation of NO and a decrease in its bioavailability (Sazonova et al., 2021). NO has a variety of vascular-protective effects, ranging from vasodilation, anti-aggregation, and anti-inflammatory effects to inhibition of lipid oxidation and vascular smooth muscle hyperplasia (Ritchie et al., 2017). Therefore, the reduction of NO production has a directly promoting effect on atherosclerosis. In addition, oxidative stress plays an important role in lipid peroxidation. Low-density lipoprotein (LDL) peroxidation to oxidized low-density lipoprotein (ox-LDL) accumulates in blood vessels, leading to apoptosis and necrosis of foam cells, forming a necrotic lipid core, generating unstable atherosclerotic plaque, and triggering acute cardiovascular events (Li et al., 2018). Furthermore, studies have found that ox-LDL could increase the formation of ROS in cells in a dose- and time-dependent manner (Chen et al., 2007). In general, oxidative stress promotes the occurrence and development of AS by inhibiting NO production and promoting lipid peroxidation in a pathophysiological perspective.

From a genetic point of view, oxidative stress would cause genetic damage and abnormal DNA demethylation. Due to high oxidation, ROS and its complexes could oxidize large molecules, such as DNA, lipids, and proteins, and alter biological functions. Notably, ROS can induce abnormalities in precise DNA methylation patterns by directly damaging the DNA. One of the most common oxidized derivatives of oxidative damage to DNA is guanine bases from the oxidation product 8-hydroxy-2'-deoxyguanosine (8-OHDG), which is often used as a marker for the determination of oxidative damage (O'Hagan et al., 2011). After DNA damage, methylation patterns were reconstructed during repair, and DNMT1 and related complexes enrichment in chromatin at the damaged site was observed. On the other hand, oxidative damage can also interfere the methylation patterns by inducing abnormalities in DNA demethylation (Niu et al., 2015). The pivotal epigenetic enzyme TET protein catalyzes the demethylation of 5-MC hydroxyethyl to 5-hydroxymethyl cytosine (5-hMC), utilizing Fe(II) as co-factors (Tahiliani et al., 2009), while  $H_2O_2$  inhibits the reduction of ferric iron to ferric iron (Niu et al., 2015). As a result, the demethylation of TET protein decreased, and the methylation pattern changed. For atherosclerotic lesions, ROS usually alters DNA methylation markers in a similar manner.

Fortunately, within the blood vessels, there exist antioxidant molecules and systems which become a powerful weapon against oxidative damage. Antioxidants work by reducing ROS

production and removing or degrading ROS and/or other oxidants. There are many endogenous and exogenous small-molecule antioxidants like uric acid, glutathione, bilirubin, coenzyme Q, lipid acid, melatonin, anthocyanins, and polyphenols (Salvayre et al., 2016). Another important antioxidant system in the body is superoxide dismutase (Sod) family including Sod1, 2, and 3. Researchers have found that increased oxidative stress in older mice causes hypomethylation in the promoter of Sod2 (encoded mitochondrial Mn-SOD). Aged mice suffer from an altered endothelial function, but NO-dependent dilatory pathway was not observed probably because the Mn-SOD antioxidant enzyme maintains the overall endothelial function (Nguyen et al., 2016).

Briefly speaking, oxidative stress not only inhibits the production of NO and promotes lipid peroxidation but also directly causes oxidative damage to DNA bases and induce the abnormal demethylation of TNT enzyme to disrupt DNA methylation patterns, more or less accelerating the progression of AS.

## Changes in DNA Methylation Associated With Aging

AS is a chronic process, with a progressive course over many years, but it can cause acute clinical events, including acute coronary syndromes (ACS), myocardial infarction (MI), and stroke (Ferreira et al., 2021). Accumulating evidence links cardiovascular aging to epigenetic alterations encompassing a complex interplay of DNA methylation, histone posttranslational modifications, and dynamic nucleosome occupancy governed by numerous epigenetic factors (Zhang et al., 2018). With increasing age, the body is exposed to more and more external stimulus factors such as oxidative stress, smoking (Yang et al., 2019), sitting, and mental stress. Changes in diet and lifestyle contribute to endothelial damage, vasoconstriction, and a series of physiological changes. In this process, epigenetic modification, particularly DNA methylation, occurs, which can well explain the relationship between gene expression and response to the changing environment in adulthood (Cavalli and Heard, 2019). Therefore, understanding the epigenetic mechanism may better explain the aging process (Pagiatakis et al., 2021). Nowadays, DNA methylation is considered to be a significant biomarker of health linked with age (Wang et al., 2020).

Firstly, some common signs have been found in aging individuals, such as genetic material change, including genomic instability increases, telomere shortening, epigenetic change, then nutrition metabolism disorder, mitochondrial dysfunction, aging cells and organelles, and interstitial cell signaling changes. These characteristics in atherosclerosis disease also have a certain embodiment (López-Otín et al., 2013). In this article, we focus on epigenetic changes with aging. Epigenetic drift and epigenetic clock are two phenomena underlying the relationship between DNA methylation and aging (Field et al., 2018). Epigenetic drift means real-time DNA methylation changes are associated with age in an individual but not common across all individuals. The epigenetic clock, on the other hand, represents those sites that are

associated with age across all individuals (Jones et al., 2015), so that is one way to understand why patients of the same age may have different levels of methylation. As mentioned earlier, in AS lesions, global methylation level showed an age-dependent decreasing trend, and hypermethylation at some gene sites was observed.

Secondly, vascular senescence is another important feature of body senescence, which is usually manifested by endothelial dysfunction and decreased elasticity of vascular sclerosis (Jin et al., 2019). During vascular aging, DNA methylation also contributes to oxidative stress in the blood vessels. The expression of endogenous nitric oxide synthase (NOS3/eNOS) is specific to ECs in assisting to produce NO and regulate the vascular function (Ambrosini et al., 2020). The promoter region of NOS3 gene encoding eNOS has a low methylation level under physiological state, while hypermethylation occurs under a pathological state, inhibiting the expression of NOS3 and the production of NO.

Thirdly, aging could lead to impaired vascular mitochondrial function, and enhanced mitophagy accelerates AS (Tyrrell et al., 2020). Mitochondrial damage is one of the important markers of aging. Interestingly, recent studies have found that mitochondrial DNA copy number can affect human mortality and cardiovascular disease by changing the nuclear DNA methylation pattern, causing the differential expression of specific genes and changing the signal transduction (Castellani et al., 2020).

Furthermore, aging affects the immune system in many ways, and immune system disorders are crucial in the process of AS lesions. With the increase of age, the regenerative ability of bone marrow hematopoietic stem cells decreases, but the absolute number of various immune cells (such as macrophages, T cells, B cells, etc.) increases as their function decreases, leading to a decrease of anti-inflammatory ability (Nikolich-Zugich, 2018). What is more, the number of megakaryocytes increases, which could produce platelets, leading to thrombosis. With the increase of the release of inflammatory mediators *in vivo*, the body is in a state of chronic inflammation for a long time, which will accelerate the occurrence of inflammation-related diseases, such as atherosclerotic diseases. On the other hand, a recent study compared the DNA methylation level of monocytes in young and old people and showed that there was hypomethylation at the CpG sites related to the molecules of human leukocyte antigen (HLA) in the elderly, which may affect the anti-inflammatory ability (Saare et al., 2020).

## DNA Methylation Influenced by High Homocysteine

Homocysteine (HCys) has proved to be associated with cardiovascular disease for decades (Skovierova et al., 2016). Under normal conditions, HCys binds to plasma proteins to form a complex, with less than 1% in the free state (Skovierova et al., 2016). When necessary factors of metabolism like vitamin B<sub>6</sub>, vitamin B<sub>12</sub>, and folic acid are deficient or if methionine intake is excessive, too much HCys is produced and cannot be metabolized out of the body, leading to HCys accumulation

**TABLE 2 |** Atherosclerosis-specific genes modulated via DNA methylation during the disease.

	Gene	Involvement	DNAme level of AS	Reference
Lipid oxidation	KLF2	Immune and homeostasis	Hypermethylation	Zafeiropoulos et al. (2021)
	ABCA1	Outflow of phospholipid and cholesterol	Hypermethylation	Hedman et al. (2017)
Endothelial dysfunction	PCSK9	Cholesterol and fatty acid metabolism	Hypermethylation	Davies et al. (2013)
Inflammation (macrophage)	KLF2	Inflammatory response	Hypermethylation	Zafeiropoulos et al. (2021)
	PPAR- $\gamma$	Anti-inflammatory	Hypermethylation	Eshghjoo et al. (2021)
	MCP-1	Migration and gathering of monocytes	Hypomethylation	Kumar et al. (2013)
VSMC	Contractile protein	Vasoconstriction	Hypomethylation	Elia et al. (2019)
Oxidative stress	Mn-SOD	Antioxidant	Hypomethylation	O'Hagan et al. (2011)
Aging	NOS3	Produce NO	Hypermethylation	Jones et al. (2015)
	HLA	Anti-inflammatory	Hypomethylation	Castellani et al. (2020)
Hyperhomocysteinemia	PDGF p66shc	Proliferation of VECs	Hypomethylation	Tinelli et al. (2019)
	ER- $\alpha$	Decrease the level of NO synthase Atheroprotective	Hypomethylation	Han et al. (2014)
			Hypermethylation	Luo et al. (2012)

(Fiorito et al., 2014). The plasma homocysteine (free HCys) concentrations in normal adults range from 5 to 10  $\mu\text{mol/L}$  and do not exceed 15  $\mu\text{mol/L}$ . Clinically, elevations above 15  $\mu\text{mol/L}$  are defined as hyperhomocysteinemia (HHCys) (Tinelli et al., 2019). HHCys is an independent risk factor for various cardiovascular diseases, particularly vascular endothelial injury leading to AS. Persistent HHCys can increase the production of reactive oxygen species and cause oxidative stress injury and apoptosis of endothelial cells. It can also cause lipid accumulation, inhibit fibrinolysis, and promote thrombosis. In addition, HHCys can also affect the progression of AS disease through epigenetic mechanisms by changing the dynamic balance of SAM/SAH, leading to DNA methylation or hypermethylation.

HCys is closely related to the biosynthesis and metabolism of methionine (Met), which plays an important role in cell life metabolism. The Met cycle produces SAM as a methyl donor and, at the same time, HCys as a by-product. After SAM participates in the methylation reaction, S-adenosine homocysteine (SAH) is generated (Aavik et al., 2019). High levels of SAH in cells will inhibit DNA methylation by binding to DNA methylation enzymes and result in a passive loss of methylation in triplicating DNA. Thus, the dynamic balance of SAM/SAH affects the global methylation level (Shen et al., 2020). The HCys so obtained can be metabolized by two reactions. In re-methylation, HCys can be remethylated to methionine, catalyzed by transmethylase, in most tissues. This process requires folic acid and vitamin B12 as cofactors. Another way is called trans-sulfuration; through this way, cysteine will be produced to continue the metabolism catalyzed by cysteine- $\beta$ -synthase requiring vitamin B6 as a cofactor in a small number of tissues (Tinelli et al., 2019). In summary, an increased level of HCys would interfere with the methionine cycle, and an increased level of HCys is widely associated with DNA hypomethylation.

As an independent predisposing factor of coronary heart disease, HCys can affect smooth muscle cell proliferation, promote endothelial cell dysfunction, and increase inflammatory mediators (Tinelli et al., 2019). Platelet growth factor (PDGF) can promote the proliferation of vascular endothelial cells. Studies on cultured human umbilical vein endothelial cells (VSMC) *in vitro* showed that increased HCys

can induce the hypomethylation of the PDGF promoter, increase mRNA and protein expression levels, and promote the proliferation of VSMC (Han et al., 2014).

Otherwise, as a strong oxidant, HCys can induce the release of ROS, C-reactive protein (CRP), and other superoxide anions through the MAPK, NF- $\kappa$  B, and other pathways. HCys inhibit the production of nitrogen monoxide (NO), the most powerful vasodilator produced by the endothelium and by the increase of oxidative stress following the production of ROS (Luo et al., 2012). The linkage protein *p66shc* could promote the oxidative stress response of tissue cells and decrease the level of nitric oxide synthase *in vivo*, worsening the apoptosis of endothelial cells. Studies have found that the concentration of HCys is positively correlated with the concentration of *p66shc* mainly because the increase of HCys will lead to the decrease of the methylation level of *p66shc* promoter (Xiao et al., 2019).

In addition, high levels of homocysteine lead to hypermethylation in the promoter region of the estrogen receptor- $\alpha$  (ER- $\alpha$ ) gene. ER- $\alpha$  are considered human atheroprotective genes regulating the beneficial estrogenic effects on ECs and SMCs (Grimaldi et al., 2015).

While the level of HCys is affected by the level of nutrient supply, such as one-carbon unit donor nutrient folic acid, deficiencies in folic acid and other nutrients, such as vitamins B6 and B12, will increase the homocysteine levels and induce endothelial dysfunction (Hou and Zhao, 2021). Therefore, supplemental nutrients are needed, which can improve the DNA methylation status, reduce the level of inflammatory factors, and delay the progression of atherosclerosis (Hou and Zhao, 2021). A meta-regression analysis reported a positive association between supplementary folic acid dose and methylation levels; folic acid was also the only identified factor among other nutrient supplements (ElGendy et al., 2018). In mice, a folate-deficient diet can influence the mRNA levels of one-carbon metabolic and epigenetic enzymes and reduce the levels of SAM (Bahous et al., 2019). In theory, folic acid deficiency decreased the methyl donors and methylation levels. However, in large human, randomized, controlled clinical trials, it was found that folic acid supplementation reduced the serum homocysteine levels relative to placebo and did not delay the progression of AS (van Dijk et al., 2015). There is no clear

evidence that the treatment for hyperhomocysteinemia alters the methylation process and has an exactly curative effect to CHD.

In conclusion, Hcys influenced AS in various ways, such as interfering endothelial cell homeostasis, oxidative stress, and affecting DNA methylation dynamics by SAM/SAH (Table 2).

## Clinical Study and Limitation

In the clinical treatment of atherosclerotic diseases, lowering the blood lipid level is still the most important means for the treatment of related diseases, but pure anti-inflammatory drugs and those with lipid-lowering effects are increasingly limited.

At present, drugs targeting the epigenetic mechanisms have been well developed. Azacytidine, a DNA methyltransferase inhibitor, has been reported to play a certain role in the treatment of hematological tumors (Falchi et al., 2020). When it comes to treatment of cardiovascular diseases, it may play a role in reducing pathological vascular remodeling (Strand et al., 2020). Another potent DNMTs inhibitor, 5-aza-2'-deoxycytidine (5-aza-dC), has been successfully used in the treatment of leukemia and lymphoma. Studies have shown that it can inhibit the macrophages but raise and activate other immune cells to improve AS lesions (Cao et al., 2014), but there have been no reports to determine whether the two drugs can be used in the clinical treatment of AS.

Drug therapy targeting methylation has not been specifically used in AS, possibly because methylation is a widely regulated mode in various tissues, and precision treatment cannot be well achieved. Therefore, more significant further studies of DNA methylation patterns may help to find some new biological diagnostic markers and guide future clinical approaches to treat the disease.

## CONCLUSION

AS is a major cause of morbidity and mortality all over the world. The basic pathological process involves lipid accumulation together with a maladaptive immune response and alterations of vascular cells within the arterial wall (Jackson et al., 2018).

With modern molecules in the rapid development of biology, genomics, and epigenetics technology, the treatment of diseases is mainly focused on the micro-molecular level, including the study of pathway targets. Nowadays, the regulation of pre-epigenetics has become a new therapeutic target and a hotspot for the AS mechanism—for example, hyperlipidemia can be explained in part by genetics, but not all patients with hyperlipidemia develop an atherosclerotic cardiovascular disease. Some patients with no associated risk factors may still have the disease. Thus, environmental factors (environmental pollution, stress, and insomnia) may epigenetically contribute to the development of atherosclerosis.

As an important supplement to traditional genetics, epigenetics contributes to gene modification through DNA methylation/demethylation, histone modification, and non-

coding RNA (Stratton et al., 2019; Yuan et al., 2020). DNA methylation has been studied in depth due to its stable chemical properties and easy detection. Studies have found the expression of abnormal DNA methylation in AS, which plays a role in plaque formation and regulation of monocytes/macrophages. EC and VSMC function and the degree of lesion of AS have important functions. DNA methylation affects the formation of AS by regulating gene expression in some methylated regions and in the differentiation of vascular smooth muscle cells. Research on the methylation of AS-related genes has become a hot trend. The occurrence and development of AS is the result of the combined effects of multiple gene methylation and different methylation levels of different genes.

As observed clinically, the final formation of atherosclerotic lesions is closely related to environmental factors and personal living habits. Epigenetics can well coordinate the relationship between innate genes and acquired environment and influence the disease process from many aspects (Law and Holland, 2019). DNA methylation is an important part of epigenetic modification, and the methylation degree of the gene promoter is inversely correlated with the transcription level. While the “inflammatory immune theory” and “lipid-driven theory” in AS have long been well known, the epigenetic mechanisms are far from understood. Factors like inflammatory stimulation, lipid oxidation, hyperhomocysteinemia, oxidative stress, and aging are all linked to the multi-layered regulation mechanisms of DNA methylation in AS. HHCys and oxidative stress injury are common risk factors for atherosclerotic cardiovascular diseases. Hcys, as a by-product of methylation response *in vivo*, can increase or decrease the methylation level by interfering with SAM/SAH dynamic balance. Oxidative stress can induce the formation of new methylation patterns through direct oxidative damage to DNA and interfere with the demethylation process to change the DNA methylation patterns. The aging process is often accompanied by a gradual decline in genome-wide methylation, but the genes involved in atherosclerotic protection show abnormal hypermethylation.

Other epigenetic regulatory mechanisms were not discussed, such as ATP-dependent chromatin-remodeling complexes, DNA and histone modifications, and non-coding RNAs, which also play an important role in the etiology and pathogenesis of AS.

## AUTHOR CONTRIBUTIONS

YD wrote the paper. DC helped in reviewing the paper, and TX modified the paper.

## FUNDING

This study was supported by funds from the National Natural Science Foundation of China (Grant No. 82070454).



## REFERENCES

- Aavik, E., Babu, M., and Ylä-Herttuala, S. (2019). DNA Methylation Processes in Atherosclerotic Plaque. *Atherosclerosis* 281, 168–179. doi:10.1016/j.atherosclerosis.2018.12.006
- Aavik, E., Lumivuori, H., Leppanen, O., Wirth, T., Hakkinen, S.-K., Brasen, J.-H., et al. (2015). Global DNA Methylation Analysis of Human Atherosclerotic Plaques Reveals Extensive Genomic Hypomethylation and Reactivation at Imprinted Locus 14q32 Involving Induction of a miRNA Cluster. *% Eur. Heart J.* 36, 993–1000. doi:10.1093/eurheartj/ehu437
- Ambrosini, S., Mohammed, S. A., Lüscher, T. F., Costantino, S., and Paneni, F. (2020). New Mechanisms of Vascular Dysfunction in Cardiometabolic Patients: Focus on Epigenetics. *High Blood Press. Cardiovasc. Prev.* 27, 363–371. doi:10.1007/s40292-020-00400-2
- Annema, W., and Tietge, U. J. (2012). Regulation of Reverse Cholesterol Transport - a Comprehensive Appraisal of Available Animal Studies. *Nutr. Metab.* 9, 25. doi:10.1186/1743-7075-9-25
- Bahous, R. H., Cosín-Tomás, M., Deng, L., Leclerc, D., Malysheva, O., Ho, M. K., et al. (2019). Early Manifestations of Brain Aging in Mice Due to Low Dietary Folate and Mild MTHFR Deficiency. *Mol. Neurobiol.* 56, 4175–4191. doi:10.1007/s12035-018-1375-3
- Bakshi, C., Vijayvergiya, R., and Dhawan, V. (2019). Aberrant DNA Methylation of M1-Macrophage Genes in Coronary Artery Disease. *Sci. Rep.* 9, 1429. doi:10.1038/s41598-018-38040-1
- Bhutani, N., Burns, D. M., and Blau, H. M. (2011). DNA Demethylation Dynamics. *Cell* 146, 866–872. doi:10.1016/j.cell.2011.08.042
- Botts, S. R., Fish, J. E., and Howe, K. L. (2021). Dysfunctional Vascular Endothelium as a Driver of Atherosclerosis: Emerging Insights into Pathogenesis and Treatment. *Front. Pharmacol.* 12, 787541. doi:10.3389/fphar.2021.787541
- Cao, Q., Wang, X., Jia, L., Mondal, A. K., Diallo, A., Hawkins, G. A., et al. (2014). Inhibiting DNA Methylation by 5-Aza-2'-Deoxycytidine Ameliorates Atherosclerosis through Suppressing Macrophage Inflammation. *Endocrinology* 155, 4925–4938. doi:10.1210/en.2014-1595
- Castellani, C. A., Longchamps, R. J., Sumpter, J. A., Newcomb, C. E., Lane, J. A., Grove, M. L., et al. (2020). Mitochondrial DNA Copy Number Can Influence Mortality and Cardiovascular Disease via Methylation of Nuclear DNA CpGs. *Genome Med.* 12, 84. doi:10.1186/s13073-020-00778-7
- Cavalli, G., and Heard, E. (2019). Advances in Epigenetics Link Genetics to the Environment and Disease. *Nature* 571, 489–499. doi:10.1038/s41586-019-1411-0
- Chen, T., Ueda, Y., Dodge, J. E., Wang, Z., and Li, E. (2003). Establishment and Maintenance of Genomic Methylation Patterns in Mouse Embryonic Stem Cells by Dnmt3a and Dnmt3b. *Mol. Cell Biol.* 23, 5594–5605. doi:10.1128/mcb.23.16.5594-5605.2003
- Chen, X. P., Xun, K. L., Wu, Q., Zhang, T. T., Shi, J. S., and Du, G. H. (2007). Oxidized Low Density Lipoprotein Receptor-1 Mediates Oxidized Low Density Lipoprotein-Induced Apoptosis in Human Umbilical Vein Endothelial Cells: Role of Reactive Oxygen Species. *Vascul Pharmacol.* 47, 1–9. doi:10.1016/j.vph.2007.01.004
- Chistiakov, D. A., Orekhov, A. N., and Bobryshev, Y. V. (2017). Treatment of Cardiovascular Pathology with Epigenetically Active Agents: Focus on Natural and Synthetic Inhibitors of DNA Methylation and Histone Deacetylation. *Int. J. Cardiol.* 227, 66–82. doi:10.1016/j.ijcard.2016.11.204
- Clarke, M., and Bennett, M. (2006). The Emerging Role of Vascular Smooth Muscle Cell Apoptosis in Atherosclerosis and Plaque Stability. *Am. J. Nephrol.* 26, 531–535. doi:10.1159/000097815
- Davies, P. F., Civelek, M., Fang, Y., and Fleming, I. (2013). The Atherosusceptible Endothelium: Endothelial Phenotypes in Complex Haemodynamic Shear Stress Regions In Vivo. *Cardiovasc. Res.* 99, 315–327. doi:10.1093/cvr/cvt101
- Davis, F. M., and Gallagher, K. A. (2019). Epigenetic Mechanisms in Monocytes/Macrophages Regulate Inflammation in Cardiometabolic and Vascular Disease. *Arterioscler Thromb. Vasc. Biol.* 39, 623–634. doi:10.1161/ATVBAHA.118.312135
- Ehrlich, M. (2019). DNA Hypermethylation in Disease: Mechanisms and Clinical Relevance. *Epigenetics* 14, 1141–1163. doi:10.1080/15592294.2019.1638701
- ElGendy, K., Malcomson, F. C., Lara, J. G., Bradburn, D. M., and Mathers, J. C. (2018). Effects of Dietary Interventions on DNA Methylation in Adult Humans: Systematic Review and Meta-Analysis. *Br. J. Nutr.* 120, 961–976. doi:10.1017/S000711451800243X
- Elia, L., Kunderfranco, P., Carullo, P., Vacchiano, M., Farina, F. M., Hall, I. F., et al. (2018). UHRF1 Epigenetically Orchestrates Smooth Muscle Cell Plasticity in Arterial Disease. *J. Clin. Invest.* 128, 2473–2486. doi:10.1172/JCI96121
- Elia, L., Condorelli, G., and Biology, C. (2019). The Involvement of Epigenetics in Vascular Disease Development. *Int. J. Biochem. Cell Biol.* 107, 27–31. doi:10.1016/j.biocel.2018.12.005
- Eshghjoo, S., Jayaraman, A., Sun, Y., and Alaniz, R. C. (2021). Microbiota-Mediated Immune Regulation in Atherosclerosis. *Molecules* 26. doi:10.3390/molecules26010179
- Falchi, L., Ma, H., Klein, S., Lue, J. K., Montanari, F., Marchi, E., et al. (2020). Combined Oral 5-Azacytidine and Romidepsin Are Highly Effective in Patients with PTCL: A Multicenter Phase 2 Study. *Blood* 137, 2161–2170. doi:10.1182/blood.2020009004
- Ferreira, J. P., Cleland, J. G., Lam, C. S. P., Anker, S. D., Mehra, M. R., van Veldhuisen, D. J., et al. (2021). Heart Failure Re-hospitalizations and Subsequent Fatal Events in Coronary Artery Disease: Insights from COMMANDER-HF, EPHEUS, and EXAMINE. *Clin. Res. Cardiol.* 110, 1554–1563. doi:10.1007/s00392-021-01830-1
- Field, A. E., Robertson, N. A., Wang, T., Havas, A., Ideker, T., and Adams, P. D. (2018). DNA Methylation Clocks in Aging: Categories, Causes, and Consequences. *Mol. Cell* 71, 882–895. doi:10.1016/j.molcel.2018.08.008
- Fiorito, G., Guarrera, S., Valle, C., Ricceri, F., Russo, A., Grioni, S., et al. (2014). B-vitamins Intake, DNA-Methylation of One Carbon Metabolism and Homocysteine Pathway Genes and Myocardial Infarction Risk: the EPICOR Study. *Nutr. Metab. Cardiovasc. Dis.* 24, 483–488. doi:10.1016/j.numecd.2013.10.026
- Ghaznavi, H., Mahmoodi, K., and Soltanpour, M. S. (2018). A Preliminary Study of the Association between the ABCA1 Gene Promoter DNA Methylation and Coronary Artery Disease Risk. *Mol. Biol. Res. Commun.* 7, 59–65. doi:10.22099/mbr.2018.28910.1312
- Grimaldi, V., Vietri, M. T., Schiano, C., Picascia, A., De Pascale, M. R., Fiorito, C., et al. (2015). Epigenetic Reprogramming in Atherosclerosis. *Curr. Atheroscler. Rep.* 17, 476. doi:10.1007/s11883-014-0476-3
- Gujar, H., Weisenberger, D. J., and Liang, G. (2019). The Roles of Human DNA Methyltransferases and Their Isoforms in Shaping the Epigenome. *Genes (Basel)* 10, 172. doi:10.3390/genes10020172
- Han, X. B., Zhang, H. P., Cao, C. J., Wang, Y. H., Tian, J., Yang, X. L., et al. (2014). Aberrant DNA Methylation of the PDGF Gene in Homocysteine-Mediated VSMC Proliferation and its Underlying Mechanism. *Mol. Med. Rep.* 10, 947–954. doi:10.3892/mmr.2014.2249
- Harith, H. H., Di Bartolo, B. A., Cartland, S. P., Genner, S., and Kavurma, M. M. (2016). Insulin Promotes Vascular Smooth Muscle Cell Proliferation and Apoptosis via Differential Regulation of Tumor Necrosis Factor-Related Apoptosis-Inducing Ligand. *J. Diabetes* 8, 568–578. doi:10.1111/1753-0407.12339
- Hedman, Å., Mendelson, M., Marioni, R., Gustafsson, S., Joehanes, R., Irvin, M. R., et al. (2017). Epigenetic Patterns in Blood Associated with Lipid Traits Predict Incident Coronary Heart Disease Events and Are Enriched for Results from Genome-wide Association Studies. *Circ. Cardiovasc. Genet.* 10, e001487. doi:10.1161/circgenetics.116.001487
- Hou, H., and Zhao, H. (2021). Epigenetic Factors in Atherosclerosis: DNA Methylation, Folic Acid Metabolism, and Intestinal Microbiota. *Clin. Chim. Acta* 512, 7–11. doi:10.1016/j.cca.2020.11.013
- Izzo, C., Vitillo, P., Di Pietro, P., Visco, V., Strianese, A., Virtuoso, N., et al. (2021). The Role of Oxidative Stress in Cardiovascular Aging and Cardiovascular Diseases. *Life (Basel)* 11, 60. doi:10.3390/life11010060
- Jackson, A. O., Regine, M. A., Subrata, C., and Long, S. (2018). Molecular Mechanisms and Genetic Regulation in Atherosclerosis. *Int. J. Cardiol. Heart Vasc.* 21, 36–44. doi:10.1016/j.ijcha.2018.09.006
- Jeong, K., Murphy, J., Kim, J., Campbell, P. M., Park, H., Rodriguez, Y. A. R., et al. (2021). FAK Activation Promotes SMC Dedifferentiation via Increased DNA Methylation in Contractile Genes. *Circ. Res.* 129, e215–e233. doi:10.1161/circresaha.121.319066

- Jia, S. J., Gao, K. Q., and Zhao, M. (2017). Epigenetic Regulation in Monocyte/macrophage: A Key Player during Atherosclerosis. *Cardiovasc. Ther.* 35, e12262. doi:10.1111/1755-5922.12262
- Jiang, W., Chen, M., Huang, J., Shang, Y., Qin, C., Ruan, Z., et al. (2021). Proteinuria Is Independently Associated with Carotid Atherosclerosis: a Multicentric Study. *BMC Cardiovasc. Disord.* 21, 554. doi:10.1186/s12872-021-02367-x
- Jin, J., Liu, Y., Huang, L., and Tan, H. (2019). Advances in Epigenetic Regulation of Vascular Aging. *Rev. Cardiovasc. Med.* 20, 19–25. doi:10.31083/j.rcm.2019.01.3189
- Jones, M. J., Goodman, S. J., and Kobor, M. S. (2015). DNA Methylation and Healthy Human Aging. *Aging Cell* 14, 924–932. doi:10.1111/acel.12349
- Jones, P. A. (2012). Functions of DNA Methylation: Islands, Start Sites, Gene Bodies and beyond. *Nat. Rev. Genet.* 13, 484–492. doi:10.1038/nrg3230
- Khyzha, N., Alizada, A., Wilson, M. D., and Fish, J. E. (2017). Epigenetics of Atherosclerosis: Emerging Mechanisms and Methods. *Trends Mol. Med.* 23, 332–347. doi:10.1016/j.molmed.2017.02.004
- Kumar, A., Kumar, S., Vikram, A., Hoffman, T. A., Naqvi, A., Lewarchik, C. M., et al. (2013). Histone and DNA Methylation-Mediated Epigenetic Downregulation of Endothelial Kruppel-like Factor 2 by Low-Density Lipoprotein Cholesterol. *Arterioscler Thromb. Vasc. Biol.* 33, 1936–1942. doi:10.1161/ATVBAHA.113.301765
- Lacey, M., Baribault, C., Ehrlich, K. C., and Ehrlich, M. (2019). Atherosclerosis-associated Differentially Methylated Regions Can Reflect the Disease Phenotype and Are Often at Enhancers. *Atherosclerosis* 280, 183–191. doi:10.1016/j.atherosclerosis.2018.11.031
- Laukkanen, M. O., Kivelä, A., Rissanen, T., Rutanen, J., Karkkainen, M. K., Leppanen, O., et al. (2002). Adenovirus-mediated Extracellular Superoxide Dismutase Gene Therapy Reduces Neointima Formation in Balloon-Denuded Rabbit Aorta. *Circulation* 106, 1999–2003. doi:10.1161/01.cir.0000031331.05368.9d
- Law, P. P., and Holland, M. L. (2019). DNA Methylation at the Crossroads of Gene and Environment Interactions. *Essays Biochem.* 63, 717–726. doi:10.1042/EBC20190031
- Li, D., Yan, J., Yuan, Y., Wang, C., Wu, J., Chen, Q., et al. (2018). Genome-wide DNA Methylome Alterations in Acute Coronary Syndrome. *Int. J. Mol. Med.* 41, 220–232. doi:10.3892/ijmm.2017.3220
- Liu, Y., Peng, W., Qu, K., Lin, X., Zeng, Z., Chen, J., et al. (2018). TET2: A Novel Epigenetic Regulator and Potential Intervention Target for Atherosclerosis. *DNA Cel Biol* 37, 517–523. doi:10.1089/dna.2017.4118
- Liu, Y., Tian, X., Liu, S., Liu, D., Li, Y., Liu, M., et al. (2020). DNA Hypermethylation: A Novel Mechanism of CREG Gene Suppression and Atherosclerogenic Endothelial Dysfunction. *Redox Biol.* 32, 101444. doi:10.1016/j.redox.2020.101444
- López-Otin, C., Blasco, M. A., Partridge, L., Serrano, M., and Kroemer, G. (2013). The Hallmarks of Aging. *Cell* 153, 1194–1217. doi:10.1016/j.cell.2013.05.039
- Lovren, F., and Verma, S. (2013). Evolving Role of Microparticles in the Pathophysiology of Endothelial Dysfunction. *Clin. Chem.* 59, 1166–1174. doi:10.1373/clinchem.2012.199711
- Ludmer, P. L., Selwyn, A. P., Shook, T. L., Wayne, R. R., Mudge, G. H., Alexander, R. W., et al. (1986). Paradoxical Vasoconstriction Induced by Acetylcholine in Atherosclerotic Coronary Arteries. *N. Engl. J. Med.* 315, 1046–1051. doi:10.1056/NEJM198610233151702
- Luo, X., Xiao, Y., Song, F., Yang, Y., Xia, M., and Ling, W. (2012). Increased Plasma S-Adenosyl-Homocysteine Levels Induce the Proliferation and Migration of VSMCs through an Oxidative Stress-Erk1/2 Pathway in apoE(-/-) Mice. *Cardiovasc. Res.* 95, 241–250. doi:10.1093/cvr/cvs130
- Nguyen, A., Leblond, F., Mamarbachi, M., Geoffroy, S., and Thorin, E. (2016). Age-Dependent Demethylation of Sod2 Promoter in the Mouse Femoral Artery. *Oxid Med. Cel Longev* 2016, 8627384. doi:10.1155/2016/8627384
- Nikolich-Zugich, J. (2018). The Twilight of Immunity: Emerging Concepts in Aging of the Immune System. *J. Nat. Immunol.* 19, 10–19. doi:10.1038/s41590-017-0006-x
- Niu, Y., DesMarais, T. L., Tong, Z., Yao, Y., and Costa, M. (2015). Oxidative Stress Alters Global Histone Modification and DNA Methylation. *Free Radic. Biol. Med.* 82, 22–28. doi:10.1016/j.freeradbiomed.2015.01.028
- O'Hagan, H. M., Wang, W., Sen, S., Destefano Shields, C., Lee, S. S., Zhang, Y. W., et al. (2011). Oxidative Damage Targets Complexes Containing DNA Methyltransferases, SIRT1, and Polycomb Members to Promoter CpG Islands. *Cancer Cell* 20, 606–619. doi:10.1016/j.ccr.2011.09.012
- Pagiatakis, C., Musolino, E., Gornati, R., Bernardini, G., and Papait, R. (2021). Epigenetics of Aging and Disease: a Brief Overview. *Aging Clin. Exp. Res.* 33, 737–745. doi:10.1007/s40520-019-01430-0
- Papin, C., Le Gras, S., Ibrahim, A., Salem, H., Karimi, M. M., Stoll, I., et al. (2020). CpG Islands Shape the Epigenome Landscape. *J. Mol. Biol.* 433, 166659. doi:10.1016/j.jmb.2020.09.018
- Parry, A., Rulands, S., and Reik, W. (2021). Active Turnover of DNA Methylation during Cell Fate Decisions. *Nat. Rev. Genet.* 22, 59–66. doi:10.1038/s41576-020-00287-8
- Patani, H., Rushton, M. D., Higham, J., Teijeiro, S. A., Oxley, D., Cutillas, P., et al. (2020). Transition to Naïve Human Pluripotency Mirrors Pan-Cancer DNA Hypermethylation. *Nat. Commun.* 11, 3671. doi:10.1038/s41467-020-17269-3
- Peng, P., Wang, L., Yang, X., Huang, X., Ba, Y., Chen, X., et al. (2014). A Preliminary Study of the Relationship between Promoter Methylation of the ABCG1, GALNT2 and HMGR Genes and Coronary Heart Disease. *PLoS One* 9, e102265. doi:10.1371/journal.pone.0102265
- Rask-Andersen, M., Martinsson, D., Ahsan, M., Enroth, S., Ek, W. E., Gyllenstein, U., et al. (2016). Epigenome-wide Association Study Reveals Differential DNA Methylation in Individuals with a History of Myocardial Infarction. *Hum. Mol. Genet.* 25, 4739–4748. doi:10.1093/hmg/ddw302
- Ritchie, R. H., Drummond, G. R., Sobey, C. G., De Silva, T. M., and Kemp-Harper, B. K. (2017). The Opposing Roles of NO and Oxidative Stress in Cardiovascular Disease. *Pharmacol. Res.* 116, 57–69. doi:10.1016/j.phrs.2016.12.017
- Rizzacasa, B., Amati, F., Romeo, F., Novelli, G., and Mehta, J. L. (2019). Epigenetic Modification in Coronary Atherosclerosis: JACC Review Topic of the Week. *J. Am. Coll. Cardiol.* 74, 1352–1365. doi:10.1016/j.jacc.2019.07.043
- Saare, M., Tserel, L., Haljasmägi, L., Taalberg, E., Peet, N., Eimre, M., et al. (2020). Monocytes Present Age-Related Changes in Phospholipid Concentration and Decreased Energy Metabolism. *Aging Cell* 19, e13127. doi:10.1111/acel.13127
- Salvayre, R., Negre-Salvayre, A., and Camaré, C. (2016). Oxidative Theory of Atherosclerosis and Antioxidants. *Biochimie* 125, 281–296. doi:10.1016/j.biochi.2015.12.014
- Sazonova, M. A., Sinyov, V. V., Ryzhkova, A. I., Sazonova, M. D., Kirichenko, T. V., Khotina, V. A., et al. (2021). Some Molecular and Cellular Stress Mechanisms Associated with Neurodegenerative Diseases and Atherosclerosis. *Int. J. Mol. Sci.* 22, 699. doi:10.3390/ijms22020699
- Schiano, C., Benincasa, G., Franzese, M., Della Mura, N., Pane, K., Salvatore, M., et al. (2020). Epigenetic-sensitive Pathways in Personalized Therapy of Major Cardiovascular Diseases. *Pharmacol. Ther.* 210, 107514. doi:10.1016/j.pharmthera.2020.107514
- Sharma, P., Garg, G., Kumar, A., Mohammad, F., Kumar, S. R., Tanwar, V. S., et al. (2014). Genome Wide DNA Methylation Profiling for Epigenetic Alteration in Coronary Artery Disease Patients. *Gene* 541, 31–40. doi:10.1016/j.gene.2014.02.034
- Shen, W., Gao, C., Cueto, R., Liu, L., Fu, H., Shao, Y., et al. (2020). Homocysteine-methionine Cycle Is a Metabolic Sensor System Controlling Methylation-Regulated Pathological Signaling. *Redox Biol.* 28, 101322. doi:10.1016/j.redox.2019.101322
- Shyamala, N., Gundapaneni, K., Galimudi, R., Tupurani, M. A., Padala, C., Puranam, K., et al. (2021). PCSK9 Genetic (Rs11591147) and Epigenetic (DNA Methylation) Modifications Associated with PCSK9 Expression and Serum Proteins in CAD Patients. *J. Gene Med.* 23, e3346. doi:10.1002/jgm.3346
- Skovierova, H., Vidomanova, E., Mahmood, S., Sopková, J., Drgová, A., Červeňová, T., et al. (2016). The Molecular and Cellular Effect of Homocysteine Metabolism Imbalance on Human Health. *Int. J. Mol. Sci.* 17, 1733. doi:10.3390/ijms17101733
- Strand, K. A., Lu, S., Mutryn, M. F., Li, L., Zhou, Q., Enyart, B. T., et al. (2020). High Throughput Screen Identifies the DNMT1 (DNA Methyltransferase-1) Inhibitor, 5-Azacytidine, as a Potent Inducer of PTEN (Phosphatase and Tensin Homolog): Central Role for PTEN in 5-Azacytidine Protection against Pathological Vascular Remodeling. *Arterioscler Thromb. Vasc. Biol.* 40, 1854–1869. doi:10.1161/ATVBAHA.120.314458
- Stratton, M. S., Farina, F. M., and Elia, L. (2019). Epigenetics and Vascular Diseases. *J. Mol. Cel Cardiol* 133, 148–163. doi:10.1016/j.jymcc.2019.06.010
- Swirski, F. K., Libby, P., Aikawa, E., Alcaide, P., Luscinskas, F. W., Weissleder, R., et al. (2007). Ly-6C<sup>hi</sup> Monocytes Dominate Hypercholesterolemia-Associated

- Monocytosis and Give Rise to Macrophages in Atheromata. *J. Clin. Invest.* 117, 195–205. doi:10.1172/JCI29950
- Tabaei, S., and Tabaei, S. S. (2019). DNA Methylation Abnormalities in Atherosclerosis. *Artif. Cell Nanomed Biotechnol* 47, 2031–2041. doi:10.1080/21691401.2019.1617724
- Tabas, I., and Bornfeldt, K. E. (2016). Macrophage Phenotype and Function in Different Stages of Atherosclerosis. *Circ. Res.* 118, 653–667. doi:10.1161/CIRCRESAHA.115.306256
- Tabas, I., García-Cardena, G., and Owens, G. K. (2015). Recent Insights into the Cellular Biology of Atherosclerosis. *J. Cell Biol* 209, 13–22. doi:10.1083/jcb.201412052
- Tahiliani, M., Koh, K. P., Shen, Y., Pastor, W. A., Bandukwala, H., Brudno, Y., et al. (2009). Conversion of 5-methylcytosine to 5-hydroxymethylcytosine in Mammalian DNA by MLL Partner TET1. *Science* 324, 930–935. doi:10.1126/science.1170116
- Tinelli, C., Di Pino, A., Ficulle, E., Marcelli, S., and Feligioni, M. (2019). Hyperhomocysteinemia as a Risk Factor and Potential Nutraceutical Target for Certain Pathologies. *Front. Nutr.* 6, 49. doi:10.3389/fnut.2019.00049
- Tyrrell, D. J., Blin, M. G., Song, J., Wood, S. C., Zhang, M., Beard, D. A., et al. (2020). Age-Associated Mitochondrial Dysfunction Accelerates Atherogenesis. *Circ. Res.* 126, 298–314. doi:10.1161/CIRCRESAHA.119.315644
- Valencia-Morales, M. P., Zaina, S., Heyn, H., Carmona, F. J., Varol, N., Sayols, S., et al. (2015). The DNA Methylation Drift of the Atherosclerotic Aorta Increases with Lesion Progression. *BMC Med. Genomics* 8, 7. doi:10.1186/s12920-015-0085-1
- van Dijk, S. C., Enneman, A. W., Swart, K. M., van Wijngaarden, J. P., Ham, A. C., Brouwer-Brolsma, E. M., et al. (2015). Effects of 2-year Vitamin B12 and Folic Acid Supplementation in Hyperhomocysteinemic Elderly on Arterial Stiffness and Cardiovascular Outcomes within the B-PROOF Trial. *J. Hypertens.* 33, 1897–1906. discussion 906. doi:10.1097/HJH.0000000000000647
- Veland, N., Lu, Y., Hardikar, S., Gaddis, S., Zeng, Y., Liu, B., et al. (2019). DNMT3L Facilitates DNA Methylation Partly by Maintaining DNMT3A Stability in Mouse Embryonic Stem Cells. *Nucleic Acids Res.* 47, 152–167. doi:10.1093/nar/gky947
- Veljkovic, N., Zaric, B., Djuric, I., Obradovic, M., Sudar-Milovanovic, E., Radak, D., et al. (2018). Genetic Markers for Coronary Artery Disease. *Medicina (Kaunas)* 54, 36. doi:10.3390/medicina54030036
- Wang, J., Jiang, Y., Yang, A., Sun, W., Ma, C., Ma, S., et al. (2013). Hyperhomocysteinemia-Induced Monocyte Chemoattractant Protein-1 Promoter DNA Methylation by Nuclear Factor-KB/DNA Methyltransferase 1 in Apolipoprotein E-Deficient Mice. *Biores Open Access* 2, 118–127. doi:10.1089/biores.2012.0300
- Wang, X., Liu, A. H., Jia, Z. W., Pu, K., Chen, K. Y., and Guo, H. (2018). Genome-wide DNA Methylation Patterns in Coronary Heart Disease. *Herz* 43, 656–662. doi:10.1007/s00059-017-4616-8
- Wang, C., Ni, W., Yao, Y., Just, A., Heiss, J., Wei, Y., et al. (2020). DNA Methylation-Based Biomarkers of Age Acceleration and All-Cause Death, Myocardial Infarction, Stroke, and Cancer in Two Cohorts: The NAS, and KORA F4. *EBioMedicine* 63, 103151. doi:10.1016/j.ebiom.2020.103151
- Xia, Y., Brewer, A., and Bell, J. T. (2021). DNA Methylation Signatures of Incident Coronary Heart Disease: Findings from Epigenome-wide Association Studies. *Clin. Epigenetics* 13, 186. doi:10.1186/s13148-021-01175-6
- Xiao, Y., Xia, J., Cheng, J., Huang, H., Zhou, Y., Yang, X., et al. (2019). Inhibition of S-Adenosylhomocysteine Hydrolase Induces Endothelial Dysfunction via Epigenetic Regulation of P66shc-Mediated Oxidative Stress Pathway. *Circulation* 139, 2260–2277. doi:10.1161/CIRCULATIONAHA.118.036336
- Yan, Z., Deng, Y., Jiao, F., Guo, J., and Ou, H. (2017). Lipopolysaccharide Downregulates Kruppel-like Factor 2 (KLF2) via Inducing DNMT1-Mediated Hypermethylation in Endothelial Cells. *Inflammation* 40, 1589–1598. doi:10.1007/s10753-017-0599-0
- Yang, Y., Gao, X., Just, A. C., Colicino, E., Wang, C., Coull, B. A., et al. (2019). Smoking-Related DNA Methylation Is Associated with DNA Methylation Phenotypic Age Acceleration: The Veterans Affairs Normative Aging Study. *Int. J. Environ. Res. Public Health* 16, 2356. doi:10.3390/ijerph16132356
- Yu, J., Qiu, Y., Yang, J., Bian, S., Chen, G., Deng, M., et al. (2016). DNMT1-PPAR $\gamma$  Pathway in Macrophages Regulates Chronic Inflammation and Atherosclerosis Development in Mice. *Sci. Rep.* 6, 30053. doi:10.1038/srep30053
- Yuan, Y., Xu, L., Geng, Z., Liu, J., Zhang, L., Wu, Y., et al. (2020). The Role of Non-coding RNA Network in Atherosclerosis. *Life Sci.* 265, 118756. doi:10.1016/j.lfs.2020.118756
- Zafeiropoulos, S., Farmakis, I., Kartas, A., Arvanitaki, A., Pagiantza, A., Boulmpou, A., et al. (2021). Reinforcing Adherence to Lipid-Lowering Therapy after an Acute Coronary Syndrome: A Pragmatic Randomized Controlled Trial. *Atherosclerosis* 323, 37–43. doi:10.1016/j.atherosclerosis.2021.03.013
- Zaina, S., Heyn, H., Carmona, F. J., Varol, N., Sayols, S., Condom, E., et al. (2014). DNA Methylation Map of Human Atherosclerosis. *Circ. Cardiovasc. Genet.* 7, 692–700. doi:10.1161/CIRCGENETICS.113.000441
- Zhang, W., Song, M., Qu, J., and Liu, G. H. (2018). Epigenetic Modifications in Cardiovascular Aging and Diseases. *Circ. Res.* 123, 773–786. doi:10.1161/CIRCRESAHA.118.312497
- Zhang, Y., Mei, J., Li, J., Zhang, Y., Zhou, Q., and Xu, F. (2021). DNA Methylation in Atherosclerosis: A New Perspective. *Evid. Based Complement. Alternat Med.* 2021, 6623657. doi:10.1155/2021/6623657
- Zhao, D., Liu, J., Wang, M., Zhang, X., and Zhou, M. (2019). Epidemiology of Cardiovascular Disease in China: Current Features and Implications. *Nat. Rev. Cardiol.* 16, 203–212. doi:10.1038/s41569-018-0119-4
- Zhong, Y., Chen, L., Li, J., Yao, Y., Liu, Q., Niu, K., et al. (2021). Integration of Summary Data from GWAS and eQTL Studies Identified Novel Risk Genes for Coronary Artery Disease. *Medicine (Baltimore)* 100, e24769. doi:10.1097/md.00000000000024769

**Conflict of Interest:** The authors declare that the research was conducted in the absence of any commercial or financial relationships that could be construed as a potential conflict of interest.

**Publisher's Note:** All claims expressed in this article are solely those of the authors and do not necessarily represent those of their affiliated organizations or those of the publisher, the editors, and the reviewers. Any product that may be evaluated in this article or claim that may be made by its manufacturer is not guaranteed or endorsed by the publisher.

Copyright © 2022 Dai, Chen and Xu. This is an open-access article distributed under the terms of the Creative Commons Attribution License (CC BY). The use, distribution or reproduction in other forums is permitted, provided the original author(s) and the copyright owner(s) are credited and that the original publication in this journal is cited, in accordance with accepted academic practice. No use, distribution or reproduction is permitted which does not comply with these terms.



# Pyroptosis-Related Inflammasome Pathway: A New Therapeutic Target for Diabetic Cardiomyopathy

Zhengyao Cai<sup>1</sup>, Suxin Yuan<sup>1</sup>, Xingzhao Luan<sup>2</sup>, Jian Feng<sup>1\*</sup>, Li Deng<sup>3</sup>, Yumei Zuo<sup>4</sup> and Jiafu Li<sup>1</sup>

<sup>1</sup>Key Laboratory of Medical Electrophysiology, Ministry of Education and Medical Electrophysiological Key Laboratory of Sichuan Province, Department of Cardiology, Institute of Cardiovascular Research, The Affiliated Hospital of Southwest Medical University, Southwest Medical University, Luzhou, China, <sup>2</sup>Department of Neurosurgery, The Affiliated Hospital of Southwest Medical University, Luzhou, China, <sup>3</sup>Department of Rheumatology, The Affiliated Hospital of Southwest Medical University, Luzhou, China, <sup>4</sup>Department of outpatient, The 13th Retired Cadre Recuperation Clinic Of Chengdu, Institute of Cardiovascular Research, Chengdu, China

## OPEN ACCESS

### Edited by:

Xianwei Wang,  
Xinxiang Medical University, China

### Reviewed by:

Keshav Gopal,  
University of Alberta, Canada  
Owais Bhat,  
Virginia Commonwealth University,  
United States

### \*Correspondence:

Jian Feng  
jerryfeng@swmu.edu.cn

### Specialty section:

This article was submitted to  
Cardiovascular and Smooth Muscle  
Pharmacology,  
a section of the journal  
Frontiers in Pharmacology

**Received:** 23 December 2021

**Accepted:** 07 February 2022

**Published:** 07 March 2022

### Citation:

Cai Z, Yuan S, Luan X, Feng J, Deng L,  
Zuo Y and Li J (2022) Pyroptosis-  
Related Inflammasome Pathway: A  
New Therapeutic Target for  
Diabetic Cardiomyopathy.  
Front. Pharmacol. 13:842313.  
doi: 10.3389/fphar.2022.842313

Pyroptosis is a highly specific type of inflammatory programmed cell death that is mediated by Gasdermine (GSDM). It is characterized by inflammasome activation, caspase activation, and cell membrane pore formation. Diabetic cardiomyopathy (DCM) is one of the leading diabetic complications and is a critical cause of fatalities in chronic diabetic patients, it is defined as a clinical condition of abnormal myocardial structure and performance in diabetic patients without other cardiac risk factors, such as hypertension, significant valvular disease, etc. There are no specific drugs in treating DCM despite decades of basic and clinical investigations. Although the relationship between DCM and pyroptosis is not well established yet, current studies provided the impetus for us to clarify the significance of pyroptosis in DCM. In this review, we summarize the recent literature addressing the role of pyroptosis and the inflammasome in the development of DCM and summary the potential use of approaches targeting this pathway which may be future anti-DCM strategies.

**Keywords:** pyroptosis, diabetes mellitus, diabetic cardiomyopathy, nod-like receptor protein 3, gasdermine

## 1 INTRODUCTION

Diabetes mellitus (DM) is a significant public health issue all over the world (Kim, 2018; Rendra et al., 2019). Diabetic complications remain the main cause of morbidity and mortality in diabetic patients, with cardiovascular disease being the leading cause of death. Diabetic cardiomyopathy (DCM) is phenotypically defined as the structural or functional changes of the heart occurring in a diabetic patient independent of other comorbidities such as hypertension, coronary disease, and valvular disease as well as independent of other conventional cardiovascular risk factors, resulting in either the systolic or diastolic dysfunction (Rubler et al., 1972), causing a substantial detriment to the patient's quality of life (Yap et al., 2019). There are growing lines of evidence indicating myocardial inflammation as a key process in DCM development (Boudina and Abel, 2007; Mann, 2015; Prabhu

**Abbreviations:** CVDs, Cardiovascular diseases; caspase-1, Cysteine specific protease-1; DM, Diabetes mellitus; DCM, Diabetic cardiomyopathy; GSDM, Gasdermine; NLRP3, NOD-like receptor protein 3; Nrf2, Nuclear factor erythroid 2-related factor 2; NF-kB, Nuclear Factor-kB; ROS, Reactive Oxygen Species; TXNIP, Thioredoxin interacting/inhibiting protein; TLR4, Toll-like receptor 4; T1DM, Type 1 diabetes; T2DM, Type 2 diabetes.



and Frangogiannis, 2016). Hyperglycemia-induced reactive oxygen species (ROS) generation is considered to be responsible for the progression and development of DCM (Cai, 2006; Cai et al., 2006). The increased ROS could induce many cytokines and inflammatory factors, such as nuclear factor- $\kappa$ B (NF- $\kappa$ B), thioredoxin interacting/inhibiting protein (TXNIP), and inflammasome (Bryant and Fitzgerald, 2009; Devi et al., 2012; Tsai et al., 2012). Although inflammasome was shown to be involved in the pathogenic mechanisms of diabetes and its complications, the potential role and regulatory mechanism of the inflammasome in DCM has remained largely unexplored.

Pyroptosis, an emerging type of programmed cell death (Man et al., 2017; Wang et al., 2018a), is associated with the inflammatory response and is activated by bacteria, pathogens, or their endotoxins, leading to the subsequent activation of the caspase family, accompanied by cell swelling, cell membrane pore formation, cell membrane rupture, inflammasome activation, as well as the release of cell contents and inflammatory mediators, resulting in a robust inflammatory response. In recent years, pyroptosis has gradually become a very important therapeutic target for inflammation. DCM is closely related to chronic inflammation, and accumulating evidence implicated pyroptosis as a critical contributor to myocardial inflammation in DCM (Li et al., 2014; Luo et al., 2014; Luo et al., 2017; Yang et al., 2018a; Yang et al., 2018b). This review focuses on the molecular and pathophysiological mechanisms of the pyroptosis-related inflammasomes pathway in the development of DCM are summarized. With this review, we attempted to provide new insights for researchers regarding the development of potential therapies for DCM.

## 2 PYROPTOSIS: A NEWLY DISCOVERED TYPE OF PROGRAMMED CELL DEATH

### 2.1 The Relationship Between Cell Death and Pyroptosis

Cell death is a ubiquitous life phenomenon that is mainly divided into cell necrosis and programmed death, of which programmed death includes apoptosis, autophagy, pyroptosis, and other modes (Soengas et al., 1999; Levine et al., 2011; Strowig et al., 2012; Pasparakis and Vandenabeele, 2015; Wallach et al., 2016). Pyroptosis is a newly discovered type of programmed cell death associated with inflammatory responses. Compared with apoptosis, pyroptosis is characterized by cell swelling, perforation, lysis, and release of cell contents. Pyroptosis occurs in many cell lines including endothelial cells, smooth muscle cells, and cardiac myocytes, and it is widely involved in the pathophysiological processes of various diseases (Pan et al., 2018; Yu et al., 2018). Pyroptosis is mediated by numerous inflammasomes that can detect exogenous or endogenous danger signals and is characterized by activation of nod-like receptor protein-3 (NLRP3) inflammasome and caspase and the release of interleukin (IL)-1 $\beta$  and IL-18 (Xia et al., 2019; Yu et al., 2020), thereby playing a critical role in multiple inflammatory and immune-mediated diseases (Yang et al., 2014; Wang et al., 2018b; Johnson et al., 2018; Wu et al.,

2019). Interestingly, pyroptosis is like a “double-edged sword” in cell function. On one hand, it rapidly eliminates intracellular pathogens by coordinating antimicrobial host defenses (Kleinbongard et al., 2018) and helps protect multicellular organisms from bacterial infection. On the other hand, uncontrolled pyroptosis will result in a severe impact on cellular environmental homeostasis through pathological and inflammatory cascades (Shi et al., 2017), finally leading to chronic low-grade inflammation. This contradiction may be attributed to differences in the virulence strategies used and the cell types targeted by different pathogens (Miao et al., 2010).

In 2015, two studies published in *Nature* identified gasdermin D (GSDMD) as a substrate for inflammatory caspases and showed that it was essential for inflammatory caspases-dependent pyroptosis and IL-1 $\beta$  secretion (Kayagaki et al., 2015; Shi et al., 2015). In 2018, the Nomenclature Committee on Cell Death redefined pyroptosis as a programmed death of plasma membrane pores formed by GSDM protein family members, which is an inflammatory reaction, often (but not always) as a consequence of inflammatory caspase activation (Galluzzi et al., 2018). recent studies have shown that proteolytic activation of GSDME, GSDMB, and GSDMC by certain caspases and granzymes can lead to pyroptosis (Rogers et al., 2017; Wang et al., 2017; Broz et al., 2020; Hou et al., 2020; Zhang et al., 2020; Zhou et al., 2020). GSDM members can be cleaved by a variety of proteases that are activated or inactivated, and most of the proteases that induce pyroptosis can also induce apoptosis in the absence of the corresponding GSDM protein, which means that GSDM can convert apoptosis into pyroptosis (Table 1).

### 2.2 Types and Processes of Pyroptosis

Inflammatory caspases cleave the GSDM protein to trigger pyroptosis and result in pore formation in the membrane, the release of proinflammatory cytokines, and, finally, programmed cell death (Yuan et al., 2016). Currently, pyroptosis can be divided into four types (Figure 1) according to different initiate activation modes, namely classical pyroptosis pathway, nonclassical pyroptosis pathway, caspase-3-dependent pyroptosis pathway, and caspase-8-dependent pyroptosis pathway. Notably, in humans, GSDM family members are composed of six members: GSDMA, B, C, D, E, and Pejvakin, and all have a highly conserved N-terminal domain that induces pyroptosis when expressed ectopically, except for PJVKNT (Broz et al., 2020). For example, caspase-3 and caspase-8 can induce pyroptosis via the cleavage of GSDME and GSDMD, respectively (Kayagaki et al., 2015; Jorgensen et al., 2017; Wang et al., 2017). Although these four types have their characteristics, they are related to each other. In addition, they share a common endpoint event which is to process IL-18 and IL-1 $\beta$ , activate the perforating protein GSDMD, and eventually cause the cell membrane to break and release IL-18 and IL-1 $\beta$  (Ding et al., 2016; Kovacs and Miao, 2017).

#### 2.2.1 Canonical Inflammasome Pathway Associated With Pyroptosis

Under the stimulation of dangerous signals, cysteinyl aspartate specific protease-1 (caspase-1) is activated by the assembled and

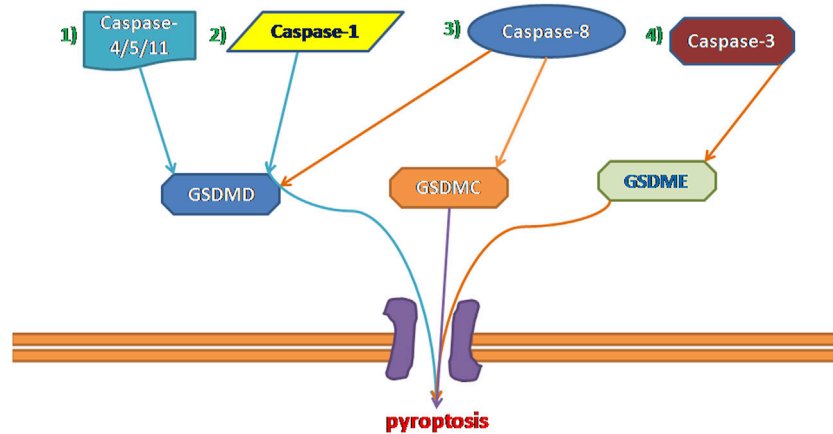


**FIGURE 1 |** Four types of pyroptosis: 1) Non-canonical Inflammasome Pathways Associated With Pyroptosis. 2) canonical Inflammasome Pathways Associated With Pyroptosis. 3) Caspase-8-dependent pyroptosis pathway. 4) Caspase-3-dependent pyroptosis pathway.

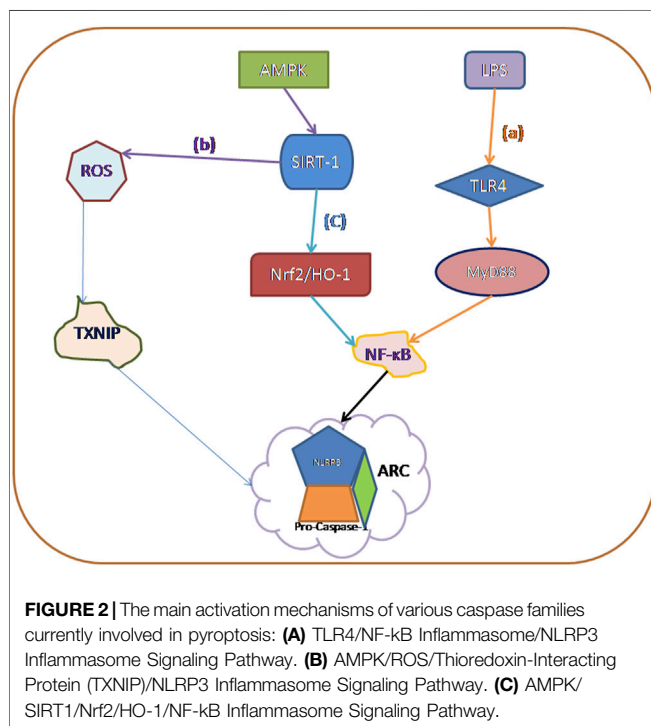


**FIGURE 2 |** The main activation mechanisms of various caspase families currently involved in pyroptosis: (A) TLR4/NF-κB Inflammasome/NLRP3 Inflammasome Signaling Pathway. (B) AMPK/ROS/Thioredoxin-Interacting Protein (TXNIP)/NLRP3 Inflammasome Signaling Pathway. (C) AMPK/SIRT1/Nrf2/HO-1/NF-κB Inflammasome Signaling Pathway.

activated inflammasome complex; this induces further cell membrane degradation, leading to cell death and release of mature IL-1 $\beta$  and mature IL-18 (Russo et al., 2016; Błażejowski et al., 2017). This caspase-1-dependent pyroptosis is known as the canonical inflammasome pathway. The specific steps are as follows:

The cells activate their respective inflammasomes, including NLRP3, absent in melanoma 2, or pyrin through the action of pathogen-associated molecular patterns and danger-associated molecular patterns under the stimulation of various external factors, such as hyperglycemia,

inflammation, and hyperlipidemia. The activation of NLRP3 initiates pro-caspase-1 self-cleavage to form a caspase-1 mature body. On the one hand, activated caspase-1 recognizes inactive IL- $\beta$  and IL-18 precursors and converts them into mature inflammatory cytokines. On the other hand, caspase-1 cleaves GSDMD that mediate the formation of membrane pores. The formation of membrane pores promotes the release of inflammatory factors, cell swelling, and finally, pyroptosis (Afonina et al., 2017; Man et al., 2017).

### 2.2.2 Non-Canonical Inflammasome Pathways Associated With Pyroptosis

In 2011, Kayagaki et al. (2011) discovered non-canonical pyroptotic pathways. In contrast to canonical pyroptotic pathways, the cell wall LPS of Gram-negative bacteria bypasses TLR4 and directly combines with the pro-caspase (-4 and -5 in humans and -11 in murine) to form activated caspase-4/5/11, and then cleaves the 53-kDa precursor form of GSDMD (pro-GSDMD) to generate N-terminal of mature GSDMD p30 fragment (Kayagaki et al., 2015), which further causes membrane pore formation, the release of IL-1b and IL-18 in the cell and induces pyroptosis (Hagar et al., 2013; Shi et al., 2014; Shi et al., 2017). This pathway does not involve caspase-1; in the absence of caspase-1, human caspase-4/5 and murine caspase-11 can also induce pyroptosis with all associated morphological characteristics (Broz et al., 2020). Although the activation pathways are different, the downstream signaling pathways are all activated caspases that cleave GSDMD and release the N-terminal domain to form membrane pores, eventually leading to pyroptosis. In other words, GSDMD is a necessary downstream component of both the canonical and non-canonical inflammasome pathways associated with pyroptosis (Kayagaki et al., 2015; Shi et al., 2015; Aglietti et al., 2016; Liu et al., 2016; Sborgi et al., 2016). However, the current understanding of the noncanonical caspase-11/4/5 pathway mainly focuses on its role

**TABLE 1 |** Discrimination between apoptosis and pyroptosis.

	Apoptosis	Pyroptosis
Common point	Programmed cell death	
Characteristic	Cell shrinkage Membrane blebbing Nuclear DNA fragmentation Nuclear condensation —	Cell enlarging Membrane broken Organelles deforming DNA randomly degraded Chromatin condensation
Dependence on caspases	Transformation to apoptosis and pyroptosis	
	Caspase 3, 6, 7, 8, 9, 10 caspases that activate GSDM members: ①GSDMC by caspase-8 Watabe et al. (2001); ②GSDMD by caspase-1, and to a lesser extent, by caspase-8 Orning et al. (2018), Sarhan et al. (2018); ③GSDME by caspase-3 Rogers et al. (2017), Wang et al. (2017)	Caspase 1, 3, 4, 5, 11

in infectious diseases (Shi et al., 2014; Yi, 2017). The role of caspase-11/4/5 in cardiovascular disease is rarely reported; this may be a research direction in the future cardiovascular field.

### 2.2.3 Caspase-3-Dependent Pyroptosis Pathway

Caspase-3 is traditionally only induced apoptosis, however, recent studies have shown that caspase-3 also plays an important role in pyroptosis. Due to the presence of a natural caspase-3 cleavage site in the N- terminal and C- terminal structural domains of GSDME, activated caspase-3 is capable of cleaving a specific site of GSDME to release an active N-terminal domain and perforating the plasma membrane to induce pyroptosis (Rogers et al., 2017). Another study has recently also reported that GSDME has the same function as GSDMD, and can also activate the intrinsic pathway downstream of inflammasome activation (Rogers et al., 2019). Briefly, GSDME is activated by caspase-3 to further generate the GSDME-N fragments and then cause the pore-forming effect of the cell membrane to mediate pyroptosis. However, the study of caspase-3 induced pyroptosis is still very limited, and future studies should focus on the mechanism of caspase-3 induced pyroptosis.

### 2.2.4 Caspase-8-Dependent Pyroptosis Pathway

As mentioned above, the cleavage of GSDMD and membrane pore formation is key to pyroptosis, a recent study by Orning et al. showed that recombinant mouse GSDMD is cleaved by purified active caspase-8 (Orning et al., 2018), although it was less efficient at GSDMD processing in comparison with caspase-1, its activity was sufficient to trigger pyroptotic cell death in murine macrophages. In recent years, many independent studies have revealed synchronicity between caspase-8 activity and GSDMD-mediated pyroptosis in multiple scenarios. In Chen/Demarco (Chen et al., 2019) et al.'s study, they found that the Caspase-8 activity led to cleavage at position D276, the cleavage site used by caspase-1 generating the p30 fragment, which means that caspase-8 generated the same pyroptosis-mediating p30 fragment as caspase-1. Various signs suggest that there may be a close relationship between caspase-8 and pyroptosis, but given that not enough attention has been paid to caspase-8 by scholars, the mechanism by which caspase-8 induced pyroptosis needs to be further explored.

## 2.3 Diabetes and Pyroptosis

Although the pathogenesis of type 1 diabetes (T1DM) and type 2 diabetes (T2DM) is differentiated, studies have found that they are each closely related to pyroptosis. Generating a T1DM model is to induce pancreatic damage using streptozotocin (STZ) while the most usual approach to developing a T2DM model is to feed animals with a high-fat diet (HFD). Previously, it was believed that the pathogenesis of T1DM involved adaptive immunity mediated by T cells. However, an increasing number of studies have shown that the Toll-like receptor (TLR)-mediated innate immune system also plays an important role in the pathogenesis of T1DM (Needell and Zipris, 2017). Carlos et al. confirmed that NLRP3-dependent IL-1  $\beta$  production mediated by mDNA leads to T1DM. The important pathological features of T2DM are insulin resistance and impaired insulin secretion from pancreatic  $\beta$ -cells. Insulin resistance is closely associated with inflammation. Numerous evidence suggests elevated expression of inflammasome components (NLRP3 caspase-1 and ASC) in untreated T2DM patients (Joya-Galeana et al., 2011; Lee et al., 2013). And the secretion of IL-1 $\beta$  and IL-18, caused by activation of the NLRP3 inflammasome, is emerging as a powerful determinant of metabolic inflammation and insulin resistance in T2DM patients (Stienstra et al., 2010; Wen et al., 2011). Consistent with these findings, higher serum levels of IL-1 $\beta$  and IL-18 have been reported in drug-naïve T2DM patients compared with healthy subjects (Lee et al., 2013). Under a hyperglycemic environment, ROS activates the NLRP3 inflammasome in  $\beta$  cells, elevating caspase-1-dependent IL-1 $\beta$  secretion; this mediates dysfunction of  $\beta$ -cell insulin secretion and promotes obesity and insulin resistance, finally leading to pyroptosis and the development of T2DM.

## 2.4 Pyroptosis and Diabetic Cardiomyopathy

Pyroptosis is triggered by various pathological stimuli, such as oxidative stress, hyperglycemia, inflammation, and it is crucial for controlling microbial infections. It was first identified in the macrophage in 1992, which presented rapid lysis after infection with *Shigella flexneri*, (Cookson and Brennan, 2001) and the name was coined in 2001 (Cookson and Brennan, 2001). Pyroptosis is a highly regulated cell death process, and it plays a

pivotal role in the pathogenesis of various cardiovascular diseases (CVDs) such as myocardial infarction (Gonzalez-Pacheco et al., 2017; Yang et al., 2017), hypertension (Bruder-Nascimento et al., 2016; Zhu et al., 2017), and cardiomyopathy (Pereira et al., 2018), and involves endothelial cells (Zhang et al., 2018a), VSMCs (Pan et al., 2018) and so on. Therefore, this process is a potential target for therapeutic intervention to prevent CVDs.

Today, increasing evidence suggests that pyroptosis is involved in the pathogenesis of cardiomyocyte injury, especially in DCM (Qiu et al., 2017). DCM, a complication of diabetes, is characterized by myocardial fibrosis, left ventricular hypertrophy, and damaged left ventricular systolic and diastolic function (Jia et al., 2018a). Inflammation is implicated in the pathogenesis of diabetic cardiomyopathy (Zhang et al., 2017). Oxidative stress, coupled with the activation of downstream pro-inflammatory and cell-death pathways, induces DCM-associated pathological changes (Althunibat et al., 2019). Therefore, anti-inflammatories may be useful for the prevention and treatment of diabetic complications. In recent years, the role of the NLRP3 inflammasome in diabetic cardiomyopathy has drawn much attention. And NLRP3 also plays an important role in the development of pyroptosis. By activating NLRP3, stimulates the production of IL-1 $\beta$  and IL-18 (Zeng et al., 2017; Ge et al., 2018), triggers pyroptosis, and ultimately leads to the development of diabetic cardiomyopathy.

Due to the different modeling methods of T1DM and T2DM, the pathophysiological mechanism of DCM caused by them will also change accordingly (Hölscher et al., 2016). Insulin may be one of the reasons for this difference. Insulin signaling in two types of diabetes is very different. T1DM is characterized by insulin deficiency, and T2DM is characterized by insulin resistance. However, recent studies have shown that no matter what type of diabetic cardiomyopathy leads to diabetes, the final manifestation is cardiac diastolic dysfunction (Hölscher et al., 2016). Although the etiology of these two types of diabetes is different, there are still some common molecular changes in the myocardium (Hölscher et al., 2016). In both two types of diabetes, proper glycemic control (Salvatore et al., 2021) is a key factor to prevent DCM progression from heart failure.

What's more, in the diabetic heart, the NLRP3 inflammasome responds to hyperglycemia-induced toxicity and initiates the progression of pyroptosis (Luo et al., 2014; Luo et al., 2017; Zhou et al., 2018). In recent years, a growing body of evidence suggests that inhibition of the NLRP3 inflammasome may slow pyroptosis in diabetes and associated complications (Yang et al., 2018b; Wu et al., 2018; Song et al., 2019). But there remain some problems, though DCM is a common clinical complication in patients with diabetes, there are few studies about the mechanism between DCM and pyroptosis, and the mechanism of how to activate NLRP3 is still not clear too.

### 3 SIGNALING PATHWAYS RELATED TO THE PYROPTOSIS OF DIABETIC CARDIOMYOPATHY

Mitochondrial ROS have a central role in NLRP3 inflammasome activation (Zhou et al., 2011; Zhong et al., 2013). One study demonstrated that the production of intracellular ROS induces

NLRP3 translocation to the cytoplasm from the nucleus in LPS treated neonatal rat cardiomyocytes. And NLRP3 cytoplasmic translocation can be prevented by the elimination of ROS (Li et al., 2019a). And the accelerated ROS production induced by high glucose plays a key role in the progression of diabetic cardiovascular disease and cardiomyocyte pyroptosis (Chen et al., 2017). A recent study showed that Gypenosides, a traditional Chinese medicine, can reduce activation of the NLRP3 inflammasome by inhibiting ROS production, and this can improve damage to the myocardium induced by high glucose (Zhang et al., 2018b). And GSDMD cleavage occurs downstream of ROS release. In conclusion, excessive generation of ROS and NLRP3 inflammasome activation trigger inflammation and pyroptosis in diabetes. But the specific mechanism by which NLRP3 triggers anxiety in DCM is still unclear.

#### 3.1 TLR4/NF- $\kappa$ B/NLRP3 Inflammasome Signaling Pathway

Toll-like receptor 4 (TLR4), Myeloid differentiation factor 88 (MyD88), and nuclear factor kappa-light-chain- enhancer of activated B cells (NF- $\kappa$ B) pathway contribute to NLRP3 inflammasome activation (Bauernfeind et al., 2009). NF- $\kappa$ B is closely associated with NLRP3 and plays a crucial part in the regulation of genes involved in immunity and inflammation (Sun, 2017). On the one hand, NF- $\kappa$ B binds to the NLRP3 promoter region and affects transcriptional regulation of NLRP3 (Qiao et al., 2012). On the other hand, blockage of NF- $\kappa$ B exacerbates the activation of the NLRP3-dependent inflammasome (Afonina et al., 2017). Then, NLRP3 inflammasome forms a complex with its adaptor apoptosis-associated speck-like protein containing a CARD (ASC) which leads to the enhancement of pro-caspase-1 and the formation of an active caspase-1 (Latz et al., 2013). The activated caspase-1 converts pro-IL-1 $\beta$  and IL-18 into its mature forms and then induces pyroptosis (Shi et al., 2015; Youm et al., 2015; Sanchez-Lopez et al., 2019). This process has a protective effect during the initial inflammation. Nevertheless, when IL-1 $\beta$  and IL-18 are continually released and accumulated in the cell, they induce pyroptosis, tissue damage, and organ dysfunction (Green et al., 2018). The above idea was demonstrated in the rat model of Hepatic ischemia/reperfusion injury by Alaa El-Din El-Sayed (El-Sisi et al., 2021; Zhang et al., 2021) and in the premature ovarian failure model made by Cairong Zhang et al. (2021). Moreover, Wang Y. et al. found that chemical GSDMD-related pyroptosis of tubular cells in diabetic kidney disease is dependent on the TLR4/NF- $\kappa$ B signaling pathway (Wang et al., 2019). In summary, we speculate that pyroptosis can be associated with DCM through the TLR4/NF- $\kappa$ B/NLRP3 Inflammasome Signaling Pathway, but there are very few scholars studying this pathway in DCM, and future directions can focus on the understanding of this pathway.

#### 3.2 AMPK/ROS/Thioredoxin-Interacting Protein (TXNIP)/NLRP3 Inflammasome Signaling Pathway

In recent years, TXNIP has been recognized as a central contributor to diabetic vascular complications (Li et al., 2017;



Lu et al., 2018; Gu et al., 2019). TXNIP levels will be increased in hyperglycemic cultured cells as well as in peripheral blood and tissues of diabetic animals (Li et al., 2017; Gu et al., 2019). The TXNIP/NLRP3 pathway was activated due to increased ROS production induced by high glucose. All NLRP3 agonists trigger the production of ROS, which leads to activation of the NLRP3 inflammasome via the ROS-sensitive TXNIP protein (Schroder et al., 2010). Mitochondrial dysfunction can produce a large number of reactive oxygen species (ROS), and this, in turn, induces dissociation of TXNIP and thioredoxin. TXNIP then binds to NLRP3 through the leucine-rich repeat domain, prompting activation of the NLRP3 inflammasome (Strowig et al., 2012; Qiu and Tang, 2016; Han et al., 2018).

TXNIP is a potential regulator involved in high glucose-induced cardiomyocytes. A recent study showed that glucose-treated H9c2 cardiomyocytes produced excessive ROS in a concentration-dependent manner, and the level of TXNIP showed a similar expression pattern in response to glucose (Bauer et al., 2014). Recently, the role of AMPK on TXNIP has also gradually attracted attention. The activation of AMPK is driven by oxidative stress via ROS-dependent phosphorylation (Mungai et al., 2011). Previous studies revealed that AMPK is a key regulator of energy metabolism and inflammation in DCM (Jia et al., 2018a; Jia et al., 2018b). In high glucose-treated cardiomyocytes, a slight increase in phosphorylated AMPK was observed. Activated AMPK degenerates TXNIP to manipulate the activity of the NLRP3 inflammasome (Wu et al., 2013). What's more, in experiments by Wei H et al., they also confirmed an anti-pyrototic pathway mediated by the ROS-AMPK-TXNIP pathway, which regulates the activity of inflammasome and caspase-1 in diabetic cardiomyocytes. In summary, the ROS-AMPK-TXNIP pathway can serve as a link between oxidative stress and cardiac inflammation in various CVDs (Wei et al., 2019).

### 3.3 AMPK/SIRT1/Nrf2/HO-1/NF-κB Inflammasome Signaling Pathway

SIRT1 is a member of the sirtuin family, which is involved in many diseases and bioprocesses such as cancer development, oxidative stress, and pyroptosis (Simic et al., 2013; Ma et al., 2016; Qu et al., 2017; Chen et al., 2018). The AMPK/SIRT1 pathway could modulate the function of vascular endothelial cells in diversiform ways, for instance, activating PGC-1α, Nrf2, and FoxO3 and inhibiting the activity of various inflammation-related proteins such as p38MAPK and NF-κB pathway. Endothelial dysfunction is closely related to DCM, so we supposed that the AMPK/SIRT1 pathway plays an important role in the pathological progress of DCM.

As one of the most essential transcription factors, nuclear factor erythroid 2-related factor 2 (Nrf2) exerts antioxidant, anti-apoptotic, and anti-inflammatory effects by interacting with multiple signaling pathways (Loboda et al., 2016; Hao et al., 2019), with an important role in cytoprotection, is activated under stress conditions when excessive ROS is detected (Tsushima et al., 2019; Ungvari et al., 2019). Many studies are showing that SIRT1/PGC-1α/Nrf2 signaling can regulate both

pyroptosis and oxidative stress in different situations such as cancer or liver oxidative stress (Do et al., 2014; Zhao et al., 2019). The Nrf2/HO-1 pathway has garnered increased interest (Wardyn et al., 2015). Importantly, in Hao Li et al.'s research, they found that in diabetic cardiomyopathy, piceatannol alleviates inflammation and oxidative stress by activating the Nrf2/HO-1 pathway while inhibiting NF-κB activation in Rat H9c2 cardiac myoblasts. The same phenomenon was found in human umbilical vein endothelial cells by Tang, Qian et al. Knockdown of Nrf2 suppressed enhancement of HO-1 expression and abolished the anti-inflammatory effects (Wardyn et al., 2015). Nrf2 is one of the upstream targets of inflammation induced by NF-κB. Besides, studies also showed that activating the Nrf2 signaling pathway could inhibit NLRP3 inflammasome-dependent pyroptosis in vascular endothelial cells (Li et al., 2019b). Nrf2 is one of the upstream targets of inflammation induced by NF-κB. Therefore, it is not difficult for us to deduce that AMPK/SIRT1/Nrf2/HO-1/NF-κB Inflammasome Signaling Pathway plays an important role in the anxiety process of diabetic cardiomyopathy.

### 3.4 Other Signaling Pathways

In recent years, some other pathways related to the pyroptosis of DCM have been discovered. 1) FoxO3a/ARC/caspase-1 Signaling Pathway: FoxO3a has been reported to inhibit cell death by targeting its downstream protein ARC in glucose-treated cardiomyocytes (Li et al., 2014). 2) AMPK/mTOR/autophagy pathway: Yang F et al. demonstrated that metformin can suppress the NLRP3 inflammasome through the AMPK/mTOR/autophagy pathway (Yang et al., 2019a). 3) Kcnq1ot1/miR-214-3p/caspase-1 pathway: The long non-coding RNA Kcnq1ot1 was overexpressed in the serum of diabetic patients, as well as in HG-treated cardiac fibroblasts and cardiac tissue of diabetic mice. Kcnq1ot1 targeted caspase-1 and regulated the expression of NLRP3 and its downstream inflammatory cytokines by sponging miR-214-3p. Silencing Kcnq1ot1 inhibited the miR-214-3p/caspase-1 pathway to relieve pyroptosis in DCM models, and ameliorate cardiac function and fibrosis *in vivo* (Yang et al., 2018b). Interestingly, a novel circular RNA, named caspase-1-associated circRNA (CACR), also promotes caspase-1 expression by targeting miR-214-3p, thus inducing pyroptosis in HG-treated cardiomyocytes (Yang et al., 2019b). However, there are few studies on the above pathways in diabetic cardiomyopathy, and the specific mechanism needs to be further explored.

## 4 DISCUSSION

Pyroptosis is a new mode of programmed death, which is closely related to the inflammatory response and has been a research hotspot in recent years. Previous studies have focused on demonstrating the relationship between pyroptosis and various diseases, but there is a lack of research on specific mechanisms, and even if there are specific mechanisms of research, few researchers integrate these mechanisms, which is the original intention of our writing of this paper. As mentioned above,

pyroptosis is closely related to the inflammatory response, and DCM can be classified as a type of chronic inflammatory disease, and the current study also shows that there is a close link between DCM and pyroptosis. So, it will be of interest if the relationship between DCM and pyroptosis can be studied in-depth and the development of DCM can be inhibited by regulating some of these molecular mechanisms.

In this review, we describe in detail the four ways to trigger pyroptosis, which were previously three, and now with the deepening of research, new mechanisms have emerged, and perhaps in the future, we will find more mechanisms to trigger pyroptosis. Then we summarized three main signaling pathways that currently trigger diabetic cardiomyopathy (Figure 2): 1) TLR4/NF- $\kappa$ B Inflammatory/NLRP3 Inflammatory Signaling Pathway; 2) AMPK/ROS/TXNIP/NLRP3 Inflammatory Signaling Pathway; and 3) AMPK/SIRT1/Nrf2/HO-1/NF- $\kappa$ B Inflammatory Signaling Pathway, which can be used to design DCM-related drugs through the above signaling pathways in the future.

However, through our study, it is found that there are still the following problems to be solved in this direction of DCM-induced pyroptosis: Firstly, the detailed mechanism underlying the function of the gasdermin family in DCM in the downstream pathway of pyroptosis remains unclear. Secondly, small-molecule inhibitors targeting TLR4, NLRP3, and other inflammatory components are potential therapeutic options for DCM. However, there are still many unknown pathways and targets, and corresponding inhibitors, related to the occurrence and development of DCM related to pyroptosis awaiting further exploration. These insights may provide research ideas for developing new mechanisms, drugs, and technologies for DCM. Based on the current summary, we propose the following research targets.

First, the mechanism of pyroptosis triggered by diabetic cardiomyopathy proposed in this review needs more experiments to verify its feasibility. And the independent

dependence of each pathway has not been explored, which provides a direction for future studies.

Second, pyroptosis is a double-edged sword, and most of the current research focuses on its bad side. Can we use the advantages of pyroptosis for DCM?

Finally, more attention should be paid to the pathophysiology of DCM, and to understand the possible potential pathways of the pyroptosis-related inflammasome, which can offer new methods and technologies for the clinical treatment of DCM.

## AUTHOR CONTRIBUTIONS

ZC and SY conceived, designed, or planned the idea. All authors collected and read the literature. ZC drafted the manuscript. YZ and JF revised the manuscript. All authors read and approved the final manuscript.

## FUNDING

This research was funded by the fund (KeyME-KeyME-2020-004) of the Key Laboratory of Medical Electrophysiology, the Fund (xtcx2019-13) of Collaborative Innovation Center for Prevention and Treatment of Cardiovascular Disease of Sichuan Province; Southwest Medical University, Teaching reform project of southwest medical university (2020XSJG-C01-19).

## SUPPLEMENTARY MATERIAL

The Supplementary Material for this article can be found online at: <https://www.frontiersin.org/articles/10.3389/fphar.2022.842313/full#supplementary-material>

## REFERENCES

- Afonina, I. S., Zhong, Z., Karin, M., and Beyaert, R. (2017). Limiting Inflammation—The Negative Regulation of NF- $\kappa$ B and the NLRP3 Inflammasome. *Nat. Immunol.* 18, 861–869. doi:10.1038/ni.3772
- Aglietti, R. A., Estevez, A., Gupta, A., Ramirez, M. G., Liu, P. S., Kayagaki, N., et al. (2016). GsdmD P30 Elicited by Caspase-11 during Pyroptosis Forms Pores in Membranes. *Proc. Natl. Acad. Sci. U S A.* 113, 7858–7863. doi:10.1073/pnas.1607769113
- Althunibat, O. Y., Al Hroob, A. M., Abukhalil, M. H., Germoush, M. O., Bin-Jumah, M., and Mahmoud, A. M. (2019). Fisetin Ameliorates Oxidative Stress, Inflammation and Apoptosis in Diabetic Cardiomyopathy. *Life Sci.* 221, 83–92. doi:10.1016/j.lfs.2019.02.017
- Bauer, P. M., Luo, B., Li, B., Wang, W., Liu, X., Xia, Y., et al. (2014). NLRP3 Gene Silencing Ameliorates Diabetic Cardiomyopathy in a Type 2 Diabetes Rat Model. *PLoS ONE* 9.
- Bauernfeind, F. G., Horvath, G., Stutz, A., Alnemri, E. S., MacDonald, K., Speert, D., et al. (2009). Cutting Edge: NF- $\kappa$ B Activating Pattern Recognition and Cytokine Receptors License NLRP3 Inflammasome Activation by Regulating NLRP3 Expression. *J. Immunol.* 183, 787–791. doi:10.4049/jimmunol.0901363
- Błażejowski, A. J., Thiemann, S., Schenk, A., Pils, M. C., Gálvez, E. J. C., Roy, U., et al. (2017). Microbiota Normalization Reveals that Canonical Caspase-1 Activation Exacerbates Chemically Induced Intestinal Inflammation. *Cell Rep* 19, 2319–2330. doi:10.1016/j.celrep.2017.05.058
- Boudina, S., and Abel, E. D. (2007). Diabetic Cardiomyopathy Revisited. *Circulation* 115, 3213–3223. doi:10.1161/CIRCULATIONAHA.106.679597
- Broz, P., Pelegrin, P., and Shao, F. (2020). The Gasdermins, a Protein Family Executing Cell Death and Inflammation. *Nat. Rev. Immunol.* 20, 143–157. doi:10.1038/s41577-019-0228-2
- Bruder-Nascimento, T., Ferreira, N. S., Zanotto, C. Z., Ramalho, F., Pequeno, I. O., Olivon, V. C., et al. (2016). NLRP3 Inflammasome Mediates Aldosterone-Induced Vascular Damage. *Circulation* 134, 1866–1880. doi:10.1161/CIRCULATIONAHA.116.024369
- Bryant, C., and Fitzgerald, K. A. (2009). Molecular Mechanisms Involved in Inflammasome Activation. *Trends Cel Biol* 19, 455–464. doi:10.1016/j.tcb.2009.06.002
- Cai, L. (2006). Suppression of Nitrate Damage by Metallothionein in Diabetic Heart Contributes to the Prevention of Cardiomyopathy. *Free Radic. Biol. Med.* 41, 851–861. doi:10.1016/j.freeradbiomed.2006.06.007
- Cai, L., Wang, Y., Zhou, G., Chen, T., Song, Y., Li, X., et al. (2006). Attenuation by Metallothionein of Early Cardiac Cell Death via Suppression of Mitochondrial Oxidative Stress Results in a Prevention of Diabetic Cardiomyopathy. *J. Am. Coll. Cardiol.* 48, 1688–1697. doi:10.1016/j.jacc.2006.07.022
- Chen, A., Chen, Z., Xia, Y., Lu, D., Yang, X., Sun, A., et al. (2018). Liraglutide Attenuates NLRP3 Inflammasome-dependent Pyroptosis via Regulating

- SIRT1/NOX4/ROS Pathway in H9c2 Cells. *Biochem. Biophys. Res. Commun.* 499, 267–272. doi:10.1016/j.bbrc.2018.03.142
- Chen, K. W., Demarco, B., Heilig, R., Shkarina, K., Boettcher, A., Farady, C. J., et al. (2019). Extrinsic and Intrinsic Apoptosis Activate Pannexin-1 to Drive NLRP3 Inflammasome Assembly. *EMBO J.* 38, e101638. doi:10.15252/embj.2019101638
- Chen, W., Zhao, M., Zhao, S., Lu, Q., Ni, L., Zou, C., et al. (2017). Activation of the TXNIP/NLRP3 Inflammasome Pathway Contributes to Inflammation in Diabetic Retinopathy: a Novel Inhibitory Effect of Minocycline. *Inflamm. Res.* 66, 157–166. doi:10.1007/s00011-016-1002-6
- Cookson, B. T., and Brennan, M. A. (2001). Pro-inflammatory Programmed Cell Death. *Trends Microbiol.* 9, 113–114. doi:10.1016/s0966-842x(00)01936-3
- Devi, T. S., Lee, I., Hüttemann, M., Kumar, A., Nantwi, K. D., and Singh, L. P. (2012). TXNIP Links Innate Host Defense Mechanisms to Oxidative Stress and Inflammation in Retinal Muller Glia under Chronic Hyperglycemia: Implications for Diabetic Retinopathy. *Exp. Diabetes Res.* 2012, 438238. doi:10.1155/2012/438238
- Ding, J., Wang, K., Liu, W., She, Y., Sun, Q., Shi, J., et al. (2016). Pore-forming Activity and Structural Autoinhibition of the Gasdermin Family. *Nature* 535, 111–116. doi:10.1038/nature18590
- Do, M. T., Kim, H. G., Choi, J. H., and Jeong, H. G. (2014). Metformin Induces microRNA-34a to Downregulate the Sirt1/Pgc-1 $\alpha$ /Nrf2 Pathway, Leading to Increased Susceptibility of Wild-type P53 Cancer Cells to Oxidative Stress and Therapeutic Agents. *Free Radic. Biol. Med.* 74, 21–34. doi:10.1016/j.freeradbiomed.2014.06.010
- El-Sisi, A. E. E., Sokar, S. S., Shebl, A. M., Mohamed, D. Z., and Abu-Risha, S. E. (2021). Octreotide and Melatonin Alleviate Inflammasome-Induced Pyroptosis through Inhibition of TLR4-NF-K $\beta$ -NLRP3 Pathway in Hepatic Ischemia/reperfusion Injury. *Toxicol. Appl. Pharmacol.* 410, 115340. doi:10.1016/j.taap.2020.115340
- Galluzzi, L., Vitale, I., Aaronson, S. A., Abrams, J. M., Adam, D., Agostinis, P., et al. (2018). Molecular Mechanisms of Cell Death: Recommendations of the Nomenclature Committee on Cell Death 2018. *Cell Death Differ* 25, 486–541. doi:10.1038/s41418-017-0012-4
- Ge, X., Li, W., Huang, S., Yin, Z., Xu, X., Chen, F., et al. (2018). The Pathological Role of NLRs and AIM2 Inflammasome-Mediated Pyroptosis in Damaged Blood-Brain Barrier after Traumatic Brain Injury. *Brain Res.* 1697, 10–20. doi:10.1016/j.brainres.2018.06.008
- Gonzalez-Pacheco, H., Vargas-Alarcon, G., Angeles-Martinez, J., Martinez-Sanchez, C., Perez-Mendez, O., Herrera-Maya, G., et al. (2017). The NLRP3 and CASP1 Gene Polymorphisms Are Associated with Developing of Acute Coronary Syndrome: a Case-Control Study. *Immunol. Res.* 65, 862–868. doi:10.1007/s12026-017-8924-0
- Green, J. P., Yu, S., Martín-Sánchez, F., Pelegrin, P., Lopez-Castejon, G., Lawrence, C. B., et al. (2018). Chloride Regulates Dynamic NLRP3-dependent ASC Oligomerization and Inflammasome Priming. *Proc. Natl. Acad. Sci. U S A.* 115, E9371–E9380. doi:10.1073/pnas.1812744115
- Gu, C., Liu, S., Wang, H., and Dou, H. (2019). Role of the Thioredoxin Interacting Protein in Diabetic Nephropathy and the Mechanism of Regulating NOD-like Receptor Protein 3 Inflammatory Corpuscle. *Int. J. Mol. Med.* 43 (6), 2440–2450. doi:10.3892/ijmm.2019.4163
- Hagar, J. A., Powell, D. A., Aachoui, Y., Ernst, R. K., and Miao, E. A. (2013). Cytoplasmic LPS Activates Caspase-11: Implications in TLR4-independent Endotoxic Shock. *Science* 341, 1250–1253. doi:10.1126/science.1240988
- Han, Y., Xu, X., Tang, C., Gao, P., Chen, X., Xiong, X., et al. (2018). Reactive Oxygen Species Promote Tubular Injury in Diabetic Nephropathy: The Role of the Mitochondrial Ros-Txnip-Nlrp3 Biological axis. *Redox Biol.* 16, 32–46. doi:10.1016/j.redox.2018.02.013
- Hao, Y., Liu, J., Wang, Z., Yu, L. L., and Wang, J. (2019). Piceatannol Protects Human Retinal Pigment Epithelial Cells against Hydrogen Peroxide Induced Oxidative Stress and Apoptosis through Modulating PI3K/Akt Signaling Pathway. *Nutrients* 11. doi:10.3390/nut11071515
- Hölscher, M. E., Bode, C., and Bugger, H. (2016). Diabetic Cardiomyopathy: Does the Type of Diabetes Matter? *Int. J. Mol. Sci.* 17, 2136.
- Hou, J., Zhao, R., Xia, W., Chang, C. W., You, Y., Hsu, J. M., et al. (2020). PD-L1-mediated Gasdermin C Expression Switches Apoptosis to Pyroptosis in Cancer Cells and Facilitates Tumour Necrosis. *Nat. Cel Biol* 22, 1264–1275. doi:10.1038/s41556-020-0575-z
- Jia, G., Hill, M. A., and Sowers, J. R. (2018). Diabetic Cardiomyopathy: An Update of Mechanisms Contributing to This Clinical Entity. *Circ. Res.* 122, 624–638. doi:10.1161/CIRCRESAHA.117.311586
- Jia, G., Whaley-Connell, A., and Sowers, J. R. (2018). Diabetic Cardiomyopathy: a Hyperglycaemia- and Insulin-Resistance-Induced Heart Disease. *Diabetologia* 61, 21–28. doi:10.1007/s00125-017-4390-4
- Johnson, D. C., Taabazuing, C. Y., Okondo, M. C., Chui, A. J., Rao, S. D., Brown, F. C., et al. (2018). DPP8/DPP9 Inhibitor-Induced Pyroptosis for Treatment of Acute Myeloid Leukemia. *Nat. Med.* 24, 1151–1156. doi:10.1038/s41591-018-0082-y
- Jorgensen, I., Rayamajhi, M., and Miao, E. A. (2017). Programmed Cell Death as a Defence against Infection. *Nat. Rev. Immunol.* 17, 151–164. doi:10.1038/nri.2016.147
- Joya-Galeana, J., Fernandez, M., Cervera, A., Reyna, S., Ghosh, S., Triplitt, C., et al. (2011). Effects of Insulin and Oral Anti-diabetic Agents on Glucose Metabolism, Vascular Dysfunction and Skeletal Muscle Inflammation in Type 2 Diabetic Subjects. *Diabetes Metab. Res. Rev.* 27, 373–382. doi:10.1002/dmrr.1185
- Kayagaki, N., Stowe, I. B., Lee, B. L., O'Rourke, K., Anderson, K., Warming, S., et al. (2015). Caspase-11 Cleaves Gasdermin D for Non-canonical Inflammasome Signalling. *Nature* 526, 666–671. doi:10.1038/nature15541
- Kayagaki, N., Warming, S., Lamkanfi, M., Vande Walle, L., Louie, S., Dong, J., et al. (2011). Non-canonical Inflammasome Activation Targets Caspase-11. *Nature* 479, 117–121. doi:10.1038/nature10558
- Kim, C. H. (2018). Microbiota or Short-Chain Fatty Acids: Which Regulates Diabetes? *Cell Mol Immunol* 15, 88–91. doi:10.1038/cmi.2017.57
- Kleinbongard, P., Amanakis, G., Skyschally, A., and Heusch, G. (2018). Reflection of Cardioprotection by Remote Ischemic Preconditioning in Attenuated ST-Segment Elevation during Ongoing Coronary Occlusion in Pigs: Evidence for Cardioprotection from Ischemic Injury. *Circ. Res.* 122, 1102–1108. doi:10.1161/CIRCRESAHA.118.312784
- Kovacs, S. B., and Miao, E. A. (2017). Gasdermins: Effectors of Pyroptosis. *Trends Cel Biol* 27, 673–684. doi:10.1016/j.tcb.2017.05.005
- Latz, E., Xiao, T. S., and Stutz, A. (2013). Activation and Regulation of the Inflammasomes. *Nat. Rev. Immunol.* 13, 397–411. doi:10.1038/nri3452
- Lee, H. M., Kim, J. J., Kim, H. J., Shong, M., Ku, B. J., and Jo, E. K. (2013). Upregulated NLRP3 Inflammasome Activation in Patients with Type 2 Diabetes. *Diabetes* 62, 194–204. doi:10.2337/db12-0420
- Levine, B., Mizushima, N., and Virgin, H. W. (2011). Autophagy in Immunity and Inflammation. *Nature* 469, 323–335. doi:10.1038/nature09782
- Li, H., Shi, Y., Wang, X., Li, P., Zhang, S., Wu, T., et al. (2019). Piceatannol Alleviates Inflammation and Oxidative Stress via Modulation of the Nrf2/HO-1 and NF-K $\beta$  Pathways in Diabetic Cardiomyopathy. *Chem. Biol. Interact* 310, 108754. doi:10.1016/j.cbi.2019.108754
- Li, N., Zhou, H., Wu, H., Wu, Q., Duan, M., Deng, W., et al. (2019). STING-IRF3 Contributes to Lipopolysaccharide-Induced Cardiac Dysfunction, Inflammation, Apoptosis and Pyroptosis by Activating NLRP3. *Redox Biol.* 24, 101215. doi:10.1016/j.redox.2019.101215
- Li, X., Du, N., Zhang, Q., Li, J., Chen, X., Liu, X., et al. (2014). MicroRNA-30d Regulates Cardiomyocyte Pyroptosis by Directly Targeting Foxo3a in Diabetic Cardiomyopathy. *Cell Death Dis* 5, e1479. doi:10.1038/cddis.2014.430
- Li, X., Kover, K. L., Heruth, D. P., Watkins, D. J., Guo, Y., Moore, W. V., et al. (2017). Thioredoxin-interacting Protein Promotes High-Glucose-Induced Macrovascular Endothelial Dysfunction. *Biochem. Biophys. Res. Commun.* 493, 291–297. doi:10.1016/j.bbrc.2017.09.028
- Liu, X., Zhang, Z., Ruan, J., Pan, Y., Magupalli, V. G., Wu, H., et al. (2016). Inflammasome-activated Gasdermin D Causes Pyroptosis by Forming Membrane Pores. *Nature* 535, 153–158. doi:10.1038/nature18629
- Loboda, A., Damulewicz, M., Pyza, E., Jozkowicz, A., and Dulak, J. (2016). Role of Nrf2/HO-1 System in Development, Oxidative Stress Response and Diseases: an Evolutionarily Conserved Mechanism. *Cell Mol Life Sci* 73, 3221–3247. doi:10.1007/s00018-016-2223-0
- Lu, L., Lu, Q., Chen, W., Li, J., Li, C., and Zheng, Z. (2018). Vitamin D3 Protects against Diabetic Retinopathy by Inhibiting High-Glucose-Induced Activation of the ROS/TXNIP/NLRP3 Inflammasome Pathway. *J. Diabetes Res.* 2018, 8193523. doi:10.1155/2018/8193523

- Luo, B., Huang, F., Liu, Y., Liang, Y., Wei, Z., Ke, H., et al. (2017). NLRP3 Inflammasome as a Molecular Marker in Diabetic Cardiomyopathy. *Front. Physiol.* 8, 519. doi:10.3389/fphys.2017.00519
- Luo, B., Li, B., Wang, W., Liu, X., Xia, Y., Zhang, C., et al. (2014). NLRP3 Gene Silencing Ameliorates Diabetic Cardiomyopathy in a Type 2 Diabetes Rat Model. *PLoS one* 9, e104771. doi:10.1371/journal.pone.0104771
- Ma, Y., Gong, X., Mo, Y., and Wu, S. (2016). Polydatin Inhibits the Oxidative Stress-Induced Proliferation of Vascular Smooth Muscle Cells by Activating the eNOS/SIRT1 Pathway. *Int. J. Mol. Med.* 37, 1652–1660. doi:10.3892/ijmm.2016.2554
- Man, S. M., Karki, R., and Kanneganti, T. D. (2017). Molecular Mechanisms and Functions of Pyroptosis, Inflammatory Caspases and Inflammasomes in Infectious Diseases. *Immunol. Rev.* 277, 61–75. doi:10.1111/imr.12534
- Mann, D. L. (2015). Innate Immunity and the Failing Heart: The Cytokine Hypothesis Revisited. *Circ. Res.* 116, 1254–1268. doi:10.1161/CIRCRESAHA.116.302317
- Miao, E. A., Leaf, I. A., Treuting, P. M., Mao, D. P., Dors, M., Sarkar, A., et al. (2010). Caspase-1-induced Pyroptosis Is an Innate Immune Effector Mechanism against Intracellular Bacteria. *Nat. Immunol.* 11, 1136–1142. doi:10.1038/ni.1960
- Mungai, P. T., Waypa, G. B., Jairaman, A., Prakriya, M., Dokic, D., Ball, M. K., et al. (2011). Hypoxia Triggers AMPK Activation through Reactive Oxygen Species-Mediated Activation of Calcium Release-Activated Calcium Channels. *Mol. Cell Biol.* 31, 3531–3545. doi:10.1128/MCB.05124-11
- Needell, J. C., and Zipris, D. (2017). Targeting Innate Immunity for Type 1 Diabetes Prevention. *Curr. Diab Rep.* 17, 113. doi:10.1007/s11892-017-0930-z
- Orning, P., Weng, D., Starheim, K., Ratner, D., Best, Z., Lee, B., et al. (2018). Pathogen Blockade of TAK1 Triggers Caspase-8-dependent Cleavage of Gasdermin D and Cell Death. *Science* 362, 1064–1069. doi:10.1126/science.aau2818
- Pan, J., Han, L., Guo, J., Wang, X., Liu, D., Tian, J., et al. (2018). AIM2 Accelerates the Atherosclerotic Plaque Progressions in ApoE<sup>-/-</sup> Mice. *Biochem. Biophys. Res. Commun.* 498, 487–494. doi:10.1016/j.bbrc.2018.03.005
- Pasparakis, M., and Vandenabeele, P. (2015). Necroptosis and its Role in Inflammation. *Nature* 517, 311–320. doi:10.1038/nature14191
- Pereira, N. S., Queiroga, T. B. D., Nunes, D. F., Andrade, C. M., Nascimento, M. S. L., Do-Valle-Matta, M. A., et al. (2018). Innate Immune Receptors over Expression Correlate with Chronic Chagasic Cardiomyopathy and Digestive Damage in Patients. *Plos Negl. Trop. Dis.* 12, e0006589. doi:10.1371/journal.pntd.0006589
- Prabhu, S. D., and Frangogiannis, N. G. (2016). The Biological Basis for Cardiac Repair after Myocardial Infarction: From Inflammation to Fibrosis. *Circ. Res.* 119, 91–112. doi:10.1161/CIRCRESAHA.116.303577
- Qiao, Y., Wang, P., Qi, J., Zhang, L., and Gao, C. (2012). TLR-induced NF-Kb Activation Regulates NLRP3 Expression in Murine Macrophages. *FEBS Lett.* 586, 1022–1026. doi:10.1016/j.febslet.2012.02.045
- Qiu, Y. Y., and Tang, L. Q. (2016). Roles of the NLRP3 Inflammasome in the Pathogenesis of Diabetic Nephropathy. *Pharmacol. Res.* 114, 251–264. doi:10.1016/j.phrs.2016.11.004
- Qiu, Z., Lei, S., Zhao, B., Wu, Y., Su, W., Liu, M., et al. (2017). NLRP3 Inflammasome Activation-Mediated Pyroptosis Aggravates Myocardial Ischemia/Reperfusion Injury in Diabetic Rats. *Oxid Med. Cell Longev* 2017, 9743280. doi:10.1155/2017/9743280
- Qu, H., Lin, K., Wang, H., Wei, H., Ji, B., Yang, Z., et al. (2017). 1,25(OH)<sub>2</sub>D<sub>3</sub> Improves Cardiac Dysfunction, Hypertrophy, and Fibrosis through PARP1/SIRT1/mTOR-Related Mechanisms in Type 1 Diabetes. *Mol. Nutr. Food Res.* 61. doi:10.1002/mnfr.201600338
- Rendra, E., Riabov, V., Mossel, D. M., Sevastyanova, T., Harmsen, M. C., and Kzyshkowska, J. (2019). Reactive Oxygen Species (ROS) in Macrophage Activation and Function in Diabetes. *Immunobiology* 224, 242–253. doi:10.1016/j.imbio.2018.11.010
- Rogers, C., Erkes, D. A., Nardone, A., Aplin, A. E., Fernandes-Alnemri, T., and Alnemri, E. S. (2019). Gasdermin Pores Permeabilize Mitochondria to Augment Caspase-3 Activation during Apoptosis and Inflammasome Activation. *Nat. Commun.* 10, 1689. doi:10.1038/s41467-019-09397-2
- Rogers, C., Fernandes-Alnemri, T., Mayes, L., Alnemri, D., Cingolani, G., and Alnemri, E. S. (2017). Cleavage of DFNA5 by Caspase-3 during Apoptosis Mediates Progression to Secondary Necrotic/pyroptotic Cell Death. *Nat. Commun.* 8, 14128. doi:10.1038/ncomms14128
- Rubler, S., Dlugash, J., Yuceoglu, Y. Z., Kumral, T., Branwood, A. W., and Grishman, A. (1972). New Type of Cardiomyopathy Associated with Diabetic Glomerulosclerosis. *Am. J. Cardiol.* 30, 595–602. doi:10.1016/0002-9149(72)90595-4
- Russo, H. M., Rathkey, J., Boyd-Tressler, A., Katsnelson, M. A., Abbott, D. W., and Dubyak, G. R. (2016). Active Caspase-1 Induces Plasma Membrane Pores that Precede Pyroptotic Lysis and Are Blocked by Lanthanides. *J. Immunol.* 197, 1353–1367. doi:10.4049/jimmunol.1600699
- Salvatore, T., Pafundi, P. C., Galiero, R., Albanese, G., Di Martino, A., Caturano, A., et al. (2021). The Diabetic Cardiomyopathy: The Contributing Pathophysiological Mechanisms. *Front. Med. (Lausanne)* 8, 695792. doi:10.3389/fmed.2021.695792
- Sanchez-Lopez, E., Zhong, Z., Stubelius, A., Sweeney, S. R., Booshehri, L. M., Antonucci, L., et al. (2019). Choline Uptake and Metabolism Modulate Macrophage IL-1 $\beta$  and IL-18 Production. *Cell Metab* 29, 1350e1357–e7. doi:10.1016/j.cmet.2019.03.011
- Sarhan, J., Liu, B. C., Muendlein, H. I., Li, P., Nilson, R., Tang, A. Y., et al. (2018). Caspase-8 Induces Cleavage of Gasdermin D to Elicit Pyroptosis during Yersinia Infection. *Proc. Natl. Acad. Sci. U S A.* 115, E10888–E10897. doi:10.1073/pnas.1809548115
- Sborgi, L., Rühl, S., Mulvihill, E., Pipercevic, J., Heilig, R., Stahlberg, H., et al. (2016). GSDMD Membrane Pore Formation Constitutes the Mechanism of Pyroptotic Cell Death. *EMBO J.* 35, 1766–1778. doi:10.15252/embj.201694696
- Schroder, K., Zhou, R., and Tschopp, J. (2010). The NLRP3 Inflammasome: a Sensor for Metabolic Danger? *Science* 327, 296–300. doi:10.1126/science.1184003
- Shi, J., Gao, W., and Shao, F. (2017). Pyroptosis: Gasdermin-Mediated Programmed Necrotic Cell Death. *Trends Biochem. Sci.* 42, 245–254. doi:10.1016/j.tibs.2016.10.004
- Shi, J., Zhao, Y., Wang, K., Shi, X., Wang, Y., Huang, H., et al. (2015). Cleavage of GSDMD by Inflammatory Caspases Determines Pyroptotic Cell Death. *Nature* 526, 660–665. doi:10.1038/nature15514
- Shi, J., Zhao, Y., Wang, Y., Gao, W., Ding, J., Li, P., et al. (2014). Inflammatory Caspases Are Innate Immune Receptors for Intracellular LPS. *Nature* 514, 187–192. doi:10.1038/nature13683
- Simic, P., Williams, E. O., Bell, E. L., Gong, J. J., Bonkowski, M., and Guarente, L. (2013). SIRT1 Suppresses the Epithelial-To-Mesenchymal Transition in Cancer Metastasis and Organ Fibrosis. *Cel Rep* 3, 1175–1186. doi:10.1016/j.celrep.2013.03.019
- Soengas, M. S., Alarcón, R. M., Yoshida, H., Giaccia, A. J., Hakem, R., Mak, T. W., et al. (1999). Apaf-1 and Caspase-9 in P53-dependent Apoptosis and Tumor Inhibition. *Science* 284, 156–159. doi:10.1126/science.284.5411.156
- Song, Y., Yang, L., Guo, R., Lu, N., Shi, Y., and Wang, X. (2019). Long Noncoding RNA MALAT1 Promotes High Glucose-Induced Human Endothelial Cells Pyroptosis by Affecting NLRP3 Expression through Competitively Binding miR-22. *Biochem. Biophys. Res. Commun.* 509, 359–366. doi:10.1016/j.bbrc.2018.12.139
- Stienstra, R., Joosten, L. A., Koenen, T., van Tits, B., van Diepen, J. A., van den Berg, S. A., et al. (2010). The Inflammasome-Mediated Caspase-1 Activation Controls Adipocyte Differentiation and Insulin Sensitivity. *Cel Metab* 12, 593–605. doi:10.1016/j.cmet.2010.11.011
- Strowig, T., Henao-Mejia, J., Elinav, E., and Flavell, R. (2012). Inflammasomes in Health and Disease. *Nature* 481, 278–286. doi:10.1038/nature10759
- Sun, S. C. (2017). The Non-canonical NF-Kb Pathway in Immunity and Inflammation. *Nat. Rev. Immunol.* 17, 545–558. doi:10.1038/nri.2017.52
- Tsai, K. H., Wang, W. J., Lin, C. W., Pai, P., Lai, T. Y., Tsai, C. Y., et al. (2012). NADPH Oxidase-Derived Superoxide Anion-Induced Apoptosis Is Mediated via the JNK-dependent Activation of NF-Kb in Cardiomyocytes Exposed to High Glucose. *J. Cel Physiol* 227, 1347–1357. doi:10.1002/jcp.22847
- Tsushima, M., Liu, J., Hirao, W., Yamazaki, H., Tomita, H., and Itoh, K. (2019). Emerging Evidence for Crosstalk between Nrf2 and Mitochondria in Physiological Homeostasis and in Heart Disease. *Arch. Pharm. Res.* 43, 286–296. doi:10.1007/s12272-019-01188-z
- Ungvari, Z., Tarantini, S., Nyúl-Tóth, Á., Kiss, T., Yabluchanskiy, A., Csipo, T., et al. (2019). Nrf2 Dysfunction and Impaired Cellular Resilience to Oxidative Stressors in the Aged Vasculature: from Increased Cellular Senescence to the



- Pathogenesis of Age-Related Vascular Diseases. *GeroScience* 41, 727–738. doi:10.1007/s11357-019-00107-w
- Wallach, D., Kang, T. B., Dillon, C. P., and Green, D. R. (2016). Programmed Necrosis in Inflammation: Toward Identification of the Effector Molecules. *Science* 352, aaf2154. doi:10.1126/science.aaf2154
- Wang, J., Sahoo, M., Lantier, L., Warawa, J., Cordero, H., Deobald, K., et al. (2018). Caspase-11-dependent Pyroptosis of Lung Epithelial Cells Protects from Melioidosis while Caspase-1 Mediates Macrophage Pyroptosis and Production of IL-18. *Plos Pathog.* 14, e1007105. doi:10.1371/journal.ppat.1007105
- Wang, Y., Gao, W., Shi, X., Ding, J., Liu, W., He, H., et al. (2017). Chemotherapy Drugs Induce Pyroptosis through Caspase-3 Cleavage of a Gasdermin. *Nature* 547, 99–103. doi:10.1038/nature22393
- Wang, Y., Jia, L., Shen, J., Wang, Y., Fu, Z., Su, S. A., et al. (2018). Cathepsin B Aggravates Coxsackievirus B3-Induced Myocarditis through Activating the Inflammasome and Promoting Pyroptosis. *Plos Pathog.* 14, e1006872. doi:10.1371/journal.ppat.1006872
- Wang, Y., Zhu, X., Yuan, S., Wen, S., Liu, X., Wang, C., et al. (2019). TLR4/NF- $\kappa$ B Signaling Induces GSDMD-Related Pyroptosis in Tubular Cells in Diabetic Kidney Disease. *Front. Endocrinol. (Lausanne)* 10, 603. doi:10.3389/fendo.2019.00603
- Wardyn, J. D., Ponsford, A. H., and Sanderson, C. M. (2015). Dissecting Molecular Cross-Talk between Nrf2 and NF- $\kappa$ B Response Pathways. *Biochem. Soc. Trans.* 43, 621–626. doi:10.1042/BST20150014
- Watabe, K., Ito, A., Asada, H., Endo, Y., Kobayashi, T., Nakamoto, K., et al. (2001). Structure, Expression and Chromosome Mapping of MLZE, a Novel Gene Which Is Preferentially Expressed in Metastatic Melanoma Cells. *Jpn. J. Cancer Res.* 92, 140–151. doi:10.1111/j.1349-7006.2001.tb01076.x
- Wei, H., Bu, R., Yang, Q., Jia, J., Li, T., Wang, Q., et al. (2019). Exendin-4 Protects against Hyperglycemia-Induced Cardiomyocyte Pyroptosis via the AMPK-TXNIP Pathway. *J. Diabetes Res.* 2019, 8905917. doi:10.1155/2019/8905917
- Wen, H., Gris, D., Lei, Y., Jha, S., Zhang, L., Huang, M. T., et al. (2011). Fatty Acid-Induced NLRP3-ASC Inflammasome Activation Interferes with Insulin Signaling. *Nat. Immunol.* 12, 408–415. doi:10.1038/ni.2022
- Wu, C., Lu, W., Zhang, Y., Zhang, G., Shi, X., Hisada, Y., et al. (2019). Inflammasome Activation Triggers Blood Clotting and Host Death through Pyroptosis. *Immunity* 50, 1401–e4. doi:10.1016/j.immuni.2019.04.003
- Wu, D., Yan, Z. B., Cheng, Y. G., Zhong, M. W., Liu, S. Z., Zhang, G. Y., et al. (2018). Deactivation of the NLRP3 Inflammasome in Infiltrating Macrophages by Duodenal-jejunal Bypass Surgery Mediates Improvement of Beta Cell Function in Type 2 Diabetes. *Metabolism* 81, 1–12. doi:10.1016/j.metabol.2017.10.015
- Wu, N., Zheng, B., Shaywitz, A., Dagon, Y., Tower, C., Bellinger, G., et al. (2013). AMPK-dependent Degradation of TXNIP upon Energy Stress Leads to Enhanced Glucose Uptake via GLUT1. *Mol. Cell* 49, 1167–1175. doi:10.1016/j.molcel.2013.01.035
- Xia, X., Wang, X., Zheng, Y., Jiang, J., and Hu, J. (2019). What Role Does Pyroptosis Play in Microbial Infection? *J. Cell Physiol* 234, 7885–7892. doi:10.1002/jcp.27909
- Yang, C. C., Yao, C. A., Yang, J. C., and Chien, C. T. (2014). Sialic Acid Rescues Repurified Lipopolysaccharide-Induced Acute Renal Failure via Inhibiting TLR4/PKC/gp91-mediated Endoplasmic Reticulum Stress, Apoptosis, Autophagy, and Pyroptosis Signaling. *Toxicol. Sci.* 141, 155–165. doi:10.1093/toxsci/kfu121
- Yang, F., Li, A., Qin, Y., Che, H., Wang, Y., Lv, J., et al. (2019). A Novel Circular RNA Mediates Pyroptosis of Diabetic Cardiomyopathy by Functioning as a Competing Endogenous RNA. *Mol. Ther. Nucleic Acids* 17, 636–643. doi:10.1016/j.omtn.2019.06.026
- Yang, F., Qin, Y., Lv, J., Wang, Y., Che, H., Chen, X., et al. (2018). Silencing Long Non-coding RNA Kcnq1ot1 Alleviates Pyroptosis and Fibrosis in Diabetic Cardiomyopathy. *Cell Death Dis* 9, 1000. doi:10.1038/s41419-018-1029-4
- Yang, F., Qin, Y., Wang, Y., Li, A., Lv, J., Sun, X., et al. (2018). LncRNA KCNQ1OT1 Mediates Pyroptosis in Diabetic Cardiomyopathy. *Cell Physiol Biochem* 50, 1230–1244. doi:10.1159/000494576
- Yang, F., Qin, Y., Wang, Y., Meng, S., Xian, H., Che, H., et al. (2019). Metformin Inhibits the NLRP3 Inflammasome via AMPK/mTOR-dependent Effects in Diabetic Cardiomyopathy. *Int. J. Biol. Sci.* 15, 1010–1019. doi:10.7150/ijbs.29680
- Yang, T. C., Chang, P. Y., and Lu, S. C. (2017). L5-LDL from ST-Elevation Myocardial Infarction Patients Induces IL-1 $\beta$  Production via LOX-1 and NLRP3 Inflammasome Activation in Macrophages. *Am. J. Physiol. Heart Circ. Physiol.* 312, H265–H274. doi:10.1152/ajpheart.00509.2016
- Yap, J., Tay, W. T., Teng, T. K., Anand, I., Richards, A. M., Ling, L. H., et al. (2019). Association of Diabetes Mellitus on Cardiac Remodeling, Quality of Life, and Clinical Outcomes in Heart Failure with Reduced and Preserved Ejection Fraction. *J. Am. Heart Assoc.* 8, e013114. doi:10.1161/JAHA.119.013114
- Yi, Y. S. (2017). Caspase-11 Non-canonical Inflammasome: a Critical Sensor of Intracellular Lipopolysaccharide in Macrophage-Mediated Inflammatory Responses. *Immunology* 152, 207–217. doi:10.1111/imm.12787
- Youm, Y. H., Nguyen, K. Y., Grant, R. W., Goldberg, E. L., Bodogai, M., Kim, D., et al. (2015). The Ketone Metabolite  $\beta$ -hydroxybutyrate Blocks NLRP3 Inflammasome-Mediated Inflammatory Disease. *Nat. Med.* 21, 263–269. doi:10.1038/nm.3804
- Yu, S. Y., Dong, B., Tang, L., and Zhou, S. H. (2018). LncRNA MALAT1 Sponges miR-133 to Promote NLRP3 Inflammasome Expression in Ischemia-Reperfusion Injured Heart. *Int. J. Cardiol.* 254, 50. doi:10.1016/j.ijcard.2017.10.071
- Yu, Z. W., Zhang, J., Li, X., Wang, Y., Fu, Y. H., and Gao, X. Y. (2020). A New Research Hot Spot: The Role of NLRP3 Inflammasome Activation, a Key Step in Pyroptosis, in Diabetes and Diabetic Complications. *Life Sci.* 240, 117138. doi:10.1016/j.lfs.2019.117138
- Yuan, J., Najafav, A., and Py, B. F. (2016). Roles of Caspases in Necrotic Cell Death. *Cell* 167, 1693–1704. doi:10.1016/j.cell.2016.11.047
- Zeng, J., Chen, Y., Ding, R., Feng, L., Fu, Z., Yang, S., et al. (2017). Isoliquiritigenin Alleviates Early Brain Injury after Experimental Intracerebral Hemorrhage via Suppressing ROS- And/or NF- $\kappa$ B-Mediated NLRP3 Inflammasome Activation by Promoting Nrf2 Antioxidant Pathway. *J. Neuroinflammation* 14, 119. doi:10.1186/s12974-017-0895-5
- Zhang, C. R., Zhu, W. N., Tao, W., Lin, W. Q., Cheng, C. C., Deng, H., et al. (2021). Moxibustion against Cyclophosphamide-Induced Premature Ovarian Failure in Rats through Inhibiting NLRP3-/Caspase-1/gsdmd-dependent Pyroptosis. *Evid. Based Complement. Alternat Med.* 2021, 8874757. doi:10.1155/2021/8874757
- Zhang, H., Chen, X., Zong, B., Yuan, H., Wang, Z., Wei, Y., et al. (2018). Gypenosides Improve Diabetic Cardiomyopathy by Inhibiting ROS-Mediated NLRP3 Inflammasome Activation. *J. Cel Mol Med* 22, 4437–4448. doi:10.1111/jcmm.13743
- Zhang, X., Pan, L., Yang, K., Fu, Y., Liu, Y., Chi, J., et al. (2017). H3 Relaxin Protects against Myocardial Injury in Experimental Diabetic Cardiomyopathy by Inhibiting Myocardial Apoptosis, Fibrosis and Inflammation. *Cell Physiol Biochem* 43, 1311–1324. doi:10.1159/000481843
- Zhang, Y., Liu, X., Bai, X., Lin, Y., Li, Z., Fu, J., et al. (2018). Melatonin Prevents Endothelial Cell Pyroptosis via Regulation of Long Noncoding RNA MEG3/miR-223/NLRP3 axis. *J. Pineal Res.* 64. doi:10.1111/jpi.12449
- Zhang, Z., Zhang, Y., Xia, S., Kong, Q., Li, S., Liu, X., et al. (2020). Gasdermin E Suppresses Tumour Growth by Activating Anti-tumour Immunity. *Nature* 579, 415–420. doi:10.1038/s41586-020-2071-9
- Zhao, M. W., Yang, P., and Zhao, L. L. (2019). Chlorpyrifos Activates Cell Pyroptosis and Increases Susceptibility on Oxidative Stress-Induced Toxicity by miR-181/SIRT1/PGC-1 $\alpha$ /Nrf2 Signaling Pathway in Human Neuroblastoma SH-Sy5y Cells: Implication for Association between Chlorpyrifos and Parkinson's Disease. *Environ. Toxicol.* 34, 699–707. doi:10.1002/tox.22736
- Zhong, Z., Zhai, Y., Liang, S., Mori, Y., Han, R., Sutterwala, F., et al. (2013). TRPM2 Links Oxidative Stress to the NLRP3 Inflammasome Activation (P1268). *J. Immunol.* 190, 1611. doi:10.1038/ncomms2608
- Zhou, R., Yazdi, A. S., Menu, P., and Tschopp, J. (2011). A Role for Mitochondria in NLRP3 Inflammasome Activation. *Nature* 469, 221–225. doi:10.1038/nature09663
- Zhou, W., Chen, C., Chen, Z., Liu, L., Jiang, J., Wu, Z., et al. (2018). NLRP3: A Novel Mediator in Cardiovascular Disease. *J. Immunol. Res.* 2018, 5702103. doi:10.1155/2018/5702103

- Zhou, Z., He, H., Wang, K., Shi, X., Wang, Y., Su, Y., et al. (2020). Granzyme A from Cytotoxic Lymphocytes Cleaves GSDMB to Trigger Pyroptosis in Target Cells. *Science* 368, eaaz7548. doi:10.1126/science.aaz7548
- Zhu, J., Yang, Y., Hu, S. G., Zhang, Q. B., Yu, J., and Zhang, Y. M. (2017). T-lymphocyte Kv1.3 Channel Activation Triggers the NLRP3 Inflammasome Signaling Pathway in Hypertensive Patients. *Exp. Ther. Med.* 14, 147–154. doi:10.3892/etm.2017.4490
- Zychlinsky, A., Prevost, M. C., and Sansonetti, P. J. (1992). Shigella Flexneri Induces Apoptosis in Infected Macrophages. *Nature* 358, 167–169. doi:10.1038/358167a0

**Conflict of Interest:** The authors declare that the research was conducted in the absence of any commercial or financial relationships that could be construed as a potential conflict of interest.

**Publisher's Note:** All claims expressed in this article are solely those of the authors and do not necessarily represent those of their affiliated organizations, or those of the publisher, the editors and the reviewers. Any product that may be evaluated in this article, or claim that may be made by its manufacturer, is not guaranteed or endorsed by the publisher.

Copyright © 2022 Cai, Yuan, Luan, Feng, Deng, Zuo and Li. This is an open-access article distributed under the terms of the Creative Commons Attribution License (CC BY). The use, distribution or reproduction in other forums is permitted, provided the original author(s) and the copyright owner(s) are credited and that the original publication in this journal is cited, in accordance with accepted academic practice. No use, distribution or reproduction is permitted which does not comply with these terms.



# A Multitarget Therapeutic Peptide Derived From Cytokine Receptors Based on in Silico Analysis Alleviates Cytokine-Stimulated Inflammation

Chun-Chun Chang<sup>1,2</sup>, Shih-Yi Peng<sup>3</sup>, Hao-Hsiang Tsao<sup>3</sup>, Hsin-Ting Huang<sup>3</sup>, Xing-Yan Lai<sup>4</sup>, Hao-Jen Hsu<sup>4\*†</sup> and Shinn-Jong Jiang<sup>3\*†</sup>

<sup>1</sup>Department of Laboratory Medicine, Hualien Tzu Chi Hospital, Hualien, Taiwan, <sup>2</sup>Department of Laboratory Medicine and Biotechnology, College of Medicine, Tzu Chi University, Hualien, Taiwan, <sup>3</sup>Department of Biochemistry, School of Medicine, Tzu Chi University, Hualien, Taiwan, <sup>4</sup>Department of Life Sciences, College of Medicine, Tzu Chi University, Hualien, Taiwan

## OPEN ACCESS

### Edited by:

Xianwei Wang,  
Xinxiang Medical University, China

### Reviewed by:

Constantino López-Macías,  
Mexican Social Security Institute  
(IMSS), Mexico  
Uzma Saqib,  
Indian Institute of Technology Indore,  
India

### \*Correspondence:

Hao-Jen Hsu  
hjhsu32@mail.tcu.edu.tw  
Shinn-Jong Jiang  
sjjiang@mail.tcu.edu.tw

<sup>†</sup>These authors have contributed  
equally to this work

### Specialty section:

This article was submitted to  
Cardiovascular and Smooth Muscle  
Pharmacology,  
a section of the journal  
Frontiers in Pharmacology

**Received:** 13 January 2022

**Accepted:** 18 February 2022

**Published:** 10 March 2022

### Citation:

Chang C-C, Peng S-Y, Tsao H-H,  
Huang H-T, Lai X-Y, Hsu H-J and  
Jiang S-J (2022) A Multitarget  
Therapeutic Peptide Derived From  
Cytokine Receptors Based on in Silico  
Analysis Alleviates Cytokine-  
Stimulated Inflammation.  
Front. Pharmacol. 13:853818.  
doi: 10.3389/fphar.2022.853818

Septicemia is a severe inflammatory response caused by the invasion of foreign pathogens. Severe sepsis-induced shock and multiple organ failure are the two main causes of patient death. The overexpression of many proinflammatory cytokines, such as TNF- $\alpha$ , IL-1 $\beta$ , and IL-6, is closely related to severe sepsis. Although the treatment of sepsis has been subject to many major breakthroughs of late, the treatment of patients with septic shock is still accompanied by a high mortality rate. In our previous research, we used computer simulations to design the multifunctional peptide KCF18 that can bind to TNF- $\alpha$ , IL-1 $\beta$ , and IL-6 based on the binding regions of receptors and proinflammatory cytokines. In this study, proinflammatory cytokines were used to stimulate human monocytes to trigger an inflammatory response, and the anti-inflammatory ability of the multifunctional KCF18 peptide was further investigated. Cell experiments demonstrated that KCF18 significantly reduced the binding of proinflammatory cytokines to their cognate receptors and inhibited the mRNA and protein expressions of TNF- $\alpha$ , IL-1 $\beta$ , and IL-6. It could also reduce the expression of reactive oxygen species induced by cytokines in human monocytes. KCF18 could effectively decrease the p65 nucleus translocation induced by cytokines, and a mice endotoxemia experiment demonstrated that KCF18 could reduce the expression of IL-6 and the increase of white blood cells in the blood stimulated by lipopolysaccharides. According to our study of tissue sections, KCF18 alleviated liver inflammation. By reducing the release of cytokines in plasma and directly affecting vascular cells, KCF18 is believed to significantly reduce the risk of vascular inflammation.

**Keywords:** sepsis, cytokine, inflammation, peptide drug, reactive oxygen species, tumor necrosis factors (TNF)- $\alpha$

## INTRODUCTION

Cytokines are mostly 8–25 kDa water-soluble proteins and glycoproteins that are involved in cell signaling. For their main functions, cytokines promote cell proliferation, activation, and differentiation and participate in inflammation, immune response regulation, and tissue repair (Cannon, 2000). Cytokines include chemokines, interferons (IFNs), interleukins (ILs), and tumor necrosis factors (TNFs). When the human body is infected by pathogens, it causes macrophages to

secrete numerous proinflammatory cytokines, such as IL-1, IL-6, IL-8, and TNF- $\alpha$ . These proinflammatory cytokines facilitate the activation of white blood cells; they prompt the accumulation of white blood cells, enhance the activation of endothelial cells, increase the permeability of blood vessels, produce inflammatory responses, remove foreign pathogens, and induce the generation of acquired immune responses. Therefore, constant cytokines are crucial for maintaining body health. However, when cytokines are overexposed, they may cause cell damage and further injury to organs. This phenomenon is called a cytokine storm, which eventually leads to the occurrence of diseases (Kilroy et al., 2007; Sun et al., 2012; D'elia et al., 2013) such as sepsis, cytokine release syndrome, and systemic inflammatory response syndrome.

Reactive oxygen species (ROS) are highly biologically active substances produced during the process of oxidative metabolism in the human body (Devasagayam et al., 2004; Pacher et al., 2007) and are exemplified by molecules such as superoxide radicals ( $O_2^{\bullet-}$ ), hydroxyl radicals ( $OH^{\bullet}$ ), and hydrogen peroxide ( $H_2O_2$ ). An appropriate amount of ROS is involved in cellular signal transduction and regulation of cell growth (Radi, 2013). In addition, white blood cells and macrophages can produce  $O_2^{\bullet-}$ ,  $H_2O_2$ , and other ROS to eliminate foreign pathogens (Prolo et al., 2014). However, excessive ROS will destroy the integrity of the antioxidant defense system in the body and cause oxidative stress and oxidative damage in the organism (Radi, 2013; Prolo et al., 2014); for example, 1) ROS may attack the polyunsaturated fatty acids on the cell membrane of the body, causing lipid peroxidation and then destroying the integrity of cell membranes. 2) ROS may change the protein structure or denature proteins, leading to a loss of enzyme activity that catalyzes metabolic reactions. 3) They may damage the base structure of DNA molecules and further cause gene mutations or toxicity. 4) ROS may stimulate white blood cells and macrophages to release cytokines and cause inflammation. These reactions can cause cell damage, destruction, and even cell death. The destruction and accumulation of these ROS are key reasons for the occurrence of aging-related phenomena and diseases, such as degenerative diseases, cancer, cardiovascular disease, diabetes, and autoimmune disease, as described in many studies (Muller et al., 2007; Sinha et al., 2014). Although oxidative stress is considered to be a phenomenon that accompanies inflammation, increasing evidence has shown that oxidative stress can be an early stage in the development of inflammation-related diseases (West et al., 2011; Kvietyis and Granger, 2012; Craige et al., 2015). The clearance of ROS plays a vital role in the prevention and treatment of inflammation-related diseases. NF- $\kappa$ B is a significant transcription factor in the signal transmission pathway and is closely related to inflammation, apoptosis, and tumorigenesis (Yamamoto and Gaynor, 2001; Lawrence, 2009). NF- $\kappa$ B is a dimer composed of various subunits, including p50, p52, p65 (RelA), RelB, and c-Rel. It regulates the expression of cytokines, chemoattractant factors, and adhesion molecules. NF- $\kappa$ B is mainly a heterodimer formed by p50 and p65, and it usually combines with I $\kappa$ B to form an inactive form in cytoplasm. When NF- $\kappa$ B is activated by cytokines (such as IL-1 $\beta$  or TNF- $\alpha$ ), proinflammatory

substances (such as ROS), or bacterial products (such as lipopolysaccharides [LPS]), I $\kappa$ B will be phosphorylated and separated from NF- $\kappa$ B, which enables NF- $\kappa$ B to enter the cell nucleus; moreover, phosphorylated p65 can bind to DNA for transcriptional regulation, which consists of 1) promoting the expression of proinflammatory cytokines and chemoattractant factors such as TNF- $\alpha$ , IL-1, and IL-6, which activate immune cells. Additionally, the transcriptional regulation 2) may entail the induction of adhesion molecules, such as ICAM, VCAM, E-selectin, and P-selectin, to promote the migration of immune cells and 3) increasing the expression of COX-2 and iNOS to exacerbate inflammatory responses. The increase in the amount of NF- $\kappa$ B is closely related to the severity of the inflammatory reaction (Lawrence, 2009).

In recent years, the possibility of developing peptides into therapeutic drugs has gradually come to be valued by many scientists (Otvos and Wade, 2014). Numerous pharmaceutical and biotech companies are engaged in developing peptide drugs, mainly because peptide drugs have comparative advantages in affinity and cell penetration—superior to natural proteins (Otvos and Wade, 2014; Fosgerau and Hoffmann, 2015)—which can trigger or inhibit the occurrence of signal transmission, overcome the limitations of existing drugs, and improve permeability for entering tissues. In addition, peptide drugs have predictable metabolic pathways, safety, and tolerability; hence, researchers can determine whether peptide drugs will cause damage to other tissues and organs. By contrast, the disadvantage of peptide drugs is their short half-life in the blood, which may render them unable to achieve the purpose of treatment (Komin et al., 2017). Therefore, the improvement and design of peptide drugs are of critical importance.

At present, the treatment of sepsis is mainly based on antibiotic treatment, cardiovascular and pulmonary support therapy, and other treatment methods intended to maintain the normal physiological function of a patient's body. No effective treatment method can reduce the cytokine storm induced by sepsis. KCF18 is a multifunctional peptide, the design of which is mainly based on the receptors of TNF- $\alpha$ , IL-1 $\beta$ , and IL-6. In previous computer simulations and surface plasmon resonance experiments, KCF18 has been proven to bind to TNF- $\alpha$ , IL-1 $\beta$ , and IL-6 simultaneously and to effectively reduce the adhesion of monocytes induced by LPS (Jiang et al., 2019). The adhesion of monocytes is closely related to the expression of proinflammatory cytokines in blood vessels (Chang et al., 2012). The KCF18 peptide may be able to bind to these proinflammatory cytokines and reduce the stimulation of cytokines to alleviate the severity of sepsis. In this study, we investigated how the KCF18 peptide modulates the functional changes of macrophages under the inflammatory response induced by cytokines and decreases the severity of sepsis in an endotoxemia mouse model.

## MATERIALS AND METHODS

### Cell Culture

The human monocytic cell line THP-1 was cultivated in RPMI-1640 medium containing 10% fetal bovine serum (FBS). The



human microvascular endothelial cells HMEC-1 (ATCC, No CRL-10636) were maintained in MCDB131 medium containing endothelial cell growth supplement (Millipore, Billerica, MA, United States) and 15% FBS, as previously described (Dinarello, 2000).

### Cell Viability Assays

THP-1 ( $2 \times 10^4$  cells/well) cells were grown in 96-well plates overnight. In the beginning, a medium containing KCF18 at various concentrations was added. After 24 and 48 h incubation periods, the viability of cells was evaluated using the WST-1 assay (Roche, Indianapolis, IN, United States), according to the manufacturer's instructions.

### Cytokine Assays

THP-1 cells were pretreated with PMA (40 nM) for 24 h to differentiate into macrophages. After 24 h, the cells were washed three times with 1×HBSS. PMA-pretreated cells were cultivated with cytokines at a concentration of 20 ng/ml or cytokines pretreated with KCF18 for 1 h. Cultures were incubated for 24 h at 37°C. After stimulation, conditioned medium was collected, and TNF- $\alpha$ , IL-6, and IL-1 $\beta$  were detected using commercial ELISA kits.

### Measurement of ROS Production

Intracellular ROS production was assayed using 2,7-dichlorofluorescein diacetate (H2DCFDA; Invitrogen). Cytokines were pretreated with KCF18 for 1 h and then incubated with THP-1 cells for 20 min. THP-1 cells were then cultivated with H2DCFDA (10  $\mu$ M) for 5 min at 37°C. Images were obtained using a fluorescence microscope (IX-71, Olympus). Fluorescence intensity was obtained using ImageJ software, averaged, and normalized to the control value.

### Oxidized Low-Density Lipoprotein Uptake Assay

Low-density lipoprotein (LDL) was added to 5  $\mu$ M CuSO<sub>4</sub>, and the mixture was incubated in an incubator (37°C, 5% CO<sub>2</sub>) for 24 h to oxidize the LDL. Subsequently, 250  $\mu$ M EDTA was added to stop the oxidation reaction, and the mixture was stored in a 4°C refrigerator. THP-1 cells ( $3 \times 10^5$  cells) were added into a 12-well plate (1 ml/well) and cocultured with 50  $\mu$ g/ml oxLDL in serum-free medium for 24 h to promote oxLDL phagocytosis by macrophages. After 24 h, the cells were washed with PBS, and 4% paraformaldehyde (1 ml/well) was added to fix the cells at room temperature for 1 h. After 1 h, the paraformaldehyde was removed, and the cells were washed with ddH<sub>2</sub>O. Sixty percent isopropanol (500  $\mu$ L/well) was added at room temperature for 5 min. Subsequently, the isopropanol was removed, Oil Red O dye (500  $\mu$ L/well) was added, and the cell mixture was incubated at room temperature for 2 h. After 2 h, the cells were washed with ddH<sub>2</sub>O, and the image thereof was taken with a Zeiss Axio Vert A1 fluorescent microscope. Ethyl alcohol (99.5%, 500  $\mu$ L/well) was added to the cells to extract the Oil Red O. The Thermo Scientific Multiskan Spectrum was used to detect absorbance at 540 nm.

### Transient Transfection and Luciferase Assays

Endothelial cells at 80% confluence were transiently transfected with plasmids using Lipofectamine (Invitrogen), according to the manufacturer's protocol. Briefly, 0.5  $\mu$ g of pGL3-4 kB-Luc or 0.1  $\mu$ g of pCMV- $\beta$ -gal was mixed with the Lipofectamine reagent; the mixture was then added to cells for 6 h. Nontransfected reagents were washed, and culture medium was added to cells. After 18 h, cytokines were pretreated with KCF18 for 1 h and incubated with cells for 6 h. Lysis buffer was added to the cells to lyse them, and luciferase and  $\beta$ -galactosidase activities were assessed using a luciferase assay kit (Promega, Madison, WI, United States) according to the manufacturer's instructions. Luciferase activity was normalized with respect to  $\beta$ -galactosidase activity and expressed as a percentage of control activity.

### RNA Isolation and Quantitative Polymerase Chain Reaction Assays

The HMEC-1 and THP-1 cells were grown to confluence in 6 cm<sup>2</sup> culture plates and then treated with cytokines at a concentration of 20 ng/ml or cytokines pretreated with KCF18 for 1 h. Cultures were incubated for 4 h at 37°C. Total RNA was isolated using Trizol Reagent (Invitrogen), according to the manufacturer's suggested protocol. An aliquot (5  $\mu$ g) of purified RNA was reverse transcribed into first-strand complementary DNA (cDNA) by using a 2,720 Thermal Cycler (Applied Biosystems, Grand Island, NY, United States), 200 U/ $\mu$ L M-MLV reverse transcriptase (Invitrogen), and 0.5 mg/ $\mu$ L oligo (dT)-adapter primers (Invitrogen) in a 20- $\mu$ L reaction mixture. The quantitative polymerase chain reaction (qPCR) assays for TNF- $\alpha$ , IL-1 $\beta$ , IL-6, and glyceraldehyde 3-phosphate dehydrogenase (GAPDH) were performed with a Roche LightCycler 480 System (Roche, Indiana CA, United States). The oligonucleotide primers used were specific for TNF- $\alpha$  (5'-AGG GAC CTC TCT CTA ATC AG-3' and 5'-TGG GAG TAG ATG AGG TAC AG-3'), IL-1 $\beta$  (5'-AAA CAG ATG AAG TGC TCC TTC-3' and 5'-TGG AGA ACA CTT GTT GCT-3'), IL-6 (5'-GCC GCC CCA CAC AGA CA-3' and 5'-CCG TCG AGG ATG TAC CGA AT-3'), and GAPDH (5'-ACG GAT TTG GTC GTA TTG GG-3' and 5'-TGA TTT TGG AGG GAT CTC GC-3'). The oligonucleotide primers used for mice TNF- $\alpha$  (5'-GCT CCC TCT CAT CAG TTC TAT-3' and 5'-TTT GCT ACG ADC TGG GCT A-3'), IL-1 $\beta$  (5'-CAA CCA ACA AGT GTA TTC TCC AT-3' and 5'-GTG TGC CGT CTT TCA TTA-3'), IL-6 (5'-GCT ACC AAA CTG GAT ATA ATC AGG-3' and 5'-CCA GGT AGC TAT GGT ACT CCA GAA-3'), MCP-1 (5'-CCC CAG TCA CCT GCT GTT AT-3' and 5'-CCA CAA TGG TCT TGA AGA TCA C-3'), and GAPDH (5'-TTC ACC ATG GAG AAG-3' and 5'-GGC ATG GAC TGT GGT CAT GA-3'). Thermal cycling conditions involved an initial denaturation step at 95°C followed by 35 amplification cycles (15 s at 95°C and 20 s at 60°C) and subsequent melt curve analysis (72–98°C). Quantitation of gene expression was conducted, with expression assessed relative to GAPDH expression levels.

## Animals and Endotoxemia Model

The animal experiments used 8-to-10-week-old male BABL/c mice as an animal model. These mice were purchased from the National Laboratory Animal Breeding and Research Center, Taipei. The mice were housed in a temperature-controlled, light-cycled facility, and this study was conducted in strict accordance with the recommendations of the Guide for the Care and Use of Laboratory Animals of the National Institutes of Health. The animal experiments performed by Dr. Shih-Yi Peng were permitted by the Tzu Chi University Institutional Animal Care and Use Committee (Permit Number: 101070). For *in vivo* experiments, mice received a single dose (10 mg/kg) of LPS (*Escherichia coli* 0,111:B4, SIGMA) administered *i. v.* After 4 h, the mice were injected with normal saline or 5 mg/kg KCF18 peptide. At 18 h after LPS injection, the mice were euthanized through exposure to CO<sub>2</sub>.

## Determination of Serum IL-6 in Mice

Blood was collected, and serum was separated through centrifugation (4°C, 3,000 rpm, 10 min). The levels of serum IL-6 were determined using the sandwich ELISA method according to the instructions provided with the reagent kits. The values are expressed as pg/mL of sera based on the appropriate standard curve.

## Histopathological Observation of Liver Tissues

The liver tissues of mice were fixed in 10% neutral phosphate buffered formalin solution, and they were then dehydrated and embedded in paraffin to make conventional paraffin sections. The sections were cut to be 4-μm thick and stained with hematoxylin and eosin (H&E). The histopathological changes of liver tissues were observed under an optical microscope.

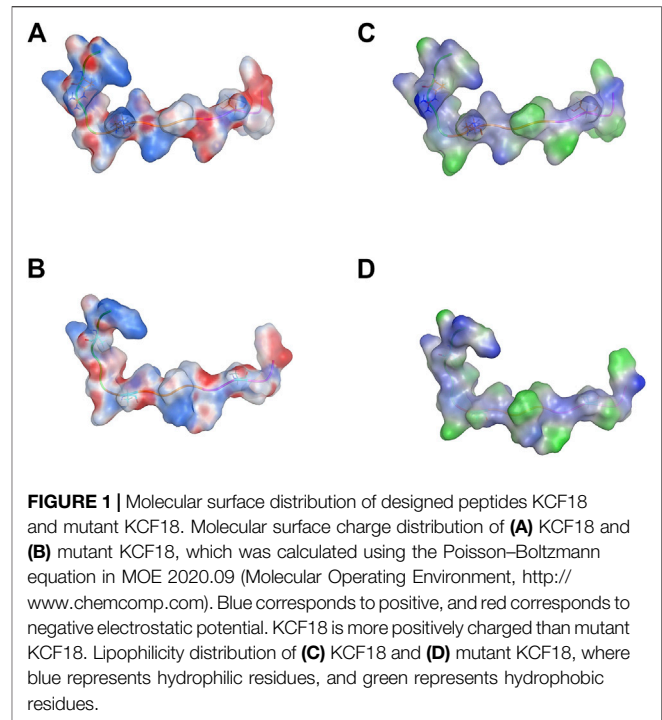
## Statistical Analysis

The results are expressed as the means ± SD from at least three independent experiments. Differences between groups were assessed using a one-way analysis of variance.  $p < 0.05$  was considered statistically significant.

## RESULTS

### Molecular Surface Distribution of Peptides KCF18 and Mutant KCF18

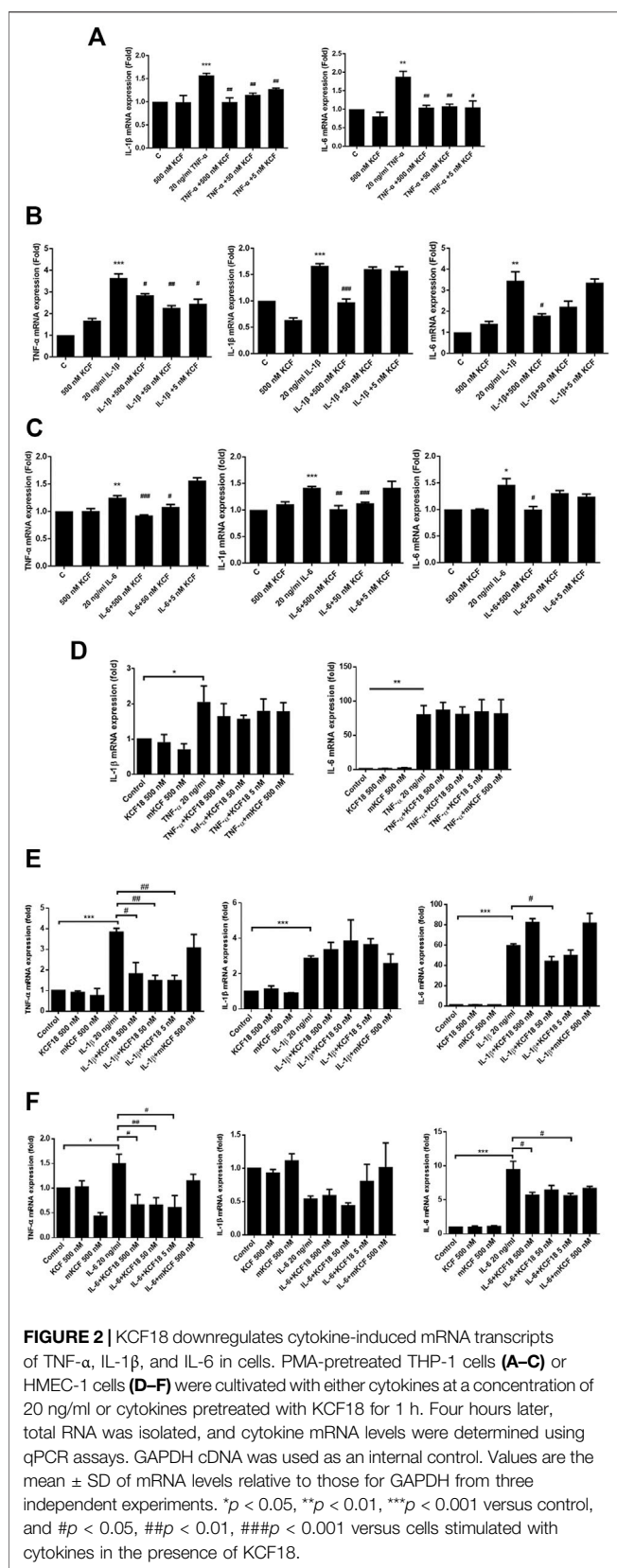
The designed combinational peptide KCF18 is truncated from the binding regions of cytokine receptors to cytokines (TNF-α, IL-1β, and IL-6), as shown in our previous study (Jiang et al., 2019). The molecular surface charge distribution of KCF18 indicated amphiphilic properties, with one side more positively charged and the other more negatively charged (Figure 1A). The lipophilicity of KCF18 was also more hydrophilic on one side and more hydrophobic on the other side (Figure 1C). However, the mutant peptide KCF18 (mKCF18) with three residues mutated to alanine (R3A, K8A, and T15A) exhibited fewer positively charged and more hydrophobic regions in the



molecular surface distributions of charge and lipophilicity (Figures 1B,D). The mutant KCF18 exhibited less binding affinity to these cytokines than wild KCF18 and the specificity of KCF18 binding to these three cytokines was further validated in the following cellular experiments.

### Anti-Inflammatory Effect of KCF18 on TNF-α-, IL-1β-, and IL-6-Induced Proinflammatory Cytokine Transcription and Expression

To investigate whether KCF18 affects the expression of cytokines by endothelial cells and macrophages, proinflammatory cytokines (TNF-α, IL-1β, or IL-6) were pretreated with KCF18 for 1 h to bind the proinflammatory cytokines. After 1 h, the coculture medium was added to the cells, and mRNA was extracted after 4 h qPCR assays were used to quantify the effects of KCF18 at various concentrations on the expression of TNF-α, IL-1β, and IL-6 mRNA. Compared with the control cells, TNF-α, IL-1β, and IL-6 mRNA levels were significantly increased when macrophages (Figures 2A–C) and endothelial cells (Figures 2D–F) were cultured with TNF-α (Figures 2A,D), IL-1β (Figure 2B and E), and IL-6 (Figures 2C,F). We also performed the experiments of TNF-α mRNA expression in cells stimulated with TNF-α (Supplementary Figure S1) and the results were similar with our previous publication (Shih et al., 2021). However, KCF18 significantly decreased cytokine-mediated expression of TNF-α, IL-1β, and IL-6 mRNA. In addition, no significant difference was observed in the mRNA expression levels between the KCF18-treated and control cells (Figure 2). The conditioned medium from 24 h was also collected



to detect the secretion of TNF- $\alpha$ , IL-1 $\beta$ , and IL-6 in macrophages by using ELISA. As depicted in **Figure 3**, when IL-6 was added, the TNF- $\alpha$  (**Figure 3A**) and IL-1 $\beta$  (**Figure 3B**) secretions of macrophages increased significantly. TNF- $\alpha$  also induced IL-6 expression in macrophages (**Figure 3C**). By incubating with various concentrations of KCF18, the expression level of IL-6 was reduced, exhibiting a downward trend (**Figure 3C**). In the results for IL-6 stimulation, the secretion of TNF- $\alpha$  was upregulated nearly 200% by macrophages; however, 500, 50, and 5 nM KCF18 decreased the expression levels of TNF- $\alpha$  by 27, 25, and 40%, respectively (**Figure 3A**;  $p < 0.05$  and 0.005). KCF18 also had the similar effects on IL-6 induced IL-1 $\beta$  expression (**Figure 3B**) and TNF- $\alpha$  induced IL-6 secretion (**Figure 3C**). The results indicated that KCF18 can bind to TNF- $\alpha$ , IL-1 $\beta$ , and IL-6, thereby reducing the activating effects of these cytokines on macrophages. To detect whether KCF18 is cytotoxic to monocytes, 500 nM KCF18 and mKCF peptides were added to THP-1 cells for 24 and 48 h, and cell viability was measured using WST-1 reagent. As depicted in **Figure 3D**, no significant difference between the control, KCF18, and mKCF groups was evident, confirming that 500 nM KCF18 and mKCF did not cause cytotoxicity to both cell lines. Hence, causing decreased cell viability is not the mechanism by which KCF18 acts on TNF- $\alpha$ , IL-1 $\beta$ , and IL-6 to reduce their induced mRNA transcript and protein expression.

## Inhibitory Effect of KCF18 on the Production of Cytokine-Induced ROS in Macrophages

Many studies have shown that overexpression of ROS is closely related to inflammation (Kvietys and Granger, 2012). Therefore, we further explored whether KCF18 can ameliorate the oxidative stress induced by TNF- $\alpha$ , IL-1 $\beta$ , and IL-6 by detecting the level of intracellular ROS production. As predicted, TNF- $\alpha$ , IL-1 $\beta$ , and IL-6 treatment induced the fluorescence intensity of ROS in the cells, increasing the intensity by 1.66-, 1.92-, and 2.37-fold, respectively (**Figures 4A–C**). However, 500, 50, and 5 nM KCF18 pretreatment decreased the TNF- $\alpha$ -induced ROS expression in a dose-dependent manner to 0.64-, 0.78-, and 0.87-fold, respectively (**Figure 4A**;  $p < 0.01$  and 0.05). KCF18 pretreatment reduced IL-1 $\beta$ -induced ROS expression by 0.57-fold and 0.91-fold, respectively (**Figure 4B**; 500 and 50 nM,  $p < 0.005$  and 0.05). KCF18 pretreatment also reduced IL-6-induced ROS production by 0.81-, 0.76-, and 1.2-fold (**Figure 4C**; 500, 50, and 5 nM,  $p < 0.01$  and 0.05). The preceding results revealed that KCF18 can inhibit TNF- $\alpha$ , IL-1 $\beta$ , and IL-6-induced ROS production by macrophages.

## Effect of KCF18 on Cytokine-Induced Phagocytosis of oxLDL by Macrophages

The oxLDL that accumulates on the inner wall of blood vessels can cause damage to endothelial cells and induce secretion of cytokines, attract monocytes to the inner wall of blood vessels, and differentiate into macrophages to phagocytose oxLDL. When

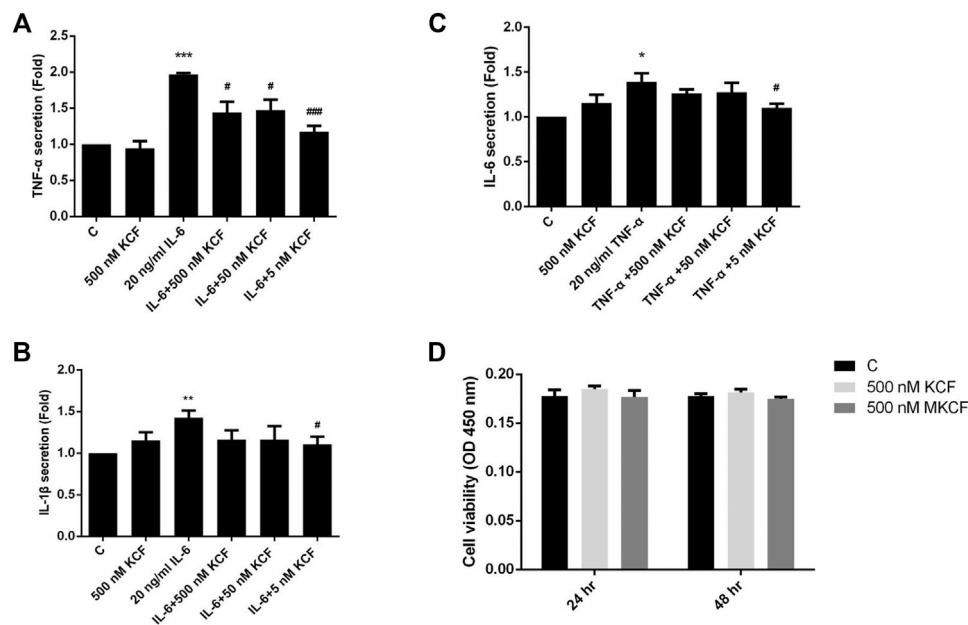


**FIGURE 3 |** KCF18 reduces cytokine-induced secretions of TNF- $\alpha$ , IL-1 $\beta$ , and IL-6 in cells. PMA-pretreated THP-1 cells were incubated with either cytokines or cytokines pretreated with KCF18 for 1 h. Conditioned medium was collected 24 h later, and TNF- $\alpha$  (A), IL-1 $\beta$  (B), and IL-6 (C) secretions were detected. (D) THP-1 cells in a 96-well microplate were treated with various concentrations of KCF18. After a 24 and 48 h incubation, cell viability was evaluated using the colorimetric WST-1 assay. Values are the mean  $\pm$  SD from three independent experiments.

macrophages converge into foam cells, which accumulate on the inner wall of blood vessels to form fibrotic plaque, it increases the risk of atherosclerosis (Bobryshev et al., 2016). We further validated whether KCF18 modulates the ability of macrophages to engulf oxLDL under the inflammation induced by cytokines. **Figure 5A** demonstrates that the phagocytosis of oxLDL by macrophages was increased by 1.26-fold after TNF- $\alpha$  stimulation. By contrast, 500 and 50 nM KCF18 decreased the oxLDL engulfment by 1.11-fold and 0.96-fold, respectively ( $p < 0.01$ ). Furthermore, KCF18 reduced the phagocytosis of oxLDL by macrophages induced by IL-1 $\beta$  and IL-6 (**Figures 5B,C**). The amount of oxLDL phagocytosed by macrophages increased by 1.16-fold when IL-1 $\beta$  was added, whereas 500 and 50 nM KCF18 pretreatment reduced oxLDL phagocytosis to 0.96-fold ( $p < 0.01$ ). IL-6 stimulated macrophages to phagocytose oxLDL 1.25-fold, whereas various concentrations of KCF18 (500, 50, and 5 nM) decreased oxLDL engulfment by 0.94, 1.02, and 1.12 times, respectively ( $p < 0.05$ ). The results corroborated that KCF18 could alleviate cytokine-induced oxLDL phagocytosis by macrophages.

### Inhibitory Effect of KCF18 on the Nuclear Translocation of p65 Stimulated by Cytokines

NF- $\kappa$ B activation plays a crucial role in cytokine-stimulated inflammation (Yamamoto and Gaynor, 2001). The main

activated state of NF- $\kappa$ B is a heterodimer formed by p50 and p65, which usually combines with I $\kappa$ B to generate an inactive state in the cytoplasm. When the NF- $\kappa$ B pathway is activated, I $\kappa$ B will be phosphorylated and separated from NF- $\kappa$ B, allowing NF- $\kappa$ B to enter the nucleus and regulate target gene transcription. Therefore, we surveyed the participation of NF- $\kappa$ B in the inflammation-inhibitory effects of KCF18 in cells. To assess whether NF- $\kappa$ B activation by cytokines was suppressed through pretreatment with KCF18, Western blotting assay for p65, a subunit of NF- $\kappa$ B and a marker of its activation, was implemented. From the nuclear lysate of macrophages, IL-1 $\beta$  and IL-6 treatment induced p65 translocation into the nucleus 2.3- and 1.5-fold, respectively (**Figures 6A,B**). Pretreatment with 500, 50, and 5 nM KCF18 decreased the IL-1 $\beta$ -induced p65 translocation in a dose-dependent manner to 1.4-, 1.4-, and 1.1-fold, respectively. KCF18 pretreatment also reduced p65 nuclear translocation by 1.1-, 1.3-, and 1.0-fold for IL-6 stimulation (**Figure 6B**). However, the scramble peptide mKCF18 did not display the ability to inhibit p65 nuclear translocation. In addition, transient transfections were performed using an NF- $\kappa$ B-dependent luciferase reporter plasmid to further examine the effects of KCF18 on NF- $\kappa$ B transcriptional activity in endothelial cells. Treatment with TNF- $\alpha$  and IL-1 $\beta$  activated NF- $\kappa$ B luciferase in HMEC-1 cells (**Figures 7A,B**), whereas KCF18 effectively reduced TNF- $\alpha$ - and IL-1 $\beta$ -induced NF- $\kappa$ B luciferase activity. However, IL-6 did not induce NF- $\kappa$ B luciferase activity obviously (**Figure 7C**). These data indicate that KCF18 can regulate the translocation of p65



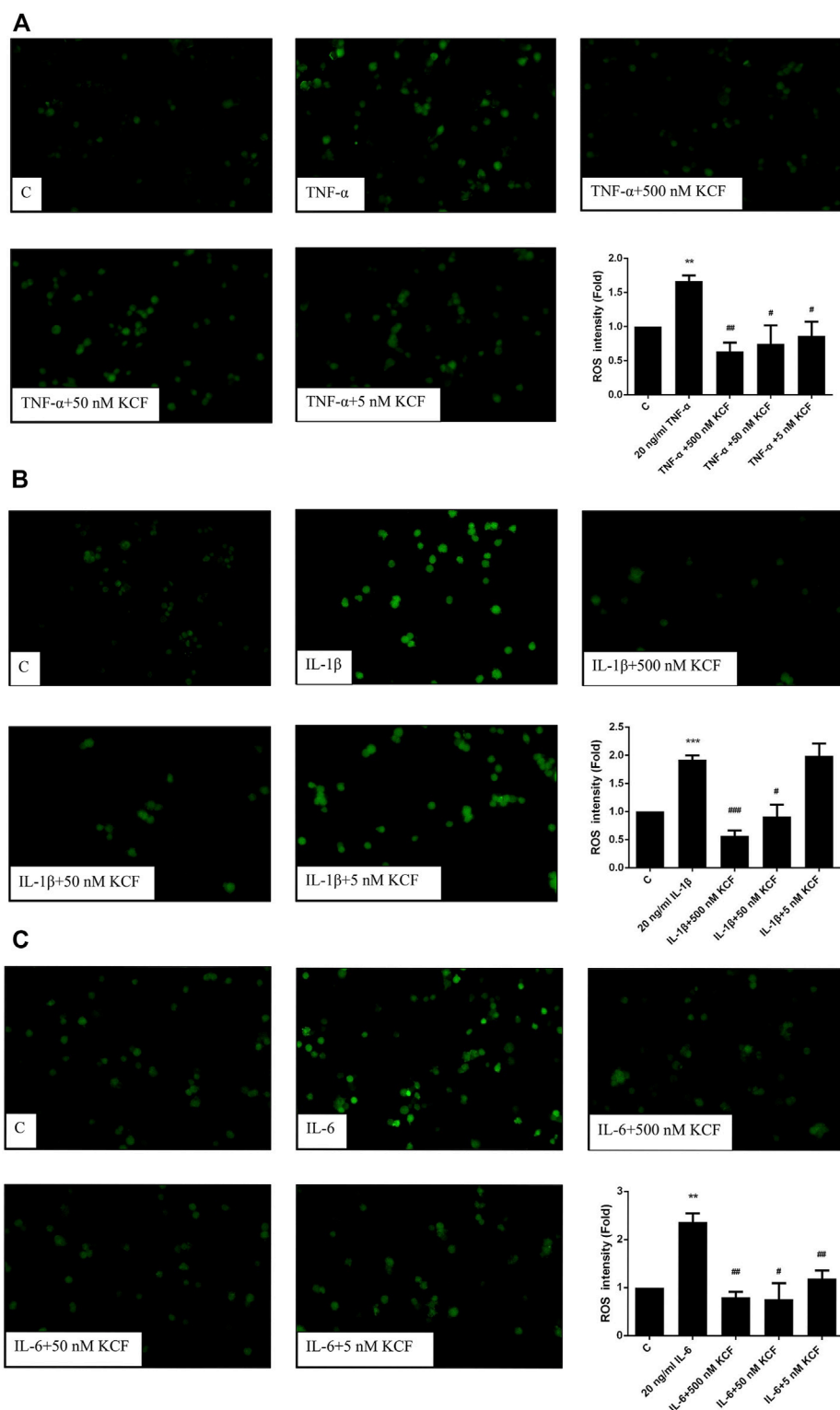


**FIGURE 4** | KCF18 reduces the production of cytokine-induced ROS in macrophages. ROS production induced by TNF- $\alpha$  (**A**), IL-1 $\beta$  (**B**), and IL-6 (**C**) was detected as described in the Materials and Methods section. Values are the mean  $\pm$  SD of fluorescent intensities versus control from three independent experiments. \*\* $p < 0.01$  versus control and # $p < 0.05$ , ## $p < 0.01$  versus cells stimulated with cytokines in the presence of KCF18.

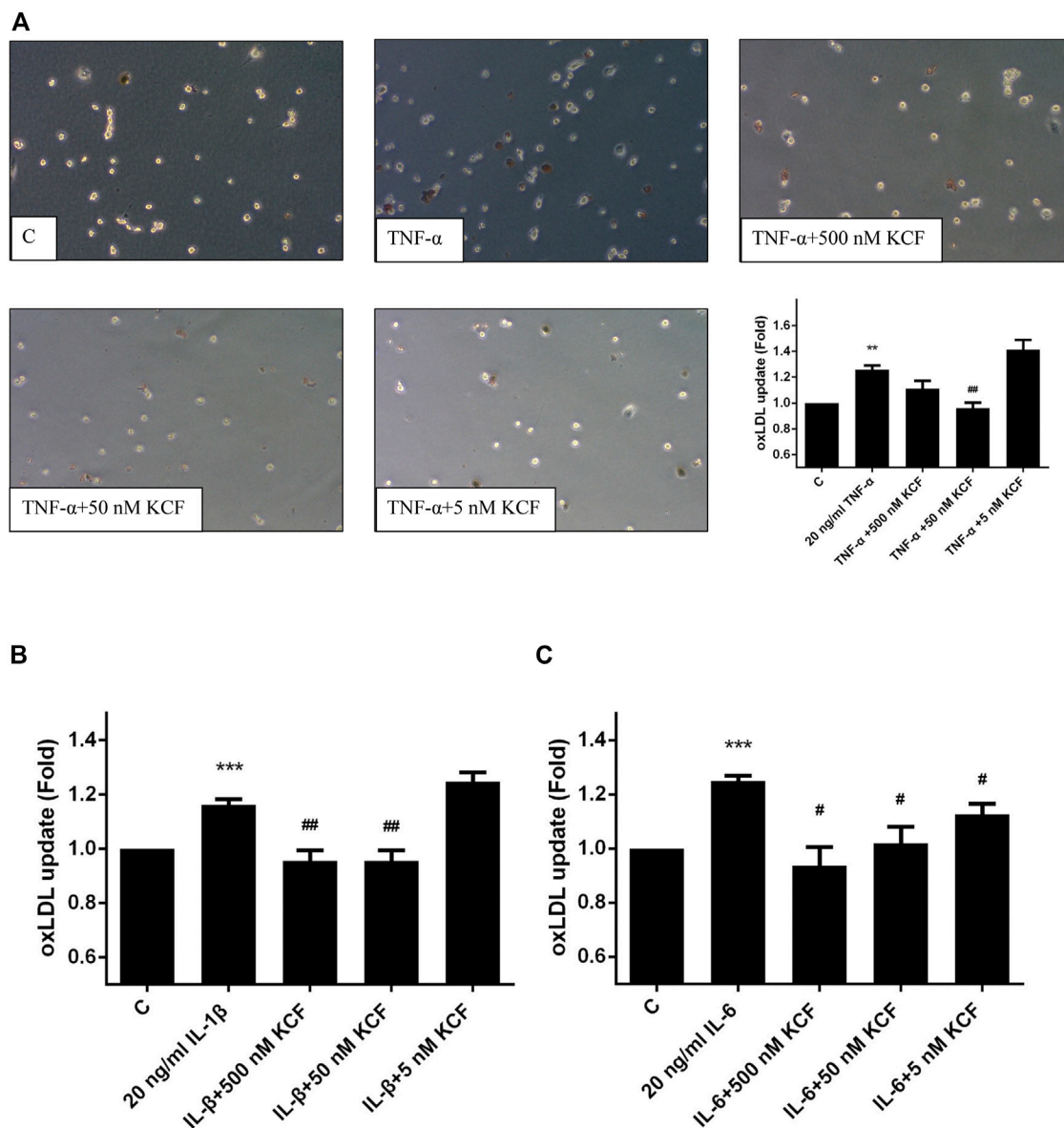


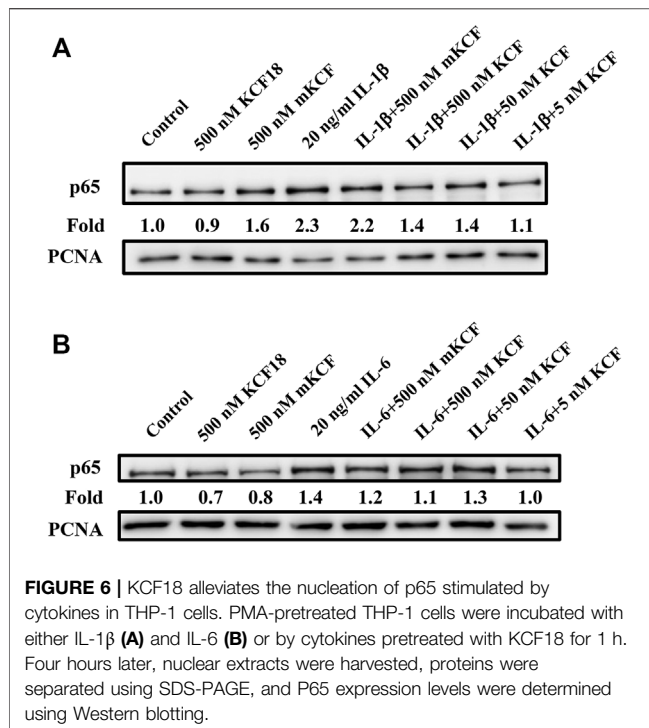
**FIGURE 5 |** KCF18 decreases cytokine-induced phagocytosis of oxLDL by macrophages. oxLDL engulfment induced by TNF- $\alpha$  (A), IL-1 $\beta$  (B), and IL-6 (C) was determined. Values are the mean  $\pm$  SD of fluorescent intensities versus control from three independent experiments. \*\* $p$  < 0.01, \*\*\* $p$  < 0.001 versus control and # $p$  < 0.05, ## $p$  < 0.01 versus cells stimulated with cytokines in the presence of KCF18.

into the nucleus by binding to cytokines, thereby reducing the severity of the inflammatory response.

### Anti-Inflammatory Effect of KCF18 on the Expression of Proinflammatory Cytokine mRNA in the Liver of Mice With Endotoxemia

Sepsis is a systemic inflammatory disease caused by infection. Studies have indicated that the overexpression of cytokines is closely related to the severity of sepsis (Chaudhry et al., 2013). To evaluate the inflammation inhibitory activity of KCF18 in

endotoxemia mice model, the TNF- $\alpha$  (Figure 8A), IL-1 $\beta$  (Figure 8B), IL-6 (Figure 8C), and MCP-1 (Figure 8D) mRNA levels in the mouse liver were determined using qPCR. TNF- $\alpha$ , IL-1 $\beta$ , IL-6, and MCP-1 mRNA levels in the liver sample were dramatically enhanced in the LPS-injected group compared with the normal group ( $p$  < 0.01; Figure 8). However, treatment with KCF18 at 5 mg/kg reduced LPS-induced IL-1 $\beta$  and IL-6 mRNA levels and significantly decreased TNF- $\alpha$  and MCP-1 mRNA levels when compared with the LPS group ( $p$  < 0.05). This indicated that KCF18 alleviated the mRNA expression levels of the inflammatory cytokines TNF- $\alpha$ , IL-1 $\beta$ , IL-6, and MCP-1 in an endotoxemia mouse model with liver injury.



## Anti-Inflammatory Effect of KCF18 on IL-6 Expression and White Blood Cell Count in the Blood of Mice With Endotoxemia

To further investigate the anti-inflammatory effects of KCF18 on LPS-induced endotoxemia in mice, the IL-6 expression level and white blood cell (WBC) count in the blood were detected. As shown in **Figure 9A**, IL-6 was induced in the LPS-injected group, and KCF18 reduced IL-6 expression in the KCF18-injected group. The WBC count was also decreased in the KCF18-injected group compared with the LPS-injected group (**Figure 9B**). However, mKCF did not express the inhibitory effects. This indicated that KCF18 could inhibit proinflammatory

cytokine expression by reducing the expression of WBC in LPS-induced endotoxemia mice.

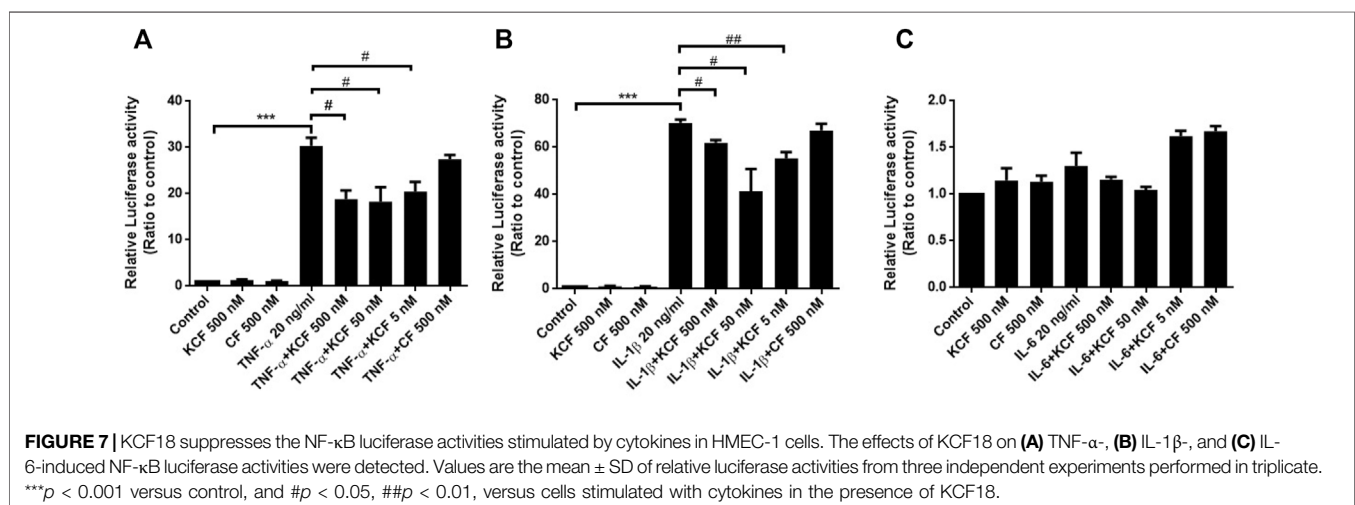
## Effect of KCF18 on the Tissue Injury of Liver Histopathology in Mice With Endotoxemia

To assess whether KCF18 could preserve liver tissue when such tissue is subjected to LPS-induced liver injury, a liver histopathological test was also performed. In the normal group, the liver tissues were intact, and the hepatocytes were regularly arranged, as depicted in **Figure 9C**. In the LPS group, the basic architecture of liver cells disappeared, and liver cells swelled. By contrast, treatment with KCF18 significantly improved the degree of liver histopathological alterations.

## DISCUSSION

Sepsis is a disease caused by complex interactions between pathogenic bacteria and host immune response. Infection by pathogenic bacteria can cause the production of cytokine storms, which will destroy the integrity of the vascular endothelial layer, leading to hypotension and coagulation disorders and ultimately to tissue damage and organ failure (Chaudhry et al., 2013). Clinical studies have found that in patients with severe sepsis, the blood levels of TNF- $\alpha$ , IL-1 $\beta$ , IL-6, IL-8, IFN- $\gamma$ , and MCP-1 are significantly increased (Bozza et al., 2007). An increase in the level of TNF- $\alpha$  in the serum of patients with sepsis increases the risk of mortality (Gogos et al., 2000); moreover, the level of IL-6 in the serum of patients with sepsis decreases, which helps patients with sepsis recover from the illness (Kumar et al., 2009). Therefore, reducing the cytokine levels in the plasma of septic patients is helpful for decreasing the severity and mortality of the patient and provides a suitable therapeutic method.

Many anti-inflammatory drugs that inhibit cytokines have been developed to retard the inflammation caused by pathogenic bacteria; however, the treatment of TNF- $\alpha$  neutralizing antibodies, soluble TNF receptors, and IL-1 receptor



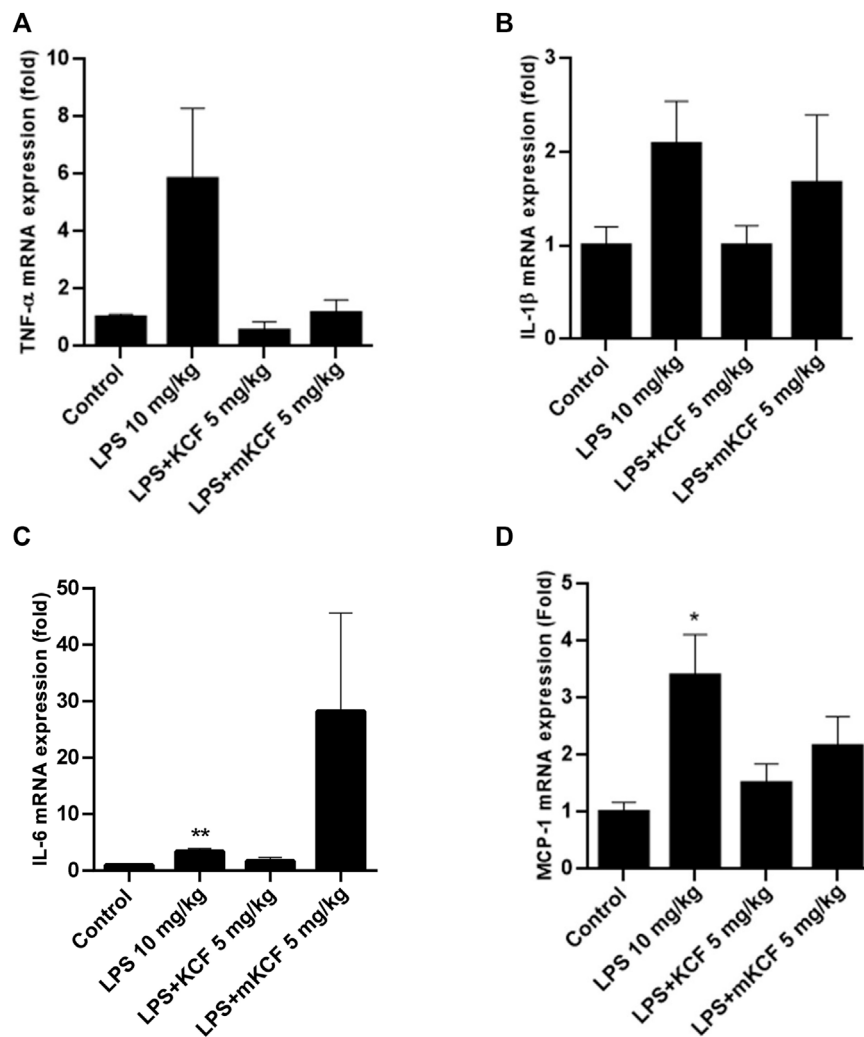


**FIGURE 8 |** KCF18 reduced the expression of proinflammatory cytokine mRNA in the livers of mice with endotoxemia. In the LPS-induced endotoxemia mouse model, liver tissue was isolated, and TNF- $\alpha$  (A), IL-1 $\beta$  (B), IL-6 (C) and MCP-1 (D) mRNA levels were determined using qPCR assays as described in the Materials and Methods section. GAPDH cDNA was used as an internal control. Values are the mean  $\pm$  SD of mRNA levels relative to those for GAPDH from three independent experiments. \*\* $p$  < 0.01, \*\*\* $p$  < 0.001 versus control and # $p$  < 0.05, ## $p$  < 0.01 versus mice stimulated with LPS in the presence of KCF18 injection.

antagonists had no therapeutic effect on patients with sepsis in clinical trials (Clark et al., 1998; Dinarello, 2000). Therefore, it should not only inhibit one cytokine unilaterally. In addition, the purification and preparation of antibodies takes a long time and has a high production cost. Peptide drugs have a short production time and a high degree of specificity as well as predictable metabolic pathways. Therefore, peptide drugs may be the trend of future drug development. Previously, we used computer simulations to calculate the binding free energies of TNF- $\alpha$ , IL-1 $\beta$ , and IL-6 to their cognate receptors and designed a multifunctional peptide, KCF18, that can bind to TNF- $\alpha$ , IL-1 $\beta$ , and IL-6 (Jiang et al., 2019). We first explored whether KCF18 affects the expression of proinflammatory cytokines secreted by macrophages. As presented in Figure 2, when cytokines (TNF- $\alpha$ , IL-1 $\beta$ , and IL-6) are incubated with cells, they will increase the expression of TNF- $\alpha$ , IL-1 $\beta$ , and IL-6 mRNA and proteins in

macrophages. However, pretreatment with various concentrations of KCF18 (500 nM, 50 nM, and 5 nM) can attenuate the mRNA and protein expressions of proinflammatory cytokines induced by TNF- $\alpha$ , IL-1 $\beta$ , and IL-6. Similar results were also observed with KCF18 pretreatment in endothelial cells by IL-1 $\beta$  and IL-6 stimulation (Figures 2E,F). However, the effect of KCF18 on TNF- $\alpha$  stimulation in endothelial cells is not as obvious as in macrophage (Figure 2D). The cause we cannot exclude may be the different cofactors or repressors which involve TNF- $\alpha$  receptor binding, express or bind on the surfaces of two cells to interfere the KCF18 interaction with TNF- $\alpha$  receptor in HMEC-1 cells. Since only 6 amino acids were designed for targeting TNF- $\alpha$  receptor binding, this interference by such cofactors or repressors might be enough to disrupt the binding of KCF18 to receptor. In contrast, the interference is not strong enough to interrupt the



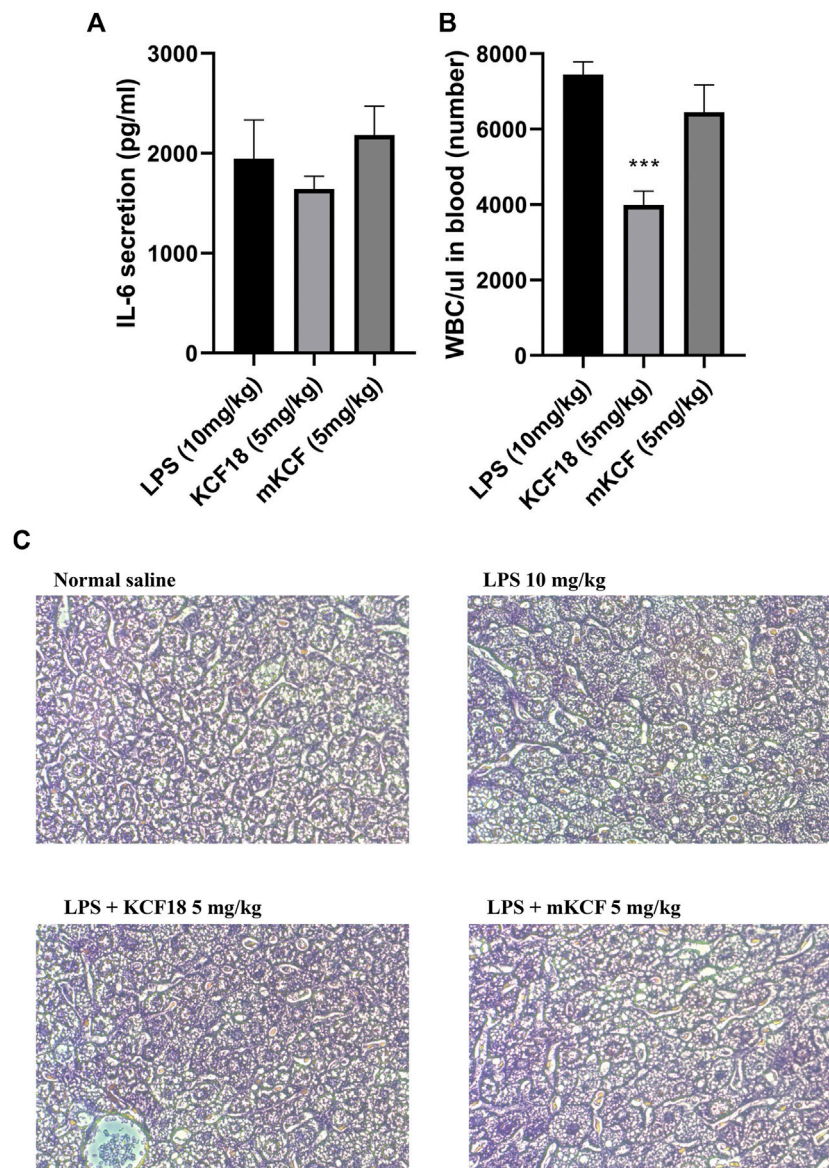


**FIGURE 9 |** KCF18 reduced the IL-6 expression and WBC count in the blood of mice and alleviated tissue injury on liver histopathology with endotoxemia. LPS-induced endotoxemia mouse model was divided into Control, LPS, LPS + KCF18 (5 mg/kg) and LPS + mKCF (5 mg/kg) groups. IL-6 expression in the mice serum (**A**) was detected using an ELISA kit, WBC count (**B**) was determined, and histopathological changes in liver tissues (**C**) were observed under optical microscope by Hematoxylin and eosin staining, magnification 200 $\times$ . LPS treatment mice had more severe liver injury and hepatocyte degeneration.

whole TNF- $\alpha$  molecule binding to its receptor. To discover whether the inhibitory effect of KCF18 on the decrease of proinflammatory cytokine expression induced by TNF- $\alpha$ , IL-1 $\beta$ , and IL-6 is due to the cytotoxicity to THP-1 cells, we used WST-1 reagent to confirm the cell growth status. As presented in **Figure 3D**, the cell viability of cocultivation of KCF18 with THP-1 cells did not extend the difference compared with the control group. This indicated that KCF18 decreased the transcription and expression of proinflammatory cytokines induced by TNF- $\alpha$ , IL-1 $\beta$ , and IL-6. However, in the experimental results, we observed that high concentrations of KCF18 were not necessarily the optimal inhibitory concentrations of cytokines. Sometimes a

low KCF18 concentration had a significant inhibitory effect, meaning that the KCF18 effect may be unstable and may not be dose dependent or that the intensity of the message may not be directly proportional to the number of receptors (Bazzoni and Beutler, 1996). In addition, it is possible that a high KCF18 concentration promotes the formation of chemical bonds between peptides, causing the configuration of KCF18 to change, in which case the effect of KCF18 may not achieve the expected results. In addition, we also found that the most effective KCF18 concentration is not necessarily the same at the mRNA and protein levels. We speculated that this may be related to the posttranslational modification of cells and the protein

degradation mechanism (Mann and Jensen, 2003; Vucic et al., 2011), which lead to different levels of mRNA and protein expression.

In the process of systemic inflammation, cytokines stimulate macrophages to release a large amount of ROS to remove foreign pathogens. When the concentration of ROS in tissue increases, the antioxidant capacity decreases or a large amount of reactive oxygen species is produced. This causes oxidative pressure in the tissue. In patients with severe sepsis and septic shock, a considerable amount of ROS is produced, which causes great oxidative pressure in tissues; in turn, this causes multiple organ failure (Crimi et al., 2006). In addition, active oxygen can interact with polyunsaturated fats. The acids interact with each other to increase the lipid peroxidation of fatty acids on the cell membrane, causing damage to the cell membrane function and affecting the normal physiological functions of the cell (Radi, 2013). Therefore, we explored whether KCF18 affects the expression of ROS secreted by macrophages under the stimulation of cytokines. The results shown in **Figure 6** indicate that TNF- $\alpha$ , IL-1 $\beta$ , and IL-6 can promote the secretion of large amounts of ROS by macrophages, and when different concentrations of KCF18 are added, they could effectively inhibit the production of ROS induced by cytokines in a dose-dependent manner. In the study of Zughaier et al., positively charged antimicrobial peptides could reduce the TNF- $\alpha$  and NO secreted by human and mouse macrophages stimulated by LPS but could also promote the respiratory burst of macrophages (respiratory burst), which produces a large amount of ROS (Zughaier et al., 2005). However, our designed peptide can effectively reduce the production of ROS stimulated by cytokines. Therefore, compared with antibacterial peptides for treating sepsis, our designed peptide has greater therapeutic potential to reduce the severity of sepsis.

A large amount of ROS promotes the lipid peroxidation of LDL to form oxLDL. Studies have shown that oxLDL plays a key role in the damage of vascular endothelial function (Parthasarathy et al., 2010), and it also plays a vital role in the early development of arteriosclerosis (Li and Mehta, 2005; Parthasarathy et al., 2010). Therefore, reducing ROS production and LDL oxidation may help alleviate the development of early arteriosclerosis. To investigate whether KCF18 affects the ability of macrophages to engulf oxLDL, oxLDL uptake induced by cytokines was assessed. The addition of cytokines induced the ability of macrophages to phagocytose oxLDL (**Figure 5**). When cells were pretreated with KCF18, macrophage phagocytosis induced by cytokines was reduced. The results proved that KCF18 could retard the ability of macrophages to produce ROS and inhibit the phagocytosis of oxLDL. Therefore, in various cardiovascular diseases (such as atherosclerosis), the designed peptide may also have the potential for use in treatment.

NF- $\kappa$ B is an essential transcription factor that regulates inflammatory responses. When a pathogen invades, the LPS on the pathogen is recognized by the TLR4 receptor, triggering the transmission of downstream messages that activate the NF- $\kappa$ B pathway (Bachert and Geveart, 1999), which promotes cells to express a large number of

cytokines—this amplifies the occurrence of inflammation. When NF- $\kappa$ B is activated, it facilitates the phosphorylation of p65 and enters the nucleus to regulate the DNA transcription of downstream genes. Studies have indicated that NF- $\kappa$ B in patients with sepsis increases greatly, which is related to a higher mortality rate and slower recovery after illness (Bohrer et al., 1997; Arnalich et al., 2000; Liu and Malik, 2006). Therefore, we explored whether the reduction of cytokine production by KCF18 was affected by inactivation of the NF- $\kappa$ B pathway. **Figure 7** shows that when cytokines stimulated the cells, the nuclear translocation of p65 was increased. However, the induction of p65 translocation was suppressed when KCF18 was pretreated with cells. A similar result was also observed in endothelial cells when the NF- $\kappa$ B-dependent luciferase reporter assay was conducted.

A lower KCF18 concentration exhibited a superior inhibitory ability. Surface charge may affect macrophage phagocytosis. The negatively charged sialic acid on the surface of macrophages can bind to positively charged nanoparticles and phagocytose the nanoparticles into the cell (Gallagher et al., 1987). Charged nanoparticles are also more likely to be swallowed by macrophages than are uncharged nanoparticles (Roser et al., 1998; Xiao et al., 2011). Therefore, a higher concentration of positively charged KCF18 (**Figure 1**) may accelerate macrophage phagocytosis, thereby reducing the effect of KCF18. This needs to be clarified in the future.

The biggest disadvantage of peptide drugs is their short half-life in the blood and low bioavailability. However, in the mice endotoxemia model, as expected, LPS injection indeed upregulated the expressions of TNF- $\alpha$ , IL-1 $\beta$ , IL-6, and MCP-1 mRNA. In contrast, KCF18 decreased LPS-induced expressions of TNF- $\alpha$ , IL-1 $\beta$ , IL-6, and MCP-1 mRNA in the liver even though no statistical difference (**Figure 8**). The reason may be due to the individual differences in mice. Another evidence was also proofed that WBC count in the blood was reduced by KCF18 (**Figure 9B**). The liver tissue in the normal control group displayed normal hepatocytic architecture. Conversely, a remarkable liver pathological changes such as vacuolization, and liver lobule destruction were observed in LPS group. The liver lobules of the mice in the LPS/w KCF18 group had less liver tissue structural damage, with clearer liver lobules (**Figure 9C**). The results confirmed that KCF18 decreased the severity of inflammation in the endotoxemia model. Gutschmann et al. designed anti-lipopolysaccharide peptides and revealed available suppression of LPS-induced cytokine secretion and conservation from lethal septic shock *in vivo* (Gutschmann et al., 2010). On the other hand, our collaborator Shih et al. also showed that KCF18 can alleviate liver injury in endotoxemia mice (Shih et al., 2021). In another study they used a peptide that only targets TNF- $\alpha$  and eased liver injury to mice (Chang et al., 2020). It indicates that peptide drugs have excellent potential for future pharmacological application. Our designed peptide KCF18 was derived from the complex structures of cytokine-receptor, which could target three major proinflammatory cytokines, TNF- $\alpha$ , IL-1 $\beta$ , and IL-6. Due to the complexity of inflammation responses and specificity of ligand-protein binding, peptide KCF18 could not target all inflammation-related cytokines, but only these three

major proinflammatory cytokines. In addition, the limitation of peptide drugs is their short half-life in the blood; therefore, a new conjugation material might be constructed to ameliorate this problem. In the previous reports, Baig's group showed that signaling pathways through toll-like receptor 4 (TLR4) stimulate several transcription factors such as NF- $\kappa$ B, Signal Transducers and Activators of Transcription family of transcription factors (STAT1), Interferon regulatory factors (IRF's), and activator protein 1 (AP1), which are the major mediators regulating the inflammatory response (Roy et al., 2016). They claimed that repression of these objectives and their upstream signaling molecules supplies a latent therapeutic approach to cure inflammatory diseases. Meng's group also showed that endotoxin lipopolysaccharides via TLR4 signaling pathway to activate translocation of NF- $\kappa$ B and further regulate expression of pro-inflammatory genes, including TNF- $\alpha$ , IL-6, and IL-1 $\beta$  during sepsis (Jiang et al., 2015). Similarly, KCF18 could alleviate inflammation mediated by blocking the interactions of TNF- $\alpha$ , IL-6, and IL-1 $\beta$  with their cognate receptors, reducing the translocation of NF- $\kappa$ B and reduction the inflammatory gene expressions. This proved that KCF18 can prevent inflammation and may provide a new direction and therapeutic treatment method for inflammation-related vascular diseases such as sepsis.

## DATA AVAILABILITY STATEMENT

The original contributions presented in the study are included in the article/**Supplementary Material**, further inquiries can be directed to the corresponding authors.

## REFERENCES

- Arnalich, F., Garcia-Palmero, E., López, J., Jiménez, M., Madero, R., Renart, J., et al. (2000). Predictive Value of Nuclear Factor kappaB Activity and Plasma Cytokine Levels in Patients with Sepsis. *Infect. Immun.* 68, 1942–1945. doi:10.1128/iai.68.4.1942-1945.2000
- Bachert, C., and Geveart, P. (1999). Effect of Intranasal Corticosteroids on Release of Cytokines and Inflammatory Mediators. *Allergy* 54 Suppl 57 (54 Suppl. 1), 116–123. doi:10.1111/j.1398-9995.1999.tb04413.x
- Bazzoni, F., and Beutler, B. (1996). The Tumor Necrosis Factor Ligand and Receptor Families. *N. Engl. J. Med.* 334, 1717–1725. doi:10.1056/NEJM199606273342607
- Bobryshev, Y. V., Ivanova, E. A., Chistiakov, D. A., Nikiforov, N. G., and Orekhov, A. N. (2016). Macrophages and Their Role in Atherosclerosis: Pathophysiology and Transcriptome Analysis. *Biomed. Res. Int.* 2016, 9582430. doi:10.1155/2016/9582430
- Böhrer, H., Qiu, F., Zimmermann, T., Zhang, Y., Jllmer, T., Männel, D., et al. (1997). Role of NFkappaB in the Mortality of Sepsis. *J. Clin. Invest.* 100, 972–985. doi:10.1172/JCI119648
- Bozza, F. A., Salluh, J. I., Japiassu, A. M., Soares, M., Assis, E. F., Gomes, R. N., et al. (2007). Cytokine Profiles as Markers of Disease Severity in Sepsis: a Multiplex Analysis. *Crit. Care* 11, R49. doi:10.1186/cc5783
- Cannon, J. G. (2000). Inflammatory Cytokines in Nonpathological States. *News Physiol. Sci.* 15, 298–303. doi:10.1152/physiologyonline.2000.15.6.298
- Chang, C. Y., Hsu, H. J., Foo, J., Shih, H. J., and Huang, C. J. (2020). Peptide-Based TNF-Alpha-Binding Decoy Therapy Mitigates Lipopolysaccharide-Induced Liver Injury in Mice. *Pharmaceuticals (Basel)* 13, 280. doi:10.3390/ph13100280
- Chang, F. M., Reyna, S. M., Granados, J. C., Wei, S. J., Innis-Whitehouse, W., Maffi, S. K., et al. (2012). Inhibition of Neddylation Represses Lipopolysaccharide-Induced Proinflammatory Cytokine Production in Macrophage Cells. *J. Biol. Chem.* 287, 35756–35767. doi:10.1074/jbc.M112.397703
- Chaudhry, H., Zhou, J., Zhong, Y., Ali, M. M., McGuire, F., Nagarkatti, P. S., et al. (2013). Role of Cytokines as a Double-Edged Sword in Sepsis. *In Vivo* 27, 669–684.
- Clark, M. A., Plank, L. D., Connolly, A. B., Streat, S. J., Hill, A. A., Gupta, R., et al. (1998). Effect of a Chimeric Antibody to Tumor Necrosis Factor-Alpha on Cytokine and Physiologic Responses in Patients with Severe Sepsis-Aa Randomized, Clinical Trial. *Crit. Care Med.* 26, 1650–1659. doi:10.1097/00003246-199810000-00016
- Craige, S. M., Kant, S., and Keaney, J. F., Jr (2015). Reactive Oxygen Species in Endothelial Function - from Disease to Adaptation -. *Circ. J.* 79, 1145–1155. doi:10.1253/circj.CJ-15-0464
- Crimi, E., Sica, V., Slutsky, A. S., Zhang, H., Williams-Ignarro, S., Ignarro, L. J., et al. (2006). Role of Oxidative Stress in Experimental Sepsis and Multisystem Organ Dysfunction. *Free Radic. Res.* 40, 665–672. doi:10.1080/10715760600669612
- D'elia, R. V., Harrison, K., Oyston, P. C., Lukaszewski, R. A., and Clark, G. C. (2013). Targeting the "cytokine Storm" for Therapeutic Benefit. *Clin. Vaccin. Immunol* 20, 319–327. doi:10.1128/CI.00636-12
- Devasagayam, T. P., Tilak, J. C., Boloor, K. K., Sane, K. S., Ghaskadbi, S. S., and Lele, R. D. (2004). Free Radicals and Antioxidants in Human Health: Current Status and Future Prospects. *J. Assoc. Physicians India* 52, 794–804.
- Dinarello, C. A. (2000). Proinflammatory Cytokines. *Chest* 118, 503–508. doi:10.1378/chest.118.2.503
- Fosgerau, K., and Hoffmann, T. (2015). Peptide Therapeutics: Current Status and Future Directions. *Drug Discov. Today* 20, 122–128. doi:10.1016/j.drudis.2014.10.003

## ETHICS STATEMENT

The animal study was reviewed and approved by the Tzu Chi University Institutional Animal Care and Use Committee (Permit Number: 108080).

## AUTHOR CONTRIBUTIONS

H-JH, C-CC, and S-JJ, conceived and designed the experiments. X-YL and H-JH provided the peptide and performed the molecular modeling. H-HT, H-TH, and S-JJ performed the cellular experiments. S-YP, H-HT, and H-TH performed the animal experiments. C-CC, H-JH, and S-JJ wrote the paper. All authors read and approved the final manuscript. All authors have read and agreed to the published version of the manuscript.

## FUNDING

This research was funded by Hualien Tzu Chi Hospital, Buddhist Tzu Chi Medical Foundation, Hualien, Taiwan (Grant Numbers: TCRD111-062) Tzu Chi University (Grant Numbers: TCMRC-P-108010, TCMRC-P-109005) and Buddhist Tzu Chi Medical Foundation (Grant Numbers: TCMMP110-01, TCAS-111-03).

## SUPPLEMENTARY MATERIAL

The Supplementary Material for this article can be found online at: <https://www.frontiersin.org/articles/10.3389/fphar.2022.853818/full#supplementary-material>



- Gallagher, J. E., George, G., and Brody, A. R. (1987). Sialic Acid Mediates the Initial Binding of Positively Charged Inorganic Particles to Alveolar Macrophage Membranes. *Am. Rev. Respir. Dis.* 135, 1345–1352. doi:10.1164/arrd.1987.135.6.1345
- Gogos, C. A., Drosou, E., Bassaris, H. P., and Skoutelis, A. (2000). Pro- versus Anti-inflammatory Cytokine Profile in Patients with Severe Sepsis: a Marker for Prognosis and Future Therapeutic Options. *J. Infect. Dis.* 181, 176–180. doi:10.1086/315214
- Gutsmann, T., Razquin-Olazarán, I., Kowalski, I., Kaconis, Y., Howe, J., Bartels, R., et al. (2010). New Antiseptic Peptides to Protect against Endotoxin-Mediated Shock. *Antimicrob. Agents Chemother.* 54, 3817–3824. doi:10.1128/AAC.00534-10
- Jiang, Q., Yi, M., Guo, Q., Wang, C., Wang, H., Meng, S., et al. (2015). Protective Effects of Polydatin on Lipopolysaccharide-Induced Acute Lung Injury through TLR4-MyD88-NF- $\kappa$ B Pathway. *Int. Immunopharmacol.* 29, 370–376. doi:10.1016/j.intimp.2015.10.027
- Jiang, S. J., Tsai, P. I., Peng, S. Y., Chang, C. C., Chung, Y., Tsao, H. H., et al. (2019). A Potential Peptide Derived from Cytokine Receptors Can Bind Proinflammatory Cytokines as a Therapeutic Strategy for Anti-inflammation. *Sci. Rep.* 9, 2317. doi:10.1038/s41598-018-36492-z
- Kilroy, G. E., Foster, S. J., Wu, X., Ruiz, J., Sherwood, S., Heifetz, A., et al. (2007). Cytokine Profile of Human Adipose-Derived Stem Cells: Expression of Angiogenic, Hematopoietic, and Pro-inflammatory Factors. *J. Cell Physiol.* 212, 702–709. doi:10.1002/jcp.21068
- Komin, A., Russell, L. M., Hristova, K. A., and Searson, P. C. (2017). Peptide-based Strategies for Enhanced Cell Uptake, Transcellular Transport, and Circulation: Mechanisms and Challenges. *Adv. Drug Deliv. Rev.* 110–111, 52–64. doi:10.1016/j.addr.2016.06.002
- Kumar, A. T., Sudhir, U., Punith, K., Kumar, R., Ravi Kumar, V. N., and Rao, M. Y. (2009). Cytokine Profile in Elderly Patients with Sepsis. *Indian J. Crit. Care Med.* 13, 74–78. doi:10.4103/0972-5229.56052
- Kvietys, P. R., and Granger, D. N. (2012). Role of Reactive Oxygen and Nitrogen Species in the Vascular Responses to Inflammation. *Free Radic. Biol. Med.* 52, 556–592. doi:10.1016/j.freeradbiomed.2011.11.002
- Lawrence, T. (2009). The Nuclear Factor NF- $\kappa$ B Pathway in Inflammation. *Cold Spring Harb Perspect. Biol.* 1, a001651.
- Li, D., and Mehta, J. L. (2005). Oxidized LDL, a Critical Factor in Atherogenesis. *Cardiovasc. Res.* 68, 353–354. doi:10.1016/j.cardiores.2005.09.009
- Liu, S. F., and Malik, A. B. (2006). NF- $\kappa$ B Activation as a Pathological Mechanism of Septic Shock and Inflammation. *Am. J. Physiol. Lung Cell Mol. Physiol.* 290, L622–L645. doi:10.1152/ajplung.00477.2005
- Mann, M., and Jensen, O. N. (2003). Proteomic Analysis of post-translational Modifications. *Nat. Biotechnol.* 21, 255–261. doi:10.1038/nbt0303-255
- Muller, F. L., Lustgarten, M. S., Jang, Y., Richardson, A., and Van Remmen, H. (2007). Trends in Oxidative Aging Theories. *Free Radic. Biol. Med.* 43, 477–503. doi:10.1016/j.freeradbiomed.2007.03.034
- Otvos, L., Jr., and Wade, J. D. (2014). Current Challenges in Peptide-Based Drug Discovery. *Front. Chem.* 2, 62. doi:10.3389/fchem.2014.00062
- Pacher, P., Beckman, J. S., and Liaudet, L. (2007). Nitric Oxide and Peroxynitrite in Health and Disease. *Physiol. Rev.* 87, 315–424. doi:10.1152/physrev.00029.2006
- Parthasarathy, S., Raghavamenon, A., Garelnabi, M. O., and Santanam, N. (2010). Oxidized Low-Density Lipoprotein. *Methods Mol. Biol.* 610, 403–417. doi:10.1007/978-1-60327-029-8\_24
- Prolo, C., Alvarez, M. N., and Radi, R. (2014). Peroxynitrite, a Potent Macrophage-Derived Oxidizing Cytotoxin to Combat Invading Pathogens. *Biofactors* 40, 215–225. doi:10.1002/biof.1150
- Radi, R. (2013). Peroxynitrite, a Stealthy Biological Oxidant. *J. Biol. Chem.* 288, 26464–26472. doi:10.1074/jbc.R113.472936
- Roser, M., Fischer, D., and Kissel, T. (1998). Surface-modified Biodegradable Albumin Nano- and Microspheres. II: Effect of Surface Charges on *In Vitro* Phagocytosis and Biodistribution in Rats. *Eur. J. Pharm. Biopharm.* 46, 255–263. doi:10.1016/s0939-6411(98)00038-1
- Roy, A., Srivastava, M., Saqib, U., Liu, D., Faisal, S. M., Sugathan, S., et al. (2016). Potential Therapeutic Targets for Inflammation in Toll-like Receptor 4 (TLR4)-Mediated Signaling Pathways. *Int. Immunopharmacol.* 40, 79–89. doi:10.1016/j.intimp.2016.08.026
- Shih, H. J., Chang, C. Y., Chiang, M., Le, V. L., Hsu, H. J., and Huang, C. J. (2021). Simultaneous Inhibition of Three Major Cytokines and its Therapeutic Effects: A Peptide-Based Novel Therapy against Endotoxemia in Mice. *J. Pers. Med.* 11, 436. doi:10.3390/jpm11050436
- Sinha, J. K., Ghosh, S., Swain, U., Giridharan, N. V., and Raghunath, M. (2014). Increased Macromolecular Damage Due to Oxidative Stress in the Neocortex and hippocampus of WNIN/Ob, a Novel Rat Model of Premature Aging. *Neuroscience* 269, 256–264. doi:10.1016/j.neuroscience.2014.03.040
- Sun, Y., Jin, C., Zhan, F., Wang, X., Liang, M., Zhang, Q., et al. (2012). Host Cytokine Storm Is Associated with Disease Severity of Severe Fever with Thrombocytopenia Syndrome. *J. Infect. Dis.* 206, 1085–1094. doi:10.1093/infdis/jis452
- Vucic, D., Dixit, V. M., and Wertz, I. E. (2011). Ubiquitylation in Apoptosis: a post-translational Modification at the Edge of Life and Death. *Nat. Rev. Mol. Cell Biol.* 12, 439–452. doi:10.1038/nrm3143
- West, A. P., Brodsky, I. E., Rahner, C., Woo, D. K., Erdjument-Bromage, H., Tempst, P., et al. (2011). TLR Signalling Augments Macrophage Bactericidal Activity through Mitochondrial ROS. *Nature* 472, 476–480. doi:10.1038/nature09973
- Xiao, K., Li, Y., Luo, J., Lee, J. S., Xiao, W., Gonik, A. M., et al. (2011). The Effect of Surface Charge on *In Vivo* Biodistribution of PEG-Oligocholic Acid Based Micellar Nanoparticles. *Biomaterials* 32, 3435–3446. doi:10.1016/j.biomaterials.2011.01.021
- Yamamoto, Y., and Gaynor, R. B. (2001). Therapeutic Potential of Inhibition of the NF- $\kappa$ B Pathway in the Treatment of Inflammation and Cancer. *J. Clin. Invest.* 107, 135–142. doi:10.1172/JCI11914
- Zughaier, S. M., Shafer, W. M., and Stephens, D. S. (2005). Antimicrobial Peptides and Endotoxin Inhibit Cytokine and Nitric Oxide Release but Amplify Respiratory Burst Response in Human and Murine Macrophages. *Cell Microbiol.* 7, 1251–1262. doi:10.1111/j.1462-5822.2005.00549.x

**Conflict of Interest:** The authors declare that the research was conducted in the absence of any commercial or financial relationships that could be construed as a potential conflict of interest.

**Publisher's Note:** All claims expressed in this article are solely those of the authors and do not necessarily represent those of their affiliated organizations, or those of the publisher, the editors and the reviewers. Any product that may be evaluated in this article, or claim that may be made by its manufacturer, is not guaranteed or endorsed by the publisher.

Copyright © 2022 Chang, Peng, Tsao, Huang, Lai, Hsu and Jiang. This is an open-access article distributed under the terms of the Creative Commons Attribution License (CC BY). The use, distribution or reproduction in other forums is permitted, provided the original author(s) and the copyright owner(s) are credited and that the original publication in this journal is cited, in accordance with accepted academic practice. No use, distribution or reproduction is permitted which does not comply with these terms.





# Development and Validation of Ischemic Events Related Signature After Carotid Endarterectomy

Chunguang Guo<sup>1†</sup>, Zaoqu Liu<sup>2†</sup>, Can Cao<sup>3†</sup>, Youyang Zheng<sup>4</sup>, Taoyuan Lu<sup>5</sup>, Yin Yu<sup>6</sup>, Libo Wang<sup>7</sup>, Long Liu<sup>7</sup>, Shirui Liu<sup>1</sup>, Zhaohui Hua<sup>1\*</sup>, Xinwei Han<sup>2\*</sup> and Zhen Li<sup>1\*</sup>

<sup>1</sup>Department of Endovascular Surgery, The First Affiliated Hospital of Zhengzhou University, Zhengzhou, China, <sup>2</sup>Department of Interventional Radiology, The First Affiliated Hospital of Zhengzhou University, Zhengzhou, China, <sup>3</sup>Institute for Cardiovascular Physiology, Goethe University, Frankfurt, Germany, <sup>4</sup>Department of Cardiology, The First Affiliated Hospital of Zhengzhou University, Zhengzhou, China, <sup>5</sup>Department of Cerebrovascular Disease, Zhengzhou University People's Hospital, Zhengzhou, China, <sup>6</sup>Department of Pathophysiology, School of Basic Medical Sciences, The Academy of Medical Science, Zhengzhou University, Zhengzhou, China, <sup>7</sup>Department of Hepatobiliary and Pancreatic Surgery, The First Affiliated Hospital of Zhengzhou University, Zhengzhou, China

## OPEN ACCESS

### Edited by:

Xianwei Wang,  
Xinxiang Medical University, China

### Reviewed by:

Anton G. Kutikhin,  
Russian Academy of Medical  
Sciences, Russia  
Diansan Su,  
Shanghai JiaoTong University, China

### \*Correspondence:

Zhaohui Hua  
huazhaohuisfy@163.com  
Xinwei Han  
fcchanxw@zzu.edu.cn  
Zhen Li  
lizhen1029@hotmail.com

<sup>†</sup>These authors have contributed  
equally to this work and share first  
authorship

### Specialty section:

This article was submitted to  
Molecular and Cellular Pathology,  
a section of the journal  
Frontiers in Cell and Developmental  
Biology

**Received:** 13 October 2021

**Accepted:** 04 March 2022

**Published:** 17 March 2022

### Citation:

Guo C, Liu Z, Cao C, Zheng Y, Lu T,  
Yu Y, Wang L, Liu L, Liu S, Hua Z,  
Han X and Li Z (2022) Development  
and Validation of Ischemic Events  
Related Signature After  
Carotid Endarterectomy.  
Front. Cell Dev. Biol. 10:794608.  
doi: 10.3389/fcell.2022.794608

**Background:** Ischemic events after carotid endarterectomy (CEA) in carotid artery stenosis patients are unforeseeable and alarming. Therefore, we aimed to establish a novel model to prevent recurrent ischemic events after CEA.

**Methods:** Ninety-eight peripheral blood mononuclear cell samples were collected from carotid artery stenosis patients. Based on weighted gene co-expression network analysis, we performed whole transcriptome correlation analysis and extracted the key module related to ischemic events. The biological functions of the 292 genes in the key module were annotated via GO and KEGG enrichment analysis, and the protein-protein interaction (PPI) network was constructed via the STRING database and Cytoscape software. The enrolled samples were divided into train ( $n = 66$ ), validation ( $n = 28$ ), and total sets ( $n = 94$ ). In the train set, the random forest algorithm was used to identify critical genes for predicting ischemic events after CEA, and further dimension reduction was performed by LASSO logistic regression. A diagnosis model was established in the train set and verified in the validation and total sets. Furthermore, fifty peripheral venous blood samples from patients with carotid stenosis in our hospital were used as an independent cohort to validate the model by RT-qPCR. Meanwhile, GSEA, ssGSEA, CIBERSORT, and MCP-counter were used to enrichment analysis in high- and low-risk groups, which were divided by the median risk score.

**Results:** We established an eight-gene model consisting of *PLSCR1*, *ECRP*, *CASP5*, *SPTSSA*, *MSRB1*, *BCL6*, *FBP1*, and *LST1*. The ROC-AUCs and PR-AUCs of the train, validation, total, and independent cohort were 0.891 and 0.725, 0.826 and 0.364, 0.869 and 0.654, 0.792 and 0.372, respectively. GSEA, ssGSEA, CIBERSORT, and MCP-counter analyses further revealed that high-risk patients presented enhanced immune signatures, which indicated that immunotherapy may improve clinical outcomes in these patients.

**Conclusion:** An eight-gene model with high accuracy for predicting ischemic events after CEA was constructed. This model might be a promising tool to facilitate the clinical management and postoperative surveillance of carotid artery stenosis patients.

**Keywords:** ischemic events, carotid endarterectomy, diagnosis model, machine learning, immune infiltration

## 1 INTRODUCTION

Ischemic events, mainly ischemic heart disease and ischemic stroke, are the leading cause of death and disability worldwide (Murray and Lopez, 1997; Campbell et al., 2019). The main etiology of ischemic events is atherosclerosis formation, which arises from inflammation, lipid deposition and plaque fibrosis in the vascular endothelium over decades (Franceschini et al., 2018; Libby et al., 2019). Therefore, it is necessary to accurately identify atherosclerotic patients who are more prone to ischemic events. With developments in medicine and technology, multiple diagnostic techniques have been used to identify people at high risk of ischemic events, including noninvasive (such as computed tomography, biomarkers, stress testing and nuclear scanning) and invasive (such as selective and superselective arteriography) techniques (Dagvasumberel et al., 2012; Zhang et al., 2017; Martinez et al., 2020; Varasteh et al., 2021). Nonetheless, these methods have only moderate prediction accuracies, and some high-risk patients are not identified early, which leads to ischemic events (Penalvo et al., 2016). Thus, new methods to identify patients at high risk for ischemic events are urgently needed.

Indeed, substantial efforts have been made to cope with the occurrence of ischemic events, and carotid endarterectomy (CEA) has been indicated to be one of the most critical techniques (Howell, 2007). Unstable plaque shedding of the carotid intima is an important cause of cardiovascular and cerebrovascular occlusion, especially at the carotid bifurcation. In clinical practice, CEA is the optimal treatment modality to prevent ischemic events in patients with atheromatous disease at the carotid bifurcation (Howell, 2007; Rerkasem et al., 2020). However, this prophylactic surgery does not provide complete prevention, and some patients who undergo regular CEA surgery may still experience ischemic events (Folkersen et al., 2012). The recurrence of ischemic events (including ischemic stroke and myocardial infarction) after CEA is an important and urgent issue, but few studies have focused on it (Folkersen et al., 2012; Zenonos et al., 2012).

With the development of bioinformatics and machine learning, elegant studies have broadly applied artificial intelligence in the medical field because it better describes the complexity and unpredictability of human physiology (Deo, 2015; Rajkomar et al., 2019). Compared with traditional imaging diagnostic methods, machine learning can extract the most critical characteristics of the disease from high-dimensional variables to improve the performance of predicting ischemic events after CEA (Heo et al., 2019). With the help of these algorithms (such as random forest (Svetnik et al., 2003), and least absolute shrinkage and selection operator (LASSO) (Tibshirani, 1997)), researchers could identify the key factors

in predicting recurrent ischemic events after CEA from massive data.

In this study, we retrieved gene expression data and clinical information from GEO for 97 patients. The hub genes of recurrent ischemic events after CEA were identified by machine learning algorithms and validated in an independent cohort (which included 50 samples from our hospital). Finally, we developed and validated a diagnostic model for predicting the probability of ischemic events after CEA. Based on this model, it is possible to intervene recurrent ischemic events after CEA in advance and improve clinical outcomes.

## 2 MATERIALS AND METHODS

### 2.1 Data Source

The workflow of the overall analysis is shown in **Figure 1**. The gene expression and clinical annotation data of GSE21545 (Folkersen et al., 2012) were retrieved from the Gene Expression Omnibus (GEO) database. This dataset was based on an Affymetrix® platform (GPL570) and included 97 peripheral blood mononuclear cell samples. The raw data were processed using the robust multichip analysis (RMA) algorithm implemented in the “Affy” R package. RMA was used to perform background adjustment, quantile normalization, and final summarization of oligonucleotides per transcript using the median polish algorithm (Liu et al., 2022a). The baseline clinical data of patients were presented in **Supplementary Table S1**.

### 2.2 Weighted Gene Co-Expression Network Analysis

Based on gene expression profiles, a total of 22,880 genes were identified from the samples. All genes were sorted in descending order according to their expression variability, which was calculated by the median absolute deviation in the entire dataset. To ensure the rationality of network construction, we excluded the outlier samples using an optimal version of hierarchical clustering, which applied Euclidean distance and averaging methods to rearrange the samples. Next, based on the top 5,000 genes, a gene co-expression network was constructed using the “WGCNA” R package (Langfelder and Horvath, 2008). We used step-by-step methods to construct gene networks. To meet the criterion of scale-free network distribution, the Pearson correlation coefficient between paired genes was calculated, and the optimum soft threshold  $\beta$  was selected. First, the Pearson's correlation value between paired genes was used to acquire a similarity matrix. Next, with the optimum soft threshold value, the similarity matrix was

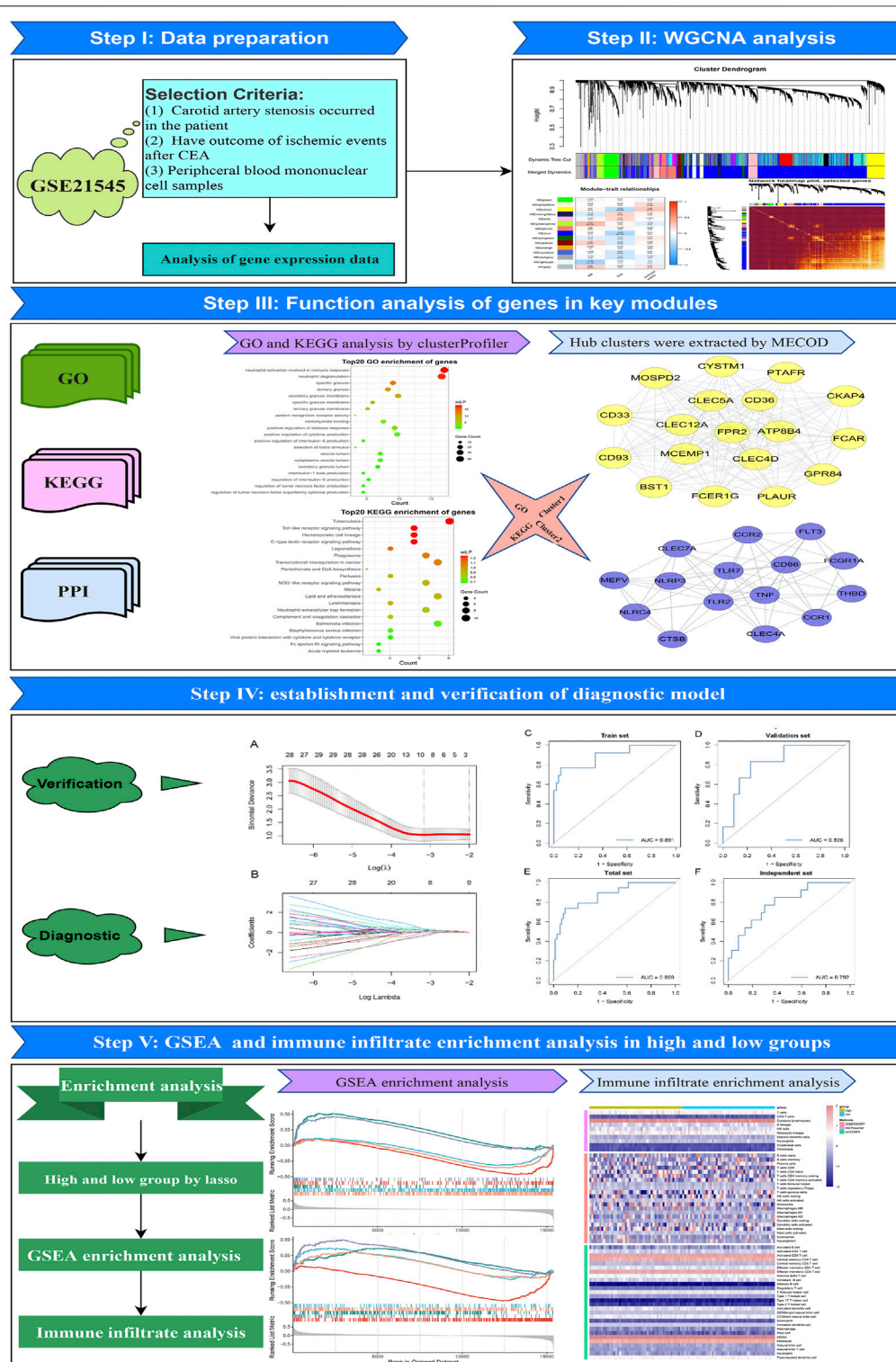


**FIGURE 1 |** Flowchart of the analysis procedure.

transformed to an adjacency matrix. The adjacency matrix was calculated by setting the parameter  $am_n = |cm_n|^\beta$  ( $cm_n$  = Pearson's correlation between genes  $m$  and  $n$ ;  $am_n$  =

adjacency between genes  $m$  and  $n$ ). Subsequently, the adjacency matrix was transformed into a topological overlap matrix (TOM), which was used to describe the similarity of

gene expression, and 1-TOM was used to describe the dissimilarity between genes. Finally, a dynamic tree algorithm was used to partition the modules of the hierarchical clustering results (minimum module size = 30; deep-split = 2; cut tree height = 0.99; merge module height = 0.25). To further investigate the module, the dissimilarity of the module eigengene (ME) was calculated. A cut line for the module dendrogram was selected, and then the modules with cutting height <0.25 were merged (Guo et al., 2022).

## 2.3 Identification of Clinically Significant Modules

MEs were used for the component analysis of each module, and modules with similar expression profiles showed highly correlated eigengenes. The relevant modules were identified by calculating the correlation between the ME and ischemic events. The gene module with the highest correlation coefficient and a  $p < 0.05$  was considered the most relevant module to ischemic events and was defined as the key module.

## 2.4 Protein-Protein Interaction Network Construction

All genes in the key module with a minimum level of confidence greater than 0.4 were submitted to the Search Tool for the Retrieval of Interacting Genes/Proteins (STRING) (<https://string-db.org/>) database version 11.0 (Szklarczyk et al., 2017; Szklarczyk et al., 2019). Protein interaction data obtained from the STRING database were used to calculate the degrees of genes by Cytoscape software (version 3.8.0; <https://cytoscape.org/>) (Shannon et al., 2003). Based on the maximal clique centrality (MCC) algorithm, significant modules with strong protein interactions were calculated and selected by Molecular Complex Detection (MCODE), which is a plugin in Cytoscape. The parameter settings for MCODE were as follows: degree cut  $\geq 2$ , K-core  $\geq 2$ , node score cut  $\geq 2$ , and maximum depth = 100.

## 2.5 Functional Enrichment Analysis

“ClusterProfiler” (Yu et al., 2012; Liu et al., 2021a), a Bioconductor package, was used to perform Gene Ontology (GO) and Kyoto Encyclopedia of Genes and Genomes (KEGG) pathway enrichment analysis. The terms with  $p < 0.05$  were considered significant.

## 2.6 Random Forest

To identify genes associated with ischemic events, random forest was employed. Random forest, originally proposed by Breiman (Mantero and Ishwaran, 2021), is an ensemble learning algorithm that can construct abundant trees and predict outcomes by voting across all trees. In this study, the expression values of all genes in the key module were extracted and merged with the clinical characteristic information of the samples. Then, all samples were randomly divided into train (75% of samples,  $n = 66$ ) and validation datasets (25% of samples,  $n = 28$ ). Finally, “randomForestSRC” version 2.9.3 (which provides fast

computing of unified random forests for survival, regression, and classification), a package in R, was used to screen out key genes associated with ischemic events in the train dataset.

## 2.7 LASSO Logistic Regression Model

To further identify genes associated with ischemic events after CEA, the LASSO regression algorithm (Lockhart et al., 2014) was used to obtain the coefficient for each key gene selected by random forest. To achieve this purpose, we used the “glmnet” (Friedman et al., 2010) R package (which is used for LASSO and elastic-net regularized generalized linear models). The alpha parameter of glmnet was set to 1, and the lambda value was chosen by cross-fold validation of the key gene set (5-fold cross-validation). Ultimately, the diagnostic model achieved the best lambda value, and its predictive accuracy in the train and validation sets was assessed by receiver operating characteristic (ROC) curve and precision recall (PR) curve.

## 2.8 Human Carotid Artery Stenosis Specimens

Participants fulfilling all of the following inclusion criteria are eligible for the study: 1) Imaging revealed carotid artery stenosis; 2) have clearly defined indications for surgery; 3) Patients with valvular heart disease, blood diseases, and malignant tumors were excluded. A total of 50 peripheral venous blood samples were collected from patients with carotid stenosis in the First Affiliated Hospital of Zhengzhou University. The baseline clinical data of patients were presented in **Supplementary Table S1**. The specimens obtained upon admission to the hospital and stored at  $-80^{\circ}\text{C}$  until use in quantitative real-time qPCR (RT-qPCR). The Research Ethics Committee of the First Affiliated Hospital of Zhengzhou University approved this study, which was consistent with the Declaration of Helsinki, and the TRN is 2019-KW-94.

## 2.9 RNA Isolation and RT-qPCR

Total RNA was isolated from peripheral blood using RNAiso Plus (Takara, Dalian, China) according to the manufacturer's instructions. The integrity and purity of the extracted total RNA were measured using NanoDrop One (Thermo Fisher Scientific, Waltham, United States) ultra-micro UV spectrophotometer. Reverse transcription was performed using the PrimeScript RT reagent Kit (Takara, Dalian, China) with gDNA Eraser. Serum RNA was reverse transcribed into cDNA using a RevertAid H Minus First Strand cDNA Synthesis Kit (Thermo Fisher Scientific, Waltham, United States) under the following conditions:  $25^{\circ}\text{C}$  for 5 min,  $42^{\circ}\text{C}$  for 60 min, and  $70^{\circ}\text{C}$  for 5 min. The product was immediately stored at  $-80^{\circ}\text{C}$  until use.

The RT-qPCR was performed on a QuantStudio five Real-Time PCR System (Applied Biosystems, Foster City, United States) using a Hieff qPCR SYBR Green Master Mix kit (Yeasen, Shanghai, China). The RT-qPCR reaction was performed  $95^{\circ}\text{C}$  for 5 min, followed by 40 cycles of  $95^{\circ}\text{C}$  for 10 s and a primer-specific annealing temperature of  $60^{\circ}\text{C}$  for 30 s. The RT-qPCR primer sequences were provided in



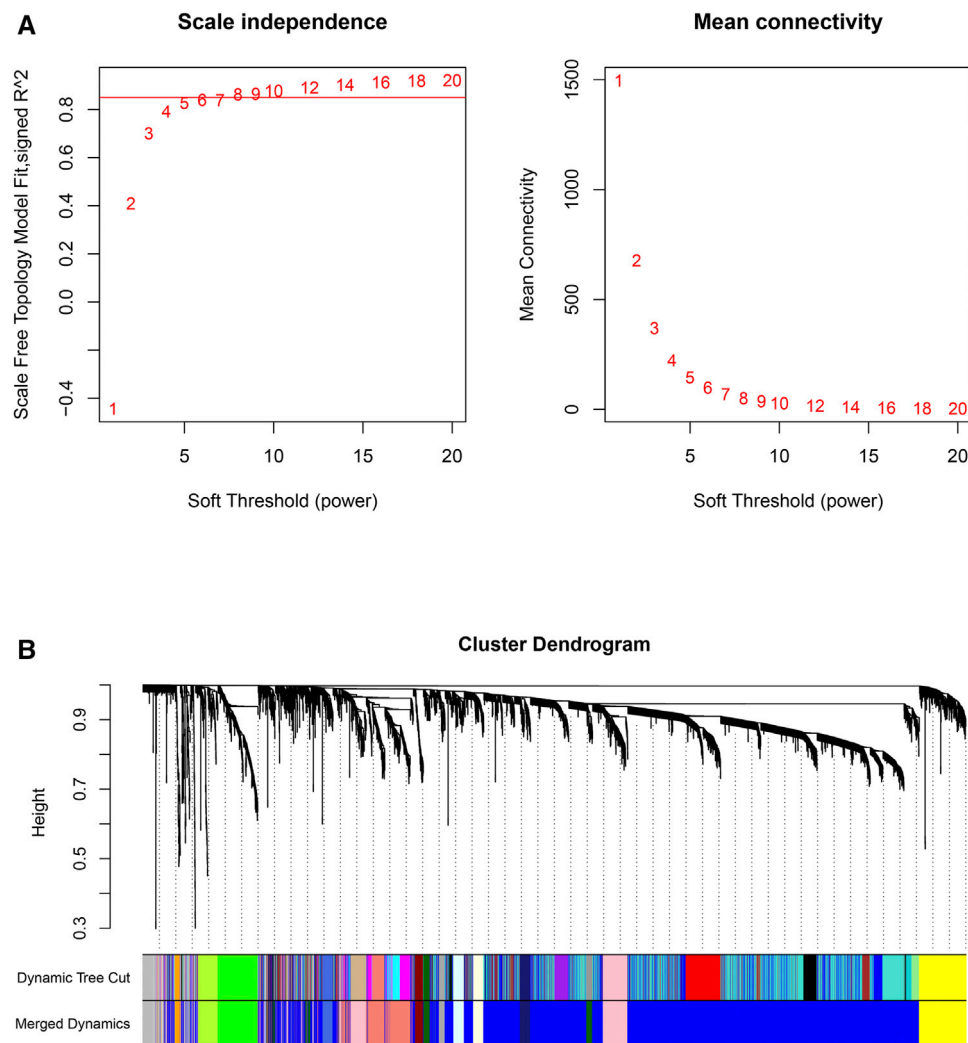


**FIGURE 2 |** Scale-free networks were constructed, and genes were clustered by WGCNA. **(A):** Scale-free network analysis under different soft-thresholding powers. The left panel shows scale-free topological indices at different soft-thresholding powers. The right panel shows the correlation analysis between the soft-thresholding powers and average connectivity of the network. **(B):** Gene clustering diagram based on hierarchical clustering under optimal soft-thresholding power. (Dynamic Tree Cut: before module merging; Merged Dynamics: after module merging).

**Supplementary Table S1.** The relative quantification values for RNA were calculated by the 2- $\Delta\Delta C_t$  method. GAPDH was used as an endogenous control for normalization.

## 2.10 Gene Set Enrichment Analysis and Immune Infiltration Profiles

Based on the median risk score of each sample, the entire study cohort was divided into high- and low-risk groups. The differential genes between the high- and low-risk groups were identified by the “limma” package and sequenced by the log2 (fold change) value. GSEA was used to decipher the underlying biological mechanisms of the genes in this model using GO and KEGG terms (Molecular Signatures database, version: c5. go.v7.4. symbols.gmt and c2. cp.kegg.v7.4. symbols.gmt). After that, the CIBERSORT (Newman et al., 2015; Liu et al., 2022b), MCP-

counter (Shi et al., 2020; Liu et al., 2021b) and single-sample gene set enrichment analysis (ssGSEA) (Yi et al., 2020; Liu et al., 2022c) algorithms were used to explore the infiltration abundance of different immune cells between the high- and low-risk groups. Heatmaps and boxplots were used to uncover the degree of difference in the responses of various immune cell subsets between the two groups under different algorithms.

## 2.11 Statistical Analysis

All data processing, statistical analyses and plotting were completed using the R program (version 4.03). The unpaired Student’s t-test and Wilcoxon test were used to compare the differences between two groups. The Benjamin-Hochberg method was used to further calculate the false discovery rate (FDR). For every analysis, statistical significance was considered at  $p < 0.05$ .

**TABLE 1** | Number of genes contained in the merged module.

Modules	Numbers	Modules	Numbers	Modules	Numbers
Blue	2,981	Grey	176	Lightyellow	64
Salmon	372	Greenyellow	121	Royalblue	63
Pink	289	Darkgreen	116	Darkred	48
Yellow	292	Midnightblue	88	Darkgrey	38
Green	244	Lightcyan	77	Orange	31

### 3 RESULTS

#### 3.1 Preparation of Data for WGCNA

In this section, we cleaned the raw gene profiles for WGCNA. Based on the 97 PBMC samples with 22,880 gene expression profiles, we calculated the median absolute deviation (MAD) of each gene and retained the top 5,000 genes sorted by the MAD.

The hierarchical clustering algorithm was further used for three outlier samples. After removing the three samples, we obtained a clean dataset consisting of 94 PBMC samples with 5,000 gene expression profiles.

#### 3.2 Co-Expression Network Construction

First, the pickSoftThreshold function (from the “WGCNA” R package) was used to select the optimal soft threshold. Under the premise that the absolute value of the correlation coefficient is greater than 0.8, we chose 8 as the optimal soft threshold for constructing scale-free networks (**Figure 2A**). Next, we employed the cutreeDynamic function (from the “dynamicTreeCut” R package) to identify co-expression modules in the network (**Figure 2B**), and all genes were clustered among the 26 modules. To reduce the complexity of the network, modules with similarity greater than 0.75 were merged. MergeCloseModules, a function in the “WGCNA” R package,

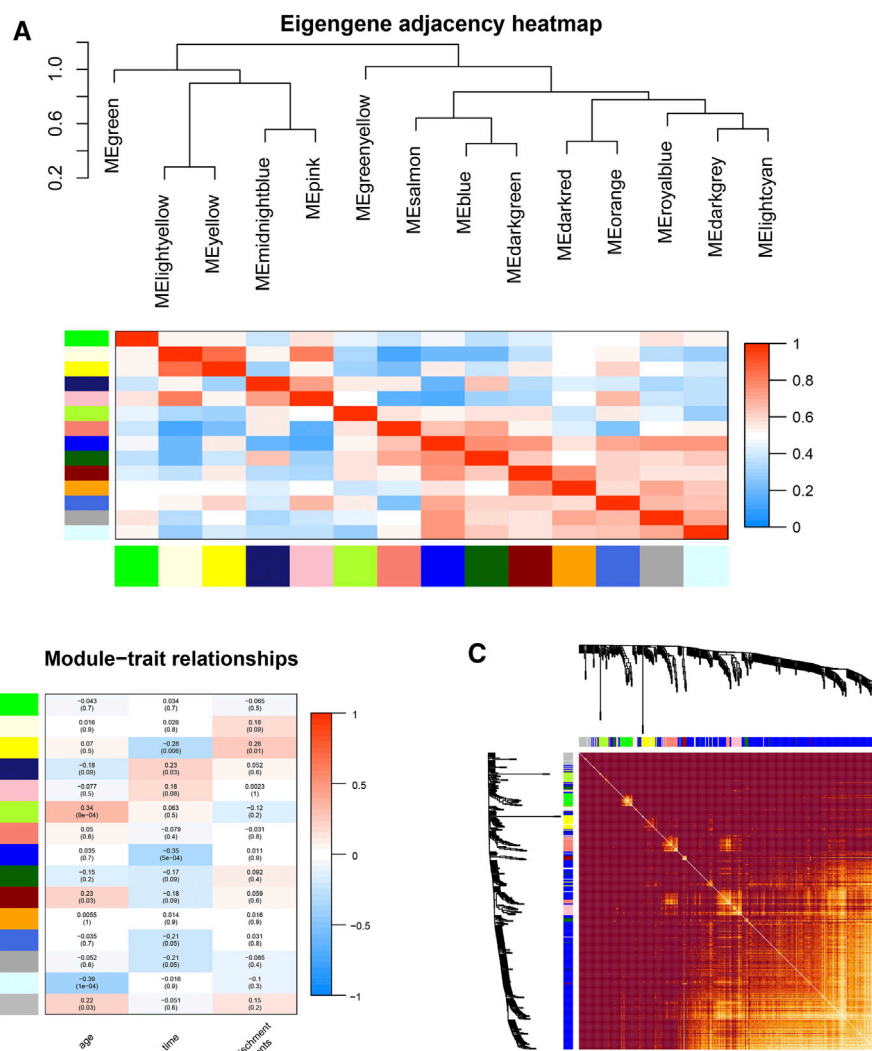
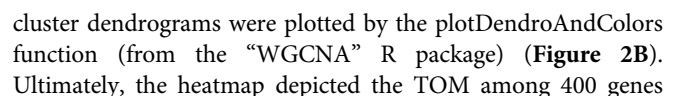


**FIGURE 3** | Gene module analysis based on WGCNA. **(A)**: Heat map of the eigengene adjacency. **(B)**: Heatmap between gene modules and clinical characteristics. **(C)**: Heatmap of the topological overlap matrix of genes selected by WGCNA.



(which were randomly selected from all genes) in WGCNA (Figure 3C).

### 3.3 Identifying Key Clinically Significant Modules

An eigengene adjacency heatmap (Figure 3A) was plotted by the plotEigengeneNetworks function (from the “WGCNA” R package) to explore the correlations between modules. In this research, the parameters of 94 samples included ischemic events, age, and time (postprocedure to ischemic event). The occurrence of ischemic events after CEA is an urgent problem to be solved, so our research focused on the early diagnosis of ischemic events. The yellow module (including 292 genes) ( $r = 0.26$ ,  $p < 0.01$ ) was the most notable module and had the strongest biological association with ischemic events in patients after CEA (Figure 3B).

### 3.4 GO and KEGG Enrichment Analysis and PPI Network Construction

To further investigate the functional features of the 292 genes in the yellow module, the enrichGO and enrichKEGG functions (from the “clusterProfiler” R package) were used to perform GO and KEGG enrichment analysis. Overall, the top 20 enriched GO terms and KEGG pathways from GO and KEGG enrichment analysis were plotted by the ggplot function (from the “ggplot2” R package) (Figures 4A,B). Among the GO terms, “neutrophil activation involved in immune response”, “neutrophil degranulation”, “specific granule”, “tertiary granule”, and “secretory granule membrane” were significantly enriched. Similarly, among the KEGG pathways, “Tuberculosis”, “Toll-like receptor signaling pathway”, “Hematopoietic cell lineage”, “C-type lectin receptor signaling pathway” and “Legionellosis” were significantly enriched. Based on the STRING database and Cytoscape software, a PPI network of the key genes within the yellow module was constructed (Figure 4C). Two key modules in the PPI network were identified by the MCODE plugin. The first module (score = 16.353, nodes = 18, edges = 139) consisted of 18 target genes, including *MOSPD2*, *CYSTM1*, *PTAFR*, *CKAP4*, *CD36*, *CLEC5A*, *CD33*, *CLEC12A*, *FPR2*, *ATP8B4*, *FCAR*, *CD93*, *MCEMP1*, *CLEC4D*, *GPR84*, *BST1*, *FCER1G*, and *PLAUR* (Figure 4D). The second module (score = 9.429, nodes = 15, edges = 66) consisted of 15 target genes, including *CLEC7A*, *CCR2*, *FLT3*, *MEFV*, *NLRP3*, *TLR7*, *CD86*, *FCGR1A*, *NLR4*, *TLR2*, *TNF*, *THBD*, *CCR1*, *CLEC4A*, and *CTSB* (Figure 4E).

### 3.5 Identification of Optimal Diagnostic Biomarkers for Predicting Ischemic Events

According to the results of WGCNA, the yellow module is most associated with the occurrence of ischemic events after CEA. Using the expression of the genes in the yellow module in the train set, the random forest algorithm was applied. We retained 79 genes with relative importance >0.5. To further simplify the diagnostic model and reduce overfitting, LASSO

regression was performed. Eventually, we obtained an eight-gene model, including *RLSCR1*, *ECRP*, *CASP5*, *SPTSSA*, *MSRB1*, *BCL6*, *FBP1* and *LST1* (Figures 5A,B). The final model formula was as follows: risk score =  $-1.61 - 0.24 \times PLSCR1 + 0.37 \times ECRP + 0.13 \times CASP5 + 0.20 \times SPTSSA - 0.38 \times MSRB1 + 0.34 \times BCL6 + 0.24 \times FBP1 + 0.23 \times LST1$ . According to this formula, we calculated the risk score of each patient. Logistic regression analysis showed that the eight-gene model was an independent predictor of ischemic events after CEA in the train dataset (odds ratio [OR] and 95% confidence interval [CI], 2.57 [1.33–7.24];  $p = 0.005$ ), validation dataset (OR and 95% CI, 10.64 [1.82–188.51];  $p = 0.033$ ) and total dataset (OR and 95% CI, 3.60 [1.60–9.08];  $p = 0.003$ ). ROC and PR curve analysis of the diagnostic model for predicting ischemic events was conducted in the train cohort, validation cohort, and total cohort. The ROC-AUCs value was 0.891 in the train cohort, 0.826 in the validation cohort and 0.869 in the total cohort (Figures 5C–E). The PR-AUCs value was 0.725 in the train cohort, 0.364 in the validation cohort and 0.654 in the total cohort (Figures 6A–C). These findings suggested that our model had a high accuracy performance.

### 3.6 Verification of the Eight-Gene Model Using RT-qPCR

RT-qPCR assays were performed in 50 samples. The risk score for the samples was calculated by the expression of the eight genes and risk score formula. ROC curve analysis of the diagnostic model for predicting ischemic events was conducted in the independent validation cohort. The ROC-AUC (Figure 5F) and PR-AUC (Figure 6D) value was 0.792 and 0.372 in the independent validation cohort.

### 3.7 GSEA

A total of 94 samples were divided into high- ( $n = 47$ ) and low-risk ( $n = 47$ ) groups according to the median risk score. GSEA revealed significant GO terms (Figures 6E,F) and KEGG pathways (Figures 6G,H) in which the differentially expressed genes were concentrated between the two risk subtypes. These were mainly inflammatory and immune infiltration-related functions or pathways, including “lipid and atherosclerosis” (normalized enrichment score (NES) = 1.528, FDR = 0.035), “cytokine-cytokine receptor interaction” (NES = 1.464, FDR = 0.035), “interleukin-6 production” (NES = 2.070, FDR = 0.002), “B cell activation” (NES = -1.891, FDR = 0.002) and “Toll-like receptor signaling pathway” (NES = 1.842, FDR = 0.002). These results indicated that our model has a close connection with inflammatory responses.

### 3.8 Immune Infiltration Analysis

To explore the infiltration abundance of immune cells between the high- and low-risk groups, three algorithms, CIBERSORT, MCP-counter and ssGSEA, were performed to ensure the stability and reproduction of our results. We calculated the score of different cell subpopulations in 94 samples (Figure 7A). Interestingly, we found significant immune cell



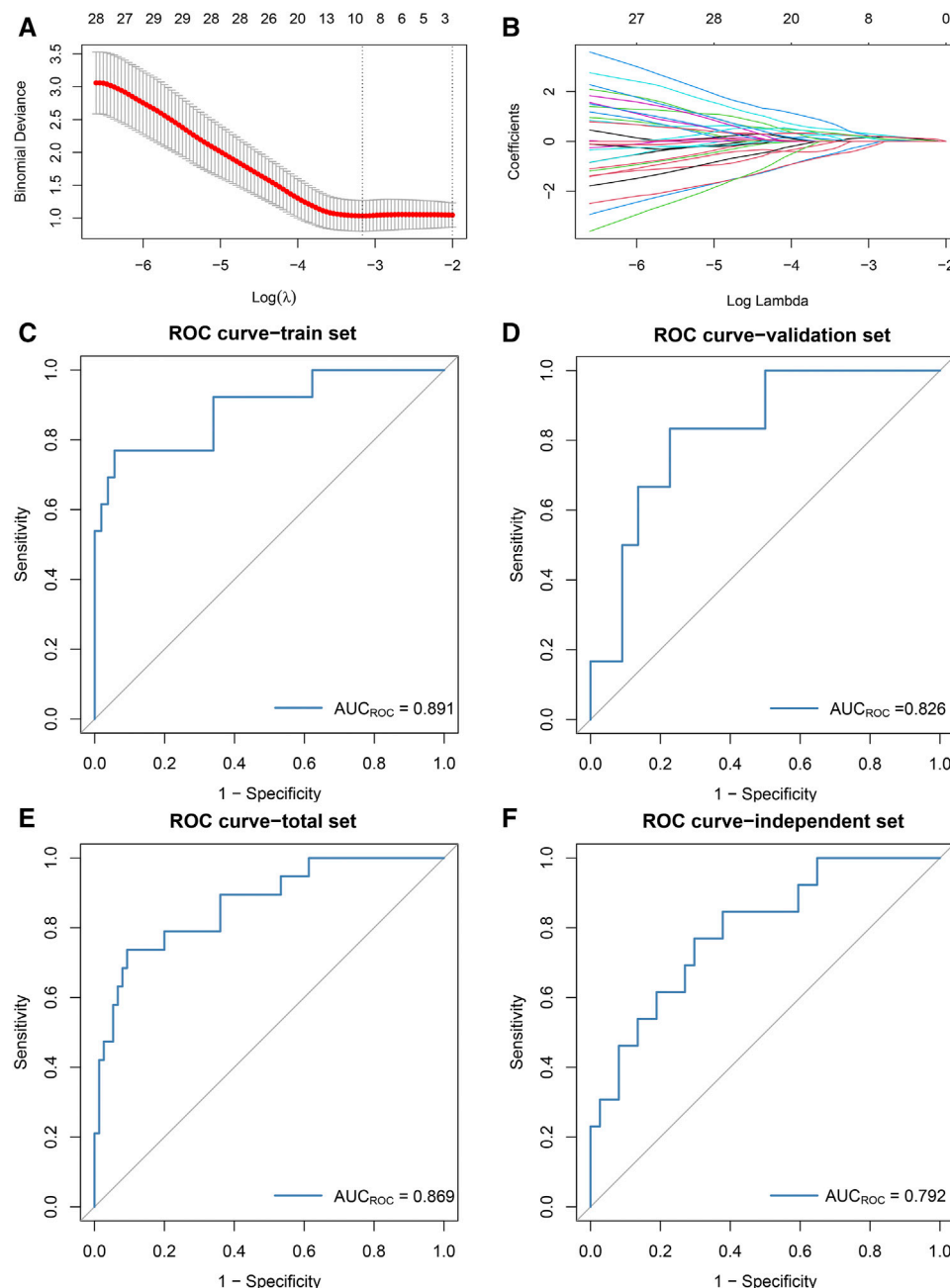


**FIGURE 5 |** The development and validation of the diagnostic model based on the random forest and LASSO regression algorithms. **(A):** The  $\log(\lambda)$  value was optimally selected by 5-fold cross-validation and plotted by the partial likelihood deviance. **(B):** The processes of LASSO regression for screening variables and mapping each variable to a curve. **(C–F):** ROC curves were used to predict ischemic events after CEA in the train **(C):** AUC = 0.891], validation **(D):** AUC = 0.826], total **(E):** AUC = 0.869] sets and independent cohort **(F):** AUC = 0.792].

abundance differences between the two subtypes (Figures 7B–D), especially B cell subtypes (such as naive B cells, activated B cells, and immature B cells) and T cell subtypes (such as activated memory CD4 T cells, regulatory T cells, activated CD8 T cells, gamma delta T cells, and type 17 T helper cells). Overall, the high-risk group had higher immune assessment scores than the low-risk group.

## 4 DISCUSSION

Ischemic events are treacherous events that occur in cardiovascular and cerebrovascular diseases, which are the leading causes of death and long-term disability worldwide (Collaborators, 2019; Campbell and Khatri, 2020; Iadecola et al., 2020). In recent years, substantial machine learning

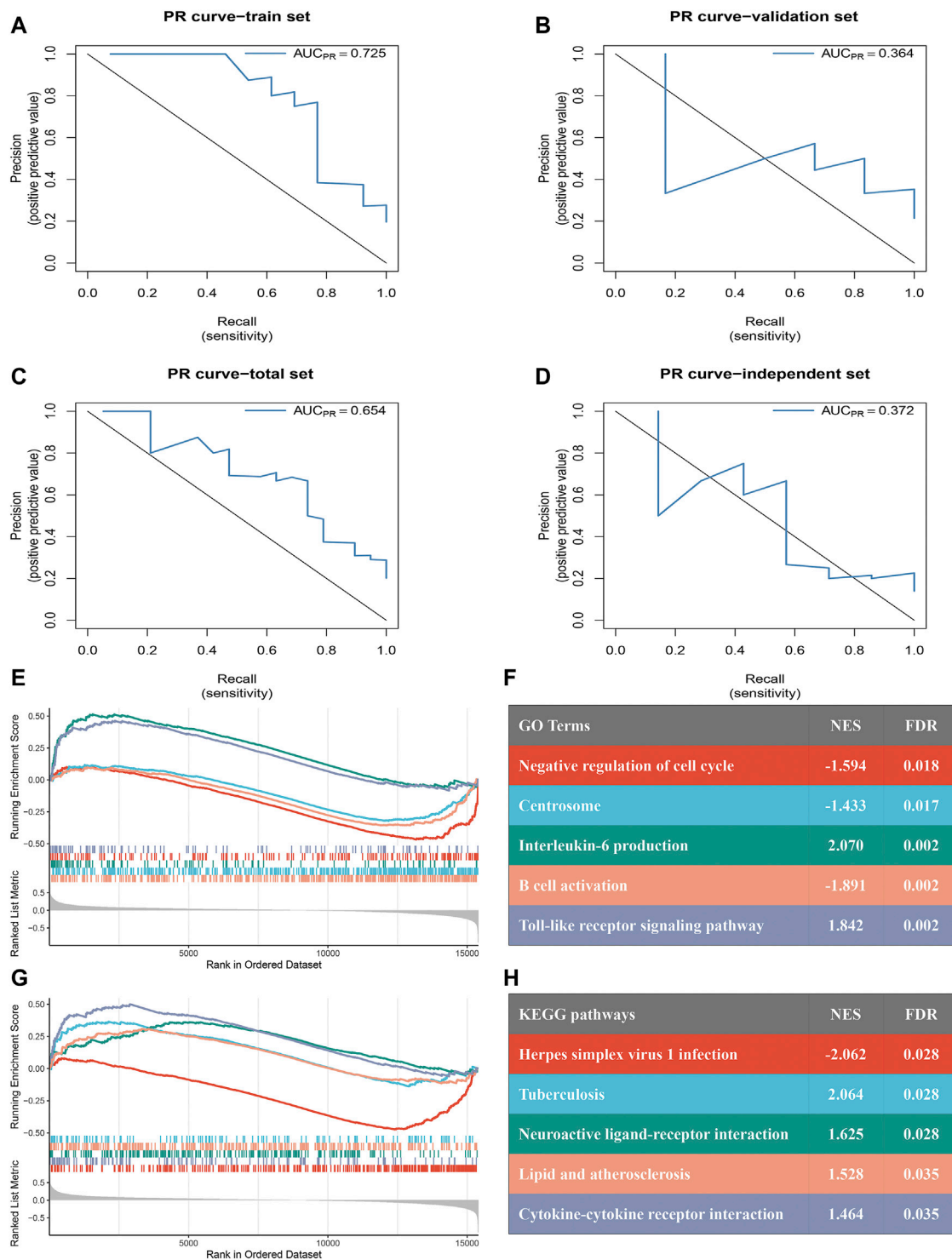
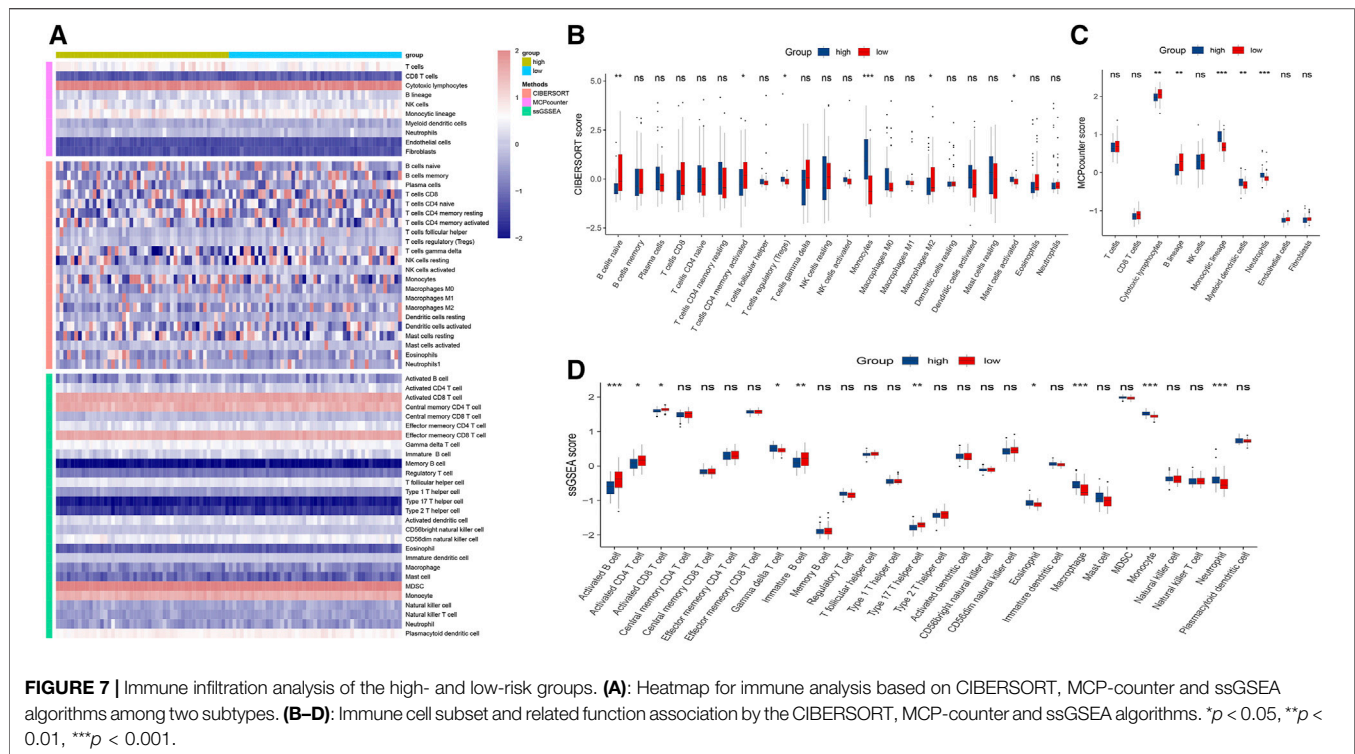


**FIGURE 6 |** PR curves assess the accuracy of the eight-gene model and GSEA of the two subtypes. **(A–D)**: PR curves were used to predict ischemic events after CEA in the train **(A)**: AUC = 0.725, validation **(B)**: AUC = 0.364, total **(C)**: AUC = 0.654 sets and independent cohort **(D)**: AUC = 0.372. **(E–F)**: Top five GO terms of differential genes in the high- and low-risk groups. **(G,H)**: Top five KEGG pathways of differentially expressed genes in the high- and low-risk groups.

models have been applied to improve the clinical outcomes of diseases because they show better potential in diagnosis and prevention and improve the undesirable therapeutic status of

patients (Vallee et al., 2019; Qiao et al., 2020). In addition, CEA is widely applied as a classic surgery to prevent ischemic events (Rerkasem et al., 2020). However, the detailed mechanisms



underlying ischemic events and accurate diagnostic models for predicting ischemic events after CEA remain to be investigated.

In our study, we extracted a yellow module (including 292 genes) significantly related to ischemic events after CEA, according to the WGCNA results. GO and KEGG enrichment analyses were further used to identify the potential functions and mechanisms of these 292 genes. KEGG analysis showed that these genes mainly participated in “Tuberculosis”, “Toll-like receptor signaling pathway”, “Hematopoietic cell lineage”, “C-type lectin receptor signaling pathway” and “Legionellosis”. GO analysis further revealed that neutrophil activation, with terms such as “neutrophil activation involved in immune response”, “neutrophil degranulation”, “specific granule”, “tertiary granule” and “secretory granule membrane”, was the most significantly enriched functional module. A recent study found that patients with tuberculous meningitis (TBM) were more vulnerable to subsequent stroke (up to 57%), especially children or those with advanced stages and severe illness (Shulman and Cervantes-Arslanian, 2019). Zhang et al. reported that the inactivation of the Toll-like receptor signaling pathway protects neurological function in patients with ischemic events (Zhang et al., 2012). Moreover, both immune and inflammatory responses were activated in the acute and chronic phases following ischemic events, which played a double-edged role in pathophysiology (Pothinini et al., 2017; Jayaraj et al., 2019; Ketelhuth, 2019; Iadecola et al., 2020). Therefore, our results suggested that the genes in the yellow module played key roles in the progression of ischemic events.

Afterwards, to establish a diagnostic model for predicting recurrent ischemic events after CEA and further eliminate the effect of multicollinearity, we performed an integrated analysis of the relationships between gene expression and clinical characteristics in the cohort and used random forest and LASSO to screen the genes in the yellow module. Finally, we found that an eight-gene model (including *PLSCR1*, *ECRP*, *CASP5*, *SPTSSA*, *MSRB1*, *BCL6*, *FBP1* and *LST1*) was highly accurate for predicting ischemic events after CEA. Previous studies revealed that *BCL6* is a candidate gene for spontaneous hypertension and stroke (Watanabe et al., 2015), but further investigation into the mechanisms of these genes and ischemic events is necessary. Univariate logistic regression analysis revealed that the eight-gene model was an independent predictor. The higher the score calculated by the formula was, the higher the risk of ischemic events after CEA. More importantly, the ROC-AUCs and PR-AUCs of the train, validation, total, and independent cohort were 0.891 and 0.725, 0.826 and 0.364, 0.869 and 0.654, 0.792 and 0.372, respectively. The time window for the treatment of ischemic events is narrow, and it is difficult for most patients to receive treatment in a timely manner after onset, which leads to serious adverse consequences (Catanese et al., 2017; Gaafar et al., 2017). Therefore, it is particularly important to predict and accurately diagnose ischemic events after CEA.

Subsequently, we further explored the association of these eight genes with ischemic events after CEA. Previous study has shown that *PLSCR1-TRPC5* was a signaling complex mediating phosphatidylserine externalization and apoptosis in neurons and that plays a pathological role in cerebral-ischemia reperfusion

injury (Guo et al., 2020). Zhang et al. (2020) reported that *CASP5* gene overexpression can significantly promote the angiogenesis ability of vascular endothelial cells by promoting the *VEGF* signaling pathway. This affected the formation of atherosclerosis and played a potential role in the development of ischemic events. Furthermore, *MSRB1* controlled immune response *in vivo* and anti-inflammatory cytokine release in macrophages (Guo et al., 2020). As we know, inflammatory factors were abundantly released and immune response was activated in ischemic events after CEA, thus, *MSRB1* may serve a protective role against events. *BCL6* may attenuate oxidative stress-induced neuronal damage by targeting the *miR-31/PKD1* axis and five novel single-nucleotide polymorphisms loci were identified in the *SLT1* locus to be associated with myocardial infarction (Iida et al., 2003; Wei et al., 2021). The above results further demonstrate that the eight-gene module affected ischemic events through multiple pathways, although three genes (*ECRP*, *SPTSSA* and *FBP1*) need to be further validated. Noteworthy, immune response played an important role in these pathways, which warrants further attention.

We further evaluated the immune infiltration among the two risk subtypes, which were divided by the diagnostic model, and more abundant immune infiltration was found in the high-risk group. A previous study demonstrated that a high abundance of immune infiltration is a risk factor for ischemic events (Iadecola et al., 2020). In the acute phase of ischemic events, immune cells attack the ischemic tissue, thereby aggravating the degree of ischemia. Metabolic substances released from ischemic tissue enter the circulatory system and eventually suppress the immune system, which leads to serious complications such as infection (Iadecola et al., 2020). These lines of evidence suggest that our research findings are persuasive. Therefore, the application of anti-immune and anti-inflammatory drugs may be a new strategy for the treatment of ischemic events after CEA.

Our work was a comprehensive study to develop an accurate eight-gene model for predicting ischemic events after CEA. Our research has the following advantages. 1) In this study, biomarkers were used to predict ischemic events after CEA, which was conducive to clinical transformation. 2) This diagnostic model has high accuracy, and the ROC-AUCs for the train, validation and total sets were all above or approach 0.8. 3) We validated the accuracy of the model in an independent cohort by RT-qPCR. 4) We found that the high-risk group of patients had abundant immune infiltration, which provided theoretical support for anti-immune and anti-inflammatory therapy in patients with ischemic events after CEA. However, although the diagnostic model was satisfactory in terms of its performance, several limitations remain in our research. First, some clinical features of samples were obscured in public datasets, which may affect our comprehensive exploration of the relationship between gene expression and clinical features (smoking, obesity, dyslipidemia, etc.). Second, compared the

RNA-seq data, proteomics data can provide more favorable pathophysiological support, but proteomics analysis cannot be performed due to the lack of data. Although further studies are necessary, the proposed model still has great clinical value.

## 5 CONCLUSION

In conclusion, an efficient diagnostic model for predicting the occurrence of ischemic events after CEA was constructed. A population at high risk of recurrent ischemic events after CEA can be identified by this model. More importantly, the establishment of the eight-gene model provides new ideas for precise prevention and anti-immune and anti-inflammatory therapy in patients with ischemic events after CEA.

## DATA AVAILABILITY STATEMENT

The datasets presented in this study can be found in online repositories. The names of the repository/repositories and accession number(s) can be found in the article/Supplementary Material.

## ETHICS STATEMENT

The studies involving human participants were reviewed and approved by The Ethics Committee of The First Affiliated Hospital of Zhengzhou University. The patients/participants provided their written informed consent to participate in this study.

## AUTHOR CONTRIBUTIONS

CG and ZL designed this work. CG, ZL, CC, YZ, TL, and XH integrated and analyzed the data. CG, LW, LL, SL, and ZH wrote this manuscript. CG, ZL, CC, ZH, XH, and ZL edited and revised the manuscript. All authors approved this manuscript.

## FUNDING

This study was supported by the National Natural Science Foundation of China (81873527).

## SUPPLEMENTARY MATERIAL

The Supplementary Material for this article can be found online at: <https://www.frontiersin.org/articles/10.3389/fcell.2022.794608/full#supplementary-material>



## REFERENCES

- Campbell, B. C. V., De Silva, D. A., Macleod, M. R., Coutts, S. B., Schwamm, L. H., Davis, S. M., et al. (2019). Ischaemic Stroke. *Nat. Rev. Dis. Primers* 5, 70. doi:10.1038/s41572-019-0118-8
- Campbell, B. C. V., and Khatri, P. (2020). Stroke. *The Lancet* 396, 129–142. doi:10.1016/S0140-6736(20)31179-X
- Catanese, L., Tarsia, J., and Fisher, M. (2017). Acute Ischemic Stroke Therapy Overview. *Circ. Res.* 120, 541–558. doi:10.1161/CIRCRESAHA.116.309278
- Collaborators, G. B. D. S. (2019). Global, Regional, and National burden of Stroke, 1990–2016: a Systematic Analysis for the Global Burden of Disease Study 2016. *Lancet Neurol.* 18, 439–458. doi:10.1016/S1474-4422(19)30034-1
- Dagvasumberel, M., Shimabukuro, M., Nishiuchi, T., Ueno, J., Takao, S., Fukuda, D., et al. (2012). Gender Disparities in the Association between Epicardial Adipose Tissue Volume and Coronary Atherosclerosis: a 3-dimensional Cardiac Computed Tomography Imaging Study in Japanese Subjects. *Cardiovasc. Diabetol.* 11, 106. doi:10.1186/1475-2840-11-106
- Deo, R. C. (2015). Machine Learning in Medicine. *Circulation* 132, 1920–1930. doi:10.1161/CIRCULATIONAHA.115.001593
- Folkersen, L., Persson, J., Ekstrand, J., Agardh, H. E., Hansson, G. K., Gabrielsen, A., et al. (2012). Prediction of Ischemic Events on the Basis of Transcriptomic and Genomic Profiling in Patients Undergoing Carotid Endarterectomy. *Mol. Med.* 18, 669–675. doi:10.2119/molmed.2011.00479
- Franceschini, N., Giambartolomei, C., de Vries, P. S., Finan, C., Bis, J. C., Huntley, R. P., et al. (2018). GWAS and Colocalization Analyses Implicate Carotid Intima-media Thickness and Carotid Plaque Loci in Cardiovascular Outcomes. *Nat. Commun.* 9, 5141. doi:10.1038/s41467-018-07340-5
- Friedman, J., Hastie, T., and Tibshirani, R. (2010). Regularization Paths for Generalized Linear Models via Coordinate Descent. *J. Stat. Softw.* 33, 1–22. doi:10.18637/jss.v033.i01
- Gaafar, T., Attia, W., Mahmoud, S., Sabry, D., Aziz, O. A., Rasheed, D., et al. (2017). Cardioprotective Effects of Wharton Jelly Derived Mesenchymal Stem Cell Transplantation in a Rodent Model of Myocardial Injury. *Ijsc* 10, 48–59. doi:10.15283/ijsc16063
- Guo, C., Liu, Z., Yu, Y., Zhou, Z., Ma, K., Zhang, L., et al. (2022). EGR1 and KLF4 as Diagnostic Markers for Abdominal Aortic Aneurysm and Associated with Immune Infiltration. *Front. Cardiovasc. Med.* 9, 781207. doi:10.3389/fcvm.2022.781207
- Guo, J., Li, J., Xia, L., Wang, Y., Zhu, J., Du, J., et al. (2020). Transient Receptor Potential Canonical 5-Scramblase Signaling Complex Mediates Neuronal Phosphatidylserine Externalization and Apoptosis. *Cells* 9, 547. doi:10.3390/cells9030547
- Heo, J., Yoon, J. G., Park, H., Kim, Y. D., Nam, H. S., and Heo, J. H. (2019). Machine Learning-Based Model for Prediction of Outcomes in Acute Stroke. *Stroke* 50, 1263–1265. doi:10.1161/STROKEAHA.118.024293
- Howell, S. J. (2007). Carotid Endarterectomy. *Br. J. Anaesth.* 99, 119–131. doi:10.1093/bja/aem137
- Iadecola, C., Buckwalter, M. S., and Anrather, J. (2020). Immune Responses to Stroke: Mechanisms, Modulation, and Therapeutic Potential. *J. Clin. Invest.* 130, 2777–2788. doi:10.1172/JCI135530
- Iida, A., Ozaki, K., Ohnishi, Y., Tanaka, T., and Nakamura, Y. (2003). Identification of 46 Novel SNPs in the 130-kb Region Containing a Myocardial Infarction Susceptibility Gene on Chromosomal Band 6p21. *J. Hum. Genet.* 48, 476–479. doi:10.1007/s10038-003-0054-y
- Jayaraj, R. L., Azimullah, S., Beiram, R., Jalal, F. Y., and Rosenberg, G. A. (2019). Neuroinflammation: Friend and Foe for Ischemic Stroke. *J. Neuroinflammation* 16, 142. doi:10.1186/s12974-019-1516-2
- Ketelhuth, D. F. J. (2019). The Immunometabolic Role of Indoleamine 2,3-dioxygenase in Atherosclerotic Cardiovascular Disease: Immune Homeostatic Mechanisms in the Artery wall. *Cardiovasc. Res.* 115, 1408–1415. doi:10.1093/cvr/cvz067
- Langfelder, P., and Horvath, S. (2008). WGCNA: an R Package for Weighted Correlation Network Analysis. *BMC Bioinformatics* 9, 559. doi:10.1186/1471-2105-9-559
- Libby, P., Buring, J. E., Badimon, L., Hansson, G. K., Deanfield, J., Bittencourt, M. S., et al. (2019). Atherosclerosis. *Nat. Rev. Dis. Primers* 5, 56. doi:10.1038/s41572-019-0106-z
- Liu, Z., Guo, C., Dang, Q., Wang, L., Liu, L., Weng, S., et al. (2022b). Integrative Analysis from Multi-center Studies Identifies a Consensus Machine Learning-Derived lncRNA Signature for Stage II/III Colorectal Cancer. *EBioMedicine* 75, 103750. doi:10.1016/j.ebiom.2021.103750
- Liu, Z., Guo, C., Li, J., Xu, H., Lu, T., Wang, L., et al. (2021a). Somatic Mutations in Homologous Recombination Pathway Predict Favourable Prognosis after Immunotherapy across Multiple Cancer Types. *Clin. Translational Med.* 11, e619. doi:10.1002/ctm.2.619
- Liu, Z., Liu, L., Guo, C., Yu, S., Meng, L., Zhou, X., et al. (2021b). Tumor Suppressor Gene Mutations Correlate with Prognosis and Immunotherapy Benefit in Hepatocellular Carcinoma. *Int. Immunopharmacology* 101, 108340. doi:10.1016/j.intimp.2021.108340
- Liu, Z., Liu, L., Weng, S., Guo, C., Dang, Q., Xu, H., et al. (2022c). Machine Learning-Based Integration Develops an Immune-Derived lncRNA Signature for Improving Outcomes in Colorectal Cancer. *Nat. Commun.* 13, 816. doi:10.1038/s41467-022-28421-6
- Liu, Z., Xu, H., Weng, S., Ren, Y., and Han, X. (2022a). Stemness Refines the Classification of Colorectal Cancer with Stratified Prognosis, Multi-Omics Landscape, Potential Mechanisms, and Treatment Options. *Front. Immunol.* 13, 828330. doi:10.3389/fimmu.2022.828330
- Lockhart, R., Taylor, J., Tibshirani, R. J., and Tibshirani, R. (2014). A Significance Test for the Lasso. *Ann. Statist.* 42, 413–468. doi:10.1214/13-AOS1175
- Mantero, A., and Ishwaran, H. (2021). Unsupervised Random Forests. *Stat. Anal. Data Min: ASA Data Sci. J.* 14, 144–167. doi:10.1002/sam.11498
- Martinez, E., Martorell, J., and Rimbau, V. (2020). Review of Serum Biomarkers in Carotid Atherosclerosis. *J. Vasc. Surg.* 71, 329–341. doi:10.1016/j.jvs.2019.04.488
- Murray, C. J., and Lopez, A. D. (1997). Alternative Projections of Mortality and Disability by Cause 1990–2020: Global Burden of Disease Study. *The Lancet* 349, 1498–1504. doi:10.1016/S0140-6736(96)07492-2
- Newman, A. M., Liu, C. L., Green, M. R., Gentles, A. J., Feng, W., Xu, Y., et al. (2015). Robust Enumeration of Cell Subsets from Tissue Expression Profiles. *Nat. Methods* 12, 453–457. doi:10.1038/nmeth.3337
- Peñalvo, J. L., Fernández-Friera, L., López-Melgar, B., Uzhova, I., Oliva, B., Fernández-Alvira, J. M., et al. (2016). Association between a Social-Business Eating Pattern and Early Asymptomatic Atherosclerosis. *J. Am. Coll. Cardiol.* 68, 805–814. doi:10.1016/j.jacc.2016.05.080
- Pothineni, N. V. K., Subramany, S., Kuriakose, K., Shirazi, L. F., Romeo, F., Shah, P. K., et al. (2017). Infections, Atherosclerosis, and Coronary Heart Disease. *Eur. Heart J.* 38, 3195–3201. doi:10.1093/eurheartj/ehx362
- Qiao, J., Sui, R., Zhang, L., and Wang, J. (2020). Construction of a Risk Model Associated with Prognosis of Post-Stroke Depression Based on Magnetic Resonance Spectroscopy. *Ndt* 16, 1171–1180. doi:10.2147/NDT.S245129
- Rajkomar, A., Dean, J., and Kohane, I. (2019). Machine Learning in Medicine. *N. Engl. J. Med.* 380, 1347–1358. doi:10.1056/NEJMra1814259
- Rerkasem, A., Orrapin, S., Howard, D. P., and Rerkasem, K. (2020). Carotid Endarterectomy for Symptomatic Carotid Stenosis. *Cochrane Database Syst. Rev.* 9, CD001081. doi:10.1002/14651858.CD001081.pub4
- Shannon, P., Markiel, A., Ozier, O., Baliga, N. S., Wang, J. T., Ramage, D., et al. (2003). Cytoscape: a Software Environment for Integrated Models of Biomolecular Interaction Networks. *Genome Res.* 13, 2498–2504. doi:10.1101/gr.1239303
- Shi, J., Jiang, D., Yang, S., Zhang, X., Wang, J., Liu, Y., et al. (2020). LPAR1, Correlated with Immune Infiltrates, Is a Potential Prognostic Biomarker in Prostate Cancer. *Front. Oncol.* 10, 846. doi:10.3389/fonc.2020.00846
- Shulman, J. G., and Cervantes-Arslanian, A. M. (2019). Infectious Etiologies of Stroke. *Semin. Neurol.* 39, 482–494. doi:10.1055/s-0039-1687915
- Svetnik, V., Liaw, A., Tong, C., Culberson, J. C., Sheridan, R. P., and Feuston, B. P. (2003). Random forest: a Classification and Regression Tool for Compound Classification and QSAR Modeling. *J. Chem. Inf. Comput. Sci.* 43, 1947–1958. doi:10.1021/ci034160g
- Szklarczyk, D., Gable, A. L., Lyon, D., Junge, A., Wyder, S., Huerta-Cepas, J., et al. (2019). STRING V11: Protein-Protein Association Networks with Increased Coverage, Supporting Functional Discovery in Genome-wide Experimental Datasets. *Nucleic Acids Res.* 47, D607–D613. doi:10.1093/nar/gky1131
- Szklarczyk, D., Morris, J. H., Cook, H., Kuhn, M., Wyder, S., Simonovic, M., et al. (2017). The STRING Database in 2017: Quality-Controlled Protein-Protein

- Association Networks, Made Broadly Accessible. *Nucleic Acids Res.* 45, D362–D368. doi:10.1093/nar/gkw937
- Tibshirani, R. (1997). The Lasso Method for Variable Selection in the Cox Model. *Statist. Med.* 16, 385–395. doi:10.1002/(sici)1097-0258(19970228)16:4<385::aid-sim380>3.0.co;2-3
- Vallée, A., Cinaud, A., Blachier, V., Lelong, H., Safar, M. E., and Blacher, J. (2019). Coronary Heart Disease Diagnosis by Artificial Neural Networks Including Aortic Pulse Wave Velocity index and Clinical Parameters. *J. Hypertens.* 37, 1682–1688. doi:10.1097/HJH.0000000000002075
- Varasteh, Z., De Rose, F., Mohanta, S., Li, Y., Zhang, X., Miritsch, B., et al. (2021). Imaging Atherosclerotic Plaques by Targeting Galectin-3 and Activated Macrophages Using (89Zr)-DFO- Galectin3-F(ab')<sub>2</sub> mAb. *Theranostics* 11, 1864–1876. doi:10.7150/thno.50247
- Watanabe, Y., Yoshida, M., Yamanishi, K., Yamamoto, H., Okuzaki, D., Nojima, H., et al. (2015). Genetic Analysis of Genes Causing Hypertension and Stroke in Spontaneously Hypertensive Rats: Gene Expression Profiles in the Kidneys. *Int. J. Mol. Med.* 36, 712–724. doi:10.3892/ijmm.2015.2281
- Wei, P., Chen, H., Lin, B., Du, T., Liu, G., He, J., et al. (2021). Inhibition of the BCL6/miR-31/PKD1 axis Attenuates Oxidative Stress-Induced Neuronal Damage. *Exp. Neurol.* 335, 113528. doi:10.1016/j.expneurol.2020.113528
- Yi, M., Nissley, D. V., McCormick, F., and Stephens, R. M. (2020). ssGSEA Score-Based Ras Dependency Indexes Derived from Gene Expression Data Reveal Potential Ras Addiction Mechanisms with Possible Clinical Implications. *Sci. Rep.* 10, 10258. doi:10.1038/s41598-020-66986-8
- Yu, G., Wang, L.-G., Han, Y., and He, Q.-Y. (2012). clusterProfiler: an R Package for Comparing Biological Themes Among Gene Clusters. *OMICS: A J. Integr. Biol.* 16, 284–287. doi:10.1089/omi.2011.0118
- Zenonos, G., Lin, N., Kim, A., Kim, J. E., Governale, L., and Friedlander, R. M. (2012). Carotid Endarterectomy with Primary Closure: Analysis of Outcomes and Review of the Literature. *Neurosurgery* 70, 646–655. doi:10.1227/NEU.0b013e3182351de0
- Zhang, B., Gu, J., Qian, M., Niu, L., Zhou, H., and Ghista, D. (2017). Correlation between Quantitative Analysis of wall Shear Stress and Intima-media Thickness in Atherosclerosis Development in Carotid Arteries. *Biomed. Eng. Online* 16, 137. doi:10.1186/s12938-017-0425-9
- Zhang, L., Chopp, M., Liu, X., Teng, H., Tang, T., Kassis, H., et al. (2012). Combination Therapy with VELCADE and Tissue Plasminogen Activator Is Neuroprotective in Aged Rats after Stroke and Targets microRNA-146a and the Toll-like Receptor Signaling Pathway. *Arterioscler Thromb. Vasc. Biol.* 32, 1856–1864. doi:10.1161/ATVBAHA.112.252619
- Zhang, Y., Yuan, Z., Shen, R., Jiang, Y., Xu, W., Gu, M., et al. (2020). Identification of Biomarkers Predicting the Chemotherapeutic Outcomes of Capecitabine and Oxaliplatin in Patients with Gastric Cancer. *Oncol. Lett.* 20, 1. doi:10.3892/ol.2020.12153

**Conflict of Interest:** The authors declare that the research was conducted in the absence of any commercial or financial relationships that could be construed as a potential conflict of interest.

**Publisher's Note:** All claims expressed in this article are solely those of the authors and do not necessarily represent those of their affiliated organizations, or those of the publisher, the editors and the reviewers. Any product that may be evaluated in this article, or claim that may be made by its manufacturer, is not guaranteed or endorsed by the publisher.

Copyright © 2022 Guo, Liu, Cao, Zheng, Lu, Yu, Wang, Liu, Liu, Hua, Han and Li. This is an open-access article distributed under the terms of the Creative Commons Attribution License (CC BY). The use, distribution or reproduction in other forums is permitted, provided the original author(s) and the copyright owner(s) are credited and that the original publication in this journal is cited, in accordance with accepted academic practice. No use, distribution or reproduction is permitted which does not comply with these terms.



# Honokiol Inhibits Atrial Metabolic Remodeling in Atrial Fibrillation Through Sirt3 Pathway

Guang Zhong Liu<sup>1,2</sup>, Wei Xu<sup>3</sup>, Yan Xiang Zang<sup>3</sup>, Qi Lou<sup>3</sup>, Peng Zhou Hang<sup>4</sup>, Qiang Gao<sup>3</sup>, Hang Shi<sup>3</sup>, Qi Yun Liu<sup>1,2</sup>, Hong Wang<sup>3</sup>, Xin Sun<sup>1,2</sup>, Cheng Liu<sup>1,2</sup>, Peng Zhang<sup>1,2</sup>, Hua Dong Liu<sup>1,2\*</sup> and Shao Hong Dong<sup>1,2\*</sup>

<sup>1</sup>Department of Cardiology, Shenzhen Cardiovascular Minimally Invasive Medical Engineering Technology Research and Development Center, Shenzhen People's Hospital, Shenzhen, China, <sup>2</sup>Shenzhen People's Hospital, The Second Clinical Medical College, Jinan University; The First Affiliated Hospital, Southern University of Science and Technology, Shenzhen, China, <sup>3</sup>Department of Cardiology, the First Affiliated Hospital, Harbin Medical University, Harbin, China, <sup>4</sup>Department of Pharmacy, Clinical Medical College, Yangzhou University, Northern Jiangsu People's Hospital, Yangzhou, China

## OPEN ACCESS

### Edited by:

Xianwei Wang,  
Xinxiang Medical University, China

### Reviewed by:

Zhan Chengchuang,  
The First Affiliated Hospital of  
Soochow University, China  
Yu-Chan Chang,  
National Yang-Ming University, Taiwan

### \*Correspondence:

Shao Hong Dong  
dshsxnk@163.com  
Hua Dong Liu  
lhd2578@163.com

### Specialty section:

This article was submitted to  
"Cardiovascular and Smooth Muscle  
Pharmacology",  
a section of the journal  
Frontiers in Pharmacology

Received: 11 November 2021

Accepted: 12 January 2022

Published: 17 March 2022

### Citation:

Liu GZ, Xu W, Zang YX, Lou Q,  
Hang PZ, Gao Q, Shi H, Liu QY,  
Wang H, Sun X, Liu C, Zhang P, Liu HD  
and Dong SH (2022) Honokiol Inhibits  
Atrial Metabolic Remodeling in Atrial  
Fibrillation Through Sirt3 Pathway.  
Front. Pharmacol. 13:813272.  
doi: 10.3389/fphar.2022.813272

**Background and Purpose:** Atrial metabolic remodeling plays a critical role in the pathogenesis of atrial fibrillation (AF). Sirtuin3 (Sirt3) plays an important role in energy homeostasis. However, the effect of Sirt3 agonist Honokiol (HL) on AF is unclear. Therefore, the aim of this study is to determine the effect of HL on atrial metabolic remodeling in AF and to explore possible mechanisms.

**Experimental Approach:** Sirt3 and glycogen deposition in left atria of AF patients were examined. Twenty-one rabbits were divided into sham, P (pacing for 3 weeks), P + H treatment (honokiol injected with pacing for 3 weeks). The HL-1 cells were subjected to rapid pacing at 5 Hz for 24 h, in the presence or absence of HL and overexpression or siRNA of Sirt3 by transfection. Metabolic factors, circulating metabolites, atrial electrophysiology, ATP level, and glycogens deposition were detected. Acetylated protein and activity of its enzymes were detected.

**Key Results:** Sirt3 was significantly down-regulated in AF patients and rabbit/HL-1 cell model, resulting in the abnormal expression of its downstream metabolic key factors, which were significantly restored by HL. Meanwhile, AF induced an increase of the acetylation level in long-chain acyl-CoA dehydrogenase (LCAD), AceCS2 and GDH, following decreasing of activity of its enzymes, resulting in abnormal alterations of metabolites and reducing of ATP, which was inhibited by HL. The Sirt3 could regulate acetylated modification of key metabolic enzymes, and the increase of Sirt3 rescued AF induced atrial metabolic remodeling.

**Conclusion and Implications:** HL inhibited atrial metabolic remodeling in AF via the Sirt3 pathway. The present study may provide a novel therapeutic strategy for AF.

**Keywords:** Honokiol, atrial fibrillation, metabolism remodeling, sirt3, acetylation

## INTRODUCTION

Atrial fibrillation (AF) is the most common sustained arrhythmia in clinical practice and may eventually be associated with morbidity and mortality. Recently, metabolomic and proteomic studies in humans and experimental AF have reported changes in the expression of molecules involved in metabolic pathways, indicating a role for metabolic alterations in the pathogenesis of AF (Mayr et al., 2008; Tu et al., 2014b). However, it is not clear that the precise mechanism underlying the impact of atrial metabolic remodeling on AF persistence.

Sirtuins are a family of nicotinamide adenine dinucleotide-(NAD<sup>+</sup>) dependent histone deacetylases and thus their function is intrinsically linked to cellular metabolism (Chang and Guarente, 2014; van de Ven et al., 2017). Sirt3 is a deacetylase that regulates the activity of the key enzymes *via* deacetylation, resulting in regulating mitochondrial energy metabolism (Lombard et al., 2007; Rardin et al., 2013). Sirt3-mediated deacetylation modifies and activates long-chain acyl-CoA dehydrogenase (LCAD) (Hirschey et al., 2010), and regulates other enzymes of fatty acid oxidation, such as medium chain-specific acyl-CoA dehydrogenase (ACADM) (Yang et al., 2016). In addition, Sirt3 deacetylates essential enzymes of acetyl-CoA synthetase 2 (AceCS2) (Schwer et al., 2006) and isocitrate dehydrogenase 2 (IDH2) (Yu et al., 2012) are involved in the tricarboxylic acid (TCA) cycle, and the glutamate dehydrogenase (GDH) in the urea cycle of metabolism (Kim et al., 2012). Our previous studies found that AF induced an expressed imbalance of the metabolic factor involved in fatty acid and glucose oxidation, which is involved in the down-regulation of PPAR- $\alpha$ /sirtuin1/PPAR co-activator  $\alpha$  (PGC-1 $\alpha$ ) pathway (Liu et al., 2016). However, the identity and role of Sirt3 under AF remains unknown.

Honokiol (HL) is a small molecular weight natural compound derived from *Magnolia grandiflora*, which is used as a traditional Chinese herb. A report has shown that HL could ameliorate cardiac hypertrophy by binding to Sirt3, activating it and increasing Sirt3 levels and its enzymatic activity (Pillai et al., 2015). Furthermore, activation of Sirt3 by Honokiol increased ATP production as well as reduced ROS and lipid peroxidation by improving fatty acid oxidation resulting in the inhibition of acute kidney injury induced by cisplatin (Li et al., 2020). However, the effects of HL on the atrial metabolic remodeling associated with AF are not completely understood.

Therefore, our study was designed to investigate whether HL prevented atrial metabolic remodeling in AF through regulating acetylated modification of key metabolic enzyme by the Sirt3 pathway.

## MATERIALS AND METHODS

### Ethics Statement

The use of animals and all procedures were in accordance with the Guide for the Care and Use of Laboratory Animals (NIH Publication 2011; eighth edition) and were approved by the Animal Care and Use Committee of the Harbin Medical

University. All animals received a standard laboratory diet and filtered water *ad libitum*. They were housed in individual cages in a temperature-controlled room at 23–25°C under a 12 h light-dark cycle. All animal procedures were conducted in accordance with the ARRIVE guidelines (Kilkenny et al., 2010; McGrath et al., 2010).

### Clinic Patient Selection

The study abided by the principles that govern the use of human tissues outlined in the Declaration of Helsinki. All patients recruited into the study provided informed consent for their samples to be used. Left atrial appendages were obtained as surgical specimens from patients undergoing cardiac surgery for mitral valve replacement following established procedures approved by the local Ethics Committee (application approval numbers: 201551). Samples were collected from patients with sinus rhythm (SR,  $n = 7$ , without history of AF) and permanent AF ( $n = 7$ , documented arrhythmia for >6 months before surgery). Patients were excluded from the study if they had other cardiac diseases, such as severe congestive heart failure, or serious systemic diseases such as thyroid disease, impaired glucose tolerance or diabetes mellitus. The specimens were immediately fixed in 4% paraformaldehyde for 48 h at 4°C and stored at –80°C. The clinical subject characteristics were shown in Table 1.

### Rabbit AF Model

The twenty-one New Zealand white rabbits (male, 2.5–3.0 kg) were provided by the Experimental Animal Center of the First Affiliated Hospital of Harbin Medical University and were randomly chosen in accordance with its weight divided into three groups: sham surgery group (sham,  $n = 7$ ) with sutured electrodes and no pacing; Pacing group (P,  $n = 7$ ) with an AF model induced by rapid right atrial pacing for 3 week at 600 beats/min; Honokiol treatment group (P + H group,  $n = 7$ ) with Honokiol intraperitoneally injected (MedChemExpress, Cat.No HY-N0003) at a dose of 5 mg kg<sup>–1</sup> day<sup>–1</sup> for 21 days (Chiang et al., 2009; Sulakhiya et al., 2014) and pacing the right atria for 3 weeks. The AF model was established according to our previous studies (Li et al., 2007; Liu et al., 2013). All rabbits were allowed to recover for 1 week after the surgery. The rabbits were anaesthetized with ketamine (30–35 mg/kg) and xylazine (sigma; 5 mg/kg *i. m.*). All blood samples were collected after an overnight fast and serum was separated and stored at –80°C prior to analysis.

### Cell Culture and Transfection

The HL-1 cells were cultured in flasks in Claycomb medium (Sigma-Aldrich, United States) supplemented with 10% foetal calf serum, 1% penicillin/streptomycin, and Norepinephrine (0.1 mM, SigmaAldrich, United States), and L-glutamine (2mM, Sigma-Aldrich, United States) at 37°C in 5% CO<sub>2</sub>. HL-1 cells were cultured in well plates and subjected to tachypacing by the stimulator (YC-2 stimulator) as described according to previous studies (Yang et al., 2005; Brundel et al., 2006). Cells ( $\geq 1 \times 10^6$  myocytes) were stimulated at the parameter (5 Hz with square pulses of 5 ms duration, pulse voltage of 1.5 V/cm). HL-1



**TABLE 1 |** The clinical subject characteristics (mean  $\pm$  SEM).

	SR n = 7	PAF n = 7	p Value
Age(years)	49.29 $\pm$ 4.05	57.86 $\pm$ 2.82	0.108
BW(kg)	70.29 $\pm$ 6.90	66.29 $\pm$ 5.49	0.653
BMI(kg/m <sup>2</sup> )	24.51 $\pm$ 1.68	23.78 $\pm$ 1.55	0.753
EF (%)	61.00 $\pm$ 2.36 (n = 5)	63.80 $\pm$ 4.14 (n = 5)	0.573
Medication spiro lactone	7/7	7/7	
furosemide	7/7	7/7	
AngiotensinIIreceptor blocker (ARB)	1/6	0/6	
NYHA class (II/III)	5/2	4/3	

The data were expressed as mean  $\pm$  SEM. SR, sinus rhythm; PAF, permanent atrial fibrillation; BW, body weight; BMI, body mass index; EF, ejection fraction; NYHA, new york heart association classification.

cells were transfected with 100  $\mu$ M Sirt3 siRNA after 24 h plating by using Lipofectamine 2000 (Invitrogen) in OptiMem (Gibco) media. Cells were returned to growth media for 6 h after transfection. To specifically overexpress Sirt3, plasmid (OriGene Technologies, Inc.) was constructed. HL-1 cells were transfected with 2  $\mu$ g plasmid after 24 h plating.

## Electrophysiological Stud

The atrial electrophysiology detection was performed as described in previous study (Zhao et al., 2010). 8 basic stimuli (S1) were followed by a premature extra stimulus (S2), and the S1S1 cycle were both 150 and 200 ms basic cycle lengths (BCLs). The interval of S1-S2 was decreased by 10 ms and then decreased in 2 ms steps until S2 failed to capture the depolarization which was defined as the AERP value. The AERP value was tested 2 times at both BCLs: 200 ms (AERP<sub>200</sub>) and 150 ms (AERP<sub>150</sub>) to obtain the mean value of the 2 AERPs. AF vulnerability was determined as the percentage of AF and the atrial arrhythmia recorded with an intracardiac electrode sustained for  $\geq 1$  s induced by a train of 10 Hz, 2 ms stimuli to the right atrium at each interval of 2 min.

## Real-Time RT-PCR

Total RNA was extracted with reagent (Axygen, United States). The quantitative real-time reverse transcriptase-polymerase chain reaction (RT-PCR) was used according to a previously described procedure (Zhao et al., 2017). The real-time PCR was performed on the Applied Bio-system (Foster City, CA, United States). The primers of related genes used in the study are listed in Table 2.

## Western Blotting

The western blotting procedures were performed as described in a previous study (Anfuso et al., 2017). The 30–50  $\mu$ g proteins were transferred to a polyvinylidene fluoride membrane. Membranes were blocked by 5% non-fat milk for 1 h. Then, the membranes were incubated overnight at 4°C with primary antibodies against Sirt3 (1:500, Abcam, 28kD), AceCS2 (1:500, Abclonal, 75kD), LCAD (1:500, Abclonal, 47kD), GDH (1:500, Abcam, 89kD), and  $\beta$ -actin (1:500, sigma, 42kD). Chemiluminescent signal was developed by using ECL kit. The western-blotting was quantified by scanning densitometry (Chemi-DOC, Bio-Rad, United States).

## Analysis of Plasma Metabolite by High-Resolution Mass Spectrometry

The plasma samples were homogenized in ultrapure water containing 50% methanol at a ratio of 1:5 (w/v), and 20  $\mu$ l of the homogenate was added to 180  $\mu$ l of precipitator containing an internal standard (methanol: acetonitrile = 1:1), mixed by vortexing for 60 s, and centrifuged at 10,000 g for 10 min. Then 5  $\mu$ l of the sample was used for analysis using a QE-Orbitrap high-resolution mass spectrometer. This detailed procedure was the same as in the literature (Ji et al., 2020).

## Immunoprecipitation Assay

A total of 200  $\mu$ g of lysates was incubated with 2  $\mu$ g/ml anti-acetyl-lysine antibodies (1:1,000, Abcam) overnight at 4°C, and then 1/4 of volume protein A/G-agarose beads was added to each sample and incubated on a rotator for 2 h at 4°C as previously described (Fukushima et al., 2016). After 2 h, samples were washed and centrifuged at 15,000 g for 5 min. The prepared samples were detected by western-blotting. The extent of acetylation protein was then subjected to immunoblot analysis as the ratio of acetylated protein/total protein band intensities.

## ATP and Activity of ATP Enzyme Measurement

ATP level and activity of ATP enzyme measurement kits were obtained from Jiancheng Biological Technical Institute (China). In brief, this testing procedure follows as the kits instruct.

## Assay Activity of Metabolic Enzyme

In brief, protein was extracted from atrial tissue or cells lysate with adding protease inhibitors, it was centrifugated at 13,000 rpm/20 min; and then supernatant was taken after centrifugation. IP antibodies were added into supernatant 500ul: LCAD, GDH and AceCS2 antibodies were 1.5 ul, respectively, and incubated overnight in a shaker at 4°C. Reactive protein A-Agarose was taken and washed 3 times with PBS. After washing, about 50% suspension was prepared with PBS. 50 ul of 50% protein A-Agarose suspension was added to the prepared sample and incubated for 2 h on A shaker at 4°C. The supernatant was centrifuged at 4°C for 1,500 g for 3 min after incubation. The protein A-Agarose-

**TABLE 2 |** Primers for real-time PCR.

Gene name	Primer sequences	Product size (bp)
Sirt3 forward primer	TGCCAGAGGGTGGTGGTCAT	169
Sirt3 reverse primer	GACCTCCATCAGCCCCAAA	
LCAD forward primer	GGGTGGTTAAGTGATGTTGT	127
LCAD reverse primer	GTAGCTTCTGTCCCTTGATA	
LDHa forward primer	ACGGCAGCAAGAGGGAGAAA	313
LDHa reverse primer	GTACCGGAAGCGGGCTGAAT	
AceCS2 forward primer	GCGTTTGCCCTTCGTGTGAT	101
AceCS2 reverse primer	CGGCGTATTGGCGATTTT	
PGC-1 $\alpha$ forward primer	TGATGACAGCGAAGATGA	133
	AAGTG	
PGC-1 $\alpha$ reverse primer	TTTGGGTGGTGACACGGAAT	114
NDUFA9 forward primer	GCAGACGCCGAGGGAAAAC	
NDUFA9 reverse primer	CAAGGGGTATGGGAGGAAGG	
GLUT1 forward primer	GGCAGATGATGCGGGAGAAG	235
GLUT1 reverse primer	ACGAACAGCGATACGACGGT	
PDK4 forward primer	CTTCAGTTACACATACTC	86
	CACCGC	
PDK4 reverse primer	GTAACCCGTAACCGAAACCAG	150
PDH forward primer	GCCAATCATAAAAGACGCTG	
PDH reverse primer	ATGCCAAACATCCCCAAGT	
GDH forward primer	CTGGATGAAGCGGGAAGGG	288
GDH reverse primer	GGGCGGCACGGAGAAGTAGA	
CROT forward primer	GGCTTCGACCGTCACCTTCT	216
CROT reverse primer	CCTGTGCTCTCGGATGTGGT	
SDHa forward primer	GGGGAGTGTCGTGGTGTATC	109
SDHa reverse primer	TGAAGTAAGTGCGCCCATAGC	
$\beta$ -actin forward primer	AGATCGTGCGGGACATCAAG	182
$\beta$ -actin reverse primer	CAGGAAGGAGGCTGGAAGA	

antibody-protein complex was washed 3 times with pre-cooled PBS. 250  $\mu$ l  $\times$ PBS was added to above complex for resolution testing.

LCAD activity was measured according to the method described (Bharathi et al., 2013). Preparing for reaction compound: 100 mM hydroxylamine, 50 mM TrisHCl, 20 mM potassium acetate, 10 mM  $MgCl_2$ , 10 mM ATP, 2 mM DTT, 1 mM ETF-FITC and 1 mM CoA. 20  $\mu$ l LCAD-IP product and 100  $\mu$ l double-steam water were added to the bottom hole of the sample, and then 20  $\mu$ l LCAD-IP product and 100  $\mu$ l reaction compound was added into the sample reaction hole. The fluorescence value was read for 5 min after reaction under 35°C.

GDH activity was detected as follows: preparing for reaction compound (50 mM HEPES, pH 7.5, 100 mM NaCl, 1 mM NADH, and 200  $\mu$ M iodonitrotetrazolium chloride), which was preheated in water bath at 25°C. 180  $\mu$ l reaction compound was added with 20  $\mu$ l GDH-IP product, and the fluorescence values were determined at 20 s (background value) and 5 min 20 s (sample reaction value). At the same time, the ultra-pure water fluorescence value was taken as the background value.

AceCS2 activity was detected as follows: preparation of reaction compound (100 mM hydroxylamine, 50 mM Tris-HCl, 20 mM potassium acetate, 10 mM  $MgCl_2$ , 10 mM ATP, 2 mM DTT, 1 mM ETF-FITC and 1 mM CoA). 20  $\mu$ l AceCS2-IP product and 100  $\mu$ l double-steam water were added to the bottom hole of the sample, and then 20  $\mu$ l AceCS2-IP product and 100  $\mu$ l reaction compound were added into the sample reaction

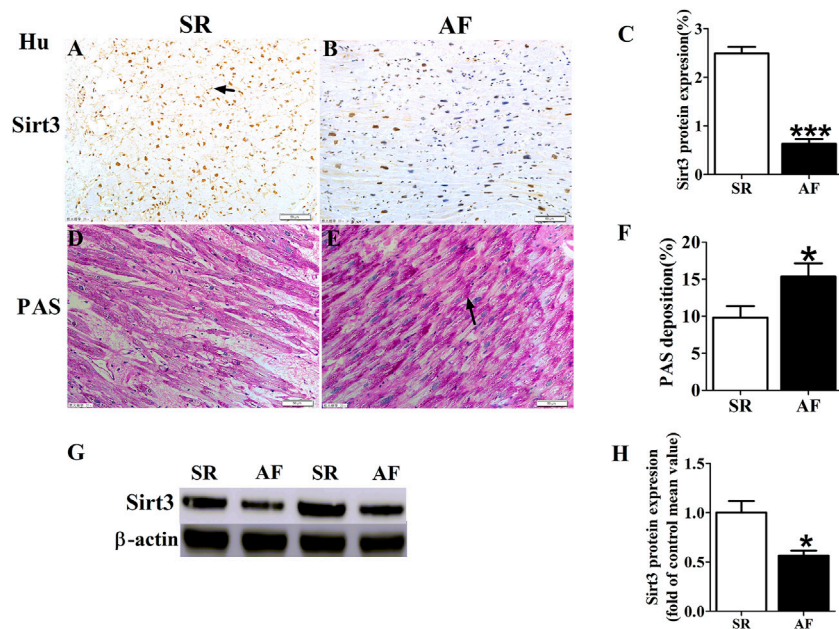


**FIGURE 1 |** Changes of Sirt3 and glycogen in AF patients. (A,B and C) Representative images and statistical results for protein expression of Sirt3 in the atria of patients. (D,E and F) Representative images and statistical results for the accumulation of glycogen in both groups of patients. (G and H) Representative bands and statistical analyzing for protein expression of Sirt3 in patients. The magnification is  $\times 20$ . \* $p < 0.05$  vs. SR group, Data from these proteins were normalized to  $\beta$ -actin,  $n = 6$  each group.

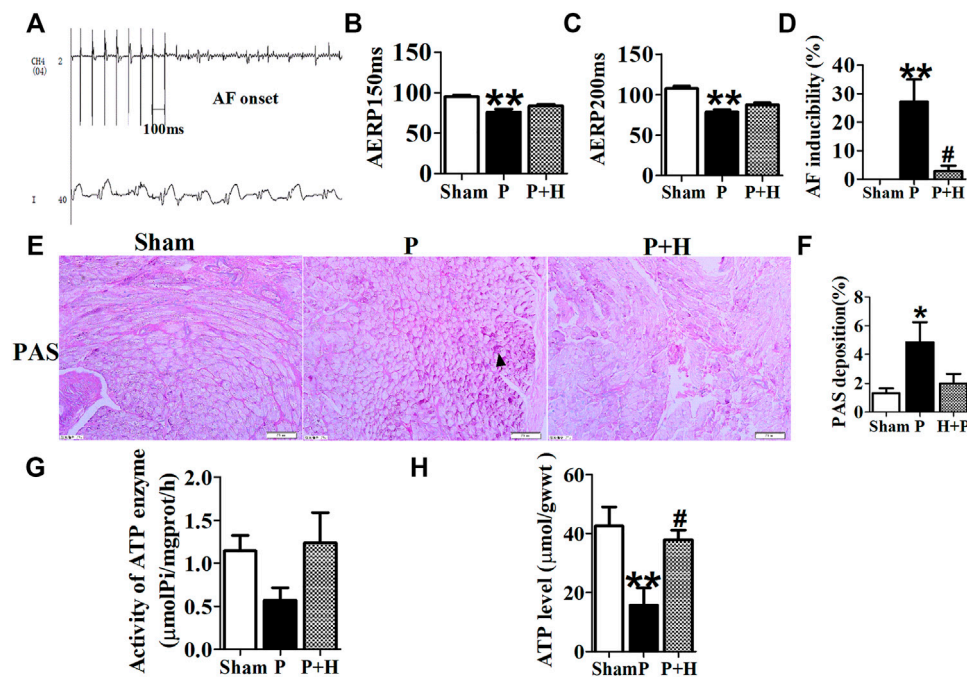


**FIGURE 2 |** Electrophysiology detection and assay of glycogen and ATP. **(A)** AF was induced after rapid-pacing. **(B,C)** AERP150 ms and AERP200 ms, **(D)** AF inducibility.  $n = 6$  each group. **(E and F)** Representative images and statistical results of the glycogen accumulation in the atria of rabbits, the magnification is  $\times 20$ . **(G and H)** Statistical analyzes of activity in ATP enzyme and level of ATP. \* $p < 0.05$  vs. sham group, \*\* $p < 0.01$  vs. sham group, # $p < 0.05$  vs. P group,  $n = 6$  each group.

hole. The fluorescence value was read for 5 min after reaction under  $35^{\circ}\text{C}$ .

### Immunohistochemical Analysis

The immunohistochemical analysis was determined with the procedures as described previously (Ma et al., 2020). Atria (including appendage and free wall) tissues were fixed in 10% formalin, and then processed for paraffin sections and rehydrated first in xylene and ethanol solutions. The sections were incubated with anti-Sirt3 (1:500; Cell Signaling Technology, United States) overnight at  $4^{\circ}\text{C}$ . The tissue sections were then reacted with peroxidase conjugated rabbit anti-goat IgG (1:1,000, Zhongshan, Beijing, China) at  $37^{\circ}\text{C}$ . Periodic acid Schiff (PAS) staining kit (BA-4044A, Baso, Taiwan) was used to analyze the glycogen distribution in myocytes. There was applied to evaluate the expression of target proteins by the digital image analysis system (HPISA-1000, Olympus, Japan). Positive cell area density was defined as positive cell area/total area of statistical fields.

### Statistical Analysis

All data are represented as mean  $\pm$  SEM. Statistical significance between different groups was determined by an unpaired  $t$ -test or a one-way analysis of variance (ANOVA) with the Tukey-test to compare all pairs of columns. When  $p$  values were less than 0.05, the difference was considered statistically significant.

## RESULTS

### Characteristics of Patients

There were no statistically significant differences in age, weight, body mass index, EF% and medication history between SR group and PAF group (see Table 1).

### Changes of Sirt3 and Glycogen in AF Patients

We detected the protein expression of Sirt3 in left atrial appendages from SR and AF patients (Figure 1). The immunohistochemical determination and western-blot found that the expression of Sirt3 protein in the AF patients was significantly down-regulated (Figures 1A–C; Figures G,H). Abnormal glycogen accumulation is a remarkable feature of atrial metabolic disturbance. PAS staining showed that AF induced an accumulation of glycogen in the atria, as shown in Figures 1D–F. A large number of red granules were observed in the atrial tissue.

### Electrophysiology Detection and Assay of Glycogen and ATP

The results of electrophysiology detection as Figure 2 showed that the AERP<sub>150</sub> (Figure 2B) and AERP<sub>200</sub> (Figure 2C) were significantly decreased in the pacing group of rabbits with

**TABLE 3 |** The average changes of metabolites (VIP>1) in plasma contributing to discrimination between P group and H + P or Sham group in PLS-DA models (Mean ± SD).

Metabolites	VIP value	H + P/P	Sham/P
LysoPC(18:1 (11Z))	8.7538	109.87 ± 33.22↑	197.17 ± 67.06↑
SM(d18:0/16:1 (9Z))	4.8505	54.61 ± 12.07	66.04 ± 7.89
(7S,8S)-DihODE	4.5799	1.45 ± 0.95	13.21 ± 29.05
PC(16:1 (9Z)/20:3 (8Z,11Z,14Z))	3.8339	71.35 ± 4.49	70.49 ± 24.6
PC(18:0/20:4 (8Z,11Z,14Z,17Z))	3.5755	79.71 ± 16.44	72.6 ± 13.99
9Z,12Z,15Z)-(7S,8S)-Dihydroxyoctadeca-9,12,15-trienoic acid	3.4277	2.26 ± 1.9	16.36 ± 38.53
SM(d18:1/16:0)	3.2129	54.72 ± 12.42	65.97 ± 8.35
L-Leucine	2.9912	71.56 ± 29.07	42.1 ± 16.1
SM(d18:1/22:0)	2.3943	12,414.9 ± 7,455.65↑	29,165.99 ± 3,567.52↑
L-Acetylcarnitine	2.2603	64.79 ± 51.66	45.15 ± 28.72
LysoPC(16:1 (9Z))	2.1503	120.16 ± 48.19↑	194.67 ± 87.07↑
PC(14:0/22:1 (13Z))	2.1434	158.9 ± 45.95↑	131.21 ± 27.05↑
Phytosphingosine	1.9513	39.7 ± 17.08	73.56 ± 19.06
SM(d18:0/24:1 (15Z))	1.9409	238,784.35 ± 16,798.01↑	224,709.69 ± 51,002.03↑
LysoPC(20:3 (5Z,8Z,11Z))	1.9336	124.21 ± 44.74↑	234.11 ± 81.87↑
Valerylcarnitine	1.8434	21.37 ± 41.91	4.55 ± 3.63
PC(16:1 (9Z)/22:5 (7Z,10Z,13Z,16Z,19Z))	1.8362	96.12 ± 11.15	67.12 ± 22.14
L-Carnitine	1.8091	107.89 ± 66.08↑	154.27 ± 122.87↑
PC(18:1 (9Z)/20:4 (5Z,8Z,11Z,14Z))	1.808	88.54 ± 4.69	80.66 ± 16.74
Linoleic acid	1.6941	79.54 ± 52.93	58.38 ± 66.65
2-Hydroxybutanoic acid	1.6393	78.68 ± 23.79	54.8 ± 22.73
Linoleyl carnitine	1.597	25.31 ± 32.4	13.39 ± 11.23
LysoPC(20:2 (11Z,14Z))	1.579	130.59 ± 40.76↑	229.5 ± 90.19↑
Hypoxanthine	1.5743	81.07 ± 121.41	332.17 ± 485.44↑
(9Z)-(7S,8S)-Dihydroxyoctadecenoic acid	1.5368	4.24 ± 1.78	9.27 ± 16.36
Hexadecaspheganine	1.5018	104.14 ± 29.52↑	80.52 ± 73.25
L-Valine	1.4966	76.8 ± 28.95	85.28 ± 31.63
Propionylcarnitine	1.4793	31.05 ± 59.64	13.22 ± 13.6
Chenodeoxycholic acid	1.4612	46.59 ± 80.13	31.65 ± 29.27
L-Proline	1.4518	83.38 ± 39.72	155.89 ± 22↑
PC(18:2 (9Z,12Z)/P-18:1 (9Z))	1.4426	70.52 ± 12.35	51.71 ± 10.66
11Z-Octadecenylcarnitine	1.3778	29.63 ± 19.96	25.66 ± 13.56
Lactic acid	1.328	76.2 ± 89.3	93.93 ± 91.29
isocitric acid	1.2934	106.34 ± 54.33↑	155.03 ± 39.4↑
SM(d18:1/20:0)	1.2732	395.62 ± 392.34↑	853.05 ± 512.89↑
Arachidonic acid	1.2628	76 ± 43.85	39.16 ± 33.48
Niacinamide	1.249	90.59 ± 64.88	48.99 ± 13.67
PC(14:0/22:0)	1.2306	176.7 ± 79.76↑	146.02 ± 32.71↑
SM(d18:1/18:1 (11Z))	1.1903	41.67 ± 9.75	60.37 ± 17.48
Sphingosine 1-phosphate	1.175	135.9 ± 36.87↑	228.98 ± 127.85↑
PC(o-16:1 (9Z)/18:0)	1.1643	203.38 ± 75.24↑	176.82 ± 91↑
SM(d18:0/18:1 (11Z))	1.1307	77.2 ± 18.12	69.39 ± 24.83
SM(d18:1/24:0)	1.1032	11,122.94 ± 656.4↑	8,706.75 ± 2,919.36↑
LysoPC(14:0)	1.1012	101.44 ± 60.3↑	244.67 ± 184.72↑
PC(o-18:1 (9Z)/20:4 (8Z,11Z,14Z,17Z))	1.0912	79.45 ± 8.38	63.32 ± 14.59
succinic acid	1.0772	64.08 ± 115.03	17.72 ± 15.59
SM(d18:1/22:1 (13Z))	1.0645	200.5 ± 70.03↑	207.66 ± 59.26↑
PC(14:0/22:5 (4Z,7Z,10Z,13Z,16Z))	1.0426	76.11 ± 15.64	82.2 ± 26.1
PC(o-16:1 (9Z)/18:2 (9Z,12Z))	1.0415	64.27 ± 11.47	56.95 ± 5.5
Uric acid	1.036	77.53 ± 93.78	15.96 ± 10.2
Vaccenic acid	1.0322	74.45 ± 46.36	74.33 ± 102.24
Sphinganine	1.0199	64.08 ± 12.87	80.79 ± 36.63

Arrow indicates significantly up-regulated, but no arrow down-regulated metabolites in the H + P and sham groups compared with P group, each group n = 6.

compared with the sham group, but HL treatment partially inhibited the shorting of AERP by rapid-pacing the atria of rabbits. The AF inducibility was markedly increased in the pacing group compared with the sham rabbits at baseline, but the treatment of Honokiol reversed it (**Figure 2D**). PAS staining showed that rapid-pacing induced an increase in

the glycogen accumulation in the atria, which was partially abrogated by HL (**Figures 2E–H**). The rapid-pacing induced a decreased in the activity of ATP enzyme, but HL partly inhibited the reduction of ATP enzyme activity, although the activity of ATP enzyme among the three group was not different statistically (**Figure 2G**). The level of ATP in the



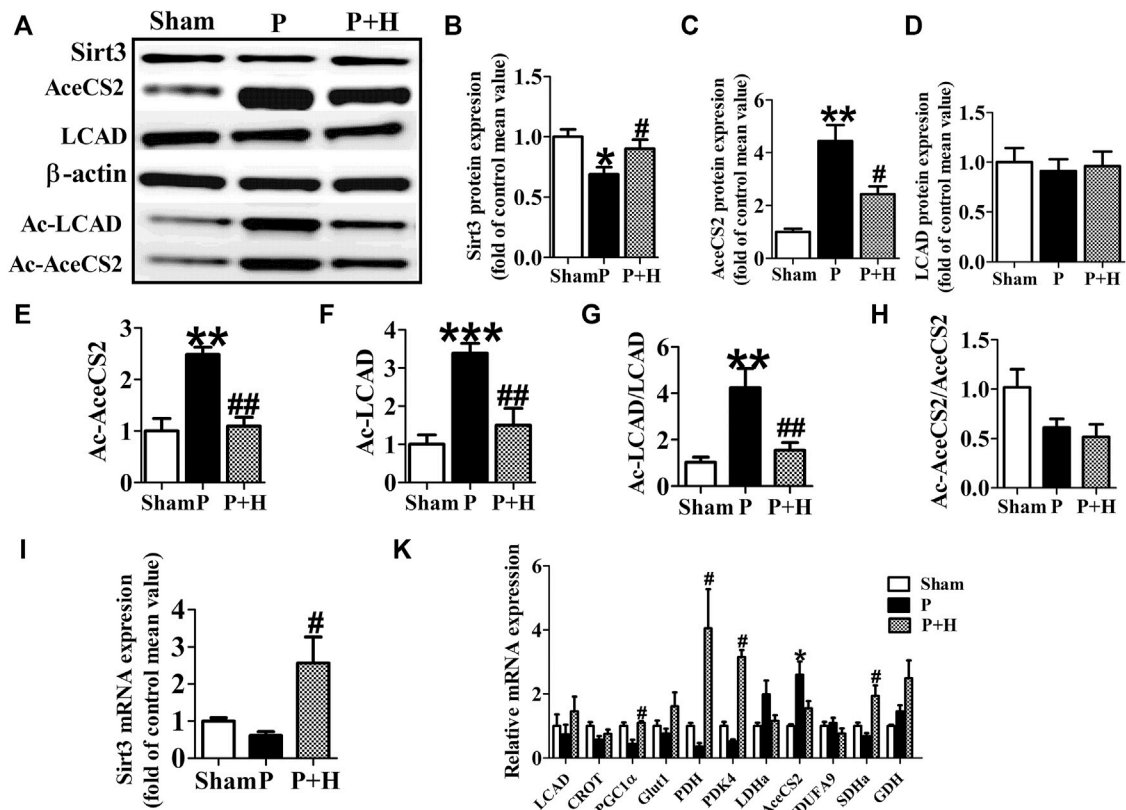


**FIGURE 3 |** HL inhibited the remodeling of metabolic factors and acetylation level of key metabolic enzyme in rabbit of AF model. **(A)** Representative bands of protein expression of Sirt3, AceCS2, Ac-LCAD and Ac-AceCS2. **(B,C,D,E,F)** Quantification analyzing of protein expression of Sirt3, AceCS2, Ac-LCAD and Ac-AceCS2. **(G and H)** Statistical results for ratio of Ac-LCAD/LCAD and Ac-AceCS2/AceCS2. **(I)** Statistical results for expression of Sirt3 gene. **(K)** Statistical results for expression of LCAD, CROT, PGC1 $\alpha$ , PDH, PDK4, LDHa, AceCS2, NDUFA9, SDHa and GDH genes. Data from these proteins were normalized to  $\beta$ -actin, and genes were normalized to  $\beta$ -actin. \* $p$  < 0.05 vs. sham group, \*\* $p$  < 0.01 vs. sham group, \*\*\* $p$  < 0.001 vs. sham group; # $p$  < 0.05 vs. P group, ## $p$  < 0.01 vs. P group, n = 6 each group.

pacing group was significantly decreased compared with sham group, however, HL inhibited this change (Figure 2H).

## HL Reversed the AF-Induced Alterations in Circulating Biochemical Metabolites

As shown in Table 3, circulating metabolites were identified and data were processed as described in previous studies (Xie et al., 2018). The metabolomics analysis illustrated that the sham, pacing (P) and HL treatment groups (H + P) could be completely separated (Supplementary Figure S1). Model quality parameters were Accuracy = 0.8, R<sup>2</sup> = 0.62, Q<sup>2</sup> = 0.89, 53 plasma metabolites in the atria had VIP > 1 involved in fatty acid metabolism, glucose and amino acid metabolism, 18 metabolites were increased and 35 of which were decreased in sham/P group, indicating rapid-pacing induced a decline of 18 circulating metabolites and a rising trend of 35 metabolites in the pacing group. Similarly, 17 showed a rising trend and 36 showed a downward trend in H + P/P group, suggesting 17 metabolites were decreased and 36 were increased in pacing group, but HL reversed the changes. MetaboAnalyst4.0 software was used to analyze the main differential endogenous metabolites with VIP value > 1, and the main metabolic pathway

with impact value greater than 0.1 was selected. The hearts of Sirt3-deficient mice exhibited more than a 50% reduction in basal ATP content (Ahn et al., 2008), and led to impaired fatty acid oxidation which was correlated with hyperacetylation of LCAD (Hirschey et al., 2010). KEGG analysis was performed on all 53 metabolites with significant differences, and the results showed that fatty acid metabolic pathways, indicating Sirt3, may regulate fatty acid metabolism activated by HL.

## HL Inhibited the Remodeling of Metabolic Factors and Acetylation Level of Key Metabolic Enzyme in Rabbit of AF Model

The atria in rabbits that were exposed to rapid pacing significantly decreased the protein and gene expression levels of Sirt3, which was restored by HL (Figures 3A,B,I). Because key metabolic enzymes are acetylated and acetylation can directly affect the enzyme activity or stability, we detected the acetylation level of acetyl-CoA synthetase 2 (AceCS2), a key enzyme involved in tricarboxylic acid cycle metabolism, and of LCAD in fatty acid oxidation. In our study, rapid-pacing induced up-regulated expression of AceCS2 protein (Figures 3A–C), but expression

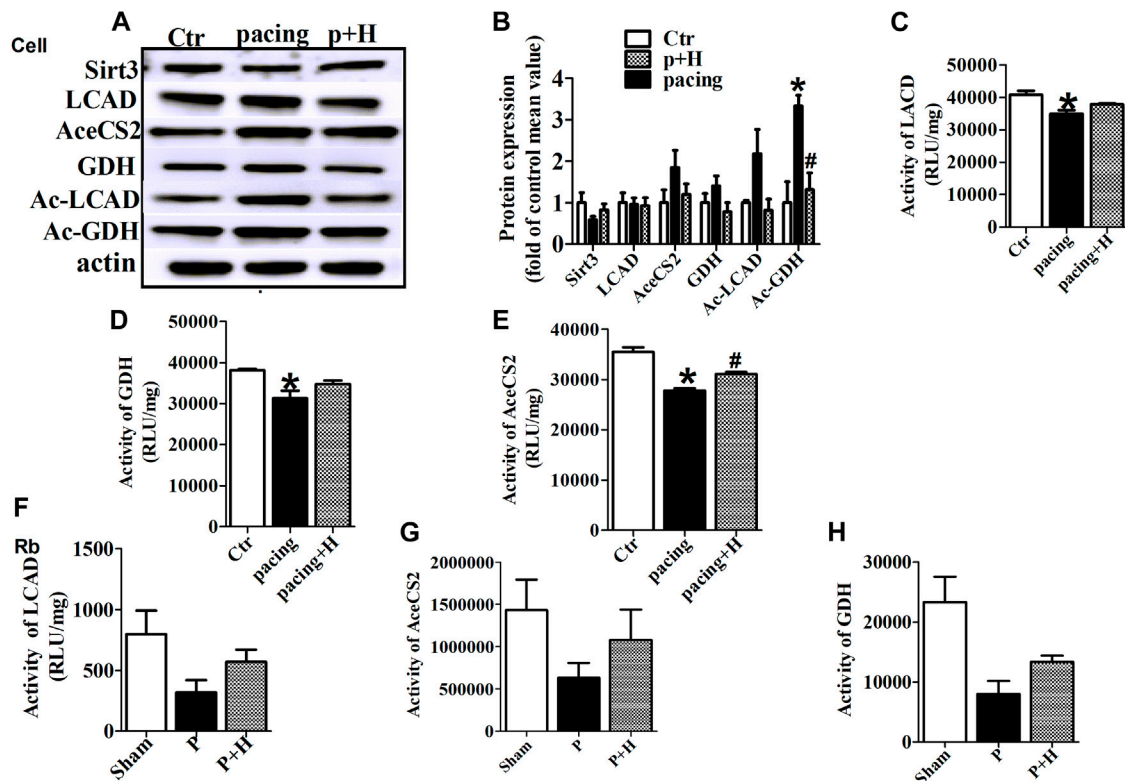


**FIGURE 4 |** HL inhibited abnormal expression and acetylation of key metabolic enzyme and restored the activity of these enzymes during AF. **(A and B)** Representative bands and statistical results of Sirt3, LCAD, AceCS2, GDH, Ac-LCAD, Ac-GDH in pacing-HL-1 cells. Data from these proteins were normalized to  $\beta$ -actin. **(C,D and E)** Statistical results for activity of LCAD, GDH and AceCS2 in pacing-HL-1 cells. \* $p < 0.05$  vs. sham group, # $p < 0.05$  vs. pacing group,  $n = 3$  each group. **(F,G and H)** Statistical results for activity of LCAD, GDH and AceCS2 in all groups of rabbits.  $n = 5$  each group.

of LCAD protein was not statistically different among all groups of rabbits (Figures 3A–D). However, the acetylation level of AceCS2 and LCAD protein obviously were up-regulated in the pacing group compared with the sham group of rabbits, which was reversed by HL (Figures 3A,E,F). The increased ratio of acetylated AceCS2/AceCS2 protein was found in the pacing group, but HL inhibited this change (Figure 3G).

Next, we detected the mRNA level of metabolic factors including LCAD, CROT, PGC1 $\alpha$ , Glut1, PDH, PDK4, LDHa, AceCS2, NDUFA9, SDHa, GDH. Rapid pacing significantly inhibited the expression of LCAD and enhanced AceCS2 mRNA expression; slightly down-regulated CROT, PGC1 $\alpha$ , Glut1 and PDH gene expression, and up-regulated LDHa, AceCS2, NDUFA9, SDHa, GDH in atria of pacing group. These changes in expression were restored by HL (Figure 3H).

Similarly, HL-1 cells were pretreated with HL (20  $\mu$ M, Sigma-Aldrich, St. Louis, MO, United States) for 1 h (Supplementary Table S1) and then stimulated with rapid pacing for 24 h. The Sirt3 expression levels was decreased, and the acetylation level of LCAD and GDH were increased in the rapid pacing HL-1 cells, but HL inhibited these changes (Figure 4).

## HL Restored the Activity of Key Metabolic Enzyme During Rapid-Pacing Atria

Acetylation is a novel regulatory mechanism for mitochondrial metabolism and controls the activity of key metabolic enzymes. We assessed that rapid-pacing induced a decrease in the activity of LCAD, AceCS2 and GDH *in vivo* and *in vitro* model of AF, and HL administration inhibited the reduction of activity in these metabolic enzymes (Figures 4C,D–F).

## HL Inhibited AF-Induced Metabolic Remodeling via Sirt3 Dependent Manner

To investigate the role of Sirt3 in regulating the acetylation of key metabolic enzymes in atria of AF, we knocked down Sirt3 expression with siRNA in HL-1 cells. Our data showed that Sirt3 siRNA markedly down-regulated the Sirt3 protein expression after transfection for 48 h (Figures 5A,B), which led to an increase of the mitochondrial acetylation level of GDH and LCAD (Figures 5A,F,G), and a significant decrease of ppho-AMPK $\alpha$ 1 expression and an increase GDH expression (Figures 5A,C,E). The above results demonstrate that Sirt3 is a key metabolic regulator that regulates the level of acetylation in metabolic enzymes and improves metabolic capacity.

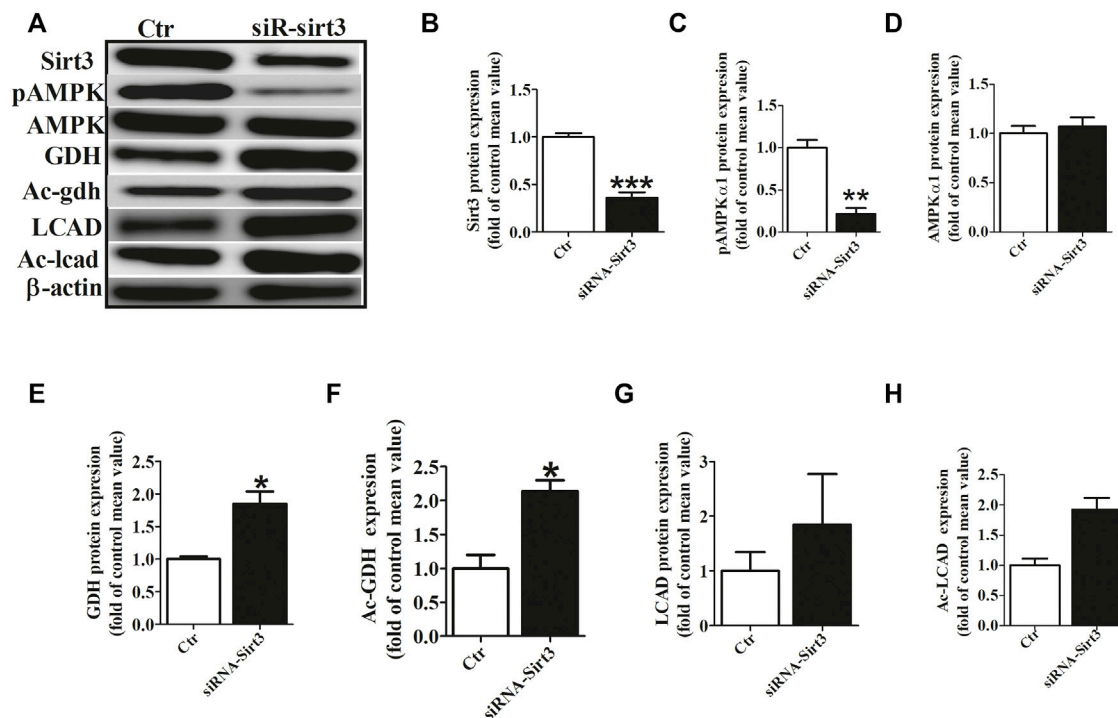


**FIGURE 5 |** Sirt3 siRNA up-regulated the acetylation level of metabolic enzymes. **(A)** Representative bands of Sirt3, pAMPKα1, AMPKα1, GDH, Ac-GDH (Ac-gdh), LCAD and Ac-LCAD expression. **(B)** Statistical results for Sirt3 expression. **(C,D)** Statistical results for pAMPKα1 and AMPKα1 expression. **(E,F)** Statistical results for GDH and Ac-GDH expression. **(G,H)** Statistical results for LCAD and Ac-LCAD expression. \* $p < 0.05$  vs. control group, \*\* $p < 0.05$  vs. control group, \*\*\* $p < 0.05$  vs. control group,  $n = 3$  each group.

To further determine whether the inhibitory effect of HL on atrial metabolic remodeling during AF was dependent on Sirt3 activation, HL-1 cells transfected with the Sirt3 plasmid was used in our study. The HL-1 cells were pretreated with transfection of Sirt3 plasmid for 48 h followed by pacing stimulation or without for 24 h. The expression of Sirt3 was significantly decreased in the pacing group compared to the control group, but the transfection with Sirt3 plasmid abrogated the down-regulation of Sirt3 induced by pacing.

Finally, we assessed the acetylation level of key metabolic enzymes controlled by the Sirt3 pathway *in vitro*. **Figure 6** shows that the level of GDH and LCAD expression were down-regulated in the Sirt3 plasmid group, but there was no significant difference among the three groups (**Figures 6A,C,E**). However, the acetylation level of LCAD and GDH were up-regulated in the pacing group compared with the control group (**Figures 6A,D,F,G**), which was reversed by Sirt3 plasmid. Similarly, rapid-pacing induced the down-regulation of pAMPKα1, but transfection with Sirt3 plasmid inhibited this change. The above results indicate that HL inhibits the atrial metabolic remodeling of AF *via* a Sirt3-dependent pathway.

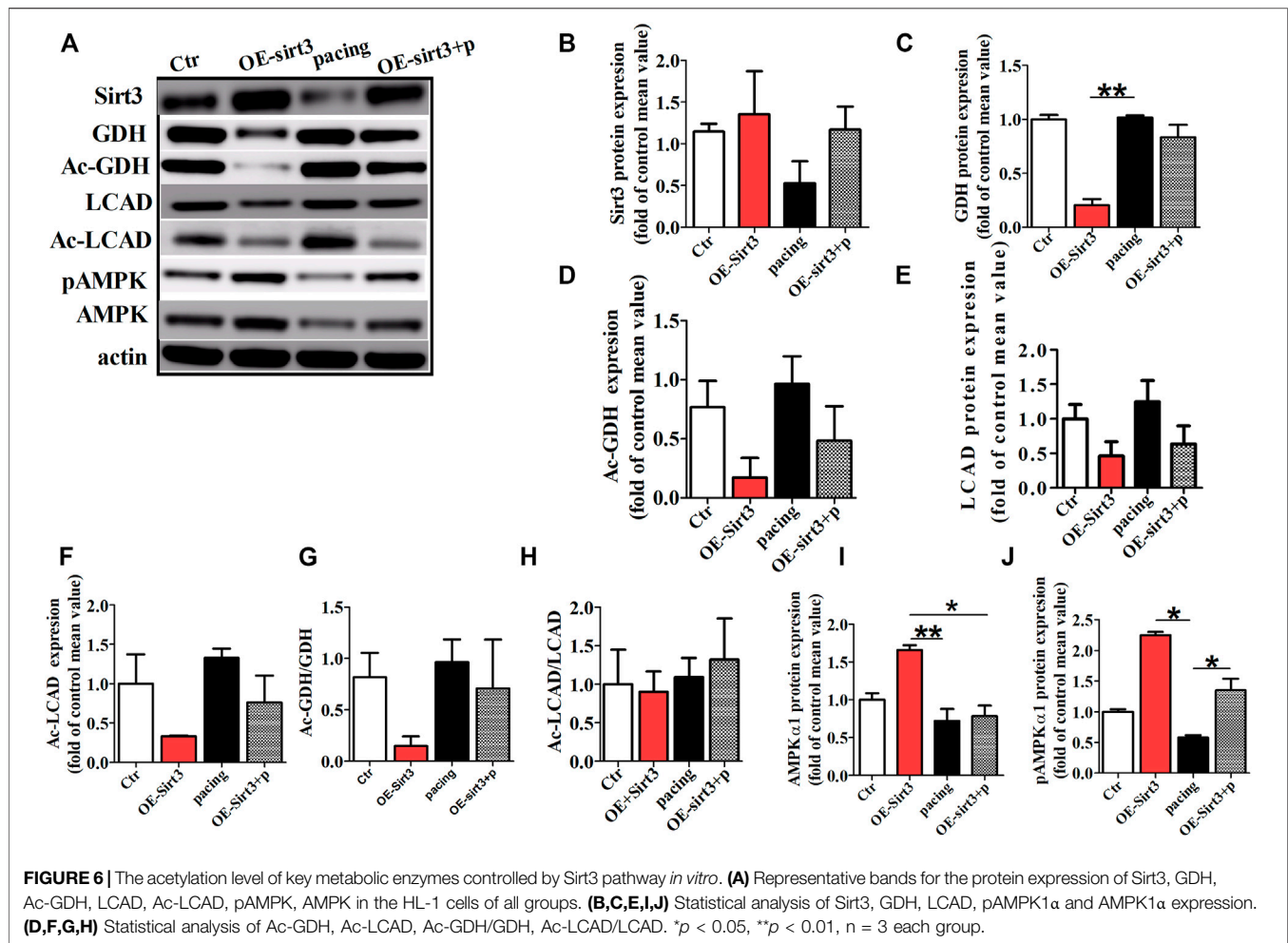
## DISCUSSION

This study identified that the down-regulation of Sirt3 in AF patients and the *vivo* and *vitro* of the AF model. We found that the increase in acetylation of enzymes involved in mitochondrial

fatty acid β-oxidation, glucose oxidation and amino acid metabolism in atria of AF, which led to abnormal changes of metabolites, glycogen deposit, reducing ATP levels, shortening of AERP, and increasing of AF vulnerability. HL reversed the increasing acetylation levels of LCAD, AceCS2 and GDH in animal and cells model of AF. The acetylation modification of key metabolic enzymes was controlled by the overexpression or depletion of Sirt3. Collectively, HL prevented the atrial metabolic remodeling of AF through the Sirt3 dependent pathway.

## HL Reversed AF-Induced Abnormal Atrial Metabolic Remodeling

Our and previous studies found glycogen accumulation and adenine nucleotide reduction in both animal models and humans with AF (Ausma et al., 2000; Liu et al., 2016). HL increased ATP production and reduced lipid peroxidation through the improving mitochondrial function in mice of cisplatin-induced renal injury model (Li et al., 2020). We demonstrated that rapid-pacing caused the reduction of ATP enzyme activity, the level of ATP, and the accumulation of glycogen in rabbits of with the AF model. Our study found an increase in the circulating lactate and ketone body levels in rabbits subjected to rapid-pacing for 1 week (Liu et al., 2016). Similarly, by using metabolomics analysis, we demonstrated that rapid-pacing induced the discordant metabolic alterations of circulating metabolites, which included fatty acid metabolism, glucose



oxidation and amino acid metabolism. The results suggest that AF induced metabolic disorder was reversed by HL.

The results in both studies showed the significant down-regulation of transcripts and proteins involved in fatty acid oxidation (Barth et al., 2005; Tu et al., 2014b). Lipid metabolic related gene PGC1α and very-long chain acyl-CoA dehydrogenase (VLCAD) was downregulated in human persistent AF and chronic AF animal models (Bai et al., 2019; Liu et al., 2020). Similarly, we found that rapid-pacing induced a mild decrease of transcript level in LCAD and CROT in atria, indicating AF led to the decrease of fatty acid metabolism, resulting in a reduced level of ATP. As shown in a study and our previous study, the reports suggest that the expression of LDH increased and the expression of Glut4 and PDH decreased in the animal model of AF (Liu et al., 2016; Liu et al., 2020). Consistent with these findings, we found down-regulation of Glut1 and PDH, NDUFA9 and SDH gene, and up-regulation of protein and gene expression in AceCS2 and GDH in both *in vitro* and *in vivo* models of AF, but HL inhibited these alterations. We found that HL treatment partially inhibited the shorting of AERP and the inducibility of AF, and although there is no statistical difference in AERP, it may be related to individual differences in animals.

The above results suggest AF induced dysfunction of glucose transportation and TCA cycle metabolism, increasing glycolysis pathway in atria.

## HL Inhibited Acetylation Modification of Metabolic Enzymes Induced by AF

Post-transcriptional acetylation modification is a potential “regulating valve” of cardiac energy metabolism in AF (Tu et al., 2014a). A previous study found HDAC (Histone deacetylase) inhibitor attenuates atrial remodeling and delays the onset of AF in mice (Scholz et al., 2019). AceCS2 is a key enzyme involved in tricarboxylic acid cycle (TCA) metabolism (Yamamoto et al., 2004), and LCAD is a key enzyme in fatty acid oxidation. Both studies demonstrated that mammalian AceCSS and LCAD were regulated by acetylation and that sirtuins activate AceCS2 and LCAD by deacetylation (Hallows et al., 2006; Hirschey et al., 2010). Moreover, Sirt3 deacetylated GDH and increased its activity (Kim et al., 2012). A study found that cardiac metabolic proteins were hyperacetylated in mice with high-fat diets, which was associated with a decrease in Sirt3 expression (Alrob et al., 2014). Our investigation demonstrated that rapid-pacing induced the increase of acetylation levels in LCAD, AceCS2 and GDH, and led to a decrease in the enzyme activity of



LCAD, AceCS2 and GDH during AF, indicating AF induced a decrease in the metabolic capability of fatty acid oxidation, TCA cycle and amino acid metabolism, which were reversed by HL.

## HL Prevented the Atrial Metabolic Remodeling of AF Through Sirt3 Dependent Pathway

Sirt3 plays a critical role in regulating the acetylation of key metabolic enzymes (He et al., 2019). LCAD is deacetylated in wild-type mice under fasting conditions and by Sirt3 *in vitro* and *in vivo*, and LCAD is hyperacetylated in the absence of Sirt3<sup>7</sup>. AceCS2 is abundant in heart and skeletal muscle and it plays an important role in acetate conversion for energy production. AceCS2 is a highly conserved and metabolic enzyme from bacteria to human, catalyzes the conversion of acetate to acetyl-CoA, and enables peripheral tissues to utilize acetate during fasting conditions (Shimazu et al., 2010). The acetyl-CoA is an important substrate for the tricarboxylic acid cycle. Accumulating biochemical studies have linked Sirt3 with activation of the mitochondrial enzyme AceCS2 that Sirt3 can regulate acetylated-modification of AceCS2 (Hallows et al., 2006; Schwer et al., 2006). In our study, we demonstrated AF induced an increase of acetylated LCAD and AceCS2 protein levels, following the reduction of its enzyme activity, indicating a decrease of metabolic capacity in the fatty acid  $\beta$ -oxidation and tricarboxylic acid cycle during AF. Furthermore, GDH is an amino-acid metabolic enzyme that promotes the metabolism of glutamate and glutamine, resulting in the generation of ATP, which promotes insulin secretion. There is a similar effect of acetylated-GDH level and its enzyme activity, which is regulated by Sirt3 (Kim et al., 2012). Consistent with our results, AF increased acetylation level of GDH, following a decrease of its activity, and indicating AF induced the decrease of amino-acid metabolism in atria.

The above study was consistent with our research, and our results demonstrate that overexpression or depletion of Sirt3 could regulate the acetylated-modification of LCAD, AceCS2 and GDH enzymes *in vitro* model of AF, in contrast change of activity in key metabolic enzymes. Further, increasing Sirt3 could improve metabolic capacity by regulating the acetylation level in metabolic enzymes. The above results indicated Sirt3 is a key metabolic regulator.

Sirt3 agonist HL could ameliorate cardiac hypertrophy by activating Sirt3 (Pillai et al., 2015) and improving fatty acid oxidation resulting in the inhibition of acute kidney injury induced by cisplatin (Li et al., 2020). However, the effects of HL on AF are not known. Our present study found a significant down-regulation of Sirt3 expression in rabbits, cell models of AF, and AF patients, followed by a reduction in LCAD, AceCS2 and GDH activity, and the acetylation level of its expression, following a decrease of fatty acid metabolism, TCA and amino-acid metabolism, but HL reversed the above changes. Interestingly, these small changes in the expression of metabolic factors in AF rabbits induced the derangement of atrial fatty acid metabolism, glucose and amino acid metabolism, which was consistent with the findings of previous studies (Liu et al., 2016), (Liu et al., 2020). In this study, HL prevented the atrial metabolic remodeling of AF through the Sirt3 dependent pathway.

Sirt3 has been implicated in various cardiac pathologies and it deacetylates multiple enzymes in mitochondrial metabolism (Yamamoto et al., 2004). A previous study reported that Sirt3 and AMPK stimulated mitochondrial biogenesis, which increased mitochondrial turnover and cardiomyocyte regeneration (Xin and Lu, 2020). In our study, the increase or decrease of Sirt3 could regulate the expression of p-AMPK $\alpha$ 1, suggesting Sirt3 is a controller of AMPK. In the present study, HL could up-regulate the expression of Sirt3, resulting in improving atrial metabolic remodeling and inhibiting AF. These findings indicated that HL inhibited metabolic remodeling of AF *via* regulating the Sirt3 signaling pathway.

## CONCLUSION

We demonstrated that the Sirt3 dependent pathway participated in atrial metabolic remodeling during AF and that HL inhibited atrial metabolic remodeling by regulating the Sirt3 dependent pathway. Thus, this pathway may provide a new potential therapeutic method for AF. Our study provided a novel insight into the pharmacological role of HL against AF and atrial metabolic remodeling.

## DATA AVAILABILITY STATEMENT

The original contributions presented in the study are included in the article/**Supplementary Materials**, further inquiries can be directed to the corresponding authors.

## ETHICS STATEMENT

The studies involving human participants were reviewed and approved by the Ethics Committee of the First Affiliated Hospital of Harbin Medical University. The patients/participants provided their written informed consent to participate in this study. The animal study was reviewed and approved by the Animal Care and Use Committee of the Harbin Medical University. Written informed consent was obtained from the owners for the participation of their animals in this study. Written informed consent was not obtained from the individual(s) for the publication of any potentially identifiable images or data included in this article.

## AUTHOR CONTRIBUTIONS

GZL and WX designed and conducted the experiments, analyzed the data, and wrote the manuscript. YZ, QL, PH, QG, HS, QL, HW, XS, CL, and PZ conducted the experiments. GZL, SHD, and HDL designed the experiment and revised the manuscript; and all authors approved the final version of the manuscript.

## FUNDING

This study was supported by the Province Natural Science Foundation of Heilongjiang (No. LH 2021H042), the National Natural Science Foundation of China (No. 81700305, 81770496, 81870191, 82070517), Science and Technology Planning Project of Shenzhen Municipality (No. JCYJ20190806153207263, No. KCFZ202002011009124) and Natural Science Foundation of Shen Zhen (No. JCYJ20190807145015194); The Doctorial Innovation Fund of Harbin Medical University (No. YJSCX 2014-30 HYD).

## REFERENCES

- Ahn, B. H., Kim, H. S., Song, S., Lee, I. H., Liu, J., Vassilopoulos, A., et al. (2008). A Role for the Mitochondrial Deacetylase Sirt3 in Regulating Energy Homeostasis. *Proc. Natl. Acad. Sci. U S A.* 105 (38), 14447–14452. doi:10.1073/pnas.0803790105
- Alrob, O. A., Sankaralingam, S., Ma, C., Wagg, C. S., Fillmore, N., Jaswal, J. S., et al. (2014). Obesity-induced Lysine Acetylation Increases Cardiac Fatty Acid Oxidation and Impairs Insulin Signalling. *Cardiovasc. Res.* 103 (4), 485–497. doi:10.1093/cvr/cvu156
- Anfuso, C. D., Olivieri, M., Fidilio, A., Lupo, G., Rusciano, D., Pezzino, S., et al. (2017). Gabapentin Attenuates Ocular Inflammation: *In Vitro* and *In Vivo* Studies. *Front. Pharmacol.* 8, 173. doi:10.3389/fphar.2017.00173
- Ausma, J., Coumans, W. A., Duimel, H., Van der Vusse, G. J., Allessie, M. A., and Borgers, M. (2000). Atrial High Energy Phosphate Content and Mitochondrial Enzyme Activity during Chronic Atrial Fibrillation. *Cardiovasc. Res.* 47 (4), 788–796. doi:10.1016/s0008-6363(00)00139-5
- Bai, F., Liu, Y., Tu, T., Li, B., Xiao, Y., Ma, Y., et al. (2019). Metformin Regulates Lipid Metabolism in a Canine Model of Atrial Fibrillation through AMPK/PPAR- $\alpha$ /VLCAD Pathway. *Lipids Health Dis.* 18 (1), 109. doi:10.1186/s12944-019-1059-7
- Barth, A. S., Merk, S., Arnoldi, E., Zwermann, L., Kloos, P., Gebauer, M., et al. (2005). Reprogramming of the Human Atrial Transcriptome in Permanent Atrial Fibrillation: Expression of a Ventricular-like Genomic Signature. *Circ. Res.* 96 (9), 1022–1029. doi:10.1161/01.res.0000165480.82737.33
- Bharathi, S. S., Zhang, Y., Mohsen, A. W., Uppala, R., Balasubramani, M., Schreiber, E., et al. (2013). Sirtuin 3 (SIRT3) Protein Regulates Long-Chain Acyl-CoA Dehydrogenase by Deacetylating Conserved Lysines Near the Active Site. *J. Biol. Chem.* 288 (47), 33837–33847. doi:10.1074/jbc.M113.510354
- Brundel, B. J., Shiroshita-Takeshita, A., Qi, X., Yeh, Y. H., Chartier, D., van Gelder, I. C., et al. (2006). Induction of Heat Shock Response Protects the Heart against Atrial Fibrillation. *Circ. Res.* 99 (12), 1394–1402. doi:10.1161/01.RES.0000252323.83137.fe
- Chang, H. C., and Guarente, L. (2014). SIRT1 and Other Sirtuins in Metabolism. *Trends Endocrinol. Metab.* 25 (3), 138–145. doi:10.1016/j.tem.2013.12.001
- Chiang, J., Shen, Y. C., Wang, Y. H., Hou, Y. C., Chen, C. C., Liao, J. F., et al. (2009). Honokiol Protects Rats against Eccentric Exercise-Induced Skeletal Muscle Damage by Inhibiting NF- $\kappa$ B Induced Oxidative Stress and Inflammation. *Eur. J. Pharmacol.* 610 (1–3), 119–127. doi:10.1016/j.ejphar.2009.03.035
- Fukushima, A., Alrob, O. A., Zhang, L., Wagg, C. S., Altamimi, T., Rawat, S., et al. (2016). Acetylation and Succinylation Contribute to Maturation Alterations in Energy Metabolism in the Newborn Heart. *Am. J. Physiol. Heart Circ. Physiol.* 311 (2), H347–H363. doi:10.1152/ajpheart.00900.2015
- Hallows, W. C., Lee, S., and Denu, J. M. (2006). Sirtuins Deacetylate and Activate Mammalian Acetyl-CoA Synthetases. *Proc. Natl. Acad. Sci. U S A.* 103 (27), 10230–10235. doi:10.1073/pnas.0604392103
- He, X., Zeng, H., and Chen, J. X. (2019). Emerging Role of SIRT3 in Endothelial Metabolism, Angiogenesis, and Cardiovascular Disease. *J. Cel Physiol* 234 (3), 2252–2265. doi:10.1002/jcp.27200

## ACKNOWLEDGMENTS

We would like to thank Bai-chun Wang MD for his cardiac surgery support.

## SUPPLEMENTARY MATERIAL

The Supplementary Material for this article can be found online at: <https://www.frontiersin.org/articles/10.3389/fphar.2022.813272/full#supplementary-material>

- Hirschey, M. D., Shimazu, T., Goetzman, E., Jing, E., Schwer, B., Lombard, D. B., et al. (2010). SIRT3 Regulates Mitochondrial Fatty-Acid Oxidation by Reversible Enzyme Deacetylation. *Nature* 464 (7285), 121–125. doi:10.1038/nature08778
- Ji, H., Song, N., Ren, J., Li, W., Xu, B., Li, H., et al. (2020). Metabonomics Reveals Bisphenol A Affects Fatty Acid and Glucose Metabolism through Activation of LXR in the Liver of Male Mice. *Sci. Total Environ.* 703, 134681. doi:10.1016/j.scitotenv.2019.134681
- Kilkenny, C., Browne, W., Cuthill, I. C., Emerson, M., and Altman, D. G. (2010). Animal Research: Reporting *In Vivo* Experiments: the ARRIVE Guidelines. *J. Physiol.* 588 (7), 2519–2521. doi:10.1111/j.1476-5381.2010.00872.x.10.1113/jphysiol.2010.192278
- Kim, E. A., Yang, S. J., Choi, S. Y., Lee, W. J., and Cho, S. W. (2012). Inhibition of Glutamate Dehydrogenase and Insulin Secretion by KHG26377 Does Not Involve ADP-Ribosylation by SIRT4 or Deacetylation by SIRT3. *BMB Rep.* 45 (8), 458–463. doi:10.5483/bmbrep.2012.45.8.040
- Li, M., Li, C. M., Ye, Z. C., Huang, J., Li, Y., Lai, W., et al. (2020). Sirt3 Modulates Fatty Acid Oxidation and Attenuates Cisplatin-Induced AKI in Mice. *J. Cel Mol Med* 24 (9), 5109–5121. doi:10.1111/jcmm.15148
- Li, Y., Li, W. M., Gong, Y. T., Li, B. X., Liu, W., Han, W., et al. (2007). The Effects of Cilazapril and Valsartan on the mRNA and Protein Expressions of Atrial Calpains and Atrial Structural Remodeling in Atrial Fibrillation Dogs. *Basic Res. Cardiol.* 102 (3), 245–256. doi:10.1007/s00395-007-0641-8
- Liu, G. Z., Hou, T. T., Yuan, Y., Hang, P. Z., Zhao, J. J., Sun, L., et al. (2016). Fenofibrate Inhibits Atrial Metabolic Remodelling in Atrial Fibrillation through PPAR-A/sirtuin 1/PGC-1 $\alpha$  Pathway. *Br. J. Pharmacol.* 173 (6), 1095–1109. doi:10.1111/bph.13438
- Liu, Y., Bai, F., Liu, N., Zhang, B., Qin, F., Tu, T., et al. (2020). Metformin Improves Lipid Metabolism and Reverses the Warburg Effect in a Canine Model of Chronic Atrial Fibrillation. *BMC Cardiovasc. Disord.* 20 (1), 50. doi:10.1186/s12872-020-01359-7
- Liu, Y., Geng, J., Liu, Y., Li, Y., Shen, J., Xiao, X., et al. (2013).  $\beta$ 3-adrenoceptor Mediates Metabolic Protein Remodeling in a Rabbit Model of Tachypacing-Induced Atrial Fibrillation. *Cell Physiol Biochem* 32 (6), 1631–1642. doi:10.1159/000356599
- Lombard, D. B., Alt, F. W., Cheng, H. L., Bunkenborg, J., Streeper, R. S., Mostoslavsky, R., et al. (2007). Mammalian Sir2 Homolog SIRT3 Regulates Global Mitochondrial Lysine Acetylation. *Mol. Cel Biol* 27 (24), 8807–8814. doi:10.1128/mcb.01636-07
- Ma, S., Ma, J., Tu, Q., Zheng, C., Chen, Q., and Lv, W. (2020). Isoproterenol Increases Left Atrial Fibrosis and Susceptibility to Atrial Fibrillation by Inducing Atrial Ischemic Infarction in Rats. *Front. Pharmacol.* 11, 493. doi:10.3389/fphar.2020.00493
- Mayr, M., Yusuf, S., Weir, G., Chung, Y. L., Mayr, U., Yin, X., et al. (2008). Combined Metabolomic and Proteomic Analysis of Human Atrial Fibrillation. *J. Am. Coll. Cardiol.* 51 (5), 585–594. doi:10.1016/j.jacc.2007.09.055
- McGrath, J. C., Drummond, G. B., McLachlan, E. M., Kilkenny, C., and Wainwright, C. L. (2010). Guidelines for Reporting Experiments Involving Animals: the ARRIVE Guidelines. *Br. J. Pharmacol.* 160 (7), 1573–1576. doi:10.1111/j.1476-5381.2010.00873.x
- Pillai, V. B., Samant, S., Sundaresan, N. R., Raghuraman, H., Kim, G., Bonner, M. Y., et al. (2015). Honokiol Blocks and Reverses Cardiac Hypertrophy in Mice by

- Activating Mitochondrial Sirt3. *Nat. Commun.* 6, 6656. doi:10.1038/ncomms7656
- Rardin, M. J., Newman, J. C., Held, J. M., Cusack, M. P., Sorensen, D. J., Li, B., et al. (2013). Label-free Quantitative Proteomics of the Lysine Acetylome in Mitochondria Identifies Substrates of SIRT3 in Metabolic Pathways. *Proc. Natl. Acad. Sci. U S A.* 110 (16), 6601–6606. doi:10.1073/pnas.1302961110
- Scholz, B., Schulte, J. S., Hamer, S., Himmler, K., Pluteanu, F., Seidl, M. D., et al. (2019). HDAC (Histone Deacetylase) Inhibitor Valproic Acid Attenuates Atrial Remodeling and Delays the Onset of Atrial Fibrillation in Mice. *Circ. Arrhythm Electrophysiol.* 12 (3), e007071. doi:10.1161/circep.118.007071
- Schwer, B., Bunkenborg, J., Verdin, R. O., Andersen, J. S., and Verdin, E. (2006). Reversible Lysine Acetylation Controls the Activity of the Mitochondrial Enzyme Acetyl-CoA Synthetase 2. *Proc. Natl. Acad. Sci. U S A.* 103 (27), 10224–10229. doi:10.1073/pnas.0603968103
- Shimazu, T., Hirsche, M. D., Huang, J. Y., Ho, L. T., and Verdin, E. (2010). Acetate Metabolism and Aging: An Emerging Connection. *Mech. Ageing Dev.* 131 (7–8), 511–516. doi:10.1016/j.mad.2010.05.001
- Sulakhiya, K., Kumar, P., Jangra, A., Dwivedi, S., Hazarika, N. K., Baruah, C. C., et al. (2014). Honokiol Abrogates Lipopolysaccharide-Induced Depressive like Behavior by Impeding Neuroinflammation and Oxido-Nitrosative Stress in Mice. *Eur. J. Pharmacol.* 744, 124–131. doi:10.1016/j.ejphar.2014.09.049
- Tu, T., Zhou, S., and Liu, Q. (2014a). Acetylation: a Potential "regulating Valve" of Cardiac Energy Metabolism during Atrial Fibrillation. *Int. J. Cardiol.* 177 (1), 71–72. doi:10.1016/j.ijcard.2014.09.022
- Tu, T., Zhou, S., Liu, Z., Li, X., and Liu, Q. (2014b). Quantitative Proteomics of Changes in Energy Metabolism-Related Proteins in Atrial Tissue from Valvular Disease Patients with Permanent Atrial Fibrillation. *Circ. J.* 78 (4), 993–1001. doi:10.1253/circj.cj-13-1365
- van de Ven, R. A. H., Santos, D., and Haigis, M. C. (2017). Mitochondrial Sirtuins and Molecular Mechanisms of Aging. *Trends Mol. Med.* 23 (4), 320–331. doi:10.1016/j.molmed.2017.02.005
- Xie, W., Zhang, W., Ren, J., Li, W., Zhou, L., Cui, Y., et al. (2018). Metabonomics Indicates Inhibition of Fatty Acid Synthesis,  $\beta$ -Oxidation, and Tricarboxylic Acid Cycle in Triclocarban-Induced Cardiac Metabolic Alterations in Male Mice. *J. Agric. Food Chem.* 66 (6), 1533–1542. doi:10.1021/acs.jafc.7b05220
- Xin, T., and Lu, C. (2020). SirT3 Activates AMPK-Related Mitochondrial Biogenesis and Ameliorates Sepsis-Induced Myocardial Injury. *Aging (Albany NY)* 12 (16), 16224–16237. doi:10.18632/aging.103644
- Yamamoto, J., Ikeda, Y., Iguchi, H., Fujino, T., Tanaka, T., Asaba, H., et al. (2004). A Kruppel-like Factor KLF15 Contributes Fasting-Induced Transcriptional Activation of Mitochondrial Acetyl-CoA Synthetase Gene AceCS2. *J. Biol. Chem.* 279 (17), 16954–16962. doi:10.1074/jbc.M312079200
- Yang, W., Nagasawa, K., Münch, C., Xu, Y., Satterstrom, K., Jeong, S., et al. (2016). Mitochondrial Sirtuin Network Reveals Dynamic SIRT3-Dependent Deacetylation in Response to Membrane Depolarization. *Cell* 167 (4), 985–1000. doi:10.1016/j.cell.2016.10.016
- Yang, Z., Shen, W., Rottman, J. N., Wikswo, J. P., and Murray, K. T. (2005). Rapid Stimulation Causes Electrical Remodeling in Cultured Atrial Myocytes. *J. Mol. Cel. Cardiol.* 38 (2), 299–308. doi:10.1016/j.yjmcc.2004.11.015
- Yu, W., Dittenhafer-Reed, K. E., and Denu, J. M. (2012). SIRT3 Protein Deacetylates Isocitrate Dehydrogenase 2 (IDH2) and Regulates Mitochondrial Redox Status. *J. Biol. Chem.* 287 (17), 14078–14086. doi:10.1074/jbc.M112.355206
- Zhao, D., Wang, Y., Du, C., Shan, S., Zhang, Y., Du, Z., et al. (2017). Honokiol Alleviates Hypertrophic Scar by Targeting Transforming Growth Factor- $\beta$ /Smad2/3 Signaling Pathway. *Front. Pharmacol.* 8, 206. doi:10.3389/fphar.2017.00206
- Zhao, J., Li, J., Li, W., Li, Y., Shan, H., Gong, Y., et al. (2010). Effects of Spironolactone on Atrial Structural Remodelling in a Canine Model of Atrial Fibrillation Produced by Prolonged Atrial Pacing. *Br. J. Pharmacol.* 159 (8), 1584–1594. doi:10.1111/j.1476-5381.2009.00551.x

**Conflict of Interest:** The authors declare that the research was conducted in the absence of any commercial or financial relationships that could be construed as a potential conflict of interest.

**Publisher's Note:** All claims expressed in this article are solely those of the authors and do not necessarily represent those of their affiliated organizations, or those of the publisher, the editors and the reviewers. Any product that may be evaluated in this article, or claim that may be made by its manufacturer, is not guaranteed or endorsed by the publisher.

Copyright © 2022 Liu, Xu, Zang, Lou, Hang, Gao, Shi, Liu, Wang, Sun, Liu, Zhang, Liu and Dong. This is an open-access article distributed under the terms of the Creative Commons Attribution License (CC BY). The use, distribution or reproduction in other forums is permitted, provided the original author(s) and the copyright owner(s) are credited and that the original publication in this journal is cited, in accordance with accepted academic practice. No use, distribution or reproduction is permitted which does not comply with these terms.



# Role of Adiponectin Receptor 1 in Promoting Nitric Oxide-Mediated Flow-Induced Dilation in the Human Microvasculature

Katie E. Cohen<sup>1,2</sup>, Boran Katunaric<sup>2,3</sup>, Mary E. Schulz<sup>2,3</sup>, Gopika SenthilKumar<sup>2,3,4</sup>, Micaela S. Young<sup>1,2</sup>, James E. Mace<sup>5</sup> and Julie K. Freed<sup>2,3,4\*</sup>

<sup>1</sup>Department of Medicine-Division of Cardiovascular Medicine, Medical College of Wisconsin, Milwaukee, WI, United States, <sup>2</sup>Cardiovascular Center, Medical College of Wisconsin, Milwaukee, WI, United States, <sup>3</sup>Department of Anesthesiology, Medical College of Wisconsin, Milwaukee, WI, United States, <sup>4</sup>Department of Physiology, Medical College of Wisconsin, Milwaukee, WI, United States, <sup>5</sup>Department of Surgery-Division of Adult Cardiothoracic Surgery, Medical College of Wisconsin, Milwaukee, WI, United States

## OPEN ACCESS

### Edited by:

Min Zhang,  
King's College London,  
United Kingdom

### Reviewed by:

William F. Jackson,  
Michigan State University,  
United States  
Masashi Mukohda,  
Okayama University of Science, Japan

### \*Correspondence:

Julie K. Freed  
jfreed@mcw.edu

### Specialty section:

This article was submitted to  
Cardiovascular and Smooth Muscle  
Pharmacology,  
a section of the journal  
Frontiers in Pharmacology

**Received:** 14 February 2022

**Accepted:** 21 March 2022

**Published:** 04 April 2022

### Citation:

Cohen KE, Katunaric B, Schulz ME, SenthilKumar G, Young MS, Mace JE and Freed JK (2022) Role of Adiponectin Receptor 1 in Promoting Nitric Oxide-Mediated Flow-Induced Dilation in the Human Microvasculature. *Front. Pharmacol.* 13:875900. doi: 10.3389/fphar.2022.875900

Chronic administration of exogenous adiponectin restores nitric oxide (NO) as the mediator of flow-induced dilation (FID) in arterioles collected from patients with coronary artery disease (CAD). Here we hypothesize that this effect as well as NO signaling during flow during health relies on activation of Adiponectin Receptor 1 (AdipoR1). We further posit that osmotin, a plant-derived protein and AdipoR1 activator, is capable of eliciting similar effects as adiponectin. Human arterioles (80–200  $\mu$ m) collected from discarded surgical adipose specimens were cannulated, pressurized, and pre-constricted with endothelin-1 (ET-1). Changes in vessel internal diameters were measured during flow using videomicroscopy. Immunofluorescence was utilized to compare expression of AdipoR1 during both health and disease. Administration of exogenous adiponectin failed to restore NO-mediated FID in CAD arterioles treated with siRNA against AdipoR1 (siAdipoR1), compared to vessels treated with negative control siRNA. Osmotin treatment of arterioles from patients with CAD resulted in a partial restoration of NO as the mediator of FID, which was inhibited in arterioles with decreased expression of AdipoR1. Together these data highlight the critical role of AdipoR1 in adiponectin-induced NO signaling during shear. Further, osmotin may serve as a potential therapy to prevent microvascular endothelial dysfunction as well as restore endothelial homeostasis in patients with cardiovascular disease.

**Keywords:** adiponectin, nitric oxide, microvascular, endothelium, flow, dilation

**Abbreviations:** AdipoR1, adiponectin receptor 1; CAD, coronary artery disease; cPTIO, 2-4-carboxyphenyl-4,4,5,5-tetramethylimidazole-1-oxyl-3-oxide; DM, diabetes mellitus; FID, flow-induced dilation; H<sub>2</sub>O<sub>2</sub>, hydrogen peroxide; L-NAME, N<sup>ω</sup>-nitro-L-arginine; MACE, major adverse cardiac events; NO, nitric oxide; nonCAD, non-coronary artery disease; PEG-Catalase, polyethylene glycol-catalase; ROS, reactive oxygen species.



## INTRODUCTION

The traditional view of the microvasculature as a network of small resistance arterioles that regulate end-organ perfusion has expanded to being a critical modulator of underlying parenchyma which can prevent or promote cardiovascular disease. Coronary, as well as peripheral systemic microvascular dysfunction, are powerful predictors of future major adverse cardiac events (MACE) (TPvd et al., 2014). Microvascular endothelial dysfunction, or a state of reduced nitric oxide (NO) bioavailability due to increased oxidative stress, can be assessed by determining the endothelial vasoactive mediator formed during flow that results in dilation (flow-induced dilation; FID). Under physiological conditions, the FID mediator generated is NO, an anti-inflammatory, anti-thrombotic compound whereas arterioles from patients with CAD rely on the formation of the pro-inflammatory, pro-atherosclerotic compound  $H_2O_2$  to elicit dilation.

We have previously shown that chronic exposure (16–20 h) to adiponectin, or a nonselective adiponectin receptor agonist (AdipoRON), is capable of restoring NO-mediated FID in human microvessels collected from patients diagnosed with CAD (Schulz et al., 2019). Adiponectin is a unique adipokine with many reported beneficial effects on the vasculature. These vascular effects include but are not limited to, triggering NO formation through activation of endothelial nitric oxide (Hattori et al., 2003) (eNOS) and promoting breakdown of ceramide (Holland et al., 2011), a sphingolipid that when elevated in plasma predicts future MACE and induces microvascular endothelial dysfunction (Freed et al., 2014a; Akhiyat et al., 2021). Targeting the adiponectin pathway may offer a therapeutic strategy to prevent or reverse microvascular endothelial dysfunction before the formation of large artery disease. Here we hypothesized that activation of adiponectin receptor 1 (AdipoR1) is responsible for the restoration of NO-mediated FID in microvessels from subjects with disease. The question was addressed here by examining 1) the expression of AdipoR1 in microvessels from patients with and without CAD, 2) the role of AdipoR1 in adiponectin-induced restoration of NO as the primary mediator of FID in diseased arterioles, and 3) whether osmotin, a plant-derived stress protein whose receptor shares homology with AdipoR1, can serve in the same capacity and promote vasodilation that relies on the formation of NO. The translational studies reported here highlight the importance of AdipoR1 signaling and offer mechanistic insight into the role of adiponectin, and potentially osmotin, in promoting a quiescent human microvascular endothelium.

## MATERIALS AND METHODS

### Human Tissue Acquisition

Fresh human adipose deemed discarded was collected at the time of surgery and placed in ice-cold HEPES buffer (pH 7.4). Discarded tissue was transported to the Pathology department (honest broker) housed within the hospital, then sent to the laboratory for dissection. De-identified patient data is collected

using RedCap, a clinical research database at the Medical College of Wisconsin. In addition to the de-identified discard collection, clinical research coordinators are approved to screen for operations that will likely result in discard tissue from the procedure and consent patients to collect their surgical discard tissue along with more detailed patient information. All protocols were approved by the local Institutional Review Board (IRB) at the Medical College of Wisconsin.

### Videomicroscopy for Microvascular Function Studies

The microvascular functional study technique has been extensively used by our laboratory (Miura et al., 2003). In an organ chamber, both ends of the resistance vessel (80–200  $\mu$ m) are cannulated with glass micropipettes filled with physiological saline solution and pressurized (60 mmHg) prior to measuring internal diameter change using videomicroscopy. Administration of endothelin-1 (2 nM) was used to pre-constrict the vessel to 30–70% of its passive diameter prior to initiating flow. Flow-induced dilation (FID) was measured as originally described by Kuo, et al. (Kuo et al., 1990) using pipettes of matched impedance. Changing the height of each reservoir in equal amounts in opposite directions generated flow without changing vessel central pressure (Kuo et al., 1990). Data are reported as diameter at a given flow rate or pressure gradient.

Internal diameters were assessed 5 min (steady-state) after each change. Two flow-response curves were generated, one after adding vehicle, and one after inhibitors (e.g. L-NAME). The concentration of agents was determined by multiplying the  $ED_{50} \times 2$  for inhibition or activation for each specific compound. Based on our previous studies, 16–20 h is an adequate duration of incubation for assessing the chronic effect of pharmacological agents. Acute treatment is defined as 30 min - 4 h of drug exposure either in the chamber bath, or in a dish containing culture media. L-NAME (100  $\mu$ M) or cPTIO (100  $\mu$ M) were added to the chamber bath to determine the role of NO in FID whereas the addition of PEG-catalase (500 U) was used to assess the contribution of  $H_2O_2$  to dilation. Smooth muscle function was assessed at the completion of each flow experiment by measuring the dilator response to papaverine (100  $\mu$ M).

### siRNA Transfection

Knockdown of AdipoR1 was achieved as previously described (Kadlec et al., 2017). Silencer Select Negative Control siRNA was used as a control. Briefly, arterioles were cannulated and transfused with the negative control or target protein siRNA (50 nM) with Lipofectamine RNAiMAX (Invitrogen). The ends of each arteriole were tied off to allow for intraluminal exposure and endothelial targeted knockdown of AdipoR1. Vessels were then incubated for 4 h in fresh medium. The following day, ties were cut off the ends of the arterioles prior to cannulation for functional studies. Knockdown efficiency was evaluated using immunofluorescence.

### Immunofluorescence

Dissected resistance arterioles from human adipose tissue were fixed in 10% neutral buffer formalin for up to 72 h. After fixation, tissues

were dehydrated through graded ethanol, cleared with xylene, and paraffin infiltrated using automated tissue processing (Sakura Tissue TEK VIP5 and VIP6). Tissue cassettes are embedded into paraffin blocks following processing. Tissue blocks were sectioned at 4  $\mu$ m and mounted on poly-L-lysine coated slides until subsequent staining. Staining was performed on a Leica Bond RX automated staining platform. Deparaffinization and citrate buffer retrieval was performed prior to staining protocol. After protein blocking (30 min, DAKO X0909) antibodies for AdipoR1 and CD31 were combined as a cocktail and incubated for 1 h at room temperature. After TBST washing, Donkey anti Mouse-488 (Invitrogen A10037) was cocktailed with Donkey anti Rabbit Cy3 (Jackson Immuno 715-166-152) and incubated 45 min at room temperature. Nuclei were stained with DAPI (Sigma, D8417). Omission of primary antibody performed for negative reagent controls. Fluorescent images of the vessel cross sections were acquired on an Olympus inverted fluorescent microscope. Image analysis was completed in Image J by outlining the outer and inner layer of the endothelium (marked by CD31) and applying the outline to quantify endothelium specific AdipoR1. The mean gray value of the endothelial lining is reported as mean  $\pm$  SEM.

## MATERIALS

Adiponectin (Recombinant Human gAcrp30/Adipolean, PeproTech US, Rocky Hill, NJ, United States) was reconstituted in 0.1% 1% bovine serum albumin (BSA). Endothelin-1 (MilliporeSigma, St. Louis, MO, United States) was dissolved in 1% BSA solution.  $\omega$ -nitro-L-arginine methyl ester (L-NAME) and polyethylene glycol-catalase (PEG-catalase) (Millipore Sigma) and 2-(4-carboxyphenyl)-4,4,5,5-tetramethylimidazole-1-oxyl-3-oxide (cPTIO) (Cayman Chemical, Ann Arbor, MI, United States) were dissolved in water. Osmotin (Abcam, Cambridge, United Kingdom) was diluted in a Tris/glycine buffer at pH 7.4. Anti-AdipoR1 antibody (ab126611) was also obtained from Abcam. Anti-AdipoR1 siRNA (s27410) and negative control siRNA (Silencer Select Negative Control #1) were obtained from Invitrogen by Thermo Fisher (Thermo Fisher Scientific, Waltham, MA, United States).

## Statistical Analysis

All data presented are expressed as mean  $\pm$  SEM. Percent maximal dilation is calculated as a percentage of maximal relaxation following constriction with endothelin-1. 100% dilation is full relaxation to the maximum diameter observed from the addition of the smooth muscle relaxant papaverine at the end of the flow experiment. A 2-way ANOVA was used with treatment and flow gradient used as parameters. The Holm-Sidak multiple comparisons test was used when significant differences ( $p < 0.05$ ) were observed between treatments. Statistical analysis was performed using GraphPad Prism, version 9.3.0. Statistical significance was defined as  $p < 0.05$ .

## RESULTS

Discarded surgical adipose was collected from a total of 36 patients for this study. The majority of microvessels were

**TABLE 1 |** Patient Demographics. CAD, coronary artery disease; BMI, body mass index; M, male; F, female. n indicates number of patients.

Characteristics	NonCAD (n = 6)	CAD (n = 30)
Sex, M/F	6	21/9
Age, years (average $\pm$ SD)	44 $\pm$ 12	66 $\pm$ 8
BMI (average $\pm$ SD)	31 $\pm$ 4	32 $\pm$ 5
Race	Caucasian (n = 5) Hispanic (n = 1)	Caucasian (n = 26) African American (n = 5) Asian/Pacific Islander (n = 1) Unknown (n = 1)
Underlying diseases/risk factors		
Coronary artery disease	0	30
Hypertension	1	22
Hyperlipidemia	1	22
Diabetes mellitus	0	9
Active smoker	0	5
Congestive heart failure	0	7
None of the above	4	0

dissected from adipose collected from patients formally diagnosed with CAD (30) with the remaining (6) collected from nonCAD patients who had 0–1 risk factor for CAD (hypertension, hyperlipidemia, diabetes mellitus, congestive heart failure, active smoker). Demographic data including age, sex, BMI, race, and underlying disease or risk factors is presented in **Table 1**.

## Expression of AdipoR1 in the Human Microcirculation

Resistance arterioles were dissected from human adipose tissue collected from both nonCAD and CAD patients for detection of AdipoR1. **Figure 1** shows representative images of human arterioles treated with immunofluorescent antibodies against AdipoR1. AdipoR1 expression in arterioles from nonCAD patients is shown in **Figure 1A** and patients diagnosed with CAD in **Figure 1B**. Microvessels from individuals with and without CAD were treated intraluminally with siRNA against AdipoR1 **Figure 1C**. Cross-sections of the arterioles were immunolabeled for CD31 to outline the endothelium and allow for identification of endothelial AdipoR1. **Figure 1D** summarizes the immunofluorescent intensity in all 3 groups. AdipoR1 is expressed in human microvessels during both health and disease and expression is significantly decreased in arterioles treated with siAdipoR1.

## Decreased Expression of AdipoR1 Impairs Restoration of Nitric Oxide-Mediated Flow-Induced Dilation

We have previously shown that chronic exposure to exogenous adiponectin restores NO as the mediator of FID in arterioles collected from patients with CAD (Schulz et al., 2019). To determine whether AdipoR1 is responsible for this effect, microvessels from patients with CAD were first treated with siRNA against AdipoR1 for 4 h prior to incubation with exogenous adiponectin for 16–20 h. As shown in **Figure 2A**, FID is significantly impaired in vessels treated with both siAdipoR1 and

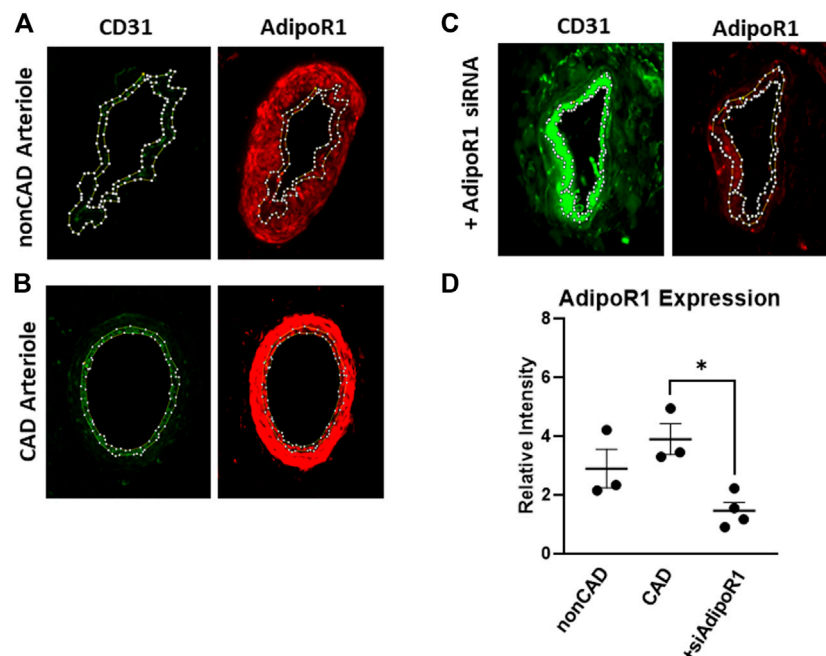


**FIGURE 1 |** AdipoR1 expression in human microvessels. Representative images showing expression of CD31 (green) and AdipoR1 (red) in arterioles from patients without CAD (A), with CAD (B) and arterioles treated with siAdipoR1 (C). CD31 was used to identify the endothelium to allow for measurement of AdipoR1 in the intimal layer of the vessel. (D) Measured relative intensity of AdipoR1 in all groups. ( $n = 3$  for nonCAD and CAD,  $n = 4$  for vessels treated with siAdipoR1; 3 nonCAD, 1 CAD),  $^*p < 0.05$ ).

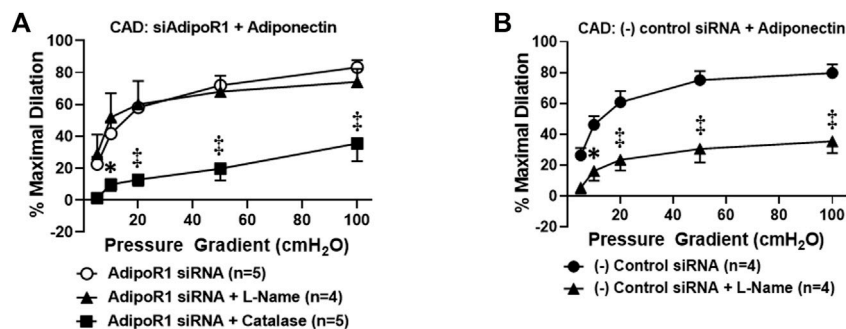


**FIGURE 2 |** Adiponectin restores NO-dependent FID via activation of AdipoR1 in CAD microvessels. (A) FID is significantly decreased in arterioles collected from patients with CAD treated with both siAdipoR1 and adiponectin in the presence of PEG-catalase ( $n = 5$ ) compared to vessels treated with siAdipoR1 alone ( $n = 5$ ) whereas L-Name had no effect ( $n = 4$ ). (B) Intraluminal treatment with negative control siRNA does not impair adiponectin-induced restoration of NO as the mediator of FID as dilation is inhibited in the presence of L-NAME ( $n = 4$ ) compared to negative control siRNA alone ( $n = 5$ ).  $^{\dagger}p < 0.01$ ,  $^*p < 0.05$  versus AdipoR1 siRNA alone.  $n$  indicates the number of patients.

adiponectin in the presence of PEG-catalase [%maximal dilation (MD)  $35.5 \pm 11.1$ ,  $n = 4$ ,  $^{\dagger}p < 0.01$  versus  $83.2 \pm 4.6$ ,  $n = 5$ ; siAdipoR1 alone] whereas L-NAME had no effect (%MD  $74.1 \pm 8.1$ ,  $n = 4$ ), suggesting that the primary mediator remains H<sub>2</sub>O<sub>2</sub> despite treatment with adiponectin. Restoration of NO-mediated FID was achieved in arterioles from patients with disease treated with a negative control siRNA (4 h) prior to adiponectin (16–20 h) as evidenced by significant decreased dilation during exposure to L-NAME (%MD  $35.4 \pm 7.6$ ,  $n = 4$  versus  $80.0 \pm 4.3$ ,  $n = 5$ ; negative control siRNA alone, **Figure 2B**).

## Role of AdipoR1 in Flow-Induced Dilation During Health and Disease

Prior studies have shown that adiponectin receptors have the intrinsic ability to hydrolyze ceramide to sphingosine (Vasiliauskaitė-Brooks et al., 2017) and thus can prevent accumulation of intracellular ceramide. We have previously shown that exogenous ceramide is capable of triggering the transition in FID mediator from NO to H<sub>2</sub>O<sub>2</sub> in arterioles from healthy, nonCAD adults, the same change in mechanism that occurs between health and disease (Freed et al., 2014b). To

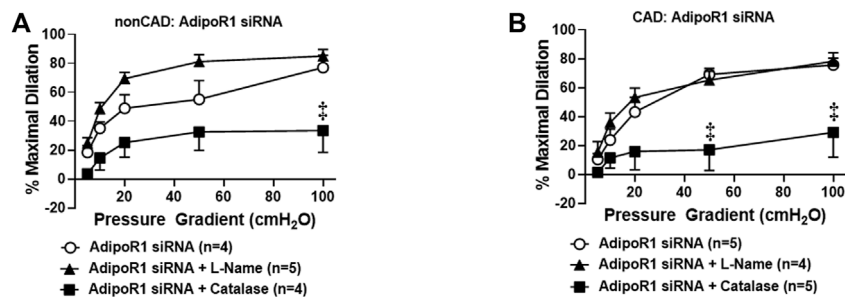


**FIGURE 3 |** Role of AdipoR1 in FID within the human microvasculature. **(A)** FID in nonCAD arterioles with reduced expression of AdipoR1 was significantly impaired in the presence of PEG-catalase ( $n = 4$ ) compared to siAdipoR1 alone ( $n = 4$ ,  $^{\dagger}p < 0.01$ ) whereas L-NAME had no effect ( $n = 5$ ). **(B)** Dilatation to flow in arterioles from CAD subjects treated with siAdipoR1 and PEG-Catalase ( $n = 5$ ) was significantly decreased compared to vessels treated with siAdipoR1 alone ( $n = 6$ ,  $^{\dagger}p < 0.01$ ), however L-NAME had no effect ( $n = 4$ ).

understand the role of adipoR1 in the mediator formed due to flow during health, AdipoR1 expression was decreased in arterioles from nonCAD adults prior to functional analysis. **Figure 3A** illustrates that following knock-down of AdipoR1, FID is impaired in arterioles exposed to PEG-catalase (%MD  $33.4 \pm 15.0$ ,  $n = 4$ ) compared to siAdipoR1 alone (%MD  $77.1 \pm 8.4$ ,  $n = 4$ ,  $^{\dagger}p < 0.01$ ). Treatment with L-NAME had no effect on maximal dilation in response to flow (%MD  $84.9 \pm 4.6$ ,  $n = 5$ ) confirming that decreased expression of AdipoR1 alone may promote H<sub>2</sub>O<sub>2</sub>-dependent FID.

The mechanism of FID was also examined in arterioles from CAD patients treated with siAdipoR1 as shown in **Figure 3B**. Following treatment with siAdipoR1, FID remained dependent on H<sub>2</sub>O<sub>2</sub> as vasodilatory capacity was significantly decreased during exposure to PEG-catalase (%MD  $29.0 \pm 17.2$ ,  $n = 5$ ; PEG-catalase versus  $75.8 \pm 4.6$ ,  $n = 5$ ; siAdipoR1 alone) whereas L-NAME had no effect (%MD  $78.3 \pm 6.0$ ,  $n = 4$ ).

## Osmotin as a Potential Activator of AdipoR1 in the Human Microvasculature

Our prior work has suggested that restoration of NO-mediated FID in arterioles from CAD patients is also achieved using AdipoRON (Schulz et al., 2019), a nonselective activator of AdipoR1 and R2 (Liu et al., 2019; Salvator et al., 2021). Osmotin is a plant-derived protein that has proven crucial to tolerate stress in most fruits and vegetables (Qureshi et al., 2007) and exhibits structural and functional homology with adiponectin (Min et al., 2004). This stress protein activates PHO36, a receptor found in plants and whose homolog in humans is AdipoR1 (Narasimhan et al., 2005). We therefore hypothesized that exogenous treatment with osmotin would restore NO-mediated FID in arterioles from diseased patients, similar to what is observed with exogenous adiponectin. To test this, arterioles from patients with CAD were incubated with osmotin (0.3  $\mu$ M, 16–20 h) prior to functional studies to determine the mediator produced during flow. Here, arterioles from subjects with CAD dilated to flow in the presence of the NO scavenger, cPTIO (%MD  $66.1 \pm 15.2$ ,  $n = 4$ ) or PEG-catalase (%MD  $52.2 \pm 11.8$ ,  $n = 5$ ) compared to osmotin with no inhibitors (%MD  $76.2 \pm 5.9$ ,  $n = 6$ ). Although maximal dilation

was reduced, FID was only significantly impaired when both agents were added simultaneously to the bath (%MD  $46.3 \pm 14.3$ ,  $n = 3$ , **Figure 4A**), suggesting that both of these mediators may be contributing to dilation from flow. The dual mediator phenotype is abolished in CAD vessels treated with both siAdipoR1 and osmotin as L-NAME had no effect on dilation (%MD  $88.7 \pm 8.4$ ,  $n = 4$ , **Figure 4B**) whereas PEG-catalase significantly reduced vasodilatory capacity compared to vessels with no inhibitor present (%MD  $7.6 \pm 5.2$ ,  $n = 4$  versus  $84.3 \pm 2.8$ ,  $n = 5$ , respectively). Interestingly, arterioles from diseased patients treated with negative control siRNA and osmotin did not display the dual mediator phenotype (**Figure 4C**). FID remained dependent on H<sub>2</sub>O<sub>2</sub> as only the presence of PEG-catalase significantly reduced maximal dilation compared to vessels not treated with inhibitors (%MD  $33.2 \pm 11.5$ ,  $n = 5$  versus  $81.7 \pm 5.3$ ,  $n = 5$ , respectively) whereas L-NAME had no effect (%MD  $70.0 \pm 9.3$ ,  $n = 7$ ).

## DISCUSSION

The novel findings of this study are 4-fold; 1) AdipoR1 is present in human peripheral resistance arterioles during both health and disease, 2) the adiponectin-mediated restoration of NO-mediated FID in microvessels from individuals with CAD is dependent on AdipoR1, 3) AdipoR1 expression is necessary to maintain NO as the primary mediator of FID during health whereas loss of AdipoR1 does not impair the ability of an arteriole to dilate to flow during disease, and 4) osmotin, a plant-derived protein whose receptor in plants shares homology with AdipoR1, may potentially serve as an adiponectin receptor activator to improve microvascular endothelial health. Microvascular endothelial dysfunction is considered a precursor to ischemic heart disease and potentially heart failure with preserved ejection fraction (HFpEF) (Paulus and Tschöpe, 2013; Sabbatini and Kararigas, 2020). Strategies which promote a healthy microvascular endothelium therefore may prevent or reverse course of disease. This is the first study to highlight



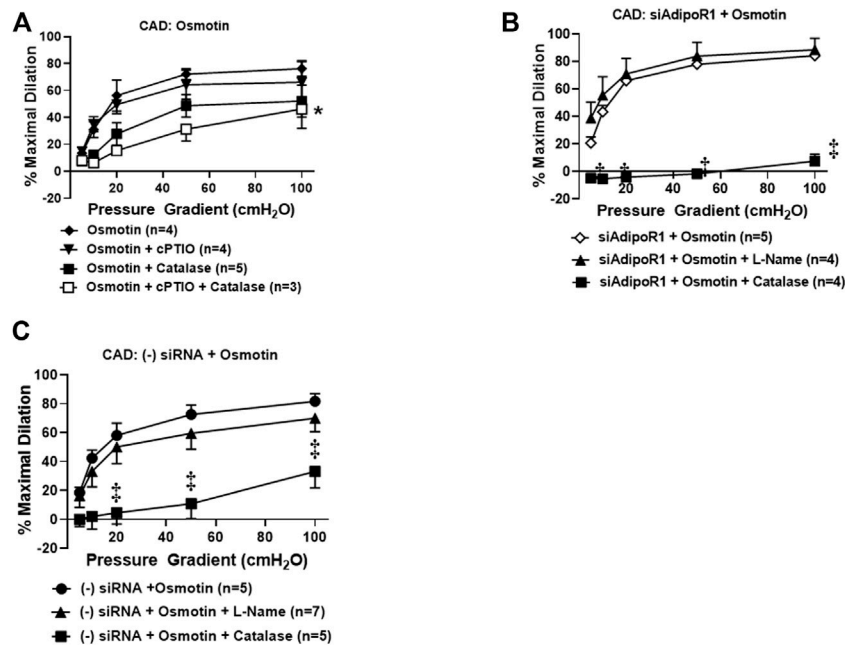


**FIGURE 4 |** Osmotin as potential activator of AdipoR1. **(A)** FID in CAD arterioles treated with osmotin (0.3  $\mu$ M, 16–20 h) was not reduced in the presence of the NO scavenger cPTIO ( $n = 4$ ) or PEG-catalase ( $n = 5$ ). Significant reduction of maximal dilation was only observed with both inhibitors ( $n = 3$ , \* $p < 0.05$ ). **(B)** The effect of osmotin was eliminated in arterioles from CAD patients with reduced expression of AdipoR1 as PEG-catalase significantly decreased overall dilation ( $n = 4$ ) compared to siAdipoR1 and osmotin ( $n = 5$ , † $p < 0.01$ ) whereas L-Name had no effect ( $n = 4$ ). **(C)** The primary mediator of FID remains dependent on H<sub>2</sub>O<sub>2</sub> despite osmotin treatment in arterioles treated with negative control siRNA ( $n = 5$  for both PEG-catalase treated and no inhibitor, ‡ $p < 0.01$ ) as opposed to NO ( $n = 7$ ; L-Name).

the importance of adiponectin receptors, specifically AdipoR1, in restoration and maintenance of a quiescent microvascular endothelium.

## Adiponectin and Vascular Health

Adiponectin is a protein released from adipocytes that exists in three oligomeric forms (high, medium, and low molecular weight) as well as a globular arrangement. The vast majority of studies on adiponectin focus on its role as a regulator of metabolism and energy homeostasis. Hypoadiponectinemia is observed in individuals who are obese, diabetic, and suffering from cardiovascular disease (Pischon et al., 2004). These observations, and the fact that adiponectin has both anti-inflammatory and anti-atherosclerotic effects on arteries (Matsuda et al., 2002; Yamauchi et al., 2003), add strength to the concept that it promotes vascular health. Despite the strong association between low plasma adiponectin and disease, few studies have investigated how the compound affects vascular function *in vivo*. Torigoe et al. demonstrated that reduced HMW adiponectin serves as an independent risk factor for impaired brachial artery flow-mediated dilation (FMD) therefore plasma levels may predict endothelial dysfunction prior to onset of disease (Torigoe et al., 2007), however the findings of this study are limited as it only included healthy men.

Even less is known about the effects of adiponectin on the microvasculature, however we have shown that chronic exposure to either globular adiponectin or AdipoRON, a nonselective adiponectin receptor agonist, restores NO-mediated FID in

arterioles from patients diagnosed with CAD (Schulz et al., 2019). The current study confirms that activation of AdipoR1 is necessary to restore NO as the primary mediator of FID as decreased expression of the receptor abolished the effect. Interestingly, AdipoR1 is expressed in arterioles from both healthy individuals as well as those with CAD. Therefore AdipoR1 may be a potential target to improve microvascular health in times of disease.

## Adiponectin and Nitric Oxide Signaling

Two receptors (AdipoR1/R2) have been identified in endothelial cells, however the expression of AdipoR1 is approximately 5-fold higher compared to AdipoR2 (Addabbo et al., 2011). Direct administration of adiponectin triggers the formation of NO in endothelial cells primarily *via* activation of AMPK, PPAR $\alpha$ , and PI3k/Akt pathways (da Silva Rosa et al., 2021; Cohen et al., 2022). Upon adiponectin binding to AdipoR1/2, an adapter protein known as APPL1 is necessary for these downstream events and subsequent phosphorylation of endothelial nitric oxide synthase (eNOS) at Ser1177 (Dimmeler et al., 1999). Additionally, adiponectin also stimulates Hsp90 binding to eNOS (Xi et al., 2005) and increases bioavailability of tetrahydrobiopterin (Margaritis et al., 2013), both of which promote NO formation. It was more recently discovered that adiponectin receptors themselves have the intrinsic ability to hydrolyze lipids, specifically sphingolipids including ceramide (Holland et al., 2011). When elevated in plasma this stress lipid serves as an independent risk factor for MACE (Havulinna et al., 2016) and is a known trigger of human microvascular endothelial

dysfunction *in vitro*<sup>11</sup>. Intracellular ceramide concentrations increase in the absence of adiponectin receptors and while the receptors have basal ceramidase activity, the breakdown of ceramide to sphingosine increases dramatically (~20-fold) in the presence of adiponectin (Vasiliauskaitė-Brooks et al., 2017). Here we show that not only activation of AdipoR1 is necessary to restore NO-mediated FID, but decreased expression of AdipoR1 alone is sufficient to promote endothelial dysfunction. Vasodilation to flow was maintained and remained dependent on H<sub>2</sub>O<sub>2</sub> in vessels from subjects with CAD suggesting that loss of AdipoR1 does not alter the ability to dilate nor the mechanism of dilation during disease. It is possible that basal ceramidase activity in AdipoR1, the most abundant adiponectin receptor within the endothelium (Addabbo et al., 2011), is critical in preventing ceramide accumulation and the transition to H<sub>2</sub>O<sub>2</sub>-dependent FID.

### AdipoR1 as a Therapeutic Target

Although they do not specifically target adiponectin receptors, medications to treat diabetes may also increase plasma adiponectin. These include metformin as well as thiazolidinediones which are known to increase the HMW form that correlates with cardiovascular disease (Miyazaki et al., 2004; Su et al., 2016). These diabetic medications have proven beneficial effects on the vasculature. For instance, vascular endothelial function, as assessed by acetylcholine-induced dilation, was shown to improve in mesenteric arteries from insulin-resistant rats (Katakam et al., 2000) as well as obese, non-diabetic rats treated with metformin (Lobato et al., 2012). It remains unknown whether the increase in adiponectin is responsible for the beneficial vascular effects observed with metformin and other diabetic medications.

Considerable effort has been directed towards the development of adiponectin receptor agonists as they may offer a treatment strategy for metabolic syndrome. AdipoRON, a nonselective, small molecule adiponectin receptor agonist has emerged as a promising agent as it orally active, and through activation of AdipoR1/2, activates AMPK to reduce fasting glucose in obese mice (Okada-Iwabu et al., 2013) similar to metformin, and even prolong their lifespan (Okada-Iwabu et al., 2013). As with exogenous adiponectin, AdipoRON is also capable of restoring NO-mediated FID in vessels from diseased individuals (Schulz et al., 2019). In addition to small molecule agonists it has been suggested that osmotin, a member of the plant pathogenesis-related (PR) protein family, is capable of activating adiponectin receptors (Narasimhan et al., 2005). Exogenous osmotin (0.1–0.3 μM) has been shown to protect against increases in inflammatory cytokines and improve cell viability in an AdipoR1-dependent manner (Liu et al., 2017). Osmotin itself does not share sequence homology with adiponectin however they do both contain a β-barrel (Min et al., 2004) and the receptors they bind to (PHO36 and AdipoR for osmotin and adiponectin, respectively) share similar sequences. This stress protein is critical for plant survival and is found in almost all plants but is abundant in tomatoes, peppers, and potatoes (Anil Kumar et al., 2015). Osmotin suppresses inflammatory signaling, vascular cell adhesion molecule-1, E-selectin, and significantly decreases atherosclerotic plaque accumulation in ApoE<sup>-/-</sup> following chronic infusion (Takahashi

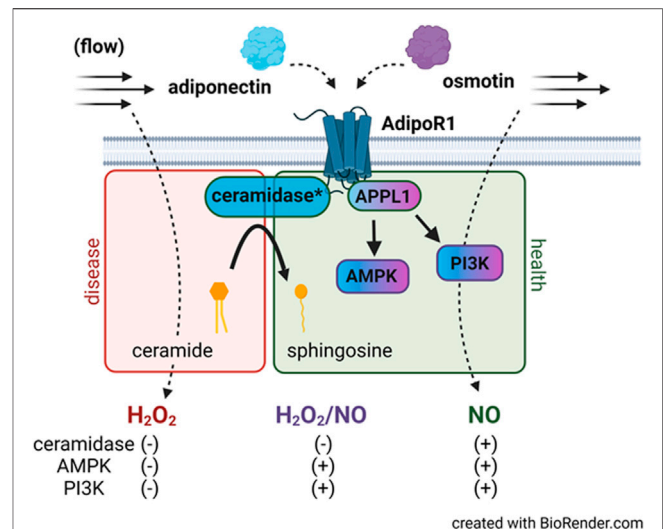


**FIGURE 5 |** AdipoR1 signaling in the microvascular endothelium.

Activation of AdipoR1 by adiponectin (blue) can activate multiple downstream pathways including AMPK and PI3K via the adapter protein APPL1. Adiponectin receptors have intrinsic ceramidase activity that allows for hydrolysis of ceramide to sphingosine. Exogenous adiponectin promotes NO-mediated FID in vessels from patients with CAD while accumulation of ceramide in healthy vessels promotes formation of H<sub>2</sub>O<sub>2</sub> during flow. Osmotin (purple) like adiponectin activates AdipoR1, APPL1, AMPK, and PI3K however dilation to both NO and H<sub>2</sub>O<sub>2</sub> is observed in arterioles from subjects with disease. Whether osmotin is capable of triggering the ceramidase activity in AdipoR1 remains unknown. \*ceramidase activity is within the adiponectin receptor.

et al., 2018). Positive effects have also been confirmed *in vivo* as osmotin through activation of the AdipoR1/2, APPL1, AMPK pathway, reduced blood glucose levels, decreased insulin resistance, and increased fatty acid oxidation and mitochondrial function (Ahmad et al., 2019). Like adiponectin osmotin can also trigger activation of the PI3k/Akt pathway to promote eNOS phosphorylation (Liu et al., 2017).

Here we show that following incubation with osmotin (16 h, 0.3 μM), human arterioles from CAD patients were able to dilate to both NO and H<sub>2</sub>O<sub>2</sub> in response to flow. It was only when both L-Name and PEG-catalase were administered simultaneously that a decrease in FID was observed. This plasticity has also been observed in arterioles treated with both adiponectin and ceranib-1, an inhibitor of ceramidase that promotes ceramide accumulation. Although osmotin has proven beneficial effects and like adiponectin, activates the AdipoR-PI3k/Akt-eNOS pathway, it unknown whether osmotin is capable of inducing ceramidase activity within adiponectin receptors. It is possible that activation of the PI3k/Akt-eNOS pathway is allowing for production of NO during flow however when inhibited, the increased ceramide allows for a compensatory pathway in which H<sub>2</sub>O<sub>2</sub> can be produced to elicit dilation (Figure 5). Although the dose used in this study (0.3 μM) has produced protective effects in cultured endothelial cells, it could be that a higher concentration is needed to achieve complete restoration of NO-mediated FID. Although other studies have shown that siRNA can be used in human vessels without causing damage (Kadlec et al., 2017), it is also plausible that the transfection reagent induces

endothelial dysfunction and the effect of osmotin at this concentration produces a more modest effect than adiponectin. Future studies are needed to determine whether osmotin can trigger ceramidase activity in adiponectin receptors and effectively reduce ceramide levels to improve (micro)vascular function.

## CONCLUSION

The data presented here highlights the importance of AdipoR1 in promoting NO-mediated signaling during flow within the human microvasculature. Endothelial dysfunction within the microvascular network is increasingly recognized as the driver of future large artery disease and cardiac events. Although vasodilation to flow can occur *via* either NO or H<sub>2</sub>O<sub>2</sub>, the effects that each compound has on the surrounding parenchyma is drastically different with the preferred mediator being the anti-inflammatory and anti-atherosclerotic NO. Interventions to treat endothelial dysfunction and restore NO as the primary substance formed during shear may offer an effective treatment strategy to prevent future heart disease. AdipoR1 receptors are present in human arterioles during health and disease and their presence appears critical to maintain NO-mediated FID. AdipoR1 activation can occur through administration of small molecule agonists (AdipoRON) and possibly plant-derived proteins such as osmotin. NO signaling during flow may be promoted by osmotin results in a dual mediator phenotype that may offer plasticity in FID signaling during times of decreased NO bioavailability.

## REFERENCES

- Addabbo, F., Nacci, C., De Benedictis, L., Leo, V., Tarquinio, M., Quon, M. J., et al. (2011). Globular Adiponectin Counteracts VCAM-1-Mediated Monocyte Adhesion *via* AdipoR1/NF-KB/cox-2 Signaling in Human Aortic Endothelial Cells. *Am. J. Physiol. Endocrinol. Metab.* 301, E1143–E1154. doi:10.1152/ajpendo.00208.2011
- Ahmad, A., Ali, T., Kim, M. W., Khan, A., Jo, M. H., Rehman, S. U., et al. (2019). Adiponectin Homolog Novel Osmotin Protects Obesity/diabetes-Induced NAFLD by Upregulating AdipoRs/PPARα Signaling in Ob/ob and Db/db Transgenic Mouse Models. *Metabolism* 90, 31–43. doi:10.1016/j.metabol.2018.10.004
- Akhiyat, N., Vasile, V., Jaffe, A., and Lerman, A. (2021). Plasma Ceramide Levels Are Elevated in Patients with Early Coronary Atherosclerosis and Microvascular Endothelial Dysfunction. *J. Am. Coll. Cardiol.* 77, 164. doi:10.1016/s0735-1097(21)01523-0
- Anil Kumar, S., Hima Kumari, P., Shravan Kumar, G., Mohanalatha, C., and Kavi Kishor, P. B. (2015). Osmotin: a Plant sentinel and a Possible Agonist of Mammalian Adiponectin. *Front. Plant Sci.* 6, 163. doi:10.3389/fpls.2015.00163
- Cohen, K. E., Katunarić, B., SenthilKumar, G., McIntosh, J. J., and Freed, J. K. (2022). Vascular Endothelial Adiponectin Signaling across the Life Span. *Am. J. Physiol. Heart Circ. Physiol.* 322, H57–H65. doi:10.1152/ajpheart.00533.2021
- da Silva Rosa, S. C., Liu, M., and Sweeney, G. (2021). Adiponectin Synthesis, Secretion and Extravasation from Circulation to Interstitial Space. *Physiology (Bethesda)* 36, 134–149. doi:10.1152/physiol.00031.2020
- Dimmeler, S., Fleming, I., Fisslthaler, B., Hermann, C., Busse, R., and Zeiher, A. M. (1999). Activation of Nitric Oxide Synthase in Endothelial Cells by Akt-dependent Phosphorylation. *Nature* 399, 601–605. doi:10.1038/21224
- Freed, J. K., Beyer, A. M., LoGiudice, J. A., Hockenberry, J. C., and Gutterman, D. D. (2014). Ceramide Changes the Mediator of Flow-Induced Vasodilation from

## DATA AVAILABILITY STATEMENT

The original contributions presented in the study are included in the article/Supplementary Material, further inquiries can be directed to the corresponding author.

## AUTHOR CONTRIBUTIONS

KEC, BK, MES, GS, MSY, and JKF contributed to the research design, execution of experiments, and data analysis. KEC, BK, MES, GS, MSY, JEM, and JKF contributed to the assembly and final editing of the manuscript.

## FUNDING

This work was supported by a National Institutes of Health K08 HL141562 (JKF) and a R38 HL143561 (M.E.W. and M.E.).

## ACKNOWLEDGMENTS

The authors wish to thank the surgeons and nurses at Froedtert Memorial Lutheran Hospital and the Ascension Healthcare Group for assistance in providing human tissue as well as the Children's Research Institute (CRI) histology core for assistance with the immunofluorescence studies.

- Nitric Oxide to Hydrogen Peroxide in the Human Microcirculation. *Circ. Res.* 115, 525–532. doi:10.1161/CIRCRESAHA.115.303881
- Freed, J. K., Beyer, A. M., LoGiudice, J. A., Hockenberry, J. C., and Gutterman, D. D. (2014). Ceramide Changes the Mediator of Flow-Induced Vasodilation from Nitric Oxide to Hydrogen Peroxide in the Human Microcirculation. *Circ. Res.* 115, 525–532. doi:10.1161/CIRCRESAHA.115.303881
- Hattori, Y., Suzuki, M., Hattori, S., and Kasai, K. (2003). Globular Adiponectin Upregulates Nitric Oxide Production in Vascular Endothelial Cells. *Diabetologia* 46, 1543–1549. doi:10.1007/s00125-003-1224-3
- Havulinna, A. S., Sysi-Aho, M., Hilvo, M., Kauhanen, D., Hurme, R., Ekroos, K., et al. (2016). Circulating Ceramides Predict Cardiovascular Outcomes in the Population-Based FINRISK 2002 Cohort. *Arterioscler Thromb. Vasc. Biol.* 36, 2424–2430. doi:10.1161/ATVBAHA.116.307497
- Holland, W. L., Miller, R. A., Wang, Z. V., Sun, K., Barth, B. M., Bui, H. H., et al. (2011). Receptor-mediated Activation of Ceramidase Activity Initiates the Pleiotropic Actions of Adiponectin. *Nat. Med.* 17, 55–63. doi:10.1038/nm.2277
- Kadlec, A. O., Chabowski, D. S., Ait-Aissa, K., Hockenberry, J. C., Otterson, M. F., Durand, M. J., et al. (2017). PGC-1α (Peroxisome Proliferator-Activated Receptor γ Coactivator 1-α) Overexpression in Coronary Artery Disease Recruits NO and Hydrogen Peroxide during Flow-Mediated Dilation and Protects against Increased Intraluminal Pressure. *Hypertension* 70, 166–173. doi:10.1161/hypertensionaha.117.09289
- Katakam, P. V., Ujhelyi, M. R., Hoenig, M., and Miller, A. W. (2000). Metformin Improves Vascular Function in Insulin-Resistant Rats. *Hypertension* 35, 108–112. doi:10.1161/01.hyp.35.1.108
- Kuo, L., Davis, M. J., and Chilian, W. M. (1990). Endothelium-dependent, Flow-Induced Dilation of Isolated Coronary Arterioles. *Am. J. Physiol.* 259, H1063–H1070. doi:10.1152/ajpheart.1990.259.4.H1063
- Liu, B., Liu, J., Wang, J., Sun, F., Jiang, S., Hu, F., et al. (2019). Adiponectin Protects against Cerebral Ischemic Injury through AdipoR1/AMPK Pathways. *Front. Pharmacol.* 10, 597. doi:10.3389/fphar.2019.00597

- Liu, J., Sui, H., Zhao, J., and Wang, Y. (2017). Osmotin Protects H9c2 Cells from Simulated Ischemia-Reperfusion Injury through AdipoR1/PI3K/AKT Signaling Pathway. *Front. Physiol.* 8, 611. doi:10.3389/fphys.2017.00611
- Lobato, N. S., Filgueira, F. P., Hagihara, G. N., Akamine, E. H., Pariz, J. R., Tostes, R. C., et al. (2012). Improvement of Metabolic Parameters and Vascular Function by Metformin in Obese Non-diabetic Rats. *Life Sci.* 90, 228–235. doi:10.1016/j.lfs.2011.11.005
- Margaritis, M., Antonopoulos, A. S., Digby, J., Lee, R., Reilly, S., Coutinho, P., et al. (2013). Interactions between Vascular wall and Perivascular Adipose Tissue Reveal Novel Roles for Adiponectin in the Regulation of Endothelial Nitric Oxide Synthase Function in Human Vessels. *Circulation* 127, 2209–2221. doi:10.1161/CIRCULATIONAHA.112.001133
- Matsuda, M., Shimomura, I., Sata, M., Arita, Y., Nishida, M., Maeda, N., et al. (2002). Role of Adiponectin in Preventing Vascular Stenosis. The Missing Link of Adipo-Vascular axis. *J. Biol. Chem.* 277, 37487–37491. doi:10.1074/jbc.M206083200
- Min, K., Ha, S. C., Hasegawa, P. M., Bressan, R. A., Yun, D. J., and Kim, K. K. (2004). Crystal Structure of Osmotin, a Plant Antifungal Protein. *Proteins* 54, 170–173. doi:10.1002/prot.10571
- Miura, H., Bosnjak, J. J., Ning, G., Saito, T., Miura, M., and Gutterman, D. D. (2003). Role for Hydrogen Peroxide in Flow-Induced Dilation of Human Coronary Arterioles. *Circ. Res.* 92, e31–40. doi:10.1161/01.res.0000054200.44505.ab
- Miyazaki, Y., Mahankali, A., Wajsborg, E., Bajaj, M., Mandarino, L. J., and DeFronzo, R. A. (2004). Effect of Pioglitazone on Circulating Adipocytokine Levels and Insulin Sensitivity in Type 2 Diabetic Patients. *J. Clin. Endocrinol. Metab.* 89, 4312–4319. doi:10.1210/jc.2004-0190
- Narasimhan, M. L., Coca, M. A., Jin, J., Yamauchi, T., Ito, Y., Kadowaki, T., et al. (2005). Osmotin Is a Homolog of Mammalian Adiponectin and Controls Apoptosis in Yeast through a Homolog of Mammalian Adiponectin Receptor. *Mol. Cell* 17, 171–180. doi:10.1016/j.molcel.2004.11.050
- Okada-Iwabu, M., Yamauchi, T., Iwabu, M., Honma, T., Hamagami, K., Matsuda, K., et al. (2013). A Small-Molecule AdipoR Agonist for Type 2 Diabetes and Short Life in Obesity. *Nature* 503, 493–499. doi:10.1038/nature12656
- Paulus, W. J., and Tschöpe, C. (2013). A Novel Paradigm for Heart Failure with Preserved Ejection Fraction: Comorbidities Drive Myocardial Dysfunction and Remodeling through Coronary Microvascular Endothelial Inflammation. *J. Am. Coll. Cardiol.* 62, 263–271. doi:10.1016/j.jacc.2013.02.092
- Pischon, T., Girman, C. J., Hotamisligil, G. S., Rifai, N., Hu, F. B., and Rimm, E. B. (2004). Plasma Adiponectin Levels and Risk of Myocardial Infarction in Men. *JAMA* 291, 1730–1737. doi:10.1001/jama.291.14.1730
- Qureshi, M. I., Qadir, S., and Zolla, L. (2007). Proteomics-based Dissection of Stress-Responsive Pathways in Plants. *J. Plant Physiol.* 164, 1239–1260. doi:10.1016/j.jplph.2007.01.013
- Sabbatini, A. R., and Kararigas, G. (2020). Menopause-Related Estrogen Decrease and the Pathogenesis of HFpEF: JACC Review Topic of the Week. *J. Am. Coll. Cardiol.* 75, 1074–1082. doi:10.1016/j.jacc.2019.12.049
- Salvator, H., Grassin-Delyle, S., Brollo, M., Couderc, L. J., Abrial, C., Victoni, T., et al. (2021). Adiponectin Inhibits the Production of TNF- $\alpha$ , IL-6 and Chemokines by Human Lung Macrophages. *Front. Pharmacol.* 12, 718929. doi:10.3389/fphar.2021.718929
- Schulz, M. E., Katunarić, B., Hockenberry, J. C., Gutterman, D. D., and Freed, J. K. (2019). Manipulation of the Sphingolipid Rheostat Influences the Mediator of Flow-Induced Dilation in the Human Microvasculature. *J. Am. Heart Assoc.* 8, e013153. doi:10.1161/JAHA.119.013153
- Su, J. R., Lu, Z. H., Su, Y., Zhao, N., Dong, C. L., Sun, L., et al. (2016). Relationship of Serum Adiponectin Levels and Metformin Therapy in Patients with Type 2 Diabetes. *Horm. Metab. Res.* 48, 92–98. doi:10.1055/s-0035-1569287
- Takahashi, Y., Watanabe, R., Sato, Y., Ozawa, N., Kojima, M., Watanabe-Kominato, K., et al. (2018). Novel Phytopeptide Osmotin Mimics Preventive Effects of Adiponectin on Vascular Inflammation and Atherosclerosis. *Metabolism* 83, 128–138. doi:10.1016/j.metabol.2018.01.010
- Torigoe, M., Matsui, H., Ogawa, Y., Murakami, H., Murakami, R., Cheng, X. W., et al. (2007). Impact of the High-Molecular-Weight Form of Adiponectin on Endothelial Function in Healthy Young Men. *Clin. Endocrinol. (Oxf)* 67, 276–281. doi:10.1111/j.1365-2265.2007.02876.x
- TPvd, Hoef, MAV, Lavieren, Damman, P., Delewi, R., Piek, M. A., Chamuleau, S. A. J., et al. (2014). Physiological Basis and Long-Term Clinical Outcome of Discordance between Fractional Flow Reserve and Coronary Flow Velocity Reserve in Coronary Stenoses of Intermediate Severity. *Circ. Cardiovasc. Interventions* 7, 301–311.
- Vasiliauskaitė-Brooks, I., Sounier, R., Rochaix, P., Bellot, G., Fortier, M., Hoh, F., et al. (2017). Structural Insights into Adiponectin Receptors Suggest Ceramidase Activity. *Nature* 544, 120–123. doi:10.1038/nature21714
- Xi, W., Satoh, H., Kase, H., Suzuki, K., and Hattori, Y. (2005). Stimulated HSP90 Binding to eNOS and Activation of the PI3-Akt Pathway Contribute to Globular Adiponectin-Induced NO Production: Vasorelaxation in Response to Globular Adiponectin. *Biochem. Biophys. Res. Commun.* 332, 200–205. doi:10.1016/j.bbrc.2005.04.111
- Yamauchi, T., Kamon, J., Waki, H., Imai, Y., Shimozawa, N., Hioki, K., et al. (2003). Globular Adiponectin Protected Ob/ob Mice from Diabetes and ApoE-Deficient Mice from Atherosclerosis. *J. Biol. Chem.* 278, 2461–2468. doi:10.1074/jbc.M209033200

**Conflict of Interest:** The authors declare that the research was conducted in the absence of any commercial or financial relationships that could be construed as a potential conflict of interest.

**Publisher's Note:** All claims expressed in this article are solely those of the authors and do not necessarily represent those of their affiliated organizations, or those of the publisher, the editors and the reviewers. Any product that may be evaluated in this article, or claim that may be made by its manufacturer, is not guaranteed or endorsed by the publisher.

Copyright © 2022 Cohen, Katunarić, Schulz, SenthilKumar, Young, Mace and Freed. This is an open-access article distributed under the terms of the Creative Commons Attribution License (CC BY). The use, distribution or reproduction in other forums is permitted, provided the original author(s) and the copyright owner(s) are credited and that the original publication in this journal is cited, in accordance with accepted academic practice. No use, distribution or reproduction is permitted which does not comply with these terms.





# Farrerol Alleviates Myocardial Ischemia/Reperfusion Injury by Targeting Macrophages and NLRP3

Lin Zhou<sup>1,2</sup>, Shuhui Yang<sup>3</sup> and Xiaoming Zou<sup>1\*</sup>

<sup>1</sup>The Fifth Affiliated Hospital, Southern Medical University, Guangzhou, China, <sup>2</sup>Department of Thoracic Surgery, Yuebei People's Hospital Affiliated to Shantou University Medical College, Shaoguan, China, <sup>3</sup>Department of Pathology, Yuebei People's Hospital Affiliated to Shantou University Medical College, Shaoguan, China

## OPEN ACCESS

### Edited by:

Xianwei Wang,  
Xinxiang Medical University, China

### Reviewed by:

Mohammad H. Abukhalil,  
Al-Hussein Bin Talal University, Jordan  
Yerra Koteswara Rao,  
National Biotechnology Research Park  
(NBRP), Taiwan

### \*Correspondence:

Xiaoming Zou  
nanfangxm\_z@163.com

### Specialty section:

This article was submitted to  
Cardiovascular and Smooth Muscle  
Pharmacology,  
a section of the journal  
Frontiers in Pharmacology

**Received:** 19 February 2022

**Accepted:** 28 March 2022

**Published:** 13 April 2022

### Citation:

Zhou L, Yang S and Zou X (2022)  
Farrerol Alleviates Myocardial  
Ischemia/Reperfusion Injury by  
Targeting Macrophages and NLRP3.  
Front. Pharmacol. 13:879232.  
doi: 10.3389/fphar.2022.879232

Myocardial ischemia/reperfusion (I/R) injury is associated with high mortality and morbidity, however, it has no curative treatment. Farrerol (FA), an active compound extracted from rhododendron, has antibacterial, anti-inflammatory, and antioxidant activities, but its effect and mechanism of FA in I/R injury remain unclear. Here, we found that FA alleviated myocardial I/R *in vivo*, and decreased the secretion of myocardial injury factors (CK-MB, LDH, troponin-1, and NT-proBNP) while inhibiting the release of inflammatory factors (IL-1 $\beta$ , IL-6, and TNF- $\alpha$ ). FA could also alleviate excessive oxidative stress by elevating the level of antioxidant enzymes and reducing oxidation products; and decreased reduced the expression of apoptosis-associated proteins (cleaved caspase-3, Bax, and Bcl-2). However, inhibiting the autophagic pathway or knocking out the *Nrf2* gene did not eliminate the myocardial protective effect of FA, but interestingly, macrophage clearance and *Nlrp3* deficiency effectively blocked the myocardial protective effect of FA. In addition, FA suppressed NLRP3 inflammasome activation by interfering with NLRP3 and NEK7. In conclusion, these results support drug-targeted macrophage therapy for myocardial I/R and indicate that FA may be used as an immunomodulator in clinical therapy for myocardial I/R.

**Keywords:** myocardial ischemia/reperfusion, farrerol, macrophage, NLRP3, NEK7

## INTRODUCTION

Myocardial ischemia/reperfusion (I/R) injury is a pathological process of progressive aggravation of tissue injury when the ischemic myocardium is restored to normal perfusion after a period of partial or complete acute coronary artery occlusion. According to the World Health Statistics 2021 report, 33.2 million deaths from the four major chronic diseases (cancer, cardiovascular disease (CVD), diabetes, and chronic respiratory disease) occurred in 2019; of which 17.9 million died from cardiovascular disease, ranking the highest mortality rate. The previous studies found that myocardial I/R injury is a major obstacle in CVD therapy (Maarman et al., 2012; Ait-Aissa et al., 2019). Currently, myocardial infarction is the leading cause of CVD-associated death worldwide (Zagidullin et al., 2020). Myocardial I/R causes oxidative stress and inflammation, thus increasing the infarct size and aggravating myocardial injury (Venkatachalam et al., 2009; Yeung et al., 2015). To date, clinical treatment methods to avoid myocardial I/R injury are lacking, thus hindering coronary heart disease therapy. Therefore, studying the pathophysiological mechanism of I/R is important to find effective prevention and treatment methods, and develop new therapeutic drugs to improve the prognosis of patients with coronary heart disease.

Many studies have examined the mechanism of I/R injury; which is mainly thought to be associated with the inflammatory effects of the massive production of intracellular oxygen free radicals, calcium overloading, the inflammatory effects of leukocytes, and the absence of high-energy phosphoric compounds (Kalogeris et al., 2012; Yan et al., 2020). I/R injury is characterized by the massive generation of free radicals, mitochondrial dysfunction, increased lipid peroxides, myocardial cell necrosis, apoptosis, weakened left ventricular contractility, malignant arrhythmias, decreased indoor pressure, and myocardial function inhibition (Ibáñez et al., 2015; Dong et al., 2019). Previous studies have shown that drug-activated nuclear factor erythroid 2-associated factor 2 (NRF2) protects against myocardial oxidative stress and myocardial injury (Shen et al., 2019). Autophagy protects I/R-induced myocardial injury by activating the AMPK protein kinase, thus decreasing apoptosis (Shi et al., 2019). In addition, blocking the release of proinflammatory cytokines from macrophages decreases cardiac inflammation (Frangogiannis, 2014). In contrast, macrophage-induced inflammation also mediates the progression of I/R, in which NLRP3 inflammasome activation is a major mechanism inducing inflammation (Nazir et al., 2017; Zhang T et al., 2020).

Farrerol (FA), naturally found in *Rhododendron dauricum* L. leaves, is a dihydro flavonoid active substance with antibacterial, anti-inflammatory, antioxidant, and other biological activities (Li et al., 2013; Ran et al., 2018; Li et al., 2019). Given its strong anti-inflammatory and antioxidant effects, it may have a protective effect against myocardial I/R injury. Therefore, this study explored whether FA might protect the heart against I/R-induced cardiac injury, and clarified the potential mechanism of FA by examining a variety of signaling pathways.

## MATERIALS AND METHODS

### Reagents

FA (95403-16), adenosine triphosphate (ATP) (A2383), lipopolysaccharide (LPS) (L7770), anti-Flag (F2555), anti-VSV (V4888), and anti-GAPDH (G9545) were purchased from Sigma. Anti-NLPR3 (AG-20B-0014) and anti-Caspase-1 (P20) (AG-20B-0042) were purchased from AdipoGen. Anti-IL-1 $\beta$  (P17) (AF-401-NA) was purchased from R&D Systems. anti-LC3B (A19665), anti-Nrf2 (A1244), anti-pro-Caspase-1 (A16792), anti-Cleaved Caspase-3 (A11021), and anti-pro-IL-1 $\beta$  (A11369) were purchased from Abclonal. anti-Cleaved PARP1 (sc-56196), anti-Bcl2 (sc-7382), anti-Bax (sc-7480), anti-ATG3 (sc-393660), anti-ASC (sc-514414), and anti-NEK7 (sc-393539) were obtained from Santa Cruz Biotechnology.

### Animals and Drug Treatments

The experimental procedure and protocol were approved by the Ethical Use Committee of Shantou University. Wild-type (WT) mice, and *Nrf2*<sup>-/-</sup> and *Nlrp3*<sup>-/-</sup> mice in a C57BL/6J background were purchased from GemPharmatech. C57BL/6J mice were administered FA or an equal volume of carrier 7 days before reperfusion. The mice were divided into five groups: 1) Sham

group ( $n = 10$ ), this group only received simple skin incision; 2) I/R group ( $n = 10$ ), C57BL/6J mice were injected with normal saline at the same dose for 7 days before I/R; 3) I/R + FA (10 mg/kg/day) group ( $n = 10$ ); 4) I/R + FA (40 mg/kg/day) group ( $n = 10$ ); 5) FA group, C57BL/6J mice were intraperitoneally injected with FA (40 mg/kg/day) for 7 days before I/R.

To explore whether FA might play a protective role in the myocardium through the NRF2 pathway, we divided *Nrf2*<sup>-/-</sup> mice into four groups: a WT (I/R) group ( $n = 10$ ), WT (I/R + FA) group ( $n = 10$ ), *Nrf2*<sup>-/-</sup> (I/R) group ( $n = 10$ ), and *Nrf2*<sup>-/-</sup> (I/R + FA) group ( $n = 10$ ). The FA group was intraperitoneally injected with FA (40 mg/kg/day) for 7 days before I/R, and the other groups were injected with the same volume of normal saline.

To explore whether FA might play a protective role in the myocardium through the autophagy-dependent pathway, we injected 3-methyladenine (3-MA) (Xia et al., 2021) (30 mg/kg) followed by 40 mg/kg FA administered 2 h afterward daily for 7 days.

In the macrophage clearance experiment, mice were pretreated with clodronate liposomes (van Rooijen and van Kesteren-Hendriks, 2002; Moreno, 2018) (200  $\mu$ l/mouse) or control liposomes daily, followed by 40 mg/kg of FA for 7 days.

### I/R Model

Myocardial I/R injury models of C57BL/6J, *Nrf2*<sup>-/-</sup>, and *Nlrp3*<sup>-/-</sup> mice were established as described previously (Zhao et al., 2019). In brief, mice were anesthetized by intraperitoneal injection of pentobarbital sodium at 50 mg/kg. Open the neck first, expose the trachea, and connect the small animal ventilator visually. Needle electrodes were fixed under the skin of the limbs of mice to monitor the changes in limb lead II electrocardiograms. Open the thoracic cavity layer by layer between the third and fourth intercostal space of the left chest. The pericardium was separated, and the heart was exposed. The left anterior descending artery was ligated with silk thread and a PE10 tube for 30 min. After 30 min of ischemia, the PE10 suture was removed. After 24 h of reperfusion, the blood and hearts of mice were collected for testing of various indexes. Mice in the sham operation group underwent the same procedure as those in the model group, but only the silk thread was retained under the left anterior descending artery without ligation or reperfusion.

### Cell Culture and Extraction of Cell Supernatant Protein

Bone marrow cells from the femur and tibia in C57BL/6J mice were collected. Bone marrow-derived macrophages (BMDM) were cultured and differentiated in RPMI-1640 medium containing 10% fetal bovine serum, 2 mM L-glutamine, 1 mM sodium pyruvate, and 50 ng/ml mouse macrophage cluster stimulating factor for 7 days. To extract cell supernatant proteins, cell supernatants were collected and centrifuged at 1,000 g for 5 min. After dead cells were removed, 600  $\mu$ l of supernatant was carefully transferred to another clean EP tube. An equal volume of pre-cooled methanol and 1/4 volume of chloroform were added and vortexed. The supernatant was

**TABLE 1** | Primer for real-time RT-PCR was used in this study.

Gene	Sequences	Species
<i>Il-1b</i>	Forward: CACAGCAGCACATCAACAAG Reverse: GTGCTCATGTCTCATCTCTG	Mouse
<i>Il-6</i>	Forward: CTCTGGGAAATCGTGGAAT Reverse: CCAGTTTGGTAGCATCCATC	Mouse
<i>Tnfa</i>	Forward: GACGTGGAAGTGGCAGAAAGAG Reverse: TTGGTGGTTGTGAGTGTGAG	Mouse
<i>Gapdh</i>	Forward: AGGTCCGTGTGAACGGATTG Reverse: TGTAGACCATGTAGTTGAGGTCA	Mouse

aspirated, 500 µl of pre-cooled methanol was added and vortexed, and the tubes were centrifuged at 13,000 r/min for 5 min. The supernatant was carefully removed and discarded. The EP tube loaded with precipitate was placed in a drying chamber at 37°C for 5 min and dissolved in 30 µl 2.5× loading buffer. After boiling at 95°C for 5 min, samples were loaded for western blot analysis.

## H&E Staining

The heart tissues from each group of mice were fixed with 4% paraformaldehyde overnight at 4°C and embedded in paraffin. The paraffin was sliced 5 µm thick and incubated with hematoxylin and eosin (H&E) with an H&E staining kit (C0105S, Beyotime, China) according to the manufacturer's protocol.

## Enzyme-Linked Immunosorbent Assay

The expression of CK-MB (MU30025, Bioswamp, China), LDH (MU30023, Bioswamp, China), troponin-1 (MU30421, Bioswamp, China), NT-proBNP (MU30252, Bioswamp, China), IL-1β (MU30369, Bioswamp, China), IL-6 (MU30044, Bioswamp, China), and TNF-α (MU30030, Bioswamp, China) in cells, tissues, or serum samples was determined with an ELISA kit according to the kit instructions.

## RT-qPCR

The relative expression of *Il-b*, *Il-6*, *Tnfa*, and *F4/80* in cells and tissues was detected by RT-qPCR. TRIzol reagent was used to extract total RNA from cells and tissues. First-strand cDNA was generated with a Reverse Transcription System Kit (Thermo Fisher Scientific), and RT-qPCR was performed with an SYBR Green PCR kit (Thermo Fisher Scientific) according to the manufacturer's instructions. All qRT-PCR was performed on a Biosystems 7300 Real-Time PCR system (Thermo Fisher Scientific). Relative gene expression levels were calculated with the  $2^{-\Delta\Delta C_t}$  method. The primer sequences are shown in Table 1.

## Assessment of Oxidative Stress in Heart Tissue

Mice in each experimental group were euthanized, and the hearts were removed and washed retrogradely with Krebs-Ringer solution maintained at 37°C. The hearts were then weighed, and the cardiac tissue was homogenized on ice in chilled phosphate-buffered saline (PBS) containing 1 mM EDTA. Centrifuge at 7,000 rpm/min for 10 min. Measure the protein

concentration of the supernatant. The supernatant was used to analyze lipid peroxidation levels and glutathione peroxidase (GSH-Px), superoxide dismutase (SOD), and malondialdehyde (MDA) levels. The vascular nicotinamide adenine dinucleotide phosphate (NADPH) oxidase is a major source of ROS and the NOX4 is the major NAD(P)H oxidase isoform in cardiomyocytes, so we use Western blotting to detect the expression level of NOX4.

## Western Blot Analysis

Total protein was isolated from tissues and cells with 1× radioimmunoprecipitation assay (RIPA) buffer containing phosphatase and protease inhibitors. After protein concentrations were determined, samples were separated by SDS-PAGE and transferred to a PVDF membrane. The membrane was blocked in Tris-buffered saline-Tween 20 (TBST) buffer containing 5% BSA for 1 h, and incubated with primary antibody (anti-Flag (1:500), anti-VSV (1:1,000), anti-GAPDH (1:10,000), Anti-NLPR3 (1:500), Anti-caspase-1 (P20) (1:1,000), Anti-IL-1β (P17) (1:1,000), Anti-LC3B (1:1,000), anti-Nrf2 (1:1,000), Anti-pro-caspase-1 (1:1,000), anti-pro-interleukin-1β (pro-IL-1β) (1:1,000), Anti-PARP1 (1:1,000), anti-Bcl2 (1:1,000), anti-Bax (1:1,000), anti-ATG3 (1:1,000), anti-ASC (1:1,000), Anti-caspase-1 (1:1,000), and anti-NEK7 (1:1,000).) at 4°C overnight. After being washed with TBST buffer three times, membranes were incubated with HRP labeled mouse or rabbit secondary antibody (1:5,000 diluted) at room temperature for 1.5 h. They were then incubated on a shaker for 1 h. The membranes were then washed with TBST five times for 5 min each. Chemiluminescence reagent was used for luminescence development. The analysis was performed with Quantity One 4.4 software.

## Immunoprecipitation

For endogenous interaction, BMDM cells in each experimental group were lysed in NP-40 buffer mixed with protease inhibitors and centrifuged at 4°C for 15 min. The cell lysates were collected and incubated with IP antibodies [NEK7 (1:100) or ASC (1:100)] overnight at 4°C. Protein A/G beads were added and incubated for 4 h at 4°C. Protein A/G beads pulled down the target protein for detection using Western blotting. For exogenous interaction, HEK-293T cells were transfected with Lipofectamine 2000 according to the kit instructions. After 24 h, cells were collected and lysed in NP-40 buffer mixed with protease inhibitors. Cell lysates were immunoprecipitated with the anti-Flag agarose gels (1:100, Sigma, A2220) and detected using Western blotting.

## Statistical Analysis

Results are shown as mean ± standard deviation from three independent experiments or are representative of three independent experiments. SPSS19.0 software was used for statistical analysis. For most experiments, differences between the two groups were assessed using two-tailed unpaired Student's t-tests and one-way analysis of variance. Non-parametric Mann-Whitney tests were used to compare the differences between more than two groups when the variances were significantly different. If a *p*-value was <0.05, the difference was considered statistically significant.

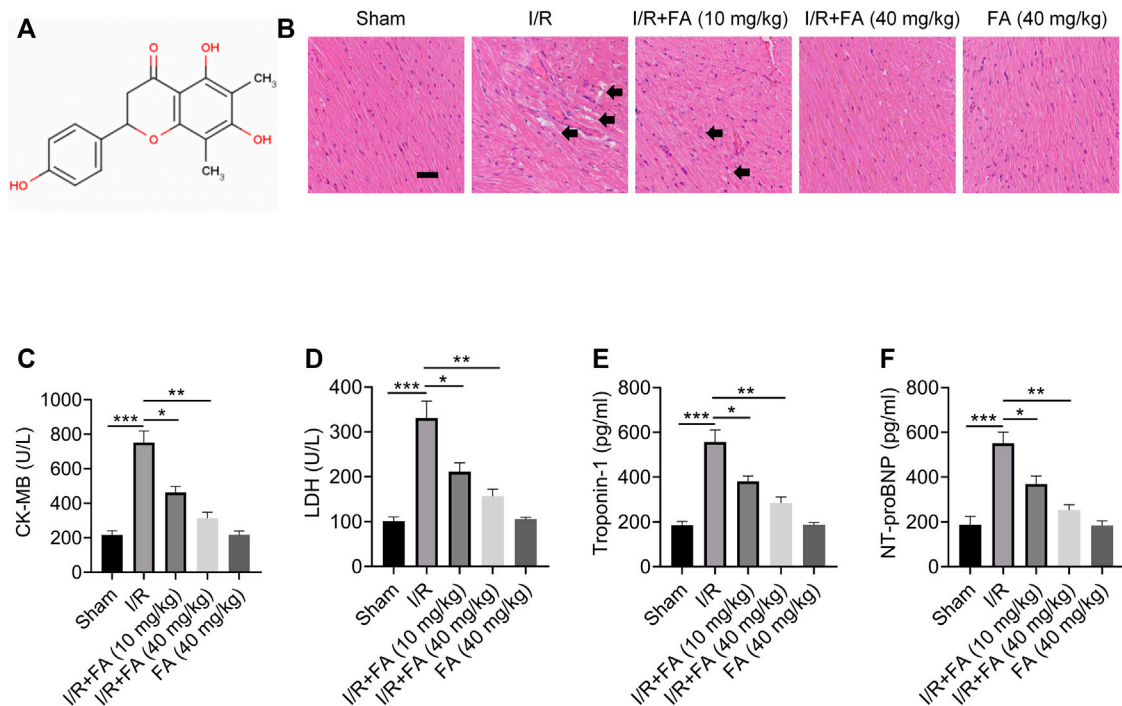


**FIGURE 1 |** The protective effect of FA against I/R-induced myocardial injury in mice. **(A)** Chemical structural formula of FA. **(B)** HE staining results of heart tissue sections in each experimental group of WT mice. **(C–F)** Expression of CK-MB, LDH, troponin-1, and NT-proBNP in the serum in each experimental group of WT mice, detected by ELISA. Data are expressed as the means  $\pm$  sd from three independent experiments. \* $p < 0.05$ , \*\* $p < 0.01$ , and \*\*\* $p < 0.001$ .

## RESULTS

### FA Has a Protective Effect Against I/R-Induced Myocardial Injury in Mice

After the successful establishment of the mouse model, treatment with FA (structure in **Figure 1A**) was performed. HE staining results indicated significant injury in the I/R group, whereas the I/R + FA (10 mg/kg or 40 mg/kg) treatment group showed significantly less histological injury caused by I/R (**Figure 1B**). In addition, FA significantly decreased the expression of CK-MB, LDH, troponin-1, and NT-proBNP induced by I/R, and FA alone treatment group did not affect the heart, immune system, and other tissue functions in healthy mice (**Figures 1C–F**). Therefore, FA effectively protects against I/R-induced myocardial injury.

### FA Alleviates the Inflammatory Response to I/R-Induced Myocardial Injury in Mice

As shown in **Figure 2**, I/R treatment increased the expression of IL-1 $\beta$ , IL-6, and TNF- $\alpha$  in the serum, whereas FA treatment decreased the expression of these inflammatory factors (**Figure 2A–C**). In addition, the RT-qPCR I/R treatment significantly upregulated the mRNA levels of these inflammatory factors in the heart tissues, while FA treatment significantly decreased their expression (**Figures 2D–F**). Thus, FA alleviates the inflammatory response that leads to myocardial injury in mice after I/R.

### FA Alleviate IR I/R-Induced Oxidative Stress in Mice

The results in **Figure 3** showed that Lipid hydroperoxide concentration and MDA level were significantly higher in the IR group than those in the sham group and IR + FA group ( $p < 0.05$ ), whereas the levels of SOD and GSH-Px were significantly lower in the IR group compared with IR + FA group. Furthermore, the NOX4 expression was significantly decreased in the IR + FA group when compared with the IR group. We did not find significant changes in these antioxidant enzymes and reductive oxidation products between the sham-operated group and the FA-only group. Therefore, these data indicate that FA can alleviate oxidative stress caused by IR.

### FA Inhibits I/R-Induced Apoptosis in Mice

The results showed that FA significantly decreased the protein expression of cleaved CASP3, cleaved PARP1 and Bax while increasing Bcl-2 expression in the heart tissues (**Figure 4A–E**). Therefore, FA alleviates I/R-induced apoptosis in I/R mice.

### FA Increases Nrf2 Expression, but Nrf2 Knockout Does not Eliminate the Myocardial Protective Effect of FA

To further determine whether the protective effect of FA against myocardial injury NRF2-dependent, we used *Nrf2*<sup>-/-</sup> mice. FA significantly increased NRF2 expression levels in I/R-treated WT mice in the heart tissues (**Figure 5A,B**). However, in *Nrf2*<sup>-/-</sup> mice,



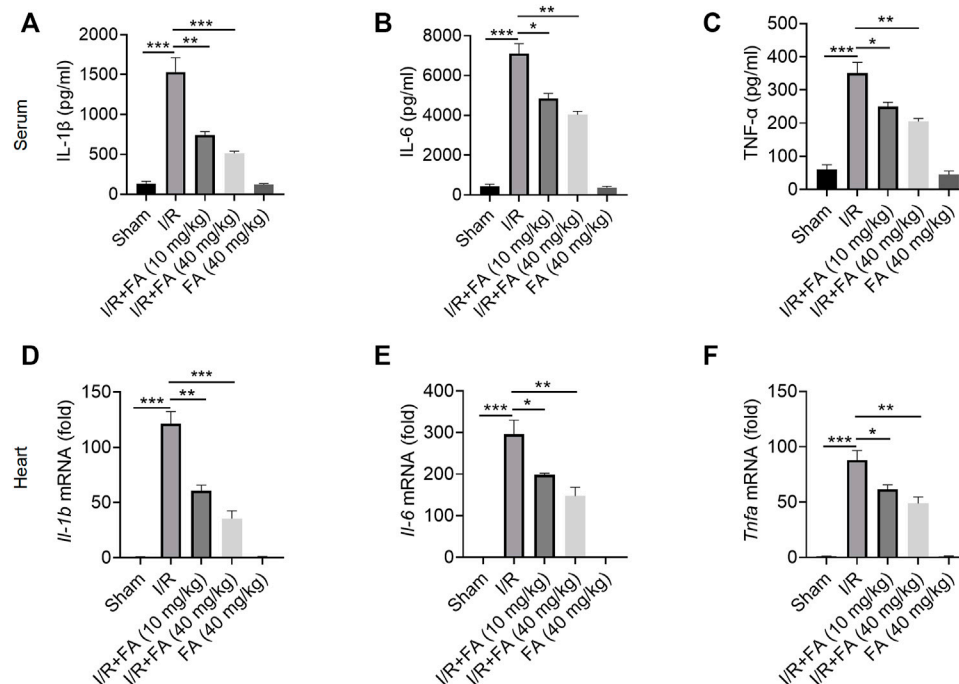


**FIGURE 2** | FA alleviates the inflammatory response to I/R-induced myocardial injury in mice. **(A–C)** Expression of the inflammatory factors IL-1 $\beta$ , IL-6, and TNF- $\alpha$  in WT mice was detected by ELISA. **(D–F)** mRNA expression of the inflammatory cytokines IL-1 $\beta$ , IL-6, IL-17, and Tnf $\alpha$  in heart tissue of WT mice in each experimental group, detected by RT-PCR. Data are expressed as the means  $\pm$  sd from three independent experiments. \* $p$  < 0.05, \*\* $p$  < 0.01, and \*\*\* $p$  < 0.001.

HE staining indicated that the protective effect of FA was unaffected, and the I/R-induced cardiac tissue damage was more severe in Nrf2 $^{-/-}$  mice than in WT mice (**Figure 5C**). Furthermore, FA significantly decreased the increases in CK-MB, LDH, troponin-1, and NT-proBNP in the serum (**Figure 5D–G**). These data suggest that the presence of NRF2 does not affect the protective effect of FA against I/R-induced myocardial injury, but the increase in NRF2 warrants further exploration.

## FA Does Not Alleviate I/R-Induced Injury Through Autophagy

Protective autophagy has been found to alleviate I/R-induced myocardial injury (Li et al., 2020). The widely used autophagy inhibitor 3-MA significantly inhibited the expression of autophagy marker ATG3 and decreased the ratio of the autophagy marker LC3II/LC3I at the experimental dose (**Figure 6A–C**). As shown in **Figure 6D**, after autophagy was inhibited by 3-MA, HE staining indicated that FA still alleviated I/R-induced injury. In addition, FA significantly decreased the increases in CK-MB, LDH, troponin-1, and NT-proBNP in the serum (**Figure 6D–H**). Accordingly, FA does not alleviate I/R-induced injury by inducing autophagy.

## Macrophage Clearance Inhibits the Myocardial Protective Effect of FA

Immune inflammation is an important factor in I/R induced myocardial injury, and macrophages are the main infiltrating

inflammatory cells acting after myocardial injury (Vilahur and Badimon, 2014). FA might exert protective effects in the myocardium by modulating macrophage-mediated inflammation. To test this hypothesis, we used clodronate liposomes to remove macrophages. F4/80 (Austyn and Gordon, 1981; van den Berg and Kraal, 2005) mRNA in clodronate-treated mouse hearts was significantly lower than in control liposomes (**Figure 7A**), thus suggesting that clodronate effectively depleted macrophages. In mice injected with liposomes in the control group, FA alleviated the I/R-induced increases in the CK-MB, LDH, troponin-1, and NT-proBNP levels in the serum. After injection of clodronate, HE staining indicated that FA was no longer protected in the myocardium (**Figure 7B**). We observed no significant changes in CK-MB, LDH, troponin-1, and NT-proBNP in the FA group compared to the control group in the serum (**Figure 7C–F**). Therefore, the protective effect of FA against I/R-induced myocardial injury may rely on its targeting of macrophages.

## FA Inhibits I/R-Induced Myocardial Injury by Inhibiting NLRP3 Inflammasome Activation

According to prior reports (Lopez-Castejon and Brough, 2011; Maruyama et al., 2019), activation of inflammasomes in macrophages is a key pathway for IL-1 $\beta$  secretion. Moreover, NLRP3 inflammasome activation is an important pathological factor leading to I/R myocardial injury. First, we examined whether FA might affect NLRP3 inflammasome activation in

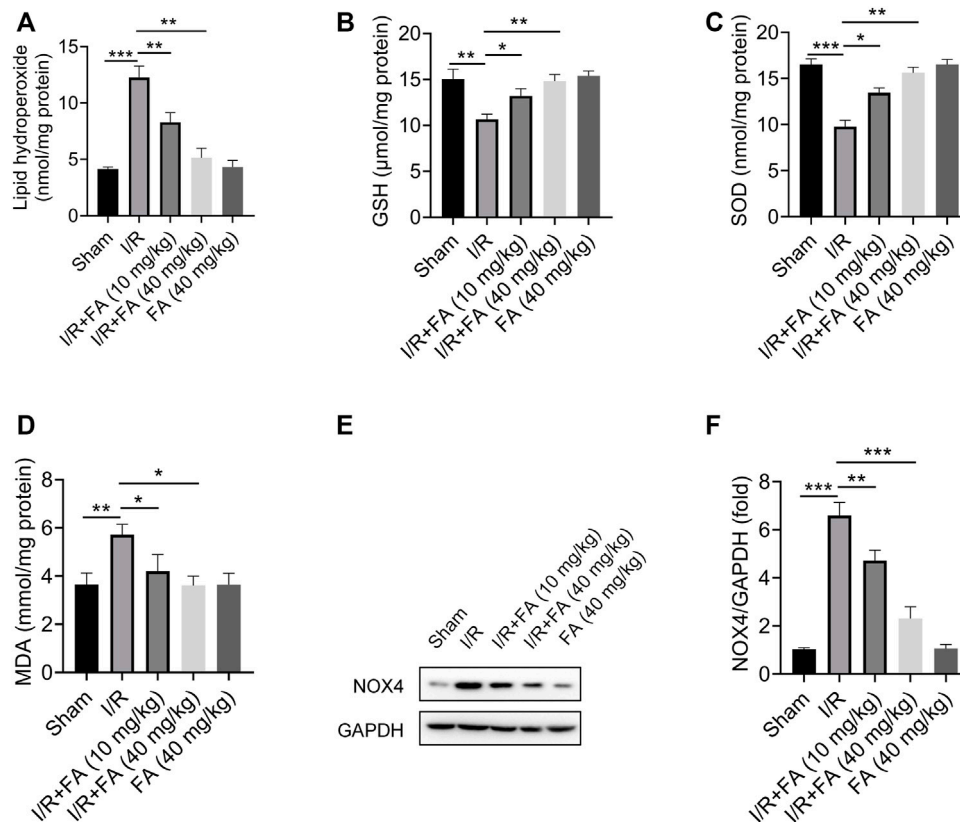


**FIGURE 3 |** Effect of FA on oxidative stress in the cardiac tissue homogenate. **(A)** Lipid hydroperoxide, **(B)** glutathione peroxidase, **(C)** superoxide dismutase, **(D)** malondialdehyde, **(E–F)** Western blotting analysis of NOX4 in the mice myocardium. Data are expressed as the mean  $\pm$  SD from three independent experiments or are representative of three independent experiments. \* $p < 0.05$ , \*\* $p < 0.01$ , and \*\*\* $p < 0.001$ .

WT I/R mice. FA significantly decreased the protein expression of NLRP3, caspase-1, IL-1 $\beta$ , and pro-IL-1 $\beta$  in WT mice, but did not significantly alter levels of the pro-caspase-1 protein (**Figures 8A–F**). However, in *Nlrp3*<sup>−/−</sup> mice, the protective effect of FA in the myocardium was eliminated (**Figure 8G**). Meanwhile, in NLRP3 knockout mice, FA did not affect the expression of IL-1 $\beta$  and caspase-1 (**Figures 8H–K**), thus, suggesting that FA affects NLRP3 inflammasome activation. Furthermore, in *Nlrp3*<sup>−/−</sup> mice, FA did not inhibit the levels of CK-MB, LDH, troponin-1, and NT-proBNP in the serum (**Figures 8L–O**). Therefore, these results suggest that FA protects against I/R-induced myocardial injury by inhibiting NLRP3 inflammasome activation.

### FA Inhibits NLRP3 Inflammasome Activation by Interfering With NLRP3 Binding to NEK7 in Macrophages

Next, we investigated whether FA might inhibit NLRP3 inflammasome activation in macrophages. First, we examined the effect of FA on macrophage toxicity. The CCK8 results indicated that FA (0–40  $\mu$ M) did not affect the proliferation of BMDM (**Figure 9A**). According to ELISA, FA decreased the release of IL-1 $\beta$  in BMDM (**Figure 9B**). Western blot results indicated that FA also inhibited the

expression of IL-1 $\beta$  and caspase-1 in cell supernatants (**Figure 9C**), thus suggesting that FA effectively inhibits NLRP3 inflammasome activation in macrophages. Endogenous IP experiments indicated that FA inhibited NLRP3 and ASC binding in macrophages (**Figure 9D**). Unexpectedly, exogenous IP revealed that FA did not affect NLRP3 interaction with ASC in HEK-293T cells (**Figure 9E**), thus, suggesting that FA does not inhibit NLRP3 inflammasome activation by affecting NLRP3's interaction with ASC. Furthermore, FA did not influence the NLRP3-NLRP3 interaction (**Figure 9F**). The interaction between NEK7 and NLRP3 plays a key role in ASC recruitment and NLRP3 oligomerization. We then studied the effect of FA on the interaction between NLRP3 and NEK7. Based on endogenous IP, FA inhibited the NEK7-NLRP3 interaction in BMDM (**Figure 10A**). In agreement with this finding, exogenous IP results also indicated that FA directly interfered with NEK7-NLRP3 interaction (**Figure 10B**). To study the reversibility of the interaction between FA and NLRP3, we analyzed the binding properties of FA and NLRP3. Washing experiments revealed that FA inhibited ATP-induced IL-1 $\beta$  secretion and caspase-1 activation after washing, thus suggesting that the inhibition of FA was irreversible (**Figure 10C,D**). Together, these results suggested that FA inhibits the activation of the NLRP3 inflammasome by blocking the NEK7-NLRP3 interaction.

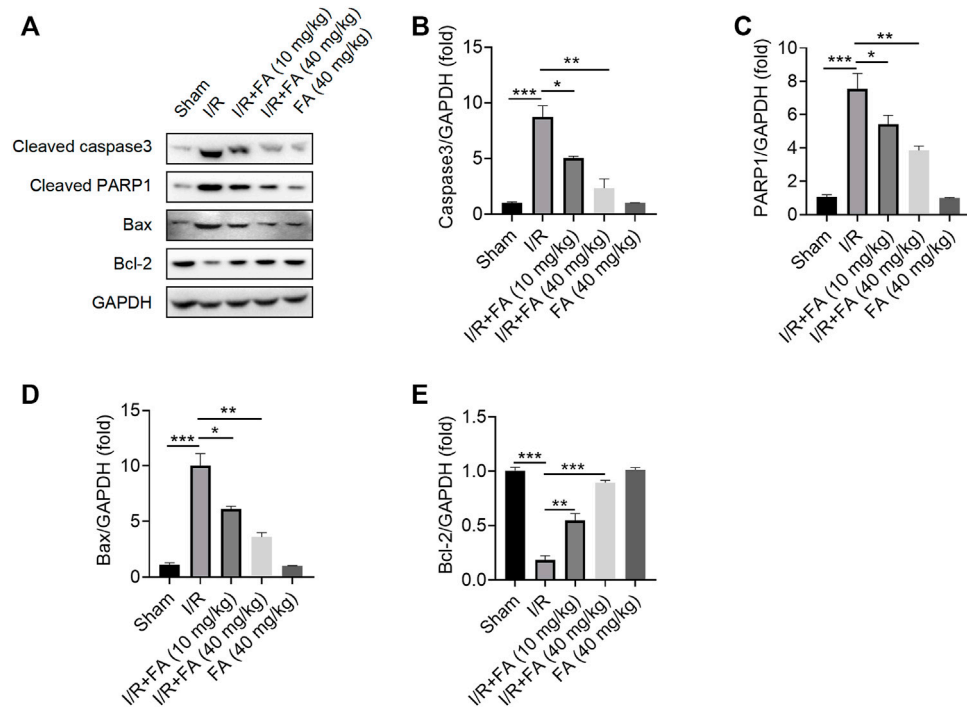


**FIGURE 4 |** FA inhibits I/R-induced apoptosis in mice. **(A–E)** Western blotting detection of the expression of the apoptosis-associated proteins cleaved PARP1, cleaved caspase-3, Bcl-2, and Bax in WT mice in each experimental group. Data are expressed as the means  $\pm$  sd and are representative of three independent experiments. \* $p < 0.05$ , \*\* $p < 0.01$ , and \*\*\* $p < 0.001$ .

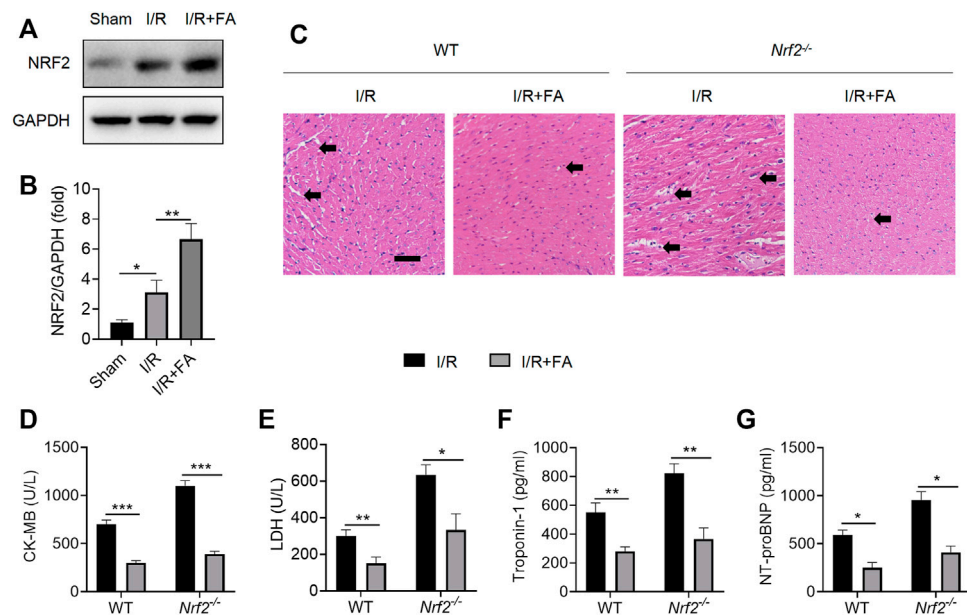


**FIGURE 5 |** FA induces an increase in NRF2, but NRF2 knockout does not eliminate the myocardial protective effect of FA. **(A,B)** The expression of NRF2 protein in each group of WT mice was detected by western blotting. **(C)** HE staining results of heart tissue sections in WT mice and *Nrf2*<sup>-/-</sup> mice in each experimental group. **(D–G)** Expression of CK-MB, LDH, troponin-1, and NT-proBNP in the serum of each experimental group in WT mice and *Nrf2*<sup>-/-</sup> mice. Data are expressed as the means  $\pm$  sd from three independent experiments or are representative of three independent experiments. \* $p < 0.05$ , \*\* $p < 0.01$ , and \*\*\* $p < 0.001$ .

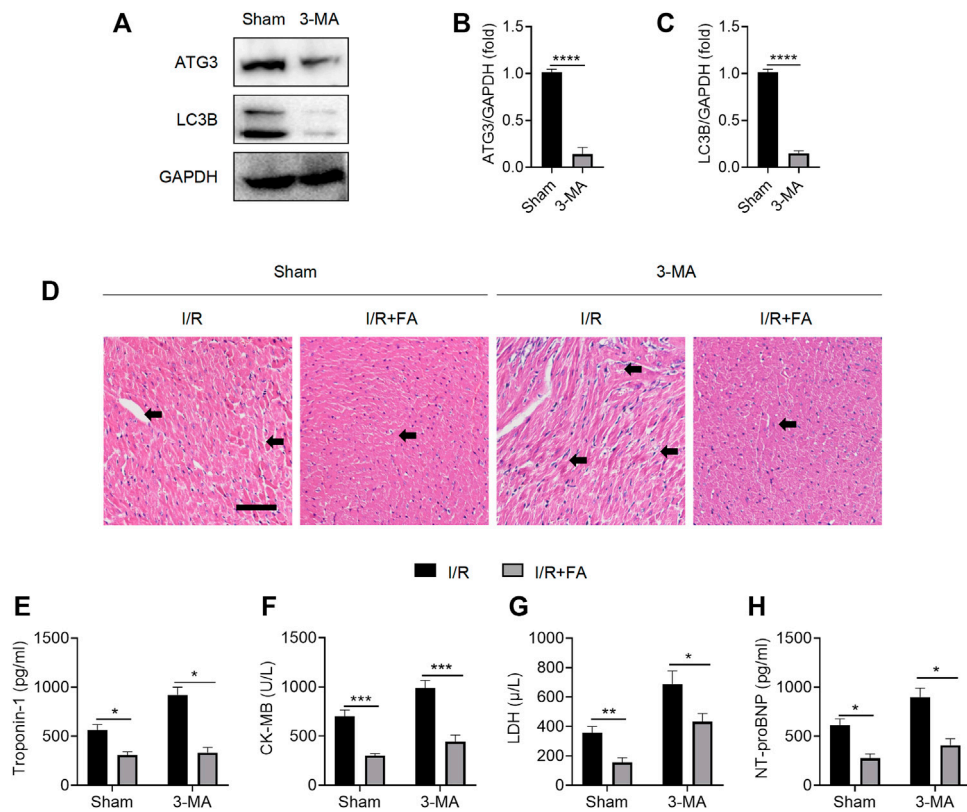


**FIGURE 6** | FA does not alleviate I/R-induced myocardial injury through autophagy. **(A–C)** Western blotting detection of the expression of ATG3 and LC3B proteins in the heart tissue of WT mice treated with saline or 3-MA. **(D)** HE staining results of heart tissue sections in WT mice treated with saline or 3-MA. **(E–H)** Expression of CK-MB, LDH, troponin-1, and NT-proBNP in the serum of each experimental group, detected by ELISA. Data are expressed as the means  $\pm$  sd from three independent experiments or are representative of three independent experiments. \* $p < 0.05$ , \*\* $p < 0.01$ , \*\*\* $p < 0.001$ , and \*\*\*\* $p < 0.0001$ .

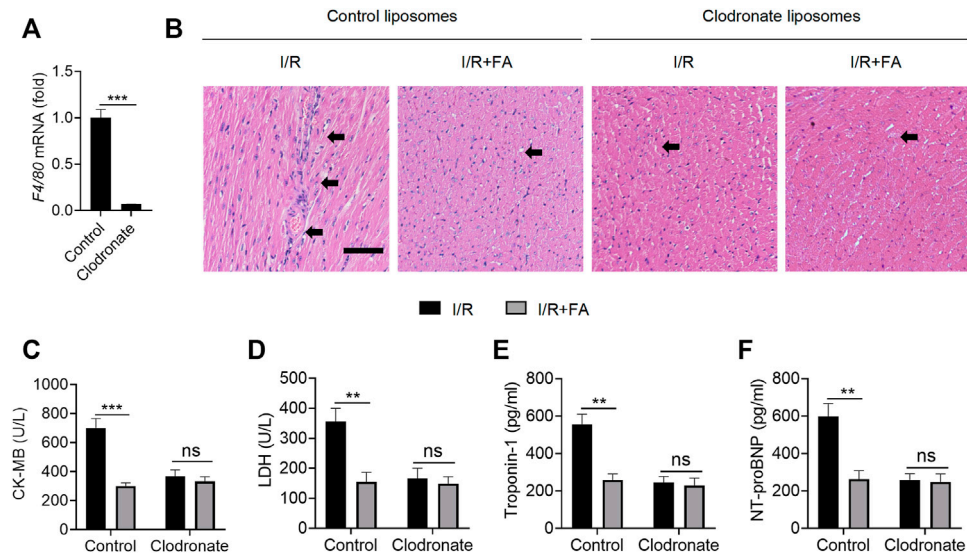


**FIGURE 7** | Macrophage clearance inhibits the myocardial protective effect of FA. **(A)** The mRNA expression of F4/80 in the heart tissue of WT mice treated with clodronate liposomes was detected by RT-PCR. **(B)** HE staining of heart tissue sections in each experimental group after treatment with clodronate liposomes or control liposomes. **(C–F)** Expression of CK-MB, LDH, troponin-1, and NT-proBNP in the serum of each experimental group after treatment with clodronate liposomes and control liposomes. Data are expressed as the means  $\pm$  sd from three independent experiments. \*\* $p < 0.01$ , \*\*\* $p < 0.001$ ; ns indicates no significance.



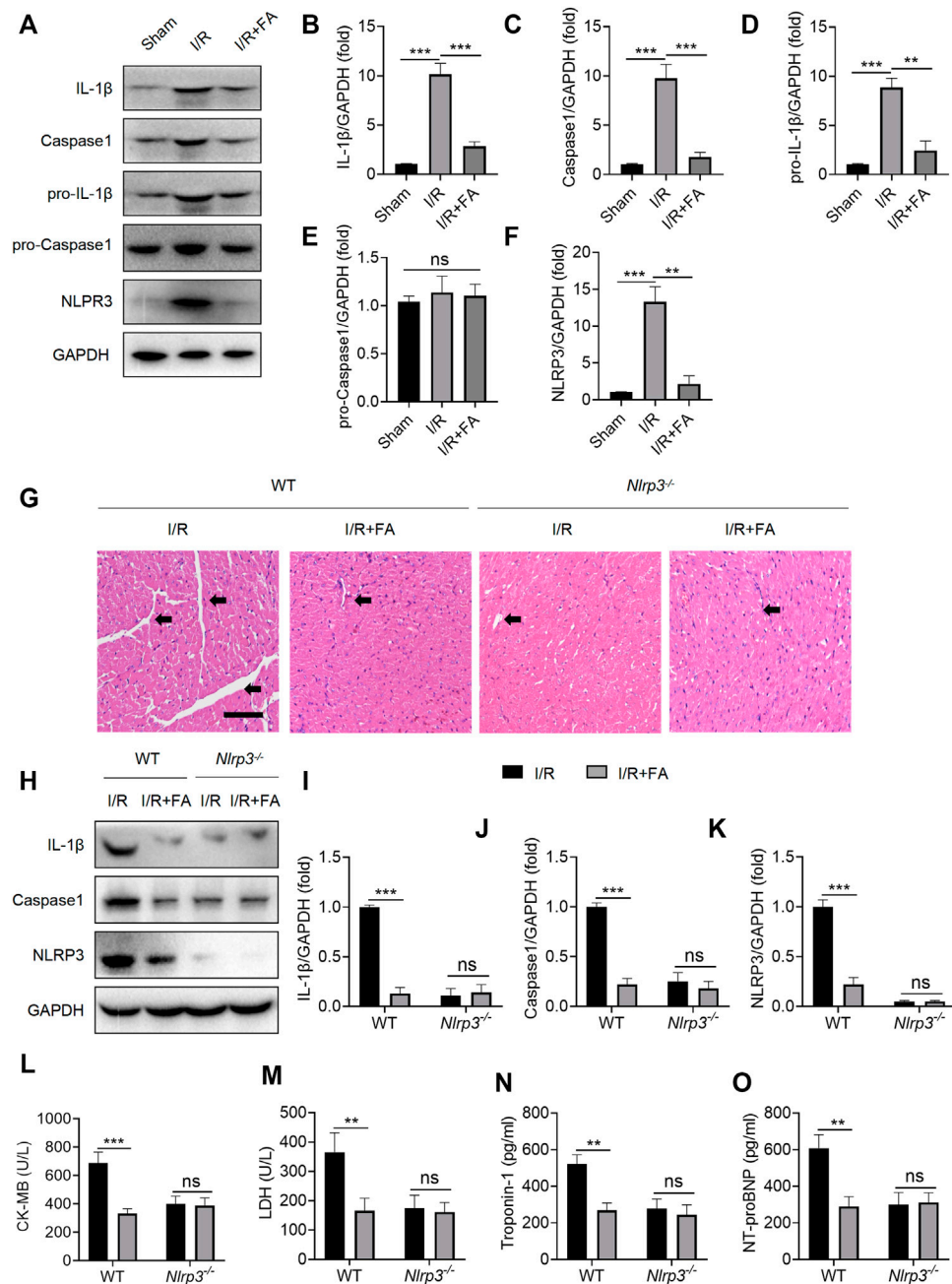


**FIGURE 8** | FA inhibits I/R-induced myocardial injury by inhibiting NLRP3 inflammasome activation. **(A–F)** Expression of NLRP3, pro-caspase-1, caspase-1, pro-IL-1 $\beta$ , and IL-1 $\beta$  in the heart tissue of WT mice was detected by western blotting. **(G)** HE staining of heart tissue sections in WT mice and *Nlrp3*<sup>-/-</sup> mice. **(H–K)** Expression of IL-1 $\beta$ , caspase-1, and NLRP3 in heart tissues of WT mice and *Nlrp3*<sup>-/-</sup> mice in each experimental group, detected by western blotting. **(L–O)** Expression of CK-MB, LDH, troponin-1, and NT-proBNP in the serum of each experimental group in WT mice and *Nlrp3*<sup>-/-</sup> mice, determined by ELISA. Data are expressed as the means  $\pm$  sd from three independent experiments or are representative of three independent experiments. \*\* $p$  < 0.01, \*\*\* $p$  < 0.001; ns indicates no significance.

## DISCUSSION

Despite significant advances in technology and drugs for the treatment of CVD, the disease remains the leading cause of death worldwide, with coronary heart disease being a key factor (Mokhtari-Zaer et al., 2018; Silvis et al., 2021). After acute

myocardial infarction, the blood flow to the ischemic myocardium must be rapidly restored, but this restoration may lead to additional complications and the aggravation of myocardial injury, known as myocardial I/R injury (Mehta et al., 2016). Therefore, exploring how to decrease the myocardial injury caused by I/R may have high therapeutic value.

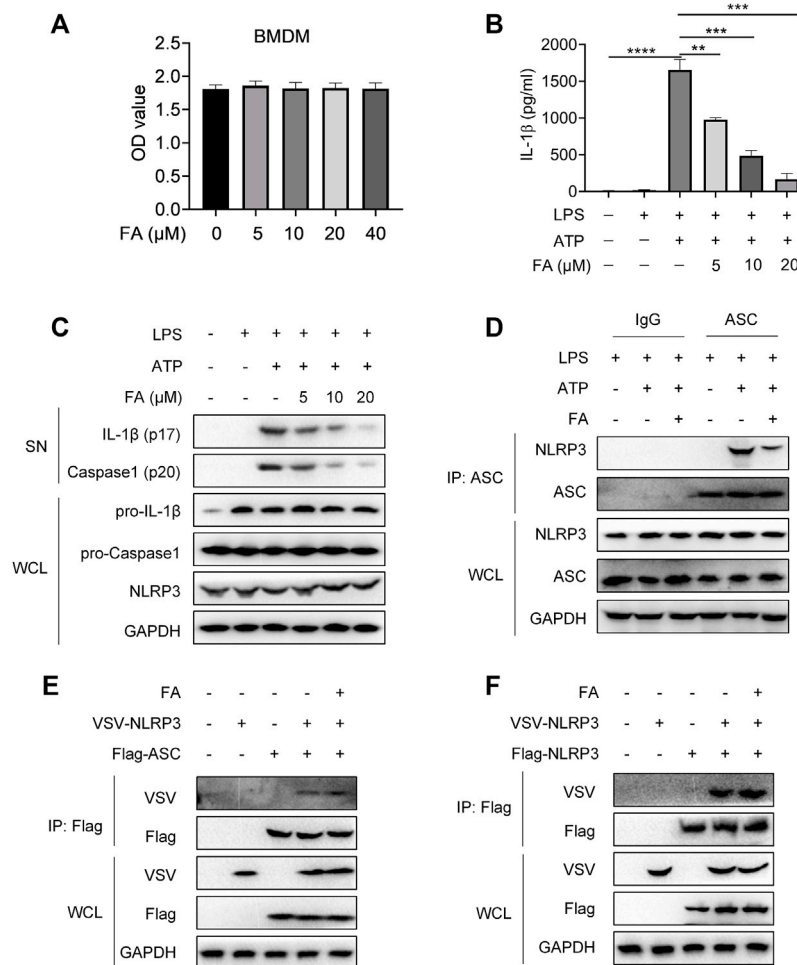


**FIGURE 9** | FA does not affect the interaction between NLRP3 and ASC or NLRP3. LPS-primed BMDMs were treated with various concentrations of FA (20 μM) for 15 min and then stimulated with ATP for 30 min. **(A)** Expression of IL-1 β in each group after treatment with different concentrations of FA, detected by ELISA. **(B)** Western blotting detection of the expression of IL-1β and caspase-1 (P20) in cell supernatants (SN), and pro-IL-1β and pro-caspase-1 in total protein. **(C)** CCK-8 detection of the effects of different concentrations of FA on the viability of BMDMs. **(D)** Endogenous IP with ASC antibody or IgG, performed in LPS-primed BMDMs stimulated with ATP in the presence or absence of FA (20 μM). **(E)** IP and western blot analysis of NLRP3 and ASC interaction in the presence or absence of FA (20 μM) in HEK-293T cells. **(F)** IP and western blot analysis of NLRP3 and NLRP3 interaction in the presence or absence of FA (20 μM) in HEK-293T cells. Data from three independent experiments or are representative of three independent experiments.

FA, found to be naturally present in *Rhododendron dauricum* L. leaves, is a natural dihydro flavonoid active substance with antibacterial, anti-inflammatory, antioxidant, and other biological activities (Li et al., 2013; Ran et al., 2018; Li et al., 2019; Qin et al., 2022). In this study, we aimed to find its role and mechanism in I/R-induced injury.

Autophagy is widespread in normal cells, acting as scavengers to meet the metabolic needs of cells and enable the renewal of some organelles (Kamynina et al., 2021). When tissues and cells are injured by various physical and chemical factors, the autophagic lysosomes increase greatly and protect cell injury (Ichimiya et al., 2020). In myocardial I/R, many immune cells and myocardial cells are injured and die, inducing autophagy to remove these dead cells and protect the myocardium (Tschöpe et al., 2021). A previous study has reported that FA promotes autophagy, and thus, protects the liver (Wang et al., 2019).

Therefore, we hypothesized that the cardiac protective effect of FA might be associated with autophagy. Here, we blocked autophagy using the widely used autophagy inhibitor 3-MA. Unexpectedly, 3-MA pretreatment did not eliminate the myocardial protective effect of FA, thus, suggesting that FA does not play a protective role in the myocardium through the autophagy-dependent pathway. The protective mechanism of FA in the heart differs from that in liver disease.

The elevated production of reactive oxygen species plays an important role during myocardial I/R injury (Cadenas, 2018). NRF2, a transcription factor, induces gene expression of a range of antioxidant enzymes, such as heme oxygenase-1 (HO-1), superoxide dismutase (SOD), glutathione catalase (GPx), NAD(P)H: quinone oxidoreductase 1 (NQO1), and γ-glutamylcysteine synthase (γ-GCS) to combat oxidative stress (Harris and DeNicola, 2020). Previous studies have shown that

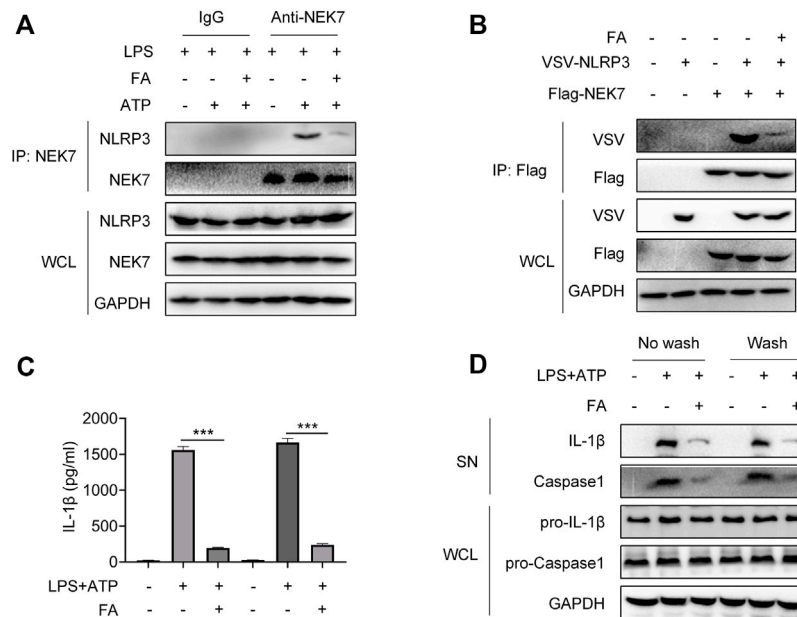


**FIGURE 10 |** FA inhibits NLRP3 inflammasome activation by interfering with NLRP3 and NEK7. LPS-primed BMDMs were treated with various concentrations of FA (20  $\mu$ M) for 15 min and then stimulated with ATP for 30 min. **(A)** Endogenous immunoprecipitation (IP) with NEK7 antibody or IgG in LPS-primed BMDMs stimulated with ATP in the presence or absence of FA (20  $\mu$ M). **(B)** IP and western blot analysis of NEK7-NLRP3 interaction in HEK-293T cells treated with FA (20  $\mu$ M). LPS-primed BMDMs were treated with FA (20  $\mu$ M) for 15 min, washed three times, and then stimulated with ATP for 30 min. ELISA analysis of IL-1 $\beta$  in supernatants in each group in the presence or absence of FA (20  $\mu$ M) **(C)**, and western blot analysis of cleaved IL-1 $\beta$  and caspase-1 (p20) in SN, and pro-IL-1 $\beta$  and pro-caspase-1 in the whole-cell lysates (WCL) **(D)**. Data are expressed as the means  $\pm$  sd from three independent experiments or are representative of three independent experiments. \*\* $p$  < 0.01, \*\*\* $p$  < 0.001, and \*\*\*\* $p$  < 0.0001.

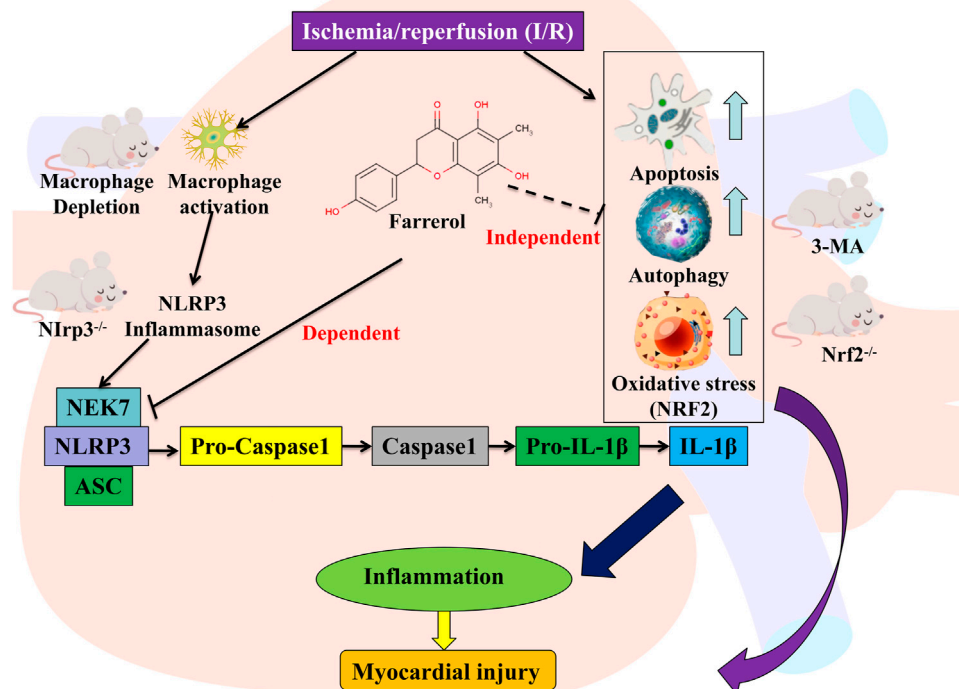


**FIGURE 11 |** Graphic abstract for major findings and proposed mechanism. FA inhibits the NEK7-NLRP3 interaction, thereby inhibiting NLRP3 inflammasome assembly and activation, resulting in an effective inhibition to alleviate myocardial ischemia/reperfusion injury. Schematic representation of the mechanism of action of FA.

FA activates NRF2 by protecting a variety of cells (Cui et al., 2019; Wang et al., 2019; Harris and DeNicola, 2020). Therefore, we used *Nrf2*<sup>-/-</sup> mice to explore whether the cardiac protective effects of FA might be associated with the NRF2 pathway. In an *Nrf2*<sup>-/-</sup> mouse I/R model, FA still exerted a protective effect in the myocardium. In addition, FA could alleviate excessive oxidative stress by elevating the level of antioxidant enzymes and reducing oxidation products in the cardiac tissue. These data suggest that NRF2 is not a key target for cardioprotection by FA.

Since FA still protected against I/R-induced myocardial injury in *Nrf2*<sup>-/-</sup> mice and WT mice with autophagy inhibition, FA does not appear to play a protective role in the myocardium through affecting NRF2 pathways and autophagy. Given that immune-mediated inflammatory responses play important roles in myocardial I/R injury, we hypothesized that FA might affect myocardial cell function by directly regulating immune cells. Because macrophages have important functions as a key factor in myocardial injury (Fan et al., 2019; Peet et al., 2020), we wondered whether FA's protective role might rely on its action on macrophages. To test this hypothesis, we used clodronate liposomes to deplete macrophages to verify that the cardioprotective effects of FA were associated with macrophages. In control mice injected with liposomes, FA alleviated I/R-induced myocardial injury, whereas the protective effect of FA was weakened after chlorophosphate injection. Moreover, FA did not decrease the increases in CK-MB, LDH, troponin-1, and NT-proBNP in the serum. Therefore, we concluded that FA alleviates I/R-induced myocardial injury by targeting macrophages. However, how does FA act on macrophages?

I/R-induced myocardial injury would produce a large amount of metabolin, which triggers NLRP3 inflammasome activation (Qiu et al., 2017; Zhang J et al., 2020). When inflammatory cells infiltrate the heart, numerous NLRP3 inflammasome spots appear in macrophages (Nazir et al., 2017; Dai et al., 2020). Might FA play a protective role by inhibiting NLRP3 inflammasome in macrophages? We tested this hypothesis by examining the expression of related factors after NLRP3 inflammasome activation. NLRP3 inflammasomes regulate caspase-1 activation and promote the maturation and secretion of IL-1 $\beta$  during the natural immune defense (Burke et al., 2021); they also regulate caspase-1-dependent programmed apoptosis and induce cell death under inflammatory and stressful pathological conditions (Swanson et al., 2019). As shown in **Figure 8**, we concluded that FA protects against I/R injury by inhibiting NLRP3 inflammasomes in macrophages. Which part of the NLRP3 inflammasome does FA act on?

The NLRP3 inflammasomes are composed of NLRP3, ASC, and caspase-1. When cells are stimulated, NLRP3 is activated and recruited pro-caspase-1 by binding ASCs and forming NLRP3

inflammasomes (Swanson et al., 2019). In response to NLRP3 inflammasomes, pro-caspase-1 is activated and forms caspase-1, which leads to the maturation and secretion of IL-1 $\beta$ , as well as a series of inflammatory responses (He et al., 2016; Shrivastava et al., 2016). NEK7 has been found to be involved in the formation and activation of the NLRP3 inflammasome, and the deletion of NEK7 specifically blocks NLRP3 inflammasome activation (He et al., 2016). Therefore, we tested the expression of these proteins to provide further verification. FA blocked the assembly of NLRP3 inflammasomes by interfering with the interaction of NEK7 and NLRP3 but did not affect the interaction of NLRP3 with ASC and NLRP3. Thus, FA inhibits NLRP3 inflammasome activation.

In summary, the experimental results of this study showed that the protective effect of FA did not through *Nrf2*-dependent or autophagy-dependent pathways, but may be due to its effect on macrophages rather than a direct effect on cardiomyocytes. After the depletion of macrophages, the protective effect of FA decreased dramatically suggesting that FA indirectly protects cardiomyocytes by targeting macrophages. Further studies showed that the protective effect of FA against I/R-induced myocardium injury involves blocking NLRP3 inflammasome assembly by interfering with the interaction between NLRP3 and NEK7, thereby inhibiting NLRP3 inflammasome activation (**Figure 11**). In conclusion, this study demonstrates a novel role of FA as a potential myocardial protective agent in the protection and treatment of I/R-induced myocardial injury by targeting NLRP3 in macrophages.

## DATA AVAILABILITY STATEMENT

The original contributions presented in the study are included in the article/Supplementary Material, further inquiries can be directed to the corresponding author.

## ETHICS STATEMENT

The animal study was reviewed and approved by Institutional Bio-Safety Committee (or Ethics Committee) of Shantou University.

## AUTHOR CONTRIBUTIONS

Conception and design: XZ Collection, analysis, and interpretation of data: LZ. Drafting of the manuscript: LZ and SY. Final approval of the article: LZ and XZ. All authors have read and agreed to the published version of the manuscript.

## REFERENCES

- Ait-Aissa, K., Heisner, J. S., Norwood Toro, L. E., Bruemmer, D., Doyon, G., Harmann, L., et al. (2019). Telomerase Deficiency Predisposes to Heart Failure and Ischemia-Reperfusion Injury. *Front. Cardiovasc. Med.* 6, 31. doi:10.3389/fcvm.2019.00031
- Austyn, J. M., and Gordon, S. (1981). F4/80, a Monoclonal Antibody Directed Specifically against the Mouse Macrophage. *Eur. J. Immunol.* 11 (10), 805–815. doi:10.1002/eji.1830111013



- Burke, R. M., Dale, B. L., and Dholakia, S. (2021). The NLRP3 Inflammasome: Relevance in Solid Organ Transplantation. *Int. J. Mol. Sci.* 22 (19), 10721. doi:10.3390/ijms221910721
- Cadenas, S. (2018). ROS and Redox Signaling in Myocardial Ischemia-Reperfusion Injury and Cardioprotection. *Free Radic. Biol. Med.* 117, 76–89. doi:10.1016/j.freeradbiomed.2018.01.024
- Cui, B., Zhang, S., Wang, Y., and Guo, Y. (2019). Farrerol Attenuates  $\beta$ -amyloid-induced Oxidative Stress and Inflammation through Nrf2/Keap1 Pathway in a Microglia Cell Line. *Biomed. Pharmacother.* 109, 112–119. doi:10.1016/j.biopha.2018.10.053
- Dai, Y., Wang, S., Chang, S., Ren, D., Shali, S., Li, C., et al. (2020). M2 Macrophage-Derived Exosomes Carry microRNA-148a to Alleviate Myocardial Ischemia/reperfusion Injury via Inhibiting TXNIP and the TLR4/NF-Kb/nlrp3 Inflammasome Signaling Pathway. *J. Mol. Cel Cardiol* 142, 65–79. doi:10.1016/j.yjmcc.2020.02.007
- Dong, Y., Chen, H., Gao, J., Liu, Y., Li, J., and Wang, J. (2019). Molecular Machinery and Interplay of Apoptosis and Autophagy in Coronary Heart Disease. *J. Mol. Cel Cardiol* 136, 27–41. doi:10.1016/j.yjmcc.2019.09.001
- Fan, Q., Tao, R., Zhang, H., Xie, H., Lu, L., Wang, T., et al. (2019). Dectin-1 Contributes to Myocardial Ischemia/Reperfusion Injury by Regulating Macrophage Polarization and Neutrophil Infiltration. *Circulation* 139 (5), 663–678. doi:10.1161/circulationaha.118.036044
- Frangogiannis, N. G. (2014). The Inflammatory Response in Myocardial Injury, Repair, and Remodelling. *Nat. Rev. Cardiol.* 11 (5), 255–265. doi:10.1038/nrcardio.2014.28
- Harris, I. S., and DeNicola, G. M. (2020). The Complex Interplay between Antioxidants and ROS in Cancer. *Trends Cel Biol* 30 (6), 440–451. doi:10.1016/j.tcb.2020.03.002
- He, Y., Hara, H., and Núñez, G. (2016). Mechanism and Regulation of NLRP3 Inflammasome Activation. *Trends Biochem. Sci.* 41 (12), 1012–1021. doi:10.1016/j.tibs.2016.09.002
- Ibáñez, B., Heusch, G., Ovize, M., and Van de Werf, F. (2015). Evolving Therapies for Myocardial Ischemia/reperfusion Injury. *J. Am. Coll. Cardiol.* 65 (14), 1454–1471. doi:10.1016/j.jacc.2015.02.032
- Ichimiya, T., Yamakawa, T., Hirano, T., Yokoyama, Y., Hayashi, Y., Hirayama, D., et al. (2020). Autophagy and Autophagy-Related Diseases: A Review. *Int. J. Mol. Sci.* 21 (23), 8974. doi:10.3390/ijms21238974
- Kalogeris, T., Baines, C. P., Krenz, M., and Korthuis, R. J. (2012). Cell Biology of Ischemia/reperfusion Injury. *Int. Rev. Cel Mol Biol* 298, 229–317. doi:10.1016/b978-0-12-394309-5.00006-7
- Kamyntina, M., Tskhovrebova, S., Fares, J., Timashev, P., Laevskaya, A., and Ulasov, I. (2021). Oncolytic Virus-Induced Autophagy in Glioblastoma. *Cancers (Basel)* 13 (14), 3482. doi:10.3390/cancers13143482
- Li, J. K., Ge, R., Tang, L., and Li, Q. S. (2013). Protective Effects of Farrerol against Hydrogen-Peroxide-Induced Apoptosis in Human Endothelium-Derived EA.Hy926 Cells. *Can. J. Physiol. Pharmacol.* 91 (9), 733–740. doi:10.1139/cjpp-2013-0008
- Li, Y., Liang, P., Jiang, B., Tang, Y., Liu, X., Liu, M., et al. (2020). CARD9 Promotes Autophagy in Cardiomyocytes in Myocardial Ischemia/reperfusion Injury via Interacting with Rbicon Directly. *Basic Res. Cardiol.* 115 (3), 29. doi:10.1007/s00395-020-0790-6
- Li, Y., Zeng, Y., Meng, T., Gao, X., Huang, B., He, D., et al. (2019). Farrerol Protects Dopaminergic Neurons in a Rat Model of Lipopolysaccharide-Induced Parkinson's Disease by Suppressing the Activation of the AKT and NF-Kb Signaling Pathways. *Int. Immunopharmacology* 75, 105739. doi:10.1016/j.intimp.2019.105739
- Lopez-Castejon, G., and Brough, D. (2011). Understanding the Mechanism of IL-1 $\beta$  Secretion. *Cytokine Growth Factor. Rev.* 22 (4), 189–195. doi:10.1016/j.cytogfr.2011.10.001
- Maarman, G., Marais, E., Lochner, A., and du Toit, E. F. (2012). Effect of Chronic CPT-1 Inhibition on Myocardial Ischemia-Reperfusion Injury (I/R) in a Model of Diet-Induced Obesity. *Cardiovasc. Drugs Ther.* 26 (3), 205–216. doi:10.1007/s10557-012-6377-1
- Maruyama, K., Nemoto, E., and Yamada, S. (2019). Mechanical Regulation of Macrophage Function - Cyclic Tensile Force Inhibits NLRP3 Inflammasome-dependent IL-1 $\beta$  Secretion in Murine Macrophages. *Inflamm. Regen.* 39, 3. doi:10.1186/s41232-019-0092-2
- Mehta, L. S., Beckie, T. M., DeVon, H. A., Grines, C. L., Krumholz, H. M., Johnson, M. N., et al. (2016). Acute Myocardial Infarction in Women: A Scientific Statement from the American Heart Association. *Circulation* 133 (9), 916–947. doi:10.1161/cir.0000000000000351
- Mokhtari-Zaer, A., Marefati, N., Atkin, S. L., Butler, A. E., and Sahebkar, A. (2018). The Protective Role of Curcumin in Myocardial Ischemia-Reperfusion Injury. *J. Cel Physiol* 234 (1), 214–222. doi:10.1002/jcp.26848
- Moreno, S. G. (2018). Depleting Macrophages *In Vivo* with Clodronate-Liposomes. *Methods Mol. Biol.* 1784, 259–262. doi:10.1007/978-1-4939-7837-3\_23
- Nazir, S., Gadi, I., Al-Dabet, M. M., Elwakil, A., Kohli, S., Ghosh, S., et al. (2017). Cytoprotective Activated Protein C Averts Nlrp3 Inflammasome-Induced Ischemia-Reperfusion Injury via mTORC1 Inhibition. *Blood* 130 (24), 2664–2677. doi:10.1182/blood-2017-05-782102
- Peet, C., Ivetic, A., Bromage, D. I., and Shah, A. M. (2020). Cardiac Monocytes and Macrophages after Myocardial Infarction. *Cardiovasc. Res.* 116 (6), 1101–1112. doi:10.1093/cvr/cvz336
- Qin, X., Xu, X., Hou, X., Liang, R., Chen, L., Hao, Y., et al. (2022). The Pharmacological Properties and Corresponding Mechanisms of Farrerol: a Comprehensive Review. *Pharm. Biol.* 60 (1), 9–16. doi:10.1080/13880209.2021.2006723
- Qiu, Z., Lei, S., Zhao, B., Wu, Y., Su, W., Liu, M., et al. (2017). NLRP3 Inflammasome Activation-Mediated Pyroptosis Aggravates Myocardial Ischemia/Reperfusion Injury in Diabetic Rats. *Oxid Med. Cel Longev* 2017, 9743280. doi:10.1155/2017/9743280
- Ran, X., Li, Y., Chen, G., Fu, S., He, D., Huang, B., et al. (2018). Farrerol Ameliorates TNBS-Induced Colonic Inflammation by Inhibiting ERK1/2, JNK1/2, and NF-Kb Signaling Pathway. *Int. J. Mol. Sci.* 19 (7), 2037. doi:10.3390/ijms19072037
- Shen, Y., Liu, X., Shi, J., and Wu, X. (2019). Involvement of Nrf2 in Myocardial Ischemia and Reperfusion Injury. *Int. J. Biol. Macromol* 125, 496–502. doi:10.1016/j.ijbiomac.2018.11.190
- Shi, B., Ma, M., Zheng, Y., Pan, Y., and Lin, X. (2019). mTOR and Beclin1: Two Key Autophagy-Related Molecules and Their Roles in Myocardial Ischemia/reperfusion Injury. *J. Cel Physiol* 234 (8), 12562–12568. doi:10.1002/jcp.28125
- Shrivastava, G., León-Juárez, M., García-Cordero, J., Meza-Sánchez, D. E., and Cedillo-Barrón, L. (2016). Inflammasomes and its Importance in Viral Infections. *Immunol. Res.* 64 (5-6), 1101–1117. doi:10.1007/s12026-016-8873-z
- Silvis, M. J. M., Demkes, E. J., Fiolet, A. T. L., Dekker, M., Bosch, L., van Hout, G. P. J., et al. (2021). Immunomodulation of the NLRP3 Inflammasome in Atherosclerosis, Coronary Artery Disease, and Acute Myocardial Infarction. *J. Cardiovasc. Transl. Res.* 14 (1), 23–34. doi:10.1007/s12265-020-10049-w
- Swanson, K. V., Deng, M., and Ting, J. P. (2019). The NLRP3 Inflammasome: Molecular Activation and Regulation to Therapeutics. *Nat. Rev. Immunol.* 19 (8), 477–489. doi:10.1038/s41577-019-0165-0
- Tschöpe, C., Ammirati, E., Bozkurt, B., Caforio, A. L. P., Cooper, L. T., Felix, S. B., et al. (2021). Myocarditis and Inflammatory Cardiomyopathy: Current Evidence and Future Directions. *Nat. Rev. Cardiol.* 18 (3), 169–193. doi:10.1038/s41569-020-00435-x
- van den Berg, T. K., and Kraal, G. (2005). A Function for the Macrophage F4/80 Molecule in Tolerance Induction. *Trends Immunol.* 26 (10), 506–509. doi:10.1016/j.it.2005.07.008
- van Rooijen, N., and van Kesteren-Hendrikx, E. (2002). Clodronate Liposomes: Perspectives in Research and Therapeutics. *J. Liposome Res.* 12 (1-2), 81–94. doi:10.1081/lpr-120004780
- Venkatachalam, K., Prabhu, S. D., Reddy, V. S., Boylston, W. H., Valente, A. J., and Chandrasekar, B. (2009). Neutralization of Interleukin-18 Ameliorates Ischemia/reperfusion-Induced Myocardial Injury. *J. Biol. Chem.* 284 (12), 7853–7865. doi:10.1074/jbc.M808824200
- Vilaur, G., and Badimon, L. (2014). Ischemia/reperfusion Activates Myocardial Innate Immune Response: the Key Role of the Toll-like Receptor. *Front. Physiol.* 5, 496. doi:10.3389/fphys.2014.00496
- Wang, L., Wei, W., Xiao, Q., Yang, H., and Ci, X. (2019). Farrerol Ameliorates APAP-Induced Hepatotoxicity via Activation of Nrf2 and Autophagy. *Int. J. Biol. Sci.* 15 (4), 788–799. doi:10.7150/ijbs.30677
- Xia, Y., Wang, P., Yan, N., Gonzalez, F. J., and Yan, T. (2021). Withaferin A Alleviates Fulminant Hepatitis by Targeting Macrophage and NLRP3. *Cell Death Dis* 12 (2), 174. doi:10.1038/s41419-020-03243-w
- Yan, H. F., Tuo, Q. Z., Yin, Q. Z., and Lei, P. (2020). The Pathological Role of Ferroptosis in Ischemia/reperfusion-Related Injury. *Zool Res.* 41 (3), 220–230. doi:10.24272/zj.issn.2095-8137.2020.042

- Yeung, H. M., Hung, M. W., Lau, C. F., and Fung, M. L. (2015). Cardioprotective Effects of Melatonin against Myocardial Injuries Induced by Chronic Intermittent Hypoxia in Rats. *J. Pineal Res.* 58 (1), 12–25. doi:10.1111/jpi.12190
- Zagidullin, N., Motloch, L. J., Gareeva, D., Hamitova, A., Lakman, I., Krioni, I., et al. (2020). Combining Novel Biomarkers for Risk Stratification of Two-Year Cardiovascular Mortality in Patients with ST-Elevation Myocardial Infarction. *J. Clin. Med.* 9 (2), 550. doi:10.3390/jcm9020550
- Zhang, J., Huang, L., Shi, X., Yang, L., Hua, F., Ma, J., et al. (2020). Metformin Protects against Myocardial Ischemia-Reperfusion Injury and Cell Pyroptosis via AMPK/NLRP3 Inflammasome Pathway. *Aging (Albany NY)* 12 (23), 24270–24287. doi:10.18632/aging.202143
- Zhang, T., Yang, W. X., Wang, Y. L., Yuan, J., Qian, Y., Sun, Q. M., et al. (2020). Electroacupuncture Preconditioning Attenuates Acute Myocardial Ischemia Injury through Inhibiting NLRP3 Inflammasome Activation in Mice. *Life Sci.* 248, 117451. doi:10.1016/j.lfs.2020.117451
- Zhao, J., Li, X., Hu, J., Chen, F., Qiao, S., Sun, X., et al. (2019). Mesenchymal Stromal Cell-Derived Exosomes Attenuate Myocardial Ischaemia-Reperfusion Injury through miR-182-Regulated Macrophage Polarization. *Cardiovasc. Res.* 115 (7), 1205–1216. doi:10.1093/cvr/cvz040
- Conflict of Interest:** The authors declare that the research was conducted in the absence of any commercial or financial relationships that could be construed as a potential conflict of interest.
- Publisher's Note:** All claims expressed in this article are solely those of the authors and do not necessarily represent those of their affiliated organizations, or those of the publisher, the editors and the reviewers. Any product that may be evaluated in this article, or claim that may be made by its manufacturer, is not guaranteed or endorsed by the publisher.

Copyright © 2022 Zhou, Yang and Zou. This is an open-access article distributed under the terms of the Creative Commons Attribution License (CC BY). The use, distribution or reproduction in other forums is permitted, provided the original author(s) and the copyright owner(s) are credited and that the original publication in this journal is cited, in accordance with accepted academic practice. No use, distribution or reproduction is permitted which does not comply with these terms.



# Association of TGF- $\beta$ Canonical Signaling-Related Core Genes With Aortic Aneurysms and Aortic Dissections

Jicheng Chen and Rong Chang\*

Department of Vasculocardiology, Shenzhen Longhua District Central Hospital, Guangdong Medical University, Shenzhen, China

## OPEN ACCESS

### Edited by:

Xianwei Wang,  
Xinxiang Medical University, China

### Reviewed by:

Alex Boye,  
University of Cape Coast, Ghana  
Venkateswara Reddy Gogulamudi,  
The University of Utah, United States

### \*Correspondence:

Rong Chang  
qhschanrong@126.com

### Specialty section:

This article was submitted to  
Cardiovascular and Smooth Muscle  
Pharmacology,  
a section of the journal  
Frontiers in Pharmacology

**Received:** 03 March 2022

**Accepted:** 04 April 2022

**Published:** 20 April 2022

### Citation:

Chen J and Chang R (2022)  
Association of TGF- $\beta$  Canonical  
Signaling-Related Core Genes With  
Aortic Aneurysms and  
Aortic Dissections.  
Front. Pharmacol. 13:888563.  
doi: 10.3389/fphar.2022.888563

Transforming growth factor-beta (TGF- $\beta$ ) signaling is essential for the maintenance of the normal structure and function of the aorta. It includes SMAD-dependent canonical pathways and noncanonical signaling pathways. Accumulated genetic evidence has shown that TGF- $\beta$  canonical signaling-related genes have key roles in aortic aneurysms (AAs) and aortic dissections and many gene mutations have been identified in patients, such as those for transforming growth factor-beta receptor one TGFBR1, TGFBR2, SMAD2, SMAD3, SMAD4, and SMAD6. Aortic specimens from patients with these mutations often show paradoxically enhanced TGF- $\beta$  signaling. Some hypotheses have been proposed and new AA models in mice have been constructed to reveal new mechanisms, but the role of TGF- $\beta$  signaling in AAs is controversial. In this review, we focus mainly on the role of canonical signaling-related core genes in diseases of the aorta, as well as recent advances in gene-mutation detection, animal models, and *in vitro* studies.

**Keywords:** TGF- $\beta$  signaling, aortic aneurysm, aortic dissection, SMADs, smooth muscle cells

## INTRODUCTION

Aortic aneurysm (AAs) and aortic dissections (ADs) are degenerative vascular diseases associated with high mortality. The main pathological manifestations are degeneration of the media layer, extracellular matrix (ECM) remodeling, infiltration of inflammatory cells into the aorta, progressive dilation of the aortic diameter and, finally, sudden death of the patient due to aorta rupture (Rabkin, 2017; Bossone and Eagle, 2021). AAs and ADs account for 1–2% of all deaths in Western countries, aortic aneurysm is the second most prevalent aortic disease following atherosclerosis and accounts for the ninth-leading cause of death overall, the estimated incidence is 2.79 per 100 000 individuals (Sampson et al., 2014).

In recent years, accumulating evidence has indicated that genetic factors, particularly transforming growth factor (TGF- $\beta$ ) signaling, play a key role in the development of aortic aneurysms, in addition to regulating many aspects of physiological homeostasis in embryonic and adult tissues (Lindsay and Dietz, 2014; Isselbacher et al., 2016; Tzavlaki and Moustakas, 2020). Several mutated genes have been identified from patients with AAs, many of these mutated genes belong to members of the TGF- $\beta$  signaling family. However, the role of TGF- $\beta$  signaling in AAs is controversial (Jones et al., 2009; Lin and Yang, 2010).

In this review, we focus mainly on the role of canonical signaling-related core genes in diseases of the aorta.

## OVERVIEW OF TGF- $\beta$ SIGNALING

TGF- $\beta$  superfamily is one of main signaling pathways in humans. Initially, it was found to have a crucial role in growth and development. Subsequent studies revealed it to be involved in regulation of various cellular processes: proliferation, differentiation, adhesion, metastasis, and apoptosis (Wu et al., 2014; Meng et al., 2016; Tzavlaki and Moustakas, 2020). In recent years, it has been revealed that dysregulation of the TGF- $\beta$  signaling pathway is closely related to several human diseases.

The transforming growth factor-beta (TGF- $\beta$ ) superfamily is comprised of over forty members, such as TGF- $\beta$ s, anti-mullerian hormone, nodal, activin, and bone morphogenetic proteins (BMPs), growth differentiation factors (GDFs). It can be divided into two subfamilies: TGF- $\beta$ /Activin/Nodal and BMP/GDF/MIS (Muellerian inhibiting substance) (MacFarlane et al., 2017; Miyazawa and Miyazono, 2017).

There are three types of TGF- $\beta$  ligands, TGF- $\beta$ 1, TGF- $\beta$ 2 and TGF- $\beta$ 3, and they have amino-acid homology of 64–82% (Perrella et al., 1998). Expression of these ligands is specific to tissues. TGF- $\beta$ s undertake very important regulatory process in the ECM. If an inactive cleaved peptide fragment, such as latent associated protein (LAP), is secreted by cells, it forms a large latent complex (LLC) with latent transforming growth factor binding protein (LTBP). Fibrillin-1 binds LTBP and anchors LLC to the ECM (Wrana et al., 1992; Isogai et al., 2003; Shi et al., 2011). TGF- $\beta$ s can activate only the corresponding receptor after dissociation from LAP; this regulatory process can concentrate and regulate the concentration of TGF- $\beta$ s to meet the different needs of cells.

TGFBRI and TGFBRII are single transmembrane glycoproteins. Their cytoplasmic regions have serine/threonine kinase activities. Seven type I receptors and five type II receptors have been identified in humans (Heldin and Moustakas, 2016). Binding of TGF- $\beta$ s, activin or nodal to receptors can lead to activation of canonical signals and TGFBRII can trans-phosphorylate and activate TGFBRI to form activated receptor dimers. Downstream SMADs proteins are activated further by activated receptor dimers (Wrana et al., 1992; Peng, 2003). The SMADs protein family is present in the cytoplasm and can transmit signals from the cell membrane directly to the nucleus. They can be divided into three subfamilies according to their structure and function: (i) receptor-activated SMADs (R-SMADs), including SMAD1, 2, 3, 5, 8, and 9; (ii) common-partner SMADs (Co-SMADs), only SMAD4 in mammals can interact with activated R-SMADs, and is the core transcription factor of the TGF- $\beta$  signal; (iii) inhibitor SMAD (I-SMADs), including SMAD6 and 7, which block receptor-mediated phosphorylation of R-SMAD and inhibit the formation of activated R-SMAD and Co-SMAD isopolymers. SMAD6 preferentially inhibits SMAD signaling initiated by the bone morphogenetic protein (BMP) type I receptors ALK-3 and ALK-6, whereas SMAD7 inhibits both transforming growth factor  $\beta$  (TGF- $\beta$ )- and BMP-induced Smad signaling (Hanyu et al., 2001; Goto et al., 2007; Miyazawa and Miyazono, 2017). I-SMADs can also bind competitively to activated receptors or R-SMADs to form

**TABLE 1 |** Protein-receptor pairing in the TGF- $\beta$  superfamily.

Ligands	Type I receptors	Type II receptors
TGF- $\beta$ s	TGFBRI (Alk5)	TGFBRII
Nodal	AcvR-Ib, AcvR-IC	AcvR-II, AcvR-IIb
Myostatin	AcvR-Ib, TGFBRI (Alk5)	AcvR-II, AcvR-IIb
Activin	TGFBRI (Alk5)	AcvR-II, AcvR-IIb
BMPs, GDFs	AcvRL-I (ALK1), AcvR-I (Alk2)	AcvR-II, AcvR-IIb, BMPRII
	BMPRIa (Alk3)	—
	BMPRIb (Alk6)	—

*TGFBRI*, transforming growth factor-beta receptors; *AcvRs*, activin A receptors; *BMPs*, Bone morphogenetic proteins; *GDFs*, growth and differentiation factors; *AcvRL-I*, activin A receptor like type 1; *BMPRI*, bone morphogenetic protein receptors.

inactive complexes, thereby inhibiting Co-SMAD-mediated gene expression (Derynck and Zhang, 2003; Park, 2005; Hata and Chen, 2016).

In the inactive state, SMAD4 is distributed in the cytoplasm and nucleus, R-SMADs are located mainly in the cytoplasm, and I-SMADs are mainly in the nucleus. If the receptor is activated, SMAD2 and SMAD3 are phosphorylated and activated to form a complex and transferred to the nucleus. The phosphorylated SMAD2/3 interacts with SMAD4 to form a Smad complex and synergistically regulates transcription of the target gene with other transcription factors (Moustakas et al., 2001; Feng and Derynck, 2005).

The downstream signal transduction of BMP differs from TGF- $\beta$  signal in that it depends on SMAD1/5/8. BMPs and GDFs bind to BMP type I receptors, including ALK-1 (activin receptor-like kinase 1), ALK-2, ALK-3/BMPRIa, or ALK-6/BMPRIb, nodal signals through ALK-4, the major type I receptor for activins, whereas myostatin signals through ALK-4 or ALK-5 (Table 1) (Morikawa et al., 2016), and then activate SMAD1/5/8 to form a complex with SMAD4 (Figure 1). The Smads complex translocates to the nucleus and regulates BMP-specific target genes, while inhibitory ligands, such as Noggin, block ligand-receptor binding and pathway activation (Chang et al., 2002). However, the pairing between receptors and ligands is not absolute, but there is some crossover. For example, TGF- $\beta$ s-activated TGFBRII not only interacts with TGFBRI, but also binds to ALK-1, thus leading to activation of both SMAD2 and SMAD3, also SMAD1, SMAD5, and SMAD8 in cells that express both ALK-1 (Goumans et al., 2003).

Studies have shown that SMADs in the TGF- $\beta$  canonical signaling pathway play a very important part in AAs and ADs, and many gene mutations have been identified in patients (Takeda et al., 2018). Studies in animal models have revealed some new molecular mechanisms. In this review, we focus on the research progress of these core genes in AAs and ADs. In addition, TGF- $\beta$  can activate many other signaling pathways that do not involve SMADs directly: extracellular-signal regulated kinase 1 and 2 (ERK1/2), c-Jun N-terminal kinase (JNK) (Lee et al., 2007; Sorrentino et al., 2008; Yamashita et al., 2008), phosphoinositide 3-kinase-Akt (PI3K-Akt) (Wilkes et al., 2005), and p38 mitogen-activated protein kinase (MAPK) (Li and Kong, 2020). We do not elaborate on TGF- $\beta$  non-classical signaling pathways.



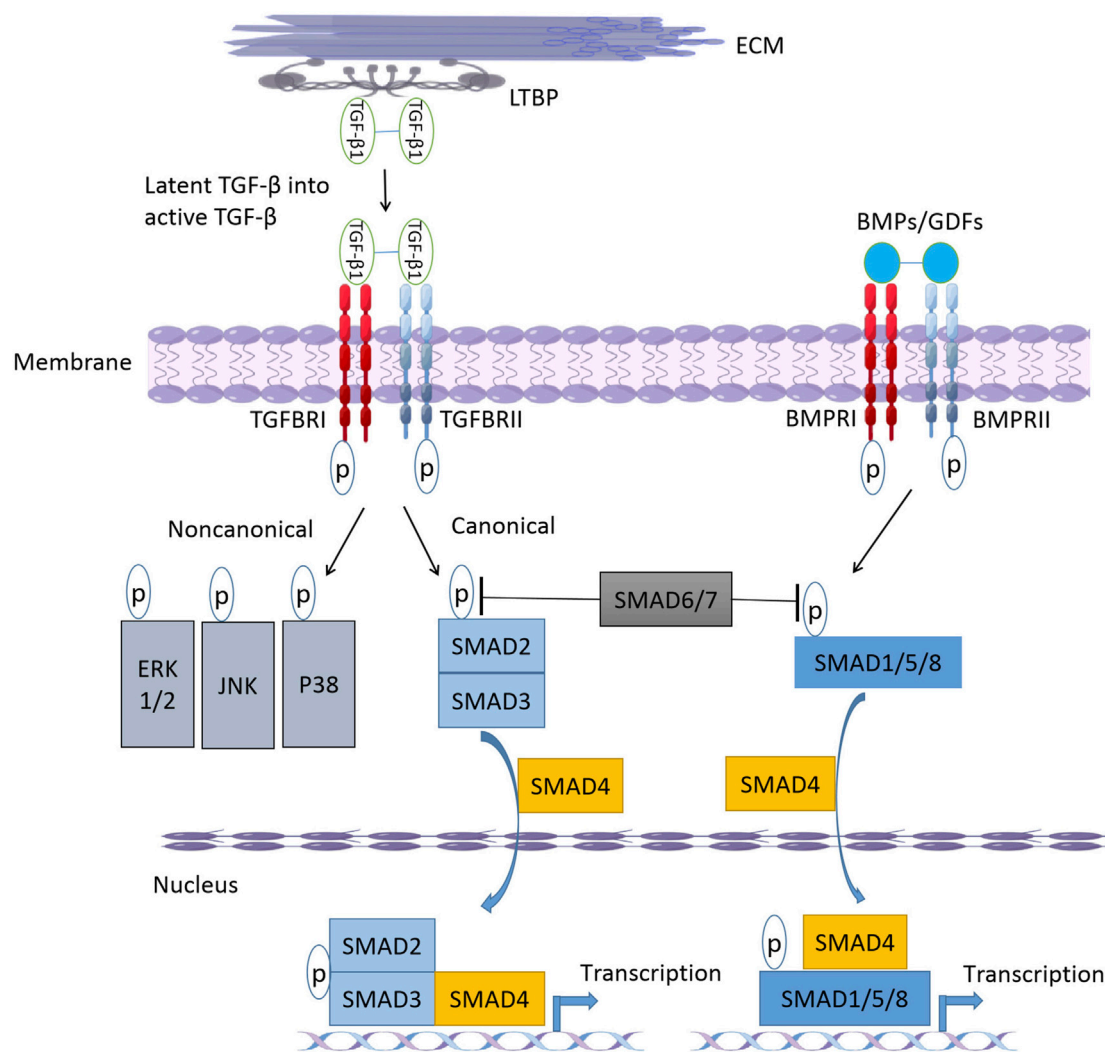


**FIGURE 1 |** The  $\beta$ /BMP signaling pathway. After cellular secretion, latent TGF- $\beta$  forms a large latent complex (LLC) with latent transforming growth factor binding protein (LTBP). Upon release from the LTBP, TGF- $\beta$  binds to receptors and TGFBR2 can trans-phosphorylate and activate TGFBR1 to form activated receptor dimers. Activation of receptor complex initiates canonical and non-canonical TGF- $\beta$  signaling pathways. After binding to active ligands BMPs or GDFs, BMPRI1 and BMPRI2 form phosphorylated dimers and activate downstream SMAD1/5/8. SMAD6 and SMAD7 can inhibit TGF- $\beta$  and BMP signaling pathways by inhibiting SMAD2/3 and SMAD1/5/8 phosphorylation, respectively. ECM, extracellular matrix; TGF- $\beta$ s, transforming growth factor- $\beta$ ; TGFBRs, transforming growth factor- $\beta$  receptors; BMPs, Bone morphogenetic proteins; GDFs, growth and differentiation factors; SMADs, *drosophila* mothers against decapentaplegic proteins; ERK, extracellular signal-regulated kinases; JNK, c-Jun N-terminal kinase.

## TGFBR1 AND TGFBR2 GENES

TGFBR1 is located on chromosome 9q. TGFBR2 is located on chromosome 3p. TGFBR1 and TGFBR2 are transmembrane proteins with serine/threonine kinase motifs, containing nine and seven exons, respectively. Early sequencing studies showed pathogenic mutations of TGFBR1 and TGFBR2 genes to be associated with a series of other pathological changes in addition to AAs, named Loeys-Dietz syndrome 1 (LDS1) and LDS2, respectively. **Table 2** gives an overview of important genetic defects leading to AAs and ADs formation in human. Most mutations in TGFBR1 and TGFBR2 genes are loss-of-function mutations, mainly in the evolutionarily conserved

serine/threonine kinase region. One-third of the TGFBR mutations are identified in TGFBR1, whereas the remainder is found in TGFBR2 (Loeys et al., 2005; Pannu et al., 2005; Loeys et al., 2006).

LDS is an autosomal-dominant genetic disorder. Although LDS shows clinical overlap with Marfan syndrome (MFS), it can be distinguished clinically from MFS (Meester et al., 2017). Except for AAs, the common features include pectus deformities, scoliosis, and arachnodactyly. Distinguishing findings are craniosynostosis, hypertelorism, cleft palate or bifid uvula, club feet, instability in the cervical spine and, most importantly, widespread arterial aneurysms with tortuosity and aortic rupture occur earlier. Moreover, in more severe cases of

**TABLE 2 |** Loss-of-function genetic defects causing AAs and ADs in human.

Gene	Chromosomal locus	Associated syndrome	Main clinical features	References (Pmid)
TGFBR1	9q22.33	Loeys-Dietz syndrome type I	Widespread arterial aneurysms with tortuosity ND ortic dissections occur earlier, pectus deformities, scoliosis, arachnodactyly, craniosynostosis, hypertelorism, cleft palate or bifid uvula, club feet	15731757 16928994
TGFBR2	3p24.1	Loeys-Dietz syndrome type II	Wildespread arterial aneurysms with tortuosity and aortic dissections occur earlier, pectus deformities, scoliosis, arachnodactyly, craniosynostosis, hypertelorism, cleft palate or bifid uvula, club feet	15731757 16928994
SMAD2	18q21.1	Loeys-Dietz syndrome type IV	Arterial aneurysms and dissections, valve abnormalities, hypertelorism, scoliosis, complex cogential heart disease	26247899
SMAD3	15q22.33	Aneurysm-osteoarthritis syndrome	Wildspread and aggressive arterial aneurysms and dissections, arterial tortuosity, early-onsetosteoarthritis, hypertelorism, bifid uvula	21217753 22167769
SMAD4	18q21.2	Juvenile polyposis syndrome and hereditary hemorrhagic telangiectasia	Aortic dilatation, Gastrointestinal hamartomatous polyps, epistaxis, telangiectasia and arteriovenous malformations	28874282
SMAD6	15q22.31	Bicuspid aortic valve	Thoracic aortic aneurysm and dissections, bicuspid aortic valve, aortic isthmus stenosis, dilated cardiomyopathy, hyperplasia of cardiac valves	28659821 32748548
SMAD7	38.p13	No report	—	—

AAs, Aortic aneurysms; ADs, Aortic dissections; TGFBRs, transforming growth factor-beta receptors; SMADs, drosophila mothers against decapentaplegic proteins.

LDS, cervical instability or cleft lip and palate may be present. The arteriopathy observed in LDS is disseminated, with AAs and ADs occurring in peripheral arterial beds and the aorta. Conversely, ectopia lentis (a finding highly specific to dysfunction of fibrillin-1 protein) is common in MFS but is not observed in LDS (Tran-Fadulu et al., 2009; Van Laer et al., 2014; MacFarlane et al., 2017). Interestingly, heterozygous deletion of TGFBR1 does not cause vascular disease. Heterozygous mutations in the TGFBR1 gene have been shown to cause multiple self-healing squamous epithelioma (MSSE). Most mutations in MSSE are extracellular ligand-binding domains or truncation mutations of the kinase domain, whereas most mutations in LDS are missense (Goudie et al., 2011; Fujiwara et al., 2019).

Abnormally enhanced TGF- $\beta$  signaling has been observed in aortic-tissue samples from patients with LDS. Co-transfection of wild-type and mutant TGFBR1 or TGFBR2 receptors in equal quantities results in reduced TGF- $\beta$  signaling, indicating that mutant receptors cannot propagate a signal even in the presence of their wild-type counterpart (Mizuguchi et al., 2004; Horbelt et al., 2010; Gallo et al., 2014). It has been revealed that mice carrying TGFBR1 and TGFBR2 heterozygous missense mutations, but not which are not haplo-sufficient for TGF- $\beta$  receptor alleles, recapitulate LDS phenotypically, which suggests that the presence of mutant TGFBR is necessary to cause disease (Gallo et al., 2014). **Table 3** gives an overview of mouse models associated with disturbed TGF- $\beta$  signaling pathway.

Smooth muscle cell-specific (SMC) knockout of TGFBR1 or TGFBR2 can lead to AAs, but TGFBR1 knockout is more destructive to the aorta. Enhanced ERK signaling in the aortic wall before causing structural degeneration has been observed in TGFBR1 SMC knockout mice. Inhibition of ERK phosphorylation or blockade of the angiotensin II type I receptor can prevent aneurysmal degeneration of Tgfr1-deficient aortas (Yang et al., 2016). In tamoxifen-induced

TGFBR2 SMC knockout mice, loss of the TGF- $\beta$  signaling pathway impairs the contractile apparatus of vascular smooth muscle, damages elastin, increases the number of macrophage markers, and increases cell proliferation and matrix accumulation (Li et al., 2014; Hu et al., 2015). Angiotensin II-induced disease in the abdominal aorta is exacerbated by systemic TGF- $\beta$  blockade, and thoracic aortic disease is exacerbated by SMC-specific loss of TGFBR2, which suggest that TGF- $\beta$  signaling prevents abdominal and thoracic aneurysmal disease by different mechanisms (Angelov et al., 2017). Those mouse experiments demonstrated that, as core molecules of the TGF- $\beta$  signaling family, TGFBR1 and TGFBR2 are essential for maintaining the structural integrity of the aorta after normal embryonic development.

## Receptor-Mediated SMADs (R-SMADs)

SMAD2 and SMAD3 mutations are important predisposing factors for AAs and ADs. They are located on the long arms of chromosomes 18 and 15, and are composed of 11 and 9 exons, respectively (Schepers et al., 2018). SMAD2 and SMAD3 proteins belong to the R-Smad family and are important downstream effectors of the canonical TGF- $\beta$  signaling pathway.

## -SMAD2 Gene

Pathogenic variants in SMAD2 have been reported in to be associated with AAs and ADs in only a few studies. Whole-exome sequencing was undertaken in 365 patients with AAs or ADs without FBN1, TGFBR1, TGFBR2, ACTA2, or MYH11 mutations: three SMAD2 loss-of function variants were identified. They were located in the MH2 region of the SMAD2 (Micha et al., 2015). Then, a novel missense mutation in SMAD2 in a Chinese family with early-onset AAs was identified (Zhang et al., 2017). Studies have shown that two distinct phenotypes are associated with pathogenic variants in SMAD2: (i) complex congenital heart disease with or without

**TABLE 3 |** Mouse models associated with disturbed TGF- $\beta$  signaling pathway.

Gene	Mouse model	Phenotype	Mechanism	References (Pmid)
TGFB1	KO	Embryonic lethal, angiogenesis defects	—	11285230
	Tgfb1 <sup>M318R/+</sup> heterozygous missense	Enlarged aortas and accelerated aortic root, recapitulate LDS	Increased TGF- $\beta$ signaling contributes to postnatal aneurysm progression, losartan prevents aortic aneurysm	24355923
	Postnatal SMC-specific tamoxifen injection	Aortic rupture and aneurysmal degeneration, 100% penetrance of ascending thoracic aortas	Inhibition of ERK phosphorylation or blockade of the ATR1 can prevent aneurysmal degeneration of Tgfb1-deficient aortas	27739498
	EC-KO	Embryonically lethal, severe defects in vascular development	—	18029401
TGFB2	KO	Embryonic lethal, angiogenesis defects	—	8873772
	Postnatal SMC-specific	Significantly lower degree of aneurysmal degeneration than TGFB1 KO	Treatment with rapamycin restored a quiescent smooth muscle phenotype and prevented dissection	24401272 26494233 27739498
	Tgfb1 <sup>M318R/+</sup> heterozygous missense	Enlarged aortas and accelerated aortic root, recapitulate LDS	Increased TGF- $\beta$ signaling contributes to postnatal aneurysm progression, losartan prevents aortic aneurysm	24355923
SMAD2	KO	Die before embryonic day 8.5 due to defective elongation of egg cylinders and germ-layer formation	—	9529255 9689088
	Neural crest cells-KO	Reduced numbers of SMCs in the media, thinner elastic lamina, and reduced vessel-wall thickness of carotid arteries	—	23817199
SMAD3	KO	Progressive dilation of aortic roots and the ascending aorta	Administration of anti-GM-CSF monoclonal antibodies to KO mice resulted in significantly less dilation in the aortic root	27688095 23585475
	Angiotensin II-infused SMAD3 KO	Significant aortic dilatation, medial and adventitial thickening	Administration of clodronate-liposomes depleted macrophage, and inhibition of iNOS restored elastin content and alleviated aortic dilation	23782924
	CaCl <sub>2</sub> induced SMAD3 KO	Abdominal aortic aneurysm	Enhanced staining for phosphorylated-SMAD2 and phosphorylated-ERK	25985281
SMAD4	KO	Pre-angiogenesis lethality	—	17895899
	EC-KO	Died at embryonic day 10.5 due to cardiovascular defects	—	17724086
	Postnatal SMC-specific	Aortic aneurysm and dissection, severe inflammatory cells infiltrate into the aorta	Macrophage infiltration contributes to the progression of aortic aneurysms. Therapeutic targeting of IL-1b improved aortic disease	26699655 29150241
SMAD6	KO	Embryonic and postnatal lethality with moderate penetrance, hyperplastic thickening of the cardiac valves, skeletal defects	—	30098998 10655064
SMAD7	KO	Majority die <i>in utero</i> due to cardiovascular defects. impaired cardiac functions and severe arrhythmia	—	18952608
	Hepatocyte-specific Smad7-knockout	Liver hepcidin expression and develop an iron deficiency phenotype	Increased phosphorylation of SMAD2/3 in atrioventricular cushion and endocardium	29575577

TGFBs, transforming growth factor-beta receptors; SMADs, drosophila mothers against decapentaplegic proteins; KO, knock out; LDS, Loeys-Dietz syndrome; SMCs, smooth muscle, smooth muscle cells; ATR1, angiotensin II, type 1 receptor; EC-KO, endothelial cell-knock out; GM-CSF, granulocyte-macrophage colony stimulating factor; iNOS, inducible nitric oxide synthase; IL-1b, Interleukin-1, beta.

laterality defects and other congenital anomalies; (ii) a late-onset vascular phenotype characterized by arterial aneurysms with connective-tissue abnormalities (Granadillo et al., 2018). Recently, studies have identified a SMAD2 nonsense variant and four missense variants, which are all located in the MH2 domain. In addition to AAs, these affected individuals present with a connective-tissue pathological phenotype (Cannaerts et al., 2019). Those studies suggest that screening for SMAD2 mutations is warranted in patients with AAs or ADs.

A striking feature is the reported increase in phosphorylated-SMAD2 expression and TGF- $\beta$  signaling in the aortic wall of patients with AAs or ADs caused by wide types of genetic mutations (Gomez et al., 2009; Fukuda et al., 2018), such as Fibrillin-1, SMAD3, SMAD4, TGFB1, TGFB2, TGFB3, and

TGFB2. This has caused controversy regarding the role of TGF- $\beta$  signaling in terms of the pathogenic mechanisms leading to AAs. Different hypotheses have arisen to address this issue, but experimental validation is needed. Evidence suggests that one of the mechanisms of overactivation of SMAD2 promoters is associated with excess transcriptional activity (a process associated with epigenetic modification of the SMAD2 promoter). This action is accompanied by switching from repression of SMAD2 expression in a healthy state to p53-dependent activation of SMAD2 by switching from myc-dependent aneurysmal VSMCs in humans (Loinard et al., 2014).

Mice embryos with SMAD2 knockout die before embryonic day-8.5 due to defective elongation of egg cylinders and germ-layer formation. Therefore, the pathological condition of the

aorta cannot be detected (Waldrip et al., 1998; Weinstein et al., 1998). SMAD2 is critical for VSMC differentiation from NCCs *in vivo*. Specific knockout of SMAD2 in NCCs leads to defective differentiation of NCCs to VSMCs in aortic-arch arteries during embryonic development. Reduced layers and numbers of VSMCs in the media, thinner elastic lamina, and reduced vessel-wall thickness of carotid arteries has been observed in SMAD2 NCC knockout mice (Xie et al., 2013). SMAD3 is important for the differentiation of SMCs from mesenchymal progenitors (Qiu et al., 2005). Evidence of AAs or ADs caused by SMAD3 deletion has not been reported in mouse models, which may be related to the compensatory effect caused by other genes. In future studies, tissue-specific knockout of SMAD3 and induction with other chemical agents (e.g., angiotensin II or  $\text{CaCl}_2$ ) may permit discovery of this association in mice.

### -SMAD3 Gene

SMAD3 plays an indispensable part in the homeostasis, remodeling, and fibrosis of connective tissue. The N-terminal MH1 domain of SMAD3 protein mediates binding to DNA, and the C-terminal MH2 domain is involved in protein-protein interactions (Schepers et al., 2018). Mutation of the MH2 domain of SMAD3 was first identified to cause AAs and ADs in patients (van de Laar et al., 2011). In contrast with other aneurysm syndromes, most of these affected individuals presented with early-onset osteoarthritis. Therefore, the syndrome caused by SMAD3 mutations is called “aneurysms-osteoarthritis syndrome” (AOS). Because of the many common clinical features with LDS (hypertelorism, bifid uvula, arterial tortuosity, and widespread AAs and ADs), it is now also classified as “LDS type 3” (van de Laar et al., 2012; MacCarrick et al., 2014). AOS is an autosomal-dominant connective-tissue disorder characterized by AAs and tortuosity, early-onset osteoarthritis, as well as mild craniofacial, skeletal and cutaneous anomalies. However, not all patients with a SMAD3 mutation present with osteoarthritis (Regalado et al., 2011). In contrast to MFS, cerebrovascular abnormalities occur frequently in AOS and LDS (van der Linde et al., 2012). Studies have further reported AOS to be caused by mutations at other SMAD3 sites (Liao et al., 2018).

SMAD3 mutations are responsible for 2% of familial thoracic AAs and ADs (Regalado et al., 2011). Sixty-seven mutations have been identified in SMAD3, including missense, nonsense, frameshift, and splice-site mutations, which are spread over the entire gene. There are no significant “hotspots” for SMAD3 mutations, but most of the reported haploinsufficiency or missense variants are concentrated in the MH2 domain. The latter is responsible for the direct binding of SMAD3 and SMAD4 to form a complex that mediates transcriptional regulation of TGF- $\beta$  downstream signals (Zhang et al., 2015; Schepers et al., 2018).

A SMAD3 knockout model in mice was used to elucidate the molecular mechanism of SMAD3 involvement in AA pathogenesis. Significant aortic dilatation, medial and adventitial thickening as well as luminal enlargement were observed in angiotensin II-infused SMAD3 knockout mice. Increased vascular inflammation (not hypertension) initiated

the AAs. AngII-infused SMAD3 mice showed increased inducible nitric oxide (iNOS)-derived production of nitric oxide and macrophage infiltration in aortas. Administration of clodronate-liposomes depleted macrophage/monocytes, and inhibition of iNOS by aminoguanidine restored elastin content and alleviated aortic dilation significantly (Tan et al., 2013). In another study, SMAD3 deficiency led to progressive dilation of aortic roots and the ascending aorta in adult C57BL/6 mice even without induction by angiotensin II. *Smad3*<sup>-/-</sup> (SMAD3 translation-initiation site was deleted) mice had a vascular phenotype similar to that observed in AOS: the aorta had chronic infiltration of inflammatory cells. Granulocyte macrophage-colony stimulating factor (GM-CSF) oversecreted from CD4<sup>+</sup>T cells in *Smad3*<sup>-/-</sup> mice has a key role in AA pathogenesis. GM-CSF has been shown to induce monocyte accumulation in the aortic root. In addition, administration of anti-GM-CSF monoclonal antibodies to *Smad3*<sup>-/-</sup> mice resulted in significantly less matrix metalloproteinase activity and dilation in the aortic root. GM-CSF overexpression has also been detected in the aorta of AOS patients with SMAD3 mutations (Ye et al., 2013). Those data strongly suggest that SMAD3 deletion in peripheral inflammatory cells is an important cause of AA, but we cannot exclude the contribution of SMAD3 deficiency in SMCs to AA occurrence. Therefore, further studies on the pathogenesis of tissue-specific SMAD3 deficiency or mutation must be done.

Another study also supported the role of SMAD3 in protecting vessel-wall integrity and suppressing inflammation in the pathogenesis of  $\text{CaCl}_2$ -induced AAAs.  $\text{CaCl}_2$  treatment induced robust infiltration by T cells and macrophages, activation of nuclear factor-kappa B and ERK 1/2 signaling pathways, and upregulation of SMAD 2/4 expression in the abdominal aorta of *Smad3*<sup>-/-</sup> mice (Dai et al., 2015). Interestingly, there was no increase in ECM accumulation, excessive collagen accumulation, or loss of SMCs in *Smad3*<sup>-/-</sup> mice. The aorta of *Smad3*-deficient mice showed enhanced staining for phosphorylated-SMAD2 and phosphorylated-Erk, but expression of TGF- $\beta$ -activated target genes was not upregulated. Instead, the aortas of fibulin-4<sup>R/R</sup>-deficient mice show increased ECM remodeling and a greater downstream transcriptional response (Ye et al., 2013). Those data further suggested that different mutations in patients with AA had different pathogenesis. Switching of the VSMC phenotype also plays an important part in TAAD. miR-21 expression has been found to be increased in an angiotensin II-infused *Smad3*<sup>+/-</sup> TAAD mouse model and in patients with ascending TAA. miR-21 deficiency in *Smad3*<sup>+/-</sup> mice exacerbates TAAD formation after infusion with angiotensin II; the increased SMAD7 expression and suppressed canonical TGF- $\beta$  signaling causes SMCs to switch from a contractile phenotype to a synthetic phenotype. Silencing of SMAD7 expression with lentivirus can prevent angiotensin II-induced TAAD formation in *Smad3*<sup>+/-</sup> miR-21<sup>-/-</sup> mice (Huang et al., 2018). Taken together, those independent studies using different lines of SMAD3 knockout mice demonstrated that SMAD3 is critical for protecting vessel walls from aneurysm formation. An excessive inflammatory response is a common feature in AA development, immunosuppression may be an effective option for treatment of patients with SMAD3 mutations.



As the core component of aortic walls, SMC disorders are an important cause of AA formation. Several *in vitro* studies have explored the role of SMAD3 in SMCs. SMAD3 has a vascular-protective role because it regulates vascular SMCs and matrix regulation. c-Ski inhibits the proliferation of aortic smooth muscle in A10 rats by suppressing SMAD3 signaling (Li et al., 2013). Furthermore, miR-26b suppresses AD development by targeting regulation of the HMGA2 and TGF- $\beta$ /SMAD3 signaling pathways; knockdown of miR-26b expression inhibited VSMC proliferation in a SMAD3-dependent way (Yang et al., 2020). Experiments on the response to vascular injury showed that the loss of SMAD3 in mice resulted in enhanced intima hyperplasia. In addition, studies have shown expression of the lncRNA CRNDE to be downregulated in AAA tissues and angiotensin II-stimulated VSMCs. CRNDE overexpression promoted VSMC proliferation and repressed apoptosis in AAA by upregulating SMAD3 expression via B-cell lymphoma 3 (Kobayashi et al., 2005; Zhou et al., 2019). TGF- $\beta$ /SMAD3 also interacts with canonical wntless type signaling to regulate the proliferation and apoptosis of SMCs (DiRenzo et al., 2016).

SMAD3 is also involved in regulation of some proinflammatory and cytokines. Connective-tissue growth factor (CTGF) is a key factor regulating ECM production. Peroxisome proliferator-activated receptor gamma binds directly to SMAD3 to inhibit induction of CTGF expression by TGF- $\beta$  signaling (Fu et al., 2001). TGF- $\beta$ 1-based inhibition of iNOS and IL-6 expression was shown to be blocked completely in Smad3-deficient VSMCs (Feinberg et al., 2004). Those studies emphasized that the role of SMAD3 in SMCs is very complex. Indeed, the function of SMAD3 in lineage-specific VSMCs may be different. SMAD3 is essential for the differentiation of cardiovascular progenitor cell-VSMCs but not for the differentiation of neural crest stem cell-VSMCs. SMAD3 deficiency leads to reduced contractility of cardiovascular progenitor cell-VSMCs (Gong et al., 2020). It has also been reported that SMAD3 knockout resulted in myocardial-cell necrosis in mice with a 129 genetic background and aortic rupture in C57BL/6J mice; different genetic backgrounds may be responsible for these differences (Kashyap et al., 2017).

## Co-SMAD -SMAD4 Gene

As a key transcription factor of the TGF- $\beta$  signaling pathway, SMAD4 is essential for developmental and postnatal cardiovascular homeostasis (Lan et al., 2007; Xu et al., 2019). SMAD4 loss-of-function mutations are associated with juvenile polyposis syndrome (JPS) and a combined JPS-hereditary hemorrhagic telangiectasia (HHT) known as “JPS-HHT syndrome”, and some affected individuals present with aortic dilatation (Larsen Haidle et al., 1993; Jelsig et al., 2016). Several genetic studies have shown that Smad4 mutation is a risk factor for aortic dilatation in JPS-HHT (Andrabi et al., 2011; Teekakirikul et al., 2013; Wu, 2017; Inoguchi et al., 2019).

A single nucleotide polymorphism (SNP) rs12455792 located in the transcription-factor binding site of SMAD4 leads to decreased transcription activity and proteoglycan degradation,

apoptosis of vascular smooth muscle cells (VSMCs) and fiber accumulation, which are involved in the pathological progression of TAAD (Wang et al., 2018). SMAD4 missense variants c.290G > T, p. (Arg97Leu) have been identified in one family associated with thoracic aortic disease. Experiments based on adenovirus transfection have revealed that the mutated site leads to increased ubiquitination-mediated degradation of Smad4 protein in SMCs (Duan et al., 2019). However, patients do not show the typical characteristics of JPS or HHT, though few cases have been reported (Schepers et al., 2018). These observations suggest that SMAD4 mutations are associated independently with aortic dilatation. In a clinical analysis, comparing the degree of dilatation of aortic roots and the ascending aorta between other HHT patients (ENG and ACVRL1 mutations) and non-HHT controls, SMAD4 mutation was found to be a significant risk factor (Vorselaars et al., 2017). Those studies demonstrated that SMAD4 mutations predispose to aortic dilatation, which suggests that screening for cardiovascular disease is necessary for JPS-HHT patients to prevent premature death due to AD or aortic rupture, which is clinically important. However, gain-of-function mutations in SMAD4 lead to Myhre syndrome; a rare, distinctive syndrome that mostly affects patients with cardiovascular abnormalities who do not have aortic dilatation (Lin et al., 2016; Meerschaut et al., 2019). The evidence stated above further emphasizes the importance of SMAD4 in the cardiovascular system.

With regard to the importance of SMAD4 and SMCs in the aorta, we conducted a mouse experiment to study how SMAD4 participates in AAs and ADs. SMAD4 deletion in SMCs led to AAs and ADs, which suggested a direct correlation between SMAD4 and AAs and ADs. Immunohistochemical assays showed that, in Smad4-deficient mice, many macrophages and cluster of differentiation (CD) $4^{+}$ T cells invaded the aorta, and expression of SMC-derived proinflammatory factors and chemokines was increased significantly. Selective clearance of macrophages and blockade of a chemokine signaling axis (CCL2-CCR2) could alleviate AAs in Smad4-deficient mice (Zhang et al., 2016). Those results suggest that the inflammatory response caused by SMAD4 loss in SMCs may be crucial for the pathogenesis of AAs and ADs. This view was confirmed by a subsequent study. Deletion of SMC-specific SMAD4 induced by tamoxifen in adult mice caused AA formation. SMAD4 ablation in SMCs activated inflammation early in the media and induced interleukin (IL)-1 $\beta$  production, and therapeutic targeting of IL-1 $\beta$  improved aortic disease and AA dilatation induced by SMC-specific SMAD4 inactivation (Da Ros et al., 2017). Interestingly, specific knockout of TGFBR2 in SMCs did not cause severe inflammatory responses and AA progression was much more moderate in mice (Zhang et al., 2016). Those data suggested that compensatory activation of TGF- $\beta$  non-canonical signaling in Smad4-deficient mice contributed significantly to the “inflammatory outburst” in the aorta.

MicroRNAs also play an important role in cardiovascular disease (Tang et al., 2021). Several researchers have studied the involvement of microRNAs (miRs) or long noncoding RNAs (lncRNAs) targeting SMAD4 in AAs and ADs. miR-146a-5p expression in circulating blood was increased

significantly in patients with thoracic aortic dissection, and upregulated expression of miR-146a-5p targeted SMAD4 to promote the proliferation and migration of VSMCs (Xue et al., 2019). The lncRNA SNHG5 acts as a “molecular sponge” for miR-205, and its expression is downregulated in abdominal aortic aneurysm (AAA) patients. Downregulation of SNHG5 expression enhances the inhibitory effect of miR-205--5p on SMAD4 and, thus, inhibits the proliferation, migration, and apoptosis of VSMCs (Nie et al., 2021). miR-26a expression has also been found to be downregulated in two mouse models of AAA and human aortic SMCs. Inhibition of miR-26A expression can increase SMAD4 expression, which enhances switching from a contractile phenotype to a synthetic phenotype (Leeper et al., 2011).

## I- SMAD Genes

### -SMAD6 Gene

As an inhibitory SMAD, SMAD6 is involved in regulation of the TGF- $\beta$  signaling pathway through various pathways. SMAD6 inhibits the formation of heteromerization with SMAD4 by binding to phosphorylated-SMAD2, but does not inhibit the activity of SMAD3. It also negatively regulates non-canonical TGF- $\beta$ 1 signaling by recruiting the deubiquitinase A20 to TRAF6 and inhibiting the TAK1-p38 MAPK/JNK pathway (Hata et al., 1998; Jung et al., 2013). Studies have revealed a crucial role for SMAD6 in the development and homeostasis of the cardiovascular system in Smad6-mutant mice. SMAD6 mutants have hyperplasia of cardiac valves and septation defects of outflow tracts, which is indicated by the development of aortic ossification and increased blood pressure (Galvin et al., 2000; Wylie et al., 2018). Individuals with a SMAD6 missense mutation present a complex cardiac pathological phenotype, such as aortic isthmus stenosis, a severe cardiac phenotype, and dilated cardiomyopathy (Kloth et al., 2019). SMAD6 is closely related to the occurrence of a bicuspid aortic valve (BAV). The latter is a heterogeneous disorder inherited primarily in an autosomal-dominant pattern with incomplete penetrance and variable expressivity. TAAs or acute ADs are common complications in inpatients with BAV. NOTCH1, TGFBR2, ACTA2, GATA5, NKX2.5, SMAD6, or ROBO4 mutations are the most commonly identified genetic causes of familial non-syndromic BAV (Musfee et al., 2020). However, there is little direct evidence that SMAD6 mutations in individuals lead to AAs or ADs. Whole-exome sequencing in 129 cases of sporadic TAAD revealed a 58-year-old male with a SMAD6 mutation (Li et al., 2021a). A clinical analysis showed limited contribution of the SMAD6 mutation to TAA development in BAV patients (Luyckx et al., 2019). Those data suggest that there may be other sites of genetic susceptibility involved in TAA. How SMAD6 participates in AAs requires *in vitro* and *in vivo* evidence.

### -SMAD7 Gene

SMAD7 is a key negative regulator of TGF- $\beta$  signaling, it antagonizes TGF- $\beta$  signaling through multiple mechanisms in the context of different cell types, and altered expression of SMAD7 is often associated with cancer, tissue fibrosis and

inflammatory diseases (Miyazawa and Miyazono, 2017). However, the genetic association between SMAD7 and aortic aneurysm and dissection has not been identified to date. Some studies suggest that SMAD7 also plays an important role in the cardiovascular system. Deletion of the MH2 domain of SMAD7 produced embryos with outflow tract, ventricular septum, ventricular compaction, and cardiac function defects (Chen et al., 2009).

Overexpression of SMAD7 suppressed differentiation and proliferation of VSMCs and reiterated defects in adult BMP9/10 double mutants mice (Wang et al., 2021). Homozygous knockdown of SMAD7 produced primarily fourth-related arch artery defects (Papangeli and Scambler, 2013), which indicates that SMAD7 is required for great vessel development. In addition, SMAD7 can be a microRNA target involved in SMCs function maintenance. Lentivirus knockdown of SMAD7 prevented AngII-induced Smad3<sup>+/+</sup>-Mir-21<sup>-/-</sup> mouse TAAD formation (Huang et al., 2018), and VSMC-specific miRNA-214 knockout inhibits AngII-induced hypertension through up-regulation of SMAD7 (Li et al., 2021b). The *in vivo* role of SMAD7 in the maintenance of aortic structure and function remains to be explored.

## Medical Therapy Targeting Abnormal TGF- $\beta$ Signaling

Progressive expansion of AAs can lead to life-threatening aortic dissection and aortic rupture. So far, surgery or endovascular intervention has been the primary treatment, but medical therapy also plays an important role in slowing AAs dilation, and as the pathogenesis of AAs becomes clearer, it is expected that more effective drug therapy will be available.

Substantial evidence shows that the canonical TGF- $\beta$  signaling abnormalities plays a central role in the formation of hereditary AAs, higher circulating TGF- $\beta$  levels are associated with more advanced stages and higher rates of aortic dilatation in TAA patients (Franken et al., 2015). In addition, it interacts with the Renin-angiotensin system (RAS) at multiple levels. Ang II can directly increase TGF- $\beta$  mRNA production, TGF- $\beta$  protein expression and TGF- $\beta$  activity upstream of signal. Abnormal upregulation of ACE and elevated local RAS signaling has been demonstrated in patients with AAs induced by abnormalities of the TGF- $\beta$  classical signaling and in mouse models (van Dorst et al., 2021). Therefore, these two signaling pathways are important targets for drug therapy. Such as TGF- $\beta$  neutralizing antibodies or Ang II type 1 receptor blocker (ARB) losartan. In addition, irbesartan, statins, and  $\beta$ -blockers are also common treatment options.

Almost all drug treatments have performed in MFS individuals, which provides a paradigm for LDS and other types of AAs, although the mutated gene loci are different, abnormal TGF- $\beta$  signaling enhancement are a common feature. Several studies have shown that aortic dilatation was decreased after the use of neutralizing inhibitors against TGF- $\beta$  or ARB in MFS mouse model (Yang et al., 2009; Habashi et al., 2011). Based on the validity of animal experiments, the first clinical trial evaluated the treatment effect of ARB on 18 pediatric

patients with MFS, the use of ARB therapy significantly slowed the rate of progressive aortic-root dilation, but the distal ascending aorta is not affected. The results were confirmed by several subsequent randomized controlled clinical trials, and the beneficial effects of losartan are independent of its effects on blood pressure (Brooke et al., 2008; Groenink et al., 2013; Lacro et al., 2014). It is speculated that the inhibitory effect on TGF- $\beta$  and ERK1/2-signaling may be the mechanism of losartan slowing down the progression of aortic aneurysms.

Several clinical trials have compared the efficacy of ARBs versus  $\beta$ -blockers in preventing aortic dilation in patients with MFS. Losartan was compared with the  $\beta$ -blocker atenolol in 608 patients with MFS, demonstrating that both drugs were equally effective in reducing aortic root dilation. Overall, the combined use of ARBs and  $\beta$ -Blockers not only significantly delayed aortic aneurysm dilation, but also prevented long-term adverse outcomes, according to a large number of clinical trials (Lacro et al., 2014; Forteza et al., 2016). Unfortunately, the clinical therapeutic effect of ARBs on MFS patients is not as significant as that of preclinical results. The time window of treatment, the type and dose of inhibitors used, and genetic heterogeneity in MFS patients may be responsible for this difference. Therefore, the effect of ARBs on genetic AA patients other than MFS needs to be carefully evaluated in consideration of the difference in the impact of gene heterogeneity on the therapeutic effect. It is necessary to conduct more genetic tests and studies on these individual patients.

## DISCUSSION AND PERSPECTIVES

TGF- $\beta$  signaling pathway plays a central role in aortic diseases, but the mechanism is very complex. The genes TGFBR1, TGFBR2, SMAD2, SMAD3, SMAD4, SMAD6 and SMAD7 reviewed in this paper. Although they belong to the same TGF- $\beta$  canonical signaling core genes family, patients with different gene mutations present very different clinical phenotype. A common phenotype of these gene mutations is aortic aneurysm or dissection, and aneurysm rupture is the main cause of death in these mutation patients. Therefore, in the clinical examination, it is necessary to screen for the cardiovascular system, especially the aorta, in patients with these mutations.

Loss-of-function mutations or deficiency of SMAD2, SMAD3, and SMAD4 genes in mice or humans lead to the formation of aortic aneurysms or dissections, suggesting that basal TGF-

$\beta$ signaling canonical signaling is indispensable for maintaining the integrity of aortic structure and function. Functional abnormalities of VSMCs, a core component of the aortic structure, caused by SMADs mutations are the most well studied, these SMADs mutations cause VSMCs to switch from contractile to secretory. Another common mechanism is activation of non-canonical signaling pathways, such as ERK1/2 and MAPK, which initiate severe inflammatory responses and protease secretion, leading to aortic ECM remodeling. Interestingly, although only a few clinical cases have been reported and the permeability is low, the mutation of I-Smad SMAD6 still leads to the formation of aortic aneurysms. This further increases the complexity of the role of TGF- $\beta$ signaling pathway in maintaining aortic structure. Whether loss of SMAD6 leads to overactivation of non-canonical signaling pathways? As far as we know, there is no AAs mouse model caused by SMAD6 gene deletion at present, and its mechanism needs to be further explored in the future.

On the other hand, although the aortic tissues of these mutated patients showed abnormal enhancement of TGF- $\beta$  signaling pathways, studies of molecular mechanisms in mouse models and cells suggest that the pathogenesis is very different.

Current drug therapies may only be suitable for a small subset of high-risk patients, and a better understanding of the underlying genetic mechanisms will help identify patient populations that respond to specific treatments. This heterogeneity of pathogenesis with different mutated genes means that targeted therapies may be the trend of the future. More efficient gene sequencing and editing techniques make this trend possible. In the study of mechanism, the efficient construction of locus mutation mouse model can better recapitulate the real human disease situation, which is more convenient for the study of pathogenesis and evaluation of potential drug targets, which will contribute to the development of personalized drug therapy.

## AUTHOR CONTRIBUTIONS

JC collated and analyzed literatures, and wrote the manuscript. RC edited the manuscript.

## FUNDING

This work was supported by the grants from Guangdong Regional Joint Fund (Grant No. 2021A151511224).

## REFERENCES

- Andrabi, S., Bekheirnia, M. R., Robbins-Furman, P., Lewis, R. A., Prior, T. W., and Potocki, L. (2011). SMAD4 Mutation Segregating in a Family with Juvenile Polyposis, Aortopathy, and Mitral Valve Dysfunction. *Am. J. Med. Genet. A* 155A (5), 1165–1169. doi:10.1002/ajmg.a.33968
- Angelov, S. N., Hu, J. H., Wei, H., Airhart, N., Shi, M., and Dichek, D. A. (2017). TGF- $\beta$  (Transforming Growth Factor- $\beta$ ) Signaling Protects the Thoracic and Abdominal Aorta from Angiotensin II-Induced Pathology by Distinct Mechanisms. *Atvb* 37 (11), 2102–2113. doi:10.1161/ATVBAHA.117.309401
- Bossone, E., and Eagle, K. A. (2021). Epidemiology and Management of Aortic Disease: Aortic Aneurysms and Acute Aortic Syndromes. *Nat. Rev. Cardiol.* 18 (5), 331–348. doi:10.1038/s41569-020-00472-6
- Brooke, B. S., Habashi, J. P., Judge, D. P., Patel, N., Loeys, B., and Dietz, H. C., 3rd (2008). Angiotensin II Blockade and Aortic-Root Dilation in Marfan's Syndrome. *N. Engl. J. Med.* 358 (26), 2787–2795. doi:10.1056/NEJMoa0706585

- Cannaerts, E., Kempers, M., Maugeri, A., Marcelis, C., Gardeitchik, T., Richer, J., et al. (2019). Novel Pathogenic SMAD2 Variants in Five Families with Arterial Aneurysm and Dissection: Further Delineation of the Phenotype. *J. Med. Genet.* 56 (4), 220–227. doi:10.1136/jmedgenet-2018-105304
- Chang, H., Brown, C. W., and Matzuk, M. M. (2002). Genetic Analysis of the Mammalian Transforming Growth Factor-Beta Superfamily. *Endocr. Rev.* 23 (6), 787–823. doi:10.1210/er.2002-0003
- Chen, Q., Chen, H., Zheng, D., Kuang, C., Fang, H., Zou, B., et al. (2009). Smad7 Is Required for the Development and Function of the Heart. *J. Biol. Chem.* 284 (1), 292–300. doi:10.1074/jbc.M807233200
- Da Ros, F., Carnevale, R., Cifelli, G., Bizzotto, D., Casaburo, M., Perrotta, M., et al. (2017). Targeting Interleukin-1 $\beta$  Protects from Aortic Aneurysms Induced by Disrupted Transforming Growth Factor  $\beta$  Signaling. *Immunity* 47 (5), 959–e9. doi:10.1016/j.immuni.2017.10.016
- Dai, X., Shen, J., Annam, N. P., Jiang, H., Levi, E., Schworer, C. M., et al. (2015). SMAD3 Deficiency Promotes Vessel wall Remodeling, Collagen Fiber Reorganization and Leukocyte Infiltration in an Inflammatory Abdominal Aortic Aneurysm Mouse Model. *Sci. Rep.* 5, 10180. doi:10.1038/srep10180
- Derynck, R., and Zhang, Y. E. (2003). Smad-dependent and Smad-independent Pathways in TGF- $\beta$  Family Signalling. *Nature* 425 (6958), 577–584. doi:10.1038/nature02006
- DiRenzo, D. M., Chaudhary, M. A., Shi, X., Franco, S. R., Zent, J., Wang, K., et al. (2016). A Crosstalk between TGF- $\beta$ /Smad3 and Wnt/ $\beta$ -Catenin Pathways Promotes Vascular Smooth Muscle Cell Proliferation. *Cell Signal* 28 (5), 498–505. doi:10.1016/j.cellsig.2016.02.011
- Duan, X. Y., Guo, D. C., Regalado, E. S., Shen, H., University of Washington Center for Mendelian, G., Coselli, J. S., et al. (2019). SMAD4 Rare Variants in Individuals and Families with Thoracic Aortic Aneurysms and Dissections. *Eur. J. Hum. Genet.* 27 (7), 1054–1060. doi:10.1038/s41431-019-0357-x
- Feinberg, M. W., Watanabe, M., Lebedeva, M. A., Depina, A. S., Hanai, J., Mammoto, T., et al. (2004). Transforming Growth Factor-Beta1 Inhibition of Vascular Smooth Muscle Cell Activation Is Mediated via Smad3. *J. Biol. Chem.* 279 (16), 16388–16393. doi:10.1074/jbc.M309664200
- Feng, X. H., and Derynck, R. (2005). Specificity and Versatility in Tgf-Beta Signaling through Smads. *Annu. Rev. Cell Dev Biol* 21, 659–693. doi:10.1146/annurev.cellbio.21.022404.142018
- Forteza, A., Evangelista, A., Sánchez, V., Teixidó-Turà, G., Sanz, P., Gutiérrez, L., et al. (2016). Efficacy of Losartan vs. Atenolol for the Prevention of Aortic Dilation in Marfan Syndrome: a Randomized Clinical Trial. *Eur. Heart J.* 37 (12), 978–985. doi:10.1093/eurheartj/ehv575
- Franken, R., Radonic, T., den Hartog, A. W., Groenink, M., Pals, G., van Eijk, M., et al. (2015). The Revised Role of TGF- $\beta$  in Aortic Aneurysms in Marfan Syndrome. *Neth. Heart J.* 23 (2), 116–121. doi:10.1007/s12471-014-0622-0
- Fu, M., Zhang, J., Zhu, X., Myles, D. E., Willson, T. M., Liu, X., et al. (2001). Peroxisome Proliferator-Activated Receptor Gamma Inhibits Transforming Growth Factor Beta-Induced Connective Tissue Growth Factor Expression in Human Aortic Smooth Muscle Cells by Interfering with Smad3. *J. Biol. Chem.* 276 (49), 45888–45894. doi:10.1074/jbc.M105490200
- Fujiwara, T., Takeda, N., Ishii, S., Morita, H., and Komuro, I. (2019). Unique Mechanism by Which TGFBR1 Variants Cause 2 Distinct System Diseases - Loeys-Dietz Syndrome and Multiple Self-Healing Squamous Epithelioma. *Circ. Rep.* 1 (11), 487–492. doi:10.1253/circrep.CR-19-0098
- Fukuda, H., Aoki, H., Yoshida, S., Tobinaga, S., Otsuka, H., Shojima, T., et al. (2018). Characterization of SMAD2 Activation in Human Thoracic Aortic Aneurysm. *Ann. Vasc. Dis.* 11 (1), 112–119. doi:10.3400/avd.0a.17-00114
- Gallo, E. M., Loch, D. C., Habashi, J. P., Calderon, J. F., Chen, Y., Bedja, D., et al. (2014). Angiotensin II-dependent TGF- $\beta$  Signaling Contributes to Loeys-Dietz Syndrome Vascular Pathogenesis. *J. Clin. Invest.* 124 (1), 448–460. doi:10.1172/JCI69666
- Galvin, K. M., Donovan, M. J., Lynch, C. A., Meyer, R. I., Paul, R. J., Lorenz, J. N., et al. (2000). A Role for Smad6 in Development and Homeostasis of the Cardiovascular System. *Nat. Genet.* 24 (2), 171–174. doi:10.1038/72835
- Gomez, D., Al Haj Zen, A., Borges, L. F., Philippe, M., Gutierrez, P. S., Jondeau, G., et al. (2009). Syndromic and Non-syndromic Aneurysms of the Human Ascending Aorta Share Activation of the Smad2 Pathway. *J. Pathol.* 218 (1), 131–142. doi:10.1002/path.2516
- Gong, J., Zhou, D., Jiang, L., Qiu, P., Milewicz, D. M., Chen, Y. E., et al. (2020). *In Vitro* Lineage-Specific Differentiation of Vascular Smooth Muscle Cells in Response to SMAD3 Deficiency: Implications for SMAD3-Related Thoracic Aortic Aneurysm. *Arterioscler Thromb. Vasc. Biol.* 40 (7), 1651–1663. doi:10.1161/ATVBAHA.120.313033
- Goto, K., Kamiya, Y., Imamura, T., Miyazono, K., and Miyazawa, K. (2007). Selective Inhibitory Effects of Smad6 on Bone Morphogenetic Protein Type I Receptors. *J. Biol. Chem.* 282 (28), 20603–20611. doi:10.1074/jbc.M702100200
- Goudie, D. R., D'Alessandro, M., Merriman, B., Lee, H., Szeverényi, I., Avery, S., et al. (2011). Multiple Self-Healing Squamous Epithelioma Is Caused by a Disease-specific Spectrum of Mutations in TGFBR1. *Nat. Genet.* 43 (4), 365–369. doi:10.1038/ng.780
- Goumans, M. J., Valdimarsdottir, G., Itoh, S., Lebrin, F., Larsson, J., Mummery, C., et al. (2003). Activin Receptor-like Kinase (ALK)1 Is an Antagonistic Mediator of Lateral TGF $\beta$ /ALK5 Signaling. *Mol. Cell* 12 (4), 817–828. doi:10.1016/s1097-2765(03)00386-1
- Granadillo, J. L., Chung, W. K., Hecht, L., Corsten-Janssen, N., Wegner, D., Nij Bijvank, S. W. A., et al. (2018). Variable Cardiovascular Phenotypes Associated with SMAD2 Pathogenic Variants. *Hum. Mutat.* 39 (12), 1875–1884. doi:10.1002/humu.23627
- Groenink, M., den Hartog, A. W., Franken, R., Radonic, T., de Waard, V., Timmermans, J., et al. (2013). Losartan Reduces Aortic Dilatation Rate in Adults with Marfan Syndrome: a Randomized Controlled Trial. *Eur. Heart J.* 34 (45), 3491–3500. doi:10.1093/eurheartj/ehs334
- Habashi, J. P., Doyle, J. J., Holm, T. M., Aziz, H., Schoenhoff, F., Bedja, D., et al. (2011). Angiotensin II Type 2 Receptor Signaling Attenuates Aortic Aneurysm in Mice through ERK Antagonism. *Science* 332 (6027), 361–365. doi:10.1126/science.1192152
- Hanyu, A., Ishidou, Y., Ebisawa, T., Shimanuki, T., Imamura, T., and Miyazono, K. (2001). The N Domain of Smad7 Is Essential for Specific Inhibition of Transforming Growth Factor-Beta Signaling. *J. Cell Biol* 155 (6), 1017–1027. doi:10.1083/jcb.200106023
- Hata, A., and Chen, Y. G. (2016). TGF- $\beta$  Signaling from Receptors to Smads. *Cold Spring Harb Perspect. Biol.* 8 (9). doi:10.1101/cshperspect.a022061
- Hata, A., Lagna, G., Massagué, J., and Hemmati-Brivanlou, A. (1998). Smad6 Inhibits BMP/Smad1 Signaling by Specifically Competing with the Smad4 Tumor Suppressor. *Genes Dev.* 12 (2), 186–197. doi:10.1101/gad.12.2.186
- Heldin, C. H., and Moustakas, A. (2016). Signaling Receptors for TGF- $\beta$  Family Members. *Cold Spring Harb Perspect. Biol.* 8 (8). doi:10.1101/cshperspect.a022053
- Horbelt, D., Guo, G., Robinson, P. N., and Knaus, P. (2010). Quantitative Analysis of TGFBR2 Mutations in Marfan-Syndrome-Related Disorders Suggests a Correlation between Phenotypic Severity and Smad Signaling Activity. *J. Cell Sci* 123 (Pt 24), 4340–4350. doi:10.1242/jcs.074773
- Hu, J. H., Wei, H., Jaffe, M., Airhart, N., Du, L., Angelov, S. N., et al. (2015). Postnatal Deletion of the Type II Transforming Growth Factor- $\beta$  Receptor in Smooth Muscle Cells Causes Severe Aortopathy in Mice. *Arterioscler Thromb. Vasc. Biol.* 35 (12), 2647–2656. doi:10.1161/ATVBAHA.115.306573
- Huang, X., Yue, Z., Wu, J., Chen, J., Wang, S., Wu, J., et al. (2018). MicroRNA-21 Knockout Exacerbates Angiotensin II-Induced Thoracic Aortic Aneurysm and Dissection in Mice with Abnormal Transforming Growth Factor- $\beta$ -SMAD3 Signaling. *Arterioscler Thromb. Vasc. Biol.* 38 (5), 1086–1101. doi:10.1161/ATVBAHA.117.310694
- Inoguchi, Y., Kaku, B., Kitagawa, N., and Katsuda, S. (2019). Hereditary Hemorrhagic Telangiectasia with SMAD4 Mutations Is Associated with Fatty Degeneration of the Left Ventricle, Coronary Artery Aneurysm, and Abdominal Aortic Aneurysm. *Intern. Med.* 58 (3), 387–393. doi:10.2169/internalmedicine.1287-18
- Isogai, Z., Ono, R. N., Ushiro, S., Keene, D. R., Chen, Y., Mazzieri, R., et al. (2003). Latent Transforming Growth Factor Beta-Binding Protein 1 Interacts with Fibrillin and Is a Microfibril-Associated Protein. *J. Biol. Chem.* 278 (4), 2750–2757. doi:10.1074/jbc.M209256200
- Isselbacher, E. M., Lino Cardenas, C. L., and Lindsay, M. E. (2016). Hereditary Influence in Thoracic Aortic Aneurysm and Dissection. *Circulation* 133 (24), 2516–2528. doi:10.1161/CIRCULATIONAHA.116.009762
- Jelsing, A. M., Tørring, P. M., Kjeldsen, A. D., Qvist, N., Bojesen, A., Jensen, U. B., et al. (2016). JP-HHT Phenotype in Danish Patients with SMAD4 Mutations. *Clin. Genet.* 90 (1), 55–62. doi:10.1111/cge.12693
- Jones, J. A., Spinale, F. G., and Ikonomidou, S. S. (2009). Transforming Growth Factor-Beta Signaling in Thoracic Aortic Aneurysm Development: a Paradox in Pathogenesis. *J. Vasc. Res.* 46 (2), 119–137. doi:10.1159/000151766



- Jung, S. M., Lee, J. H., Park, J., Oh, Y. S., Lee, S. K., Park, J. S., et al. (2013). Smad6 Inhibits Non-canonical TGF- $\beta$ 1 Signalling by Recruiting the Deubiquitinase A20 to TRAF6. *Nat. Commun.* 4, 2562. doi:10.1038/ncomms3562
- Kashyap, S., Warner, G., Hu, Z., Gao, F., Osman, M., Al Saiegh, Y., et al. (2017). Cardiovascular Phenotype in Smad3 Deficient Mice with Renovascular Hypertension. *PLoS One* 12 (10), e0187062. doi:10.1371/journal.pone.0187062
- Kloth, K., Bierhals, T., Johannsen, J., Harms, F. L., Juusola, J., Johnson, M. C., et al. (2019). Biallelic Variants in SMAD6 Are Associated with a Complex Cardiovascular Phenotype. *Hum. Genet.* 138 (6), 625–634. doi:10.1007/s00439-019-02011-x
- Kobayashi, K., Yokote, K., Fujimoto, M., Yamashita, K., Sakamoto, A., Kitahara, M., et al. (2005). Targeted Disruption of TGF- $\beta$ -Smad3 Signaling Leads to Enhanced Neointimal Hyperplasia with Diminished Matrix Deposition in Response to Vascular Injury. *Circ. Res.* 96 (8), 904–912. doi:10.1161/01.RES.0000163980.55495.44
- Lacro, R. V., Dietz, H. C., Sleeper, L. A., Yetman, A. T., Bradley, T. J., Colan, S. D., et al. (2014). Atenolol versus Losartan in Children and Young Adults with Marfan's Syndrome. *N. Engl. J. Med.* 371 (22), 2061–2071. doi:10.1056/NEJMoa1404731
- Lan, Y., Liu, B., Yao, H., Li, F., Weng, T., Yang, G., et al. (2007). Essential Role of Endothelial Smad4 in Vascular Remodeling and Integrity. *Mol. Cell Biol.* 27 (21), 7683–7692. doi:10.1128/MCB.00577-07
- Larsen Haidle, J., MacFarland, S. P., Howe, J. R., Adam, M. P., Ardinger, H. H., Pagon, R. A., et al. (1993). In *Juvenile Polyposis Syndrome* GeneReviews(R). Seattle (WA).
- Lee, M. K., Pardoux, C., Hall, M. C., Lee, P. S., Warburton, D., Qing, J., et al. (2007). TGF- $\beta$  Activates Erk MAP Kinase Signalling through Direct Phosphorylation of ShcA. *EMBO J.* 26 (17), 3957–3967. doi:10.1038/sj.emboj.7601818
- Leeper, N. J., Raiesdana, A., Kojima, Y., Chun, H. J., Azuma, J., Maegdefessel, L., et al. (2011). MicroRNA-26a Is a Novel Regulator of Vascular Smooth Muscle Cell Function. *J. Cell Physiol.* 126 (4), 1035–1043. doi:10.1002/jcp.22422
- Li, J., Li, P., Zhang, Y., Li, G. B., Zhou, Y. G., Yang, K., et al. (2013). c-Ski Inhibits the Proliferation of Vascular Smooth Muscle Cells via Suppressing Smad3 Signaling but Stimulating P38 Pathway. *Cell Signal* 25 (1), 159–167. doi:10.1016/j.cellsig.2012.09.001
- Li, W., Li, Q., Jiao, Y., Qin, L., Ali, R., Zhou, J., et al. (2014). Tgfb2 Disruption in Postnatal Smooth Muscle Impairs Aortic wall Homeostasis. *J. Clin. Invest.* 124 (2), 755–767. doi:10.1172/JCI69942
- Li, Y., Fang, M., Yang, J., Yu, C., Kuang, J., Sun, T., et al. (2021a). Analysis of the Contribution of 129 Candidate Genes to Thoracic Aortic Aneurysm or Dissection of a Mixed Cohort of Sporadic and Familial Cases in South China. *Am. J. Transl. Res.* 13 (5), 4281–4295.
- Li, Y., Li, H., Xing, W., Li, J., Du, R., Cao, D., et al. (2021b). Vascular Smooth Muscle Cell-specific miRNA-214 Knockout Inhibits Angiotensin II-induced Hypertension through Upregulation of Smad7. *FASEB J.* 35 (11), e21947. doi:10.1096/fj.202100766RR
- Li, Z., and Kong, W. (2020). Cellular Signaling in Abdominal Aortic Aneurysm. *Cell Signal* 70, 109575. doi:10.1016/j.cellsig.2020.109575
- Liao, M. F., Gong, Q. W., Liu, L., Xiong, X. Y., Zhang, Q., Gong, C. X., et al. (2018). Association Between Polymorphism of SMAD3 Gene and Risk of Sporadic Intracranial Arterial Aneurysms in the Chinese Han Population. *J. Clin. Neurosci.* 47, 269–272. doi:10.1016/j.jocn.2017.09.006
- Lin, A. E., Michot, C., Cormier-Daire, V., L'Ecuier, T. J., Matherne, G. P., Barnes, B. H., et al. (2016). Gain-of-Function Mutations in SMAD4 Cause a Distinctive Repertoire of Cardiovascular Phenotypes in Patients with Myhre Syndrome. *Am. J. Med. Genet. A.* 170 (10), 2617–2631. doi:10.1002/ajmg.a.37739
- Lin, F., and Yang, X. (2010). TGF- $\beta$  Signaling in Aortic Aneurysm: Another Round of Controversy. *J. Genet. Genomics* 37 (9), 583–591. doi:10.1016/S1673-8527(09)60078-3
- Lindsay, M. E., and Dietz, H. C. (2014). The Genetic Basis of Aortic Aneurysm. *Cold Spring Harb Perspect. Med.* 4 (9), a015909. doi:10.1101/cshperspect.a015909
- Loeys, B. L., Chen, J., Neptune, E. R., Judge, D. P., Podowski, M., Holm, T., et al. (2005). A Syndrome of Altered Cardiovascular, Craniofacial, Neurocognitive and Skeletal Development Caused by Mutations in TGFBR1 or TGFBR2. *Nat. Genet.* 37 (3), 275–281. doi:10.1038/ng1511
- Loeys, B. L., Schwarze, U., Holm, T., Callewaert, B. L., Thomas, G. H., Pannu, H., et al. (2006). Aneurysm Syndromes Caused by Mutations in the TGF- $\beta$  Receptor. *N. Engl. J. Med.* 355 (8), 788–798. doi:10.1056/NEJMoa055695
- Loinard, C., Basatemur, G., Masters, L., Baker, L., Harrison, J., Figg, N., et al. (2014). Deletion of Chromosome 9p21 Noncoding Cardiovascular Risk Interval in Mice Alters Smad2 Signaling and Promotes Vascular Aneurysm. *Circ. Cardiovasc. Genet.* 7 (6), 799–805. doi:10.1161/CIRCGENETICS.114.000696
- Luyckx, I., MacCarrick, G., Kempers, M., Meester, J., Geryl, C., Rombouts, O., et al. (2019). Confirmation of the Role of Pathogenic SMAD6 Variants in Bicuspid Aortic Valve-Related Aortopathy. *Eur. J. Hum. Genet.* 27 (7), 1044–1053. doi:10.1038/s41431-019-0363-z
- MacCarrick, G., Black, J. H., 3rd, Bowdin, S., El-Hamamsy, I., Frischmeyer-Guerrero, P. A., Guerrero, A. L., et al. (2014). Loeys-Dietz Syndrome: a Primer for Diagnosis and Management. *Genet. Med.* 16 (8), 576–587. doi:10.1038/gim.2014.11
- MacFarlane, E. G., Haupt, J., Dietz, H. C., and Shore, E. M. (2017). TGF- $\beta$  Family Signaling in Connective Tissue and Skeletal Diseases. *Cold Spring Harb Perspect. Biol.* 9 (11). doi:10.1101/cshperspect.a022269
- Meerschaut, I., Beyens, A., Steyaert, W., De Ryck, R., Bonte, K., De Backer, T., et al. (2019). Myhre Syndrome: A First Familial Recurrence and Broadening of the Phenotypic Spectrum. *Am. J. Med. Genet. A.* 179 (12), 2494–2499. doi:10.1002/ajmg.a.61377
- Meester, J. A. N., Verstraeten, A., Schepers, D., Alaerts, M., Van Laer, L., and Loeys, B. L. (2017). Differences in Manifestations of Marfan Syndrome, Ehlers-Danlos Syndrome, and Loeys-Dietz Syndrome. *Ann. Cardiothorac. Surg.* 6 (6), 582–594. doi:10.21037/acs.2017.11.03
- Meng, X. M., Nikolic-Paterson, D. J., and Lan, H. Y. (2016). TGF- $\beta$ : the Master Regulator of Fibrosis. *Nat. Rev. Nephrol.* 12 (6), 325–338. doi:10.1038/nrneph.2016.48
- Micha, D., Guo, D. C., Hilhorst-Hofstee, Y., van Kooten, F., Atmaja, D., Overwater, E., et al. (2015). SMAD2 Mutations Are Associated with Arterial Aneurysms and Dissections. *Hum. Mutat.* 36 (12), 1145–1149. doi:10.1002/humu.22854
- Miyazawa, K., and Miyazono, K. (2017). Regulation of TGF- $\beta$  Family Signaling by Inhibitory Smads. *Cold Spring Harb Perspect. Biol.* 9 (3). doi:10.1101/cshperspect.a022095
- Mizuguchi, T., Colod-Beroud, G., Akiyama, T., Abifadel, M., Harada, N., Morisaki, T., et al. (2004). Heterozygous TGFBR2 Mutations in Marfan Syndrome. *Nat. Genet.* 36 (8), 855–860. doi:10.1038/ng1392
- Morikawa, M., Derynck, R., and Miyazono, K. (2016). TGF- $\beta$  and the TGF- $\beta$  Family: Context-dependent Roles in Cell and Tissue Physiology. *Cold Spring Harb Perspect. Biol.* 8 (5), a021873. doi:10.1101/cshperspect.a021873
- Moustakas, A., Souchelnyskiy, S., and Heldin, C. H. (2001). Smad Regulation in TGF- $\beta$  Signal Transduction. *J. Cell Sci.* 114 (Pt 24), 4359–4369. doi:10.1242/jcs.114.24.4359
- Musfee, F. I., Guo, D., Pinard, A. C., Hostetler, E. M., Blue, E. E., Nickerson, D. A., et al. (2020). Rare Deleterious Variants of NOTCH1, GATA4, SMAD6, and ROBO4 Are Enriched in BAV with Early Onset Complications but Not in BAV with Heritable Thoracic Aortic Disease. *Mol. Genet. Genomic Med.* 8 (10), e1406. doi:10.1002/mgg3.1406
- Nie, H., Zhao, W., Wang, S., and Zhou, W. (2021). Based on Bioinformatics Analysis Lncrna SNHG5 Modulates the Function of Vascular Smooth Muscle Cells through mir-205-5p/SMAD4 in Abdominal Aortic Aneurysm. *Immun. Inflamm. Dis.* 9 (4), 1306–1320. doi:10.1002/iid3.478
- Pannu, H., Fadulu, V. T., Chang, J., Lafont, A., Hasham, S. N., Sparks, E., et al. (2005). Mutations in Transforming Growth Factor- $\beta$  Receptor Type II Cause Familial Thoracic Aortic Aneurysms and Dissections. *Circulation* 112 (4), 513–520. doi:10.1161/CIRCULATIONAHA.105.537340
- Papangeli, I., and Scambler, P. J. (2013). Tbx1 Genetically Interacts with the Transforming Growth Factor- $\beta$ /bone Morphogenetic Protein Inhibitor Smad7 during Great Vessel Remodeling. *Circ. Res.* 112 (1), 90–102. doi:10.1161/CIRCRESAHA.112.270223
- Park, S. H. (2005). Fine Tuning and Cross-Talking of TGF- $\beta$  Signal by Inhibitory Smads. *J. Biochem. Mol. Biol.* 38 (1), 9–16. doi:10.5483/bmbrep.2005.38.1.009
- Peng, C. (2003). The TGF- $\beta$  Superfamily and its Roles in the Human Ovary and Placenta. *J. Obstet. Gynaecol. Can.* 25 (10), 834–844. doi:10.1016/s1701-2163(16)30674-0

- Perrella, M. A., Jain, M. K., and Lee, M. E. (1998). Role of TGF-Beta in Vascular Development and Vascular Reactivity. *Miner Electrolyte Metab.* 24 (2-3), 136–143. doi:10.1159/000057361
- Qiu, P., Ritchie, R. P., Fu, Z., Cao, D., Cumming, J., Miano, J. M., et al. (2005). Myocardin Enhances Smad3-Mediated Transforming Growth Factor-Beta1 Signaling in a CARg Box-independent Manner: Smad-Binding Element Is an Important Cis Element for SM22alpha Transcription *In Vivo*. *Circ. Res.* 97 (10), 983–991. doi:10.1161/01.RES.0000190604.90049.71
- Rabkin, S. W. (2017). The Role Matrix Metalloproteinases in the Production of Aortic Aneurysm. *Prog. Mol. Biol. Transl. Sci.* 147, 239–265. doi:10.1016/bs.pmbts.2017.02.002
- Regalado, E. S., Guo, D. C., Villamizar, C., Avidan, N., Gilchrist, D., McGillivray, B., et al. (2011). Exome Sequencing Identifies SMAD3 Mutations as a Cause of Familial Thoracic Aortic Aneurysm and Dissection with Intracranial and Other Arterial Aneurysms. *Circ. Res.* 109 (6), 680–686. doi:10.1161/CIRCRESAHA.111.248161
- Sampson, U. K., Norman, P. E., Fowkes, F. G., Aboyans, V., Yanna Song, S., Harrell, F. E., Jr., et al. (2014). Global and Regional burden of Aortic Dissection and Aneurysms: Mortality Trends in 21 World Regions, 1990 to 2010. *Glob. Heart* 9 (1), 171–e10. doi:10.1016/j.gheart.2013.12.010
- Schepers, D., Tortora, G., Morisaki, H., MacCarrick, G., Lindsay, M., Liang, D., et al. (2018). A Mutation Update on the LDS-Associated Genes TGF $\beta$ 2/3 and SMAD2/3. *Hum. Mutat.* 39 (5), 621–634. doi:10.1002/humu.23407
- Shi, M., Zhu, J., Wang, R., Chen, X., Mi, L., Walz, T., et al. (2011). Latent TGF- $\beta$  Structure and Activation. *Nature* 474 (7351), 343–349. doi:10.1038/nature10152
- Sorrentino, A., Thakur, N., Grimsby, S., Marcusson, A., von Bulow, V., Schuster, N., et al. (2008). The Type I TGF-Beta Receptor Engages TRAF6 to Activate TAK1 in a Receptor Kinase-independent Manner. *Nat. Cell Biol.* 10 (10), 1199–1207. doi:10.1038/ncb1780
- Takeda, N., Hara, H., Fujiwara, T., Kanaya, T., Maemura, S., and Komuro, I. (2018). TGF- $\beta$  Signaling-Related Genes and Thoracic Aortic Aneurysms and Dissections. *Int. J. Mol. Sci.* 19 (7). doi:10.3390/ijms19072125
- Tan, C. K., Tan, E. H., Luo, B., Huang, C. L., Loo, J. S., Choong, C., et al. (2013). SMAD3 Deficiency Promotes Inflammatory Aortic Aneurysms in Angiotensin II-Infused Mice via Activation of iNOS. *J. Am. Heart Assoc.* 2 (3), e000269. doi:10.1161/JAHA.113.000269
- Tang, Y., Fan, W., Zou, B., Yan, W., Hou, Y., Kwabena Agyare, O., et al. (2021). TGF- $\beta$  Signaling and microRNA Cross-Talk Regulates Abdominal Aortic Aneurysm Progression. *Clin. Chim. Acta* 515, 90–95. doi:10.1016/j.cca.2020.12.031
- Teekakirikul, P., Milewicz, D. M., Miller, D. T., Lacro, R. V., Regalado, E. S., Rosales, A. M., et al. (2013). Thoracic Aortic Disease in Two Patients with Juvenile Polyposis Syndrome and SMAD4 Mutations. *Am. J. Med. Genet. A.* 161A (1), 185–191. doi:10.1002/ajmg.a.35659
- Tran-Fadulu, V., Pannu, H., Kim, D. H., Vick, G. W., 3rd, Lonsford, C. M., Lafont, A. L., et al. (2009). Analysis of Multigenerational Families with Thoracic Aortic Aneurysms and Dissections Due to TGFBR1 or TGFBR2 Mutations. *J. Med. Genet.* 46 (9), 607–613. doi:10.1136/jmg.2008.062844
- Tzavlaki, K., and Moustakas, A. (2020). TGF- $\beta$  Signaling. *Biomolecules* 10 (3). doi:10.3390/biom10030487
- van de Laar, I. M., Oldenburg, R. A., Pals, G., Roos-Hesselink, J. W., de Graaf, B. M., Verhagen, J. M., et al. (2011). Mutations in SMAD3 Cause a Syndromic Form of Aortic Aneurysms and Dissections with Early-Onset Osteoarthritis. *Nat. Genet.* 43 (2), 121–126. doi:10.1038/ng.744
- van de Laar, I. M., van der Linde, D., Oei, E. H., Bos, P. K., Bessems, J. H., Bierma-Zeinstra, S. M., et al. (2012). Phenotypic Spectrum of the SMAD3-Related Aneurysms-Osteoarthritis Syndrome. *J. Med. Genet.* 49 (1), 47–57. doi:10.1136/jmedgenet-2011-100382
- van der Linde, D., van de Laar, I. M., Bertoli-Avella, A. M., Oldenburg, R. A., Bekkers, J. A., Mattace-Raso, F. U., et al. (2012). Aggressive Cardiovascular Phenotype of Aneurysms-Osteoarthritis Syndrome Caused by Pathogenic SMAD3 Variants. *J. Am. Coll. Cardiol.* 60 (5), 397–403. doi:10.1016/j.jacc.2011.12.052
- van Dorst, D. C. H., de Wagenaar, N. P., van der Pluijm, I., Roos-Hesselink, J. W., Essers, J., and Danser, A. H. J. (2021). Transforming Growth Factor- $\beta$  and the Renin-Angiotensin System in Syndromic Thoracic Aortic Aneurysms: Implications for Treatment. *Cardiovasc. Drugs Ther.* 35 (6), 1233–1252. doi:10.1007/s10557-020-07116-4
- Van Laer, L., Dietz, H., and Loey, B. (2014). Loey-Dietz Syndrome. *Adv. Exp. Med. Biol.* 802, 95–105. doi:10.1007/978-94-007-7893-1\_7
- Vorselaars, V. M. M., Diederik, A., Prabhudesai, V., Velthuis, S., Vos, J. A., Snijder, R. J., et al. (2017). SMAD4 Gene Mutation Increases the Risk of Aortic Dilation in Patients with Hereditary Haemorrhagic Telangiectasia. *Int. J. Cardiol.* 245, 114–118. doi:10.1016/j.ijcard.2017.06.059
- Waldrip, W. R., Bikoff, E. K., Hoodless, P. A., Wrana, J. L., and Robertson, E. J. (1998). Smad2 Signaling in Extraembryonic Tissues Determines Anterior-Posterior Polarity of the Early Mouse Embryo. *Cell* 92 (6), 797–808. doi:10.1016/s0092-8674(00)81407-5
- Wang, L., Rice, M., Swist, S., Kubin, T., Wu, F., Wang, S., et al. (2021). BMP9 and BMP10 Act Directly on Vascular Smooth Muscle Cells for Generation and Maintenance of the Contractile State. *Circulation* 143 (14), 1394–1410. doi:10.1161/CIRCULATIONAHA.120.047375
- Wang, Y., Yin, P., Chen, Y. H., Yu, Y. S., Ye, W. X., Huang, H. Y., et al. (2018). A Functional Variant of SMAD4 Enhances Macrophage Recruitment and Inflammatory Response via TGF- $\beta$  Signal Activation in Thoracic Aortic Aneurysm and Dissection. *Aging (Albany NY)* 10 (12), 3683–3701. doi:10.18632/aging.101662
- Weinstein, M., Yang, X., Li, C., Xu, X., Gotay, J., and Deng, C. X. (1998). Failure of Egg cylinder Elongation and Mesoderm Induction in Mouse Embryos Lacking the Tumor Suppressor Smad2. *Proc. Natl. Acad. Sci. U S A.* 95 (16), 9378–9383. doi:10.1073/pnas.95.16.9378
- Wilkes, M. C., Mitchell, H., Penheiter, S. G., Doré, J. J., Suzuki, K., Edens, M., et al. (2005). Transforming Growth Factor-Beta Activation of Phosphatidylinositol 3-kinase Is Independent of Smad2 and Smad3 and Regulates Fibroblast Responses via P21-Activated Kinase-2. *Cancer Res.* 65 (22), 10431–10440. doi:10.1158/0008-5472.CAN-05-1522
- Wrana, J. L., Attisano, L., Cárcamo, J., Zentella, A., Doody, J., Laiho, M., et al. (1992). TGF Beta Signals through a Heteromeric Protein Kinase Receptor Complex. *Cell* 71 (6), 1003–1014. doi:10.1016/0092-8674(92)90395-s
- Wu, J., Niu, J., Li, X., Wang, X., Guo, Z., and Zhang, F. (2014). TGF- $\beta$ 1 Induces Senescence of Bone Marrow Mesenchymal Stem Cells via Increase of Mitochondrial ROS Production. *BMC Dev. Biol.* 14, 21. doi:10.1186/1471-213X-14-21
- Wu, L. (2017). Functional Characteristics of a Novel SMAD4 Mutation from Thoracic Aortic Aneurysms (TAA). *Gene* 628, 129–133. doi:10.1016/j.gene.2017.07.042
- Wylie, L. A., Mouillesseaux, K. P., Chong, D. C., and Bautch, V. L. (2018). Developmental SMAD6 Loss Leads to Blood Vessel Hemorrhage and Disrupted Endothelial Cell Junctions. *Dev. Biol.* 442 (2), 199–209. doi:10.1016/j.ydbio.2018.07.027
- Xie, W. B., Li, Z., Shi, N., Guo, X., Tang, J., Ju, W., et al. (2013). Smad2 and Myocardin-Related Transcription Factor B Cooperatively Regulate Vascular Smooth Muscle Differentiation from Neural Crest Cells. *Circ. Res.* 113 (8), e76–86. doi:10.1161/CIRCRESAHA.113.301921
- Xu, J., Gruber, P. J., and Chien, K. R. (2019). SMAD4 Is Essential for Human Cardiac Mesodermal Precursor Cell Formation. *Stem Cells* 37 (2), 216–225. doi:10.1002/stem.2943
- Xue, L., Luo, S., Ding, H., Liu, Y., Huang, W., Fan, X., et al. (2019). Upregulation of miR-146a-5p Is Associated with Increased Proliferation and Migration of Vascular Smooth Muscle Cells in Aortic Dissection. *J. Clin. Lab. Anal.* 33 (4), e22843. doi:10.1002/jcla.22843
- Yamashita, M., Fatyol, K., Jin, C., Wang, X., Liu, Z., and Zhang, Y. E. (2008). TRAF6 Mediates Smad-independent Activation of JNK and P38 by TGF-Beta. *Mol. Cell* 31 (6), 918–924. doi:10.1016/j.molcel.2008.09.002
- Yang, H. H., Kim, J. M., Chum, E., van Breemen, C., and Chung, A. W. (2009). Long-term Effects of Losartan on Structure and Function of the Thoracic Aorta in a Mouse Model of Marfan Syndrome. *Br. J. Pharmacol.* 158 (6), 1503–1512. doi:10.1111/j.1476-5381.2009.00443.x
- Yang, P., Schmit, B. M., Fu, C., DeSart, K., Oh, S. P., Berceli, S. A., et al. (2016). Smooth Muscle Cell-specific Tgfr1 Deficiency Promotes Aortic Aneurysm Formation by Stimulating Multiple Signaling Events. *Sci. Rep.* 6, 35444. doi:10.1038/srep35444
- Yang, P., Wu, P., Liu, X., Feng, J., Zheng, S., Wang, Y., et al. (2020). MiR-26b Suppresses the Development of Stanford Type A Aortic Dissection by

- Regulating HMGA2 and TGF- $\beta$ /Smad3 Signaling Pathway. *Ann. Thorac. Cardiovasc. Surg.* 26 (3), 140–150. doi:10.5761/atcs.0a.19-00184
- Ye, P., Chen, W., Wu, J., Huang, X., Li, J., Wang, S., et al. (2013). GM-CSF Contributes to Aortic Aneurysms Resulting from SMAD3 Deficiency. *J. Clin. Invest.* 123 (5), 2317–2331. doi:10.1172/JCI67356
- Zhang, P., Hou, S., Chen, J., Zhang, J., Lin, F., Ju, R., et al. (2016). Smad4 Deficiency in Smooth Muscle Cells Initiates the Formation of Aortic Aneurysm. *Circ. Res.* 118 (3), 388–399. doi:10.1161/CIRCRESAHA.115.308040
- Zhang, W., Zeng, Q., Xu, Y., Ying, H., Zhou, W., Cao, Q., et al. (2017). Exome Sequencing Identified a Novel SMAD2 Mutation in a Chinese Family with Early Onset Aortic Aneurysms. *Clin. Chim. Acta* 468, 211–214. doi:10.1016/j.cca.2017.03.007
- Zhang, W., Zhou, M., Liu, C., Liu, C., Qiao, T., Huang, D., et al. (2015). A Novel Mutation of SMAD3 Identified in a Chinese Family with Aneurysms-Osteoarthritis Syndrome. *Biomed. Res. Int.* 2015, 968135. doi:10.1155/2015/968135
- Zhou, Y., He, X., Liu, R., Qin, Y., Wang, S., Yao, X., et al. (2019). LncRNA CRNDE Regulates the Proliferation and Migration of Vascular Smooth Muscle Cells. *J. Cel Physiol* 234, 16205–16214. doi:10.1002/jcp.28284

**Conflict of Interest:** The authors declare that the research was conducted in the absence of any commercial or financial relationships that could be construed as a potential conflict of interest.

**Publisher's Note:** All claims expressed in this article are solely those of the authors and do not necessarily represent those of their affiliated organizations, or those of the publisher, the editors and the reviewers. Any product that may be evaluated in this article, or claim that may be made by its manufacturer, is not guaranteed or endorsed by the publisher.

Copyright © 2022 Chen and Chang. This is an open-access article distributed under the terms of the Creative Commons Attribution License (CC BY). The use, distribution or reproduction in other forums is permitted, provided the original author(s) and the copyright owner(s) are credited and that the original publication in this journal is cited, in accordance with accepted academic practice. No use, distribution or reproduction is permitted which does not comply with these terms.



# Propofol Protects Myocardium From Ischemia/Reperfusion Injury by Inhibiting Ferroptosis Through the AKT/p53 Signaling Pathway

Shengqiang Li<sup>1</sup>, Zhen Lei<sup>1</sup>, Xiaomei Yang<sup>1</sup>, Meng Zhao<sup>1</sup>, Yonghao Hou<sup>1</sup>, Di Wang<sup>2</sup>, Shuhai Tang<sup>1</sup>, Jingxin Li<sup>3\*</sup> and Jingui Yu<sup>1\*</sup>

<sup>1</sup>Department of Anesthesiology, Qilu Hospital, Cheeloo College of Medicine, Shandong University, Jinan, China, <sup>2</sup>Department of Anesthesiology, The Second Hospital, Cheeloo College of Medicine, Shandong University, Jinan, China, <sup>3</sup>Department of Physiology, School of Basic Medical Science, Cheeloo College of Medicine, Shandong University, Jinan, Shandong, China

## OPEN ACCESS

### Edited by:

Xianwei Wang,  
Xinxiang Medical University, China

### Reviewed by:

Ruo-Peng Liang,  
First Affiliated Hospital of Zhengzhou  
University, China  
Huan He,  
Nanchang University, China

### \*Correspondence:

Jingxin Li  
ljingxin@sdu.edu.cn  
Jingui Yu  
yujingui1109@126.com

### Specialty section:

This article was submitted to  
Cardiovascular and Smooth Muscle  
Pharmacology,  
a section of the journal  
Frontiers in Pharmacology

**Received:** 22 December 2021

**Accepted:** 21 February 2022

**Published:** 16 March 2022

### Citation:

Li S, Lei Z, Yang X, Zhao M, Hou Y, Wang D, Tang S, Li J and Yu J (2022) Propofol Protects Myocardium From Ischemia/Reperfusion Injury by Inhibiting Ferroptosis Through the AKT/p53 Signaling Pathway. *Front. Pharmacol.* 13:841410. doi: 10.3389/fphar.2022.841410

The molecular mechanism underlying the protective role of propofol against myocardial ischemia/reperfusion (I/R) injury remains poorly understood. Previous studies have shown that ferroptosis is an imperative pathological process in myocardial I/R injury. We hypothesized that propofol prevents myocardial I/R injury by inhibiting ferroptosis via the AKT/p53 signaling pathway. The ferroptosis-inducing agent erastin (E) and AKT inhibitor MK2206 (MK) were used to investigate the role of propofol in myocardial I/R injury. H9C2 cells treated without any reagents, erastin for 24 h, propofol for 1 h before adding erastin were assigned as the control (C), E, and E + P group, respectively. Cell viability, reactive oxygen species (ROS), and the expression of antioxidant enzymes, including ferritin heavy chain 1 (FTH1), cysteine/glutamate transporter (XCT), and glutathione peroxidase 4 (GPX4) in H9C2 cells. Rat hearts from the I/R + P or I/R groups were treated with or without propofol for 20 min before stopping perfusion for 30 min and reperfusion for 60 min. Rat hearts from the I/R + P + MK or I/R + MK groups were treated with or without propofol for 20 min, with a 10-min treatment of MK2206 before stopping perfusion. Myocardial histopathology, mitochondrial structure, iron levels, and antioxidant enzymes expression were assessed. Our results demonstrated that erastin increased H9C2 cell mortality and reduced the expression of antioxidant enzymes. I/R, which reduced the expression of antioxidant enzymes and increased iron or p53 ( $p < 0.05$ ), boosted myocardium pathological and mitochondrion damage. Propofol inhibited these changes; however, the effects of propofol on I/R injury were antagonized by MK ( $p < 0.05$ ). In addition, AKT siRNA inhibited the propofol-induced expression of antioxidant enzymes ( $p < 0.05$ ). Our findings confirm that propofol protects myocardium from I/R injury by inhibiting ferroptosis via the AKT/p53 signal pathway.

**Keywords:** Akt, ferroptosis, heart, ischemia/reperfusion injury, propofol, p53



## INTRODUCTION

Propofol (2,6-diisopropyl phenol), a popular intravenous anesthetic, is widely used in the induction and maintenance of general anesthesia (Bovill, 2006). Emerging data have shown that propofol exerts profound protective effects on myocardial ischemia/reperfusion (I/R) injury (Suleiman et al., 2015) by scavenging ROS (Zhao et al., 2019), reducing calcium overload (Zhou et al., 1997), and inhibiting polymorphonuclear neutrophils (PMN) adhesion (Szekely et al., 2000). Nevertheless, the specific underlying mechanism remains unclear.

Ferroptosis is a newly recognized form of cell death (Chen et al., 2020) that is distinct from apoptosis, necrosis, and autophagy (Macías-Rodríguez et al., 2020), characterized by cell membrane rupture and vesiculation, mitochondrial atrophy, ridge reduction, and nuclear-lacking chromatin aggregation (Yagoda et al., 2007; Yang and Stockwell, 2008). Under the action of divalent iron (Dixon et al., 2012) or iron-containing enzymes (Yang et al., 2016), unsaturated fatty acids of the cell membrane undergo lipid peroxidation to induce ferroptosis. The expression level of glutathione peroxidase 4 (GPX4) (Zhang et al., 2021), as the core enzyme of the antioxidant system, decreases during ferroptosis.

Ferroptosis is associated with a range of diseases, such as myocardial I/R injury, cancer, degenerative disease, and acute kidney injury (Han et al., 2020). As a critical role in the pathological process of myocardial injury (Stockwell et al., 2017), ferroptosis is closely related to p53 (Kruse and Gu, 2009). When cells are hypoxic, the stability and activity of p53 are enhanced. Subsequently, p53 enters the nucleus to regulate the expression of its downstream targets and promote the development of ferroptosis (Jiang et al., 2015). The activity of p53 is negatively regulated by AKT (also known as protein kinase B, PKB), a serine/threonine-specific protein kinase that is critical for regulating myocardial I/R injury (Yin et al., 2013). Phosphorylation of AKT promotes the combination of murine double minute 2 (MDM2) and p53, which leads to the degradation of p53 to inhibit ferroptosis (Freedman et al., 1999). A previous study has shown that propofol protects hepatic I/R injury by activating AKT phosphorylation (Wei et al., 2021) and p53 expression. Nevertheless, the effect of propofol on myocardial I/R injury remains unclear. Thus, we hypothesized that propofol may protect the myocardium by inhibiting myocardial ferroptosis through the AKT/p53 signaling pathway.

To test the above hypothesis, a series of *in vitro* and *in vivo* experiments were performed to investigate the effect and underlying mechanism of propofol on ferroptosis. This study demonstrates that propofol inhibits ferroptosis of both H9C2 cells and rat myocardium via the AKT/p53 signaling pathway, and it protects the myocardium from I/R injury.

## MATERIALS AND METHODS

### Cell Culture

H9C2 cells were obtained from KeyGEN BioTECH (KG444, Nanjing, China), and cultured in high-glucose Dulbecco's modified Eagle's medium (DMEM, 0030034DJ, GIBCO,

New York, USA) supplemented with 10% fetal bovine serum (FBS, 16140071, GIBCO, New York, USA) and 1% penicillin/streptomycin (15140122, GIBCO, New York, USA). The cells were incubated in a tri-gas incubator with 5% CO<sub>2</sub> at 37°C.

### Cell Viability Assay

Cells were inoculated at 3,000–4,000/well in 96-well plates. After treatment, 10% cell counting kit-8 (CCK-8, HY-K0301, MCE, New Jersey, United States) reagent was added and incubated for 1–3 h. The absorbance was measured using a Microplate Reader (Thermo Fisher Scientific, Massachusetts, United States) at 450 nm.

### Experimental Grouping and Corresponding Treatment

H9C2 cells were treated with no reagents (C), erastin (5 µM, GC16630, California, GLP BIO, United States) for 24 h (E), and propofol (50 µM, D126608, Sigma, Missouri, United States) for 1 h before erastin (E + P). Each experiment was repeated three times (Figure 1A).

### Trypan Blue Assay

H9C2 cells were inoculated in 12-well plates and treated as described above. Next, 0.4% trypan blue solution (T8070, Solarbio, Beijing, China) was added to the cells for 3 min. Cell viability was calculated by a cell counter (Countstar® BioTech, ALIT Life Science, Shanghai, China).

### Assessment of ROS Production

H9C2 cells were inoculated into 12-well plates overnight and treated as described above, then 10 µM dihydroethidium solution (DHE, S0063, Beyotime, Shanghai, China) was added to each well and the plates were incubated in the dark for 30 min at 37°C. The cells were observed under a fluorescence microscope (Nikon, Tokyo, Japan) and analyzed with Image J software (National Institutes of Health, Maryland, United States).

### Malondialdehyde, Iron Levels, and Superoxide Dismutase Activity Measurement

H9C2 cells from each group were collected and used to generate a 10% homogenate, which was placed at –20°C and repeatedly thawed on ice 3 times. The supernatant was centrifuged at 2,500 r/min for 10 min at 4°C. The MDA levels and SOD activity were determined according to the kit instruction (A003-1-2 and A001-3-2, Nanjing Jiancheng Bioengineering Institute, Nanjing, China). The iron levels in H9C2 cells were detected using a kit (DIFE-250, BioAssay Systems, California, USA) and in the myocardium were determined according to the kit instructions (A039-2-1, Nanjing Jiancheng Bioengineering Institute, Nanjing, China). The protein concentration was measured with a BCA kit (P0012S, Beyotime, Shanghai, China).

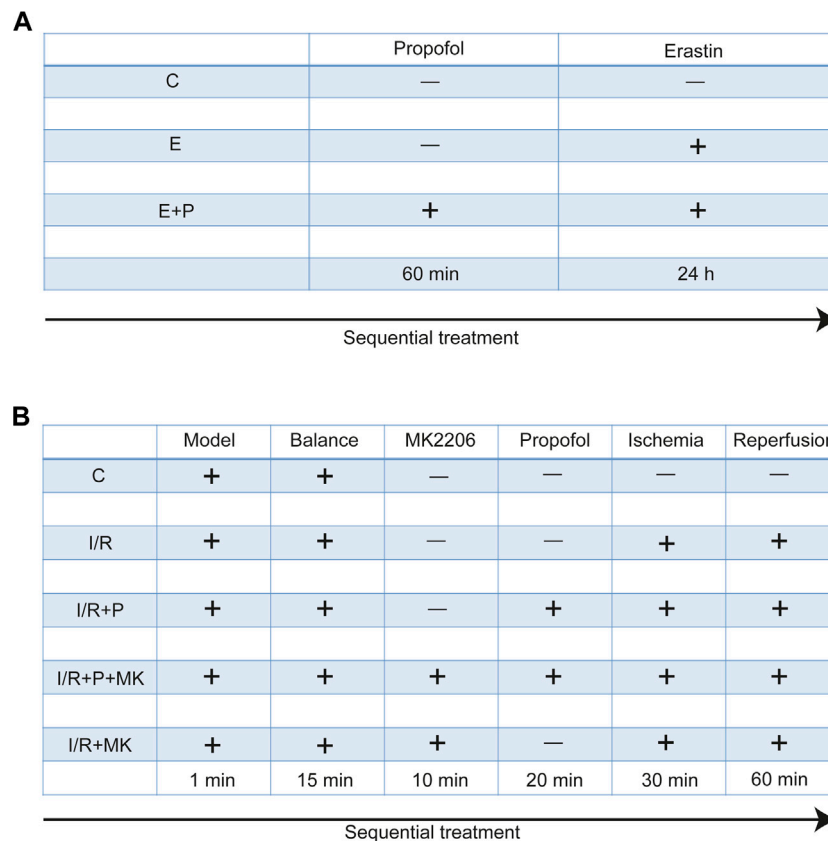


**FIGURE 1 |** Experimental grouping and corresponding treatment. Experimental grouping and corresponding treatment on H9C2 cells **(A)** and rat hearts **(B)**.

## Detection of Antioxidant Expressions in AKT siRNA-Transfecting H9C2 Cells

After incubation in 12-well plates for 24 h, the H9C2 cell medium was replaced with a serum-free medium (Opti-MEM I, Thermo Fisher Scientific, Massachusetts, United States). The siRNA (Gene Pharma, Shanghai, China) was diluted in serum-free medium and mixed with diluted Lipofectamine 2000 (Lipo 2000, Thermo Fisher Scientific, Massachusetts, USA) for 20 min at room temperature. Then, the mixture was added into 12-well plates and incubated for 6–8 h, replacing the medium with a complete medium once. After being incubated for 24 h, the cells were treated for follow-up experiments as the design above. Proteins were extracted from H9C2 cells and handled as western blot analysis. The siRNA sequence of AKT was as follows: F: 5'-CCAAGCACC GUGUGACCAUTT-3', R: 5'-AUGGUCACACGGUGCUUG GTT-3'.

## Animals

Adult male rats (Wistar, weight 180–240 g), purchased from the Experimental Animal Center of Shandong University, were housed in a constant temperature ( $25 \pm 2^\circ\text{C}$ ) room, fed with standard water and laboratory diet.

## Langendorff Heart Preparation

Rats were acclimatized to the laboratory environment for 3 days, anesthetized by 10% chloral hydrate, and sequentially injected with heparin (250 U/kg, H8060, Solarbio, Beijing, China). The hearts were rapidly resected and dipped into 40 ml ice-cold KH solution (pH 7.4, containing in mM: NaCl 115,  $\text{MgSO}_4$  1.2, KCl 4.7,  $\text{KH}_2\text{PO}_4$  1.2,  $\text{CaCl}_2$  1.8, glucose 11, and  $\text{NaHCO}_3$  25). Finally, the hearts were cannulated using a retrofitted Langendorff apparatus and perfused with KH at a velocity of 10 ml/min, which was gassed with 5%  $\text{CO}_2$  and 95%  $\text{O}_2$  at  $37^\circ\text{C}$ . Myocardial ischemia was caused by stopping perfusion for 30 min, and reperfusion resulted from recanalization for another 60 min.

## Animal Grouping and Treatment

All rats were randomly divided into five groups. After stabilizing for 15 min, rat hearts were treated with KH for 120 min (C), with (I/R + P) or without (I/R) propofol for 20 min before stopping perfusion for 30 min and reperfusion for 60 min, with (I/R + P + MK) or without propofol (I/R + MK) after MK2206 (15 nM, GC16304, New York, GLP BIO, USA) for 10 min before stopping perfusion ( $N = 6$ , Figure 1B).

## MDA, Iron Levels, and Glutathione/Oxidized Glutathione (GSH/GSSG) Ratio Determination

After recanalization, the rat heart left ventricle anterior wall was cut. MDA, iron levels (A039-2-1, A039-2-1, Nanjing Jiancheng Bioengineering Institute, Nanjing, China), and the GSH/GSSG ratio (S0053, Beyotime, Shanghai, China) were assessed using their respective assay kits. The concentration of protein was detected by a BCA kit and the absorbance was determined with a microplate reader.

## Myocardial Fiber Assessment

Hearts were fixed overnight in 4% paraformaldehyde, dehydrated with alcohol, and made transparent with xylene. They were then fixed in paraffin and finally cut into 3–4- $\mu$ m-thick slices, which were placed in xylene and alcohol and then stained with hematoxylin-eosin (HE) (C0105S, Beyotime, Shanghai, China). Finally, the sections were sealed with neutral resin and imaged under a microscope (Nikon, Tokyo, Japan).

## Mitochondrial Morphology Assessment

After reperfusion as described above, the left ventricle anterior wall was cut into a size of 2 mm  $\times$  5 mm  $\times$  10 mm and fixed overnight in electron microscope fixative (G1102, Servicebio, Wuhan, China). The sections were then embedded in phosphate buffer and baked in the oven. Sequentially, they were cut to a size 50–60 nm and stained with 2% uranyl acetate lead. Images were acquired under a transmission electron microscope (HITACHI, Tokyo, Japan).

## Western Blot Analysis

Proteins were extracted from H9C2 cells and myocardium lysates of the left ventricle anterior wall. Protein was separated by 12% SDS-PAGE, transferred to polyvinylidene fluoride (PVDF) membranes, blocked with 5% non-fatty milk for 60 min, and incubated with primary antibodies overnight at 4°C. Then, the membranes were incubated with secondary antibodies for 60 min and detected with enhanced chemiluminescence (ECL) detection system. Images were analyzed by ImageJ software.

## Immunofluorescence Assessment

After dewaxing and rehydrating according to a previous description, paraffin sections were repaired in citrate solution (P0083, Beyotime, Shanghai, China) for 30 min, blocked with 5% bovine serum albumin (BSA) for 60 min, and incubated with primary antibodies overnight at 4°C. Subsequently, they were incubated with secondary antibodies for 60 min and DAPI (C1002, Beyotime, Shanghai, China) for 15 min, followed by visualization using an immunofluorescence microscope and analyzed with ImageJ software.

## Antibodies

The following antibodies were used: anti-AKT (ab179463, Abcam, Cambridgeshire, UK), anti-AKT (phospho Ser473, 4060, CST, Boston, United States), anti-P53 (2,524, CST, Boston, United States), anti-P53 (phospho S392, ab33889, Abcam, Cambridgeshire, UK), anti-Ferritin (ab75973, Abcam, Cambridgeshire, UK), anti-GPX4 (ab125066, Abcam,

Cambridgeshire, UK), anti-XCT (ab175186, Abcam, Cambridgeshire), anti- $\alpha$ -tubulin (ab7291, Abcam, Cambridgeshire, UK). HRP-conjugated secondary antibodies (ZB-2301 or ZB-2305, ZSGB-BIO, Beijing, China) and fluorochrome conjugated secondary antibody (ab150064, Abcam, Cambridgeshire).

## Statistical Analysis

Data are expressed as mean  $\pm$  standard deviation (SD) and were analyzed by one-way ANOVA with Tukey's post hoc test or the *t*-test. GraphPad Prism version 9.0 (San Diego, California, United States) was used for analysis, and a *p* value < 0.05 was considered to indicate a significant difference.

## RESULTS

### Effect of Propofol on Erastin-Induced H9C2 Cells Ferroptosis

First, we examined the effect of erastin on H9C2 cells and found a linear inhibition of cell viability with increasing erastin concentrations using the CCK-8 assay. We found that 2.5  $\mu$ M erastin markedly decreased cell viability; hence it was selected for follow-up experiments (**Figure 2A**). The cell viability was lower in Group E than in Group C, as revealed by the optical microscope and the trypan blue assay, which was increased by propofol pretreatment (**Figures 2B,D,E**). Similarly, the ROS, MDA, and iron levels were higher in Group E than in Group C as revealed by DHE staining, MDA, and iron test. All of these parameters were also reduced by propofol pretreatment (**Figures 2C,F–H**). The change of SOD activity was similar to the trypan blue results (**Figure 2I**). In addition, western blot analysis showed a significant decrease in the expression of anti-ferroptosis enzymes (FTH1 and GPX4) in Group E compared with Group C, which was again reduced by propofol pretreatment (**Figures 2J–L**). Taken together, these results demonstrated that erastin induced ferroptosis in H9C2 cells and propofol pretreatment alleviates this form of death, suggesting an important protective role of propofol in the H9C2 cells ferroptosis.

### Effect of Propofol on AKT Knockdown in H9C2 Cells

Given the central role of AKT in myocardial protection, we investigated whether AKT was involved in the anti-ferroptosis effect of propofol. We first knocked out the AKT gene of H9C2 cells with AKT siRNA. Western blot analysis showed that AKT siRNA significantly reduced AKT and P-AKT expressions levels (**Figures 3A–C**). In addition, it showed that AKT siRNA significantly reduced the expression of anti-ferroptosis enzymes (FTH1, XCT, and GPX4) in H9C2 cells, which was further reduced by erastin, while propofol slightly inhibited the effect of erastin (**Figures 3D–G**). Similarly, the cell viability of H9C2 cells in the CCK8 experiment was similar to the above enzymes (**Figure 3H**). These results indicated that propofol might inhibit ferroptosis in H9C2 cells through the AKT signaling pathway.

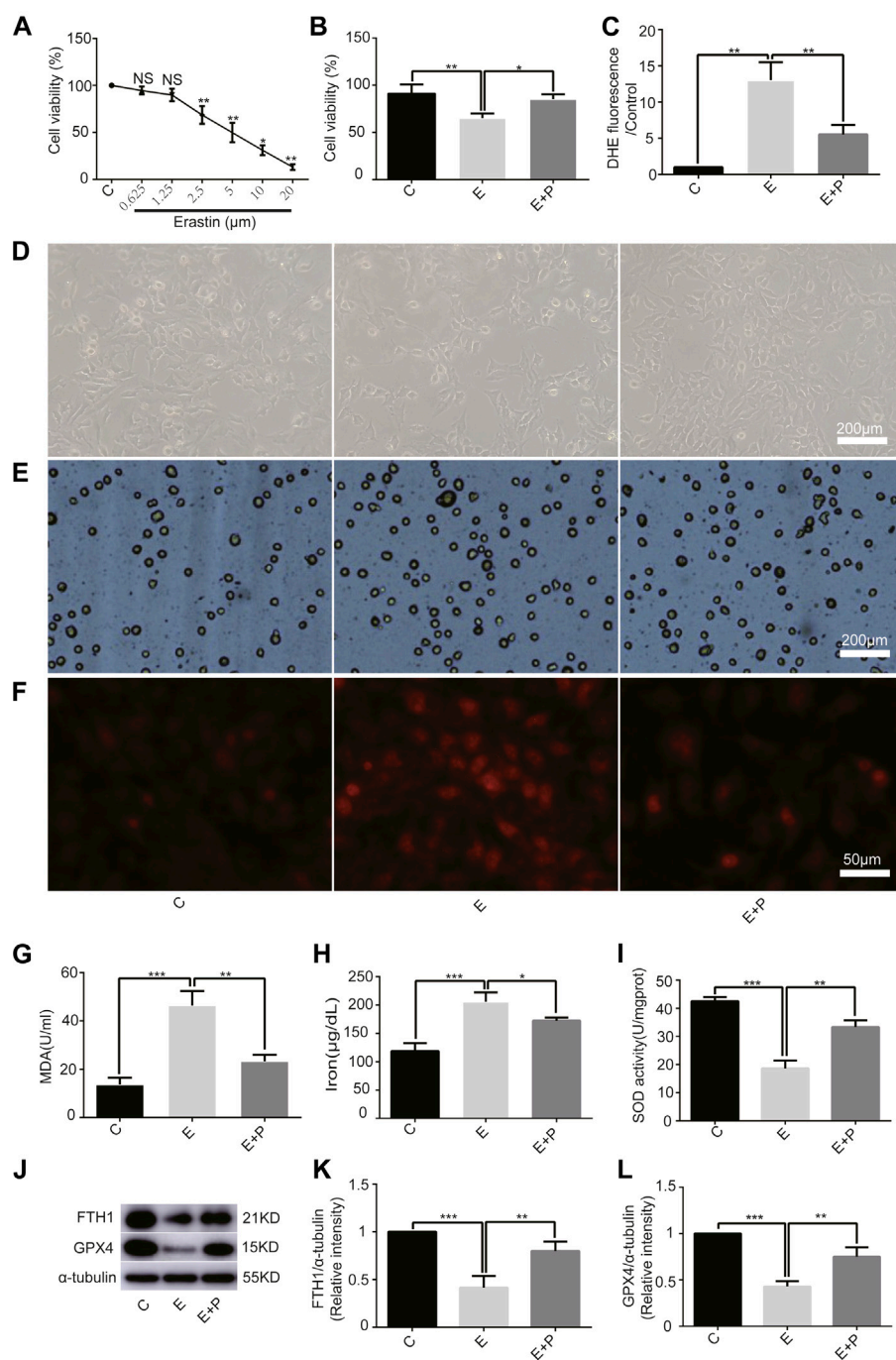


**FIGURE 2 |** Effect of propofol on erastin-induced H9C2 cell ferroptosis. **(A)** Cell viability of H9C2 cells treated with erastin (0–20  $\mu$ M). **(B,D,E)** Effect of propofol on erastin-induced cell death. Dead cells were stained with trypan blue. Scale bar: 200  $\mu$ m. **(C,F)** Effect of propofol on reactive oxygen species (ROS) production. Quantification of ROS is expressed as DHE. Scale bar: 50  $\mu$ m. Effect of propofol on MDA **(G)**, iron **(H)**, and SOD **(I)** production. **(J–L)** Influence of propofol on antioxidant enzymes (FTH1 and GPX4).  $N = 3$ . Data are expressed as the mean  $\pm$  SD. Significance was calculated using one-way ANOVA with Tukey's post hoc test or the  $t$ -test.  $p$ -values  $< 0.05$  were considered statistically significant. \* $p < 0.05$ , \*\* $p < 0.01$ , \*\*\* $p < 0.001$ .



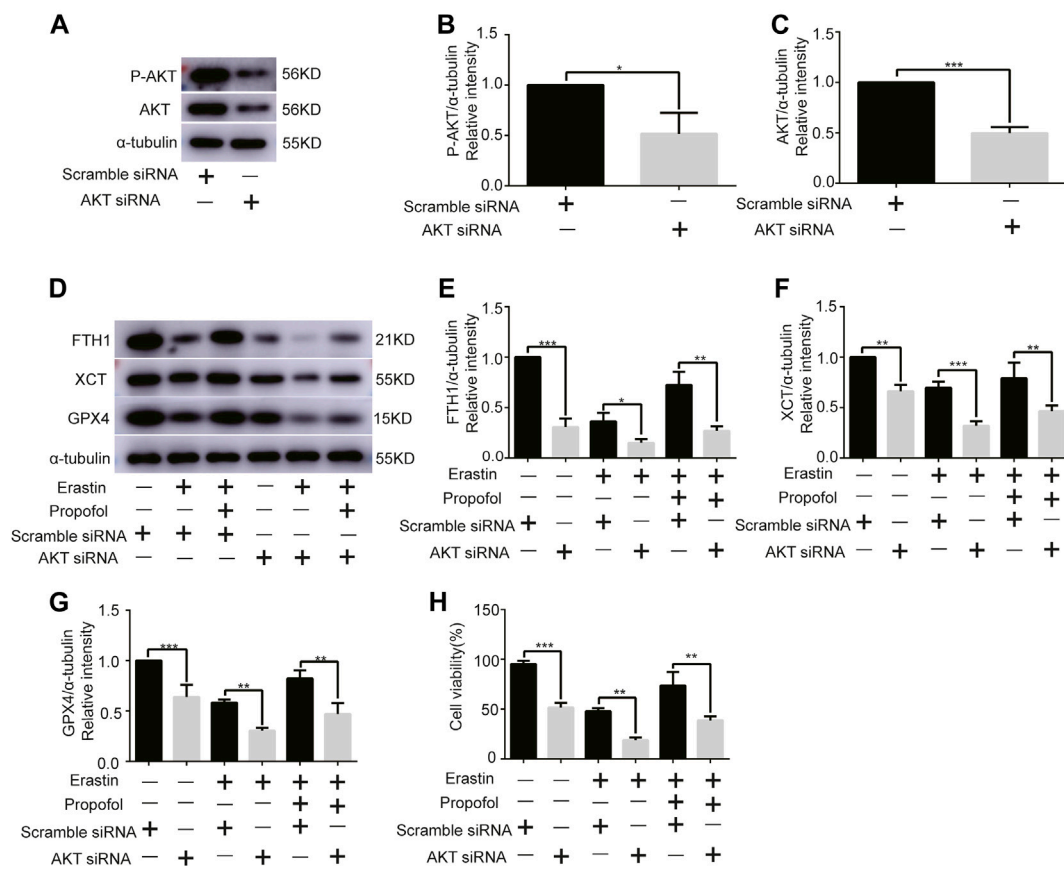


**FIGURE 3 |** Effect of AKT knockdown on H9C2 cell ferroptosis with propofol pre-treatment. **(A–C)** Expression of AKT and p-AKT in H9C2 cells transfected with AKT and scramble siRNA. **(D–G)** Levels of FTH1, XCT, and GPX4 in H9C2 cells transfected with AKT and scramble siRNA with propofol pre-treatment. **(H)** Change in the viability of H9C2 cells transfected with AKT and scramble siRNA with propofol pre-treatment. N = 3. Data are expressed as the mean  $\pm$  SD. Significance was calculated using one-way ANOVA with Tukey's post hoc test or the *t*-test. *p*-values < 0.05 were considered statistically significant. \**p* < 0.05, \*\**p* < 0.01, \*\*\**p* < 0.001.

## Influence of I/R-Induced Myocardial Ferroptosis

To understand the effect of propofol on myocardial tissue ferroptosis, we established an isolated myocardial I/R model with the Langendorff system. Similarly, MDA and iron levels were higher in Group I/R than in Group C, as revealed by the MDA and iron test; they were also reduced by propofol pretreatment (**Figures 4A,B**). In addition, western blot analysis revealed a significant decrease in the expression of anti-ferroptosis enzymes (FTH1, XCT, and GPX4) in the I/R compared with Group C, which was also reduced by propofol pretreatment (**Figures 4C–F**). Taken together, these results demonstrated that I/R induced myocardial tissue ferroptosis and propofol pretreatment alleviates this phenomenon.

## Influence of AKT Inhibitor on Myocardium Ferroptosis With Propofol Pre-Treatment

Next, we investigated whether AKT was involved in the anti-ferroptosis effect of propofol on the myocardium. We

pretreated myocardial tissue with AKT inhibitor (MK2206). I/R showed a lower GSH/GSSG ratio than C, which was reversed with propofol. However, MK2206 inhibited all the effects of propofol (**Figure 4G**). MK2206 significantly increased myocardium iron levels in Group I/R + MK compared with Group I/R and inhibited the effect of propofol (**Figure 4H**). Similarly, HE staining showed an abundance of severely wavy and injured myofibers in Group I/R compared with Group C, which was prevented by propofol (**Figure 4I**). TEM revealed that enlarging or distorting myocardial mitochondrial ridges in Group I/R compared with Group C, which was significantly diminished in Group I/R + P. MK2206 attenuated all these effects (**Figure 4J**). Changes in p53 and p-p53 protein were common with increased myocardium iron (**Figure 4K–M**). In addition, western blot showed that the changes in anti-ferroptosis enzymes (FTH1, XCT, and GPX4) were similar to those in the GSH/GSSG ratio (**Figures 5A–D**). These results suggest that propofol pretreatment inhibits ferroptosis in myocardial tissue through the AKT/p53 signaling pathway.

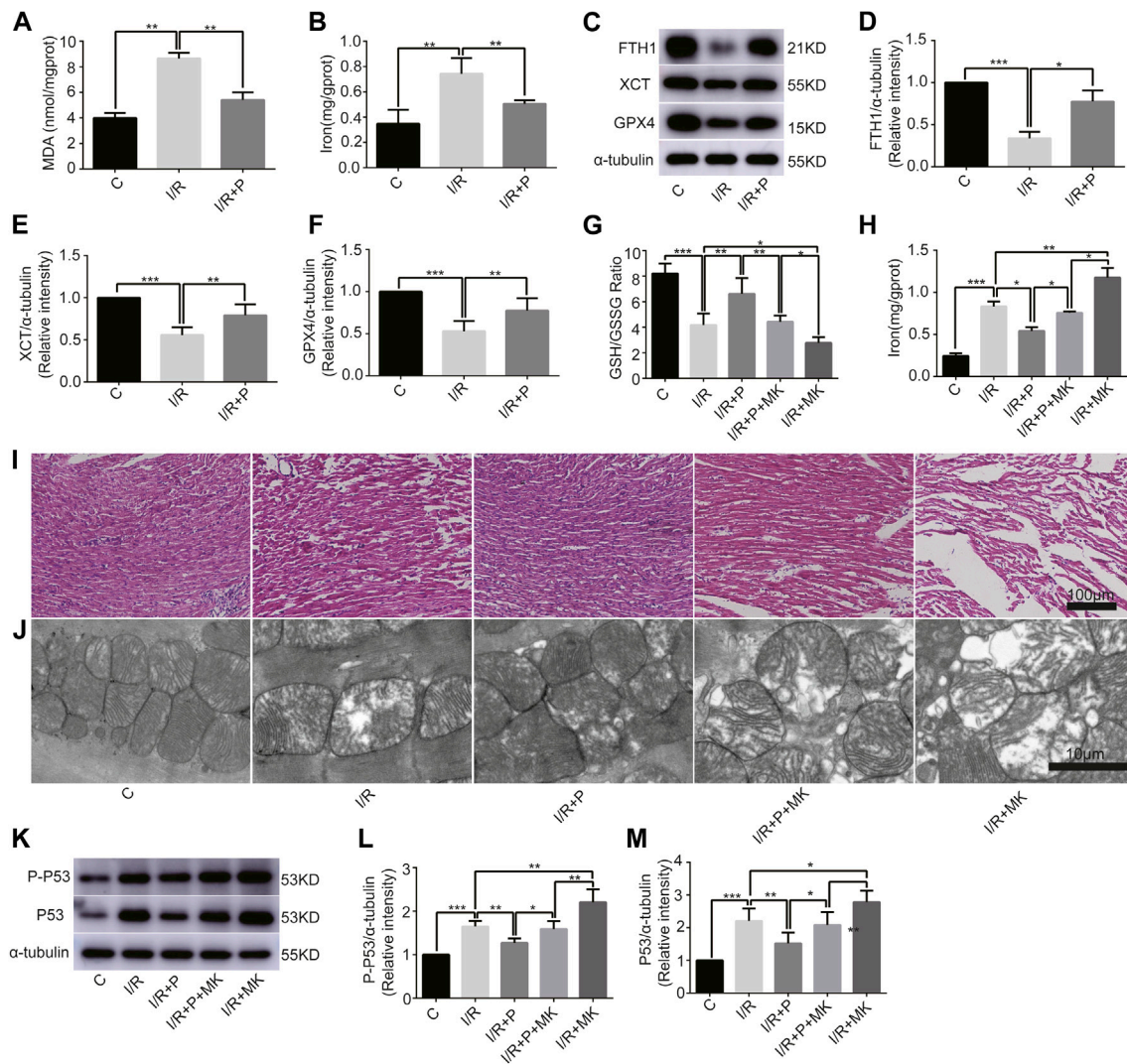


**FIGURE 4 |** Influence of AKT inhibitor on myocardial ferroptosis with propofol pretreatment. **(A–F)**: Effect of propofol on I/R-induced myocardial MDA, iron, and antioxidant enzymes expressions. **(G–H)**: GSH/GSSG ratio and iron changes in the myocardium. **(I)** Structural changes in myocardial fibers based on HE staining. Scale bar: 100  $\mu$ m. **(J)** Mitochondrial changes under electron microscopy. Scale bar: 10  $\mu$ m. **(K–M)**: Expression of p53 and p-p53 in myocardium based on the western blot assay. N = 6. Data are expressed as the mean  $\pm$  SD. Significance was calculated using one-way ANOVA with Tukey's post hoc test or the *t*-test. *p*-values < 0.05 were considered statistically significant. \**p* < 0.05, \*\**p* < 0.01, \*\*\**p* < 0.001.

## Change of AKT Activity by Propofol

Western blot analysis showed that AKT phosphorylation, which was inhibited by I/R or MK2206, was activated by propofol (Figures 5E,F). Immunofluorescence levels showing P-AKT phosphorylation were identical to the western blot results shown above (Figures 5G,H). There was no difference in immunofluorescence levels of AKT among the groups (Figures 5I,J).

## DISCUSSION

The major finding of this study was that propofol pretreatment inhibited ferroptosis in H9C2 cells and rat myocardium by

reducing the expression of ROS, iron, and lipid peroxidation as well as increasing the expression of anti-ferroptosis enzymes. Therefore, propofol protects the myocardium from I/R injury through the AKT/P53 signaling pathway. To the best of our knowledge, this is the first study demonstrating that propofol inhibits myocardial ferroptosis and the underlying molecular mechanism.

Investigating the death processes and underlying mechanisms of cardiomyocytes may provide insights into novel therapeutic approaches for heart diseases, especially I/R injury (Whelan et al., 2010). Ferroptosis, which is distinct from conventional cell death, including apoptosis, necroptosis, and autophagy-dependent cell death, has recently been identified as a key pathological process connecting oxidative stress, inflammation, and cardiovascular

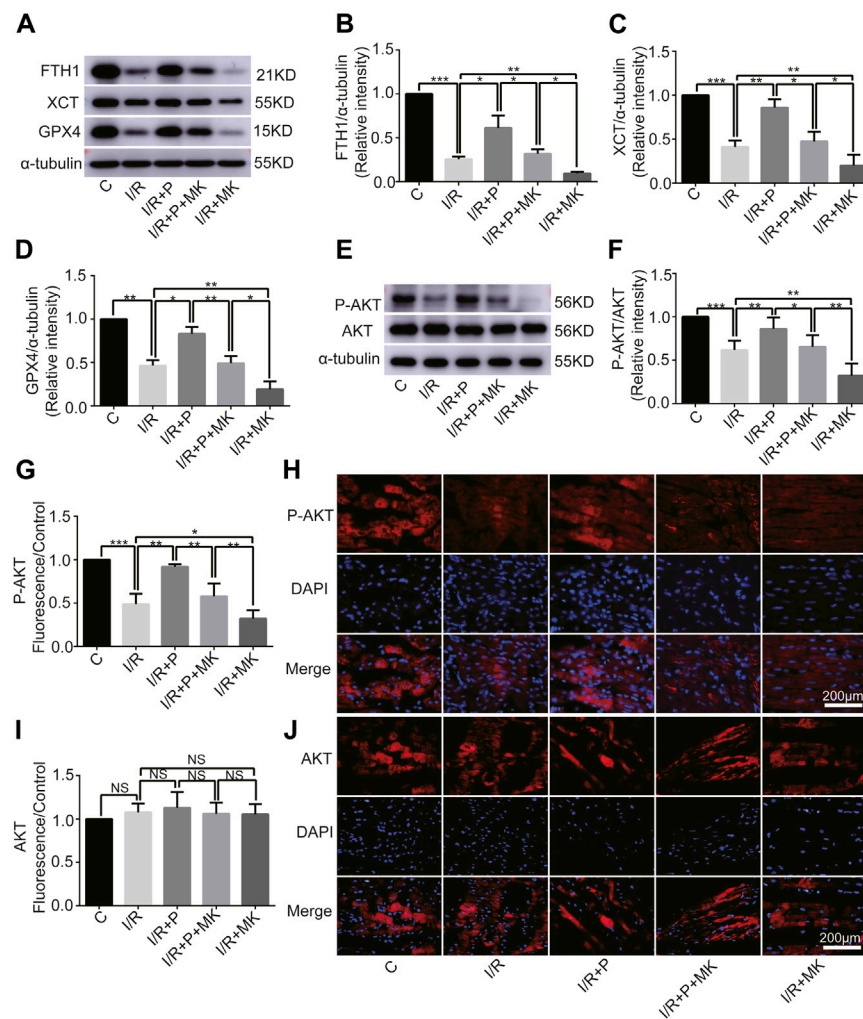


**FIGURE 5 |** Changes in protein levels in response to propofol. **(A–D)**: Influence of propofol on I/R-induced antioxidant enzyme expression. **(E–F)**: Expression of AKT and p-AKT in myocardium based on western blot analysis. **(G–J)**: Expression of AKT and P-AKT by immunofluorescence. N = 6. Data are expressed as the mean  $\pm$  SD. Scale bar: 20  $\mu$ m. Significance was calculated using one-way ANOVA with Tukey's post hoc test or the *t*-test. *p*-values < 0.05 were considered statistically significant. \**p* < 0.05, \*\**p* < 0.01, \*\*\**p* < 0.001.

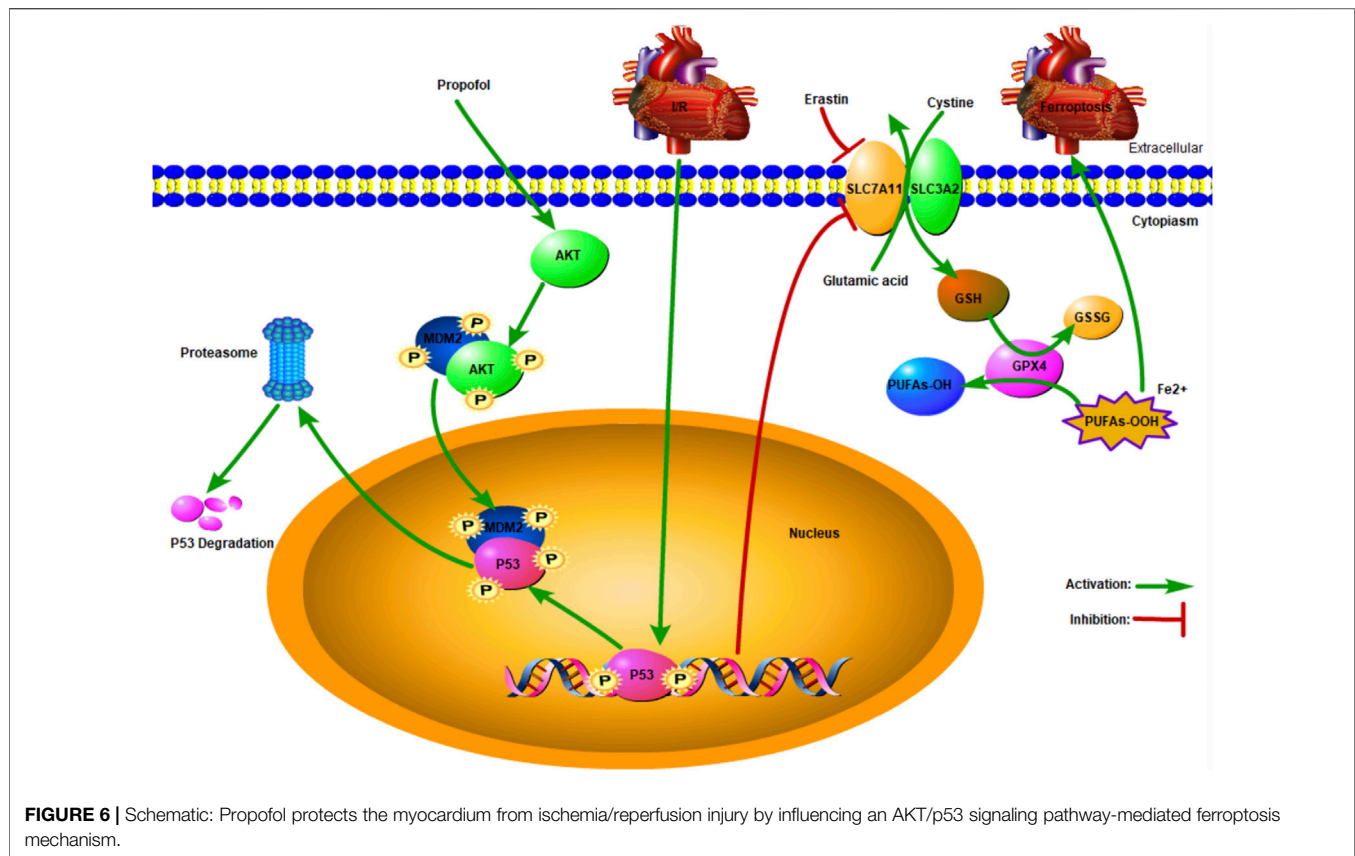
diseases (Yu et al., 2021). Ferroptosis, an iron-dependent type of cell death that is mainly caused by oxidation-reduction imbalance, differs from conventional cell death processes characterized by typical cell shrinkage, mitochondrial fragmentation, and nuclear condensation. With the increasing understanding of the molecular mechanisms of ferroptosis, ferroptosis has become a potential novel diagnostic and therapeutic target of cardiomyopathy. In this study, our results demonstrated that ferroptosis played an essential role in myocardial injury induced by erastin or I/R following previous findings (Fang et al., 2019; Li et al., 2020). Briefly, erastin or I/R triggered iron accumulation and then damaged cardiomyocytes due to oxidative stress (Olivieri, 1994).

A number of studies have reported that propofol protects the myocardium from I/R injury (Kobayashi et al., 2008; Li et al., 2019), but the mechanism is not clear. Our study showed that

p53, which promoted fatal lipid ROS accumulation and resulted in cardiomyocyte's ferroptosis, was upregulated in I/R-induced myocardial injury, which is consistent with the previous study (Tang et al., 2021). Notably, we found that propofol, which significantly inhibited p53 expression, inhibited myocardial ferroptosis caused by erastin or I/R.

Our results also demonstrated that erastin or I/R induced antioxidant enzyme damage and ROS accumulation, resulting in cell ferroptosis. Recent studies have shown that GPX4 improves iron absorption by directly decomposing peroxides, catalyzing the transformation of reduced glutathione (GSH) to oxidized GSH (GSSG) (Imai et al., 2017), and inhibiting the expression of ferritin heavy chain 1 (FTH1) (Sun et al., 2016). In the present study, we found that propofol improved the antioxidant capacity of cardiomyocytes by improving the levels of FTH1, XCT, or





GPX4 and reducing iron levels. Another study has shown that p53 inhibits cystine absorption by downregulating XCT expression (Magri et al., 2021), resulting in the inhibition of cystine-dependent glutathione oxidase activity and increased cell lipid ROS, leading to ferroptosis (Jiang et al., 2015). Our results showing propofol downregulation of p53 and reduction of cardiomyocyte dysfunction are consistent with the previous study (Lai et al., 2011).

A recent study showed that AKT plays a pivotal role in p53 degradation (Chibaya et al., 2021), which is inconsistent with the present findings. The p53 was degraded by binding with MDM2 (Wang et al., 2020), and this process was accelerated by AKT phosphorylation at ser166 or 188 (Feng et al., 2004). As shown in our study, propofol protected the myocardium from I/R-induced injury by AKT phosphorylation (Shravah et al., 2014). The expression of p53 increased after MK2206 pretreatment, indicating that signaling pathways other than AKT were involved in p53 degradation. When DNA is damaged, ataxia telangiectasia-mutated (ATM) activation induces p53 activation, resulting in cell aging or apoptosis (Jiang and Chen, 2020). Calcium-dependent kinase 5 (CDK5) and CDK9 activate p53 by phosphorylating ser33, which enhances the binding abilities of cyclic adenosine monophosphate (AMP) response element-binding protein (CREB) binding protein (CBP), thus raising p53 transcription activity (Zhang et al., 2002) (Figure 6).

Our study has some limitations. First, the Langendorff model rather than the rat I/R model was used in this study. However, the rat Langendorff model is easy to prepare, and the experimental results are reproducible (Finegan et al., 2000), which is consistent with best practices for reduction fine displacement (3R) (Flecknell, 2002). Second, the protective effects of AKT, which is the key survival signaling component in the heart, are associated with numerous factors. Recent studies have shown that propofol plays a protective role in the heart by activating the AKT/eNOS (Yan et al., 2021), ser473/thr308 (Lou et al., 2015), or PI3K/AKT (Wu et al., 2012) signal pathways. In our study, we only explored one biological process of AKT; other regulatory effects require further investigation. Third, the animal experiments were complicated and difficult, with a low success rate and inconsistent results (De Villiers and Riley, 2020). Fourth, propofol was used at a single concentration (50  $\mu$ M) according to a previous study (Yu et al., 2018), in which propofol (50  $\mu$ M) pretreatment was able to protect myocardium from I/R injury in the rat Langendorff model. The single concentration of propofol used in this study could limit our understanding of its role in I/R injury. Finally, we measured only the expression levels of FTH1, XCT, and GPX4 but not those of other antioxidant enzymes.

In conclusion, propofol pretreatment inhibits myocardial ferroptosis through the AKT/p53 signaling pathway, reducing



ROS, iron, and lipid peroxidation and increasing antioxidant enzyme expression. These data may explain why propofol reduces perioperative complications associated with myocardial I/R injury, including arrhythmias, decreasing systolic and diastolic function, and myocardial stunning.

## DATA AVAILABILITY STATEMENT

The original contributions presented in the study are included in the article/**Supplementary Material**, further inquiries can be directed to the corresponding authors.

## ETHICS STATEMENT

The animal study was reviewed and approved by The Experimental Animals Medical Ethics Committee in Shandong University (ECSBMSSDU 2019-2-048).

## AUTHOR CONTRIBUTIONS

Study conception/design: SL and JY. Experimental execution: SL, ZL, and XY. Data analysis: SL, MZ, and YH. Drafting of paper: SL,

DW, and ST. Manuscript editing/revision: SL, JL, and JY. Manuscript reading/final approval: all authors.

## FUNDING

This study was supported by the National Natural Science Foundation of China (No. 26010105131548), Shandong Province Natural Science Foundation (ZR2017BH041), and Key Research and Development Program of Shandong Province (No. 2018GSF118079).

## ACKNOWLEDGMENTS

The authors would like to thank the colleagues at Shandong University and the reviewers for their insightful comments on the manuscript.

## SUPPLEMENTARY MATERIAL

The Supplementary Material for this article can be found online at: <https://www.frontiersin.org/articles/10.3389/fphar.2022.841410/full#supplementary-material>

## REFERENCES

- Bovill, J. G. (2006). Intravenous Anesthesia for the Patient with Left Ventricular Dysfunction. *Semin. Cardiothorac. Vasc. Anesth.* 10, 43–48. doi:10.1177/108925320601000108
- Chen, Y., Hua, Y., Li, X., Arslan, I. M., Zhang, W., and Meng, G. (2020). Distinct Types of Cell Death and the Implication in Diabetic Cardiomyopathy. *Front. Pharmacol.* 11, 42. doi:10.3389/fphar.2020.00042
- Chibaya, L., Karim, B., Zhang, H., and Jones, S. N. (2021). Mdm2 Phosphorylation by Akt Regulates the P53 Response to Oxidative Stress to Promote Cell Proliferation and Tumorigenesis. *Proc. Natl. Acad. Sci. USA* 118 (2021), e2003193118. doi:10.1073/pnas.2003193118
- De Villiers, C., and Riley, P. R. (2020). Mouse Models of Myocardial Infarction: Comparing Permanent Ligation and Ischaemia-Reperfusion. *Dis. Model. Mech.* 13, dmm046565. doi:10.1242/dmm.046565
- Dixon, S. J., Lemberg, K. M., Lamprecht, M. R., Skouta, R., Zaitsev, E. M., Gleason, C. E., et al. (2012). Ferroptosis: An Iron-dependent Form of Nonapoptotic Cell Death. *Cell* 149, 1060–1072. doi:10.1016/j.cell.2012.03.042
- Fang, X., Wang, H., Han, D., Xie, E., Yang, X., Wei, J., et al. (2019). Ferroptosis as a Target for protection against Cardiomyopathy. *Proc. Natl. Acad. Sci. USA* 116, 2672–2680. doi:10.1073/pnas.1821022116
- Feng, J., Tamaskovic, R., Yang, Z., Brazil, D. P., Merlo, A., Hess, D., et al. (2004). Stabilization of Mdm2 via Decreased Ubiquitination Is Mediated by Protein Kinase B/Akt-dependent Phosphorylation. *J. Biol. Chem.* 279, 35510–35517. doi:10.1074/jbc.M404936200
- Finegan, B. A., Gandhi, M., Clanachan, A. S., and cardiology, c. (2000). Phentolamine Prevents the Adverse Effects of Adenosine on Glycolysis and Mechanical Function in Isolated Working Rat Hearts Subjected to Antecedent Ischemia. *J. Mol. Cell Cardiol* 32, 1075–1086. doi:10.1006/jmcc.2000.1144
- Flecknell, P. (2002). Replacement, Reduction and Refinement. *ALTEX* 19, 73–78.
- Freedman, D. A., Wu, L., Levine, A. J., and Cmls, m. l. s. (1999). Functions of the MDM2 Oncoprotein. *Cell Mol Life Sci* 55, 96–107. doi:10.1007/s000180050273
- Han, C., Liu, Y., Dai, R., Ismail, N., Su, W., and Li, B. (2020). Ferroptosis and its Potential Role in Human Diseases. *Front. Pharmacol.* 11, 239. doi:10.3389/fphar.2020.00239
- Imai, H., Matsuoka, M., Kumagai, T., Sakamoto, T., and Koumura, T. (2017). Lipid Peroxidation-dependent Cell Death Regulated by GPx4 and Ferroptosis. *Curr. Top. Microbiol. Immunol.* 403, 143–170. doi:10.1007/82\_2016\_508
- Jiang, L., Kon, N., Li, T., Wang, S. J., Su, T., Hibshoosh, H., et al. (2015). Ferroptosis as a P53-Mediated Activity during Tumour Suppression. *Nature* 520, 57–62. doi:10.1038/nature14344
- Jiang, S., and Chen, J. (2020). WRN Inhibits Oxidative Stress-Induced Apoptosis of Human Lensepithelial Cells through ATM/p53 Signaling Pathway and its Expression Is Downregulated by DNA Methylation. *Mol. Med.* 26, 68. doi:10.1186/s10020-020-00187-x
- Kobayashi, I., Kokita, N., and Namiki, A. (2008). Propofol Attenuates Ischaemia-Reperfusion Injury in the Rat Heart *In Vivo*. *Eur. J. Anaesthesiol* 25, 144–151. doi:10.1017/S0265021507001342
- Kruse, J. P., and Gu, W. (2009). Modes of P53 Regulation. *Cell* 137, 609–622. doi:10.1016/j.cell.2009.04.050
- Lai, H. C., Yeh, Y. C., Wang, L. C., Ting, C. T., Lee, W. L., Lee, H. W., et al. (2011). Propofol Ameliorates Doxorubicin-Induced Oxidative Stress and Cellular Apoptosis in Rat Cardiomyocytes. *Toxicol. Appl. Pharmacol.* 257, 437–448. doi:10.1016/j.taap.2011.10.001
- Li, W., Li, W., Leng, Y., Xiong, Y., and Xia, Z. (2020). Ferroptosis Is Involved in Diabetes Myocardial Ischemia/Reperfusion Injury through Endoplasmic Reticulum Stress. *DNA Cell Biol* 39, 210–225. doi:10.1089/dna.2019.5097
- Li, Y. m., Sun, J. g., Hu, L. h., Ma, X. c., Zhou, G., and Physiology, X. z. H. J. J. o. C. (2019). Propofol-mediated Cardioprotection Dependent of microRNA-451/HMGB1 against Myocardial Ischemia-reperfusion Injury. *J. Cell Physiol* 234, 23289–23301. doi:10.1002/jcp.28897
- Lou, P. H., Lucchinetti, E., Zhang, L., Affolter, A., Gandhi, M., Zhakupova, A., et al. (2015). Propofol (Diprivan®) and Intralipid® Exacerbate Insulin Resistance in Type-2 Diabetic Hearts by Impairing GLUT4 Trafficking. *Anesth. Analg* 120, 329–340. doi:10.1213/ane.0000000000000558
- Macías-Rodríguez, R. U., Inzaugarat, M. E., Ruiz-Margáin, A., Nelson, L. J., and Cubero, F. J. J. I. J. o. M. S. (2020). Reclassifying Hepatic Cell Death during Liver Damage: Ferroptosis—A Novel Form of Non-apoptotic Cell Death? *Int. J. Mol. Sci.* 21, 1651.
- Magri, J., Gasparetto, A., Conti, L., Calautti, E., Cossu, C., Ruiui, R., et al. (2021). Tumor-Associated Antigen xCT and Mutant-P53 as Molecular Targets for

- New Combinatorial Antitumor Strategies. *Cells* 10, 108. doi:10.3390/cells10010108
- Olivieri, P. L. a. N. (1994). Iron Overload Cardiomyopathies. *Cardiovasc. Drugs Ther.* 8, 101–110.
- Shravah, J., Wang, B., Pavlovic, M., Kumar, U., Chen, D. D., Luo, H., et al. (2014). Propofol Mediates Signal Transducer and Activator of Transcription 3 Activation and Crosstalk with Phosphoinositide 3-kinase/AKT. *JAKSTAT* 3, e29554. doi:10.4161/jkst.29554
- Stockwell, B. R., Friedmann Angeli, J. P., Bayir, H., Bush, A. I., Conrad, M., Dixon, S. J., et al. (2017). Ferroptosis: A Regulated Cell Death Nexus Linking Metabolism, Redox Biology, and Disease. *Cell* 171, 273–285. doi:10.1016/j.cell.2017.09.021
- Suleiman, M. S., Underwood, M., Imura, H., and Caputo, M. (2015). Cardioprotection during Adult and Pediatric Open Heart Surgery. *Biomed. Res. Int.* 2015, 712721. doi:10.1155/2015/712721
- Sun, X., Ou, Z., Chen, R., Niu, X., Chen, D., Kang, R., et al. (2016). Activation of the P62-Keap1-NRF2 Pathway Protects against Ferroptosis in Hepatocellular Carcinoma Cells. *Hepatology* 63, 173–184. doi:10.1002/hep.28251
- Szekely, A., Heindl, B., Zahler, S., Conzen, P. F., and Becker, B. F. (2000). Nonuniform Behavior of Intravenous Anesthetics on Postischemic Adhesion of Neutrophils in the guinea Pig Heart. *Anesth. Analg* 90, 1293–1300. doi:10.1097/00000539-200006000-00007
- Tang, L.-J., Zhou, Y.-J., Xiong, X.-M., Li, N.-S., Zhang, J.-J., Luo, X.-J., et al. (2021). Ubiquitin-specific Protease 7 Promotes Ferroptosis via Activation of the p53/TfR1 Pathway in the Rat Hearts after Ischemia/reperfusion. *Free Radic. Biol. Med.* 162, 339–352. doi:10.1016/j.freeradbiomed.2020.10.307
- Wang, W., Qin, J. J., Rajaei, M., Li, X., Yu, X., Hunt, C., et al. (2020). Targeting MDM2 for Novel Molecular Therapy: Beyond Oncology. *Med. Res. Rev.* 40, 856–880. doi:10.1002/med.21637
- Wei, L., Chen, W., Hu, T., Tang, Y., Pan, B., Jin, M., et al. (2021). Effect and Mechanism of Propofol in Hepatic Ischemia/reperfusion Injury of Rat. *J. Cell Physiol* 25, 4185. doi:10.26355/eurev\_202106\_26115
- Whelan, R. S., Kaplinskiy, V., and Kitsis, R. N. (2010). Cell Death in the Pathogenesis of Heart Disease: Mechanisms and Significance. *Annu. Rev. Physiol.* 72, 19–44. doi:10.1146/annurev.physiol.010908.163111
- Wu, K. L., Chen, C. H., and Shih, C. D. (2012). Nontranscriptional Activation of PI3K/Akt Signaling Mediates Hypotensive Effect Following Activation of Estrogen Receptor  $\beta$  in the Rostral Ventrolateral Medulla of Rats. *J. Biomed. Sci.* 19, 76. doi:10.1186/1423-0127-19-76
- Yagoda, N., von Rechenberg, M., Zaganjor, E., Bauer, A. J., Yang, W. S., Fridman, D. J., et al. (2007). RAS-RAF-MEK-dependent Oxidative Cell Death Involving Voltage-dependent Anion Channels. *Nature* 447, 864–868. doi:10.1038/nature05859
- Yan, J.-H., Tang, Y., and Guo, K. (2021). Evaluation of Propofol in Inhibiting Proliferation of Cardiac Fibroblasts in Angiotensin II-Induced Mouse. *Crit. Rev. Eukaryot. Gene Expr.* 31, 71–78. doi:10.1615/CritRevEukaryotGeneExpr.2021037483
- Yang, W. S., Kim, K. J., Gaschler, M. M., Patel, M., Shchepinov, M. S., and Stockwell, B. R. (2016). Peroxidation of Polyunsaturated Fatty Acids by Lipoxygenases Drives Ferroptosis. *Proc. Natl. Acad. Sci. U S A.* 113, E4966–E4975. doi:10.1073/pnas.1603244113
- Yang, W. S., and Stockwell, B. R. (2008). Synthetic Lethal Screening Identifies Compounds Activating Iron-dependent, Nonapoptotic Cell Death in Oncogenic-RAS-Harboring Cancer Cells. *Chem. Biol.* 15, 234–245. doi:10.1016/j.chembiol.2008.02.010
- Yin, Y., Guan, Y., Duan, J., Wei, G., Zhu, Y., Quan, W., et al. (2013). Cardioprotective Effect of Danshensu against Myocardial Ischemia/reperfusion Injury and Inhibits Apoptosis of H9c2 Cardiomyocytes via Akt and ERK1/2 Phosphorylation. *Eur. J. Pharmacol.* 699, 219–226. doi:10.1016/j.ejphar.2012.11.005
- Yu, X., Sun, X., Zhao, M., Hou, Y., Li, J., Yu, J., et al. (2018). Propofol Attenuates Myocardial Ischemia Reperfusion Injury Partly through Inhibition of Resident Cardiac Mast Cell Activation. *Int. Immunopharmacol* 54, 267–274. doi:10.1016/j.intimp.2017.11.015
- Yu, Y., Yan, Y., Niu, F., Wang, Y., Chen, X., Su, G., et al. (2021). Ferroptosis: a Cell Death Connecting Oxidative Stress, Inflammation and Cardiovascular Diseases. *Cell Death Discov* 7, 193. doi:10.1038/s41420-021-00579-w
- Zhang, J., Krishnamurthy, P. K., and Johnson, G. V. (2002). Cdk5 Phosphorylates P53 and Regulates its Activity. *J. Neurochem.* 81, 307–313. doi:10.1046/j.1471-4159.2002.00824.x
- Zhang, Y., Swanda, R. V., Nie, L., Liu, X., Wang, C., Lee, H., et al. (2021). mTORC1 couples cyst(e)ine availability with GPX4 protein synthesis and ferroptosis regulation. *Nat. Commun.* 12, 1589. doi:10.1038/s41467-021-21841-w
- Zhao, L., Zhuang, J., Wang, Y., Zhou, D., Zhao, D., Zhu, S., et al. (2019). Propofol Ameliorates H9c2 Cells Apoptosis Induced by Oxygen Glucose Deprivation and Reperfusion Injury via Inhibiting High Levels of Mitochondrial Fusion and Fission. *Front. Pharmacol.* 10, 61. doi:10.3389/fphar.2019.00061
- Zhou, W., Fontenot, H. J., Liu, S., and Kennedy, R. H. (1997). Modulation of Cardiac Calcium Channels by Propofol. *Anesthesiology* 86, 670–675. doi:10.1097/00000542-199703000-00020

**Conflict of Interest:** The authors declare that the research was conducted in the absence of any commercial or financial relationships that could be construed as a potential conflict of interest.

**Publisher's Note:** All claims expressed in this article are solely those of the authors and do not necessarily represent those of their affiliated organizations, or those of the publisher, the editors and the reviewers. Any product that may be evaluated in this article, or claim that may be made by its manufacturer, is not guaranteed or endorsed by the publisher.

Copyright © 2022 Li, Lei, Yang, Zhao, Hou, Wang, Tang, Li and Yu. This is an open-access article distributed under the terms of the Creative Commons Attribution License (CC BY). The use, distribution or reproduction in other forums is permitted, provided the original author(s) and the copyright owner(s) are credited and that the original publication in this journal is cited, in accordance with accepted academic practice. No use, distribution or reproduction is permitted which does not comply with these terms.



# Adenosine in Acute Myocardial Infarction-Associated Reperfusion Injury: Does it Still Have a Role?

Corrado De Marco<sup>1,2</sup>, Thierry Charron<sup>1,2</sup> and Guy Rousseau<sup>1,3\*</sup>

<sup>1</sup>CIUSSS du Nord-de-l'Île-de-Montréal, Hôpital du Sacré-Coeur, Department of Medicine, QC, Montréal, Canada, <sup>2</sup>Department of Medicine, Université de Montréal, Montréal, QC, Canada, <sup>3</sup>Department of Pharmacology and Physiology, Université de Montréal, Montréal, QC, Canada

The mainstay of acute myocardial infarction has long been timely reperfusion of the culprit obstruction. Reperfusion injury resulting from a multitude of pathophysiological processes has been demonstrated to negatively affect myocardial recovery and function post-infarction. Adenosine interacts directly with the sequential pathophysiological processes culminating in reperfusion injury by inhibiting them upstream. The evidence for adenosine's benefit in acute myocardial infarction has produced mixed results with regards to myocardial salvage and long-term mortality. The heterogenous evidence with regards to benefits on clinical outcomes has resulted in modest uptake of adenosine in the clinical setting. However, it is critical to analyze the variability in study methodologies. The goal of this review is to evaluate how adenosine dose, route of administration, timing of administration, and site of administration play essential roles in the molecule's efficacy. The benefits of adenosine, as highlighted in the following review, are clear and its role in the treatment of acute myocardial infarction should not be discounted

**Keywords:** myocardial infarction, no-reflow, reperfusion injury, adenosine, reperfusion, myocardial ischemia

## OPEN ACCESS

### Edited by:

Xianwei Wang,  
Xinxiang Medical University, China

### Reviewed by:

Gerd Heusch,  
University of Duisburg-Essen,  
Germany

### \*Correspondence:

Guy Rousseau  
guy.rousseau@umontreal.ca

### Specialty section:

This article was submitted to  
Cardiovascular and Smooth Muscle  
Pharmacology,  
a section of the journal  
Frontiers in Pharmacology

**Received:** 17 January 2022

**Accepted:** 26 April 2022

**Published:** 13 May 2022

### Citation:

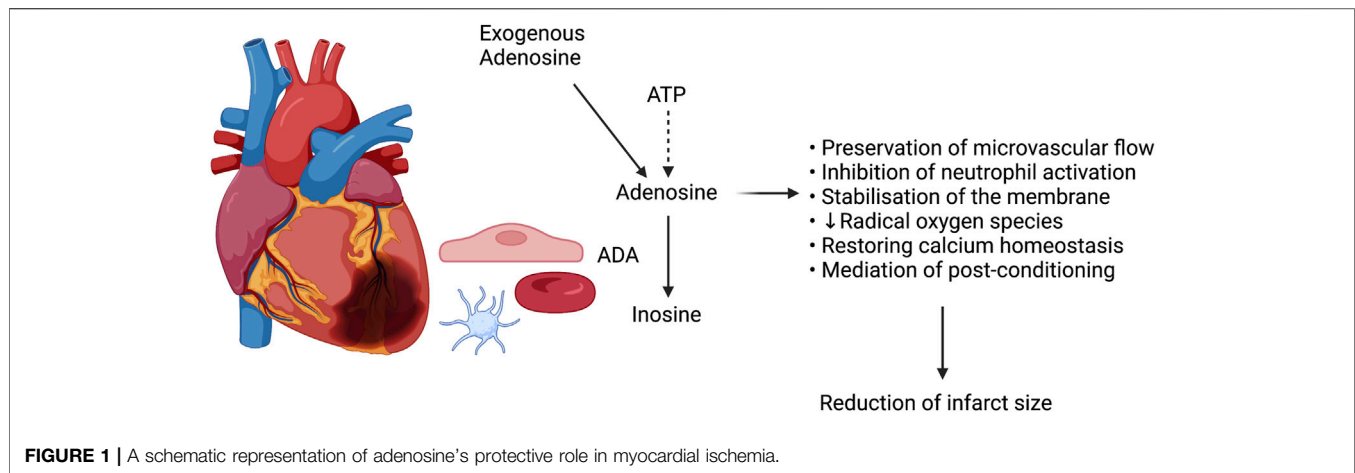
De Marco C, Charron T and  
Rousseau G (2022) Adenosine in  
Acute Myocardial Infarction-  
Associated Reperfusion Injury: Does it  
Still Have a Role?  
Front. Pharmacol. 13:856747.  
doi: 10.3389/fphar.2022.856747

## INTRODUCTION

Reperfusion therapy for acute myocardial infarction (AMI) has been established as the mainstay of therapy for reduction of the extent of myocardial damage and, ultimately, of mortality (Fibrinolytic Therapy Trialists' (FTT) Collaborative Group, 1994). Moreover, earlier reperfusion is related to improved survival (GUSTO Angiographic Investigators, 1993). That said, reperfusion itself has been associated with certain deleterious effects, including myocyte death, microvascular injury, myocardial stunning, no-reflow, and reperfusion arrhythmias (Kloner, 1993).

Nowadays, the first-choice therapy for ST-elevation myocardial infarction (STEMI) is percutaneous coronary intervention (PCI) (Keeley et al., 2003). Although PCI is successful in most cases, up to 40% of patients do not achieve complete myocardial reperfusion despite successful angioplasty of the culprit lesion (Gao et al., 2015). Critically, the myocardial outcome of the "ischemia-reperfusion" sequence exhibited in AMI depends not only on the time delay between ischemia and reperfusion, but so too on whether lethal reperfusion injury occurs (Monassier, 2008a).

A multitude of therapeutic options aimed at minimizing reperfusion injury, and thereby optimising results and outcomes of coronary artery revascularization following AMI, have historically been proposed. Adenosine, an endogenous nucleoside produced by the degradation of adenosine triphosphate (ATP) (Forman et al., 2006), figures among them. Adenosine has been shown to act on all mechanisms of reperfusion injury, distal embolization excluded, by promoting



preservation of microvascular flow, inhibiting neutrophils and the resultant inflammatory cascade, stabilizing cellular membranes and reducing synthesis of radical oxygen species, restoring calcium homeostasis, and mediating post-conditioning (**Figure 1**) (Forman et al., 2006; Monassier, 2008b).

Three large, randomised trials of adenosine completed in the late 1990s and early 2000s showed variable results. While adenosine consistently showed benefit in terms of minimizing infarct size, none of the studies were able to demonstrate a statistically significant mortality benefit, be it all-cause or cardiovascular mortality (Mahaffey et al., 1999; Quintana et al., 2003; Ross et al., 2005).

A systematic review published in 2015 (Gao et al., 2015) confirmed the same findings demonstrated in the three randomised control trials discussed above. Adenosine treatment was not found to have any effect on mortality or re-infarction, though did appear to offer beneficial effects on myocardial reperfusion, no reflow, and post-infarction left ventricular ejection fraction (Gao et al., 2015). Multiple hypotheses for the lack of consistent beneficial effects of adenosine have been emitted, including the inconsistent route of adenosine administration and the timing of infusion (Gao et al., 2015).

The conflicting findings in the literature, as well as the lack of statistically significant benefits in terms of endpoints pertaining to mortality and re-infarction, have resulted in sparse uptake in use of adenosine in the treatment of acute myocardial infarction.

## REVISITING THE CONCEPTS OF REPERFUSION INJURY

Monassier succinctly summarizes the concept of reperfusion injury by separating it into its two main facets: no-reflow, resulting from endothelial microvascular injury, and reperfusion syndrome, involving cardiomyocytes (Monassier, 2008b). The no-reflow phenomenon was initially described in 1966 by Krug et al (Krug et al., 1966). This phenomenon results from microvascular dysfunction

caused by increased capillary permeability and consequent edema in the infarcted/reperfused area, endothelial and vascular smooth muscle damage as well as release of vasoconstrictive substances from atherosclerotic lesions with resulted impaired vasomotion, and neutrophil infiltration and aggregation, all of which culminate in capillary destruction and hemorrhage (Heusch and Gersh, 2017; Heusch, 2019).

Consensus states that a large part of cell death resulting from reperfusion injury occurs within minutes of reperfusion. In addition to the mechanisms of microvascular dysfunction and vasoconstriction contributing to reperfusion injury, there seems to be an as-of-yet obscure but equally critical role mediated by the mitochondrial permeability transition pore (MPTP). Free radical oxygen species generation, which occurs during the ischemic event, and delivery to the infarcted area, which occurs following reperfusion, may contribute to MPTP opening. Opening of the MPTP appears to induce sarcolemmal rupture within the first minutes of reperfusion, potentially through the hypercontracture of neighbouring myocytes induced by high calcium levels in the presence of ATP (Komamura et al., 1994; Hausenloy et al., 2017; Heusch, 2020).

Reperfusion of the culprit lesion in AMI equally results in embolization of microthrombi and particles of plaque material downstream, thereby plugging small arteries and arterioles (Heusch and Gersh, 2017; Heusch, 2020; Kleinbongard and Heusch, 2022). These distal microinfarcts result in an inflammatory response and, moreover, reduce contractile function in the surviving myocardium around the distal microinfarcts via a mechanism of inflammatory signal-mediated myofibrillar oxidation (Kleinbongard and Heusch, 2022). Microvascular dysfunction in both the culprit artery, but so too in adjacent arteries via collateral vessels, may subsequently be induced by such embolic events (Heusch and Gersh, 2017; Heusch, 2020).

The processes above coalesce to ultimately contribute to abnormalities of potassium, sodium, and calcium homeostasis in injured myocytes, to an inability to restore myocyte energy



balance, and to microvascular injury that are the hallmarks of the no-reflow phenomenon (Forman et al., 2006).

## UNDERSTANDING ADENOSINE AND THE RATIONALE FOR ITS USE AS A CARDIOPROTECTIVE AGENT

Adenosine is a naturally occurring purine nucleoside comprised of an adenine molecule linked to a ribose sugar moiety via a beta-N9-glycosidic bond (Layland et al., 2014). It is synthesized in the intracellular space by purine synthesis or it may accumulate as a result of the breakdown of adenosine triphosphate (ATP) (Layland et al., 2014). Concentrations of intracellular adenosine have been shown to increase in situations in which there is a mismatch between ATP synthesis and use (e.g., ischemia) (Saito et al., 1999).

Adenosine's transportation occurs rapidly into vascular endothelial cells and erythrocytes, where it is catabolized by adenosine deaminase to inosine (Layland et al., 2014). Notably, adenosine deaminase is found on the plasmatic membranes of erythrocytes and platelets (Franco et al., 1990). Understanding adenosine's transportation and, most importantly, its short half-life is critical to comprehending its pharmacokinetics. Adenosine, when administered via the intra-coronary route, has a peak effect of < 10 s and a duration of action of roughly 20 s (Layland et al., 2014).

The four receptors that bind adenosine are A1, A2A, A2B, and A3 (Shryock and Belardinelli, 1997). Adenosine A2A receptors are found on neutrophils, endothelial cells, vascular smooth muscle, and platelets (Vinten-Johansen et al., 1999). Activation of the A2A and A2B receptors increases adenylate cyclase activity and cAMP levels via coupling to G<sub>s</sub> proteins (Heusch, 2010), consequently resulting in potent vasodilation of the coronary circulation and an increase in myocardial blood flow (Shryock and Belardinelli, 1997; Vinten-Johansen et al., 1999; Heusch, 2010). Furthermore, adenylate cyclase activation *via* the A2A receptor results in inhibition of neutrophil superoxide generation and adherence to the endothelium (Vinten-Johansen et al., 1999). Therein, adenosine and its receptor-ligand induction of adenylate cyclase target neutrophil aggregation and adherence, reducing neutrophilic arterial plugging that has been evoked as one of the central mechanisms of reperfusion injury. Additionally, adenosine's inhibition of neutrophil activation targets and prevents what is otherwise one of the initiating factors of the inflammatory cascade that culminates in reperfusion injury (Vinten-Johansen et al., 1999).

Adenosine's administration initiates a multitude of metabolic events that could be beneficial in the setting of ischemia and reperfusion (Forman et al., 2006). Exogenous adenosine is responsible for the restoration of ATP levels in viable but energy-deficient ischemic cells, as demonstrated in a study wherein the presence of an adenosine deaminase inhibitor resulted increased levels of ATP following reperfusion (Forman and Velasco, 1991).

Studies suggest that adenosine may play a critical role in promoting vascular repair and in accelerating the development

of new blood vessels following vascular injury (Dubey et al., 2002; Montesinos et al., 2004). These properties of adenosine are attributable to its stimulation of angiogenic factors such as IL-8, vascular endothelial growth factor, and basic fibroblast growth factor from microvascular endothelial cells (Feoktistov et al., 2003). One may infer from the above properties that adenosine may play an integral role in the repair of injured endothelium after reperfusion and, thereby, prevent ventricular remodeling by favouring collateral blood flow.

Ischemic pre-conditioning is a phenomenon wherein a brief period of ischemia renders the myocardium more resistant to injury following a subsequent episode of ischemia (Vinten-Johansen et al., 1999). Seminal work done by Schulz et al (Schulz et al., 1995) has highlighted the integral role that endogenous release of adenosine plays in limitation of infarct size. The group's work (Schulz et al., 1995), published in 1994, compared four groups: a first group subjected to 90 min of ischemia, a second group subjected to an initial 10-minute period of ischemia (i.e., ischemic pre-conditioning) followed by a 15-minute period of reperfusion prior to a 90-minute period of ischemia, a third group receiving intra-coronary infusion of adenosine deaminase maintained throughout the 90-minute ischemic period, and a final group undergoing ischemic pre-conditioning with concomitant adenosine deaminase infusion and subsequent 90-minute ischemia. Their results demonstrated a significantly reduced infarct size in the ischemic pre-conditioning alone (i.e., without adenosine deaminase infusion) group (Schulz et al., 1995). In so doing, this pioneering article confirmed the central role of endogenous adenosine in ischemic pre-conditioning in swine hearts, since the infarct size reduction in ischemic pre-conditioning was significantly attenuated when catabolism of adenosine was increased through administration of adenosine deaminase (Schulz et al., 1995). A similar principle, dubbed ischemic post-conditioning, is a phenomenon whereby repetitive short episodes of ischemia following a longer, more prolonged ischemic episode result in significantly decreased myocardial damage (Liu et al., 1991; Zhao et al., 2003). Adenosine, *via* A1 receptor-induced activation of protein kinase C and subsequent protein function modulation by phosphorylation mediates and potentiates the phenomena of pre- and post-conditioning (Vinten-Johansen et al., 1999). Lending further credence to this theory, research demonstrated that pre-conditioning protection could be blocked by use of adenosine receptor blocking agents (Liu et al., 1991; Schulz et al., 1995), and was conversely potentiated by use of an A1-specific agonist (Liu et al., 1991). The A2A and A3 receptors may equally play a role in pre- and post-conditioning, though this has been less well established.

Moreover, the ischemic pre-conditioning triggered by adenosine has been demonstrated to be unique when compared to that triggered by other molecules mediating pre-conditioning, such as acetylcholine, bradykinin, and opioids (Cohen et al., 2001). More specifically, it has been

demonstrated that the pre-conditioning induced by adenosine release, unlike that of the other molecules mentioned, seems independent of either free radicals or mitochondrial  $K_{ATP}$  channels (Cohen et al., 2001). The evidence supports that it is therefore most likely that adenosine results in direct activation of protein kinases (Cohen et al., 2001), more specifically protein kinase C, whose role in ischemic pre-conditioning is well established (Vinten-Johansen et al., 1999).

The beneficial effects of adenosine on myocardial blood flow and on limitation of infarct size have been extensively studied and demonstrated in animals (Boucher et al., 2004; Yetgin et al., 2015).

## HIGHLIGHTING THE IMPORTANCE OF THE ADMINISTRATION ROUTE

Early studies of adenosine in the setting of AMI in humans were performed with administration of adenosine *via* the intravenous route.

In the AMISTAD (Mahaffey et al., 1999; Ross et al., 2005) trials, low (50 mcg/kg/min) and high (70 mcg/kg/min) infusions of adenosine started within 15 min of thrombolysis or before coronary intervention were compared in a 1:1:1 fashion to placebo. AMISTAD II demonstrated no difference in the primary endpoint of new congestive heart failure > 24 h after randomization or first re-hospitalization for congestive heart failure, or death from any cause within 6 months, but that patients treated with adenosine had a tendency towards smaller infarct sizes (17% of the left ventricular size versus 27%,  $p = 0.074$ ). Furthermore, infarct size was shown to be significantly related ( $p < 0.001$ ) to the occurrence of the primary endpoint.

In the ATTAC (Quintana et al., 2003) study, a single dose (10mcg/kg/min) of adenosine was infused at the time of thrombolysis and maintained for 6 h and was compared to placebo. No beneficial effect of adenosine was found regarding echocardiographic indices of left ventricular systolic or diastolic function. Despite the trial being stopped early due to lack of apparent effect after an interim analysis, 12-month follow-up data showed that cardiovascular mortality was 8.9% with adenosine and 12.1% with placebo (OR 0.71, 95% CI 0.4-1.2,  $p = 0.2$ ) and 8.4 versus 14.6% (OR 0.53, 95% CI 0.23-1.24,  $p = 0.09$ ) in patients with anterior AMI.

The primary limitation pertaining to intravenous adenosine administration is that maximal doses are difficult to achieve because of the marked systemic hypotension associated with higher adenosine doses (Charron et al., 2013). Whether maximal doses of adenosine were achieved in studies employing the intravenous route is unclear. The cardioprotective properties observed, however, are non-negligible and highlight that even intravenous adenosine, despite potentially sub-optimal dosing, may result in stimulation of remote pathways of cardioprotection. Intracoronary administration of adenosine, unlike intravenous administration, enables delivery of much higher doses without direct systemic effects, most notably hypotension.

## PROPERLY TIMING ADENOSINE ADMINISTRATION

Recalling that the pathophysiology underpinning reperfusion injury is, as the name implies, coronary reperfusion, it is inherently logical that the optimal timing for adenosine administration be prior to reperfusion, whether achieved with thrombolysis or percutaneous coronary intervention. If administered late, once reperfusion has already occurred, the pathophysiological cascade culminating in reperfusion injury will already have been triggered, and adenosine's inhibitory effects on this chain of events are more likely to be inefficient.

To the above point, an animal study on rats published in 2004 (Boucher et al., 2004) compared the effects of early versus late administration of an adenosine A2A agonist (CGS21680) on infarct size, which was calculated as a percentage of the area at risk by occlusion of the target coronary artery—in this case, the left anterior descending artery. In the study, the early administration group received CGS21680 5 min prior to reperfusion, whereas the late administration group received adenosine 5 min after the initiation of reperfusion. Study groups were compared to control subjects. Infarct size was significantly reduced in the early compared to the control group ( $25.7 \pm 5.3\%$  versus  $46.5 \pm 5.3\%$ ,  $p < 0.05$ ). Conversely, there was no statistically significant difference when comparing the late group infarct size area ( $38.2 \pm 6.2\%$ ) to that of the control group. Indeed, such a study lends credence to the belief that timing adenosine administration before reperfusion is crucial for optimising treatment effects.

To date, there has been inconsistency in study methodology as it pertains to adenosine administration (Yetgin et al., 2015). Ultimately, results have been mixed, though there is a demonstrable trend towards improved outcomes in terms of infarct size limitation with earlier administration of adenosine.

## ESTABLISHING AN OPTIMAL DURATION OF ADENOSINE INFUSION

Duration of infusion represents yet another point of discussion when examining adenosine's role in AMI. The early intravenous studies (Mahaffey et al., 1999; Quintana et al., 2003; Ross et al., 2005), most notably AMISTAD, AMISTAD II, and ATTACC, used variable infusion durations ranging from one to six h. That said, the limitations of intravenous adenosine administration have been discussed previously and, indeed, dose adjustments to infusion rates were often made in these studies because of adverse effects related to the adenosine infusion.

In contrast, while there may be no human studies evaluating continuous infusions of adenosine *via* the intracoronary route, an animal study on porcine subjects (Yetgin et al., 2015) did compare bolus with prolonged infusions of intracoronary adenosine. Results of said study (Yetgin et al., 2015) demonstrated that only the prolonged, high-dose infusion of adenosine was able to limit infarct size ( $46 \pm 4\%$  of the area at risk versus  $59 \pm 3\%$  in the

control group,  $p = 0.02$ ) and no reflow ( $26 \pm 6\%$  of the infarct area versus  $49 \pm 6\%$  in the control group,  $p = 0.03$ ), with bolus administration of adenosine without subsequent prolonged infusion yielding results that were similar to those of the control group.

Given the extremely short half-life of adenosine, it stands to reason that bolus injections, unless perfectly timed and optimally delivered, may be inadequate when treating reperfusion injury in AMI. Conversely, more prolonged intracoronary delivery initiated just prior to reperfusion may increase local drug concentrations multi-fold and may achieve adequate levels in the target microvascular bed, thereby potentially improving therapeutic efficacy. That said, There remains at present a lack of evidence in the literature to support this hypothesis.

## THE IMPORTANCE OF LOCATION OF ADENOSINE ADMINISTRATION

The logical question stemming from growing interest in intracoronary administration of adenosine pertains to selection of the optimal location for such intracoronary delivery. Studies to date have employed various methodologies, with intracoronary injection sites being quite variable. The three main intracoronary administration sites identified and examined in the literature thus far are at the catheter site, at the site of percutaneous coronary intervention, or distal to the occlusion site (Yetgin et al., 2015).

An animal study (Charron et al., 2013) in male pigs harmonizes many of the elements discussed above by comparing three different doses of adenosine—2, 4, and 8 mg—administered prior to reperfusion as a bolus either intra-coronary, downstream of the occlusion site, or extra-coronary. Results demonstrated a significant reduction ( $p < 0.05$ ) in infarct size expressed as a percentage of area at risk in the 4 mg ( $33 \pm 6\%$ ) and 8 mg ( $30 \pm 5\%$ ) intra-coronary groups compared to the placebo group ( $46 \pm 3\%$ ). Critically, there was no statistically significant reduction in the 2 mg intra-coronary group ( $38 \pm 2\%$ ) and, most interestingly, in the 8 mg intracoronary group in whom adenosine was injected upstream of the occlusion site ( $47 \pm 6\%$ ).

Translation of such animal studies to humans, with the beneficial effects of intra-coronary adenosine downstream of the occlusion site prior to the onset of reperfusion, has been demonstrated by Marzilli et al. (Marzilli et al., 2000). Such an administration route was associated with beneficial effects on both coronary blood flow and ventricular function, indicating likely minimization of the mechanisms underpinning reperfusion injury (Marzilli et al., 2000). In fact, a meta-analysis comparing randomized controlled trials studying intracoronary adenosine versus control to trials studying intravenous adenosine versus control found improved clinical outcomes in terms of less heart failure in patients administered intracoronary adenosine (Bulluck et al., 2016).

## DISCUSSION

The mainstay of therapy for patients with AMI remains reperfusion, either *via* timely percutaneous coronary intervention in capable centers or *via* thrombolysis. Successful reperfusion has been extensively demonstrated to reduce cardiac mortality and minimize infarct size and left ventricular damage. That said, reperfusion, as discussed extensively in this review, may itself induce injury deleterious to left ventricular function both in the short- and long-term. Therefore, exploration and identification of therapy tailored to those at the highest risk of reperfusion injury may provide additional avenues dedicated to improving left ventricular function and clinical outcomes.

Adenosine has widely been demonstrated to have multiple favorable effects in mitigating no-reflow and reperfusion injury, primarily but not exclusively through inhibition of neutrophil-mediated vascular plugging and vascular damage. In experimental models, both intravenous and intracoronary routes of administration resulted in marked reduction of infarct size. In human trials, intravenous adenosine has similarly shown benefit in infarct size reduction, though this benefit has yet to translate to concrete clinical endpoints, most notably cardiovascular mortality and heart failure hospitalization.

While use of adenosine in the acute treatment of AMI has yet to garner uptake at large, it remains an avenue of interest worth exploring further. Most critically, the varying study methodologies make it difficult to draw broad conclusions from the existing evidence. The evidence is becoming increasingly clearer that dose, timing of administration, route of administration, and site of administration play critical roles in adenosine's ultimate efficacy. An understanding of adenosine's pharmacokinetics and pharmacodynamics is critical when examining studies done to date and when planning and executing future studies. In the case of intra-coronary administration, especially, the presence of blood in the catheter may lead to rapid inactivation of adenosine, recalling that adenosine deaminase is found on the plasmatic membrane of erythrocytes and platelets, prior to its arrival at the target site. Overall, by drawing from the literature, it appears as though a bolus of adenosine delivered intra-coronary distal to the occlusion site at or just prior to reperfusion is most effective in reducing reperfusion injury, though this hypothesis has yet to be tested in human subjects.

## CONCLUSION

It is critical that reperfusion injury be seen not only as a theoretical phenomenon, but rather as an important determinant of final infarct size and consequent ventricular dysfunction. Adenosine, despite its perceived lack of benefit relative to clinical outcomes, remains one of the few molecules to consistently reduce infarct size,

especially in anterior AMI, by directly combatting the pathophysiological underpinnings of reperfusion injury. Its clinical use and continued study in well-designed experiments is not only necessary, but so too vital to the goal of improving patient outcomes in AMI.

## REFERENCES

- Boucher, M., Pesant, S., Falcao, S., de Montigny, C., Schampaert, E., Cardinal, R., et al. (2004). Post-ischemic Cardioprotection by A2A Adenosine Receptors: Dependent of Phosphatidylinositol 3-kinase Pathway. *J. Cardiovasc Pharmacol.* 43, 416–422. doi:10.1097/00005344-200403000-00013
- Bulluck, H., Sirker, A., Loke, Y. K., Garcia-Dorado, D., and Hausenloy, D. J. (2016). Clinical Benefit of Adenosine as an Adjunct to Reperfusion in ST-Elevation Myocardial Infarction Patients: An Updated Meta-Analysis of Randomized Controlled Trials. *Int. J. Cardiol.* 202, 228–237. doi:10.1016/j.ijcard.2015.09.005
- Charron, T., Tran Quang, T., Gosselin, A., and Rousseau, G. (2013). Dose-dependent Effect of a Single Dose of Adenosine Given Just before Reperfusion in the Coronary Artery Downstream the Occlusion Site Reduces Infarct Size. *Can. Jour Car* 29, 344–345. doi:10.1016/j.cjca.2013.07.588
- Cohen, M. V., Yang, X. M., Liu, G. S., Heusch, G., and Downey, J. M. (2001). Acetylcholine, Bradykinin, Opioids, and Phenylephrine, but Not Adenosine, Trigger Preconditioning by Generating Free Radicals and Opening Mitochondrial K(ATP) Channels. *Circ. Res.* 89, 273–278. doi:10.1161/hh1501.094266
- Dubey, R. K., Gillespie, D. G., and Jackson, E. K. (2002). A(2B) Adenosine Receptors Stimulate Growth of Porcine and Rat Arterial Endothelial Cells. *Hypertension* 39, 530–535. doi:10.1161/hy0202.103075
- Feoktistov, I., Ryzhov, S., Goldstein, A. E., and Biaggioni, I. (2003). Mast Cell-mediated Stimulation of Angiogenesis: Cooperative Interaction between A2B and A3 Adenosine Receptors. *Circ. Res.* 92, 485–492. doi:10.1161/01.RES.0000061572.10929.2D
- Fibrinolytic Therapy Trialists' (Ftt) Collaborative Group (1994). Indications for Fibrinolytic Therapy in Suspected Acute Myocardial Infarction: Collaborative Overview of Early Mortality and Major Morbidity Results from All Randomised Trials of More Than 1000 Patients. Fibrinolytic Therapy Trialists' (FTT) Collaborative Group. *Lancet* 343, 311–322.
- Forman, M. B., Stone, G. W., and Jackson, E. K. (2006). Role of Adenosine as Adjunctive Therapy in Acute Myocardial Infarction. *Cardiovasc Drug Rev.* 24, 116–147. doi:10.1111/j.1527-3466.2006.00116.x
- Forman, M. B., and Velasco, C. E. (1991). Role of Adenosine in the Treatment of Myocardial Stunning. *Cardiovasc Drugs Ther.* 5, 901–908. doi:10.1007/BF00053551
- Franco, R., Aran, J. M., Colomer, D., Matutes, E., and Vives-Corrons, J. L. (1990). Association of Adenosine Deaminase with Erythrocyte and Platelet Plasma Membrane: an Immunological Study Using Light and Electron Microscopy. *J. Histochem Cytochem* 38, 653–658. doi:10.1177/38.5.2332624
- Gao, Q., Yang, B., Guo, Y., and Zheng, F. (2015). Efficacy of Adenosine in Patients with Acute Myocardial Infarction Undergoing Primary Percutaneous Coronary Intervention: A PRISMA-Compliant Meta-Analysis. *Med. Baltim.* 94 (32), e1279. doi:10.1097/MD.0000000000001279
- Gusto Angiographic Investigators (1993). The Effects of Tissue Plasminogen Activator, Streptokinase, or Both on Coronary-Artery Patency, Ventricular Function, and Survival after Acute Myocardial Infarction. *N. Engl. J. Med.* 329, 1615–1622. doi:10.1056/NEJM199311253292204
- Hausenloy, D. J., Botker, H. E., Engstrom, T., Erlinge, D., Heusch, G., Ibanez, B., et al. (2017). Targeting Reperfusion Injury in Patients with ST-Segment Elevation Myocardial Infarction: Trials and Tribulations. *Eur. Heart J.* 38, 935–941. doi:10.1093/eurheartj/ehw145
- Heusch, G. (2010). Adenosine and Maximum Coronary Vasodilation in Humans: Myth and Misconceptions in the Assessment of Coronary Reserve. *Basic Res. Cardiol.* 105, 1–5. doi:10.1007/s00395-009-0074-7
- Heusch, G. (2019). Coronary Microvascular Obstruction: the New Frontier in Cardioprotection. *Basic Res. Cardiol.* 114, 45. doi:10.1007/s00395-019-0756-8
- Heusch, G., and Gersh, B. J. (2017). The Pathophysiology of Acute Myocardial Infarction and Strategies of Protection beyond Reperfusion: a Continual Challenge. *Eur. Heart J.* 38, 774–784. doi:10.1093/eurheartj/ehw224
- Heusch, G. (2020). Myocardial Ischaemia-Reperfusion Injury and Cardioprotection in Perspective. *Nat. Rev. Cardiol.* 17, 773–789. doi:10.1038/s41569-020-0403-y
- Keeley, E. C., Boura, J. A., and Grines, C. L. (2003). Primary Angioplasty versus Intravenous Thrombolytic Therapy for Acute Myocardial Infarction: a Quantitative Review of 23 Randomised Trials. *Lancet* 361, 13–20. doi:10.1016/S0140-6736(03)12113-7
- Kleinbongard, P., and Heusch, G. (2022). A Fresh Look at Coronary Microembolization. *Nat. Rev. Cardiol.* 19, 265–280. doi:10.1038/s41569-021-00632-2
- Kloner, R. A. (1993). Does Reperfusion Injury Exist in Humans? *J. Am. Coll. Cardiol.* 21, 537–545. doi:10.1016/0735-1097(93)90700-b
- Komamura, K., Kitakaze, M., Nishida, K., Naka, M., Tamai, J., Uematsu, M., et al. (1994). Progressive Decreases in Coronary Vein Flow during Reperfusion in Acute Myocardial Infarction: Clinical Documentation of the No Reflow Phenomenon after Successful Thrombolysis. *J. Am. Coll. Cardiol.* 24, 370–377. doi:10.1016/0735-1097(94)90290-9
- Krug, A., Du Mesnil De Rochemont, W., and Korb, G. (1966). Blood Supply of the Myocardium after Temporary Coronary Occlusion. *Circ. Res.* 19, 57–62. doi:10.1161/01.res.19.1.57
- Layland, J., Carrick, D., Lee, M., Oldroyd, K., and Berry, C. (2014). Adenosine: Physiology, Pharmacology, and Clinical Applications. *JACC Cardiovasc Interv.* 7 (6), 581–591. doi:10.1016/j.jcin.2014.02.009
- Liu, G. S., Thornton, J., Van Winkle, D. M., Stanley, A. W., Olsson, R. A., and Downey, J. M. (1991). Protection against Infarction Afforded by Preconditioning Is Mediated by A1 Adenosine Receptors in Rabbit Heart. *Circulation* 84, 350–356. doi:10.1161/01.cir.84.1.350
- Mahaffey, K. W., Puma, J. A., Barbagelata, N. A., DiCarli, M. F., Leeser, M. A., Browne, K. F., et al. (1999). Adenosine as an Adjunct to Thrombolytic Therapy for Acute Myocardial Infarction: Results of a Multicenter, Randomized, Placebo-Controlled Trial: the Acute Myocardial Infarction Study of Adenosine (AMISTAD) Trial. *J. Am. Coll. Cardiol.* 34, 1711–1720. doi:10.1016/s0735-1097(99)00418-0
- Marzilli, M., Orsini, E., Marraccini, P., and Testa, R. (2000). Beneficial Effects of Intracoronary Adenosine as an Adjunct to Primary Angioplasty in Acute Myocardial Infarction. *Circulation* 101, 2154–2159. doi:10.1161/01.cir.101.18.2154
- Monassier, J. P. (2008). Reperfusion Injury in Acute Myocardial Infarction: from Bench to Cath Lab. Part II: Clinical Issues and Therapeutic Options. *Arch. Cardiovasc Dis.* 101 (9), 565–575. doi:10.1016/j.acvd.2008.06.013
- Monassier, J. P. (2008). Reperfusion Injury in Acute Myocardial Infarction. From Bench to Cath Lab. Part I: Basic Considerations. *Arch. Cardiovasc Dis.* 101 (7–8), 491–500. doi:10.1016/j.acvd.2008.06.014
- Montesinos, M. C., Shaw, J. P., Yee, H., Shamamian, P., and Cronstein, B. N. (2004). Adenosine A(2A) Receptor Activation Promotes Wound Neovascularization by Stimulating Angiogenesis and Vasculogenesis. *Am. J. Pathol.* 164, 1887–1892. doi:10.1016/S0002-9440(10)63749-2
- Quintana, M., Hjendahl, P., Sollevi, A., Kahan, T., Edner, M., Rehnqvist, N., et al. (2003). Left Ventricular Function and Cardiovascular Events Following Adjuvant Therapy with Adenosine in Acute Myocardial Infarction Treated with Thrombolysis, Results of the ATTenuation by Adenosine of Cardiac Complications (ATTACC) Study. *Eur. J. Clin. Pharmacol.* 59, 1–9. doi:10.1007/s00228-003-0564-8
- Ross, A. M., Gibbons, R. J., Stone, G. W., Kloner, R. A., and Alexander, R. W. (2005). A Randomized, Double-Blinded, Placebo-Controlled Multicenter Trial of Adenosine as an Adjunct to Reperfusion in the Treatment of Acute

## AUTHOR CONTRIBUTIONS

All authors listed have made a substantial, direct, and intellectual contribution to the work and approved it for publication. The figure was made with www.Biorender.com.



- Myocardial Infarction (AMISTAD-II). *J. Am. Coll. Cardiol.* 45, 1775–1780. doi:10.1016/j.jacc.2005.02.061
- Saito, H., Nishimura, M., Shinano, H., Makita, H., Tsujino, I., Shibuya, E., et al. (1999). Plasma Concentration of Adenosine during Normoxia and Moderate Hypoxia in Humans. *Am. J. Respir. Crit. Care Med.* 159, 1014–1018. doi:10.1164/ajrccm.159.3.9803100
- Schulz, R., Rose, J., Post, H., and Heusch, G. (1995). Involvement of Endogenous Adenosine in Ischaemic Preconditioning in Swine. *Pflugers Arch.* 430, 273–282. doi:10.1007/BF00374659
- Shryock, J. C., and Belardinelli, L. (1997). Adenosine and Adenosine Receptors in the Cardiovascular System: Biochemistry, Physiology, and Pharmacology. *Am. J. Cardiol.* 79, 2–10. doi:10.1016/s0002-9149(97)00256-7
- Vinten-Johansen, J., Thourani, V. H., Ronson, R. S., Jordan, J. E., Zhao, Z. Q., Nakamura, M., et al. (1999). Broad-spectrum Cardioprotection with Adenosine. *Ann. Thorac. Surg.* 68, 1942–1948. doi:10.1016/s0003-4975(99)01018-8
- Yetgin, T., Uitterdijk, A., Te Lintel Hekkert, M., Merkus, D., Krabbendam-Peters, I., van Beusekom, H. M. M., et al. (2015). Limitation of Infarct Size and No-Reflow by Intracoronary Adenosine Depends Critically on Dose and Duration. *JACC Cardiovasc Interv.* 8, 1990–1999. doi:10.1016/j.jcin.2015.08.033
- Zhao, Z. Q., Corvera, J. S., Halkos, M. E., Kerendi, F., Wang, N. P., Guyton, R. A., et al. (2003). Inhibition of Myocardial Injury by Ischemic Postconditioning during Reperfusion: Comparison with Ischemic Preconditioning. *Am. J. Physiol. Heart Circ. Physiol.* 285, H579–H588. doi:10.1152/ajpheart.01064.2002

**Conflict of Interest:** The authors declare that the research was conducted in the absence of any commercial or financial relationships that could be construed as a potential conflict of interest.

**Publisher's Note:** All claims expressed in this article are solely those of the authors and do not necessarily represent those of their affiliated organizations, or those of the publisher, the editors and the reviewers. Any product that may be evaluated in this article, or claim that may be made by its manufacturer, is not guaranteed or endorsed by the publisher.

Copyright © 2022 De Marco, Charron and Rousseau. This is an open-access article distributed under the terms of the Creative Commons Attribution License (CC BY). The use, distribution or reproduction in other forums is permitted, provided the original author(s) and the copyright owner(s) are credited and that the original publication in this journal is cited, in accordance with accepted academic practice. No use, distribution or reproduction is permitted which does not comply with these terms.



# Qiliqiangxin Modulates the Gut Microbiota and NLRP3 Inflammasome to Protect Against Ventricular Remodeling in Heart Failure

Yingdong Lu<sup>1†</sup>, Mi Xiang<sup>1†</sup>, Laiyun Xin<sup>1,2</sup>, Yang Zhang<sup>1,2</sup>, Yuling Wang<sup>1</sup>, Zihuan Shen<sup>1</sup>, Li Li<sup>1\*</sup> and Xiangning Cui<sup>1\*</sup>

<sup>1</sup>Department of Cardiovascular, Guang'anmen Hospital, China Academy of Chinese Medical Sciences, Beijing, China, <sup>2</sup>First Clinical Medical School, Shandong University of Chinese Medicine, Jinan, China

## OPEN ACCESS

### Edited by:

Xianwei Wang,  
Xinxiang Medical University, China

### Reviewed by:

Jianying Ma,  
Fudan University, China  
Xinli Li,  
Nanjing Medical University, China

### \*Correspondence:

Li Li  
REAZON@VIP.163.com  
Xiangning Cui  
cuixiangning@126.com

<sup>†</sup>These authors share first authorship

### Specialty section:

This article was submitted to  
Cardiovascular and Smooth Muscle  
Pharmacology,  
a section of the journal  
Frontiers in Pharmacology

Received: 27 March 2022

Accepted: 13 April 2022

Published: 02 June 2022

### Citation:

Lu Y, Xiang M, Xin L, Zhang Y, Wang Y,  
Shen Z, Li L and Cui X (2022)  
Qiliqiangxin Modulates the Gut  
Microbiota and NLRP3 Inflammasome  
to Protect Against Ventricular  
Remodeling in Heart Failure.  
Front. Pharmacol. 13:905424.  
doi: 10.3389/fphar.2022.905424

**Aims:** Pathological left ventricular (LV) remodeling induced by multiple causes often triggers fatal cardiac dysfunction, heart failure (HF), and even cardiac death. This study is aimed to investigate whether qiliqiangxin (QL) could improve LV remodeling and protect against HF via modulating gut microbiota and inhibiting nod-like receptor pyrin domain 3 (NLRP3) inflammasome activation.

**Methods:** Rats were respectively treated with QL (100 mg/kg/day) or valsartan (1.6 mg/kg/day) by oral gavage after transverse aortic constriction or sham surgery for 13 weeks. Cardiac functions and myocardial fibrosis were assessed. In addition, gut microbial composition was assessed by 16S rDNA sequencing. Furthermore, rats' hearts were harvested for histopathological and molecular analyses including immunohistochemistry, immunofluorescence, terminal-deoxynucleotidyl transferase-mediated 2'-deoxyuridine 5'-triphosphated nick end labeling, and Western blot.

**Key findings:** QL treatment preserved cardiac functions including LV ejection fractions and fractional shortening and markedly improved the LV remodeling. Moreover, HF was related to the gut microbial community reorganization like a reduction in *Lactobacillus*, while QL reversed it. Additionally, the protein expression levels like IL-1 $\beta$ , TNF- $\alpha$ , NF- $\kappa$ B, and NLRP3 were decreased in the QL treatment group compared to the model one.

**Conclusion:** QL ameliorates ventricular remodeling to some extent in rats with HF by modulating the gut microbiota and NLRP3 inflammasome, which indicates the potential therapeutic effects of QL on those who suffer from HF.

**Keywords:** gut microbiota, NLRP3 inflammasome, qiliqiangxin, heart failure, ventricular remodeling

## INTRODUCTION

As one of the most prevalent cardiac dysfunctions, heart failure (HF) is caused by multiple cardiac diseases like coronary heart disease, hypertension, arrhythmia, and viral myocarditis (Zhong et al., 2021), characterized by high morbidity and mortality (Ren et al., 2021; Sokolski et al., 2022). A significant pathological basis of HF is cardiac remodeling, which is thought to play a key part in the clinical outcomes of heart diseases (Liu et al., 2021) and occurs through various complex

mechanisms, leading to changes such as pathological cardiac hypertrophy, interstitial fibrosis, increased degradation of the myocardial extracellular matrix, impaired heart functions, and even HF (Hao et al., 2021; Ni et al., 2022; Ren et al., 2021). Cardiac remodeling in HF is typically characterized by myocardial hypertrophy (Zhong et al., 2021), which is initially an adaptive and compensatory response to maintain the ejection fraction under increased pressure load, while irreversible damage could be induced if pathological overload persists, along with inflammatory responses, vascular dysfunction, increased extracellular matrix deposition, myocardial fibrosis, and all pathologic changes resulting in cardiac dysfunction (Nemska et al., 2021; Tsuda, 2021; Zhong et al., 2021). Although several interventions are currently used in HF treatment, aiming to decrease cardiac afterload, there are no drugs available that target the initial inflammation and myocardial remodeling at the origin of hypertrophy (Nemska et al., 2021). It is, therefore, necessary to thoroughly elucidate the underlying pathogenesis of ventricular remodeling in HF and find new therapeutic targets.

A hypothesis, named “gut hypothesis of heart failure”, has attracted widespread attention recently, in which a decreased cardiac output and elevated systemic congestion were thought to cause intestinal mucosal ischemia and/or edema, increased bacterial translocation, augmented circulating endotoxins, and eventually underlying inflammatory response in HF patients (Tang et al., 2017). Gut microbiota can affect the host *via* various processes, including the interaction of their signaling molecules such as lipopolysaccharides (LPSs) and peptidoglycans with cells on the mucosal surface usually *via* pattern recognition receptors (PRRs) that can affect distal organs directly or indirectly and some other processes (Tang et al., 2017). PRRs are primarily composed of toll-like receptors (TLRs) and nod-like receptor (NLR) inflammasomes, among which nod-like receptor pyrin domain 3 (NLRP3) is the best characterized inflammasome (Herrmann et al., 2021). Accumulating evidence has demonstrated that NLRP3 plays a vital role in LV remodeling in HF. In the transverse aortic constriction (TAC) models, the NLRP3 inflammasome was demonstrated to form in cardiomyocytes where NLRP3 signaling promoted left ventricle maladaptive response to pressure overload (Suetomi et al., 2018) and cause LV dysfunction, hypertrophy, and fibrosis (Dang et al., 2020). The pharmacological inhibition of NLRP3 or NLRP3 knockout reduced myocardial inflammation, fibrosis, myocardial hypertrophy, and cardiac dysfunction (Gan et al., 2018; Willeford et al., 2018; Zhang et al., 2020). Mechanistically, the NLRP3 macromolecules accelerate caspase-1 activation as well as the secretion and accumulation of proinflammatory cytokines like IL-1 $\beta$  and IL-18 afterward (Mauro et al., 2019). Nevertheless, it is uncertain whether blocking NLRP3 can reverse the cardiac remodeling following HF (Zhang et al., 2020).

Qiliqiangxin (QL) is a well-known compound preparation of traditional Chinese medicine with extracts from 11 herbs including astragali radix, ginseng radix et rhizoma, aconiti lateralis radix preparata, salviae miltiorrhizae radix et rhizoma, descursainiae semen lepidii semen, alismatis rhizoma, cinnamomi ramulus, periplocae cortex, carthami flos, polygonati odorati rhizoma, and citri reticulatae pericarpium (Cheng et al., 2020; Fu et al., 2018). QL

has been approved by the National Medical Products Administration for the treatment of HF for more than a decade. In addition, a multicenter randomized double-blind study demonstrated the cardioprotective effect of QL in cardiac patients with HF (Li et al., 2013). Moreover, QL has been reported to ameliorate cardiac remodeling through increasing cardiac contractility and regulating inflammation in the treatment of chronic HF (Xiao et al., 2009). Finally, our previous study has reported that QL can attenuate cardiac remodeling *via* NF- $\kappa$ B signaling pathways in a rat model of myocardial infarction (Han et al., 2018). Most of these studies were focused on PPAR gamma, TGF- $\beta$ 1/Smads, or cardiac metabolism. Nevertheless, what remains unknown is whether QL prevents hearts from ventricular remodeling through regulating the intestinal function and the NLRP3 inflammasome. In the present study, therefore, we explored the role of QL in ventricular remodeling *via* comparison with valsartan using Sprague–Dawley (SD) rats with the model of TAC. We hypothesized QL’s pharmacological interventions in the microbial community structure and NLRP3-inflammatory corpuscle signaling, which thereby alleviated ventricular remodeling in HF.

## MATERIALS AND METHODS

### Model Induction of Heart Failure Through Pressure Overload

Male SD rats (220–250 g), purchased from Beijing Vital River Laboratory Animal Technology Co., Ltd. [Animal license number: SCXK (Beijing) 2017–0302], were fed adaptively for 3 days. A model of HF was established surgically through transverse aortic constriction (TAC) operation as has been described (Ruppert et al., 2020), which is one of the most widespread preclinical models of cardiac hypertrophy and HF induced by pressure overload (Boccella et al., 2021). Following anesthesia with sodium pentobarbital (40 mg/kg) and subsequently a left anterolateral thoracotomy, the aortic arch between the brachiocephalic trunk and the left common carotid artery was exposed and then constricted to the size of a 21-gauge needle. The rats in the sham-operation group underwent the same procedure but without aortic constriction. Following the modeling, the surviving rats with HF were randomly divided into three groups, which were the model group (Model,  $n = 5$ ), QL group (Model + QL,  $n = 7$ ), and valsartan group (Model + Valsartan,  $n = 6$ ). There are finally four groups including the sham group (Sham,  $n = 7$ ) with sham operation. The animals in the four groups were maintained under the same conditions for 13 weeks, which were kept in a relatively constant temperature room ( $24^{\circ}\text{C} \pm 1^{\circ}\text{C}$ ) with a natural day/night cycle light and given *ad libitum* access to standard chow and water. All the experimental procedures were approved by the Institutional Animal Care and Use Committee of Guang’anmen Hospital, China Academy of Chinese Medical Sciences, in accordance with the regulations on the management and use of experimental animals.

### Interventions

The QL capsule, which was obtained from Shijiazhuang Yiling Pharmaceutical Co., Ltd. (Shijiazhuang, Hebei, China), and

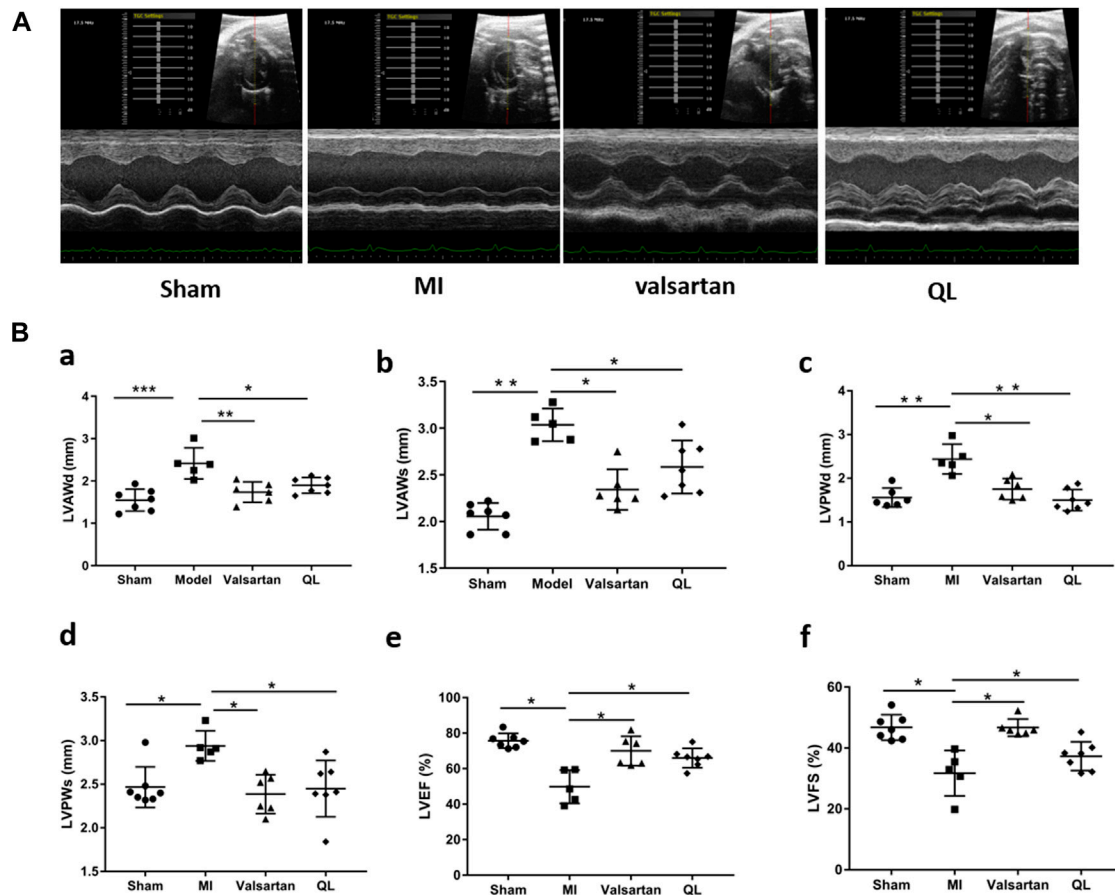


**FIGURE 1 |** QL protected cardiac functions in HF. **(A)** Representative echocardiograms of rats in four groups. **(B)** Comparison of echocardiography parameters in the four groups. LVAWd: LV end-diastolic anterior wall thicknesses, LVAWs: LV end-systolic anterior wall thicknesses, LVPWd: LV end-diastolic posterior wall thicknesses, LVPWs: LV end-systolic posterior wall thicknesses, LVEF: LV ejection fraction, and LVFS: LV fractional shortening. The data are the mean  $\pm$  standard deviation ( $\bar{x} \pm s$ ) ( $n = 5, 6$ , or  $7$  per group),  $^*p < 0.05$ ,  $^{**}p < 0.01$ , and  $^{***}p < 0.001$ .

valsartan, which was purchased from Beijing Novartis Pharmaceutical Co., Ltd. (Beijing, China) as the positive control, were dissolved separately in sterile water. The rats were respectively treated with QL and valsartan at doses of 100 mg/(kg. d) and 1.6 mg/(kg. d) by oral gavage once a day starting on day 1 following surgery for 13 weeks. The rats in the sham and model groups were given equal volumes of physiological saline solution.

## Echocardiography

Thirteen weeks after the interventions, noninvasive transthoracic echocardiography was performed on rats anesthetized with sodium pentobarbital (40 mg/kg) using an animal-specific Vevo 2100 high-resolution imaging system (Visual Sonics Inc., Toronto, Ontario, Canada). M-mode echocardiograms of the LV short axis were captured at the level of the papillary muscle for determining LV ejection fractions (LVEFs), LV fractional shortening (LVFS), LV end-diastolic anterior wall thickness (LVAWd), LV end-systolic anterior wall thickness (LVAWs), LV end-diastolic posterior wall thickness (LVPWd), and end-

systolic posterior wall thickness (LVPWs). These parameters were obtained and averaged from the three cardiac cycles.

## Histopathology, Immunohistochemistry, Immunofluorescence, and TUNEL

After euthanasia, the heart was immediately excised, irrigated clean with cold saline, and transversely dissected into two parts at the maximum transverse diameter. During our experiment, the heart tissues were fixed with 4% paraformaldehyde, embedded in paraffin, and sectioned into 4  $\mu$ m for hematoxylin and eosin (H&E), Masson, and Sirius Red staining. Image pro plus 6.0 was used to quantify the ratio of fibrosis area to the entire surface.

For assessing the expression of several important proteins through immunohistochemistry, the paraffin slices were put into an autoclave and boiled for 3 min to repair the antigen. After that, the slices were placed at 60°C for 2 h, deparaffinized, hydrated with xylene and ethanol followed by phosphate-buffered saline (PBS), and then incubated with primary antibodies overnight at



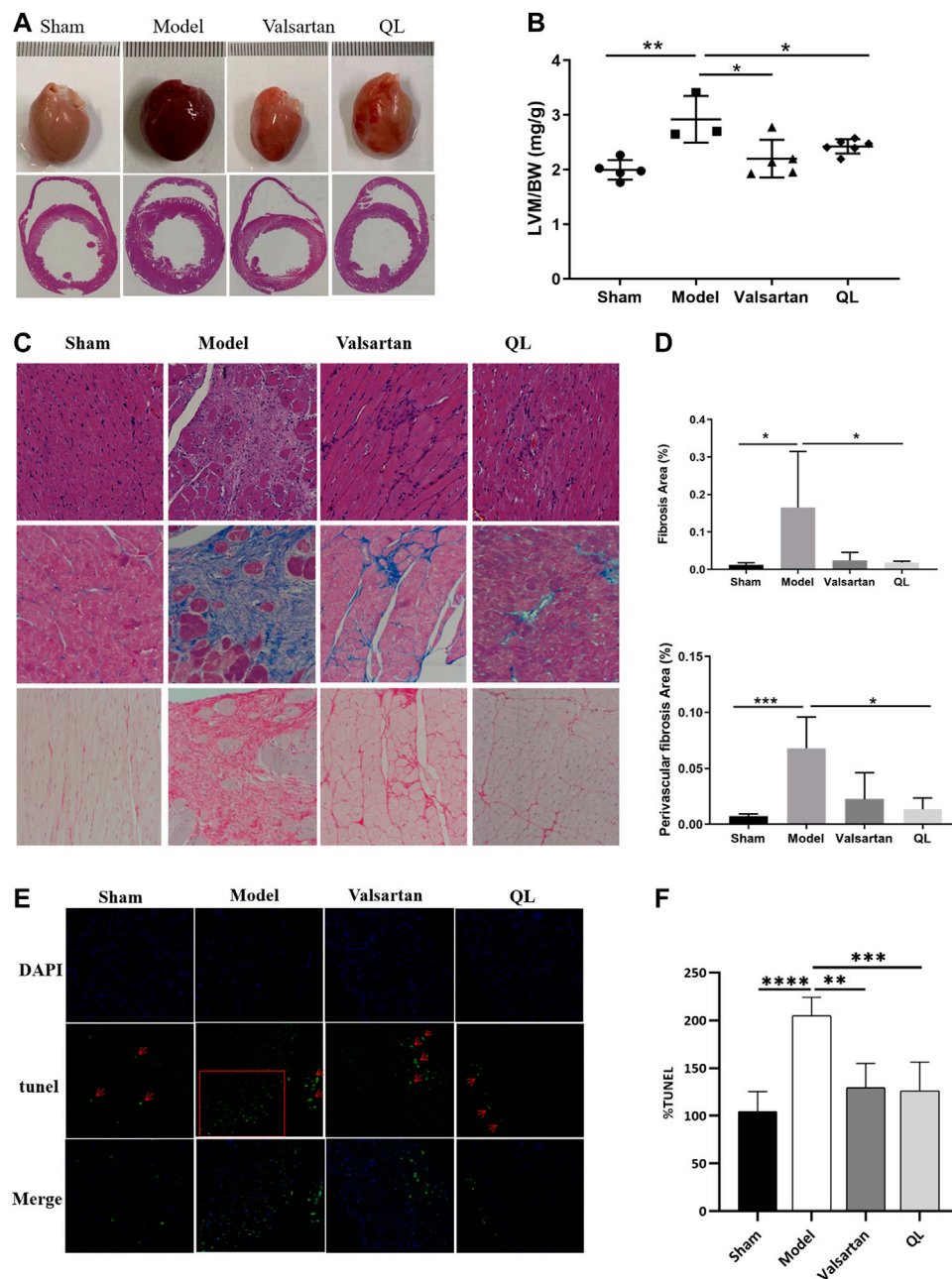


**FIGURE 2 |** QL reversed ventricular remodeling and alleviate cardiomyocyte apoptosis of rats with HF. **(A)** Appearance and transverse section of the heart. **(B)** Left ventricular mass to total body weight. **(C)** Histopathologic changes of the cardiac tissue with H&E staining and myocardial fibrosis observed with Masson staining and Sirius Red staining (Scale bar = 100  $\mu$ m). **(D)** Quantification of heart fibrosis area. **(E)** TUNEL staining for cell apoptosis rate. **(F)** Relative apoptosis rate of the myocardial cells. The data are the mean  $\pm$  standard deviation ( $\bar{x} \pm s$ ) ( $n = 3, 4, 5$ , or 6 per group) \* $p < 0.05$ , \*\* $p < 0.01$ , \*\*\* $p < 0.001$ , \*\*\*\* $p < 0.0001$ .

4°C: NLRP3 antibody (1:200, R30750, NSJBIO, United States), PYCARD antibody (ASC) (1:200, DF6304, Affinity Biosciences, CHN), cleaved-IL-1 $\beta$  (Asp116) antibody (1:250, AF4006, Affinity Biosciences, CHN), IL1 $\beta$  antibody (1:120, AF5103, Affinity Biosciences, CHN), and TNF- $\alpha$  antibody (1:250, ab66579, Abcam, United States). The slices were afterward incubated with horseradish peroxidase (HRP)-conjugated goat antirabbit immunoglobulin G (IgG) at 37°C for 30 min, followed by staining

with a diaminobenzidine (DAB) color kit (ZLI-9017, ZSGB-BIO, and CHN).

For the immunofluorescence staining, the paraffin-embedded colon sections (4  $\mu$ m) were deparaffinized for citrate-ethylenediaminetetraacetic acid (EDTA) antigen retrieval and incubated with occludin antibodies (1:200 dilution, ab216327, Abcam). Having been placed at 4°C overnight, the colon sections were then washed with PBS and added with a fluorescent

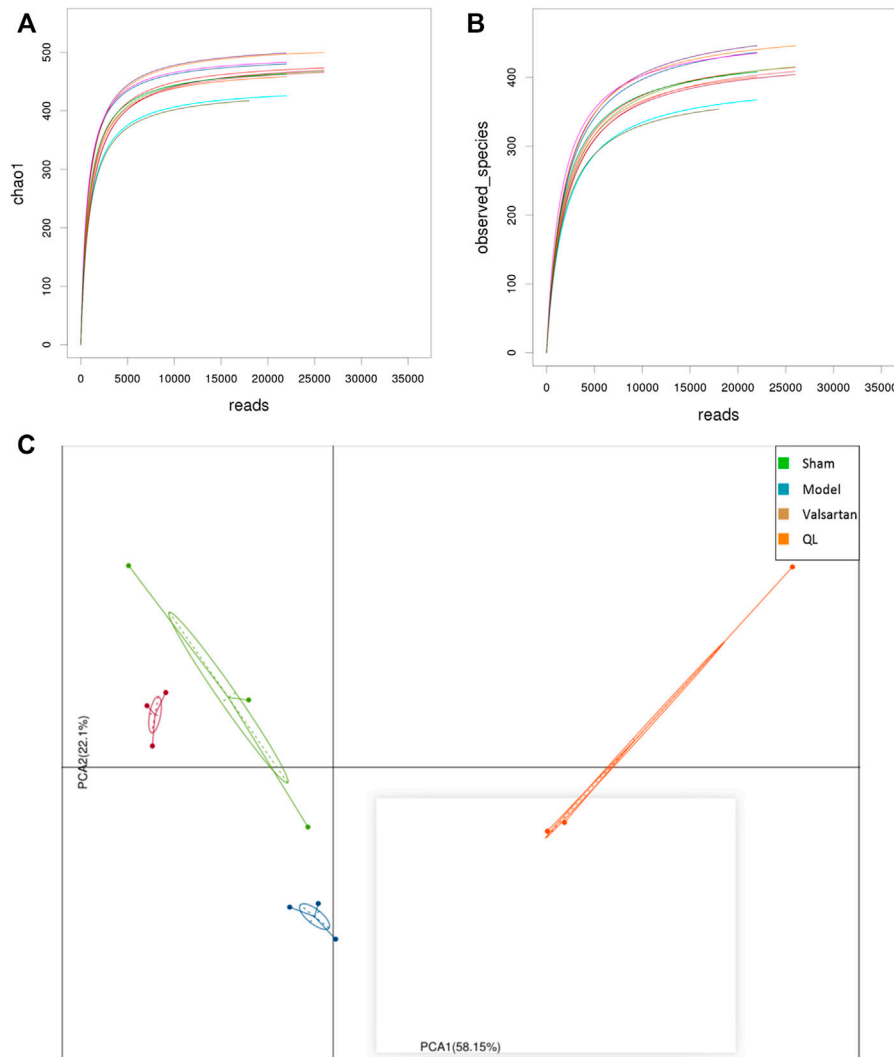


**FIGURE 3 |** QL regulates the composition of gut microbiota. **(A,B)** Dilution curves of species richness alpha diversity in samples. **(C,D)** PCA results of different microbiota, respectively, in all levels and the genus level. **(E,F)** Relative abundance of gut microbiota at the genus level. The data are the mean  $\pm$  standard deviation ( $\bar{x} \pm s$ ) ( $n = 3$  per group).

secondary antibody. The images were generated by using a confocal laser scanning microscope (Olympus, FV1000) and eventually analyzed by ImageJ.

Apoptosis of cardiomyocytes was finally analyzed through the terminal-deoxynucleotidyl transferase-mediated 2'-deoxyuridine 5'-triphosphated nick-end-labeling (TUNEL) method (Roche, 11684795910).

## Measurement of Gut Microbiota

Gut microbial composition was assessed through 16S rDNA gene sequencing. The rat feces from the cecum were collected using sterile cryotubes and then stored at  $-80^{\circ}\text{C}$  until processing, and the DNA sample was extracted using a Power Fecal DNA Isolation Kit (Qiagen-Mobio, German). The V3-V4 variable regions of the 16S rDNA were amplified by PCR; then, a library was constructed. The PCR products were sequenced

using an Illumina MiSeq Sequencer (SeqMatic, United States). The raw data were filtered to obtain clean reads, and paired-end reads with the overlap were merged into the tags that were clustered to operational taxonomic units (OTUs) constituting sequences with  $\geq 97\%$  similarity. The Ribosomal Database Project was used to make taxonomic annotation. The complexity of species diversity was analyzed through Chao1 richness, Simpson index, and Shannon index, and the relative abundance of each OTU in each sample was obtained according to the OTU abundance information.

## Western Blot

A total of 20  $\mu\text{g}$  of the cardiac protein extract was separated by 10% or 12% TGX stain-free™ fastcast™ acrylamide kit (1610183/1610185, Bio-Rad, United States) and then transferred to the trans-blot turbo mini 0.2  $\mu\text{m}$  PVDF transfer packs (1704156, Bio-

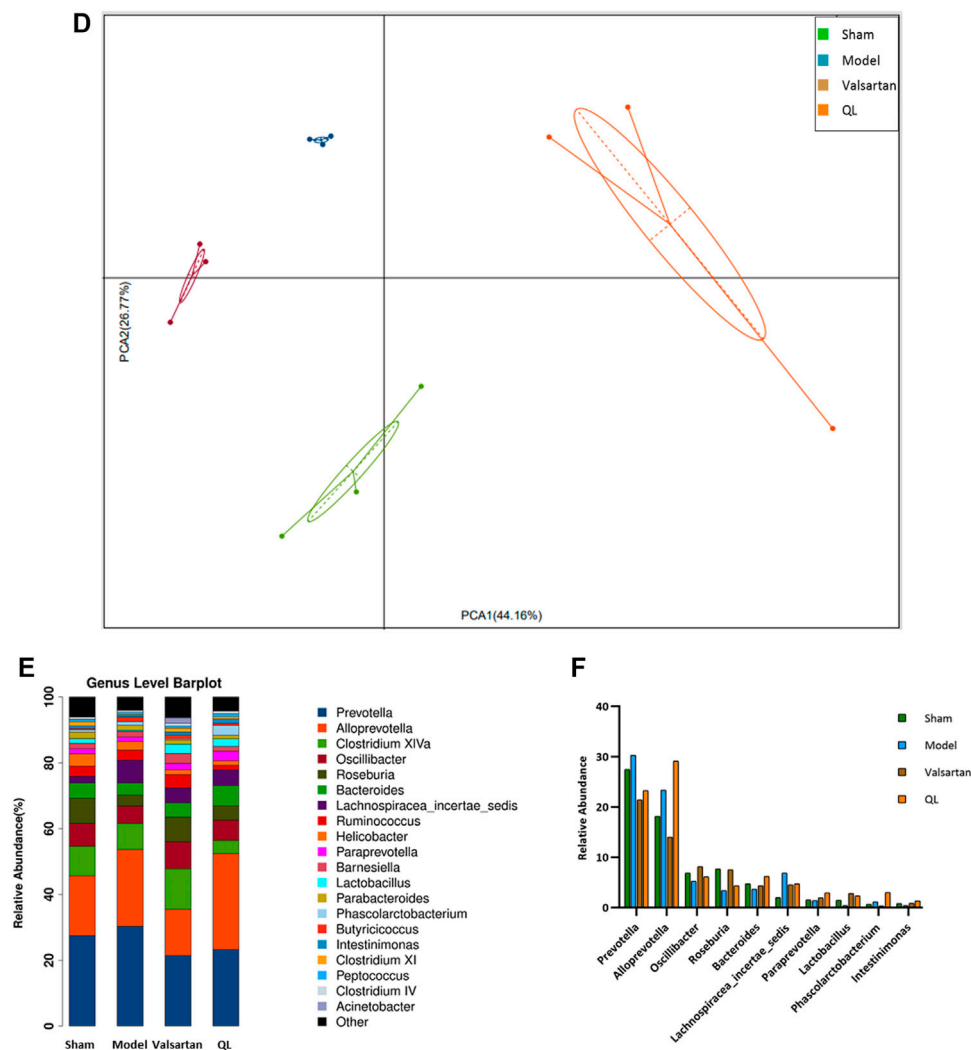


FIGURE 3 | (Continued).

Rad, United States). After blocking with 5% nonfat dry milk (9999S, Cell Signaling, United States) at room temperature for 2 h, we incubated the PVDF membrane with primary antibodies at 4°C overnight: anti-NF- $\kappa$ B p105/p50 antibody (1: 5000, ab32360, Abcam, United Kingdom), NLRP3 antibody/NALP3 (1:500, R30750, NSJBIO, United States), PYCARD antibody (ASC) (1:1000, DF6304, Affinity Biosciences, CHN), cleaved-IL-1 $\beta$  (Asp116) antibody (1:1000, AF4006, Affinity Biosciences, CHN), IL1 $\beta$  antibody (1:1000, AF5103, Affinity Biosciences, CHN), TNF- $\alpha$  antibody (1:1000, ab66579, Abcam, United States), and caspase-1 antibody (D-3) (1:500, sc-392736, Santa Cruz, United States). The PVDF membranes were afterward incubated with the HRP-conjugated goat antirabbit IgG (H&L) (1: 10000, bs-40295G-HRP, Bioss, CHN) or HRP-conjugated goat antimouse IgG (H&L) (1: 1000, A0216, Beyotime, CHN) at room temperature for 1 h. The PVDF membranes were eventually visualized using Gel Doc™ XR + System (Bio-Rad, United States) and Image Lab Software (Bio-

Rad, United States) with the ECL substrate (1705062, Bio-Rad, United States), followed by quantification using ImageJ (NIH, United States), and the results expressed as density values were normalized to GAPDH or tubulin.

### Enzyme-Linked Immunosorbent Assay

Concentrations of TNF- $\alpha$  and IL-1 $\beta$  in serum were determined, respectively, using a QuantiCyto® Rat TNF- $\alpha$  ELISA kit (ERC102a.48, NeoBioscience, CHN) and QuantiCyto® Rat IL-1 $\beta$  ELISA kit (ERC007.48, NeoBioscience, CHN). The standard substance at known concentrations and serum were pipetted into the wells of microplate strips, incubated for 90 min at 37°C, away from light. Next, the biotinylated antibodies were incubated for 60 min with TNF- $\alpha$  and the IL-1 $\beta$  antigen, respectively. Then, the bound enzyme and chromogenic substrate were added successively. Finally, The OD<sub>450</sub> values were detected, which corresponded to the TNF- $\alpha$  and IL-1 $\beta$  concentrations, and the ultimate data were expressed as pg/ml of protein.

## Statistical Analysis

GraphPad Prism software (version 8.0) was used for statistical analysis and drawing of the data, with assays independently repeated at least three times. The values for all the measurements were displayed as the mean  $\pm$  standard deviation ( $\bar{x} \pm s$ ). Comparisons between multiple groups were performed through repeated one-way analysis of variance (ANOVA), with  $p < 0.05$  considered statistically significant.

## RESULTS

### QL Improved Cardiac Functions in Heart Failure

We first used echocardiography to determine the phenotype establishment of TAC-induced HF and the effects of QL on the cardiac functions. Representative two-dimensional echocardiograms and comparison of various parameters in all groups are illustrated in **Figure 1**. Significant remodeling manifestations appeared in the model rats 13 weeks following TAC, evidenced by augmentation in LVAWd, LVAWs, LVPWd, and LVPWs (**Figure 1B(a–d)**). In addition, the cardiac function of the model group was worse than that of the sham group with the reduction in LVEF and LVFS (**Figure 1B(e,f)**). However, all these parameters were improved by the application of QL versus model group, and no significant difference could be detected between the sham group and QL group.

### QL Reversed LV Remodeling and Cardiomyocytes Apoptosis in Heart Failure

The results observed through transverse section area of hearts and further quantified by the left ventricular mass to total body weight (LVM/BW) showed slight cardiac hypertrophy in the HF rats and improved conditions by both QL and valsartan (**Figure 2A,B**). Through the histological analysis and quantification of heart fibrosis area in each group, the irregularly arranged cardiac myocytes, inflammatory infiltration, fibroblast proliferation, fibrous scar formation, and enlarged fibrosis area were observed in the heart of the model rats with HF. The histopathological changes above mentioned were ameliorated by QL and valsartan to varying degrees maintaining the integrity of myocardial cells, and QL appears to display a more significant improvement compared with valsartan (**Figure 2C,D**). Moreover, as shown in **Figure 2E,F** for TUNEL staining of the cardiac tissue, the rate of cardiomyocyte apoptosis in the model group increased, while it decreased in both the QL group and valsartan group, especially after QL treatment.

### QL Alters the Composition of Gut Microbiota

When analyzing gut microbiota composition, the operational taxonomic units (OTUs) were obtained by clustering with 97% similarity, and each OTU was considered as a species. As shown in **Figure 3A,B**, the alpha diversity reflects the species diversity

within a single sample, including the observed species index and Chao 1 index, in which each curve represents a sample. The curves of each sample tended to be plateaued as the sequencing depth increased, meaning that the amount of sequencing data is reasonable and the entire microbial community was captured. The principal component analysis (PCA) results of different species in either all the levels or the genus level implied that the flora composition of the four groups can be well distinguished and the differences between each group were well identified (**Figure 3C, D**). Based on the species annotation results, the top 20 microbiota in abundance at the genus level were selected for each group to generate a column accumulation diagram of relative abundance (**Figure 3E**). Focused on different expressions among the four groups, our results show differences in the abundance of some microbiota in the HF rats with an increase in *Prevotella*, *Alloprevotella*, and *Lachnospiraceae\_incertae\_sedis*, but these three genera were reduced after valsartan intervention and *Prevotella* and *Lachnospiraceae\_incertae\_sedis* in the QL group express lower as well. Some other microbiota in the model group, nevertheless, demonstrated decreased expression including *Oscillibacter*, *Roseburia*, *Bacteroides*, and *Lactobacillus*, and those of the valsartan group and QL group were conversely increased to some extent. In addition, through QL intervention, *Paraprevotella*, *Phascolarctobacterium*, and *Intestinimonas* increased significantly compared with the other three groups. The relative abundances of significantly different microbiota at the genus level are exhibited in **Figure 3F**.

### QL Improves the Gut Barrier

In order to confirm the protection of QL on the gut barrier, we evaluated the intestinal injury in the colon of rats in four groups. As shown in **Figure 4A**, the HF animals were observed with the edematous, severed, or denuded intestinal villi, along with the significantly increased gap between the epithelial cells, which were, however, ameliorated after receiving QL and valsartan treatment. Furthermore, the intestinal epithelial tight junction protein occludin was used as an indicator to evaluate the function of the intestinal barrier, whose expression was disrupted following HF but restored by QL and valsartan nearly to the normal levels (**Figure 4B,C**).

### QL Inhibits the Expression of NF- $\kappa$ B-Related Signaling Molecules

Subsequently, the levels of IL-1 $\beta$ , NF- $\kappa$ B, and TNF- $\alpha$  in the heart tissue were respectively detected by Western blot and immunohistochemical analysis to determine how disrupted gut microbiota and the damaged gut barrier affect the heart. The results showed that the expressions of IL-1 $\beta$ , NF- $\kappa$ B, and TNF- $\alpha$  were increased in the cardiac tissue of modeling rats relative to those of the sham one but decreased following QL and valsartan treatment (**Figure 5A,B**). Consistent with these results, the serum levels of proinflammatory cytokines IL-1 $\beta$  and TNF- $\alpha$  were rapidly and persistently enhanced after TAC surgery but decreased after the interventions of QL and valsartan (**Supplementary Figure S1A–B**).



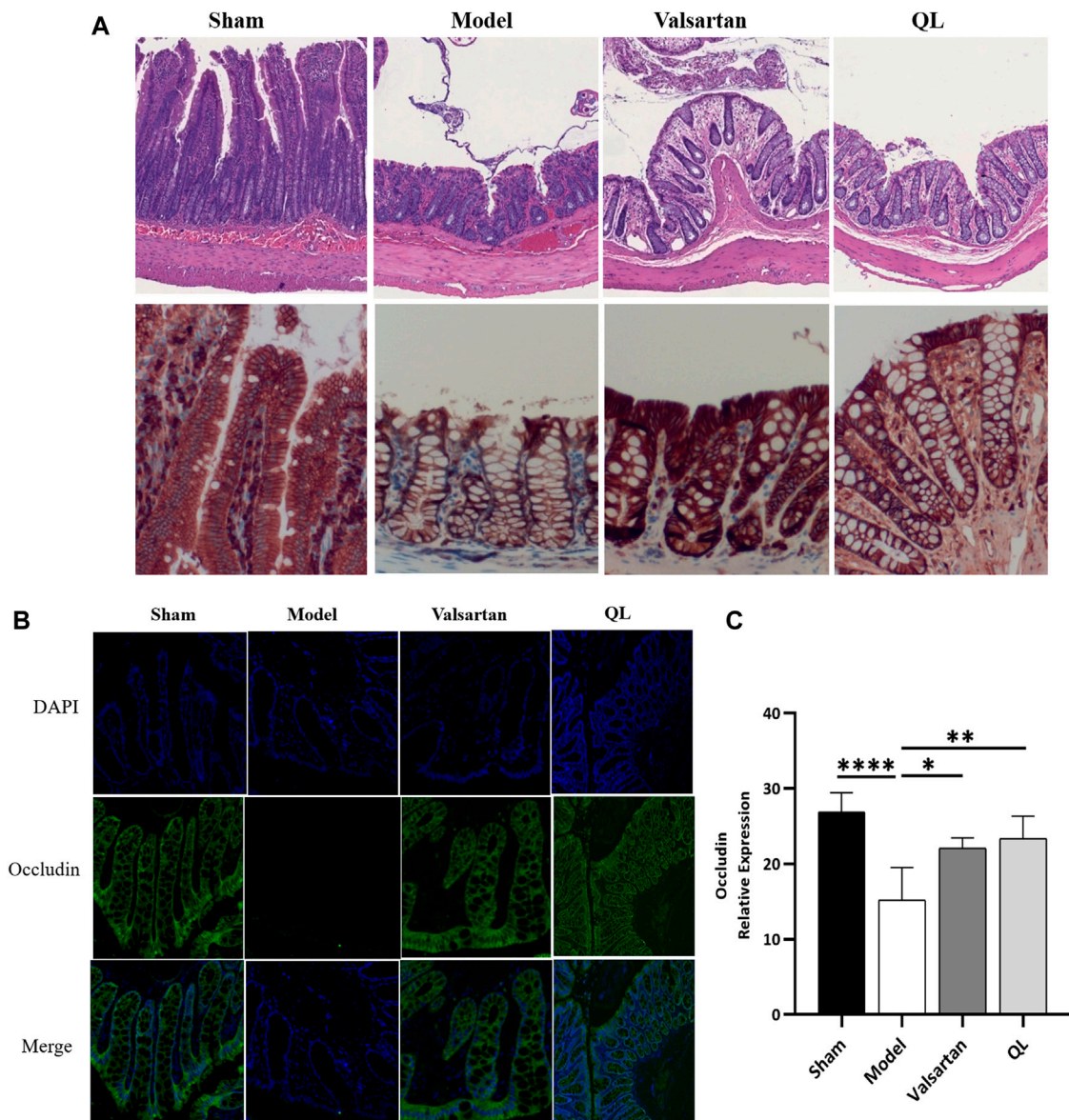


**FIGURE 4 |** QL ameliorates the pathological damage of the intestinal barrier in HF. **(A)** Pathological changes of the colonic mucosa under a light microscope with H&E staining (scale bar = 300  $\mu$ m). **(B,C)** Expression of occludin detected with immunofluorescence staining. The data are the mean  $\pm$  standard deviation ( $\bar{x} \pm s$ ) (n = 5 or 6 per group); \* $p$  < 0.05, \*\* $p$  < 0.01, and \*\*\*\* $p$  < 0.0001.

## QL Inhibited Inflammasomes in Heart Failure

To further verify the pathologic changes shown through inflammasomes, the relative tissue protein expression levels of NLRP3 and its associated proteins in the cardiac tissue were detected through Western blot and immunohistochemistry. The results revealed significantly higher NLRP3 generation in the model group compared with the healthy control group, while treatment of valsartan and QL blocked these effects. Moreover, the protein expressions of ASC, caspase-1, and cleaved-IL-1 $\beta$  were upregulated in the model group but downregulated *via*

valsartan and QL intervention, especially the latter one. These results inspired us to conclude that NLRP3 and its associated signaling pathways might be the targets of QL in the pathological process of ventricular remodeling.

## DISCUSSION

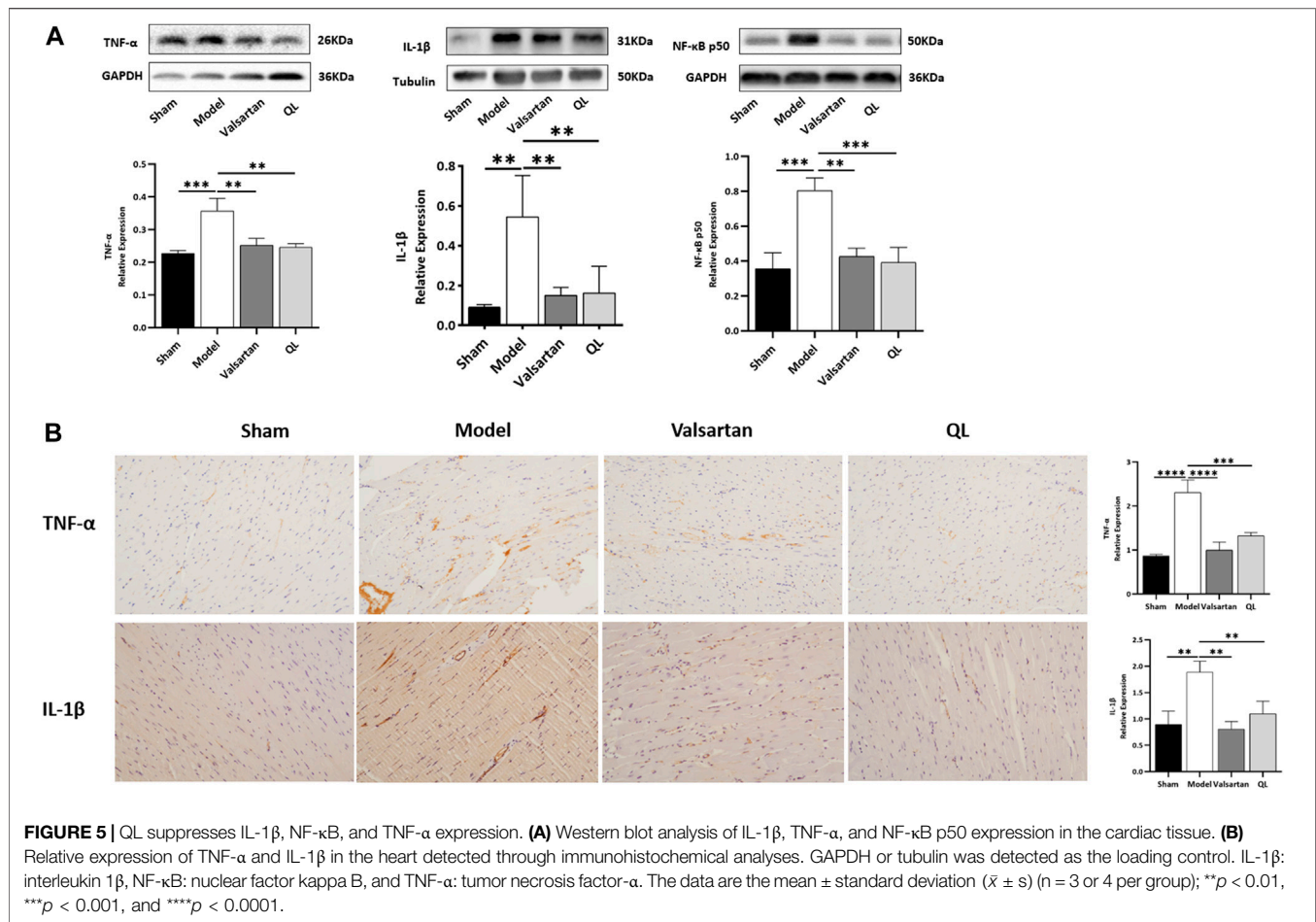
As previously mentioned, cardiac remodeling, caused or exacerbated by varying pathological changes, will eventually result in serious consequences, for which there are no effective

drugs (Hao et al., 2021; Ni et al., 2022; Ren et al., 2021). New therapeutic strategies are needed to be introduced clinically for protecting against pressure overload-induced cardiac injury (Li X. et al., 2021) or targeting adverse post-MI left ventricle remodeling (Germano et al., 2020). Researchers highlight the potential of intestinal microbiota and NLRP3 inflammasomes to impact ventricular remodeling, which hold promise as effective targets for improving cardiac functions in HF (Boccella et al., 2021; Zhao et al., 2021). The beneficial effects of QL on cardiac hypertrophy, ventricular remodeling, and HF through multiple pathways have been widely reported (Gao et al., 2018; Lu et al., 2020; Wang et al., 2017). Valsartan, an angiotensin II (ANG II) receptor blocker, exerts positive effects in improving chronic inflammation, promoting scar repair, maintaining cardiomyocyte integrity, alleviating ventricular remodeling, and thus preserving cardiac functions (Shi et al., 2020). Further studies indicated that valsartan administration could affect the intestinal microbiota composition and SCFA generation and blunted the LPS-induced elevations of inflammatory cytokines (Iwashita et al., 2013; Qi et al., 2021). In the present study, therefore, with valsartan as the control intervention, we verified the effects of QL on ventricular remodeling of rats with HF. We found the protective effects of QL on the LV remodeling with the regulation of gut microbiota. Furthermore, we revealed that QL intervention could block the inflammasome formation and inflammatory cytokine release in the cardiomyocytes, which were consistent with those from the previous studies (Zhang et al., 2019; Zou et al., 2012).

Ventricular remodeling involves the alteration of the ventricular structure, with the geometry changes including conversation in wall thickness and cavity diameter, along with a progression from elliptical to spherical configuration (Tomoia et al., 2019). In addition, it might result in the deterioration of cardiac functions like the declined systolic function (Zhang XX. et al., 2021). The reduced parameters like LVAWd, LVAWs, LVPWd, and LVPWs, along with the slightly improved LVEF and LVFS, showed that pressure overload-induced deterioration of the cardiac structure and functions was partially reversed by QL, suggesting the salutary role of QL against remodeling in HF. Mechanistically, it was thought that ventricular remodeling is primarily attributed to cardiomyocyte reduction and poor development of surviving cardiomyocytes and the extracellular matrix (Zhang XX. et al., 2021). When chronic LV pressure overloads, the cardiomyocytes become hypertrophied and alter their cellular properties, whereas cardiac fibroblasts convert into an activated state, proliferate, and/or increase extracellular matrix deposition (Li X. et al., 2021). These pathological changes ultimately lead to the HF development and poor prognosis (Li X. et al., 2021). The results of histological analysis and fibrosis area quantification additionally revealed the ameliorated histopathological changes by QL to a certain extent.

A growing body of evidence derived from the epidemiological and animal model studies uncovers that altered gut microbiota and gut functions are closely related to the development of

adverse cardiac remodeling and HF (Boccella et al., 2021; Carrillo-Salinas et al., 2020). In chronic heart failure patients, the wall thickness and permeability of the intestine increase, the bacterial populations adhering to the intestinal mucosa release, and bacteria or their toxins transfer from the intestine to the blood directly, which associate with systemic inflammation (Wang et al., 2021). Another research, as previously described, demonstrated that decreased cardiac output and elevated systemic congestion may cause intestinal mucosal ischemia and/or edema, increased bacterial translocation, increased circulating endotoxins, and eventually underlying inflammatory response in the HF patients (Tang et al., 2017). In the model of TAC, it was proposed that gut hypoperfusion induced by TAC may lead to intestinal microbiome dysregulation and increased gut permeability, which in turn affect systemic inflammation and contribute to cardiac dysfunction (Boccella et al., 2021). Persistent inflammation of the heart is considered as a sign of hypertrophy of myocardial hypertrophy (Zhong et al., 2021). Consequently, new challenge lying ahead is that specific microbiota, metabolites, or other microbiota-targeted/driven interventions need to be further explored in the human clinical intervention studies. The results shown in **Figure 3C,D** with the differences in the species composition and abundance in the four groups indicate that QL and valsartan may regulate the intestinal components. From the column accumulation diagram of relative abundance (**Figure 3E,F**), our results show underexpression of *Prevotella* and *Lachnospiraceae\_incertae\_sedis* in the QL group compared with the model group, while some other microbiota including *Oscillibacter*, *Roseburia*, *Bacteroides*, *Lactobacillus*, *Paraprevotella*, *Phascolarctobacterium*, and *Intestinimonas* were upregulated *via* QL intervention. The relative abundance changes of *Prevotella* were reported to injure the colonic epithelia, resulting in inflammation and thus inflammatory cytokine generation like IL-6, TNF- $\alpha$ , and IL-8 (Xia et al., 2021). It is also related to TMAO production (Sardu et al., 2021). *Oscillibacter* (Chen et al., 2020; Dessì et al., 2021), *Roseburia* (Cornuault et al., 2020), *Bacteroides* (Yuan et al., 2021), *Paraprevotella* (Fei et al., 2019; Zhang X. et al., 2021), *Phascolarctobacterium* (Pan et al., 2021), and *Intestinimonas* (Afouda et al., 2019; Luo et al., 2021) exert promoting effects in the SCFA generation or associate positively with its content. *Oscillibacter*, furthermore, exhibited the potential of anti-inflammation and an intestinal defense barrier (Chen et al., 2021). A study in mice revealed the alleviating effect of *Bacteroides* on the LPS-induced inflammation like restoration of LPS-induced TNF- $\alpha$  and IL-10 generation, then reducing the intestinal microbiota disorders, and maintaining the intestinal epithelium integrity and plasma LPS concentration (Tan et al., 2019). *Lactobacillus*, a well-known probiotic, is essential in maintaining intestinal barrier functions and integrity (Li L. et al., 2021), protecting hearts after MI (Li et al., 2021b; Tang et al., 2019), reducing cardiac hypertrophy and HF following MI, and improving LVEF and LVFS (Li L. et al., 2021). Additionally, we have shown the impaired gut barrier in the model group, including the damaged intestinal mucosa and a lower expression of tight junction protein occludin, while it is improved with

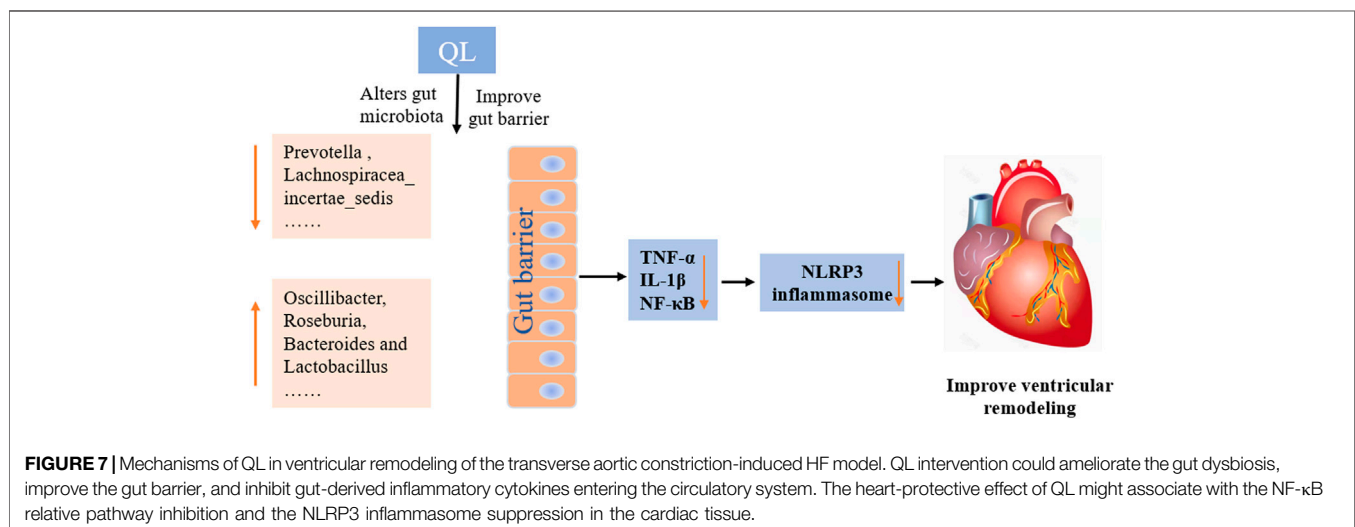
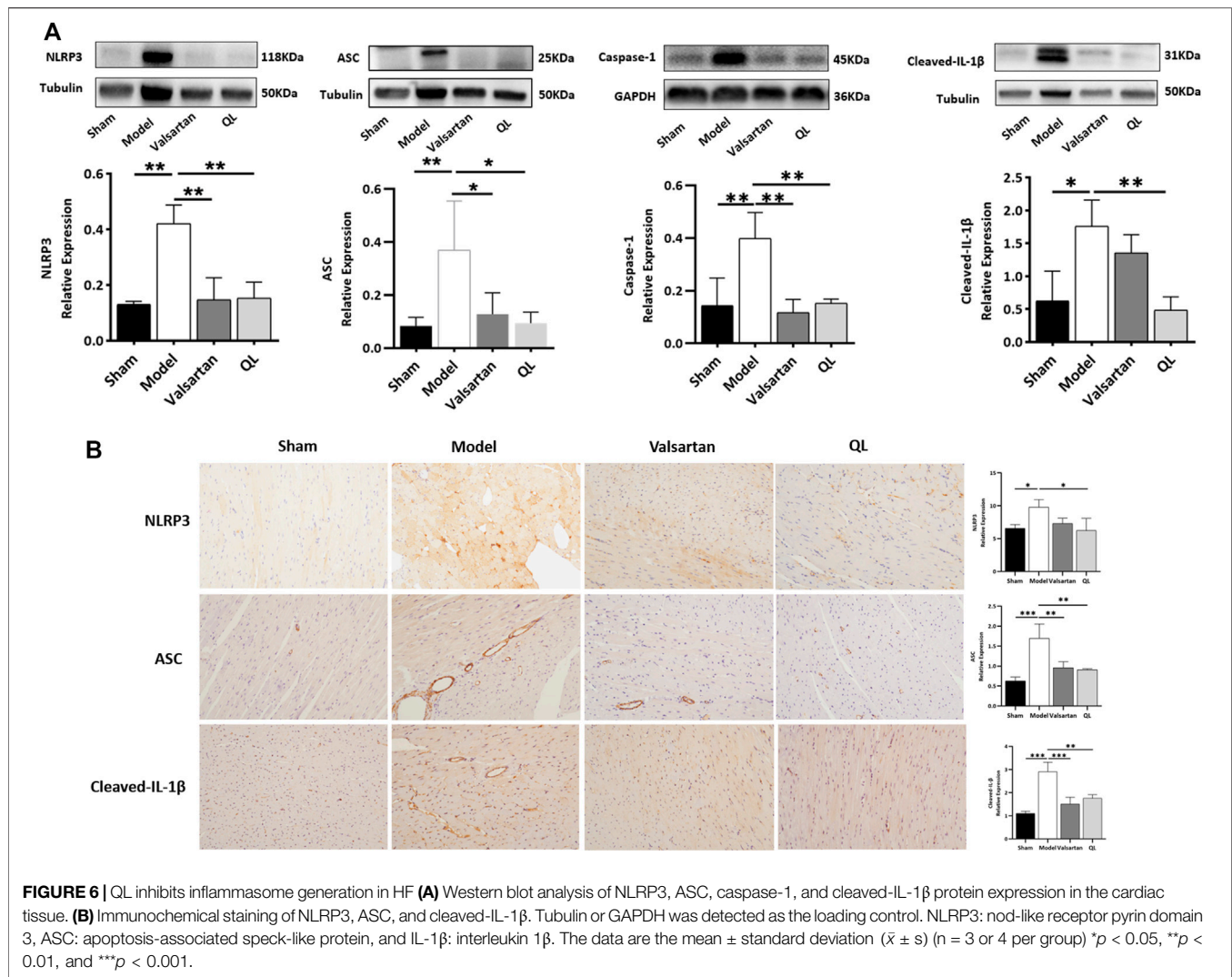


varying degrees after treatment (Figure 4). Taken together, our findings suggest that QL has partly protective effects on the gut dysbiosis and gut barrier functions, thus protecting the heart from ventricular remodeling and HF.

Recently, a lot of literature studies have implied that an imbalanced composition and function of the gut microbiome, known as dysbiosis, increases the risk of incident adverse cardiovascular events, including HF (Go et al., 2013). The current “gut hypothesis of heart failure” first proposed by Tang et al. implies that a decreased cardiac output and adaptive redistribution of systemic circulation lead to the intestinal hypoperfusion, intestinal villi ischemia, bowel wall oedema, and impaired barrier functions (Tang et al., 2019). This disruption in the intestinal barrier function in turn leads to the increase of gut permeability and circulating endotoxins (LPS), augment inflammatory-related responses, and escalated HF (Pasini et al., 2016; Sandek et al., 2014). Gut-derived LPS could trigger inflammatory responses *via* TLRs, which mediates the activation of NF- $\kappa$ B (Chen et al., 2016). NF- $\kappa$ B, a master regulator of the inflammatory gene expression, is activated in various heart diseases like congestive HF and myocardial hypertrophy (Lorenzo et al., 2011). Growing reports showed that the NF- $\kappa$ B pathway plays a critical role in regulating the

NLRP3 inflammasome (Afonina et al., 2017; Barroso et al., 2016; Lorenzo et al., 2011). A research revealed that alarmins released on necrotic cell death after AMI, such as TNF and IL-1 $\beta$ , can also act as beginning proinflammatory paracrine responses (Cohen et al., 2015; Dinarello et al., 2013; Franchi et al., 2009), which additionally activate NF- $\kappa$ B and ultimately lead to the transcriptional upregulation of the NLRP3 inflammasome. The NLRP3 inflammasome can in turn lead to cardiac fibrosis and hypertrophy *via* generating inflammatory cytokines such as IL-1 $\beta$ , IL-18, TNF- $\alpha$ , and TGF- $\beta$  (Yamaguchi et al., 2022). The inflammasome is involved in cardiac fibrosis development in HF, which can be activated under stress and formed with NLRP3 and procaspase-1 by the adaptor protein ASC. It was reported that the NLRP3 inflammasome exerts inflammatory effects through regulating proinflammatory cytokine release, including IL-1 $\beta$  and IL-18, which aggravate the cardiomyocyte dysfunction and cause ventricular remodeling and HF (Dang et al., 2020). The NLRP3 inflammasome, according to another report, could be upregulated and activated in the cardiac hypertrophy models, which aggravates cardiac fibrosis through activating the TGF- $\beta$ /Smad pathway and promotes cardiac hypertrophy through activating the MAPK pathway (Pan et al., 2019). Altogether, the activation of signaling pathways related to NF- $\kappa$ B and NLRP3







is undoubtedly a key process involved in cardiac remodeling. QL has been shown to inhibit the NF- $\kappa$ B signaling pathway activation in the previous studies (Han et al., 2018), which is consistent with our findings (Figure 5). Furthermore, as shown in Figure 6, we first demonstrated that QL treatment in HF could inhibit the expression of NLRP3, ASC, caspase-1, and cleaved IL-1 $\beta$ , which are NLRP3 inflammasome key proteins (Zhang et al., 2022).

## CONCLUSION

In conclusion, our current findings indicate that QL treatment is capable of ameliorating ventricular remodeling by inhibiting myocardial fibrosis and apoptosis and improves cardiac functions in the rat models with TAC. This study extends the understanding of the protective effect of QL, indicating that it alters the composition of gut microbiota and intestinal barrier functions and exerts potent anti-inflammatory effects by inhibiting the NLRP3 inflammasome activation (Figure 7). QL might, therefore, be a promising drug for ventricular remodeling and even HF.

## DATA AVAILABILITY STATEMENT

The datasets presented in this study can be found in online repositories. The names of the repository/repositories and accession number(s) can be found below: <https://www.ebi.ac.uk/metabolights/>, MTBLS4675.

## REFERENCES

- Afonina, I. S., Zhong, Z., Karin, M., and Beyaert, R. (2017). Limiting Inflammation-The Negative Regulation of NF- $\kappa$ B and the NLRP3 Inflammasome. *Nat. Immunol.* 18, 861–869. doi:10.1038/ni.3772
- Afouda, P., Durand, G. A., Lagier, J. C., Labas, N., Cadoret, F., Armstrong, N., et al. (2019). Noncontiguous Finished Genome Sequence and Description of *Intestinimonas Massiliensis* Sp. Nov Strain GD2T, the Second *Intestinimonas* Species Cultured from the Human Gut. *Microbiologyopen* 8, e00621. doi:10.1002/mbo3.621
- Barroso, A., Gualdrón-López, M., Esper, L., Brant, F., Araújo, R. R., Carneiro, M. B., et al. (2016). The Aryl Hydrocarbon Receptor Modulates Production of Cytokines and Reactive Oxygen Species and Development of Myocarditis during Trypanosoma Cruzi Infection. *Infect. Immun.* 84, 3071–3082. doi:10.1128/iai.00575-16
- Boccella, N., Paolillo, R., Coretti, L., D'Apice, S., Lama, A., Giugliano, G., et al. (2021). Transverse Aortic Constriction Induces Gut Barrier Alterations, Microbiota Remodeling and Systemic Inflammation. *Sci. Rep.* 11, 7404. doi:10.1038/s41598-021-86651-y
- Carrillo-Salinas, F. J., Anastasiou, M., Ngwenyama, N., Kaur, K., Tai, A., Smolgovsky, S. A., et al. (2020). Gut Dysbiosis Induced by Cardiac Pressure Overload Enhances Adverse Cardiac Remodeling in a T Cell-dependent Manner. *Gut Microbes* 12, 1–20. doi:10.1080/19490976.2020.1823801
- Chen H. H., Zhang, F., Zhang, J., Zhang, X., Guo, Y., and Yao, Q. (2020). A Holistic View of Berberine Inhibiting Intestinal Carcinogenesis in Conventional Mice Based on Microbiome-Metabolomics Analysis. *Front. Immunol.* 11, 588079. doi:10.3389/fimmu.2020.588079
- Chen, Y., Peng, L., Shi, S., Guo, G., and Wen, H. (2021). Boeravinone B Alleviates Gut Dysbiosis during Myocardial Infarction-induced Cardiotoxicity in Rats. *J. Cel Mol Med* 25, 6403–6416. doi:10.1111/jcmm.16620

## ETHICS STATEMENT

The animal study was reviewed and approved by Institutional Animal Care and Use Committee of Guang'anmen Hospital, China Academy of Chinese Medical Sciences.

## AUTHOR CONTRIBUTIONS

YL and MX contributed equally to this work. XC and LL had great contribution in the second-time revision, polishing the manuscript, and helping in revising figures. Other authors help to collect data and search the literature.

## FUNDING

This work was supported by grants from the National Natural Science Foundation of China (81973842). The publication fees is funded by Guang'anmen Hospital, China Academy of Chinese Medical Sciences.

## SUPPLEMENTARY MATERIAL

The Supplementary Material for this article can be found online at: <https://www.frontiersin.org/articles/10.3389/fphar.2022.905424/full#supplementary-material>

- Chen, Z., Zhu, S., and Xu, G. (2016). Targeting Gut Microbiota: a Potential Promising Therapy for Diabetic Kidney Disease. *Am. J. Transl. Res.* 8, 4009–4016.
- Cheng, W., Wang, L., Yang, T., Wu, A., Wang, B., Li, T., et al. (2020). Qiliqiangxin Capsules Optimize Cardiac Metabolism Flexibility in Rats with Heart Failure after Myocardial Infarction. *Front. Physiol.* 11, 805. doi:10.3389/fphys.2020.00805
- Cohen, I., Idan, C., Rider, P., Peleg, R., Vornov, E., Elena, V., et al. (2015). IL-1 $\alpha$  Is a DNA Damage Sensor Linking Genotoxic Stress Signaling to Sterile Inflammation and Innate Immunity. *Sci. Rep.* 5, 14756. doi:10.1038/srep14756
- Cornuault, J. K., Moncaut, E., Loux, V., Mathieu, A., Sokol, H., Petit, M. A., et al. (2020). The Enemy from within: a Prophage of *Roseburia Intestinalis* Systematically Turns Lytic in the Mouse Gut, Driving Bacterial Adaptation by CRISPR Spacer Acquisition. *Isme j* 14, 771–787. doi:10.1038/s41396-019-0566-x
- Dang, S., Zhang, Z. Y., Li, K. L., Zheng, J., Qian, L. L., Liu, X. Y., et al. (2020). Blockade of  $\beta$ -adrenergic Signaling Suppresses Inflammasome and Alleviates Cardiac Fibrosis. *Ann. Transl. Med.* 8, 127. doi:10.21037/atm.2020.02.31
- Dessi, P., Sánchez, C., Mills, S., Cocco, F. G., Isipato, M., Ijaz, U. Z., et al. (2021). Carboxylic Acids Production and Electrosynthetic Microbial Community Evolution under Different CO<sub>2</sub> Feeding Regimens. *Bioelectrochemistry* 137, 107686. doi:10.1016/j.bioelechem.2020.107686
- Dinarello, C. A., and van der Meer, J. W. (2013). Treating Inflammation by Blocking Interleukin-1 in Humans. *Semin. Immunol.* 25, 469–484. doi:10.1016/j.smim.2013.10.008
- Fei, Y., Wang, Y., Pang, Y., Wang, W., Zhu, D., Xie, M., et al. (2019). Xylooligosaccharide Modulates Gut Microbiota and Alleviates Colonic Inflammation Caused by High Fat Diet Induced Obesity. *Front. Physiol.* 10, 1601. doi:10.3389/fphys.2019.01601
- Franchi, L., Eigenbrod, T., and Núñez, G. (2009). Cutting Edge: TNF-Alpha Mediates Sensitization to ATP and Silica via the NLRP3 Inflammasome in

- the Absence of Microbial Stimulation. *J. Immunol.* 183, 792–796. doi:10.4049/jimmunol.0900173
- Fu, J., Chang, L., Harms, A. C., Jia, Z., Wang, H., Wei, C., et al. (2018). A Metabolomics Study of Qiliqiangxin in a Rat Model of Heart Failure: a Reverse Pharmacology Approach. *Sci. Rep.* 8, 3688. doi:10.1038/s41598-018-22074-6
- Gan, W., Ren, J., Li, T., Lv, S., Li, C., Liu, Z., et al. (2018). The SGK1 Inhibitor EMD638683, Prevents Angiotensin II-Induced Cardiac Inflammation and Fibrosis by Blocking NLRP3 Inflammasome Activation. *Biochim. Biophys. Acta (Bba) - Mol. Basis Dis.* 1864 (1), 1–10. doi:10.1016/j.bbdis.2017.10.001
- Gao, R. R., Wu, X. D., Jiang, H. M., Zhu, Y. J., Zhou, Y. L., Zhang, H. F., et al. (2018). Traditional Chinese Medicine Qiliqiangxin Attenuates Phenylephrine-Induced Cardiac Hypertrophy via Upregulating PPAR $\gamma$  and PGC-1 $\alpha$ . *Ann. Transl. Med.* 6, 153. doi:10.21037/atm.2018.04.14
- Germano, J. F., Huang, C., Sin, J., Song, Y., Tucker, K. C., Taylor, D. J. R., et al. (2020). Intermittent Use of a Short-Course Glucagon-like Peptide-1 Receptor Agonist Therapy Limits Adverse Cardiac Remodeling via Parkin-dependent Mitochondrial Turnover. *Sci. Rep.* 10, 8284. doi:10.1038/s41598-020-64924-2
- Go, A. S., Mozaffarian, D., Roger, V. L., Benjamin, E. J., Berry, J. D., Borden, W. B., et al. (2013). Executive Summary: Heart Disease and Stroke Statistics--2013 Update: a Report from the American Heart Association. *Circulation* 127, 143–152. doi:10.1161/CIR.0b013e31828124ad10.1161/CIR.0b013e318282ab8f
- Han, A., Lu, Y., Zheng, Q., Zhang, J., Zhao, Y., Zhao, M., et al. (2018). Qiliqiangxin Attenuates Cardiac Remodeling via Inhibition of TGF- $\beta$ 1/Smad3 and NF-Kb Signaling Pathways in a Rat Model of Myocardial Infarction. *Cell Physiol Biochem* 45, 1797–1806. doi:10.1159/000487871
- Hao, S., Sui, X., Wang, J., Zhang, J., Pei, Y., Guo, L., et al. (2021). Secretory Products from Epicardial Adipose Tissue Induce Adverse Myocardial Remodeling after Myocardial Infarction by Promoting Reactive Oxygen Species Accumulation. *Cell Death Dis* 12, 848. doi:10.1038/s41419-021-04111-x
- Herrmann, J., Xia, M., Gummi, M. R., Greco, A., Schacke, A., van der Giet, M., et al. (2021). Stressor-Induced "Inflammaging" of Vascular Smooth Muscle Cells via Nlrp3-Mediated Pro-inflammatory Auto-Loop. *Front. Cardiovasc. Med.* 8, 752305. doi:10.3389/fcvm.2021.752305
- Iwashita, M., Nakatsu, Y., Sakoda, H., Fujishiro, M., Kushiya, A., Fukushima, T., et al. (2013). Valsartan Restores Inflammatory Response by Macrophages in Adipose and Hepatic Tissues of LPS-Infused Mice. *Adipocyte* 2, 28–32. doi:10.4161/adip.21837
- Li, L., Zhong, S.-j., Hu, S.-y., Cheng, B., Qiu, H., and Hu, Z.-x. (2021b). Changes of Gut Microbiome Composition and Metabolites Associated with Hypertensive Heart Failure Rats. *BMC Microbiol.* 21, 141. doi:10.1186/s12866-021-02202-5
- Li, X., Braza, J., Mende, U., Choudhary, G., and Zhang, P. (2021a). Cardioprotective Effects of Early Intervention with Sacubitril/valsartan on Pressure Overloaded Rat Hearts. *Sci. Rep.* 11, 16542. doi:10.1038/s41598-021-95988-3
- Li, X., Zhang, J., Huang, J., Ma, A., Yang, J., Li, W., et al. (2013). A Multicenter, Randomized, Double-Blind, Parallel-Group, Placebo-Controlled Study of the Effects of Qili Qiangxin Capsules in Patients with Chronic Heart Failure. *J. Am. Coll. Cardiol.* 62, 1065–1072. doi:10.1016/j.jacc.2013.05.035
- Liu, J., Zheng, X., Zhang, C., Zhang, C., and Bu, P. (2021). Lcz696 Alleviates Myocardial Fibrosis after Myocardial Infarction through the sFRP-1/Wnt/ $\beta$ -Catenin Signaling Pathway. *Front. Pharmacol.* 12, 724147. doi:10.3389/fphar.2021.724147
- Lorenzo, O., Picatoste, B., Ares-Carrasco, S., Ramirez, E., Egido, J., and Tuñón, J. (2011). Potential Role of Nuclear Factor  $\kappa$ B in Diabetic Cardiomyopathy. *Mediators Inflamm.* 2011, 652097. doi:10.1155/2011/652097
- Lu, Y., Wu, J., Sun, Y., Xin, L., Jiang, Z., Lin, H., et al. (2020). Qiliqiangxin Prevents Right Ventricular Remodeling by Inhibiting Apoptosis and Improving Metabolism Reprogramming with Pulmonary Arterial Hypertension. *Am. J. Transl. Res.* 12, 5655–5669.
- Luo, L., Yan, J., Chen, B., Luo, Y., Liu, L., Sun, Z., et al. (2021). The Effect of Menthol Supplement Diet on Colitis-Induced colon Tumorigenesis and Intestinal Microbiota. *Am. J. Transl. Res.* 13, 38–56.
- Mauro, A. G., Bonaventura, A., Mezzaroma, E., Quader, M., and Toldo, S. (2019). NLRP3 Inflammasome in Acute Myocardial Infarction. *J. Cardiovasc. Pharmacol.* 74, 175–187. doi:10.1097/fjc.0000000000000717
- Nemcs, S., Gassmann, M., Bang, M. L., Frossard, N., and Tavakoli, R. (2021). Antagonizing the CX3CR1 Receptor Markedly Reduces Development of Cardiac Hypertrophy after Transverse Aortic Constriction in Mice. *J. Cardiovasc. Pharmacol.* 78, 792–801. doi:10.1097/fjc.0000000000001130
- Ni, Y., Deng, J., Bai, H., Liu, C., Liu, X., and Wang, X. (2022). CaMKII Inhibitor KN-93 Impaired Angiogenesis and Aggravated Cardiac Remodelling and Heart Failure via Inhibiting NOX2/mtROS/p-VEGFR2 and STAT3 Pathways. *J. Cel Mol Med* 26, 312–325. doi:10.1111/jcmm.17081
- Pan, X., Liu, F., Song, Y., Wang, H., Wang, L., Qiu, H., et al. (2021). Motor Stereotypic Behavior Was Associated with Immune Response in Macaques: Insight from Transcriptome and Gut Microbiota Analysis. *Front. Microbiol.* 12, 644540. doi:10.3389/fmicb.2021.644540
- Pan, X. C., Liu, Y., Cen, Y. Y., Xiong, Y. L., Li, J. M., Ding, Y. Y., et al. (2019). Dual Role of Triptolide in Interrupting the NLRP3 Inflammasome Pathway to Attenuate Cardiac Fibrosis. *Int. J. Mol. Sci.* 20 (2), 360. doi:10.3390/ijms20020360
- Pasini, E., Aquilani, R., Testa, C., Baiardi, P., Angioletti, S., Boschi, F., et al. (2016). Pathogenic Gut Flora in Patients with Chronic Heart Failure. *JACC Heart Fail.* 4, 220–227. doi:10.1016/j.jchf.2015.10.009
- Qi, Y.-Z., Jiang, Y.-H., Jiang, L.-Y., Shao, L.-L., Yang, X.-S., and Yang, C.-H. (2021). An Insight into Intestinal Microbiota of Spontaneously Hypertensive Rats after Valsartan Administration. *Dose-Response* 19 (2), 15593258211011342. doi:10.1177/15593258211011342
- Ren, F.-f., Xie, Z.-y., Jiang, Y.-n., Guan, X., Chen, Q.-y., Lai, T.-f., et al. (2021). Dapagliflozin Attenuates Pressure Overload-Induced Myocardial Remodeling in Mice via Activating SIRT1 and Inhibiting Endoplasmic Reticulum Stress. *Acta Pharmacol. Sin.* doi:10.1038/s41401-021-00805-2
- Ruppert, M., Lakatos, B. K., Braun, S., Tokodi, M., Karime, C., Oláh, A., et al. (2020). Longitudinal Strain Reflects Ventriculoarterial Coupling rather Than Mere Contractility in Rat Models of Hemodynamic Overload-Induced Heart Failure. *J. Am. Soc. Echocardiogr* 33, 1264–e4. doi:10.1016/j.echo.2020.05.017
- Sandek, A., Swidsinski, A., Schroedl, W., Watson, A., Valentova, M., Herrmann, R., et al. (2014). Intestinal Blood Flow in Patients with Chronic Heart Failure: a Link with Bacterial Growth, Gastrointestinal Symptoms, and Cachexia. *J. Am. Coll. Cardiol.* 64, 1092–1102. doi:10.1016/j.jacc.2014.06.1179
- Sardu, C., Consiglia, Trotta, M., Santella, B., D'Onofrio, N., Barbieri, M., Rizzo, M. R., et al. (2021). Microbiota Thrombus Colonization May Influence Athero-Thrombosis in Hyperglycemic Patients with ST Segment Elevation Myocardialinfarction (STEMI). Marianella Study. *Diabetes Res. Clin. Pract.* 173, 108670. doi:10.1016/j.diabres.2021.108670
- Shi, B., Huang, Y., Ni, J., Chen, J., Wei, J., Gao, H., et al. (2020). Qi Dan Li Xin Pill Improves Chronic Heart Failure by Regulating mTOR/p70S6k-Mediated Autophagy and Inhibiting Apoptosis. *Sci. Rep.* 10, 6105. doi:10.1038/s41598-020-63090-9
- Sokolksi, M., Reszka, K., Suchocki, T., Adamik, B., Doroszko, A., Drobnik, J., et al. (2022). History of Heart Failure in Patients Hospitalized Due to COVID-19: Relevant Factor of In-Hospital Complications and All-Cause Mortality up to Six Months. *Jcm* 11, 241. doi:10.3390/jcm11010241
- Suetomi, T., Willeford, A., Brand, C. S., Cho, Y., Ross, R. S., Miyamoto, S., et al. (2018). Inflammation and NLRP3 Inflammasome Activation Initiated in Response to Pressure Overload by Ca2+/Calmodulin-dependent Protein Kinase II  $\delta$  Signaling in Cardiomyocytes Are Essential for Adverse Cardiac Remodeling. *Circulation* 138, 2530–2544. doi:10.1161/circulationaha.118.034621
- Tan, H., Zhao, J., Zhang, H., Zhai, Q., and Chen, W. (2019). Novel Strains of Bacteroides Fragilis and Bacteroides Ovatus Alleviate the LPS-Induced Inflammation in Mice. *Appl. Microbiol. Biotechnol.* 103, 2353–2365. doi:10.1007/s00253-019-09617-1
- Tang, T. W. H., Chen, H. C., Chen, C. Y., Yen, C. Y. T., Lin, C. J., Prajnamitra, R. P., et al. (2019). Loss of Gut Microbiota Alters Immune System Composition and Cripples Postinfarction Cardiac Repair. *Circulation* 139, 647–659. doi:10.1161/circulationaha.118.035235
- Tang, W. H., Kitai, T., and Hazen, S. L. (2017). Gut Microbiota in Cardiovascular Health and Disease. *Circ. Res.* 120, 1183–1196. doi:10.1161/circresaha.117.309715
- Tomoaia, R., Beyer, R. S., Simu, G., Serban, A. M., and Pop, D. (2019). Understanding the Role of Echocardiography in Remodeling after Acute Myocardial Infarction and Development of Heart Failure with Preserved Ejection Fraction. *Med. Ultrason.* 21, 69–76. doi:10.11152/mu-1768
- Tsuda, T. (2021). Clinical Assessment of Ventricular Wall Stress in Understanding Compensatory Hypertrophic Response and Maladaptive Ventricular Remodeling. *Jcdd* 8, 122. doi:10.3390/jcdd8100122

- Wang, H., Zhang, X., Yu, P., Zhou, Q., Zhang, J., Zhang, H., et al. (2017). Traditional Chinese Medication Qiliqiangxin Protects against Cardiac Remodeling and Dysfunction in Spontaneously Hypertensive Rats. *Int. J. Med. Sci.* 14, 506–514. doi:10.7150/ijms.18142
- Wang, Z., Cai, Z., Ferrari, M. W., Liu, Y., Li, C., Zhang, T., et al. (2021). The Correlation between Gut Microbiota and Serum Metabolomic in Elderly Patients with Chronic Heart Failure. *Mediators Inflamm.* 2021, 5587428. doi:10.1155/2021/5587428
- Willeford, A., Suetomi, T., Nickle, A., Hoffman, H. M., Miyamoto, S., and Heller Brown, J. (2018). CaMKII $\delta$ -mediated Inflammatory Gene Expression and Inflammasome Activation in Cardiomyocytes Initiate Inflammation and Induce Fibrosis. *JCI Insight* 3. doi:10.1172/jci.insight.97054
- Xia, J., Gu, L., Guo, Y., Feng, H., Chen, S., Jurat, J., et al. (2021). Gut Microbiota Mediates the Preventive Effects of Dietary Capsaicin against Depression-like Behavior Induced by Lipopolysaccharide in Mice. *Front. Cell Infect. Microbiol.* 11, 627608. doi:10.3389/fcimb.2021.627608
- Xiao, H., Song, Y., Li, Y., Liao, Y. H., and Chen, J. (2009). Qiliqiangxin Regulates the Balance between Tumor Necrosis Factor-Alpha and Interleukin-10 and Improves Cardiac Function in Rats with Myocardial Infarction. *Cell Immunol.* 260, 51–55. doi:10.1016/j.cellimm.2009.09.001
- Yamaguchi, K., Yisireyili, M., Goto, S., Cheng, X. W., Nakayama, T., Matsushita, T., et al. (2022). Indoxyl Sulfate Activates NLRP3 Inflammasome to Induce Cardiac Contractile Dysfunction Accompanied by Myocardial Fibrosis and Hypertrophy. *Cardiovasc. Toxicol.* 22, 365–377. doi:10.1007/s12012-021-09718-2
- Yuan, Y., Lu, L., Bo, N., Chaoyue, Y., and Haiyang, Y. (2021). Allicin Ameliorates Intestinal Barrier Damage via Microbiota-Regulated Short-Chain Fatty Acids-TLR4/MyD88/NF-K $\kappa$  Cascade Response in Acrylamide-Induced Rats. *J. Agric. Food Chem.* 69, 12837–12852. doi:10.1021/acs.jafc.1c05014
- Zhang, T., Wang, H., Lu, M., Zhao, K., Yin, J., Liu, Y., et al. (2020). Astragaloside IV Prevents Myocardial Hypertrophy Induced by Mechanical Stress by Activating Autophagy and Reducing Inflammation. *Am. J. Transl. Res.* 12, 5332–5342.
- Zhang, X., Li, N., Chen, Q., and Qin, H. (2021b). Fecal Microbiota Transplantation Modulates the Gut Flora Favoring Patients with Functional Constipation. *Front. Microbiol.* 12, 700718. doi:10.3389/fmicb.2021.700718
- Zhang, X. X., Liang, B., Shao, C. L., and Gu, N. (2021a). Traditional Chinese Medicine Intervenes Ventricular Remodeling Following Acute Myocardial Infarction: Evidence from 40 Random Controlled Trials with 3,659 Subjects. *Front. Pharmacol.* 12, 707394. doi:10.3389/fphar.2021.707394
- Zhang, Y., Zhu, M., Zhang, F., Zhang, S., Du, W., and Xiao, X. (2019). Integrating Pharmacokinetics Study, Network Analysis, and Experimental Validation to Uncover the Mechanism of Qiliqiangxin Capsule against Chronic Heart Failure. *Front. Pharmacol.* 10, 1046. doi:10.3389/fphar.2019.01046
- Zhao, M., Zhang, J., Xu, Y., Liu, J., Ye, J., Wang, Z., et al. (2021). Selective Inhibition of NLRP3 Inflammasome Reverses Pressure Overload-Induced Pathological Cardiac Remodeling by Attenuating Hypertrophy, Fibrosis, and Inflammation. *Int. Immunopharmacol.* 99, 108046. doi:10.1016/j.intimp.2021.108046
- Zhong, Y., Chen, L., Li, M., Chen, L., Qian, Y., Chen, C., et al. (2021). Dangshen Erling Decoction Ameliorates Myocardial Hypertrophy via Inhibiting Myocardial Inflammation. *Front. Pharmacol.* 12, 725186. doi:10.3389/fphar.2021.725186
- Zou, Y., Lin, L., Ye, Y., Wei, J., Zhou, N., Liang, Y., et al. (2012). Qiliqiangxin Inhibits the Development of Cardiac Hypertrophy, Remodeling, and Dysfunction during 4 Weeks of Pressure Overload in Mice. *J. Cardiovasc. Pharmacol.* 59, 268–280. doi:10.1097/FJC.0b013e31823f888f

**Conflict of Interest:** The authors declare that the research was conducted in the absence of any commercial or financial relationships that could be construed as a potential conflict of interest.

**Publisher's Note:** All claims expressed in this article are solely those of the authors and do not necessarily represent those of their affiliated organizations or those of the publisher, the editors, and the reviewers. Any product that may be evaluated in this article or claim that may be made by its manufacturer is not guaranteed or endorsed by the publisher.

Copyright © 2022 Lu, Xiang, Xin, Zhang, Wang, Shen, Li and Cui. This is an open-access article distributed under the terms of the Creative Commons Attribution License (CC BY). The use, distribution or reproduction in other forums is permitted, provided the original author(s) and the copyright owner(s) are credited and that the original publication in this journal is cited, in accordance with accepted academic practice. No use, distribution or reproduction is permitted which does not comply with these terms.



# Naltrexone-Induced Cardiac Function Improvement is Associated With an Attenuated Inflammatory Response and Lipid Peroxidation in Volume Overloaded Rats

## OPEN ACCESS

### Edited by:

Zufeng Ding,

University of Arkansas for Medical Sciences, United States

### Reviewed by:

Attila Kiss,

Medical University of Vienna, Austria

Scott Levick,

The University of Sydney, Australia

Mihály Ruppert,

Semmelweis University, Hungary

Hussein Kadhem Al-Hakeim,

University of Kufa, Iraq

Attila Oláh,

Semmelweis University, Hungary

### \*Correspondence:

Shaaban A. Mousa

shaaban.mousa@charite.de

<sup>†</sup>These authors have contributed equally to this work

### Specialty section:

This article was submitted to

Cardiovascular and Smooth Muscle

Pharmacology,

a section of the journal

Frontiers in Pharmacology

**Received:** 10 February 2022

**Accepted:** 31 May 2022

**Published:** 30 June 2022

### Citation:

Dehe L, Mousa SA, Shaqura M, Shakibaei M, Schäfer M and Treskatsch S (2022) Naltrexone-Induced Cardiac Function Improvement is Associated With an Attenuated Inflammatory Response and Lipid Peroxidation in Volume Overloaded Rats. *Front. Pharmacol.* 13:873169. doi: 10.3389/fphar.2022.873169

Lukas Dehe<sup>1†</sup>, Shaaban A. Mousa<sup>1\*†</sup>, Mohammed Shaqura<sup>1</sup>, Mehdi Shakibaei<sup>2</sup>, Michael Schäfer<sup>1</sup> and Sascha Treskatsch<sup>1</sup>

<sup>1</sup>Department of Anesthesiology and Operative Intensive Care Medicine, Charité—Universitätsmedizin Berlin, Corporate Member of Freie Universität Berlin, Humboldt-Universität Zu Berlin and Berlin Institute of Health, Berlin, Germany, <sup>2</sup>Institute of Anatomy, Ludwig-Maximilians-Universität München, München, Germany

In previous studies, upregulation of myocardial opioid receptors as well as the precursors of their endogenous ligands were detected in the failing heart due to chronic volume overload. Moreover, opioid receptor blockade by naltrexone improved left ventricular function. In parallel, inflammatory processes through cytokines have been confirmed to play an important role in the pathogenesis of different forms of heart failure. Thus, the present study examined the systemic and myocardial inflammatory response to chronic volume overload and its modulation by chronic naltrexone therapy. Chronic volume overload was induced in male Wistar rats by applying an infrarenal aortocaval fistula (ACF) for 28 days during which the selective opioid receptor antagonist naltrexone ( $n = 6$ ) or vehicle ( $n = 6$ ) were administered *via* a subcutaneously implanted Alzet minipump. The ultrastructural, morphometric and hemodynamic characterization of ACF animals were performed using an intraventricular conductance catheter *in vivo* and electron microscopy *in vitro*. Co-localization of mu-, delta- and kappa-opioid receptor subtypes (MOR, DOR, and KOR respectively) with the voltage gated L-type Ca<sup>2+</sup> channel (Cav1.2), the ryanodine receptor (RyR), and mitochondria in cardiomyocytes as well as IL-6, IL-12, TNF-alpha, and Malondialdehyde (MDA) were determined using double immunofluorescence confocal microscopy, RT-PCR and ELISA, respectively. In rat left ventricular myocardium, three opioid receptor subtypes MOR, DOR, and KOR colocalized with Cav1.2, RyR and mitochondria suggesting a modulatory role of the excitation-contraction coupling. In rats with ACF-induced volume overload, signs of heart failure and myocardial ultrastructural damage, chronic naltrexone therapy improved cardiac function and reversed the systemic and myocardial inflammatory cytokine expression as well as lipid peroxidation. In conclusion, antagonism of the cardiodepressive effects of the myocardial opioid system does not only improve left ventricular function but also blunts the inflammatory response and lipid peroxidation.

**Keywords:** naltrexone, cardiac, cytokine, lipid peroxidation, volume overload



## INTRODUCTION

Heart failure is a clinical syndrome characterized by inadequate cardiac function to maintain organ perfusion (McDonagh et al., 2021; Torregroza et al., 2021). The most common causes of heart failure are the acute events of myocardial ischemia and subsequent scarring or of chronic hypertension (Goel et al., 2013; De Luca, 2020). It is well known that heart failure is associated with significant morbidity and mortality worldwide (McDonagh et al., 2021). In contrast to the well described immediate cardioprotective effects of opioids in the acute event of myocardial ischemia (Torregroza et al., 2020; Torregroza et al., 2021), recent findings raised the awareness that the chronically enhanced intrinsic tone of endogenous opioids during heart failure may have detrimental effects (Treskatsch et al., 2015; Treskatsch et al., 2016; Dehe et al., 2021). Consistently, chronic morphine treatment resulted in a higher mortality risk in patients with acute coronary syndrome (Meine et al., 2005; Ray et al., 2016; Häuser et al., 2020) as well as in patients with chronic treatment of noncancer pain patients with long-acting opioids (Ray et al., 2016; Häuser et al., 2020). Indeed, intravenous morphine administration to elderly patients (age > 75 years) suffering from congestive heart failure (CHF) increased their in-hospital mortality rate. Moreover, patients being administered morphine were more likely to develop congested heart failure (Ray et al., 2016; Häuser et al., 2020). In the ACF animal model of heart failure, the expression of myocardial opioid receptors as well as their endogenous ligands were highly up-regulated as part of a compensatory counter-regulation of the activation of the sympathetic nervous system (Treskatsch et al., 2014). In this context, persistent opioid receptor blockade by naltrexone significantly improved left ventricular function and also decreased rBNP-45 plasma concentrations in rats with volume overload (Dehe et al., 2021).

A growing body of evidence showed that neurohormones and cytokines, including IL-6 and TNF- $\alpha$ , contribute to the progression of heart failure (Seta et al., 1996). In more recent studies, inflammatory processes have been confirmed to be involved in the pathogenesis of different forms of CHF (Westermann et al., 2011; Libby et al., 2016). It is well established that particularly TNF- $\alpha$  is one of most crucial inflammatory cytokines which plays an important role in the pathogenesis and progression of heart disease (Feldman et al., 2000; Böse et al., 2007; Kleinbongard et al., 2010). Indeed, TNF- $\alpha$  is involved in multiple cellular progressions such as oxidative stress (Ozsoy et al., 2008) and apoptosis (Bryant et al., 1998; Condorelli et al., 2002; Chen et al., 2014). Oxidative stress is known to impair mitochondrial function. In addition, a previous study demonstrated a correlation between increased mitochondrial oxidative stress and the rate of transcription of pro-inflammatory cytokines such as IL-6 in chronic human diseases (Naik and Dixit, 2011).

Therefore, there is great interest towards the elucidation of the potential therapeutic strategies targeting elevated cytokines and oxidative stress during heart failure. Since persistent opioid receptor blockade by naltrexone led to improved LV function and decreased rBNP-45 plasma concentrations in volume

overloaded rats, the present study investigated whether cytokines such as IL-6, IL-12 and TNF- $\alpha$  as well as Malondialdehyde (MDA) plasma concentrations and their left ventricle myocardial content are significantly up-regulated during volume overload and whether the opioid receptor blockade by naltrexone resulted in the attenuation of this inflammatory response and lipid peroxidation.

## MATERIALS AND METHODS

### Animals

Following approval by the local animal care committee (Landesamt für Gesundheit und Soziales, Berlin, Germany), we performed the present experiments in male Wistar rats (400 g) (Harlan Winkelmann, Borcheln, Germany) according to the European Directive introducing new animal welfare and care guidelines (2010/63/EU). During the experimental period, rats were supported with standard laboratory chow and water *ad libitum* on a 12-h/12-h light–dark cycle.

### Aortocaval Fistula Induction and Naltrexone Treatment

The needle-technique to induce an infrarenal aortocaval fistula (ACF) has been described first by Garcia and Diebold using a 18 G needle (Garcia and Diebold, 1990). Here, we used an infrarenal aortocaval fistula (ACF) to induce chronic volume overload according to previous studies (Treskatsch et al., 2014). Briefly, under isoflurane anesthesia laparotomy was conducted and the aorta was penetrated with a 16 G disposable needle (Braun, Melsungen, Germany) distal to the renal arteries. Then, the needle was advanced across the aortic wall into the adjacent vena cava inferior. The aortic puncture site was sealed with cyanoacrylate glue after needle withdrawal. ACF patency was assessed by the pulsatile flow of oxygenated blood from the aorta into the vena cava inferior. Immediately at the end of ACF induction, group of 6 rats received a continuous subcutaneous administration of naltrexone (10 mg  $\times$  kg<sup>-1</sup>  $\times$  h<sup>-1</sup>) by subcutaneously implanted Alzet<sup>®</sup> minipumps (osmotic pump, model 2ML4, 2.5  $\mu$ L per hour) (“ACF/Naltrexone”) (Dehe et al., 2021). Naltrexone binds with approximately similar affinity to three opioid receptor subtypes MOR, DOR and KOR (Ananthan et al., 1999). Naltrexone, compared with naloxone, exhibits a longer-acting opioid receptor antagonist effect, with a half-life of 3.9–10.3 h vs. approximately 60 min. The other group of rats ( $n = 5$ ) with ACF also received a minipump delivering vehicle (isotonic saline) at the same volume during the whole experimental period (“ACF/Vehicle”). Sham-operated animals ( $n = 6$ ) served as controls subjected to the same operational steps except the puncture of the aorta and without any treatment. The subcutaneously injected metamizole (40 mg/kg) was used as post-surgical analgesia (Treskatsch et al., 2014).

### Hemodynamic Evaluation

The “closed chest” method was used to measure hemodynamic parameters as previously described (Treskatsch et al., 2014).

Briefly, 28 days after fistula induction in the measurements were done under tiletamine/zolazepam anesthesia (Zoletil<sup>®</sup>, 10 mg/kg s.c. followed by 50 mg/kg i.m.) in spontaneously breathing rats (Saha et al., 2007). Following anesthesia (5–10 min), rats subjected to tracheostomy to facilitate spontaneous breathing and were placed on a heating pad to maintain body temperature. In order to measure the central venous pressure (CVP) a plastic catheter (PE-50) was inserted via the left jugular vein into the superior vena cava. However, the arterial and intraventricular pressures and their derivatives were determined with a pressure micro-tip catheter (Millar<sup>®</sup>, SPR-838 NR), which was inserted into the left ventricle via the right carotid artery. All parameters were recorded and analyzed by the PowerLab<sup>®</sup>-system and software (AD Instruments, Dunedin, New Zealand). At the end of experiments, rats were decapitated and their hearts were removed by dissecting the aortic root immediately above the aortic valves and the superior vena cava above the atria; then the entire heart weight was determined. Experiments were performed in triplicate at 10 min intervals to assure stable measurement conditions.

## Immunofluorescence and Electron Microscopy

Control or rats with ACF-induced volume overload were deeply anesthetized with tiletamine/zolazepam (Zoletil<sup>®</sup>) and transcardially perfused with 100 ml warm saline, followed by 300 ml 4% (w/v) paraformaldehyde in 0.16 M phosphate buffer solution (pH 7.4) ("fixative solution"). Then, left ventricle were removed, postfixed in fixative solution, and cryoprotected overnight at 4°C in PBS containing 10% sucrose. The 10 µm thick sections of the left ventricle were mounted onto gelatin-coated slides and incubated overnight with the following primary antibodies as described previously (Treskatsch et al., 2014; Treskatsch et al., 2015; Treskatsch et al., 2016) as follows: rabbit polyclonal anti-Mu-Opioid Receptor (MOR) (1:1000) (gift from S. Schulz and V. Höllt, Magdeburg, Germany), rabbit polyclonal anti-Delta-Opioid Receptor (DOR) (Dr. R. Elde, Minneapolis, MN, United States), rabbit polyclonal anti-Kappa-Opioid Receptor (KOR) (1:1000) (gift from S. J. Watson, Michigan, United States) in combination with the mouse monoclonal anti-dihydropyridine receptor ( $\alpha_2$  subunit) antibody to identify the voltage-gated L-type Ca<sup>2+</sup> channel (anti-Cav1.2) (SIGMA<sup>®</sup>, Missouri, United States), monoclonal anti-Inositol-1,4,5-trisphosphate receptor type III (1:600) to identify ryanodine receptors (RyR) (BD Biosciences) or monoclonal anti-mitochondrion marker MTC02 (1:300) to identify mitochondrial structures (Thermo Scientific). After incubation, with primary antibodies, the tissue sections were then washed with PBS and incubated with Texas Red-conjugated goat anti-rabbit antibody (Vector Laboratories) and FITC-conjugated donkey anti-mouse secondary antibodies (Vector Laboratories, Inc. Burlingame, CA). Thereafter, sections were washed with PBS and the nuclei stained bright blue with 4'-6-diamidino-2-phenylindole (DAPI) (0.1 µg/ml in PBS) (SIGMA<sup>®</sup>, Missouri, United States). Finally, the tissues were washed in PBS, mounted on Vectashield (Vector Laboratories),

and viewed under a Zeiss LSM 510 laser scanning microscope (Carl Zeiss, Göttingen, Germany). To demonstrate specificity of staining, the following controls were included: omission of the primary antisera or the secondary antibodies, as described in previous studies (Ananthan et al., 1999; Naik and Dixit, 2011; Treskatsch et al., 2014). For electron microscopy evaluation as described previously (Treskatsch et al., 2015), samples were fixed in Karnovsky's fixative and then post-fixed in 2% OsO<sub>4</sub>/0.1 M phosphate buffer. After rinsing and dehydration in ethanol, the samples were embedded in Epon (Plano, Marburg, FRG), ultrathin cuts made on a Reichert Ultracut E, and contrasted with 2% uranyl acetate and lead citrate. A transmission electron microscope (Zeiss TEM10, Jena, Germany) was used to examine the tissue samples.

## Quantification of Immunostaining

Images were obtained on a confocal laser scanning microscope, LSM510, equipped with an argon laser (458/488/514 nm), a green helium/neon laser (543 nm), and a red helium/neon laser (633 nm; Carl Zeiss, Göttingen, Germany). Single optical slice images were taken using  $\times 10$  or  $\times 20$  Plan-Neofluar air interface or  $\times 40$  Plan-Neofluar oil interface objective lens. The settings of the confocal microscope were established using a control section and kept unchanged for all subsequent acquisitions. For the quantitative evaluation of all immunofluorescence double staining of opioid receptor subtypes with Cav1.2 or RyR, the version 1.41 of the image analysis program ImageJ<sup>®</sup> was applied (<http://rsbweb.nih.gov/ij/>) as previously described (Shimojo et al., 1997; Schneider et al., 2012). Briefly, the different color channels, each identifying distinct target structures, were separated by using the plug-in (color deconvolution), thus the color signal can quantitatively be evaluated. A manually specified area was identified for each specifically colored area. Intensity thresholds were assigned, so that a maximum degree of integrated area of stained target structure was identified, while minimizing possible background activities. Areas above the threshold value were defined as positive and indicated information about the percentage of the immunostained area in relation to the previously selected total area. Values below the threshold were eliminated as background. The threshold value was kept constant for all sections. With the help of ImageJ, the parameter percentage area (% stained area) was calculated using the software. The percentage area was defined as the specific-colored area in relation to the total area of a photographed tissue preparation. All calculated quantitative color intensities are presented as % immunoreactive area in the manuscript (see also **Supplementary Figure S1**). Data were presented as median plus range.

## Determination of Inflammatory Cytokines and Lipid Peroxidation

Blood samples from control ( $n = 6$ ), ACF/Vehicle ( $n = 5$ ) and ACF/Naltrexone ( $n = 6$ ) animals were withdrawn into EDTA-preloaded tubes after completion of hemodynamic measurements in order to measure the serum inflammatory cytokines concentrations and lipid peroxidation. Then, the blood was

centrifuged at 1,000 g for 10 min at 4°C immediately after withdrawal. Subsequently, the plasma was maintained at -80°C until further use. Finally, a sensitive enzyme-linked immunosorbent assay (ELISA) kit (Abnova, Heidelberg, Germany) was used to measure the plasma concentrations of IL-6, IL-12, TNF-alpha and Malondialdehyde (MDA).

## Quantitative RT-PCR of Myocardial Inflammatory Cytokine mRNA

PCR analysis for IL-6, IL-12, TNF-alpha and Malondialdehyde specific mRNA from rat left ventricle myocardium was performed by using the commercially available Qiazol Lysis kit, (Qiagen, Hilden, Germany) as described previously (Dehe et al., 2021). Total RNA was extracted from the entire left ventricle myocardium of Wistar rats ( $n = 6$  per experimental group) using RNeasy Kit (Qiagen, Hilden, Germany). 0.5  $\mu$ L (25 pmol) oligo dT and 2  $\mu$ L (200 pmol) random primers were added up to 1  $\mu$ g total RNA, incubated at 37°C for 15 min, then at 85°C for 5 s, finally at 4°C for transfer onto ice (according to TaKaRa® manual). cDNA was stored at -20°C. Taqman® qRT-PCR was performed with a SYBR® Green kit following the manufacturer's instructions (Applied Biosystems). The following specific primers were used: for IL-12, forward primer: GCATGTGTCAATCAGCTACC, reverse primer: AAGACACTTGGCAGGTCCAG (Ensembl, Accession Nr: NM\_053390.1); for IL-6, forward primer: GTTCTCTCCGCAA GAGACTT, reverse primer: TGGTCT GTTGTGGGTGGTATC (Ensembl, Accession NM\_012589); for TNF-alpha, forward primer: GTGATCGGTCCCAA CAAGGA, reverse primer: CGCTTGGTGGTTTGCTACG (Ensembl, Accession Nr: NM\_012675.3). Amplification was carried out for 40 cycles, each consisting of 15 s at 95°C; for cytokines specific mRNA and 18S ribosomal protein for 60 s at 60°C. A temperature just below the specific melting temperature ( $T_m$ ) was employed for detection of fluorescence specific products. IL-12, IL-6 and TNF-alpha specific mRNA were quantified using three independent samples in duplicate. The housekeeping gene S18, a ribosomal protein, was used as an internal reference gene for quantification.

## Statistical Analyses

The acquired data were expressed as medians plus their interquartile ranges. Statistical differences between the three groups were obtained using a one-way analysis of variance (ANOVA) on Ranks (Kruskal-Wallis test) followed by post hoc Dunn's test. Sigma Plot 13.0 statistical software (Systat Software GmbH, Erkrath, Germany) was used to perform all the statistical test.

## RESULTS

### Localization of Mu-Opioid Receptor, Delta-Opioid Receptor, and Kappa-Opioid Receptor in the Left Ventricle Myocardium

Our double immunofluorescence confocal microscopy showed in tissue sections of rat left ventricular myocardium the presence of

the opioid receptor subtypes MOR, DOR and KOR, their colocalization with the voltage-gated L-type  $Ca^{2+}$ -channel Cav1.2 on the outer cell membrane (Figure 1) and their colocalization with the ryanodine receptor (RyR) on the intracellular sarcoplasmic reticulum of left ventricular cardiomyocytes (Figure 2). Quantification of the immunohistochemical staining of these images by ImageJ (Version 1.52a, NIH, United States) imaging software provided the median [range]% values of the area of Cav1.2-immunoreactivity colocalizing with distinct opioid receptor subtype immunoreactivity (yellow fluorescence) of up to 56 (48–65)% for MOR, 67 (55–80)% for DOR and 78 (75–91)% for KOR. Moreover, quantification of the median (range)% values of the area of RyR-immunoreactivity colocalizing with distinct opioid receptor subtype immunoreactivity revealed an overlap (yellow fluorescence) of up to 59 (51–94)% for MOR, 77 (66–84)% for DOR and 63 (60–73)% for KOR (Figures 2A–L).

MOR, DOR and KOR single staining (Texas red fluorescence) were consistently demonstrated in mitochondria-like structures which were regularly arranged in rows located between cardiomyocytes (Figures 1, 2). Consistently, MOR (but also DOR and KOR, data not shown) colocalized with well-defined mitochondrial structures (mitochondrial marker MTC02) of left ventricular cardiomyocytes from controls (Figures 3A–D) compared to ACF-induced volume overload rats (Figures 3E–H).

### Cardiac Remodeling in Aortocaval Fistula Rats

28 days after fistula induction, the weight indices of heart ( $p = 0.008$ ) as well as lung ( $p = 0.006$ ) exhibited a significant increase in all rats with ACF-induced volume overload compared to controls (Table 1). However, chronic naltrexone treatment of ACF rats did not significantly affect heart and lung weight indices compared to the ACF/Vehicle treated group (Table 1).

Ultrastructural analysis of the left ventricle myocardium in normal (control) rats revealed intact myocardial tissue with specific cell-cell contacts and regular intercellular spaces, cardiomyocytes with well-organized numerous cardiomyofibers and normal mitochondrial distribution with a preserved internal architecture (Figures 4A,B). In contrast, left ventricle myocardium of ACF rats showed widening of the intercellular space, disrupted contractile structures and cellular fragmentation. Moreover, the mitochondria exhibited a poorly preserved internal architecture including size enlargement and accumulation of amorphous dense bodies (Figures 4C,D).

### Naltrexone Improved Cardiac Function

In all rats with ACF-induced volume ( $n = 5$ ) overload, there was a significant increase in biventricular filling pressures (LVEDP:  $p = 0.005$ ) and significant decrease in the diastolic blood pressure (DPB:  $p = 0.003$ ) compared to controls ( $n = 6$ ) due to the aortocaval fistula (Table 1). Chronic naltrexone treatment of ACF rats ( $n = 6$ ) caused a significant reduction in left ventricular end-diastolic pressure (LVEDP,  $p = 0.021$ ) compared to ACF rats subjected to vehicle treatment (Table 1). Moreover, global myocardial contractility as measured by  $dp/dt_{min}$  was



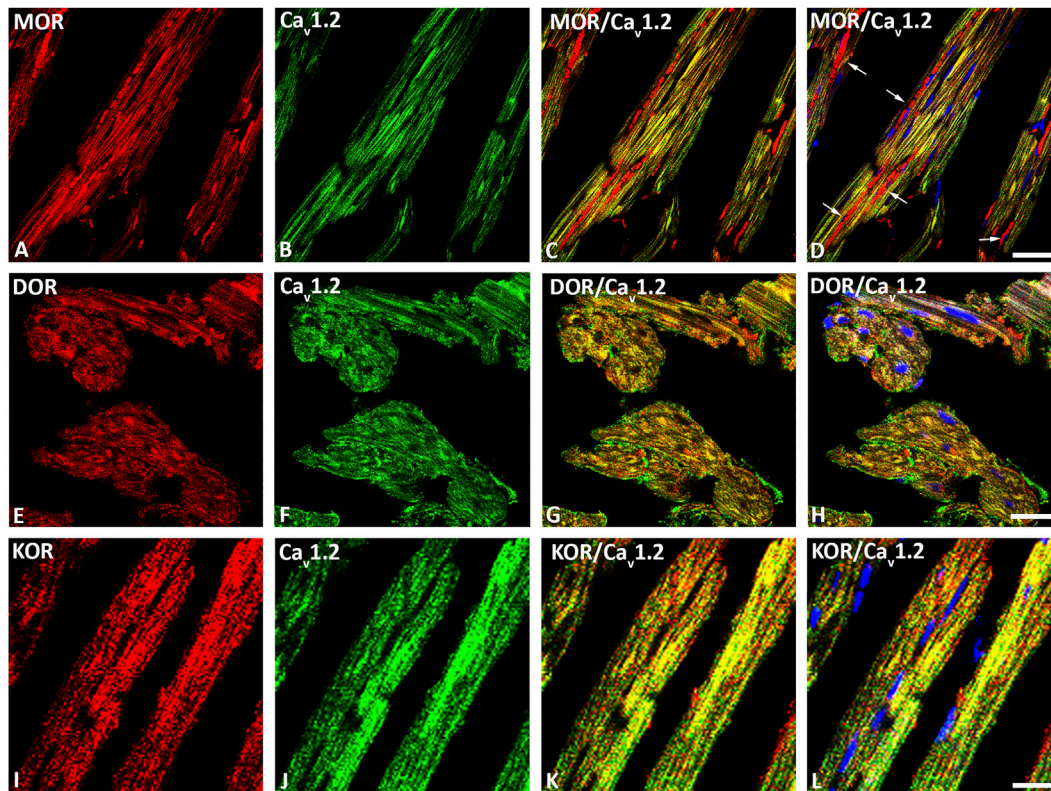


**FIGURE 1 |** Double immunofluorescence confocal microscopy of opioid receptor mu (MOR) (A), delta (DOR) (E), and kappa (KOR) (I) (Texas red immunofluorescence) with L-type  $\text{Ca}^{2+}$ -channel Cav1.2 (FITC green fluorescence) (B, F, J) in rat left ventricular myocardium. Note that rows of mitochondria are located between cardiomyocytes and are immunostained for MOR as indicated by the red fluorescence (arrow) (D). Nuclei identified by their bright blue using DAPI staining (D, H, L). (C–L) show the colocalization of opioid receptor subtypes mu, delta and kappa together with the L-type  $\text{Ca}^{2+}$ -channel Cav1.2 on cardiomyocytes of the left ventricle. Bar = 20  $\mu\text{m}$ .

significantly improved due to chronic naltrexone treatment in ACF rats ( $\text{dP/dt}_{\text{min}}$ :  $p = 0.002$ ) (Table 1). Volume overload significantly increased rBNP-45 ( $p < 0.002$ ) and angiotensin-2 ( $p < 0.001$ ) plasma levels in ACF/vehicle rats and this increase was reversed by naltrexone treatment (Table 1).

### Attenuated Cytokine Response in Rats With Naltrexone Treatment

Volume overload led to a significant increase of plasma inflammatory cytokines and lipid peroxidation in ACF/vehicle rats ( $n = 5$ ) (IL-6:  $p = 0.001$ ; IL-12:  $p = 0.001$ ; TNF- $\alpha$ :  $p = 0.018$ ; MDA:  $p = 0.005$ ) (Figures 5A–D). However, chronic naltrexone treatment in ACF rats ( $n = 6$ ) was associated with a significant reduction of the inflammatory cytokines including IL-6, IL-12 as well as TNF- $\alpha$  in the blood plasma (IL-6:  $p = 0.047$ , IL-12:  $p = 0.035$ , TNF- $\alpha$ :  $p = 0.007$ ) (Figures 5A–D). Moreover, chronic naltrexone administration in ACF rats ( $n = 6$ ) reduced lipid peroxidation as measured by malondialdehyde (MDA:  $p = 0.022$ ) (Figures 5A–D). In parallel, volume overload led to a significant increase in the mRNA transcription of the inflammatory cytokines IL-12 and TNF- $\alpha$  within the myocardium of the left ventricle of ACF/

vehicle rats (IL-12:  $p = 0.005$ , TNF- $\alpha$ :  $p = 0.008$ ) but not for IL-6 ( $p = 0.512$ ) (Figures 6A–C). Importantly, chronic naltrexone treatment in ACF rats was associated with a significant reduction of the inflammatory cytokine IL-12, and TNF- $\alpha$  mRNA (IL-12:  $p = 0.001$ , TNF- $\alpha$ :  $p = 0.008$ ) but not for IL-6 ( $p = 0.149$ ) (Figures 6A–C).

### DISCUSSION

This study confirms the co-expression of opioid receptor subtypes MOR, DOR and KOR with the voltage-gated L-type  $\text{Ca}^{2+}$ -channels Cav1.2 and the intracellular ryanodine receptor in rat LV cardiomyocytes. Moreover, opioid receptor subtypes also colocalized with mitochondria of cardiomyocytes. In rats with ACF-induced volume overload, hemodynamic signs of heart failure were associated with myocardial ultrastructural damage, an enhanced systemic (increased IL-6, IL-12, TNF- $\alpha$  plasma concentrations) as well as myocardial (increased IL-6, IL-12, TNF- $\alpha$  mRNA transcription) inflammatory response. In parallel, the mitochondrial lipid peroxidation was enhanced. Interestingly, these harmful effects were reversed by chronic naltrexone treatment in rats with ACF-induced volume



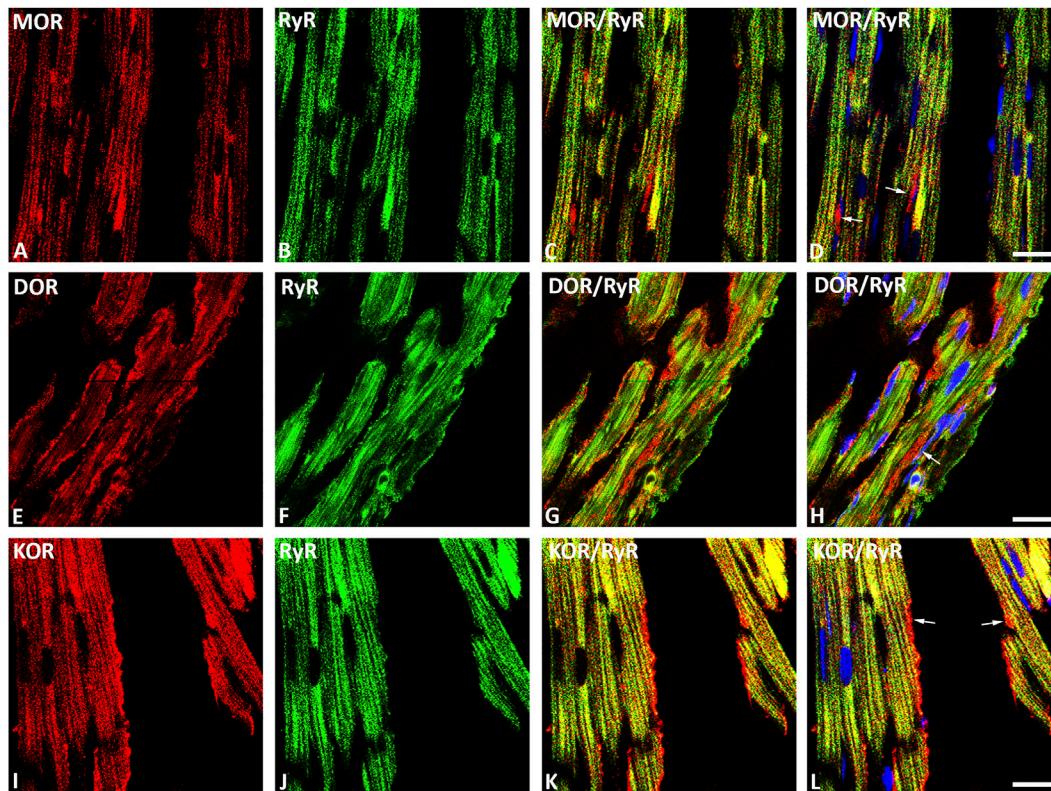


**FIGURE 2 |** Double immunofluorescence confocal microscopy of opioid receptor subtypes mu (MOR) (A), delta (DOR) (E), and kappa (KOR) (I) (Texas red immunofluorescence) in combination with the sarcoplasmic ryanodine receptor (RyR) (FITC green fluorescence) (B, F, J) in rat left ventricular myocardium. (C–L) show co-expression of opioid receptor subtypes MOR, DOR and KOR with RyR on the cardiomyocytes of the rat left ventricle (yellow fluorescence). Note that rows of mitochondria are located between cardiomyocytes and are immunostained for MOR (D), DOR (H) or KOR (L) as indicated by the red fluorescence (arrow). Nuclei are indicated by their bright blue fluorescence (D, H, L). Bar = 10  $\mu$ m.

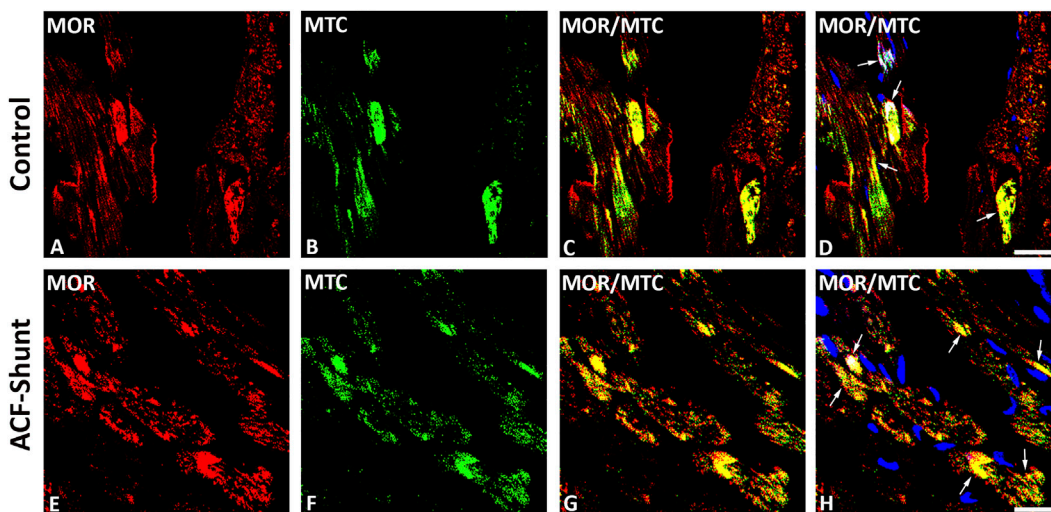


**FIGURE 3 |** Double immunofluorescence staining of mu-opioid receptor (MOR) (A, E) (red fluorescence) and mitochondrial marker MCT02 (green fluorescence) (B, F) in rat left ventricular myocardium from controls (A–D) and rats with ACF-induced volume overload (E–H). (A–D) show that some of MOR immunoreactivity colocalized intracellularly with well-defined mitochondrial structures (mitochondrial marker MCT02) (colocalization seen as yellow immunofluorescence) (arrow). (E–H) show MOR colocalized with swollen mitochondrial structures (mitochondrial marker MTC02) of rat LV cardiomyocytes. (Bar = 10  $\mu$ m).

**TABLE 1 |** Changes of morphometric and hemodynamic parameters of the weight indices of heart and lung in relation to body weights and biventricular filling pressures obtained from control rats and vehicle- (isotonic saline) or naltrexone-treated rats with ACF-induced volume overload. The data are given as medians plus interquartile ranges: HR = heart rate; SBP = systolic blood pressure; DBP = diastolic blood pressure; BW = body weight. Note that there are significant differences not only between the ACF/Vehicle and control group (P1-value) but also between the ACF/Vehicle and ACF/Naltrexone group (P2-value).  $p < 0.05$  was considered statistically significant.

	Control (n = 6)	ACF/Vehicle (n = 5)	ACF/Naltrexone (n = 6)	p-value
Body weight (g)	409 (331; 453)	415 (366; 468)	397 (356; 449)	P = 0.664
Heart weight (mg)	1550 (1425; 1900)	2225 (1790; 2825)	1942 (1625; 2410)	P <sub>1</sub> = 0.003 P <sub>2</sub> = 0.559
Heart/BW (mg/g kg)	3.6 (3.5; 4.3)	5.7 (4.3; 5.8)	4.5 (3.2; 5.5)	P <sub>1</sub> = 0.008 P <sub>2</sub> = 0.326
Lung/BW (mg/g kg)	3.9 (3.2; 4.5)	5.4 (4.9; 8.9)	5.3 (5.1; 6.2)	P <sub>1</sub> = 0.006 P <sub>2</sub> = 1.00
SBP (mmHg)	155 (141; 179)	118 (106; 130)	142 (108; 176)	P <sub>1</sub> = 0.016 P <sub>2</sub> = 0.213
DBP (mmHg)	130 (102; 153)	76 (65; 84)	94 (73; 108)	P <sub>1</sub> = 0.003 P <sub>2</sub> = 0.743
LVEDP (mmHg)	4.9 (4.6; 5.6)	10.8 (8.3; 16.4)	6.8 (6.2; 7.7)	P <sub>1</sub> = 0.005 P <sub>2</sub> = 0.021
dP/dt <sub>max</sub> (mmHg/s)	17890 (14365; 18562)	9068 (6974; 10795)	14124 (12785; 15006)	P <sub>1</sub> = 0.005 P <sub>2</sub> = 0.011
dP/dt <sub>min</sub> (mmHg/s)	-10937 (-13344; -9058)	-6659 (-7530; -3614)	-8675 (-9764; -7813)	P <sub>1</sub> = 0.002 P <sub>2</sub> = 0.026
rBNP-45 (pg/ml)	27 (17; 42)	141 (133; 171)	36 (32; 46)	P <sub>1</sub> = 0.002 P <sub>2</sub> = 0.044
Angiotensin-2 (pg/ml)	386 (371; 456)	1092 (989; 1135)	430 (393; 473)	P <sub>1</sub> = 0.001 P <sub>2</sub> = 0.059

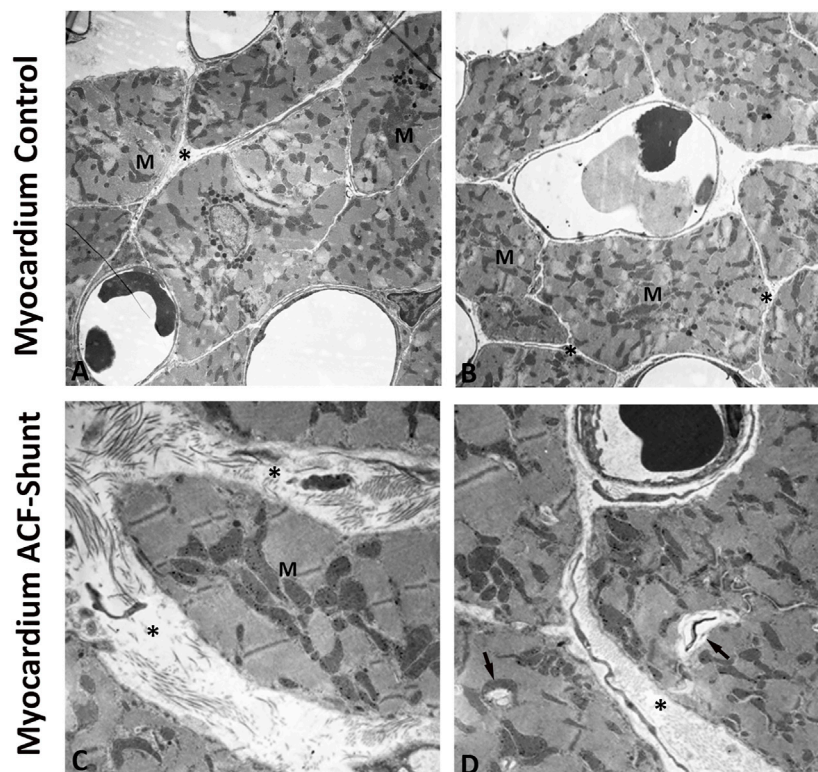


**FIGURE 4 |** Electron micrographs of the left ventricle (LV) from controls (**A, B**) and rats with ACF-induced volume overload (**C, D**). **A** and **B** display cross sections of control hearts showing intact myocardial tissue with specific cell-cell contacts and regular intercellular spaces (see \*), cardiomyocytes with well-organized numerous cardiomyofibers and intact mitochondria with a preserved internal architecture. (**C, D**) show ultrastructure changes of the left ventricle at  $28 \pm 2$  days after ACF induction. Note the widening of the intercellular space (see \*), degenerated myofibers (arrow) and disorganized cell organelles. In addition, many mitochondria (M) showed ultrastructural abnormalities such as size enlargement with amorphous dense bodies and disruption of the internal architecture. Magnification: (**A**)  $\times 10,000$ ; (**B**)  $\times 20,000$ ; bar =  $1 \mu\text{m}$ .

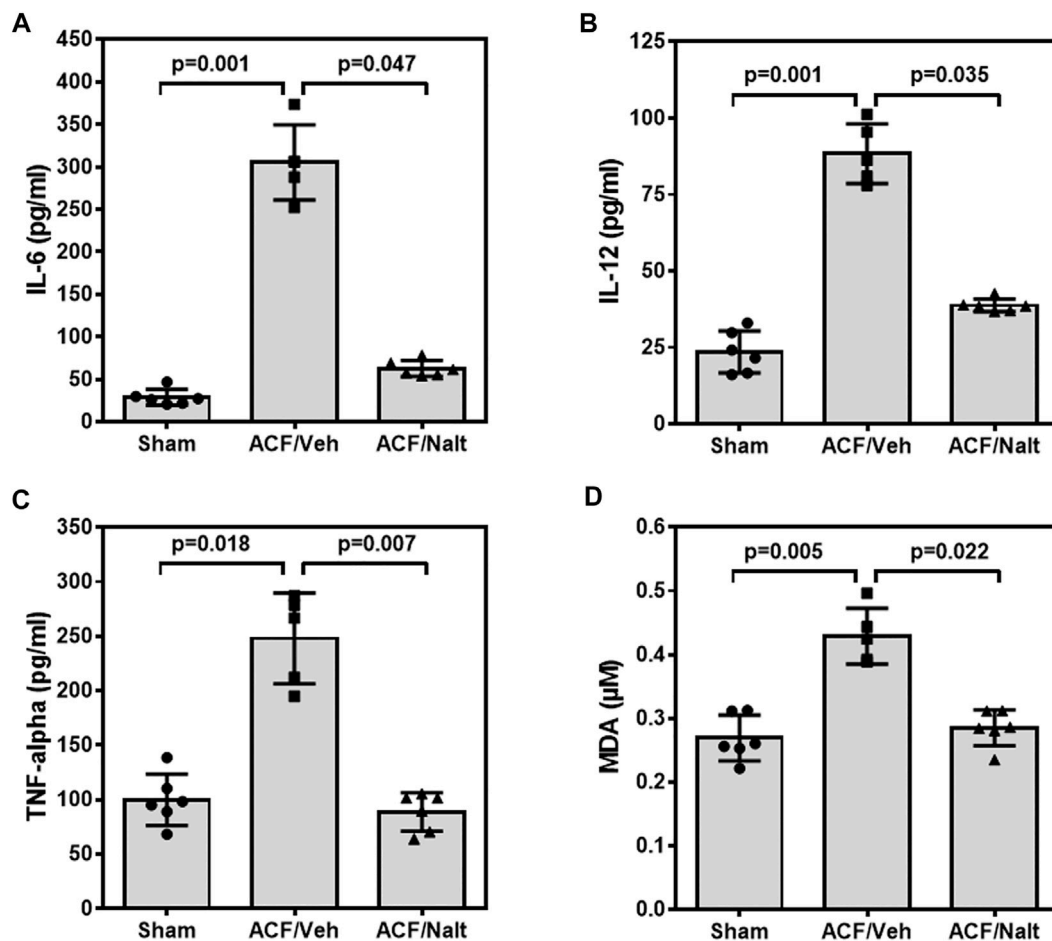


**FIGURE 5 |** Interleukin 6 (IL-6) (A), Interleukin 12 (IL-12) (B), tumor necrosis factor  $\alpha$  (TNF- $\alpha$ ) (C) and malondialdehyde (MDA) (D) values of control, ACF/Vehicle- and ACF/Naltrexone-treated rats. Values of inflammatory cytokines and malondialdehyde were significantly increased in ACF/Vehicle treated rats compared to controls (IL-6:  $p = 0.001$ ; IL-12:  $p = 0.001$ ; TNF- $\alpha$ :  $p = 0.018$ ; MDA:  $p = 0.005$ ). Chronic naltrexone treatment in ACF rats was concomitant with a significant decrease in the inflammatory cytokines and lipid-peroxidation (IL-6:  $p = 0.047$ ; IL-12:  $p = 0.035$ ; TNF- $\alpha$ :  $p = 0.007$ ; MDA:  $p = 0.022$ ). Values are medians plus interquartile ranges ( $n = 6$  rats/group). Data represent medians (range).

overload. Taken together, antagonism of the cardio-depressive effects of the myocardial opioid system does not only improve left ventricular function but also blunts the inflammatory response and lipid peroxidation.

Similar to the demonstrated colocalization of opioid receptors with voltage gated calcium channels in neurons of the central nervous system (Takasusuki and Yaksh, 2011) and the localization of G protein coupled receptors such as the adrenergic and opioid receptors in both the sarcolemma and intracellular microdomains of cardiomyocytes (Head et al., 2005), the present study shows abundant colocalization of opioid receptor subtypes with the calcium channels Cav1.2 and RyR as well as the mitochondria of rat LV cardiomyocytes. Consistently, recent study by Weis and Zamponi (Weiss and Zamponi, 2021) demonstrated the inhibitory effects of opioids on calcium channels. Collectively, these findings seem to point towards a functional link between cardiac opioid receptors and the excitation-contraction coupling within cardiomyocytes.

In animals with volume overload—due to an aorto-caval shunt—our study confirms previous findings (Garcia and Diebold, 1990; Brower et al., 1996; Dehe et al., 2021) that the significant increase of the weight indices of both the heart and lung in rats with ACF-induced volume overload was associated with a marked increase in the rBNP-45 and angiotensin-2 plasma concentrations. In parallel, there was a significant change in all hemodynamic measurements of ACF rats indicating the pronounced systolic and diastolic left ventricular dysfunction. Indeed, our ACF model is characterized by severe biventricular dilatation with signs of decompensated heart failure as shown by a significantly reduced cardiac contractility and elevated LVEDP (Treskatsch et al., 2014). Consistently, our electron microscopy analysis showed clear ultrastructural damage of the LV myocardium in ACF rats with volume overload.

Today, neurohormones and cytokines are known to play an essential role in the development of heart failure (Seta et al., 1996; Van Linthout and Tschöpe, 2017). A growing body of evidence



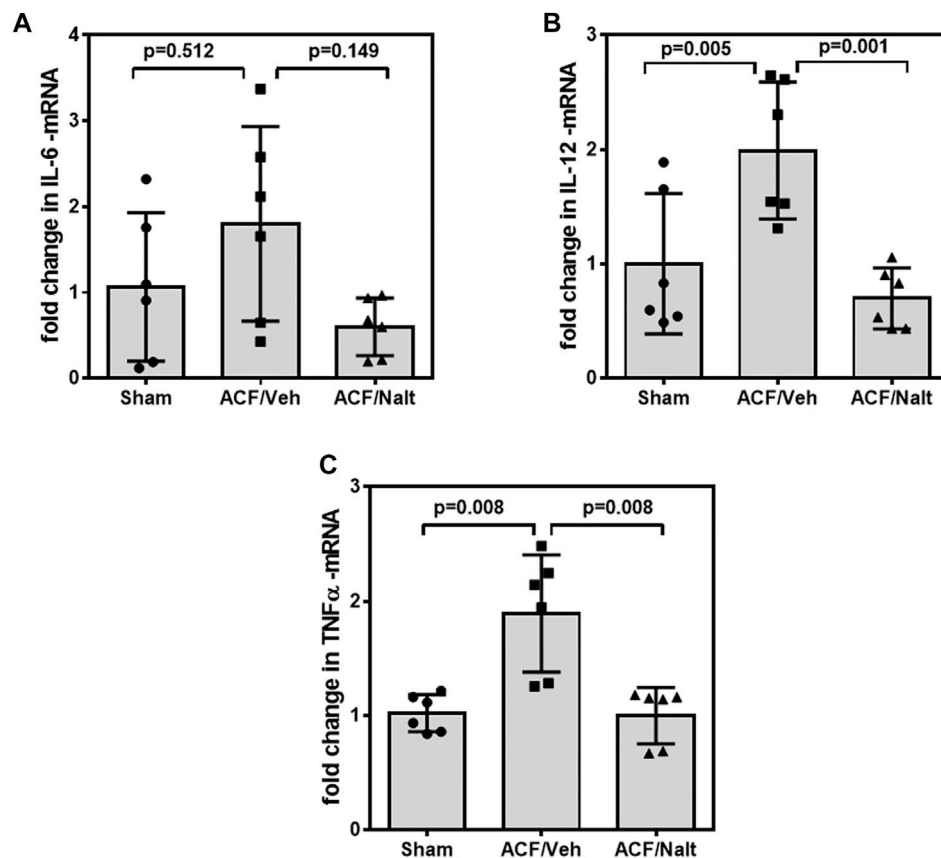


**FIGURE 6 |** Quantitative RT-PCR Interleukin 6 (IL-6) **(A)**, Interleukin 12 (IL-12) **(B)** and tumor necrosis factor  $\alpha$  (TNF- $\alpha$ ) **(C)** specific mRNA values of control, ACF/Vehicle- and ACF/Naltrexone-treated rats. Values of inflammatory cytokines were significantly increased in ACF/Vehicle treated rats compared to controls (IL-12:  $p = 0.005$ ; TNF- $\alpha$ :  $p = 0.008$ ) but not for IL-6 ( $p = 0.512$ ). Chronic naltrexone treatment in ACF rats was concomitant with a significant decrease in the inflammatory cytokine mRNA (IL-12:  $p = 0.001$ ; TNF- $\alpha$ :  $p = 0.008$ ) but not for IL-6 ( $p = 0.149$ ). Data represent medians (range) ( $n = 6$  rats/group).

shows that neurohormones and cytokines, including IL-6 and TNF- $\alpha$ , contribute to the progression of heart failure (Seta et al., 1996). Indeed, our study showed that volume overload in ACF rats caused a significant increase in systemic plasma levels of inflammatory cytokines including IL-6, IL-12 and TNF- $\alpha$  as well as lipid-peroxidation concomitant with the enhanced expression of IL-6, IL-12 and TNF- $\alpha$  mRNA within myocardium. These findings are in agreement with the notion that inflammatory processes have been recognized to be a cornerstone in the pathogenesis of different forms of CHF (Westermann et al., 2011; Libby et al., 2016) and that oxidative stress has been shown to be involved heart failure in animals and humans (Hokamaki et al., 2004; Polidori et al., 2004; LeLeiko et al., 2009). Consistent with these results, patients suffering from heart failure exhibited a correlation between enhanced expression of serum inflammatory cytokines and adverse clinical outcomes (Torre-Amione et al., 1996; Hokamaki et al., 2004). Indeed, TNF- $\alpha$ , IL-1 $\beta$  and IL-6 levels were increased in CHF patients and TNF- $\alpha$  correlated with the severity of the disease (Torre-Amione et al., 1996). Moreover, these cytokines and their corresponding receptors were independent indicators of mortality rate in patients with

progressed CHF (Deswal et al., 2001). In parallel, cytokine, including TNF- $\alpha$ , treatment reduced both contraction and the  $\text{Ca}^{2+}$  transient in rat ventricular myocytes and these effects were modulated by opioids (Duncan et al., 2007). Moreover, TNF- $\alpha$  seems to have negative inotropic effects due to the changes in intracellular  $\text{Ca}^{2+}$  homeostasis within adult cardiomyocytes (Yokoyama et al., 1993), most likely via downregulation of  $\text{Ca}^{2+}$ -regulating genes (Thaik et al., 1995; Wu et al., 2011).

Interestingly the present experiments demonstrated that the improved cardiac function in rats with ACF-induced volume overload by chronic naltrexone treatment reversed the enhanced expression of inflammatory cytokines IL-6, IL-12 and TNF- $\alpha$  within myocardium as well as in serum. Moreover, naloxone inhibited endotoxin-induced up-regulation of inflammatory molecules including IL-6 and TNF- $\alpha$  as well as NF- $\kappa\text{B}$  activation through antagonizing the L-type calcium channels (Jan et al., 2011). In contrast, chronic administration of tramadol in normal rats enhanced the expression of serum inflammatory cytokines and apoptotic markers as well as lipid peroxidation in the cerebrum of rats (Mohamed and Mahmoud, 2019).



Cardiomyocytes energy requirement is covered by mitochondria to maintain their contractile function. In case of a higher energy demand, cardiomyocytes produce new mitochondria (mitochondrial biogenesis) (Ayoub et al., 2017). The malfunction of mitochondrial biogenesis occurs in heart failure in humans and animal models of pressure overload (Sebastiani et al., 2007; Witt et al., 2008). The restriction in heart function is the consequence of apoptosis and myocardial remodeling initiated by mitochondria. In addition, oxidative stress is defined as a state when reactive oxygen species (ROS) defeat the body's antioxidant enzymes. ROS are oxygen-containing molecules that are chemically active and formed as a by-product of oxygen metabolism (Ayoub et al., 2017). In this study, the chronic blockade of the cardiac opioid system by naltrexone resulted in a reduced lipid peroxidation as a surrogate of oxidative stress. In this context, oxidative stress is known to impair mitochondrial function leading to a reduced mitochondrial capacity to generate ATP. Sharov showed this in dogs with chronic heart failure due to myocardial ischemia (Sharov et al., 1998). Extending the aforementioned studies, we showed the intracellular colocalization between opioid receptors and mitochondria in cardiomyocytes of the left ventricle in rats suggesting a modulatory role in mitochondrial function under conditions of oxidative stress.

Several limitations should be considered. Since our animal model does not represent the multimorbidity and causality of cardiac compromised patients, one cannot transfer these findings directly to a clinical situation. However, this animal model has been extensively described and, within 28 days, the animals exhibited a predictable state of nearly decompensated heart failure accompanied by a dilatative cardiomyopathy. It is characterized by significantly elevated biventricular filling pressures and reduced cardiac contractility. The rats typically show overt signs of decompensation, e.g., ascites, strained breathing, decreased mobility, and sudden arrhythmia. The study was conducted only in male Wistar rats. Female Wistar rats are prone to a more difficult ACF induction, and standardization has not been established yet. Therefore, a comprehensive analysis of this experimental model amongst female Wistar rats has yet to be conducted.

## CONCLUSION

In summary, the present findings give evidence of the essential role of the intrinsic cardiac opioid system during chronic volume overload. Morphologically, opioid receptor subtypes were colocalized with calcium channels as well as mitochondria in cardiomyocytes of the LV in rats suggesting a modulatory role of the excitation-contraction coupling. This was accompanied by an increased expression of inflammatory cytokines and TNF- $\alpha$  as well as elevated lipid peroxidation in the blood circulation and in left ventricle myocardium. Importantly, chronic naltrexone treatment attenuated these signs of a systemic and local inflammatory response and lipid peroxidation in parallel to an improved LV function and reduced rBNP-45 plasma concentration. Since the

naltrexone treatment did not completely reverse the measured parameters to baseline, it cannot be ruled out that there are also other mechanisms responsible.

## DATA AVAILABILITY STATEMENT

The original contributions presented in the study are included in the article/**Supplementary Material**, further inquiries can be directed to the corresponding authors.

## ETHICS STATEMENT

The animal study was reviewed and approved by Landesamt für Gesundheit und Soziales, Berlin, Germany; G0144/12.

## AUTHOR CONTRIBUTIONS

LD, SM were responsible for acquisition of data, analysis and interpretation, writing up of the first draft of the paper; MOS contributed to data acquisition, analysis and interpretation; SM, MES provided the EM pictures; MIS, MES helped with data analysis, manuscript composition and proofreading; SM, MIS contributed substantially to the conception and design of the study and helped with data analysis and interpretation; ST took overall responsibility for the conducted study and final revision of the manuscript, he contributed to the development of the study design.

## FUNDING

This work was supported by B. Braun-Stiftung (grant number BBST-D-14-00037) and European Association of Cardiothoracic Anaesthesiology (EACTA) (Research Grant 2016).

## ACKNOWLEDGMENTS

Petra von Kwiatkowski's technical assistance is gratefully acknowledged.

## SUPPLEMENTARY MATERIAL

The Supplementary Material for this article can be found online at: <https://www.frontiersin.org/articles/10.3389/fphar.2022.873169/full#supplementary-material>

**Supplementary Figure S1** | Example of quantitative evaluation of immunohistochemical staining within rat atria using the version 1.41 of the image analysis program ImageJ<sup>®</sup> (<http://rsbweb.nih.gov/ij/>). The additional use of the plug-in (color deconvolution) allowed the separation of the different color channels each identifying distinct target structures, whose color signal can, thus, be quantitatively evaluated. With the help of ImageJ, the parameter percentage area (% stained area) was calculated. The percentage area was defined as the specific-colored area in relation to the total area of a photographed tissue preparation.

## REFERENCES

- Ananthan, S., Kezar, H. S., 3rd, Carter, R. L., Saini, S. K., Rice, K. C., Wells, J. L., et al. (1999). Synthesis, Opioid Receptor Binding, and Biological Activities of Naltrexone-Derived Pyrido- and Pyrimidomorphinans. *J. Med. Chem.* 42 (18), 3527–3538. doi:10.1021/jm990039i
- Ayoub, K. F., Pothineni, N. V. K., Rutland, J., Ding, Z., and Mehta, J. L. (2017). Immunity, Inflammation, and Oxidative Stress in Heart Failure: Emerging Molecular Targets. *Cardiovasc Drugs Ther.* 31 (5–6), 593–608. doi:10.1007/s10557-017-6752-z
- Böse, D., Leineweber, K., Konorza, T., Zahn, A., Bröcker-Preuss, M., Mann, K., et al. (2007). Release of TNF-Alpha During Stent Implantation Into Saphenous Vein Aortocoronary Bypass Grafts and Its Relation to Plaque Extrusion and Restenosis. *Am. J. Physiol. Heart Circ. Physiol.* 292 (5).
- Brower, G. L., Henegar, J. R., and Janicki, J. S. (1996). Temporal Evaluation of Left Ventricular Remodeling and Function in Rats with Chronic Volume Overload. *Am. J. Physiol.* 271 (5 Pt 2), H2071–H2078. doi:10.1152/ajpheart.1996.271.5.H2071
- Bryant, D., Becker, L., Richardson, J., Shelton, J., Franco, F., Peshock, R., et al. (1998). Cardiac Failure in Transgenic Mice With Myocardial Expression of Tumor Necrosis Factor-Alpha. *Circulation* 97 (14), 1375–1381. doi:10.1161/01.cir.97.14.1375
- Chen, Z. W., Qian, J. Y., Ma, J. Y., Chang, S. F., Yun, H., Jin, H., et al. (2014). TNF- $\alpha$ -Induced Cardiomyocyte Apoptosis Contributes to Cardiac Dysfunction After Coronary Microembolization in Mini-Pigs. *J. Cell Mol. Med.* 18 (10), 1953–1963.
- Condorelli, G., Morisco, C., Latronico, M. V., Claudio, P. P., Dent, P., Tsichlis, P., et al. (2002). TNF-Alpha Signal Transduction in Rat Neonatal Cardiac Myocytes: Definition of Pathways Generating From the TNF-Alpha Receptor. *Faseb J.* 16 (13), 1732–1737. doi:10.1096/fj.02-0419com
- De Luca, L. (2020). Established and Emerging Pharmacological Therapies for Post-Myocardial Infarction Patients with Heart Failure: a Review of the Evidence. *Cardiovasc Drugs Ther.* 34 (5), 723–735. doi:10.1007/s10557-020-07027-4
- Dehe, L., Shaqura, M., Nordine, M., Habazettl, H., von Kwiatkowski, P., Schluchter, H., et al. (2021). Chronic Naltrexone Therapy Is Associated with Improved Cardiac Function in Volume Overloaded Rats. *Cardiovasc Drugs Ther.* 35 (4), 733–743. doi:10.1007/s10557-020-07132-4
- Deswal, A., Petersen, N. J., Feldman, A. M., Young, J. B., White, B. G., and Mann, D. L. (2001). Cytokines and Cytokine Receptors in Advanced Heart Failure: an Analysis of the Cytokine Database from the Vesnarinone Trial (VEST). *Circulation* 103 (16), 2055–2059. doi:10.1161/01.cir.103.16.2055
- Duncan, D. J., Hopkins, P. M., and Harrison, S. M. (2007). Negative Inotropic Effects of Tumour Necrosis Factor-Alpha and Interleukin-1beta are Ameliorated by Alfentanil in Rat Ventricular Myocytes. *Br. J. Pharmacol.* 150 (6), 720–726. doi:10.1038/sj.bjp.0707147
- Feldman, A. M., Combes, A., Wagner, D., Kadakomi, T., Kubota, T., Li, Y. Y., et al. (2000). The Role of Tumor Necrosis Factor in the Pathophysiology of Heart Failure. *J. Am. Coll. Cardiol.* 35 (3), 537–544. doi:10.1016/s0735-1097(99)00600-2
- Garcia, R., and Diebold, S. (1990). Simple, Rapid, and Effective Method of Producing Aorticaval Shunts in the Rat. *Cardiovasc Res.* 24 (5), 430–432. doi:10.1093/cvr/24.5.430
- Goel, K., Pinto, D. S., and Gibson, C. M. (2013). Association of Time to Reperfusion with Left Ventricular Function and Heart Failure in Patients with Acute Myocardial Infarction Treated with Primary Percutaneous Coronary Intervention: a Systematic Review. *Am. Heart J.* 165 (4), 451–467. doi:10.1016/j.ahj.2012.11.014
- Häuser, W., Schubert, T., Scherbaum, N., and Tölle, T. (2020). Long-term Opioid Therapy of Non-cancer Pain : Prevalence and Predictors of Hospitalization in the Event of Possible Misuse. *Schmerz* 34 (Suppl. 1), 8–15. doi:10.1007/s00482-018-0331-5
- Head, B. P., Patel, H. H., Roth, D. M., Lai, N. C., Niesman, I. R., Farquhar, M. G., et al. (2005). G-protein-coupled Receptor Signaling Components Localize in Both Sarcolemmal and Intracellular Caveolin-3-Associated Microdomains in Adult Cardiac Myocytes. *J. Biol. Chem.* 280 (35), 31036–31044. doi:10.1074/jbc.M502540200
- Hokamaki, J., Kawano, H., Yoshimura, M., Soejima, H., Miyamoto, S., Kajiwara, I., et al. (2004). Urinary Biopyrrins Levels Are Elevated in Relation to Severity of Heart Failure. *J. Am. Coll. Cardiol.* 43 (10), 1880–1885. doi:10.1016/j.jacc.2004.01.028
- Jan, W. C., Chen, C. H., Hsu, K., Tsai, P. S., and Huang, C. J. (2011). L-type Calcium Channels and  $\mu$ -opioid Receptors Are Involved in Mediating the Anti-inflammatory Effects of Naloxone. *J. Surg. Res.* 167 (2), e263–72. doi:10.1016/j.jss.2010.03.039
- Kleinbongard, P., Heusch, G., and Schulz, R. (2010). TNFalpha in Atherosclerosis, Myocardial Ischemia/Reperfusion and Heart Failure. *Pharmacol. Ther.* 127 (3), 295–314. doi:10.1016/j.pharmthera.2010.05.002
- LeLeiko, R. M., Vaccari, C. S., Sola, S., Merchant, N., Nagamia, S. H., Thoenes, M., et al. (2009). Usefulness of Elevations in Serum Choline and Free F2-Isoprostane to Predict 30-day Cardiovascular Outcomes in Patients with Acute Coronary Syndrome. *Am. J. Cardiol.* 104 (5), 638–643. doi:10.1016/j.amjcard.2009.04.047
- Libby, P., Nahrendorf, M., and Swirski, F. K. (2016). Leukocytes Link Local and Systemic Inflammation in Ischemic Cardiovascular Disease: An Expanded "Cardiovascular Continuum". *J. Am. Coll. Cardiol.* 67 (9), 1091–1103. doi:10.1016/j.jacc.2015.12.048
- McDonagh, T. A., Metra, M., Adamo, M., Gardner, R. S., Baumbach, A., Böhm, M., et al. (2021). 2021 ESC Guidelines for the Diagnosis and Treatment of Acute and Chronic Heart Failure. *Eur. Heart J.* 42 (36), 3599–3726. doi:10.1093/eurheartj/ehab368
- Meine, T. J., Roe, M. T., Chen, A. Y., Patel, M. R., Washam, J. B., Ohman, E. M., et al. (2005). Association of Intravenous Morphine Use and Outcomes in Acute Coronary Syndromes: Results from the CRUSADE Quality Improvement Initiative. *Am. Heart J.* 149 (6), 1043–1049. doi:10.1016/j.ahj.2005.02.010
- Mohamed, H. M., and Mahmoud, A. M. (2019). Chronic Exposure to the Opioid Tramadol Induces Oxidative Damage, Inflammation and Apoptosis, and Alters Cerebral Monoamine Neurotransmitters in Rats. *Biomed. Pharmacother.* 110, 239–247. doi:10.1016/j.biopha.2018.11.141
- Naik, E., and Dixit, V. M. (2011). Mitochondrial Reactive Oxygen Species Drive Proinflammatory Cytokine Production. *J. Exp. Med.* 208 (3), 417–420. doi:10.1084/jem.20110367
- Ozsoy, H. Z., Sivasubramanian, N., Wieder, E. D., Pedersen, S., and Mann, D. L. (2008). Oxidative Stress Promotes Ligand-Independent and Enhanced Ligand-Dependent Tumor Necrosis Factor Receptor Signaling. *J. Biol. Chem.* 283 (34), 23419–23428. doi:10.1074/jbc.M802967200
- Polidori, M. C., Praticó, D., Savino, K., Rokach, J., Stahl, W., and Mecocci, P. (2004). Increased F2 Isoprostane Plasma Levels in Patients with Congestive Heart Failure Are Correlated with Antioxidant Status and Disease Severity. *J. Card. Fail.* 10 (4), 334–338. doi:10.1016/j.cardfail.2003.11.004
- Ray, W. A., Chung, C. P., Murray, K. T., Hall, K., and Stein, C. M. (2016). Prescription of Long-Acting Opioids and Mortality in Patients with Chronic Noncancer Pain. *Jama* 315 (22), 2415–2423. doi:10.1001/jama.2016.7789
- Saha, D. C., Saha, A. C., Malik, G., Astiz, M. E., and Rackow, E. C. (2007). Comparison of Cardiovascular Effects of Tiletamine-Zolazepam, Pentobarbital, and Ketamine-Xylazine in Male Rats. *J. Am. Assoc. Lab. Anim. Sci.* 46 (2), 74–80.
- Schneider, C. A., Rasband, W. S., and Eliceiri, K. W. (2012). NIH Image to ImageJ: 25 Years of Image Analysis. *Nat. Methods* 9 (7), 671–675. doi:10.1038/nmeth.2089
- Sebastiani, M., Giordano, C., Nediani, C., Travaglini, C., Borch, E., Zani, M., et al. (2007). Induction of Mitochondrial Biogenesis Is a Maladaptive Mechanism in Mitochondrial Cardiomyopathies. *J. Am. Coll. Cardiol.* 50 (14), 1362–1369. doi:10.1016/j.jacc.2007.06.035
- Seta, Y., Shan, K., Bozkurt, B., Oral, H., and Mann, D. L. (1996). Basic Mechanisms in Heart Failure: the Cytokine Hypothesis. *J. Card. Fail.* 2 (3), 243–249. doi:10.1016/s1071-9164(96)80047-9
- Sharov, V. G., Goussev, A., Lesch, M., Goldstein, S., and Sabbah, H. N. (1998). Abnormal Mitochondrial Function in Myocardium of Dogs with Chronic Heart Failure. *J. Mol. Cell Cardiol.* 30 (9), 1757–1762. doi:10.1006/jmcc.1998.0739
- Shimojo, M., Ricketts, M. L., Petrelli, M. D., Moradi, P., Johnson, G. D., Bradwell, A. R., et al. (1997). Immunodetection of 11 Beta-Hydroxysteroid Dehydrogenase Type 2 in Human Mineralocorticoid Target Tissues: Evidence for Nuclear Localization. *Endocrinology* 138 (3), 1305–1311. doi:10.1210/endo.138.3.4994

- Takasusuki, T., and Yaksh, T. L. (2011). Regulation of Spinal Substance P Release by Intrathecal Calcium Channel Blockade. *Anesthesiology* 115 (1), 153–164. doi:10.1097/ALN.0b013e31821950c2
- Thaik, C. M., Calderone, A., Takahashi, N., and Colucci, W. S. (1995). Interleukin-1 Beta Modulates the Growth and Phenotype of Neonatal Rat Cardiac Myocytes. *J. Clin. Invest.* 96 (2), 1093–1099. doi:10.1172/jci118095
- Torre-Amione, G., Kapadia, S., Benedict, C., Oral, H., Young, J. B., and Mann, D. L. (1996). Proinflammatory Cytokine Levels in Patients with Depressed Left Ventricular Ejection Fraction: a Report from the Studies of Left Ventricular Dysfunction (SOLVD). *J. Am. Coll. Cardiol.* 27 (5), 1201–1206. doi:10.1016/0735-1097(95)00589-7
- Torregroza, C., Raupach, A., Feige, K., Weber, N. C., Hollmann, M. W., and Huhn, R. (2020). Perioperative Cardioprotection: General Mechanisms and Pharmacological Approaches. *Anesth. Analg.* 131 (6), 1765–1780. doi:10.1213/ane.00000000000005243
- Torregroza, C., Roth, S., Feige, K., Lurati Buse, G., Hollmann, M. W., and Huhn, R. (2021). Perioperative Cardioprotection - from Bench to Bedside : Current Experimental Evidence and Possible Reasons for the Limited Translation into the Clinical Setting. *Anaesthesist* 70 (5), 401–412. doi:10.1007/s00101-020-00912-5
- Treskatsch, S., Feldheiser, A., Rosin, A. T., Siffringer, M., Habazettl, H., Mousa, S. A., et al. (2014). A Modified Approach to Induce Predictable Congestive Heart Failure by Volume Overload in Rats. *PLoS One* 9 (1), e87531. doi:10.1371/journal.pone.0087531
- Treskatsch, S., Shaqura, M., Dehe, L., Feldheiser, A., Roepke, T. K., Shakibaei, M., et al. (2015). Upregulation of the Kappa Opioidergic System in Left Ventricular Rat Myocardium in Response to Volume Overload: Adaptive Changes of the Cardiac Kappa Opioid System in Heart Failure. *Pharmacol. Res.* 102, 33–41. doi:10.1016/j.phrs.2015.09.005
- Treskatsch, S., Shaqura, M., Dehe, L., Roepke, T. K., Shakibaei, M., Schäfer, M., et al. (2016). Evidence for MOR on Cell Membrane, Sarcoplasmic Reticulum and Mitochondria in Left Ventricular Myocardium in Rats. *Heart Vessels* 31 (8), 1380–1388. doi:10.1007/s00380-015-0784-8
- Van Linthout, S., and Tschöpe, C. (2017). Inflammation - Cause or Consequence of Heart Failure or Both? *Curr. Heart Fail Rep.* 14 (4), 251–265. doi:10.1007/s11897-017-0337-9
- Weiss, N., and Zamponi, G. W. (2021). Opioid Receptor Regulation of Neuronal Voltage-Gated Calcium Channels. *Cell Mol. Neurobiol.* 41 (5), 839–847. doi:10.1007/s10571-020-00894-3
- Westermann, D., Lindner, D., Kasner, M., Zietsch, C., Savvatis, K., Escher, F., et al. (2011). Cardiac Inflammation Contributes to Changes in the Extracellular Matrix in Patients with Heart Failure and Normal Ejection Fraction. *Circ. Heart Fail* 4 (1), 44–52. doi:10.1161/circheartfailure.109.931451
- Witt, H., Schubert, C., Jaekel, J., Fliegner, D., Penkalla, A., Tiemann, K., et al. (2008). Sex-specific Pathways in Early Cardiac Response to Pressure Overload in Mice. *J. Mol. Med. Berl.* 86 (9), 1013–1024. doi:10.1007/s00109-008-0385-4
- Wu, C. K., Lee, J. K., Chiang, F. T., Yang, C. H., Huang, S. W., Hwang, J. J., et al. (2011). Plasma Levels of Tumor Necrosis Factor- $\alpha$  and Interleukin-6 Are Associated with Diastolic Heart Failure through Downregulation of Sarcoplasmic Reticulum Ca<sup>2+</sup> ATPase. *Crit. Care Med.* 39 (5), 984–992. doi:10.1097/CCM.0b013e31820a91b9
- Yokoyama, T., Vaca, L., Rossen, R. D., Durante, W., Hazarika, P., and Mann, D. L. (1993). Cellular Basis for the Negative Inotropic Effects of Tumor Necrosis Factor-Alpha in the Adult Mammalian Heart. *J. Clin. Invest.* 92 (5), 2303–2312. doi:10.1172/jci116834

**Conflict of Interest:** The authors declare that the research was conducted in the absence of any commercial or financial relationships that could be construed as a potential conflict of interest.

**Publisher's Note:** All claims expressed in this article are solely those of the authors and do not necessarily represent those of their affiliated organizations, or those of the publisher, the editors and the reviewers. Any product that may be evaluated in this article, or claim that may be made by its manufacturer, is not guaranteed or endorsed by the publisher.

Copyright © 2022 Dehe, Mousa, Shaqura, Shakibaei, Schäfer and Treskatsch. This is an open-access article distributed under the terms of the Creative Commons Attribution License (CC BY). The use, distribution or reproduction in other forums is permitted, provided the original author(s) and the copyright owner(s) are credited and that the original publication in this journal is cited, in accordance with accepted academic practice. No use, distribution or reproduction is permitted which does not comply with these terms.



# AMPK Activation Alleviates Myocardial Ischemia-Reperfusion Injury by Regulating Drp1-Mediated Mitochondrial Dynamics

Jingxia Du<sup>1\*</sup>, Hongchao Li<sup>2</sup>, Jingjing Song<sup>1</sup>, Tingting Wang<sup>1</sup>, Yibo Dong<sup>1</sup>, An Zhan<sup>1</sup>, Yan Li<sup>1</sup> and Gaofeng Liang<sup>2\*</sup>

<sup>1</sup>Pharmacy Department, School of Basic Medical Sciences, Henan University of Science and Technology, Luoyang, China,

<sup>2</sup>Pathology Department, School of Basic Medical Sciences, Henan University of Science and Technology, Luoyang, China

## OPEN ACCESS

### Edited by:

Xianwei Wang,  
Xinxiang Medical University, China

### Reviewed by:

Jianjiang Wu,  
First Affiliated Hospital of Xinjiang  
Medical University, China  
Lanxin Lv,  
Xuzhou Medical University, China

### \*Correspondence:

Jingxia Du  
dujingxia2005@163.com  
Gaofeng Liang  
lgfeng990448@163.com

### Specialty section:

This article was submitted to  
Cardiovascular and Smooth Muscle  
Pharmacology,  
a section of the journal  
Frontiers in Pharmacology

**Received:** 25 January 2022

**Accepted:** 08 June 2022

**Published:** 04 July 2022

### Citation:

Du J, Li H, Song J, Wang T, Dong Y,  
Zhan A, Li Y and Liang G (2022) AMPK  
Activation Alleviates Myocardial  
Ischemia-Reperfusion Injury by  
Regulating Drp1-Mediated  
Mitochondrial Dynamics.  
Front. Pharmacol. 13:862204.  
doi: 10.3389/fphar.2022.862204

Mitochondrial dysfunction is a salient feature of myocardial ischemia/reperfusion injury (MIRI), while the potential mechanism of mitochondrial dynamics disorder remains unclear. This study sought to explore whether activation of Adenosine monophosphate-activated protein kinase (AMPK) could alleviate MIRI by regulating GTPase dynamin-related protein 1 (Drp1)-mediated mitochondrial dynamics. Isolated mouse hearts in a Langendorff perfusion system were subjected to ischemia/reperfusion (I/R) treatment, and H9C2 cells were subjected to hypoxia /reoxygenation (H/R) treatment *in vitro*. The results showed that AICAR, the AMPK activator, could significantly improve the function of left ventricular, decrease arrhythmia incidence and myocardial infarction area of isolated hearts. Meanwhile, AICAR increased superoxide dismutase (SOD) activity and decreased malondialdehyde (MDA) content in myocardial homogenate. Mechanistically, AICAR inhibited the phosphorylation of Drp1 at Ser 616 while enhanced phosphorylation of Drp1 at Ser 637. In addition, AICAR reduced the expression of inflammatory cytokines including *TNF- $\alpha$* , *IL-6*, and *IL-1 $\beta$* , as well as mitochondrial fission genes *Mff* and *Fis1*, while improved the expression of mitochondrial fusion genes *Mfn1* and *Mfn2*. Similar results were also observed in H9C2 cells. AICAR improved mitochondrial membrane potential (MMP), reduced reactive oxygen species (ROS) production, and inhibited mitochondrial damage. To further prove if Drp1 regulated mitochondrial dynamics mediated AMPK protection effect, the mitochondrial fission inhibitor Mdivi-1 was utilized. We found that Mdivi-1 significantly improved MMP, inhibited ROS production, reduced the expression of *TNF- $\alpha$* , *IL-6*, *IL-1 $\beta$* , *Fis1*, and *Mff*, and improved the expression of *Mfn1* and *Mfn2*. However, the protection effect of Mdivi-1 was not reversed by AMPK inhibitor Compound C. In conclusion, this study confirmed that activation of AMPK exerted the protective effects on MIRI, which were largely dependent on the inhibition of Drp1-mediated mitochondrial fission.

**Keywords:** AMPK, DRP1, mitochondrial dynamics, myocardial ischemia/reperfusion injury, ROS, inflammatory factors



## INTRODUCTION

Acute myocardial infarction (AMI) is the global leading cause of death in cardiovascular diseases (Tibaut et al., 2017). Restore blood supply in time to ischemic myocardium is the most effective treatment for AMI. Reperfusion is a viable therapeutic strategy for ischemic heart disease with high morbidity and mortality (Ren et al., 2021). However, reperfusion may also exacerbate myocardial damage and produce a second blow to the myocardium, such as excessively generating reactive oxygen and nitrogen species (Daiber et al., 2021), increasing release of inflammatory mediators and recruitment of inflammatory cells (Toldo et al., 2018), mitochondrial  $\text{Ca}^{2+}$  overload, and the opening of the mitochondrial permeability transition pore (MPTP) (Ong et al., 2015; Basalay et al., 2020). Cardiomyocytes are rich in mitochondria, and mitochondrial dysfunction, which induces cardiomyocytes apoptosis or necrosis, eventually leads to heart injury and dysfunction (Zhang et al., 2021a). Although AMI patients may receive timely reperfusion therapy, reperfusion after revascularization of an AMI can contribute up to 50% of the resulting infarct damage (Levent et al., 2020). Therefore, exploring the molecular mechanism and new strategies for MIRI intervention are greatly needed.

Mitochondrial dysfunction is closely related to metabolic disorders, ischemic heart disease, and many other diseases (Xue et al., 2020). During MIRI, mitochondria ATP production and mitochondrial membrane potential (MMP) are decreased, while reactive oxygen species (ROS) are excessively produced, which collectively lead to myocardial damage (Hou et al., 2018). Therefore, preventing the detrimental effects of mitochondria is an important therapeutic strategy for MIRI.

AMPK, a highly conserved serine/threonine-protein kinase and also a key regulator of cellular homeostatic balance, is activated during metabolic cellular stress such as decreased oxygen or glucose supply, or increased AMP/ATP ratio (Hardie et al., 2012). Intrinsic activation of AMPK is extremely important to hold back excess mitochondrial ROS production and consequent JNK signaling activation during reperfusion (Zaha et al., 2016). Recently, sapanone A (SA) postconditioning was demonstrated to ameliorate MIRI by regulating mitochondrial quality control *via* activating AMPK (Shi et al., 2021). Calenduloside E (CE) is effective in mitigating MIRI by modulating AMPK-mediated OPA1-related mitochondrial fusion (Wang et al., 2020). These studies strongly suggest that the activation of AMPK plays a crucial role in the prevention of MIRI by regulating the mitochondrial function.

Mitochondria are highly dynamic organelles, constantly undergoing dynamic changes controlled by mitochondrial fusion and fission (Hsu et al., 2021). Disruption of dynamic balance always leads to heterogeneity and dysfunction of mitochondria (Zhang et al., 2021b). Mitochondrial dynamics are regulated by fusion and fission genes. Mitochondrial fusion is regulated by a family of GTPases including *Mfn1* and *Mfn2* (Hall et al., 2016), while mitochondrial fission is largely regulated by the *Drp1* and the *Drp1* targeting molecule fission 1 (*Fis1*)

(Vongsak et al., 2021). *Drp1*, located in the cytosol, is essential for mitochondrial fission (Bradshaw et al., 2016). During mitochondrial fission, cytosolic *Drp1* is recruited to mitochondria, binds to adaptors on mitochondrial outer membranes, and assembles into oligomers to constrict and sever mitochondrial membranes (van der Bliek et al., 2013; Yu et al., 2021). The most characteristic mechanism of post-translational modification in *Drp1* involves phosphorylation at two key sites: *Drp1* (Ser616) and *Drp1* (Ser637) (Chang and Blackstone, 2010). Excessive mitochondrial fission results in the collapse of membrane potential, the elevation of ROS production, and consequently cellular injury or death (Xu et al., 2017).

Even though AMPK may play a crucial role in the prevention of MIRI, it is largely unknown whether AMPK activation alleviates MIRI by regulating *Drp1*-mediated mitochondrial dynamics. Herein, a mouse model of MIRI *in vitro* and a H9C2 cell model of H/R were established to investigate whether AMPK activation alleviates MIRI by regulating *Drp1*-mediated mitochondrial dynamics.

## MATERIALS AND METHODS

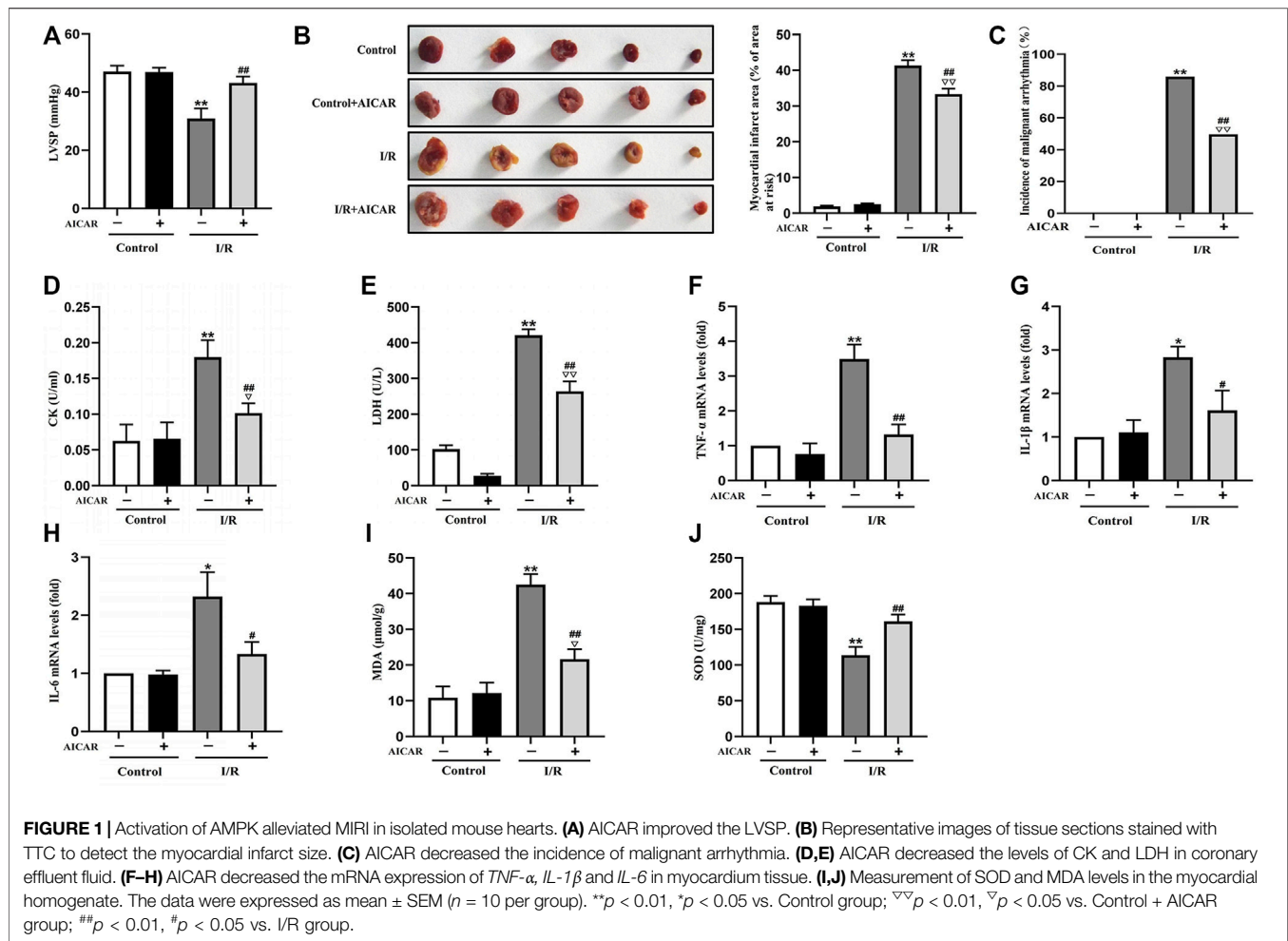
### Animals and H9C2 Cell Culture

The C57BL/6J mice (male, 20–25 g) were obtained from the Laboratory Animal Center of Henan University of Science and Technology (Luoyang, China, License number: SCXK 2020-0008). All the animal experiments were approved by the Animal Care and Ethics Committee of Henan University of Science and Technology (Luoyang, China) and performed in compliance with the guidelines for the Principles of Laboratory Animal Care and Use of Laboratory Animals published by NIH (NIH Publication, 8th Edition, 2011).

H9C2 cells were purchased from ATCC, and were cultured in a mixture of 10% fetal bovine serum (FBS) and double antibiotics (penicillin and streptomycin, 100  $\mu\text{g}/\text{ml}$ ) in Dulbecco's modified eagle medium (DMEM).

### Langendorff Perfused Heart I/R Model

Mice were intraperitoneally injected with ethyl urethane (1 g/kg) for anesthesia, and heparin (500 IU/kg) for heparinization. The hearts were taken rapidly from the thoracic cavity and fixed on the Langendorff apparatus. Isolated hearts were either continuously perfused in the control group, or balanced for 15 min, stopped perfusion for 30 min, and reperfused for 30 min to replicate the I/R experimental model. The detailed process of the MIRI model was shown in the supplementary file, **Supplementary Figure S1**. Retrograde coronary perfusion was maintained with Tyrode solution (g/L, NaCl 7.895, KCl 0.403,  $\text{MgCl}_2 \cdot 6\text{H}_2\text{O}$  0.203,  $\text{CaCl}_2$  0.200,  $\text{NaH}_2\text{PO}_4 \cdot 2\text{H}_2\text{O}$  0.052, Hepes 2.383, and glucose 1.982, PH 7.35–7.45) at constant pressure in the temperature controlled glass chamber (37.5°C). A latex balloon connected to the pressure transducer was inserted into the left ventricle. The BL-420 S biological and functional experimental system was used for monitoring heart rate, left ventricular peak pressure (LVSP), and electrocardiogram (ECG) continuously.



## Hypoxia/Reoxygenation Model in H9C2 Cells

H9C2 cells with hypoxia/reoxygenation (H/R) to mimic the I/R model *in vitro*. The hypoxic condition was achieved *via* a hypoxic incubator (95% N<sub>2</sub> and 5% CO<sub>2</sub>). The conventional culture medium was replaced with serum-free medium (100% DMEM) and incubated for 12 h in an incubator at 37°C with 95% N<sub>2</sub> and 5% CO<sub>2</sub>. Thereafter, the serum-free medium (100% DMEM) was then replaced with the conventional culture medium (90% DMEM + 10% FBS), and the cells were incubated for 12 h reoxygenation at 37°C in 95% air and 5% CO<sub>2</sub>. The cells were pre-incubated with AICAR (1 mM), Compound C (25 μM) or Mdivi-1 (50 μM) for 1 h if necessary.

## TTC Staining for Myocardial Infarction Size Measurement

The hearts were immediately taken down from the Langendorff perfusion device at the end of reperfusion, and cut into pieces about 2 mm thick, and then placed in 1% triphenyltetrazolium chloride (TTC, lot number: abs47011070, Absin) for 20 min. Then these pieces were photographed, and the area of the

non-infarct area (red) and infarct area (white) was calculated by Image-Pro Image analysis software. The percentage of infarct area to the total myocardial area was calculated according to the following formula:

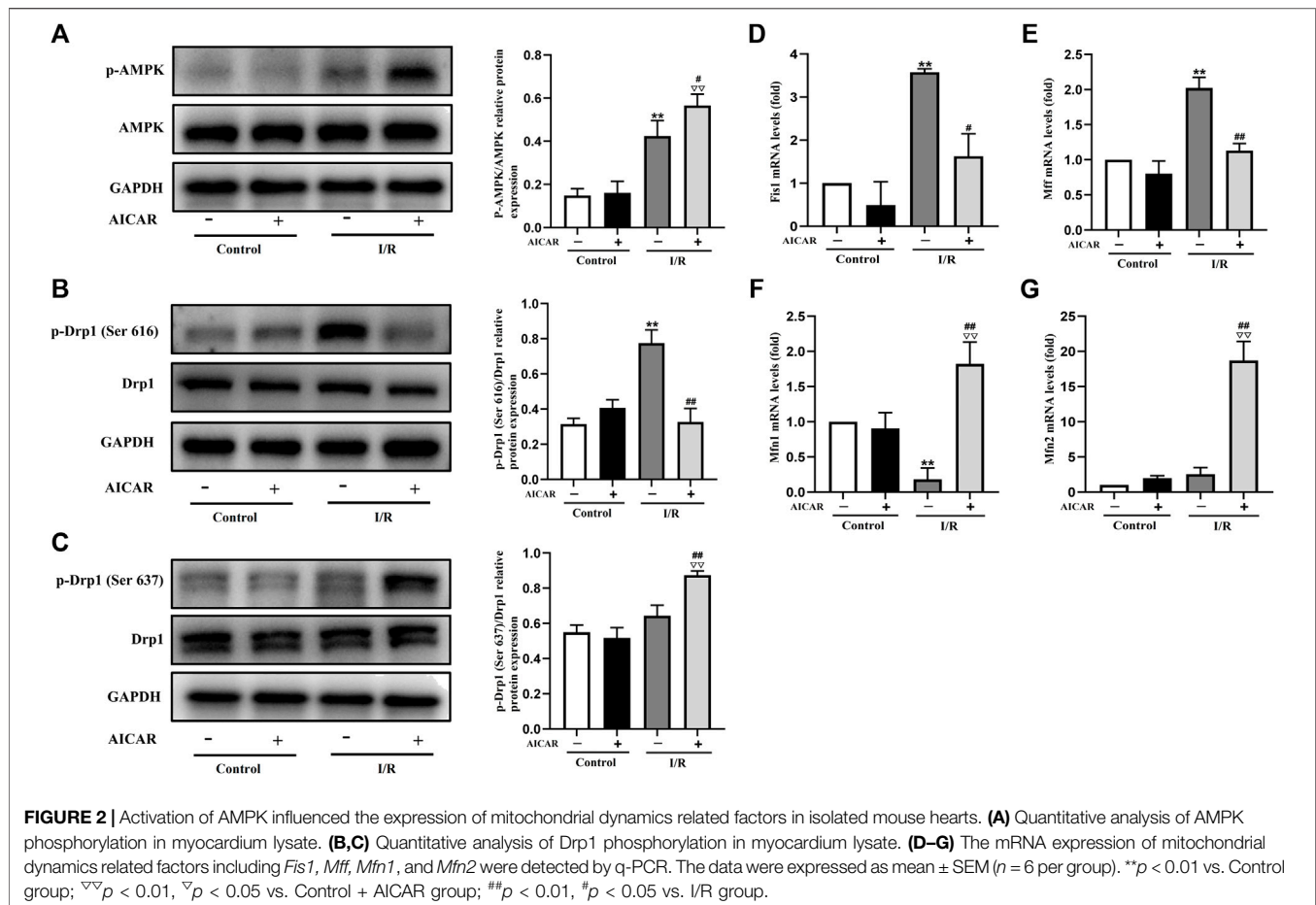
$$\text{Myocardial infarct area (\%)} = \frac{\text{myocardial infarct area}}{\text{total myocardial area}} \times 100\%$$

## Creatine Kinase and Lactate Dehydrogenase Activity Measurement

Myocardial injury was reflected by the activity of CK and LDH in the coronary effluent or the supernatant of H9C2 cell culture by using CK and LDH assay kit respectively according to the manufacturer's instructions (Nanjing Jiancheng Biotechnology, China).

## Superoxide Dismutase Activity and Malondialdehyde Content Measurement

Tissue homogenate (10%, weight/volume) was made from part of left ventricular and centrifuged at 4°C, 3,000 rpm for 15 min, and



the supernatant was obtained to detect the SOD activity and MDA content according to the manufacturer's instructions (Nanjing Jiancheng Bioengineering Institute, China).

### Intracellular ROS Assay

For intracellular ROS detection, H9C2 cells were treated with H/R, and then incubated with ROS specific fluorescent probe dye DCFH-DA (Beyotime Institute of Biotechnology, Shanghai, China) for 20 min at 37°C. Flow cytometry was performed to analyze the levels of mitochondrial ROS.

### Mitochondrial Membrane Potential Analysis

A mitochondrial membrane potential assay kit with JC-1 (Beyotime Institute of Biotechnology, Shanghai, China) was used to detect changes in the mitochondrial membrane potential by confocal laser scanning microscope (CLSM) and flow cytometry, which were performed according to the manufacturer's protocol.

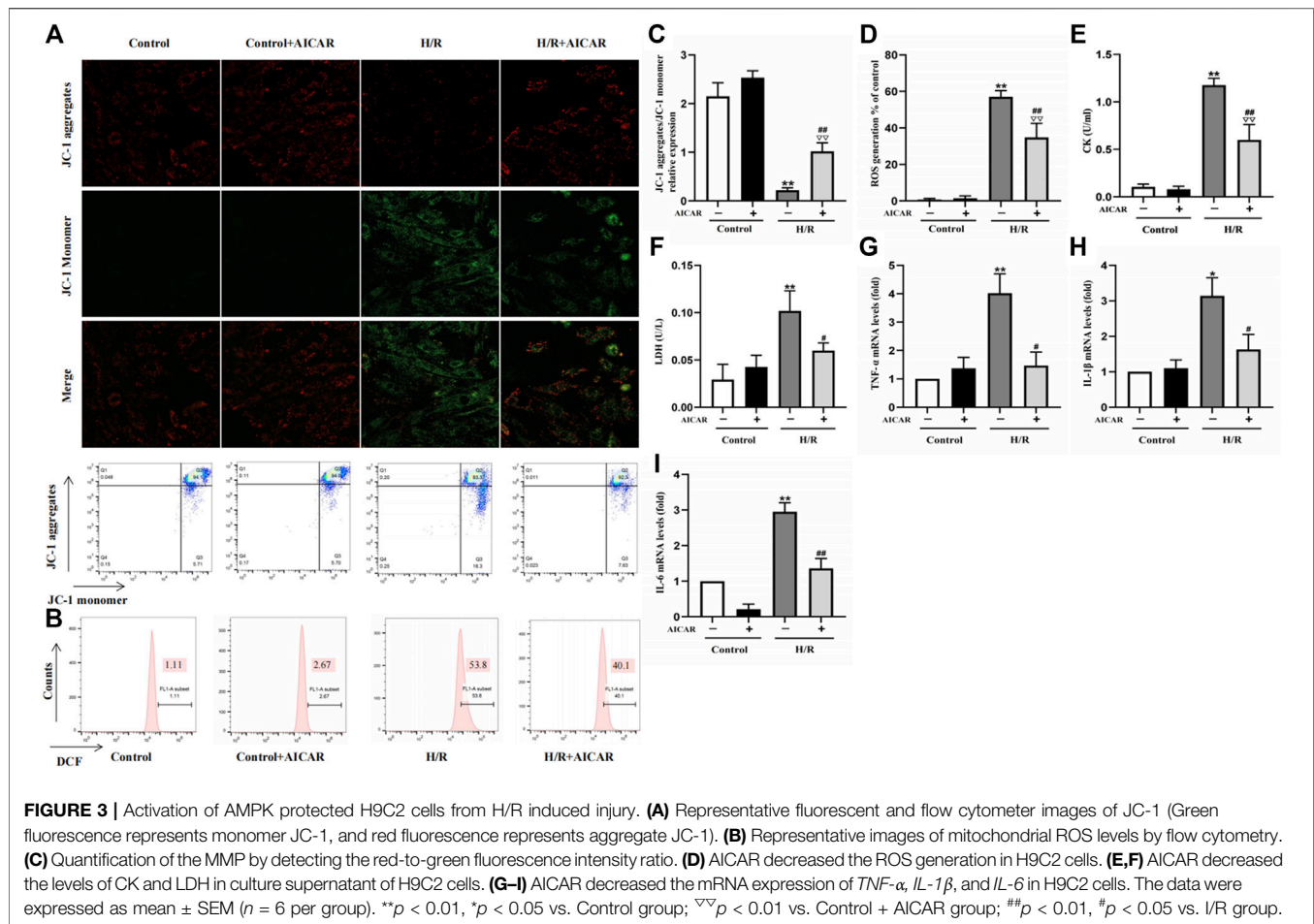
### Mitochondrial Morphological Detection by Transmission Electron Microscopy

After finishing the H/R process, the cells were collected and immediately fixation in 2.5% glutaraldehyde for 2 h, and then

soaked in 0.1 M phosphoric acid buffer for 30 min, fixed in 1% osmium tetroxide solution at 4°C for 2 h. After that, cells were dehydrated using a graded ethanol immersion series and then embedded in resin. The H9C2 cells were cut into 50–70 nm sections using an ultramicrotome (UC7, Leica), and stained with uranium acetate and lead citrate, and finally observed using an electron microscope (H-7650, HITACHI).

### Western Blot Analysis

The tissue or cell total proteins were extracted with lysis buffer (RIPA) containing protein phosphatase inhibitor (Beijing Solar Science & Technology Co., Ltd.). As reported, the quantity of protein was measured by the BCA method (Sangon Bioengineering, Shanghai). Denatured protein samples (30  $\mu$ g) were subjected to SDS-PAGE. After electrophoresis, protein was transferred to PVDF membranes, which were then blocked for 1 h by 5% nonfat dry milk in TBS-T (mM, Tris-base 24.8, NaCl 136.8, KCl 2.7, 0.1% Tween-20, pH 7.4) and subsequently incubated with primary antibody in 5% nonfat dry milk at 4°C overnight. After washing thrice with TBS-T, the membranes were incubated with anti-rabbit or anti-mouse horseradish peroxidase-conjugated secondary antibodies (1:5000 dilutions) for 1 h. The signal was detected by chemiluminescence using the ECL detection system (Amersham) (Du et al., 2020). The same



procedure was repeated for AMPK (1:1000), p-AMPK (1:1000), p-Drp1 (Ser 616) (1:1000), p-Drp1 (Ser 637), (1:1000), Drp1 (1:1000), and GAPDH (1:5000) at 4°C overnight. GAPDH was used as a loading control for total protein. Quantification of bands was performed using ImageJ Software (NIH).

## Quantitative Real-Time Polymerase Chain Reaction

Total RNA was extracted from the tissue or cells using TRIzol reagent (TaKaRa Bio, Dalian, China) and reverse-transcribed using a high-capacity complementary DNA reverse transcription kit (CWBio, Beijing, China). qPCR was performed on the 7,500 Sequence Detection System (Applied Biosystems, Foster City, CA, United States) by using SYBR™ Green PCR Master Mix kit (CWBio, Beijing, China) according to the manufacturer's protocol. The reaction system was as follows: 10 min at 95°C and then 15 s at 95°C and 1 min at 60°C for 40 cycles. The expression of inflammatory factor including tumor necrosis factor-α (*TNF-α*), Interleukin-6 (*IL-6*), Interleukin-1β (*IL-1β*), and mitochondrial dynamics regulators including *Fis1*, *Mff*, *Mfn1*, and *Mfn2* were quantified. The primers used in the present study were listed in supplementary file **Supplementary Table S1**. The  $2^{-\Delta\Delta Ct}$

method was used to quantify the genes, and *β-actin* gene was used as the internal control.

## Statistical Analysis

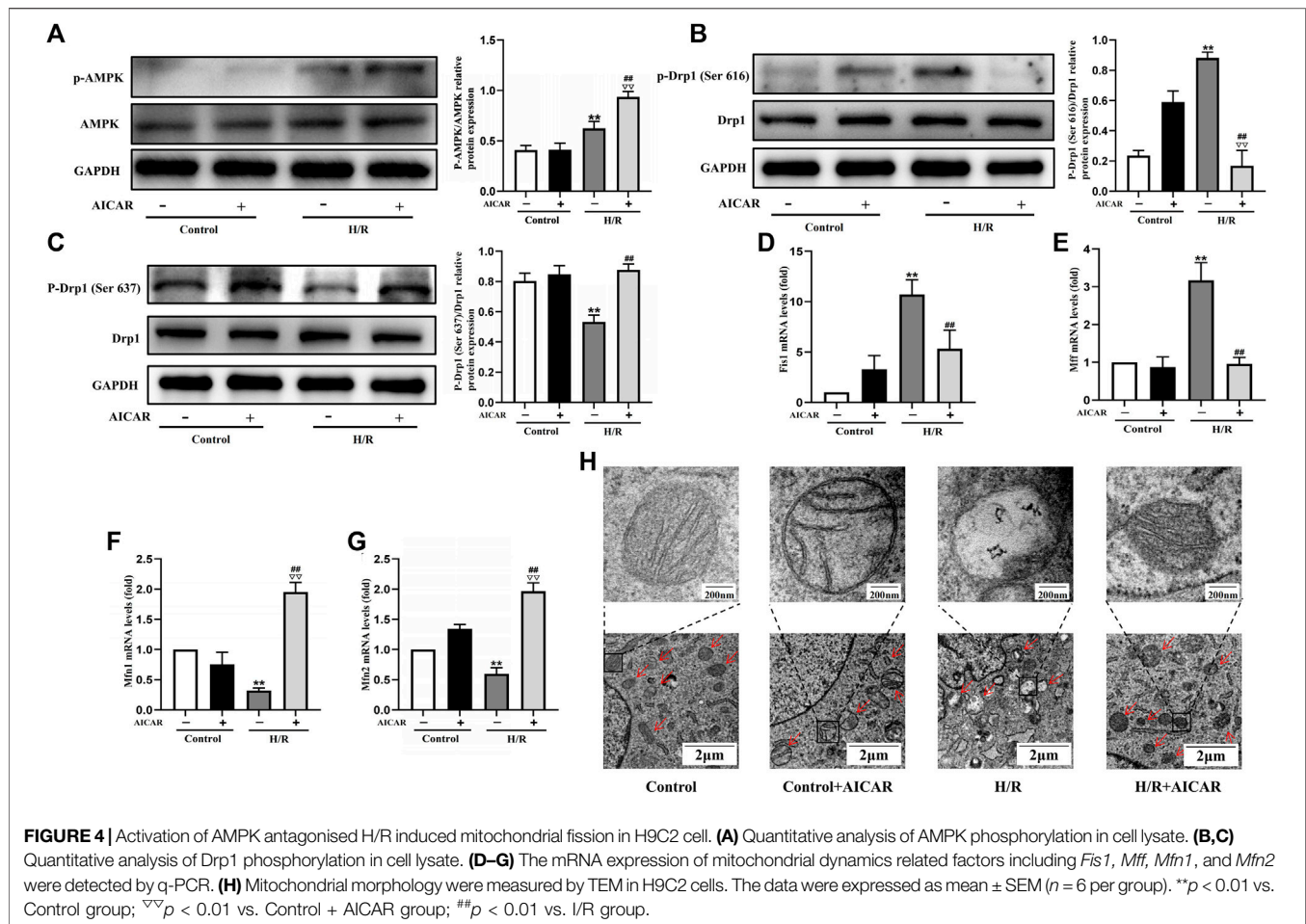
Data were expressed as means ± SEM. All experimental data were analyzed by using a one-way analysis of variance (ANOVA) followed by a Tukey multiple comparison test. A level of *p* < 0.05 was considered to be a statistically significant difference.

## RESULTS

### Activation of AMPK Alleviated MIRI in Isolated Mouse Hearts

AICAR, an AMPK agonist, was first examined for its effects on MIRI. As shown in **Figure 1**, in the isolated mouse heart model, there were no significant differences of LVSP at baseline among the different groups. AICAR treatment significantly improved LVSP (**Figure 1A**), reduced the incidence of malignant arrhythmia (**Figure 1C**), and decreased myocardial infarct size in mice subjected to I/R treatment (**Figure 1B**). AICAR also reduced CK and LDH levels of the coronary effluent in the I/R group significantly (**Figures 1D,E**). The mRNA expression levels of *TNF-α*, *IL-6*, and *IL-1β* in myocardial tissue were determined,





and the results showed that AICAR decreased the mRNA levels of *TNF- $\alpha$* , *IL-1 $\beta$* , and *IL-6* in myocardial tissue (Figures 1F–H). SOD is one of the most important antioxidant enzymes in myocardial tissue, and MDA reflects the level of lipid peroxidation. Our results showed that AICAR increased SOD activity (Figure 1J) and decreased MDA content after myocardial I/R (Figure 1I). Taken together, these results suggested that AICAR could alleviate I/R-induced myocardial tissue damage.

### Activation of AMPK Influenced the Expression of Mitochondrial Dynamics Related Factors in Isolated Mouse Hearts

Mitochondrial dynamic balance is critical for mitochondrial homeostasis. To determine the possible mechanisms of AMPK protecting against MIRI, the expression levels of mitochondrial dynamics related factors were examined by western blot or qPCR technique. As expected, AICAR significantly increased the phosphorylation level of AMPK (Figure 2A), and at the same time, the results showed that the phosphorylation level of Drp1 (Ser 637) increased (Figure 2C), while the phosphorylation level of Drp1 (Ser 616) decreased (Figure 2B). Correspondingly, we examined mitochondrial fusion and fission genes, and the results showed that AICAR could reduce the mRNA expression of

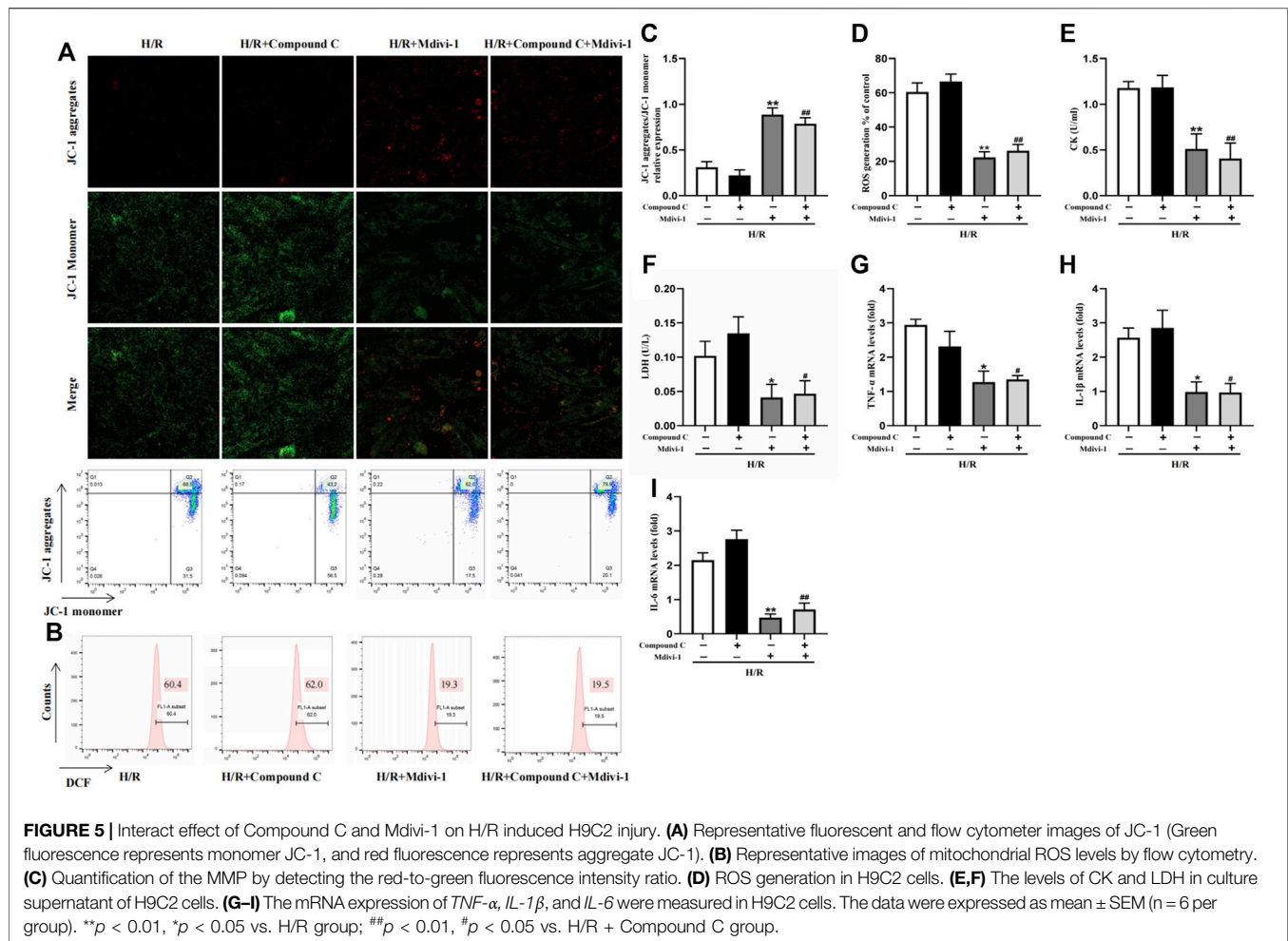
mitochondrial fission factors such as *Fis1* and *Mff* (Figures 2D,E), and promote the mRNA expression of mitochondrial fusion factors such as *Mfn1* and *Mfn2* (Figures 2F,G).

### Activation of AMPK Protected H9C2 Cells From H/R Induced Injury

As shown in Figure 3, MMP was reduced after H/R treatment in H9C2 cells (Figures 3A,C), while ROS generation was significantly increased (Figures 3B,D). AICAR treatment reversed these trends, which could improve MMP and reduce ROS levels significantly. At the same time, AICAR significantly reduced CK and LDH levels in the cell culture medium after H/R treatment (Figures 3E,F). Next, we detected the mRNA levels of inflammation factors including *TNF- $\alpha$* , *IL-1 $\beta$* , and *IL-6* in H9C2 cells after H/R treatment. The results showed that AICAR significantly decreased the mRNA levels of *TNF- $\alpha$* , *IL-1 $\beta$* , and *IL-6* in H9C2 cells (Figures 3G–I).

### Activation of AMPK Antagonised H/R Induced Mitochondrial Fission in H9C2 Cell

To determine the underlying mechanism of AMPK activation in protecting the cardiomyocytes, we evaluated the effect of AMPK activation on mitochondrial morphology and mitochondrial



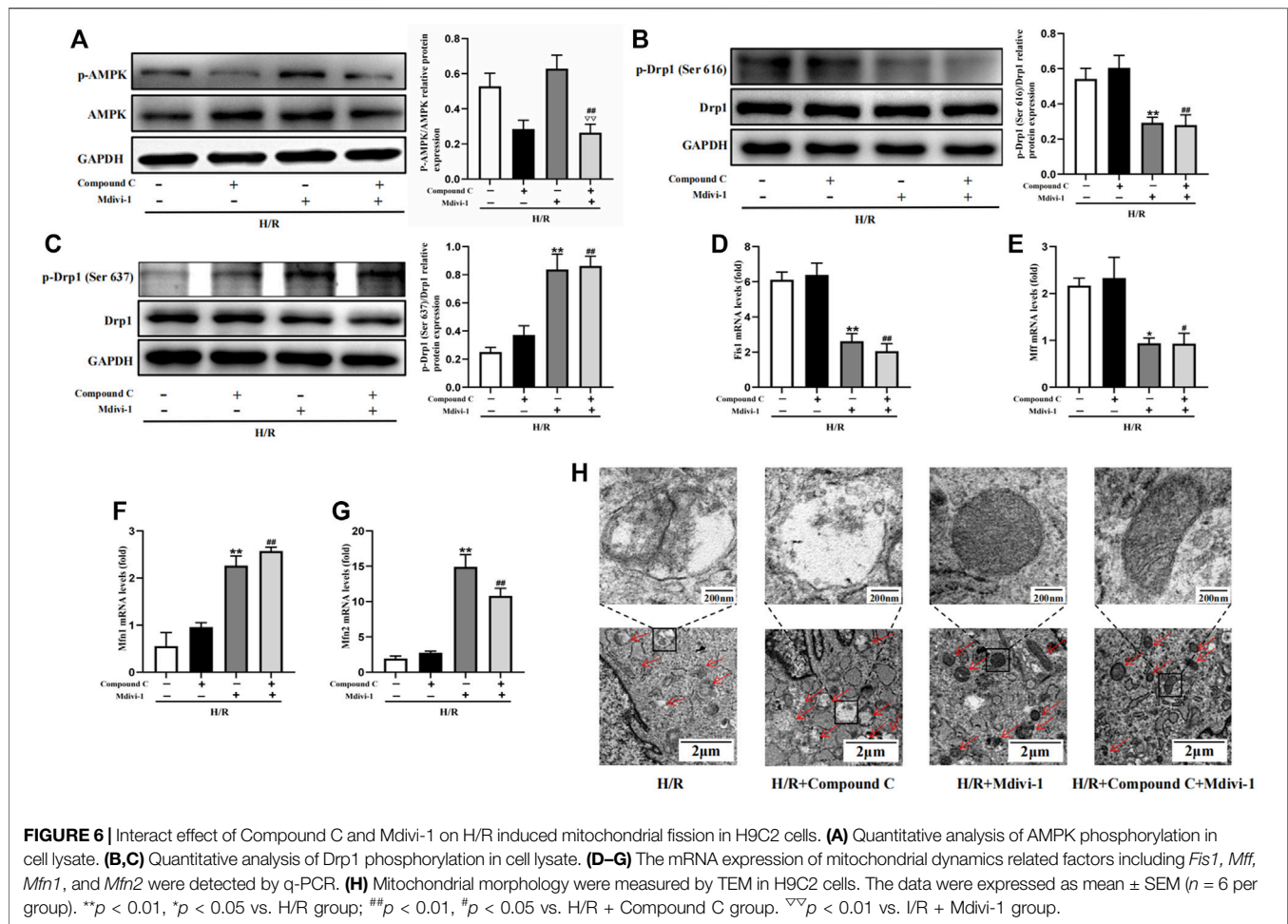
dynamic related factors in H9C2 cells. We found that H/R treatment triggered the increased phosphorylation of Drp1 at Ser 616, with a decreased phosphorylation of Drp1 at Ser 637. Compared with the H/R group, AICAR, an agonist of AMPK (Figure 4A), inhibited the phosphorylation of Drp1 at Ser 616 and increased the phosphorylation of Drp1 at Ser 637 significantly (Figures 4B,C). Next, we detected mitochondrial fusion and fission factors by qPCR, and the results were similar to those in animal experiments, which showed that AICAR reduced the expression of mitochondrial fission factors such as *Fis1*, *Mff* (Figures 4D,E), and promoted the expression of mitochondrial fusion factors such as *Mfn1* and *Mfn2* (Figures 4F,G). Considering that mitochondrial ultrastructure impairment is an early symbol of mitochondrial damage, mitochondrial morphology was further observed by TEM. The results showed that the outer membrane of mitochondria ruptured massively after H/R treatment, with mitochondrial fragmentation increases, and the mitochondrial cristae disappearance, even severe vacuolization. AICAR could restore the morphology of mitochondria, that is, reduced the outer membrane rupture of mitochondria and mitochondrial vacuolization, and reappearance of mitochondrial cristae (Figure 4H).

### AMPK Inhibitor Couldn't Block the Protection of Mitochondrial Fission Inhibitor Mdivi-1 on H/R Induced Injury in H9C2 Cells

Mdivi-1, the selective Drp1 inhibitor, was used to verify the excessive mitochondrial fission was vital in MIRI. Compared with the H/R group, Mdivi-1 caused a sharp rise in MMP (Figures 5A,C) and a dramatic decline in ROS production (Figures 5B,D). At the same time, CK and LDH levels also decreased (Figures 5E,F). Meanwhile, Mdivi-1 treatment also decreased the mRNA levels of inflammatory factors such as *TNF-α*, *IL-1β*, and *IL-6* in cells (Figures 5G-I). Furthermore, after the cells were co-incubated with Mdivi-1 and Compound C, which was the AMPK inhibitor, the results showed that Compound C couldn't block the protection effect of Mdivi-1 on H/R induced cell injury, and there was no statistically significant compared with Mdivi-1 alone.

### AMPK Inhibitor Couldn't Block the Effect of Mdivi-1 on H/R Induced Mitochondrial Fission in H9C2 Cells

Firstly, Mdivi-1 was used to investigate its effects on the expression of mitochondrial dynamic related factors. Compared with the H/R group, Mdivi-1 treatment reduced the phosphorylation of Drp1(Ser 616)



significantly, and increased the phosphorylation of Drp1(Ser 637) (Figure 6B,C). Moreover, the qPCR results showed that Mdivi-1 reduced the mRNA expression of mitochondrial fission factors such as *Fis1* and *Mff* (Figure 6D, E), and promoted the mRNA expression of mitochondrial fusion factors such as *Mfn1* and *Mfn2* (Figure 6F,G). Secondly, as the selective AMPK inhibitor, Compound C was used to further verify that Drp1-mediated mitochondrial dynamics was the downstream of AMPK signaling. As expected, Compound C inhibited the phosphorylation of AMPK in cells (Figure 6A), while it couldn't reverse the effects of Mdivi-1 on Drp1 signaling and mitochondrial dynamic related factors when co-incubated with Mdivi-1 and Compound C in H9C2 cells.

Furthermore, mitochondrial morphology was further observed by TEM, the results showed that Mdivi-1 could restore the mitochondrial morphology after H/R treatment, such as reducing the outer membrane rupture and vacuolation of mitochondria, and reappearance of mitochondrial cristae. When co-incubation with Mdivi-1 and Compound C, the latter couldn't reverse the protective effects of Mdivi-1 on mitochondrial morphology (Figure 6H).

## DISCUSSION

AMPK, a key energy sensor that regulates cellular metabolism to maintain energy homeostasis, has been reported to have multiple

organ protection functions (Trefts and Shaw, 2021). Although previous studies have indicated that the AMPK agonist AICAR decreased cardiomyocyte apoptosis, improved cardiac function, and inhibited MIRI (Fan et al., 2021), the specific mechanism remains unclear. In the present study, the effects of AICAR were examined to determine whether the activation of AMPK signaling could protect the heart against MIRI, and to explore the potential mechanism. The results showed that AICAR could protect heart or H9C2 cells from I/R or H/R-induced injury by activating the AMPK signaling, which exerted a beneficial effect on mitochondrial dynamics, enhanced mitochondrial fusion, and inhibited mitochondrial fission, which ultimately reduced the myocardial infarct size and improved left ventricular dysfunction.

Unbalanced mitochondrial dynamics is a fatal factor causing mitochondrial dysfunction and cardiomyocyte apoptosis during MIRI (Maneechote et al., 2019; Xue et al., 2020). Drp1 is the main functional protein mediating mitochondrial dynamic changes. Under stress, Drp1 can be recruited to the outer membrane of mitochondria and thus trigger the division of mitochondria (Zheng et al., 2019; Sun et al., 2021). The function of Drp1 is regulated by phosphorylation, acetylation, glycosylation, etc. (Hu et al., 2020; Sun et al., 2021). Studies have shown that phosphorylation of Drp1 at Ser 616 accelerated its recruitment to the mitochondrial membrane, while phosphorylation at Ser



637 hindered this process (Wu et al., 2020). Excessive mitochondrial translocation of Drp1 not only triggered mitochondrial fragmentation elevation, but also led to increased mitochondrial ROS generation. Meanwhile, Cytochrome C (CytC) was released into the cytoplasm, therefore triggering inflammatory response and cell apoptosis (Xu et al., 2016; Sun et al., 2021). Given the detrimental effect of sustained mitochondrial fission in ischemic heart disease, exploring new ways to attenuate Drp1-mediated mitochondrial fission is of clinical interest to combat MIRI.

In the present study, we confirmed that I/R or H/R treatment led to an imbalance of mitochondrial dynamic genes. As the qPCR results showed, the expression of mitochondrial fission factors such as *Mff* and *Fis1* increased significantly, conversely, the expression of mitochondrial fusion factors such as *Mfn1* or *Mfn2* decreased. Meanwhile, mitochondrial morphology shown by TEM further confirmed that mitochondrial fragmentation increased and mitochondria were damaged. This meant that I/R or H/R treatment induced imbalance of mitochondrial dynamic and function. The AMPK pathway was the classic downstream target of AICAR (Ahmad et al., 2021). We found AICAR could reverse these imbalances, which inhibited the expression of mitochondrial fission factors such as *Mff* and *Fis1*, and enhanced the expression of mitochondrial fusion factors such as *Mfn1* and *Mfn2*, and then maintaining the balance of mitochondrial dynamic and function, thereby inhibiting mitochondrial ROS production and inflammatory reactions. At the protein level, AICAR inhibited the phosphorylation of mitochondrial fission-associated proteins Drp1 (Ser 616), and enhanced the phosphorylation of mitochondrial fusion-associated proteins Drp1 (Ser 637) both in the mouse model of MIRI and in the cell model of H/R. Overall, these results indicated the association between AMPK signaling and Drp1 mediated mitochondrial dynamics, which was consistent with the previous reports (Sun et al., 2021).

To further verify that Drp1-mediated mitochondrial dynamics was regulated by AMPK signaling, firstly, we used Mdivi-1 to pretreat the cells, which was the mitochondrial fission inhibitor. Results showed that Mdivi-1 protected cardiomyocytes and restored the mitochondrial dynamics balance just as the AICAR did. Secondly, we used Compound C, a selective inhibitor of AMPK, we found that the protective effects of Mdivi-1 on cardiomyocytes and mitochondria were almost unaffected when they were co-incubated. These studies indicated that it was possible to regulate the phosphorylation of Drp1 as a potential therapeutic target for protecting the mitochondria and cardiomyocytes under MIRI, and AICAR suppressed Drp1-mediated mitochondrial damage dependent on AMPK signaling.

## REFERENCES

- Ahmad, I., Molyvdas, A., Jian, M.-Y., Zhou, T., Traylor, A. M., Cui, H., et al. (2021). AICAR Decreases Acute Lung Injury by Phosphorylating AMPK and Upregulating Heme Oxygenase-1. *Eur. Respir. J.* 58, 2003694. doi:10.1183/13993003.2003694-2020
- Basalay, M. V., Yellon, D. M., and Davidson, S. M. (2020). Targeting Myocardial Ischaemic Injury in the Absence of Reperfusion. *Basic Res. Cardiol.* 115, 63. doi:10.1007/s00395-020-00825-9
- Bradshaw, T. Y., Romano, L. E., Duncan, E. J., Nethisinghe, S., Abeti, R., Michael, G. J., et al. (2016). A Reduction in Drp1-Mediated Fission Compromises

## CONCLUSION

In summary, in the present report, the experiments were performed to investigate the protective mechanism of AMPK activation on MIRI. Our findings demonstrated that AICAR protected cardiomyocytes and mitochondria by activating AMPK signaling, which depended on Drp1-mediated mitochondrial dynamics. Our results not only provide a theoretical foundation for exploring the mechanism but also put forward a promising treatment target for MIRI.

## DATA AVAILABILITY STATEMENT

The original contributions presented in the study are included in the article/Supplementary Material, further inquiries can be directed to the corresponding author.

## ETHICS STATEMENT

The animal study was reviewed and approved by the Animal Care and Ethics Committee of Henan University of Science and Technology.

## AUTHOR CONTRIBUTIONS

JD designed the experiments and wrote the manuscript. HL, JS, TW, YD, and AZ carried out the experiments and analyzed the data. YL and GL supervised and corrected the manuscript.

## FUNDING

The present study was supported by the Henan Province Scientific and Technology Research Project, and Natural Science Foundation of Henan Province (Grant No. 222102310437, 202300410150).

## SUPPLEMENTARY MATERIAL

The Supplementary Material for this article can be found online at: <https://www.frontiersin.org/articles/10.3389/fphar.2022.862204/full#supplementary-material>

- Mitochondrial Health in Autosomal Recessive Spastic Ataxia of Charlevoix Saguenay. *Hum. Mol. Genet.* 25, 3232–3244. doi:10.1093/hmg/ddw173
- Chang, C. R., and Blackstone, C. (2010). Dynamic Regulation of Mitochondrial Fission through Modification of the Dynamin-Related Protein Drp1. *Ann. N. Y. Acad. Sci.* 1201, 34–39. doi:10.1111/j.1749-6632.2010.05629.x
- Daiber, A., Andreadou, I., Oelze, M., Davidson, S. M., and Hausenloy, D. J. (2021). Discovery of New Therapeutic Redox Targets for Cardioprotection against Ischemia/reperfusion Injury and Heart Failure. *Free Radic. Biol. Med.* 163, 325–343. doi:10.1016/j.freeradbiomed.2020.12.026
- Du, J., He, W., Zhang, C., Wu, J., Li, Z., Wang, M., et al. (2020). Pentamethylquercetin Attenuates Cardiac Remodeling via Activation of the



- Sestrins/Keap1/Nrf2 Pathway in MSG-Induced Obese Mice. *Biomed. Res. Int.* 2020, 3243906. doi:10.1155/2020/3243906
- Fan, H. W., Ding, R., Liu, W., Zhang, X., Li, R., Wei, B., et al. (2021). Heat Shock Protein 22 Modulates NRF1/TFAM-dependent Mitochondrial Biogenesis and DRP1-Sparked Mitochondrial Apoptosis through AMPK-Pgc1 $\alpha$  Signaling Pathway to Alleviate the Early Brain Injury of Subarachnoid Hemorrhage in Rats. *Redox Biol.* 40, 101856. doi:10.1016/j.redox.2021.101856
- Hall, A. R., Burke, N., Dongworth, R. K., Kalkhoran, S. B., Dyson, A., Vicencio, J. M., et al. (2016). Hearts Deficient in Both Mfn1 and Mfn2 Are Protected against Acute Myocardial Infarction. *Cell. Death Dis.* 7, e2238. doi:10.1038/cddis.2016.139
- Hardie, D. G., Ross, F. A., and Hawley, S. A. (2012). AMPK: a Nutrient and Energy Sensor that Maintains Energy Homeostasis. *Nat. Rev. Mol. Cell. Biol.* 13, 251–262. doi:10.1038/nrm3311
- Hou, H., Wang, Y., Li, Q., Li, Z., Teng, Y., Li, J., et al. (2018). The Role of RIP3 in Cardiomyocyte Necrosis Induced by Mitochondrial Damage of Myocardial Ischemia-Reperfusion. *Acta Biochim. Biophys. Sin. (Shanghai)* 50, 1131–1140. doi:10.1093/abbs/gmy108
- Hsu, C. C., Zhang, X., Wang, G., Zhang, W., Cai, Z., Pan, B. S., et al. (2021). Inositol Serves as a Natural Inhibitor of Mitochondrial Fission by Directly Targeting AMPK. *Mol. Cell.* 81, 3803–e7. doi:10.1016/j.molcel.2021.08.025
- Hu, Q., Gutiérrez Cortés, N., Wu, D., Wang, P., Zhang, J., Mattison, J. A., et al. (2020). Increased Drp1 Acetylation by Lipid Overload Induces Cardiomyocyte Death and Heart Dysfunction. *Circ. Res.* 126, 456–470. doi:10.1161/circresaha.119.315252
- Levent, E., Noack, C., Zelarayán, L. C., Katschinski, D. M., Zimmermann, W. H., and Tiburcy, M. (2020). Inhibition of Prolyl-Hydroxylase Domain Enzymes Protects from Reoxygenation Injury in Engineered Human Myocardium. *Circulation* 142, 1694–1696. doi:10.1161/circulationaha.119.044471
- Maneechote, C., Palee, S., Kerdphoo, S., Jaiwongkam, T., Chattipakorn, S. C., and Chattipakorn, N. (2019). Balancing Mitochondrial Dynamics via Increasing Mitochondrial Fusion Attenuates Infarct Size and Left Ventricular Dysfunction in Rats with Cardiac Ischemia/reperfusion Injury. *Clin. Sci. Lond.* 133, 497–513. doi:10.1042/cs20190014
- Ong, S. B., Samangouei, P., Kalkhoran, S. B., and Hausenloy, D. J. (2015). The Mitochondrial Permeability Transition Pore and its Role in Myocardial Ischemia Reperfusion Injury. *J. Mol. Cell. Cardiol.* 78, 23–34. doi:10.1016/j.yjmcc.2014.11.005
- Ren, D., Fedorova, J., Davitt, K., Van Le, T. N., Griffin, J. H., Liaw, P. C., et al. (2022). Activated Protein C Strengthens Cardiac Tolerance to Ischemic Insults in Aging. *Circ. Res.* 130, 252–272. doi:10.1161/circresaha.121.319044
- Shi, X., Li, Y., Wang, Y., Ding, T., Zhang, X., and Wu, N. (2021). Pharmacological Postconditioning with Sappanone A Ameliorates Myocardial Ischemia Reperfusion Injury and Mitochondrial Dysfunction via AMPK-Mediated Mitochondrial Quality Control. *Toxicol. Appl. Pharmacol.* 427, 115668. doi:10.1016/j.taap.2021.115668
- Sun, J., Liu, X., Shen, C. a., Zhang, W., and Niu, Y. (2021). Adiponectin Receptor Agonist AdipoRon Blocks Skin Inflamm-aging by Regulating Mitochondrial Dynamics. *Cell. Prolif.* 54, e13155. doi:10.1111/cpr.13155
- Tibaut, M., Mekis, D., and Petrovic, D. (2017). Pathophysiology of Myocardial Infarction and Acute Management Strategies. *Cardiovasc Hematol. Agents Med. Chem.* 14, 150–159. doi:10.2174/1871525714666161216100553
- Toldo, S., Mauro, A. G., Cutter, Z., and Abbate, A. (2018). Inflammasome, Pyroptosis, and Cytokines in Myocardial Ischemia-Reperfusion Injury. *Am. J. Physiol. Heart Circ. Physiol.* 315, H1553–H68. doi:10.1152/ajpheart.00158.2018
- Trefts, E., and Shaw, R. J. (2021). AMPK: Restoring Metabolic Homeostasis over Space and Time. *Mol. Cell.* 81, 3677–3690. doi:10.1016/j.molcel.2021.08.015
- van der Blik, A. M., Shen, Q., and Kawajiri, S. (2013). Mechanisms of Mitochondrial Fission and Fusion. *Cold Spring Harb. Perspect. Biol.* 5, 5. doi:10.1101/cshperspect.a011072
- Vongsak, J., Prachayasakul, W., Apaijai, N., Vaniyapong, T., Chattipakorn, N., and Chattipakorn, S. C. (2021). The Alterations in Mitochondrial Dynamics Following Cerebral Ischemia/Reperfusion Injury. *Antioxidants* 10, 1384. doi:10.3390/antiox10091384
- Wang, M., Wang, R. Y., Zhou, J. H., Xie, X. H., Sun, G. B., and Sun, X. B. (2020). Calendulose E Ameliorates Myocardial Ischemia-Reperfusion Injury through Regulation of AMPK and Mitochondrial OPA1. *Oxidative Med. Cell. Longev.* 2020, 1–12. doi:10.1155/2020/2415269
- Wu, X., Cui, W. W., Guo, W., Liu, H., Luo, J., Zhao, L., et al. (2020). Acrolein Aggravates Secondary Brain Injury after Intracerebral Hemorrhage through Drp1-Mediated Mitochondrial Oxidative Damage in Mice. *Neurosci. Bull.* 36, 1158–1170. doi:10.1007/s12264-020-00505-7
- Xu, S., Pi, H., Zhang, L., Zhang, N., Li, Y., Zhang, H., et al. (2016). Melatonin Prevents Abnormal Mitochondrial Dynamics Resulting from the Neurotoxicity of Cadmium by Blocking Calcium-dependent Translocation of Drp1 to the Mitochondria. *J. Pineal Res.* 60, 291–302. doi:10.1111/jpi.12310
- Xu, Y., Wang, Y., Wang, G., Ye, X., Zhang, J., Cao, G., et al. (2017). YiQiFuMai Powder Injection Protects against Ischemic Stroke via Inhibiting Neuronal Apoptosis and PKC $\delta$ /Drp1-Mediated Excessive Mitochondrial Fission. *Oxidative Med. Cell. Longev.* 2017, 1–17. doi:10.1155/2017/1832093
- Xue, W., Wang, X., Tang, H., Sun, F., Zhu, H., Huang, D., et al. (2020). Vitexin Attenuates Myocardial Ischemia/reperfusion Injury in Rats by Regulating Mitochondrial Dysfunction Induced by Mitochondrial Dynamics Imbalance. *Biomed. Pharmacother.* 124, 109849. doi:10.1016/j.biopha.2020.109849
- Yu, R., Jin, S.-B., Ankarcona, M., Lendahl, U., Nistér, M., and Zhao, J. (2021). The Molecular Assembly State of Drp1 Controls its Association with the Mitochondrial Recruitment Receptors Mff and MIEF1/2. *Front. Cell. Dev. Biol.* 9, 706687. doi:10.3389/fcell.2021.706687
- Zaha, V. G., Qi, D., Su, K. N., Palmeri, M., Lee, H. Y., Hu, X., et al. (2016). AMPK Is Critical for Mitochondrial Function during Reperfusion after Myocardial Ischemia. *J. Mol. Cell. Cardiol.* 91, 104–113. doi:10.1016/j.yjmcc.2015.12.032
- Zhang, K., Guo, M.-Y., Li, Q.-G., Wang, X.-H., Wan, Y.-Y., Yang, Z.-J., et al. (2021a). Drp1-dependent Mitochondrial Fission Mediates Corneal Injury Induced by Alkali Burn. *Free Radic. Biol. Med.* 176, 149–161. doi:10.1016/j.freeradbiomed.2021.09.019
- Zhang, Y., Ren, X., Wang, Y., Chen, D., Jiang, L., Li, X., et al. (2021b). Targeting Ferroptosis by Polydopamine Nanoparticles Protects Heart against Ischemia/reperfusion Injury. *ACS Appl. Mat. Interfaces* 13, 53671–53682. doi:10.1021/acsami.1c18061
- Zheng, X., Qian, Y., Fu, B. D., Jiao, D., Jiang, Y., Chen, P., et al. (2019). Mitochondrial Fragmentation Limits NK Cell-Based Tumor Immunosurveillance. *Nat. Immunol.* 20, 1656–1667. doi:10.1038/s41590-019-0511-1

**Conflict of Interest:** The authors declare that the research was conducted in the absence of any commercial or financial relationships that could be construed as a potential conflict of interest.

**Publisher's Note:** All claims expressed in this article are solely those of the authors and do not necessarily represent those of their affiliated organizations, or those of the publisher, the editors and the reviewers. Any product that may be evaluated in this article, or claim that may be made by its manufacturer, is not guaranteed or endorsed by the publisher.

Copyright © 2022 Du, Li, Song, Wang, Dong, Zhan, Li and Liang. This is an open-access article distributed under the terms of the Creative Commons Attribution License (CC BY). The use, distribution or reproduction in other forums is permitted, provided the original author(s) and the copyright owner(s) are credited and that the original publication in this journal is cited, in accordance with accepted academic practice. No use, distribution or reproduction is permitted which does not comply with these terms.



# AKT/PACS2 Participates in Renal Vascular Hyperpermeability by Regulating Endothelial Fatty Acid Oxidation in Diabetic Mice

Zhihao Shu<sup>1,2</sup>, Shuhua Chen<sup>3</sup>, Hong Xiang<sup>4</sup>, Ruoru Wu<sup>5</sup>, Xuewen Wang<sup>2</sup>, Jie Ouyang<sup>2</sup>, Jing Zhang<sup>2</sup>, Huiqin Liu<sup>2</sup>, Alex F. Chen<sup>6</sup> and Hongwei Lu<sup>1,2\*</sup>

<sup>1</sup>Health Management Center, Third Xiangya Hospital of Central South University, Changsha, China, <sup>2</sup>Department of Cardiology, Third Xiangya Hospital of Central South University, Changsha, China, <sup>3</sup>Department of Biochemistry, School of Life Sciences, Central South University, Changsha, China, <sup>4</sup>Center for Experimental Medicine, Third Xiangya Hospital of Central South University, Changsha, China, <sup>5</sup>Xiangya School of Medicine, Central South University, Changsha, China, <sup>6</sup>Institute for Cardiovascular Development and Regenerative Medicine, Xinhua Hospital Affiliated to Shanghai Jiaotong University School of Medicine, Shanghai, China

## OPEN ACCESS

### Edited by:

Xianwei Wang,  
Xinxiang Medical University, China

### Reviewed by:

Long Zhao,  
The Affiliated Hospital of Qingdao  
University, China  
Xiangyang Zhu,  
Mayo Clinic, United States  
Wenyan Gong,  
Hangzhou Normal University, China

### \*Correspondence:

Hongwei Lu  
hongweilu@csu.edu.cn

### Specialty section:

This article was submitted to  
Cardiovascular and Smooth Muscle  
Pharmacology,  
a section of the journal  
Frontiers in Pharmacology

**Received:** 16 February 2022

**Accepted:** 16 June 2022

**Published:** 05 July 2022

### Citation:

Shu Z, Chen S, Xiang H, Wu R,  
Wang X, Ouyang J, Zhang J, Liu H,  
Chen AF and Lu H (2022) AKT/PACS2  
Participates in Renal Vascular  
Hyperpermeability by Regulating  
Endothelial Fatty Acid Oxidation in  
Diabetic Mice.  
Front. Pharmacol. 13:876937.  
doi: 10.3389/fphar.2022.876937

Diabetes is a chronic metabolic disorder that can cause many microvascular and macrovascular complications, including diabetic nephropathy. Endothelial cells exhibit phenotypic and metabolic diversity and are affected by metabolic disorders. Whether changes in endothelial cell metabolism affect vascular endothelial function in diabetic nephropathy remains unclear. In diabetic mice, increased renal microvascular permeability and fibrosis, as well as increased MAMs and PACS2 in renal endothelial cells, were observed. Mice lacking PACS2 improved vascular leakage and glomerulosclerosis under high fat diet. *In vitro*, PACS2 expression, VE-cadherin internalization, fibronectin production, and Smad-2 phosphorylation increased in HUVECs treated with high glucose and palmitic acid (HGHF). Pharmacological inhibition of AKT significantly reduced HGHF-induced upregulation of PACS2 and p-Smad2 expression. Blocking fatty acid  $\beta$ -oxidation (FAO) ameliorated the impaired barrier function mediated by HGHF. Further studies observed that HGHF induced decreased FAO, CPT1 $\alpha$  expression, ATP production, and NADPH/NADP<sup>+</sup> ratio in endothelial cells. However, these changes in fatty acid metabolism were rescued by silencing PACS2. In conclusion, PACS2 participates in renal vascular hyperpermeability and glomerulosclerosis by regulating the FAO of diabetic mice. Targeting PACS2 is potential new strategy for the treatment of diabetic nephropathy.

**Keywords:** vascular permeability, diabetes, PACS2, fatty acid oxidation, endoplasmic reticulum, mitochondria, endothelial cell

**Abbreviations:** BUN, Blood urea nitrogen; BSA, Bovine serum albuminates; BDH1, D-beta-hydroxybutyrate dehydrogenase; CPT1 $\alpha$ , carnitine palmitoyl-transferase 1 $\alpha$ ; CHO, Total cholesterol; CRE, Creatinine; DN, Diabetic nephropathy; DKD, Diabetic kidney disease; ESRD, End-stage renal disease; EC, Endothelial cell; ECM, Extracellular matrix; ETO, Etomoxir; FN, Fibronectin; FAO, Free fatty acid oxidation; GO, Gene ontology; HFD, High-fat diet; HGHF, High glucose and high fat; ITGB4, Integrin beta 4; ITGA3, Integrin alpha 3; KEGG, Kyoto Encyclopedia of Genes and Genomes; MAMs, Mitochondria-associated membranes; MLLT4, Myeloid/lymphoid or mixed-lineage leukemia 4; OCR, Oxygen consumption rate; PACS2, Phosphofurin acidic cluster sorting protein 2; PA, Palmitic acid; STZ, Streptozocin; TG, Triglyceride; TR-F, Time-resolved fluorescence; u-mALB, Urine microalbuminuria.

## INTRODUCTION

Diabetic nephropathy (DN) is a chronic microvascular complication of diabetes and has become the leading cause of the end-stage renal disease (ESRD) (Cheng et al., 2021). Endothelial cells are essential participants in the pathogenesis of DN; they constitute the renal filtration barrier (Fu et al., 2019), mediate chronic inflammation (Jeong et al., 2017), and crosstalk with podocytes and mesangial cells (Weil et al., 2012; Kuravi et al., 2014) in progressive DN. Studies have shown that endothelial cell dysfunction, manifested as oxidative imbalance, endothelial apoptosis, abnormal angiogenesis, and decreased nitric oxide bioavailability (McDonald et al., 2019), primarily affects the progression of DN.

According to recent single-cell sequencing, endothelial cells exhibit metabolic transcriptome plasticity in health and disease (Kalucka et al., 2020; Rohlenova et al., 2020). The expression levels of genes related to the fatty acid oxidation (FAO) pathway in resting endothelial cells are 3–4 times higher than those in proliferating endothelial cells (Kalucka et al., 2018). Moreover, inhibiting endothelial glycolysis will reduce the hyperproliferation of tumor blood vessels (Cantelmo et al., 2016). However, the effect of changing endothelial metabolism on diabetes remains unclear. As a systemic metabolic disease, diabetes is often presented with both hyperglycemia and dyslipidemia. It has been reported that nutrient overload can lead to glucolipotoxicity in type 2 diabetes (Dahlby et al., 2020), and hyperglycemia alone is not enough to trigger generalized diabetic microangiopathy (Barrett et al., 2017). Therefore, we speculate that chronic high glucose and high fat (HGHF) conditions may alter endothelial metabolism, leading to diabetic renal vascular dysfunction.

Our previous studies have shown that under high glucose conditions, endothelial mitochondrial DNA damage, increased mitochondrial reactive oxidative species (mtROS) production, and subsequent mitochondrial fission lead to vascular endothelial dysfunction (Liu et al., 2019a; Xiang et al., 2021). Though we and others have explored the pathogenic role of mitochondrial dysfunction in diabetic vascular endothelial cells, the role of endothelial metabolic reprogramming in DN is still unknown. Besides, mitochondria play a central regulatory role in endothelial metabolism, closely related to cell proliferation, apoptosis, and nuclear signal transduction (Qi et al., 2017). In addition, mitochondria-associated ER membranes (MAMs), as a novel subcellular structure, have a more profound impact on endothelial function by regulating mitochondrial dynamics, lipid metabolism, and calcium signaling (Ricciardi and Gnudi, 2020). It has been reported that MAMs have multiple roles in diabetic complications (Wu et al., 2019; Cheng et al., 2020), but no endothelial cells have been concerned. Besides that, papers reported that some MAMs related proteins could play a significant role in diseases. Phosphofurin acidic cluster sorting protein 2 (PACS2) (Arruda et al., 2014) regulates cellular energy metabolism in insulin resistance, and fatty acid-CoA ligase 4 (FACL4) inhibits the eNOS/NO/cGMP signaling pathway (Yang et al., 2022). Moreover, GRP75 induces mitochondria-associated membrane formation and mitochondrial impairment

(Liang et al., 2021). As a cell type with potential metabolic plasticity, whether changes in MAMs are related to endothelial metabolism under diabetic conditions is still worth studying.

In this study, we evaluated the regulation of vascular endothelial metabolism and its role in DN. To this end, we established a streptozotocin (STZ) and high fat diet (HFD)-induced type 2 diabetic mouse model (Wang et al., 2018; Cheng et al., 2019) to evaluate the vascular damage of the kidney. Also, we used an *in vitro* endothelial cell injury model induced by high glucose plus palmitic acid (also referred to as HGHF) (Sun et al., 2021; Wu et al., 2021) to study the main molecular mechanism of barrier function changes and fibrosis.

## MATERIALS AND METHODS

### Animal Model and Study Design

All animal manipulations were approved by the Institutional Animal Care and Use Committee of Central South University, Changsha, China (#2019sydw0021). All efforts were made to minimize mouse suffering. Eight-week-old male C57BL/6J mice (wildtype, WT) and phosphofurin acidic cluster sorting protein 2 (PACS2) knockout mice (PACS2<sup>-/-</sup>) were obtained from the Nanjing Biomedical Research Institute of Nanjing University and housed under standard pathogen-free conditions at the Xiangya Medical School of Central South University.

After 1 week of acclimatization, the mice were randomly assigned to the standard chow diet (ND) group and the STZ plus HFD (STZ/HFD) group, with five mice each. The latter was fed HFD (D12109C, Research Diets, New Brunswick, NJ, USA) and intraperitoneally injected 35 mg/kg STZ (S0130, Sigma-Aldrich, San Louis, MO, USA) twice between 9 and 10 weeks. STZ was dissolved in sodium citrate-hydrochloric acid buffer solution, pH 4.5 (SSC) (Feng et al., 2019; Zhang et al., 2019; Kim et al., 2020). The ND group was injected with the same volume of SSC. Blood glucose was measured at week 11, and mice with blood glucose >11.1 mM were considered to have diabetes. The flow chart of establishing the HFD diabetic mouse model is shown in **Supplementary Figure S1A**.

### Cell Culture

The results of population studies have shown that patients with diabetes mellitus complicated with hyperlipemia have a higher incidence of rapid progression of diabetic vascular impairment (Haile and Timerga, 2020; Gebreegziabihir et al., 2021). For these patients, glucose control alone cannot reduce the final incidence of ESRD (Coca et al., 2012; Peltier et al., 2014). We believe that glucose and lipid overload are jointly involved in the pathogenesis of high-risk diabetes patients. Therefore, HGHF conditions were created in this study to simulate the disease state (Sun et al., 2021; Wu et al., 2021).

Primary human umbilical vein endothelial cells (HUVECs) were purchased from the American Type Culture Collection (ATCC, Manassas, VA, USA) and cultured in an Endothelial Cell Medium (Invitrogen, Carlsbad, CA, USA) containing 5% fetal bovine serum at 37°C in a 5% CO<sub>2</sub> incubator. Cells were treated with 30 mM glucose and 0.1 mM palmitic acid (P0500, Sigma-Aldrich, USA) dissolved in 0.5% bovine serum albumin

(BSA) for 48 h to simulate HGHF treatment. The Akt inhibitor MK-2206 2HCl was purchased from Selleck Chemicals (S1078, Houston, TX, USA).

## Measurement of Blood Metabolic Parameters

Blood was drawn through the submandibular vein at 11, 14, 17, and 20 weeks to measure serum biochemistry parameters, including total cholesterol (CHO), triglyceride (TG), blood glucose, creatinine (CRE), and blood urea nitrogen (BUN). The 24-h urine microalbuminuria (u-mALB) was measured once a week from the 8th week, but no urine was collected 1 week after each blood collection to avoid the effect of transient blood loss on renal function. All mice were sacrificed at week 20, and kidney tissues were fixed in 4% paraformaldehyde and stained with hematoxylin-eosin (HE) and Masson trichrome.

## SiRNA Transfection

To verify the function of PACS2 in HUVECs, PACS2 siRNA was delivered into cells according to the manufacturer's instructions. Briefly, cells were transfected with 50 nM PACS2 siRNA or negative control (Ribobio, Guangzhou, Guangdong, China) using Lipofectaminutase 3,000 reagent (Invitrogen) in Opti-MEM I reduced serum medium (ThermoFisher Scientific, Grand Island, NY, USA) for 12 h, and then stimulated with HGHF for another 48 h.

## Masson's Trichrome Staining

After deparaffinization and rehydration through 100, 95, and 70% ethanol, kidney tissue slides were serially stained in Weigert's iron hematoxylin working solution for 10 min and Biebrich scarlet-acid fuchsin solution for another 10–15 min. To differentiate nuclei, slides were submerged into the phosphomolybdic-phosphotungstic acid solution for 10–15 min or until the collagen was not red. Slides were then directly transferred into blue aniline solution and stained for 5–10 min. Following differentiation in 1% acetic acid solution for 2–5 min and rapid dehydration through 95% ethyl alcohol and absolute ethyl alcohol, slides were dipped into xylene and finally mounted with a resinous mounting medium.

## Vascular Leakage Assay

As an indicator of vascular permeability, albumin extravasation was evaluated in the Miles assay by measuring the extravasation of albumin-bound Evans blue. In short, mice were anaesthetized with isoflurane inhalation. Five min later, 150  $\mu$ L of Evans Blue (30 mg/ml; Sigma-Aldrich) was anaesthetized via the tail vein and allowed to circulate for 30 min, then extravasated Evans blue dye was evaluated (Shan et al., 2017). Following photographing the extravasation of Evans blue in the coronal section of kidneys. The kidneys were dried on foil at 150°C for 48 h. To extract Evans blue from the tissue, 500  $\mu$ L formamides was added and incubated at 55°C for 72 h. Plasma extravasation was quantified by measuring absorbance at 620 nm and calculated per gram of dry weight.

## FITC-Dextran Permeability Assay

Confluent HUVECs were treated with or without HGHF for 48 h on type I collagen-coated culture inserts with 0.4- $\mu$ m pores (BD

Bioscience, Franklin Lakes, NJ, USA). After that, 15  $\mu$ L of 5 mg/ml FITC-dextran 40 (Sigma-Aldrich) was added to the upper chamber and incubated at 37°C for 15, 30, and 60 min. The fluorescence intensity of FITC-dextran diffused into the lower chamber was measured at Ex/Em = 485/590 nm.

Endothelial cell permeability was detected by using an *In Vitro* Vascular Permeability Assay kit following the manufacturer's protocol (Millipore, Burlington, MA, USA). After forming a tighter monolayer and exposure to HGHF, the cells were stained with FITC-dextran 40 for 20 min. The amount of FITC-dextran 40 (Aman et al., 2012) diffused across the endothelial monolayer was observed under a fluorescent microscope with a FITC filter and quantified on a fluorescence plate reader.

Leaked ratio = Transwell lower chamber fluorescence intensity ( $Ex_{480}/Em_{590}$ )/upper chamber fluorescence intensity ( $Ex_{480}/Em_{590}$ ).

## Oxygen Consumption Assay

The kinetic changes of extracellular oxygen levels, an indicator of aerobic metabolism in living cells, were measured using the MitoXpressXtra oxygen consumption assay kit (Luxel Bioscience, Santa Clara, CA, USA) (Du et al., 2019). Antimycin A, a potent electron transport chain complex III inhibitor, was used to shut down mitochondrial respiration (zero oxygen consumption control). The uncoupling agent carbonyl cyanide 4-(trifluoromethoxy) phenylhydrazone (FCCP) that disrupts the mitochondrial proton gradient was employed to drive its maximal mitochondrial respiration rate. In principle, the phosphorescent signal of MitoXpressXtra is quenched by oxygen and produces a signal that is inversely proportional to the amount of oxygen present. Time-resolved fluorescence (TR-F) was measured at Ex/Em = 380/650 nm and the recommended delay time. The parameters of oxygen consumption included PA-based maximal oxygen consumption rate (PA-OCR) obtained by adding 2.5  $\mu$ mol/L FCCP plus PA-only-based substrate and negative control (NegOCR) obtained by adding 1  $\mu$ mol/L antimycin A in the presence of PA-only-based substrate.

## Cellular ATP Assay

Cells were seeded in triplicate in 96-well plates and treated with firefly luciferase for the indicated time. Cellular ATP levels were evaluated using an ATPlite assay (Perkin-Elmer, Waltham, MA, USA) (Liu et al., 2019a).

## NADPH/NADP Measurement

Intracellular NADPH/NADP ratio was assayed using an NADP/NADPH quantification colorimetric kit (K347-100, BioVision, Milpitas, CA, USA) as per the manufacturer's instructions.

## Immunohistochemistry

Kidney tissues were fixed in 4% glutaraldehyde at 4°C for 48 h, and then post-fixed in 1% osmium tetroxide at room temperature for 2 h. After pre-staining with barbitone acetate for 10 min, histological samples were dehydrated with acetone and embedded in paraffin wax. Immunohistochemical staining was



performed to detect PACS2 (PA5-100167, ThermoFisher) and CD31 (ab28364, Abcam, Cambridge, UK) in endothelial cells and visualized using fluorochrome-conjugated goat anti-mouse (ab150115, Abcam) or anti-rabbit IgG H&L (ab150077, Abcam). PACS2-positive cells were counted and normalized to total endothelial cells in the same field using computer-assisted morphometric analysis.

## Western Blot Analysis

Chemiluminescent based on horseradish peroxidase (HRP) were used to detect and visualize western blots. The following antibodies were used: anti-CPT1 $\alpha$  (12252S, Cell Signaling Technology, Beverly, MA, USA), PACS2 (GTX17244, GeneTex, Irvine, CA, USA), VE-cadherin (ab33168, Abcam),  $\beta$ -actin (A5441, Sigma-Aldrich), AKT (2938S, Cell Signaling Technology), p-AKT (9018S, Cell Signaling Technology), Smad2 (5339T, Cell Signaling Technology), p-Smad2 (ab280888, Abcam, UK), PPAR $\alpha$  (ab215270, Abcam, UK), and HRP conjugated goat anti-rabbit IgG secondary antibody (AS09 602, Agrisera, Vannas, Sweden).

## Electron Microscope

Cells were isolated on nickel fitters, stained with 2% uranyl acetate for 10 min, and then stained with Reynold's lead citrate for 5 min. The endoplasmic reticulum (ER)-mitochondria contacts of endothelial cells were evaluated by transmission electron microscopy (TEM; Hitachi-7650, Tokyo, Japan) at 60 kV. The ER-mitochondrial contacts were quantified as described previously (Wu et al., 2019). The images were analyzed using ImageJ (National Institutes of Health, Bethesda, MD, USA). The mitochondrial and ER membranes were delineated using the freehand tool. The selected areas were converted to a mask, and the perimeters of ER were calculated. Two independent investigators blindly quantified the images. To quantify MAMs, the total ER perimeter connected to mitochondria to the total ER perimeter was normalized.

## Immunofluorescence Microscopy

HUVECs were labelled with ER-Tracker Blue-White DPX dye (E12353, ThermoFisher Scientific) and Mito Tracker Deep Red FM (M22426, ThermoFisher Scientific) at 37°C for 30 min and observed under a confocal microscope (LSM800, Carl Zeiss Microscopy, Cambridge, MA, USA). The Pearson correlation coefficient mode, a well-defined and generally accepted means of describing the overlap between image pairs, was applied to quantify the degree of co-localization between the fluorophores representing ER-Tracker Blue and Mito Tracker Deep Red. The Pearson correlation coefficient was analyzed using the built-in Carl Zeiss co-localization analysis module from the ZEN software and the threshold obtained from single-label control samples.

## Label-Free Quantitative Proteomics

Total proteins were extracted from HUVECs in the presence or absence of HGHF. Peptide samples (2  $\mu$ g) were separated and analyzed by Kangchen Biotech (Shanghai, China) using the EASY-nLC1200 system and Q Exactive mass spectrometer (120 min/sample), respectively (Zhu et al., 2020). Differentially

expressed peptides were identified at  $p < 0.05$  and fold-change  $> 2$ , followed by gene ontology (GO) enrichment analysis by using Blast2Go 4.0.7 software.

## Untargeted Metabolomics of HUVECs

Each cell sample is slowly thawed at 4°C, mixed with 1 ml of cold methanol/acetonitrile/H<sub>2</sub>O (2:2:1, v/v/v) and vortexed adequately. The homogenates were sonicated for two cycles at low temperature, 30 min/cycle, incubated at -20°C for 60 min to precipitate proteins and centrifuged at 13,000 rpm at 4°C for 15 min. Supernatants were collected, dried under vacuum, and stored at -80°C. The dried samples were re-dissolved in 100  $\mu$ L acetonitrile/water (1:1, v/v), vortexed, and centrifuged. The resulting supernatants were used for LC-MS/MS analysis, performed at Applied Protein Technology (Shanghai, China). The metabolites were blasted against the online Kyoto Encyclopedia of Genes and Genomes (KEGG) database (<http://geneontology.org/>) to retrieve their COs and were subsequently mapped to pathways in KEGG. The corresponding KEGG pathways were finally extracted.

## Statistical Analysis

The SPSS 22.0 software (SPSS, Chicago, IL, USA) was used for statistical analysis. Data are expressed as mean  $\pm$  standard deviation (SD). Statistical differences were assessed by Student *t*-test of the means between two groups or by one-way analysis of variance of the means between multiple groups.  $p < 0.05$  was considered a significant difference.

## RESULTS

### Renal Vascular Hyperpermeability and Glomerulosclerosis in Diabetic Mice

In order to observe the pathological changes of kidney vascular vessels, we created a diabetic mouse model. Hyperglycemia and hyperlipidemia developed after 14 weeks of HFD feeding plus low-dose STZ injection (Figure 1A). Blood CRE, BUN, and u-mALB levels increased significantly at week 20, indicating that the kidney of the HFD group was dysfunctional. Consistent with the serum and urinary biochemical analysis results, HE and Masson trichrome staining showed pathological changes in renal tissues, manifested as atrophy of glomerular vascular loops (Figure 1B) and renal microvascular fibrosis (Figures 1C,D). Moreover, Evans blue extravasation demonstrated an increased renal tissue extravasation index in the HFD group (Figures 1E,F). TEM observation of renal endothelial cells showed a significant increase in MAMs of renal cortical glomerular endothelial cells, accompanied by mitochondrial swelling and crista degeneration (Figure 1G). These results indicate that mitochondria are involved in endothelial cell dysfunction induced by HGHF.

### Increased MAMs and Barrier Dysfunction in HGHF-Treated Endothelial Cells

To explore the underlying mechanism behind endothelial cell dysfunction in diabetic mice, we next examined the barrier

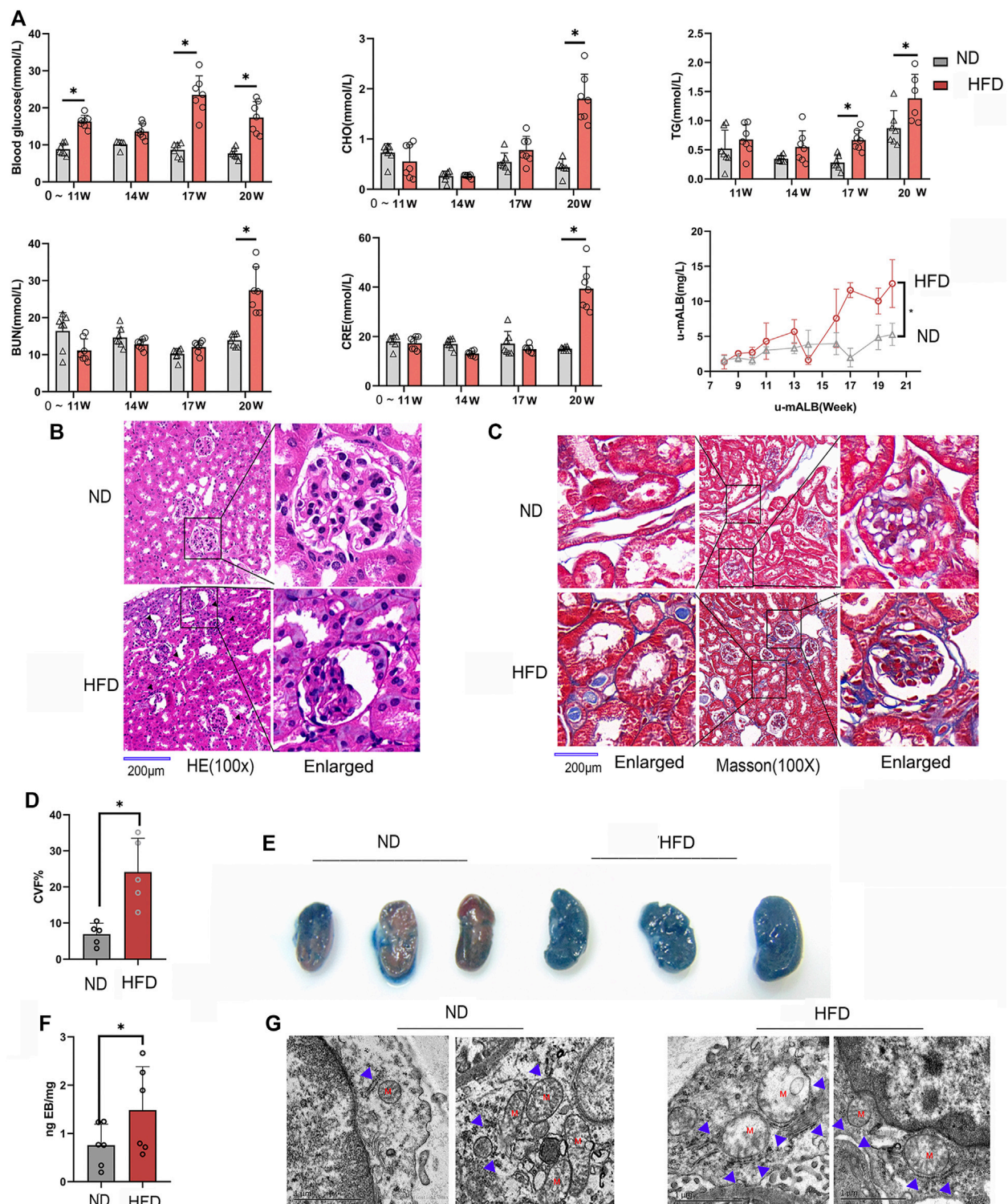


**FIGURE 1 |** Renal vascular dysfunction and endothelial mitochondria-associated ER membranes (MAMs) increased in the diabetic mice model. **(A)** Biochemical analysis of blood glucose, total cholesterol (CHO), triglyceride (TG), blood urea nitrogen (BUN), creatinine (CRE), and 24-h urine microalbumin (u-mALB) in mice fed with regular chow diet (ND) or HFD. **(B)** Hematoxylin-eosin (HE) and **(C)** Masson's trichrome staining of mouse kidney tissues. Magnification,  $\times 100$  and  $400\times$ . Scale bar,  $200\ \mu\text{m}$ . **(D)** Histogram of changes in CVF. **(E)** Photographs of Evans blue (EB)-stained mouse kidneys. **(F)** EB extravasation index. Representative images are shown, or data are represented as the mean  $\pm$  SD,  $n \geq 5$ . **(G)** Quantitative analysis of mitochondrial MAM coverage in vascular endothelial cells in kidney tissues depicted in Figure 1. Representative images are shown or data are represented as the mean  $\pm$  SD,  $n = 3$ .  $**p < 0.01$ .



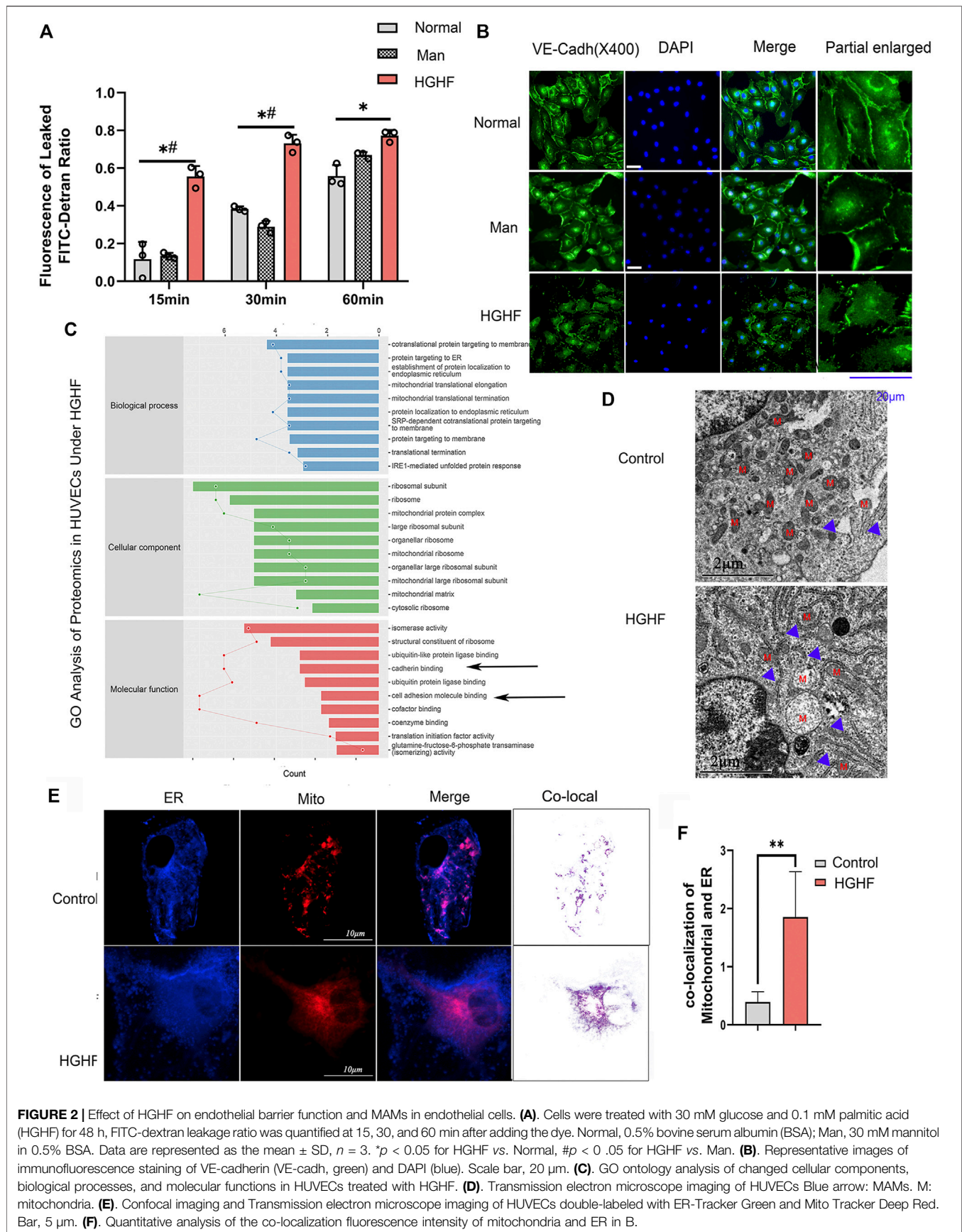


**FIGURE 2 |** Effect of HGHF on endothelial barrier function and MAMs in endothelial cells. **(A)** Cells were treated with 30 mM glucose and 0.1 mM palmitic acid (HGHF) for 48 h, FITC-dextran leakage ratio was quantified at 15, 30, and 60 min after adding the dye. Normal, 0.5% bovine serum albumin (BSA); Man, 30 mM mannitol in 0.5% BSA. Data are represented as the mean  $\pm$  SD,  $n = 3$ . \* $p < 0.05$  for HGHF vs. Normal, # $p < 0.05$  for HGHF vs. Man. **(B)** Representative images of immunofluorescence staining of VE-cadherin (VE-cadh, green) and DAPI (blue). Scale bar, 20  $\mu$ m. **(C)** GO ontology analysis of changed cellular components, biological processes, and molecular functions in HUVECs treated with HGHF. **(D)** Transmission electron microscope imaging of HUVECs. Blue arrow: MAMs. M: mitochondria. **(E)** Confocal imaging and Transmission electron microscope imaging of HUVECs double-labeled with ER-Tracker Green and Mito Tracker Deep Red. Bar, 5  $\mu$ m. **(F)** Quantitative analysis of the co-localization fluorescence intensity of mitochondria and ER in B.

function changes of endothelial cells. As shown in **Figure 2A**, FITC-dextran permeability was significantly increased in the HGHF group from 15, 30 until 60 min. VE-cadherin is the central adhesion molecule of endothelial cell-cell junctions (Lampugnani et al., 2018). The dissociation of p120-catenin and  $\beta$ -catenin from VE-cadherin complexes will increase VE-cadherin internalization and weaken the endothelial barrier (Yang et al., 2015; Juettner et al., 2019). The immunofluorescence of VE-cadherin showed a significant decrease from the cell membrane in **Figure 2B**, indicating that the adherent contact between endothelial cells was damaged.

By mining the MS reference database, protein identification was performed on data-independent acquisition (DIA) data results (identification criteria: precursor threshold, 1.0% false discovery rate (FDR) and protein threshold, 1.0% FDR). We identified 26,201 peptides and 3,678 proteins in the two sets of samples. The identified proteins were screened for differentially expressed ones between the ND and HGHF groups. The relative fold change of expression  $>1.2$  and the Student *t*-test *q*-value  $<0.05$  were used as filter criteria to process DIA quantitative data. On this basis, 320 differentially expressed proteins were selected out (**Supplementary Figure S2A**). Of them, 138 were upregulated and 182 downregulated after HGHF treatment. GO annotation analysis showed that they were mainly enriched in the unfolded protein response in the ER, and the mitochondrial translational elongation and termination processes (**Figure 2C**) indicate mitochondrial damage or ER stress. Proteomics also supported that the proteins were enriched in the mitochondria and ER (**Supplementary Figure S2B**). Several proteins related to renal damage and inflammation increased, consistent with the chronic renal inflammation state (**Supplementary Figure S2C**). We also found that the expression of the integrin-related proteins (like ITGB4, ITGA3) and cell-cell adhesions protein MLLT4 had down-regulated significantly (**Figure 2C**), which indicates damage to membrane integrity (Tremblay et al., 2014). Further, we verified the potential changes in mitochondria-ER contact *in vivo*. The same cell samples were observed under TEM, showing enrichment of ER and MAMs (**Figure 2D**) under HGHF. Double staining of mitochondria and ER revealed their more significant co-localization in HGHF-treated HUVECs (**Figures 2E,F**).

## Increased Expression of PACS2 in HGHF-Treated Endothelial Cells

Based on the TEM and immunofluorescence observations of renal endothelial cells *in vivo* and HGHF-treated HUVECs *in vitro*, we further explored the expression changes of three MAMs regulatory proteins, acyl-CoA synthetase 4 (FACL4) (Lewin et al., 2002), PACS2 (Yang et al., 2021), and glucose-regulated protein 75 (GRP75) (Liu et al., 2019b), in HUVECs under HGHF exposure. Among these regulatory proteins, PACS2 was significantly increased in HGHF-induced HUVECs (**Figures 3A,B**), and it also had an inevitable increase in diabetic mouse renal vascular tissues (**Figure 3C**). To further understand the role of PACS2, we silenced PACS2 in HUVECs using siRNA (**Figures 3D,E**). We found knocking down PACS2 could attenuate HGHF-enhanced co-localization of mitochondria and ER (**Figures**

**3F,G**). These results indicate that PACS2 is an active regulator of MAMs and may be involved in endothelial cell dysfunction in HGHF-treated endothelial cells.

## Loss of PACS2 Expression Improves HGHF-Induced Endothelial Barrier Dysfunction

PACS2 knockout mice (PACS2<sup>-/-</sup>) were used to confirm the effect of PACS2 on vascular endothelium under HGHF *in vivo*. Diabetic PACS2<sup>-/-</sup> mouse modeling was created the same as depicted in **Supplementary Figure S1**. Microscopic immunofluorescence observations verified the gene knockout efficiency (**Figure 4A**). We observed that the HFD treatment altered the biochemical parameters of renal function in WT mice. However, PACS2 knockout eliminated the increase in blood glucose, TG, CRE, and BUN caused by HFD treatment. However, it did not affect CHO (**Figure 4B**), indicating that PACS2 is implicated in HFD-induced renal dysfunction.

Compared to HFD-treated WT mice, PACS2-deficient mice showed a significant reduction in HFD-induced glomerular fibrosis in Masson staining (**Figures 4C,D**). In addition, we found that the glomerular cortex endothelial cells and vascular endothelial cell MAMs in the kidney tissues of PACS2<sup>-/-</sup> + HFD mice were significantly reduced (**Figure 4E**), as was the glomerular Evans blue leakage index (**Figures 4F,G**), suggesting that PACS2 plays a role in HFD-induced kidney injury by regulating MAMs.

## Inhibition of AKT Blocks Hyperpermeability and Fibronectin Generation Under HGHF With PACS2 Upregulation

In order to explore how HGHF-induced endothelial PACS2 and MAMs vary, the upstream regulators of PACS2 were then examined. Recent reports noted that AKT could mediate vascular barrier leakage and inhibit renal fibrosis (Lewin et al., 2002; Yang et al., 2021) and controlling MAMs integrity (Peltier et al., 2014). Therefore, we evaluated whether AKT works upstream of PACS2 in HUVECs treated with HGHF.

**Figures 5A,B** show that HGHF induced endothelial cell fibrosis, indicated by increased FN expression. At the same time, the phosphorylation levels of AKT and Smad2 were significantly increased (**Figures 5A,B**), suggesting that HGHF activates both AKT and Smad2 signaling pathways. Extracellular matrix (ECM) is secreted from endothelial cells, and its accumulation is the pathological basis of DN. However, the transcription factor Smad2 signaling mediates endothelial-related ECM deposition and renal fibrosis (Weng et al., 2020). To understand the potential role of PACS2 in the activation of AKT and Smad2, we silenced PACS2 and then treated cells with HGHF. We found that knocking down PACS2 reduced FN expression and Smad2 phosphorylation but did not inhibit AKT phosphorylation, indicating that PACS2 regulates Smad2 signaling during HGHF-induced endothelial cell fibrosis. Interestingly, MK2206, a selective AKT inhibitor, decreased HGHF-induced PACS2 expression and Smad2 phosphorylation, indicating that AKT signaling works



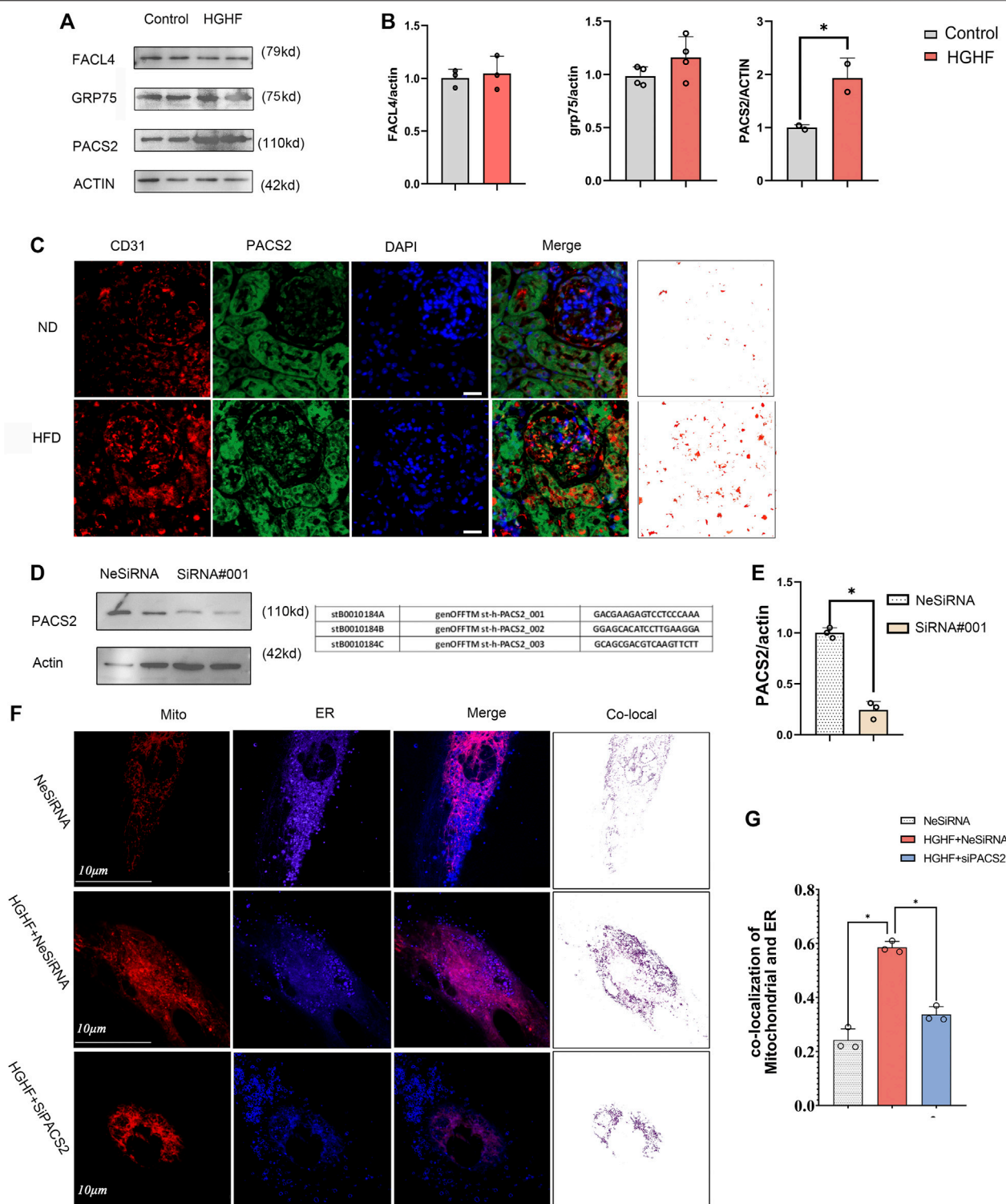


**FIGURE 3 |** PACS2 increased expression in endothelial cells response to HGHF at the MAMs. (A). Western blot analysis of MAM-related proteins. ACTIN used as loading control. (B). Quantitative analysis of the expression of FACL4, GRP75, and PACS2 in A. The band densities were quantitated and normalized to the corresponding ACTIN. (C). Immunofluorescence imaging of cells stained for CD31 (red), PACS2 (green), and nucleus (DAPI, blue) in mouse kidney tissues. (D). Transfection efficiency of PACS2 siRNA in HUVECs. (E). Quantitative analysis of PACS2 knockdown in D. (F). Confocal imaging of cells double-labeled with ER-Tracker Blue and Mito Tracker Deep Red in HUVECs. Single optical sections are shown and the purple ones indicate the co-localization of mitochondria and ER. Bar, 10  $\mu$ m. (G). Quantitative analysis of the co-localization ratio in F. Representative images are shown, or data are represented as the mean  $\pm$  SD,  $n = 3$ . \* $p < 0.05$ .

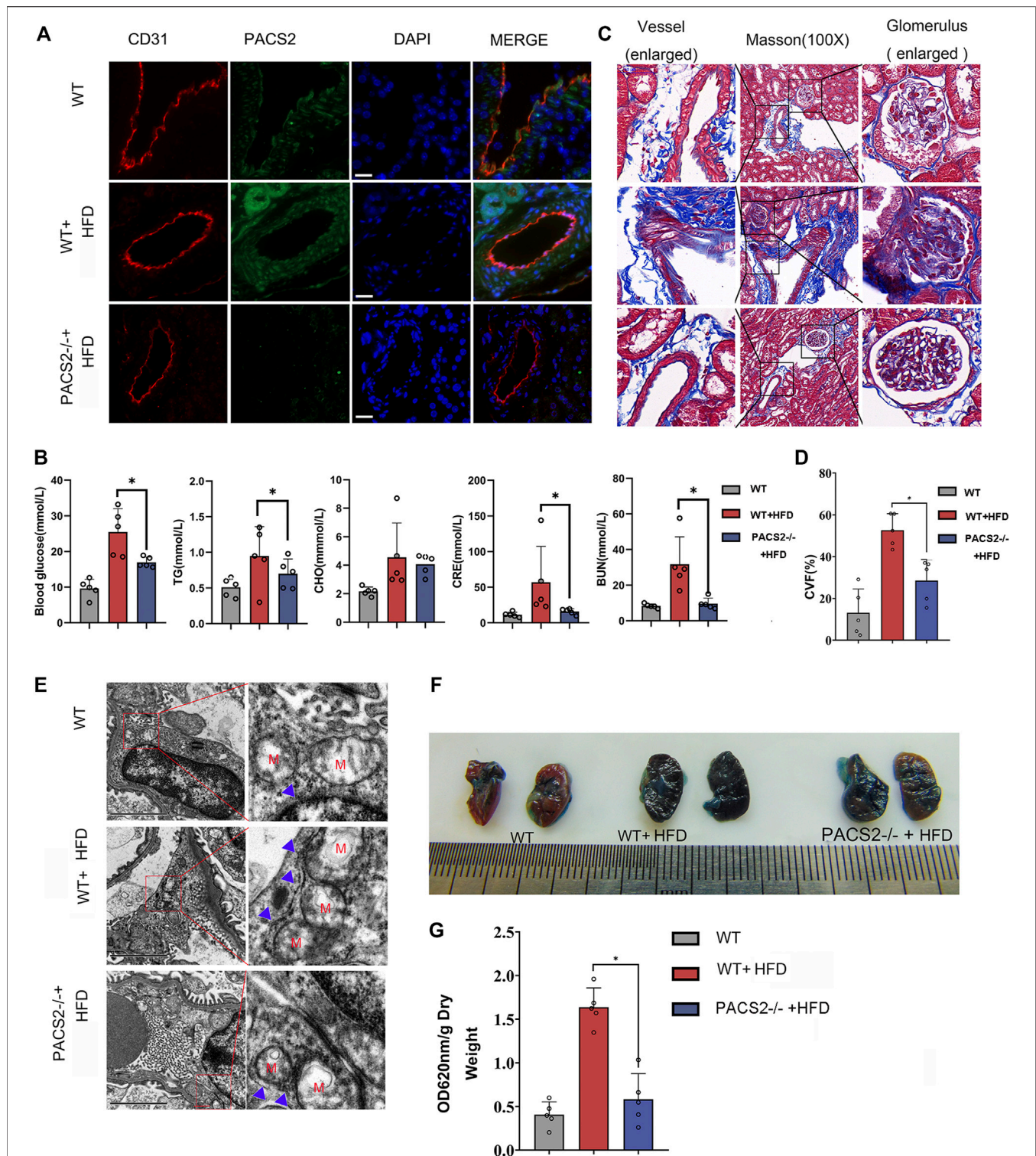
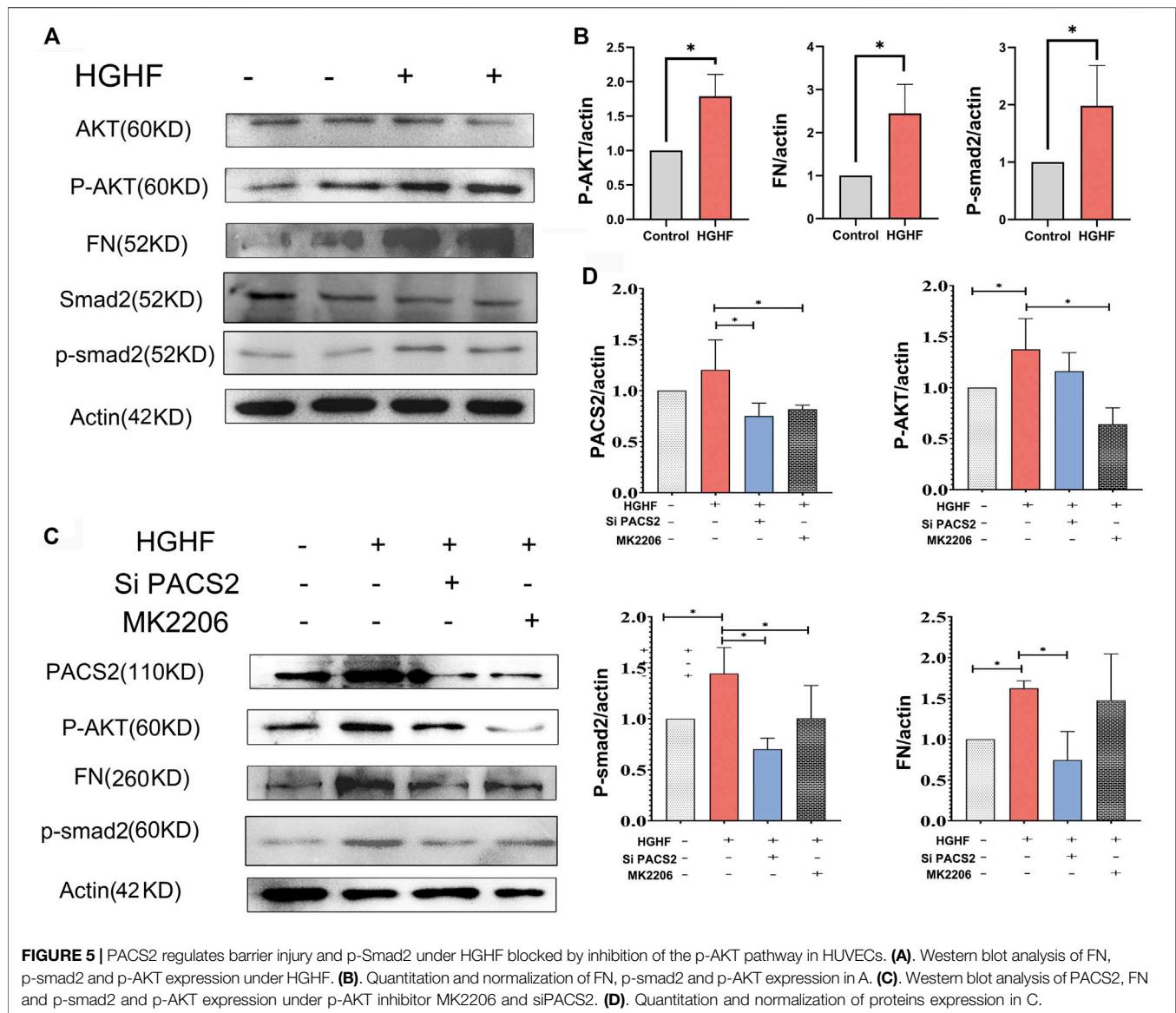


**FIGURE 4 |** Loss of PACS2 expression improves kidney barrier function and anti-fibrosis induced by HGF. **(A)** Immunofluorescence of kidney tissues. Bar, 50  $\mu$ m. **(B)** Biochemical analysis of serum parameters in wild type (WT) and PACS2<sup>-/-</sup> mice fed with or without HFD. **(C)** Masson staining of kidney tissues, Magnification,  $\times 100$ . **(D)** Histogram of CVF in B. **(E)** Transmission electron microscope imaging of mouse kidney ultrastructure. Magnification,  $\times 15,000$ . Red M, mitochondria of renal endothelial cells; blue arrow, MAMs. Images of Evans blue staining of mouse kidneys. **(F)** Photographs of Evans blue (EB)-stained mouse kidneys. **(G)** Histogram of EB extravasation index. Representative images are shown or data are represented as the mean  $\pm$  SD,  $n \geq 5$ . \* $p < 0.05$ .



upstream of PACS2 regulation under HGHF treatment (Figures 5C,D). These results indicate that HGHF-induced PACS2 upregulation in endothelial cell dysfunction is partly through the AKT signaling.

### Inhibition of AKT/PACS2 Improves Free Fatty Metabolism in HGHF-Treated HUVECs

Recent research reported that PACS2 could regulate cellular energy metabolism, in which the free fatty metabolism was also related to cell-cell junction (Xiong et al., 2018). In order to understand how AKT/PACS2 signaling impacts endothelial barrier function, we explored the metabolic index in endothelial cells. Non-targeted metabolomics were tested under HGHF induced HUVECs and FAO's key enzyme, carnitine palmitoyl-transferase 1 $\alpha$  (CPT1 $\alpha$ ), was examined in diabetic kidney tissue. KEGG pathway analysis results revealed that most differential

metabolites were enriched in the metabolism pathways (Figure 6A). Significant changes were found in adenosine monophosphate, adenosine 5'-diphosphate, glycerol 3-phosphate (phosphoglycerol 3), N-acetylglucosamine-1-phosphate, and phosphorylcholine (Supplementary Figure S2), all of which are related to fatty acid metabolism, indicating that fatty acid metabolism is easily affected by HGHF and has a role in HGHF-induced HUVEC damage.

Next, we measured FAO ability through mitochondrial respiration using PA as an energy substrate. We evaluated FAO-dependent OCR (PA-OCR) by adding FCCP or etomoxir (ETO) into cultured HUVECs. The results showed that PA-OCR was significantly reduced after HGHF exposure. However, silencing PACS2 reversed the inhibition of PA-OCR by HGHF (Figure 6B). Quantitative NADPH/NADP<sup>+</sup> (Figure 6C) and ATP (Figure 6D) analyses showed that the NADPH/NADP<sup>+</sup> ratio and ATP production in HUVECs was significantly reduced after



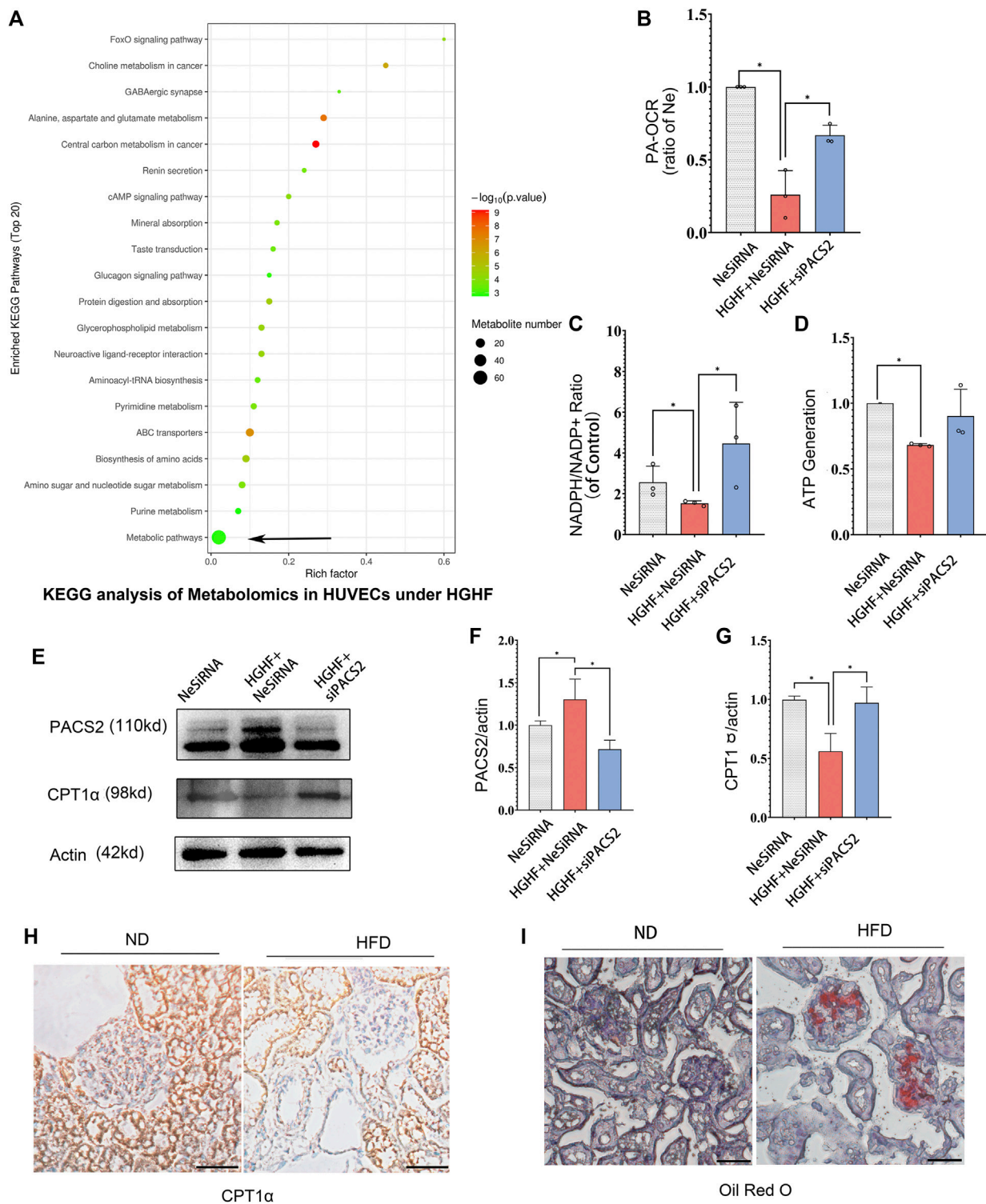


**FIGURE 6 |** Silencing PACS2 improves free fatty metabolism in HUVECs treated with HGHF. **(A)** KEGG analysis of metabolomics in HUVECs under HGHF. **(B)** Palmitic acid (PA)-based oxygen consumption rate (OCR) was measured in cells transfected with negative siRNA (NeSiRNA) or PACS2 siRNA (siPACS2) and treated with or without HGHF. **(C)** Determination of cellular NADPH/NADP ratio. **(D)** Determination of cellular ATP levels. **(E)** Western blot analysis of PACS2 and carnitine palmitoyl-transferase 1α (CPT1α) expression. **(F)** Quantitation and normalization of PACS2 expression in E. **(G)** Quantitation and normalization of CPT1α expression in E. **(H)** Immunohistochemical staining of CPT1α in mouse kidney. Magnification, ×200. **(I)** Oil Red staining of mouse kidney. Magnification, ×200. Representative images are shown or data are represented as the mean ± SD,  $n = 3$ . \* $p < 0.05$ .



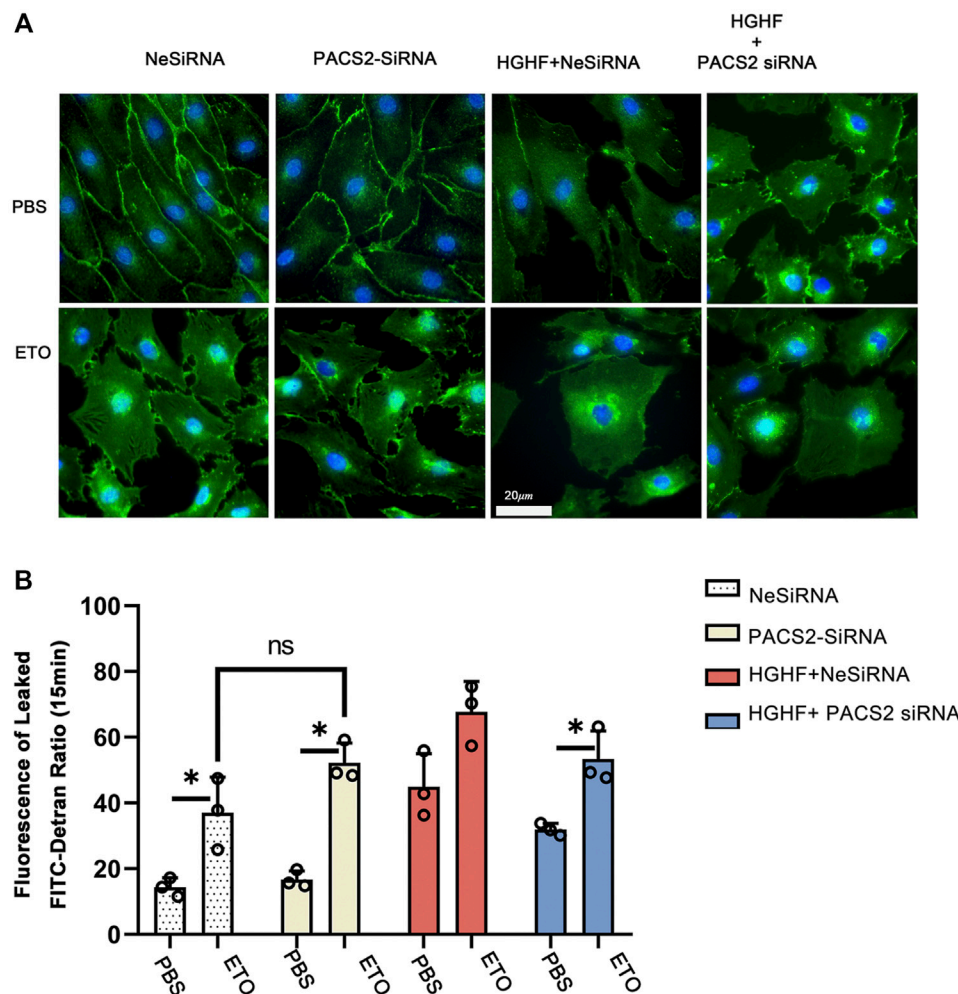


**FIGURE 7 |** Inhibition of fatty acid  $\beta$ -oxidation disturbs the barrier function of endothelial cells and eliminates the protective effect of PACS2. **(A)**. Immunofluorescence staining of VE-cadherin (green) in cells transfected with NeSiRNA or siPACS2 and treated with the fatty acid  $\beta$ -oxidation inhibitor etomoxir (ETO) or phosphate buffered saline (PBS) as vehicle control. Blue, DAPI. Bar, 20  $\mu$ m. **(B)**. Quantification of FITC-dextran leakage ratio of HUVECs within 15 min. Representative images are shown or data are represented as the mean  $\pm$  SD,  $n = 3$ . \* $p < 0.05$ .

HGHF treatment. However, knocking down PACS2 prevented the effect of HGHF on the NADPH/NADP<sup>+</sup> ratio and showed a tendency to block the effect of HGHF on ATP production. These results suggest that HGHF interferes with mitochondrial aerobic respiration, where PACS2 is a positive regulator.

We also found that, contrary to the changes in PACS2 expression, CPT1 $\alpha$  expression was significantly reduced under HGHF stress but was rescued by PACS2 knockdown (Figures 6E–G). This result was consistent with the CPT1 $\alpha$  expression in kidney tissues of diabetic mice fed with HFD and found that its protein expression was reduced (Figure 6H) in Oil red-positive tissues (Figure 6I). These results further suggest that PACS2 regulates fatty acid metabolism, possibly by disturbing the balance of endothelial redox homeostasis through NADPH production.

## Inhibition of FAO Blocks PACS2 Regulation of Endothelial Barrier Function and Hyperpermeability

As observed above, HGHF affects endothelial FAO. However, it is unclear if PACS2 regulation of barrier function under HGHF is reliable for the FAO change. Therefore, the FAO inhibitor ETO were used to block FAO in endothelial cells to test this. We found that ETO increased VE-cadherin internalization (Figure 7A) and FITC leakage (Figure 7B) under non-HGHF conditions. Moreover, PACS2 knockdown attenuated the effect of HGHF on FITC leakage and VE-cadherin internalization (Figure 7B). However, this PACS2 effect was not seen when ETO was present. These results indicate that FAO is downstream of PACS2 in regulating endothelial barrier function under HGHF.

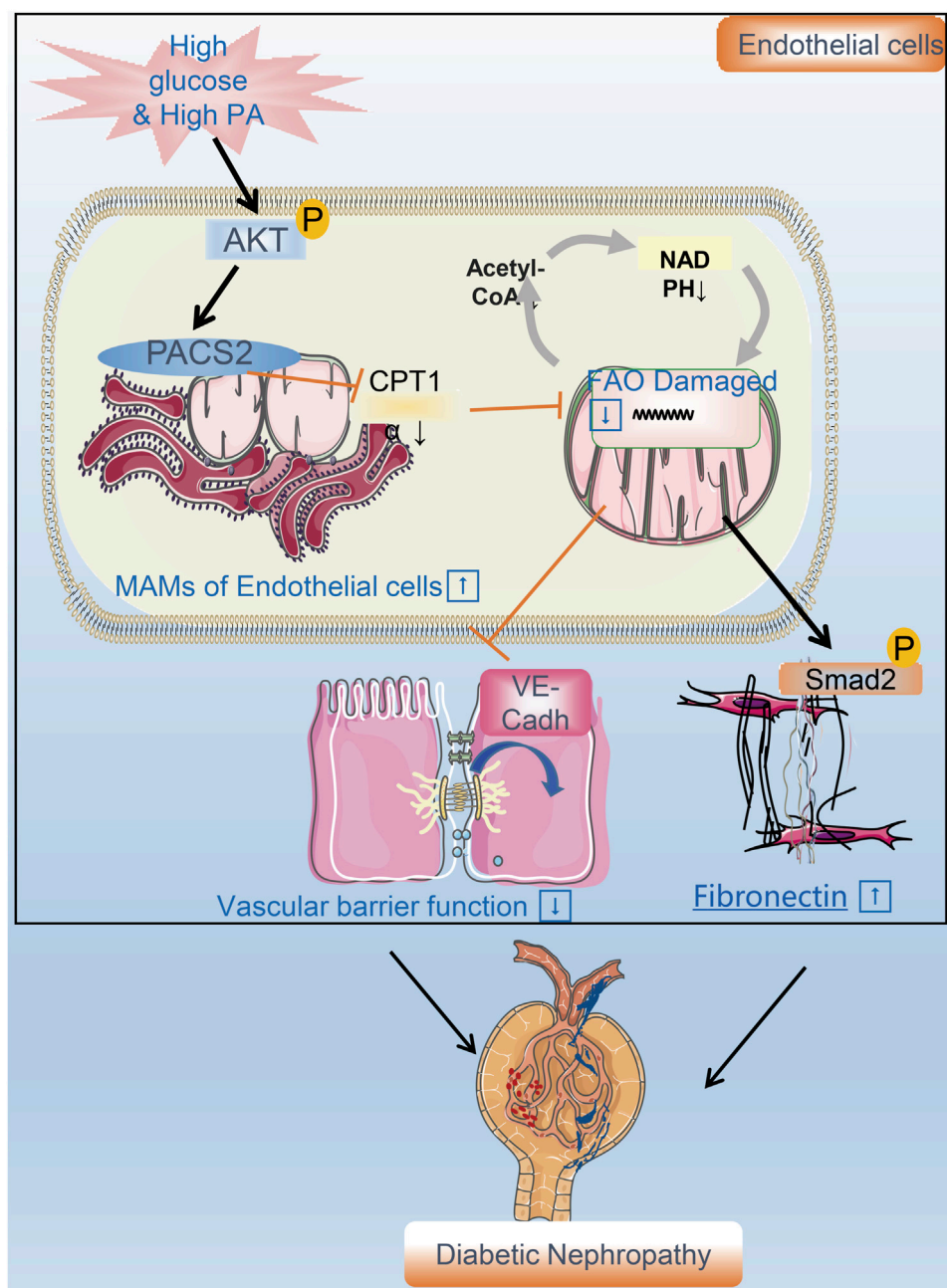


**FIGURE 8 |** A flow chart model proposal to explain the mechanism of renal vascular endothelial cell injury in DN. PACS2 is a critical component of the mechanism behind DN caused by HGHF. Under high glucose/high fat conditions, PACS2 is upregulated and increases the number of MAMs, followed by a decrease in CPT1 $\alpha$  expression, free fatty (FA)  $\beta$ -oxidation, and NADPH production in renal vascular endothelial cells. All these metabolic changes will promote the internalization of VE-cadherin, disturb the barrier function of endothelial cells, and fibrosis increased ultimately lead to pathogenesis and development of DN.

## DISCUSSION

Diabetes combined with hyperlipidemia is usually regarded as a potent risk factor to induce DN. Endothelial cells are the fundamental component of the renal filtration barrier and are directly damaged by abnormal circulating metabolites in diabetes. This study aimed to determine the function of vascular endothelial cells and their metabolic mechanisms in the

occurrence and development of DN. We found that the expression of the endothelial MAM regulatory protein PACS2 increases significantly in response to HGHF. Furthermore, the knockout of PACS2 protects renal vascular function from HGHF. Moreover, PACS2 regulates endothelial FAO and further affects VE-cadherin internalization and Smad2 activation, which damage the filtration membrane barrier and increase FN generation in the ECM. (Figure 8).

Due to the low content of mitochondria (2–6% of the cytoplasm volume), endothelial cells preferentially obtain 80% of ATP through glycolysis in a resting state (Caja and Enríquez, 2017). Although the energy supply from FAO is limited, it is essential for endothelial redox homeostasis (Kalucka et al., 2018). It was reported that when assembled into a formed network, HUVECs will increase FAO, decrease glycolysis, and increase NADPH regeneration to maintain redox homeostasis (Patella et al., 2015; Andrade et al., 2021). However, when both glucose and lipids are overloaded, malonyl-CoA will accumulate and interact with CPT1 $\alpha$ , thereby reducing the oxidation of fatty acids in the mitochondria (Fucho et al., 2017; Bellini et al., 2018). Lipid accumulation and low expression of CPT1 $\alpha$  support the damaged FAO capability (Gray et al., 2013; Ghosh et al., 2017) observed in the STZ/HFD-induced mouse kidneys. Indeed, we examined the expression of the FAO rate-limiting enzyme CPT1 $\alpha$  in HUVECs and mouse kidneys and found that it was decreased under HGHF. Besides, HGHF inhibits fatty acid utilization and increases the secretion of endothelial FN. Consistent with this, TGF- $\beta$ 1 and interleukin-1 $\beta$  can trigger endothelial-to-mesenchymal-transition by affecting acetyl-CoA levels through FAO (Xiong et al., 2018). We also found that when FAO was inhibited with or without silencing PACS2, the endothelial barrier was impaired, and Smad2 was activated. These endothelial dysfunctions caused by FAO inhibition cannot be offset by PACS2 knockdown, indicating that FAO works downstream of PACS2.

High glucose can activate endothelial nitric oxide synthase and induce mtROS that cause mitochondrial DNA damage. Our previous studies found that high glucose affects dynamin-related protein 1-mediated mitochondrial fission in endothelial cells (Liu et al., 2019a). In this study, we first observed an increase in MAMs under HGHF. Abnormally increased MAMs have been reported to evoke mitochondrial calcium overload, mitophagosome formation, and mitophagy (Gbel et al., 2020). It also has been reported that MAMs are associated with hepatocyte insulin resistance (Bassot et al., 2019) and diabetic smooth muscle cell phenotypic transformation (Moulis et al., 2019). We found that under HGHF, increased endothelial MAMs were accompanied by mitochondrial swelling and fragmentation. Thus, we explored the significance of the increase in MAMs in endothelial cells. Previous studies have shown that MAMs can regulate Ca<sup>2+</sup> signalling (Boyman et al., 2020), lipid synthesis (Balla et al., 2020), and mitochondrial fusion (Hu et al., 2021). Although we assessed three enriched proteins related to lipid metabolism (Thomas et al., 2017), including GRP75, FACL4, and PACS2, only PACS2 showed significant changes after HGHF treatment. As one of the enriched regulatory proteins of MAMs, mice lacking PACS2 still maintain relatively low levels of MAMs, which may help endothelial cells maintain a baseline crosstalk between ER and mitochondria. Previous studies have shown that downregulation of PACS2 can prevent the increase of mitochondrial Ca<sup>2+</sup>-mediated apoptosis (Barroso-González et al., 2016). However, we believe that PACS2 is a metabolic switch, not just a single specific

pathway component in endothelial cells. In metabolism-related evaluations, downregulation of PACS2 increased NADPH/NADP<sup>+</sup> ratio, ATP generation, and PA-OCR in HGHF-treated endothelial cells. Although different metabolic conditions may affect endothelial cell function, in this study, the barrier function and fibroblastic phenotype related to VE-cadherin and p-Smad2 were regulated by PACS2.

At last, extrapolating data from HUVECs *in vitro* exposure to HGHF to diabetic patients is insufficient. Ideally, studies of endothelial cells from human donors with diabetes or glomerular endothelial cell line (GEnCs) with diabetes would be used to validate the key findings. Besides that, the endothelial-specific gene knock-off animal model will be the future research plan to strengthen our evidence.

## CONCLUSION

In summary, our findings reveal the role of PACS2 in regulating free fatty acids metabolism in glomerular endothelial cells and DN. Therefore, knocking down PACS2 can alleviate vascular barrier damage and glomerulosclerosis by enhancing the FAO ability. We highlight the metabolic mechanism and provide a new target for the treatment of diabetic microvascular complications.

## DATA AVAILABILITY STATEMENT

The datasets presented in this study can be found in online repositories. The names of the repository/repositories and accession number(s) can be found below: The proteomics data has uploaded *via* PRIDE in ProteomeXchange with accession number: PXD033227.

## ETHICS STATEMENT

The animal study was reviewed and approved by Institutional Animal Care and Use Committee of Central South University, Changsha, China.

## AUTHOR CONTRIBUTIONS

ZS wrote the paper and conceived and designed the experiments. AC Helped modify and optimize the experimental design. SC and HX collected and provided the cell samples for this study. RW, XW, JO, JZ, and HuL contributed to drafting the article. All authors have read and approved the final submitted manuscript. HoL is the GUARANTOR for the article who accepts full responsibility for the study's work and conduct, has access to the data, and oversaw the decision to publish. All authors read and approved the final manuscript.

## FUNDING

This work was supported by a grant from the National Natural Science Foundation of China (grant Nos. 81870352, 81970252) and the Key Research and Development Project of Hunan Province (grant Nos. 2019SK2041, 2020SK2087).

## ACKNOWLEDGMENTS

Authors acknowledge Junpu Wang and Jing Li, Department of Pathology, Xiangya Hospital, Central South University for providing the help of TEM of MAMs. We also would like to thank Applied Protein Technology Co., Ltd. (Shanghai, China) and KangChen Biotech (Shanghai, China) for metabolomics and proteomics.

## REFERENCES

- Aman, J., van Bezu, J., Damanafshan, A., Huveneers, S., Eringa, E. C., Vogel, S. M., et al. (2012). Effective Treatment of Edema and Endothelial Barrier Dysfunction with Imatinib. *Circulation* 126, 2728–2738. doi:10.1161/CIRCULATIONAHA.112.134304
- Andrade, J., Shi, C., Costa, A. S. H., Choi, J., Kim, J., Doddaballapur, A., et al. (2021). Control of Endothelial Quiescence by FOXO-Regulated Metabolites. *Nat. Cell. Biol.* 23, 413–423. doi:10.1038/s41556-021-00637-6
- Arruda, A. P., Pers, B. M., Parlakgöl, G., Güney, E., Inouye, K., and Hotamisligil, G. S. (2014). Chronic Enrichment of Hepatic Endoplasmic Reticulum-Mitochondria Contact Leads to Mitochondrial Dysfunction in Obesity. *Nat. Med.* 20, 1427–1435. doi:10.1038/nm.3735
- Balla, T., Sengupta, N., and Kim, Y. J. (2020). Lipid Synthesis and Transport Are Coupled to Regulate Membrane Lipid Dynamics in the Endoplasmic Reticulum. *Biochim. Biophys. Acta Mol. Cell. Biol. Lipids* 1865, 158461. doi:10.1016/j.bbalip.2019.05.005
- Barrett, E. J., Liu, Z., Khamaisi, M., King, G. L., Klein, R., Klein, B. E. K., et al. (2017). Diabetic Microvascular Disease: An Endocrine Society Scientific Statement. *J. Clin. Endocrinol. Metab.* 102, 4343–4410. doi:10.1210/je.2017-01922
- Barroso-González, J., Auclair, S., Luan, S., Thomas, L., Atkins, K. M., Aslan, J. E., et al. (2016). PACS-2 Mediates the ATM and NF- $\kappa$ B-dependent Induction of Anti-apoptotic Bcl-xL in Response to DNA Damage. *Cell. Death Differ.* 23, 1448–1457. doi:10.1038/cdd.2016.23
- Bassot, A., Chauvin, M. A., Bendridi, N., Ji-Cao, J., Vial, G., Monnier, L., et al. (2019). Regulation of Mitochondria-Associated Membranes (MAMs) by NO/sGC/PKG Participates in the Control of Hepatic Insulin Response. *Cells* 8, 1319. doi:10.3390/cells8111319
- Bellini, L., Campana, M., Rouch, C., Chacinska, M., Bugliani, M., Meneyrol, K., et al. (2018). Protective Role of the ELOVL2/docosaheptaenoic Acid axis in Glucolipotoxicity-Induced Apoptosis in Rodent Beta Cells and Human Islets. *Diabetologia* 61, 1780–1793. doi:10.1007/s00125-018-4629-8
- Boyman, L., Karbowski, M., and Lederer, W. J. (2020). Regulation of Mitochondrial ATP Production: Ca<sup>2+</sup> Signaling and Quality Control. *Trends Mol. Med.* 26, 21–39. doi:10.1016/j.molmed.2019.10.007
- Caja, S., and Enriquez, J. A. (2017). Mitochondria in Endothelial Cells: Sensors and Integrators of Environmental Cues. *Redox Biol.* 12, 821–827. doi:10.1016/j.redox.2017.04.021
- Cantelmo, A. R., Conradi, L. C., Brajic, A., Goveia, J., Kalucka, J., Pircher, A., et al. (2016). Inhibition of the Glycolytic Activator PFKFB3 in Endothelium Induces Tumor Vessel Normalization, Impairs Metastasis, and Improves Chemotherapy. *Cancer Cell* 30, 968–985. doi:10.1016/j.ccell.2016.10.006
- Cheng, H.-T., Xu, X., Lim, P. S., and Hung, K.-Y. (2021). Worldwide Epidemiology of Diabetes-Related End-Stage Renal Disease, 2000–2015. *Diabetes Care* 44, 89–97. doi:10.2337/dc20-1913

## SUPPLEMENTARY MATERIAL

The Supplementary Material for this article can be found online at: <https://www.frontiersin.org/articles/10.3389/fphar.2022.876937/full#supplementary-material>

**Supplementary Figure S1** | Flow chart of STZ/HFD mouse model. A. Schematic diagram of diabetic mice model induced by streptozotocin (stz) and fed with high-fat diet (HFD) for up to 20 weeks.

**Supplementary Figure S2** | Proteomics of HUVECs under HGHF. (A). Heat map of significantly different proteins between control and HGHF(test) group. (B). Differential proteins located in mitochondria and ER (C). Proteins has been reported correlated with renal function (Test/Control).

**Supplementary Figure S3** | Metabolomics of HUVECs under HGHF. (A). PCA map of samples in metabolomics. (B). Differential metabolomic molecular in HUVECs under HGHF. (C). Long-chain free fatty acid correlated with FAO in metabolomic.

- Cheng, H., Gang, X., He, G., Liu, Y., Wang, Y., Zhao, X., et al. (2020). The Molecular Mechanisms Underlying Mitochondria-Associated Endoplasmic Reticulum Membrane-Induced Insulin Resistance. *Front. Endocrinol.* 11, 592129. doi:10.3389/fendo.2020.592129
- Cheng, Y., Yu, X., Zhang, J., Chang, Y., Xue, M., Li, X., et al. (2019). Pancreatic Kallikrein Protects against Diabetic Retinopathy in KK Cg-Ay/J and High-Fat Diet/streptozotocin-Induced Mouse Models of Type 2 Diabetes. *Diabetologia* 62, 1074–1086. doi:10.1007/s00125-019-4838-9
- Coca, S. G., Ismail-Beigi, F., Haq, N., Krumholz, H. M., and Parikh, C. R. (2012). Role of Intensive Glucose Control in Development of Renal End Points in Type 2 Diabetes Mellitus: Systematic Review and Meta-Analysis Intensive Glucose Control in Type 2 Diabetes. *Arch. Intern. Med.* 172, 761–769. doi:10.1001/archinternmed.2011.2230
- Dahlby, T., Simon, C., Backe, M. B., Dahllöf, M. S., Holson, E., Wagner, B. K., et al. (2020). Enhancer of Zeste Homolog 2 (EZH2) Mediates Glucolipotoxicity-Induced Apoptosis in  $\beta$ -Cells. *Int. J. Mol. Sci.* 21, 8016. doi:10.3390/ijms21218016
- Du, Q., Tan, Z., Shi, F., Tang, M., Xie, L., Zhao, L., et al. (2019). PGC1 $\alpha$ /CEBPB/CPT1A axis Promotes Radiation Resistance of Nasopharyngeal Carcinoma through Activating Fatty Acid Oxidation. *Cancer Sci.* 110, 2050–2062. doi:10.1111/cas.14011
- Feng, W., Lei, T., Wang, Y., Feng, R., Yuan, J., Shen, X., et al. (2019). GCN2 Deficiency Ameliorates Cardiac Dysfunction in Diabetic Mice by Reducing Lipotoxicity and Oxidative Stress. *Free Radic. Biol. Med.* 130, 128–139. doi:10.1016/j.freeradbiomed.2018.10.445
- Fu, H., Liu, S., Bastacky, S. I., Wang, X., Tian, X. J., and Zhou, D. (2019). Diabetic Kidney Diseases Revisited: A New Perspective for a New Era. *Mol. Metab.* 30, 250–263. doi:10.1016/j.molmet.2019.10.005
- Fucho, R., Casals, N., Serra, D., and Herrero, L. (2017). Ceramides and Mitochondrial Fatty Acid Oxidation in Obesity. *FASEB J.* 31, 1263–1272. doi:10.1096/fj.201601156R
- Gbel, J., Engelhardt, E., Pelzer, P., Sakthivelu, V., Jahn, H. M., Jevtic, M., et al. (2020). Mitochondria-Endoplasmic Reticulum Contacts in Reactive Astrocytes Promote Vascular Remodeling. *Cell. Metab.* 31, 791–808 e8.
- Gebreegziabih, G., Belachew, T., Mehari, K., and Tamiru, D. (2021). Prevalence of Dyslipidemia and Associated Risk Factors Among Adult Residents of Mekelle City, Northern Ethiopia. *Plos One* 16, e0243103. doi:10.1371/journal.pone.0243103
- Ghosh, A., Gao, L., Thakur, A., Siu, P. M., and Lai, C. W. K. (2017). Role of Free Fatty Acids in Endothelial Dysfunction. *J. Biomed. Sci.* 24, 50. doi:10.1186/s12929-017-0357-5
- Gray, S. P., Di Marco, E., Okabe, J., Szyndralewicz, C., Heitz, F., Montezano, A. C., et al. (2013). NADPH Oxidase 1 Plays a Key Role in Diabetes Mellitus-Accelerated Atherosclerosis. *Circulation* 127, 1888–1902. doi:10.1161/CIRCULATIONAHA.112.132159
- Haile, K., and Timerga, A. (2020). Dyslipidemia and its Associated Risk Factors Among Adult Type-2 Diabetic Patients at Jimma University Medical Center,



- Jimma, Southwest Ethiopia. *Diabetes Metab. Syndr. Obes.* 13, 4589–4597. doi:10.2147/DMSO.S283171
- Hu, Y., Chen, H., Zhang, L., Lin, X., Li, X., Zhuang, H., et al. (2021). The AMPK-MFN2 axis Regulates MAM Dynamics and Autophagy Induced by Energy Stresses. *Autophagy* 17, 1142–1156. doi:10.1080/15548627.2020.1749490
- Jeong, H. S., Hong, S. J., Cho, S. A., Kim, J. H., Cho, J. Y., Lee, S. H., et al. (2017). Comparison of Ticagrelor Versus Prasugrel for Inflammation, Vascular Function, and Circulating Endothelial Progenitor Cells in Diabetic Patients With Non-ST-Segment Elevation Acute Coronary Syndrome Requiring Coronary Stenting: A Prospective, Randomized, Crossover Trial. *JACC Cardiovasc Interv.* 10, 1646–1658. doi:10.1016/j.jcin.2017.05.064
- Juettner, V. V., Kruse, K., Dan, A., Vu, V. H., Khan, Y., Le, J., et al. (2019). VE-PTP Stabilizes VE-Cadherin Junctions and the Endothelial Barrier via a Phosphatase-independent Mechanism. *J. Cell. Biol.* 218, 1725–1742. doi:10.1083/jcb.201807210
- Kalucka, J., Bierhansl, L., Concinha, N. V., Missiaen, R., Elia, I., Brüning, U., et al. (2018). Quiescent Endothelial Cells Upregulate Fatty Acid  $\beta$ -Oxidation for Vasculoprotection via Redox Homeostasis. *Cell. Metab.* 28, 881–e13. doi:10.1016/j.cmet.2018.07.016
- Kalucka, J., de Rooij, L. P. M. H., Goveia, J., Rohlenova, K., Dumas, S. J., Meta, E., et al. (2020). Single-Cell Transcriptome Atlas of Murine Endothelial Cells. *Cell* 180, 764–e20. doi:10.1016/j.cell.2020.01.015
- Kim, D. Y., Kim, S. R., and Jung, U. J. (2020). Myricitrin Ameliorates Hyperglycemia, Glucose Intolerance, Hepatic Steatosis, and Inflammation in High-Fat Diet/Streptozotocin-Induced Diabetic Mice. *Int. J. Mol. Sci.* 21, 1870. doi:10.3390/ijms21051870
- Kuravi, S. J., McGettrick, H. M., Satchell, S. C., Saleem, M. A., Harper, L., Williams, J. M., et al. (2014). Podocytes Regulate Neutrophil Recruitment by Glomerular Endothelial Cells via IL-6-mediated Crosstalk. *J. Immunol.* 193, 234–243. doi:10.4049/jimmunol.1300229
- Lampugnani, M. G., Dejana, E., and Giampietro, C. (2018). Vascular Endothelial (VE)-Cadherin, Endothelial Adherens Junctions, and Vascular Disease. *Cold Spring Harb. Perspect. Biol.* 10, a029322. doi:10.1101/cshperspect.a029322
- Lewin, T. M., Van Horn, C. G., Krisans, S. K., and Coleman, R. A. (2002). Rat Liver Acyl-CoA Synthetase 4 Is a Peripheral-Membrane Protein Located in Two Distinct Subcellular Organelles, Peroxisomes, and Mitochondrial-Associated Membrane. *Arch. Biochem. Biophys.* 404, 263–270. doi:10.1016/s0003-9861(02)00247-3
- Liang, T., Hang, W., Chen, J., Wu, Y., Wen, B., Xu, K., et al. (2021). ApoE4 ( $\Delta$ 272-299) Induces Mitochondrial-associated Membrane Formation and Mitochondrial Impairment by Enhancing GRP75-Modulated Mitochondrial Calcium Overload in Neuron. *Cell. Biosci.* 11, 50. doi:10.1186/s13578-021-00563-y
- Liu, H., Xiang, H., Zhao, S., Sang, H., Lv, F., Chen, R., et al. (2019). Vildagliptin Improves High Glucose-Induced Endothelial Mitochondrial Dysfunction via Inhibiting Mitochondrial Fission. *J. Cell. Mol. Med.* 23, 798–810. doi:10.1111/jcmm.13975
- Liu, Y., Ma, X., Fujioka, H., Liu, J., Chen, S., and Zhu, X. (2019). DJ-1 Regulates the Integrity and Function of ER-Mitochondria Association through Interaction with IP3R3-Grp75-VDAC1. *Proc. Natl. Acad. Sci. U. S. A.* 116, 25322–25328. doi:10.1073/pnas.1906565116
- McDonald, J. D., Mah, E., Chitchumroonchokchai, C., Dey, P., Labyk, A. N., Villamena, F. A., et al. (2019). Dairy Milk Proteins Attenuate Hyperglycemia-Induced Impairments in Vascular Endothelial Function in Adults with Prediabetes by Limiting Increases in Glycemia and Oxidative Stress that Reduce Nitric Oxide Bioavailability. *J. Nutr. Biochem.* 63, 165–176. doi:10.1016/j.jnutbio.2018.09.018
- Moulis, M., Grousset, E., Faccini, J., Richetin, K., Thomas, G., and Vindis, C. (2019). The Multifunctional Sorting Protein PACS-2 Controls Mitophagosome Formation in Human Vascular Smooth Muscle Cells through Mitochondria-ER Contact Sites. *Cells* 8, 638. doi:10.3390/cells8060638
- Patella, F., Schug, Z. T., Persi, E., Neilson, L. J., Erami, Z., Avanzato, D., et al. (2015). Proteomics-based Metabolic Modeling Reveals that Fatty Acid Oxidation (FAO) Controls Endothelial Cell (EC) Permeability. *Mol. Cell. Proteomics* 14, 621–634. doi:10.1074/mcp.M114.045575
- Peltier, A., Goutman, S. A., and Callaghan, B. C. (2014). Painful Diabetic Neuropathy. *BMJ* 348, g1799. doi:10.1136/bmj.g1799
- Qi, H., Casaleña, G., Shi, S., Yu, L., Ebefors, K., Sun, Y., et al. (2017). Glomerular Endothelial Mitochondrial Dysfunction Is Essential and Characteristic of Diabetic Kidney Disease Susceptibility. *Diabetes* 66, 763–778. doi:10.2337/db16-0695
- Ricciardi, C. A., and Gnudi, L. (2020). The Endoplasmic Reticulum Stress and the Unfolded Protein Response in Kidney Disease: Implications for Vascular Growth Factors. *J. Cell. Mol. Med.* 24, 12910–12919. doi:10.1111/jcmm.15999
- Rohlenova, K., Goveia, J., García-Caballero, M., Subramanian, A., Kalucka, J., Treps, L., et al. (2020). Single-Cell RNA Sequencing Maps Endothelial Metabolic Plasticity in Pathological Angiogenesis. *Cell. Metab.* 31, 862–e14. doi:10.1016/j.cmet.2020.03.009
- Shan, K., Liu, C., Liu, B. H., Chen, X., Dong, R., Liu, X., et al. (2017). Circular Noncoding RNA HIPK3 Mediates Retinal Vascular Dysfunction in Diabetes Mellitus. *Circulation* 136, 1629–1642. doi:10.1161/CIRCULATIONAHA.117.029004
- Sun, J., Huang, X., Niu, C., Wang, X., Li, W., Liu, M., et al. (2021). aFGF Alleviates Diabetic Endothelial Dysfunction by Decreasing Oxidative Stress via Wnt/ $\beta$ -Catenin-Mediated Upregulation of HXK2. *Redox Biol.* 39, 101811. doi:10.1016/j.redox.2020.101811
- Thomas, G., Aslan, J. E., Thomas, L., Shinde, P., Shinde, U., and Simmen, T. (2017). Caught in the Act - Protein Adaptation and the Expanding Roles of the PACS Proteins in Tissue Homeostasis and Disease. *J. Cell. Sci.* 130, 1865–1876. doi:10.1242/jcs.199463
- Tremblay, A. J., Lamarche, B., Deacon, C. F., Weisnagel, S. J., and Couture, P. (2014). Effects of Sitagliptin Therapy on Markers of Low-Grade Inflammation and Cell Adhesion Molecules in Patients with Type 2 Diabetes. *Metabolism* 63, 1141–1148. doi:10.1016/j.metabol.2014.06.004
- Wang, M., Song, L., Strange, C., Dong, X., and Wang, H. (2018). Therapeutic Effects of Adipose Stem Cells from Diabetic Mice for the Treatment of Type 2 Diabetes. *Mol. Ther.* 26, 1921–1930. doi:10.1016/j.jymthe.2018.06.013
- Weil, E. J., Lemley, K. V., Mason, C. C., Yee, B., Jones, L. I., Blouch, K., et al. (2012). Podocyte Detachment and Reduced Glomerular Capillary Endothelial Fenestration Promote Kidney Disease in Type 2 Diabetic Nephropathy. *Kidney Int.* 82, 1010–1017. doi:10.1038/ki.2012.234
- Weng, C. H., Li, Y. J., Wu, H. H., Liu, S. H., Hsu, H. H., Chen, Y. C., et al. (2020). Interleukin-17A Induces Renal Fibrosis through the ERK and Smad Signaling Pathways. *Biomed. Pharmacother.* 123, 109741. doi:10.1016/j.biopha.2019.109741
- Wu, L., Liu, C., Chang, D. Y., Zhan, R., Zhao, M., Man Lam, S., et al. (2021). The Attenuation of Diabetic Nephropathy by Annexin A1 via Regulation of Lipid Metabolism Through the AMPK/PPAR $\alpha$ /CPT1b Pathway. *Diabetes* 70, 2192–2203. doi:10.2337/db21-0050
- Wu, S., Lu, Q., Ding, Y., Wu, Y., Qiu, Y., Wang, P., et al. (2019). Hyperglycemia-Driven Inhibition of AMP-Activated Protein Kinase  $\alpha$ 2 Induces Diabetic Cardiomyopathy by Promoting Mitochondria-Associated Endoplasmic Reticulum Membranes *In Vivo*. *Circulation* 139, 1913–1936. doi:10.1161/CIRCULATIONAHA.118.033552
- Xiang, H., Song, R., Ouyang, J., Zhu, R., Shu, Z., Liu, Y., et al. (2021). Organelle Dynamics of Endothelial Mitochondria in Diabetic Angiopathy. *Eur. J. Pharmacol.* 895, 173865. doi:10.1016/j.ejphar.2021.173865
- Xiong, J., Kawagishi, H., Yan, Y., Liu, J., Wells, Q. S., Edmunds, L. R., et al. (2018). A Metabolic Basis for Endothelial-To-Mesenchymal Transition. *Mol. Cell.* 69, 689–e7. doi:10.1016/j.molcel.2018.01.010
- Yang, H. Z., Xiong, W. J., Li, X., Jiang, J., and Jiang, R. (2022). Low Androgen Status Inhibits Erectile Function by Upregulating the Expression of Proteins of Mitochondria-Associated Membranes in Rat Corpus Cavernosum. *Andrology*.
- Yang, J., Yao, W., Qian, G., Wei, Z., Wu, G., and Wang, G. (2015). Rab5-mediated VE-Cadherin Internalization Regulates the Barrier Function of the Lung Microvascular Endothelium. *Cell. Mol. Life Sci.* 72, 4849–4866. doi:10.1007/s00018-015-1973-4
- Yang, M., Han, Y., Luo, S., Xiong, X., Zhu, X., Zhao, H., et al. (2021). MAMs Protect Against Ectopic Fat Deposition and Lipid-Related Kidney Damage in DN Patients. *Front. Endocrinol.* 12, 609580. doi:10.3389/fendo.2021.609580
- Zhang, F., Yuan, W., Wei, Y., Zhang, D., Duan, Y., Li, B., et al. (2019). The Alterations of Bile Acids in Rats with High-Fat Diet/streptozotocin-Induced Type 2 Diabetes and Their Negative Effects on Glucose Metabolism. *Life Sci.* 229, 80–92. doi:10.1016/j.lfs.2019.05.031

Zhu, Y., Bo, H., Chen, Z., Li, J., He, D., Xiao, M., et al. (2020). LINC00968 Can Inhibit the Progression of Lung Adenocarcinoma through the miR-21-5p/SMAD7 Signal axis. *Aging (Albany NY)* 12, 21904–21922. doi:10.18632/aging.104011

**Conflict of Interest:** The authors declare that the research was conducted in the absence of any commercial or financial relationships that could be construed as a potential conflict of interest.

**Publisher's Note:** All claims expressed in this article are solely those of the authors and do not necessarily represent those of their affiliated organizations, or those of

the publisher, the editors and the reviewers. Any product that may be evaluated in this article, or claim that may be made by its manufacturer, is not guaranteed or endorsed by the publisher.

Copyright © 2022 Shu, Chen, Xiang, Wu, Wang, Ouyang, Zhang, Liu, Chen and Lu. This is an open-access article distributed under the terms of the Creative Commons Attribution License (CC BY). The use, distribution or reproduction in other forums is permitted, provided the original author(s) and the copyright owner(s) are credited and that the original publication in this journal is cited, in accordance with accepted academic practice. No use, distribution or reproduction is permitted which does not comply with these terms.



# Cyclovirobuxine D Ameliorates Experimental Diabetic Cardiomyopathy by Inhibiting Cardiomyocyte Pyroptosis *via* NLRP3 *in vivo* and *in vitro*

Ge Gao<sup>1,2,3</sup>, Lingyun Fu<sup>1,2,3,4</sup>, Yini Xu<sup>1,2,3</sup>, Ling Tao<sup>1,3</sup>, Ting Guo<sup>1,2,3</sup>, Guanqin Fang<sup>1,2,3</sup>, Guangqiong Zhang<sup>1,2,3</sup>, Shengquan Wang<sup>1,2,3</sup>, Ti Qin<sup>1,2,3</sup>, Peng Luo<sup>1,2\*</sup> and Xiangchun Shen<sup>1,2,3,4\*</sup>

## OPEN ACCESS

### Edited by:

Xianwei Wang,  
Xinxiang Medical University, China

### Reviewed by:

Yong Zhang,  
Harbin Medical University, China  
Zhen Qiu,  
Renmin Hospital of Wuhan University,  
China

### \*Correspondence:

Peng Luo  
329572497@qq.com  
Xiangchun Shen  
shenxiangchun@126.com

### Specialty section:

This article was submitted to  
Cardiovascular and Smooth Muscle  
Pharmacology,  
a section of the journal  
Frontiers in Pharmacology

Received: 28 March 2022

Accepted: 24 May 2022

Published: 05 July 2022

### Citation:

Gao G, Fu L, Xu Y, Tao L, Guo T,  
Fang G, Zhang G, Wang S, Qin T,  
Luo P and Shen X (2022)  
Cyclovirobuxine D Ameliorates  
Experimental Diabetic  
Cardiomyopathy by Inhibiting  
Cardiomyocyte Pyroptosis *via*  
NLRP3 *in vivo* and *in vitro*.  
Front. Pharmacol. 13:906548.  
doi: 10.3389/fphar.2022.906548

<sup>1</sup>The State Key Laboratory of Functions and Applications of Medicinal Plants, Guizhou Medical University, Guiyang, China, <sup>2</sup>The Department of Pharmacology of Materia Medica (The High Efficacy Application of Natural Medicinal Resources Engineering Center of Guizhou Province and The High Educational Key Laboratory of Guizhou Province for Natural Medicinal Pharmacology and Druggability), School of Pharmaceutical Sciences, Guizhou Medical University, Guiyang, China, <sup>3</sup>The Key Laboratory of Optimal Utilization of Natural Medicine Resources (The Union Key Laboratory of Guiyang City-Guizhou Medical University), School of Pharmaceutical Sciences, Guizhou Medical University, Guiyang, China, <sup>4</sup>The Key Laboratory of Endemic and Ethnic Diseases of Ministry of Education, Guizhou Medical University, Guiyang, China

Diabetic cardiomyopathy (DCM) is one of the common complications of diabetic patients, which can induce myocardial hypertrophy, cardiac fibrosis, and heart failure. Growing evidence has shown that the occurrence and development of DCM are accompanied by pyroptosis which is an NLRP3-mediated intense inflammatory cell death. Cyclovirobuxine D (CVB-D) has been shown to significantly ameliorate DCM and anti-inflammatory effects associated with cardiomyopathy, but it is unclear whether it has an effect on cardiomyocyte pyroptosis accompanying DCM. Therefore, the purpose of the present study was to explore the ameliorating effect of CVB-D on cardiomyocyte pyroptosis associated with DCM and its molecular regulation mechanism. Type 2 diabetes in C57BL/6 mice was reproduced by the high-fat and high-glucose diet (HFD) combined with low-dose streptozotocin (STZ). The characteristics of DCM were evaluated by cardiac ultrasonography, serum detection, and histopathological staining. The results suggested that CVB-D could significantly alleviate the cardiac pathology of DCM. Then, we explored the mechanism of CVB-D on primary neonatal rat cardiomyocyte (PNRCM) injury with high glucose (HG) *in vitro* to simulate the physiological environment of DCM. Preincubation with CVB-D could significantly increase cell viability, attenuate cytopathological changes and inhibit the expression levels of pyroptosis-related proteins. Further research found that the myocardial improvement effect of CVB-D was related to its inhibition of NLRP3 expression. In conclusion, our data suggest that CVB-D can ameliorate DCM by inhibiting cardiomyocyte pyroptosis *via* NLRP3, providing a novel molecular target for CVB-D clinical application.

**Keywords:** cyclovirobuxine D, high glucose, NLRP3 inflammasome, cardiomyocytes, pyroptosis, diabetic cardiomyopathy

## INTRODUCTION

Diabetic cardiomyopathy (DCM) is a myocardial microvascular complication of diabetes, characterized by cardiac insufficiency, myocardial interstitial fibrosis, and myocardial hypertrophy, finally resulting in heart failure. Recent evidence has confirmed that DCM is independent of coronary heart disease, hypertension, and other heart diseases (Kaul et al., 2010; Mandavia et al., 2013). It is noteworthy that DCM is the main cause of death in diabetics (Boudina and Abel, 2010; Falcão-Pires and Leite-Moreira, 2012). The pathological mechanisms of DCM include metabolic changes, mitochondrial dysfunction, oxidative stress, inflammation, cell death, extracellular matrix remodeling, etc. (Hu et al., 2017). Pyroptosis is a pro-inflammatory programmed cell death pattern (Kroemer et al., 2009; Coll et al., 2011), which has biochemical and morphological characteristics of necrosis and apoptosis. Unlike apoptosis or necrosis, pyroptosis leads to activating and releasing a large number of inflammatory cytokines (Xu et al., 2014).

Pyroptosis plays a very significant role in the initiation and progression of cardiovascular diseases, so the inhibitors and drugs targeting pyroptosis pathway-related proteins have always been a research hotspot (Jia et al., 2019). More importantly, activation of pro-caspase-1 is the key to initiating pyroptosis. In 2002, Martinon et al. (2002) first identified inflammasome as molecular platforms that trigger activation of cleaved-caspase-1 and then cut pro-IL-1 $\beta$  and pro-IL-18. The inflammasome is a multiprotein complex composed of receptors, connexin ASC, and pro-caspase-1. To date, several types of inflammasome have been identified, including NLRP1, NLRP3, NLRC4, NLRP6, and AIM2 inflammasome. Among these different types of inflammasome, NLRP3 inflammasome has been extensively highlighted in a variety of mammalian cells due to its association with various autoimmune and inflammatory diseases (Zeng et al., 2019). A lot of studies found that hyperglycemia environment-induced overactivation of NLRP3 inflammasome. After the activation of NLRP3, the pyrin domain in NLRP3 binds to the pyrin domain in ASC, which then binds to pro-caspase-1 through card–card interactions. Following pro-caspase-1 is cleaved-caspase-1, an active form, which further promotes the maturation and secretion of IL-18 and IL-1 $\beta$ , and exposes the N-terminal effect domain of GSDMD, a member of the Gasdermins family of proteins. After the formation of membrane pores, pro-inflammatory cytokines and cell contents are released, leading to pyroptosis (Li et al., 2014; Wree et al., 2014; Chen et al., 2016; Xu et al., 2018). It has been reported that the expression of NLRP3, cleaved-caspase-1, and pyroptosis pathway-related proteins are upregulated in the heart of diabetic rats. Inhibition of NLRP3 expression in H9c2 cardiomyocytes can significantly prevent pyroptosis induced by high glucose (Luo et al., 2014). Therefore, several NLRP3 inflammasome inhibitors, such as colchicine, glyburide derivatives, MCC950, INF4E, dapansulide/OLT1177, 16673-34-0, and CY-09, have been identified to prevent NLRP3 oligomerization and interfere with ASC polymerization (Jiang et al., 2017; Toldo and Abbate, 2018; Toldo et al., 2018). In addition to the aforementioned drugs directly targeting NLRP3

inhibition, other molecules that indirectly inhibit NLRP3 expression may also ameliorate cardiovascular diseases. For example, Zhang et al. (2018) found that melatonin rescues endothelial cell pyroptosis by reducing pyroptosis-related protein levels *via* the MEG3/miR-223/NLRP3 signaling axis to ameliorate atherosclerosis. MicroRNA-30c-5p can inhibit NLRP3 inflammation-dependent endothelial cell pyroptosis by downregulating FOXO3 expression in atherosclerosis (Li et al., 2018). Above all, NLRP3, as the initiating signal of pyroptosis, is a potential therapeutic target for tackling cardiovascular diseases.

Cycloxanthine D (CVB-D) is a triterpenoid alkaloid, extracted from *Caulis et Ramulus Buxi Sinicae* as Chinese medicine, which is widely applied in the prevention and treatment of various cardiovascular diseases such as arrhythmia and heart failure in China. Experiments have confirmed that CVB-D can reduce cardiac hypertrophy in hyperthyroid rats by preventing cardiomyocyte apoptosis and inhibiting the P38 mitogen-activated protein kinase signaling pathway (Wu et al., 2017). It can also alleviate doxorubicin-induced cardiomyopathy by inhibiting oxidative damage and mitochondrial biogenesis disorders (Guo et al., 2015). In addition, previous studies have verified that CVB-D has a significant therapeutic effect on DCM *via* activating the Nrf2-mediated antioxidant response (Jiang et al., 2020). Research studies have reported that CVB-D suppresses lipopolysaccharide-induced inflammatory responses in murine macrophages *in vitro* by blocking the JAK-STAT signaling pathway. The results proved that the anti-inflammatory actions of CVB-D may be related to its cardioprotection (Guo et al., 2014). However, it is still unclear whether CVB-D can improve DCM by inhibiting cardiomyocyte pyroptosis. Therefore, in this study, a pathological model of DCM was established *in vivo* and *in vitro*, with CVB-D treatment. The NLRP3-mediated pyroptosis was evaluated as a signal transduction pathway to investigate the protective effect of CVB-D on DCM and its molecular regulation mechanism. Finally, we found that CVB-D can ameliorate DCM by inhibiting cardiomyocyte pyroptosis *via* NLRP3. Our results add to the evidence for cardiovascular applications of CVB-D.

## MATERIALS AND METHODS

### Experimental Animals and Groups

Sixty healthy male C57BL/6 mice, 8 weeks old, and weighing 18–24 g were used. The mice were provided by the Animal Experiment Center of Guizhou Medical University, Production License Number: SYXK (Guizhou) 2018-0001. The experiment was approved by the Animal Ethics Committee of Guizhou Medical University (No. 2000904) and followed the ethical standards of animal experiments. The mice were randomly divided into 2 groups with body weight as following: control group ( $n = 12$ , normal rat maintenance diet) and HFD group ( $n = 48$ , high-fat and high-glucose diet). The control group mice were fed with a standard diet containing 16% protein, 4% fat, and 60% carbohydrate, while the HFD group mice were fed with HFD containing 18% fat, 20% sucrose, 2% cholesterol, 0.2% cholic acid, and 59.8% normal diet (Jiang et al., 2020). The mice in two groups



were free to drink water and chew. After 12 weeks of feeding, serum was collected from the tail vein of mice in each group, and fasting blood glucose (FBG) and insulin (INS) levels were detected to calculate the insulin resistance index. The formula was as follows:  $\text{HOMA-IR} = (\text{FBG} \times \text{INS})/22.5$ . Mice in the HFD group with insulin resistance were given a single intraperitoneal injection of streptozotocin (STZ, 30 mg/kg), 10 mg/ml sodium citrate buffer (pH 4.5), and the control group was given an equal volume of sodium citrate buffer. After 4 times of continuous injections of STZ, when the FBG level was higher than 11.1 mM, the mice model of type 2 diabetes was reproduced. Then, the mice in the HFD group were randomly divided into 4 groups as follows: DCM, DCM + CVB-D. L (low dose of CVB-D, 0.5 mg/kg/day), DCM + CVB-D. H (high dose of CVB-D, 1 mg/kg/day), and DCM + Met (metformin, 250 mg/kg/day). The control and DCM groups were given saline for the next 2 months. CHO (Cholesterol, Redu Life Sciences Co., Ltd., China), TG (Triglycerides, Redu Life Sciences Co., Ltd., China), and LDH (Lactate dehydrogenase, Nanjing Jiancheng Institute of Biological Engineering, China) contents in serum were detected after the experiment.

## Cell Culture and Treatment

After extraction, isolation, purification, culture, and identification of PNRCMs (primary neonatal rat cardiomyocytes), the protective effects of CVB-D on HG (high glucose)-induced PNRCM injury were investigated. The experimental groups were as follows: Control (25 mM glucose Dulbecco's modified eagle medium, 25 mM glucose DMEM), HG (40 mM glucose); HG + CVB-D. L (0.1  $\mu\text{M}$ ), HG + CVB-D. H (1  $\mu\text{M}$ ), and HG + Met (0.5 mM), PNRCMs were preincubated with CVB-D and Met for 1 h and then treated with HG for 24 h. Preliminary basic studies have proved that CVB-D has a significant inhibitory effect on NLRP3-mediated cardiomyocyte pyroptosis. In order to further clarify the molecular mechanism of CVB-D on inhibiting PNRCM pyroptosis, NLRP3 inhibitor (MCC950, MedChemExpress, United States) and agonist (BMS-986299, MedChemExpress, United States) were added. The experimental design was as follows: Control (25 mM glucose DMEM), HG (40 mM glucose), HG + CVB-D (1  $\mu\text{M}$ ), HG + MCC950 (1  $\mu\text{M}$ ) or BMS-986299 (1  $\mu\text{M}$ ), and HG + CVB-D + MCC950 or BMS-986299. PNRCMs were pretreated with MCC950 or BMS-986299 for 1 h, then CVB-D was added for 1 h, and finally co-incubated with HG for 24 h.

## Ultrasonography

First, the mice were anesthetized by ether inhalation. The limbs of the mice were fixed after anesthesia, and then the hair on the chest was removed with hair removal cream. The coupling agent was evenly applied after the skin was exposed. The EF (left ventricular ejection fraction), FS (fractional shortening), IVSd (interventricular septal thickness at diastole), LVPWd (left ventricular posterior wall dimensions), and LVIDd (left ventricular internal diameter at end-diastole) of mice were recorded with the M-mode of small-animal ultrasonography (Feiyinuo Technology Co., Ltd., China).

## Hematoxylin-Eosin Staining

The heart tissues were fixed in 4% paraformaldehyde for more than 24 h, and then were dehydrated and embedded. The repaired wax blocks were placed in a paraffin slicer for sections and the thickness was 3  $\mu\text{m}$ . After the paraffin sections were dewaxed, the following staining steps were performed respectively: hematoxylin staining, eosin staining, dehydration, and sealing. Finally, microscopic examination, image acquisition, and analysis (Nikon, Japan) were carried out by independent pathological workers.

## Masson Staining

After the paraffin sections were dewaxed to water, we stained successively with potassium dichromate, hematoxylin, lichun red acid fuchsin, phosphomolybdic acid, and aniline blue. The sections were sealed after differentiation. Images data were analyzed using a microscope (Nikon, Japan).

## TUNEL Staining

The sections were stained according to the instructions of the terminal deoxynucleotidyl transferase-mediated dUTP-biotin nick end labeling (TUNEL) staining kits (Roche, Switzerland). DAPI was used for nuclear staining, and the sections were sealed. They were observed using a fluorescence microscope, and images were collected (Nikon, Japan).

## Immunohistochemistry

After paraffin sections' dewaxing, the following steps were conducted: antigen repair, blocking endogenous peroxidase, serum sealing, adding primary and secondary antibodies, DAB coloration, nucleus staining, dehydration, sealing, microscopic observation, and capturing images (CIC, United States).

## MTT Assay

The PNRCMs were seeded into 96-well plates and cultured for 72 h. After 24 h of treatment, 20  $\mu\text{l}$  5  $\text{mg}\cdot\text{ml}^{-1}$  MTT was added (Beijing Solaibao Technology Co., Ltd., China) to each well and incubated for 4–6 h under dark conditions. Then the supernatant of the cardiomyocytes culture was discarded. After 150  $\mu\text{l}$  DMSO was added to each well, the plate was placed on the shaker until all the crystals at the bottom dissolved. Finally, the absorbance at 490 nm wavelength was measured (Thermo scientific, United States).

## Giemsa Staining

PNRCMs were fixed with 4% paraformaldehyde for 20 min, and then stained with staining solution A and B in turn according to the instructions (Beijing Solaibao Technology Co., Ltd., China). After the sediment in the staining solution was washed out, cell morphology was observed under an inverted microscope, and images were taken (Chongqing Photoelectric Instrument Co., Ltd. China).

## Immunofluorescence

After the cells were fixed, permeated, and sealed with goat serum, the primary and secondary antibodies were dropped and incubated. The nucleus was stained with DAPI and

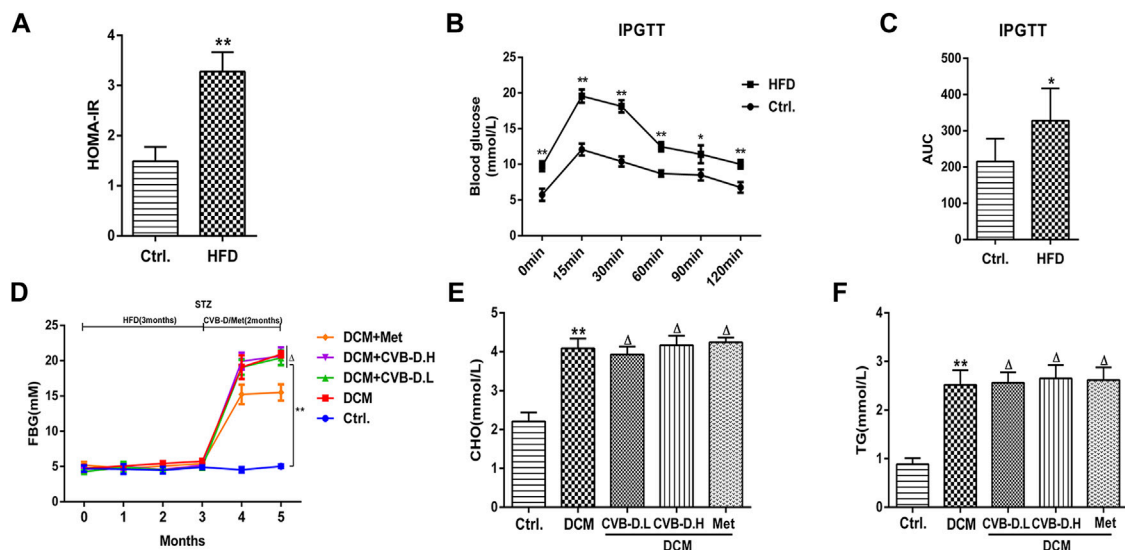


**FIGURE 1 |** HFD (high-fat and high-glucose diet) combined with STZ (streptozotocin) induces type 2 diabetes model in mice. **(A)** Insulin resistance index was calculated in mice by detecting FBG (fasting blood glucose) and INS (insulin). **(B)** After intraperitoneal injection of glucose in fasting condition, the blood glucose of mice at different time points was measured. **(C)** Histogram of AUC (area under the curve) of blood glucose at different time points in mice. **(D)** FBG of mice during modeling and treatment. **(E,F)** Effects of CVB-D on CHO (cholesterol) and TG (triglycerides) contents in serum of DCM (diabetic cardiomyopathy) mice. The data are presented as the mean  $\pm$  SEM ( $n = 6$ ),  $p < 0.05$ ,  $**p < 0.01$  versus the control group;  $\Delta p > 0.05$  versus the model group.

photographed with a fluorescence microscope (Leica, Germany). The fluorescence values of each group were detected by ImageJ software.

## Calcein-AM/PI Staining

The cells were rinsed with phosphate buffer saline (PBS) two times and incubated with Calcein-AM and PI (Shanghai Bebo Biological Technology Co., Ltd., China) at room temperature for 40 min without light, respectively. The cells were rinsed with PBS again twice and observed using the fluorescence microscope (Leica, Germany).

## ELISA

IL-18 and IL-1 $\beta$  were determined in mice serum and supernatant of cardiomyocytes culture according to the kit instructions provided by Shanghai Fanyin Biotechnology Co., Ltd. (China).

## Virus Transfection

To determine the role of NLRP3 expression in CVB-D inhibition of cardiomyocyte pyroptosis, we designed transfecting cardiomyocytes with NLRP3-shRNA lentivirus. NLRP3-shRNA and shRNA-NC were from Hunan Fenghui Biotechnology Co., Ltd. (China). For NLRP3-shRNA sequences were: GATCCGCGCAGGTTCTACTCCA TCAAAGTTCAAGAGActtgatggagtagaacctgcTTTTTGT. Virus titer:  $1.1 \times 10^8$  (TU/mL).

## Western Blotting

Mice heart tissues and cardiomyocytes were lysed with the RIPA buffer (Beijing Solaibao Technology Co., Ltd., China) to obtain total proteins. The concentration of extracted proteins was determined by using a BCA protein concentration analysis kit (Beijing Solaibao

Technology Co., Ltd., China). The proteins with equal mass were separated into EP tubes, and then they were separated by SDS-PAGE and transferred to the PVDF membrane. After blocking with 5% skim milk at room temperature for 1.5 h, the membranes were incubated with the following primary antibodies at 4°C overnight: NLRP3 (Proteintech, China), pro-caspase-1 (Changzhou Xiangtai Biotechnology Co., Ltd., China), cleaved-caspase-1 (Suzhou Ruiying Biotechnology Co., Ltd., China), IL-18 (Proteintech, China), GSDMD & GSDMD-N (Changzhou Xiangtai Biotechnology Co., Ltd., China), IL-1 $\beta$  (Changzhou Xiangtai Biotechnology Co., Ltd., China), and GAPDH (Proteintech, China). The next day, the membranes were incubated with the corresponding secondary antibody at room temperature for 1.5 h. The ECL buffer (New Sai Mei Biotechnology Co., Ltd., China) was added to the membrane. The protein bands were scanned by Bio-RAD ChemiDoc XRS + imaging system (United States). Image Lab 4.0 software was used for stripe gray value statistical analysis.

## Statistical Analysis

The experimental data were analyzed and processed by GraphPad Prism software, and the results were expressed as the mean  $\pm$  SEM.  $p < 0.05$  was considered statistically significant.

## RESULTS

### CVB-D Improves Cardiac Dysfunction in DCM Mice

The type 2 diabetes model was reproduced by HFD and intraperitoneal injection of STZ in mice. In **Figure 1A**, the model mice showed significant insulin resistance after

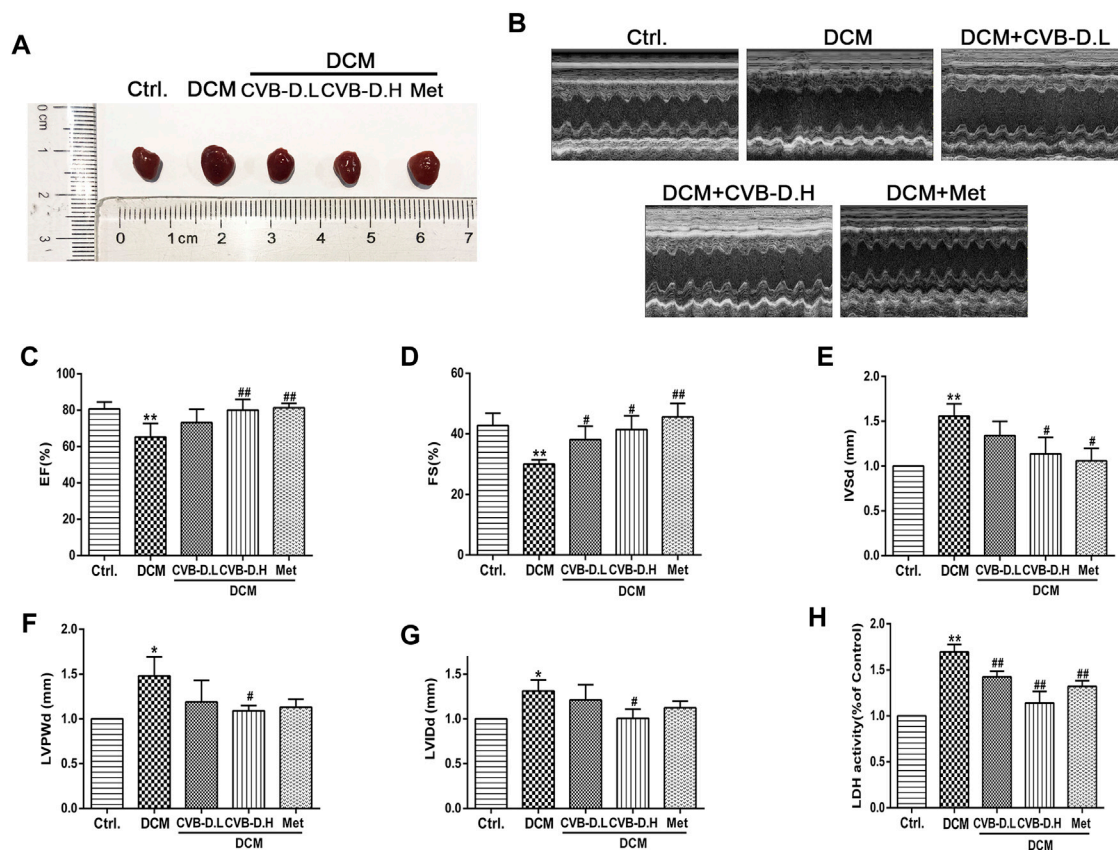


**FIGURE 2 |** CVB-D improves cardiac dysfunction in DCM mice. **(A)** Effects of CVB-D on cardiac hypertrophy in DCM mice. **(B)** Cardiac function of mice was measured by cardiac ultrasound. **(C–G)** The effect of CVB-D on EF (left ventricular ejection fraction), FS (fractional shortening), IVSd (interventricular septal thickness at diastole), LVPWd (left ventricular posterior wall dimensions), LVIDd (left ventricular internal diameter at end-diastole) of DCM mice hearts. **(H)** The content of LDH (lactate dehydrogenase) in serum of mice was detected. The data are presented as the mean  $\pm$  SEM ( $n = 6$ ), \* $p < 0.05$ , \*\* $p < 0.01$  versus the control group; # $p < 0.05$ , ## $p < 0.01$  versus the model group.

12 weeks of HFD compared with the control group. Results of IPGTT (intraperitoneal glucose tolerance test) showed that the blood glucose of mice in the HFD group was significantly higher than the control group at 0, 15, 30, 60, 90, and 120 min after intraperitoneal glucose injection (Figure 1B), and the AUC (area under the curve) of blood glucose was also larger than the control group (Figure 1C). In addition, the FBG, CHO, and TG in mice serum of the model group were significantly increased compared to those in the control group; however, CVB-D did not improve these three indicators, suggesting that CVB-D could not ameliorate metabolic disorder in type 2 diabetes mice (Figures 1D–F). Compared with the control group, the cardiac hypertrophy of mice in the model group was alleviated by CVB-D treatment for 2 months (Figure 2A). Cardiac ultrasonography was widely applied to monitor the cardiac function of mice, and our data indicated that the cardiac systolic and diastolic function deteriorated in EF, FS, IVSd, LVPWd, and LVIDd of DCM mice. After CVB-D treatment, these values were reversed and the cardiac function of mice was improved (Figures 2B–G). In addition, CVB-D was found to significantly reduce serum LDH content in DCM mice

(Figure 2H). Furthermore, compared with the control group, the serum levels of IL-18 and IL-1 $\beta$  in DCM mice were increased, and CVB-D treatment could inhibit the serum levels of these two pro-inflammatory cytokines (Figures 4D,E). Taken together, DCM can be induced by type 2 diabetes, which leads to cardiac hypertrophy, cardiac systolic and diastolic dysfunction, and the release of pro-inflammatory cytokines. All of the harmful changes can be reversed by CVB-D, and these improvement effects do not affect the metabolic disorders of DCM mice.

## CVB-D Prevents Cardiomyocyte Pyroptosis in DCM Mice

Hematoxylin–eosin (HE) staining showed that DCM mice had cardiomyocyte arrangement disorder, cell hypertrophy, and obvious inflammatory cell infiltration; however, CVB-D significantly ameliorated these pathological changes induced by DCM (Figure 3A). Masson staining, as a pathological check for fibrosis, indicates that DCM could result in severe myocardial fibrosis in mice, and CVB-D treatment significantly reduced collagen deposition (Figure 3B).



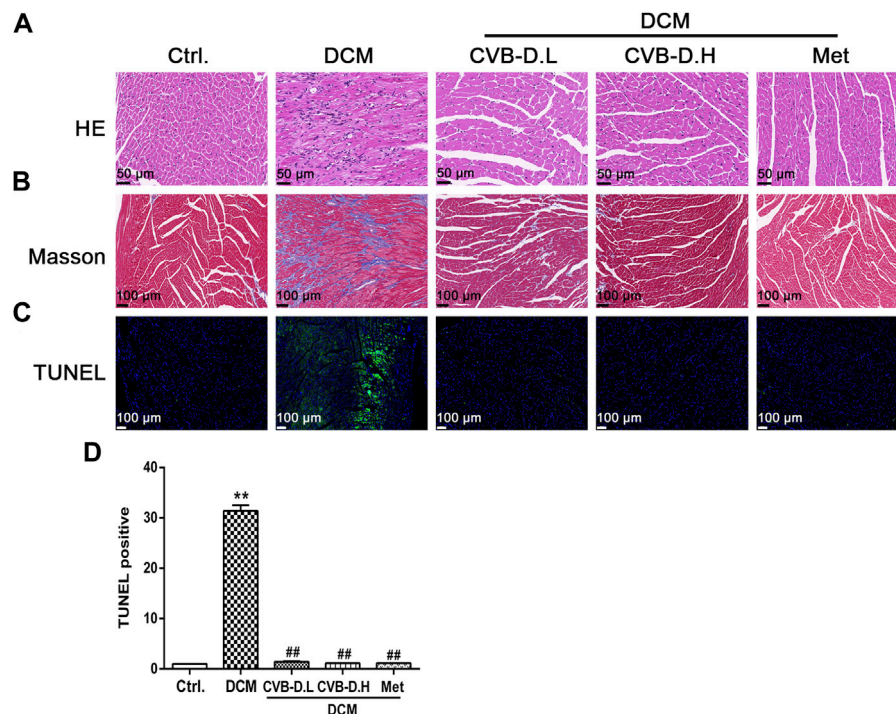


**FIGURE 3 |** CVB-D ameliorates the cardiac physiology changes in DCM mice. **(A)** HE (Hematoxylin-Eosin) staining of mice heart tissues. **(B)** Masson staining was performed in mice heart tissues. **(C,D)** Influence of CVB-D on TUNEL positive cell number. The data are presented as the mean  $\pm$  SEM ( $n = 6$ ), \* $p < 0.05$ , \*\* $p < 0.01$  versus the control group; # $p < 0.05$ , ## $p < 0.01$  versus the model group.

Pyroptosis exhibits some of the morphological characteristics of both apoptosis and necrosis, one of which is DNA fragmentation, so positive results were found in the TUNEL test (Luo et al., 2014). Experimental results suggested that nuclear DNA damage in DCM mice was more serious than in the control group, while CVB-D reversed the phenomenon of myocardial nuclear DNA fragmentation (Figures 3C,D). NLRP3-mediated cardiomyocyte pyroptosis is critical for the initiation and development of DCM, so we measured the protein expression levels of NLRP3, p-caspase-1 (pro-caspase-1), c-caspase-1 (cleaved-caspase-1), GSDMD, GSDMD-N, IL-18, and IL-1 $\beta$  in mice heart tissue by Western blot. Experiment results showed that the expression levels of NLRP3 and pyroptosis pathway-related proteins were significantly increased in the DCM group, and CVB-D could attenuate the expression of these proteins (Figures 4A,B). Immunohistochemical staining results of heart tissues were consistent with Western blot results (Figure 4C). Above all, the present results indicate that CVB-D can significantly improve the cardiac pathological changes in DCM mice, which may be related to the inhibition of NLRP3-mediated cardiomyocyte pyroptosis.

### CVB-D Improves the PNRCM Injury Induced by HG

In order to simulate the physiological environment of DCM, PNRCMs were exposed to 40 mM HG. First, PNRCMs were extracted by the trypsin digestion method and purified by the

differential speed sticking method and then cultured in DMEM medium *in vitro*. The PNRCMs were identified by immunofluorescence staining with cardiomyocyte-specific protein-cardiac troponin T (cTnT) (Figure 5A). MTT results suggested that 25 mM glucose had no effect on the viability of PNRCMs, while 40 mM HG significantly reduced the viability of PNRCMs (Figure 5B). The cytotoxicity test results of CVB-D showed that the concentration of CVB-D had no toxicity on cell viability less than 1  $\mu$ M (Figure 5C). 0.1  $\mu$ M or 1  $\mu$ M CVB-D could reverse the decreased viability of PNRCMs induced by 40 mM HG (Figure 5D). Western blot analysis indicated that HG upregulated the expression level of NLRP3 (Figures 5E,F) and induced PNRCMs pyroptosis, resulting in a significantly higher number of PI stained positive cells than the control group (Figures 5G,H).

Exposure to HG resulted in hypertrophy of PNRCMs, unclear cell membranes, spherical cells with increased oxygen consumption, and nucleus moving to the cell center by Giemsa staining. Preincubation with CVB-D could significantly ameliorate cellular morphology (Figure 5I). Further, IL-18 and IL-1 $\beta$  contents, and LDH release were determined by commercial kits in the cell culture supernatant. Experimental results showed that HG induced the secretion of large amounts of IL-18 and IL-1 $\beta$  into the culture medium, and LDH released leakage as well. The CVB-D could inhibit the increase of IL-18 and IL-1 $\beta$ , and release leakage of LDH in the medium (Figure 5J-L). To sum up, CVB-D could alleviate the



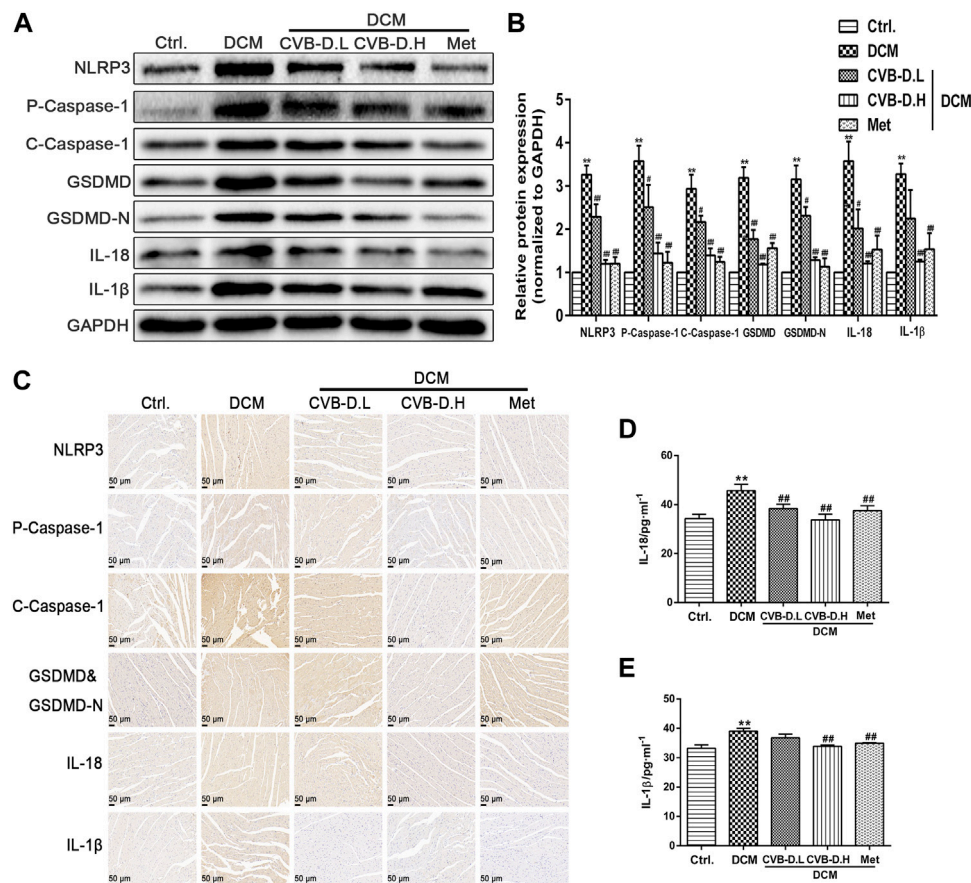


**FIGURE 4 |** CVB-D inhibits the expression of pyroptosis-related proteins in the heart tissue of DCM mice. **(A,B)** Determination of NLRP3 and pyroptosis pathway-related proteins expression in heart tissues of DCM mice by western blotting, and all proteins expression were normalized to GAPDH. **(C)** The expressions of NLRP3, P-Caspase-1 (Pro-Caspase-1), C-Caspase-1 (Cleaved-Caspase-1), GSDMD&GSDMD-N, IL-18 and IL-1β were observed by immunohistochemistry. **(D,E)** Effects of CVB-D on the contents of IL-18 and IL-1β in mice serum. The data are presented as the mean  $\pm$  SEM ( $n = 6$ ), \* $p < 0.05$ , \*\* $p < 0.01$  versus the control group; # $p < 0.05$ , ## $p < 0.01$  versus the model group.

damage and pathological changes of PNRCMs induced by HG, thus playing a protective role in the myocardium.

## CVB-D Inhibits PNRCMs Pyroptosis Induced by HG

In order to further investigate the inhibitory effect of CVB-D on PNRCMs pyroptosis induced by HG, the expression levels of NLRP3, p-caspase-1 (pro-caspase-1), c-caspase-1 (cleaved-caspase-1), GSDMD, GSDMD-N, IL-18, and IL-1β were assayed using the immunofluorescence method. The results showed that NLRP3 was greatly activated under high-glucose stimulation, and the activated NLRP3 induced pro-caspase-1 activation, as well as downstream GSDMD, GSDMD-N, IL-18, and IL-1β maturation. CVB-D inhibited the expression of these relevant proteins, that is, preventing PNRCM pyroptosis (Figures 6A–G). After extracellular proteins were extracted, the results of Western blot were consistent with the immunofluorescence staining results (Figures 6H,I). We further observed the DNA breakage and cell membrane damage of cardiomyocytes by PI

staining and found that CVB-D could significantly reduce the number of PI-stained positive cells. So, we thought CVB-D reversed PNRCMs pyroptosis induced by HG (Figures 6J,K). It was found that CVB-D improves the PNRCM pyroptosis caused by HG.

## CVB-D Ameliorates HG-Induced PNRCM Injury by Inhibiting Cardiomyocyte Pyroptosis via NLRP3

The pharmacological NLRP3 inhibitor (MCC950) and agonist (BMS-986299) were used to investigate the role of NLRP3 in CVB-D inhibition of pyroptosis in HG-induced PNRCMs. Cytotoxicity of MCC950 and BMS-986299 were determined by MTT assay (Figures 7A,G). Then, we detected LDH releasing leakage in the cell culture supernatant, NLRP3, and pyroptosis pathway-related proteins expression levels. The results suggested that MCC950 inhibited the expression of NLRP3 and downregulated the expression of pyroptosis-related proteins. Thus, MCC950 inhibited cardiomyocyte

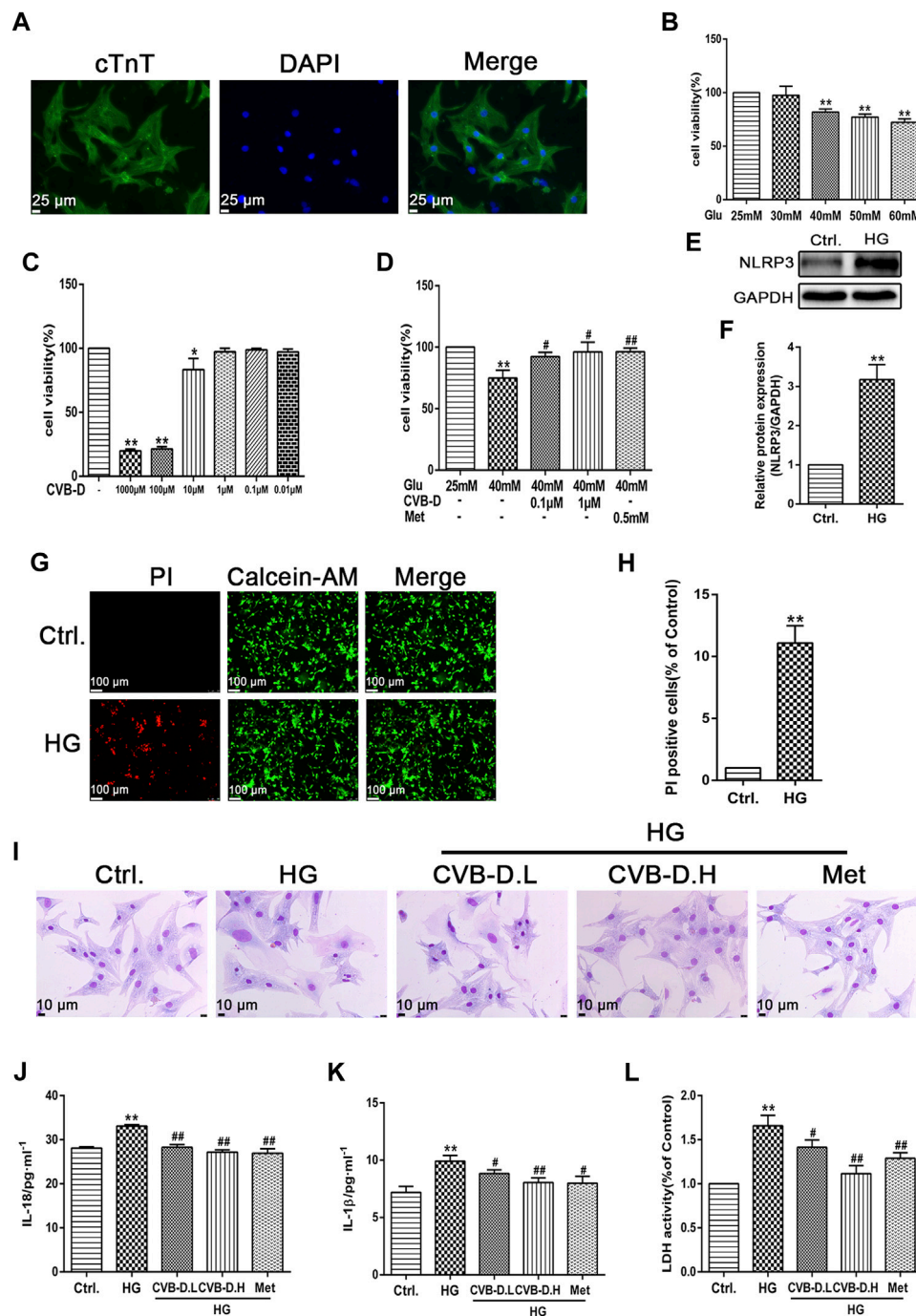


**FIGURE 5 |** CVB-D improves the PNRCMs (primary neonatal rat cardiomyocytes) injury induced by HG (high glucose). **(A)** Immunofluorescence was used to identify the purity of PNRCMs. **(B–D)** The effect of CVB-D on the decreased viability of PNRCMs induced by HG was detected by MTT assay. **(E,F)** Western blotting was used to determine the effect of HG on NLRP3 expression in PNRCMs. **(G,H)** Calcein-AM/PI staining was used to observe cardiomyocyte pyroptosis caused by HG. **(I)** Effects of CVB-D on pathological changes of PNRCMs induced by HG were observed by Giemsa staining. **(J–L)** Influence of CVB-D on the contents of IL-18, IL-1 $\beta$  and LDH in the supernatant of PNRCMs culture medium were detected by ELISA and LDH kits. The data are presented as the mean  $\pm$  SEM ( $n = 3$ ), \* $p < 0.05$ , \*\* $p < 0.01$  versus the control group; # $p < 0.05$ , ## $p < 0.01$  versus the model group.

pyroptosis and alleviated LDH leakage caused by HG. For the LDH content in the medium and Western blot, the results showed that there was no statistical difference compared to

HG + MCC950 with HG + CVB-D + MCC950 groups (**Figures 7B,E,F**). The results of the number of positive cells stained by PI were the same as the Western blot results (**Figures 7C,D**). In

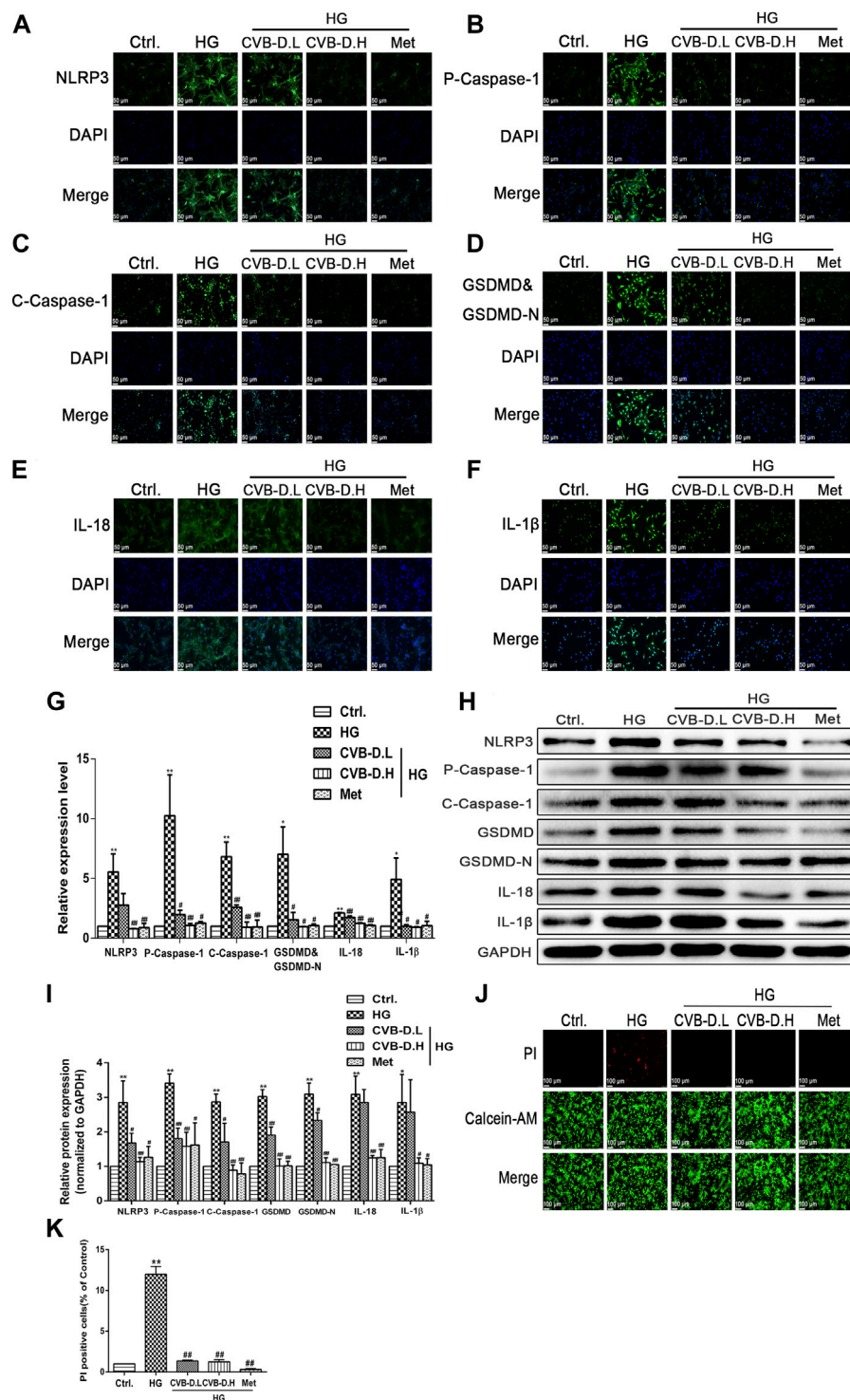


**FIGURE 6 |** CVB-D inhibits PNCrMs pyroptosis induced by HG. **(A–F)** The effect of CVB-D on the expression of pyroptosis pathway proteins was observed by immunofluorescence. **(G)** The fluorescence values of each group were counted by ImageJ software. **(H,I)** Western blotting was used to determine the expression level of pyroptosis related proteins after CVB-D treatment. **(J,K)** Pyroptosis and living cells were differentiated by Calcein-AM/PI staining after CVB-D treatment. The data are presented as the mean  $\pm$  SEM ( $n = 3$ ). \* $p < 0.05$ , \*\* $p < 0.01$  versus the control group; # $p < 0.05$ , ## $p < 0.01$  versus the model group.



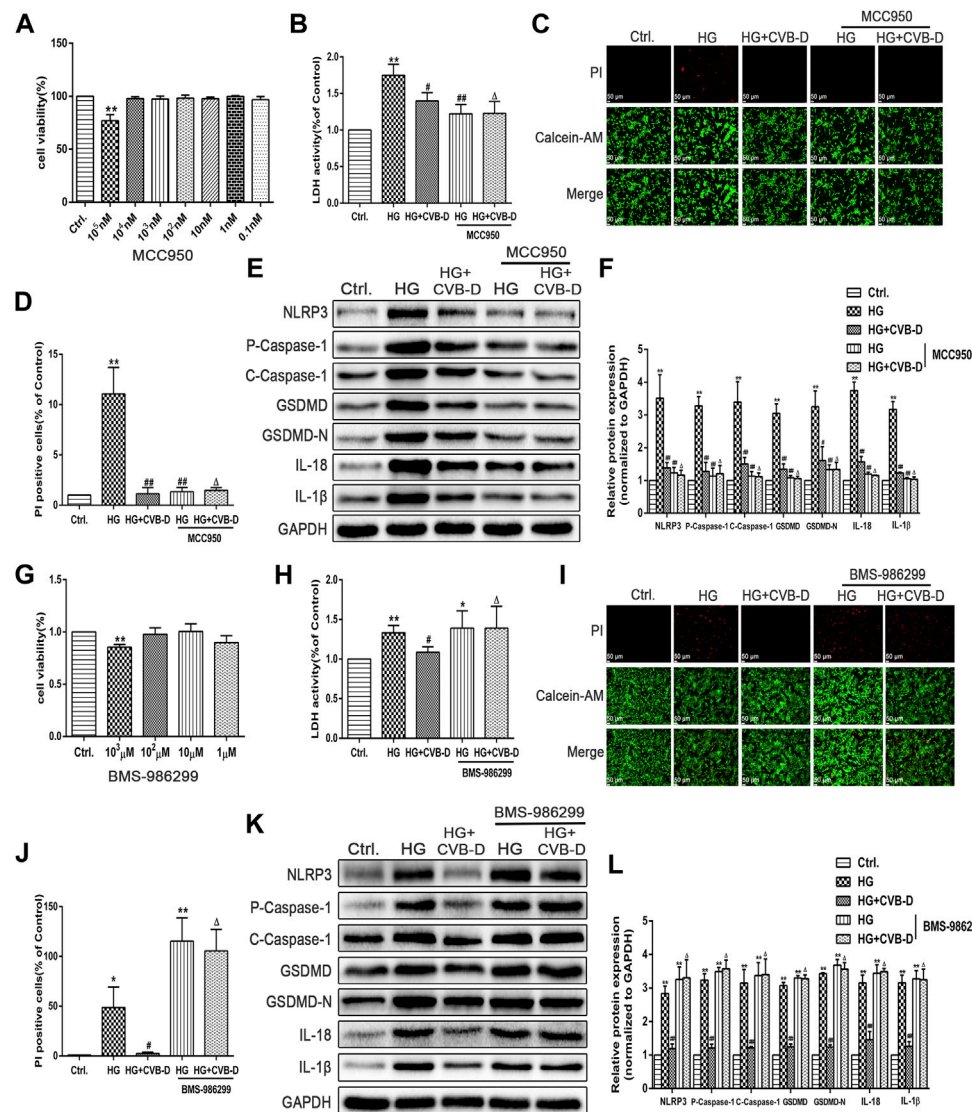


**FIGURE 7 |** CVB-D ameliorates HG-induced PNRCMs injury by inhibiting cardiomyocyte pyroptosis via NLRP3. **(A)** Cytotoxicity of MCC950 was detected by MTT assay. **(B)** After pretreatment with MCC950, LDH content in cell culture supernatant was detected. **(C,D)** The effect of MCC950 on cardiomyocyte pyroptosis was judged by the number of PI staining positive cells. **(E,F)** The expression level of pyroptosis related proteins was detected by western blotting with MCC950 pretreatment. The data are presented as the mean  $\pm$  SEM ( $n = 3$ ), \* $p < 0.05$ , \*\* $p < 0.01$  versus the control group; # $p < 0.05$ , ## $p < 0.01$  versus the model group;  $\Delta p > 0.05$  versus the HG+MCC950 group. **(G)** Cytotoxicity of BMS-986299 was detected by MTT assay. **(H)** LDH content in cell culture supernatant was detected after pretreatment with BMS-986299. **(I,J)** The effect of BMS-986299 on cardiomyocyte pyroptosis was observed by PI staining. **(K,L)** Western blotting was used to detected proteins expression in pyroptosis pathway with BMS-986299 pretreatment. The data are presented as the mean  $\pm$  SEM ( $n = 3$ ), \* $p < 0.05$ , \*\* $p < 0.01$  versus the control group; # $p < 0.05$ , ## $p < 0.01$  versus the model group;  $\Delta p > 0.05$  versus the HG+BMS-986299 group.

addition, the results of calcein-AM/PI staining suggested that the inhibition effect of CVB-D on cardiomyocyte pyroptosis was abrogated by BMS-986299, which also increased CVB-D-induced downregulation of LDH content in the medium (Figures 7H–J). The pyroptosis pathway-related protein expression was determined by Western blot. Compared with the HG + BMS-986299 group, HG + CVB-D + BMS-986299 could not further affect the expression of pyroptosis-related proteins (Figures 7K,L).

To further clarify the role of NLRP3 in CVB-D inhibition PNRCMs pyroptosis, we transfected NLRP3-shRNA lentivirus into PNRCMs. The results showed that NLRP3-shRNA and CVB-D significantly reduced the expression of NLRP3 and pyroptosis pathway-related proteins. Consistently, LDH leakage results and protein expression results showed no significant difference between the HG + NLRP3-shRNA group and the HG + NLRP3-shRNA + CVB-D group (Figures 8A–C). Our results consistently showed that



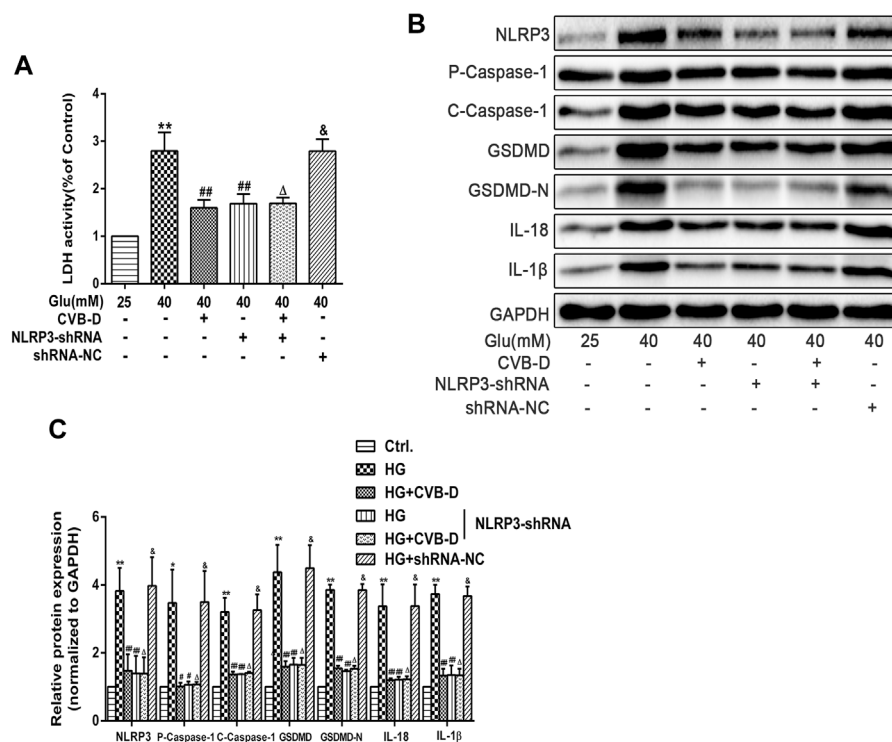


**FIGURE 8 |** NLRP3-shRNA verifies the regulation mechanism of CVB-D inhibition pyroptosis induced by HG in PNRCMs. **(A)** LDH release in cell culture supernatant was detected after NLRP3-shRNA lentivirus-infected. **(B,C)** Western blotting was used to detected proteins expression in pyroptosis pathway after NLRP3-shRNA lentivirus infection with PNRCMs. The data are presented as the mean  $\pm$  SEM ( $n = 3$ ),  $*p < 0.05$ ,  $**p < 0.01$  versus the control group;  $^{\#}p < 0.05$ ,  $^{\#\#}p < 0.01$  versus the model group;  $^{\Delta}p > 0.05$  versus the HG+NLRP3-shRNA group;  $^{\delta}p > 0.05$  versus the model group.

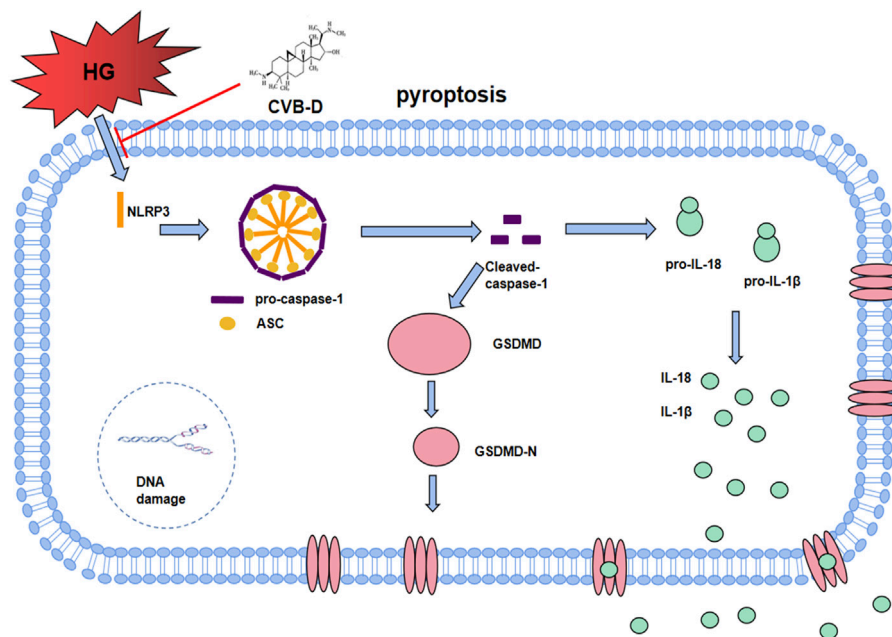


**FIGURE 9 |** The molecular regulation mechanism of CVB-D improving DCM. After HG induced NLRP3 overactivation, it assembles with ASC and pro-caspase-1 to form inflammasome. After Cleaved-caspase-1 is activated, on the one hand, it activates GSDMD-N to cause pore formation on cell membrane. On the other hand, Cleaved-caspase-1 promotes the maturation and secretion of IL-18 and IL-1β, finally leads to cardiomyocyte pyroptosis, accelerating the progress of DCM. CVB-D significantly ameliorates DCM, which may be associated with the inhibition of NLRP3-mediated cardiomyocyte pyroptosis.

CVB-D ameliorated HG-induced PNRCMs pyroptosis, at least in part, *via* NLRP3.

## DISCUSSION

Cardiovascular complications from diabetes have been the leading cause of morbidity and mortality worldwide. DCM is a descriptive pathology that can be defined as changes in the myocardial structure and function independent of other conventional cardiac risk factors, including hypertension, coronary atherosclerotic heart disease (CAD), and significant heart valve disease in diabetic patients (Bell and Goncalves, 2019). DCM has no clinical symptoms in the early stages of its progression (Jia et al., 2016). In the first stage, it mainly presents as various forms of cardiometabolic abnormalities, which may be associated with increased myocardial fibrosis and stiffness. Those harmful changes further lead to atrioventricular filling dysfunction and increased left ventricular end-diastolic pressure (Westermeyer et al., 2016). The second stage is the evolution of DCM to heart failure, followed by cardiac remodeling, left ventricular hypertrophy, myocardial interstitial fibrosis, and diastolic dysfunction, which further leads to heart failure with reduced ejection fraction (Jia et al., 2016). Due to the complexity of the pathogenesis and clinical characteristics of DCM, the clinical treatment of DCM is facing a great challenge.

Although extensive research has been carried out in the past 10 years, there is still no convincing method for the treatment of DCM. In 2008, the United States Food and Drug Administration (USFDA) also proposed that for diabetes-induced cardiovascular complications, only controlling blood glucose is not enough (Kant et al., 2019), so it is necessary to further explore the pathological basis of DCM. According to literature reports, many harmful factors, such as oxidative stress, inflammation, cardiomyocyte death, interstitial fibrosis of cardiac tissue, and cardiac stiffness, lead to diastolic and systolic dysfunction. These lesions are the initiation and progression of DCM, and ultimately result in heart failure (Palmieri et al., 2001; Levelt et al., 2016). NLRP3, the most widely studied type of inflammasome, is involved in a variety of physiological processes *in vivo* (Zeng et al., 2019). In addition, accumulating evidence has shown that NLRP3 overexpression can be induced in a hyperglycemic environment, leading to pyroptosis, a strong pro-inflammatory cell death mode (Kroemer et al., 2009; Coll et al., 2011). Recently, it is well known that pyroptosis accelerates the deterioration of DCM (Luo et al., 2014). Above all, based on the complexity of the pathological basis of DCM, combined with the laboratory preliminary studies, we have confirmed that CVB-D, an important pharmacodynamic component of Chinese medicine *Caulis et Ramulus Buxi Sinicae*, could improve DCM by activating Nrf2-mediated antioxidant reaction (Jiang et al., 2020). Therefore, we further explored the molecular regulatory mechanism of CVB-D on the improvement of DCM by

taking the NLRP3-mediated cardiomyocyte pyroptosis as the research route.

We successfully reproduced the type 2 diabetes model *in vivo* through a high-fat and high-glucose diet and low-dose STZ. The experimental results suggested that compared with the control group, DCM mice showed significant cardiac hypertrophy and cardiac systolic and diastolic dysfunction. The mice in the model group also showed many harmful changes, such as increased levels of serum inflammatory cytokines IL-18 and IL-1 $\beta$ , which were consistent with the clinical characteristics of DCM (Jia et al., 2016; Westermeyer et al., 2016). In addition, we observed the pathological changes in the heart tissue in mice and found obvious inflammatory cell infiltration, myocardial fibrosis, and DNA breakage. These results suggested that inflammation plays a key role in the progression of DCM. CVB-D alleviated the aforementioned deterioration, indicating that the improvement of DCM by CVB-D was related to the inhibition of inflammatory response.

In the NLRs family, NLRP3 has been identified as a key node-like receptor family member that can recognize microbial and non-microbial danger signals and trigger aseptic inflammatory responses in various disease conditions (Yang et al., 2018; Jin et al., 2021). Recognition signals are transduced to the inflammasome adapter ASC (apoptosis-associated speck-like protein containing a CARD) to further activate pro-caspase-1, followed by IL-18/1 $\beta$  release and GSDMD cleavage to induce pyroptosis (Zhao et al., 2018). In both *in vivo* and *in vitro* experiments, we found that a high-glucose environment significantly upregulated the expression of NLRP3 and pyroptosis pathway-related proteins, and CVB-D inhibited the expression of these proteins. Pyroptosis can deteriorate DNA breakage, so calcein/PI staining was used to identify pyroptosis and living cells. Experimental results showed that the number of PI staining positive cells in the CVB-D group was significantly lower than that in the HG group, showing that CVB-D prevented cardiomyocyte pyroptosis induced by HG. To further explore the relationship between CVB-D improving the PNRCM pyroptosis induced by HG and inhibition expression of NLRP3, we investigated the effect of pharmacological NLRP3 inhibitor (MCC950), agonist (BMS-986299), and NLRP3-shRNA lentivirus on the inhibition of PNRCM pyroptosis by CVB-D. There was no significant difference in the expression levels of NLRP3 and pyroptosis-related proteins between the two groups when the MCC950 or BMS-986299 was used in combination with CVB-D compared with the MCC950 or BMS-986299 alone under the condition of HG. The results suggested that CVB-D may ameliorate the HG-induced PNRCM injury by inhibiting cardiomyocyte pyroptosis *via* NLRP3 (Figure 9).

In summary, our experimental results are consistent with previous studies, and CVB-D has a significant improvement effect on DCM, which can reverse the cardiac dysfunction and pathological changes caused by DCM. The molecular mechanism may be involved that CVB-D inhibits cardiomyocyte pyroptosis *via* NLRP3 to improve DCM. The present results provide a novel idea for the clinical application of CVB-D.

## DATA AVAILABILITY STATEMENT

The original contributions presented in the study are included in the article/Supplementary Material; further inquiries can be directed to the corresponding authors.

## ETHICS STATEMENT

The animal study was reviewed and approved by the experiment was approved by the Animal Ethics Committee of Guizhou Medical University (No. 2000904), Guizhou Medical University, Guiyang, China.

## AUTHOR CONTRIBUTIONS

GG, GF, GZ, SW, TG, and TQ designed and performed experiments, and wrote the manuscript. LF, YX, and LT prepared figures and analyzed the data. PL and XS provided ideas, reviewed the manuscript, and provided financial support.

## REFERENCES

- Bell, D. S. H., and Goncalves, E. (2019). Heart Failure in the Patient with Diabetes: Epidemiology, Aetiology, Prognosis, Therapy and the Effect of Glucose-Lowering Medications. *Diabetes Obes. Metab.* 21 (6), 1277–1290. doi:10.1111/dom.13652
- Boudina, S., and Abel, E. D. (2010). Diabetic Cardiomyopathy, Causes and Effects. *Rev. Endocr. Metab. Disord.* 11 (1), 31–39. doi:10.1007/s11154-010-9131-7
- Chen, H., Lu, Y., Cao, Z., Ma, Q., Pi, H., Fang, Y., et al. (2016). Cadmium Induces Nlrp3 Inflammasome-dependent Pyroptosis in Vascular Endothelial Cells. *Toxicol. Lett.* 246, 7–16. doi:10.1016/j.toxlet.2016.01.014
- Coll, N. S., Eppler, P., and Dangl, J. L. (2011). Programmed Cell Death in the Plant Immune System. *Cell Death Differ.* 18 (8), 1247–1256. doi:10.1038/cdd.2011.37
- Falcão-Pires, L., and Leite-Moreira, A. F. (2012). Diabetic Cardiomyopathy: Understanding the Molecular and Cellular Basis to Progress in Diagnosis and Treatment. *Heart Fail Rev.* 17 (3), 325–344. doi:10.1007/s10741-011-9257-z
- Guo, D., Li, J. R., Wang, Y., Lei, L. S., Yu, C. L., and Chen, N. N. (2014). Cycloviobuxinum D Suppresses Lipopolysaccharide-Induced Inflammatory Responses in Murine Macrophages *In Vitro* by Blocking Jak-Stat Signaling Pathway. *Acta Pharmacol. Sin.* 35 (6), 770–778. doi:10.1038/aps.2014.16
- Guo, Q., Guo, J., Yang, R., Peng, H., Zhao, J., Li, L., et al. (2015). Cycloviobuxine D Attenuates Doxorubicin-Induced Cardiomyopathy by Suppression of Oxidative Damage and Mitochondrial Biogenesis Impairment. *Oxid. Med. Cell Longev.* 2015, 151972. doi:10.1155/2015/151972
- Hu, X., Bai, T., Xu, Z., Liu, Q., Zheng, Y., and Cai, L. (2017). Pathophysiological Fundamentals of Diabetic Cardiomyopathy. *Compr. Physiol.* 7 (2), 693–711. doi:10.1002/cphy.c160021
- Jia, G., Demarco, V. G., and Sowers, J. R. (2016). Insulin Resistance and Hyperinsulinaemia in Diabetic Cardiomyopathy. *Nat. Rev. Endocrinol.* 12 (3), 144–153. doi:10.1038/nrendo.2015.216
- Jia, C., Chen, H., Zhang, J., Zhou, K., Zhuhe, Y., Niu, C., et al. (2019). Role of Pyroptosis in Cardiovascular Diseases. *Int. Immunopharmacol.* 67, 311–318. doi:10.1016/j.intimp.2018.12.028
- Jiang, H., He, H., Chen, Y., Huang, W., Cheng, J., Ye, J., et al. (2017). Identification of a Selective and Direct Nlrp3 Inhibitor to Treat Inflammatory Disorders. *J. Exp. Med.* 214 (11), 3219–3238. doi:10.1084/jem.20171419
- Jiang, Z., Fu, L., Xu, Y., Hu, X., Yang, H., Zhang, Y., et al. (2020). Cycloviobuxine D Protects against Diabetic Cardiomyopathy by Activating Nrf2-Mediated

All authors contributed to the article and approved the submitted version.

## FUNDING

This study was supported by the National Natural Science Foundation of China (No. 82060729 and U1812403-4-4), the Fund of High-Level Innovation Talents (No. 2015-4029), the base of International Scientific and Technological Cooperation of Guizhou Province [No. (2017)5802], the National Natural Science Foundation of Guizhou Medical University (No. 19NSP076), and the Fund of 2018 Academic New Seedling Cultivation and Innovation Exploration Special project of Guizhou Medical University (No. [2018]5779-66).

## ACKNOWLEDGMENTS

We thank PL, XS, and other members of the laboratory for professional advice and financial support.

- Antioxidant Responses. *Sci. Rep.* 10 (1), 6427. doi:10.1038/s41598-020-63498-3
- Jin, X., Fu, W., Zhou, J., Shuai, N., Yang, Y., and Wang, B. (2021). Oxymatrine Attenuates Oxidized Low-density Lipoprotein-induced HUVEC Injury by Inhibiting NLRP3 Inflammasome-mediated Pyroptosis via the Activation of the SIRT1/Nrf2 Signaling Pathway. *Int. J. Mol. Med.* 48 (4), 187. doi:10.3892/ijmm.2021.5020
- Kant, R., Munir, K. M., Kaur, A., and Verma, V. (2019). Prevention of Macrovascular Complications in Patients with Type 2 Diabetes Mellitus: Review of Cardiovascular Safety and Efficacy of Newer Diabetes Medications. *World J. Diabetes* 10 (6), 324–332. doi:10.4239/wjd.v10.i6.324
- Kaul, K., Hodgkinson, A., Tarr, J. M., Kohner, E. M., and Chibber, R. (2010). Is Inflammation a Common Retinal-Renal-Nerve Pathogenic Link in Diabetes? *Curr. Diabetes Rev.* 6 (5), 294–303. doi:10.2174/157339910793360851
- Kroemer, G., Galluzzi, L., Vandenabeele, P., Abrams, J., Alnemri, E. S., Baehrecke, E. H., et al. (2009). Classification of Cell Death: Recommendations of the Nomenclature Committee on Cell Death 2009. *Cell Death Differ.* 16 (1), 3–11. doi:10.1038/cdd.2008.150
- Levelt, E., Mahmod, M., Piechnik, S. K., Ariga, R., Francis, J. M., Rodgers, C. T., et al. (2016). Relationship between Left Ventricular Structural and Metabolic Remodeling in Type 2 Diabetes. *Diabetes* 65 (1), 44–52. doi:10.2337/db15-0627
- Li, X., Du, N., Zhang, Q., Li, J., Chen, X., Liu, X., et al. (2014). MicroRNA-30d Regulates Cardiomyocyte Pyroptosis by Directly Targeting Foxo3a in Diabetic Cardiomyopathy. *Cell Death Dis.* 5 (10), e1479. doi:10.1038/cddis.2014.430
- Li, P., Zhong, X., Li, J., Liu, H., Ma, X., He, R., et al. (2018). MicroRNA-30c-5p Inhibits Nlrp3 Inflammasome-Mediated Endothelial Cell Pyroptosis through Foxo3 Down-Regulation in Atherosclerosis. *Biochem. Biophys. Res. Commun.* 503 (4), 2833–2840. doi:10.1016/j.bbrc.2018.08.049
- Luo, B., Li, B., Wang, W., Liu, X., Xia, Y., Zhang, C., et al. (2014). Nlrp3 Gene Silencing Ameliorates Diabetic Cardiomyopathy in a Type 2 Diabetes Rat Model. *PLoS One* 9 (8), e104771. doi:10.1371/journal.pone.0104771
- Mandavia, C. H., Aroor, A. R., Demarco, V. G., and Sowers, J. R. (2013). Molecular and Metabolic Mechanisms of Cardiac Dysfunction in Diabetes. *Life Sci.* 92 (11), 601–608. doi:10.1016/j.lfs.2012.10.028
- Martinon, F., Burns, K., and Tschopp, J. (2002). The Inflammasome: A Molecular Platform Triggering Activation of Inflammatory Caspases and Processing of Proil-Beta. *Mol. Cell* 10 (2), 417–426. doi:10.1016/s1097-2765(02)00599-3
- Palmieri, V., Bella, J. N., Arnett, D. K., Liu, J. E., Oberman, A., Schuck, M. Y., et al. (2001). Effect of Type 2 Diabetes Mellitus on Left Ventricular Geometry and Systolic Function in Hypertensive Subjects: Hypertension Genetic

- Epidemiology Network (Hypergen) Study. *Circulation* 103 (1), 102–107. doi:10.1161/01.cir.103.1.102
- Toldo, S., and Abbate, A. (2018). The Nlrp3 Inflammasome in Acute Myocardial Infarction. *Nat. Rev. Cardiol.* 15 (4), 203–214. doi:10.1038/nrcardio.2017.161
- Toldo, S., Mauro, A. G., Cutter, Z., and Abbate, A. (2018). Inflammasome, Pyroptosis, and Cytokines in Myocardial Ischemia-Reperfusion Injury. *Am. J. Physiol. Heart Circ. Physiol.* 315 (6), H1553–h1568. doi:10.1152/ajpheart.00158.2018
- Westermeier, F., Riquelme, J. A., Pavez, M., Garrido, V., Díaz, A., Verdejo, H. E., et al. (2016). New Molecular Insights of Insulin in Diabetic Cardiomyopathy. *Front. Physiol.* 7, 125. doi:10.3389/fphys.2016.00125
- Wree, A., Eguchi, A., Mcgeough, M. D., Pena, C. A., Johnson, C. D., Canbay, A., et al. (2014). Nlrp3 Inflammasome Activation Results in Hepatocyte Pyroptosis, Liver Inflammation, and Fibrosis in Mice. *Hepatology* 59 (3), 898–910. doi:10.1002/hep.26592
- Wu, J. B., Zhou, Y., Liang, C. L., Zhang, X. J., Lai, J. M., Ye, S. F., et al. (2017). Cycloviobuxinum D Alleviates Cardiac Hypertrophy in Hyperthyroid Rats by Preventing Apoptosis of Cardiac Cells and Inhibiting the P38 Mitogen-Activated Protein Kinase Signaling Pathway. *Chin. J. Integr. Med.* 23 (10), 770–778. doi:10.1007/s11655-015-2299-7
- Xu, J., Jiang, Y., Wang, J., Shi, X., Liu, Q., Liu, Z., et al. (2014). Macrophage Endocytosis of High-Mobility Group Box 1 Triggers Pyroptosis. *Cell Death Differ.* 21 (8), 1229–1239. doi:10.1038/cdd.2014.40
- Xu, Y. J., Zheng, L., Hu, Y. W., and Wang, Q. (2018). Pyroptosis and its Relationship to Atherosclerosis. *Clin. Chim. Acta* 476, 28–37. doi:10.1016/j.cca.2017.11.005
- Yang, F., Qin, Y., Wang, Y., Li, A., Lv, J., Sun, X., et al. (2018). Lncrna KCNQ1OT1 Mediates Pyroptosis in Diabetic Cardiomyopathy. *Cell Physiol. Biochem.* 50 (4), 1230–1244. doi:10.1159/000494576
- Zeng, C., Wang, R., and Tan, H. (2019). Role of Pyroptosis in Cardiovascular Diseases and its Therapeutic Implications. *Int. J. Biol. Sci.* 15 (7), 1345–1357. doi:10.7150/ijbs.33568
- Zhang, Y., Liu, X., Bai, X., Lin, Y., Li, Z., Fu, J., et al. (2018). Melatonin Prevents Endothelial Cell Pyroptosis via Regulation of Long Noncoding Rna Meg3/Mir-223/Nlrp3 Axis. *J. Pineal Res.* 64 (2), 1–13. doi:10.1111/jpi.12449
- Zhao, L., Xu, Y., Tao, L., Yang, Y., Shen, X., Li, L., et al. (2018). Oxymatrine Inhibits Transforming Growth Factor  $\beta$ 1 (TGF- $\beta$ 1)-Induced Cardiac Fibroblast-To-Myofibroblast Transformation (FMT) by Mediating the Notch Signaling Pathway *In Vitro. Med. Sci. Monit.* 24, 6280–6288. doi:10.12659/msm.910142

**Conflict of Interest:** The authors declare that the research was conducted in the absence of any commercial or financial relationships that could be construed as a potential conflict of interest.

**Publisher's Note:** All claims expressed in this article are solely those of the authors and do not necessarily represent those of their affiliated organizations, or those of the publisher, the editors, and the reviewers. Any product that may be evaluated in this article, or claim that may be made by its manufacturer, is not guaranteed or endorsed by the publisher.

Copyright © 2022 Gao, Fu, Xu, Tao, Guo, Fang, Zhang, Wang, Qin, Luo and Shen. This is an open-access article distributed under the terms of the Creative Commons Attribution License (CC BY). The use, distribution or reproduction in other forums is permitted, provided the original author(s) and the copyright owner(s) are credited and that the original publication in this journal is cited, in accordance with accepted academic practice. No use, distribution or reproduction is permitted which does not comply with these terms.



# Advantages of publishing in Frontiers



## OPEN ACCESS

Articles are free to read  
for greatest visibility  
and readership



## FAST PUBLICATION

Around 90 days  
from submission  
to decision



## HIGH QUALITY PEER-REVIEW

Rigorous, collaborative,  
and constructive  
peer-review



## TRANSPARENT PEER-REVIEW

Editors and reviewers  
acknowledged by name  
on published articles

## Frontiers

Avenue du Tribunal-Fédéral 34  
1005 Lausanne | Switzerland

**Visit us:** [www.frontiersin.org](http://www.frontiersin.org)

**Contact us:** [frontiersin.org/about/contact](http://frontiersin.org/about/contact)



## REPRODUCIBILITY OF RESEARCH

Support open data  
and methods to enhance  
research reproducibility



## DIGITAL PUBLISHING

Articles designed  
for optimal readership  
across devices



## FOLLOW US

@frontiersin



## IMPACT METRICS

Advanced article metrics  
track visibility across  
digital media



## EXTENSIVE PROMOTION

Marketing  
and promotion  
of impactful research



## LOOP RESEARCH NETWORK

Our network  
increases your  
article's readership